Study and applications of the H-Si bond activation of silanes by iridacycles : a contribution to the design of multicompetent catalysts

Mustapha Hamdaoui

▶ **To cite this version:**

Mustapha Hamdaoui. Study and applications of the H-Si bond activation of silanes by iridacycles : a contribution to the design of multicompetent catalysts. Other. Université de Strasbourg, 2017. English. NNT : 2017STRAF007 . tel-02003516

HAL Id: tel-02003516
https://theses.hal.science/tel-02003516

Submitted on 1 Feb 2019

HAL is a multi-disciplinary open access archive for the deposit and dissemination of scientific research documents, whether they are published or not. The documents may come from teaching and research institutions in France or abroad, or from public or private research centers.

L'archive ouverte pluridisciplinaire **HAL**, est destinée au dépôt et à la diffusion de documents scientifiques de niveau recherche, publiés ou non, émanant des établissements d'enseignement et de recherche français ou étrangers, des laboratoires publics ou privés.

UNIVERSITÉ DE STRASBOURG

ÉCOLE DOCTORALE DES SCIENCES CHIMIQUES ED222

Institut de Chimie de Strasbourg UMR 7177

THÈSE présentée par :

Mustapha HAMDAOUI

soutenue le : **30 janvier 2017**

pour obtenir le grade de : **docteur de l'université de Strasbourg**

Discipline/ Spécialité : **CHIMIE**

ÉTUDE ET APPLICATIONS DE LA RÉACTION D'ACTIVATION DES SILANES PAR LES IRIDACYCLES

Une contribution á l'élaboration de catalyseurs multicompétents

THÈSE dirigée par :

Mr DJUKIC Jean-Pierre	Directeur de Recherche CNRS, université de Strasbourg, France

RAPPORTEURS :

Mr RICHARDS Christopher John	Reader, university of East Anglia, United Kingdom
Mr GRELLIER Mary	Maître de Conférences, université Paul Sabatier,Toulouse, France

AUTRES MEMBRS DU JURY :

Mr ARMSPACH Dominique	Professeur des Universités, université de Strasbourg, France

Table of contents

Remerciements

Tout d'abord, je remercie chaleureusement Dr. Jean-Pierre Djukic, mon directeur de thèse. Jean-Pierre, je vous suis très reconnaissant de m'avoir donné l'opportunité de faire partie de ce projet de recherche. Merci de m'avoir donné ma chance, d'avoir cru en moi, et de m'avoir soutenu tout au long de notre projet. Cela a été enrichissant et passionnant de travailler au côté d'un homme d'une si grande culture intellectuelle et ouverture d'esprit. Merci d'avoir fait de moi le jeune chercheur que je suis devenu aujourd'hui, que je n'étais pas encore au début de cette thèse.

Un grand merci à vous Dr. Michel Pfeffer de m'avoir ouvert pour la toute première fois les portes de votre laboratoire lors de mon stage de master 2. Merci pour votre confiance et votre bienveillance. Merci également pour vos conseils et votre gentillesse à mon égard. Je suis fier d'avoir travaillé à vos côtés.

Je remercie tous les membres du jury. Merci Pr. Dominique Armspach. Merci Dr. Mary Grellier. Merci Pr. Christopher John Richards. Merci Dr. Vincent Ritleng. Merci à vous tous. Je vous suis très reconnaissant d'avoir accepté de juger ce travail de thèse, d'y consacrer une part non négligeable de votre temps, et pour votre généreuse disponibilité.

Je remercie Dr. Laurent Barloy et Dr. Vincent Ritleng d'avoir généreusement accepté de juger mon travail à mi-parcours.

Un grand merci à tous les étudiants qui ont collaboré avec moi pour mener à bien ce projet de recherche. J'ai eu de la chance de vous fréquenter et de vous encadrer. Dans l'ordre dans lequel chacun d'entre vous a effectué son stage au sein du laboratoire, j'exprime ma gratitude à Thomas De Oliveira, Marjolaine Ney, Antoine Paul Constant, Camille Desrousseaux et à Diane Fischer-Krauser. Merci beaucoup d'avoir contribué à ce travail de thèse, pour votre précieuse aide et pour votre convivialité. Merci également à Vivien Sarda pour avoir contribué sur la partie ITC. Les résultats décrits dans cette thèse n'auraient pas été complets sans vous.

Je tiens à remercier chaleureusement mes « colocataires » de laboratoire avec qui j'ai « cohabité » tout au long du doctorat : Milan et Dang. Vous êtes devenus naturellement mes amis. Merci pour tous ces moments partagés en dehors du laboratoire (ou pas) !

Geneviève, je te suis très reconnaissant pour ton aide apportée, pour ta gentillesse, et pour la disponibilité dont tu as fait preuve à mon égard.

Coucou ! Merci à Jennifer et Houda pour avoir apporté de la convivialité et de l'entraide. Coucou !

Merci également à Nicolas et Mélanie pour les conseils et l'aide technique apportés.

Un grand merci à toutes les autres personnes qui ont fréquenté le laboratoire durant ma thèse, en particulier Adel, Ana-Soraya et Predrag. Merci aussi à Wissam.

Le travail de thèse décrit dans ce manuscrit n'aurait pas pu être accompli sans l'aide précieuse des différents services d'analyses. Ayant passé une durée non négligeable au service RMN, je voudrais chaleureusement saluer les contributions de Bruno et de Maurice. Merci pour toute l'aide et les conseils apportés. Sachez que j'ai pris du plaisir à échanger avec vous ! Merci aussi à Lionel. Sans oublier bien entendu les véritables « yeux » et « oreilles » de cette thèse que sont les « 5 spectros » ! Merci à Hélène et Stéphanie du service masse pour votre générosité et toutes vos analyses. Merci à Martine et Noémie du service microanalyse, pour avoir analysé mes échantillons et pour m'avoir accueilli au sein de votre service avec gentillesse. Merci à Corinne et Lydia du service RX, pour toutes les analyses et le travail de résolution des structures. Grâce à vous deux, la réussite d'une bonne partie de ce projet de thèse a été possible, je vous en suis reconnaissant. Je n'oublie pas de remercier également toutes les personnes du magasin de chimie. J'ai une pensée toute particulière pour Lydia, Georges, Jonathan, Antoine et Véronique.

Durant ces trois années de travail passionnant et passionné, j'ai eu la chance rencontrer de nombreuses personnes que ce soit au sein de l'institut de chimie ou en dehors. J'ai une pensée particulière pour Thomas S. à qui j'exprime ma sympathie pour tous les moments passés ensemble. Merci aussi à Marc, Fan et Pengfei.

Comme mentionné plus haut, j'ai fait la connaissance de nombreuses personnes venant d'horizons différents et variés au sein de l'université. Discuter avec vous m'a permis d'ouvrir mon esprit à d'autres cultures et disciplines : quelle richesse ! Je dois me remémorer cette anecdote racontée par un doctorant en neurosciences : comment il a dû se battre pour franchir les contrôles douaniers sans encombre parce qu'il devait transporter du cerveau de chameau, le sujet de son étude ! A côté de moi, son doctorat ressemble aux aventures d'Indiana Jones !

Un énorme merci à toute ma famille, grâce à qui j'ai pu surmonter les difficultés. Merci pour m'avoir aidé à concrétiser mon rêve de devenir docteur en chimie (pas dentiste, ou médecin pour soigner les maux de tête comme vous aviez tendance à comprendre lorsque j'expliquais que j'étudiais pour devenir docteur !). Merci bien sûr à mes parents et à tous mes frères et sœurs. Merci à ma grande sœur, ma deuxième maman ! Saches que tu portes si naturellement ton prénom ! Merci à mon beau-frère, toi le mari de ma grande sœur, pour ta si grande générosité.

Un énorme merci à Anissa, mon amour, d'avoir été à mes côtés, de m'avoir soutenu et de m'avoir supporté tout au long de ce chemin de vie !

Je voudrais finalement remercier tous les organismes qui ont contribué au financement de ce projet de thèse ; à savoir l'université de Strasbourg, le labex CSC, l'ANR-DFG (COCOORDCHEM) et le CNRS.

A toutes les personnes que j'ai oublié de remercier, je vous demande d'avance pardon. Enfin je tiens à demander pardon à toutes les personnes que j'ai pu blesser sans le vouloir, à qui j'ai pu manquer de respect sans me rendre compte. Sachez que ce n'était pas mon intention.

Merci encore à Jean-Pierre ! Je serai à jamais marqué par cette expérience.

On l'a fait !

Je dédicace ce manuscrit à toutes les personnes que j'aime.

Abstract

The fundamental principle behind catalysis is the lowering of the highest energy barrier of a reaction through the intervention of “stabilized-forms” of transition states and intermediates. Identifying as much as possible accurately these intermediates and/or transition states is of great interest for chemists working in the field. In particular, the so-called silicon–(transition-metal)–hydrogen complexes (Si–TM–H) are considered as important catalytic intermediates in most of hydrosilylation reactions. However, due to the elusive behavior of most of these intermediates, only few studies of the literature described both experimental and theoretical methods to investigate the complex nature of the bonding within this Si–TM–H motif. In this context, the main objective of this thesis was the study of reactions between iridium complexes and silanes by various experimental and computational methods.

THIS THESIS

Combined study: NMR spectroscopy, X-ray diffraction, isothermal calorimetry titration, computational methods

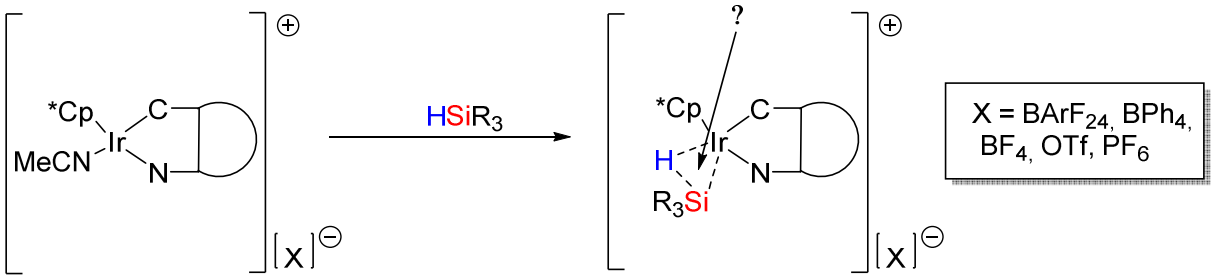

During this thesis, we have discovered a new family of highly active iridium(III)-based precatalysts [**2**][$BArF_{24}$] and [**4**][$BArF_{24}$]. These iridacycles are ionic in nature with the cationic moieties [**2**]$^+$ and [**4**]$^+$ being associated with the weakly coordinating anion [$BArF_{24}$]$^-$ ($BArF_{24}$ = tetrakis[3,5-bis(trifluoromethyl)phenyl]borate). Notably, these ionic iridacycles were found to be very stable so that their handling under air whether in solution or as solid powder was possible. Apart from the remarkable stability of [**2**][$BArF_{24}$] and [**4**][$BArF_{24}$], the relative simplicity of their molecular structures allowed us to develop a very simple and convenient synthetic protocol for their preparation on gram scale.

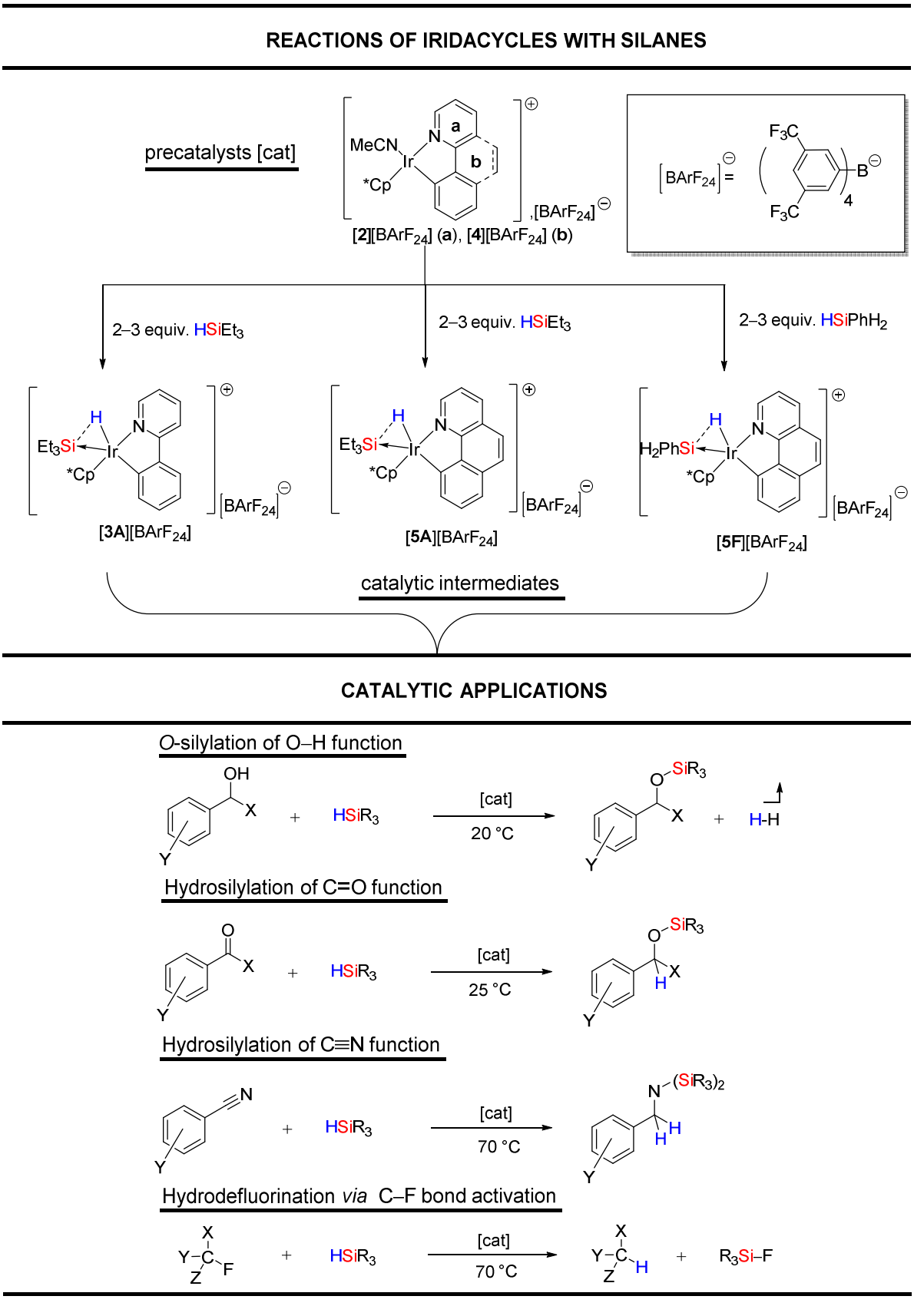

The results disclosed in this thesis provide solid evidence for the involvement of iridium(III)-silane intermediates in the catalytic activation of O—H, C=O, C≡N, and C—F bonds. Combined

experimental and theoretical studies of these intermediates point towards a Lewis donor-acceptor structural formulation of the type [Ir(III)H]→[SiR_3]. Based on these findings, a mechanism for each catalytic reaction reported herein is proposed. [**4**][$BArF_{24}$] showed to be more active than [**2**][$BArF_{24}$] in most of the reactions studied. Most notably, [**4**][$BArF_{24}$] catalyzes the *O*-silylation reaction between 1-phenylpropanol and triethylsilane with a TOF_t of ~1.16 × 10^6 h^{-1} (*t* ~3.4 s; TON = 1093). We report the first examples of an iridium-based precatalyst for the hydrosilylation of nitriles, the solvent-free C(sp^3)—F bond activation of fluorocyclohexane, and the *N*-silylation of aniline. The inhibition of the *O*-silylation of alcohols proved to be induced by the addition of substrates such as aniline and phenylacetylene, explaining why the *O*-silylation of methanol does not take place within the tandem alkyne-hydroamination – imine-hydrosilylation previously reported by the LCSOM laboratory [Iali, W. et al. *Chem. Commun.* **2012**, *48* (83), 10310.]. Overall, we believe that these results provide a significant contribution to the design of future multicompetent iridacyclic precatalysts, and constitute an original insight to the bonding within the Si—Ir(III)—H motif by considering the cation [SiR_3]$^+$ as a Z-type ligand rather than a “traditional” X ligand.

❖ Introduction

La catalyse est un concept très important en chimie. Le principe fondamental sur lequel repose le phénomène de catalyse est interprété comme suit : c'est l'abaissement de la barrière d'énergie libre d'activation ($\Delta G^{\ddagger}$) d'une réaction chimique, qui, par effet cinétique, induit ainsi une accélération des processus chimiques mis en jeu. Ainsi, il est généralement admis que cet abaissement de $\Delta G^{\ddagger}$ permet la « stabilisation » des états dits intermédiaires ou de transition. Identifier et étudier le plus en détail possible ces espèces chimiques permet aux chercheurs travaillant dans le domaine de comprendre comment et pourquoi la catalyse fonctionne pour une réaction chimique donnée. En particulier, il existe une famille de catalyseurs à base de métaux de transition qui occupe une place importante dans ce domaine (du fait de leur nature chimique et des réactions chimiques qu'ils permettent d'accélérer) que l'on nomme catalyseurs organométalliques. Parmi ces catalyseurs organométalliques, Il existe une famille bien particulière qu'on appelle les métallacycles. Comme montré dans le schéma R1a ci-dessous, les métallacycles, comme leur nom l'indique, sont des composés chimiques constitués d'une unité cyclique dont fait partie le métal de transition (palladium, rhodium, ruthénium, iridium, etc).

a) Métallacycles

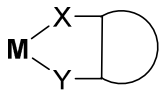

M = métal de transition
(Pd, Rh, Ru, Ir, ...)

b) Iridacycles

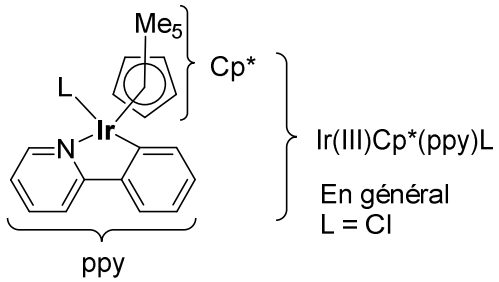

Schéma R1. a) Structure générale des métallacyles ; **b)** exemple de métallacyles à base d'iridium : iridacycles de formule Ir(III)Cp*(ppy)L.

Les métallacyles à base d'iridium (III), des ligands (κ^2-C,N)-phenylenepyridine (ppy) et η^5-pentamethylcyclopentadiène (Cp*) (schéma R1b) sont des iridacycles dont la chimie se développe de plus en plus en raison notamment de leur potentiel en catalyse homogène.[1] Cependant très peu d'études ont été réalisées en vue d'étudier plus en détail le rôle de chaque composant potentiellement apte à intervenir dans le déroulement de la catalyse impliquant ces iridacycles. De plus, on se rend compte qu'une « tradition » communément à la mode s'est mise en place parmi les pratiquants de ce champ de recherche bien particulier de la catalyse dite « homogène » et organométallique. En effet, lorsque l'on passe en revue les travaux à ce sujet dans la littérature, il apparaît que dans la grande majorité des cas les chercheurs adoptent la méthode dite de « soupe catalytique», c'est-à-dire consistant à mélanger tous les ingrédients utiles au bon fonctionnement de la catalyse sans se préoccuper des espèces chimiques clés *réellement* impliquées, et cela au détriment d'une stratégie bien plus fondamentale et dont les efforts, non moins utiles, permettraient *in fine* par exemple l'identification de la structure bien définie du précatalyseur, autrement dit la forme pré-activée du « vrai catalyseur ». On entend par précatalyseur tout composé ayant la structure chimique la plus proche possible de celle du « vrai catalyseur », en général différant l'une de l'autre par un site de coordination soit occupé par un ligand suffisamment « labile », dans le cas du précatalyseur, soit laissé « vacant », dans le cas du « vrai catalyseur ». Autant il est quasiment impossible d'identifier la structure du « vrai catalyseur », autant la structure d'au moins un intermédiaire clé est en général plus facile à observer car « plus bas en énergie ». L'objectif global de cette thèse s'inscrit dans ce cadre, c'est-à-dire la synthèse et la caractérisation de nouveaux précatalyseurs actifs ainsi que l'identification d'intermédiaires catalytiques clés.

Récemment, le laboratoire LCSOM a montré que le précatalyseur à base d'iridium **P1** permettait de promouvoir plusieurs réactions chimiques à la fois, et ce, au sein d'un même et unique mélange catalytique (schéma R2).[2] Ce système est intéressant à étudier de façon plus approfondie parce qu'il offre une voie de synthèse catalytique d'amines aromatiques chirales

[1] a) Y Corre, Y.; Iali, W.; Hamdaoui, M.; Trivelli, X.; Djukic, J.-P.; Agbossou-Niedercorn, F.; Michon, C. Efficient Hydrosilylation of Imines Using Catalysts Based on Iridium(III) Metallacycles. *Catal. Sci. Technol.* **2015**, *5* (3), 1452–1458. b) Han, Y.-F.; Jin, G.-X. Cyclometalated [Cp*M(C^X)] (M = Ir, Rh; X = N, C, O, P) complexes. *Chem. Soc. Rev.,* **2014**, *43*, 2799. c) Kennedy, A. R.; Kerr, W. J.; Moir, R.; Reid, M. Anion Effects to Deliver Enhanced Iridium Catalysts for Hydrogen Isotope Exchange Processes. *Org. Biomol. Chem.* **2014**, *12* (40), 7927–7931. d) MacDonald, J. P. Shupe, B. H.; Schreiber, J. D.; Franz, A. K. Counterion effects in the catalytic stereoselective synthesis of 2,3'-pyrrolidinyl spirooxindoles. *Chem. Commun.*, **2014**, *50*, 5242. e) Smith, M. B. Cobalt, rhodium and iridium. *Annu. Rep. Prog. Chem., Sect. A: Inorg. Chem*, **2012**, *108*, 196–210. f) Liu, J.; Wu, X.; Iggo, J. A.; Xiao, J. Half-Sandwich Iridium Complexes-Synthesis and Applications in Catalysis. *Coord. Chem. Rev.* **2008**, *252* (5–7), 782–809.

[2] Iali, W.; Paglia, F. La; Goff, X.-F. Le; Sredojević, D.; Pfeffer, M.; Djukic, J.-P. Room Temperature Tandem Hydroamination and Hydrosilation/protodesilation Catalysis by a Tricarbonylchromium-Bound Iridacycle. *Chem. Commun.* **2012**, *48* (83), 10310.

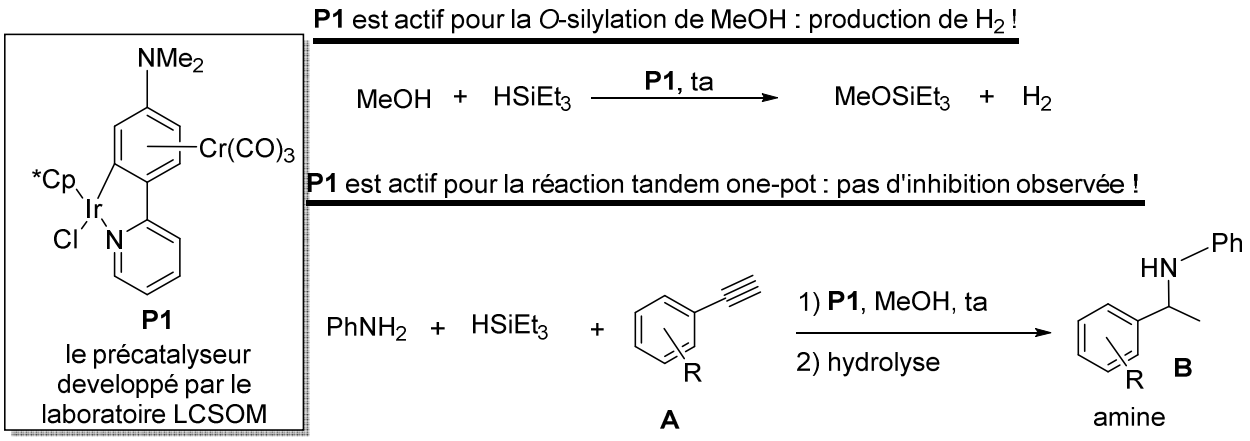

Schéma R2. Le système catalytique établi en 2012 par le LCSOM.

« directement » à partir d'alcynes par un procédé dit *tandem* et *one-pot*. En effet, ce procédé permet d'économiser l'étape de purification de l'imine intermédiaire et la dernière étape de synthèse qui consiste en l'hydrosilylation catalytique de l'imine isolée en amine. De plus, le précatalyseur **P1** utilisé est l'unique source d'acte catalytique dans le milieu car celui-ci est capable de promouvoir les deux réactions mises en jeu. Ce dernier point est très intéressant d'un point de vue économique car il constitue une rationalisation de l'usage de la quantité globale d'iridium employé dans la synthèse. La nature assez complexe d'un point de vue chimique de ce système catalytique a tout de suite suscité d'importantes interrogations. Fondamentalement, le bon déroulement de la catalyse au sein d'un système comme celui-ci indique que le précatalyseur **P1** possède des propriétés telles qu'il est capable d'effectuer les deux réactions successives (certainement différentes au niveau mécanistique) tout en supportant le milieu très complexe dans lequel il évolue. Mais par le biais de quels mécanismes cela est-il possible ? Quelles sont les intermédiaires clés qui y sont impliqués ? Ce sont ces questions, entre autres, auxquelles nous avons voulu répondre durant ce travail de thèse.

Nous avons choisi d'étudier plus spécifiquement les intermédiaires catalytiques résultant des réactions entre une nouvelle classe d'iridacycles ioniques et différents silanes $HSiR_3$ (schéma R3).

CETTE THÉSE

Étude combinée: spectroscopie RMN, diffraction aux rayons X, titration calorimétrique isotherme (ITC), calculs théoriques

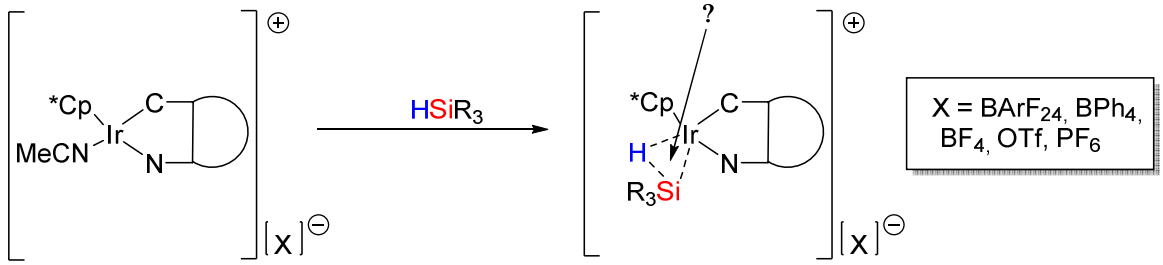

Schéma R3. Etude des réactions entre différents iridacycles ioniques et silanes $HSiR_3$.

❖ Résultats et discussions

- Synthèse de nouveaux iridacycles (neutres et ioniques)

Plusieurs iridacycles neutres et ioniques ont été préparés en suivant la stratégie de synthèse générale ci-dessous (schéma R4).

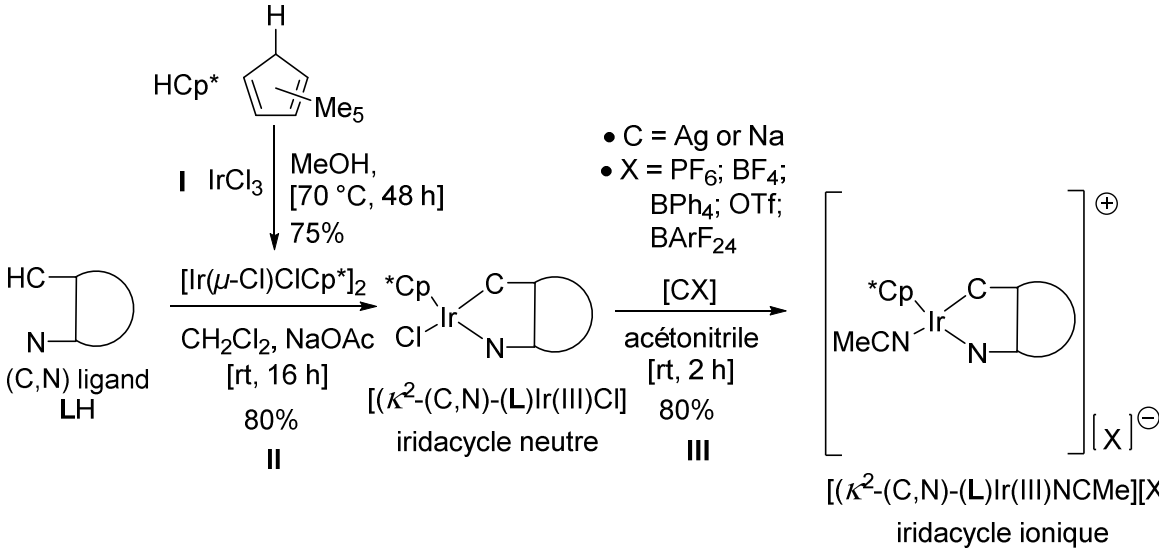

Schéma R4. Stratégie de synthèse des complexes ioniques [(κ^2-(C,N)-(**L**)Ir(III)NCMe][X].

Le procédé chimique par lequel les iridacycles ioniques de formule générale [(κ^2-(C,N)-(**L**)Ir(III)NCMe][X] ont été obtenus a été facile à mettre en œuvre et a requis seulement trois étapes de synthèse (**I–III**) avec un rendement moyen de ≥75% pour chaque étape.

Dans le schéma R5 ci-dessous est illustré tous les iridacycles synthétisés. La plupart de ces complexes ont été complétement caractérisés (spectroscopie par résonance magnétique nucléaire (RMN), spectrométrie de masse, analyses élémentaires) et la structure de plusieurs d'entre eux a été confirmée par diffraction des rayons X.

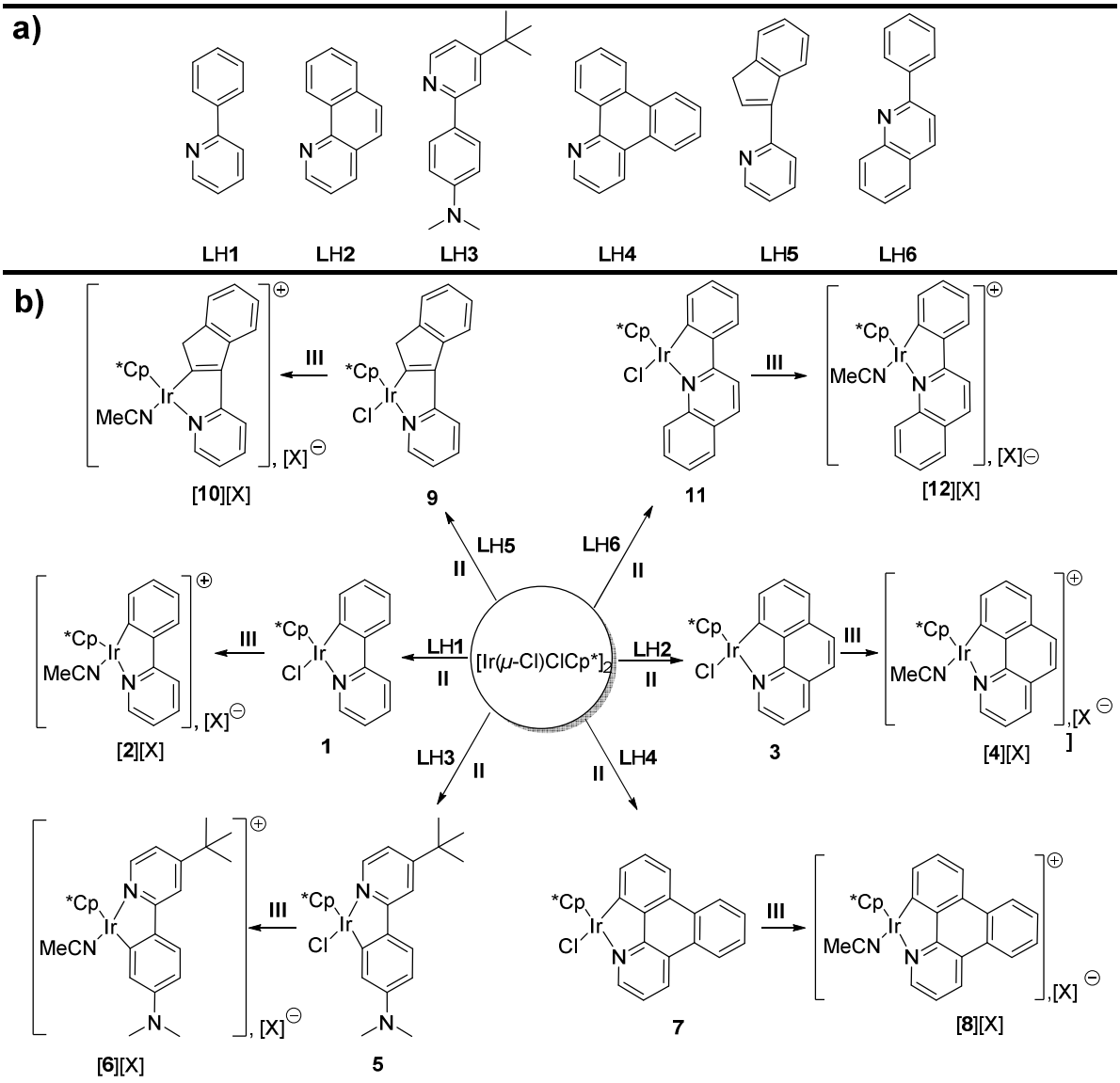

Schéma R5. Stratégie de synthèse des complexes ioniques [(κ^2-(C,N)-(**L**)Ir(III)NCMe][X].

Le rhodacycle ionique [(κ^2-(C,N)-(2-phenylenepyridine)Rh(III)NCMe][$BArF_{24}$] ([**2'**][$BArF_{24}$], schéma R6) a aussi été synthétisé et totalement caractérisé. En effet, il serait intéressant de

comparer l'effet du métal de transition (Ir *versus* Rh) sur la performance catalytique du métallacycle.

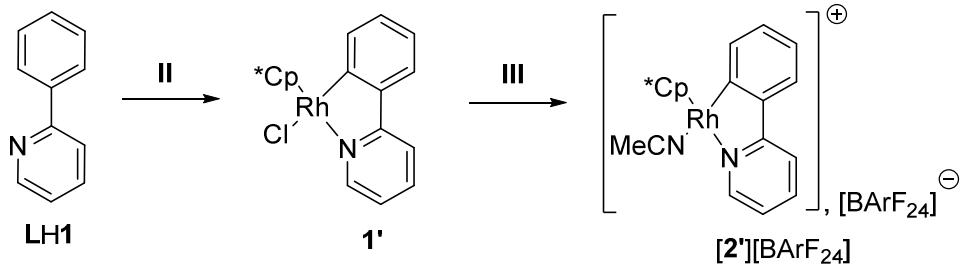

Schéma R6. Synthèse du rhodacycle ionique [(κ^2-(C,N)-(2-phenylenepyridine)Rh(III)NCMe][$BArF_{24}$], abrégé par [**2'**][$BArF_{24}$], à partir de **1'** et de Na[$BArF_{24}$] en suivant la procédure **III**.

Les complexes [**2**][X] (X = $BArF_{24}$, BPh_4, BF_4, PF_6, OTf), [**4**][X] (X = $BArF_{24}$, BPh_4, OTf), [**6**][$BArF_{24}$] et [**2'**][$BArF_{24}$] ont ensuite été testés en tant que précatalyseurs potentiels pour la réaction de *O*-silylation d'alcools. Les résultats sont résumés dans la section suivante.

- Etudes cinétique et catalytique de la réaction de *O*-silylation d'alcools

  - Pourquoi la réaction de *O*-silylation d'alcools ?

La réaction catalytique de *O*-silylation d'alcools (*O*Si) est abondamment documentée dans la littérature.[3] En général cette réaction a été étudiée comme méthode alternative en vue de produire soit les éthers de silyle (protection des alcools) soit de l'hydrogène (source d'énergie) en effectuant ce qu'on appelle un couplage déshydrogénatif d'un alcool (O–H) et d'un silane (Si–H). Dans notre cas, on s'est intéressé à cette réaction pour deux raisons principales. La première raison est pratique car elle permet le suivi cinétique direct de l'hydrogène produit en fonction du temps comme moyen de comparaison qualitatif et quantitatif entre différents systèmes catalytiques. Et la seconde raison est fondamentale dans le sens où elle permet d'établir son mécanisme de fonctionnement en ayant accès à des données cinétiques spécifiques (accès par exemple à la constante isotopique cinétique k_H/k_D). Le directeur du

[3] Par exemple : a) Cardoso, J. M. S.; Lopes, R.; Royo, B. *J.* Dehydrogenative silylation of alcohols catalysed by half-sandwich iron N-heterocyclic carbene complexes. *Organomet. Chem.* **2015**, *775*, 173-177. b) Esteruelas, M. A.; Oliván, M.; Vélez, A. POP-pincer silyl complexes of group 9: Rhodium versus iridium. *Inorg. Chem.* **2013**, *52*, 12108−12119. c) Sattler, W.; Parkin, G. Zinc Catalysts for On-Demand Hydrogen Generation and Carbon Dioxide Functionalization. *J. Am. Chem. Soc.* **2012**, *134*, 17462−17465. d) Luo, X. L.; Crabtree, R. H. Homogeneous catalysis of silane alcoholysis via nucleophilic attack by the alcohol on an Ir(η^2-$HSiR_3$) intermediate catalyzed by $[IrH_2S_2(PPh_3)_2]SbF_6$ (S = solvent). *J. Am. Chem. Soc.* **1989**, *111*, 2527-2535.

laboratoire (Dr Jean-Pierre Djukic) a conçu un dispositif qui nous a permis de suivre en direct l'évolution de la pression d'hydrogène en fonction du temps (schéma R7).

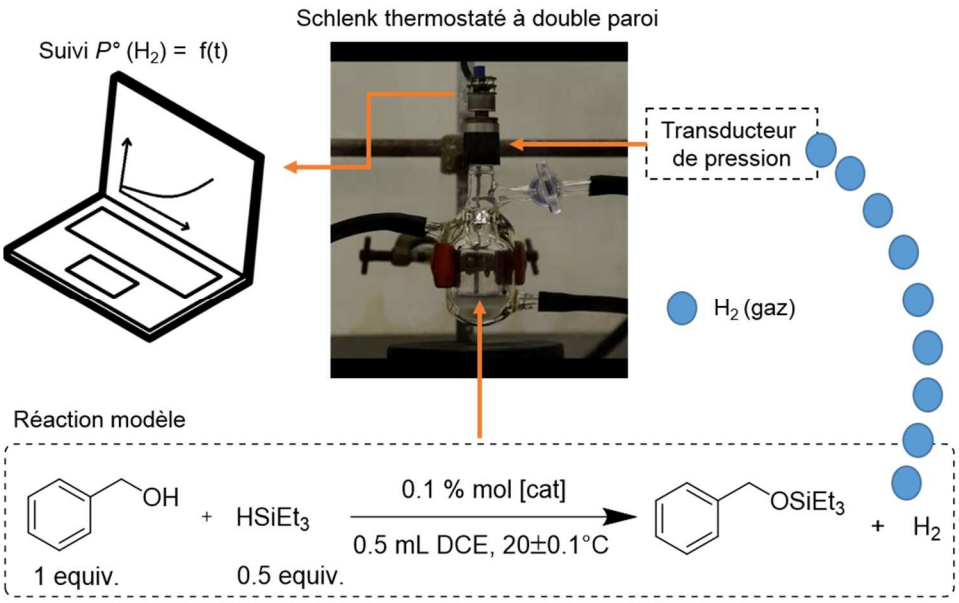

Schéma R7. Dispositif conçu par le directeur du laboratoire (Dr. Jean-Pierre Djukic) afin de suivre la pression de H_2 en fonction du temps lors des essais catalytiques de la réaction de *O*-silylation d'alcools.

- Performance des sels [**2**][X]

Avec cette méthode dite de piézométrie, nous avons ainsi comparé l'activité catalytique des différents complexes d'iridium [**2**][X], en prenant le complexe neutre **1** comme référence (schéma R5) et la réaction entre l'alcool benzylique et le triéthylsilane ($HSiEt_3$) dans le 1,2-dichloroéthane (DCE) comme solvant a servi de modèle d'étude (schéma R7). Les résultats sont rassemblés sous la forme d'une courbe modélisant l'évolution de la pression relative en H_2 (bar) en fonction du temps (s) (schéma 8). Tous les complexes testés montrent une certaine activité vis-à-vis de cette réaction. Le « meilleur » précatalyseur est le complexe [**2**][$BArF_{24}$] ($TOF_{initial}$ (10 % conversion) > 1.6×10^5 h^{-1}), et le « pire » précatalyseur est le complexe neutre **1**. Ces résultats mettent en évidence les effets positifs sur la catalyse induits par 1) l'abstraction du ligand chlorido et 2) la présence d'un anion du type $[BArF_{24}]^-$. Par contre, la nature du contre-anion peut considérablement influer sur l'efficacité en catalyse. Par ailleurs, la réaction ne montre aucun dégagement d'hydrogène en l'absence de précatalyseur.

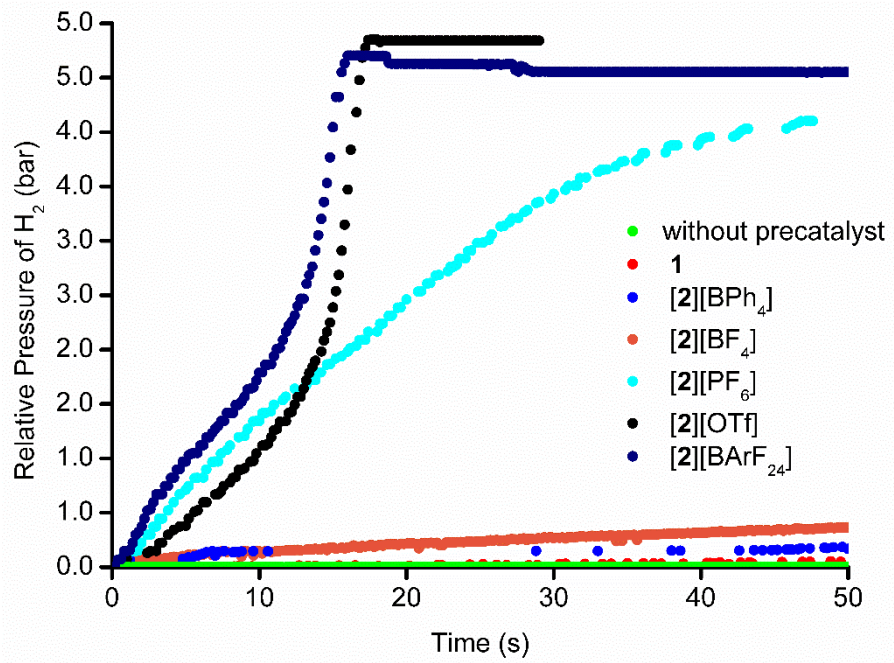

Schéma R8. Courbe modélisant la pression relative en H_2 (bar) en fonction du temps (s) : comparaison de la performance des précatalyseurs [**2**][X] (0.1 mol %, 4.8 μmol) dans la réaction entre l'alcool benzylique (9.5 mmol) et le triéthylsilane (5.0 mmol) (20±0.1 °C, 0.5 mL DCE).

- Performance des autres sels : [**4**][X] (X = $BArF_{24}$, BPh_4, OTf), [**6**][$BArF_{24}$] et [**2'**][$BArF_{24}$]

Nous avons aussi comparé l'activité catalytique des différents complexes d'iridium [**4**][$BArF_{24}$], [**6**][$BArF_{24}$] et [**2'**][$BArF_{24}$], en prenant le complexe ionique [**2**][$BArF_{24}$] comme référence (schéma R5). Ainsi, nous avons trouvé que le nouveau complexe [**4**][$BArF_{24}$] dépasse de très loin l'activité catalytique de [**2**][$BArF_{24}$] dans la réaction entre le 1-phénylpropanol et $HSiEt_3$, et ce dans les mêmes conditions qu'auparavant, se manifestant par un dégagement de tout l'hydrogène (H_2) en moins de 4 secondes ! Les résultats sont rassemblés sous la forme d'une courbe modélisant l'évolution de la pression relative en H_2 (bar) en fonction du temps (s) (schéma R9), et aussi sous la forme d'un tableau qui rassemble les données cinétiques liées à l'efficacité catalytique des différents précatalyseurs testés (tableau R1). Dans ces nouvelles conditions, nous avons trouvé que le précatalyseur [**4**][$BArF_{24}$] effectue la catalyse avec un TOF (calculé à 100% de conversion, t ~3.4 s) de ~1.16×10^6 h^{-1} ! Ce genre de performance est à notre connaissance sans précédent dans la littérature pour un catalyseur à l'iridium.

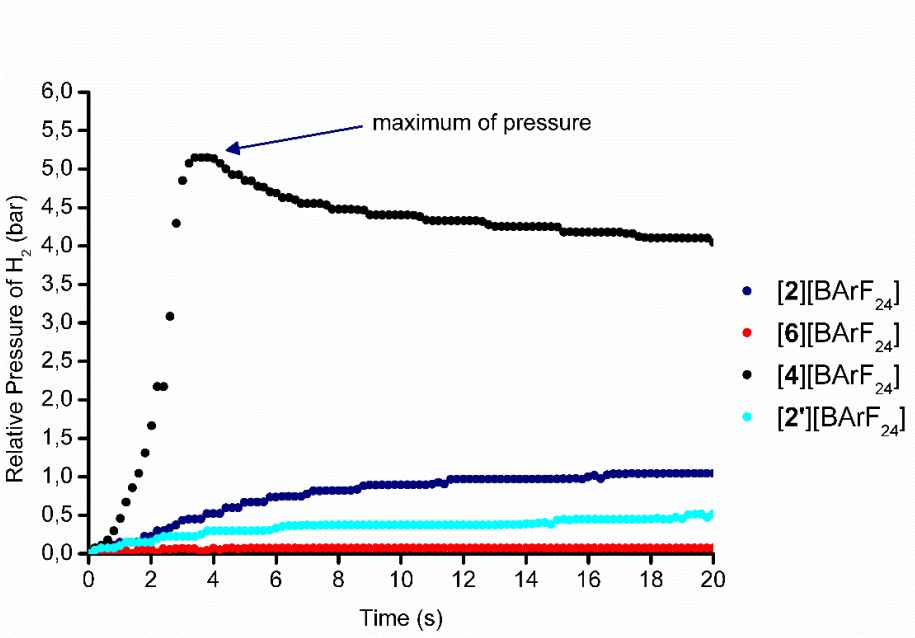

Schéma R9. Courbe modélisant la pression relative en H_2 (bar) en fonction du temps (s) : comparaison de la performance des précatalyseurs [**2**][$BArF_{24}$], [**4**][$BArF_{24}$], [**6**][$BArF_{24}$] et [**2'**][$BArF_{24}$] (0.1 mol %, 4.8 μmol) dans la réaction entre le 1-phénylpropanol (9.5 mmol) et le triéthylsilane (5.0 mmol) (20±0.1°C, 0.5 mL DCE).

Tableau R1. Performance catalytique des nouveaux sels dans la réaction d'*O*-silylation de 1-phénylpropanol avec le triéthylsilane.

Complex	t (min)	Yield [a] (%)	v_i [b] (10^{-2} M•s^{-1})	TON [c] (%) [d]	TOF$_i$ [e] (h^{-1})
[**2**][$BArF_{24}$]	60	75	3.49	500 (50)	105,662
[**2'**][$BArF_{24}$]	>10	100	1.25	99 (10)	23,750
[**4**][$BArF_{24}$]	<1	100	34.36	1000 (100)	364,490
[**4**][$BArF_{24}$]	<1	100	34.36	1000 (100)	1,157,487 [f]
[**6**][$BArF_{24}$]	>5	5	0.06	50 (5)	1539 [g]

[a] Yield in evolved H_2 for the following conditions: 9.5 mmol of alcohol, 4.8 mmol of $HSiEt_3$, 0.1 mol% of [**2**][$BArF_{24}$] (6.7 mg), 0.5 mL of 1,2-dichloroethane, 20 ± 0.1 °C. [b] $v_i = -(d[HSiEt_3]/dt)_i$. [c] TON: turnover number, calculated at the highest conversion as the molar ratio silylated alcohol:catalyst. [d] Percentage of conversion. [e] TOF$_i$: TON/time or turnover frequency calculated at a reaction time corresponding to 10% of conversion. [f] TOF$_t$ (t ~3.4 s) at 100% of conversion [g] Calculated at 5% of conversion.

Par la suite, nous avons sélectionné les précatalyseurs [**2**][$BArF_{24}$] et [**4**][$BArF_{24}$] pour leur application dans la catalyse de plusieurs systèmes réactionnels : l'hydrosilylation de carbonyles et de nitriles et l'hydrodéfluoration (HDF) de fluorocarbures par activation C–F (*vide infra*).

Mais auparavant, nous avons voulu approfondir les questions suivantes : comment expliquer l'effet du contre-anion observé ? Et quelle est la nature exacte de l'espèce catalytiquement active ? Les résultats liés à ces études sont résumés ci-après.

- Étude RMN de la réactivité de [**2**][X] vis-à-vis du triéthylsilane.

Afin d'expliquer l'effet du contre-anion sur l'activité en catalyse, les complexes [**2**][X] ont été étudiés sur la base de leur intéraction avec le triéthylsilane. La RMN a été utilisée à ces fins, et elle nous a permis d'observer plusieurs espèces chimiques dont certaines ont été inconnues jusque-là. Les résultats sont résumés dans le schéma R10 qui suit.

D'après ces observations, il a été conclu que le contre-anion joue en effet un rôle primordial sur l'issue de l'espèce catalytiquement active [**3A**][X], qui est générée *in situ via* l'addition de la liaison H–Si (rupture) sur l'iridium (*vide infra*). Les anions $[OTf]^-$ et $[BF_4]^-$ sont « la plupart du temps » suffisamment proches du centre cationique [**3A**]$^+$ pour interagir avec le silylium $[Et_3Si]^+$ en formant Et_3SiOTf et $FSiEt_3$ respectivement. Et_3SiOTf est connue pour être une source active de silylium alors que $FSiEt_3$ est une molécule relativement inerte. Ceci explique l'activité supérieure de [**2**][OTf] en catalyse en comparaison à l'activité quasi-nulle de [**2**][BF_4]. On explique l'activité supérieure de [**2**][$BArF_{24}$] par une « stabilité » suffisante de l'intermédiaire [**3A**][$BArF_{24}$] (observé par RMN et RX, *vide infra*). Ces analyses RMN nous ont aussi permis de mettre en évidence l'existence de l'espèce clé [**3B**][X] dont l'étude approfondie nous a mené à conclure à la formulation d'un dimère d'iridium où un seul ligand hydruro ponte deux atomes d'iridium (schéma R10). Dans le paragraphe suivant sont résumés les résultats d'une étude combinant méthodes expérimentales et théoriques dont le but a été d'isoler l'intermédiaire [**3A**][$BArF_{24}$] et de formuler la meilleure structure qui rationalise les résultats ainsi obtenus.

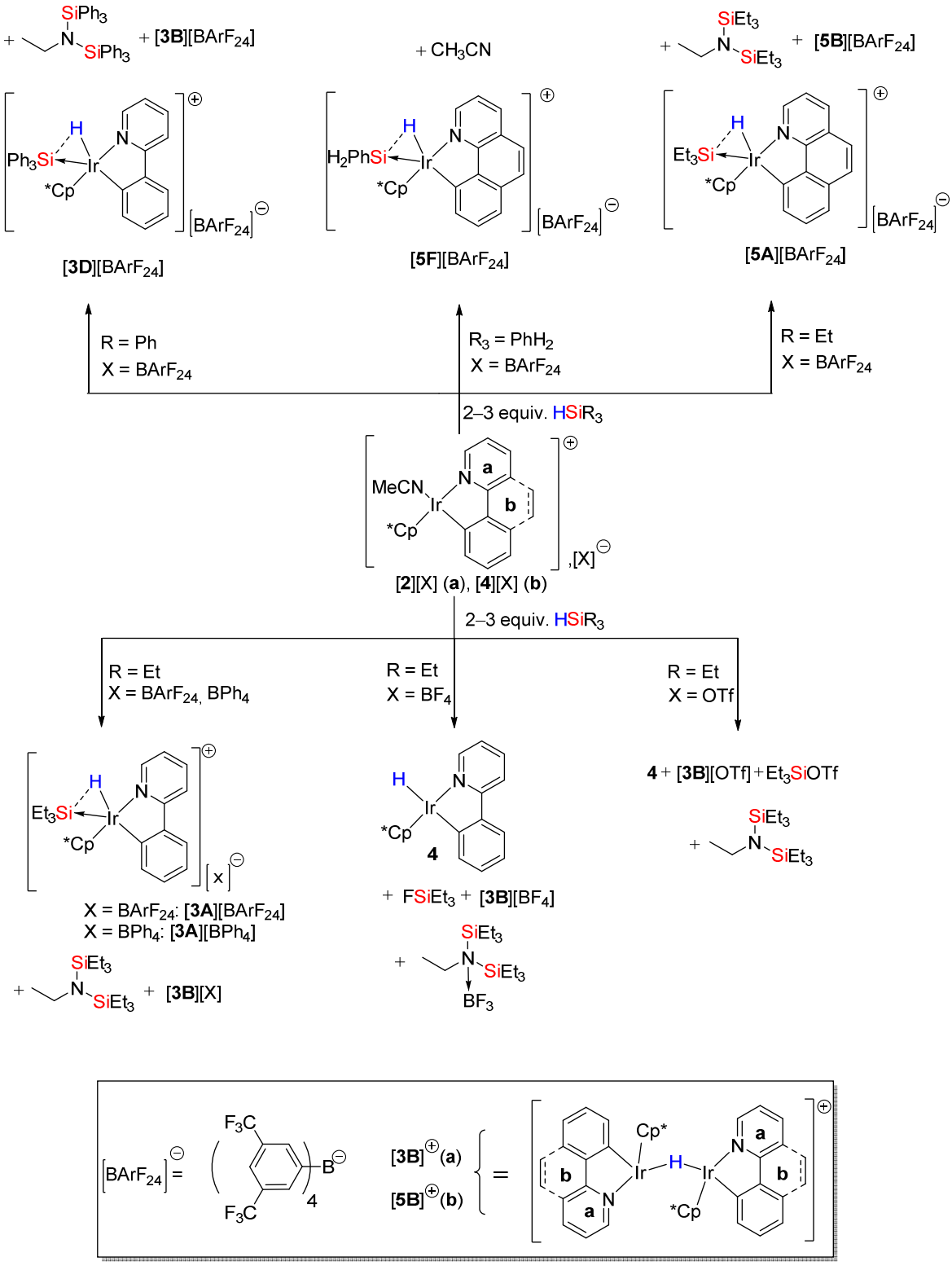

Schéma R10. Réactivité des complexes [**2**][X] et [**4**][$BArF_{24}$] vis-à-vis des silanes $HSiR_3$.

- Mise en évidence et étude des intermédiaires clés [**3A**][$BArF_{24}$] et [**5A**][$BArF_{24}$]

  - [**3A**][$BArF_{24}$]

L'intermédiaire ionique [**3A**][$BArF_{24}$] a été piégé et caractérisé par RMN et RX (schéma R11a-b). Nous avons également étudié sa réactivité vis-à-vis de plusieurs bases de Lewis. La structure RX a été étudiée en détail par les moyens de la théorie de la fonctionnelle de la densité corrigée pour l'effet de la force de London (DFT-D) (schéma R11c–d). Tous les résultats convergent vers un complexe ionique du type donneur-accepteur de Lewis, *i.e.* [**4**](donneur)→[$SiEt_3$]$^+$(accepteur), comme étant la meilleure formulation structurale de [**3A**][$BArF_{24}$].[4] Par ailleurs l'étude de la thermochimie de la réaction, *via* la méthode dite de titration isotherme micro-calorimétrique (ITC), a permis de mettre en évidence le rôle majeur de l'hydrosilylation catalytique de l'acétonitrile libérée par [**2**][$BArF_{24}$] après interaction de celui-ci avec $HSiEt_3$ pour former transitoirement [**3A**][$BArF_{24}$].

- [**5A**][$BArF_{24}$]

De la même manière que pour [**3A**][$BArF_{24}$], la réaction entre [**4**][$BArF_{24}$] et $HSiEt_3$ a été étudiée en détail. L'intermédiaire résultant de cette dernière réaction, c'est-à-dire [**5A**][$BArF_{24}$], a été piégé et caractérisé par RMN (schéma R12) et RX (schéma R13a). La structure RX a été étudiée en détail par les moyens de la théorie de la fonctionnelle de la densité corrigée pour l'effet de la force de London (DFT-D) et confirme la structure du type donneur-accepteur de Lewis similaire à [**3A**][$BArF_{24}$].

- [**5B**][$BArF_{24}$]

La réaction entre [**4**][$BArF_{24}$] et $HSiEt_3$ mène non seulement à la formation l'intermédiaire [**5A**][$BArF_{24}$], mais également au dimère d'iridium à hydrure mono-pontant [**5B**][$BArF_{24}$]. La structure RX de [**5B**][$BArF_{24}$] a été obtenue avec succès (schéma R13b) et montre une bonne similitude avec les structures RX des composés [**5B**][$BArF_{24}$] et [**5B**][$BArF_{24}$] qui ont été également établies par notre laboratoire durant ce projet de thèse. La meilleure formulation possible pour [**5B**][$BArF_{24}$] est un complexe du type donneur-accepteur de Lewis, comme il a été démontré par calculs DFT-D pour le complexe [**5B**][OTf].

[4] Hamdaoui, M.; Ney, M.; Sarda, V.; Karmazin, L.; Bailly, C.; Sieffert, N.; Dohm, S.; Hansen, A.; Grimme, S.; Djukic, J.-P. Evidence of a Donor–Acceptor (Ir–H)→SiR_3 Interaction in a Trapped Ir(III) Silane Catalytic Intermediate. *Organometallics* **2016**, *35* (13), 2207–2223.

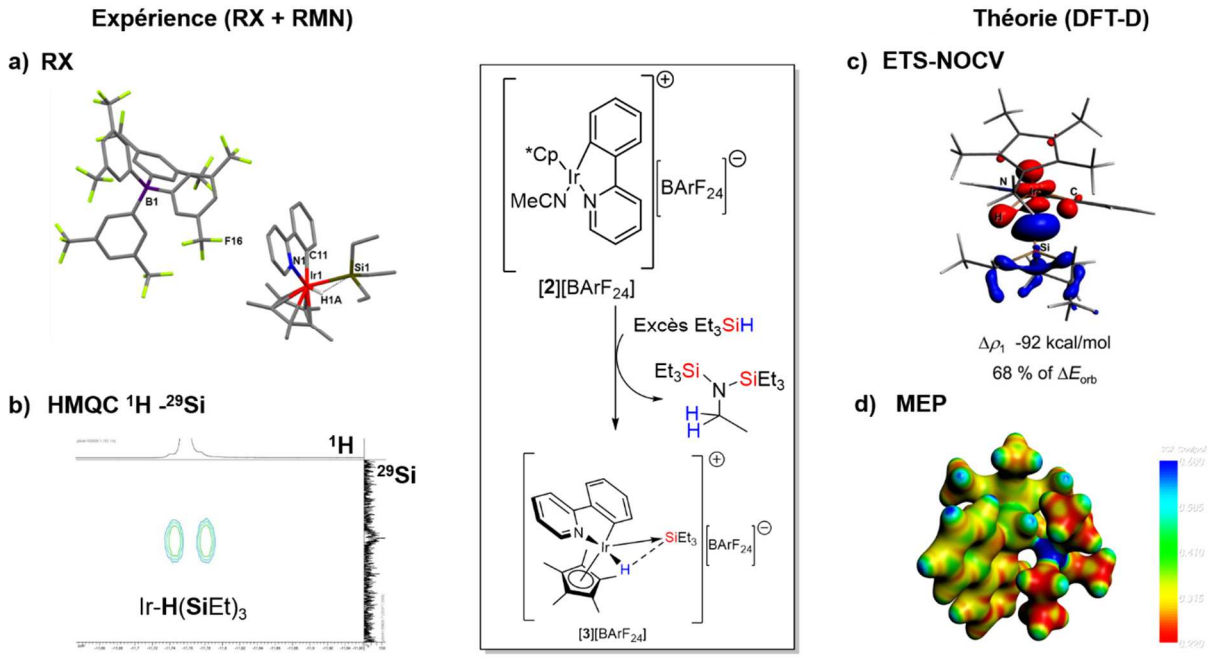

Scheme R11. Au milieu est représentée la formulation structurale proposée pour l'intermédiaire [**3A**][BArF$_{24}$] d'après les observations faites **a)** à l'état cristallin (RX) et **b)** à l'état liquide (RMN), et d'après l'étude de sa structure RX via **c)** l'analyse ETS-NOCV de la déformation de densités ρ^{orb} rendant compte de l'interaction de liaison entre les fragments à valence pleine **4** et $[SiEt_3]^+$ dans leur géométries préparées et dérivant de [**3A**]$^+$ (Le transfert de densité électronique après interaction s'opère du volume rouge vers le volume bleu) ; et **d)** l'analyse de la carte de densité électronique obtenue sur la base de l'isosurface (0.05 e bohr^{-3}) du champ « self-consistent » de densité électronique du modèle de [**3A**]$^+$ en phase gazeuse et à l'état singulet fondamental: les couleurs bleu et rouge sont associées aux régions d'augmentation et de diminution de densité électronique après interaction.

- [**5F**][BArF$_{24}$]

La réaction entre [**4**][BArF$_{24}$] et $HSiPhH_2$ mène à la formation exclusive de l'intermédiaire [**5F**][BArF$_{24}$]. La structure RX de [**5F**][BArF$_{24}$] n'a pas encore été obtenue. Cependant, nous avons la preuve spectroscopique (RMN) de l'existence de [**5F**][BArF$_{24}$].

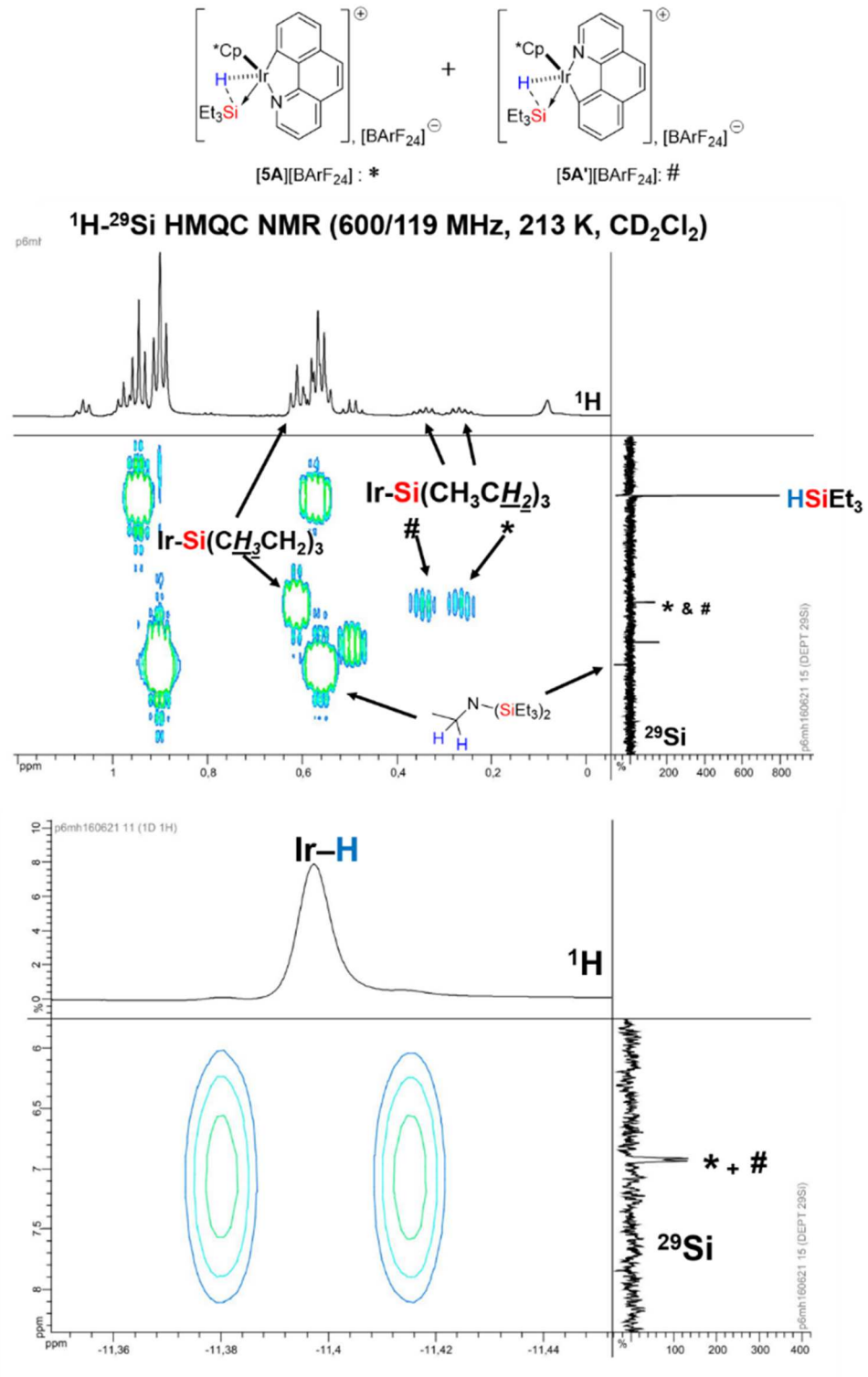

Schéma R12. Analyse spectroscopique par RMN 2D ^{29}Si-^{1}H HMQC (haut : région de Ir→SiE$_3$; bas : région de Ir–H) de la réaction entre [**4**][BArF$_{24}$] et un excès de HSiEt$_3$ (2 équiv./Ir) dans CD_2Cl_2 (–60 °C).

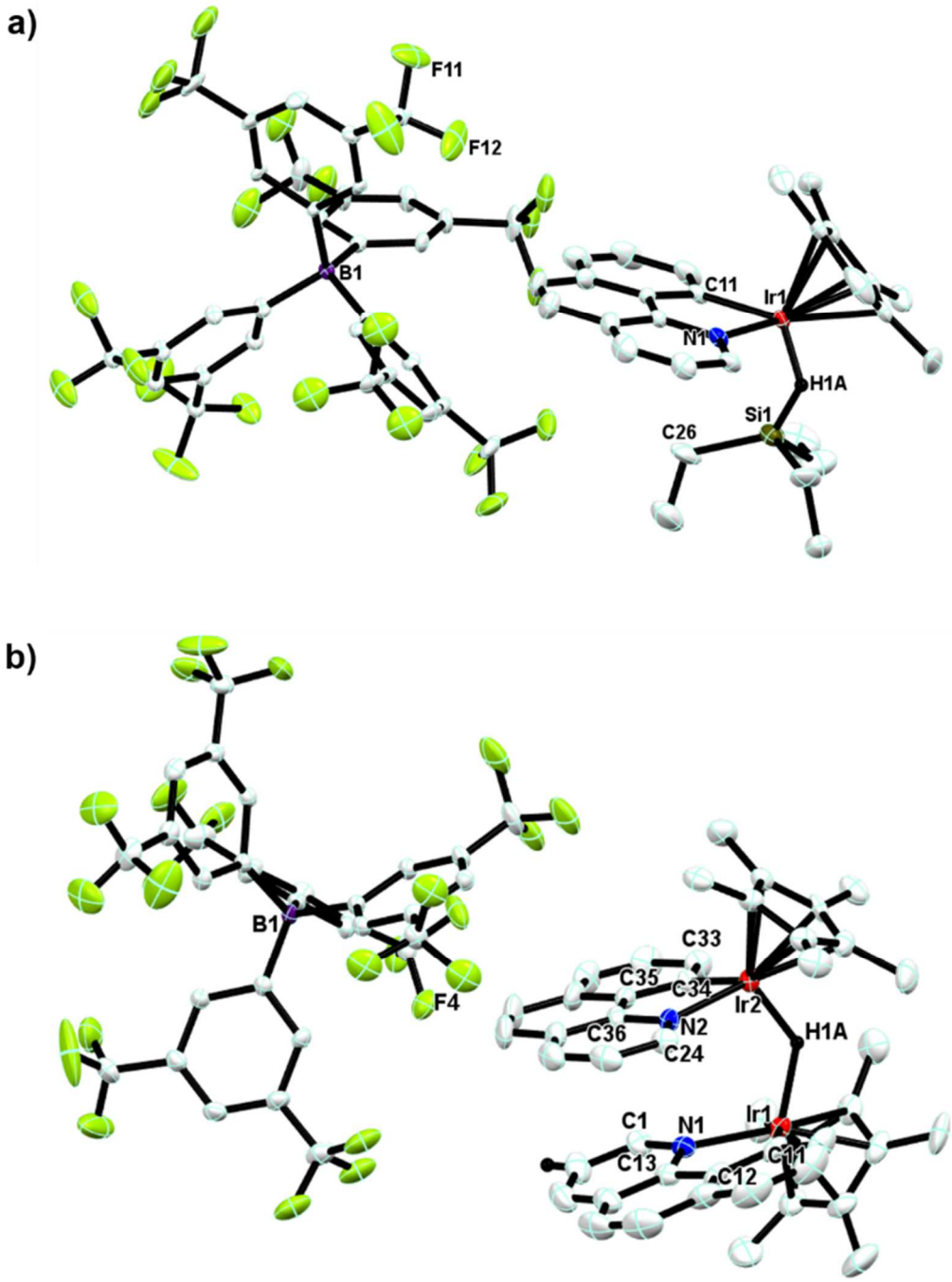

Schéma R13. Structures RX de **a)** [**5A**][BArF$_{24}$] et **b)** [**5B**][BArF$_{24}$].

- Performance de [**2**][BArF$_{24}$] et [**4**][BArF$_{24}$] dans d'autres réactions catalytiques

Nous avons montré que les complexes [**2**][BArF$_{24}$] et [**4**][BArF$_{24}$] sont d'excellents précatalyseurs pour la réaction de *O*-silylation d'alcools. Nous avons voulu tester ces complexes dans d'autres réactions. Nous avons démontré durant ce travail de thèse que [**2**][BArF$_{24}$] et [**4**][BArF$_{24}$] sont effectivement d'excellents précatalyseurs pour les réactions

d'hydrosilylation de plusieurs substrats insaturés ainsi que pour l'hydrodéfluoration catalytique de la fonction C–F (schéma R14). Cependant, le précatalyseur [**4**][$BArF_{24}$] a montré une activité bien supérieure à [**2**][$BArF_{24}$] dans toutes les réactions étudiées.

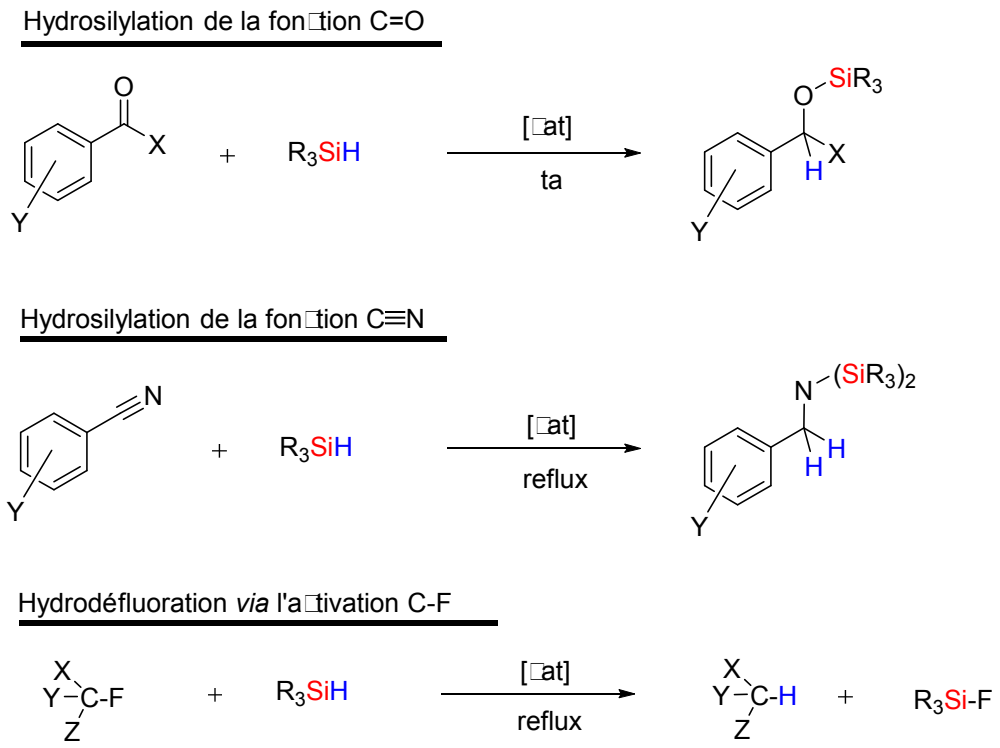

Schéma R14. Applications catalytiques des précatalyseurs [**2**][$BArF_{24}$] et [**4**][$BArF_{24}$].

- Hydrosilylation de nitriles

Nous rapportons les premiers précatalyseurs à base d'iridium que sont [**2**][$BArF_{24}$] et [**4**][$BArF_{24}$] pour l'hydrosilylation catalytique de nitriles. [**4**][$BArF_{24}$] catalyse l'hydrosilylation d'une large variété de nitriles et ce dans des conditions qui sont remarquables lorsque nous les comparons aux meilleurs systèmes catalytiques rapportés à ce jour (schéma R15).

- Hydrosilylation de carbonyls

Nous démontrons également que le complexe [**4**][$BArF_{24}$] est un excellent précatalyseur pour l'hydrosilylation d'une large variété d'aldéhydes et de cétones, et ce, dans des conditions qui

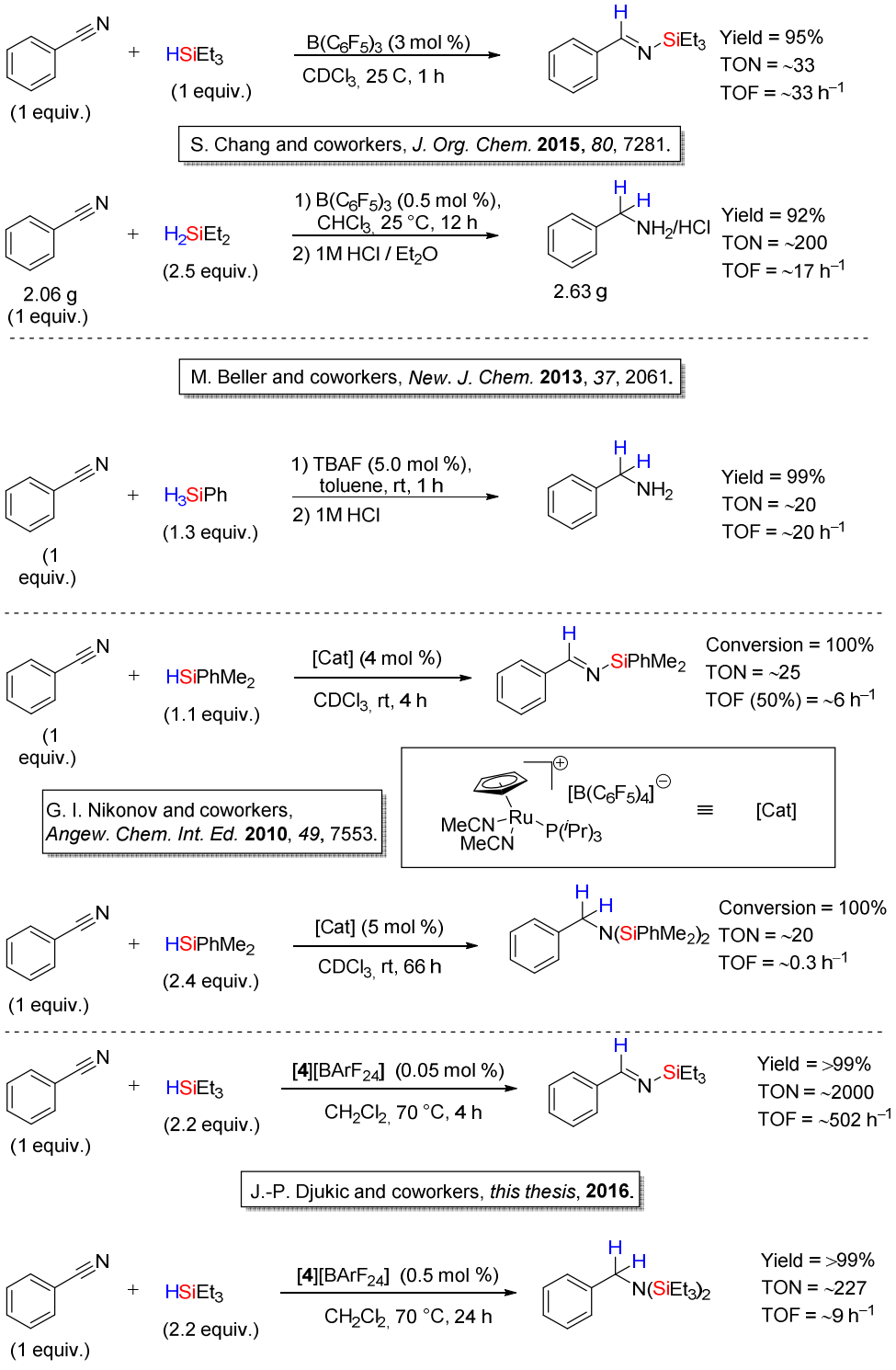

Schéma R15. Comparaison de la performance catalytique de [**4**][$BArF_{24}$] avec les meilleurs systèmes précédemment décrits pour l'hydrosilylation chimio-sélective de benzonitrile.

sont remarquablement bien supérieures à celles des meilleurs systèmes catalytiques rapportés à ce jour (tableau R2).

Tableau R2. Résumé de la performance catalytique de [**4**][$BArF_{24}$] pour l'hydrosilylation d'aldéhydes et de cétones, en comparaison aux meilleurs systèmes précédemment décrits dans la littérature.

Substrat	Précatalyseur (mol %)	TON	TOF (h^{-1})
Cyclohexanone	[(DPI)Mn] (1.0) (R. J. Trovitch et al.)[5]	6400	7.8×10^4
Acétophénone	[**4**][$BArF_{24}$] (0.1) (J.- P. Djukic et al.)	1000	1.2×10^4
	[(DPI)Mn] (0.1) (R. J. Trovitch et al.)[5]	100	1.5×10^3
	[Ir(POCOP)(acetone)H][$B(C_6F_5)_4$] (0.5) (M. Brookhart et al.) [6]	200	6.0×10^2
Aldéhydes	[**4**][$BArF_{24}$] (0.1) (J.- P. Djukic et al.)	1000	2.0×10^3
	[**4**][$BArF_{24}$] (0.5) (J.- P. Djukic et al.)	≤200	$\leq 4.0 \times 10^2$
Cétones	[**4**][$BArF_{24}$] (0.5) (J.- P. Djukic et al.)	≤200	$\leq 4.0 \times 10^2$

- Hydrodéfluoration catalytique de fluorocarbures saturés

[5] Mukhopadhyay, T. K.; Flores, M.; Groy, T. L.; Trovitch, R. J. A Highly Active Manganese Precatalyst for the Hydrosilylation of Ketones and Esters. *J. Am. Chem. Soc.* **2014**, *136* (3), 882–885.
[6] Park, S.; Brookhart, M. Hydrosilylation of Carbonyl-Containing Substrates Catalyzed by an Electrophilic η^1-Silane iridium(III) Complex. *Organometallics* **2010**, *29* (22), 6057–6064.

Le résultat le plus remarquable obtenu dans l'étude concernant l'activation catalytique de la liaison C–F est le fait que [**4**][BArF$_{24}$] (mais également [**2**][BArF$_{24}$]) est un excellent précatalyseur (0.5 mol %, 1,5 h, 70 °C) pour l'hydrodéfluoration sans solvant du fluorocyclohexane **F-Cy** en cyclohexane **H-Cy** (schéma R16).

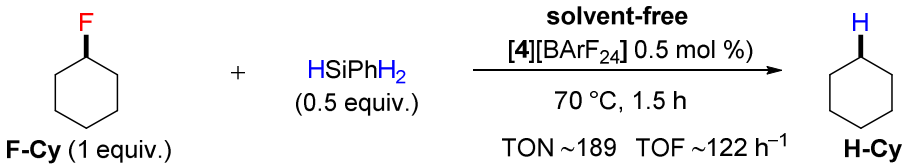

Schéma R16. [**4**][BArF$_{24}$] catalyse l'hydrodéfluoration catalytique de fluorocyclohexane avec HSiPhH$_2$ comme source d'hydrure.

- *N*-silylation catalytique de l'aniline

Nous rapportons également le premier complexe d'iridium, c'est à dire [**4**][BArF$_{24}$], qui est capable d'effectuer la *N*-silylation catalytique d'une amine primaire, en loccurrence l'aniline, dans des conditions douces et sélectives, et ce, sans avoir besoin d'autres additifs (schéma R17). Le groupe de J. F. Hartwig a décrit que le complexe d'iridum [Ir(cod)OMe]$_2$ catalyse la *N*-silylation d'amines secondaires uniquement.[7]

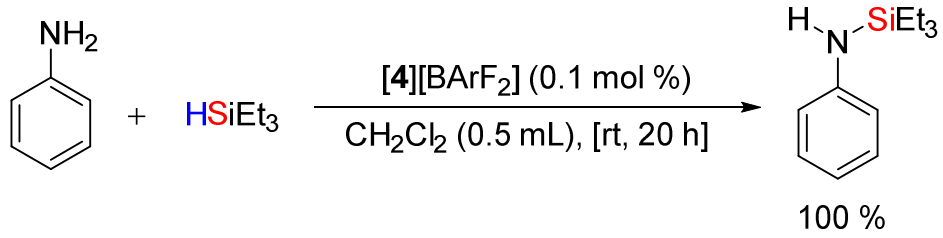

Schéma R17. La *N*-silylation catalytique de l'aniline catalysée par [**4**][BArF$_{24}$].

❖ Conclusions générales et perspectives

Une nouvelle famille de précatalyseurs homogènes a été découverte. La facilité dans leur préparation (grâce à leur simplicité structurale), leur excellente stabilité, et surtout leur efficacité catalytique dans plusieurs réactions réputées très difficiles, c.-à-d. l'hydrosilylation des nitriles

[7] Li, Q.; Driess, M.; Hartwig, J. F. Iridium-Catalyzed Regioselective Silylation of Aromatic and Benzylic C–H Bonds Directed by a Secondary Amine. *Angew. Chem. Int. Ed.* **2014**, *53* (32), 8471–8474.

et l'activation C–F, surpasse d'autres précatalyseurs organométalliques similaires connus à ce jour. Le fait le plus significatif est la mise en évidence expérimentale et théorique que les précatalyseurs en question fonctionnement comme une paire de Lewis organométallique du type donneur-accepteur s'établissant entre le complexe neutre [Ir-H] (donneur) et le ligand $[SiEt_3]^+$ (accepteur). Ce dernier ligand est un ligand Z en appliquant le formalisme de Green,[8] ce qui suggère un état d'oxidation formel autour de l'atome d'iridium de +III.

Ce projet de thèse a contribué à une meilleure compréhension de la chimie du silylium appliquée à la chimie organométallique, et a abouti à l'émergence d'un nouveau champ de recherche qui mérite d'être approfondi.

[8] Green, J. C.; Green, M. L. H.; Parkin, G. The Occurrence and Representation of Three-Centre Two-Electron Bonds in Covalent Inorganic Compounds. *Chem. Commun.* **2012**, *48* (94), 11481.

1 Objectives of the thesis

The starting point of this thesis was to understand the mechanisms of a previous catalytic system promoted by an iridium complex that has been developed by the Laboratoire de Chimie et Systémique Organo-Métalliques (LCSOM). The promising potential of this reaction laid the ground for the present project the results of which are presented in this manuscript. We provide in this section the main objectives of the thesis.

1.1 Context and problematic

1.1.1 What is the reaction we wished to study?

Dr. Wissam Iali, Dr. Jean-Pierre Djukic and coworkers showed that the iridium precatalyst **P1** catalyzes under mild conditions and in tandem and one-pot fashion the sequential hydroamination – hydrosilylation – protodesilylation reactions transforming directly the aromatic alkynes **A** into the corresponding chiral aromatic amines **B** (scheme 1).[9] Even though the process of this chemical transformation seems to be *simple* at first glance, it is interesting to study the underlying mechanistic issues.

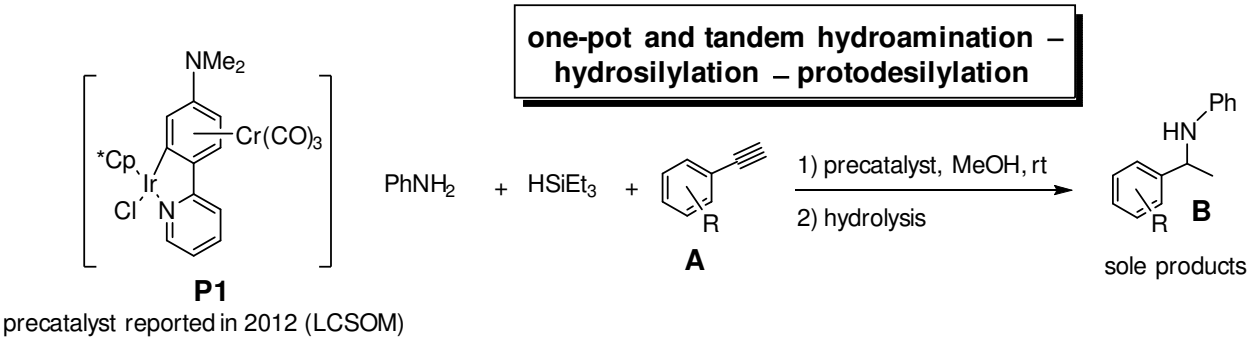

Scheme 1. The system reported by the LCSOM group in 2012. All the process is catalyzed by **P1** as a single precatalyst.

1.1.2 Why is this reaction interesting?

This newly established reaction is interesting because of 1) its atom and time economies and 2) of its simplicity in providing in one single catalytic step a variety of aromatic amines from available and simple starting materials. Aromatic amines are important intermediates in organic and organometallic chemistry.[10] The development of processes that allow their fast, simple and selective production is highly attractive for academic and industrial applications.

[9] Iali, W.; Paglia, F. La; Goff, X.-F. Le; Sredojević, D.; Pfeffer, M.; Djukic, J.-P. Room Temperature Tandem Hydroamination and Hydrosilation/protodesilation Catalysis by a Tricarbonylchromium-Bound Iridacycle. *Chem. Commun.* **2012**, *48* (83), 10310.

[10] Lawrence, S. A. In *Amines : Synthesis, Properties, and Applications*; Cambridge University Press, 2004.

1.1.3 What are the problems of this reaction?

The apparent practical simplicity of this reaction does not mean that a simple mechanism is at work. At least two surprising points emphasizing the complexity of the system should be analyzed further on. The first fact is that methanol as a solvent does not inhibit the reaction by reacting with silane through the well-known *O*-silylation (*O*Si) reaction (scheme 2).

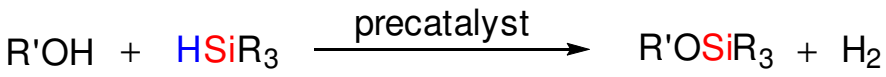

Scheme 2. The catalytic reaction of *O*-silylation of alcohols (*O*Si).

The second fact is that each elementary reaction of this synthesis occurs apparently in an ordered fashion if a given order of substrate introduction is respected. In order to deeply investigate this reaction, one has to view it as a *complex system* to avoid falling out into oversimplifications that could bring us on wrong directions and eventually missing important details. That is why we tried to keep this notion of complexity in mind during this PhD study.

1.2 What are the objectives of the thesis?

The final objective of this thesis is to get a better understanding of the mechanisms that govern this iridium-based complex catalytic system. The main hypothesis was the existence of a (or several) metal-silane intermediate(s) of crucial role(s) along this (these) complex catalytic cycle(s). However, the central objective deals with investigating the nature of these catalytically active iridium species involved in 1) the H–Si bond activation and 2) the transfer of these two atoms (Si and H) to organic substrates. To this effect, the *O*Si reaction was chosen as a model reaction of study. As the thesis project was being advanced, a major concern of interest emerged which was to understand the nature of bonding within the silicon-iridium-hydrogen unit of the catalytic intermediates that are formed upon interaction of iridium precatalysts with silanes. For this purpose, a thorough study of these intermediates by combined experimental and theoretical approaches was systematically undertaken.

2 Evidence of a donor-acceptor interaction [Ir-H]→[SiR_3] in catalytic intermediates of relevant activity

The most relevant results of this chapter have been already published [Reprinted with permission from J.-P. Djukic et al. Evidence of a Donor–Acceptor (Ir–H)→SiR_3 Interaction in a Trapped Ir(III) Silane Catalytic Intermediate. *Organometallics* **2016**, 35 (13), 2207–2223. Copyright 2016 American Chemical Society]. This paper deals with the study conducted towards the identification of an important iridium-silane catalytic intermediate featuring a Lewis donor-acceptor structure. In this chapter, we provide additional results in support of our earlier claim.

What does make the *O*-silylation of methanol inhibited in the complex system we described in chapter 1 (scheme 1)? In this chapter, we provide solid arguments that answer this question. We will show that the main argument that rationalizes these previous observations is the involvement of important iridium-silane catalytic intermediates, which feature Lewis donor-acceptor structures. After briefly introducing the emerging potential of iridacyles as (pre)catalysts, we will discuss the bonding situation within the silicon–transition-metal–hydrogen motif of catalytic intermediates considered to be involved in most hydrosilylation reactions. Then we will describe both unpublished and published results related to the synthesis and characterization of new iridium precatalysts, the study of the catalytic *O*Si of alcohols originally taken as a model reaction, the study of the reaction between several silanes and ionic iridacycles by serveral means (Nuclear Magnetic Resonance, Isothermal Titration Calorimetry, and X-ray diffraction), and most importantly the experimental characterization (X-ray diffraction) and theoretical investigation (DFT-D) of new iridium-silane catalytic intermediates. All these results will be critically discussed. Finally, we will give some insights on future perspectives of the chemistry reported herein.

2.1 General introduction

2.1.1 Iridacycles

Iridacycles belong to the large family of metallacyclic organometallic complexes. Iridacycles were however less studied than for instance palladacycles, rhodacycles and ruthenacycles.[11] Over the last years, pentamethylcyclopentadienyl iridium(III) metallacycles have particularly attracted interest due to their many rich organometallic reactions and catalytic applications.[12,13] Specifically, many recent reports highlighted the catalytic potential of $[(\kappa^2\text{-(C,N)-(PhPy)Ir(III)Cp*L'}]^q$ metallacycles (PhPy = 2-phenylenepyridine, Cp* = pentamethylcyclopentadienyl, L' = halide or solvent ligand, where *q* is the charge 0 or +1 depending on the nature of L') towards a wide range of transformations, opening promising perspectives for such simple organometallic complexes.[14] For instance, our group and collaborators (F. Agbossou-Niedercorn and coworkers, university of Lille 1) have recently shown that the cationic iridacycle $[(\kappa^2\text{-(C,N)-(PhPy)Ir(III)Cp*(solvent)}]^+$ catalyzes various hydrosilylation reactions with high efficiency and broad substrate scope.[15]

[11] Ritleng, V.; Sirlin, C.; Pfeffer, M. Ru-, Rh-, and Pd-Catalyzed C–C Bond Formation Involving C–H Activation and Addition on Unsaturated Substrates: Reactions and Mechanistic Aspects. *Chem. Rev.* **2002**, *102* (5), 1731–1770.

[12] For selected work of our group, see: a) Djukic, J. P.; Iali, W.; Pfeffer, M.; Le Goff, X. F. Synthesis of Planar Chiral Iridacycles by Cationic Metal π-Coordination: Facial Selectivity, and Conformational and Stereochemical Consequences. *Chem. - A Eur. J.* **2012**, *18* (19), 6063–6078. b) Djukic, J.-P.; Iali, W.; Pfeffer, M.; Le Goff, X.-F. Charge-Induced Facial-Selectivity in the Formation of New Cationic Planar Chiral Iridacycles Derived from Aniline. *Chem. Commun.* **2011**, *47* (12), 3631–3633. c) Scheeren, C.; Maasarani, F.; Hijazi, A.; Djukic, J.-P.; Pfeffer, M.; Zarić, S. D. .; Le Goff, X.-F.; Ricard, L. Stereoselective "Electrophilic" Cyclometalation of Planar-Prochiral (η^6-Arene)tricarbonylchromium Complexes with Asymmetric Metal Centers: Pseudo-*T*-4 $[Cp^*RhCl_2]_2$ and $[Cp^*IrCl_2]_2$. *Organometallics* **2007**, *26* (14), 3336–3345.

[13] For selected work of other groups, see: a) Turlington, C. R.; White, P. S.; Brookhart, M.; Templeton, J. L. Sequential Nitrene Transfers to an Organometallic Half-Sandwich Iridium Complex. *Organometallics* **2015**, *34* (20), 4810–4812. b) Davies, D. L.; Al-Duaij, O.; Fawcett, J.; Giardiello, M.; Hilton, S. T.; Russell, D. R. Room-Temperature Cyclometallation of Amines, Imines and Oxazolines with $[MCl_2Cp^*]_2$ (M = Rh, Ir) and $[RuCl_2(p\text{-cymene})]_2$. *Dalt. Trans.* **2003**, *2* (21), 4132–4138. c) Overman, L. E.; Owen, C. E.; Pavan, M. M.; Richards, C. J. Catalytic Asymmetric Rearrangement of Allylic N-Aryl Trifluoroacetimidates. A Useful Method for Transforming Prochiral Allylic Alcohols to Chiral Allylic Amines. *Org. Lett.* **2003**, *5* (11), 1809–1812.

[14] For recent reviews and papers, see for example: a) Michon, C.; MacIntyre, K.; Corre, Y.; Agbossou-Niedercorn, F. Pentamethylcyclopentadienyl Iridium(III) Metallacycles Applied to Homogeneous Catalysis for Fine Chemical Synthesis. *ChemCatChem* **2016**, *8* (10), 1755–1762. b) Han, Y.-F.; Jin, G.-X. Cyclometalated [Cp*M(C^X)] (M = Ir, Rh; X = N, C, O, P) complexes. *Chem. Soc. Rev.,* **2014**, *4*3, 2799. c) Kennedy, A. R.; Kerr, W. J.; Moir, R.; Reid, M. Anion Effects to Deliver Enhanced Iridium Catalysts for Hydrogen Isotope Exchange Processes. *Org. Biomol. Chem.* **2014**, *12* (40), 7927–7931. d) MacDonald, J. P. Shupe, B. H.; Schreiber, J. D.; Franz, A. K. Counterion effects in the catalytic stereoselective synthesis of 2,3'-pyrrolidinyl spirooxindoles. *Chem. Commun.*, **2014**, *50*, 5242. e) Smith, M. B. Cobalt, rhodium and iridium. *Annu. Rep. Prog. Chem., Sect. A: Inorg. Chem*, **2012**, *108*, 196–210. f) Liu, J.; Wu, X.; Iggo, J. A.; Xiao, J. Half-Sandwich Iridium Complexes-Synthesis and Applications in Catalysis. *Coord. Chem. Rev.* **2008**, *252* (5–7), 782–809.

[15] a) Corre, Y.; Rysak, V.; Capet, F.; Djukic, J.-P.; Agbossou-Niedercorn, F.; Michon, C. Selective Hydrosilylation of Esters to Aldehydes Catalysed by Iridium(III) Metallacycles through Trapping of Transient Silyl Cations. *Chem. - A Eur. J.* **2016**, *22* (39), 14036–14041. b) Corre, Y.; Iali, W.; Hamdaoui, M.; Trivelli, X.; Djukic, J.-P.; Agbossou-Niedercorn, F.; Michon, C. Efficient Hydrosilylation of Imines Using Catalysts Based on Iridium(III) Metallacycles. *Catal. Sci. Technol.* **2015**, *5* (3), 1452–1458. c) Iali, W.; Paglia, F. La; Goff, X.-F. Le; Sredojević, D.; Pfeffer, M.; Djukic, J.-P. Room Temperature Tandem Hydroamination and Hydrosilation/protodesilation Catalysis by a Tricarbonylchromium-Bound Iridacycle. *Chem. Commun.* **2012**, *48* (83), 10310.

2.1.2 Transition-metal silane complexes

Metal-silane complexes are central to many chemical transformations that aim the synthesis of high value organic molecules and materials.[16] The most documented[16,17] types of metal-silane adducts are the so-called σ-complexes ($\eta^{1 \text{ or } 2}$:H–SiR_3)$TM^{(n)}$ (*n*: formal oxidation state; TM: transition-metal) arising from the isohypsic[18] (i.e. *n* = constant, by definition the isohypsic term refers to reactions occuring at a given reactive center with no change of its formal oxidation state) metal-coordination of silane[19] and $R_3Si–M^{(n+2)}–H$ complexes arising from oxidative-addition of the H–Si bond at $M^{(n)}$.[20] However, intermediary situations considered as so-called "arrested states" towards the H–Si bond cleavage by oxidative addition were also pointed out and raised sustained attention.[21] TM–silane adducts are commonly categorized according to the bonding relationships existing within the Si–TM–H motif, i.e. 2 center - 2 electron and 3 center - 2 electron interactions.[22] Subcategories of stabilizing interactions referred to as IHI (interligand hypervalent interactions) and SISHA[23] (secondary interaction between a silicon and a hydrogen atom) were proposed. The SISHA concept, rather imprecise in its definition of the actual nature of the key secondary interaction, embraces a large number of bonding situations where the Si…H interaction within the Si–TM–H motif is weak but not negligible.[15] The complexity that may lie behind the cohesion of the Si–TM–H motif[24] was addressed theoretically

[16] a) Corey, J. Y. Reactions of Hydrosilanes with Transition Metal Complexes. *Chem. Rev.* **2016**, acs.chemrev.5b00559. b) Corey, J. Y. Reactions of Hydrosilanes with Transition Metal Complexes and Characterization of the Products. *Chem. Rev.* **2011**, *111* (2), 863–1071.
[17] Hosomi, A.; Miura, K. In *Comprehensive Organometallic Chemistry III*; Crabtree, R. H., Mingos, D. M. P., Eds.; Elsevier: Oxford, 2007, p 297-339.
[18] Burns, N. Z.; Baran, P. S.; Hoffmann, R. W. Redox Economy in Organic Synthesis. *Angew. Chem. Int. Ed.* **2009**, *48*, 2854-2867.
[19] Yang, J.; White, P. S.; Schauer, C. K.; Brookhart, M. Structural and Spectroscopic Characterization of an Unprecedented Cationic Transition-Metal η^1-Silane Complex. *Angew. Chem. Int. Ed.* **2008**, *2008*, 4141-4143.
[20] Klei, S. R.; Tilley, T. D.; Bergman, R. G. The Mechanism of Silicon–Hydrogen and Carbon–Hydrogen Bond Activation by Iridium(III): Production of a Silylene Complex and the First Direct Observation of Ir(III)/Ir(V) C−H Bond Oxidative Addition and Reductive Elimination. *J. Am. Chem. Soc.* **2000**, *122*, 1816-1817.
[21] a) Perutz, R. N.; Sabo-Etienne, S. The σ-CAM Mechanism: σ Complexes as the Basis of σ-Bond Metathesis at Late-Transition-Metal Centers. *Angew. Chem. Int. Ed.* **2007**, *46*, 2578 - 2592. b) Calimano, E.; Tilley, T. D. Synthesis and reactivity of rhodium and iridium alkene, alkyl and silyl complexes supported by a phenyl-substituted PNP pincer ligand. *Dalton Trans.* **2010**, *39*, 9250-9263. c) Martin, M.; Sola, E.; Torres, O.; Plou, P.; Oro, L. A. Versatility of Cyclooctadiene Ligands in Iridium Chemistry and Catalysis. *Organometallics* **2003**, *22*, 5406-5417.
[22] Green, J. C.; Green, M. L. H.; Parkin, G. The occurrence and representation of three-centre two-electron bonds in covalent inorganic compounds. *Chem. Commun.* **2012**, *48*, 11481-11503.
[23] Lachaize, S.; Sabo-Etienne, S. σ-Silane Ruthenium Complexes: The Crucial Role of Secondary Interactions. *Eur. J. Inorg. Chem.* **2006**, 2115-2127.
[24] a) Schubert, U.; Ackermann, K.; Worle, B. A long silicon-hydrogen bond or a short silicon-hydrogen nonbond? Neutron-diffraction study of ($\eta^5CH_3C_5H_4$)$(CO)_2$(H)MnSiF$(C_6H_5)_2$. *J. Am. Chem. Soc.* **1982**, *104*, 7378-7380. b) Nikonov, G. I. The Puzzle of $Cp(CO)_2Mn(HSiCl_3)$: Classical or Nonclassical? *Organometallics* **2003**, *22*, 1597-1598. c) Nikonov, G. I. Recent Advances in Nonclassical Interligand Si...H Interactions. *Adv. Organomet. Chem.* **2005**, *53*, 217-309. d) Vybioshchikov, S. F.; Nikonov, G. I. Unique {$H(SiR_3)_2$}, (H_2SiR_3), H($HSiR_3$), and (H_2)SiR_3 Ligand Sets Supported by the {Fe(Cp)(L)} Platform (L=CO, PR_3). *Chem. - Eur. J.* **2006**, *12*, 8518-8533.

in the past[25] although without formal consideration for non-covalent interactions. Recent recourse to X-ray diffraction multipolar refinement methods with support of the Quantum Theory of Atoms in Molecules[26] (QTAIM) has fuelled the quest for a unified picture of the electronic structure of metal-silane complexes.[27] Sustained efforts are still required to understand the mechanism of silane addition to transition metal centers particularly in coordinatively saturated complexes for which the creation of the necessary vacant site requires ligand displacement. Iridacycles of the formula $[(\kappa^2\text{-(C,N)-(L)Ir(III)Cp*L'}]^q$ (L is a heterochelating ligand) belong to such a class of coordinatively saturated complexes that can promote catalytically the hydrosilylation of imines[28] upon displacement of the ligand L' and with the assistance of the $[BArF_{24}]^-$ anion, i.e. tetrakis[3,5-bis(trifluoromethyl)phenyl]borate. The high potential of this class of organoiridium complexes for hydrogen atom transfer catalysis has also been documented by Pfeffer[29] and by Xiao[30] and coworkers. Furthermore, in all-in-one-pot conditions, iridacycles are capable of orderly and selectively achieve the hydroamination of alkynes and the subsequent hydrosilylation of imine intermediates in methanol without interference of the latter (scheme 1, page 17).[31] In this chapter, we report on the structures of key $(R_3Si)(H)Ir$ reactive intermediates arising from the reaction between new ionic iridacycles and silanes $HSiR_3$ (scheme 10, page 54). The investigation of the interaction of these ionic iridacycles with silanes and alcohols was carried out focussing on a model catalytic reaction

[25] Lin, Z. Structural and bonding characteristics in transition metal–silane complexes. *Chem. Soc. Rev.* **2002**, *31*, 239-245.
[26] Bader, R. F. W. In *Atoms in Molecules: A Quantum Theory*; Clarendon: Oxford, 1990.
[27] a) Scherer, W.; Meixner, P.; Barquera-Lozada, J. E.; Hauf, C.; Obenhuber, A.; Brück, A.; Wolstenholme, D. J.; Ruhland, K.; Leusser, D.; Stalke, D. A Unifying Bonding Concept for Metal Hydrosilane Complexes. *Angew. Chem. Int. Ed.* **2013**, *52*, 6092-6096. b) Hauf, C.; Barquera-Lozada, J. E.; Meixner, P.; Eickerling, G.; Altmannshofer, S.; Stalke, D.; Zell, T.; Schmidt, D.; Radius, U.; Scherer, W. *Z.* Remanent Si-H Interactions in Late Transition Metal Silane Complexes. *Anorg. Allg. Chem.* **2013**, *639*, 1996-2004.
[28] Corre, Y.; Iali, W.; Hamdaoui, M.; Trivelli, X.; Djukic, J.-P.; Agbossou-Niedercorn, F.; Michon, C. Efficient Hydrosilylation of Imines Using Catalysts Based on Iridium(III) Metallacycles. *Catal. Sci. Technol.* **2015**, *5* (3), 1452–1458.
[29] Pannetier, N.; Sortais, J.-B.; Issenhuth, J.-T.; Barloy, L.; Sirlin, C.; Holuigue, A.; Lefort, L.; Panella, L.; de Vries, J. G.; Pfeffer, M. Cyclometalated Complexes of Ruthenium, Rhodium and Iridium as Catalysts for Transfer Hydrogenation of Ketones and Imines. *Adv. Synth. Cat.* **2011**, *353*, 2844-2852.
[30] a) Wu, X.; Liu, J.; Li, X.; Zanotti-Gerosa, A.; Hancock, F.; Vinci, D.; Ruan, J.; Xiao, J. On water and in air: Fast and highly chemoselective transfer hydrogenation of aldehydes with iridium catalysts. *Angew. Chem., Int. Ed.* **2006**, *45*, 6718-6722. b) Wang, C.; Pettman, A.; Basca, J.; Xiao, J. Hydrogenation of imino bonds with half-sandwich metal catalysts. *Angew. Chem., Int. Ed.* **2011**, *49*, 7548-7552. c) Wang, C.; Chen, H.-Y. T.; Bacsa, J.; Catlow, C. R. A.; Xiao, J. Synthesis and X-ray structures of cyclometalated iridium complexes including the hydrides. *Dalton Trans.* **2013**, *42*, 935-940. d) Wei, Y.; Wang, C.; Jiang, X.; Xue, D.; Liu, Z.-T.; Xiao, J. Catalyst-free transformation of levulinic acid into pyrrolidinones with formic acid. *Green Chem.* **2014**, *16*, 1093-1096. e) Chen, H. Y. T.; Wang, C.; Wu, X.; Jiang, X.; Catlow, C. R. A.; Xiao, J. Iridicycle-Catalysed Imine Reduction: An Experimental and Computational Study of the Mechanism. *Chem. Eur. J.* **2015**, *21*, 16564-16577.
[31] Iali, W.; Paglia, F. La; Goff, X.-F. Le; Sredojević, D.; Pfeffer, M.; Djukic, J.-P. Room Temperature Tandem Hydroamination and Hydrosilation/protodesilation Catalysis by a Tricarbonylchromium-Bound Iridacycle. *Chem. Commun.* **2012**, *48* (83), 10310.

that is widely documented, i.e the *O*Si of alcohols (scheme 2, page 18).[32] The above mentioned (R_3Si)(H)Ir intermediates can reasonably be considered as the key catalytic species in the fast room temperature *O*Si of alcohols[24c,33] (this chapter), hydrosilylation of carbonyls and nitriles (chapter 3), and the C–F bond activation of fluorocarbons (chapter 4), and also certainly in other hydrosilylation reactions catalyzed by iridacycles of formula [(κ^2-(C,N)-(L)Ir(III)Cp*L']^q.[20,23,34]

[32] a) Cardoso, J. M. S.; Lopes, R.; Royo, B. *J.* Dehydrogenative silylation of alcohols catalysed by half-sandwich iron N-heterocyclic carbene complexes. *Organomet. Chem.* **2015**, *775*, 173-177. b) Esteruelas, M. A.; Oliván, M.; Vélez, A. POP-pincer silyl complexes of group 9: Rhodium versus iridium. *Inorg. Chem.* **2013**, *52*, 12108−12119. ❑) Luo, X. L.; Crabtree, R. H. Homogeneous catalysis of silane alcoholysis via nucleophilic attack by the alcohol on an Ir(η^2-$HSiR_3$) intermediate catalyzed by $[IrH_2S_2(PPh_3)_2]SbF_6$ (S = solvent). *J. Am. Chem. Soc.* **1989**, *111*, 2527-2535. d) Sattler, W.; Parkin, G. Zinc Catalysts for On-Demand Hydrogen Generation and Carbon Dioxide Functionalization. *J. Am. Chem. Soc.* **2012**, *134*, 17462–17465.

[33] a) Labouille, S.; Escalle-Lewis, A.; Jean, Y.; Mézailles, N.; LeFloch, P. Mechanism of the dehydrogenative silylation of alcohols catalyzed by cationic gold complexes: An experimental and theoretical study. *Chem. Eur. J.* **2011**, *17*, 2256 - 2265. b) Cardoso, J. M. S.; Lopes, R.; Royo, B. Dehydrogenative silylation of alcohols catalysed by half-sandwich iron N-heterocyclic carbene complexes. *J. Organomet. Chem.* **2015**, *775*, 173-177.

[34] Corre, Y.; Rysak, V.; Capet, F.; Djukic, J.-P.; Agbossou-Niedercorn, F.; Michon, C. Selective Hydrosilylation of Esters to Aldehydes Catalysed by Iridium(III) Metallacycles through Trapping of Transient Silyl Cations. *Chem. - A Eur. J.* **2016**, *22* (39), 14036–14041.

2.2 Results and discussion

2.2.1 Synthesis and characterization of complexes

2.2.1.1 General strategy

Several neutral and ionic iridacycles were prepared following the general synthetic strategy shown below (scheme 3). The chemical process by which the final ionic

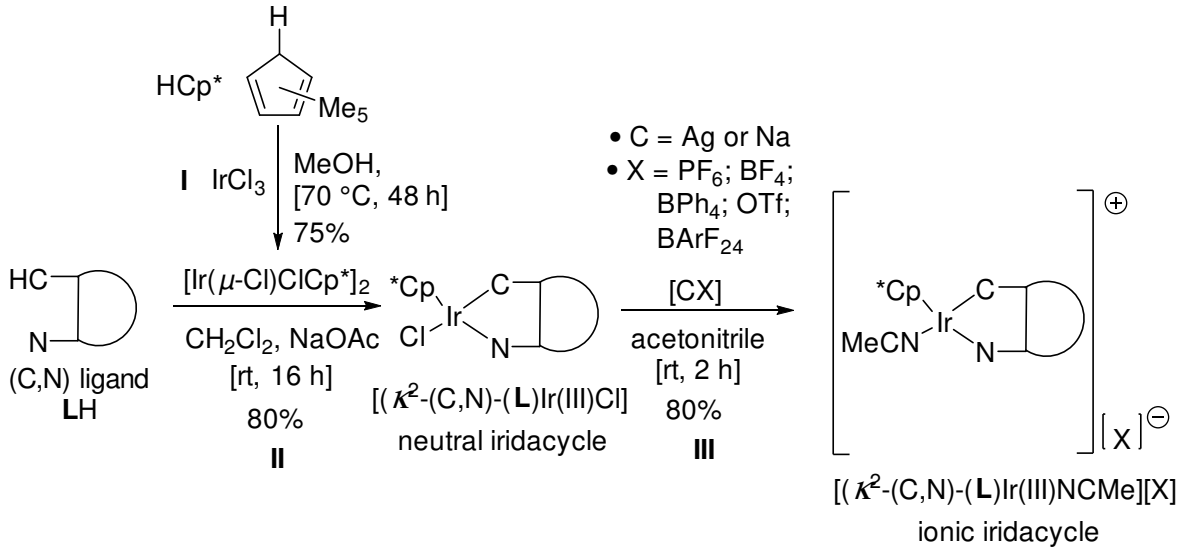

Scheme 3. General synthetic strategy used for the preparation of the iridacycles disclosed in this thesis. Neutral iridacycles [(κ^2-(C,N)-(**L**)Ir(III)Cl] were prepared from the C,N-heterobidentate ligand **L**H and the iridium precursor [Ir(μ-Cl)ClCp*]$_2$ through procedures **I–II**, whereas ionic iridacycles [(κ^2-(C,N)-(**L**)Ir(III)NCMe][X] were prepared from [(κ^2-(C,N)-(**L**)Ir(III)Cl] and salts [CX] through the procedure **III**.

iridacycles of the general formula [(κ^2-(C,N)-(**L**)Ir(III)NCMe][X] were obtained was easy to conduct, and required only three steps (**I–III**) with an average yield of ≥75% for each step in general. In step **I**, the chloro-bridged iridium dimer [Ir(μ-Cl)ClCp*]$_2$ was synthesized from $IrCl_3$ and 1,2,3,4,5-pentamethylcyclopenta-1,3-diene (HCp*) upon refluxing of methanol for at least 48 h (experimental part).[35] In step **II**, the chlorido iridacycles [(κ^2-(C,N)-(**L**)Ir(III)Cl] were suitably prepared in 80% yield in general, through the well known C–H activation of the heterobidentate C,N-ligand **L**H by the

[35] White, C.; Yates, A.; Maitlis, P. M.; Heinekey, D. M. (η^5-Pentamethylcyclopentadienyl)Rhodium and -Iridium Compounds. In *Inorganic Syntheses*; John Wiley & Sons, Inc., 2007; pp 228–234.

dimeric iridium complex [Ir(μ-Cl)ClCp*]$_2$ and with the assistance of NaOAc.[36] The synthesis was generally conducted at room temperature overnight in a minimum volume of CH_2Cl_2 (~5–10 mL) (experimental part). The last step **III** is also a very convenient way for the preparation of ionic η^1-(CH_3CN)-iridacycles [(κ^2-(C,N)-(**L**)Ir(III)NCMe][X]. [(κ^2-(C,N)-(**L**)Ir(III)NCMe][X] were prepared in 80% yield in general by chloride abstraction from [(κ^2-(C,N)-(**L**)Ir(III)Cl] with the assistance of [CX] salts (C = Ag or Na; X = PF_6, BF_4, BPh_4, OTf, $BArF_{24}$) and CH_3CN.[37] The synthesis was generally conducted at room temperature for 2 h in a minimum volume of CH_3CN (~5–7 mL) (experimental part).

2.2.1.2 Several new neutral and ionic iridacycles have been prepared

Using the 3 steps **I**–**III** of the general strategy described before, six C,N ligands **L**H**1**–**L**H**6** (scheme 4a) were used as starting material for the synthesis of several neutral (**1**, **3**, **5**, **7**, **9**, **11**) and ionic ([**2**][X], [**4**][X], [**6**][X], [**8**][X] [**10**][X], [**12**][X]) iridacycles (scheme 4b). Complexes **7**, **9**, [**2**][BPh_4], [**4**][$BArF_{24}$], [**4**][OTf], [**4**][BPh_4], [**6**][$BArF_{24}$], [**8**][$BArF_{24}$], and [**10**][$BArF_{24}$ are new. All the other neutral and ionic iridacycles are known complexes which were prepared by us and others.[38,39,40,41,42] Most of new complexes were fully characterized. The related experimental procedures and conditions, the characterization data and the NMR spectra are described in the experimental part. The ionic iridacycles showed to be very stable in solution and solid state under standard

[36] a) Scheeren, C.; Maasarani, F.; Hijazi, A.; Djukic, J. P.; Pfeffer, M.; Zarić, S. D.; Le Goff, X. F.; Ricard, L. Stereoselective "electrophilic" cyclometalation of Planar-Prochiral (η^6-Arene)tricarbonylchromium Complexes with Asymmetric Metal Centers: Pseudo-T-4 [Cp*$RhCl_2$]$_2$ and [Cp*$IrCl_2$]$_2$. *Organometallics* **2007**, *26* (14), 3336–3345. b) Davies, D. L.; Al-Duaij, O.; Fawcett, J.; Giardiello, M.; Hilton, S. T.; Russell, D. R. Room-Temperature Cyclometallation of Amines, Imines and Oxazolines with [MCl_2Cp*]$_2$ (M = Rh, Ir) and [$RuCl_2$(*p*-cymene)]$_2$. *Dalt. Trans.* **2003**, *2* (21), 4132–4138.

[37] Hamdaoui, M.; Ney, M.; Sarda, V.; Karmazin, L.; Bailly, C.; Sieffert, N.; Dohm, S.; Hansen, A.; Grimme, S.; Djukic, J.-P. Evidence of a Donor–Acceptor (Ir–H)→SiR_3 Interaction in a Trapped Ir(III) Silane Catalytic Intermediate. *Organometallics* **2016**, *35* (13), 2207–2223.

[38] For **1** and **3**, see: Li, L.; Brennessel, W. W.; Jones, W. D. An Efficient Low-Temperature Route to Polycyclic Isoquinoline Salt Synthesis via C-H Activation with [Cp*MCl_2]$_2$ (M = Rh, Ir). *J. Am. Chem. Soc.* **2008**, *130* (37), 12414–12419.

[39] For **5**, see: Djukic, J. P.; Iali, W.; Pfeffer, M.; Le Goff, X. F. Synthesis of Planar Chiral Iridacycles by Cationic Metal π-Coordination: Facial Selectivity, and Conformational and Stereochemical Consequences. *Chem. - A Eur. J.* **2012**, *18* (19), 6063–6078.

[40] For **11**, see: Liu, Z.; Habtemariam, A.; Pizarro, A. M.; Clarkson, G. J.; Sadler, P. J. Organometallic Iridium(III) Cyclopentadienyl Anticancer Complexes Containing C,N-Chelating Ligands. *Organometallics* **2011**, *30* (17), 4702–4710.

[41] For [**2**][$BArF_{24}$] (and [**2**][OTf], [**2**]BF_4]: modified procedure), see: Hamdaoui, M.; Ney, M.; Sarda, V.; Karmazin, L.; Bailly, C.; Sieffert, N.; Dohm, S.; Hansen, A.; Grimme, S.; Djukic, J.-P. Evidence of a Donor–Acceptor (Ir–H)→SiR_3 Interaction in a Trapped Ir(III) Silane Catalytic Intermediate. *Organometallics* **2016**, *35* (13), 2207–2223.

[42] For original data of [**2**][PF_6], [**2**][OTf], [**2**]BF_4]:, see: Park-Gehrke, L. S.; Freudenthal, J.; Kaminsky, W.; Dipasquale, A. G.; Mayer, J. M. Synthesis and Oxidation of CpIrIII Compounds: Functionalization of a Cp Methyl Group. *Dalt. Trans.* **2009**, *0* (11), 1972–1983.

conditions of temperature and pressure; with the exception however of [**6**][$BArF_{24}$], which decomposed in chlorinated solvents such as $CHCl_3$ and CH_2Cl_2 within few hours. This instability may be due to the labitity of the acetonitrile ligand in solution.

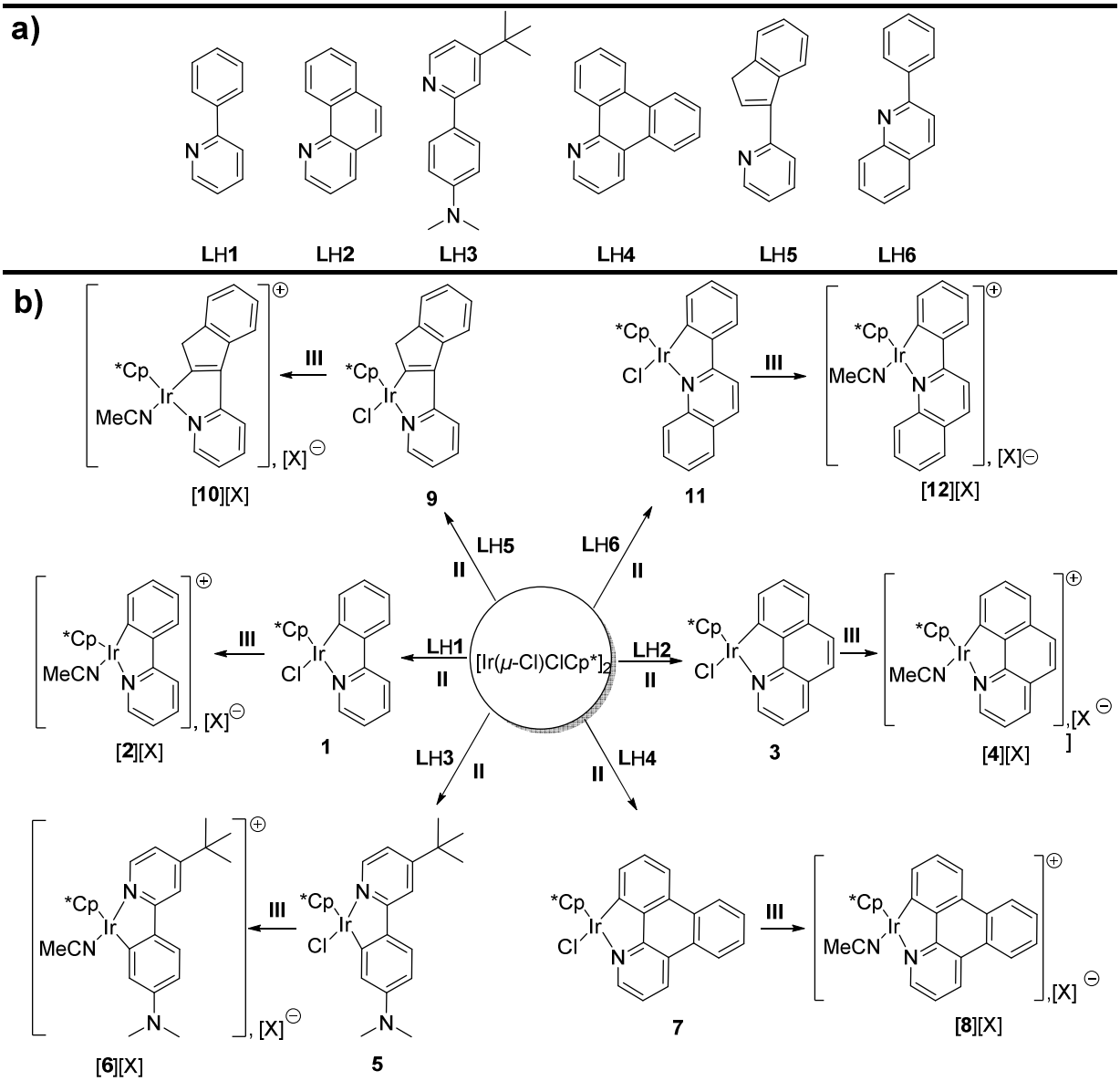

Scheme 4. The chemical structures of **a)** the C,N-heterobidentate ligands **L**H, and **b)** the related neutral iridacycles, **1**, **3**, **5**, **7**, **9** and **11**, and ionic iridacycles, [**2**][X], [**4**][X], [**6**][X], [**8**][X] [**10**][X], and [**12**][X]. For [**2**][X], X = $BArF_{24}$, BPh_4, OTf, PF_6, and BF_4; for [**4**][X], X = $BArF_{24}$, BPh_4, OTf; for [**6**][X], [**8**][X], and [**10**][X], X = $BArF_{24}$; and for [**12**][X], X = OTf.

2.2.1.3 Synthesis of the ionic rhodacycle [**2'**][$BArF_{24}$]

In order to investigate the effect of the transition metal on the catalytic performance, we also synthesized the ionic rhodacycle [(κ^2-(C,N)-(2-phenylenepyridine)Rh(III)NCMe][$BArF_{24}$] ([**2'**][$BArF_{24}$], scheme 5). Using the procedure **III**, [**2'**][$BArF_{24}$] was easily prepared from **1'** and Na[$BArF_{24}$] in 63% yield. [**2'**][$BArF_{24}$] has been fully analytically characterized (see experimental part for details).

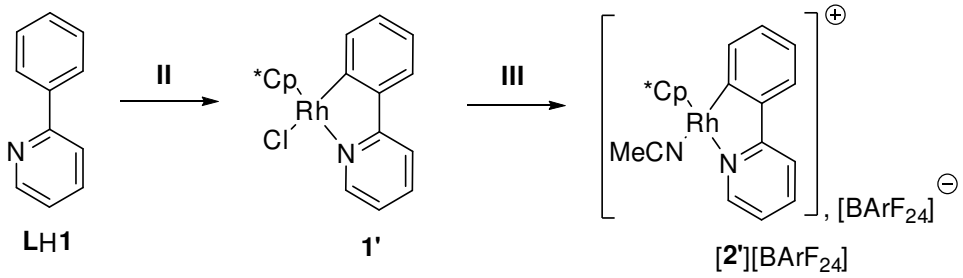

Scheme 5. Synthesis of the ionic rhodacycle [(κ^2-(C,N)-(2-phenylenepyridine)Rh(III)NCMe][$BArF_{24}$], [**2'**][$BArF_{24}$], from **1'** and Na[$BArF_{24}$] through the procedure **III**.

2.2.1.4 Single crystal X-ray diffraction studies

The structures of [**2**][$BArF_{24}$], [**2**][BPh_4], [**2**][BF_4], [**2'**][$BArF_{24}$], [**4**][$BArF_{24}$], [**4**][BPh_4] and [**6**][$BArF_{24}$] have been determined by single crystal X-ray diffraction analysis (figures 1–3).

2.2.1.4.1 X-ray structures of [**2**][$BArF_{24}$], [**2**][BPh_4] and [**2**][BF_4]

Figure 1 shows the X-ray structures of [**2**][BPh_4] (figure 1b), [**2**][BF_4] (figure 1b) and [**2**][$BArF_{24}$] (figure 1c). In table 1 are provided some typical geometrical parameters found in the latter structures, whereas table 2 lists all their pertinent structural X-ray diffraction acquisition and refinement data (see appendix for more details). The structure of [**2**][$BArF_{24}$] displays the longest cation-anion separation ($d_{Ir\text{-}B}$~ 11.1 Å), arbitrarily defined here as the shortest distance between the central atoms of each ion, i.e. the Ir atom for the cation and the B atom for the anion, within the crystal lattice. The $[BF_4]^-$ salt displays (figure 1b) the typical cation-anion separation already reported

for [**2**][OTf][43] (O as central atom of the anion) and [**2**][PF_6][44] (P as central atom of the anion), which lies within the 6.82–5.06 Å range. The $[BPh_4]^-$ salt represents an intermediary situation because the cation-anion separation is found to amount $d_{Ir\text{-}B}$ ~ 7.468(4) Å (figure 1a).

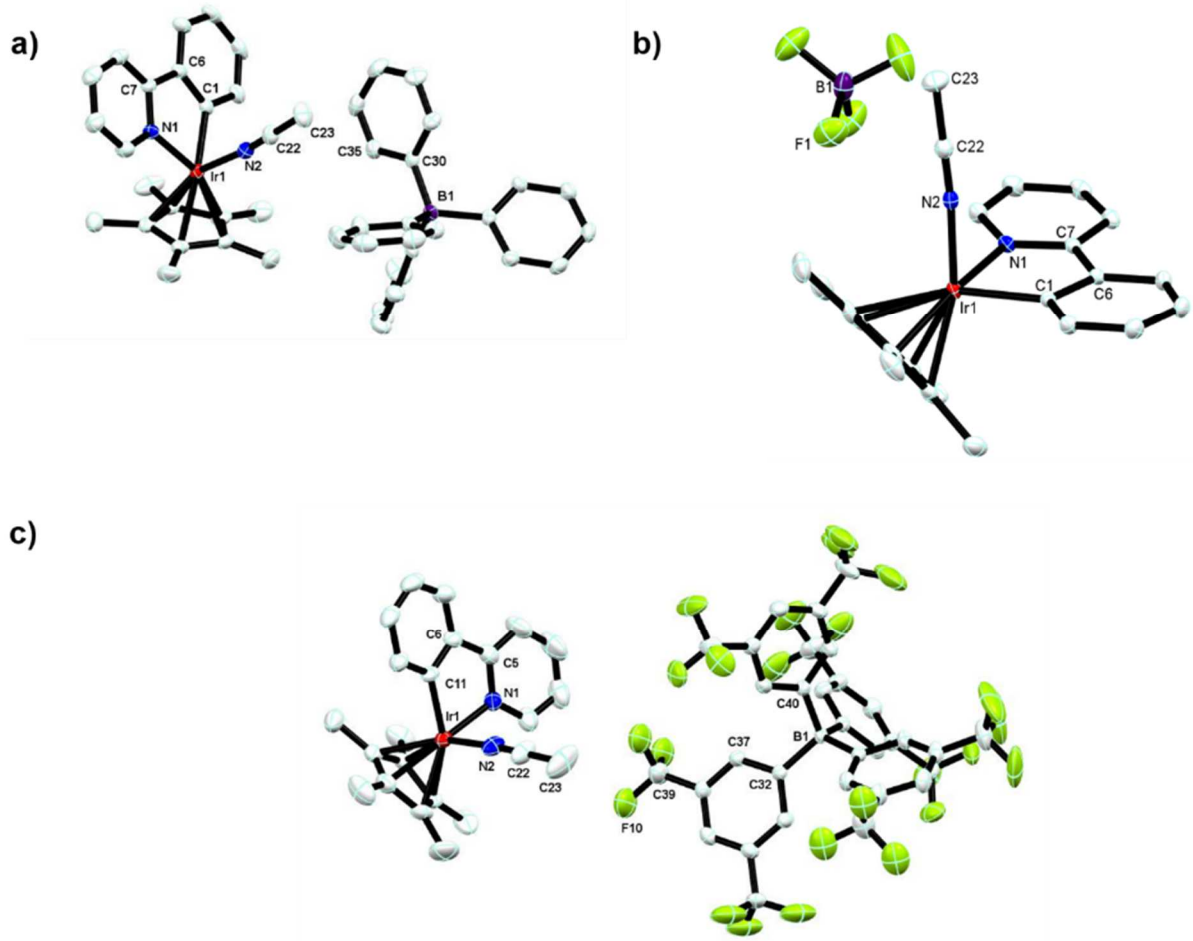

Figure 1. Ellipsoid-type diagrams drawn at the 30% probability level with partial atom numbering of the structures of **a)** [**2**][BPh_4], **b)** [**2**][BF_4] and **c)** [**2**][$BArF_{24}$]. For [**2**][BPh_4] and [**2**][BF_4], one lattice CH_2Cl_2 molecule was omitted for clarity. For all structures, hydrogen atoms were omitted for clarity, and the depicted anions are the nearest ones to the considered cation in the crystal lattice.

2.2.1.4.2 X-ray structures of [**2'**][$BArF_{24}$] and [**6**][$BArF_{24}$]

[43] Sau, Y. K.; Yi, X. Y.; Chan, K. W.; Lai, C. S.; Williams, I. D.; Leung, W. H. Insertion of Nitrene and Chalcogenolate Groups into the Ir-C σ Bond in a Cyclometalated iridium(III) Complex. *J. Organomet. Chem.* **2010**, *695* (9), 1399–1404.

[44] Hu, Y.; Li, L.; Shaw, A. P.; Norton, J. R.; Sattler, W.; Rong, Y. Synthesis, Electrochemistry, and Reactivity of New iridium(III) and rhodium(III) Hydrides. *Organometallics* **2012**, *31* (14), 5058–5064.

Table 1. Selected interatomic distances (Å), angles (deg) and torsion angles (deg) for [**2**][$BArF_{24}$], [**2**][BPh_4] and [**2**][BF_4].

Distance (Å)	**[2][$BArF_{24}$]**	**[2][BPh_4]**	**[2][BF_4]**
Ir1–N1	2.091(3)	2.085(2)	2.096(2)
Ir1–N2	2.049(4)	2.058(2)	2.044(3)
C1—Ir1	C11—Ir1, 2.049(4)	2.063(2)	2.048(3)
B1–Ir1	11.079(3)	7.468(4)	5.088(2)
Angle (°)	**[2][$BArF_{24}$]**	**[2][BPh_4]**	**[2][BF_4]**
C1–Ir1–N1	C11–Ir1–N1, 78.24(15)	78.04(8)	77.77(10)
N2—Ir1—N1	84.88(15)	83.26(8)	85.23(10)
C22—N2—Ir1	172.4(4)	173.9(2)	172.8(3)
N2—C22—C23	178.7(6)	179.3(3)	179.3(4)
	[2][$BArF_{24}$]	**[2][BPh_4]**	**[2][BF_4]**
Torsion angle (°)	C11–C6–C5–N1, 1.1(6)	C1–C6–C7–N1, –0.4(3)	C1–C6–C7–N1, –0.8(3)
	C2—C1—N1—Ir1, 178.8(4)	C10—C11—N1—Ir1, 179.3(2)	C10—C11—N1—Ir1, 176.5(2)

Figure 2 shows the X-ray structures of [**2'**][$BArF_{24}$] (figure 2a) and [**6**][$BArF_{24}$] (figure 2b). Few typical geometrical parameters found in the latter structures and all their pertinent structural X-ray diffraction acquisition and refinement data (see appendix for more details) are summarized in table 3 and table 4 respectively. When compared to the structure of [**2**][$BArF_{24}$], the structures of [**2'**][$BArF_{24}$] and [**6**][$BArF_{24}$] feature almost identical geometrical parameters, with however some slight differences. For example, the d(M–N_{NCMe}) (M = Ir, Rh) bond length provides a good indication of the degree of coordination of the NCMe ligand to the metal, at least in the solid state. One can notice that [**2'**][$BArF_{24}$] and [**6**][$BArF_{24}$] feature the longest (d(Rh–N_{NCMe}) = 2.065(3) Å) and the shortest (d(Ir–N_2) = 2.035(3) Å) d(M–N_{NCMe}) bond lengths respectively, whereas [**2'**][$BArF_{24}$] features an intermediary bond length with d(Ir–N_{NCMe}) = 2.049(4) Å. The M–N–C_{NCMe} angle is another parameter to compare. It is worth to notice that [**6**][$BArF_{24}$] features an Ir–N–C_{NCMe} angle of 178.4(3)°, which is the most quasi-linear mode of coordination of NCMe to the metal when compared to other salts (172.4(4) for [**2**][$BArF_{24}$], 170.2(4)° for [**2'**][$BArF_{24}$]).

Table 2. Table of structural X-ray diffraction acquisition and refinement data for [**2**][BF_4], [**2**][$BArF_{24}$] and [**2**][BPh_4]. Temperature of acquisition: T = 173(2) K.

compound	**[2][BF_4]**	**[2][$BArF_{24}$]**	**[2][BPh_4]**
formula	$C_{23}H_{26}IrN_2BF_4 \bullet CH_2Cl_2$	$C_{32}H_{12}BF_{24} \bullet C_{23}H_{26}IrN_2$	$C_{23}H_{26}IrN_2 \bullet C_{24}H_{20}B \bullet CH_2Cl_2$
mol. wt (g/mol)	694.39	1385.88	926.79
habit	yellow prism	yellow plate	yellow prism
cryst. size (mm)	0.30 × 0.25 × 0.20	0.22 × 0.20 × 0.06	0.32 × 0.20 × 0.18
cryst. syst.	monoclinic	triclinic	monoclinic
space group	$P2_1/c$	$P\bar{1}$	$P2_1/c$
a (Å)	14.6676(5)	12.8467(5)	11.6460(3)
b (Å)	12.8597(4)	13.2327(5)	23.1238(7)
c (Å)	15.8707(4)	17.0526(6)	18.5864(5)
α (deg)	90	91.546(1)	90
β (deg)	119.400(2)	97.457(1)	123.485(1)
γ (deg)	90	107.091(1)	90
V (Å^3)	2608.02(14)	2740.94(18)	4174.6(2)
Z	4	2	4
D_x (Mg m^{-3})	1.768	1.679	1.475
θ_{max}, θ_{min} (°)	32.0, 1.6	31.1, 1.6	32.0, 1.6
μ (mm^{-1})	5.37	2.56	3.36
h,*k*,*l* range	–21/21, –19/17, –23/23	–10/18, –19/12, –24/24	–17/17, –34/34, –27/27
measd reflns	35077	42350	59089
indept reflns	9049	17435	14481
reflns ($I>2\sigma(I)$)	7606	14177	11492
params	313	739	493
R_{int}	0.025	0.025	0.034
$R[F^2 > 2\sigma(F^2)]$	0.030	0.047	0.032
$wR(F^2)$	0.063 [a]	0.124 [b]	0.062 [c]
S	1.11	1.02	1.03

[a] $w = 1/[\sigma^2(F_o^2) + (0.0174P)^2 + 6.0988P]$ where $P = (F_o^2 + 2F_c^2)/3$. [b] $w = 1/[\sigma^2(F_o^2) + (0.0693P)^2 + 4.0848P]$ where $P = (F_o^2 + 2F_c^2)/3$. [c] $w = 1/[\sigma^2(F_o^2) + (0.0244P)^2 + 3.2725P]$ where $P = (F_o^2 + 2F_c^2)/3$.

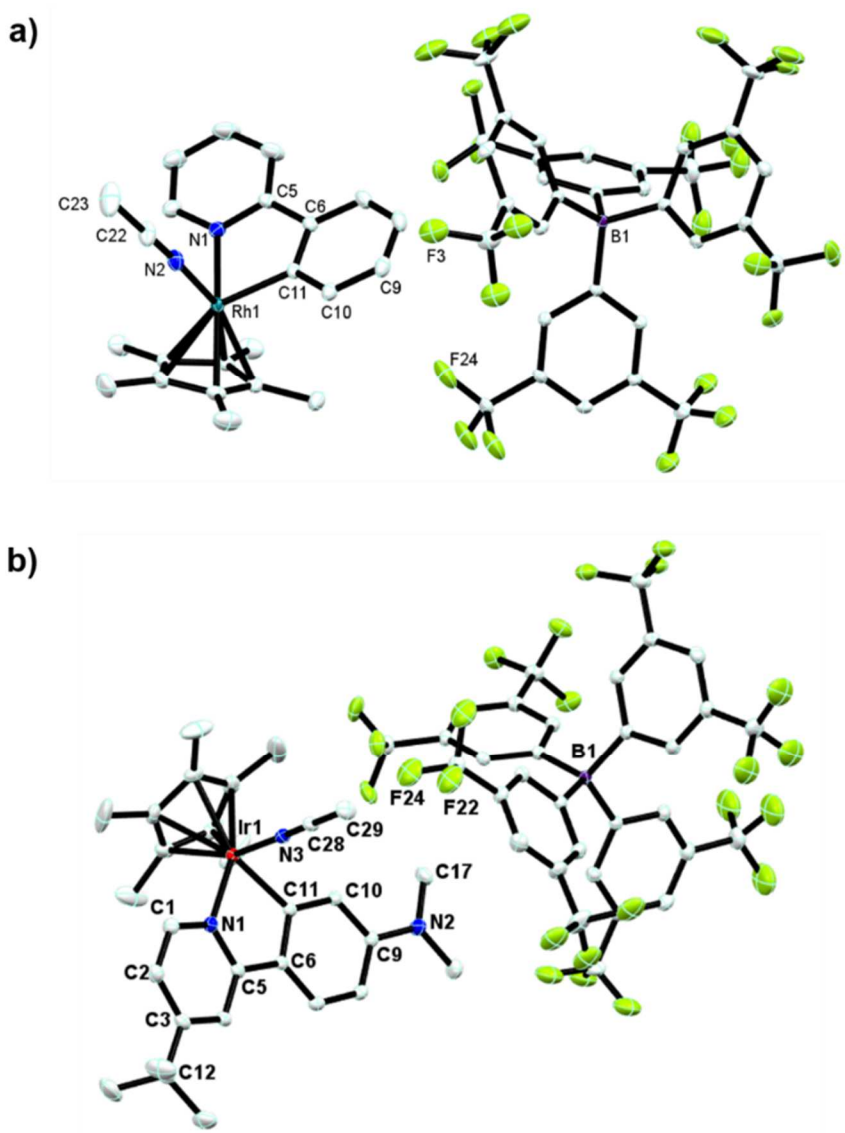

Figure 2. Ellipsoid-type diagrams drawn at the 30% probability level with partial atom numbering of the structures of **a)** [**2'**][$BArF_{24}$] and **b)** [**6**][$BArF_{24}$] (lattice hexane molecule was omitted for clarity). For both structures, all hydrogens and disordered fluorine atoms were omitted for clarity and the depicted anions are the nearest ones to the considered cation in the crystal lattice.

Another geometrical parameter to compare is the shortest *d*(M–B_{BArF24}) distance found in the crystal lattice, because it can give us an indication of the degree of the ion-pair association/separation, at least in the solid state. As mentioned before, the fact that [**2**][$BArF_{24}$] is characterized by the longest ion-pair separation of *d*(Ir–B_{BArF24}) = 11.079(3) Å holds also true when it is compared to both [**2'**][$BArF_{24}$] and [**6**][$BArF_{24}$],

Table 3. Selected interatomic distances (Å), angles (deg) and torsion angles (deg) for [**2'**][$BArF_{24}$] (M = Rh), [**6**][$BArF_{24}$], [**4**][$BArF_{24}$] and [**4**][BPh_4] (M = Ir).

Distance (Å)	**[2'][$BArF_{24}$]**	**[6][$BArF_{24}$]**	**[4][$BArF_{24}$]**	**[4][BPh_4]**
M1–N1	2.089(3)	2.106(3)	2.098(4)	2.106(2)
M1–N2	2.065(3)	2.035(3)	2.034(3)	2.037(2)
C11—M1	2.042(3)	2.053(3)	2.073(3)	C1–Ir1, 2.065(2)
B1–M1	8.504(3)	9.324(5)	8.887(2)	7.315(4)
Angle (°)	**[2'][$BArF_{24}$]**	**[6][$BArF_{24}$]**	**[4][$BArF_{24}$]**	**[4][BPh_4]**
C11–M1–N1	78.56(13)	78.8(1)	C1–M1–N1, 79.2(1)	C1–M1–N1, 78.95(9)
N2—M1—N1	86.32(14)	N3—Ir1—N1, 87.9(1)	87.1(1)	86.29(9)
C22—N2—M1	170.2(4)	C28—N3—Ir1, 178.4(3)	C24—N2—M1, 172.3(3)	C24—N2—M1, 179.0(2)
N2—C22—C23	178.7(6)	N3—C28—C29, 177.9(4)	178.0(5)	N2—C22—C23, 179.1(3)
	[2'][$BArF_{24}$]	**[6][$BArF_{24}$]**	**[4][$BArF_{24}$]**	**[4][BPh_4]**
Torsion angle (°)	N1—C5—C6—C11, –0.7(5)	N1—C5—C6—C11, 0.3(5)	N1—C12—C13—C11, 1.6(5)	N1—C12—C13—C1, –1.4(3)
	C2—C1—N1—Rh1, –178.3(4)	C2—C1—N1—Ir1, 175.9(3)	C2—C1—N1—Ir1, –175.9(4)	C12—C11—N1—Ir1, 176.8(2)

which feature shorter distances (d(Rh–B_{BArF24}) = 8.504(3) Å and d(Ir–B_{BArF24}) = 9.324(5) Å, respectively). What could explain such a difference in cation-anion separation for [**2**][$BArF_{24}$] when compared to [**2'**][$BArF_{24}$] and [**6**][$BArF_{24}$]? While the difference between [**2**][$BArF_{24}$] and [**2'**][$BArF_{24}$] may be due to the difference of the size of the transition metal S_M (Ir for [**2**]$^+$ and Rh for [**2'**]$^+$, $S_{Ir} > S_{Rh}$), the difference between [**2**][$BArF_{24}$] and [**6**][$BArF_{24}$] becomes more difficult to rationalize. Though, one can tentatively postulate that the polar (NMe_2) and the hydrophobic (^{t}Bu) substituents of the phenylenepyridine ligand in [**6**]$^+$ could favor additional electrostatic and/or non-covalent interactions between [**6**]$^+$ and [$BArF_{24}$]$^-$, thus explaining the better (closer) association between the two ions for [**6**][$BArF_{24}$] than for [**2**][$BArF_{24}$].

Table 4. Table of structural X-ray diffraction acquisition and refinement data for [**2'**][$BArF_{24}$], [**6**][$BArF_{24}$], [**4**][$BArF_{24}$] and [**4**][BPh_4]. Temperature of acquisition: T = 173(2) K.

compound	**[2'][$BArF_{24}$]**	**[6][$BArF_{24}$]**	**[4][$BArF_{24}$]**	**[4][BPh_4]**
formula	$C_{32}H_{12}BF_{24}$•$C_{23}H_{26}N_2Rh$	$C_{32}H_{12}BF_{24}$•$C_{29}H_{39}IrN_2$•C_6H_{12}	$C_{25}H_{26}IrN_2$•$C_{32}H_{12}BF_{24}$	$2(C_{25}H_{26}IrN_2)$•$2(C_{24}H_{20}B)$•$0.5(C_6H_6)$
mol. wt (g/mol)	1296.59	1485.09	1409.93	1770.82
habit	yellow prism	yellow prism	yellow prism	yellow prism
cryst.size (mm)	0.36 × 0.16 × 0.10	0.24 × 0.16 × 0.10	0.30 × 0.25 × 0.08	0.35 × 0.25 × 0.20
cryst. syst.	triclinic	triclinic	triclinic	triclinic
space group	$P\bar{1}$	$P\bar{1}$	$P\bar{1}$	$P\bar{1}$
a (Å)	12.7624(5)	14.7520(7)	12.3318(6)	12.0116(4)
b (Å)	13.2269(6)	15.3911(7)	12.9386(6)	17.9419(6)
c (Å)	16.9988(7)	16.4500(8)	18.3704(9)	19.2603(6)
α (deg)	91.752(1)	97.200	86.356(1)	92.616(1)
β (deg)	97.534(1)	96.675(1)	78.921(1)	95.995(1)
γ (deg)	107.250(1)	109.957(1)	75.034(1)	97.243(1)
V (Å^3)	2709.5(2)	3432.0 (3)	2778.6(2)	4087.9(2)
Z	2	2	2	2
D_x (Mg m^{-3})	1.589	1.534	1.685	1.439
θ_{max}, θ_{min} (°)	30.0, 1.2	30.0, 1.3	34.1, 1.6	32.0, 1.5
μ (mm^{-1})	0.44	2.05	2.52	3.30
h,*k*,*l* range	−17⁄17, −18⁄18, −23⁄23	−20⁄20, −21⁄21, −23⁄23	−19⁄19, −20⁄20, −28⁄28	−17⁄17, −26⁄26, −23⁄23
measd reflns	74316	76738	108274	105999
indept reflns	15767	20031	22760	28306
reflns (I>2σ(I))	12927	16368	19906	20690
params	727	851	748	994

R_{int}	0.032	0.046	0.026	0.036
$R[F^2 > 2\sigma(F^2)]$	0.070	0.046	0.043	0.035
$wR(F^2)$	0.200 [a]	0.122 [b]	0.121[c]	0.073 [d]
S	1.02	1.02	1.05	1.01

[a] $w = 1/[\sigma^2(F_o^2) + (0.1091P)^2 + 8.299P]$ where $P = (F_o^2 + 2F_c^2)/3$. [b] $w = 1/[\sigma^2(F_o^2) + (0.0731P)^2 + 2.5831P]$ where $P = (F_o^2 + 2F_c^2)/3$. [c] $w = 1/[\sigma^2(F_o^2) + (0.0692P)^2 + 5.3126P]$ where $P = (F_o^2 + 2F_c^2)/3$. [d] $w = 1/[\sigma^2(F_o^2) + (0.0308P)^2 + 2.4408P]$ where $P = (F_o^2 + 2F_c^2)/3$.

2.2.1.4.3 X-ray structures of [**4**][BArF$_{24}$] and [**4**][BPh$_4$]

Figure 3 shows the X-ray structures of [**4**][BArF$_{24}$] (figure 3a) and [**4**][BPh$_4$] (figure 2b). The typical geometrical parameters found in the latter structures and all their pertinent structural X-ray diffraction acquisition and refinement data (see appendix for more details) are summarized in table 3 and table 4 respectively.

When compared to the structures of [**2**][BArF$_{24}$] and [**2**][BPh$_4$], the structures of [**4**][BArF$_{24}$] and [**4**][BPh$_4$] share, with some deviations, almost the same geometrical features. For example, [**2**][BArF$_{24}$] and [**2**][BPh$_4$] both feature a slightly longer bond length d(Ir–N$_{NCMe}$) (2.049(4) Å and 2.058(2) Å respectively) than that of [**4**][BArF$_{24}$] and [**4**][BPh$_4$] (2.034(3) Å and 2.037(2) Å respectively). An Ir–N–C$_{NCMe}$ angle of 179.0(2)° is noticed for [**4**][BPh$_4$], which is markedly different from the value of 173.9(2)° found for [**2**][BPh$_4$]. An interesting feature observed in the crystal structure of [**4**][BPh$_4$] is the presence of H-π interactions that are established between the hydrogen H74A of bound-NCMe and the carbon atoms of one of the phenyl groups (arbitrarily denoted as Ph1^{BPh4} here) of the [BPh$_4$]$^-$ anion (figure 3c), characterized by the distance of d(H$_{74A}^{NCMe}$–C$_{Ph1}^{BPh4}$) = 2.660 Å (C$_{Ph1}^{BPh4}$ = centroid of Ph1 comprised of the carbons C82, C83, C84, C85, C86, C81). The H-π interactions are much likely to be considered as H-anion interactions of electrostatic type because the formal negative charge of the anion [BPh$_4$]$^-$ is largely delocalized over the four phenyl groups, more specifically at the carbon atoms. These H-anion interactions can be viewed as an electronic or charge communication "gateway" between the positively charged cation [**4**]$^+$ and the negatively charged anion [BPh$_4$]$^-$. Such interactions may also exist for all other [BArF$_{24}$]$^-$ and [BPh$_4$]$^-$ salts disclosed in this thesis, though with less efficient spatial directionality due to steric and/or lattice packing effects.

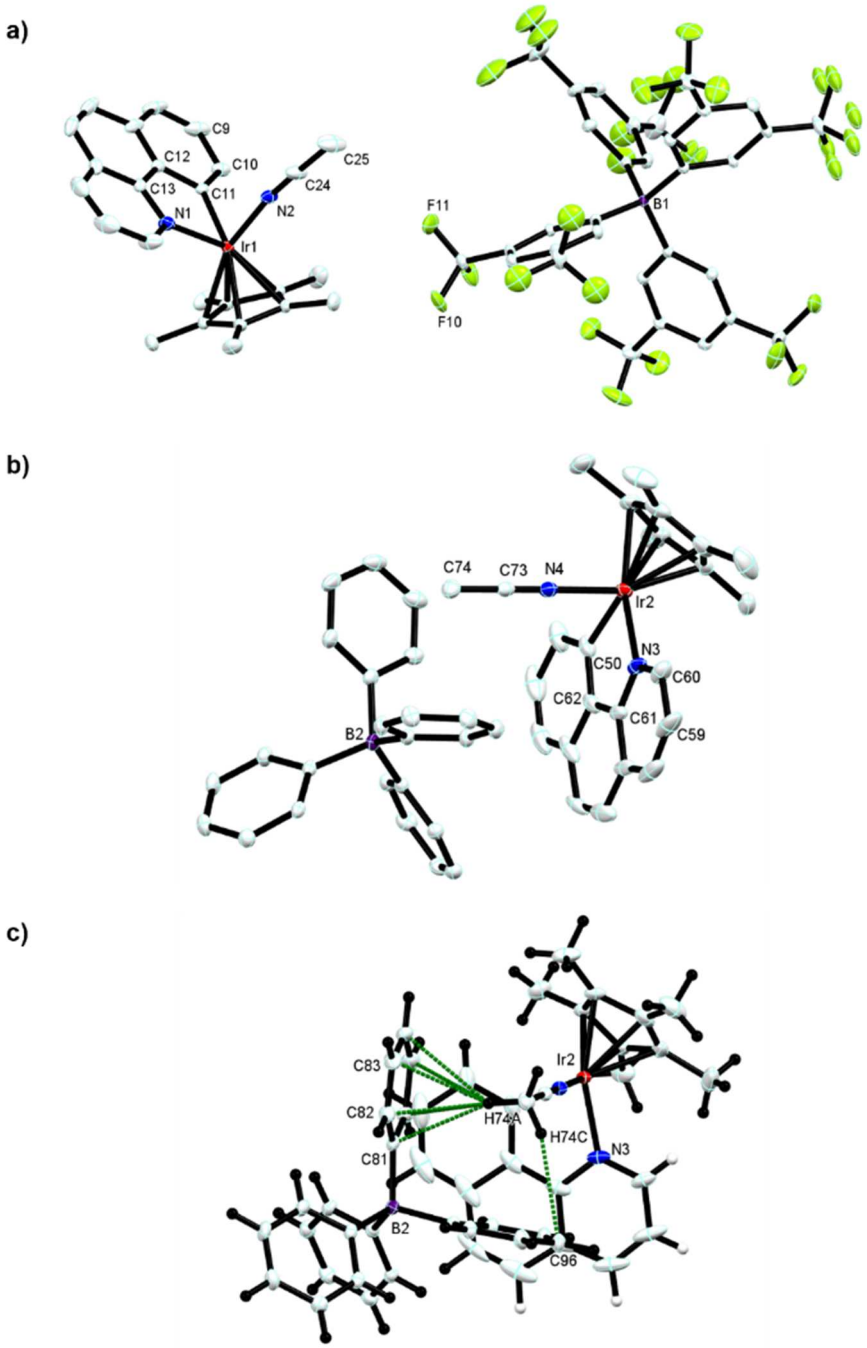

Figure 3. Ellipsoid-type diagrams drawn at the 30% probability level with partial atom numbering of the structures of **a)** [**4**][$BArF_{24}$] and **b–c)** [**4**][BPh_4] (lattice benzene and additional [**4**][BPh_4] molecules were omitted for clarity). For both structures in **a–b)**, all hydrogens and disordered fluorine atoms were omitted for clarity and the depicted anions are the nearest ones to the considered cation in the crystal lattice. For the structure in **c)**, all hydrogens atoms are shown in order to point out the so-called H-π interactions (green dots) between the CH_3CN ligand of the cation $[\mathbf{4}]^+$ (hydrogens H74A and H7AC) and one of the phenyl group of the anion $[BPh_4]^-$.

This is well illustrated for example with the structure of [**2**][BPh_4] (figure 2a, and see appendix for more details), where the shortest distance between one of the hydrogens of bound-NCMe and one of the phenyl groups of the anion is found to be $d(H_{NCMe}–Ph_1^{BPh4})$ ~2.660 Å. As mentioned before, the complex [**2**][$BArF_{24}$] is characterized by an ion-pair separation of d(Ir–B_{BArF24}) = 11.079(3) Å, which is ~2.2 Å longer that the value found for [**4**][$BArF_{24}$] (~8.887(2) Å). On the other hand, [**2**][BPh_4] features an ion-pair separation of d(Ir–B_{BPh4}) ~7.468(4) Å, ~0.15 Å longer that the value found for [**4**][BPh_4] (~7.315(4) Å).

2.2.2 Diffusion Ordered Spectroscopy (DOSY) studies

In order to study the origins of the difference in the distance $d(Ir_{cation}–B_{anion})$, which is a measure of the extent of anion-cation separation in the solid state (X-ray structures), we decided to carry-out ^1H and ^{19}F NMR diffusion-ordered spectroscopic (DOSY) analyses of the structurally characterized [**2**][$BArF_{24}$] and [**2**][BF_4]. The measurements were carried out in d_5.PhCl (ε ~ 5.6[45]) and CD_2Cl_2 (ε ~ 8.9[37]) solutions at 298 K (table 5). Hydrodynamic diffusion coefficients were determined accurately by an analytical method (figure 4a–b) and from 2D-DOSY plots (see experimental part). Both methods afforded identical values of cation and anion hydrodynamic diffusion coefficients D, which were based on ^1H and ^{19}F NMR experiments respectively. For the measures carried out in d_5.PhCl, the D_{cation}/D_{anion} ratio for [**2**][$BArF_{24}$] was found to be only slighly higher than the theoretical value of 1 for an ideal tight ion pair model (analytical D_{cation}/D_{anion}= 1.11(1), 2D-DOSY plot D_{cation}/D_{anion}= 1.1) (figure 4a, table 5), whereas for [**2**][BF_4] the ratio was closer to 1 (D_{cation}/D_{anion}= 1.01(1), 2D-DOSY plot D_{cation}/D_{anion}= 1.0) (figure 4b, table 5).[46] In CD_2Cl_2, a slightly more polar solvent, the qualitative values of D_{cation}/D_{anion} ratios extracted from 2D-DOSY plots were 1.2 and 0.9 for [**2**][$BArF_{24}$] and [**2**][BF_4] respectively.

[45] Reichardt, C. In *Solvents and Solvent Effects in Organic Chemistry*; Wiley-VCH Verlag GmbH & Co. KGaA: 2004, p 471-507.
[46] Pregosin, P. S. NMR Spectroscopy and Ion Pairing: Measuring and Understanding How Ions Interact. *Pure Appl. Chem.* **2009**, *81* (4), 615–633.

Table 5. *D* values (10^{-10} $m^2 \cdot s^{-1}$) for [**2**][X] (X = $BArF_{24}$, BF_4) as a function of solvent.

Solvent	Complex [a]	D_{cation} (^1H) [b]	D_{anion} (^{19}F) [b]	D_{cation}/D_{anion}
CD_2Cl_2	[**2**][$BArF_{24}$]	9.8	8.4	1.2
	[**2**][BF_4]	11.0	12.7	0.9
C_6D_5Cl	[**2**][$BArF_{24}$]	4.4	4.1	1.1
	[**2**][BF_4]	5.8	5.8	1.0

[a] Concentration: 8.2 mmol•L^{-1}. [b] Measured at 298 K.

A ^{19}F-^1H HOESY experiment carried out with [**2**][$BArF_{24}$] at 298 K in CD_2Cl_2 displayed no mutual through-space correlation between the signals of the two ions, which indicates that within the time scale of NMR spectroscopy the ion pair is indeed dissociated according to Pregosin's criteria.[47] These results indicate that the ion-pairing in the latter $[BArF_{24}]^-$ and $[BF_4]^-$ salts is not largely different in a solvent of moderate polarity such as d_5.PhCl and that ion-pair dissociation is only slightly enhanced in a more polar solvent such as CD_2Cl_2 because the values of the D_{cation}/D_{anion} ratio remain close to 1. Static DFT calculations of idealized ion pair dissociation enthalpies[48] $\Delta H_{cp\rightarrow\infty}$ (the cp index stands for contact ion pair and ∞ stands for the dissociated pair) for [**2**][$BArF_{24}$] ($\Delta H_{cp\rightarrow\infty}$= +15, $\Delta G_{cp\rightarrow\infty}$= −1 kcal/mol) and [**2**][BF_4] ($\Delta H_{cp\rightarrow\infty}$= +14; $\Delta G_{cp\rightarrow\infty}$= +2 kcal/mol) with a conventional conductor-like screening model of solvation[49] (COSMO) in PhCl (ε = 5.62[37], T = 298.15 K) merely[50] suggest that the slightly more favored dissociation of $[BArF_{24}]^-$ should be entropy-grounded as compared to $[BF_4]^-$ (figure 5). If one considers the total cation-anion interaction energy ΔE_{int} as defined by the Energy Decomposition Analysis[51]

[47] Pregosin, P. S. NMR Spectroscopy and Ion Pairing: Measuring and Understanding How Ions Interact. *Pure Appl. Chem.* **2009**, *81* (4), 615–633.
[48] Vanka, K.; Chan, M. S. W.; Pye, C. C.; Ziegler, T. A Density Functional Study of Ion-Pair Formation and Dissociation in the Reaction between Boron- and Aluminum-Based Lewis Acids with $(1,2\text{-}Me_2Cp)_2ZrMe_2$. *Organometallics* **2000**, *19* (10), 1841–1849.
[49] Klamt, A.; Schüürmann, G. COSMO: A New Approach to Dielectric Screening in Solvents with Explicit Expressions for the Screening Energy and Its Gradient. *J. Chem. Soc.*, *Perkin Trans. 2* **1993**, No. 5, 799–805.
[50] Hansen, A.; Bannwarth, C.; Grimme, S.; Petrovic, P.; Werlé, C.; Djukic, J. P. The Thermochemistry of London Dispersion-Driven Transition Metal Reactions: Getting the "Right Answer for the Right Reason." *ChemistryOpen* **2014**, *3* (5), 177–189.
[51] Ziegler, T.; Rauk, A. A Theoretical Study of the Ethylene-Metal Bond in Complexes between Cu(+1), Ag(+1), Au(+1), Pt(0), or Pt(+2) and Ethylene, Based on the Hartree-Fock-Slater Transition-State Method. *Inorg. Chem.* **1979**, *18* (6), 1558–1565.

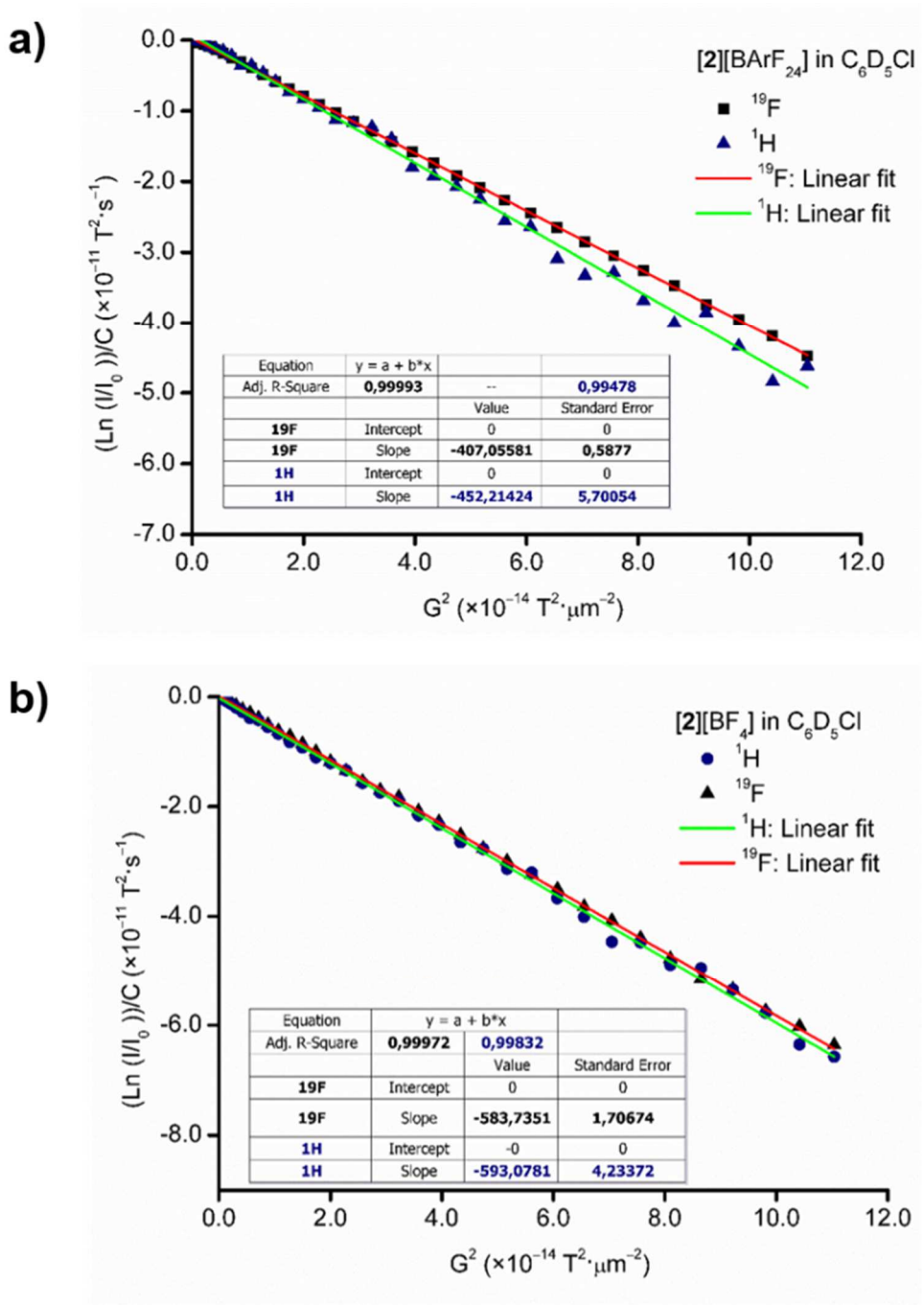

Figure 4. Analytical determination of hydrodynamic diffusion coefficients of associated ions in **a)** [**2**][$BArF_{24}$] and **b)** [**2**][BF_4] (8.2 mmol•L^{-1}in d_5.PhCl). Plot of $\ln(I/I_0)/C$ vs. G^2 (where $\ln(I/I_0) = \gamma_X^2 \bullet \delta_2 \bullet (\Delta - \delta/3 - \tau/2) \bullet D \bullet G^2$; $C = \gamma_X^2 \bullet \delta_2 \bullet (\Delta - \delta/3 - \tau/2)$). The absolute value of the hydrodynamic diffusion coefficient D are as follows: $D([BArF_{24}]^-)$ = 407.0(6) and $D([\mathbf{2}]^+)$ = 452(6) µm^2.s^{-1}. Consequently, $D([\mathbf{2}]^+)/D([BArF_{24}]^-)$ = 1.11(1). $D([BF_4]^-)$ = 584(2) and $D([\mathbf{2}]^+)$ = 593(4) μm^2.s^{-1}. Consequently, $D([\mathbf{2}]^+)/D([BF_4]^-)$ = 1.01(1). See experimental part for more details.

scheme, that is $\Delta E_{int} = (\Delta E_{Pauli})_{repulsive} + (\Delta E_{coul.} + \Delta E_{orb.} + \Delta E_{disp.})_{attractive} = \Delta E_{Pauli} + \Sigma\Delta E_{attractive}$, most of the attractive energy contribution in the ion pair arises from the coulombic ($\Delta E_{coul.}$) energy term: 83% ($\Delta E_{coul.} \times 100 / \Sigma\Delta E_{attractive}$) of the attractive term in [**2**]$^+$,[BF_4]$^-$, and 75% in [**2**]$^+$,[$BArF_{24}$]$^-$. This difference of coulombic contribution is consistent with the larger delocalization of the charge density mostly at the F atoms in the [$BArF_{24}$]$^-$ anion as compared to [BF_4]$^-$. The dispersion and orbital interaction energy terms contribute respectively to 3% and 13% of the attractive term $\Sigma\Delta E_{attractive}$ in [**2**]$^+$,[$BArF_{24}$]$^-$ and 16 % and 8 % in [**2**]+,[BF_4]$^-$. The lower value of $\Delta E_{int.}$ (solvation term included) for [**2**]$^+$,[$BArF_{24}$]$^-$ ($\Delta E_{int.}$ = −72 kcal/mol) as compared to [**2**]$^+$,[BF_4]$^-$ ($\Delta E_{int.}$ = −99 kcal/mol) is consistent with the former's ability to dissociate more readily in moderately polar solvents.

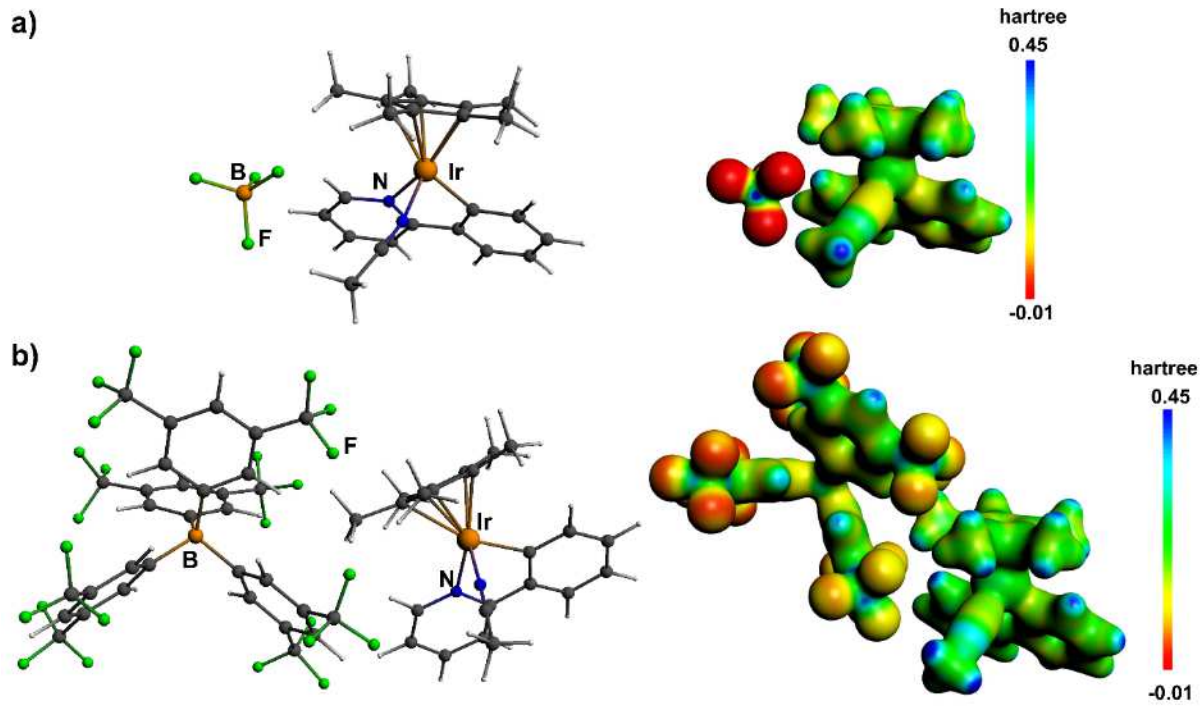

Figure 5. COSMO (PhCl) singlet ground state geometries (ZORA-PBE-D3(BJ)/ae-TZP) of ion pairs **a)** [**2**][BF_4] and **b)** [**2**][$BArF_{24}$] (left) with associated maps of electrostatic potential (MEP) drawn on the isosurface (0.05 e•bohr^{-3}) of the self-consistent field electron density (right). Interatomic distance Ir–B for [**2**][BF_4]: 5.341 Å. Shortest F–Ir distance for [**2**][BF_4]: 4.667 Å. Interatomic distance Ir–B for [**2**][$BArF_{24}$]: 8.322 Å. Shortest F–Ir distance for [**2**][$BArF_{24}$]: 5.654 Å.

2.2.3 Catalytic *O*-silylation of alcohols: kinetic study

2.2.3.1 The piezometry set-up

In scheme 6 below is represented the piezometry set-up that we used throughout this study for the measurement of the absolute pressure of hydrogen produced during the *O*Si reaction of alcohols. This technique of measurement was designed and engineered by the director of the laboratory Dr Jean-Pierre Djukic. All the measurements were done by the MSc1 student Marjolaine Ney and by myself.

2.2.3.2 [**2**][X] salts

All [**2**][X] salts (X= $BArF_{24}$, BPh_4, BF_4, PF_6, OTf) were probed for their catalytic activity in the *O*-silylation (*O*Si) of alcohols (table 6, figure 8, see experimental part for more details). All reactions were generally performed with 2:1 mixtures of neat alcohol and $HSiEt_3$ to which a limited amount (0.5 mL) of 1,2-dichloroethane (DCE) was added to allow the full solubilization of the catalyst and ensure homogeneity of the reaction medium throughout experiments.

2.2.3.2.1 $HSiEt_3$ is the best silane

As shown in figure 6 below, $HSiEt_3$ was the most reactive silane with benzyl alcohol. Noteworthy, other silanes such as $HSiPh_3$, $PhSiH_3$ and polymethylhydrosiloxane (PMHS) proved much less reactive than $HSiEt_3$ in the conditions of catalysis (20 °C, small amounts of 1,2-dichloroethane) (figure 6).

2.2.3.2.2 There is a solvent effect

It is well known that the nature of the solvent may have a detrimental effect on the rate of a reaction, especially in catalysis. For this purpose, the reaction between benzyl alcohol and $HSiEt_3$ in the presence of [**2**][$BArF_{24}$] (0.1 mol %) was studied in four solvents: 1,2-dichloroethane (DCE), tetrahydrofuran (THF), chlorobenzene (PhCl), and acetonitrile (ACN). The results are shown in figure 7. The use of ACN instead of DCE at +20 °C fully inhibited the production of H_2 and the *O*Si of alcohol: no signs of hydrosilylation of ACN were perceptible in the conditions of the catalysis. In contrast, the use of THF as solvent showed to be compatible with the conditions of the catalysis since the activity in this case was at least as good as when DCE was used as solvent (figure 7).

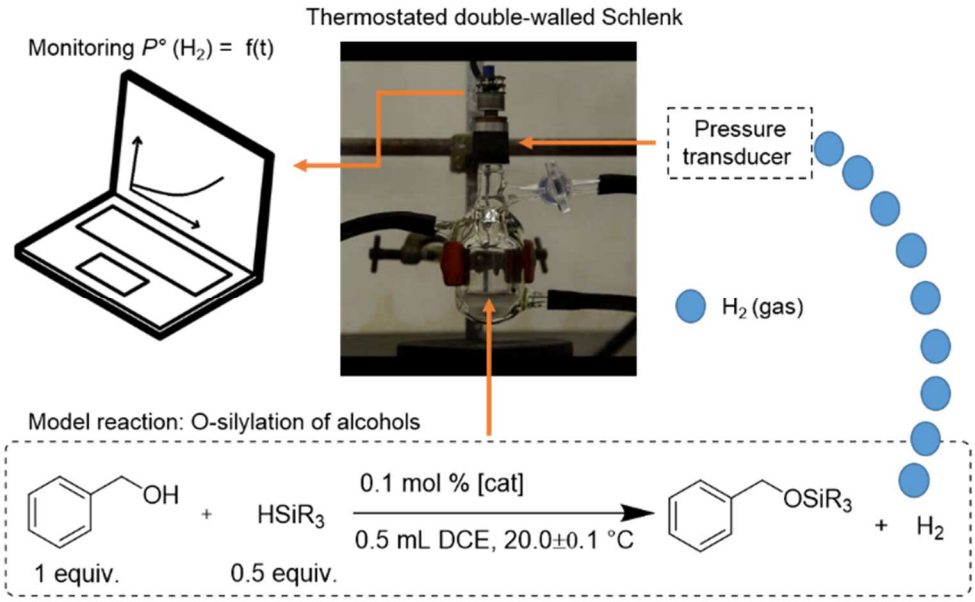

Scheme 6. Representation of the piezometry set-up used for the measurement of the absolute pressure of hydrogen (with the help of a pressure transducer connected to a Laptop) which is produced inside a thermostated double-walled Schlenk tube (V = 28.5 mL) containing all the chemical constituants for the catalytic *O*-silylation (*O*Si) reaction of alcohols in DCE.

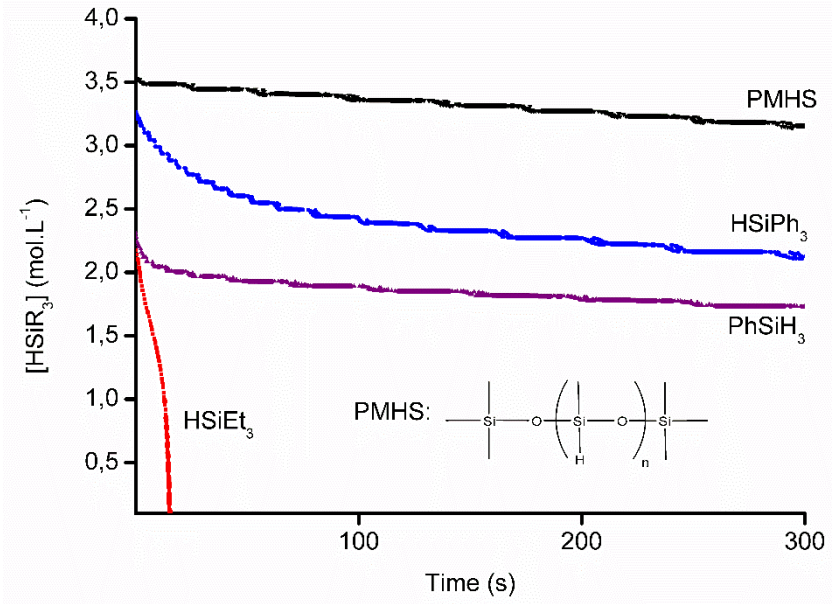

Figure 6. Reaction of benzyl alcohol (1 mL, 9.5 mmol) with various silanes (5.0 mmol) in the presence of identical amounts of [**2**][$BArF_{24}$] (0.1 mol %: 6. 7 mg, 4.8 μmol) dissolved in 1,2-dichloroethane (DCE, 0.5 mL). The concentration of silanes in solution [$HSiR_3$] has been inferred from the piezometric measure of the overhead pressure of H_2.

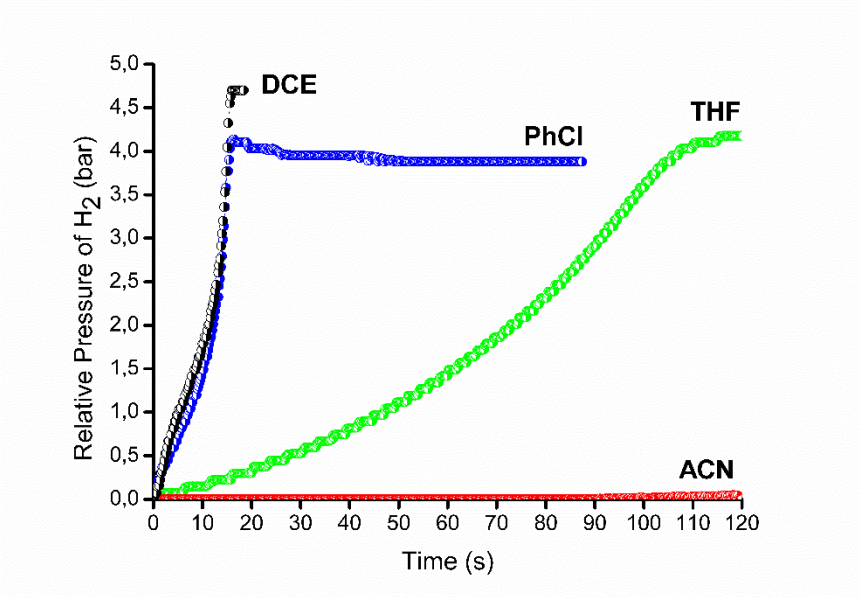

Figure 7. Reaction of benzyl alcohol (1 mL, 9.5 mmol) with $HSiEt_3$ (0.8 mL, 5.0 mmol) in four different solvents (DCE: 1,2-dichloroethane, THF: tetrahydrofuran, PhCl: chlorobenzene, ACN: acetonitrile) and in the presence of identical amounts of [**2**][$BArF_{24}$] (DCE, 0.5 mL) dissolved in the given solvent (0.5 Ml). The curve is the direct piezometric measure of the overhead pressure of H_2 (bar) as a function of time (s).

However, switching from THF to chlorobenzene (PhCl) as solvent proved to give a lower rate efficiency within the same conditions of catalysis (figure 7).

2.2.3.2.3 The inhibition of the *O*Si reaction of alcohols

We investigated the effect that could induce the addition of other competing substrates on the rate of the *O*Si reaction of alcohols. Several substrates that could be hydrosilylated under the conditions of the catalysis were tested during this study. The substrates used were: *N*-methyl-1-phenylmethanimine, aniline, phenylacetylene, phenyl-1-propyne, and acetophenone. The results are summarized in figure 8. Addition of amounts as low as 1 mol % (relative to silane) of a reasonable Lewis base (i.e. imine, aniline, alkyne) showed to inhibit alcohol *O*Si. Phenyl-1-propyne showed to induce a non-complete inhibition of the *O*Si reaction when compared to the complete inhibition induced by phenylacetylene. The latter fact might be due to the presence of the methyl group in phenyl-1-propyne, which could lead to a less efficient interaction of the alkyne function with iridium. It is interesting to see however that acetophenone

had no effect on the *O*Si reaction (figure 8, purple line) as evidenced by the release of hydrogen at the same rate as it is the case where no additive was added (figure 8, black line).

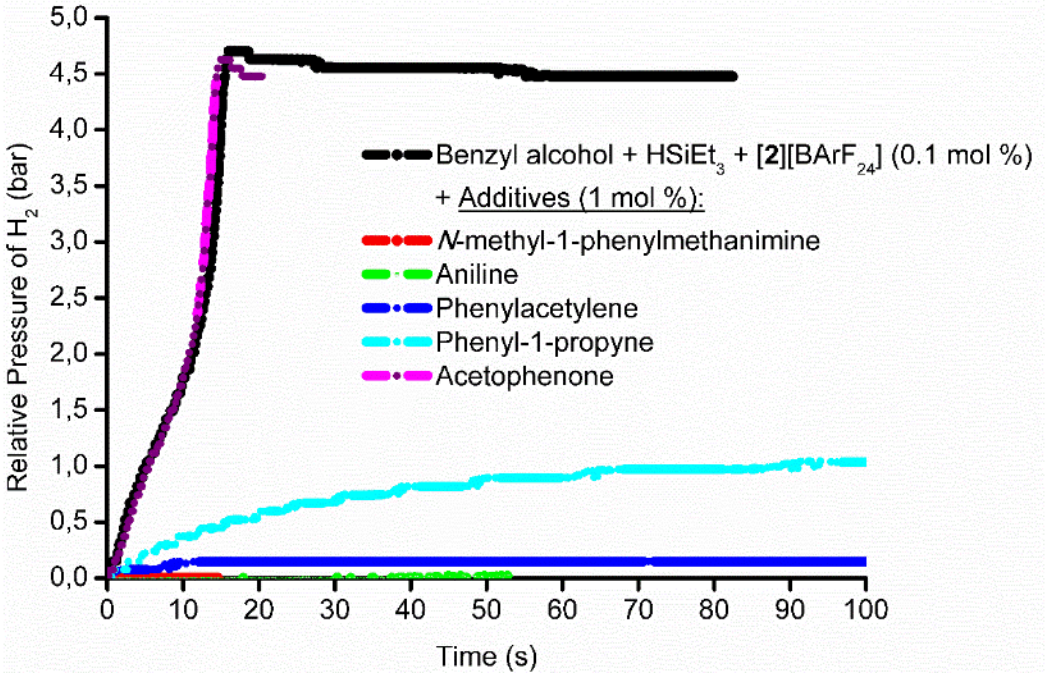

Figure 8. Reaction of benzyl alcohol with $HSiEt_3$ without additive (black line) and with additive (colored lines, 1 mol %) in the presence of identical amounts of [**2**][$BArF_{24}$] (0.1 mol %) dissolved in DCE. The curve is the direct piezometric measure of the overhead pressure of H_2 (bar) as a function of time (s).

From this study, one can conclude that substrates like imines, amines and alkynes seem to interact with iridium centre since they induce the inhibition of the *O*Si reaction when they are introduced as 10 equivalents relative to the precatalyst [**2**][$BArF_{24}$] (0.1 mo %). In contrast, carbonyl substrates like acetophenone do not seem to interact with the iridium centre because the catalytic *O*Si reaction showed to proceed normally even in the presence of acetophenone.

2.2.3.2.4 The effect of the counter-anion X in [**2**][X] on catalysis?

The nature of the counter-anion X showed to be of critical importance when the *O*Si reaction of benzyl alcohol with $HSiEt_3$ was studied with all [**2**][X] salts and **1** as precatalysts (0.1 mol %) (figure 9). [**2**][$BArF_{24}$] gave the best rate efficiency. However, [**2**][BPh_4], [**2**][BF_4] and **1** proved to be nearly catalytically inactive. [**2**][PF_6] displayed an intermediary situation with a rather moderate catalytic efficiency for this reaction. [**2**][OTf] displayed a catalytic activity similar to

that of [**2**][$BArF_{24}$] with TOF_i values higher than 10^5 h^{-1} for $PhCH_2OH$ (figure 9) and (4-MeO)benzyl alcohol (figure 10, table 6). As shown below with the DOSY NMR study, the lack of catalytic activity for [**2**][BF_4] is not related to the ion-pair separation.

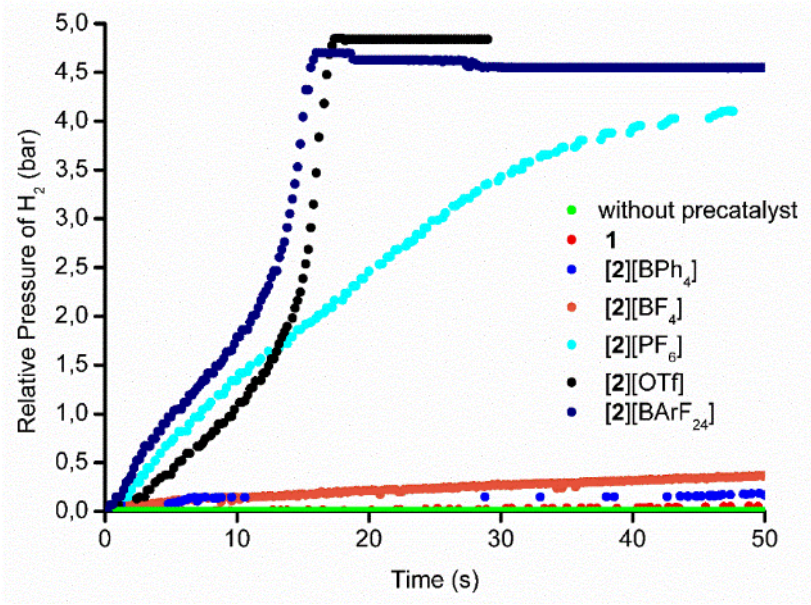

Figure 9. Pressure of hydrogen (bar) as a function of time (s): comparison of the catalytic performance of DCE (0.5 mL) solutions of [**2**][X] (X = $BArF_{24}$, BPh_4, BF_4, PF_6, OTf) and **1** (4.8 µmol) in the *O*-silylation reaction of benzyl alcohol (1 mL, 9.5 mmol) with $HSiEt_3$ (0.8 mL, 5.0 mmol); molar precatalyst:alcohol:$HSiEt_3$ ratio was 1:2000:1000 in all experiments.

2.2.3.2.5 [**2**][$BArF_{24}$] catalyzes the *O*Si reaction of various alcohols

The *O*Si reaction of primary benzylic alcohols and methanol was achieved quantitatively within a few seconds up to a few minutes at 20.0 ± 0.1 °C with loadings in [**2**][$BArF_{24}$] as low as 0.1 mol % (relative to $HSiEt_3$) (table 6, figure 10). Notably, a very high TOF_i value of ~2 × 10^5 h^{-1} was reached when (4-MeO)-benzyl alcohol was used (table 6).

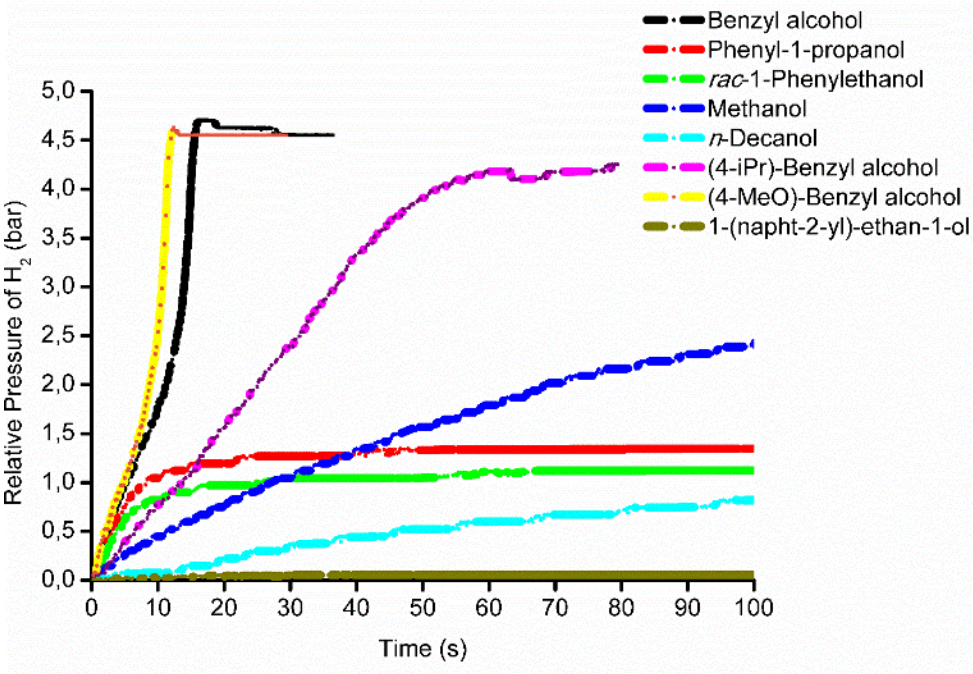

Figure 10. Pressure of hydrogen (bar) as a function of time (s) as measured with the piezometry set-up: comparison of various alcohols (9.5 mmol) in the *O*-silylation reaction with $HSiEt_3$ (0.8 mL, 5.0 mmol) catalyzed by [**2**][$BArF_{24}$]. Molar precatalyst:alcohol:$HSiEt_3$ ratio was 1:2000:1000 in all experiments.

Table 6. Catalytic performance of [**2**][$BArF_{24}$] in the *O*-silylation of selected alcohols with $HSiEt_3$.

Alcohol	t (min)	Yield [a] (%)	v_i [b] (10^{-2} M•s^{-1})	TON [c]	TOF_i [d] (h^{-1})
Benzyl alcohol	<1	100	8.39	1040	163,636
(4-MeO)-benzyl alcohol	<1	100	8.87	832	192,100
(4-^{i}Pr)-benzyl alcohol	<1	100	2.90	934	58,004
Methanol	10	100	2.69	1008	38,504
n-Decanol	10	43	3.00	450	8266
1-(Napht-2-yl)-ethan-1-ol	10	1	0.25	12	-

[a] Yield in evolved H_2 for the following conditions: 9.5 mmol of alcohol, 4.8 mmol of $HSiEt_3$, 0.1 mol% of [**2**][$BArF_{24}$] (6.7 mg), 0.5 mL of 1,2-dichloroethane, 20 ± 0.1 °C. [b] $v_i = -(d[HSiEt_3]/dt)_i$. [c] TON: turnover number, calculated at the highest conversion as the molar ratio silylated alcohol:catalyst. [d] TOF_i: TON/time or turnover frequency calculated at a reaction time corresponding to 10% of conversion.

2.2.3.2.6 Kinetic studies

In order to get kinetic information that could give insight on the the mechanism at work in the *O*-silylation reaction, we have undertaken *in situ* kinetic measurements of the catalytic system. The method of piezometry, as described previously in scheme 6, proved to serve as a useful tool because it gave us direct access to critical kinetic parameters such as the order in precatalyst and the initial kinetic isotope effect (KIE) values k_H^{init}/k_D^{init}.

Order in catalyst. Figure 11 below shows the pressure of hydrogen produced from the reaction between benzyl alcohol and $HSiEt_3$, which was monitored over time for five different concentrations of [**2**][$BArF_{24}$] (0.5 mL of DCE, 20.0 ± 0.1 °C). A blank experiment without any loading in [**2**][$BArF_{24}$] showed to give any release of hydrogen (0 mol %: green line, figure 11).

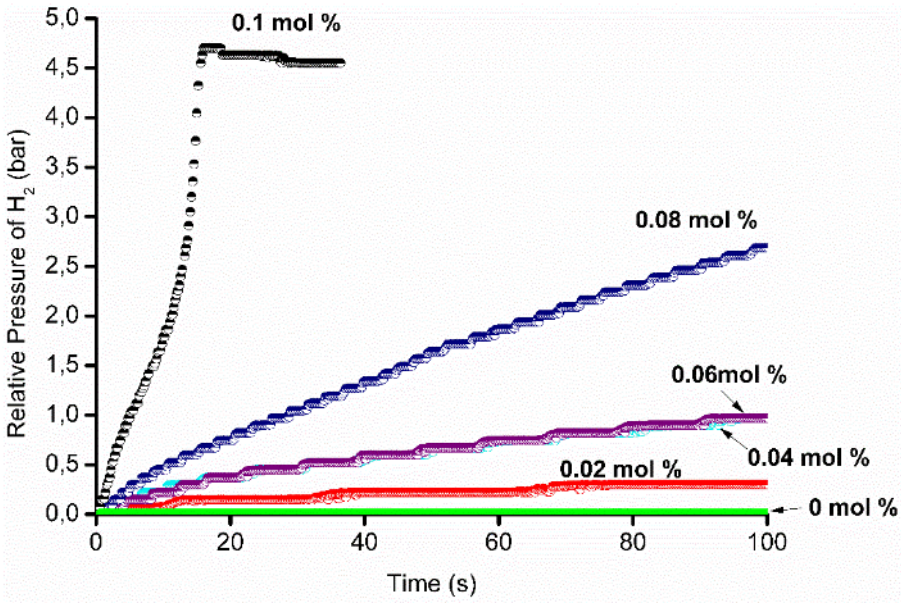

Figure 11. Pressure of hydrogen (bar) as a function of time (s) as measured with the piezometry set-up: influene of the concentration of the precatalyst [**2**][$BArF_{24}$] on the rate of the *O*Si reaction between benzyl alcohol (1 mL, 9.5 mmol) with $HSiEt_3$ (0.8 mL, 5.0 mmol) at 20.0 ± 0.1 °C. See experimental part for details.

A partial second order in [**2**][$BArF_{24}$] for the reaction between $HSiEt_3$ and 2 equiv. of benzyl alcohol was inferred from a set of 5 catalytic runs carried out with different concentrations of

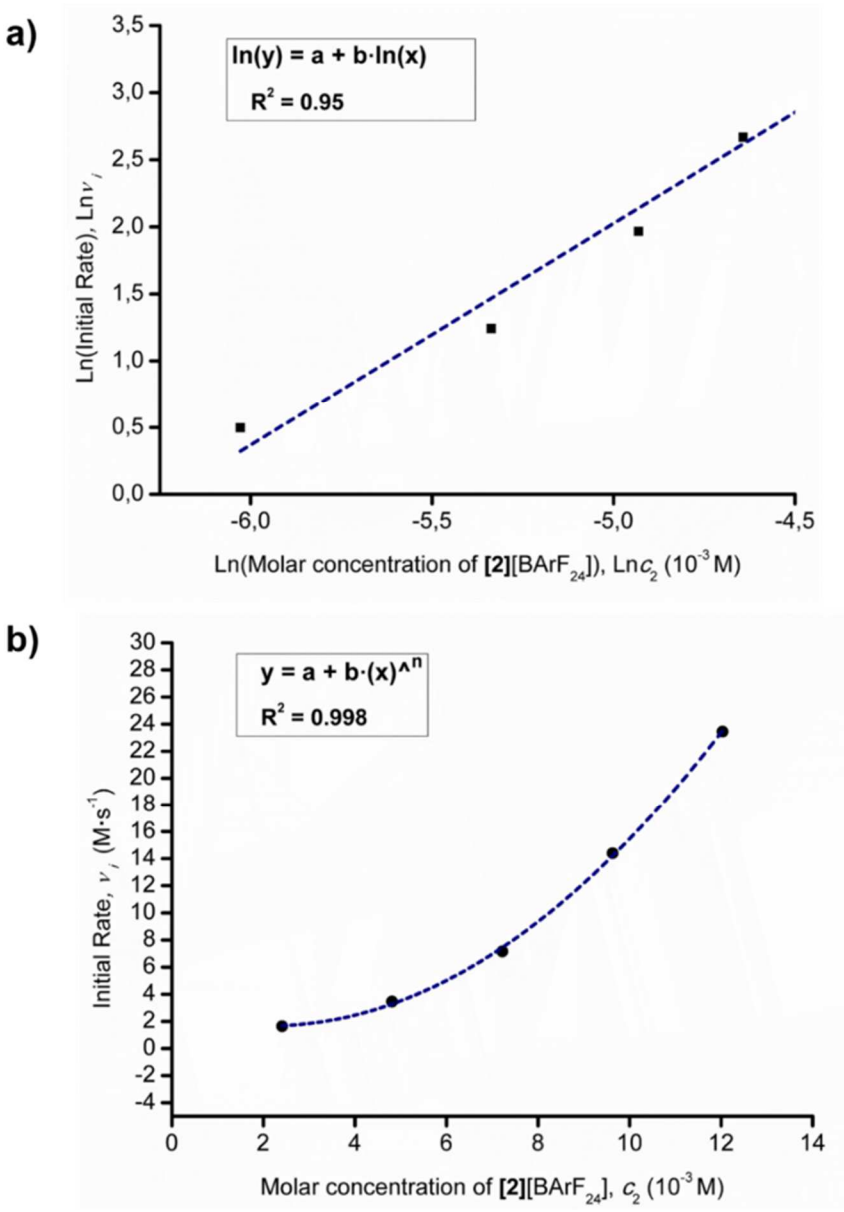

Figure 12. a) Linear curve fit of the plot of ln(v_i) as a function of ln(c_2) for [**2**][$BArF_{24}$]. **b)** Power-type curve fit of the plot of v_i ($M \cdot s^{-1}$) as a function of c_2 for [**2**][$BArF_{24}$]. The intial rates v_i ($= -(d[HSiEt_3]/dt)_i$) were measured from the slopes of the curves (only the initial points of a straight curve were considered) that monitor the concentration of $HSiEt_3$ (inferred from the measured pressure of hydrogen (bar)) as a function of time (s). The measure of hydrogen was monitored by using the piezometry set-up: benzyl alcohol (9.5 mmol), $HSiEt_3$ (0.8 mL, 5.0 mmol), [**2**][$BArF_{24}$], c_2(10^{-3} M): 2.41 (0.02mol %), 4.81 (0.04 mol %), 7.22 (0.06 mol %), 9.63 (0.08 mol %), 12.0 (0.1 mol %), 1,2-dichloroethane (0.5 mL), 20 °C.

[**2**][$BArF_{24}$] by the piezometric monitoring of the pressure of H_2 (or HD) developed in the overhead volume of a sealed thermostated reactor as a function of time (figure 12a–b). A linear curve fit of $\ln(v_i)$ vs. $\ln(c_2)$ plot[52] afforded an order of 1.6(2) (R^2: 0.95) (figures 12a) and a non-linear curve fit of a v_i vs. c_2 plot (taking $v_i = a + b\bullet(c_2)^n$ as model where n is the partial order in [**2**][$BArF_{24}$] afforded an order of 2.2(2) (R^2: 0.99) in catalyst (figure 12b): v_i is the initial reaction rate and c_2 the initial concentration in [**2**][$BArF_{24}$]. This partial second order in [**2**][$BArF_{24}$] might suggest the involvement of two differents active species during the mechanism of the *O*Si reaction of alcohols with $HSiEt_3$.

Kinetic Isotope Effect (KIE), k_H^{init}/k_D^{init}. Comparative catalytic runs carried out with MeOD(or H), $HSiEt_3$ and [**2**][$BArF_{24}$] were also monitored by piezometry to determine the kinetic isotope effect (KIE)[53] k_H/k_D (based on initial reaction rates, figure 13a–b, see experimental part for details). A value of 2.7 ± 0.2 for the KIE (figure 13a) suggests that the rate-determining step is the RO-H bond cleavage in the last step of formation of $MeOSiEt_3$ that most likely implies reaction of a $[RO(H)(SiEt_3)]^+$ species with an Ir-bound hydrido ligand (*vide infra*).[54] Similar experiments carried out with D-$SiEt_3$ (or -H) produced an inverse KIE (IKIE) k_H/k_D of 0.73 ± 0.01 the origin of which was not assigned at the present stage of our investigations (figure 13b). Such inverse KIE in metal-promoted H–Si bond activation of silanes has been assigned in one case to the H–Si bond activation assitance by remote groups.[55]

2.2.3.2.7 What about new salts?

Salts [**2'**][$BArF_{24}$], [**4**][$BArF_{24}$], and [**6**][$BArF_{24}$] were also tested for their catalytic performance in the *O*-silylation reaction of 1-phenylpropanol with $HSiEt_3$, in DCE solutions (0.5 mL) of the precatalysts with loadings as low as 0.1 % mol (20.0 ± 0.1 °C) (table 7, figure 14). When [**4**][$BArF_{24}$] (0.1 mol % relative to $HSiEt_3$) was used as precatalyst, the *O*Si reaction of benzyl alcohol with $HSiEt_3$ was so extremely rapid in terms of hydrogen gas release that we preferred to switch to 1-phenylpropanol, which is known to be less reactive. Surprisingly, when

[52] Espenson, J. H. *Chemical Kinetics and Reaction Mechanisms*; McGraw-Hill Book Company: New York, 1981.
[53] Gómez-Gallego, M.; Sierra, M. A. Kinetic Isotope Effects in the Study of Organometallic Reaction Mechanisms. *Chem. Rev. (Washington, DC, United States)* **2011**, *111* (8), 4857–4963.
[54] Luo, X. L.; Crabtree, R. H. Homogeneous Catalysis of Silane Alcoholysis via Nucleophilic Attack by the Alcohol on an Ir(η^2-$HSiR_3$) Intermediate Catalyzed by $[IrH_2S_2(PPh_3)_2]SbF_6$ (S = Solvent). *J. Am. Chem. Soc.* **1989**, *111*, 2527–2535.
[55] Nolin, K. A.; Krumper, J. R.; Pluth, M. D.; Bergman, R. G.; Toste, F. D. Analysis of an Unprecedented Mechanism for the Catalytic Hydrosilylation of Carbonyl Compounds. *J. Am. Chem. Soc.* **2007**, *129* (47), 14684–14696.

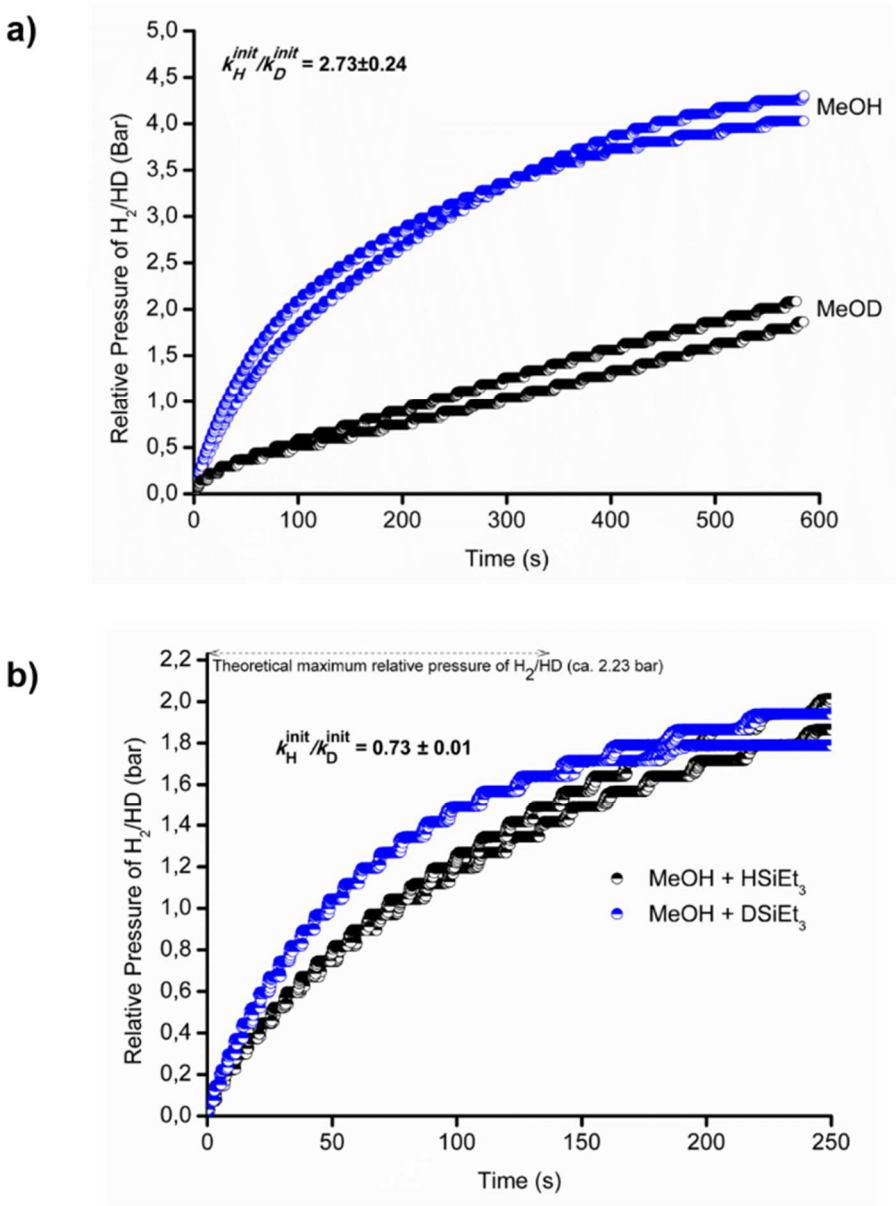

Figure 13. Pressure of hydrogen (bar) as a function of time (s) in [**2**][$BArF_{24}$] catalyzed *O*-silylation of methanol with triethylsilane: **a)** MeOD/$HSiEt_3$ or MeOH/$HSiEt_3$, **b)** $DSiEt_3$/MeOH or $HSiEt_3$/MeOH. The theoretical maximum pressure corresponds to 100% conversion of silane into the corresponding alkoxysilanes. See experimental part for details.

the experiment was reproduced with 1-phenylpropanol instead of benzyl alcohol, the reaction was also extremely rapid so that all the hydrogen gas was released within ~3 seconds (figure 14) as measured with the piezometry set-up. When compared to the other salts tested, [**4**][$BArF_{24}$] is by far the most efficient which is characterized by a TOF_i of ~3.6 × 10^5 h^{-1}, whereas the TOF_i obtained with [**2**][$BArF_{24}$] was ~1.05 × 10^5 h^{-1}. The ionic rhodacycle

Table 6. Catalytic performance of the new salts in the *O*-silylation of benzyl alcohol with $HSiEt_3$.

Complex	t (min)	Yield [a] (%)	v_i [b] (10^{-2} M•s^{-1})	TON [c] (%) [d]	TOF_i [e] (h^{-1})
[**2**][$BArF_{24}$]	60	75	3.49	500 (50)	105,662
[**2'**][$BArF_{24}$]	>10	100	1.25	99 (10)	23,750
[**4**][$BArF_{24}$]	<1	100	34.36	1000 (100)	364,490
[**2**][$BArF_{24}$]	60	75	3.49	500 (50)	770 [f]
[**4**][$BArF_{24}$]	<1	100	34.36	1093 (100)	1,157,487 [g]
[**6**][$BArF_{24}$]	>5	5	0.06	50 (5)	1539 [h]

[a] Yield in evolved H_2 for the following conditions: 9.5 mmol of alcohol, 4.8 mmol of $HSiEt_3$, 0.1 mol% of [**2**][$BArF_{24}$] (6.7 mg), 0.5 mL of 1,2-dichloroethane, 20 ± 0.1 °C. [b] $v_i = -(d[HSiEt_3]/dt)_i$. [c] TON: turnover number, calculated at the highest conversion as the molar ratio silylated alcohol:catalyst. [d] Percentage of conversion. [e] TOF_i: TON/time or turnover frequency calculated at a reaction time corresponding to 10% of conversion. [f] TOF_t (t ~60 min) at 75% of conversion. [g] TOF_t (t ~3.4 s) at 100% of conversion. [h] Calculated at 5% of conversion.

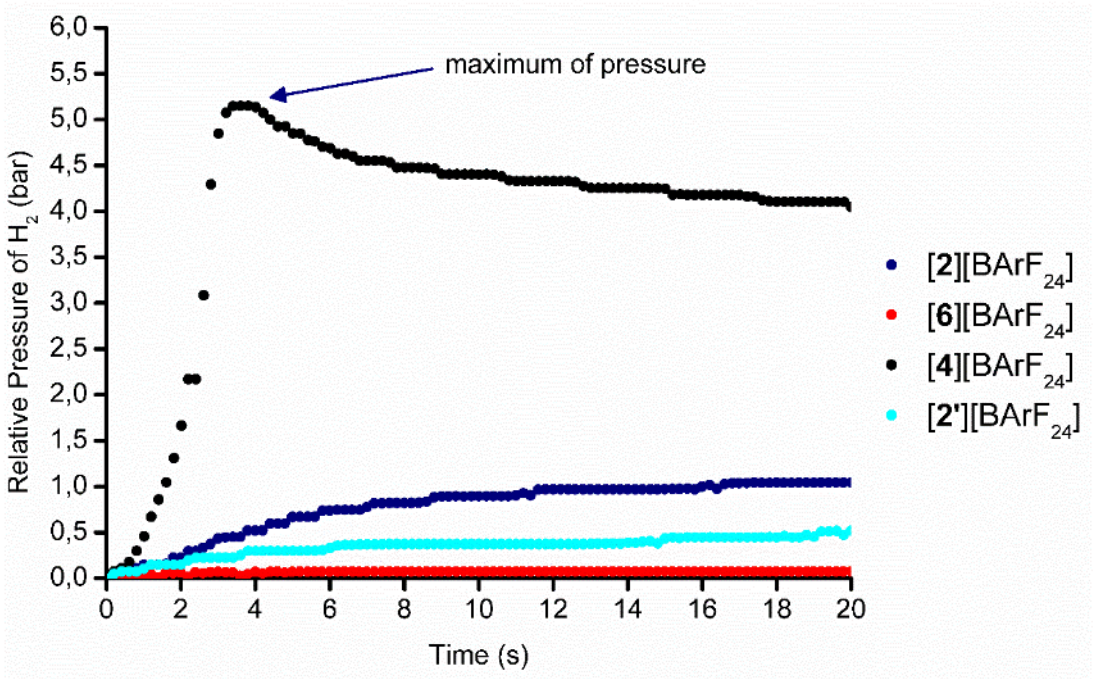

Figure 14. Pressure of hydrogen (bar) as a function of time (s): comparison of the catalytic performance of DCE (0.5 mL) solutions of [**2**][$BArF_{24}$], [**4**][$BArF_{24}$], [**6**][$BArF_{24}$] and [**2'**][$BArF_{24}$] (4.8 μmol, 0.1 mol %) in the *O*-silylation of 1-phenylpropanol alcohol (1.32 mL, 9.5 mmol) with $HSiEt_3$ (0.8 mL, 5.0 mmol); molar precatalyst:alcohol:$HSiEt_3$ ratio was 1:2000:1000 in all experiments.

[**2'**][$BArF_{24}$] showed non-negligible activity (TOF_i ~2.4 × 10^4 h^{-1}) when compared to its iridacyclic counterparts [**2**][$BArF_{24}$] and [**6**][$BArF_{24}$]. In contrast, [**6**][$BArF_{24}$] showed the "worst" catalytic efficiency (TOF_i ~1.5× 10^3 h^{-1}). The catalytic efficiency is somehow underestimated by the method we chose to calculate the TOF_i of [**4**][$BArF_{24}$], as it was estimated at only 10% of conversion. The calculation at 100% of conversion (t ~3.4 s) provides a TOF_t of ~1.16 × 10^6 h^{-1}!

2.2.4 Evidence for the *N*-silylation of aniline catalyzed by [**4**][$BArF_{24}$]

The reaction between aniline and $HSiEt_3$ is readily catalyzed by [**4**][$BArF_{24}$] (0.1 mol %) at room temperature in CH_2Cl_2 as solvent (scheme 7). The silazane product, that is 1,1,1-triethyl-*N*-phenylsilanamine, formed selectively and quantitatively within 20 h of reaction.

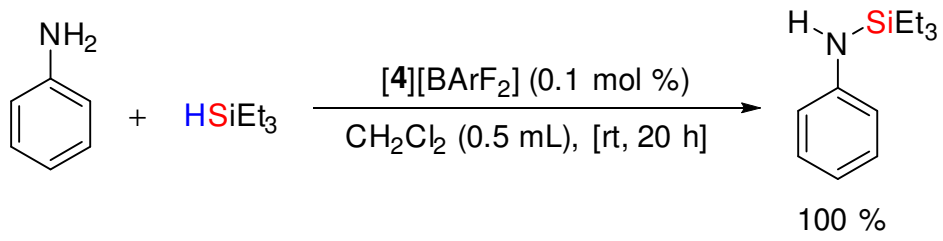

Scheme 7. The catalytic *N*-silylation of aniline catalyzed by [**4**][$BArF_{24}$].

The formation of the product was evidenced from ^{1}H NMR spectroscopy ($CDCl_3$, 298 K, 400 MHz) and electro-spray ionization (ESI) analysis of the crude reaction mixture (see experimental part for details).

This result is rather surprising because we expected, as previsously shown, the inhibition of the catalysis due to the hypothetical coordination of aniline to iridium. This reaction might represent a potential inhibition or "reactive" pathway for the tandem reaction described in scheme 1.

2.2.5 [**4**][$BArF_{24}$] catalyzes the tandem hydroamination – hydrosilylation of phenylacetylene (Iali-Djukic reaction)

The tandem reaction previously described by our group,[56] has been repeated under identical conditions using the new precatalyst [**4**][$BArF_{24}$] (scheme 8) instead of the originaly used precatalyst **P1** (scheme 1).

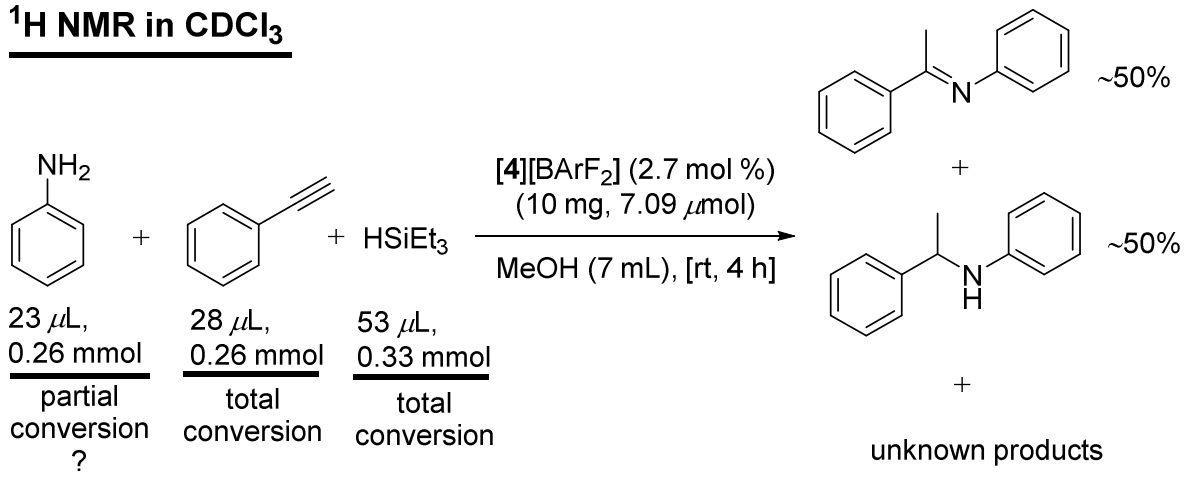

Scheme 8. Repetition of the "Iali-Djukic" reaction reported in 2012, under the same catalytic conditions but using the newly established ionic iridacycle [**4**][$BArF_{24}$] as precatalyst (2.7 mol %). The procedure was as follows: in a Schlenk tube was added 1) aniline, 2) phenylacetylene, 3) MeOH, 4) [**4**][$BArF_{24}$], then 5) $HSiEt_3$. The yellow-colored reaction mixture was stirred at room temperature for 4 h. The reaction was then analyzed by ^1H NMR spectroscopy ($CDCl_3$, 298 K, 400 MHz).

After 4 h of reaction, the ^1H NMR analysis showed incomplete formation of the expected amine product. Instead, the reaction mixture was composed of the intermediate imine product and the amine product in a ratio of 1:1. While phenylacetylene was completely consumed, the doubt still resides about the fate of aniline, as it seemed that it was still present in the reaction mixture (comparison of its ^1H NMR peaks with those of an authentic sample in $CDCl_3$ showed a slight downfield chemical shift of its typical ^1H NMR peaks in the aromatic region). When the reaction was repeated where phenylacetylene was first added to a solution of [**4**][$BArF_{24}$] in MeOH (7 mL), the color of the reaction immediately changed from yellow to deep brown, which might be the result of alkyne insertion into the Ir–C bond of the iridacycle. To this reaction mixture was added aniline and $HSiEt_3$ respectivey. The color of the solution remained deep brown. After 4

[56] Iali, W.; Paglia, F. La; Goff, X.-F. Le; Sredojević, D.; Pfeffer, M.; Djukic, J.-P. Room Temperature Tandem Hydroamination and Hydrosilation/protodesilation Catalysis by a Tricarbonylchromium-Bound Iridacycle. *Chem. Commun.* **2012**, *48* (83), 10310.

h of stirring, an ^{1}H NMR analysis ($CDCl_3$) of the latter reaction mixture showed no characteristic peaks of phenylacetylene anymore, whereas those of aniline could be clearly distinguished.

2.2.6 Reactions between [**2**][X] and silanes

Our initial hypothesis was that an iridium-silane adduct [(κ^2-(C,N)-(**L**)Ir(III)($HSiR_3$)][X] (scheme 9) could be one of the key active intermediates involved in the catalytic systems reported herein. To identify such iridium-silane intermediates, [**2**][X] salts (X = $BArF_{24}$, BPh_4, BF_4, OTf, PF_6) were studied based on their reaction with different silanes $HSiR_3$ (scheme 10). The main questions we wanted to address were: what are the features of the Si–Ir–H motif? How does the addition of silane to iridium proceed? Ir(III) or Ir(V)?

The results of this study are summarized in scheme 10, and the related experimental conditions as well as the NMR spectra can be found in the experimental part.

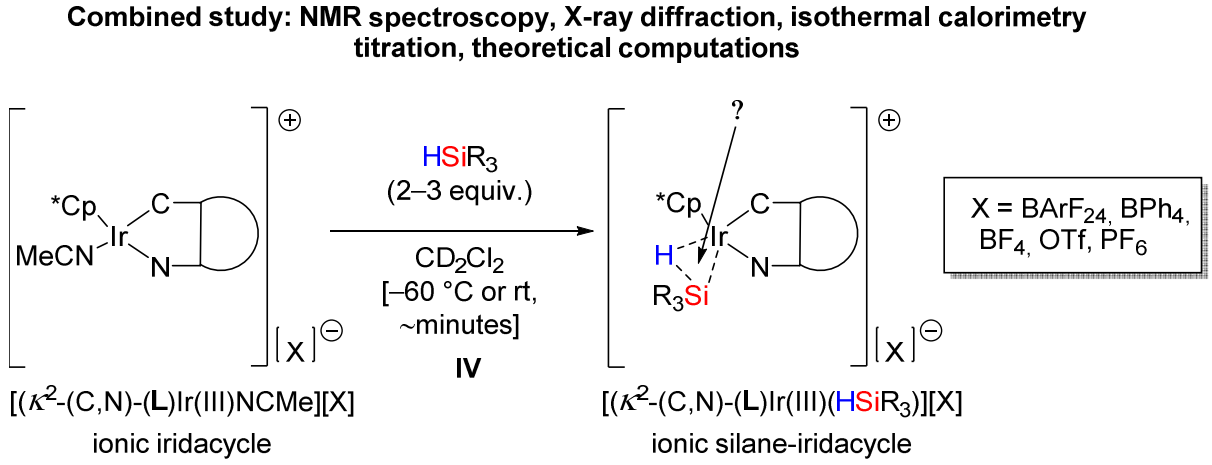

Scheme 9. Strategy for the investigation of iridium-silane intermediates: stoichiometric reaction between ionic iridacycles [(κ^2-(C,N)-(**L**)Ir(III)NCMe][X] (where X = $BArF_{24}$, BPh_4, BF_4, OTf, PF_6) and silanes $HSiR_3$ (R = Et, Ph, H).

2.2.6.1 [**2**][X] + $HSiEt_3$

The study of the reaction between [**2**][X] salts and $HSiEt_3$ (scheme 10) allowed us to provide a rationale for the influence of the anion $[X]^-$ in [**2**][X] on the rate of alcohol *O*Si. We have recently published the results of this study, which are also included in this thesis. The main conclusions of the published results were that $[BArF_{24}]^-$ was in fact the “only” anion (among anions studied)

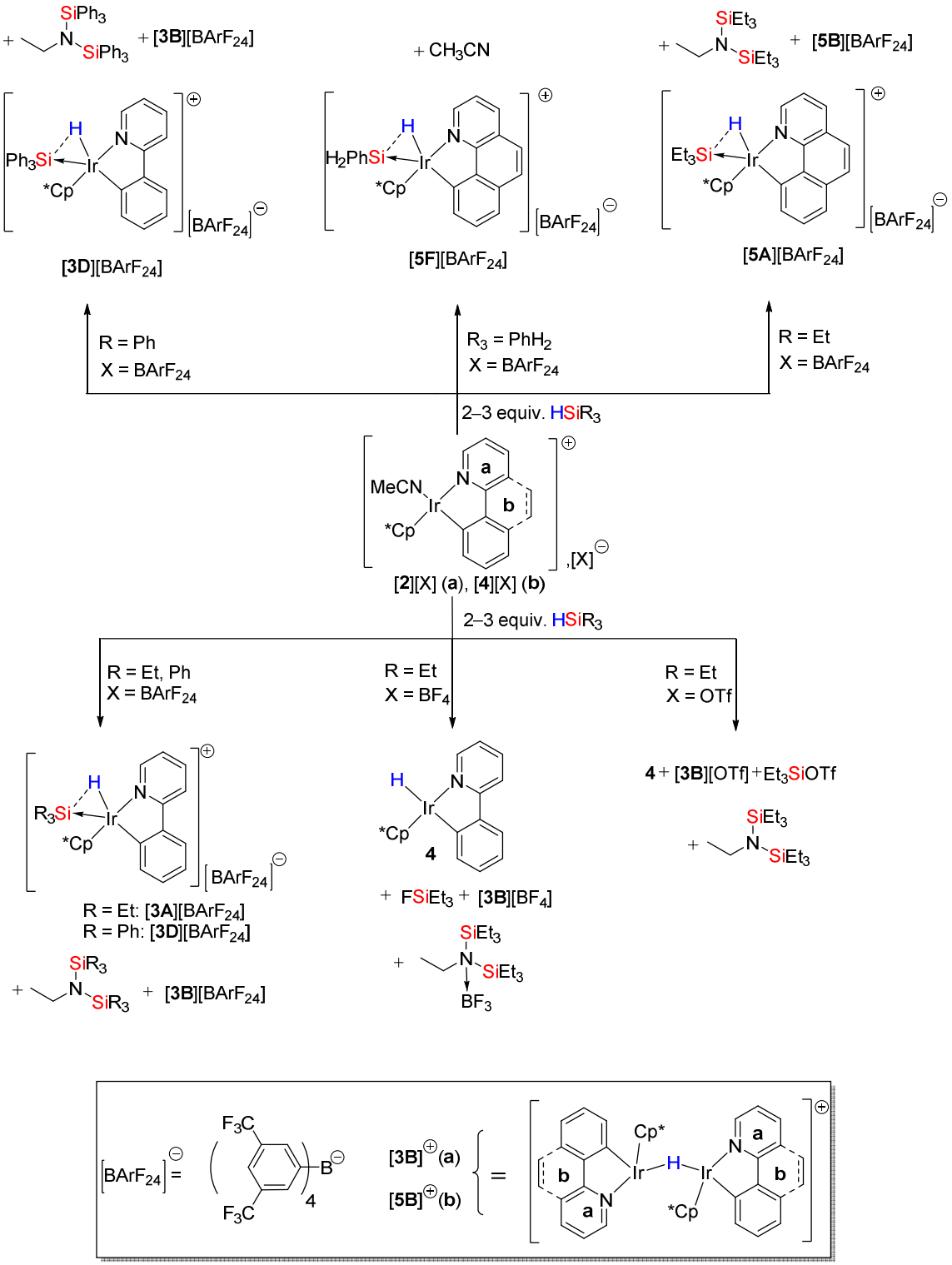

Scheme 10. Study of the reaction of [**2**][X] and [**4**][X] salts (X= $BArF_{24}$, BPh_4, BF_4, or OTf) with silanes $HSiR_3$ (R = Et, Ph; $R_3 = PhH_2$).

not affected by the the presence of the electrophilic silylium cation $[Et_3Si]^+$ within the coordination sphere of iridium. In contrast, anions such as $[OTf]^-$ and $[BF_4]^-$ reacted with $[Et_3Si]^+$ to give Et_3SiOTf and $FSiEt_3$ respectively.

2.2.6.2 [**2**][$BArF_{24}$]

The fate of [**2**][$BArF_{24}$] in catalysis, which in principle requires the departure of the bound CH_3CN molecule to allow $HSiEt_3$ to interact with the Ir(III) center, was investigated by various methods, i.e. ^1H and ^{29}Si NMR spectroscopic monitoring and isothermal titration calorimetry (ITC[57]) at 20.0 °C. ^1H NMR monitoring of the reaction of [**2**][$BArF_{24}$] in CD_2Cl_2 with excess $HSiEt_3$ (6 equiv./Ir) revealed the swift and exothermic *in situ* formation of $(Et_3Si)_2NEt$,[58] i.e. the product of the double hydrosilylation of CH_3CN.[59] More importantly the ^1H NMR spectrum revealed the complete conversion of [**2**][$BArF_{24}$] mainly into [**3A**][$BArF_{24}$] (scheme 10), which is characterized by a hydridic signal at $\delta = -11.7$ ppm showing up about 3.5 ppm downfield of the typical signal of the neutral hydrido complex **4** reported by Norton and co-workers.[60] ^1H and ^{29}Si HMQC NMR experiments (experimental part) confirmed the existence of coupling between the Si nucleus (δ ^{29}Si = 7.0 ppm) and the hydridic proton (δ (^1H) = –11.7 ppm) of [**3A**][$BArF_{24}$] with a H–Si coupling constant $J_{Si\text{-}H}$ of ~20 Hz, suggesting a rather weak H–Si interaction.[61] It was also noted that another new species was present besides [**3A**][$BArF_{24}$] (scheme 10), i.e. [**3B**][$BArF_{24}$], displaying a typical hydridic proton signal at around $\delta = -23$ ppm. Under these conditions (6 equiv. of $HSiEt_3$/Ir) the [**3A**][$BArF_{24}$]:[**3B**][$BArF_{24}$] ratio was 1.5:1. The latter ratio reversed to 1:1.3 when only 3 equiv. of $HSiEt_3$ were added to a solution of [**2**][$BArF_{24}$]. With 2 equiv. of $HSiEt_3$/Ir the ratio (2.6:1) was again favorable to [**3A**][$BArF_{24}$], the presence of $(Et_3Si)_2NEt$ was noted and traces of unreacted [**2**][$BArF_{24}$] were detected. These results suggested at first that

---

[57] a) Martinho Simoes, J. A.; Minas da Piedade, M. E. *Molecular Energetics Condensed-Phase Thermochemical Techniques*; Oxford University Press: New York, 2008. b) Krell, T.; Lacal, J.; Garcia-Fontana, C.; Silva-Jimenez, H.; Rico-Jimenez, M.; Lugo, A. C.; Darias, J. A. R.; Ramos, J.-L. Characterization of molecular interactions using isothermal titration calorimetry. *Methods Mol. Biol.* **2014**, *1149*, 193-203.

[58] Pérez, M.; Qu, Z.-W.; Caputo, C. B.; Podgorny, V.; Hounjet, L. J.; Hansen, A.; Dobrovetsky, R.; Grimme, S.; Stephan, D. W. Hydrosilylation of ketones, imines and nitriles catalysed by electrophilic phosphonium cations: Functional group selectivity and mechanistic considerations. *Chem. Eur. J.* **2015**, *21*, 6491-6500.

[59] a) Gandhamsetty, N.; Jeong, J.; Park, J.; Park, S.; Chang, S. Boron-Catalyzed Silylative Reduction of Nitriles in Accessing Primary Amines and Imines. *J. Org. Chem.* **2015**, *80*, 7281-7287. b) Yang, Y.-F.; Chung, L. W.; Zhang, X.; Houk, K. N.; Wu, Y.-D. Ligand-Controlled Reactivity, Selectivity, and Mechanism of Cationic Ruthenium-Catalyzed Hydrosilylations of Alkynes, Ketones, and Nitriles: A Theoretical Study. *J. Org. Chem.* **2014**, *79*, 8856-8864.

[60] Hu, Y.; Li, L.; Shaw, A. P.; Norton, J. R.; Sattler, W.; Rong, Y. Synthesis, electrochemistry, and reactivity of new iridium(III) and rhodium(III) hydrides. *Organometallics* **2012**, *31*, 5058-5064.

[61] a) Corey, J. Y. Reactions of Hydrosilanes with Transition Metal Complexes. *Chem. Rev.* **2016**, acs.chemrev.5b00559. b) Corey, J. Y. Reactions of Hydrosilanes with Transition Metal Complexes and Characterization of the Products. *Chem. Rev.* **2011**, *111* (2), 863–1071.

[**3B**][$BArF_{24}$] might be a resting state possibly resulting from the reaction of transient **4** with [**2**][$BArF_{24}$] (Eq. 1) or from a reaction of [**3A**][$BArF_{24}$] with [**2**][$BArF_{24}$] (Eq. 2).

$$[\mathbf{2}]^+ + \mathbf{4} \longrightarrow [\mathbf{3B}]^+ + MeCN \quad (1)$$

$$[\mathbf{2}]^+ + [\mathbf{3A}]^+ \longrightarrow [\mathbf{3B}]^+ + [MeCN\text{-}SiEt_3]^+ \quad (2)$$

Isolation of [**3B**][$BArF_{24}$] was attempted by crystallization from a reaction aliquot at low temperature, which afforded two sets of moisture-sensitive red-orange ([**3B**][$BArF_{24}$]) and pale yellow crystals ([**3A**][$BArF_{24}$], *vide infra*). Owing to the low quality of the grown crystals only a preliminary structure of [**3B**][$BArF_{24}$] could be obtained showing a ca. 3.2 Å separation of the two Ir centers. The precise localization of the hydride atom bridging the two Ir centers has proven particularly difficult. This is due to many residual peaks of electronic density which could not be eliminated without affecting the quality of the structure. This problem is unfortunately an intrinsic limitation found in most of X-ray diffractometers which cannot accurately localize hydride ligands, particularly those bound to heavy atoms like transiton-metals. The problem of X-ray diffraction analyses of mono-hydrido-brigded complexes have been discused in the literature, especially by R. Bau and coworkers.[62] As shown below, [**3B**][X] is a side-product in all reactions of [**2**][X] with $HSiEt_3$ in CD_2Cl_2.

It must be noted that addition of 2 equiv. of *N,N*-dimethylaminopyridine (DMAP) to a solution containing [**3A**][$BArF_{24}$] and [**3B**][$BArF_{24}$] in a 2.6:1 ratio resulted in the formation of **4** and in the increase of the relative amount of [**3B**][$BArF_{24}$] (**4**:[**3B**][$BArF_{24}$] ~1:1, see experimental part). Similarly, addition of excess amounts of [*n*NBu_4][OTf] to a 7.7:1 mixture of [**3A**][$BArF_{24}$] and [**3B**][$BArF_{24}$] in CD_2Cl_2 caused the full consumption of [**3A**][$BArF_{24}$] to yield a new mixture containing **4** and [**3B**][$BArF_{24}$] in a 50:1 ratio and Et_3SiOTf (see experimental part). These two experiments indicate that the triethylsilylium moiety can be readily abstracted from [**3A**]$^+$ by Lewis bases.

2.2.6.3 [**2**][BF_4]

[62] Teller, G.; Kirtley, W.; Koetzle, F. Structures of Transition-Metal Hydride Complexes. *Acc. Chem. Res.* **1979**, *1928* (1969), 176–183.

^{1}H NMR monitoring of the reaction of 2 equiv. of $HSiEt_3$ with [**2**][BF_4] (experimental part) in CD_2Cl_2 indicated the swift formation of complexes **4** and [**3B**][BF_4] in a 2.6:1 ratio, and the formation of $FSiEt_3$, the NMR signature of which matched literature data[63] (δ (^{29}Si) = 33.1 ppm, δ (^{19}F) = −176.9 ppm, $J_{Si\text{-}F}$ = 287 Hz). The formation of **4** can be explained[64] by the abstraction of one fluoride from $[BF_4]^-$ by the Lewis-acidic[65] silylium fragment $[Et_3Si]^+$ of putative transient [**3**][BF_4].

2.2.6.4 [**2**][OTf]

Very similar behavior was observed in the reaction of [**2**][OTf] with 2 equiv. of $HSiEt_3$. ^{1}H NMR spectroscopic monitoring (see experimental part) of the reaction revealed the rapid formation of **4** and [**3B**][OTf] in a 1.1:1 ratio, and the presence of Et_3SiOTf, the spectroscopic signature of which was firmly established by comparison with that of an authentic sample. Rather interesting is the catalytic performance of [**3B**][OTf] displayed in figure 15, which is comparable to that of reference compound **1** and by far much lower than that of [**2**][OTf].

Treatment of a CD_2Cl_2 solution of [**3B**][OTf] with excess amounts of $HSiEt_3$ (6 equiv./Ir) in a sealed NMR sample tube led according to ^{1}H NMR spectroscopy to the formation of very low amounts of **4**; the [**3B**][OTf]:**4** ratio being approximately 4:1 (ca. 1/9th of the iridacyclic content of [**3B**][OTf] converted into **4**). It was also noted that the characteristic *H*–Si ^{1}H NMR signal of $HSiEt_3$ at ca. δ = 3.65 ppm[66] vanished. New peaks assigned to dissolved H_2 and possible Et_4Si[67] were observed at δ = 4.59 (singlet) ppm and at δ = 0.94 (triplet) and δ = 0.54 (quartet) ppm respectively. It is speculated that upon reaction of excess $HSiEt_3$ with [**3B**][OTf] the release of Et_3SiOTf (and **4**) promotes the formation of the putative transient $[(Et_3Si)_2H][OTf]$,

---

[63] Vela, J.; Smith, J. M.; Yu, Y.; Ketterer, N. A.; Flaschenriem, C. J.; Lachicotte, R. J.; Holland, P. L. Synthesis and Reactivity of Low-Coordinate Iron(II) Fluoride Complexes and Their Use in the Catalytic Hydrodefluorination of Fluorocarbons. *J. Am. Chem. Soc.* **2005**, *127*, 7857-7870.

[64] a) Luo, X. L.; Crabtree, R. H. Homogeneous Catalysis of Silane Alcoholysis via Nucleophilic Attack by the Alcohol on an Ir(η^2-$HSiR_3$) Intermediate Catalyzed by $[IrH_2S_2(PPh_3)_2]SbF_6$ (S = Solvent). *J. Am. Chem. Soc.* **1989**, *111*, 2527-2535. b) Bassindale, A. R.; Stout, T. On the non-existence of trimethylsilyl tetrafluoroborate in acetone and acetonitrile : the generation of boron trifluoride in weakly coordinating solvents. *Tetrahedron Lett.* **1984**, *25*, 1631-1632.

[65] a) Hoffmann, S. P.; Kato, T.; Tham, F. S.; Reed, C. A. Structure and Solution Reactivity of (Triethylsilylium)triethylsilane Cations. *Chem. Commun.* **2006**, 767-769. b) Nava, M.; Reed, C. A. Triethylsilyl perfluoro-tetraphenylborate, $[Et_3Si^+][F_{20}$-$BPh_4]$, a widely used nonexistent compound. *Organometallics* **2011**, *30*, 4798-4800. c) Connelly, S. J.; Kaminsky, W.; Heinekey, D. M. Structure and Solution Reactivity of (Triethylsilylium)triethylsilane Cations. *Organometallics* **2013**, *32*, 7478-7481.

[66] Chen, J.; Chen, E. Y. X. Elusive Silane–Alane Complex [Si[BOND]H···Al]: Isolation, Characterization, and Multifaceted Frustrated Lewis Pair Type Catalysis. *Angew. Chem., Int. Ed.* **2015**, *54*, 6842-6846.

[67] Einholz, W.; Gollinger, W.; Haubold, W. *Z.* Rhodium-Catalyzed Hydrosilylation of Ketones: Catalyst Development and Mechanistic Insights. *Naturforsch., B: Chem. Sci.* **1990**, *45*, 25-30.

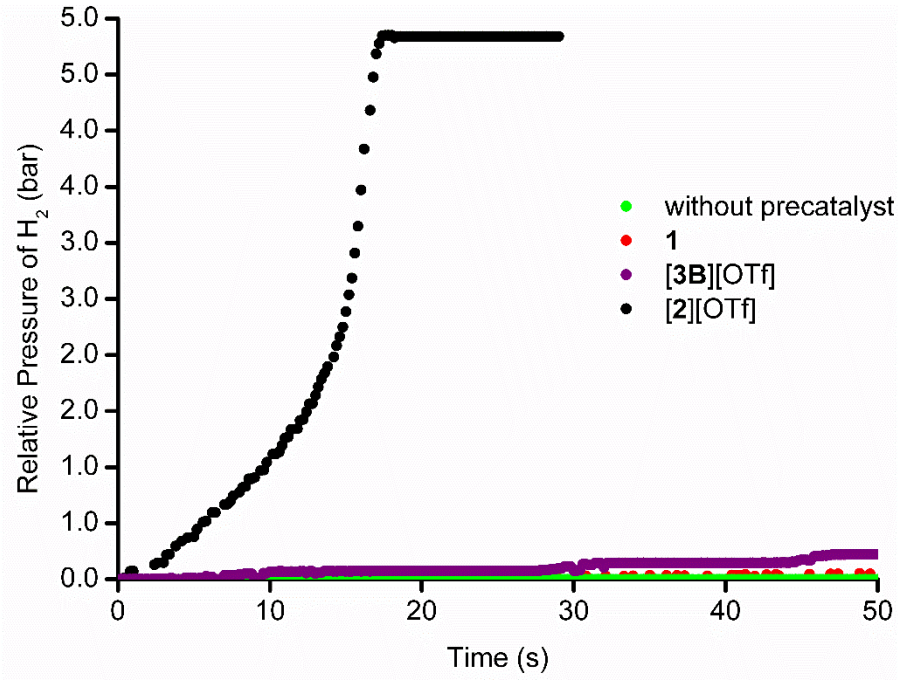

Figure 15. Pressure of hydrogen (bar) as a function of time (s): comparison of the catalytic performance of DCE (0.5 mL) solutions of [**2**][OTf], [**3B**][OTf] and **1** (4.8 *μ*mol) in the *O*-silylation of benzyl alcohol (1 mL, 9.5 mmol) with $HSiEt_3$ (0.8 mL, 5.0 mmol); molar precatalyst:alcohol:$HSiEt_3$ ratio was 1:2000:1000 in all experiments.

a stabilized form of the highly electrophilic silylium $[Et_3Si]^+$ cation according to Heinekey[65c] and Reed[65a,b], which is responsible for the transformation of $HSiEt_3$ into Et_4Si.[65c]

2.2.6.5 [**2**][BPh_4]

^1H NMR monitoring of the reaction of 2 equiv. of $HSiEt_3$ with [**2**][BPh_4] in CD_2Cl_2 indicated the formation of similar species observed for [**2**][$BArF_{24}$] (scheme 10), i.e. the product of the double hydrosilylation of CH_3CN ($(Et_3Si)_2NEt$), the iridium-silane intermediate [**3A**][BPh_4], which is characterized by a broad hydridic signal at $\delta \sim -11.7$ ppm, and the hydrido-bridged iridium complex [**3B**][BPh_4]. The three species were present in a ratio of ~1.2:1:1 (see experimental part). There is no sign of any reaction between $[BPh_4]^-$ and the Lewis-acidic silylium fragment $[Et_3Si]^+$ of transient [**3A**][BPh_4].

2.2.7 [**2**][$BArF_{24}$] + $HSiPh_3$

^{1}H NMR monitoring of the reaction of 2 equiv. of $HSiPh_3$ with [**2**][$BArF_{24}$] in CD_2Cl_2 indicated the formation of similar species observed for [**2**][$BArF_{24}$] with $HSiEt_3$ (scheme 10), i.e. the product of the double hydrosilylation of CH_3CN which is $(Ph_3Si)_2NEt$, the iridium-silane intermediate [**3D**][$BArF_{24}$], which is characterized by a broad hydridic signal at $\delta \sim -11.9$ ppm, and the hydrido-bridged iridium complex [**3B**][BPh_4]. The three species were present in a ratio of ~1:1:0.1 (see experimental part). There is no sign of any reaction between $[BArF_{24}]^-$ and the Lewis-acidic silylium fragment $[Ph_3Si]^+$ of the the intermediate [**3D**][$BArF_{24}$].

2.2.8 [**4**][$BArF_{24}$] + $HSiR_3$

In a similar manner as for [**2**][$BArF_{24}$], [**4**][$BArF_{24}$] presented comparable reactivity with silanes such as $HSiEt_3$ and $HSiPhH_2$ (scheme 10).

2.2.8.1 $HSiEt_3$

We treated a CD_2Cl_2 solution of [**4**][$BArF_{24}$] with excess amounts of $HSiEt_3$ (2 equiv./Ir) in a sealed NMR sample tube. Multinuclear NMR analysis (at –60 °C) of the reaction revealed the total conversion of [**4**][$BArF_{24}$] to [**5A**][$BArF_{24}$], [**5A'**][$BArF_{24}$] (isomer of [**5A**][$BArF_{24}$]), [**5B**][$BArF_{24}$], $(Et_3Si)_2NEt$ along with unconsumed $HSiEt_3$ in a ratio of ~1:1:0.1:1.2:1.2 (see experimental part for full NMR data). The X-ray structures of [**5A**][$BArF_{24}$] and [**5A'**][$BArF_{24}$] feature identical ^{1}H peaks of H_{Ar} B[*h*]Q (C,N ligand = benzo[*h*]quinolin-10-yl) and Cp*, except for bound $[Et_3Si]^+$ moieties which feature slightly distinct ^{1}H and ^{29}Si chemical shifts. The latter non-equivalence in ^{1}H and ^{29}Si chemical shifts for $[Et_3Si]^+$ signals is attributed to the two possible isomers [**5A**][$BArF_{24}$], [**5A'**][$BArF_{24}$], the X-ray structures of which could be successfully determined (*vide infra*). Additional 2D ^{29}Si-^{1}H HMQC analysis of the reaction mixture provide solid evidence for the involvement of the two latter isomers in solution as well (scheme 11, see experimental part for more details). [**5A**][$BArF_{24}$] (and [**5A'**][$BArF_{24}$]) features the typical hydride signal at $\delta = -11.4$ ppm, and a ^{29}Si chemical shift at $\delta = 6.9$ ppm; these signals are very close to the ones found for [**3A**][$BArF_{24}$] (δ (^{1}H) = –11.7 ppm, and a δ (^{29}Si) = 7.1 ppm). A coupling constant $J_{Si\text{-}H}$ of ~20 Hz was found for [**5A**][$BArF_{24}$] (and [**5A'**][$BArF_{24}$]), suggesting a rather weak H–Si interaction as it has been observed for the intermediate [**3A**][$BArF_{24}$] (*vide supra*). The X-ray structure of [**5B**][$BArF_{24}$] was obtained, and confirmed the expected hydrido-bridged iridium dimer bonding (*vide infra*).

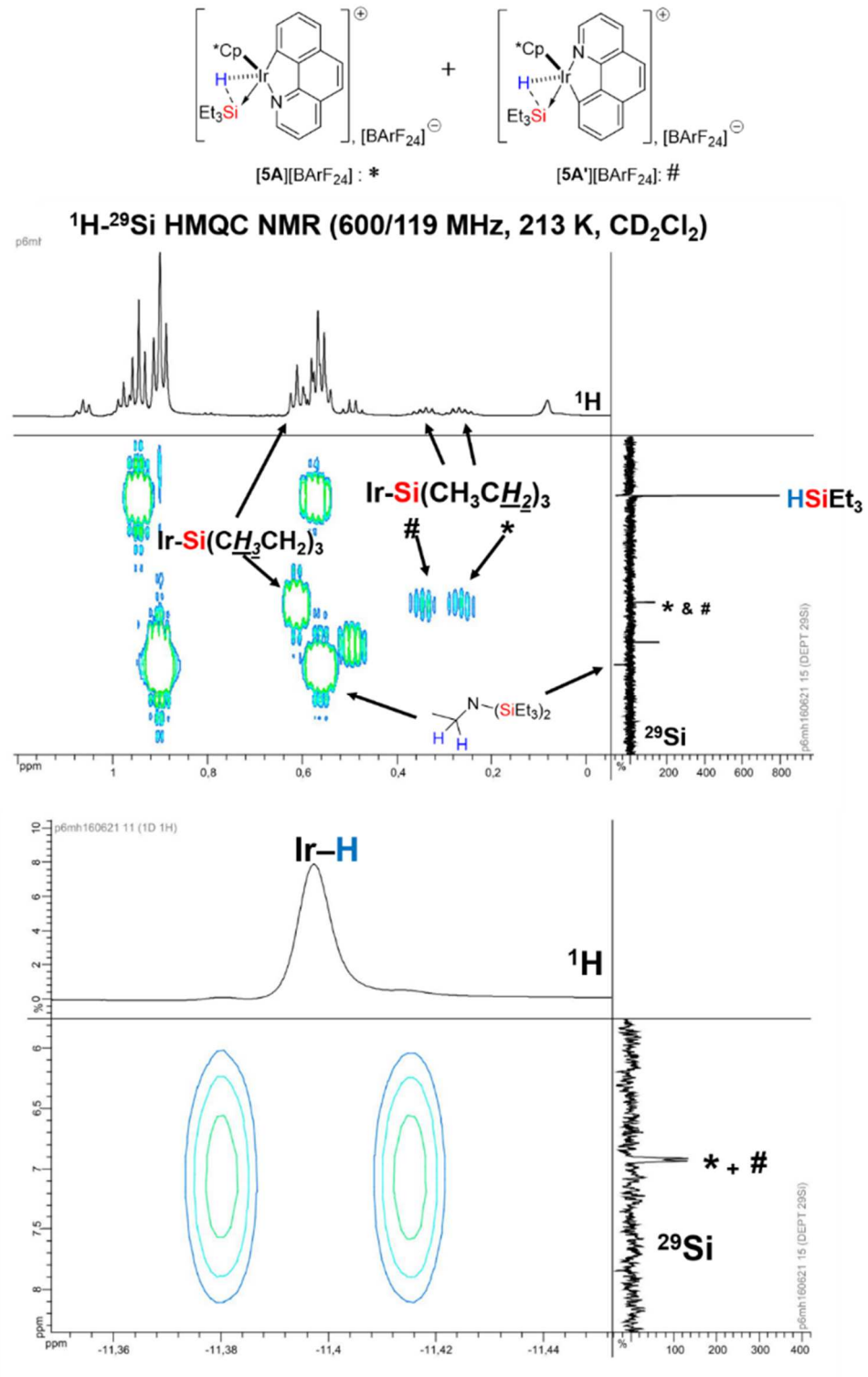

Scheme 11. 2D ^{29}Si-^{1}H HMQC NMR spectroscopy analysis (top: Ir→SiE_3 region; bottom: Ir–H region) of the reaction between [**4**][$BArF_{24}$] and excess amounts of $HSiEt_3$ (2 equiv./Ir) in CD_2Cl_2 (– 60 °C).

2.2.8.1.1 $HSiPhH_2$

We treated a CD_2Cl_2 solution of [**4**][$BArF_{24}$] with excess amounts of $HSiPhH_2$ (2 equiv./Ir) in a sealed NMR sample tube. Multinuclear NMR analysis (at –60 °C) of the reaction revealed the total and exclusive conversion of [**4**][$BArF_{24}$] to [**5F**][$BArF_{24}$], along with unconsumed $HSiPhH_2$ and released CH_3CN (from [**4**][$BArF_{24}$]) in a ratio of ~1:1:3 (scheme 10, see experimental part for full NMR data). There was no sign of hydrosilyation of CH_3CN, as one equivalent (per Ir) of free CH_3CN was observed (singlet at δ =1.98 ppm in CD_2Cl_2). The identity of the silane-iridium intermediate [**5F**][$BArF_{24}$] was assessed by the observation of the typical Ir–H signal at δ = –11.5 ppm (broad singlet), whith no detectable H–Si coupling. [**5F**][$BArF_{24}$] features a ^{29}Si chemical shift at δ = –35.6 ppm, which is ~23 ppm downfiled than the value found for "free" $HSiPhH_2$ (δ = –56.7 ppm). Unfortunately, after several attempts the X-ray structure of [**5F**][$BArF_{24}$] has not been determined.

2.2.9 Structure and bonding in [**3B**][OTf]

Compound [**3B**][OTf] was synthesized by reaction of [**2**][OTf] with excess $HSiEt_3$, fully analytically characterized (see experimental part) and its structure resolved by X-ray diffraction analysis. Figure 16 displays the ellipsoid-type diagram of the structure of [**3B**][OTf] whereas in tabe 8 are provided some typical geometrical parameters found in the latter structures, and in table 9 are listed all their pertinent structural X-ray diffraction acquisition and refinement data (see appendix for more details). In this complex the position of the bridging hydrido ligand was determined from Fourier difference maps and refined. The Ir1–H1 and Ir2–H1 distances are slightly different and amount respectively 1.63(6) and 1.79(6) Å. This apparent difference nonetheless lies within the limits of accuracy defined by standard deviation and could be an artefact of the localization from Fourier difference maps. In a perfectly symmetric molecule a C2 rotation axis would be positioned at the bridging hydrogen atom somewhat parallel to the Ir-N bonds, and would bisect perpendicularly the Ir1–Ir2 segment. The structure drawn in figure 16 indicates π-π stacking interactions with a pyridyl-to-pyridyl inter-centroid distance of ca. 3.4 Å, a structural feature similar to that reported previously for another catalytically inactive μ-hydrido-bridged bisruthenacycle.[68] A rationale similar to that proposed for the formation of

[68] Petrović, P.; Djukic, J.-P.; Hansen, A.; Bannwarth, C.; Grimme, S. In *Non-Covalent Interactions in the Synthesis and Design of New Compounds*; Maharramov, A. M., Kamran T. Mahmudov, Kopylovich, M. N., Pombeiro, A. J. L., Eds.; John Wiley & Sons: 2016, p 115-143.

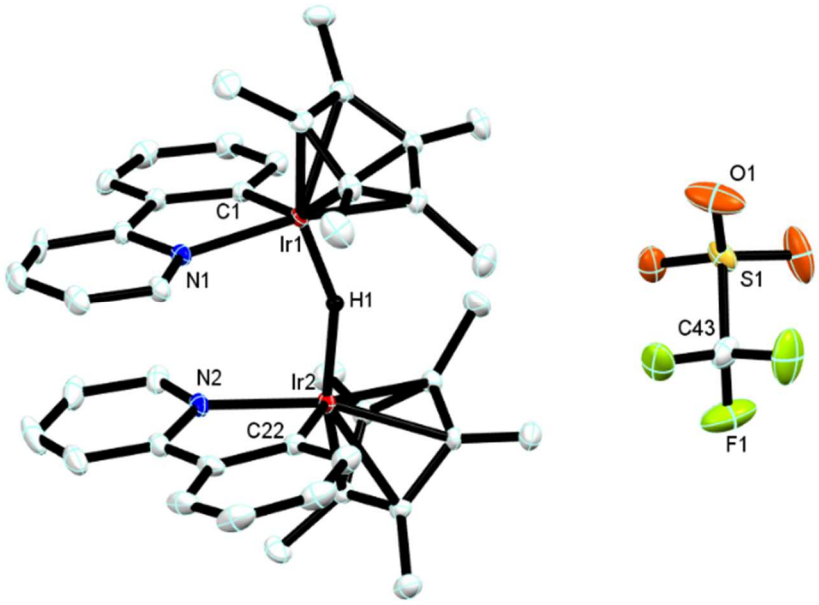

Figure 16. Ellipsoid-type diagram of the structure of [**3B**][OTf] drawn at the 30% probability level with partial atom numbering. Note that hydridic H1 atom was located from Fourier difference maps and its position refined. Dichloromethane molecules and most of hydrogen atoms were omitted for clarity.

[**3B**][$BArF_{24}$] can be made for [**3B**][OTf]; the latter stems from a reaction of **4** with [**2**][OTf] with the concomitant displacement of MeCN and its capture by Et_3SiOTf in the early stages of the reaction.

Symmetry-unconstrained DFT geometry optimization carried out with a gas-phase singlet ground state model of [**3B**]$^+$ (ZORA – PBE-D3(BJ)/ae-TZP level) produced a more symmetric geometry in which the Ir–H–Ir motif displays Ir–H distances of the same order (1.743 and 1.737 Å). The π-π interaction is localy materialized by blue-colored NCI isosurfaces in figure 17b depicting non-bonded van der Waals contacts. Bonding within cation [**3B**]$^+$ was further analyzed assuming an equivalent [$\mathbf{4}_{H}\rightarrow\mathbf{2+}_{Ir}$]$^+$ donor-acceptor pair formulation, where **2+** is the 16-electron cationic iridacycle resulting from the departure of MeCN from [**2**]$^+$, H and Ir indexes specify atoms involved in the main bonding interactions taking place between fragments **4** and [**2+**]$^+$. This fragmentation scheme, although artificial, is of great use to outline the peculiar

Table 8. Selected interatomic distances (Å), angles (deg) and torsion angles (deg) for [**3B**][OTf], [**3A**][$BArF_{24}$], [**5A**][$BArF_{24}$] and [**5B**][$BArF_{24}$].

Distance (Å)	**[3B][OTf]**	**[3A][$BArF_{24}$]**	**[5A][$BArF_{24}$]**	**[5B][$BArF_{24}$]**
Ir1–Si1	-	2.5008(8)	2.566(2)	-
Ir1–H1A	Ir1–H1, 1.63(6); Ir2–H1, 1.79(6)	1.47	1.4312	Ir1–H1A, 1.8568; Ir2–H1A, 1.7869
Si1–H1A	-	2.10	1.574	-
Ir1–N1	Ir1–N1, 2.082(3); N2–Ir2, 2.079(3)	2.0754(19)	2.099(4)	Ir1–N1, 2.088(7); N2–Ir2, 2.090(6)
C11—Ir1	C1–Ir1, 2.037(4); C22–Ir2, 2.040(4)	2.089(2)	2.079(4)	C11—Ir1, 2.078(6); C34—Ir2, 2.040(8)
B1–Ir1	-	10.077(2)	7.809(4)	B1–Ir1, 10.004(7); B1–Ir2, 8.777(7)
Angle (°)	**[3B][OTf]**	**[3A][$BArF_{24}$]**	**[5A][$BArF_{24}$]**	**[5B][$BArF_{24}$]**
C11–Ir1–N1	C1–Ir1–N1, 78.5(1); C22–Ir2–N2, 108.3(2)	77.60(8)	78.5(2)	C1–Ir1–N1, 78.7(3); C34–Ir2–N2, 79.1(3)
C11–Ir1–Si1	-	86.32(14)	97.6(1)	-
N1–Ir1–Si1	-	99.78(6)	80.7(1)	-
N1–Ir1–H1A	N1–Ir1–H1, 98(2); N2–Ir2–H1, 97(2)	76.2	83.4	N1–Ir1–H1A, 111.0; N2–Ir2–H1A, 108.7
Ir1–H1-Ir2	155.1(4).	-	-	Ir1–H1A-Ir2, 131.50

propensity of **4** to form donor-acceptor complexes[69] (*vide infra*). Extended transition state – natural orbital for chemical valence[70] (ETS-NOCV) analysis was performed to visualize electron density transfer upon orbital interaction between the latter two fragments in their so-called *prepared* geometry, that is the geometry preceding the establishment of inter-fragment bonds leading to [**3B**]$^+$ The two fragments were defined as resulting from the cleavage of the longest Ir–H distance (1.743 Å) in [**3B**]$^+$. It was found that the main orbital interaction energy component (–48 kcal/mol) arises from the interaction materialized by density deformation $\Delta\rho_1$ (figure 17b) which represents 61% of the inter-fragment orbital interaction energy (ΔE_{orb}= –77 kcal/mol).

[69] Turlington, C. R.; Harrison, D. P.; White, P. S.; Brookhart, M.; Templeton, J. L. Probing the oxidation chemistry of half-sandwich iridium complexes with oxygen atom transfer reagents. *Inorg. Chem.* **2013**, *52*, 11351-11360.

[70] a) Mitoraj, M. P.; Michalak, A.; Ziegler, T. On the Nature of the Agostic Bond between Metal Centers and β-Hydrogen Atoms in Alkyl Complexes. An Analysis Based on the Extended Transition State Method and the Natural Orbitals for Chemical Valence Scheme (ETS-NOCV). *Organometallics* **2009**, *28*, 3727-3733. b) Mitoraj, M. P.; Michalak, A.; Ziegler, T. A Combined Charge and Energy Decomposition Scheme for Bond Analysis. *J. Chem. Theory Comput.* **2009**, *5*, 962-975.

Table 9. Table of structural X-ray diffraction acquisition and refinement data for [**3B**][OTf], [**3A**][$BArF_{24}$], [**5A**][$BArF_{24}$] and [**5B**][$BArF_{24}$]. Temperature of acquisition: T = 173(2) K.

compound	**[3B][OTf]**	**[3A][$BArF_{24}$]**	**[5A][$BArF_{24}$]**	**[5B][$BArF_{24}$]**
formula	$C_{42}H_{47}Ir_2N_2$•CF_3O_3S •2(CH_2Cl_2)	$C_{32}H_{12}BF_{24}$•$C_{27}H_{39}IrNS$ i•0.5(C_6H_{14})	$C_{32}H_{12}BF_{24}$•$C_{29}H_{39}IrNSi$	$C_{32}H_{12}BF_{24}$•$C_{46}H_{47}Ir_2$ N_2
mol. wt (g/mol)	1283.14	1504.19	1485.12	1875.48
habit	orange prism	yellow block	yellow prism	red prism
cryst.size (mm)	0.40 × 0.35 × 0.30	0.38 × 0.35 × 0.30	0.34 × 0.25 × 0.16	0.38 × 0.30 × 0.22
cryst. syst.	monoclinic	triclinic	monoclinic	monoclinic
space group	$P2_1/c$	$P\bar{1}$	$P2_1/c$	$P2_1/c$
a (Å)	10.9779(9)	12.614(5)	12.5087(6)	13.1813(5)
b (Å)	23.2754(19)	13.698(5)	19.5739(10)	14.6406(6)
c (Å)	21.0040(13)	19.789(5)	25.5683(13)	37.7769(14)
α (deg)	90	81.064(5)	90	90
β (deg)	120.899(3)	71.685(5)	98.955(1)	96.152(1)
γ (deg)	90	79.438(5)	90	90
V (Å^3)	4605.1(6)	3173.5(19)	6183.9(5)	7248.3(5)
Z	4	2	4	4
D_x (Mg m^{-3})	1.851	1.574	1.595	1.719
θ_{max}, θ_{min} (°)	34.0, 2.3	32.1, 1.5	33.1, 1.3	32.0, 1.5
μ (mm^{-1})	6.11	2.23	2.29	3.78
h,*k*,*l* range	–14/17, –36/35, –33/13	–18/18, –20/20, –29/29	–19/8, –28/30, –36/39	–19/19, –21/21, –56/56
measd reflns	74913	83067	141138	175516
indept reflns	18826	22017	23408	25132
reflns (I>2σ(I))	15330	19600	17366	19373
params	555	820	820	944

R_{int}	0.033	0.023	0.043	0.038
$R[F^2>2\sigma(F^2)]$	0.041	0.033	0.066	0.082
$wR(F^2)$	0.083 [a]	0.124 [b]	0.167 [c]	0.198 [d]
S	1.15	1.02	1.02	1.22

[a] $w = 1/[\sigma^2(F_o^2) + (0.021P)^2 + 18.0829P]$ where $P = (F_o^2 + 2F_c^2)/3$. [b] $w = 1/[s^2(F_o^2) + (0.0415P)^2 + 2.3317P]$ where $P = (F_o^2 + 2F_c^2)/3$. [c] $w = 1/[\sigma^2(F_o^2) + (0.0772P)^2 + 23.8188P]$ where $P = (F_o^2 + 2F_c^2)/3$. [d] $w = 1/[\sigma^2(F_o^2) + (0.0461P)^2 + 90.7306P]$ where $P = (F_o^2 + 2F_c^2)/3$.

The electron density transfer associated with $\Delta\rho_1$ entails donation from d orbitals at Ir and from the s orbital at the hydrido H atom. Furthermore, natural bonding orbital (NBO) analysis of the Lewis structure of [**3B**]$^+$ provided an explicit formulation for one Ir–H natural bonding orbital as a linear combination of atomic orbital components. The electron occupation of the latter fell above the standard threshold value of 1.5 electron below which bonding interactions are not considered within the NBO valence scheme. This natural bonding orbital located on the shortest interatomic H–Ir segment is formulated as $\psi_{Ir-H}(1.545\ e) = 0.71(s)_H + 0.70(sd^{2.59})_{Ir}$.

2.2.10 Isothermal Titration Calorimetry (ITC) experiments

2.2.10.1 A brief introduction to ITC

It is well known that almost any chemical reaction/interaction or physical change gives rise to a change in heat or enthalpy. Isothermal Titration Calorimetry (ITC) is a method of measure of the heat released (exothermic) or consumed (endothermic) during a chemical reaction or a physical change. This technique became a powerful method, especially for biologists, as it allows the access to important thermodynamic and kinetic parameters of a catalytic reaction[71] or the active site of an enzyme[72] for example. The method is powerful because very small heats (~0.1 mcal; 0.4 mJ) can be measured with the most modern instruments.[73] Our group successfully applied this method to the study of organometallic systems, especially for the

[71] Blackmond, D. G.; Rosner, T.; Pfaltz, A. Comprehensive Kinetic Screening of Catalysts Using Reaction Calorimetry. *Org. Process Res. Dev.* **1999**, *3* (4), 275–280.
[72] Ghai, R.; Falconer, R. J.; Collins, B. M. Applications of Isothermal Titration Calorimetry in Pure and Applied Research-Survey of the Literature from 2010. *J. Mol. Recognit.* **2012**, *25* (1), 32–52.
[73] Freyer, M. W.; Lewis, E. A. Isothermal Titration Calorimetry: Experimental Design, Data Analysis, and Probing Macromolecule/Ligand Binding and Kinetic Interactions. *Methods Cell Biol.* **2008**, *84* (7), 79–113.

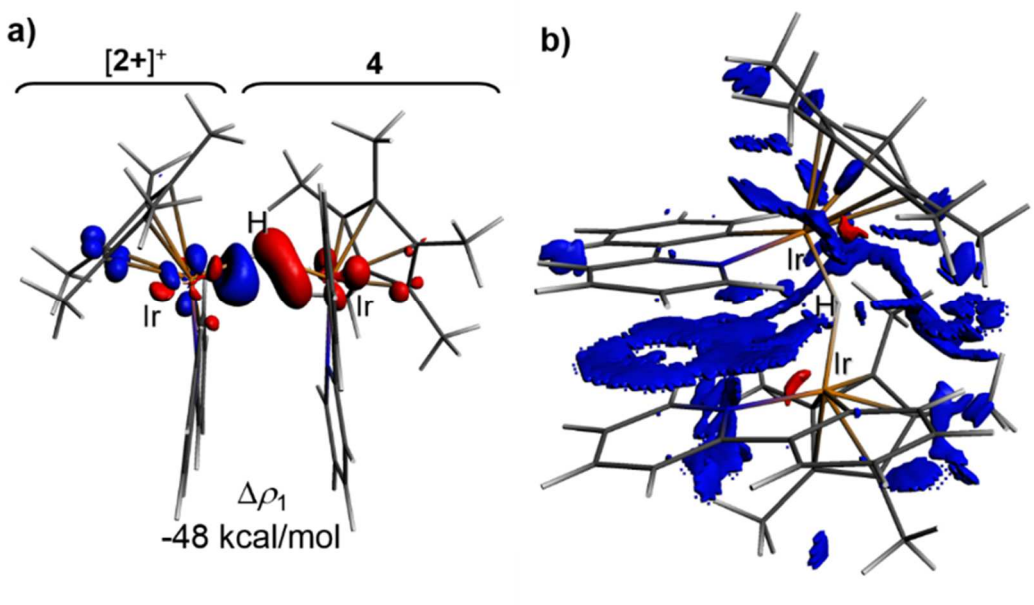

Figure 17. a) ETS-NOCV analysis of the bonding interaction between closed-shell fragments **4** and [**2+**]$^+$ in their prepared geometry in [**3B**]$^+$. Deformation density isosurface plot $\Delta\rho_1$ (0.005 e.bohr^{-3}) is associated with an orbital interaction energy of –48 kcal/mol. Electron density transfer operates from the red to the blue colored volumes upon interaction. **b)** ADFview2013 plots of non-covalent interaction (NCI) regions materialized by reduced density gradient isosurfaces (cut-off value s = 0.02 a.u., ρ =0.05 a.u.) colored according to the sign of the signed density $\lambda_2\rho$ for a singlet ground state model of [**3B**]$^+$. Red (attractive) and blue (Pauli repulsion or non-bonded van der Waals) colors are associated to negatively and positively signed terms respectively.

investigation of the contribution of London dispersion forces to the so-called non-covalent interactions in these systems.[74]

2.2.10.2 The enthalpy of activation of [**2**][BArF$_{24}$]

The enthalpy of activation of [**2**][BArF$_{24}$] with HSiEt$_3$ in PhCl at 20 °C was studied by ITC. The measure was performed by the sequential addition of small volumes of a PhCl solution of HSiEt$_3$ into 1 mL of a solution of [**2**][BArF$_{24}$]. Under such conditions the side-formation of [**3B**][BArF$_{24}$] was expected to be minimized. Three experiments were run independently; they all indicated

[74] a) Hansen, A.; Bannwarth, C.; Grimme, S.; Petrovic, P.; Werlé, C.; Djukic, J. P. The Thermochemistry of London Dispersion-Driven Transition Metal Reactions: Getting the "Right Answer for the Right Reason." *ChemistryOpen* **2014**, *3* (5), 177–189. b) Iali, W.; Petrović, P.; Pfeffer, M.; Grimme, S.; Djukic, J.-P. The Inhibition of Iridium-Promoted Water Oxidation Catalysis (WOC) by Cucurbit[n]urils. *Dalt. Trans.* **2012**, *41* (39), 12233–12243.

that thermochemical stationary state was reached with 3 equiv. of $HSiEt_3$ with an associated (exothermic) enthalpy of reaction of -46 ± 3 kcal/mol (figure 18). This value of enthalpy can be decomposed as the sum of three main thermochemical contributions (scheme 12): 1) the reaction of [**2**][$BArF_{24}$] with $HSiEt_3$ leading to [**3A**][$BArF_{24}$], MeCN, [**3B**][$BArF_{24}$] and the possible partial conversion of [**3A**]$^+$ into **4** and the silylium-chlorobenzene cation[75] [$(Et_3Si)(PhCl)$]$^+$ (ΔH_1), 2) the catalyzed hydrosilylation of the released MeCN into $(Et_3Si)N{=}C(H)Me$ (ΔH_2) and 3) the hydrosilylation of the latter into $(Et_3Si)_2NEt$ (ΔH_3).

Computation of the thermochemistry[76] of the latter two steps was carried out at the B3LYP-NL/def2-QZVP level with zero-point energy and solvation corrections (see computational methods in the experimental part) using the COSMO-RS[77] procedure. The computed values of ΔH_2 (−16.5 kcal/mol) and ΔH_3 (−28.1 kcal/mol) suggest a dominant thermochemical contribution of the hydrosilylation of MeCN to the total enthalpy of reaction. For convenience, the enthalpy of the single reaction of [**2**][$BArF_{24}$] with $HSiEt_3$ leading to [**3A**][$BArF_{24}$] and MeCN, i.e. ΔH_1*, was computed by substituting $[BArF_{24}]^-$ by $[BF_4]^-$. Assuming contact ion pairs for [**2**][BF_4] and [**3**][BF_4], ΔH_1* was found to be slightly endothermic with a value of +1.2 kcal/mol (ΔG_1*= +4.5 kcal/mol); the total found to be slightly endothermic with a value of +1.2 kcal/mol (ΔG_1*= +4.5 kcal/mol); the total computed reaction enthalpy amounting $\Delta H_{tot} = \Delta H_1^* + \Delta H_2 + \Delta H_3 = -43.5$ kcal/mol ($\Delta G_{298\ K} = -24$ kcal/mol). It must be noted that performing the calculation without inclusion of the counter-anion had a minor effect on the value of ΔH_1*. According to DFT calculations, it can be stated that the catalyzed hydrosilylation of MeCN assists the departure of MeCN from [**2**]$^+$ and enables the formation of [**3A**]$^+$, which is thermodynamically not favored according to the computed positive value of ΔG_1*.

[75] Connelly, S. J.; Kaminsky, W.; Heinekey, D. M. Structure and Solution Reactivity of (Triethylsilylium)triethylsilane Cations. *Organometallics* **2013**, *32*, 7478-7481.
[76] Hansen, A.; Bannwarth, C.; Grimme, S.; Petrović, P.; Werlé, C.; Djukic, J.-P. The Thermochemistry of London Dispersion-Driven Transition Metal Reactions: Getting the 'Right Answer for the Right Reason'. *ChemistryOpen* **2014**, *3*, 177-189.
[77] Klamt, A. Conductor-like Screening Model for Real Solvents: A New Approach to the Quantitative Calculation of Solvation Phenomena. *J. Phys. Chem.* **1995**, *99*, 2224-2235.

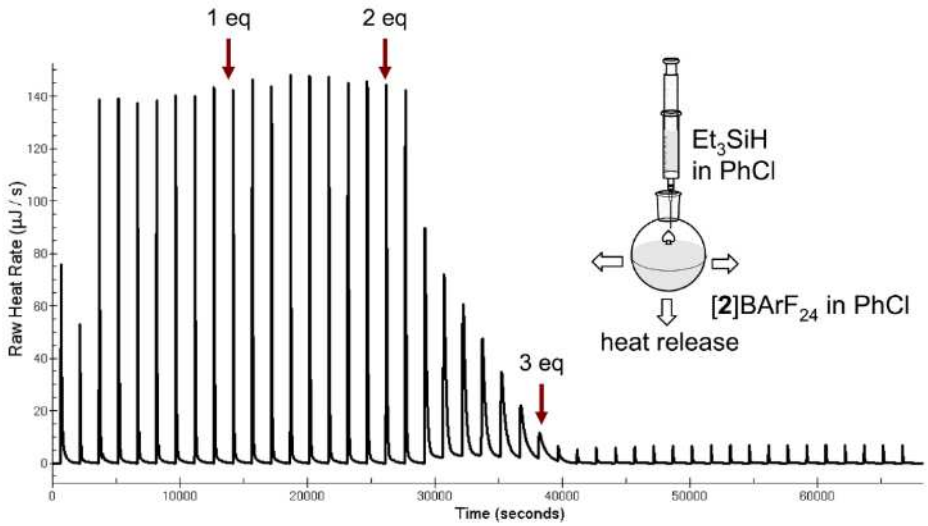

Figure 18. Calorigram of the isothermal (T= 293.15 K) titration (ITC) of [**2**][$BArF_{24}$] in PhCl (c = 1.0 mmol•L^{-1}) by sequential injections (v = 2 μL, time delay between injections = 1500 s) of $HSiEt_3$ (c = 78.4 mmol•L^{-1}).

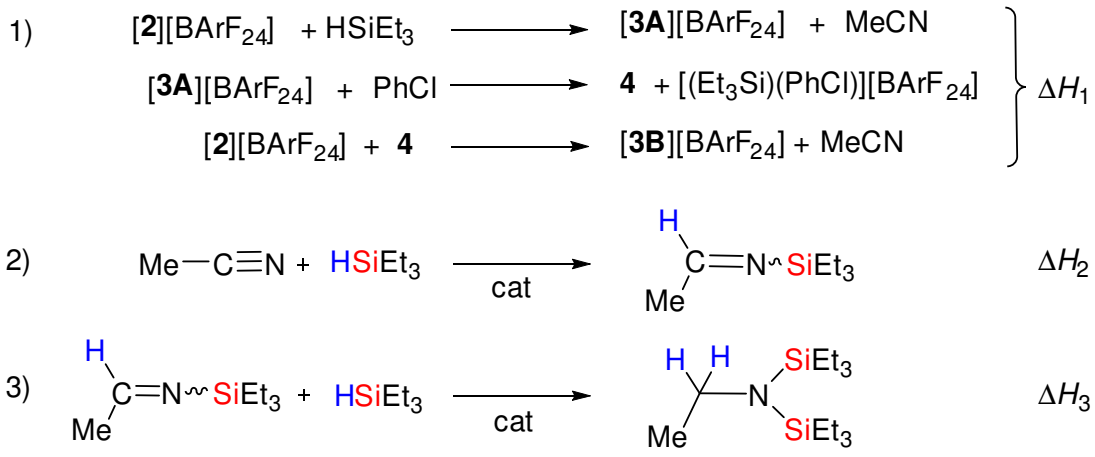

Scheme 12. Among the three thermochemical contributions identified for the activation of [**2**][$BArF_{24}$] by $HSiEt_3$ in PhCl, ΔH_2 and ΔH_3 are the dominant ones, according to COSMO-RS/DFT-D computations.

2.2.11 Structural characterization of intermediates [**3A**][$BArF_{24}$], [**5A**][$BArF_{24}$] and [**5A'**][$BArF_{24}$]

2.2.11.1 Attempt to synthesize [**3A**][$BArF_{24}$]

We tried to isolate the intermediate [**3A**][$BArF_{24}$] by reacting [**2**][$BArF_{24}$] with $HSiEt_3$ at room temperature in CH_2Cl_2 (scheme 13). Instead of the desired product, the new complex

[**3C**][BArF$_{24}$] has been isolated as red/orange crystals. The structure of [**3C**][BArF$_{24}$] has been confirmed by full analytical characterization of the crystals (see experimental part for details). Unfortunately, no X-ray diffraction structure of [**3C**][BArF$_{24}$] could be obtained at this stage.

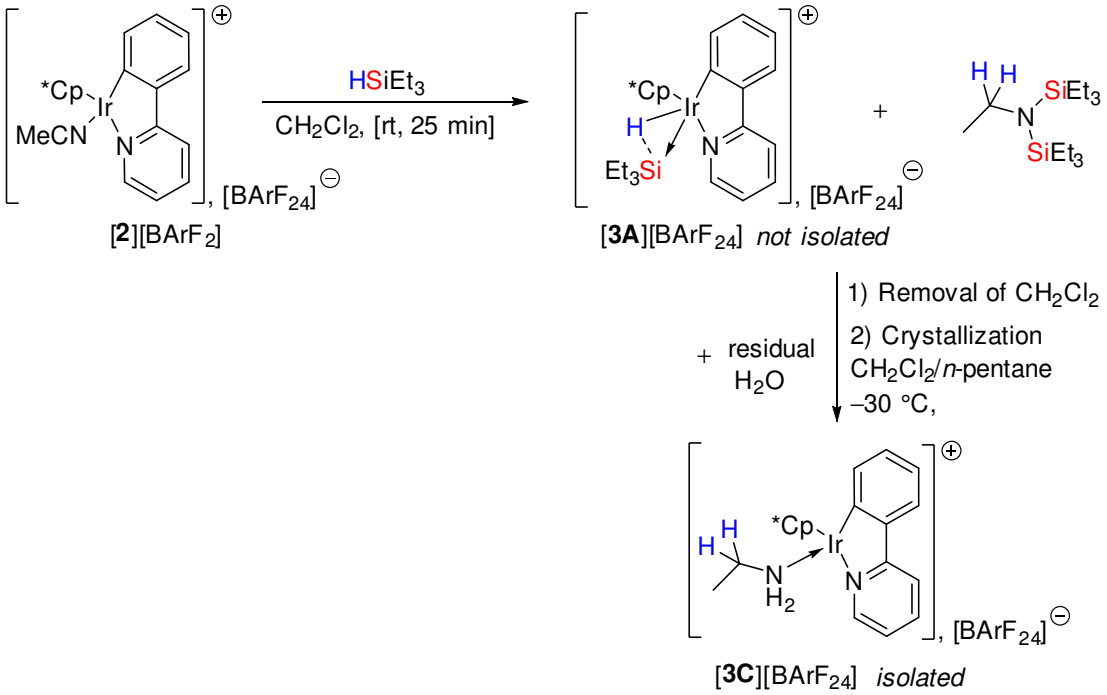

Scheme 13. Attempt for the synthesis of [**2A**][BArF$_{24}$] led to the isolation of the ionic iridacycle [(κ^2-(C,N)-(2-phenylenepyridine)Ir(III)N(H)$_2$Et][BArF$_{24}$], [**2C**][BArF$_{24}$], from [**2**][BArF$_{24}$] and HSiEt$_3$.

2.2.11.2 X-ray diffraction characterization of [**3A**][BArF$_{24}$]

Owing to its high reactivity and sensitivity to moisture [**3A**][BArF$_{24}$] could not be isolated and fully characterized analytically. Nonetheless, as already mentioned above, crystals were grown by the solvent diffusion technique at –20°C directly from reaction aliquots, thus affording samples suitable for X-ray diffraction analysis. Close analysis of diffraction data of two different crystals suggested that [**3A**][BArF$_{24}$] exists under two distinct diastereomeric forms that differ by the position of the SiEt$_3$ group and the hydridic H atom relatively to the iridacycle. Those two isomers are isoergonic (298.15 K) within 1 kcal/mol according to gas-phase singlet ground state DFT calculations. According to NMR data that display a single signal for the hydridic proton around δ = –11.7 ppm, it is speculated that the two isomers [**3A**][BArF$_{24}$] are either engaged in a fast mutual exchange or that their respective ^{1}H NMR spectra coincide. Figure

19a displays the structure of [**3A**][BArF$_{24}$] above its computed model (figure 19b), which displays a geometry consistent with the X-ray diffraction data.

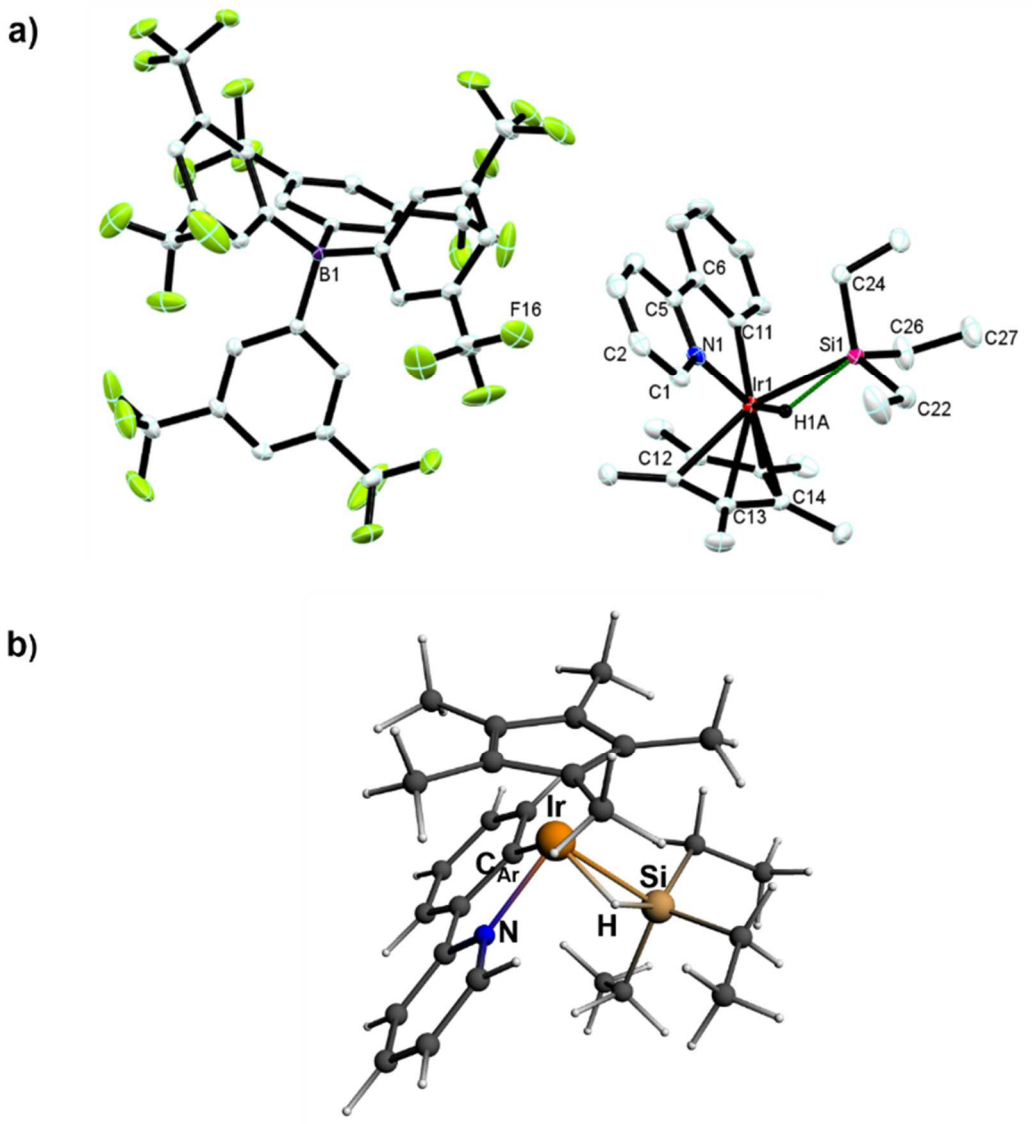

Figure 19. **a)** Ellipsoid-type diagram of the structure of [**3A**][BArF$_{24}$] drawn at the 30 % probability level with partial atom numbering. Note that hydridic H1A atom was located from Fourier difference maps and its position frozen during refinement. Green dots show the Si1–H1A interaction. Pentane molecule and most of hydrogen atoms were omitted for clarity. **b)** Gas phase singlet ground state geometry of [**3A**]$^{+}$ computed at the ZORA-PBE0-dDsC/ae-TZP level. Selected interatomic distances (Å): Ir–Si 2.514, Ir–H 1.583, Si–H 1.913, C_{Ar}–Ir 2.056, N–Ir 2.069.

Incomplete structural data of the other diastereomer of [**3A**][$BArF_{24}$] (named as [**3A'**][$BArF_{24}$]) was obtained. Table 8 summarizes some characteristic geometrical parameters found in the X-ray structure of [**3A**][$BArF_{24}$], whereas table 9 displays its acquisition and refinement data. The coordination geometry of [**3A**][$BArF_{24}$] suggests an heptacoordinate Ir center displaying the main feature of a SISHA-type adduct[78], i.e. an experimental H–Si distance (ca. 2.10 Å) slightly longer than the generally accepted limit value of 1.9 Å.[79] The Ir–Si distance of ca. 2.50 Å is only slightly longer than that reported by R.G. Bergman, T. D. Tilley and co-workers for $[(Ph_3Si)(Me_3P)IrCp^*]^+$ (2.41 Å).[80] The Ir–H distance of ca. 1.47 Å is akin to that reported for complex **4** (1.52 Å) by J. R. Norton and co-workers.[81]

2.2.11.3 X-ray diffraction characterization of [**5A**][$BArF_{24}$] and [**5A'**][$BArF_{24}$]

Crystals of [**5A**][$BArF_{24}$] were grown by the solvent diffusion technique at –30°C directly from the stoichiometric reaction between $HSiEt_3$ and [**4**][$BArF_{24}$], thus affording samples suitable for X-ray diffraction analysis. Similar diffraction data than those found for [**3A**][$BArF_{24}$] were noticed for [**5A**][$BArF_{24}$] as well, as it is showed in the X-ray diffraction structure depicted in figure 20 and table 8. In table 9 can be found the acquisition and refinement data for [**5A**][$BArF_{24}$] (see appendix for more details). Similarly, [**5A**][$BArF_{24}$] gave two crystals which, after analysis, unambigously confirmed that [**5A**][$BArF_{24}$] exists under two distinct diastereoisomeric forms that differ by the position of the $SiEt_3$ group and the hydridic H atom relatively to the iridacycle. The X-ray structure of the diastereoisomer of [**5A**][$BArF_{24}$], denoted as [**5A'**][$BArF_{24}$], is provided in the appendix. The latter two isomers were showed to exist in solution as 1/1 mixture, as supported by NMR spectroscopy analysis (*vide supra*). Indeed, NMR data display single signals for the hydridic proton around δ = –11.7 ppm, the aromatic protons of the C,N heterobidentate ligand (δ = 7.54–8.67 ppm) and the Cp* protons (δ = 1.69 ppm), and distinct signals for the methylene protons for $SiEt_3$ at around δ = 0.29 ppm ([**5A**][$BArF_{24}$]) and δ = 0.22 ppm ([**5A'**][$BArF_{24}$]) (see experimental part for details). Moreover, ^{29}Si NMR data clearly show two disctinct, though very close, signals at around δ = 6.93 ppm ([**5A**][$BArF_{24}$]) and

[78] Lachaize, S.; Sabo-Etienne, S. *σ*-Silane Ruthenium Complexes: The Crucial Role of Secondary Interactions. *Eur. J. Inorg. Chem.* **2006**, 2115-2127.
[79] Corey, J. Y. Reactions of Hydrosilanes with Transition Metal Complexes and Characterization of the Products. *Chem. Rev.* **2011**, *111*, 863-1071.
[80] Klei, S. R.; Tilley, T. D.; Bergman, R. G. The Mechanism of Silicon-Hydrogen and Carbon-Hydrogen Bond Activation by Iridium (III): Production of a Silylene Complex and the First Direct Observation of Ir (III)/Ir(V) C-H Bond Oxidative Addition and Reductive Elimination. *J. Am. Chem. Soc.* **2000**, *122*, 1816-1817.
[81] Hu, Y.; Li, L.; Shaw, A. P.; Norton, J. R.; Sattler, W.; Rong, Y. Synthesis, electrochemistry, and reactivity of new iridium(III) and rhodium(III) hydrides. *Organometallics* **2012**, *31*, 5058-5064.

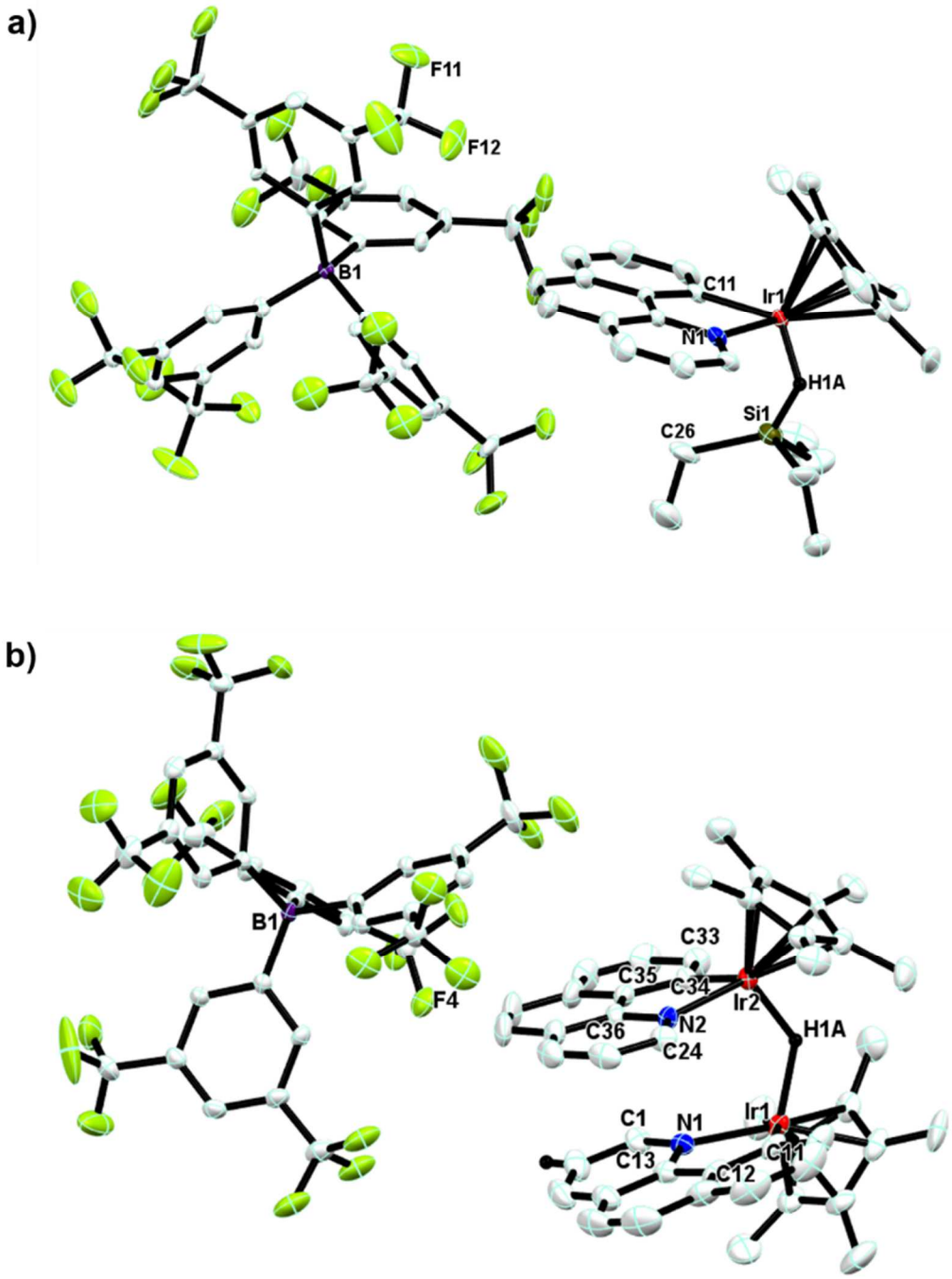

Figure 20. Ellipsoid-type diagram of the structure of **a)** [**5A**][$BArF_{24}$] and **b)** [**5B**][$BArF_{24}$] drawn at the 30 % probability level with partial atom numbering. Note that hydridic H1 atom of both structures was located from Fourier difference maps and its position was fixed without refinement. In **a)** and **b)**, disordered fluorine atoms and most of hydrogen atoms were omitted for clarity. In **a)**, ½ molecule of benzene and disordered carbon carbon atoms were omitted for clarity.

δ = 6.90 ppm ([**5A'**][$BArF_{24}$]) (see experimental part for details). It is speculated that the $[Et_3Si]^+$ fragment of the two isomers [**5A**][$BArF_{24}$] and [**5A'**][$BArF_{24}$] "feels" slightly different electronic environment depending on its position within the [IrH] motif (see X-ray structures). Therefore, we propose that $[Et_3Si]^+$ [**5A**][$BArF_{24}$] has a slightly more electrophilic Si atom due to its closer spatial position with the carbanionic C11 atom (figure 20a) than it is the case for [**5A'**][$BArF_{24}$] (see appendix), thus explaining the slightly highfiled ^1H and downfield ^{29}Si chemical shifts of $[Et_3Si]^+$ in [**5A**][$BArF_{24}$] when compared to [**5A'**][$BArF_{24}$].

The structure of [**5A**][$BArF_{24}$] (figure 20a), displays a particular geometry within the Ir1–H1A–Si1 motif, which is at first glance reminiscent of an η^1-$HiSEt_3$ coordination mode to iridium. However, the Ir1–H1A bond length of ~1.43 Å is not precise enough as the position of the hydride H1A could not be refined, though located from Fourier difference maps. As a consequence, the H1A–Si1distance of ~1.57 Å is by far shorter from what it is expected for a almost totally cleaved H–Si bond ($J_{H–Si}$ =20 Hz) as it was observed for [**3A**][$BArF_{24}$] (H–Si distance of ~2.10 Å). DFT-D calculations conducted on [**5A**][$BArF_{24}$] (not described in this thesis) showed that actually this complex has very similar geometrical, structural and electronic parameters as those found for [**3A**][$BArF_{24}$].

The structure of [**5B**][$BArF_{24}$] (figure 20b), displays very similar geometrical features than those of [**3B**][OTf] (table 8). However, a closer analysis within the bonding of the Ir1–H1A–Ir2 motif and its comparison to those of [**3B**][OTf] revealed a slightly longer Ir1–HA1 distance which amounts ~1.86 Å as compared to 1.63(6) Å for [**3B**][OTf]. In contrast, the Ir2–H1A of ~1.79 Å in [**5B**][$BArF_{24}$] is identical to the Ir2–H1 distance of ~1.79(6) Å found in [**3B**][OTf]. Even though the position of the hydride H1A could not be refined, it was however located from Fourier difference maps. As we have recently shown with a deep analysis study of the similar ionic complex [**3B**][OTf],[82] the difference between Ir1–H1A and Ir2–H1A distances in [**5B**][$BArF_{24}$] is the result of the intrinsic Lewis donor-acceptor interaction established between the Lewis donor [IrH] and the Lewis acceptor $[Ir]^+$ (*vide infra*). The structure of [**5B**][$BArF_{24}$] indicates π–π stacking interactions between the two C,N ligands, a structural feature similar to that reported previously for [**3B**][OTf] (figure 16) and another catalytically inactive μ-hydrido-bridged bisruthenacycle.

[82] Hamdaoui, M.; Ney, M.; Sarda, V.; Karmazin, L.; Bailly, C.; Sieffert, N.; Dohm, S.; Hansen, A.; Grimme, S.; Djukic, J.-P. Evidence of a Donor–Acceptor (Ir–H)→SiR_3 Interaction in a Trapped Ir(III) Silane Catalytic Intermediate. *Organometallics* **2016**, *35* (13), 2207–2223.

2.2.12 Investigation of the structure of [**3A**][$BArF_{24}$] by DFT methods.

To establish the bonding relationship within the critical Si–Ir–H motif of [**3A**][$BArF_{24}$], DFT investigations were carried out using DFT-D functionals[83] that reproduce the effect of non-local dispersion interactions.[84,85] Computations carried out with generalized gradient approximation (GGA), meta-GGA and hydrid functionals (ZORA PBE-D3(BJ), TPSS-D3(BJ) and PBE0-dDsC, respectively) associated with a Slater-type basis set (TZP) produced geometries displaying good match with the X-ray diffraction-based structure (figure 19b). Geometry optimizations using GGA and hybrid functionals (PBE-D3 and PBE0-D3, respectively) associated with an effective core potential gaussian-type basis set (ECP SDD) performed satisfactorily as well. The map of electrostatic potential (MEP) shown in figure 21a clearly shows that the Si atom carries the greatest charge density depletion in [**3A**]$^+$, which according to Natural Population Analysis[86] (NPA, figure 22) assigns to the Si atom the highest partial positive natural charge. Figure 21b displays Non-Covalent Interaction (NCI) regions determined on the basis of the reduced density gradients method.[87]

Apart from the blue-colored isosurfaces that depict non-bonded van der Waals interactions and Pauli repulsion areas, the typical red-colored NCI isosurface ring that surrounds the Si–Ir bond and the Si–H interaction within a so-called *covalent through*[88] indicates that the Si center interacts covalently with the Ir center.

---

[83] a) Grimme, S.; Ehrlich, S.; Goerigk, L. Effect of the damping function in dispersion corrected density functional theory. *J. Comp. Chem.* **2011**, *32*, 1456-1465. b) Steinmann, S. N.; Corminboeuf, C. Comprehensive Benchmarking of a Density-Dependent Dispersion Correction. *J. Chem. Theor. Comp.* **2011**, *7*, 3567-3577.

[84] a) Hyla-Kryspin, I.; Grimme, S.; Djukic, J.-P. The Cr–Mn Interaction in syn-Facial [Tricarbonyl(benzyl)chromium]manganesetricarbonyl Complexes: A Non-Covalent Metal–Metal Bond. *Organometallics* **2009**, *28*, 1001-1013. b) Schwabe, T.; Grimme, S.; Djukic, J.-P. Noncovalent Metal–Metal Interactions: The Crucial Role of London Dispersion in a Bimetallic Indenyl System. *J. Am. Chem. Soc.* **2009**, *131*, 14156-14157. c) Grimme, S.; Djukic, J.-P. The Crucial Role of Dispersion in the Cohesion of Nonbridged Binuclear Os → Cr and Os → W Adducts. *Inorg. Chem.* **2010**, *49*, 2911-2919. d) Grimme, S.; Djukic, J.-P. Cation–Cation "Attraction": When London Dispersion Attraction Wins over Coulomb Repulsion. *Inorg. Chem.* **2011**, *50*, 2619-2628. e) Werlé, C.; Karmazin, L.; Bailly, C.; Ricard, L.; Djukic, J.-P. Stabilization of an Electron-Unsaturated Pd(I)-Pd(I) Unit by Double Hemichelation. *Organometallics* **2015**, *34*, 3055-3064.

[85] Petrović, P.; Djukic, J.-P.; Hansen, A.; Bannwarth, C.; Grimme, S. In *Non-Covalent Interactions in the Synthesis and Design of New Compounds*; Maharramov, A. M., Kamran T. Mahmudov, Kopylovich, M. N., Pombeiro, A. J. L., Eds.; John Wiley & Sons: 2016, p 115-143.

[86] Weinhold, F. In *Encyclopedia of Computational Chemistry*; von Ragué-Schleyer, P., Allinger, N. L., Clark, T., Gasteiger, J., Kollman, P. A., Schaefer, H. F., Schreiner, P. R., Eds.; John Wiley & Sons, Chichester, UK: 1998; Vol. 3, p 1792-1811.

[87] a) Contreras-Garcia, J.; Johnson, E. R.; Keinan, S.; Chaudret, R.; Piquemal, J. P.; Beratan, D. N.; Yang, W. NCIPLOT: A Program for Plotting Noncovalent Interaction Regions. *J. Chem. Theor. Comput.* **2011**, *7*, 625-632. b) Johnson, E.; Keinan, S.; Mori-Sanchez, P.; Contreras-Garcia, J.; Cohen, A. J.; Yang, W. Revealing Noncovalent Interactions. *J. Am. Chem. Soc.* **2010**, *132*, 6498-6506.

[88] Werlé, C.; Karmazin, L.; Bailly, C.; Ricard, L.; Djukic, J.-P. Stabilization of an Electron-Unsaturated Pd(I)–Pd(I) Unit by Double Hemichelation. *Organometallics* **2015**, *34*, 3055-3064.

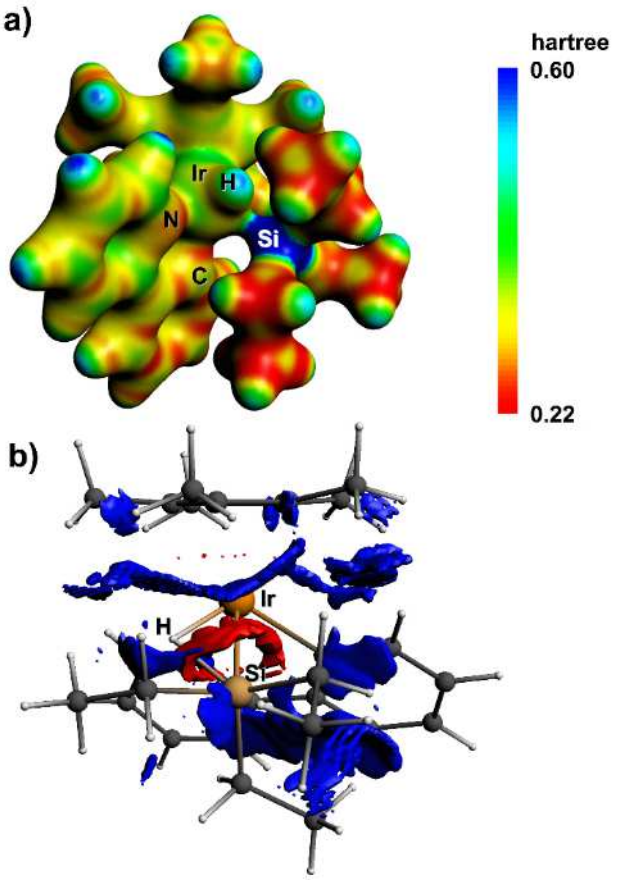

Figure 21. a) Map of electrostatic potential (MEP) drawn on the isosurface (0.05 e•bohr^{-3}) of the self-consistent field electron density of a gas phase singlet ground state model of [**3A**]$^{+}$. **b)** ADFview2013 plots of non-covalent interaction (NCI) regions materialized by reduced density gradient isosurfaces (cut-off value s = 0.02 a.u., ρ =0.05 a.u.) colored according to the sign of the signed density $\lambda_2\rho$. Red (attractive) and blue (Pauli repulsive or non-bonded van der Waals) isosurfaces are associated with negatively and positively signed terms respectively.

Topological analysis of the electron density following the Quantum Theory of Atoms in Molecules[89] (QTAIM from the AIMAll[90] software) was performed at the PBE0-D3 and PBE-D3 levels with effective core potential (ECP) gaussian-type Stuttgart/Dresden (SDD) contracted and diffuse basis sets. Table 10 lists the main topological electron density parameters for the Si–Ir–H motif, i.e. the electron density ρ_β at bond critical points (3,-1), the laplacian of the density $\nabla^2\rho_\beta$, the bond ellipticity (ε) and the interatomic electron delocalization index (δ(A,B)). This QTAIM analysis reveals that bond critical points (BCP (3,–1)) exist for Ir–Si and Ir–H bond paths

[89] Bader, R. F. W. In *Atoms in Molecules: A Quantum Theory*; Clarendon: Oxford, 1990.
[90] Keith, T. A.; TK Gristmill Software: Overland Park KS, USA, 2016.

(table 10). However, no BCP (3,−1) and bond path were found for a Si–H interaction. Identical conclusions were drawn from QTAIM investigations carried out with hybrid PBE0-dDsC, meta-GGA TPSS-D3(BJ) or GGA PBE-D3(BJ) functionals associated with Slater-type basis sets of various sizes and number of polarization functions (with or without scalar ZORA correction, using all electron TZP or TZ2P basis sets fit with diffuse functions in the case of the PBE0 functional). The observed basis-set dependence of the computed value of $\nabla^2\rho_\beta$ at BCPs of Ir–H and Ir–Si bonds (table 10) is a known behavior of QTAIM for heteropolar bonds.[91] It is also generally considered that the laplacian for such bonds can adopt either a positive or negative value.[92] The delocalization index δ(A,B),[93] which provides a measure of electron delocalization probability between two atomic basins, follows the trend of Wiberg indexes (figure 22 and table 10) for the Si–Ir–H motif: δ(Ir,H)>δ(Ir,Si) >> δ(H,Si) (table 10). Its value clearly suggests a stronger Ir–H bond and a weaker Ir–Si interaction. The low but significant value of δ(H,Si) suggests an evanescent interaction that cannot be dismissed as unimportant to the cohesion of the complex. The value of the bond ellipticity ε[94,95] for the Ir–H bond ($\varepsilon \sim 0$, table) is consistent with a cylindrically symmetric bond and a more localized bonding interaction directed towards the Ir center. In the case of the Ir–Si bond the value of the elllipticity ($0.5 < \varepsilon < 1$, table 10) might indicate delocalization of the respective bonding electrons. On the main QTAIM features, all computations suggest a strong Ir–H bond, a weaker Ir–Si bond and the absence of a significant covalent H–Si interaction. Finally, figure 23 displays the so-called localization domains for two different isosurface plots of the electron localization function[96] (ELF) $\eta(r)$ (values of $\eta(r)$ greater than 0.5 usually denote larger electron localization).[9755] Monosynaptic core (C(Ir) and C(Si) and C(C)), disynaptic and polysynaptic basins (V(C,H), V(Ir,Si), V(Ir,H)) are drawn at two values of the ELF ($\eta(r)$= 0.55 and 0.70 in figure 23).

---

[91] Jabłonski, M.; Palusiak, M. Basis Set and Method Dependence in Quantum Theory of Atoms in Molecules Calculations for Covalent Bonds. *J. Phys. Chem. A* **2010**, *114*, 12498-12505.
[92] Grimme, S.; Djukic, J.-P. The Crucial Role of Dispersion in the Cohesion of Nonbridged Binuclear Os → Cr and Os → W Adducts. *Inorg. Chem.* **2010**, *49*, 2911-2919.
[93] a) Fradera, X.; Poater, J.; Simon, S.; Duran, M.; Sola, M. Electron-pairing analysis from localization and delocalization indices in the framework of the atoms-in-molecules theory. *Theor. Chem. Acc.* **2002**, *108*, 214-224. b) Bader, R. F. W.; Streitwieser, A.; Neuhaus, A.; Laidig, K. E.; Speers, P. Electron Delocalization and the Fermi Hole. *J. Am. Chem. Soc.* **1996**, *118*, 4959-4965.
[94] Bader, R. F. W. In *Atoms in Molecules: A Quantum Theory*; Clarendon: Oxford, 1990.
[95] Lopez, C. S.; de Lera, A. R. Bond Ellipticity as a Measure of Electron Delocalization in Structure and Reactivity. *Curr. Org. Chem.* **2011**, *15*, 3576-3593.
[96] Savin, A.; Nesper, R.; Wengert, S.; Fässler, T. F. ELF: The Electron Localization Function. *Angew. Chem. Int. Ed. Eng.* **1997**, *36*, 1808-1832.
[97] Fowe, E. P.; Therrien, B.; Suss-Fink, G.; Daul, C. A Combined Charge and Energy Decomposition Scheme for Bond Analysis. *Inorg. Chem.* **2008**, *47*, 42-48.

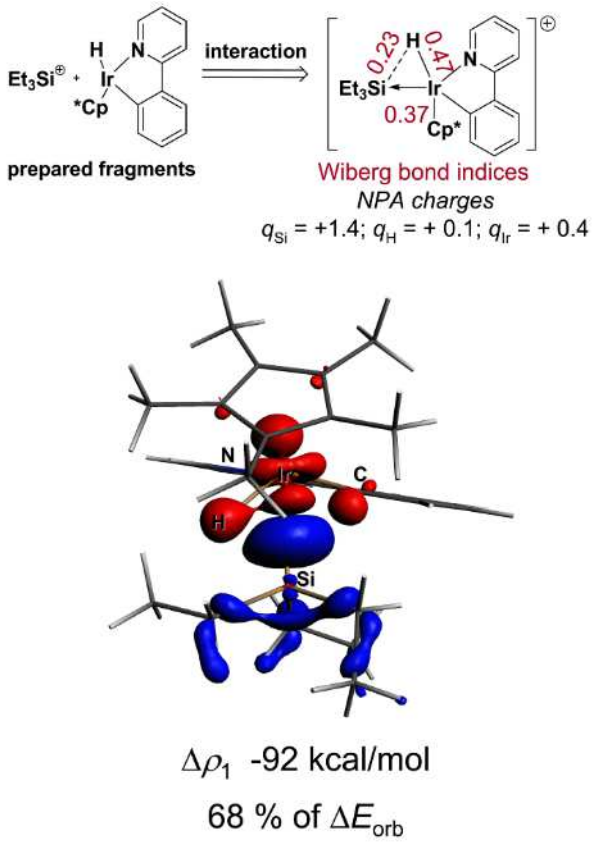

Figure 22. Wiberg bond indexes and NPA[72] charges at atoms of interest (top) computed at the ZORA-PBE-D3(BJ)/ae-TZP level. ADFview2013 isosurface plot of deformation density $\Delta\rho_1$ (0.005 e•bohr^{-3}) produced by an ETS-NOCV[98] analysis according to the realistic fragmentation scheme chosen for [**3A**]$^+$: electron density transfer operates from the red to the blue-colored volumes upon interaction.

At values 0.55 < $\eta(r)$ <0.7, the ELF disynaptic basin located at the Ir–Si segment merges partly with the Ir,H valence basin. Figure 23 displays the same disynaptic basin located at the Ir–Si segment for $\eta(r)$ = 0.7, which further supports the hypothesis of a dominant dative Ir→Si component within the slightly delocalized (Ir–H)→Si interaction.

Extended transition state – natural orbital for chemical valence (ETS-NOCV) analysis[90] was carried out considering the fragmentation scheme displayed in figure 22. The latter

[98] a) Mitoraj, M. P.; Michalak, A.; Ziegler, T. On the Nature of the Agostic Bond between Metal Centers and β-Hydrogen Atoms in Alkyl Complexes. An Analysis Based on the Extended Transition State Method and the Natural Orbitals for Chemical Valence Scheme (ETS-NOCV). *Organometallics* **2009**, *28*, 3727-3733. b) Mitoraj, M. P.; Michalak, A.; Ziegler, T. A Combined Charge and Energy Decomposition Scheme for Bond Analysis. *J. Chem. Theory Comput.* **2009**, *5*, 962-975.

Table 10. QTAIM and NBO analysis of [**3A**][$BArF_{24}$] performed on three different geometries.

Geometry opt. level [c]	Analysis level [d]	Path	QTAIM [a]				NBO [b]
			ρ_β	$\nabla^2\rho_\beta$	ε	δ(A,B)	WBI
ZORA-PBE0-dDsC/	PBE0-D3/	Ir-Si	0.0723	–0.0689	0.68	0.43	0.43
ae-TZP	SDD	Ir-H	0.1618	0.0036	0.05	0.85	0.55
	6-311++G** [e]	Si…H	[f]	[f]	[f]	0.14	0.21
ZORA-PBE0-dDsC/	PBE0-D3/	Ir-Si	0.0741	–0.0701	0.69	0.40	0.42
ae-TZP	SDD	Ir-H	0.1646	–0.0234	0.08	0.87	0.55
	def2-TZVPP	Si…H	[f]	[f]	[f]	0.13	0.20
PBE0-D3/	PBE0-D3/	Ir-Si	0.0728	–0.0706	0.98	0.40	0.42
SDD	SDD	Ir-H	0.1610	–0.0108	0.08	0.86	0.55
def2-TZVPP	def2-TZVPP	Si…H	[f]	[f]	[f]	0.14	0.22
PBE-D3/	PBE-D3/	Ir-Si	0.0720	–0.0658	0.55	0.49	0.44
SDD	SDD	Ir-H	0.1589	–0.0242	0.08	0.84	0.55
def2-TZVPP	def2-TZVPP	Si…H	[f]	[f]	e	0.14	0.19
ZORA-PBE0-dDsC/	ZORA-PBE0-dDsC/	Ir-Si	0.0734	–0.0605	[g]	[g]	0.35
ae-TZP	ae-TZ2P	Ir-H	0.1639	0.0111	[g]	[g]	0.45
		Si…H	[f]	[f]	[g]	[g]	0.26
ZORA-PBE0-dDsC/	ZORA-PBE0-dDsC/	Ir-Si	0.0738	0.0169	[g]	[g]	[g]
ae-TZP	ae-QZ4P	Ir-H	0.1632	0.0041	[g]	[g]	[g]
		Si…H	[f]	[f]	[g]	[g]	[g]

[a] QTAIM analysis: electron density (ρ_β), laplacian of the electron density ($\nabla^2\rho_\beta$) and bond ellipticity (ε) at bond critical points, delocalization index δ(A,B) between the pair of atoms (A,B) (all values are given in au). [b] Wiberg bond index (WBI), as obtained from NBO analysis. [c] Level of theory used in the structure optimization. [d] Level of theory used in QTAIM and NBO analyses. [e] identical results were obtained with a 6-311+G** basis set. [f] No value because no bond critical point (3,-1) was localized for this interaction. [g] not computed.

fragmentation scheme is not artificial though: it was chosen on the basis of the experimentally established reactivity of [**3A**][$BArF_{24}$] (*vide supra*, DMAP and TfO^- quenching experiments) that behaves as a source of electrophilic $[Et_3Si]^+$ moiety. This "realistic" scheme entails a donor-acceptor pair formulation such that [**3A**][$BArF_{24}$] ≡ [$\mathbf{4}_{Ir}\rightarrow SiEt_3$][$BArF_{24}$]. Plot of the deformation density isosurface $\Delta\rho_1$ (corresponding to 68 % of the total orbital interaction energy $\Delta E_{orb.} = -135$ kcal/mol) suggests that upon interaction between prepared geometries of **4** and $[Et_3Si]^+$ electron

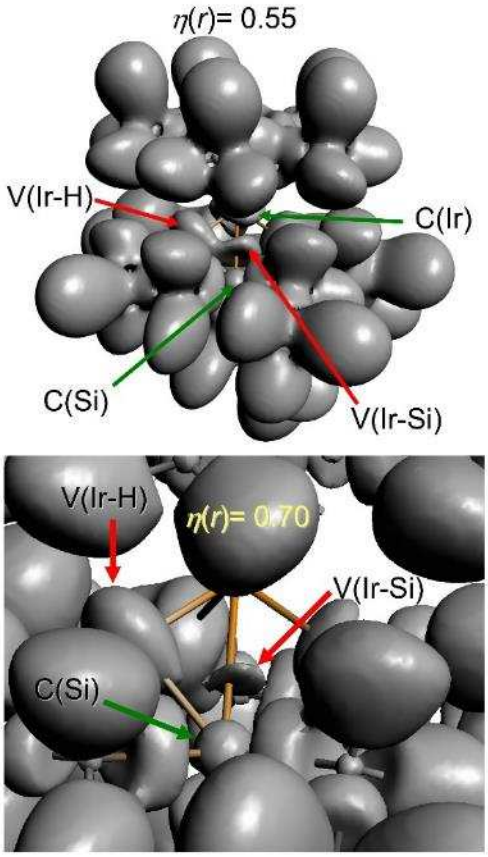

Figure 23. Isosurface plots of the ELF[88] of [**3A**]+ with values of $\eta(r)$ of 0.55 (top) and 0.77 (bottom) with enlarged view of the localization basins for the Si–Ir–H motif.

density donation operates 1) from the Ir center and to a lesser extent 2) from the Ir-bound H atom and chelate's C_{Ar} atom. This density donation operates towards a broad volume of space (blue-colored in figure 22) surrounding the Ir–Si segment and the σ Si–C bonds at the Et_3Si fragment.

This comprehensive analysis converges to a rather "simplified" picture of the bonding situation within the Si–Ir–H motif, that is a donor-acceptor interaction between the Ir–H unit and the Si atom with a largely dominant contribution of the Ir–Si interaction and a minor one of the Si–H interaction.

2.2.13 [**3A**][$BArF_{24}$]: Ir(III) or Ir(V)?

The reactivity of [**3A**][$BArF_{24}$] towards Lewis donors serves as a base to establish the formal oxidation state of the Ir center. According to Tilley and Bergman, Ir(V) species might play an

important role in C–H and E–H activation reactions.[99] A priori, [**3A**][$BArF_{24}$] could be formulated as an 18 electron $[ML_3X_4]^+$ Ir(V) complex (of neutral equivalent formula $[ML_2X_5]$) according to Green's formalism.[100] However, the fact that the silylium fragment can putatively be abstracted by weak Lewis bases such as $[BF_4]^-$ or $[OTf]^-$ and also by the stronger DMAP[101] to give **4** is clear evidence that the Et_3Si moiety in [**3A**][$BArF_{24}$] is a Z ligand and not an X ligand.[102] The silylium $[Et_3Si]^+$ is indeed isoelectronic to neutral boranes BR_3 that are prototypical Z-type ligands. Therefore, a $[ML_3X_3Z]$ formulation would be more appropriate for [**3A**][$BArF_{24}$].[96a] Furthermore, the electron density donation from the Ir center towards the Si center in [**3A**][$BArF_{24}$] is too weak to consider the Ir center as holding a +V formal oxidation state according to DFT calculations. The difference of the sum of atomic natural charges at the Et_3Si moiety in [**3A**][$BArF_{24}$] and at the "gas-phase" silylium, i.e. $\Delta\Sigma q(SiEt_3) = [(\Sigma q_i)_{[3]+} - 1]$, where q_i stands for the natural charge of atom *i* in the Et_3Si moiety and 1 is the charge of the gas-phase silylium, provides a hint on the extent of the charge density transfer from the Ir towards the Et_3Si moiety. It must be noted that natural charges (NPA) follow properly the trend of the charge density and can be used to characterize the overall electron density enrichment or depletion at given molecular fragments.[103,104] The value of $\Delta\Sigma q(SiEt_3)$ amounts −0.16 ($(\Sigma q_i)_{[3]+}$ = +0.84) for the Et_3Si moiety in [**3A**][$BArF_{24}$], which means that only 1/6th of the positive charge of [**3A**]$^+$ is borne by fragment **4** in [**3A**]$^+$. The conversion of [**2**][$BArF_{24}$] into [**3A**][$BArF_{24}$] can therefore be considered as isohypsic at Ir, i.e. as taking place at a constant formal +III oxidation state. Consequently, it is proposed that the mechanism of formation of [**3A**][$BArF_{24}$] implies the hydride transfer from $HSiEt_3$ to the Ir center of transient [**2+**][$BArF_{24}$] and the concerted bonding of the silylium cation to the new hydrido-iridium unit (scheme 14), rather than a conventional oxidative-addition step, an hypothesis that is currently under investigation. Whether the transfer

---

[99] Klei, S. R.; Tilley, T. D.; Bergman, R. G. The Mechanism of Silicon-Hydrogen and Carbon-Hydrogen Bond Activation by Iridium (III): Production of a Silylene Complex and the First Direct Observation of Ir(III)/Ir(V) C-H Bond Oxidative Addition and Reductive Elimination. *J. Am. Chem. Soc.* **2000**, *122*, 1816-1817.

[100] Parkin, G. Valence, Oxidation Number, and Formal Charge: Three Related but Fundamentally Different Concepts. *J. Chem. Ed.* **2006**, *83*, 791.

[101] a) Gutsulyak, D. V.; van der Est, A.; Nikonov, G. I. Facile Catalytic Hydrosilylation of Pyridines. *Angew. Chem. Int. Ed.* **2011**, *50*, 1384 -1387. b) Osakada, K. 1,4-Hydrosilylation of pyridine by ruthenium catalyst: A new reaction and mechanism. *Angew. Chem. Int. Ed.* **2011**, *50*, 3845 - 3846.

[102] a) Green, M. L. H. A new approach to the formal classification of covalent compounds of the elements. *J. Organomet. Chem.* **1995**, *500*, 127-148. b) Amgoune, A.; Bourissou, D. σ-Acceptor, Z-type ligands for transition metals. *Chem. Commun.* **2011**, *47*, 859-871.

[103] Hyla-Kryspin, I.; Grimme, S.; Djukic, J.-P. The Cr–Mn Interaction in syn-Facial [Tricarbonyl(benzyl)chromium]manganesetricarbonyl Complexes: A Non-Covalent Metal–Metal Bond. *Organometallics* **2009**, *28*, 1001-1013.

[104] a) Djukic, J.-P.; Fetzer, L.; Czysz, A.; Iali, W.; Sirlin, C.; Pfeffer, M. One-Pot Generation of a Tris-cationic Homobimetallic Planar-Chiral Ruthenacycle. *Organometallics* **2010**, *29*, 1675-1679. b) Djukic, J.-P.; Iali, W.; Pfeffer, M.; Le Goff, X.-F. Synthesis of Planar Chiral Iridacycles by Cationic Metal π-Coordination: Facial Selectivity, and Conformational and Stereochemical Consequences. *Chem. - Eur. J.* **2012**, *18*, 6063-6078.

of the silylium cation to Ir is concerted or not is still an unsettled question. However, an alternative proposal is that the heterolytic H–Si bond cleavage can be viewed to occur with an "asymmetric" manner, that is to say through a hydride transfer from Si to Ir followed by the "trapping" of the $[Et_3Si]^+$ moiety by molecule **4**, thus giving rise to the donor-acceptor structure that we propose for [**3A**][$BArF_{24}$]. The latter proposal is supported by DFT calculations (in collaboration with Stephan Grimme and coworkers, not published). Indeed, the polar character of the H–Si bond in $HSiEt_3$ characterized by marked negative natural charge (NPA computed at the ZORA-PBE-D3(BJ)/ae-TZP level, *q*(Si-*H*)= –0.19) at the (Si-bound) H atom and positive partial natural charge at the Si atom (NPA, *q*(*Si*-H)= +1.22) creates a predisposition to hydride transfer that is well documented.[105]

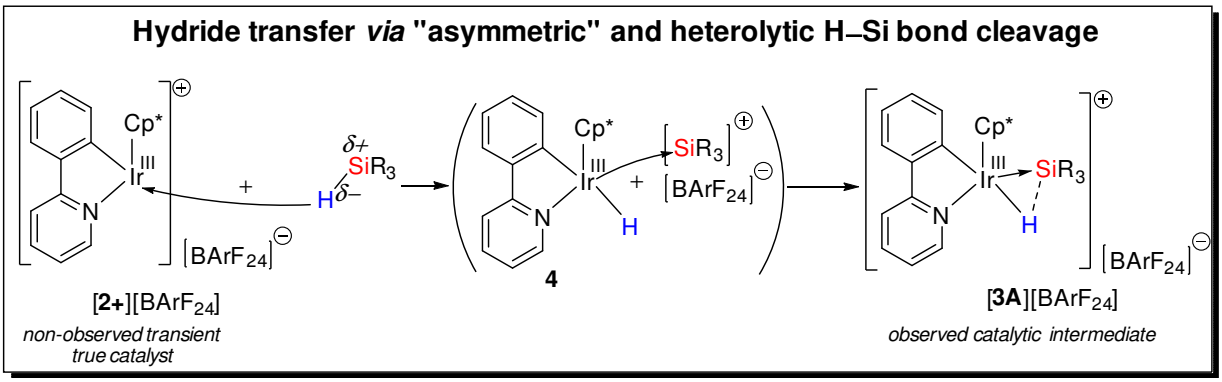

Scheme 14. Proposed mechanism for the formation of [**3A**][$BArF_{24}$] from $HSiEt_3$ and [**2+**][$BArF_{24}$].

2.2.14 Proposed catalytic cycle for the *O*-silylation of alcohols

The results disclosed point to complex $[\mathbf{3A}]^+$ as the most direct product of the activation of $[\mathbf{2}]^+$ by $HSiEt_3$. As such its capability to readily release the $[Et_3Si]^+$ cation is central to the catalysis, for the *O*-silylation of alcohols to take place the silylium cation must be transferred from $[\mathbf{3A}]^+$ in the early stages of the reaction in a way similar to that depicted by Brookhart and co-workers

[105] a) Carey, F. A.; Tremper, H. S. Carbonium ion-silane hydride transfer reactions. I. Scope and stereochemistry. *J. Amer. Chem. Soc.* **1968**, *90*, 2578-2583. b) Carey, F. A.; Tremper, H. S. Carbonium ion-silane hydride transfer reactions. II. 2-Phenyl-2-norbornyl cation. *J. Org. Chem.* **1969**, *34*, 4-6. c) Carey, F. A.; Hsu, C.-L. W. Carbonium ion-silane hydride transfer reactions IV. Structure and reactivity at silicon. *J. Organomet. Chem.* **1969**, *19*, 29-41. d) Carey, F. A.; Tremper, H. S. Carbonium ion-silane hydride transfer reactions. V. tert-Alkyl cations. *J. Org. Chem.* **1971**, *36*, 758-761. e) Chojnowski, J.; Wilczek, L.; Fortuniak, W. The mechanism of hydride transfer from silicon to a carbenium ion in a weakly nucleophilic medium. *J. Organomet. Chem.* **1977**, *135*, 13-22. f) Mayr, H.; Basso, N.; Hagen, G. Kinetics of hydride-transfer reactions from hydrosilanes to carbenium ions. Substituent effects in silicenium ions. *J. Am. Chem. Soc.* **1992**, *114*, 3060-3066. g) Voskoboynikov, A. Z.; Parshina, I. N.; Shestakova, A. K.; Butin, K. P.; Beletskaya, I. P.; Kuz'mina, L. G.; Howard, J. A. K. Reactivity of Lanthanide and Yttrium Hydrides and Hydrocarbyls toward Organosilicon Hydrides and Related Compounds. *Organometallics* **1997**, *16*, 4041-4055.

for the catalyzed cleavage of alkyl ethers with $HSiEt_3$.[106] Whether the transfer occurs within the coordination sphere of the Ir center in [**3A**]$^+$ with the concerted deprotonation of the [R-O(H)-SiR'$_3$]$^+$ intermediate, or inter-molecularly in the solution bulk is not settled. Scheme 15 depicts a simplified outer-sphere mechanism[107] that accounts for the KIE observed with MeOD(H). This

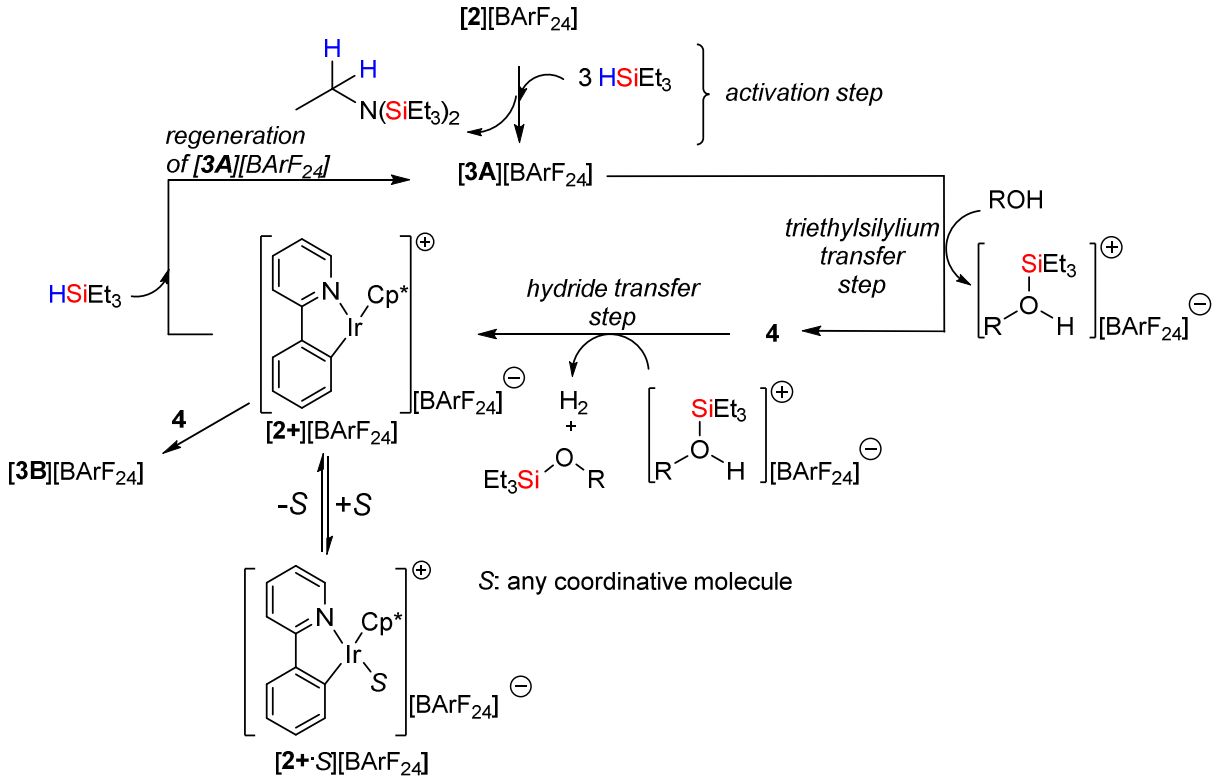

Scheme 15. Proposed catalytic cycle for the *O*-silylation of alcohols promoted by [**2**][BArF$_{24}$].

mechanism is of course valid for both [**2**]$^+$ and [**4**]$^+$ precatalysts, and more generally for every catalytically active complex disclosed in this thesis. The renewal of [**3A**][BArF$_{24}$] in the cycle results from reaction of transient [**2+**][BArF$_{24}$] with $HSiEt_3$. [**2+**][BArF$_{24}$] can be produced by reaction of **4** with the Brønsted acid [R-O(H)-SiR'$_3$]$^+$. Complex [**3B**][BArF$_{24}$], can therefore arise from a reaction of **4** with transient [**2+**][BArF$_{24}$] or its solvated form [**2+**•*S*][BArF$_{24}$] (*S*= alcohol, alkoxytriethylsilane, etc…). Even though [**3B**]$^+$ was shown to produce low amounts of **4** in the

[106] Yang, J.; White, P. S.; Brookhart, M. Scope and Mechanism of the Iridium-Catalyzed Cleavage of Alkyl Ethers with Triethylsilane. *J. Am. Chem. Soc.* **2008**, *130*, 17509-17518.

[107] a) Metsanen, T. T.; Hrobarik, P.; Klare, H. F. T.; Kaupp, M.; Oestreich, M. Insight into the mechanism of carbonyl hydrosilylation catalyzed by Brookhart's cationic iridium(III) pincer complex. *J. Am. Chem. Soc. Rev.* **2014**, *136*, 6912- 6915. b) Iglesias, M.; Fernandez-Alvarez, F. J.; Oro, L. A. Outer-sphere ionic hydrosilylation catalysis. *ChemCatChem* **2014**, *6*, 2486 - 2489.

presence $HSiEt_3$, the poor catalytic activity of this dinuclear species seemingly disqualifies it for any major contribution to the *O*Si reaction.

The origin of the above mentioned kinetic second order in [**2**][$BArF_{24}$] determined from initial reaction rates cannot be assigned with certainty at this stage. Finally, in the case of [**2**][OTf] a similar outer-sphere catalytic cycle (not shown here) devoid of [**3A**]$^+$ involving the reaction of the *in situ*-formed Et_3SiOTf with the alcohol can be envisaged.

2.2.15 Hydrido-iridium(III) complex **4**, an ambident Lewis donor.

Our results echo recent claims by Templeton et al. on the Lewis donor character of **4**.[108] The latter authors reported the adventitious formation of [**4**→Ag←**4**]$^+$ from reaction of **4** with silver(I) salts. Several other examples of donor-acceptor metal-silver and metal-metalloid complexes have been reported by Braunschweig et al.[109] The crystal structure of [**4**→Ag←**4**]$^+$ (Cambridge Structural Database refcode BIQGOZ) reveals geometric features akin to those of [**3A**][$BArF_{24}$]: the piano stool subunits that are related by an inversion center located at the bridging Ag atom are four-legged and the Ir centers are formally heptacoordinated. Even though Templeton et al. did not localize the two hydrido ligands in the published X-ray diffraction structure, the position of the Ag atom in this hetero-trimetallic complex leaves no doubts about their respective positions closeby the silver center.

Having in scope the emerging property of Ir(III) complex **4** as a peculiar Lewis donor we undertook a DFT study of Templeton's complex, looking for possible similarities with [**3A**][$BArF_{24}$]. The gas phase singlet ground state geometry of [**4**→Ag←**4**]$^+$ was optimized at the ZORA-PBE-D3(BJ)/ae-TZP level with the C_i symmetry. Figure 24 displays the corresponding geometry decorated with a NCI region plot. The main interatomic distances match the structural X-ray diffraction analysis data. More interesting are the Ir–H distances of ca. 1.66 Å and the hydridic H-to-Ag distances of 1.90 Å, which corroborate Templeton's report

[108] Turlington, C. R.; Harrison, D. P.; White, P. S.; Brookhart, M.; Templeton, J. L. Probing the oxidation chemistry of half-sandwich iridium complexes with oxygen atom transfer reagents. *Inorg. Chem.* **2013**, *52*, 11351-11360.

[109] a) Braunschweig, H.; Gruss, K.; Radacki, K. Interaction between d- and p-block metals: synthesis and structure of platinum-alane adducts. *Angew. Chem. Int. Ed.* **2007**, *46*, 7782 -7784. b) Braunschweig, H.; Brunecker, C.; Dewhurst, R. D.; Schneider, C.; Wennemann, B. Lewis Acid Binding and Transfer as a Versatile Experimental Gauge of the Lewis Basicity of Fe0, Ru0, and Pt0 Complexes. *Chem. Eur. J.* **2015**, *21*, 19195 -19201. c) Braunschweig, H.; Dewhurst, R. D.; Hupp, F.; Schneider, C. Silver(I) and thallium(I) cations as unsupported bridges between two metal bases. *Chem. Commun.* **2014**, *50*, 15685-15688. d) Braunschweig, H.; Dewhurst, R. D.; Hupp, F.; Kaufmann, C.; Phukan, A. K.; Schneidera, C.; Yea, Q. Gauging metal Lewis basicity of zerovalent iron complexes via metal-only Lewis pairs. *Chem. Sci.* **2014**, *5*, 4099-4104. e) Bauer, J.; Bertermann, R.; Braunschweig, H.; Gruss, K.; Hupp, F.; Kramer, T. New Metal-Only Lewis Pairs : Elucidating the Electronic In fl uence of. *Inorg. Chem.* **2012**, *51*, 5617–5626.

of a significant $J_{H\text{-}Ag}$ coupling constant in the ^{1}H NMR spectrum of [**4**→Ag←**4**]$^+$.[101] The attractive NCI domain is located in the close vicinity of the Ag–Ir segment; part of it contains a covalent through that surrounds the H–Ag and Ir–H segments whereas the remaining plain NCI isosurface somewhat eclipses the Ir–C_{Ar} bond of the neighboring iridacycle.

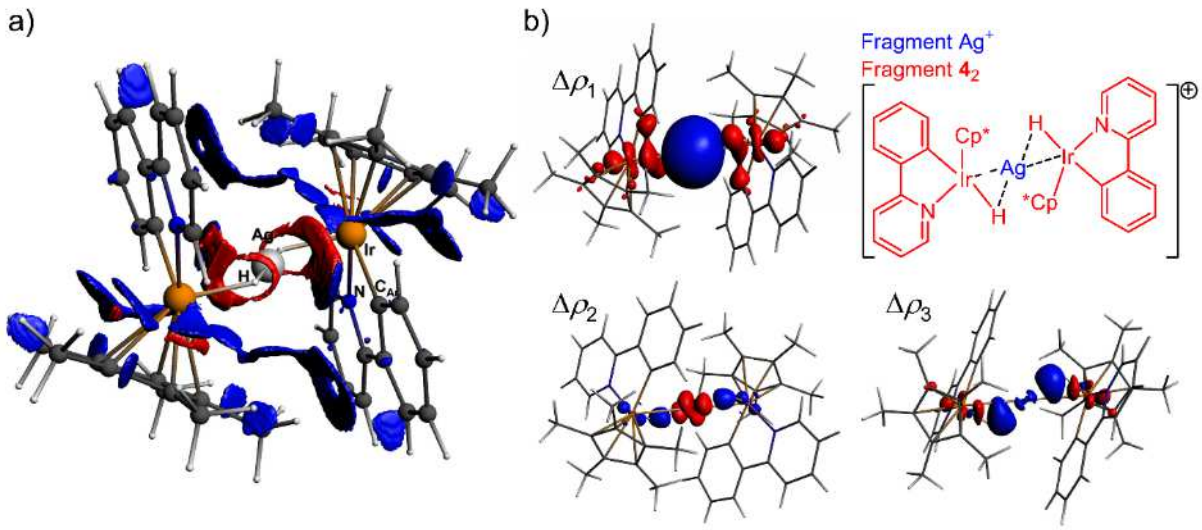

Figure 24. **a)** Gas-phase singlet ground state geometry of Templeton's [**4**→Ag←**4**]$^+$ complex optimized at the ZORA-PBE-D3(BJ)/ae-TZP level decorated with an ADFview2013 plot of non-covalent interaction (NCI) regions (ZORA-PBE0-dDsC/ae-TZP) within [**4**→Ag←**4**]$^+$ materialized by reduced density gradient isosurfaces (cut-off value s = 0.02 a.u., ρ =0.05 a.u.) colored according to the sign of the signed density $\lambda_2\rho$. Red (attractive) and blue (Pauli repulsive or non-bonded van der Waals) isosurfaces are associated with negatively and positively signed terms respectively. Selected interatomic distances (Å) and angles (°):Ir–H 1.661, H–Ag 1.902, Ir–Ag 2.736 (exptl ~2.716), Ir–C_{Ar} 2.058 (exptl 2.055), Ir–N 2.079 (exptl 2.031), Ag–Ir–CAr 67.8 (exptl 71.3) and Ag–Ir–N 103.3 (exptl 108.2). **b)** ADFview2013 isosurface plots of deformation densities $\Delta\rho_1$, $\Delta\rho_2$ and $\Delta\rho_3$ (0.002 e•bohr^{-3}) produced by an ETS-NOCV[90] analysis according to the depicted fragmentation scheme chosen for [**4**→Ag←**4**]$^+$: electron density transfer operates from the red to the blue colored volumes upon interaction.

QTAIM analysis (ZORA-PBE0-DdSc/ae-TZ2P) indicates no BCP (3,–1) and bond path in the Ir–Ag segments (Wiberg bond index w= 0.10). Within the Ir–H–Ag motif the only existing BCPs (3,–1) are for Ir–H (w= 0.50, ρ_β= 0.134, $\nabla^2\rho_\beta$= 0.072) and Ag–H (w= 0.15, ρ_β= 0.069, $\nabla^2\rho_\beta$= 0.140) bond paths. The latter two interactions match the criteria of relatively strong and weak

polar bonds, respectively. Analysis of the NPA natural charges (q_{Ir}= +0.47, q_{H}=–0.08 q_{Ag}= +0.65) indicates that a moderate portion of the positive charge of this cation is distributed over the two fragments **4** (+0.35, i.e. a charge of +0.17 on each fragment **4**), the remaining charge residing at the silver(I) center. Standard ETS-NOCV[90] analysis was performed assuming fragmentation of the molecule into the Ag^+ ion and a fictitious fragment made of the two molecules of **4** in their prepared geometry and position in [**4**→Ag←**4**]$^+$ (figure 24b). Density deformation plot $\Delta\rho_1$ (33% of the total orbital interaction energy ΔE_{orb}= –121 kcal/mol) corresponds to a density donation mostly from the two Ir–H motifs towards a broad area surrounding the silver atom. $\Delta\rho_2$ (8 % of ΔE_{orb}) corresponds to back-donation from a *d* orbital at silver towards two areas located in the Ag–H segments, whereas $\Delta\rho_3$ (12% of ΔE_{orb}) corresponds to density donation from a *d* orbital at Ir atoms towards a broad area that embraces the Ir–Ag and H–Ag segments. Combined theoretical analyses suggest indeed a delocalized and NCI-supported donor-acceptor (Ir–H)→Ag^+←(Ir–H) interaction of overall weak covalent character,[110,111,112] wherein the Ir–Ag interactions seem to be dominantly non-covalent according to QTAIM analysis (no BCPs, no bond paths). Having in sight the electronic structures of [**3B**][OTf], [**3A**][$BArF_{24}$], [**5A**][$BArF_{24}$] and [**4**→Ag←**4**]$^+$, and in full support to earlier statements by Templeton et al.,[113] complex **4** can indeed be considered as an ambident Lewis donor capable of binding Z-type Lewis acceptors (Z= fragment [**2**]$^+$ in [**3B**]$^+$, [Et_3Si]$^+$ in [**3A**]$^+$ and [**5A**]$^+$, and Ag^+ in [**4**→Ag←**4**]$^+$) either by the Ir atom, the hydridic hydrogen atom or both atoms of the Ir–H motif (scheme 16).

[110] Schwabe, T.; Grimme, S.; Djukic, J.-P. Noncovalent Metal–Metal Interactions: The Crucial Role of London Dispersion in a Bimetallic Indenyl System. *J. Am. Chem. Soc.* **2009**, *131*, 14156-14157.
[111] Grimme, S.; Djukic, J.-P. The Crucial Role of Dispersion in the Cohesion of Nonbridged Binuclear Os → Cr and Os → W Adducts. *Inorg. Chem.* **2010**, *49*, 2911-2919.
[112] Werlé, C.; Bailly, C.; Karmazin-Brelot, L.; Goff, X. F. L.; Pfeffer, M.; Djukic, J. P. First Stabilization of 14-Electron Rhodium(I) Complexes by Hemichelation. *Angew. Chem. Int. Ed.* **2014**, *53*, 9827-9831.
[113] Turlington, C. R.; Harrison, D. P.; White, P. S.; Brookhart, M.; Templeton, J. L. Probing the oxidation chemistry of half-sandwich iridium complexes with oxygen atom transfer reagents. *Inorg. Chem.* **2013**, *52*, 11351-11360.

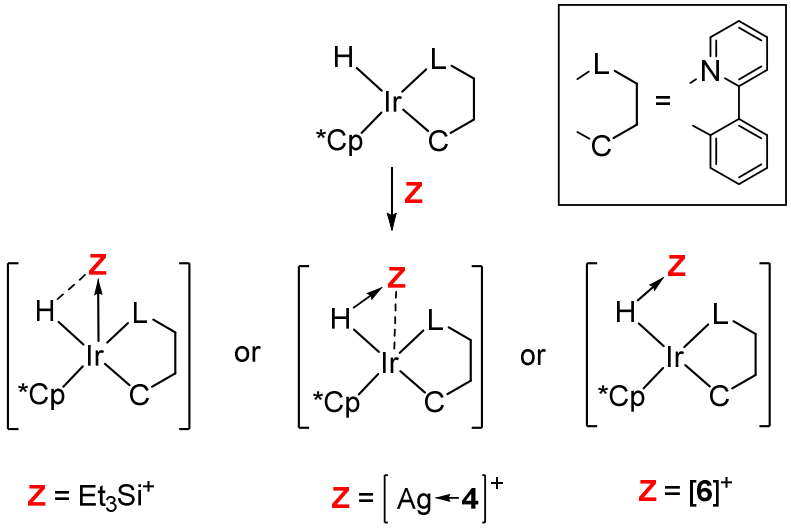

Scheme 16. Binding sites at **4** for a *Z* acceptor.

2.3 Conclusions and perspectives

[**2**][$BArF_{24}$] and [**4**][$BArF_{24}$] are highly efficient precatalysts for the *O*-silylation of primary and secondary alcohols, a reaction that nonetheless can be readily quenched by addition of Lewis bases such as aniline, phenylacetylene, phenyl-1-propyne, and *N*-methyl-1-phenylmethanimine. Acetophenone showed to be tolerated when added to the *O*-silylation reaction mixture of benzylic alcohol and $HSiEt_3$, suggesting that the alcohol function is more reactive than the carbonyl function within the conditions of the catalysis. [**4**][$BArF_{24}$] has shown to be catalytically active in the room temperature *N*-silylation of aniline. The inhibition induced by aniline in the *O*-silylation reaction of alcohols is a solid support towards the fact that *N*-silylation of aniline might be preferentially at work, thus suppressing the expected *O*-silylation reaction. These results bring a new light into our earlier observations of the lack of major interference of the reaction solvent, i.e. methanol, in a tandem (sequential) hydroamination-hydrosilylation of terminal alkynes promoted by a catalyst structurally similar to **P1** (scheme 1). The activation of [**2**][$BArF_{24}$] and [**4**][$BArF_{24}$] by $HSiEt_3$ entails the formation of highly reactive (hydrido-Ir(III))-silylium adducts, i.e. [**3A**][$BArF_{24}$] and [**5A**][$BArF_{24}$], which most probably result from hydride transfer from the silane to the iridium(III) center with no change of the formal oxidation state of the latter. In catalysis, both intermediates [**3A**][$BArF_{24}$] and [**5A**][$BArF_{24}$] have a bifacetted behavior; i.e. a source of a highly electrophilic silylium and a hydride donor. ITC proved to be a valuable analytical tool for establishing not only the stoichiometry in $HSiEt_3$ required for the activation [**2**][$BArF_{24}$], but also the enthalpy of activation of [**2**][$BArF_{24}$] in PhCl.

According to COSMO-RS/DFT calculations, the activation of [**2**][$BArF_{24}$] is enabled by the largely exothermic catalyzed consumption of the released MeCN by a double hydrosilylation process. Similar studies conducted on [**4**][$BArF_{24}$] point towards the same features as for [**2**][$BArF_{24}$]. The metallacyclic heptacoordinate Ir(III) complex [**3A**]$^+$ can be formulated as a Lewis donor-acceptor pair established between the hydrido-iridium complex **4** (donor) and the triethylsilylium cation (Z-type acceptor), wherein a rather weak Si···H interaction contributes to cohesion. The fact that the silylium cation can readily be transfered to a Lewis base (DMAP or TfO^-) from intermediate [**3A**]$^+$ sheds a new light on the possible role of akin Ir intermediates in the catalytic hydrosilylation of imines promoted by akin iridacycles. Related to the Lewis pair character of [**3A**]$^+$ is the issue of the nature of the associated anion. Quite tangible is the assumption that [**3A**]$^+$ does also form in the early stages of the reaction of [**2**][BF_4] or [**2**][OTf] with $HSiEt_3$. The highly electrophilic silylium fragment of putative [**3A**][OTf] can be captured by any Lewis donors present in the medium (TfO^-, MeCN, alcohol and any Lewis base) and at least by the triflate anion itself if no better base is present leading to a still catalytically effective **4**/Et_3SiOTf combination. The X-ray structure of [**4**][BPh_4] features non-covalent H-π interactions established between one of the hydrogens of bound Ir-NCMe and one of the phenyl of $[BPh_4]^-$. Even though intermediate [**5A**][BPh_4], i.e. the product of reaction between [**4**][BPh_4] and $HSiEt_3$, could be clearly identified by ^1H NMR spectroscopy, it is still unclear why [**4**][BPh_4] is inactive in catalysis. We have shown that the catalysis in *O*-silylation of alcohols can be inhibited if abstraction of the $[Et_3Si]^+$ moiety leads to inert X-SiR_3 species devoid of the electrophilic character (such as $FSiEt_3$ in the case of [**2**][BF_4]) necessary for the activation of so-called organic hydride-acceptors (ketones and imines for example). The X-ray structure of the novel iridium-silane intermediate [**5A**][$BArF_{24}$] (and of its isomer [**5A'**][$BArF_{24}$]) and of the inactive hydrido-bridged iridium dimer [**5B**][$BArF_{24}$], were successfully obtained. NMR spectroscopy and several DFT-D calculations all converge towards a donor-acceptor structural formulation for [**5A**][$BArF_{24}$], i.e. the second example of the kind after [**3A**][$BArF_{24}$]. In chapter 3 and 4 of this manuscript, we describe that [**4**][$BArF_{24}$] is a better precatalyst than [**2**][$BArF_{24}$] for the hydrosilylation of carbonyls (chapter 3) and for the C–F bond activation of saturated substrates (chapter 4). In future studies our group will try to understand what are the fundamental reasons behind such a difference in the catalytic activity between [**2**][$BArF_{24}$] and [**4**][$BArF_{24}$] despite their very similar structural features. Finally, the formation of [**3B**]$^+$ and [**5B**]$^+$ are major downsides of the considered catalytic systems as they constitute catalytically inactive forms of the iridacycles. It is speculated that this issue can be addressed by proper molecular engineering.

3 Catalytic hydrosilylation of carbonyls and nitriles

In this chapter, we provide a brief survey of the hydrosilylation reaction with a particular focus on recent advances in the hydrosilylation of aldehydes, ketones and nitriles catalyzed by transition-metal complexes. We also describe our results of the catalytic and mechanistic studies related to the hydrosilylation of aldehydes, ketones and nitriles. Following the discussion of the results, we propose a plausible mechanism for each class of reaction. Finally, a conclusion is given that highlights the significance as well as the limitations of our results along with the identification of the future challenges in the field.

3.1 General introduction

3.1.1 What is a hydrosilylation reaction?

The hydrosilylation reaction is a chemical reduction of an unsaturated bond with a silane (H–Si). This method has been shown to work for a variety of double and triple bonds, and the most studied of all include C≡C, C=C, C=O and C=N bonds (scheme 17). [114]

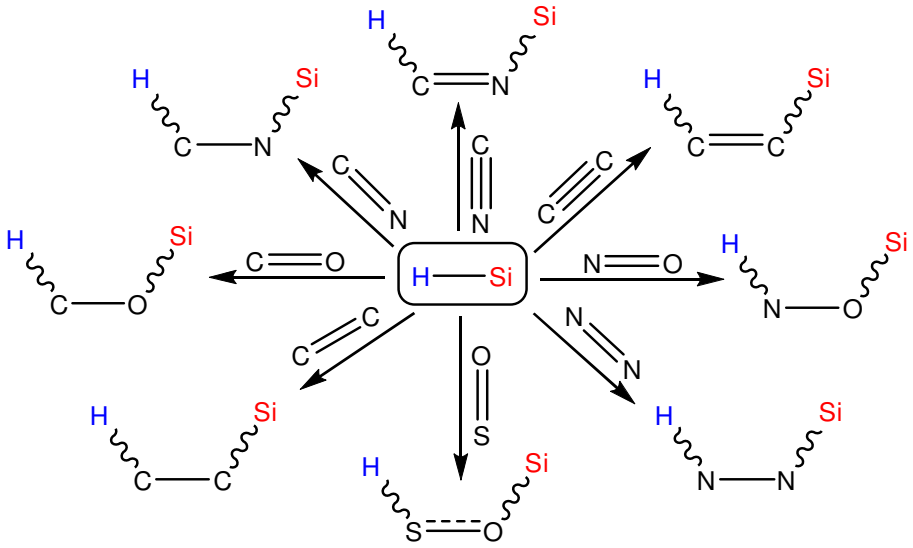

Scheme 17. Schematic representations describing the hydrosilylation of unsaturated bonds.

3.1.2 Why hydrosilylation as a method of reduction?

A general review of the literature[114,115,116] on the hydrosilylation reaction provides the commonly invoked reasons that explain the popularization of this reaction which are 1) the relative low cost and non-toxicity of silicon reagents compared for example to their tin, germanium, boron and aluminum counterparts, 2) together with the mild reaction conditions required and the relative usefulness of their reaction products for subsequent functionalization.

[114] Marciniec, B; Macie-jewski, H; Pietraszuk, C.; Pawluć, P. In *Hydrosilylation A Comprehensive Review on Recent Advances*, Marciniec, B., Ed.; Springer: Berlin Heidelberg, 2009; Vol. 1.
[115] Lewis, L. N.; Lewis, N.; Uriarte, R. J. Hydrosilylation. In Advances in Chemistry Series; ACS, Ed.; ACS, 1992; Vol. 230; pp 541–549.
[116] Ojima, I. The Hydrosilylation reaction. In The Chemistry of Organic Silicon Compounds, Patai, S; Rappoport, Z., Eds.; Wiley, 1989; Parts 1–2; pp 1479–1526.

3.1.3 What is known about catalytic hydrosilylation?

The hydrosilylation of various functional groups has been proven to be catalyzed by several means. The route that uses transition metal complexes (TMCs) as (pre)catalysts is certainly the most popular because of its mildness compared for example to the silyl radical generation method[117] (thermal cleavage and/or homolytic decomposition by free-radical initiators of the H–Si bond in silicon hydrides). This also stems from the unique property of TMCs to behave as versatile activators for the polar H–Si bond, providing a variety of metal hydride intermediates that are capable of selectively reducing a large panel of carbon-carbon and carbon-heteroatom bonds. This is well illustrated by successful uses of TMCs in most industrial hydrosilylation processes which are mostly based on noble metals such as platinum and rhodium due to their high catalytic performances (very high turnover number (TON) and turnover number frequency (TOF)). Platinum (pre)catalysts are the most commonly used for the hydrosilylation of olefins principally for the so-called "curing/hardening" of silicone polymer, while rhodium catalysts are mostly used for the hydrosilylation of alkynes and carbonyls, palladium complexes are preferentially applied to the hydrosilylation of conjugated dienes, and iridium complexes are specifically employed in the hydrosilylation of allyl electrophiles.[118] Historically the gain in interest for the hydrosilylation reaction has been attributed to the pioneer contributions of J. L. Speier and coworkers in 1957,[119] A. J. Chalk and J. F. Harold in 1965,[120] B. D. Karstedt and coworkers in 1973,[121] and E. Lukevics and coworkers in 1987,[122] with respect to the discovery of platinum precatalysts (so-called Speier's, Karstedt's and Lukevic's precatalysts) and the mechanistic proposal for the this reaction (so-called Chalk-Harrod mechanism) (scheme 18). Olefins were the first unsaturated substrates to be reduced by the catalyzed hydrosilylation reaction.[123]

---

[117] Marciniec, B. Catalytic aspects of hydrosilylation. In *Comprehensive Handbook on Hydrosilylation*, Marciniec, B., Ed.; Pergamon Press, 1992, pp 8–11.
[118] Yamamoto, K.; Hayashi, T. Hydrosilylations. In *Transition Metals for Organic Synthesis*, Beller, M.; Bolm, C.; Wiley-VCH Verlag GmbH: Weinheim, Germany; pp 167–191.
[119] Speier, J. L.; Webster, J. A.; Barnes, G. H. The Addition of Silicon Hydrides to Olefinic Double Bonds. Part II. The Use of Group VIII Metal Catalysts. *J. Am. Chem. Soc.* **1957**, *79* (4), 974–979.
[120] Chalk, A. J.; Harrod, J. F. Homogeneous Catalysis. II. The Mechanism of the Hydrosilation of Olefins Catalyzed by Group VIII Metal Complexes [1]. *J. Am. Chem. Soc.* **1965**, *87* (1), 16–21.
[121] Karstedt, B. D. Karstedt. P latinum Complexes of Unsaturated Siloxanes and Platinum Containing Organopolysiloxanes. U.S. Patent 3,775,452, November 27, 1973. Assigned to General Electric Corporation.
[122] Iovel, I. G.; Goldberg, Y. S.; Shymanska, M. V.; Lukevics, E. Quaternary Onium Hexachloroplatinates: Novel Hydrosilylation Catalysts. *Organometallics* **1987**, *6* (7), 1410–1413.
[123] Sommer, L. H.; Pietrusza, E. W.; Whitmore, F. C. Peroxide-Catalyzed Addition of Trichlorosilane to 1-Octene. *J. Am. Chem. Soc.* **1947**, *69* (1), 188.

a) First [Pt] precatalysts applied to "homogeneous" olefin hydrosilylation (eq. 1)

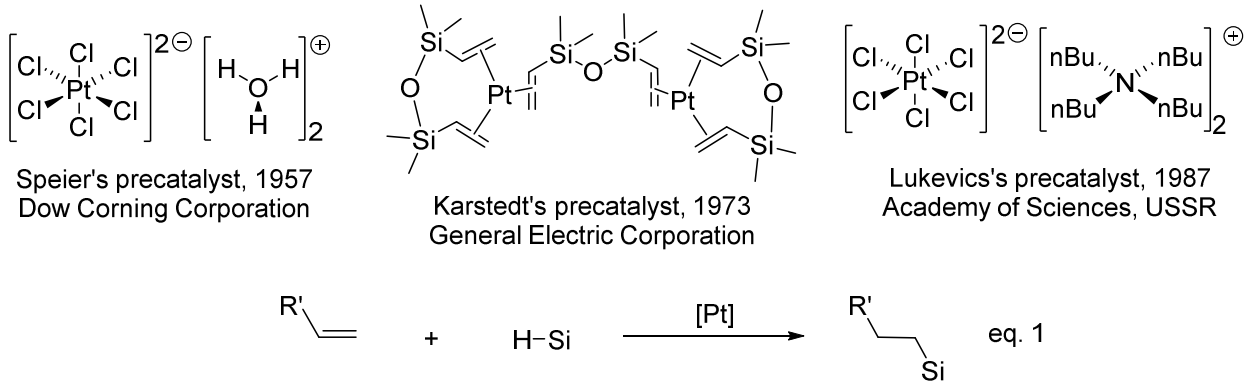

b) First [Pt]-based (left) and modified (right) Chalk-Harrod mechanism proposals for olefin hydrosilylation

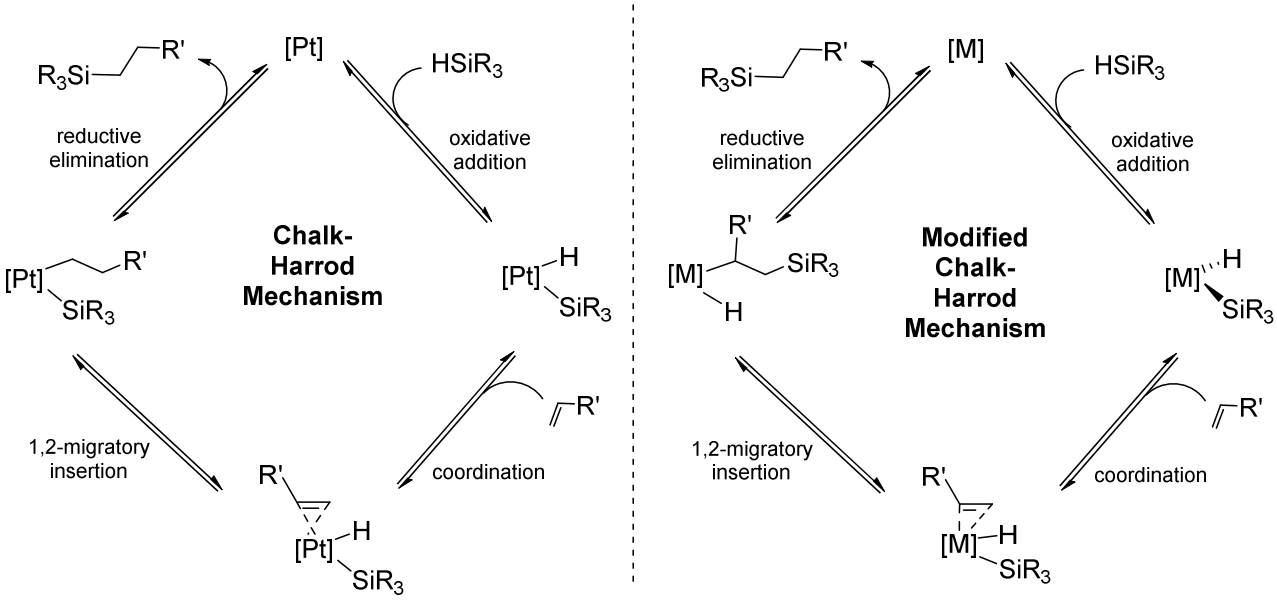

Scheme 18. Hydrosilylation of olefins with **a)** Speier's, Karstedt's and Lukevic's [Pt] precatalysts and **b)** its so-called "Chalk-Harrod" (with [Pt]) and "modified Chalk-Harrod" (with other metals) mechanism proposals.

Nowadays the hydrosilylation reaction is one of the most important reactions in chemistry. This is for example demonstrated by the common use in laboratories of the commercially available Speier's ($PtH_2Cl_6 \cdot 6H_2O$) and Karstedt's ($Pt_2[(Me_2SiCH{=}CH_2)_2O]_3$) precatalysts for the reduction

of olefins,[124] and the incorporation of silicon into zeolites, polymers, and dendrimers into a variety of materials.[125]

3.1.4 Mechanisms of the hydrosilylation of olefins catalyzed by [Pt]: a brief state of the art

The hydrosilylation of olefins has been througouly studied with a notable contribution from A. J. Chalk and J. F. Harrod who were the first to propose a mechanism of this reaction using the Speier's precatalyst (PtH_2Cl_6•$6H_2O$).[126] In two seminal papers published by S. B. Duckett and R. N. Perutz,[127] and by F. Seitz and M. S. Wrighton,[128] the authors proposed modified versions of the [Pt] "Chalk-Harrod mechanism", that are the "two-silicon" and "modified Chalk-Harrod" mechanisms respectively. There are several groups that reported results in support of the latter mechanisms. One can cite the contributions of P. M. Maitlis, D. L. Beach, I. Ojima, L. A. Oro, B. E. Grant, M. S. Wrighton and S. Murai and coworkers who found that a rather different mechanism is at work for rhodium,[129] iridium,[130] cobalt[131] and iron[132] complexes leading to the so-called "modified Chalk-Harrod" mechanism. The research groups of J. Y. Corey and coworkers,[133] T. D. Tilley and coworkers,[134] T. Takahashi, E. Negishi and coworkers,[135] among others were involved in the establishment of the so-called "σ-bond-metathesis" mechanism at work for d^0 transition metals. These mechanisms are widely accepted until today even though

[124] Nakajima, Y.; Shimada, S. Hydrosilylation Reaction of Olefins: Recent Advances and Perspectives. *RSC Adv.* **2015**, *5* (26), 20603–20616.
[125] Van Leeuwen, Piet W.N.M. Hydrosilylation. In *Homogeneous Catalysis*; Springer Netherlands: Dordrecht, 2004.
[126] Chalk, A. J.; Harrod, J. F. Homogeneous Catalysis. II. The Mechanism of the Hydrosilation of Olefins Catalyzed by Group VIII Metal Complexes [1]. *J. Am. Chem. Soc.* **1965**, *87* (1), 16–21.
[127] Duckett, S. B.; Perutz, R. N. Mechanism of Homogeneous Hydrosilation of Alkenes by (.eta.5-Cyclopentadienyl)rhodium. *Organometallics* **1992**, *11* (1), 90–98.
[128] Seitz, F.; Wrighton, M. S. Photochemical Reaction of $[(CO)_4Co(SiEt_3)]$ with Ethylene: Implications for Cobaltcarbonyl-Catalyzed Hydrosilation of Alkenes. *Angew. Chem. Int. Ed.* **1988**, *27* (2), 289–291.
[129] a) Millan, A.; Towns, E.; Maitlis, P. M. The Direct Conversion of α-Olefins into Vinyl- and Allyl-Silances Catalysed by Rhodium Complexes. *J. Chem. Soc., Chem. Commun.* **1981**, *0* (14), 673–674. b) Onopchenko, A.; Sabourin, E. T.; Beach, D. L. Rhodium(I)-Catalyzed Hydrosilylation of Styrene. *J. Org. Chem.* **1983**, *48* (25), 5101–5105. c) Ojima, I.; Fuchikami, T.; Yatabe, M. The Reactions of Hydrosilanes with Trifluoropropene and Pentafluorostyrene Catalyzed by Ruthenium, Rhodium and Palladium Complexes. *J. Organomet. Chem.* **1984**, *260* (3), 335–346.
[130] Oro, L. A.; Fernandez, M. J.; Esteruelas, M. A.; Jimenez, M. S. Hydrosilylation of Alkenes by Iridium Complexes. *J. Mol. Catal.* **1986**, *37* (2), 151–156.
[131] a) Reichel, C. L.; Wrighton, M. S. Photochemistry of Cobalt Carbonyl Complexes Having a Cobalt-Silicon Bond and Its Importance in Activation of Catalysis. *Inorg. Chem.* **1980**, *19* (12), 3858–3860. b) Brookhart, M.; Grant, B. E. Mechanism of a cobalt(III)-Catalyzed Olefin Hydrosilation Reaction: Direct Evidence for a Silyl Migration Pathway. *J. Am. Chem. Soc.* **1993**, *115* (6), 2151–2156. c) Chatani, N.; Kodama, T.; Kajikawa, Y.; Murakami, H.; Kakiuchi, F.; Ikeda, S.-I.; Murai, S. The $Co_2(CO)_8$-Catalyzed Hydrosilylation of Oxygen-Containing Olefins: Silylmetalation as a Key Step. *Chem. Lett.* **2000**, (1), 14–15.
[132] Mitchener, J. C.; Wrighton, M. S. Photogeneration of Very Active Homogeneous Catalysts Using Laser Light Excitation of Iron Carbonyl Precursors. *J. Am. Chem. Soc.* **1981**, *103* (4), 975–977.
[133] Gountchev, T. I.; Tilley, T. D. Hydrosilylation Catalysis by C_2-Symmetric Bis(silylamido) Complexes of Yttrium. *Organometallics* **1999**, *18* (26), 5661-5667.
[134] Corey, J. Y.; Zhu, X. H. Reactions of Hydrosilanes and Olefins in the Presence of Cp_2MCl_2/BuLi. *Organometallics* **1992**, *11* (2), 672–683.
[135] Takahashi, T.; Hasegawa, M.; Suzuki, N.; Saburi, M.; Rousset, C. J.; Fanwick, P. E.; Negishi, E. Zirconium-Catalyzed Highly Regioselective Hydrosilation Reaction of Alkenes and X-Ray Structures of Silyl(hydrido)zirconocene Derivatives. *J. Am. Chem. Soc.* **1991**, *113* (22), 8564–8566.

studies show that they can vary depending on the nature of the metal complexes or the catalytic conditions. For example, P. B. Glaser and T. D. Tilley proposed an original mechanism in support of the high anti-Markovnikov regioselectivity observed for a silylene ruthenium complex (scheme 19).[136] It implies an H–Si bond insertion into the C=C bond of the olefin without the intervention of the metallic center, which is in total contrast with the "classical" Chalk-Harrod mechanism.

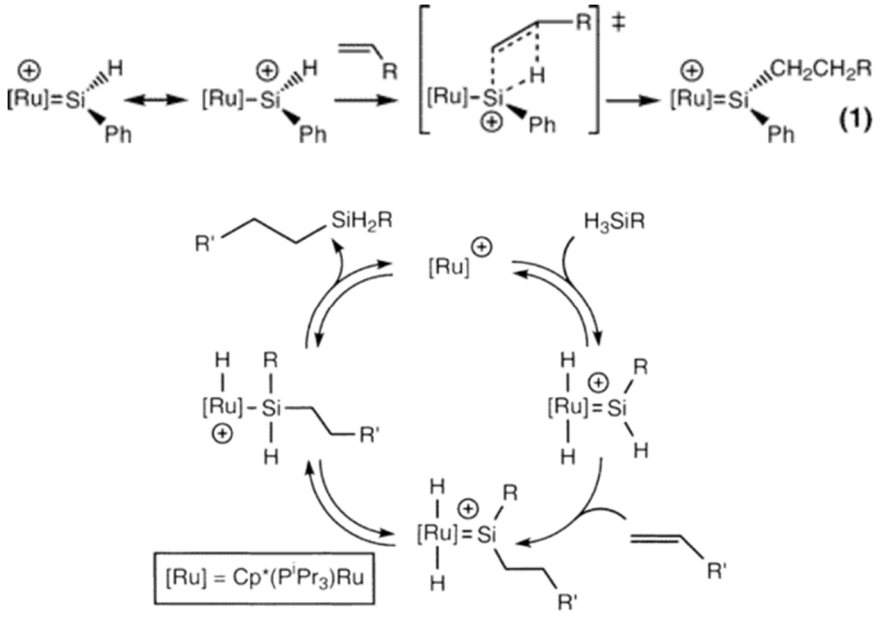

Scheme 19. Hydrosilylation of olefins catalyzed by silylene [Ru]-based complexes, as proposed by P. B. Glaser and T. D. Tilley.[136] Reprinted with permission from Glaser, P. B.; Tilley, T. D. *J. Am. Chem. Soc.* **2003**, *125* (45), 13640. Copyright 2003 American Chemical Society.

Another good example is the work of F. Ozawa and coworkers who showed that a class of ruthenium precatalysts can follow both the Chalk-Harrod and the modified Chalk-Harrod mechanisms depending on the steric environment created by the surrounding ligands.[137]

The hydrosilylation of olefins is beyond of this thesis project. As a consequence, we will not discuss in detail the mechanisms mentioned before. For more details, the reader is oriented

[136] Glaser, P. B.; Tilley, T. D. Catalytic Hydrosilylation of Alkenes by a Ruthenium Silylene Complex. Evidence for a New Hydrosilylation Mechanism. *J. Am. Chem. Soc.* **2003**, *125* (45), 13640–13641.
[137] Yooichiroh Maruyama; Kunihiro Yamamura; Takashi Sagawa; Hiroyuki Katayama, and; Ozawa, F. Mechanisms of C–Si and C–H Bond Formation on the Reactions of Alkenylruthenium(II) Complexes with Hydrosilanes. *Organometallics* **2000**, *19* (7), 1308–1318.

into the original publications previously quoted.[126–137] Recently, one critical review[138] and one excellent research article[139] also appeared in this field.

3.1.5 Application of silyl derivatives

Industrially, hydrosilylation finds strategically important applications, though limited in use, for example in the production of adhesives and coupling agents.[140] Despite the high price of platinum ($31 per gram),[141] the Speier's precatalyst remains the organometallic complex of choice for the large scale hydrosilylation of olefins. This is due to its very high efficiency with remarkable TON (turnover number) and TOF (turnover frequency).[142] However, since platinum is among the most expensive (and least abundant) noble metals this only fact calls for its replacement. Silyl derivatives are used in a very broad range of applications, for example as coupling agents for the modification of various types of sensitive surfaces (e.g. cloths, glass, conservation of archaeological treasures) and for the synthesis of polysiloxane derivatives that find important applications (e.g. organic electronics).[143]

[138] Marciniec, B. Hydrosilylation of Alkenes and Their Derivatives. In *Hydrosilylation A Comprehensive Review on Recent Advances*; Springer Netherlands: Dordrecht, 2009; pp 3–51.
[139] Meister, T. K.; Riener, K.; Gigler, P.; Stohrer, J.; Herrmann, W. A.; Kühn, F. E. Platinum Catalysis Revisited—Unraveling Principles of Catalytic Olefin Hydrosilylation. *ACS Catal.* **2016**, *6* (2), 1274–1284.
[140] Brook, M. A. In Silicon in Organic, Organometallic, and Polymer Chemistry; Wiley-VCH Verlag, 2000.
[141] http://www.apmex.com/spotprices/platinum-price (Visited on 10th of October 2016)
[142] Marciniec, B. Catalytic aspects of hydrosilylation. In *Comprehensive Handbook on Hydrosilylation*, Marciniec, B., Ed.; Pergamon Press, 1992; pp 8–11.
[143] Larry N. Lewis; Judith Stein; Yan Gao; Robert E. Colborn; Gudrun Hutchins. Platinum Catalysts Used in the Silicones Industry. *Platinum. Met. Rev.* **1997**, *41* (2), 66.

3.2 Hydrosilylation of aldehydes and ketones

3.2.1 Introduction

3.2.1.1 Some properties of silicon that make the hydrosilylation of carbonyls a good target reaction

Silicon (Si) at the formal oxidation state of +IV in neutral molecules like trialkyl (or aryl) silyl hydrides ($HSiR_3$) for example, is considered to be generally inert towards a variety of neutral reagents like water or alcohols, while it is known that Si forms strong bonds to more electronegative elements (E) such as oxygen (O), nitrogen (N), and fluorine (F). There are principally two ways that lead to the Si–E bond formation as represented in scheme 20 (of course all the elements Si, O, N, and F are initially involved in neutral or ionic molecules): 1) interaction of the electro-deficient cationic silicon (Si^+) with a neutral element E (scheme 20a), and 2) interaction of the neutral silicon Si with an anionic element E^- (scheme 20b).

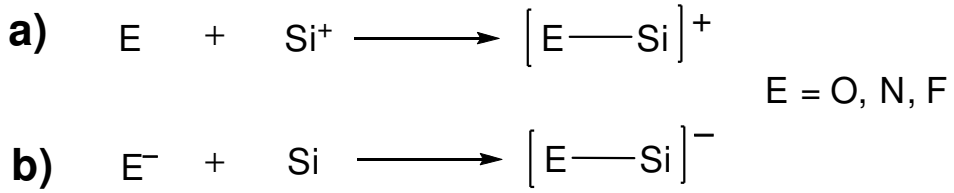

Scheme 20. Schematic representation of the interaction between silicon atom (Si) and E atoms (E = O, N, F).

This combination of properties allows Si–N, Si–O and Si-F bonds to be chemoselectively accessible under appropriate conditions. More specifically, the hydrosilylation of C=O functional groups has attracted a special attention due to the oxophilicity of silicon which is driven by the strength of the Si–O bond. However, as mentioned previously, the H–Si bond is relatively stable and needs consequently to be activated for an efficient Si–O bonding interaction to occur. For example, the uncatalyzed and direct hydrosilylation of ketones is prevented by a very high free-energy barrier of ~43.1 kcal•mol^{-1} (~180.3 kJ•mol^{-1}) under ambient conditions.[144] As a consequence, strategies towards "solving" this kinetic problem have concentrated on the catalytic H–Si bond activation. In this context, transition metals that mediate H–Si bond activation provide a rich chemistry especially in the catalytic hydrosilylation of aldehydes and ketones.

[144] Pérez, M.; Qu, Z. W.; Caputo, C. B.; Podgorny, V.; Hounjet, L. J.; Hansen, A.; Dobrovetsky, R.; Grimme, S.; Stephan, D. W. Hydrosilylation of Ketones, Imines and Nitriles Catalysed by Electrophilic Phosphonium Cations: Functional Group Selectivity and Mechanistic Considerations. *Chem. - A Eur. J.* **2015**, *21* (17), 6491–6500.

No general and selective method for the catalytic hydrosilylation of aldehydes and ketones has been developed yet even though a large array of systems has been reported. The interest in the hydrosilylation of C=O bond of aldehydes and ketones mainly stems from potential applications in the syntheses of fine chemicals and intermediates.[145] Moreover, the latter reaction provides a more interesting route into silyl ethers (scheme 21, **path A**) over the indirect two-step route using in general stoichiometric amounts of 1) non-safe and non-selective alumino or boro-hydrides as reducing agents,[146] and of 2) a combination of a base with a halogenosilane as the silylation procedure[147] (scheme 21, **path B**). Furthermore, the resulting O–Si bond can be easily hydrolyzed to yield an alcohol, allowing more functionalization if necessary (scheme 21, path **A**). Finally, hydrosilylation is considered as a safest and less time demanding reduction method of carbonyls to alcohols compared to the traditional process that generally requires high pressure of H_2[148] (scheme 21, **path C**).

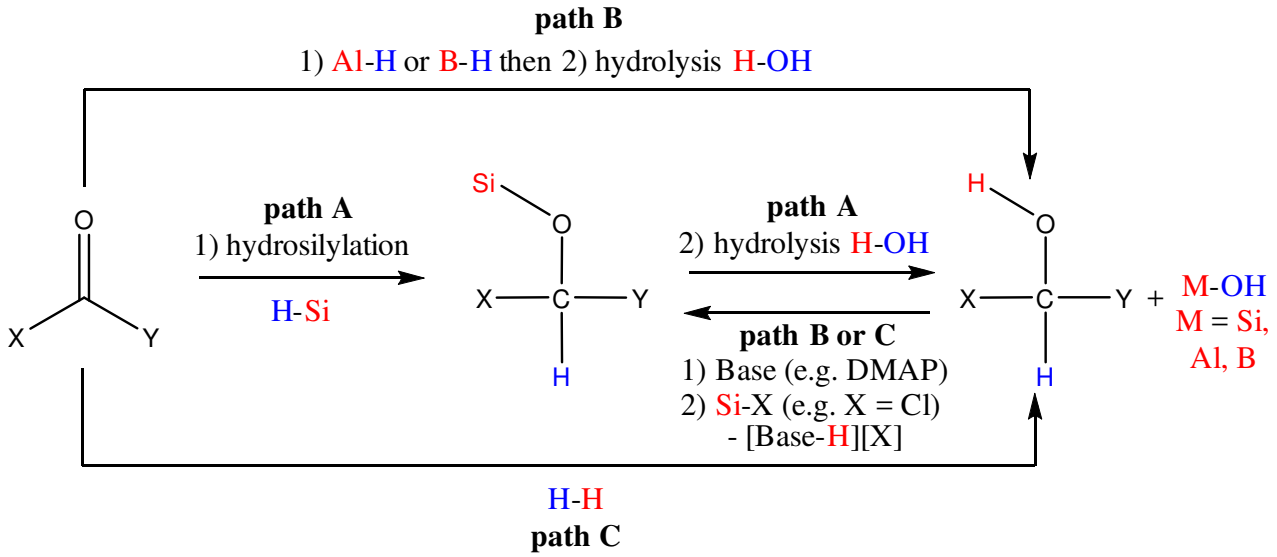

Scheme 21. Common reduction methods of aldehydes and ketones for the synthesis of silyl ethers either directly by hydrosilylation (path **A**) or indirectly by 1) reduction to alcohols and then 2) *O*-silylation of the latter (paths **B** and **C**).

[145] Bhaduri, S.; Mukesh, D. In *Homogeneous Catalysis: Mechanisms and Industrial Applications.*; Wiley-Interscience, 2000.
[146] Seyden-Penne, J. Reduction of Double Bonds. In *Reductions by the Alumino-and Borohydrides in Organic Synthesise*, 2nd Edition; Wiley-VCH, 1997; pp 37–45.
[147] Greene, Theodora; W. Wuts, Peter G. M. Protection for the Hydroxyl Group, Including 1,2- and 1,3-Diols. In *Greene's Protective Groups in Organic Synthesis*; John Wiley & Sons, Inc.: Hoboken, NJ, USA, 2007; Vol. 9, pp 165–221.
[148] Ohkuma, T.; Noyori, R. Homogeneous Hydrogenations—Carbonly Reductions. In *Transition Metals for Organic Synthesis*; Wiley-VCH Verlag GmbH: Weinheim, Germany, 2004; Vol. 1, pp 29–95.

Over the last years, several reviews and book chapters summarized the last achievements in TM-based catalytic hydrosilylation of carbonyls.[149,150,151,152,153,154,155,156] In particular, TM-based catalytic hydrosilylation of aldehydes and ketones is becoming one of the most studied and convenient reductive synthetic route to prepare primary (from aldehydes) and secondary alcohols (from ketones). Almost all transition metals in combination with various ligands (phosphines and NHCs are certainly the most used of all) have been tested as (pre)catalyst systems, and most of them belong to the group VIII of the periodic table. Apart from the "TM catalyst system", other catalyst systems are known for this reaction from at least the 1960's, which are mainly based on nucleophile/electrophile combinations such as amines, phosphines or halide ions as nucleophiles, and metal salts (e.g. $ZnCl_2$) or main-group elements (e.g $BF_3.(Et_2O)$ and $B(C_6F_5)_3$) as Lewis acids; fluoride salts such as TBAF or CsF; and the silyl radical generation chemical methods (based on H–Si bond cleavage upon thermal decomposition or free-radical initiation). One has also to mention the use of heterogeneous colloidal or supported metallic systems (mainly 5% platinum on carbon support, and reduced Ni^0 from $NiCl_2/HSiEt_3$ refluxing).[157]

While writing this section, it was figured that actually the literature abounds with publications dealing with TMCs catalyzed hydrosilylation of carbonyls, and for this reason we will only specify in the following paragraph some examples reported to date mainly on iridium complexes. The reader is oriented to specialized reviews[149–157] and original papers[158–167] for more complete informations.

---

[149] Qin, X.; Liu, X.; Guo, C.; Wu, H.; Xiaofei, Q.; Xiaoyan, L.; Caihong, G.; Haishun, W. Reaction Mechanisms of Carbonyl Compounds Hydrosilylation Catalyzed by Group VIII Transition Metal Complexes. *Chinese J. Org. Chem.* **2016**, *36* (1), 60.
[150] Chakraborty, S.; Bhattacharya, P.; Dai, H.; Guan, H. Nickel and Iron Pincer Complexes as Catalysts for the Reduction of Carbonyl Compounds. *Acc. Chem. Res.* **2015**, *48* (7), 1995–2003.
[151] Marciniec, B. Hydrosilylation of Unsaturated Carbon—Heteroatom Bonds. In *Hydrosilylation A Comprehensive Review on Recent Advances*; Marciniec, B., Ed.; Springer Netherlands: Dordrecht, 2009; Vol. 1, pp 289–339.
[152] Roy, A. K. A Review of Recent Progress in Catalyzed Homogeneous Hydrosilation (Hydrosilylation). *Adv. Organomet. Chem.* **2007**, *55*, 1–59.
[153] H. Nishiyama. Hydrosilylations of carbonyl and imine compounds. In *Transition Metals for Organic Synthesis: Building Blocks and Fine Chemicals*; Beller, M., Bolm, C., Eds; Wiley-VCH, Weinheim, 2004; vol. 1, pp 182-188.
[154] Riant, O.; Mostefaï, N.; Courmarcel, J. Recent Advances in the Asymmetric Hydrosilylation of Ketones, Imines and Electrophilic Double Bonds. *Synthesis (Stuttg).* 2004, ***2004*** (18), 2943–2958.
[155] Carpentier, J.-F.; Bette, V. Chemo- and Enantioselective Hydrosilylation of Carbonyl and Imino Groups. An Emphasis on Non-Traditional Catalyst Systems. *Curr. Org. Chem.* **2002**, *6* (10), 913–936.
[156] a) ojima, I.; li, Z.; zhu, J. Recent advances in the hydrosilylation and related reactions. In *The Chemistry of Organic Silicon Compounds*; Rappoport, Z.; Apeloig, Y., Eds.; Wiley,1998; Vol. 2, pp 1733–1742. b) Ojima, I. The Hydrosilylation reaction. In *The Chemistry of Organic Silicon Compounds*, Patai, S.; Rappoport, Z., Eds.; Wiley, 1989; Parts 1–2; pp 1479–1526.
[157] Marciniec, B.; Gulinski, J.; Urbaniak, W.; Kornetka, Z. W. In *Comprehensive Handbook on Hydrosilylation*; Pergamon Press, 1992.

3.2.1.3 Selected examples of catalytic systems from the literature

In order to give a more synoptic overview, we have summarized in table 11 and scheme 22 the efficiency of various catalytic systems for the hydrosilylation of acetophenone by various hydrosilanes $HSiR_3$.[158,159,160,161,162,163,164,165,166,167,168,169,170,171,172,173,174,175]

[158] For boron, see: Parks, D. J.; Piers, W. E. Tris(pentafluorophenyl)boron-Catalyzed Hydrosilation of Aromatic Aldehydes, Ketones, and Esters. *J. Am. Chem. Soc.* **1996**, *118* (39), 9440–9441.

[159] For potassium, see: Revunova, K.; Nikonov, G. I. Base-Catalyzed Hydrosilylation of Ketones and Esters and Insight into the Mechanism. *Chem. - A Eur. J.* **2014**, *20* (3), 839–845.

[160] For zinc, see: Sattler, W.; Ruccolo, S.; Rostami Chaijan, M.; Nasr Allah, T.; Parkin, G. Hydrosilylation of Aldehydes and Ketones Catalyzed by a Terminal Zinc Hydride Complex, [κ^3-Tptm]ZnH. *Organometallics* **2015**, *34* (19), 4717–4731.

[161] For copper, see: Brunner, H.; Amberger, K. Asymmetrische Katalysen. *J. Organomet. Chem.* **1991**, *417* (3), C63–C65.

[162] For gold, see: Corma, A.; González-Arellano, C.; Iglesias, M.; Sánchez, F. Gold Nanoparticles and Gold(III) Complexes as General and Selective Hydrosilylation Catalysts. *Angew. Chem. Int. Ed.* **2007**, *46* (41), 7820–7822.

[163] For nickel, see: Bheeter, L. P.; Henrion, M.; Brelot, L.; Darcel, C.; Chetcuti, M. J.; Sortais, J. B.; Ritleng, V. Hydrosilylation of Aldehydes and Ketones Catalyzed by an N-Heterocyclic Carbene-Nickel Hydride Complex under Mild Onditions. *Adv. Synth. Catal.* **2012**, *354* (14–15), 2619–2624.

[164] For palladium, see: Chouthaiwale, P. V.; Rawat, V.; Sudalai, A. Pd-Catalyzed Selective Hydrosilylation of Aryl Ketones and Aldehydes. *Tetrahedron Lett.* **2012**, *53* (2), 148–150.

[165] For platinum, see: Caseri, W.; Pregosin, P. S. Hydrosilylation Chemistry and Catalysis with *cis*-$PtCl_2(PhCH{=}CH_2)_2$. *Organometallics* **1988**, *7* (6), 1373–1380.

[166] For cobalt, see: Brunner, H.; Amberger, K. Asymmetrische Katalysen. LXXV. Enantioselektive Hydrosilylierung von Acetophenon Mit Pyridinyloxazolin-kobalt(I)-Komplexen Als Katalysatoren. *J. Organomet. Chem.* **1991**, *417* (3), C63–C65.

[167] For rhodium, see: Yiğit, M.; Özdemir, I.; Çetinkaya, B.; Çetinkaya, E. Novel N-Heterocyclic-Carbene–rhodium Complexes as Hydrosilylation Catalysts. *J. Mol. Catal. A Chem.* **2005**, *241* (1), 88–92.

[168] For iridium, see: Park, S.; Brookhart, M. Hydrosilylation of Carbonyl-Containing Substrates Catalyzed by an Electrophilic η^1-Silane iridium(III) Complex. *Organometallics* **2010**, *29* (22), 6057–6064.

[169] For iron, see: Ruddy, A. J.; Kelly, C. M.; Crawford, S. M.; Wheaton, C. A.; Sydora, O. L.; Small, B. L.; Stradiotto, M.; Turculet, L. (*N*-Phosphinoamidinate)Iron Pre-Catalysts for the Room Temperature Hydrosilylation of Carbonyl Compounds with Broad Substrate Scope at Low Loadings. *Organometallics* 2013, *32* (19), 5581–5588.

[170] For ruthenium, see: Gutsulyak, D. V.; Vyboishchikov, S. F.; Nikonov, G. I. Cationic Silane σ-Complexes of Ruthenium with Relevance to Catalysis. *J. Am. Chem. Soc.* **2010**, *132* (17), 5950–5951.

[171] For manganese, see: Mukhopadhyay, T. K.; Flores, M.; Groy, T. L.; Trovitch, R. J. A Highly Active Manganese Precatalyst for the Hydrosilylation of Ketones and Esters. *J. Am. Chem. Soc.* **2014**, *136* (3), 882–885.

[172] For rhenium, see: Du, G.; Abu-Omar, M. M. Catalytic Hydrosilylation of Carbonyl Compounds with Cationic Oxorhenium(V) Salen. *Organometallics* **2006**, *25* (20), 4920–4923.

[173] For molybdenum, see: McLeod, N. A.; Kuzmina, L. G.; Korobkov, I.; Howard, J. A. K.; Nikonov, G. I. Hydridosilylamido Complexes of Ta and Mo Isolobal with Berry's Zirconocenes: Syntheses, β-Si–H Agostic Interactions, Catalytic Hydrosilylation, and Insight into Mechanism. *Dalt. Trans.* **2016**, *45* (6), 2554–2561.

[174] For tungsten, see: Gądek, A.; Szymańska-Buzar, T. Activation of the SiH Bond of Silanes in Photochemical Reactions with $W(CO)_6$: Hydrosilylation of Ketones and Dehydrosilylation of Alcohol by H_2SiPh_2. *Polyhedron* **2006**, *25* (6), 1441–1448.

[175] For titanium, see: Halterman, R. L.; Ramsey, T. M.; Chen, Z. Catalytic Asymmetric Hydrosilation of Aryl Alkyl Ketones with C_2-Symmetric Chiral Metallocene Complexes. *J. Org. Chem.* **1994**, *59* (9), 2642–2644.

Table 11. General overview on TM-based catalyzed hydrosilylation of acetophenone with hydrosilanes $HSiR_3$ (taken as reference reaction). The abbreviations used stand for: [cat] ((pre)catalyst), t (time), T (temperature), y (yield), c° (conversion), OH (hydrolysis or methanolysis), THF (tetrahydrofuran), DMF (dimethylformamide),* (chiral ligand), *hv* (light irradiation), [Ref] (publication reference number).

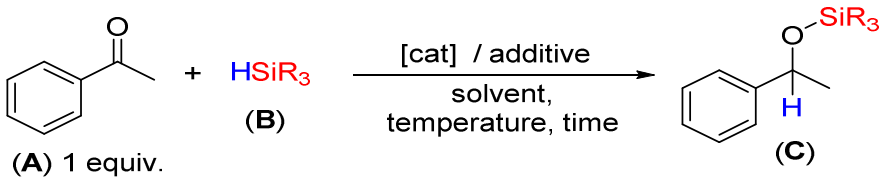

Metal	[cat] / additive (mol%)	B (equiv)	solvent	T (°C)	t (h)	C (%)	[Ref]
B	$B(C_6F_5)_3$ (2.0)	$HSiPh_3$ (1.0)	benzene	rt	-	97 (y)	158
K	KO^tBu (0.1)	H_3SiPh (1.1)	THF	rt	< 0.1	98 (c°)	159
Zn	[κ^3-Tptm]ZnH (1.0)	H_3SiPh (1.0)	C_6D_6	rt	0.75	100 (mixture)	160
Cu	CuO^tBu (0.3)+DIOP (0.35)	H_2SiPh_2 (1.0)	neat	0→rt	15	100 (OH)	161
Au	1Au-(MCM-41) (5.0)	H_2SiPh_2 (2.0)	Toluene	70	8	100 (c°)	162
Ni	[NiNHC-Cl] (5.0)+$NaHBEt_3$ (10.0)	H_2SiPh_2 (1.0)	THF	rt	17	88 (OH)	163
Pd	$Pd(OAc)_2$ (0.5)	$HSiEt_3$ (1.2)	DMF	rt	1	98 (y)	164
Pt	cis-Pt(Cl_2)$(styrene)_2$ / aniline (0.05)	$HSiMeCl_2$ (1.0)	neat	rt	32	84	165
Co	$[Co(Py)_6][BPh_4]$	H_2SiPh_2 (1.0)	neat	0-20	18	100	166
Rh	[RhNHC-Cl] (0.5)	$HSiEt_3$ (1.3)	neat	90	2	95	167
Ir	$[Ir(POCOP)(acetone)H][B(C_6F_5)_4]$ (0.5)	$HSiEt_3$ (3.0)	C_6D_5Cl	rt	0.3	100 (c°)	168
Fe	[(κ^2-PN)$Fe(N(SiMe_3)_2]$ (0.015)	H_3SiPh (0.6)	Toluene	rt	4	99 (c°, OH)	169
Ru	$[RuCp(NCMe)_2][B(C_6F_5)_4]$ (5.0)	$HSiPhMe_2$ (1.0)	$CDCl_3$	rt	24	30 (c°)	170
Mn	[(PDI)Mn] (0.1)	H_3SiPh (1.0)	neat	rt	< 0.1	99 (c°)	171
Re	[Re(O)(NCMe)] $[B(C_6F_5)_4]$ (1.0)	$HSiEt_3$ (1.5)	CD_2Cl_2	rt	2.5	97 (y)	172
Mo	[MoH] (5.0)	H_3SiPh (1.0)	C_6D_6	rt	10	35 (y)	173
W	$[W(CO)_6]$ (2.0)	H_2SiPh_2 (0.3)	n-Heptane	rt	1 (*hv*)	10 (c°)	174
Ti	[Ti*] (0.5) / n-BuLi (1.0)	$HSi(EtO)_3$ (2.5)	THF	−78→rt	13	100 (y)	175

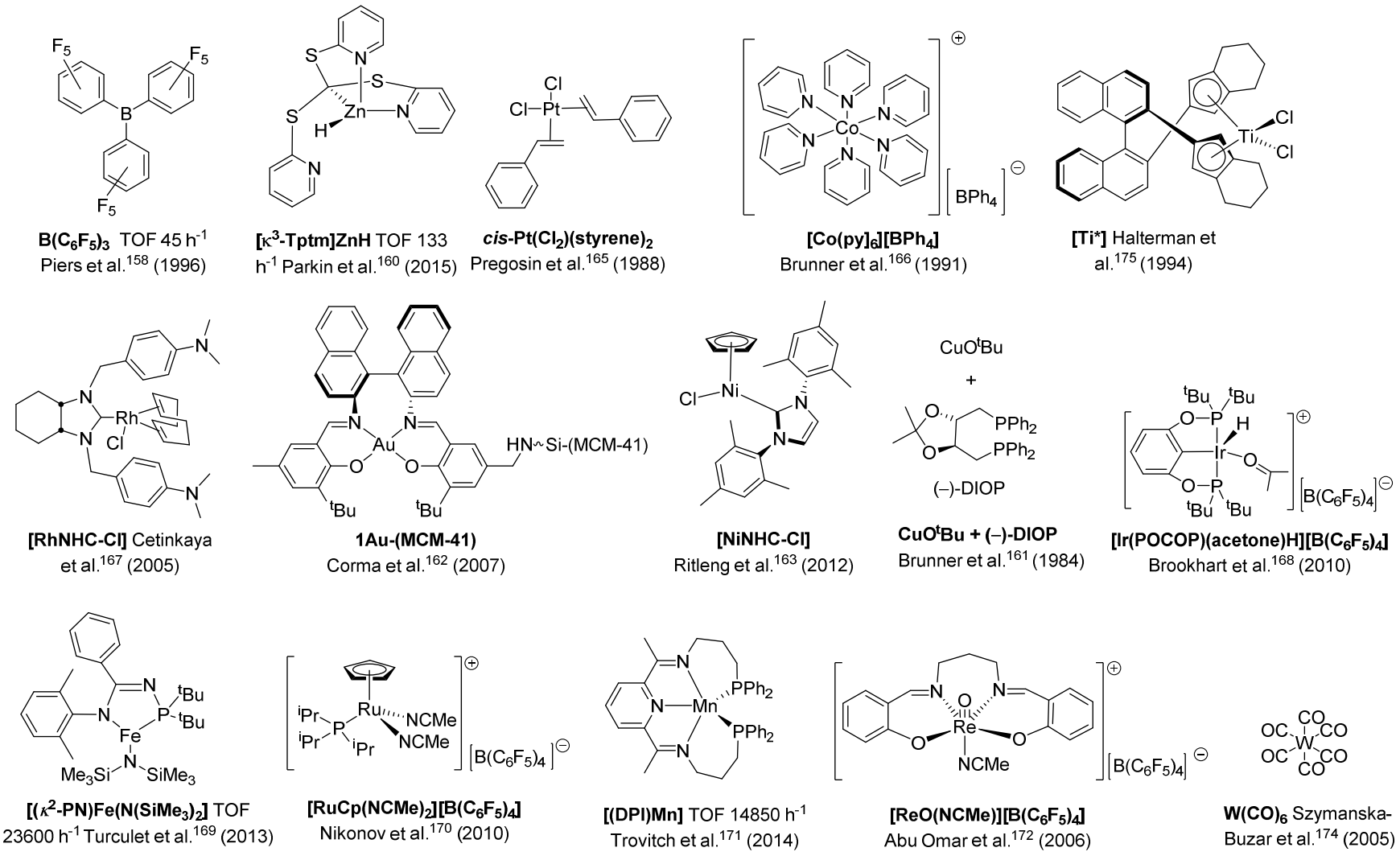

$B(C_6F_5)_3$ TOF 45 h^{-1} Piers et al.[158] (1996)

[κ^3-Tptm]ZnH TOF 133 h^{-1} Parkin et al.[160] (2015)

***cis*-$Pt(Cl_2)(styrene)_2$** Pregosin et al.[165] (1988)

$[Co(py)_6][BPh_4]$ Brunner et al.[166] (1991)

[Ti*] Halterman et al.[175] (1994)

[RhNHC-Cl] Cetinkaya et al.[167] (2005)

1Au-(MCM-41) Corma et al.[162] (2007)

[NiNHC-Cl] Ritleng et al.[163] (2012)

CuO^tBu + (–)-DIOP Brunner et al.[161] (1984)

$[Ir(POCOP)(acetone)H][B(C_6F_5)_4]$ Brookhart et al.[168] (2010)

[(κ^2-PN)$Fe(N(SiMe_3)_2)_2$] TOF 23600 h^{-1} Turculet et al.[169] (2013)

$[RuCp(NCMe)_2][B(C_6F_5)_4]$ Nikonov et al.[170] (2010)

[(DPI)Mn] TOF 14850 h^{-1} Trovitch et al.[171] (2014)

$[ReO(NCMe)][B(C_6F_5)_4]$ Abu Omar et al.[172] (2006)

$W(CO)_6$ Szymanska-Buzar et al.[174] (2005)

Scheme 22. Molecular structures of (pre)catalysts depicted in table 11 (see previous page) along with their TON (turnover number), TOF (turnover number frequency), and publication reference number.

3.2.1.4 Catalysis with iridium

In general, iridium complexes have been little studied as hydrosilylation catalysts in comparison to the more traditionally used Pt(0) and Pt(II) complexes and the corresponding Rh(I) and Rh(III) complexes. However, several research groups reported iridium based homogenous catalysis applied for the hydrosilylation of aldehydes and ketones. The efficiency of these systems varies and mostly depends on the nature of the ligand, the silane, the substrate, the solvent, etc. An efficient iridium-based catalytic system that works under general conditions for a variety of substrates is still lacking, as it is the case for other TMs. In 1972, I. Ojima and coworkers showed that the Wilkinson's [$RhCl(PPh_3)_3$] complex could catalyze within a few minutes the reaction between cyclohexanone and $HSiEt_3$ to give cyclohexyloxytriethylsilane (98%).[176] Surprisingly the related [$IrCl(PPh_3)_3$] complex showed no activity at all.[177] In 1985, T. A. Nile and coworkers found that [$Ir(COE)_2Cl_2]_2$ (COE = *cis*-cyclooctene) and [$Ir(COD)Cl]_2$ (COD = *cis*,*cis*-1,5-cyclooctadiene) precursors, sometimes in combination with phosphines, were active precatalysts in the hydrosilylation of *α*,*β*-unsaturated ketones.[178] In 1998, E. Lukevics and coworkers utilized the so-called Vaska's [$IrCl(CO)(PPh_3)_2$] complex as precatalyst for the hydrosilylation of aromatic aldehydes with $HSiEt_3$, which showed superior activity when compared to the Ru, Pd and Pt counterparts.[179] In 2002, R. G. Bergman and coworkers reported that the iridium(III) complex [$Cp^*(PMe_3)Ir(SiPh_2)(H)][B(C_6F_5)_4$] catalyzes the hydrosilylation of acetophenone with H_2SiPh_2 with rather low activity and selectivity (scheme 23).[180] In 2002, Doherty and coworkers showed that combining [$Ir(COD)Cl]_2$ with iminophosphine ligands within the same reaction vessel permits the catalytic hydrosilylation of acetophenone under mild conditions.[181]

[176] Ojima, I.; Nihonyanagi, M.; Nagai, Y. Rhodium Complex Catalysed Hydrosilylation of Carbonyl Compounds. *J. Chem. Soc. Chem. Commun.* **1972**, No. 16, 938a.
[177] Bennett, M.; Charles, R.; Fraser, P. Oxidative Addition of Monosilanes to Planar iridium(I) Complexes and Carbonylation of the Resulting Adducts. *Aust. J. Chem.* **1977**, *30* (6), 1201.
[178] Apple, D. C.; Brady, K. A.; Chance, J. M.; Heard, N. E.; Nile, T. A. Iridium Complexes as Hydrosilylation Catalysts. *J. Mol. Catal.* **1985**, *29* (1), 55–64.
[179] Iovel, I.; Popelis, J.; Gaukhman, A.; Lukevics, E. Hydrosilylation of Unsaturated (Hetero)aromatic Aldehydes and Related Compounds Catalyzed by Transition Metal Complexes. *J. Organomet. Chem.* **1998**, *559* (1), 123–130.
[180] Klei, S. R.; Tilley, T. D.; Bergman, R. G. Stoichiometric and Catalytic Behavior of Cationic Silyl and Silylene Complexes. *Organometallics* **2002**, *21* (22), 4648–4661.
[181] Doherty, S.; Knight, J. G.; Scanlan, T. H.; Elsegood, M. R.; Clegg, W. Iminophosphines: Synthesis, Formation of 2,3-Dihydro-1H-benzo[1,3]azaphosphol-3-Ium Salts and N-(Pyridin-2-Yl)-2-Diphenylphosphinoylaniline, Coordination Chemistry and Applications in Platinum Group Catalyzed Suzuki Coupling Reactions and Hydrosilylations. *J. Organomet. Chem.* **2002**, *650* (1), 231–248.

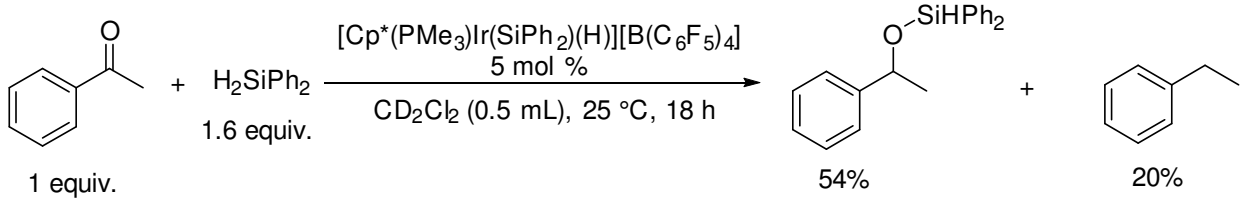

Scheme 23. Hydrosilylation of acetophenone catalyzed by the complex $[Cp^*(PMe_3)Ir(SiPh_2)(H)][B(C_6F_5)_4]$, as reported by R. G. Bergman and coworkers.[180]

In 2010, M. Brookhart and coworkers successfully applied the complex $[Ir(POCOP)(acetone)H][B(C_6F_5)_4]$ (where POCOP = 2,6- $[OP(^tBu)_2]_2C_6H_3$]) to the hydrosilylation of aliphatic and aromatic ketones and aldehydes with $HSiEt_3$ showing good rates but rather limited substrate scope (scheme 24).[182] To date, the latter iridium precatalyst $[Ir(POCOP)(acetone)H][B(C_6F_5)_4]$ is presumably the best homogeneous iridium system applied in the hydrosilylation of aldehydes and ketones (until our system described in this thesis).

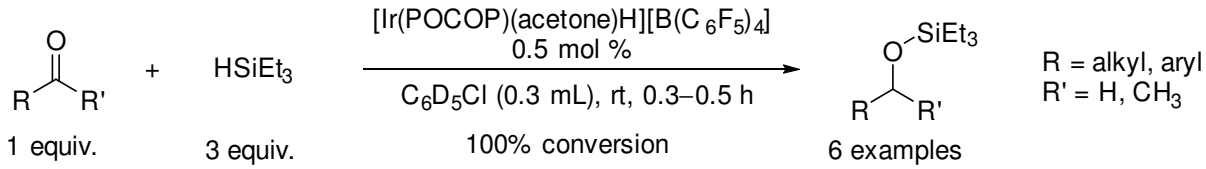

Scheme 24. The complex $[Ir(POCOP)(acetone)H][B(C_6F_5)_4]$ is an active iridium precatalyst for the hydrosilylation of ketones and aldehydes, as reported by M. Brookhart and coworkers.[182] POCOP = 2,6-$[OP(^tBu)_2]_2C_6H_3$].

3.2.1.5 Asymmetric hydrosilylation of ketones

3.2.1.5.1 Motivation, general principle, and historical background

Asymmetric hydrosilylation of ketones is an interesting reaction to study because it can be a valuable method for the synthesis of enantiopure alcohol derivatives. The principle that makes this reaction useful to explore is that ketones RR'C=O are pro-chiral (schemes 25–26). The latter point offers the possibility to afford selectively an enantiomeric excess of *R* or *S* as stereogenic centers. However, the nature of the metal and its ligands are crucial parameters that will determine the most favorable attacking face (*Si* or *Re*) of the ketone (scheme 26).

[182] Park, S.; Brookhart, M. Hydrosilylation of Carbonyl-Containing Substrates Catalyzed by an Electrophilic η^1-Silane iridium(III) Complex. *Organometallics* **2010**, *29* (22), 6057–6064.

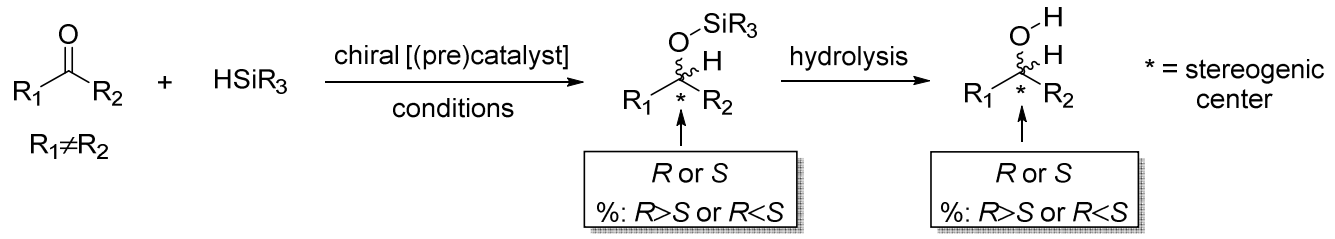

Scheme 25. General reaction scheme for asymmetric hydrosilylation of ketones.

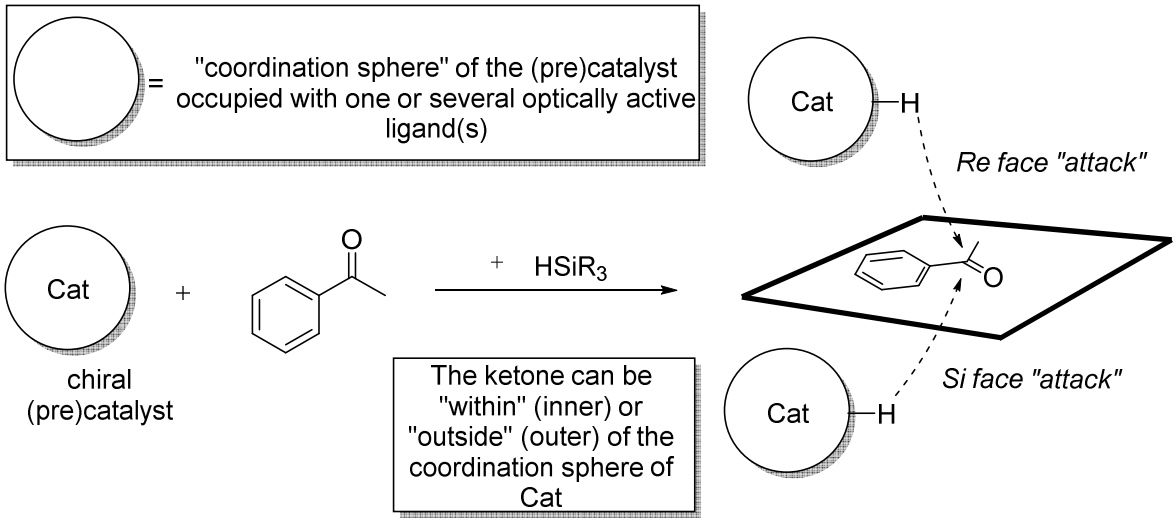

Scheme 26. Schematic representation of the principle behind asymmetric hydrosilylation of ketones. The example with acetophenone as substrate is given for illustrating this principle.

In this context, many TM-based catalytic systems have been developed.[183,184] H. Kumada and coworkers reported the first study on asymmetric hydrosilylation of ketones by using a [Pt] precatalyst with combination of either (+)-(*R*)-benzylmethylphenyl-phosphine or (–)-(*R*)-methylphenyl-*n*-propylphosphine as chiral ligands.[185] This seminal work was followed within the same period by the studies of H. Kumada and coworkers, Ojima and coworkers, and Kagan and coworkers, using the complex $[Rh\{(R)\text{-}(PhCH_2)MePhP\}_2(H)_2(S)_2][ClO_4]$ (S = solvent),[186] a

[183] Marciniec, B; Macie-jewski, H; Pietraszuk, C.; Pawluć, P. Asymmetric Hydrosilylation of Unsaturated Carbon–Heteroatom Bonds. In *Hydrosilylation: A Comprehensive Review on Recent Advances*, Marciniec, B., Ed.; Springer: Berlin Heidelberg, 2009; Vol. 1, pp 342–382.
[184] Nishiyama, H.;. Itoh, K. Asymmetric Hydrosilylation and Related Reactions. In *Catalytic Asymmetric Synthesis*, 2nd edition; Ojima, I., Ed.; Wiley-VCH, 2000; pp 111-145.
[185] Yamamoto, K.; Hayashi, T.; Kumada, M. Asymmetric Hydrosilylation of Ketones Catalyzed by Chiral Phosphine-platinum(II) Complexes. *J. Organomet. Chem.* **1972**, *46* (2), C65–C67.
[186] Yamamoto, K.; Kumada, M. Asymmetric Hydrosilylation of Ketones Catalyzed by a Chiral Cationic Rhodium Complex. *J. Organomet. Chem.* **1973**, *54*, 45–47.

combination of [Rh(1,5-hexadiene)Cl)$_2$ or [Rh(cyclooctadiene)Cl]$_2$ with (–)-(*S*)-benzylmethylphenylphosphine) (optical purity 62%) as ligand,[187] and a supported heterogeneous [Rh^I]/(optically-pure phosphine) complex[188] respectively. Since these early publications, numerous reports have been published with the highest enantioselectivities ever reached come generally from oxazoline-based ligand systems (scheme 27).[189]

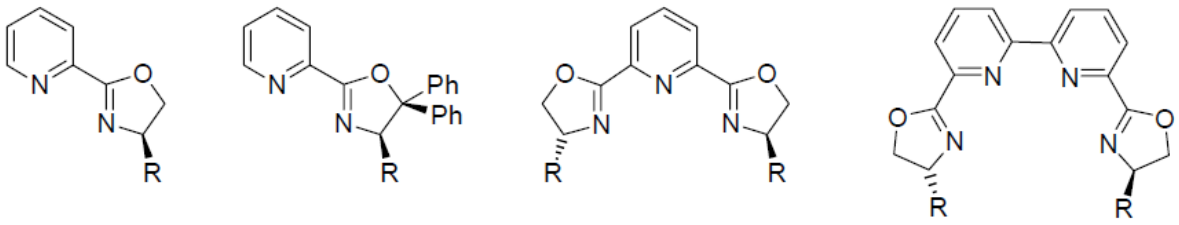

Scheme 27. Representative examples of typically employed pyridineoxazoline ligands in the asymmetric hydrosilylation of ketones.[189] Van Leeuwen, Piet W.N.M. Hydrosilylation. In *Homogeneous Catalysis*; Springer Netherlands: Dordrecht, 2004; p 381. © 2004 Kluwer Academic Publishers. With permission of Springer.

3.2.1.5.2 The case of iridium complexes: seminal works

Concerning iridium, the first asymmetric hydrosilylation of ketones was reported in 1995 by S. Uemura and coworkers, giving highly enantioselective reaction (>90% *ee*) (*ee* = enantiomer excess) with chiral (*S*,*S*,*S*)-diphenyloxazolinyl- ferrocenylphosphine ((*S*,*S*,*S*)-DIPOF, scheme) as ligand.[190] A mixture of DIPOF (1 mol %) and [Ir(COD)Cl]$_2$ precursor (0.5 mol %) proved to be a useful tool for the hydrosilylation of acetophenone (100 mol %) with H_2SiPh_2 (130 mol %). 1-Phenylethanol was obtained within 20 h at 0°C in high yield and with an *ee* of 96% and (*S*) as absolute configuration. An intriguing fact pointed out by the authors was the formation of 1-phenylethanol with a lower *ee* and with the opposite absolute configuration (*R*) when the same reaction was conducted with [Rh(COD)Cl]$_2$ in place of [Ir(COD)Cl]$_2$ as precatalyst (scheme 28).

[187] Ojima, I.; Kogure, T.; Nagai, Y. Asymmetric Reduction of Ketones *via* Hydrosilylation Catalyzed by a Rhodium(I) Complex with Chiral Phosphine Ligands. *Chem. Lett.* **1973**, *2* (6), 541–544.
[188] Poulin, J. C.; Dumont, W.; Dang, T. P.; Kagan, H. B. C. R. Préparation d'une diphosphine chirale liée à une résine polystyrène insoluble et exemple d'utilisation en catalyse asymétrique. *Acad. Sci., Ser. C*, **1973**, *277*, 41.
[189] Van Leeuwen, Piet W.N.M. Hydrosilylation. In *Homogeneous Catalysis*; Springer Netherlands: Dordrecht, 2004; pp 371–385.
[190] Nishibayashi, Y.; Segawa, K.; Ohe, K.; Uemura, S. Chiral Oxazolinylferrocene-Phosphine Hybrid Ligand for the Asymmetric Hydrosilylation of Ketones. *Organometallics* **1995**, *14* (12), 5486–5487.

Other ketones were showed to be compatible with these catalytic conditions, affording enantioenriched alcohols with *ee* values >90%.[190]

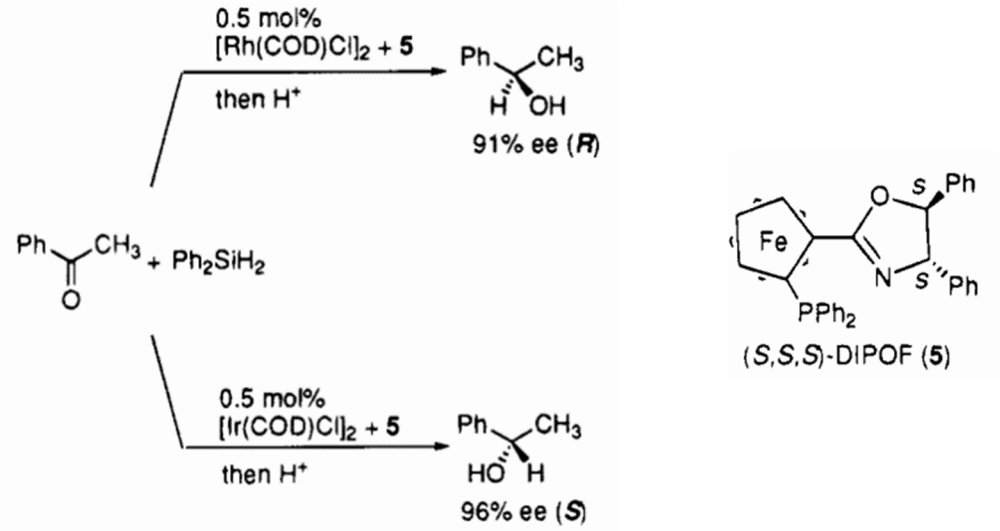

Scheme 28. First example of iridium-catalyzed asymmetric hydrosilylation of ketones, as reported by S. Uemura and coworkers.[190] Reprinted with permission from Nishibayashi, Y.; Segawa, K.; Ohe, K.; Uemura, S. *Organometallics* **1995**, *14* (12), 5486. Copyright 1995 American Chemical Society.

3.2.1.6 Proposed mechanisms

Many different mechanisms of carbonyl (aldehydes and ketones in general) hydrosilylation have been proposed.[191,192,193,194,195] Upon reviewing the literature on the subject, it is intriguing to see such a variety of possible catalytic routes that were proposed over the years. Actually, important issues are still unsolved regarding the actual *key intermediates (and steps)* involved in several catalytic systems. Overall, it seems like "complex" chemistry is at work when TM (also non-TM)-based (pre)catalysts, silanes and carbonyls are mixed together, making difficult

[191] Lipke, M. C.; Liberman-Martin, A. L.; Tilley, T. D. Electrophilic Activation of Silicon-Hydrogen Bonds in Catalytic Hydrosilations. *Angew. Chem. Int. Ed.* **2017**, *56* (9), 2260–2294.
[192] Qin, X.; Liu, X.; Guo, C.; Wu, H.; Xiaofei, Q.; Xiaoyan, L.; Caihong, G.; Haishun, W. Reaction Mechanisms of Carbonyl Compounds Hydrosilylation Catalyzed by Group VIII Transition Metal Complexes. *Chinese J. Org. Chem.* **2016**, *36* (1), 60.
[193] Chakraborty, S.; Bhattacharya, P.; Dai, H.; Guan, H. Nickel and Iron Pincer Complexes as Catalysts for the Reduction of Carbonyl Compounds. *Acc. Chem. Res.* **2015**, *48* (7), 1995–2003.
[194] Riener, K.; Högerl, M. P.; Gigler, P.; Kühn, F. E. Rhodium-Catalyzed Hydrosilylation of Ketones: Catalyst Development and Mechanistic Insights. *ACS Catal.* **2012**, *2* (4), 613–621.
[195] Marciniec, B. Hydrosilylation of Unsaturated Carbon—Heteroatom Bonds. In *Hydrosilylation A Comprehensive Review on Recent Advances*; Marciniec, B., Ed.; Springer Netherlands: Dordrecht, 2009; Vol. 1, pp 289–339.

any common rationale on how and why chemical reactions occur in general. One of the key steps are the breaking of the H–Si bond and the formation of the Si–O bond. The real mechanism explaining how electrons are redistributed between these two bonds is of critical importance yet remains still largely not understood. Saying differently, what are the key clues that make this H–Si bond in good predisposition for the activation to occur and why? On the other hand, the formation of the C–H bond at the carbonyl function, commonly accepted to occur *via* a metal-mediated hydride transfer route, that is the so-called hydride mechanism, is still a matter of debate among researchers working in the field. The doubt resides on the origin of the hydride donor (H^D) source. Even though there are solid evidences towards metal-hydrides (MH) as the H^D source, in some cases other sources of H^D cannot be excluded, at least MH moieties cannot be clearly identified to be involved as such. [193,196,197,198]

In the following paragraphs, after a brief overview on different mechanisms, we will mention in detail only those proposed with iridium complexes as (pre)catalysts, and discuss their validity in terms of experimental evidences (if sufficiently reported) from which the related mechanisms are postulated. If the reader needs more details, a good review has recently appeared which deals with silane activation mechanisms for a broad spectrum of hydrosilylation catalysts, ranging from main group Lewis acids into silylene and η^3-silane organometallic complexes.[191]

One can distinguish two general mechanisms that are currently proposed to explain the hydrosilylation of carbonyls depending on the nature of the (pre)catalyst and the silane, namely the Ojima (scheme 29) and the ionic hydrosilylation (scheme 30) mechanisms. In 1975, I. Ojima and coworkers proposed the first mechanism for the hydrosilylation of various carbonyls catalyzed by the Wilkinson's [$Rh(PPh)_3Cl$] complex (scheme 29a).[199] The mechanism is believed to proceed *via* an inner-sphere catalytic cycle similar to that previously proposed by A. J. Chalk and J. F. Harrod for the hydrosilylation of alkenes,[200] with the main steps as follows: 1) oxidative addition of the silane, 2) coordination of the carbonyl compound, 3) migratory insertion into the M−Si bond and 4) reductive elimination of the silyl ether product. G. Z. Zheng,

[196] Khalimon, A. Y.; Shirobokov, O. G.; Peterson, E.; Simionescu, R.; Kuzmina, L. G.; Howard, J. A. K.; Nikonov, G. I. Mechanistic Aspects of Hydrosilylation Catalyzed by (ArN=)Mo(H)(Cl)(PMe_3)$_3$. *Inorg. Chem.* **2012**, *51* (7), 4300–4313.
[197] Shirobokov, O. G.; Kuzmina, L. G.; Nikonov, G. I. Nonhydride Mechanism of Metal-Catalyzed Hydrosilylation. *J. Am. Chem. Soc.* **2011**, *133* (17), 6487–6489.
[198] Bhattacharya, P.; Krause, J. A.; Guan, H. Iron Hydride Complexes Bearing Phosphinite-Based Pincer Ligands: Synthesis, Reactivity, and Catalytic Application in Hydrosilylation Reactions. *Organometallics* **2011**, *30* (17), 4720–4729.
[199] Ojima, I.; Nihonyanagi, M.; Kogure, T.; Kumagai, M.; Horiuchi, S.; Nakatsugawa, K.; Nagai, Y. Reduction of Carbonyl Compounds via Hydrosilylation. *J. Organomet. Chem.* **1975**, *94* (3), 449–461.
[200] Chalk, A. J.; Harrod, J. F. Homogeneous Catalysis. II. The Mechanism of the Hydrosilation of Olefins Catalyzed by Group VIII Metal Complexes. *J. Am. Chem. Soc.* **1965**, *87* (1), 16–21.

T. H. Chan and coworkers (in 1995), and P. Hofmann, L. H. Gade and coworkers (in 2009) proposed other [Rh]-based catalytic mechanisms (scheme 29b–c).[201,202] The relative deviations from the Ojima mechanism have been attributed to the difference in the nature of catalytic intermediates involved upon going from monohydro silanes (Ojima) into di- and trihydro silanes (Zheng-Chan and Hofmann-Gade mechanisms), as it has been recently discussed in a review reported by F. E. Kühn and coworkers.[203] The Zheng-Chan (scheme 29b) and Hofmann-Gade (scheme 29c) mechanisms differ in that they propose divergent hydride transfer routes to the C=O function. In the former proposal, the hydride is transferred from the coordinated Si atom, while in the latter one the hydride is transferred from the Rh center. In 2003, F. D. Toste and coworkers proposed an original mechanistic rationale accounting for the observations made with high valent [Re]-catalyzed hydrosilylation of carbonyl compounds ([Re] = *cis*-$Re(O)_2I(PPh_3)_2$, scheme 30a).[204] However, M. M. Abu-Omar and coworkers reported in 2007 a detailed mechanistic study where they concluded that other alternative mechanism could be at work for other [Re]-catalyzed hydrosilylation of carbonyls (for example where [Re] = $Re(O)Cl_3(PPh_3)_2$), scheme 30b). The authors argued that "the postulated mechanism for *cis*-$Re(O)_2I(PPh_3)_2$ [Toste-mechanism] is likely to be the exception rather than the rule for hydrosilylation reactions catalyzed by high-valent oxorhenium complexes".[205] The latter points illustrate again the difficulty in postulating general mechanisms for a (at best) given family of (pre)catalysts, which seems to be more pronounced in the case of hydrosilylation reactions in general. By the way, other mechanisms have been proposed for [Mo], and [Co]-based catalysis by G. I. Nikonov and coworkers (2009) (scheme 30c), and by J. C. Peters and coworkers (2015) (scheme 30d) respectively.[206,207] The so-called ionic hydrosilylation mechanism is the other major alternative mechanism proposed for the catalytic hydrosilylation of carbonyls compounds.

---

[201] Zheng, G. Z.; Chan, T. H. Regiocontrolled Hydrosilation of *α*,*β*-Unsaturated Carbonyl Compounds Catalyzed by Hydridotetrakis(triphenylphosphine)rhodium(I). *Organometallics* **1995**, *14* (1), 70–79.

[202] Schneider, N.; Finger, M.; Haferkemper, C.; Bellemin-Laponnaz, S.; Hofmann, P.; Gade, L. H. Metal Silylenes Generated by Double Silicon-Hydrogen Activation: Key Intermediates in the Rhodium-Catalyzed Hydrosilylation of Ketones. *Angew. Chem. Int. Ed.* **2009**, *48* (9), 1609–1613.

[203] Riener, K.; Högerl, M. P.; Gigler, P.; Kühn, F. E. Rhodium-Catalyzed Hydrosilylation of Ketones: Catalyst Development and Mechanistic Insights. *ACS Catal.* **2012**, *2* (4), 613–621.

[204] Kennedy-Smith, J. J.; Nolin, K. A.; Gunterman, H. P.; Toste, F. D. Reversing the Role of the Metal–Oxygen *π*-Bond. Chemoselective Catalytic Reductions with a rhenium(V)-Dioxo Complex. *J. Am. Chem. Soc.* **2003**, *125* (14), 4056–4057.

[205] Du, G.; Fanwick, P. E.; Abu-Omar, M. M. Mechanistic Insight into Hydrosilylation Reactions Catalyzed by High Valent Re≡X (X = O, NAr, or N) Complexes: The Silane (SiH) Does Not Add across the Metal–Ligand Multiple Bond. *J. Am. Chem. Soc.* **2007**, *129* (16), 5180–5187.

[206] Peterson, E.; Khalimon, A. Y.; Simionescu, R.; Kuzmina, L. G.; Howard, J. A. K.; Nikonov, G. I. Diversity of Catalysis by an Imido-Hydrido Complex of Molybdenum. Mechanism of Carbonyl Hydrosilylation and Silane Alcoholysis. *J. Am. Chem. Soc.* **2009**, *131* (3), 908–909.

[207] Nesbit, M. A.; Suess, D. L. M.; Peters, J. C. E–H Bond Activations and Hydrosilylation Catalysis with Iron and Cobalt Metalloboranes. *Organometallics* **2015**, *34* (19), 4741–4752.

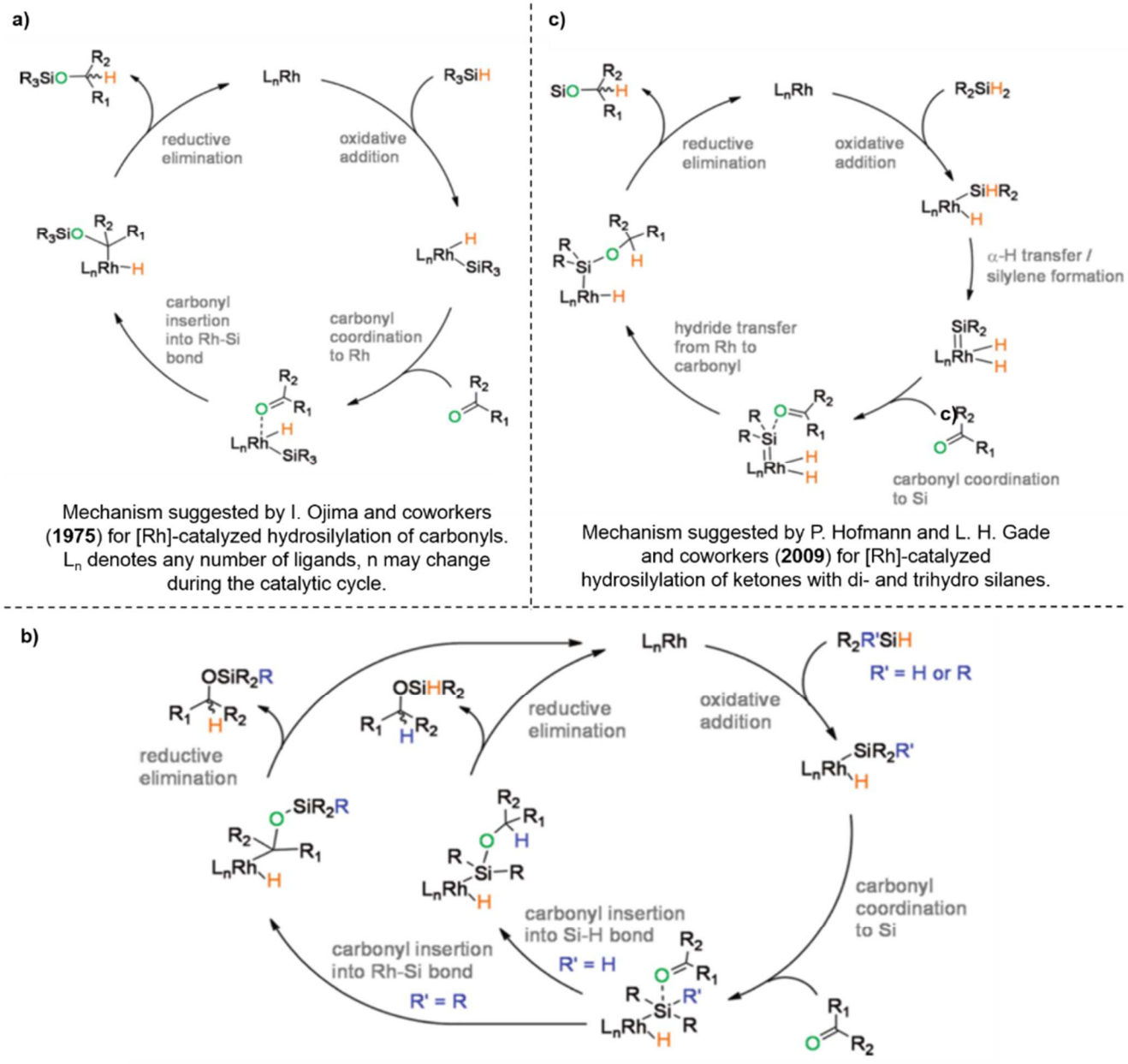

Scheme 29. Proposed mechanisms for the [Rh]-catalyzed hydrosilylation of aldehydes and ketones, as proposed by **a)** I. Ojima and coworkers,[199] **b)** G. Z. Zheng, T. H. Chan and coworkers,[201] and **c)** P. Hofmann, L. H. Gade and coworkers.[202] Reprinted with permission from Riener, K.; Högerl, M. P.; Gigler, P.; Kühn, F. E. *ACS Catal.* **2012**, *2* (4), 613. Copyright 2012 American Chemical Society.

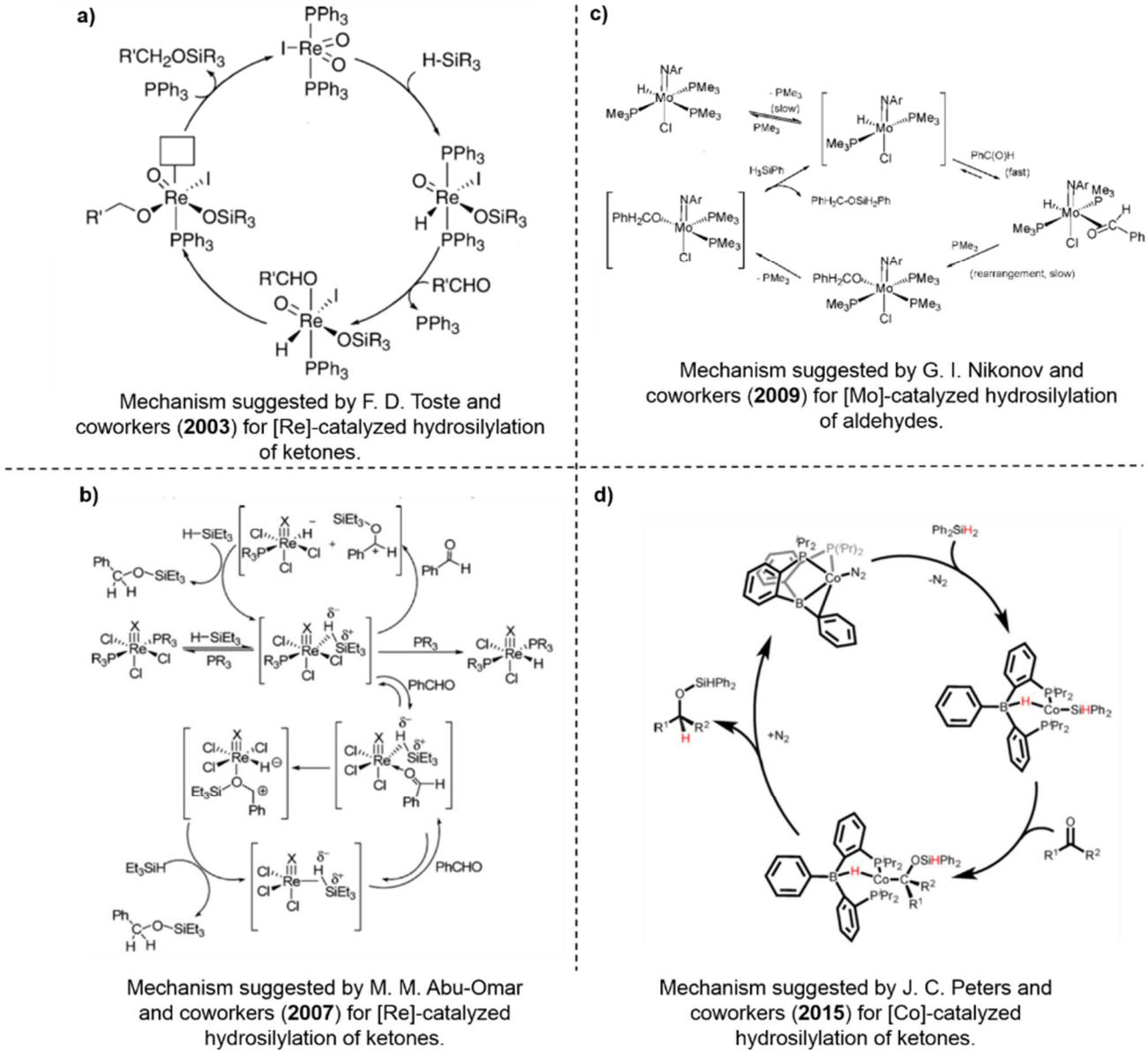

Scheme 30. Proposed mechanisms for **a**–**b**) [Re], **c**) [Mo], and **d**) [Co]-catalyzed hydrosilylation of aldehydes and ketones, as proposed by **a)** F. D. Toste and coworkers (Reprinted with permission from Nolin, K. A.; Krumper, J. R.; Pluth, M. D.; Bergman, R. G.; Toste, F. D. *J. Am. Chem. Soc.* **2007**, *129* (47), 14684. Copyright 2007 American Chemical Society),[204] **b)** M. M. Abu-Omar and coworkers (Reprinted with permission from Du, G.; Fanwick, P. E.; Abu-Omar, M. M. *J. Am. Chem. Soc.* **2007**, *129* (16), 5180. Copyright 2007 American Chemical Society),[205] **c)** G. I. Nikonov and coworkers (Reprinted with permission from Peterson, E.; Khalimon, A. Y.; Simionescu, R.; Kuzmina, L. G.; Howard, J. A. K.; Nikonov, G. I. *J. Am. Chem. Soc.* **2009**, *131* (3), 908. Copyright 2009 American Chemical Society),[206] and **d)** J. C. Peters and coworkers (Reprinted with permission from Nesbit, M. A.; Suess, D. L. M.; Peters, J. C. *Organometallics* **2015**, *34* (19), 4741 Copyright 2015 American Chemical Society).[207]

In 2000 W. E. Piers and coworkers were the first to propose such a mechanism with the Lewis acid $B(C_6F_5)_3$ as a catalyst (scheme 31a).[208] The authors provided solid evidences towards an original ionic H–Si bond activation mechanism based on the observations that the least basic substrates are hydrosilylated at the fastest rates. They consequently proposed that the Lewis basic H–Si bond is activated by the Lewis acidic borane catalyst leading to an heterolytic cleavage of the H–Si bond, assisted by the coordination of the C=O function of the carbonyl to $[R_3Si]^+$. This reaction mechanism has been confirmed with the study reported by M. Oestreich and co-workers, who elegantly demonstrated the S_N2-Si mechanism for the H–Si bond dissociation.[209] Due to the elusive behavior of the intermediate $[Et_3Si–H–B(C_6F_5)_3]$, the "more stable" Lewis pair intermediate $[R_3Si–H–BR'_3]$ has been characterized (2014) by X-ray crystallography by H. M. Tuononen, W. E. Piers and coworkers, thus confirming their earlier proposals.[210] In 2015, S. Grimme, D. W. Stephan and coworkers provided a DFT-based ionic hydrosilylation mechanism as a possible explanation of the catalysis observed with the Lewis acid $[(C_6F_5)_3PF][B(C_6F_5)_4]$ (scheme 31b).[211] Later on in 2010, M. Brookhart and coworkers, and G. I. Nikonov and coworkers adopted a similar ionic hydrosilylation mechanism as plausible rationale for the catalysis mediated with $[Ir(POCOP)(acetone)H][B(C_6F_5)_4]$ (scheme 31c) and $[(P(^iPr)_3(Cp)Ru(NCMe)_2][B(C_6F_5)_4]$ (scheme 31d) complexes respectively.[212,213] In 2014, P. Hrobárik, M. Oestreich and coworkers proposed a more detailed (revisited) version of the Brookhart's mechanism, opening some controversy about the "true" hydride donor source involved within this complex catalysis (*vide infra*).[214] The common feature of the above proposed ionic hydrosilylation mechanisms involves the silylium $[R_3Si]^+$ ion abstraction by the O atom of the C=O function as the key step, which gives rise to the formation of $[C=O\rightarrow SiR_3]^+$ and [M]-H (M = B, Ir, P, Ru) as catalytic intermediates.

---

[208] Parks, D. J.; Blackwell, J. M.; Piers, W. E. Studies on the Mechanism of $B(C_6F_5)_3$-Catalyzed Hydrosilation of Carbonyl Functions. *J. Org. Chem.* **2000**, *65* (10), 3090–3098.

[209] Rendler, S.; Oestreich, M. Conclusive Evidence for an SN_2-Si Mechanism in the $B(C_6F5)_3$-Catalyzed Hydrosilylation of Carbonyl Compounds: Implications for the Related Hydrogenation. *Angew. Chem. Int. Ed.* **2008**, *47* (32), 5997–6000.

[210] Houghton, A. Y.; Hurmalainen, J.; Mansikkamäki, A.; Piers, W. E.; Tuononen, H. M. Direct Observation of a Borane-Silane Complex Involved in Frustrated Lewis-Pair-Mediated Hydrosilylations. *Nat. Chem.* **2014**, *6* (11), 983–988.

[211] Pérez, M.; Qu, Z. W.; Caputo, C. B.; Podgorny, V.; Hounjet, L. J.; Hansen, A.; Dobrovetsky, R.; Grimme, S.; Stephan, D. W. Hydrosilylation of Ketones, Imines and Nitriles Catalysed by Electrophilic Phosphonium Cations: Functional Group Selectivity and Mechanistic Considerations. *Chem. - A Eur. J.* **2015**, *21* (17), 6491–6500.

[212] Park, S.; Brookhart, M. Hydrosilylation of Carbonyl-Containing Substrates Catalyzed by an Electrophilic η^1-Silane iridium(III) Complex. *Organometallics* **2010**, *29* (22), 6057–6064.

[213] Gutsulyak, D. V.; Vyboishchikov, S. F.; Nikonov, G. I. Cationic Silane σ-Complexes of Ruthenium with Relevance to Catalysis. *J. Am. Chem. Soc.* **2010**, *132* (17), 5950–5951.

[214] Metsänen, T. T.; Hrobárik, P.; Klare, H. F. T.; Kaupp, M.; Oestreich, M. Insight into the Mechanism of Carbonyl Hydrosilylation Catalyzed by Brookhart's Cationic Iridium(III) Pincer Complex. *J. Am. Chem. Soc.* **2014**, *136* (19), 6912–6915.

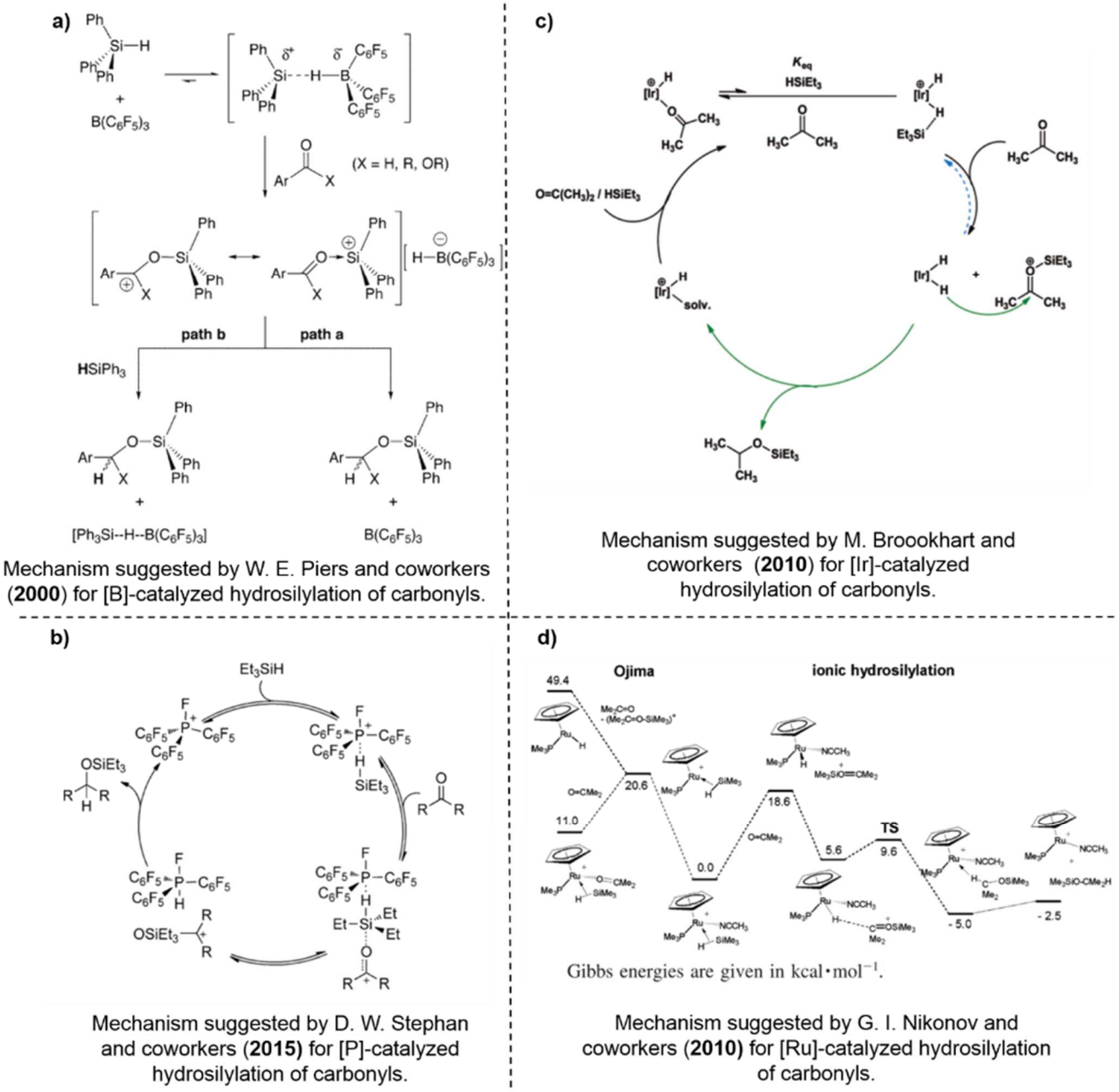

Scheme 31. Proposed ionic mechanisms for the hydrosilylation of aldehydes and ketones, as reported by **a)** E. Piers and coworkers (Reprinted with permission from Parks, D. J.; Blackwell, J. M.; Piers, W. E. *J. Org. Chem*. **2000**, *65* (10), 3090. Copyright 2000 American Chemical Society),[208] **b)** Grimme, D. W. Stephan and coworkers, (Reprinted with permission from Pérez, M.; Qu, Z. W.; Caputo, C. B.; Podgorny, V.; Hounjet, L. J.; Hansen, A.; Dobrovetsky, R.; Grimme, S.; Stephan, D. *Chem. - A Eur. J.* **2015**, *21* (17), 6491. Copyright 2015 Wiley Materials), [211] **c)** M. Brookhart and coworkers (Reprinted with permission from Park, S.; Brookhart, M. *Organometallics* **2010**, *29* (22), 6057. Copyright 2010 American Chemical Society),[212] and **d)** G. I. Nikonov and coworkers (Reprinted with permission from Gutsulyak, D. V.; Vyboishchikov, S. F.; Nikonov, G. I. *J. Am. Chem. Soc*. **2010**, *132* (17), 5950. Copyright 2010 American Chemical Society) [213]

From inspection of these mechanisms, it is postulated then that both $[C{=}O{\rightarrow}SiR_3]^+$ (which can reasonably be considered as a more or less stabilized carbocationic intermediate $[C^+–O\text{-}SiR_3]$) and [M] –H intermediates react with each other affording the silyl ether product [C(H)–O– SiR_3] and regenerating the catalyst $[M]^+$ or [M] for further cycles.

To our knowledge, the only available mechanisms which involve an iridium complex as a (pre)catalyst are those proposed by the research groups of M. Brookhart and coworkers (original version, scheme 31c) and M. Oestreich and coworkers (revisited version, scheme 32c), which both deal with the complex $[Ir(POCOP)(acetone)H][B(C_6F_5)_4]$.[215,216] The latter mechanisms have been recently discussed in two recent papers reported by M. Iglesias, L. A. Oro and coworkers (2014), and by T. D. Tilley and coworkers (2016).[217,218] The conflict resides on the nature of the hydride donor source (H^D), as either $[Ir^{III}]$–H or $[Ir^V](H)(SiR_3)$ have been proposed to act as such by the groups of M. Brookhart and M. Oestreich respectively. However, the merit should be recognized to the M. Brookhart's team who was the first to provide a solid evidence supporting an ionic-nature of the proposed catalytic hydrosilylation of carbonyls. The X-ray diffraction analysis of the trapped single crystal of the $[Ir(POCOP)(\eta^1\text{-}SiEt_3)H][B(C_6F_5)_4]$ (scheme 32a–b) complex proved to be the best structural evidence to support the latter mechanism.[219] The particularity of this H–Si σ-complex is the presence, as revealed by its X-ray structure, of a linear Ir–H–Si arrangement allowed by the η^1-$HSiEt_3$ coordination mode to Ir. The latter point is invoked as the major reason why this complex is so active in catalysis when paralleling its structure-function to similar observations obtained with $R_3Si–HSiR_3$,[220] $R'_3B–HSiR_3$[221] and $R''_3Al–HSiR_3$[222] adducts of linear Si–H–Si, B–H–Si and Al–H–Si angles respectively.

---

[215] Park, S.; Brookhart, M. Hydrosilylation of Carbonyl-Containing Substrates Catalyzed by an Electrophilic η^1-Silane iridium(III) Complex. *Organometallics* **2010**, *29* (22), 6057–6064.

[216] Metsänen, T. T.; Hrobárik, P.; Klare, H. F. T.; Kaupp, M.; Oestreich, M. Insight into the Mechanism of Carbonyl Hydrosilylation Catalyzed by Brookhart's Cationic Iridium(III) Pincer Complex. *J. Am. Chem. Soc.* **2014**, *136* (19), 6912–6915.

[217] Iglesias, M.; Fernández-Alvarez, F. J.; Oro, L. A. Outer-Sphere Ionic Hydrosilylation Catalysis. *ChemCatChem* **2014**, *6* (9), 2486–2489.

[218] Lipke, M. C.; Liberman-Martin, A. L.; Tilley, T. D. Electrophilic Activation of Silicon-Hydrogen Bonds in Catalytic Hydrosilations. *Angew. Chem. Int. Ed.* **2017**, *56* (9), 2260–2294.

[219] Yang, J.; White, P. S.; Schauer, C. K.; Brookhart, M. Structural and Spectroscopic Characterization of an Unprecedented Cationic Transition-Metal η^1-Silane Complex. *Angew. Chem. Int. Ed.* **2008**, *47* (22), 4141–4143.

[220] a) Hoffmann, S. P.; Kato, T.; Tham, F. S.; Reed, C. A. Novel Weak Coordination to Silylium Ions: Formation of Nearly Linear Si-H-Si Bonds. *Chem. Commun.* **2006**, *31* (7), 767–769. b) Connelly, S. J.; Kaminsky, W.; Heinekey, D. M. Structure and Solution Reactivity of (Triethylsilylium)triethylsilane Cations. *Organometallics* **2013**, *32* (24), 7478–7481.

[221] Houghton, A. Y.; Hurmalainen, J.; Mansikkamäki, A.; Piers, W. E.; Tuononen, H. M. Direct Observation of a Borane-Silane Complex Involved in Frustrated Lewis-Pair-Mediated Hydrosilylations. *Nat. Chem.* **2014**, *6* (11), 983–988.

[222] Chen, J.; Chen, E. Y. X. Elusive Silane Alane Complex [Si-H…Al]: Isolation, Characterization, and Multifaceted Frustrated-Lewis-Pair-Type Catalysis. *Angew. Chem. Int. Ed.* **2015**, *54* (32),6842–6846.

a)

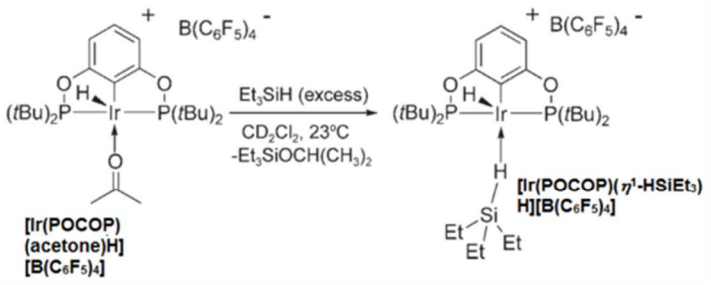

M. Brookhart's original study on the reaction leading to [Ir(POCOP)(η^1-HSiEt$_3$)(H)][B(C$_6$F$_5$)$_4$], identified as key catalytic intermediate.

b)

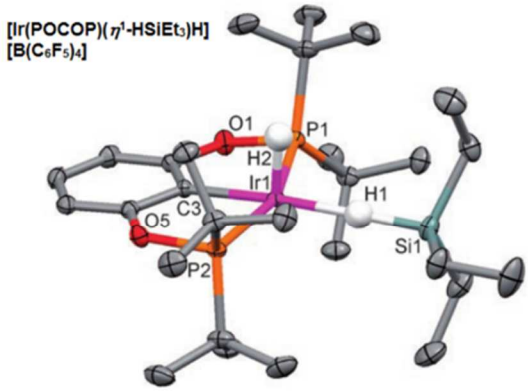

M. Brookhart's original study on the X-ray structure of [Ir(POCOP)(η^1-HSiEt$_3$)(H)][B(C$_6$F$_5$)$_4$], identified as key catalytic intermediate.

c)

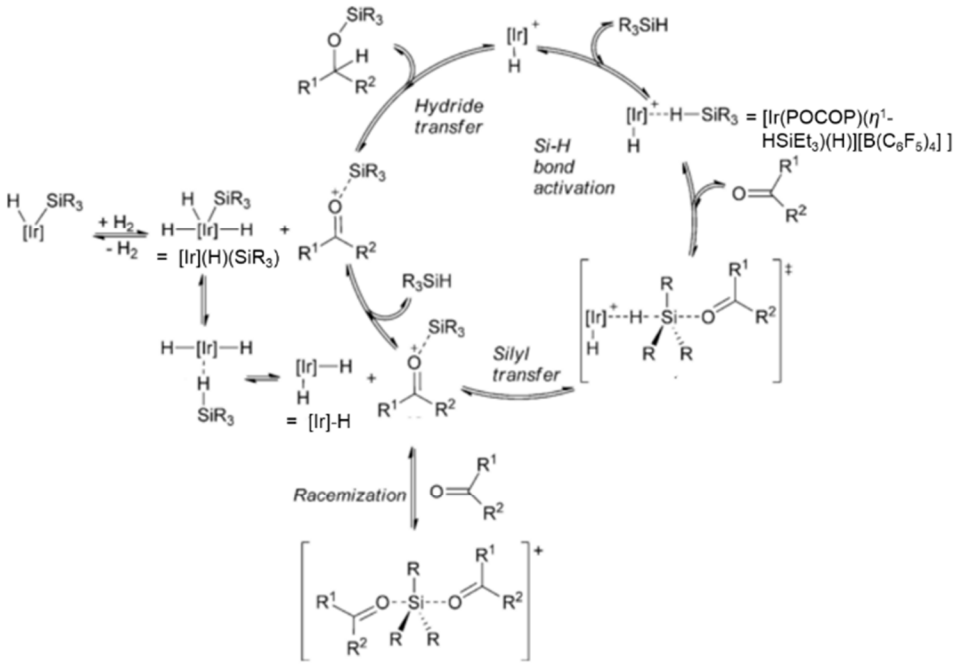

M. Oestreich's revisited study on the catalytic mechanism for the hydrosilylation of ketones and aldehydes, involving [Ir(POCOP)(η^1-HSiEt$_3$)(H)][B(C$_6$F$_5$)$_4$] as the key catalytic intermediate.

Scheme 32. a–b) Original M. Brookhart and coworkers' study, which shed light on the nature of [Ir(POCOP)(η^1-SiEt$_3$)H][B(C$_6$F$_5$)$_4$], proposed to be the active catalytic intermediate in the hydrosilylation of aldehydes and ketones (Reprinted with permission from Yang, J.; White, P. S.; Schauer, C. K.; Brookhart, M. *Angew. Chem. Int. Ed.* **2008**, *47* (22), 4141. Copyright 2008 Wiley Materials).[219] **c)** Revisited mechanism of M. Oestreich and coworkers' (Reprinted with permission from Metsänen, T. T.; Hrobárik, P.; Klare, H. F. T.; Kaupp, M.; Oestreich, M. J. *Am. Chem. Soc.* **2014**, *136* (19), 6912. Copyright 2014 American Chemical Society).[216]

Another solid evidence in support of the ionic hydrosilylation mechanism came also from the M. Brookhart's group; with the crystallization of the ether stabilized silyl cation intermediate $[SiEt_3OEt_2][B(C_6F_5)_4]$ from a mixture of diethylether and $HSiEt_3$ in the presence of the *in-situ* generated catalytic intermediate $[Ir(POCOP)(\eta^1\text{-}SiEt_3)H][B(C_6F_5)_4]$ (scheme 33).[223]

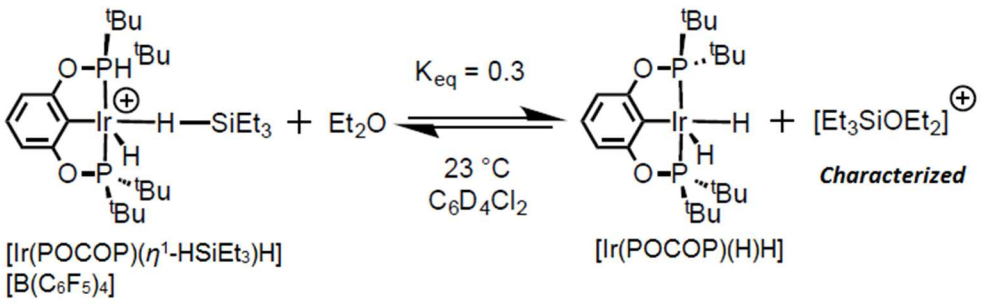

Scheme 33. Proposed mechanism for the the formation of the diethyether-triethylsilylium Lewis pair intermediate $[SiEt_3OEt_2][B(C_6F_5)_4]$.[223] Reprinted with permission from Yang, J.; White, P. S.; Brookhart, M. Scope and Mechanism of the Iridium-Catalyzed Cleavage of Alkyl Ethers with Triethylsilane. *J. Am. Chem. Soc.* **2008**, *130* (51), 17509. Copyright 2008 American Chemical Society.

However, these remarkable bodies of evidence provided by the M. Brookhart's group did not include any clear evidence about the involvement of [Ir]–H as a catalytic intermediate, even though the logic should point towards that conclusion. In this context, the study conducted by M. Oestreich and coworkers was a deeper examination of the role that [Ir]–H could play as a possible H^D source.[224] The authors concluded that at least a more complex variation of the ionic hydrosilylation mechanism originally suggested by M. Brookhart and coworkers should be considered. The main argument provided by the authors was based on the observation that the neutral [Ir]–H complex is less prompt for transferring its hydride to $[R'_2C{=}O{\rightarrow}SiR_3]^+$ than $[Ir](H)(SiR_3)$ (which is the product of addition of $HSiR_3$ to [Ir]–H) does. The latter point was supported by a DFT study, which indicated that $[Ir](H)(SiR_3)$ is a better H^D (more "hydridic") than

[223] Yang, J.; White, P. S.; Brookhart, M. Scope and Mechanism of the Iridium-Catalyzed Cleavage of Alkyl Ethers with Triethylsilane. *J. Am. Chem. Soc.* **2008**, *130* (51), 17509–17518.
[224] Metsänen, T. T.; Hrobárik, P.; Klare, H. F. T.; Kaupp, M.; Oestreich, M. Insight into the Mechanism of Carbonyl Hydrosilylation Catalyzed by Brookhart's Cationic Iridium(III) Pincer Complex. *J. Am. Chem. Soc.* **2014**, *136* (19), 6912–6915.

[Ir]-H. However, a contradiction still exists since [Ir](H)(SiR_3) can also be viewed as a less efficient H^D source than [Ir]–H if we only take into consideration the steric environment created at Ir and H atoms. Indeed, because of its additional SiR_3 ligand, [Ir](H)(SiR_3) might be less easily accessible for transferring its hydride when compared to the less sterically encumbred [Ir]–H. Additional studies are needed to clarify the situation of the latter controversy.

Overall, one can conclude that the nature of the hydrosilylation mechanism which is at work at least for aldehydes and ketones is strongly influenced by the catalytic system of study. However, a huge progress has been made in the field with the remarkable contribution of several research groups, the results of which should be regarded as important pieces of a large puzzle that might give rise to future fundamental understandings. The most important challenge in the future is to elucidate as precisely as possible the nature of the key species and/or steps that are involved in this particular reaction.

3.2.2 Results and discussion

In chapter 2 of this manuscript, we described the *O*Si of alcohols catalyzed by precatalysts [**2**][X] and [**4**][X], and described the related mechanism based on experimental and theoretical evidences. In light of these observations, we decided to investigate the hydrosilylation of aldehydes and ketones. The results of this study are summarized in tables 12 and 13, while the related experimental procedures, optimization studies and characterization of products can be found in the experimental part.

3.2.2.1 hydrosilylation of acetophenone as starting point

We first carried out a preliminary test with the hydrosilylation of one equivalent of acetophenone with 1.2 equivalents of $HSiEt_3$ in the presence of 0.1 mol % of [**4**][$BArF_{24}$] and CD_2Cl_2 as solvent (0.5 mL) upon stirring at room temperature (scheme 34). The reaction was extremely exothermic. After ~5 minutes, the reaction was analyzed by ^1H NMR which showed selective and complete conversion (>99%) of the substrates into (triethylsiloxy)ethylbenzene (scheme 34), corresponding to a TON of 1000 and a TOF of 1.2×10^4 h^{-1} (scheme 34).

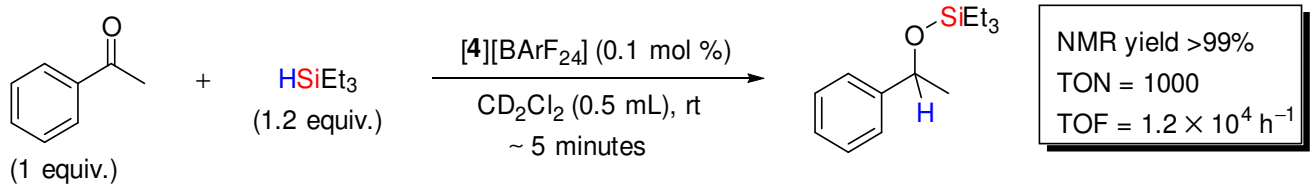

Scheme 34. [**4**][$BArF_{24}$] mediated catalytic hydrosilylation of acetophenone with $HSiEt_3$ (^1H NMR analysis: CD_2Cl_2, 298 K, 400 MHz).

Acetophenone was also found to be efficiently converted (97%) within 15 minutes when using only 0.05 mol % of [**4**][$BArF_{24}$], corresponding to a TON of ~2000 and a TOF of ~7.8×10^3 h^{-1}. This outstanding reactivity encouraged us to study the substrate scope of this catalyst system (aldehydes and ketones). Several optimization studies were conducted with acetophenone as substrate, which mostly consisted in varying the nature of the silane, the precatalyst and the solvent (experimental part). The following optimized conditions were selected for the substrate scope study: ketone or aldehyde (1 equivalent) and silane (1.2 equivalents) were mixed

together prior to addition of a solution containing 0.1 mol % of [**4**][$BArF_{24}$] in CH_2Cl_2 (0.5 mL). After stirring for 30 minutes at room temperature, a solution of tri-*tert*-butylbenzene (as the ^1H NMR internal reference) in CH_2Cl_2 or C_6D_6 (~0.2 mL) was introduced to the reaction mixture, then an aliquot was taken for ^1H NMR analysis (C_6D_6). These conditions will be called "standard conditions" in the next sections, and any deviation from these standard conditions will be clearly specified. By using the latter standard conditions several ketones and aldehydes were tested, and the related results are summarized in table 12 and table 13 respectively.

3.2.2.2 Substrate scope: hydrosilylation of ketones

Several ketones were found to be readily and quantitatively hydrosilylated (table 12). Most of the ketones tested were totally converted under the standard conditions but raising the precatalyst loading from 0.1 to 0.5 mol % was necessary to ensure completion. Some substrates showed however some reluctance to complete reduction under the standard conditions, so that a prolonged time of reaction was necessary. For example, 4'-(trifluoromethyl)acetophenone was partially converted (30%) within 18h of reaction. Similarly, when 2-acetylpyridine and 4-acetylbenzonitrile were used, the respective products were obtained in both cases in 54% yield. The latter observations at first view contradict the fact that electron-withdrawing groups should make the carbon atom of the C=O bond more electrophilic, thus making the nucleophilic attack of the hydride more favorable. However, one can explain the latter contradiction if we look at what would happen at the oxygen atom of the C=O bond upon decreasing the electron density with introduction of electron-withdrawing substituents. The fact that the rate of hydrosilylation becomes lower can be rationalized in terms of lower Lewis basicity at the oxygen atom of the ketone in that cases. Indeed, if we consider that the activation of the C=O bond occurs through the coordination of the Lewis basic oxygen atom to the Lewis acidic silylium group $[SiEt_3]^+$, one can easily postulate that a lower Lewis basicity at oxygen will lower the reaction efficiency with $[SiEt_3]^+$, making the C=O bond less activated. These results provide at first glance a good support towards an ionic-like hydrosilylation mechanism of the catalytic reaction described herein. Moreover, these findings are reminiscent of the ones described by M. Brookhart and coworkers for the carbonyl hydrosilylation precatalyst [Ir(POCOP)(acetone)H][$B(C_6F_5)_4$] (schemes 24 and 31c). The authors noticed a similar behavior during the substrate scope study, which was that acetophenone was 4 times

Table 12. [**4**][$BArF_{24}$]-catalyzed hydrosilylation of ketones.

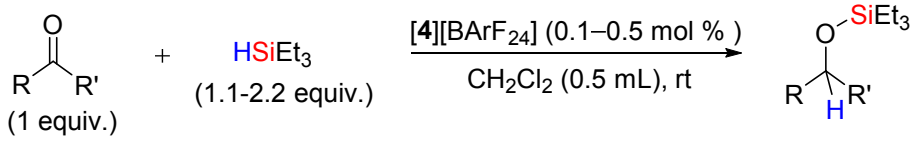

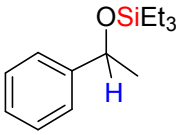

a

0.05 mol %
15 min
97%

b

0.1 mol %
30 min
>99%

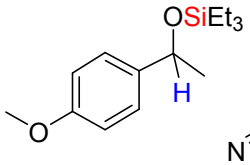

0.5 mol %
30 min
>99%

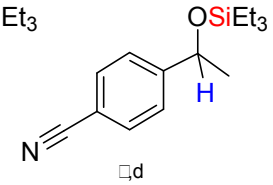

,d

0.5 mol %
30 min
54%

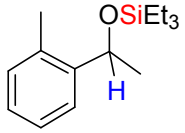

0.5 mol %
30 min
>99%

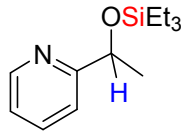

,d

0.5 mol %
18 h
54%

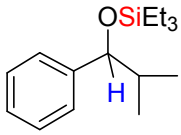

,d

0.5 mol %
30 min
>99%

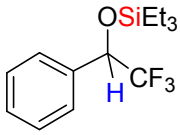

0.5 mol %
18h
30%

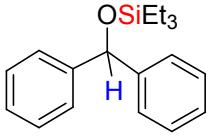

0.5 mol %
30min
>99%

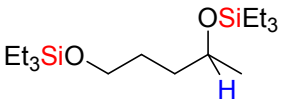

,d,e

0.5 mol %
30 min
>99%

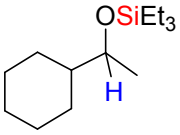

0.1 mol %
30 min
<1%

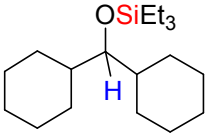

0.5 mol %
30 min
96%

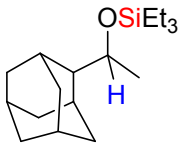

0.5 mol %
30 min
<1%

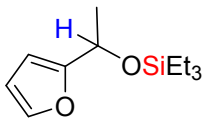

,d

0.5 mol %
2 h
>99%

a) Conditions: a□etophenone (0.2 mL, 1.71 mmol), $HSiEt_3$ (0.30 mL, 1.89 mmol), [**4**][$BArF_{24}$] (1.2 mg, 8.57×10^{-4} mmol, [0.05 mol %]), rt. When 0.1 mol % of [**4**][$BArF_{24}$] and a ratio of 1:1.2 in a□etophenone:$HSiEt_3$ were used, >99% of produ□t formed after only 5 min, □orresponding to a TON of 1000 and a TOF of 1.2×10^4 h^{-1}. b) Conditions: ketone (1.8 mmol), $HSiEt_3$ (0.31 mL, 1.96 mmol), [**4**][$BArF_{24}$] (2.5 mg, 1.77×10^{-3} mmol, [0.1 mol %]), rt. □) Conditions: ketone (1.1 mmol), $HSiEt_3$ (0.19 mL, 1.20 mmol), [**4**][$BArF_{24}$] (7.7 mg, 5.48×10^{-3} mmol [0.5 mol %]), rt. d) 2.2 equivalents of $HSiEt_3$ (0.38 mL, 2.40 mmol) were used. e) The OH fun□tion was *O*-silylated. Yields were determined by ^{1}H NMR using 1,3,5-tri-*tert*-butylbenzene as internal referen□e.

more reactive than 4'-(trifluoromethyl)acetophenpone,[225] consistent with the silylium-based ionic hydrosilylation mechanism they proposed. It is worth to notice that functional groups such as methoxy, nitrile and furanyl were tolerated, although in the latter two cases their total consumption proved to be difficult for the reasons discussed above. It is expected however that increasing the precatalyst loading to 1 mol % should lead to quantitative conversion of the two latter substrates. However, the OH functional group is not tolerated because the *O*-silylation reaction is competing with the hydrosilylation of ketone. But it is interesting to note that when 2.2 equivalents of $HSiEt_3$ were used, quantitative formation of the product that contains the two protected alcohol functions was observed. It is also interesting to see that the catalytic system could support sterically demanding substrates as illustrated with the total conversion of benzophenone, dicyclohexylmethanone and 2-methyl-1-phenylpropan-1-one when 0.5 mol % of [**4**][$BArF_{24}$] was used under standard conditions. Finally, cyclohexanone was also quantitatively transformed when 0.5 mol % of [**4**][$BArF_{24}$] were used under standard conditions, whereas the more challenging 1-acetyladamantane substrate was unreactive under the standard conditions of catalysis (30 minutes, room temperature, 0.5 mol % of [**4**][$BArF_{24}$]).

3.2.2.3 Substrate scope: hydrosilylation of aldehydes

A similar study was conducted with aldehydes as substrates, and the related results are summarized in table 13. Most of aliphatic and (hetero)aryl aldehydes selected for this study were quantitatively converted within 30 minutes (9 examples). Remarkably, a precatalyst loading of only 0.1 mol % or 0.5 mol % was necessary for all the substrates. Substituents like methyl, methoxy, bromo and trifluoromethyl were tolerated. Unactivated aliphatic substrates were found more reluctant to reduction. For example, priopionaldehyde was partially hydrosilylated in 76% yield (0.5 mol % in precatalyst). However, the *α,β*-unsaturated compound but-2-enal proved to be less active because the C=O function was hydrosilylated in only 11% yield when using the standard conditions.

[225] Park, S.; Brookhart, M. Hydrosilylation of Carbonyl-Containing Substrates Catalyzed by an Electrophilic η^1-Silane iridium(III) Complex. *Organometallics* **2010**, *29* (22), 6057–6064.

Table 13. [**4**][BArF$_{24}$]-catalyzed hydrosilylation of aldehydes.

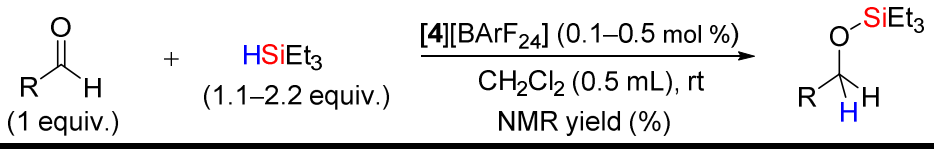

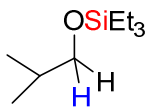

b

0.5 mol %
30 min
76%

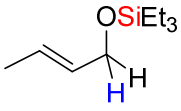

a

0.1 mol %
30 min
11%

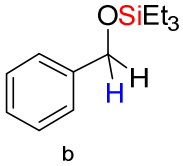

b

0.5 mol %
30 min
>99%

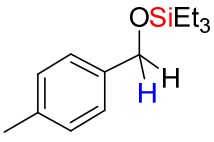

a

0.1 mol %
30 min
97%

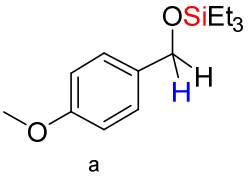

a

0.1 mol %
30 min
>99%

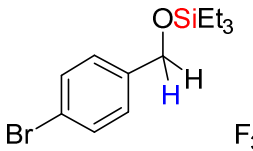

b,c

0.5 mol %
30 min
>99%

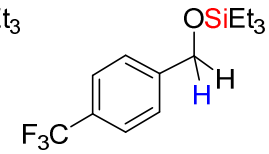

b

0.5 mol %
18h
68%

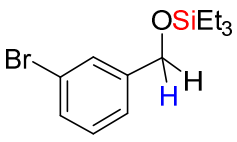

b,c

0.5 mol %
30 min
>99%

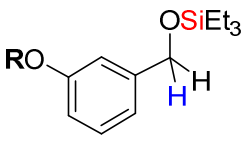

b,c,d

0.5 mol %, 30 min
Conversion: >99%
R = H: 17%; **R** = SiEt$_3$: 83%

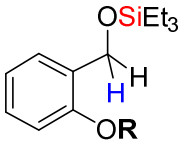

b,c,d

0.5 mol %, 30 min
Conversion: >99%
R = H: 39%; **R** = SiEt$_3$: 61%

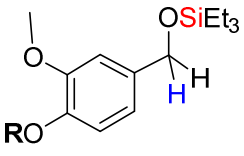

b,c,d

0.5 mol %, 30 min
Conversion: >99%
R = H: 75%; **R** = SiEt$_3$: 25%

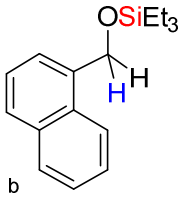

b

0.5 mol %
30 min
>99%

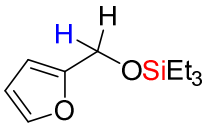

b,c'

0.4 mol %
2h
79%

a) Conditions: aldehyde (1.8 mmol), HSiEt$_3$ (0.31 mL, 1.96 mmol), [**4**][BArF$_{24}$] (2.5 mg [0.1 mol %]), rt. b) Conditions: aldehyde (1.1 mmol), HSiEt$_3$ (0.19 mL, 1.20 mmol), [**4**][BArF$_{24}$] (7.7 mg, 7.7 μL, [0.5 mol %]), rt. c) 2.2 equivalents of HSiEt$_3$ (0.38 mL, 2.41 mmol) were used. c') aldehyde (0.11 mL, 1.33 mmol), 1.8 equivalents of HSiEt$_3$ (0.38 mL, 2.41 mmol), [**4**][BArF$_{24}$] (7.7 mg, 7.7 μL, [0.4 mol %]) were the conditions used. d) The OH function was *O*-silylated. Yields were determined by ^{1}H NMR using 1,3,5-tri-*tert*-butylbenzene as internal reference.

2-Naphthaldehyde was easily hydrosilylated using 0.5 mol % of precatalyst within 30 minutes, affording triethyl(naphthalen-2-ylmethoxy)silane in >99% yield.. However, by using an excess of $HSiEt_3$, alcohol and acetyl functional groups were also easily hydrosilylated in addition to the targeted aldehyde function. Even though this method showed not to be chemoselective in the aldehyde hydrosilylation when alcohol and acetyl functional groups are present, its potential to give access to aromatic compounds containing several alcohol groups is demonstrated, thanks to the possibility offered by the catalytic system to mediate *O*-silylation and hydrosilylation reactions in the same time without any detrimental inhibition. An interesting comparison to make is that 0.5 mol % in precatalyst was necessary to fully transform benzaldehyde to the related product, whereas only 0.05 mol % loading showed to be sufficient for acetophenone. This latter observation also contradicts what is usually reported in the literature for benzaldehyde, which is said to be generally more prone to hydrosilylation than acetophenone. The latter fact can be rationalized if we consider the nature of the substituent R attached to (Ph)(R)C=O in acetophenone (R = Me) and benzaldehyde (R = H). The Me substituent is more electron-donating than H, thus the C=O bond becomes more electron-rich if substituted with the former group than just with H. As a consequence, the Lewis basic oxygen atom can be considered as more electron-rich in acetophenone when compared to benzaldehyde, making the formation of the O–Si bond more favorable in the former case, which overall gives rise to a higher rate of hydrosilylation observed with acetophenone as substrate. Again our observation is in accord with what was previously postulated, which is that an ionic-like hydrosilylation mechanism seems to be at work within this catalytic system.

3.2.2.4 Mechanistic considerations towards a plausible catalytic cycle

One plausible catalytic cycle for the hydrosilylation of aldehydes and ketones catalyzed by [**4**][$BArF_{24}$] is shown in scheme 35. Of course, this mechanism is only a preliminary proposal since deep mechanistic investigations need to be conducted to shed light on the real mechanism at work. However, taking into the account the previous results reported in this manuscript regarding the catalytic *O*-silylation of alcohols, and most importantly the isolation of the relevant catalytic intermediate [**5A**][$BArF_{24}$] upon interaction of the precatalyst [**4**][$BArF_{24}$] with $HSiEt_3$, and also the results of the catalysis reported in this chapter, we can propose a mechanism which consistently rationalize all the data set that have been showed until now.

In the conditions of the catalysis described herein, the remarkable efficiency seems to stem from the combination of several favorable factors of critical importance regarding the complexity of the system. First of all, the precatalyst [**4**][$BArF_{24}$] interacts with the excess of $HSiEt_3$ resulting in the activation of the H–Si bond of $HSiEt_3$ at the iridium center and the concomitant exothermic double hydrosilylation of the released acetonitrile ligand. The latter processes constitute the *activation step* which overall lead to the irreversible product of the double hydrosilylation of acetonitrile and the formation of the *key catalytic intermediate* [**5A**][$BArF_{24}$] (scheme 35). Second, the donor-acceptor property of [**5A**][$BArF_{24}$] permits to accommodate within the same environment and as "masked" forms the hydride $[H]^-$ and the silylium $[Et_3Si]^+$, where the hydrido iridium(III) moiety acts as the Lewis donor for the stabilization of the very unstable silylium moiety $[Et_3Si]^+$ which acts as the Lewis acid acceptor. The $BArF_{24}$ anion is also of tremendous importance, it is believed to bring sufficient stabilization for the cationic catalytic species that are generated during the catalysis, although its exact role(s) still remain(s) a mystery.

The *in situ* generated catalytic intermediate [**5A**][$BArF_{24}$] initiates the catalysis by transferring the silylium Lewis acid $[Et_3Si]^+$ to the Lewis basic oxygen atom of the C=O function of the substrate ([**C=O**]) affording the (triethylsilyl)carboxonium ([**C=O**]→$SiEt_3^+$) and the hydrido iridium(III) (**13**) species as catalytic intermediates; this step is denoted as the *triethylsilylium transfer step* (Si^+_t). Then, the catalytic intermediates [**C=O**]→$SiEt_3^+$ and **13** react with each other through a *hydride transfer step* (H^-_t) (path **A**, scheme 35), the hydride being transferred from iridium to the electrophilic carbocation-like carbon of [**C=O**]→$SiEt_3^+$, affording the triethylsilyl ether product [**CH–O**]–$SiEt_3$ and the transient ionic pair [**4+**][$BArF_{24}$]. Even though we do not any have conclusive evidence at this stage, we cannot exclude a concurrent pathway for the H^-_t step, which is the hydride transfer mediated by $HSiEt_3$ (denoted as pathway **C** in scheme 35). As an example, M. Oestreich and coworkers reported that $HSiEt_3$ can effectively reduce silyliminiums intermediates to silylamines.[226] Further experiments are underway in order to clarify which pathway is more viable for the H^-_t step. [**4+**][$BArF_{24}$] can reasonably be considered as the *true iridium catalyst* due to the coordination vacancy created at iridium. [**4+**][$BArF_{24}$] can react through at least two different pathways, which are the regeneration of [**5A**][$BArF_{24}$] after the reaction with $HSiEt_3$, and the formation of the monohydrido-bridged

[226], K.; Mohr, J.; Oestreich, M. Silylium Ion Promoted Reduction of Imines with Hydrosilanes. *Organometallics* **2013**, *32* (22), 6643–6646.

diiridium complex [**5B**][BArF$_{24}$] resulting from the reaction with **13**. [**5B**][BArF$_{24}$] as such is believed to be *inactive in catalysis*.

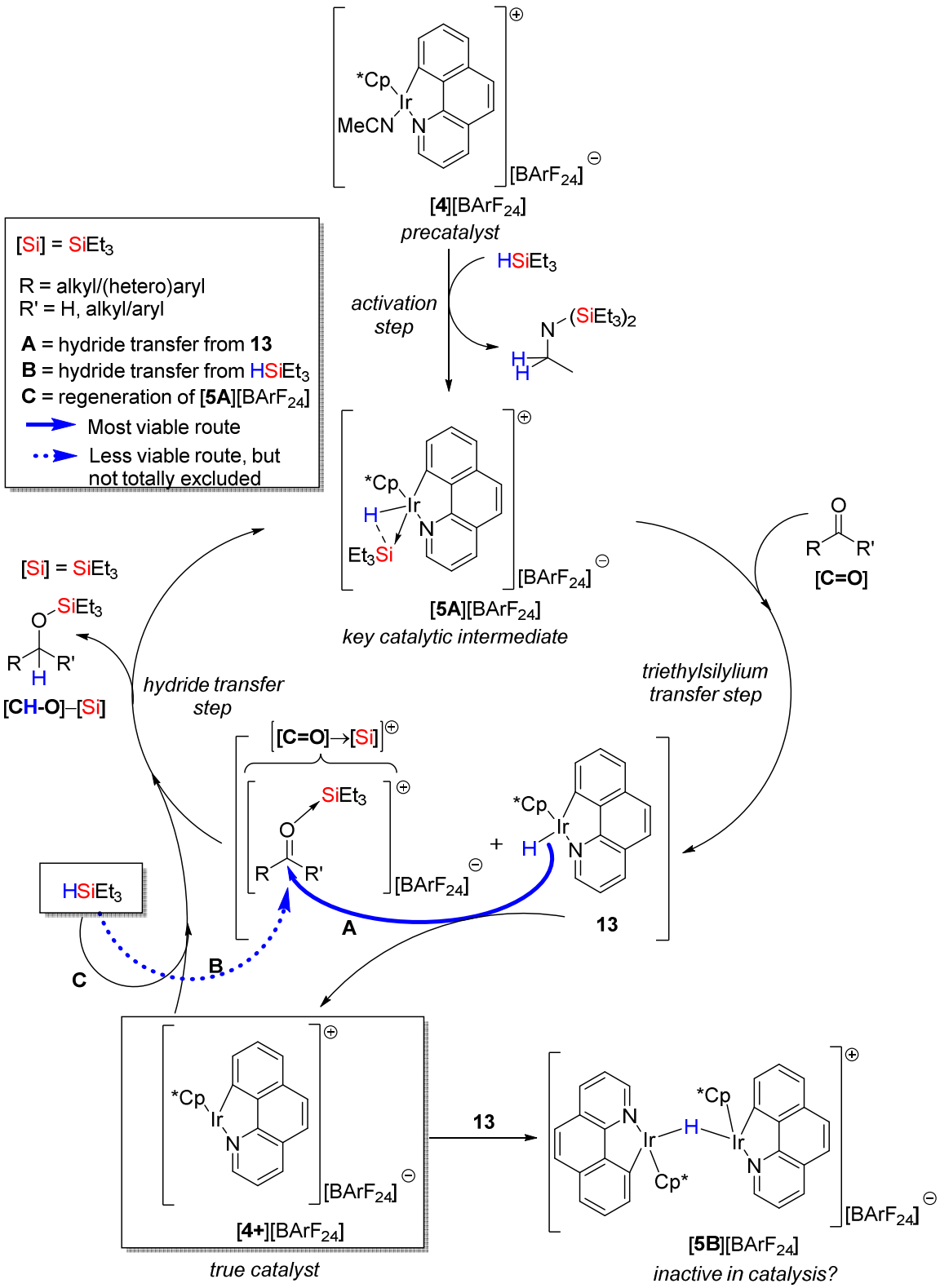

Scheme 35. Proposed catalytic cycle for the hydrosilylation of aldehydes and ketones.

3.2.3 Conclusions and perspectives

We have shown in this chapter that [**4**][$BArF_{24}$] catalyzes the hydrosilylation of several aldehydes and ketones with excellent yields (in most cases, >99%), good rates (in most cases, TOF of 1200 h^{-1}) and a good selectivity towards the targeted silyl ethers products. [**2**][$BArF_{24}$] is a less efficient precatalyst than [**4**][$BArF_{24}$] for the catalytic hydrosilylation of acetophenone with $HSiEt_3$. To the best of our knowledge, [**4**][$BArF_{24}$] is the first iridium precatalyst which shows such large substrate scope and rate efficiencies for the hydrosilylation of aldehydes and ketones. [**4**][$BArF_{24}$] is with no doubt more efficient than the previously reported Brookhart's team precatalyst [Ir(POCOP)(acetone)H][$B(C_6F_5)_4$] (schemes 24 and 31c), which was considered to be the best iridium precatalyst for the carbonyl hydrosilylation.[227] As an illustration (table 14), [**4**][$BArF_{24}$] catalyzes the hydrosilylation of acetophenone in ~5 minutes with a TON of 1000 and a TOF of 1.2×10^4 h^{-1}, whereas [Ir(POCOP)(acetone)H][$B(C_6F_5)_4$] (scheme 22) catalyzes the same reaction (3 equivalents of $HSiEt_3$ instead of 1.2 equivalents in our case) within 20 minutes with a TON of 200 and a TOF of 600 h^{-1}. Notably, among all homogeneous transition metal complexes [**4**][$BArF_{24}$] can be classified among the best precatalysts reported to date for the hydrosilylation of aldehydes and ketones. In 2014, R. J. Trovitch and coworkers reported a TOF of 7.8×10^4 h^{-1} for a Mn(II) precatalyst (table 14, scheme 22), that is probably one of the highest TOFs ever reached to date for a carbonyl hydrosilylation reaction catalyzed by a TM-based (pre)catalyst.[228] However, even if manganese precursors are cheaper than iridium ones, the preparation of the latter Mn(II) precatalyst is challenging and because of its paramagnetic property and air sensitivity it requires handling inside a dry glovebox. Moreover, the catalysis mediated by this complex is hugely dependant on the nature of the substrate. In our case, [**4**][$BArF_{24}$] is remarkably stable under air both in solution and as pure solid, thus simplifying its handling. More importantly, because of its structural simplicity, [**4**][$BArF_{24}$] is easily prepared on gram scale within few hours, from the commercially available chlorido iridacycle (scheme 3). In addition, the presence of an alcohol functional group on the substrate is not detrimental for the carbonyl hydrosilylation catalysis, because [**4**][$BArF_{24}$] is also an excellent *O*-silylation precatalyst, so that products with two

[227] Park, S.; Brookhart, M. Hydrosilylation of Carbonyl-Containing Substrates Catalyzed by an Electrophilic η^1-Silane iridium(III) Complex. *Organometallics* **2010**, *29* (22), 6057–6064.
[228] Mukhopadhyay, T. K.; Flores, M.; Groy, T. L.; Trovitch, R. J. A Highly Active Manganese Precatalyst for the Hydrosilylation of Ketones and Esters. *J. Am. Chem. Soc.* **2014**, *136* (3), 882–885.

alcohol functions can be obtained. However, some limitations of the system arise when substrates with electron-withdrawing substituents are tested, for which the rate of hydrosilylation tend to decrease, so that a prolonged time of reaction and a higher loading of the precatalyst were generally necessary.

Table 14. Summary of the catalytic performance of [**4**][$BArF_{24}$] for the hydrosilylation of aldehydes and ketones, and its comparison to previous relevant systems.

Substrate	**Precatalyst (mol %)**	**TON**	**TOF (h^{-1})**
Cyclohexanone	[(DPI)Mn] (1.0) (R. J. Trovitch et al.)[128]	6400	7.8×10^4
Acetophenone	[**4**][$BArF_{24}$] (0.1) (J.- P. Djukic et al.)	1000	1.2×10^4
	[(DPI)Mn] (0.1) (R. J. Trovitch et al.)[128]	100	1.5×10^3
	[Ir(POCOP)(acetone)H][$B(C_6F_5)_4$] (0.5) (M. Brookhart et al.)[127]	200	6.0×10^2
Aldehydes	[**4**][$BArF_{24}$] (0.1) (J.- P. Djukic et al.)	1000	2.0×10^3
	[**4**][$BArF_{24}$] (0.5) (J.- P. Djukic et al.)	≤200	$\leq 4.0 \times 10^2$
Ketones	[**4**][$BArF_{24}$] (0.5) (J.- P. Djukic et al.)	≤200	$\leq 4.0 \times 10^2$

We proposed a plausible mechanism for this reaction, but further investigations are currently undertaken. The high efficiency of [**4**][$BArF_{24}$] is believed to derive from the structural features of the key catalytic intermediate [**5A**][$BArF_{24}$], which behaves as a Lewis donor-acceptor pair. By this way, the reactivity of the highly electrophilic moiety $[SiEt_3]^+$ can be controlled by moderating its Lewis acidity with the stabilizing Lewis type interaction which is established with the donating hydrido-iridium(III) group (**13**). The latter picture rationally explains the high turnover rates that were achieved for the hydrosilylation of several aldehydes and ketones. A rationale design of new precatalysts with potentially better activities is underway. For example, we believe that choosing a more electron-rich C,N-chelate ligand would potentially enhance the electron density at iridium thus providing a better stabilization of the Lewis acidic moiety $[SiEt_3]^+$.

3.3 Hydrosilylation of nitriles

3.3.1 Introduction

3.3.1.1 General overview

Hydrosilylation of nitriles into *N*,*N*-bis(silyl)amines gives access to primary amines of important added value. Mild and selective catalytic hydrosilylation of nitriles is known to be difficult to achieve as illustrated by the very few studies conducted in the field. The main difficulty arises from the strong C≡N bond (BDE = 179.3 kcal/mol; 750.0 kJ/mol)[229] which makes its reduction problematic. However, some TM-based and so-called metal-free catalyst systems have recently emerged for the hydrosilylation of nitriles with some important improvements. In 1961, R. Calas and coworkers reported the first transition-metal based catalytic hydrosilylation of nitriles using $ZnCl_2$ (scheme. 36).[230]

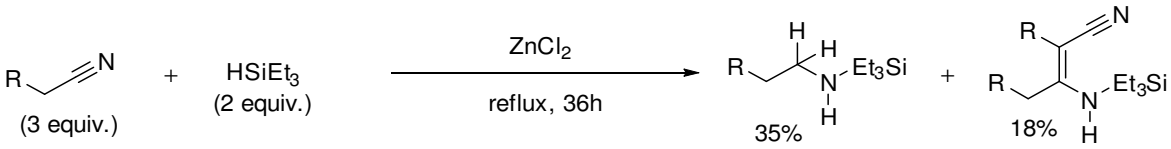

Scheme 36. First transition-metal complex catalyzed hydrosilylation of nitriles.[230]

Other studies that followed this seminal report successfully applied cobalt, [231] rhenium,[232] rhodium,[233] ruthenium[234] and zinc[235] based complexes as precatalysts. However, in most cases heating at 100 °C combined with high catalyst loadings is necessary to achieve a rather

[229] BDE is defined as the *bond dissociation enthalpy*, and the C≡N BDEs values have been taken from the following reference: Luo, Y.-R. In *Comprehensive Handbook of Chemical Bond Energies*; CRC Press, 2007.
[230] Calas, R.; Frainnet, E.; Bazouin, A. Compt. Rend. **1961**, *252*, 420.
[231] Murai, T.; Sakane, T.; Kato, S. Cobalt Carbonyl Catalyzed Reduction of Aromatic Nitriles with a Hydrosilane Leading to -Disilylamines. *Tetrahedron Lett.* **1985**, *26* (42), 5145–5148.
[232] Cabrita, I.; Fernandes, A. C. A Novel Efficient and Chemoselective Method for the Reduction of Nitriles Using the System Silane/oxo-Rhenium Complexes. *Tetrahedron* **2011**, *67* (42), 8183–8186.
[233] a) Huckaba, A. J.; Hollis, T. K.; Reilly, S. W. Homobimetallic Rhodium NHC Complexes as Versatile Catalysts for Hydrosilylation of a Multitude of Substrates in the Presence of Ambient Air. *Organometallics* **2013**, *32* (21), 6248–6256. b) Itagaki, S.; Sunaba, H.; Kamata, K.; Yamaguchi, K.; Mizuno, N. Hydrosilylation of Various Multiple Bonds by a Simple Combined Catalyst of a Tungstate Monomer and Rhodium Acetate. *Chem. Lett.* **2013**, *42* (9), 980–982. c) Campos, J.; Rubio, M.; Esqueda, A. C.; Carmona, E. Large-Scale Preparation and Labelling Reactions of Deuterated Silanes. *J. Label. Compd. Radiopharm.* **2012**, *55* (1), 29–38. d) Caporusso, A. M.; Panziera, N.; Pertici, P.; Pitzalis, E.; Salvadori, P.; Vitulli, G.; Martra, G. Hydrosilylation of Aromatic Nitriles Promoted by Solvated Rhodium Atom-Derived Catalysts. *J. Mol. Catal. A Chem.* **1999**, *150* (1), 275–285.
[234] Gutsulyak, D. V.; Nikonov, G. I. Chemoselective Catalytic Hydrosilylation of Nitriles. *Angew. Chem. Int. Ed.* **2010**, *49* (41), 7553–7556.
[235] a) Rit, A.; Zanardi, A.; Spaniol, T. P.; Maron, L.; Okuda, J. A Cationic Zinc Hydride Cluster Stabilized by an N-Heterocyclic Carbene: Synthesis, Reactivity, and Hydrosilylation Catalysis. *Angew. Chem. Int. Ed.* **2014**, *53* (48), 13273–13277. b) Boone, C.; Korobkov, I.; Nikonov, G. I. Unexpected Role of Zinc Hydride in Catalytic Hydrosilylation of Ketones and Nitriles. *ACS Catal.* **2013**, *3* (10), 2336–2340.

limited substrate scope and selectivity. In 2010, G. I. Nikonov and coworkers described that $[Ru(^{i}Pr_3P)(NCMe)_2][B(C_6F_5)_4]$ (4–5 mol %) catalyzes, with quite good chemoselectively, the hydrosilylation of a broad scope of nitriles to silylimines, while the complete reduction to bis(silyl)amines was generally inefficient (scheme 37).[236] This study constitutes the best

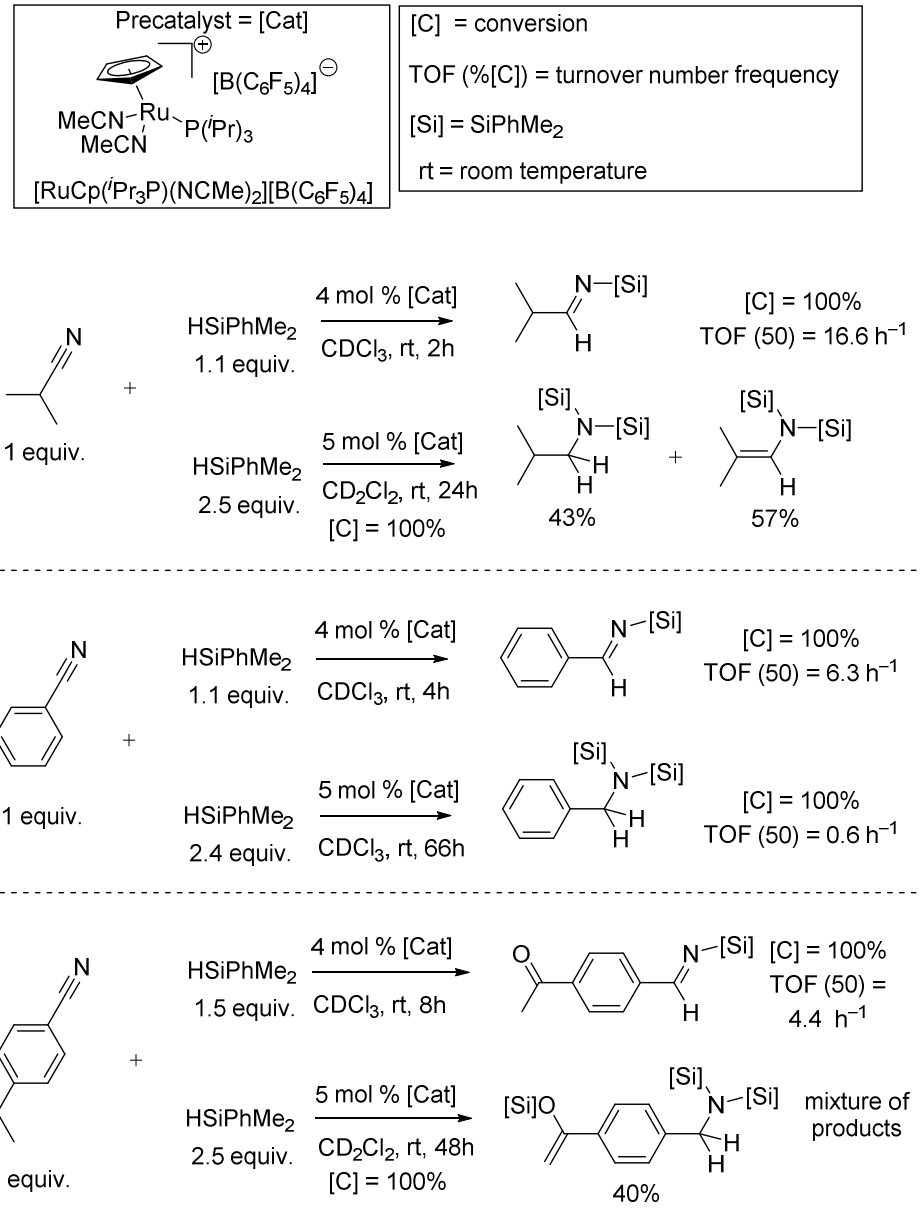

Scheme 37. Selected examples of $[Ru(^{i}Pr_3P)(NCMe)_2][B(C_6F_5)_4]$ (4–5 mol %) catalyzed hydrosilylation of nitriles, as reported by G. I. Nikonov and coworkers.[236]

[236] Gutsulyak, D. V.; Nikonov, G. I. Chemoselective Catalytic Hydrosilylation of Nitriles. *Angew. Chem. Int. Ed.* **2010**, *49* (41), 7553–7556.

example to date in terms of reaction rates, substrate scope and selectivity for a TM-based catalytic system in the hydrosilylation of nitriles (until our work described herein).

Apart from TM-based catalyst systems, other systems based on main-group metals and fluoride salts have shown to catalyze the hydrosilylation of nitriles. In 2015, S. Chang and coworkers achieved a significant advance by employing tris(pentafluorophenyl)borane [$B(C_6F_5)_3$] (1–3 mol %) as catalyst for the rapid hydrosilylation of a wide variety of alkyl and (hetero)aryl nitriles at room temperature.[237] Interestingly, good functional group tolerance and selective formation of imines or amines depending on the nature of the silane were observed. The authors reported also silylative reduction of conjugated nitriles using the same [$B(C_6F_5)_3$]-based catalytic system (5 mol %).[238] In the same period, D. W. Stephan and coworkers showed that the electrophilic phosphonium salt [$P(C_6F_5)_3F$][$B(C_6F_5)_4$] (1.5 mol %) was active in the hydrosilylation of nitriles but heating at 100 °C and prolonged times (24 h) were necessary for complete conversion.[239] In 2013, M. Beller and co-workers reported that tetra-*n*-butylammonium fluoride (TBAF, 5–10 mol %) catalyzes the hydrosilylation of diverse aryl nitriles at 25–60 °C affording the resulting amines after hydrolysis in 62–96 isolated yields.[240]

Other methods of synthesis of primary amines are known. The Gabriel synthesis[241] and the reductive amination of carbonyls[242] reactions are commonly employed in organic synthesis, but the limitations come from the need of first preparing the substrates to be reduced and from the formation of side products. The nitriles are also reduced either stoichiometrically with traditional metal hydrides (R_3AlH or R_3BH)[243] or catalytically *via* direct addition of hydrogen gas.[244] The main limitations of the latter methods reside in their lack of selectivity associated with high level

---

[237] Gandhamsetty, N.; Jeong, J.; Park, J.; Park, S.; Chang, S. Boron-Catalyzed Silylative Reduction of Nitriles in Accessing Primary Amines and Imines. *J. Org. Chem.* **2015**, *80* (14), 7281–7287.

[238] Gandhamsetty, N.; Park, J.; Jeong, J.; Park, S.-W.; Park, S.; Chang, S. Chemoselective Silylative Reduction of Conjugated Nitriles under Metal-Free Catalytic Conditions: *β*-Silyl Amines and Enamines. *Angew. Chem. Int. Ed.* **2015**, *54* (23), 6832–6836.

[239] Pérez, M.; Qu, Z.-W.; Caputo, C. B.; Podgorny, V.; Hounjet, L. J.; Hansen, A.; Dobrovetsky, R.; Grimme, S.; Stephan, D. W. Hydrosilylation of Ketones, Imines and Nitriles Catalysed by Electrophilic Phosphonium Cations: Functional Group Selectivity and Mechanistic Considerations. *Chem. - A Eur. J.* **2015**, *21* (17), 6491–6500.

[240] Bornschein, C.; Werkmeister, S.; Junge, K.; Beller, M. TBAF-Catalyzed Hydrosilylation for the Reduction of Aromatic Nitriles. *New J. Chem.* **2013**, *37* (7), 2061.

[241] a) Gibson, M. S.; Bradshaw, R. W. The Gabriel Synthesis of Primary Amines. *Angew. Chem. Int. Ed.* **1968**, *7* (12), 919–930. b) Gabriel, S. Ueber Eine Darstellungsweise Primärer Amine Aus Den Entsprechenden Halogenverbindungen. *Chem. Ber.* **1887**, *20* (2), 2224–2236.

[242] See for example: Lehmann, F.; Scobie, M. Rapid and Convenient Microwave-Assisted Synthesis of Primary Amines via Reductive N-Alkylation of Methyl Carbamate with Aldehydes. *Synthesis* **2008** (11), 1679–1681.

[243] See for example: Amundsen, L. H.; Nelson, L. S. Reduction of Nitriles to Primary Amines with Lithium Aluminum Hydride. *J. Am. Chem. Soc.* **1951**, *73* (1), 242–244.

[244] Bagal, D. B.; Bhanage, B. M. Recent Advances in Transition Metal-Catalyzed Hydrogenation of Nitriles. *Adv. Synth. Catal.* **2015**, *357* (5), 883–900.

of risks and potential hazards. Primary azides were found to be reduced to primary amines by using a $CeCl_3 \cdot 7H_2O$/NaI stoichiometric system.[245]

3.3.1.2 Catalysis with iridium

To the best of our knowledge, catalytic hydrosilylation of nitriles with iridium has not been described yet. The only known example of an attempted nitrile hydrosilylation with an iridium complex was reported by R. G. Bergman and coworkers in 2002 (scheme 38).[246] When iridium silyl complexes were combined with nitriles, C–C bond cleavage of the R-C≡N function (R = Me, Ph) followed by intramolecular C≡N insertion into the Ir–Si bond were observed instead of the expected hydrosilylation reaction.

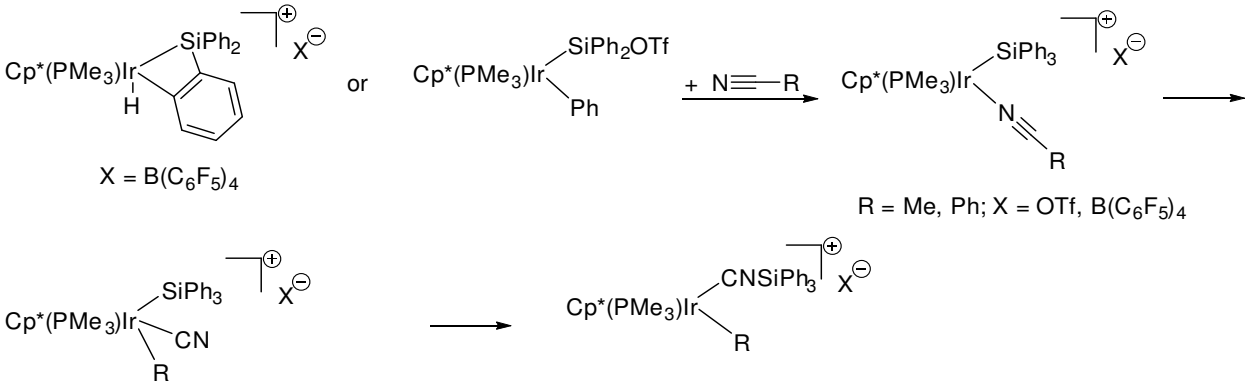

Scheme 38. The postulated mechanism for the C–C bond cleavage of nitriles (R–C≡N), as proposed by R. G. Bergman and coworkers.[239]

3.3.1.3 Different mechanisms were proposed

Little experimental evidence is known in support of mechanisms at play in the catalytic hydrosilylation of nitriles in general. However, experimental and theoretical studies have suggested rather divergent mechanism proposals, mainly because of the specificity of the studied system. We will discuss in a non-exhaustive way some of the mechanisms that have been proposed for the hydrosilylation of nitriles.

[245] Bartoli, G.; Di Antonio, G.; Giovannini, R.; Giuli, S.; Lanari, S.; Paoletti, M.; Marcantoni, E. Efficient Transformation of Azides to Primary Amines Using the Mild and Easily Accessible $CeCl_3.7H_2O$/NaI System. *J. Org. Chem.* **2008**, *73* (5), 1919–1924.
[246] Klei, S. R.; Tilley, T. D.; Bergman, R. G. Stoichiometric and Catalytic Behavior of Cationic Silyl and Silylene Complexes. *Organometallics* **2002**, *21* (22), 4648–4661.

In 2006, H. Tobita described a stoichiometric reaction mechanism for the “outer-sphere” hydrosilylation of nitriles observed with some hydrido(hydrosilylene)tungsten complexes, for instance $Cp'(CO)_2(H)W{=}Si(H)[C(SiMe_3)_3]$ (scheme 39).[247] The reaction between the latter complex and nitriles is believed to generate the solvated (donor-acceptor) intermediate that undergoes thermal intramolecular rearrangement with sequential hydride transfer to the carbon atom of the C≡N bond followed either by coordination of N to W or by hydride migration from Si to W.

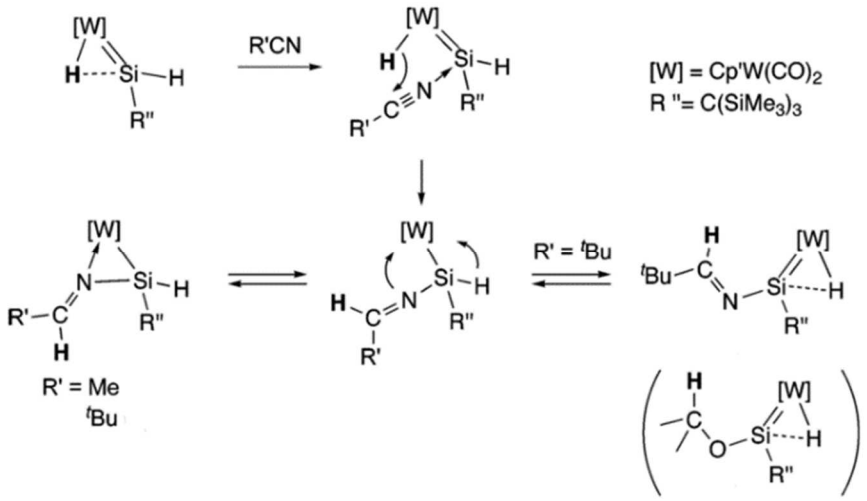

Scheme 39. Stoichiometric reaction mechanism for the “outer-sphere” hydrosilylation of nitriles mediated by a [W](H)(SiR”H) complex, as proposed by H. Tobita and coworkers.[247] Reprinted with permission from Watanabe, T.; Hashimoto, H.; Tobita, H. *J. Am. Chem. Soc.* **2006***, 128* (7), 2176. Copyright 2006 American Chemical Society.

In 2008, a theoretical study conducted on the latter system was reported by Y.-D. Wu and coworkers.[248] The authors concluded that the hydrosilylation of nitrile occurs through a silyl migration mechanism, analogous to the modified Chalk–Harrod mechanism, and predicted the difficult possibility of these tungsten complexes to mediate catalytically the hydrosilylation of nitriles. The arguments invoked for the latter assumption were that the calculated tungsten–silylene or tungsten–silyl products are too “stable, which could prevent their easy conversion to the starting hydrido(hydrosilylene)tungsten complexes when reacting with a

[247] Watanabe, T.; Hashimoto, H.; Tobita, H. Stoichiometric Hydrosilylation of Nitriles with Hydrido(hydrosilylene)tungsten Complexes: Formation of W–Si–N Three-Membered Ring Complexes and Their Unique Thermal Behaviors. *J. Am. Chem. Soc.* **2006**, *128* (7), 2176–2177.
[248] Zhang, X.-H.; Chung, L. W.; Lin, Z.; Wu, Y.-D. A DFT Study on the Mechanism of Hydrosilylation of Unsaturated Compounds with Neutral Hydrido(hydrosilylene)tungsten Complex. *J. Org. Chem.* **2008**, *73* (3), 820–829.

hydrosilane substrate. In 2011, a second stoichiometric reaction mechanism was proposed by H. Tobita and coworkers with another family of W and Mo complexes (scheme 40).[249] In this case, an "inner-sphere" activation of the nitrile (**A**→**B**) was proposed to take place prior to intramolecular insertion of the C≡N bond to the M-Si bond (**B**→**C**) and hydride transfer to the resulting (M)C=N(Si) bond (**C**→**D**). The authors did not notice any catalytic activity for these complexes. In 2012, G. I. Nikonov and coworkers managed to make catalytic the hydrosilylation of nitriles mediated by a (ArN=)$MoCl_2(PMe_3)_3$ (Ar = 2,6-diisopropylphenyl) complex.[250] However, the catalysis showed to be very limited which prevented the authors to get any experimental information on the mechanism.

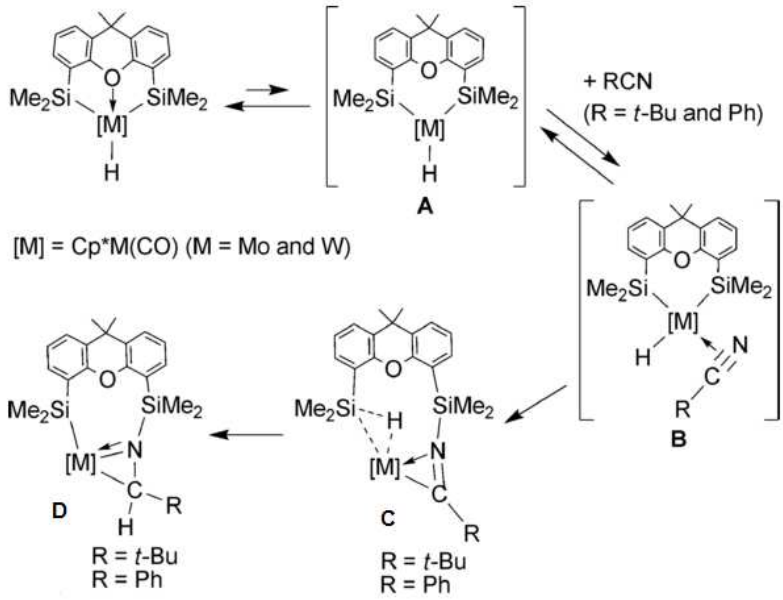

Scheme 40. Stoichiometric reaction mechanism for the "inner-sphere" hydrosilylation of nitriles mediated by [M](H)((κ^3 Si,Si,O-xantsil) complexes (M = Mo, W), proposed by H. Tobita and coworkers.[249] Reproduced from Ref. 242 with permission from The Royal Society of Chemistry.

In 2013, G. I. Nikonov and coworkers reported the hydrosilylation of nitriles catalyzed by a zinc hydride complex ([**Zn**]H) and proposed the related mechanism (scheme 41).[251] The authors proposed that the substrate attacks the intermediate [**Zn**]H($HSiR_3$) complex *via* a cyclic, 6e σ-

[249] Komuro, T.; Begum, R.; Ono, R.; Tobita, H. Synthesis and Characterisation of Hydrido Molybdenum and Tungsten Complexes Having a Hemilabile Tridentate Si,Si,O-Ligand: Observation of Stepwise Hydrosilylation of a Nitrile to Form an N-Silylimine on the Metal Centre. *Dalt. Trans.* **2011**, *40* (10), 2348–2357.
[250] Khalimon, A. Y.; Shirobokov, O. G.; Peterson, E.; Simionescu, R.; Kuzmina, L. G.; Howard, J. A. K.; Nikonov, G. I. Mechanistic Aspects of Hydrosilylation Catalyzed by (ArN=)Mo(H)(Cl)$(PMe_3)_3$. *Inorg. Chem.* **2012**, *51* (7), 4300–4313.
[251] Boone, C.; Korobkov, I.; Nikonov, G. I. Unexpected Role of Zinc Hydride in Catalytic Hydrosilylation of Ketones and Nitriles. *ACS Catal.* **2013**, *3* (10), 2336–2340.

aromatic transition state. However, although it is an elegant proposal important inconsisties remain partly because no structural (and theoretical) evidence in support for the proposed intermediate and/or the transition state was provided. In 2010, G. I. Nikonov proposed an interesting mechanism based on the observations they made from the hydrosilylation of nitriles catalyzed by [[Ru](NCMe)($HSiR_3$)][$B(C_6F_5)_4$] intermediates ([Ru] = Ru(^{i}Pr$_3$P)Cp), which formed upon addition of silanes to [[Ru](NCMe)$_2$][$B(C_6F_5)_4$] precursors (scheme 42a).[252] The authors explained their mechanisms based on the considerations that [[Ru](NCMe)($HSiR_3$)][$B(C_6F_5)_4$] undergo nucleophilic abstraction of the silylium moiety [R_3Si^+] by the nitrile substrate (L) to form [[Ru](NCMe)(H)]. The silylium ion abstraction pathway was supported by previous DFT studies conducted by the same authors with the carbonyl hydrosilylation reaction, which concluded that the latter reaction pathway was favored over the dissociative Ojima-type pathway.[253]

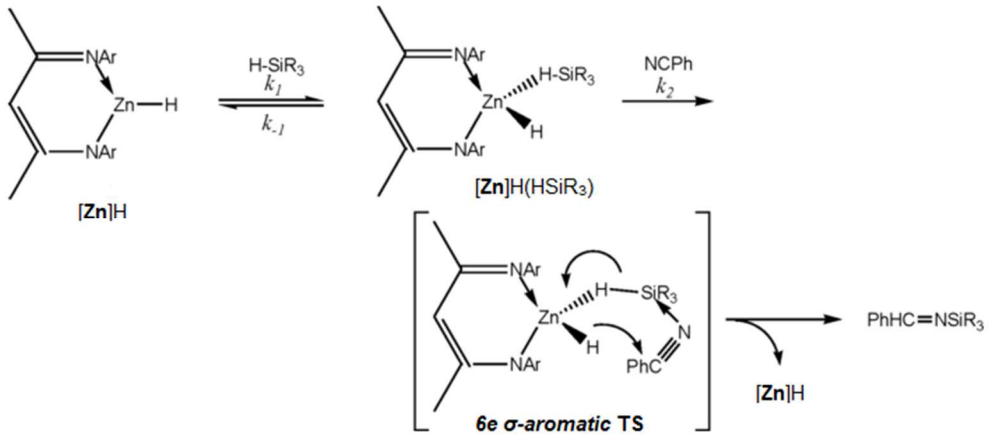

Scheme 41. Mechanism proposal for the hydrosilylation of nitriles catalyzed by a [**Zn**]H complex, as reported by G. I. Nikonov and coworkers.[251] Reprinted with permission from Boone, C.; Korobkov, I.; Nikonov, G. I. *ACS Catal.* **2013**, *3* (10), 2336. Copyright 2013 American Chemical Society.

More recently, a DFT study conducted by Y.-D. Wu and coworkers reached similar conclusions.[254] The authors proposed a similar outer-sphere silylium abstraction pathway (scheme 42b), with the involvement of the "S_N2-Si" (**TS44-P**) transition state as possible

[252] Gutsulyak, D. V.; Nikonov, G. I. Chemoselective Catalytic Hydrosilylation of Nitriles. *Angew. Chem. Int. Ed.* **2010**, *49* (41), 7553–7556.
[253] Gutsulyak, D. V.; Vyboishchikov, S. F.; Nikonov, G. I. Cationic Silane σ-Complexes of Ruthenium with Relevance to Catalysis. *J. Am. Chem. Soc.* **2010**, *132* (17), 5950–5951.
[254] Yang, Y.-F.; Chung, L. W.; Zhang, X.; Houk, K. N.; Wu, Y.-D. Ligand-Controlled Reactivity, Selectivity, and Mechanism of Cationic Ruthenium-Catalyzed Hydrosilylations of Alkynes, Ketones, and Nitriles: A Theoretical Study. *J. Org. Chem.* **2014**, *79* (18), 8856–8864.

"interaction picture" between the substrates and the Ru catalytic intermediate. In 2015, Stephan and coworkers proposed a DFT-based mechanism rational that explains the hydrosilylation of nitriles, carbonyls and imines catalyzed by $[(C_6F_5)_3PF][B(C_6F_5)_4]$ (scheme 31b).

a)

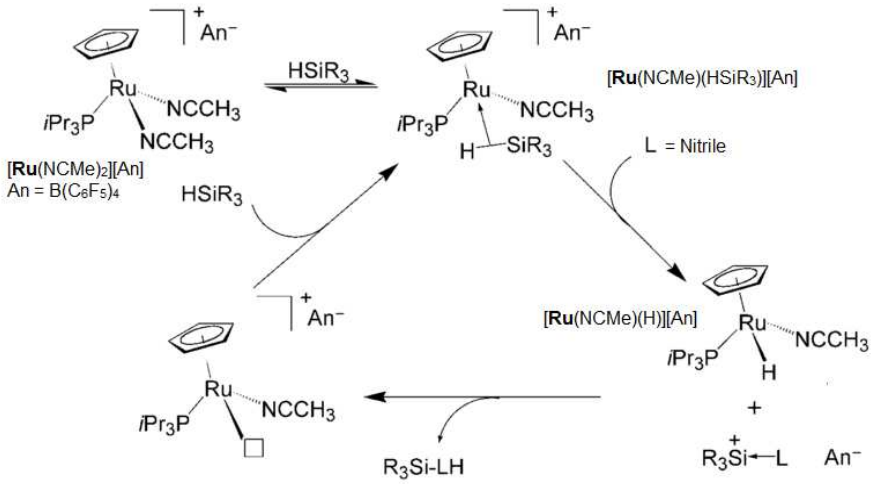

b)

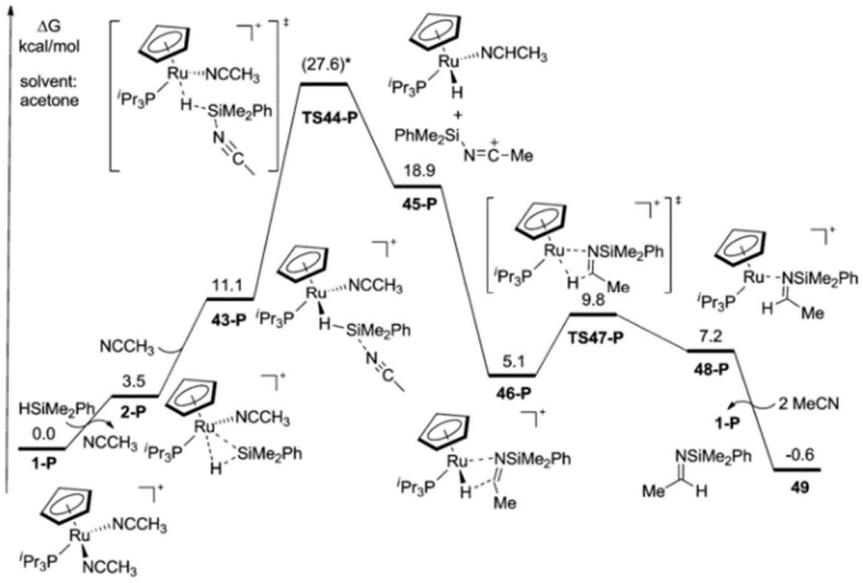

Scheme 42. a) Mechanism proposal for the hydrosilylation of nitriles catalyzed by [Ru(^{i}Pr$_3$P)Cp NCMe)(HSiR$_3$)][B(C_6F_5)$_4$], as reported by G. I. Nikonov and coworkers.[252] Reprinted with permission from Gutsulyak, D. V.; Nikonov, G. I. *Angew. Chem. Int. Ed*. **2010**, *49* (41), 7553. Copyright 2010 Wiley Materials. **b)** DFT calculated energy profile (Gibbs energies are given in kcal•mol^{-1}) of acetonitrile hydrosilylation with precatalyst **1-P** ([Ru(^{i}Pr$_3$P)Cp (NCMe)(HSiR$_3$)][B(C_6F_5)$_4$]), as reported by Y.-D. Wu and coworkers.[254] Reprinted with permission from Yang, Y.-F.; Chung, L. W.; Zhang, X.; Houk, K. N.; Wu, Y.-D. *J. Org. Chem.* **2014**, *79* (18), 8856. Copyright 2014 American Chemical Society.

The authors calculated the energy profile by considering the hydrosilylation of carbonyls, and argued that the related mechanism they proposed could also be at work for nitriles as substrates without further explanations.[255]

3.3.2 Results and discussions

3.3.2.1 Stoichiometric hydrosilylation of the acetonitrile ligand with $HSiEt_3$

Previously in this manuscript, we have shown that the overall efficiency of precatalysts [**2**][$BArF_{24}$] and [**4**][$BArF_{24}$] is partly conditioned by one key parameter which is the hydrosilylation of the released acetonitrile ligand (CH_3CN) upon addition of triethylsilane to iridium. Indeed the stoichiometric reaction between [**2**][$BArF_{24}$] and $HSiEt_3$ performed in CD_2Cl_2 at room temperature was *in situ* monitored by ^1H NMR. The resulting ^1H spectrum showed quantitative conversion of the acetonitrile bound ligand to *N,N*-bis(triethylsilyl)ethylamine **6** (scheme 43) within few minutes provided that an excess of $HSiEt_3$ was used. The same features were observed in the reaction between [**4**][$BArF_{24}$] and $HSiEt_3$.

This observation can be best rationalized if we consider the bifacetted role played by the *in situ* generated catalytic intermediates [**3A**][$BArF_{24}$] and [**5A**][$BArF_{24}$]. As a consequence, two sequential transfer steps can be imagined for the hydrosilylation reaction: 1) transfer of the silylium cation to acetonitrile and (silyl)iminium intermediates (activation steps *via* coordination to nitrogen), and 2) transfer of the hydride to C≡N and C=N bonds respectively. Based on these plausible mechanistic considerations, we were curious to study the catalytic hydrosilylation of nitriles with [**2**][$BArF_{24}$] and [**4**][$BArF_{24}$], the results of which are reported below.

3.3.2.2 [**3**][$BArF_{24}$] catalyzes the solvent-free hydrosilylation of acetonitrile and benzonitrile

3.3.2.2.1 Acetonitrile is not selectively hydrosilylated

The starting point was to check whether the hydrosilylation of CH_3CN with $HSiEt_3$ could be possible under catalytic loadings of [**2**][$BArF_{24}$] and using the nitrile as solvent (solvent-free conditions). We first carried out the hydrosilylation of one equivalent of CH_3CN with 2

[255] Pérez, M.; Qu, Z. W.; Caputo, C. B.; Podgorny, V.; Hounjet, L. J.; Hansen, A.; Dobrovetsky, R.; Grimme, S.; Stephan, D. W. Hydrosilylation of Ketones, Imines and Nitriles Catalysed by Electrophilic Phosphonium Cations: Functional Group Selectivity and Mechanistic Considerations. *Chem. - A Eur. J.* **2015**, *21* (17), 6491–6500.

equivalents of $HSiEt_3$ in the presence of 1 mol % of [**2**][$BArF_{24}$] upon heating at 50 °C for 44 h then at 80 °C for 100 h (scheme 43).

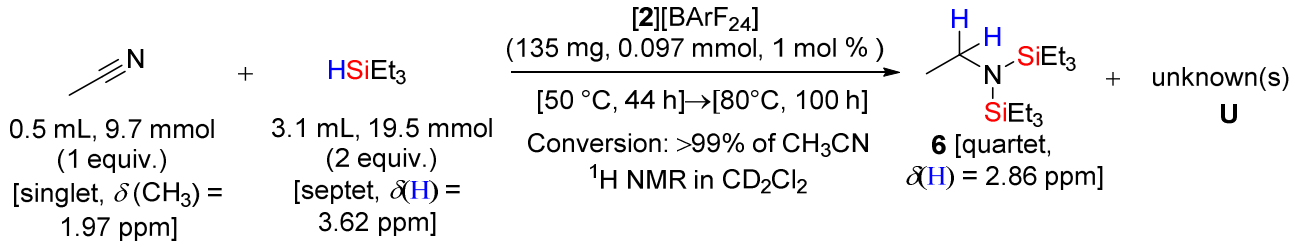

Scheme 43. [**2**][$BArF_{24}$] catalyzed hydrosilylation of acetonitrile with $HSiEt_3$ to **6** under solvent-free conditions.

Monitoring the reaction mixture by ^{1}H NMR spectroscopy (CD_2Cl_2, 298 K) showed that the evolution of the reaction mixture stopped after heating at 80 °C for 24 h. Careful analysis of the different ^{1}H signals of the NMR spectrum revealed full conversion of CH_3CN but partial conversion of $HSiEt_3$ (table 15). However, besides the typical signals of the desired product, that is *N,N*-bis(triethylsilyl)ethylamine **6** ($EtN(TES)_2$) ($CH_3C\underline{H}_2N(TES)_2$: δ = 2.86 ppm, quartet, J = 7.1 Hz), other signals belonging to four unknown products **U1–4** were also observed (characterized by a quartet at δ = 3.1 ppm (J = 7.1 Hz) for **U1**; a quintet at δ = 2.76 ppm (J = 7.2 Hz) for **U2**; a singlet at δ = 2.0 ppm for **U3**, and a singlet at δ = 1.60 ppm for **U4**). The desired product *N,N*-bis(triethylsilyl)ethylamine (**6**) and the unknown product **U2** were isolated from the reaction mixture (with impurities). Furthermore, **6** and **U2** were characterized by NMR spectroscopy and electro-spray ionization (ESI) mass analysis (see the experimental part). Et_4Si was also isolated and identified to be as such by comparison of its ^{1}H NMR data (CD_2Cl_2; δ = 0.94 ppm (triplet, J = 8 Hz), 0.54 ppm (quadruplet, J = 8 Hz)) with those previously reported by D. Heinekey and coworkers.[256] However, it is clear that Et_4Si did not form during the hydrosilylation of acetonitrile because a careful analysis of all the ^{1}H NMR spectra, resulting from the catalytic reaction mixture at different intervals, did not reveal any spectroscopic traces of Et_4Si. Therefore, the formation of Et_4Si results during either the purification of the reaction mixture or the bulb-to-bulb distillation process upon heating under vacuum the purified reaction mixture (see experimental part for more details). However, all attempts to clearly identify the molecular structure of the isolated unknown product **U2** proved to be challenging. The attempts

[256] Connelly, S. J.; Kaminsky, W.; Heinekey, D. M. Structure and Solution Reactivity of (Triethylsilylium)triethylsilane Cations. Organometallics **2013**, *32* (24), 7478–7481.

to isolate and identify the other unknown products **U1** and **U3** were unfortunately unsuccessful. However, a careful analysis and interpretation of the different ^{1}H NMR spectra of the reaction we describe here prompted us to identify some interesting features of the reaction mixture.

3.3.2.2.2 Analysis and interpretation of the ^{1}H NMR spectra

The ratios of $HSiEt_3/CH_3CN$ and $HSiEt_3/CH_3CN$/**6** were inferred from the ^{1}H NMR spectra recorded for the different conditions described in scheme 43, and the related data are combined in table 15. Of course, the goal is not about to discuss in detail all these ratios, but their careful comparison reveals an important paradoxal fact. When we look at the ratio of $HSiEt_3/CH_3CN$/**6**, it decreases over time from 23/6/1 to 2.2/0/1, a fact that points out a contradiction . This observation suggests that CH_3CN seems to be consumed without reacting just with $HSiEt_3$ to give **6** but with another molecule(s) as well. It is probable that the unknown products **U1-3** come from the reaction between CH_3CN and another constituents of the mixture. What are the other constituents which can react with CH_3CN?

Table 15. Evolution of the ratios of $HSiEt_3/CH_3CN$ and $HSiEt_3/CH_3CN$/**6** in the reaction mixture described in scheme 30. These ratios were calculated from the ^{1}H NMR spectra recorded at different time intervals of the reaction.

Conditions		**Ratio**	
T (°C)	**t (h)**	$HSiEt_3/CH_3CN$	$HSiEt_3/CH_3CN$/**6**
50	20	3.8/1	23/6/1
50	44	36/1	5.5/0.1/1
80	100	87/1	2.2/0/1

At this stage we cannot exclude any possibility, but **6** and at least one of the unknown products **U1-3** are potential candidates, even though the exact identity of **U1**, **U2** or **U3** is still unknown. The group of G. I. Nikonov and coworkers reported in 2010 a similar problem. When acetonitrile and $HSiPhMe_2$ were subjected to catalytic amounts of [**Ru**$(NCMe)(HSiR_3)$][$B(C_6F_5)_4$] (0.4 mol %) under solvent free conditions (23 h, ambient temperature), the authors noticed that 95% of CH_3CN was converted along with the formation of the desired product $CH_3(H)C{=}NSiPhMe_2$ (10%), a coupling product identified to be $CH_3(H)C{=}NCH(CH_3)N(SiMe_2Ph)_2$ (60%), and other unknown products. The authors proposed that $CH_3(H)C{=}NCH(CH_3)N(SiMe_2Ph)_2$ might result from the "N–Si addition across the C=N bond".[257] In our case, further studies are still underway in order to elucidate by which mechanism the formation of unknown products **U1–3** occurs.

3.3.2.2.3 Benzonitrile is selectively and totally hydrosilylated

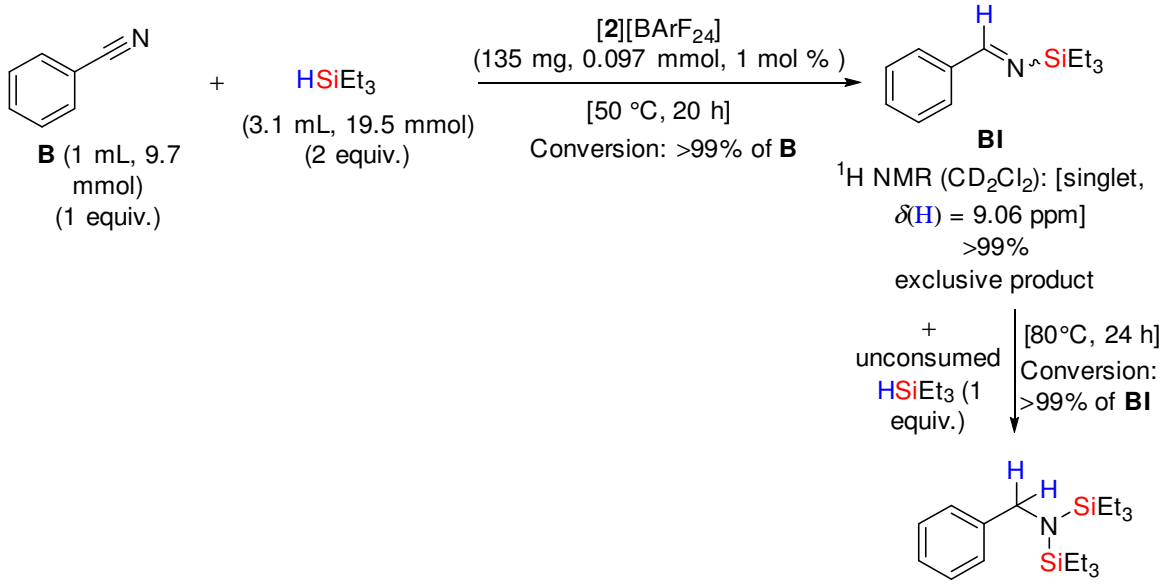

Scheme 44. [**2**][$BArF_{24}$] catalyzed selective hydrosilylation of benzonitrile with $HSiEt_3$ to **BI** and **BA** under solvent-free conditions.

[257] Gutsulyak, D. V; Nikonov, G. I. Chemoselective Catalytic Hydrosilylation of Nitriles. *Angew. Chem. Int. Ed.* **2010**, *49* (41), 7553–7556.

As shown in scheme 44, benzonitrile (**B**) reacted more readily and selectively with $HSiEt_3$ when compared to CH_3CN under the same solvent-free catalytic conditions. Indeed, when we carried out the hydrosilylation of one equivalent of **B** with two equivalents of $HSiEt_3$ in the presence of 1 mol % of [**2**][$BArF_{24}$] upon heating at 50 °C for 20 h, the ^1H NMR (CD_2Cl_2, 298 K) analysis of the reaction mixture showed the quantitative conversion of **B** (>99%) and the exclusive formation of the monohydrosilylated product, that is *N*-(triethylsilyl)benzylimine **BI** (PhCHN(TES)), characterized by its typical peak (PhC*H*N(TES), singlet) at δ = 9.06 ppm (scheme 44, see experimental part). Then when a prolonged heating of the same reaction mixture at 80 °C for 24 h was carried out, the ^1H NMR (CD_2Cl_2, 298 K) analysis showed the complete conversion of **BI** (>99%) and the exclusive formation of the bishydrosilylated product, that is *N*,*N*-bis(triethylsilyl)benzylamine **BA** ($PhCH_2N(TES)_2$), which is characterized by its typical peak ($PhCH_2N(TES)_2$, singlet) at δ = 4.20 ppm (scheme 44, see experimental part).

To conclude, we found an easy and solvent-free method for selectively forming *N*-(triethylsilyl)benzylimine or *N*,*N*-bis(triethylsilyl)benzylamine from the readily available benzonitrile and triethylsilane substrates by using the easily prepared iridium complex [**2**][$BArF_{24}$] as precatalyst. In addition, all the "solvent-free" study carried with acetonitrile and benzonitrile as nitriles was repeated with [**4**][$BArF_{24}$] as precatalyst, leading to the same results reported above but with better rate efficiencies. Then, we wondered: what could be the effect of a "co-solvent" on the efficiency of [**4**][$BArF_{24}$] in the catalytic hydrosilylation of nitriles studied before?

3.3.2.3 Catalytic hydrosilylation of nitriles in dichloromethane is also efficient

With the encouraging results that we reported before, we next conducted comparative studies on the hydrosilylation of acetonitrile, propionitrile and benzonitrile with four different silanes, and using dichloromethane (CH_2Cl_2) as solvent. The goal here was to study in a combined fashion the influence of the silane on the catalytic performance while tuning the steric encumbrement and the electronic density surrounding the C≡N bond. The results of this study are summarized in table 16.

For every nitrile, all the catalytic runs with different silanes were conducted under identical conditions (see conditions detailed in table 16). Triethylsilane appeared to be the most reactive silane for the hydrosilylation of propionitrile and benzonitrile giving the desired products in 95%

Table 16. [**4**][$BArF_{24}$] catalyzed hydrosilylation of acetonitrile, propionitrile and benzonitrile in CH_2Cl_2.

Reaction[1]	Yield (%)[2]			
	$HSiEt_3$	$HSiPh_3$	$HSiPhH_2$	PMHS
acetonitrile[a] 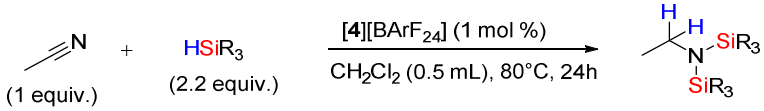	8	7	2	10
propionitrile[b] 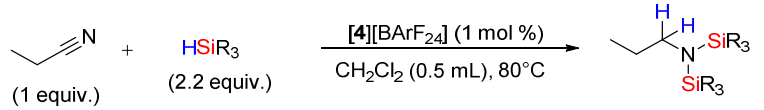	41 (24h)[b'] / 95 (72h)[b']	57	2	<1
benzonitrile[c] 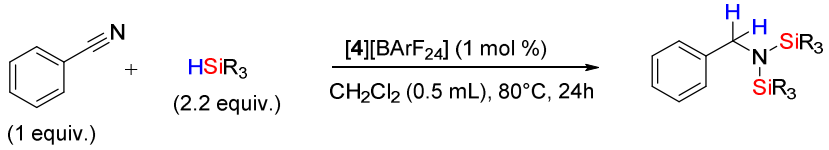	>99	11	<1	<1

1) Conditions: a) acetonitrile (0.1 mL, 1.9 mmol), silane (4.2 mmol), [**4**][$BArF_{24}$] (27 mg, 19.2 *μ*mol [1 mol %]), 80 °C; b) propionitrile (0.1 mL, 1.4 mmol), silane (3.1 mmol), [**4**][$BArF_{24}$] (20 mg, 14 *μ*mol [1 mol %]), 80 °C; b') propionitrile (0.2 mL, 2.8 mmol), $HSiEt_3$ (0.98 mL, 6.1 mmol), [**4**][$BArF_{24}$] (39 mg, 28 *μ*mol [1 mol %]), 80 °C; b') benzonitrile (0.2 mL, 1.9 mmol), silane (4.3 mmol), [**4**][$BArF_{24}$] (27 mg, 19 *μ*mol [1 mol %]), 80 °C. 2) Yields were determined by ^{1}H NMR against 1,3,5-tri-*tert*-butylbenzene as internal reference.

72h) and >99% (24h) NMR yields respectively. Benzonitrile turned out to be more reactive than propionitrile presumably because of the electron-withdrawing nature of the phenyl group which therefore activates the electrophilic carbon atom of the C≡N bond towards hydride attack. However, the reaction between acetonitrile and three of the four silanes proved to give the same mixture of products as observed for the solvent-free conditions (*vide supra*), the best

selectivity being obtained with PMHS even though minor difference in NMR yields was noticed. Indeed, when acetonitrile and triethylsilane were heated at 80 °C for 24 h in the presence of [**4**][$BArF_{24}$] (1 mol %), the ^1H NMR (CD_2Cl_2) spectrum revealed the presence of the unknown product **U2** (scheme 43) besides the desired product **6** (~8 % of NMR yield). When conducting the reaction with PMHS as silane, only the desired product was obtained in ~10 % NMR yield. We postulate that the selectivity observed with PMHS may be related to the bulkiness of the silane which prevents possible side reactions to occur.

This hypothesis is further strengthened by the observation made when $HSiPhH_2$ was reacted with acetonitrile at 80 °C for 72 h in the presence of [**4**][$BArF_{24}$] (1 mol %), affording unknown products as major species along with 18% (NMR yield) of the desired product. It is worth to note that only the desired product was observed in the case of propionitrile, showing the importance of the alkyl substituent on the selectivity of the reaction. One plausible explanation is that the ethyl group of propionitrile is a more sterically demanding group than the methyl group of acetonitrile, which makes the formation of side products less favorable in the former case, thus explaining the relative better yield of the desired product. This latter explanation tends rather to support the idea that the undesired product might the result of homo or hetero coupling reactions. Importantly, under the same conditions as above and in the absence of [**4**][$BArF_{24}$], the reaction between triethylsilane and all the nitriles used during this study gave no observable product by ^1H NMR.

We also investigated the effect of the proportion of the precatalyst on the reaction rate (table S9, experimental part). Surprisingly, we found that actually the selective mono-hydrosilyation of benzonitrile smoothly occured within 4 h (70 °C) when using only 0.05 mol % of [**4**][$BArF_{24}$], thus corresponding to a TON of ~2000 and a TOF of 502 h^{-1}. Even a more intriguing observation was made when only 0.1 mol % of [**4**][$BArF_{24}$] was used. The ^1H NMR spectrum (C_6D_6, 298 K, 400 MHz) analysis showed that actually a total conversion of *N*-(triethylsilyl)benzylimine **BI** was obtained affording the desired product *N*,*N*-bis(triethylsilyl)benzylamine **BA** (~80% yield), along with an unknown compound (~20% yield) for which a characterisitic singlet peak appeared at δ = 3.55 ppm (see experimental part). We believe that this latter compound can be considered as as intermediate because it was systemically observed when partial conversion of *N*-(triethylsilyl)benzylimine **BI** to **BA** has occured, but no traces of it could be observed when ~99% of **BA** has formed. Further studies

are underway to try identifying this unknown product and rationally explaining by which mechanism it formed.

3.3.2.4 [**4**][$BArF_{24}$] catalyzes the hydrosilylation of various aromatic nitriles

With these informations in hand, we then moved to the next catalytic studies with the focus on using only (hetero)aryl nitriles as substrates of choice to avoid the problems encountered in the previous study. Optimization studies conducted with benzonitrile and $HSiEt_3$ as substrates (experimental part) of choice allowed us to select the best conditions to apply for this substrate scope study. The conditions are as follows: a solution of CH_2Cl_2 containing one equivalent of nitrile and 2.2 equivalents of triethylsilane was charged with 0.5–1 mol % of [**4**][$BArF_{24}$], and the resulting mixture was heated at 70 °C during at least 24 h. When conducting the reaction with benzonitrile under the latter conditions but without any precatalyst, no conversion was observed. Similarly, no conversion was observed at room temperature whatever the precatalyst loading used. The results of this study are summarized in table 17.

In all cases, the simple addition of [**4**][$BArF_{24}$] to the reaction mixture led to a marked effervescence mostly because of the highly exothermic reaction between excess $HSiEt_3$ and [**4**][$BArF_{24}$]. As it is shown in table 17, various nitriles derivatives were hydrosilylated with excellent yields under the selected reaction conditions. Using only 0.5 mol % of [**4**][$BArF_{24}$], benzonitrile, 4-methylbenzonirile, 4-methylbenzonirile and 4-cyanobiphenyl were quantitatively converted to the resulting products in 24 h. Interestingly, 2-chlorobenzonitrile, 2,6-difluorobenzonitrile and 2-naphthonitrile were also quantitatively converted (24 h) to the desired products when using only 0.5 mol % of [**4**][$BArF_{24}$]. However, substrates with electron-withdrawing substituents at the para and meta position of the phenyl group such as CF_3, NO_2 (para) and Cl (meta), gave only 86% of products. However, the presence of an acetyl or alcohol group at the para position of the benzyl moiety proved to create the competitive hydrosilylation of ketone or the *O*-silylation of alcohol respectively, thus lowering the yield (not shown). Some more challenging substrates were also tested. For example, isophthalonitrile is an interesting substrate to study because its reduced form, that is 1,3-phenylenedimethanamine, is a commonly used starting material, especially in coordination chemistry, as a simple *N*,*N*-donor ligand or a precursor for more sophisticated ligands. Under our standard catalytic conditions, isophthalonitrile is conveniently reduced, though not totally, thus giving the related product in a not negligible yield 60%. Anthracene-9-carbonitrile is the other challenging substrate to be

hydrosilylated, giving the desired product in 67% yield. Under the conditions we used, substrates like nicotinonitrile and 4-aminobenzonitrile were not converted.

Table 17. [**4**][$BArF_{24}$] catalyzed hydrosilylation of (hetero)aryl nitriles.

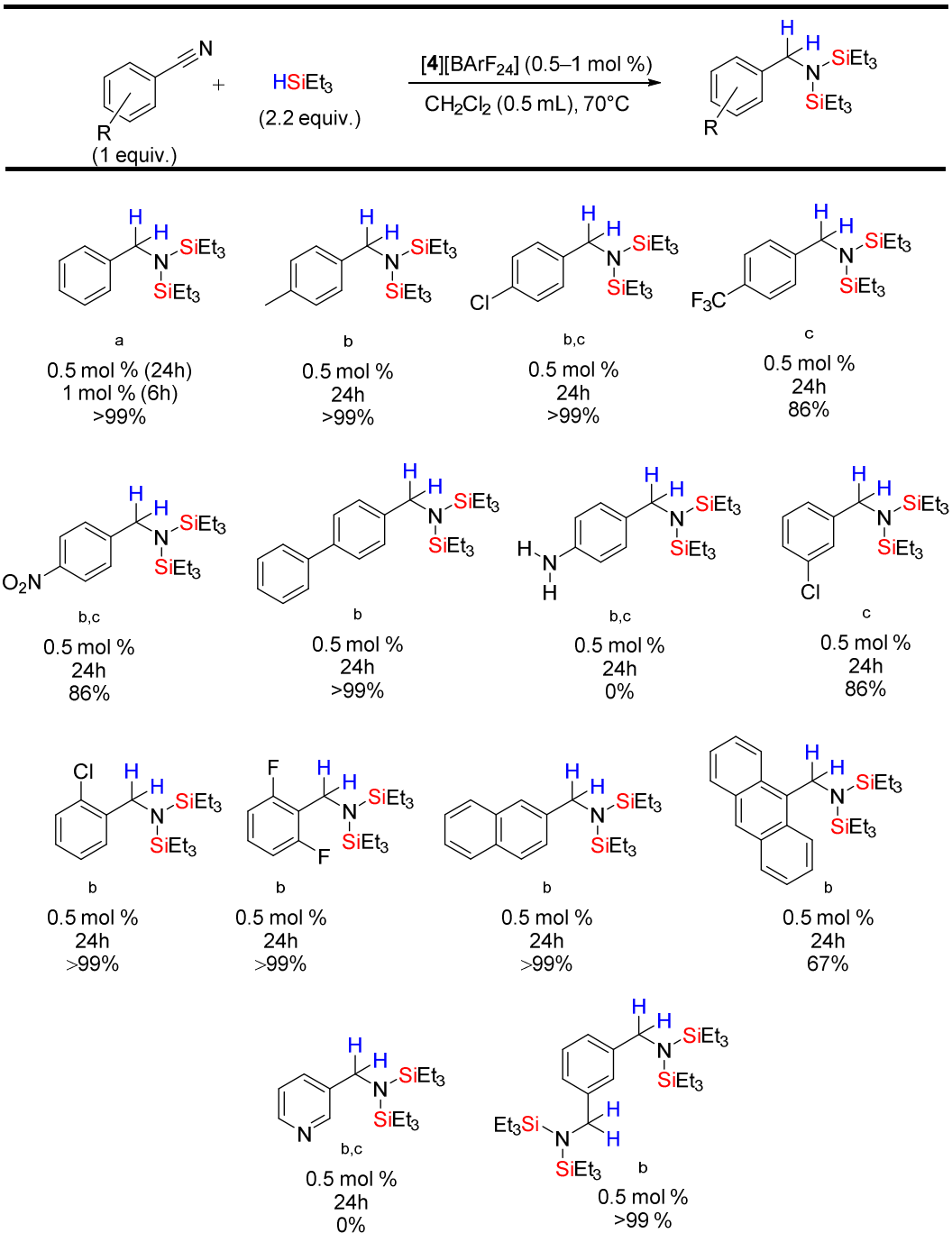

Conditions: a) nitrile (1.1 mmol), $HSiEt_3$ (0.35 mL, 2.13 mmol), [**4**][$BArF_{24}$] (6.8 mg, 4.85 μmol [0.5 mol %]; or 13.7 mg, 9.7 μmol [1 mol %]), 70 °C. b) nitrile (0.8 mmol), $HSiEt_3$ (0.3 mL, 1.85 mmol), [**4**][$BArF_{24}$] (5.89 mg, 4.2 μmol [0.5 mol %]; or 11.1 mg, 8.4 μmol [1 mol %]), 70 °C. c) Instead of 2.2 equiv. of $HSiEt_3$, 4.6 equivalents (0.60 mL, 3.76 mmol) were used. Yields were determined by ^{1}H NMR using 1,3,5-tri-*tert*-butylbenzene as internal reference.

reactivity towards hydrosilylation. This might come from either the detrimental interaction of the silylium $[Et_3Si]^+$or the iridium catalytic center with the nitrogen atom of pyridine and amine groups. On the other hand, during the mechanistic study (*vide infra*), we found that actually benzonitrile was selectively reduced to *N*-(triethylsilyl)benzylimine with high rate efficiency, corresponding to a TON of ~71 and TOF (at >99% conversion) of ~4.2×10^3 h^{-1}. In the future, we aim at undertaking further optimization studies prior to extend the substrate scope of this catalytic and selective monohydrosilylation of nitriles.

3.3.2.5 Preliminary mechanistic considerations: experiment and theory

The scheme 45 describes one of the preliminary investigations that we carried out on the mechanism of the catalytic system we described in this chapter. *In situ* ^1H NMR analysis of a mixture of benzonitrile (**B**) and $HSiEt_3$ in the conditions of the catalysis, revealed that quantitative conversion of benzonitrile to *N*-(triethylsilyl)benzylimine (**BI**) took place within few seconds (upon warming at 35–40 °C) (scheme 45).

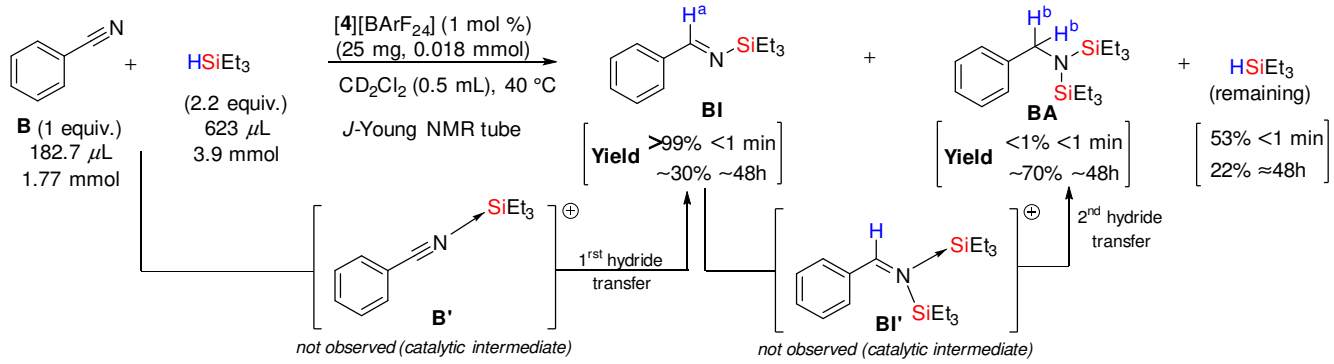

Scheme 45. ^1H NMR analysis (CD_2Cl_2, 400 MHz, 298 K) of a mixture of benzonitrile (**B**, 1 equiv.) and Et_3SiH (2.2 equiv) in the presence of a solution of 1 mol % of [**4**][$BArF_{24}$] in 0.5 mL of CD_2Cl_2. NMR yields were determined using 1,3,5-tri-*tert*-butylbenzene as internal reference (25.4 mg, 0.103 mmol), and applying the formulas *n*(**BI**) / *n*(**B**) and *n*(**BA**) / *n*(**B**) where *n* is the number of moles in mol.

Actually, upon shaking the solution of the reaction mixture before NMR analysis, a sudden color change from yellow to orange was noticed, consistent with the transformation of **B** to **BI**. With the help of the ^1H NMR spectrum (recorded immediately after the starting of the reaction), integration of the typical benzylidenic C-$\underline{H}^a$ signal of **BI** at δ = 9.2 ppm against the typical C$\underline{H}_3$ signal of 1,3,5-tri-*tert*-butylbenzene (used as internal reference) at δ = 1.48 ppm indicated that

BI formed in an NMR yield of ~99%. Similarly, the integration of the typical benzylic C-*H*^{b} signal of *N*-*N*-bis(triethylsilyl)benzylamine (**BA**) at δ = 4.31 ppm corresponded to an NMR yield of ~1% in **BA**. Unconsumed $HSiEt_3$ was estimated to amount ~53% from the integration of its typical Si-*H* signal at δ = 3.82 ppm. When the reaction (within the same J Young NMR tube) was allowed to stand for 48h (from the starting of the reaction) at room temperature, the resulting ^{1}H NMR analysis spectrum revealed that ~70% of **BI** was converted to **BA** (scheme 45).

These observations suggest that the monohydrosilylation of benzonitrile to **BI** is very facile in the conditions of catalysis, whereas the additional monohydrosilylation of **BI**, through the intermediate **BI'**, to the final product **BA** is much more difficult. The latter point can be rationalized from a kinetic point of view if one considers the difference in the free energy barriers ($\Delta G^{\ddagger}$) of the two successive reactions (mono- and bishydrosilylation) as a function of the nature of the catalytic intermediates that are involved along the reaction pathway. Intermediate **BI'**, which formed from **BI** and $[SiR_3]^+$, bears two bulky $[SiEt_3]^+$ groups on nitrogen. Thus, the hydride transfer from the iridium center to the electrophilic carbon atom (*C*-H^a) of **BI'** is hardly accessible because of the steric demand of $N(SiEt_3)_2$ (even though this steric effect may be counter-balanced by the well known elongation in N–Si bonds). Moreover, the hydride is transferred to **BI'** from the sterically demanding group [(B[*h*]Q)IrCp*(H)] (B[*h*]Q = benzo-[*h*]-quinolin-10-yl) of the catalytic intermediate [**5A**][$BArF_{24}$]. Saying differently, the second hydride transfer to **BI'** is much more energetically unfavourable when compared to the first hydride transfer to **B'**. As a consequence, a rather high $\Delta G^{\ddagger}$ for the second hydride transfer pathway is expected, thus explaining the need for heating at a higher temperature to achieve the complete hydrosilylation of nitriles to *N*-*N*-bis(triethylsilyl)amines in general. From a thermodynamic point of view, the reluctance of *N*-(triethylsilyl)benzylimine (**BI**) towards the second hydride transfer from [**5A**][$BArF_{24}$] might be the result of the *relative* low hydricity (or hydride ability)[258] of [**5A**][$BArF_{24}$] and the low hydride affinity (or hydride obtaining-ability)[258] of **BI**. Thus, the difference of reactivity between **B** and **BI** can be explained in terms of their different hydride affinity with respect to [**5A**][$BArF_{24}$], which is higher for **B** than for **BI.** Of course, a more "realistic" view would take into account a balance between kinetic and thermodynamic factors, which overall could explain the higher reactivity of **B** towards hydrosilylation relative to **BI**.

[258] Zhu, X.-Q.; Liu, Q.-Y.; Chen, Q.; Mei, L.-R. Hydride, Hydrogen, Proton, and Electron Affinities of Imines and Their Reaction Intermediates in Acetonitrile and Construction of Thermodynamic Characteristic Graphs (TCGs) of Imines as a "Molecule ID Card". *J. Org. Chem.* **2010**, *75* (3), 789-808.

Attempts to spectroscopically observe the catalytic intermediates **B'** and **BI'** *via* the stoichiometric reaction between [**4**][$BArF_{24}$], benzonitrile and $HSiEt_3$, and eventually obtaining single crystals, failed because of their elusive behavior. One of the strategies we wish to use in the near future is based on the *in situ* generation of [$SiEt_3$][$B(C_6F_5)]_4$ from [Ph_3C][$B(C_6F_5)]_4$ and $HSiEt_3$, and its stoichiometric transfer to benzonitrile, thus giving the possibility to observe (at least) by ^1H NMR spectroscopy the species **B**'. A similar experiment can be done to observe **BI'** from **BI**. However, even though there are several experimental observations and kinetic studies to conduct yet, we reported at this stage of study some evidences which point towards an ionic type mechanism for the hydrosilylation of nitriles catalyzed by [**4**][$BArF_{24}$]. As a consequence, a plausible mechanism is proposed in scheme 46.

3.3.2.6 An ionic hydrosilylation mechanism is proposed

Taking into the account the previous results reported in this manuscript regarding the catalytic *O*-silylation of alcohols and the hydrosilylation of carbonyls, the characterization of the key catalytic intermediate [**5A**][$BArF_{24}$], and also the results of the catalysis reported in this chapter, we can propose a mechanism which consistently rationalize all the data so far discussed. The main features of the ionic hydrosilylation mechanism which is proposed for the hydrosilylation of carbonyls described in scheme 35 can be considered to be present in the mechanism of the hydrosilylation of nitriles as well (scheme 46).

The *in situ* generated catalytic intermediate [**5A**][$BArF_{24}$] initiates the catalysis by transferring $[Et_3Si]^+$ to the Lewis basic nitrogen atom of the nitrile affording *N*-(triethylsilyl)benzonitrile ([**C≡N**]→$SiEt_3^+$) and the hydrido iridium(III) complex (**13**) as catalytic intermediates; this step is denoted as the *triethylsilylium transfer step* (Si^+_t). Then, the catalytic intermediates [**C≡N**]→$SiEt_3^+$ and **13** react with each other through a *hydride transfer step* (H^-_t) (path **A**, scheme 46), the hydride being transferred from iridium to the electrophilic carbocation-like carbon of [**C≡N**]→$SiEt_3^+$, affording *N*-(triethylsilyl)benzylimine as product ([**CH═N**]–$SiEt_3$). Then [**CH═N**]–$SiEt_3$ enters a new catalytic cycle involving the similar transfer steps as above, namely Si^+_t and H^-_t, which overall afford *N,N*-bis-(triethylsilyl)benzylamine as the product ([**C(H)$_2$–N**]–$(SiEt_3)_2$). Further experiments are underway in order to clarify whether $HSiEt_3$ as hydride source is a viable pathway for the H^-_t step. [**4+**][$BArF_{24}$] can reasonably be considered as the *true iridium catalyst* due to the coordination vacancy created at iridium. However, at the

moment, we can only postulate that [**5B**][BArF$_{24}$] is *inactive in catalysis*, because we lack sound experimental evidence of contrary.

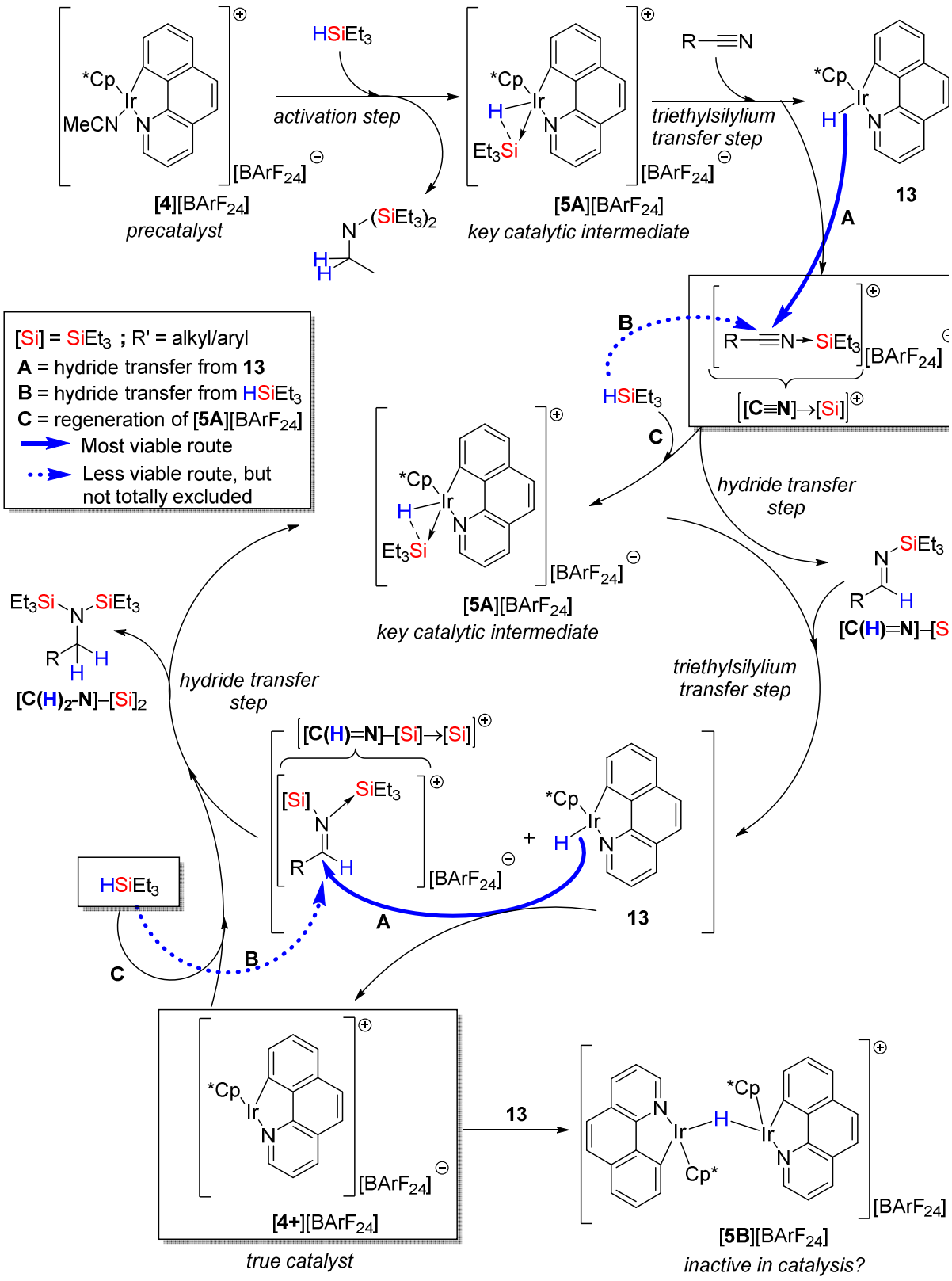

Scheme 46. Proposed catalytic cycle for the hydrosilylation of nitriles.

3.3.3 Conclusions and perspectives

To the best of our knowledge, we have reported the first examples of an iridium-based complex for the catalytic hydrosilylation of nitriles.

We have shown in this chapter that [**4**][$BArF_{24}$] is an efficient precatalyst for the hydrosilylation of various aromatic nitriles with $HSiEt_3$. Notably, we have also demonstrated the catalytic potential of [**2**][$BArF_{24}$] (1 mol %) for the solvent-free and chemoselective monohydrosilylation and bishydrosilylation of benzonitrile. On the other hand, the hydrosilylation of acetonitrile (solvent-free or CH_2Cl_2 as co-solvent) proved to give a mixture of by-products in addition to the product of double hydrosilylation, that is *N,N*-bis-(triethylsilyl)ethylamine. Since the identity of the by-products is still unknown, their formation is proposed to be the result of homo- or hetero-coupling reactions. Benzonitrile was also chemoselectively hydrosilylated to (*N*-(triethylsilyl)benzylimine under co-solvent (CH_2Cl_2) conditions with a TON of ~71 and a TOF (at >99% conversion) of ~4.2×10^3 h^{-1}. *N*-(triethylsilyl)benzylimine could also be obtained by using a lower catalytic loading of 0.05 mol % in [**4**][$BArF_{24}$], corresponding to a TON of ~2000 and a TOF of ~502 h^{-1}, whereas *N,N*-bis-(triethylsilyl)ethylamine was chemoselectively obtained ([**4**][$BArF_{24}$], 1 mol %) with a TON of ~227 and and a TOF of ~9 h^{-1}.

Scheme 47 depicted below summarizes the catalytic performance of [**4**][$BArF_{24}$] with respect to others catalytic systems of the literature for the hydrosilylation of benzonitrile. One can see that [**4**][$BArF_{24}$] competes very well with most of the other (pre)catalysts for the bishydrosilylation of benzonitrile, whereas it clearly outerperforms the best exiting catalytic systems for the chemoselective monohydrosilylation of benzonitrile, proving its good robustness and remarkable rate efficiency. However, a major limitation of the catalytic system was noticed with the apparent low tolerence of substrates substituted with electron withdrawing groups at the para position (such as NO_2) of the benzyl or nitrogen-containing substrates like pyridinyl and amino groups.

The advantages of using [**4**][$BArF_{24}$] as a precatalyst for the nitrile hydrosilylation reaction are its very good stability under air and at high temperature (at least up to 80 °C), and its relative structural simplicity. The first point allows the processing of the catalytic reaction without any special pecaution or set-up, as it is the case for most organometallic catalytic systems regarding

their sensitivity to air and heat in general. The second point allows [**4**][BArF$_{24}$] to be easily accessible within a half-day and on gram scale by carrying out during one simple single step

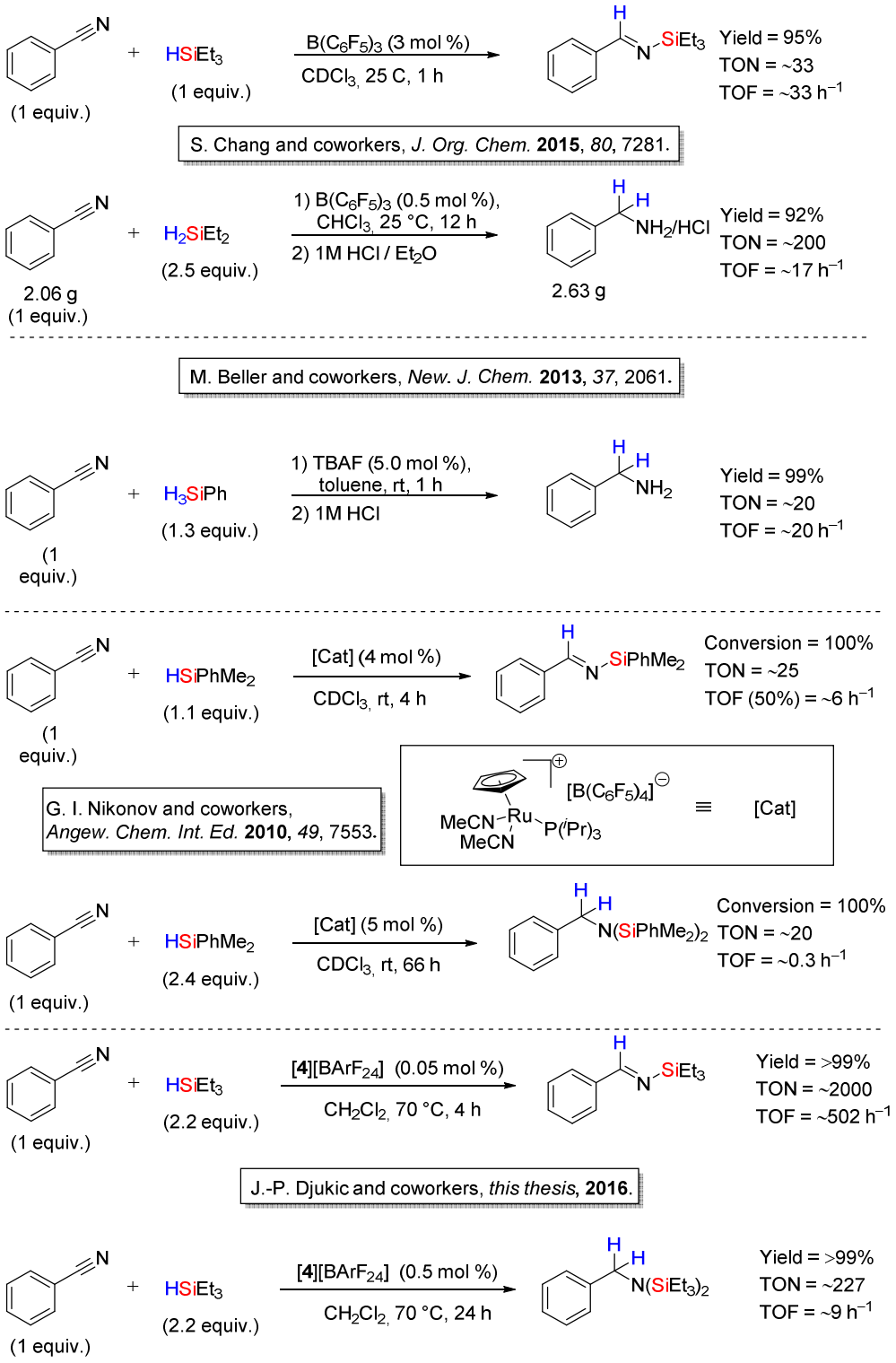

Scheme 47. Comparison of the catalytic performance of [**4**][BArF$_{24}$] with the previous relevant systems for the chemoselective hydrosilylation of benzonitrile.

the chloride abstraction reaction of the commercially available chlorido iridacycle (scheme 3) in the presence of Na[$BArF_{24}$] and acetonitrile.

In scheme 46 of this chapter, we have proposed an ionic-like mechanism for the catalytic hydrosilylation of nitriles mediated by [**4**][$BArF_{24}$] (also valid for [**2**][$BArF_{24}$] of course). The key success of the catalysis reported herein is mostly explained by the donor-acceptor property of the catalytic intermediates [**3A**][$BArF_{24}$] and [**5A**][$BArF_{24}$] which behave as both silylium ([$SiEt_3$]$^+$) and hydride ("H^-") transfer mediators towards the activation of the C–N bond of the nitrile and the intermediate imine, and the formation of the C–H bond of the imine and the amine, respectively. Even though the latter mechanism is in good accordance with our observations, some questions remain not answered yet, especially regarding the mechanism underlying the second hydride transfer step. The monohydrosilylation of benzonitrile was found to proceed by far more faster thant its bishydrosilylation. The latter observation tends to support the classical hydride mechanism which means that in our case the transfer of the hydride is most probably mediated by the catalytic intermediate iridium hydride **13**. However, it conceptually remains "hard to imagine" how such a bulky molecule (**13**) finds a way to favorably interact with the likely bulkier silylium intermediate *N,N*-bis-(triethylsilyl)benzylimine? The fact that a heating at 70–80 °C was necessary for the last hydride transfer step to proceed for the formation of the *N,N*-bis-(triethylsilyl)benzylamine products does not provide, in our opinion, a full support (though not sufficient) to the high free energy barrier explanation. This issue will be the object of future investigations in the laboratory. One idea to check is to experimentally and theoretically calculate the relative hydricity (H^D) of the hydrides donors **4**, **13** and $HSiEt_3$, together with their relative reactivity towards benzonitrile, *N*-(triethylsilyl)benzonitrile and *N,N*-bis-(triethylsilyl)benzylimine.

4 Catalytic C–F bond activation

In this chapter, we describe our contribution to the challenging and growing field of the catalytic carbon-fluorine (C–F) bond activation. After introducing the reasons of interest and the problems associated with the C–F bond activation, we provide a review on some historical breakthroughs and recent great achievements in the fields of stoichiometric and catalytic hydrodefluoration and functionalization of fluorocarbons using main group and transition metal based compounds. In this context, we will show that our laboratory obtained significant results during this thesis project, especially regarding the solvent-free and catalytic C(sp^3)–F bond activation of unactivated fluorocarbons.

4.1 Introduction

4.1.1 Why C–F bond activation?

As outlined in scheme 48 below, the carbon-fluorine (C–F) bond is considered to be the strongest single bond that carbon could form with any other element, with an average bond energy ~20 kcal•mol^{-1} higher than the carbon-hydrogen (C–H) bond (scheme 48a).[259] The main reason that explains the highly thermodynamic stability of the C–F bond is attributed to its highly ionic ($C^{\delta+}$–$F^{\delta-}$) character combined with the small size of fluorine, leading overall to a pronounced electrostatic attraction.[260] Thus, the C–F bond in a RCF_3 group will have a stronger ionic character than it does in R_2CF_2 and R_3CF groups respectively (scheme 48b).[253]

a) C-H vs C-F bond strenght: C-F bond always « wins »

Bond	Bond Energy (±)	
	kcal•mol^{-1}	kJ•mol^{-1}
H_3C–H	105 (0.1)	439.3 (0.4)
F_3C–F	130.7 (0.5)	546.8 (2.1)
H_2C=CH	110.9 (0.6)	464.2 (2.5)
F_2C=CF	130.6 (3)	564.4 (12.6)
C–H	112.9 (0.5)	472.2 (2.2)
C–F	125.6 (2)	525.2 (8.4)
C–H$_2$	89.7 (1.2)	375.5 (5.0)
C–F$_2$	98.7 (1)	412.8 (4.2)

b) C-F bond strenght increases with its ionic character

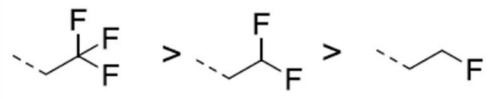

c) Perfluorocarbons (PFCs) are highly persistant pollulants

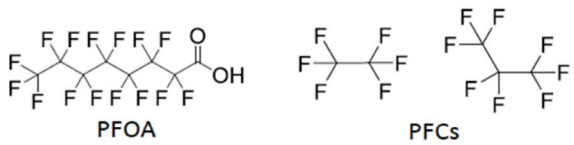

d) C-F bond activation challenges

- R ≠ H: functional-deflluoration (FDF)

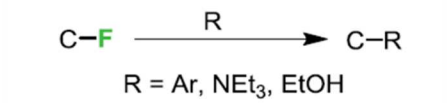

- R = H: hydrodefluoration (HDF)

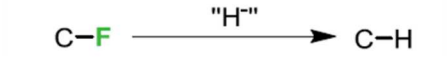

The highly toxic **HF** gas is a possible by-product!

Scheme 48. C–F bond activation problem sketch. The bonds energies listed in **a)** were taken from reference [259]. PFOA and PFCs stand for perfluorooctanoic acid and perfluorocarbons respectively.

[259] Luo, Y.-R. In Comprehensive Handbook of Chemical Bond Energies; CRC Press, 2007.
[260] O'Hagan, D. Understanding Organofluorine Chemistry. An Introduction to the C-F Bond. *Chem. Soc. Rev.* **2008**, *37* (2), 308–319.

As a consequence, perfluorocarbons (PFCs) are extraordinary inert compounds. A serious environmental concern is encountered with these PFCs because of their bio-accumulation as highly persistent pollutants.[261] In some cases, their lifetime is estimated to be more than 2000 years.[262] In addition, fluoroarenes and chlorofluorocarbons gas are known to contribute to the global warming through the greenhouse effect.[263] More revealing is the fact that traces of perfluorooctanoic acid (PFOA, scheme 48c) and perfluorooctanesulfonic acid (PFOS) have been recently detected within the blood of polar bears,[264] thus illustrating the inertness-bioaccumulation relationship problem of these PFCs in general. Moreover, PFOA is suspected to be involved in some diseases which include high cholesterol, thyroid disease, and some cancers. [265]

4.1.2 Strategies developed for the C–F bond activation

In recent decades, catalytic C–F bond activation has attracted a marked research interest.[266,267,268,269,270,271,272] One of the main objectives aim at developing valuable C–F bond

[261] a) G. B. Post, J. B. Louis, R. L. Lippincott, N. A. Procopio. Occurrence of Perfluorinated Compounds in Raw Water from New Jersey Public Drinking Water Systems. *Environ. Sci. Technol.* **2013**, *47* (23), 13266–13275. b) J. P. Benskin, D. C. G. Muir, B. F. Scott, C. Spencer, A. O. De Silva, H. Kylin, J. W. Martin, A. Morris, R. Lohmann, G. Tomy, B. Rosenberg, S Taniyasu, N. Yamashita. Perfluoroalkyl Acids in the Atlantic and Canadian Arctic Oceans. *Environ. Sci. Technol.* **2012**, *46* (11), 5815–5823.

[262] a) Paul, A. G.; Jones, K. C.; Sweetman, A. J. A First Global Production, Emission, And Environmental Inventory For Perfluorooctane Sulfonate. *Environ. Sci. Technol.* **2009**, *43* (2), 386–392. b) Ravishankara, A. R.; Turnipseed, A. A.; Jensen, N. R.; Barone, S.; Mills, M.; Howard, C. J.; Solomon, S. Do Hydrofluorocarbons Destroy Stratospheric Ozone? *Science* **1994**, *263* (5143), 71–5.

[263] a) Lu, Q.-B. Cosmic-Ray-Driven Reaction and Greenhouse Effect of Halogenated Molecules: Culprits for Atmospheric Ozone Depletion and Global Climate Change. *Int. J. Mod. Phys. B* **2013**, *27* (17), 1350073-1350111. b) Han, W.; Li, Y.; Tang, H.; Liu, H. Treatment of the Potent Greenhouse Gas, CHF_3—An Overview. *J. Fluor. Chem.* **2012**, *140*, 7–16.

[264] Vetter, W.; Gall, V.; Skírnisson, K. Polyhalogenated Compounds (PCBs, Chlordanes, HCB and BFRs) in Four Polar Bears (Ursus Maritimus) That Swam Malnourished from East Greenland to Iceland. *Sci. Total Environ.* **2015**, *533*, 290–296.

[265] a) Morrison, J. Perfluorinated chemicals taint drinking water. *Chem. Eng. News* **2016**, *94* (20), 20-22. b) Tucker, D. K.; Macon, M. B.; Strynar, M. J.; Dagnino, S.; Andersen, E. The Mammary Gland Is a Sensitive Pubertal Target in CD-1 and C57Bl/6 Mice Following Perinatal Perfluorooctanoic Acid (PFOA) Exposure. *Reprod. Toxicol.* **2015**, *54*, 26–36. c) Vieira, V. M.; Hoffman, K.; Shin, H. M.; Weinberg, J. M.; Webster, T. F.; Fletcher, T. Perfluorooctanoic Acid Exposure and Cancer Outcomes in a Contaminated Community: A Geographic Analysis. *Environ. Health Perspect.* **2013**, *121* (3), 318–323. d) Steenland, K.; Jin, C.; MacNeil, J.; Lally, C.; Ducatman, A.; Vieira, V.; Fletcher, T. Predictors of PFOA Levels in a Community Surrounding a Chemical Plant. *Environ. Health Perspect.* **2009**, *117* (7), 1083–1088.

[266] Shen, Q.; Huang, Y. G.; Liu, C.; Xiao, J. C.; Chen, Q. Y.; Guo, Y. Review of Recent Advances in C–F Bond Activation of Aliphatic Fluorides. *J. Fluor. Chem.* **2015**, *179*, 14–22.

[267] Whittlesey, M. K.; Peris, E. Catalytic Hydrodefluorination with Late Transition Metal Complexes. *ACS Catal.* **2014**, *4* (9), 3152–3159.

[268] Fernández-Alvarez, F. J.; Iglesias, M.; Oro, L. A.; Passarelli, V. Bond Activation and Catalysis. In *Comprehensive Inorganic Chemistry II: From Elements to Applications*, 2nd Ed.; Elsevier B.V.: 2013; Vol. 8, pp 399–432.

[269] Stahl, T.; Klare, H. F. T.; Oestreich, M. Main-Group Lewis Acids for C–F Bond Activation. *ACS Catal.* **2013**, *21* (3), 1578–1587.

[270] H.; Uneyama, K. C–F Bond Activation in Organic Synthesis. *Chem. Rev.* **2009**, *109* (5), 2119–2183.

[271] Richmond, T. G. Metal Reagents for Activation and Functionalization of Carbon–Fluorine Bonds. In *Activation of Unreactive Bonds and Organic Synthesis*; Mura, S., Ed.; Topics in Organometallic Chemistry Series; Springer: Berlin–Heidelberg, 1999; Vol. 3, pp 243–269.

[272] Burdeniuc, J.; Jedicka, B.; Crabtree, R. H. Recent Advances in C–F Bond Activation. *Chem. Ber.* **1997**, *130* (2), 145–154.

functionalization methodologies,[273] which could hence solve the recovery problem regarding these wasteful (per)fluorinated compounds. Several strategies have been developed towards this goal which are based on either simply replacing fluorine by hydrogen *via* the so-called hydrodefluoration (HDF) and perdefluoration reactions (schema 48d) or by replacing fluorine with any other functional element or group of elements (different from hydrogen) *via* the functional-defluoration (FDF) reaction (scheme 48d).

However, selective and efficient methods of general application are still lacking. We will only give some relevant examples on catalytic C–F bond activation methods that have been described throughout the literature with a preferential focus on HDF as a strategy. Two main HDF methods have been described in the literature, which are based on the use of main-group Lewis acids (R_3B, R_3Al, R_3Si^+) in combination with either main-group or transition metal hydrides as catalytic systems.[269] Several reviews on the various C–F activation methods have appeared last years.[267–271,274] A number of transition metal complexes have been described to mediate stoichiometric C–F bond activation.[266,272,274,275] In 1995 appeared the first catalytic version achieved by D. Milstein and coworkers with the use of rhodium complexes as catalysts for the activation of fluorobenzenes.[276] However, since this seminal work, an increasing number of reports has been published with the use of other TMs as (pre)catalysts.[267] The catalytic activation of a C–F bond within the coordination sphere of a TM center is challenging because the fundamental TM…C-F interaction is most of the time precluded by the very poor coordination ability of fluorocarbons to TMs, and whenever it becomes possible (mostly with aryl fluorides), the reaction generally ends at the stoichiometric C–F activation step because of the formation a strong TM–F bond.[271] Thus, it has appeared that one of the best strategies for the catalytic C–F bond activation is based on main group Lewis acids as catalytic systems.[269]

4.1.3 Catalytic HDF reaction with $HSiR_3$: principles and overview

The important barrier of activation associated with the C–F bond (very weak Lewis base) cleavage calls for the use of highly acidic and fluorophilic Lewis acids (LAs).[262] Lewis acids

[273] Ahrens, T.; Kohlmann, J.; Ahrens, M.; Braun, T. Functionalization of Fluorinated Molecules by Transition-Metal Mediated C–F Bond Activation To Access Fluorinated Building Blocks. *Chem. Rev.* **2015**, *115* (2), 931–972.
[274] Braun, T.; Perutz, R. N. In *Comprehensive Organometallic Chemistry III*; Crabtree, R. H., Mingos, D. M. P., Eds.; Elsevier: Oxford, Oxford, 2007; Vol. 1; pp 725–758.
[275] Torrens, H. Carbon-Fluorine Bond Activation by Platinum Group Metal Complexes. In *Coordination Chemistry Reviews*; Elsevier B.V.: 2005; Vol. 249, pp 1957–1985.
[276] Aizenberg, M.; Milstein, D. Catalytic Activation of Carbon-Fluorine Bonds by a Soluble Transition Metal Complex. *Science* **1994**, *265* (5170), 359–361.

made of boron, aluminum and silicon have been efficiently employed in the catalytic C–F bond activation of a variety of aliphatic and aromatic fluorocarbons.[269] In the case of silicon-based LAs, a pre-activation step is necessary for the generation of the highly active R_3Si^+ as LA from $HSiR_3$, by considering three different mechanisms upon which the catalysis can be initiated, as illustrated with a scheme originally published by M. Oestreich and coworkers in a recent review (scheme 49).[277]

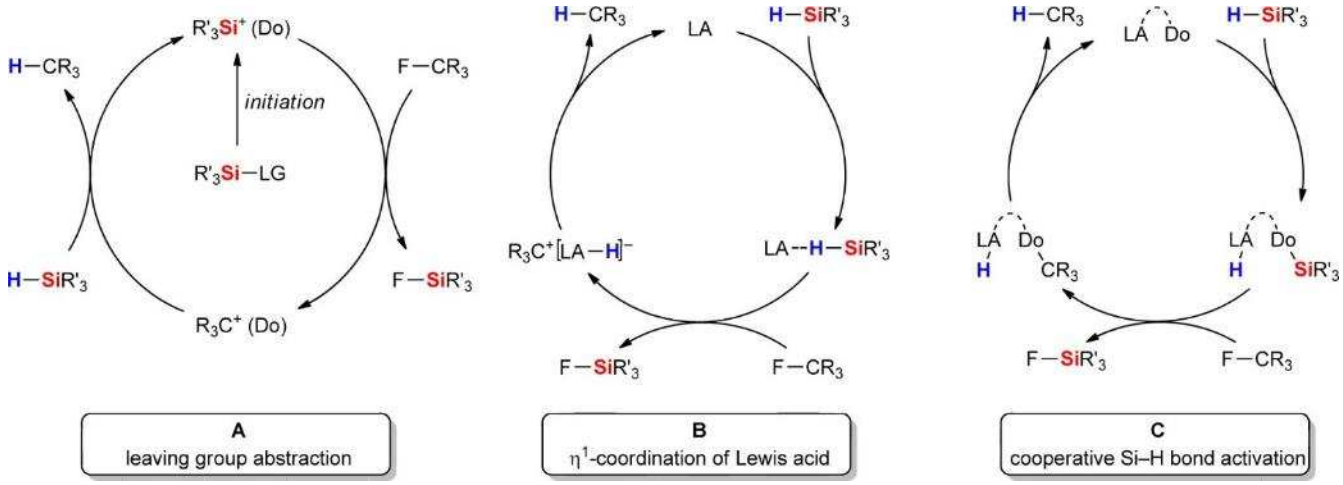

Scheme 49. Lewis-acid (LA) based strategies for the catalytic C–F bond activation with $HSiR_3$ as reducing agents. LA can be Si-, Al, B-, or TM-based (pre)catalyst. LG and Do stand for leaving grouo and for Donnor group respectively.[277] Reprinted with permission from Stahl, T.; Klare, H. F. T.; Oestreich, M. *ACS Catal*. **2013**, *21* (3), 1578. Copyright 2013 American Chemical Society.

As shown in the scheme 49, the same general principles are used, which are based on 1) the activation of the H–Si bond in $HSiR_3$, 2) the *in situ* generation of R_3Si^+, 3) the Lewis acid-base reaction between R_3'C–F and R_3Si^+ with the generation of R'_3C^+ and $FSiR_3$ respectively, and 4) the formation of R'_3C–H following the hydride transfer to R'_3C^+. It is the nature of the process used during the H–Si bond activation step which will determine the outcome of the complete reaction, as the *in situ* generated R_3Si^+ is highly electrophilic and of dramatic sensitivity to the presence of any electron donor molecule (denoted as Do in scheme 49) including solvents and counteranions. This *in situ* generated R_3Si^+ moiety can be sufficiently stabilized without losing its activity by different approaches, using either a weakly coordinating and electron donating

[277] Stahl, T.; Klare, H. F. T.; Oestreich, M. Main-Group Lewis Acids for C–F Bond Activation. *ACS Catal.* **2013**, *21* (3), 1578–1587.

anion (scheme 49, A),[278] a transition metal-based complex (scheme 49, B)[279] or a frustrated Lewis pair (FLP) (scheme 49, C).[280] Thus, several strategies have been adopted from different research groups by using $HSiR_3$ as reducing source and one of the above approaches for stabilizing the R_3Si^+ Lewis acids.

In 2005, O. Ozerov and coworkers were the first to describe the catalytic C–F bond activation of fluorocarbons, by using the approach A described in scheme 35, with $HSiEt_3$/$[Et_3Si][B(C_6F_5)_4]$ as catalytic system.[281] Later on, the same research group described a similar approach based on halogenated carboranes ($[CHB_{11}H_5Cl_6]$) as stabilizing counteranions, and showed that better TONs and substrate scope were achieved than with $[B(C_6F_5)_4]$ as counteranion.[278] This is illustrated with the highly efficient and chemoselective conversion of perfluorinated toluene into pentafluorotoluene when $[Et_3Si][CHB_{11}H_5Cl_6]$ was used as catalyst, thus corresponding to an unprecedented TON of 2700 ; whereas a TON of only 19 was obtained when $[Et_3Si][B(C_6F_5)_4]$ was used as catalyst. These studies show that by a subtle choice of counteranion, a more efficient catalysis can be achieved when highly electrophilic R_3Si^+ moieties are used as catalysts. However, the challenging several steps preparation of these halogenated carboranes may preclude the future application of for example $[Et_3Si][CHB_{11}H_5Cl_6]$ as catalyst for the C–F bond activation.[282] Similarly, the research group of T. Müller and coworkers reported in 2006 the use of hydrogen- and fluorine-bridged disilyl-cations as catalysts (2.2–4.7% mol) of the room temperature HDF reaction of fluorodecane and benzyl trifluoride to give quantitatively and within 30 minutes the corresponding alkanes.[283]

In the last few years, the research group of W. D Stephan and coworkers made significant contributions in the catalytic C–F bond activation of fluorocarbons. In 2012, they reported the catalytic HDF reaction of alkyl fluorides with $HSiEt_3$ by using $B(C_6F_5)_3$ (5 mol %) as the Lewis acid catalyst.[284] By this way, 1-fluoropentane and 1-fluoroadamantane were converted (>95%)

---

[278] Douvris, C.; Ozerov, O. V. Hydrodefluorination of Perfluoroalkyl Groups Using Silylium-Carborane Catalysts. *Science* **2008**, *321* (5893), 1188–1190.
[279] Yang, J.; Brookhart, M. Iridium-Catalyzed Reduction of Alkyl Halides by Triethylsilane. *J. Am. Chem. Soc.* **2007**, *129* (42), 12656–12657.
[280] Chen, J.; Chen, E. Y. X. Elusive Silane Alane Complex [Si-H…Al]: Isolation, Characterization, and Multifaceted Frustrated-Lewis-Pair-Type Catalysis. *Angew. Chem.- Int. Ed.* **2015**, *54* (23), 6842–6846.
[281] Scott, V. J.; Çelenligil-Çetin, R.; Ozerov, O. V. Room-Temperature Catalytic Hydrodefluorination of $C(sp^3)$–F Bonds. *J. Am. Chem. Soc.* **2005**, *127* (9), 2852–2853.
[282] Reed, C. A. Carboranes: A New Class of Weakly Coordinating Anions for Strong Electrophiles, Oxidants, and Superacids. *Acc. Chem. Res.* **1998**, *31* (3), 133–139.
[283] Panisch, R.; Bolte, M.; Müller, T. Hydrogen- and Fluorine-Bridged Disilyl Cations and Their Use in Catalytic C–F Activation. *J. Am. Chem. Soc.* **2006**, *128* (30), 9676–9682.
[284] Caputo, C. B.; Stephan, D. W. Activation of Alkyl C–F Bonds by $B(C_6F_5)_3$: Stoichiometric and Catalytic Transformations. *Organometallics* **2012**, *31* (1), 27–30.

within 5 min at room temperature into *n*-pentane and adamantane respectively. This catalytic HDF reaction seems to proceed via the mechanism B of the scheme 49. Shortly after, the same research group of W. D. Stephan and coworkers achieved a remarkable advance when they described the catalytic HDF reaction of various aliphatic and aromatic fluorocarbons, by using the phosphonium salt $[(C_6F_5)_3PF][B(C_6F_5)_3]$ as Lewis acid catalyst (1 mol %) (scheme 50).[285] In this manner, 1-fluoroadamantane, 1-fluoropentane, fluorocyclohexane, and *α*,*α*,*α*-trifluoromethyltoluene were quantitatively converted to the corresponding hydrocarbons within 3 hours, whereas bis(difluoromethyl)benzene derivatives required 24 hours (scheme 50a).

a)

R-F + Et_3SiH ⟶ R-H + Et_3SiF

Substrate	Cat. (mol %)*	t (h)	%Si–F†	%C–F‡	TON
Adamantyl-F	1	1	84	100	100
$C_5H_{11}F$	1	2	88	100	100
$C_6H_{11}F$	1	1	>95	100	100
$PhCF_3$	1	3	>95	>99	33
1,4-$C_6H_4(CF_2H)_2$	1	24	81	87	3.6
$C_6F_5CF_3$	1	24	71	98	4.1
3,5-$C_6H_3Br(CF_3)_2$	5	24	67	91	0.76
	10		77	>98	0.41
1,3,5-$C_6H_3(CF_3)_3$	5	24	49	69	0.58
	10		73	>99	0.41

b)

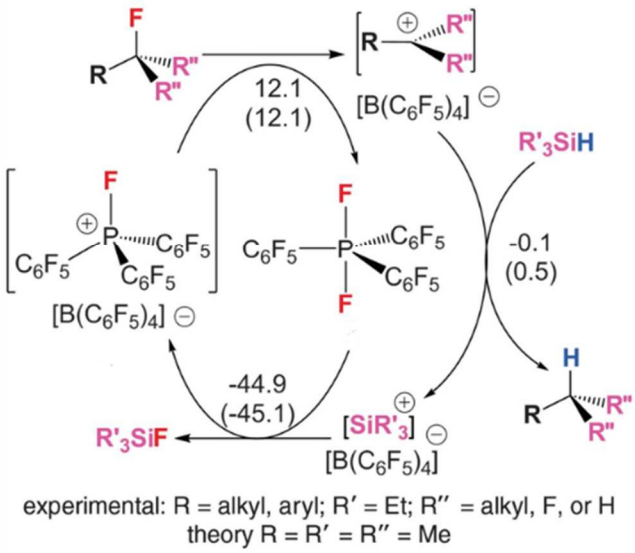

Scheme 50. Catalytic HDF reaction of fluoroalkanes by $[(C_6F_5)_3PF][B(C_6F_5)_3]$ as the Lewis acid catalyst (1 mol %; rt), reported by W. D. Stephan and coworkers.[285] **a)** Results of the catalytic HDF reaction of fluoroalkanes. (R = alkyl). **b)** Proposed reaction mechanism for phosphonium-catalyzed HDF reactions. Energies are calculated at the wB97XD/def2-TZVPP level of theory. Energy values are given in units of kcal•mol^{-1} relative to the energy of the $[(C_6F_5)_3PF]$ cation, $HSiMe_3$, and ^{t}BuF compounds; Gibbs free energies are given in parentheses. From Caputo, C. B.; Hounjet, L. J.; Dobrovetsky, R.; Stephan, D. W. *Science* **2013**, 341 (6152), 1374. Reprinted with permission from AAAS.

[285] Caputo, C. B.; Hounjet, L. J.; Dobrovetsky, R.; Stephan, D. W. Lewis Acidity of Organofluorophosphonium Salts: Hydrodefluorination by a Saturated Acceptor. *Science* **2013**, *341* (6152), 1374–1377.

Mechanistically, the authors invoked the fluorophilicity of the electrophilic phosphonium center in $[(C_6F_5)_3PF][B(C_6F_5)_3]$ balanced with the higher fluorophilicity of $[Et_3Si][B(C_6F_5)_4]$ and hydricity of $HSiEt_3$ as the key success of the catalytic system (scheme 50b).

In 2015, D. Vidovic and coworkers reported a similar observation with bicationic $[RP(C(PPh_3)_2)]^{2+}$ (R = Ph, 4-F-Ph) phosphenium salts which proved to easily activate the C–F bond of *α*,*α*,*α*- trifluoromethyltoluene.[286] In 2016, W. D Stephan and coworkers described an elegant method of derivatization of aryl and alkyl CF_3 groups with a range of arenes to give CH_2–aryl fragments by using the $[(C_6F_5)_3PF][B(C_6F_5)_3]$ phosphonium salt as Lewis acid catalyst (1.5–5 mol %).[287] The latter catalyst proved to initiate sequential benzylation or alkylation and hydrodefluorination reactions with a wide range of substrates in the presence of either $HSiEt_3$ or $HSi(^iPr)_3$ (25–80 °C, 4–16h).

4.1.4 TM-based catalytic HDF reaction

The catalytic hydrodefluoration reaction of fluorocarbons mediated by transition-metal complexes is becoming an intense research topic. In 2014, M. K. Whittlesey and E. Peris reported a review on this reaction with late transition metal complexes.[288] Several research groups have contributed to the field of stoichiometric or catalytic TM-based HDF reaction methodology.[289] Since 1920, TMs such as Pt, Ni, Pd, and Rh were first applied as heterogeneous catalytic systems in the HDF reaction of aryl fluorides with H_2 as reducing agent.[181] The limiting factor here come from the high hydrogen pressure which is usually required, besides the unselective over-reductions frequently encountered. Later, some research groups solved this limitation with the use of other heterogeneous catalytic systems such as Pd/C/NaOH (aq), providing the HDF products of aryl fluorides under milder conditions when using 2-propanol[290] or hydrazine[291] in place of H_2 as a hydrogen source. Few homogeneous systems have been reported to be able to catalyze the HDF reaction of aryl

[286] Đorđević, N.; Tay, M. Q. Y.; Muthaiah, S.; Ganguly, R.; Dimić, D.; Vidović, D. C–F Bond Activation by Transient Phosphenium Dications. *Inorg. Chem.* **2015**, *54* (9), 4180–4182.
[287] Zhu, J.; Pérez, M.; Stephan, D. W. C–C Coupling of Benzyl Fluorides Catalyzed by an Electrophilic Phosphonium Cation. *Angew. Chem.- Int. Ed.* **2016**, *55* (29), 8448–8451.
[288] Whittlesey, M. K.; Peris, E. Catalytic Hydrodefluorination with Late Transition Metal Complexes. *ACS Catal.* **2014**, *4* (9), 3152–3159.
[289] Fernández-Alvarez, F. J.; Iglesias, M.; Oro, L. A.; Passarelli, V. Bond Activation and Catalysis. In *Comprehensive Inorganic Chemistry II: From Elements to Applications*, 2nd Ed.; Elsevier B.V.: 2013; Vol. 8, pp 399–432.
[290] . Dong, Y. H.; Meng, Q. Z.; Kang, R. H. Dechlorination of aromatic chlorides in aqueous system catalyzed by functionalized MontK10 supported palladium-tin. *Chin. Chem. Lett.* **2003**, *14*, 368–370.
[291] Cellier, P. P.; Spindler, J. F.; Taillefer, M.; Cristau, H. J. Pd/C-Catalyzed Room-Temperature Hydrodehalogenation of Aryl Halides with Hydrazine Hydrochloride. *Tetrahedron Lett.* **2003**, *44* (38), 7191–7195.

fluorides. For example, in 2003 Y. Fort and coworkers described that NHC-supported [Ni^0] complexes could catalyze the HDF reaction of aryl- or heteroaryl-fluorides in combination with Et_2CHONa as a hydrogen source.[292] In 2000, W. D. Jones and collaborators described the first catalytic TM-based HDF reaction of fluoroalkanes based on the use of [$ZrH_2Cp_2^*$]/H_2 as catalytic system.[293] Many other examples followed by using a variety of TMs. It is also remarkable to notice that despite the previously mentioned problem associated with the strong TM–F bond resulting from the C–F bond activation of aryl fluorides at TMs,[294] some research groups have actually reported the challenging catalytic HDF reaction of C(sp^2)–F bonds of pentafluorpyridine and hexafluoropropene with the use of combinations of either [ZrF_2]/AlH^iBu_2[295] or [$TiCp_2F_2$]/$HSiR_3$[296] as catalytic systems. Also a breakthrough was achieved in 1996 by R. H. Crabtree and coworkers,[297] and by T. G. Richmond and coworkers,[298] when some examples of TM-based HDF reaction of alkyl perfluorocarbons were reported, by using [$FeCp^*_2$]/Zn and [$TiCp_2F_2$]/Al/$HgCl_2$ combinations as stoichiometric systems respectively. More recently, the research groups of R. G. Bergman and J. Arnold reported the catalytic mono-HDF reaction of polyfluoroarenes by using a niobium(III) imido complex and silanes as catalytic system.[299] Interestingly, the authors showed that π interactions play a key role in C–F activation of these fluoroarenes *via* the formation of a η^6-(F-arene) bound complex prior to C–F oxidative addition and C–H reductive elimination reactions. Many other TMs such as cobalt,[300] ruthenium,[301]

[292] Kuhl, S.; Schneider, R.; Fort, Y. Catalytic Carbon-Fluorine Bond Activation with Monocoordinated Nickel-Carbene Complexes: Reduction of Fluoroarenes. *Adv. Synth. Catal.* **2003**, *345* (3), 341–344.
[293] Kraft, B. M.; Lachicotte, R. J.; Jones, W. D. Aliphatic Carbon-Fluorine Bond Activation Using $(C_5Me_5)_2ZrH_2$. *J. Am. Chem. Soc.* **2000**, *122* (35), pp 8559–8560.
[294] Clot, E.; Eisenstein, O.; Jasim, N.; MacGregor, S. A.; McGrady, J. E.; Perutz, R. N. C-F and C-H Bond Activation of Fluorobenzenes and Fluoropyridines at Transition Metal Centers: How Fluorine Tips the Scales. *Acc. Chem. Res.* **2011**, *44* (5), 333–348.
[295] Jäger-Fiedler, U.; Klahn, M.; Arndt, P.; Baumann, W.; Spannenberg, A.; Burlakov, V. V.; Rosenthal, U. Room-Temperature Catalytic Hydrodefluorination of Pentafluoro-Pyridine by Zirconocene Fluoro Complexes and Diisobutylaluminumhydride. *J. Mol. Catal. A Chem.* **2007**, *261* (2), 184–189.
[296] Kühnel, M. F.; Lentz, D. Titanium-Catalyzed C-F Activation of Fluoroalkenes. *Angew. Chem. - Int. Ed.* **2010**, *49* (16), 2933–2936.
[297] Burdeniuc, J.; Crabtree, R. H. Photoinduced Catalytic Defluorination of Perfluoroalkanes To Give Perfluoroalkenes. *J. Am. Chem. Soc.* **1996**, *118* (10), 2525–2526.
[298] Kiplinger, J. L.; Richmond, T. G. Group IV Metallocene-Mediated Synthesis of Fluoroaromatics via Selective Defluorination of Saturated Perfluorocarbons. *J. Am. Chem. Soc.* **1996**, *118* (7), 1805–1806.
[299] Gianetti, T. L.; Bergman, R. G.; Arnold, J. Carbon–fluorine Bond Cleavage in Fluoroarenes via a Niobium(III) Imido Complex: From Stoichiometric to Catalytic Hydrodefluorination. *Chem. Sci.* **2014**, *5* (6), 2517–2524.
[300] Li, J.; Zheng, T.; Sun, H.; Li, X. Selectively Catalytic Hydrodefluorination of Perfluoroarenes by $Co(PMe_3)_4$ with Sodium Formate as Reducing Agent and Mechanism Study. *Dalt. Trans.* **2013**, *42* (36), 13048–13053.
[301] Stahl, T.; Klare, H. F. T.; Oestreich, M. C(sp_3)–F Bond Activation of CF_3-Substituted Anilines with Catalytically Generated Silicon Cations: Spectroscopic Evidence for a Hydride-Bridged Ru–S Dimer in the Catalytic Cycle. *J. Am. Chem. Soc.* **2013**, *135* (4), 1248–1251.

palladium,[302] rhodium,[303] iron,[304] and copper[305] were applied as homogeneous (pre)catalysts for the HDF reaction.

4.1.5 Iridium-based stoichiometric C–F bond activation

Few iridium based organometallic complexes have been employed for the stoichiometric C–F bond activation of fluorocarbons. In 1991, D. Milstein and coworkers showed for the first time that $MeIr^{I}(PEt_3)_3$ could activate the C–F bond of hexafluorobenzene affording $(C_6F_5)Ir^{I}(PEt_3)_2$ as the product of C–F bond oxidative addition.[306] In 2005, R. P. Hughes and coworkers reported that some $Cp^*Ir(PMe_3)(CF_2R_F)Y$ (R_F = F, CF_3; Y = H, D) complexes activate intramolecularly the C–F bond of the CF_2R_F ligands.[307] In 2011, K. Krogh-Jespersen, A. S. Goldman and coworkers made a significant achievement towards the stoichiometric oxidative addition of aliphatic C–F bonds to the iridium center of $(PCP)Ir^{I}$ (where PCP is κ^3-C_3H_6-2,6-$[CH_2P(^{t}Bu)_2]_2$).[308] Interestingly, the authors found that actually the oxidative addition of the C–F bond at iridium was possible because a reversible C–H bond activation initiated the process. In 2012, M. Cowie and coworkers described the C–F bond activation mediated by the diiridium complex $[Ir_2(CO)_3(\mu\text{-H})\text{-(depm)}_2]^+$.[309] The latter complex reacts stoichiometrically with vinyl fluorides, and in some cases water showed to play a key role as assistant of the C–F bond activation process. Other outstanding results were reported by the research group of A. L. Rheingold and coworkers, who prepared several Ir–F complexes through the stoichiometric activation of the C–F bond of fluorocarbons.[310]

---

[302] Sabater, S.; Mata, J.; Peris, E. Hydrodefluorination of Carbon-Fluorine Bonds by the Synergistic Action of a Ruthenium-Palladium Catalyst. *Nat. Commun.* **2013**, *4*, 2553.

[303] Lindup, R. J.; Marder, T. B., Perutz, R. N.; Whitwood, A. C. Sequential C–F Activation and Borylation of Fluoropyridines *via* Intermediate Rh(I) Fluoropyridyl Complexes: A Multinuclear NMR Investigation. *Chem. Commun.* **2007**, *95* (35), 3664.

[304] Vela, J.; Smith, J. M.; Yu, Y.; Ketterer, N. A.; Flaschenriem, J.; Lachicotte, R. J.; Holland, P. L.; Flaschenriem, C. J. Synthesis and Reactivity of Low-Coordinate Iron (II) Fluoride Complexes and Their Use in the Catalytic Hydrodefluorination of Fluorocarbons. *J. Am. Chem. Soc.* **2005**, *127*, 7857–7870.

[305] Lv, H.; Cai, Y.-B.; Zhang, J.-L. Copper-Catalyzed Hydrodefluorination of Fluoroarenes by Copper Hydride Intermediates. *Angew. Chem.- Int. Ed.* **2013**, *52* (11), 3203–3207.

[306] Blum, O.; Frolow, F.; Milstein, D. Carbon-Fluorine Bond Activation by iridium(I). A Unique Process Involving Phosphorus-Carbon Bond Cleavage, Phosphorus-Fluorine Bond Formation and Net Retention of Oxidation State. *J. Chem. Soc., Chem. Commun.* **1991**, *0* (4), 258–259.

[307] Hughes, R. P.; Laritchev, R. B.; Yuan, J.; Golen, J. A.; Rucker, A. N.; Rheingold, A. L. A Simple Route to Difluorocarbene and Perfluoroalkylidene Complexes of Iridium. *J. Am. Chem. Soc.* **2005**, *127* (43), 15020–15021.

[308] Choi, J.; Wang, D. Y.; Kundu, S.; Choliy, Y.; Emge, T. J.; Krogh-Jespersen, K.; Goldman, A. S. Net Oxidative Addition of $C(sp^3)$-F Bonds to Iridium via Initial C–H Bond Activation. *Science.* **2011**, *332* (6037), 1545-1548.

[309] Slaney, M. E.; Ferguson, M. J.; McDonald, R.; Cowie, M. Tandem C–F and C–H Bond Activation in Fluoroolefins Promoted by a Bis(diethylphosphino)methane-Bridged Diiridium Complex: Role of Water in the Activation Processes. *Organometallics* **2012**, *31* (4), 1384–1396.

[310] a) Yuan, J.; Hughes, R. P.; Rheingold, A. L. Synthesis and Crystallographic Characterization of Dimeric Perfluoroalkyl Iridium Complexes: $[Cp^*Ir(X)(RF)]_2$ (X=I, RF=CF_3, CF_2CF_3, $CF_2CF_2CF_3$, $CF(CF_3)_2$, $CF(CF_3)(CF_2CF_3)$; X=Cl and Br, RF=CF_2CF_3), and a New Perfluoroethylidene Complex $Cp^*Ir(PPh_3)(CFCF_3)$. *Inorganica Chim. Acta* **2010**, *364* (1), 96–101. b)

Catalytic C–F bond activation with iridium complexes is very rare. To our knowledge, only 3 examples have been reported so far in the literature. In 2007, M. Brookhart and coworkers reported the first catalytic C–F bond activation with the aid of an iridium complex.[311] The authors used [Ir(POCOP)(acetone)H][B(C_6F_5)$_4$] (2 mol %) in combination of $HSiEt_3$ (3 equiv.) as the catalytic system for the conversion (92%) of 1-fluoropentane (1 equiv.) to *n*-pentane within 72 h at 50 °C. However, the catalytic system showed to be more interesting to apply for the dehydrodehalogenation of chloro- and bromoalkanes. The authors proposed the catalytic cycle outlined in scheme 51.

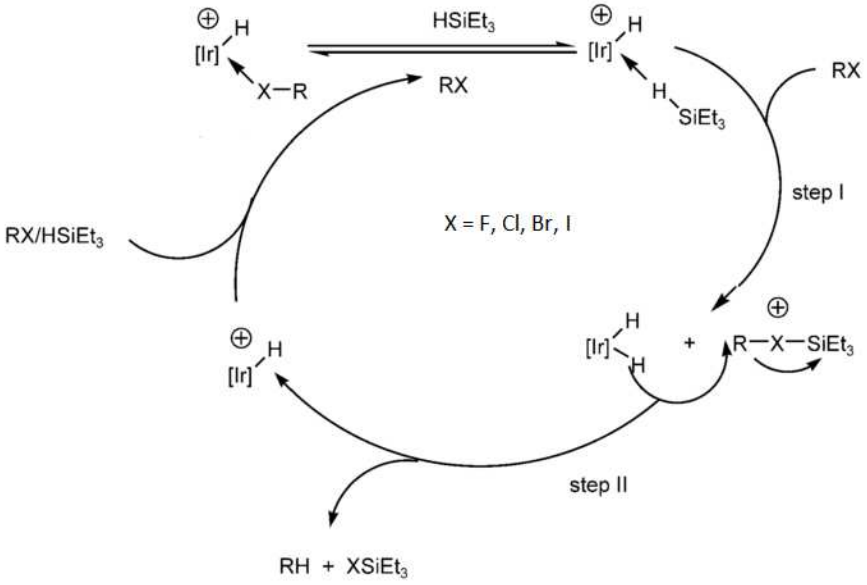

Scheme 51. Catalytic cycle proposed by M. Brookhart and coworkers for the HDF reaction of fluoropentane by [Ir(POCOP)(acetone)H][B(C_6F_5)$_4$] as precatalyst (2 mol %; 50 °C).[311] Reprinted with permission from Yang, J.; Brookhart, M. *J. Am. Chem. Soc*. **2007**, *129* (42), 12656. Copyright 2007 American Chemical Society.

The catalytic cycle was postulated to follow an ionic-type mechanism (scheme 51).[311] The first step was proposed (step I) to permit the transfer of Et_3Si^+ from the [Ir](η^1-$HSiEt_3$) intermediate

Yuan, J.; Hughes, R. P.; Rheingold, A. L. The First Example of a Bis(trifluoromethyl)carbene Transition-Metal Complex and Its Reduction to a Perfluoroallene Complex. *Eur. J. Inorg. Chem.* **2007**, *2007* (30), 4723–4725. c) Hughes, R. P.; Laritchev, R. B.; Yuan, J.; Golen, J. A.; Rucker, A. N.; Rheingold, A. L. A Simple Route to Difluorocarbene and Perfluoroalkylidene Complexes of Iridium. *J. Am. Chem. Soc.* **2005**, *127* (43), 15020–15021.

[311] Yang, J.; Brookhart, M. Iridium-Catalyzed Reduction of Alkyl Halides by Triethylsilane. *J. Am. Chem. Soc.* **2007**, *129* (42), 12656–12657.

to the fluoride substituent of the fluorocarbon RF affording $[RFSiEt_3]^+$ and $[[Ir](H)_2$ as intermediates. In the second step (step II), $[[Ir](H)_2$ transfers its hydride to $[RFSiEt_3]^+$ *via* an S_N2-like mechanism leading to the formation of $FSiEt_3$ and [Ir]H. The regeneration of the active catalytic intermediate [Ir](η^1-$HSiEt_3$) was proposed to proceed through the coordination of $HSiEt_3$ to [Ir]H.

In 2014, J. D. Weaver and coworkers reported the use of the iridium complex $[Ir(ppy)_3]$ (ppy = phenylenepyridine) as the first photocatalyst employed in a HDF reaction of a series of fluoroarenes.[312] The method showed to selectively give access to partially fluorinated arenes by using EtN^iPr_2 as the reducing agent. By this way, a remarkable achievement was made with the unprecedented TON of 22500 reached with the mono-HDF reaction of pentafluoropyridine used as a proof of concept. However, if one considers the mechanism proposed by the authors (scheme 52), one can't find any rational regarding the fate of the released fluoride anion F^-. Perhaps the hazardous HF gas is formed here.

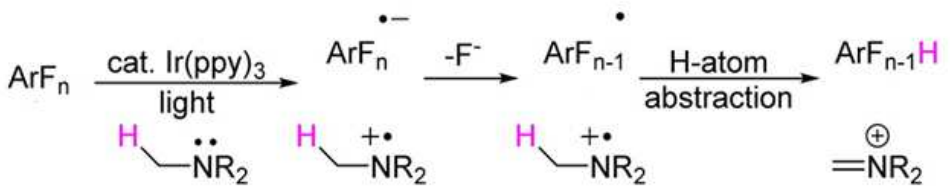

Scheme 52. First iridium-based photocatalytic HDF reaction of fluoroarenes with $[Ir(ppy)_3]$/ EtN^iPr_2 as catalytic system, as reported by J. D. Weaver and coworkers.[312] Reprinted with permission from Senaweera, S. M.; Singh, A.; Weaver, J. D. *J. Am. Chem. Soc.* **2014**, *136* (8), 3002. Copyright 2014 American Chemical Society.

In 2016, Y. Kayaki and coworkers described the first example of iridium-catalyzed HDF reaction of fluoroarenes with the hydrogen transfer methodology.[313] By employing ^{i}PrOH as the hydrogen source, the authors managed to transform in mild conditions (30 °C, 1h) and good conversions (61–100%) a variety of perfluorinated pyridines and arenes into (in general) the monohydrogentaed products.

[312] Senaweera, S. M.; Singh, A.; Weaver, J. D. Photocatalytic Hydrodefluorination: Facile Access to Partially Fluorinated Aromatics. *J. Am. Chem. Soc.* **2014**, *136* (8), 3002–3005.
[313] Matsunami, A.; Kuwata, S.; Kayaki, Y. Hydrodefluorination of Fluoroarenes Using Hydrogen Transfer Catalysts with a Bifunctional Iridium/NH Moiety. *ACS Catal.* **2016**, *6* (8), 5181–5185.

4.1.7 Our strategy

Our research laboratory became interested in this field only recently after the discovery of the bifunctional and donor-acceptor behavior of the iridium-silane catalytic intermediates that are disclosed in this thesis manuscript.[314] Because we view these intermediates as a source of Et_3Si^+ and "H^-", we wondered: is it then possible to apply them for the catalytic HDF reaction of fluorocarbons? The answer to this question can be found in the following section.

4.2 Results and discussion

4.2.1 Preliminary investigations: the C(sp^2)–F bond is not activated

At the beginning of our study, hexafluorobenzene (HFB) was checked to be inactive in the HDF reaction whatever the silane used (see experimental part). Therefore, for calculating the conversion by ^{19}F NMR analysis it was decided to use HFB as an internal reference.

Diverse fluorocarbons have been tested for the catalytic HDF reaction. We started the study by carrying out the reactions depicted in scheme 53. Fluorobenzene (C_6H_5F) (1 equiv.) and $HSiEt_3$ (2 equiv.) were mixed together prior the addition of a solution of [**2**][$BArF_{24}$] (1.4 mol %) in CD_2Cl_2 (0.5 mL). Stirring this mixture at room temperature for 2 h, and then at 50 °C for 70 h did not give any conversion of fluorobenzene (scheme 53a). The use of either [**2**][BPh_4] or [**2**][BF_4] as precatalysts led also to the same observation (see experimental part). Repeating the same experiment by using 2 mol % of [**2**][$BArF_{24}$] and heating the reaction mixture at 70 °C for 4 h (CD_2Cl_2), the ^{19}F and ^1H NMR analysis clearly showed that thermal degradation of the catalyst occured. Indeed, the typical ^{19}F NMR signals of $FSiEt_3$ and of C_6H_5F along with the only characteristic ^1H NMR signals of fluorobenzene were identified. The formation of $FSiEt_3$ might be the result of the probable reaction between the CF_3 group of $[BArF_{24}]^-$ and the transient Et_3Si^+ intermediate.

[314] Hamdaoui, M.; Ney, M.; Sarda, V.; Karmazin, L.; Bailly, C.; Sieffert, N.; Dohm, S.; Hansen, A.; Grimme, S.; Djukic, J.-P. Evidence of a Donor–Acceptor (Ir–H)→SiR_3 Interaction in a Trapped Ir(III) Silane Catalytic Intermediate. *Organometallics* **2016**, *35* (13), 2207–2223.

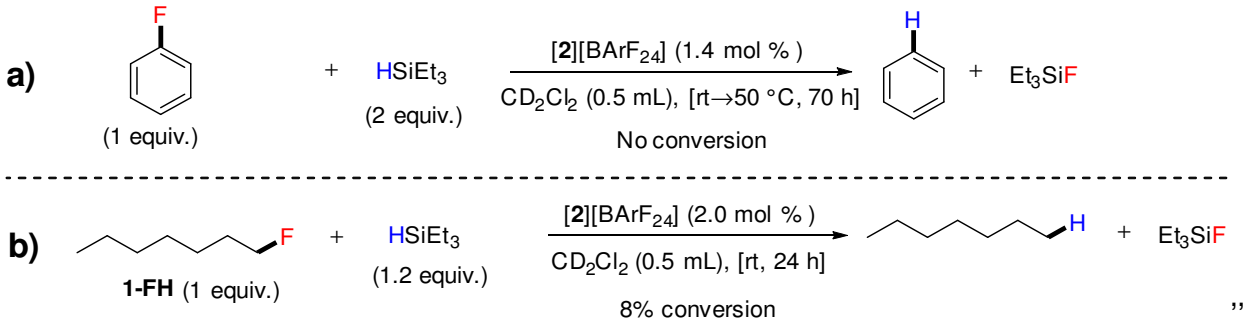

Scheme 53. Investigation of the catalytic HDF reaction of **a)** fluorobenzene and **b)** 1-fluoroheptane (**1-FH**) with [**2**][$BArF_{24}$] as precatalyst.

The HDF reaction between 1-fluoroheptane (**1-FH**) (1 equiv.) and $HSiEt_3$ (1.2 equiv.) in the presence of 2 mol % of [**2**][$BArF_{24}$] and CD_2Cl_2 (0.5 mL) was also investigated (scheme 53b). Stirring this mixture at room temperature for 24 h resulted in 8% of conversion of **1-FH** to *n*-heptane as revealed by ^{19}F NMR analysis. These preliminary investigations indicated that *a priori* a C(sp^3)–F bond is more reactive than a C(sp^2)–F towards the HDF reaction when carried out in the conditions of the catalysis that we used.

4.2.2 Full HDF reaction of 1-fluoroheptane: the importance of the nature of silane and solvent

We suspected a detrimental influence of the solvent on the fate of the catalytic HDF reaction. We could not exclude that CD_2Cl_2 could compete with the HDF reaction of fluorocarbons because its C–Cl bond activation is a plausible side reaction, as previously observed by M. Brookhart and coworkers.[315] So, we decided to turn our attention on the use of fluorobenzene as a solvent because of its inertness towards the HDF reaction (as shown with a blank test where fluorobenzene was used as substrate and solvent), its relative high boiling point (85 °C at 760 mmHg), and its ability to solubilize [**2**][$BArF_{24}$]. Using C_6H_5F (0.5 mL) as solvent and 2 mol % of [**2**][$BArF_{24}$], we first studied the influence of the nature of silane on the conversion of **1-FH** to *n*-heptane. It was found that total conversion of **1-FH** (1 equiv.) was obtained when $HSiPhH_2$ (1.2 equiv.) was used as silane upon heating the reaction mixture for 23 h at 80 °C (entry 1, table 18). [**4**][$BArF_{24}$] gave the same results as well (scheme 54). No conversion was observed with $HSiEt_3$, or PMHS as silane (entries 3–4, table 18). Indeed, ^1H and ^{19}F NMR spectroscopic data (C_6D_6, see spectra in scheme 54) showed clear evidence that total

[315] Yang, J.; Brookhart, M. Reduction of Alkyl Halides by Triethylsilane Based on a Cationic Iridium Bis(phosphinite) Pincer Catalyst: Scope, Selectivity and Mechanism. *Adv. Synth. Catal.* **2009**, *351* (1–2), 175–187.

disappearance of typical signals of **1-FH** (^{1}H [C*H*$_2$F, doublet of triplets]: δ = 4.0 to 4.2 ppm, $J^1_{H\text{-}F}$ = 47.5 Hz, $J^3_{H\text{-}H}$ = 6.1; ^{19}F [singlet]: δ = –218.6 ppm) was accompanied with the appearance of typical signals of *n*-heptane (^{1}H [C*H*$_2$, m]: δ = 1.2 ppm; [C*H*$_3$, triplet]: δ =0.9 ppm, $J^3_{H\text{-}H}$ = 7.2 Hz). 19 F NMR spectroscopy (scheme 54) showed the presence of PhSiHF2, as indicated by its typical chemical shift at ~–141 ppm (see scheme 57). However, the better reactivity of HSiPhH$_2$ when compared to other silanes in performing the HDF reaction in this case, raises a question about the real mechanism of this reaction. Indeed, as shown previously in this manuscript, HSiEt$_3$ was found to give the best activity in performing the *O*-silylation of alcohols and the hydrosilylation of carbonyls and nitriles. So, what could explain this difference?

Table 18. Influence of the nature of silane on the catalytic HDF reaction of 1-fluoroheptane.[a]

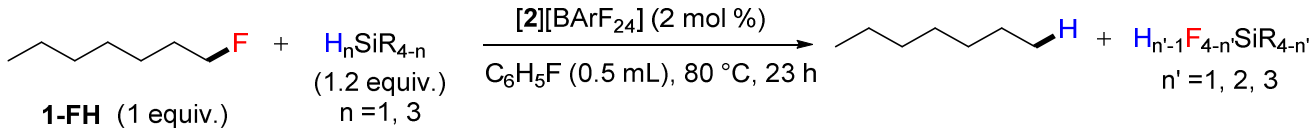

1-FH (1 equiv.)

Entry	Silane (H_nSiR_{4-n})	Conversion (%)
1	HSiPhH$_2$	>99
2	PMHS	<1
3	HSiEt$_3$	<1

[a] Conditions: **1-FH** (0.1 mL, 0.68 mmol), H$_n$SiR$_{4-n}$: for HSiEt$_3$: 0.13 mL, 0.82 mmol; for HSiPhH$_2$: 0.11 mL, 0.82 mmol; for PMHS: 0.11 mL, 0.82 mmol, [**2**][BArF$_{24}$] (20.0 mg, 0.014 mmol, 2.0 mol %), C$_6$H$_5$F (0.5 mL), 80 °C, 23 h. Conversions were determined by ^{1}H and ^{19}F NMR spectroscopy (CD$_2$Cl$_2$). PMHS stands for polymethylhydrosiloxane.

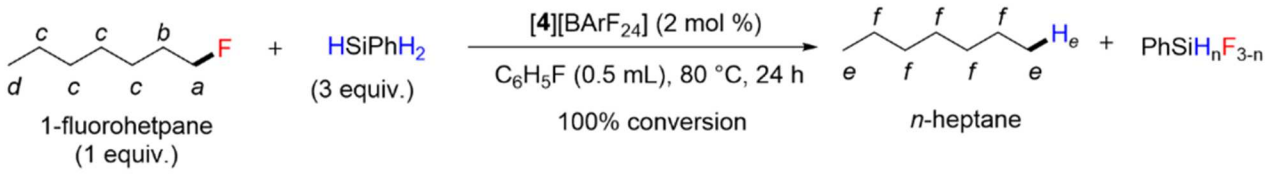

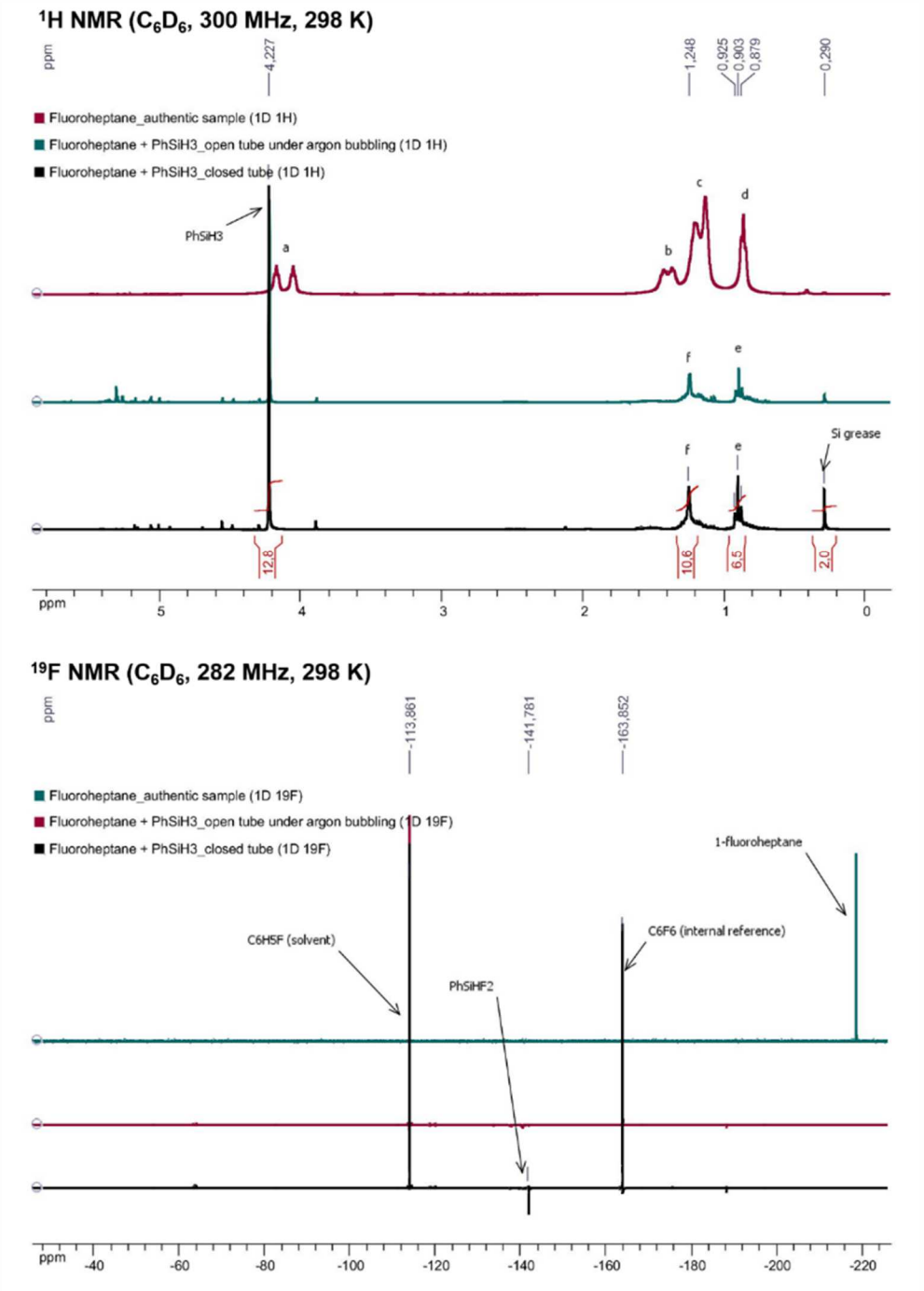

Scheme 54. ^{1}H and ^{19}F NMR spectroscopic analysis of the catalytic HDF transformation of 1-fluoropheptane to *n*-heptane using [**4**][$BArF_{24}$]/$HSiPhH_2$ as catalytic system.

To tackle this issue, further investigations are still undergoing in the laboratory, based on the postulate that the difference might come from the nature of the involved catalytic intermediate(s). Before answering the latter question, we wished first to optimize further the reaction and if possible extend the substrate scope.

4.2.3 First attempts to extend the HDF reaction study

Most of the work described in the next sections was carried by Diane Fischer-Krauser, who was a brilliant MSc1 student that I had the opportunity to supervise and to work with. We began the study by first trying the HDF reaction of the *O*-benzyl protected version of **2-FCyOH** as substrate, namely ((2-fluorocyclohexyl)oxy)benzene (**2-FCyOBn**) (table 19). **2-FCyOBn** was synthesized by the deprotonation of **2-FCyOH** with NaH to give Na[**2-FCyO**], followed by the *in situ* SN_2 dehalogenative benzylation reaction with benzyl bromide (see experimental part). However, **2-FCyOBn** has proved to be less reactive towards the HDF reaction. The results of this study are summarized in table 19, and for experimental details the reader is referred to the experimental part.

When [**4**][BPh_4] was used as precatalyst, it showed to give the highest conversion (26%, entry 1, table 19) when compared to [**4**][$BArF_{24}$] and [**4**][BF_4] which both converted only 13% of **2-FCyOBn** (entries 2–3, table 19). However, combining [**4**][BPh_4] with an excess of silane as catalytic system had a negative effect on the conversion which dropped until 17% (entry 4, table 19). The rather low conversion obtained with **2-FCyOBn** as substrate cannot be explained at this stage, but we can postulate that the OBn functional group could react with the transient $[Et_3Si]^+$ moiety *via* a donor-acceptor interaction with the oxygen atom, thereby activating the benzyloxy group towards the hydride attack by the [Ir-H] intermediate (**13,** scheme 60) leaving toluene and **R-CyOH** (**R** = **2-F** or **H**) as products.

Catalytic ether cleavage induced by iridium and hydrosilane as catalytic system has been already shown to be possible as reported by M. Brookhart and coworkers.[316] However, we can exclude at this stage this possibility because a careful analysis of the NMR spectra of the resulting reaction mixtures does not provide any clear evidence about the formation of toluene as by-product. We then tried to extend this reaction by using 2-fluorocyclohexan-1-ol (**2-**

[316] Yang, J.; White, P. S.; Brookhart, M. Scope and Mechanism of the Iridium-Catalyzed Cleavage of Alkyl Ethers with Triethylsilane. *J. Am. Chem. Soc.* **2008**, *130* (51), 17509–17518.

Table 19. Influence of the counter-anion X (X = BPh_4, $BArF_{24}$, OTf) in [**4**][X]-catalyzed HDF reaction of ((2-fluorocyclohexyl)oxy)benzene (**2-FCyOBn**) with $HSiPhH_2$.[a]

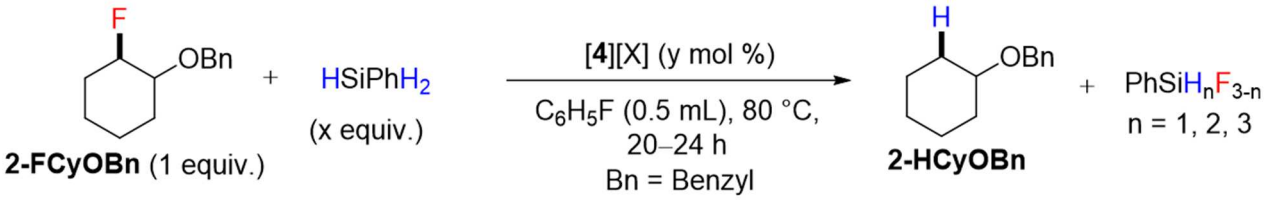

Entry	x equiv.	X (y mol %)	Conversion (%)
1	1	BPh_4 (1)	26
2	1	$BArF_{24}$ (1)	13
3	1	OTf (1)	13
4	3	BPh_4 (5)	17

[a] Conditions entries 1–3: **2-FCyOBn** (30 mg, 0.14 mmol), $HSiPhH_2$ (x = 1 equiv.: 0.02 ml, 0.14 mmol), [**4**][X] [y = 1.0 mol %] (X = $BArF_{24}$: 2.0 mg, 1.4 μmol; X = BPh_4: 1.3 mg, 1.4 μmol; X = OTf: 1.0 mg, 1.4 μmol), C_6H_5F (0.5 ml), 80 °C, 20 h. Conditions entry 4: **2-FCyOBn** (70 mg, 0.34 mmol), $HSiPhH_2$ (x = 3 equiv.: 0.13 ml, 1.05 mmol), [**4**][BPh_4] (15.0 mg, 10.6 μmol [y = 5.0 mol %]), C_6H_5F (0.5 ml), 80 °C, 24 h. Conversions were determined by NMR spectroscopy (C_6D_6) against hexafluorobenzene as ^{19}F internal reference.

FCyOH) as substrate with the idea of checking the influence of the OH-function substituent on HDF reaction. Of course, we expected that *O*-silylation of the OH function could occur very selectively, but does the resulting tandem *O*-silylation/HDF reactions could occur? This might give access to an interesting route to functionalized products derived from wasteful fluorocarbons that are difficult to eliminate otherwise.

4.2.4 One-pot and tandem *O*-silylation/HDF reactions of 2-fluorocyclohexan-1-ol

We report herein a successful one-pot and tandem procedure of the *in-situ O*-silylation and the subsequent HDF reaction of **2-FCyOH** to **2-FCyOSiEt$_3$** and **H-CyOSiEt$_3$** respectively, with the use of 5 mol % of [**4**][BArF$_{24}$] as the only catalytic source for both steps (scheme 55).

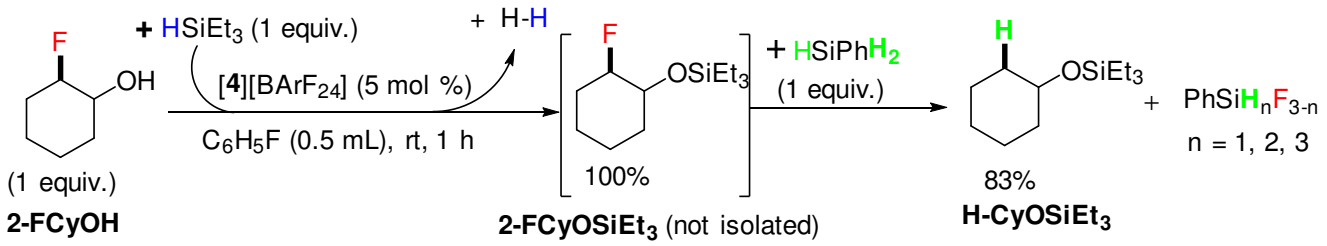

Scheme 55. Development of the one-pot and tandem procedure for the *O*-silylation and HDF reactions of **2-FCyOH** to **2-FCyOSiEt$_3$** and **H-CyOSiEt$_3$**, using 5 mol % of [**4**][BArF$_{24}$] as the only catalytic source for both steps.

The *in situ* generated *O*-silylated intermediate **2-FCyOSiEt$_3$** could be obtained quantitatively from **2-FCyOH** (1equiv.) and HSiEt$_3$ (1 equiv.) within 1 h at room temperature. One equivalent of HSiPhH$_2$ was then added to the same reaction mixture which was heated at 80 °C for 20 h with no additional loading in [**4**][BArF$_{24}$]. Interestingly, NMR analysis revealed that 83% of **2-FCyOSiEt$_3$** was converted. The quantity of [**4**][BArF$_{24}$] used was critical because with only 1 mol %, only 18% of **2-FCyOSiEt$_3$** was converted. The complex nature of the signals observed in the ^{1}H NMR spectrum precluded any satisfactory conclusion about the other products of the reaction. A better understanding of this reaction is currently under investigation especially with the help of GC-MS analysis.

4.2.5 The HDF reaction of trifluoromethyltoluene does not work well

As the catalytic activation of the C(sp^3)–F bond of an aliphatic substrate proved to be more facile than the C(sp^2)–F bond of an arene substrate, we thought to investigate the catalytic activation of the C(sp^3)–F bond of trifluoromethyltoluene (C$_6$H$_5$CF$_3$) as substrate (scheme 56). Unfortunately, after several attempts, the HDF reaction of this substrate was very difficult. However, a conversion of 31% was obtained only when heating at 100 °C for 24 h a solution containing C$_6$H$_5$CF$_3$ (as solvent), 3 equivalents of HSiPhH$_2$ and 5 mol % of [**4**][BArF$_{24}$].

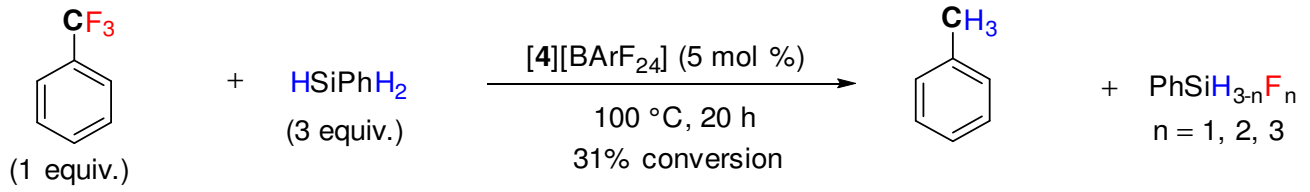

Scheme 56. Investigation of the solvent-free catalytic HDF reaction of trifluoromethyltoluene using $HPhSiH_2$ and [**4**][$BArF_{24}$] as catalyst system.

From this study, when gathered with previous observations, it seems that the extent of the C–F bond activation is critically influenced by the [**4**][$BArF_{24}$]/$HPhSiH_2$ pair as the catalytic system. The study also confirms that the solvent of use may be detrimental to the efficiency of the catalysis within our reaction conditions, because no reaction was observed until the substrate $C_6H_5CF_3$ becomes "the solvent". Overall, these results seriously question the beneficial effect of fluorobenzene as solvent, which nonetheless has proved to be necessary for the complete HDF conversion of 1-fluoroheptane to *n*-heptane.

4.2.6 [**2**][$BArF_{24}$] versus [**4**][$BArF_{24}$] in the catalytic HDF reaction of 1-fluoroheptane

We then investigated the HDF reaction of 1-fluoroheptane (**1-FH**) using [**4**][$BArF_{24}$] as precatalyst and C_6H_5F as solvent. When 2 mol % of [**4**][$BArF_{24}$] and 3 equivalents of $HSiPhH_2$ were used, full conversion of **1-FH** was observed (entry 2, table 20). Besides the typical signals of *n*-heptane that are observed in the ^1H NMR spectrum, we also identified in the ^1H and ^{19}F NMR spectra the presence of several silanes derivatives (denoted as **SiF_1**, **SiF_2** and **SiF_3**, scheme 57), the structures of which could be unequivocally derived from additional 2D NMR experiments.

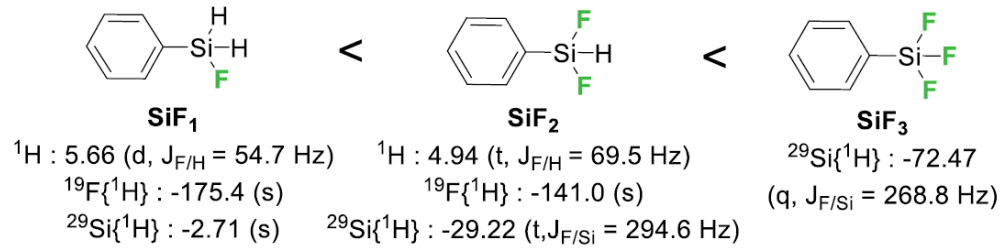

SiF_1
^1H : 5.66 (d, $J_{F/H}$ = 54.7 Hz)
$^{19}F\{^1H\}$: -175.4 (s)
$^{29}Si\{^1H\}$: -2.71 (s)

SiF_2
^1H : 4.94 (t, $J_{F/H}$ = 69.5 Hz)
$^{19}F\{^1H\}$: -141.0 (s)
$^{29}Si\{^1H\}$: -29.22 (t,$J_{F/Si}$ = 294.6 Hz)

SiF_3
$^{29}Si\{^1H\}$: -72.47
(q, $J_{F/Si}$ = 268.8 Hz)

Scheme 57. NMR (C_6D_6) spectroscopic identification of $PhSiH_{3-n}F_n$ species observed in the catalytic HDF reaction of 1-fluoroheptane (s and q stand for singlet and quartet respectively).

The species **SiF_2** and **SiF_3** in a ratio of 1:3 are the major fluorosilanes observed in the ^{19}F NMR spectrum of the reaction mixture. This observation may indicate that several types of silane species are involved in the HDF reaction, because $HSiPhH_2$, $PhSiFH_2$, and $PhSiF_2H$ could potentially be activated through the H–Si bond interaction with the active catalyst [**4+**][$BArF_{24}$] (scheme 60). However, this explanation seems to be in contradiction with the necessity of using an excess of $HSiPhH_2$ whereas 30 mol % would be enough to completely achieve the HDF reaction. It is worth to notice that without [**4**][$BArF_{24}$] as the catalyst source, there was no reaction (entry 1, table 20). As a conclusion here, we demonstrated the potential of combining together [**4**][$BArF_{24}$] and $HSiPhH_2$ as efficient catalytic system to mediate the HDF reaction of 1-fluoroheptane.

4.2.7 Solvent-free HDF reaction: preliminary substrate scope

We tried to extend the previous methodology to similar fluorocarbon substrates under solvent-free conditions. As we are still at the preliminary stage of the study, only a few examples can be reported at the moment here. As depicted in scheme 58, fluorocyclohexane (**F-Cy**) proved to be readily converted to cyclohexane (**H-Cy**) under the solvent-free conditions. The analysis of the resulting ^1H and ^{19}F NMR spectra (scheme 59) allowed us to identify the typical singlet peak of **H-Cy** at 1.40 ppm, accompanied with the ^{19}F NMR signals of the fluorosilanes **SiF_1**, **SiF_2** and **SiF_3**. **SiF_1** was the main product whereas **SiF_2** and **SiF_3** were present in a ratio of 1:3. **F-Cy** was quantitatively converted because no characteristic ^1H NMR (C_6D_6) signals could be identified ([C*H*F, doublet of septets]: δ = 4.2–4.4 ppm, $J^1_{H\text{-}F}$ = 48.8 Hz, $J^3_{H\text{-}H}$ = 3.9 Hz) and ^{19}F NMR (C_6D_6) ([singlet]: δ = –173.9 ppm). However, typical signals of cyclohexene, although neglible in intensity, were also observed, accounting for the loss of proton from the cyclohexyl cation intermediate. Overall, cyclohexane and cyclohexene contribute to 50% of the reaction products, whereas the remaining 50% could not be identified by ^1H NMR analysis due the complicated pattern within the range of δ = 0.8–1.8 ppm. As a similar result, O. V. Ozerov and coworkers identified another product ($C_{12}H_{22}$ (M/Z^+ 166), ~30%) accompanying cyclohexane (~58%) in the complete conversion of fluorocyclohexane during the HDF reaction.[317] Such an observation is not surprising if we consider the formation of the cyclohexyl cation intermediate

[317] Douvris, C.; Nagaraja, C. M.; Chen, C.-H.; Foxman, B. M.; Ozerov, O. V. Hydrodefluorination and Other Hydrodehalogenation of Aliphatic Carbon–Halogen Bonds Using Silylium Catalysis. *J. Am. Chem. Soc.* **2010**, *132* (13), 4946–4953.

of pronounced reactivity towards intermolecular electrophilic attack.

Table 20. Investigation of the catalytic HDF reaction of 1-fluoroheptane with $HSiPhH_2$ using [**4**][$BArF_{24}$] as precatalyst.[a]

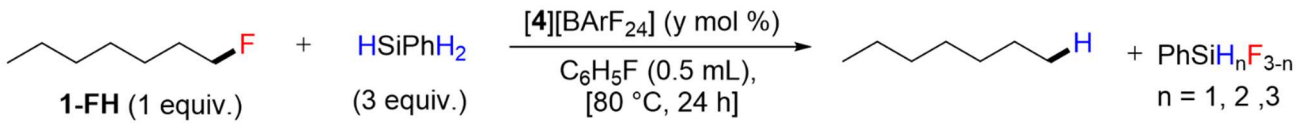

Entry	y mol %	Conversion (%)
1	0	<1
2	2	>99

[a] Conditions: **1-FH** (0.04 mL, 0.27 mmol), $HSiPhH_2$ (0.1 mL, 0.82 mmol), [**4**][$BArF_{24}$] (8.0 mg, 5.7 μmol [2.0 mol %]), C_6H_5F (0.5 mL), 80 °C, 24 h. Conversions were determined by NMR spectroscopy (C_6D_6) against hexafluorobenzene as ^{19}F internal reference.

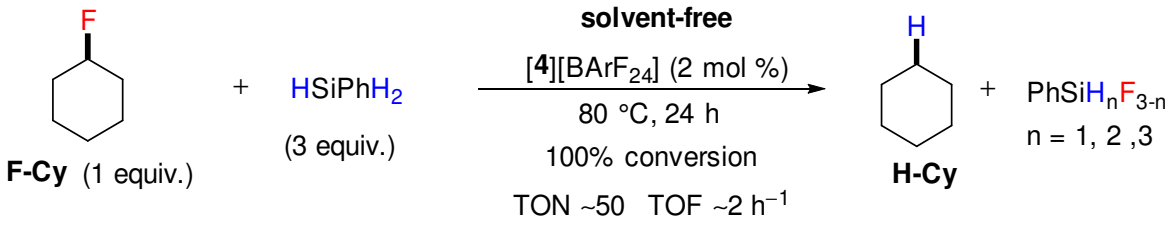

Scheme 58. Investigation of the solvent-free catalytic HDF reaction of fluorocyclohexane (**F-Cy**) with $HPhSiH_2$ as reducing agent and [**4**][$BArF_{24}$] as precatalyst.

4.2.8 Solvent-free HDF reaction of fluorocyclohexane: optimization study

We performed a remarkable improvement in the catalytic conditions. The solvent-free reaction described in the previous section (with **2-FCy**/$HPhSiH_2$/[**4**][$BArF_{24}$] as catalytic system) was optimized by tuning several parameters which include the time of reaction, temperature, the

proportion of [**4**][$BArF_{24}$], the proportion of $HPhSiH_2$, open-tube versus closed-tube of reaction, etc. The most relevant results related to this work will be discussed here, and detailed experimental procedures will be found in the experiment part.

4.2.8.1 A time of 1.5 h is sufficient for complete conversion

Significant improvement was made when the same reaction was repeated in slightly different conditions. Monitoring the conversion of **2-FCy** by ^{1}H and ^{19}F NMR, it was surprisingly found that actually a heating at 70 °C combined with a time of only 1.5 h were sufficient conditions for quantitative conversion (experimental part). However, no reaction was observed at room temperature. The presence of the precatalyst proved to be necessary as no conversion was obtained without any loading of [**4**][$BArF_{24}$]. Next, we wondered if a lower loading in [**4**][$BArF_{24}$] could also result in total conversion of **2-FCy**.

4.2.8.2 Only 0.5 equivalent of $HPhSiH_2$ proved to be necessary!

The reaction was further optimized until it was found that near quantitative conversion of **2-FCy** (91%) was obtained with only 0.5 equivalent (relative to **2-FC**) (entry 3, table 21) instead of 1 or 3 equivalents (entries 1–2, table 21). Interestingly, an inverse silane concentration rate dependence was identified from this study, in contradiction with what was observed with 1-fluoroheptane as substrate and C_6H_5F as solvent for which the rate of conversion showed a direct dependence in silane concentration (table 18). We believe that these opposite observations may indicate a different mechanism at work depending on the solvent of use in each case (either C_6H_5F/substrate as solvent system, or substrate alone as solvent). However, we cannot exclude that an excess of $HPhSiH_2$ could possibly be more sensitive to side reactions under the solvent-free conditions. We are tempted to propose the generation of $[H_2PhSi–H{\rightarrow}SiPhH_2]^+$ as a plausible donor-acceptor intermediate, where one molecule of $HSiPhH_2$ stabilizes through a hydride bridging the transient moiety $PhSiH_2^+$. Similar observations have been reported by D. M. Heinekey and coworkers who provided the crystal structure of $[Et_3Si–H{\rightarrow}SiEt_3]^+$ intermediate as highly reactive hydride donor (or H^+ acceptor to form H_2, depending on the point of view) even towards solvents (PhCl, CD_2Cl_2, etc).[318] It is essential to consider

[318] Connelly, S. J.; Kaminsky, W.; Heinekey, D. M. Structure and Solution Reactivity of (Triethylsilylium)triethylsilane Cations. *Organometallics* **2013**, *32* (24), 7478–7481.

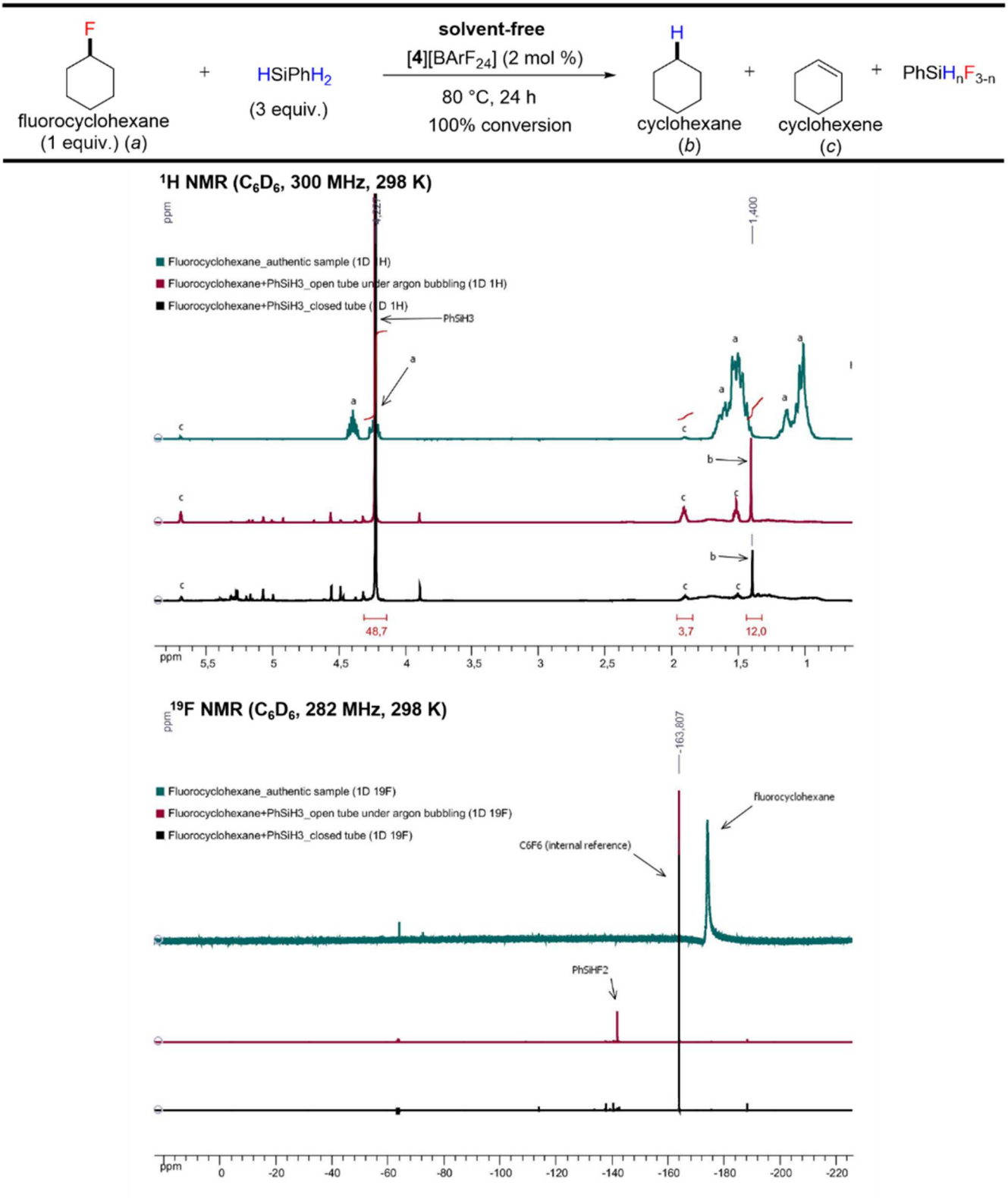

Scheme 59. ^{1}H and ^{19}F NMR spectroscopic analysis of the catalytic HDF transformation of 2-fluorocyclohexane into cyclohexane using [**4**][$BArF_{24}$]/$PhSiH_3$ as catalytic system.

Table 21. Influence of the proportion of silane on the solvent-free catalytic HDF reaction of fluorocyclohexane (**2-FCy**) with $HPhSiH_2$ using [**4**][$BArF_{24}$] as precatalyst.[a]

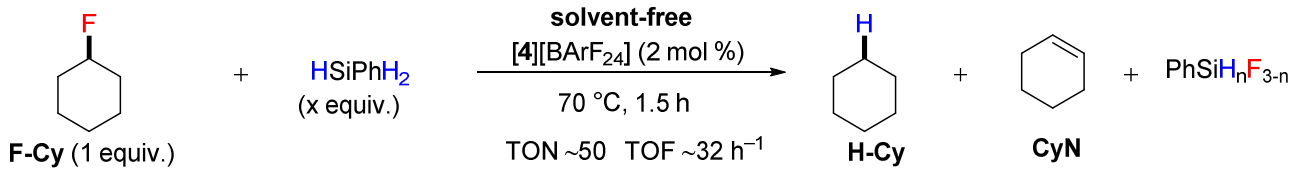

Entry	x equiv.	2-FCy (%)	CyN (%)
1	3	77	6
2	1	83	3
3	0.5	91	3

[a] Conditions: **F-Cy** (0.05 mL, 0.46 mmol), $HSiPhH_2$: (for x = 0.5 equiv.: 0.03 mL, 0.23 mmol; for x = 1.0 equiv.: 0.06 mL, 0.46 mmol; for x = 3.0 equiv.: 0.17 mL, 1.37 mmol), [**4**][$BArF_{24}$] (13.0 mg, 9.2 μmol [2.0 mol %]), 70 °C, 1.5 h. Yields and conversions were determined by NMR spectroscopy (C_6D_6) against 1,3,5-trimethylbenzene and hexafluorobenzene as ^1H and ^{19}F internal references respectively.

our catalytic system under study as a complex chemical system where many interacting chemical species and still yet unsettled reaction pathways are unknown, especially when we are manipulating such silylium species of extreme reactivity though with unpredicted behavior. As shown by many research groups especially those working at the organic/inorganic interface like J. B. Lambert and coworkers[319] and C. Reed and coworkers,[320] once silylium cations of the type R_3Si^+ are generated in solution, they can react with solvents such as benzene or toluene. On the other hand, silanes like $HSiPhH_2$ have been shown to undergo catalytic dimerization, polymerization, and redistribution as reported for example by D. Zargarian and coworkers.[321]

[319] Lambert, J. B.; Kania, L.; Zhang, S. Modern Approaches to Silylium Cations in Condensed Phase. *Chem. Rev.* **1995**, *95* (5), 1191–1201.
[320] a) Nava, M.; Reed, C. A. Triethylsilyl Perfluoro-Tetraphenylborate, [Et_3Si^+][F_{20}-BPh_4^-], a Widely Used Nonexistent Compound. *Organometallics* **2011**, *30* (17), 4798–4800. b) Reed, C. A. The Silylium Ion Problem, R_3Si^+. Bridging Organic and Inorganic Chemistry. *Acc. Chem. Res.* **1998**, *31* (6), 325–332.
[321] Hao, J.; Vabre, B.; Zargarian, D. Reactions of Phenylhydrosilanes with Pincer–Nickel Complexes: Evidence for New Si–O and Si–C Bond Formation Pathways. *J. Am. Chem. Soc.* **2015**, *137* (48), 15287–15298.

By considering these facts, even though the underlying mechanism is still unclear, we can explain the lower catalytic efficiency of the solvent-free HDF reaction when the concentration of $HSiPhH_2$ increases by the possible accumulation of $[H_2PhSi–H\rightarrow SiPhH_2]^+$ accompanied with some silane redistribution catalyzed by the highly reactive intermediate [**5F**][$BArF_{24}$].

4.2.8.3 Only 0.5 mol % of [**4**][$BArF_{24}$] is sufficient!

This study is summarized in table 22. Upon varying the proportion of [**4**][$BArF_{24}$], we arrived to an even more interesting result which showed that using only 0.5 mol % instead of 2 mol % (as systemically done for previous studies), near quantitative (97%) conversion of **2-FCy** was obtained accompanied with negligible amount of cyclohexene (**CyN**) (experimental part). However, as expected increasing the loading to 5 mol % resulted in the quantitative conversion of **2-FCy**. Further studies are currently undertaken in order to establish the minimum proportion of [**4**][$BArF_{24}$] necessary for the complete conversion of **2-FCy**.

Table 22. Influence of the proportion of [**4**][$BArF_{24}$] on the solvent-free catalytic HDF reaction of fluorocyclohexane (**2-FCy**) with $PhSiH_3$.[a]

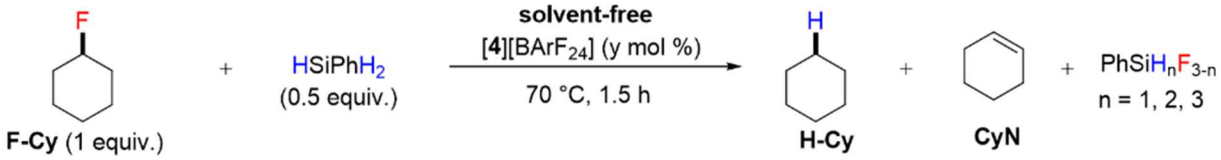

Entry	y (mol %)	2-FCy (%)[a]	CyN (%)[b]	TON	TOF (h^{-1})
1	0.5	97	6	189	122
2	2	97	3	50	32
3	5	>99	3	20	13

[a] Conditions: **F-Cy** (0.05 mL, 0.46 mmol), $HPhSiH_2$ (0.03 mL, 0.23 mmol), [**4**][$BArF_{24}$] (3.4 mg, 2.4 μmol [0.5 mol %]; 13.0 mg, 9.2 μmol [2.0 mol %]; 32.5 mg, 23.1 μmol [5.0 mol %]), 70 °C, 1.5 h. Yields and conversions were determined by NMR spectroscopy (C_6D_6) against 1,3,5-trimethylbenzene and hexafluorobenzene as ^1H and ^{19}F internal references respectively. TOFs values were determined at the highest conversion of **F-Cy**.

4.2.9 An ionic like mechanism explains most of the results

Based on the results that are disclosed in this chapter, a plausible ionic-like mechanism is presented in scheme 60.

Following the activation step of the precatalyst [**4**][$BArF_{24}$] to the intermediate [**5F**][$BArF_{24}$], the HDF reaction is initiated with the activation of the C–F bond of the fluorocarbon substrate by the transfer of $[H_2PhSi]^+$ from the intermediate [**5F**][$BArF_{24}$] to the fluorine atom leading to the formation of [[**C-F**]→$SiPhH_2$]$^+$ and **13** as catalytic intermediates. The latter intermediates then interact with each other through a hydride transfer step from **13** to [[**C-F**]→$SiPhH_2$]$^+$, following a more likely S_N1-like mechanism where the nucleophilic hydride ("H^-") attacks the electrophilic carbon atom, thus forming the hydrocarbon [**C-H**] and $FSiPhH_2$. The next catalytic cycle then becomes possible with the regeneration of [**5F**][$BArF_{24}$] from the interaction of $HSiPhH_2$ with the coordinatively unsaturated complex [**4+**][$BArF_{24}$]. At this stage, we cannot exclude the involvement of $HSiPhH_2$ as plausible candidate in the hydride transfer step. As mentionned previously, the highly active [**4+**][$BArF_{24}$] is the truly active catalyst which upon reaction with **13** affords [**5B**][$BArF_{24}$]. However, as it has been shown in chapter 2 (scheme 10), the hydrido-bridged iridium dimer [**5B**][$BArF_{24}$] was not observed upon reaction of [**4**][$BArF_{24}$] with $HSiPhH_2$, a fact that could explain the peculiar efficiency of the key active intermediate [**5F**][$BArF_{24}$] for the catalytic C–F bond activation.

By considering such a mechanism, it helps us to explain in part our observations of the better reactivity of "unactivated" and saturated fluorocarbons in terms of the Lewis acid-base concept. Indeed, as the fluorine atom of fluoroheptane and fluorocyclohexane is more electron rich than it is the case for "activated" fluorocarbons like trifluoromethylbenzene and fluorobenzene, the Lewis acid-base concept tells us that "logically" the Lewis acidic $[H_2PhSi]^+$ will interact more stronger with the most electron rich Lewis basic fluorocarbons that are fluoroheptane and fluorocyclohexane. In this manner, the present mechanistic rationale provides a good support to the ionic silylium-based transfer mechanism rather than the traditional oxidative addition of C–F bond at the iridium center. In addition, the fact that trifluoromethylbenzene and fluorobenzene are far less reactive may be indicative of the difficulty in generating unstable $Ph(CF_2)^+$ and Ph^+ as carbocationic-like intermediates, thus supporting the involvement of an S_N1 mechanism. Of course, profound mechanistic investigations are needed to support this hypothesis and to clarify the true species that are involved during the C–H bond formation.

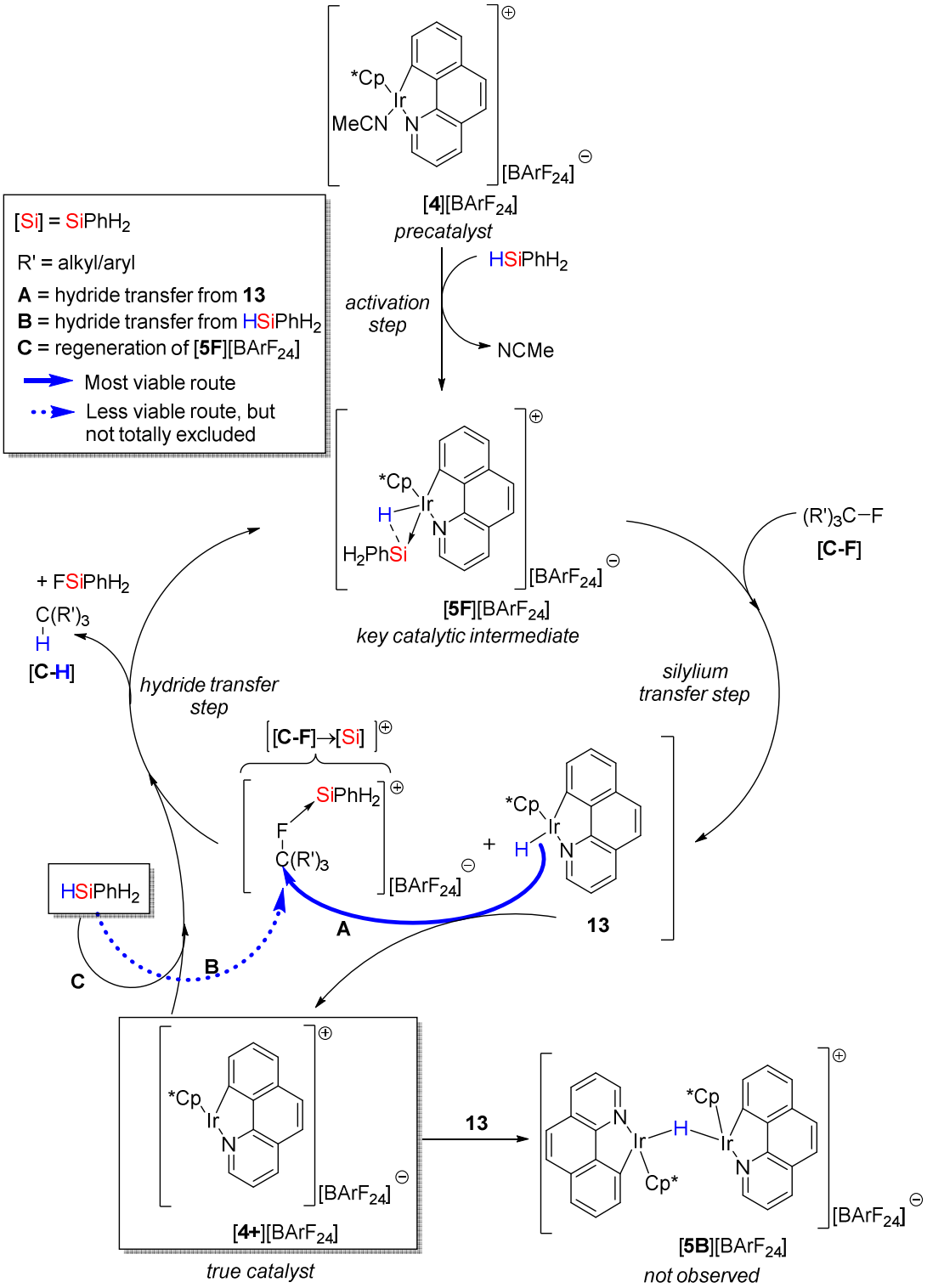

Scheme 60. Plausible mechanism for the hydrodefluoration of fluorocarbons catalyzed by [**4**][BArF$_{24}$]

4.3 Conclusions and perspectives

We have developed for the first time a straightforward methodology towards the solvent-free and catalytic hydrodefluoration (HDF) reaction of the unactivated fluorocycyclohexane. More importanty, this transformation is catalyzed by the newly established iridacycle [**4**][$BArF_{24}$] (0.5 mol %) in combination with $HSiPhH_2$ as the hydride source, corresponding to a TON of 189 and a TOF of 122 h^{-1}. Under similar catalytic conditions, 1-fluoroheptane was also completely converted to *n*-heptane using fluorobenzene as the solvent. The latter transformation will be repeated soon under solvent-free conditions as well. We have also reported the new tandem and one-pot *O*-silylation – HDF transformation of 2-fluorocyclohexan-1-ol (**2-FCyOH**) to (cyclohexyloxy)triethylsilane (**H-CyOSiEt$_3$**) in 83% yield, with the use of 5 mol % of [**4**][$BArF_{24}$] as the only catalytic source for both steps. This reaction is interesting because it offers the potential to make recoverable wasteful saturated fluorocarbons that contain alcohol functions. The application of this tandem methodology to similar (saturated) fluorinated alcohols like (hexafluoro)isopropanol (HFIP) will be, among other applications, particularly investigated.

The catalytic HDF reaction we reported herein is proposed to follow an ionic-like mechanism. Since the catalysis was showed to be promoted by the combination of $HSiPhH_2$ with the iridium precatalyst [**4**][$BArF_{24}$] (or [**2**][$BArF_{24}$]), it is believed that the process is initiated by a *silylium transfer step* which is mediated by the key catalytic iridium-silane intermediate [**5F**][$BArF_{24}$]. The fact that the C(sp^3)–F bond of fluorocyclohexane and fluoropentane is much more easier activated than the C(sp^2)–F bond of trifluoromethylbenzene and fluorobenzene is a good support to the silylium-based transfer step rather than the traditional oxidative addition of the C–F bond at the iridium center, because a C(sp^3)–F bond is considered to be stronger and more Lewis basic that a C(sp^2)–F bond. This trend of reactivity is also a good support to the assumption that carbocationic intermediates are involved, which could be generated through an S_N1-like mechanism.

The catalytic C–F bond activation methodology which is disclosed in this thesis is promising and yet it is only at its preliminary stage of study. However, several observations remain difficult to interpret. An important issue to adress is to explain the higher efficiency of $HSiPhH_2$ in serving as the hydride source for the HDF reaction in the presence of either [**2**][$BArF_{24}$] or [**4**][$BArF_{24}$] as precatalyst. The latter fact is somehow in contradiction with the observations we reported in previous chapters. Indeed, we have shown that $HSiEt_3$ was the best silane for the

hydrosilylation of O–H, C=O and C≡N functions catalyzed by either [**2**][$BArF_{24}$] or [**4**][$BArF_{24}$]. We believe that the particular success of $HSiPhH_2$ in the C–F bond activation catalysis resides in the structural and electronic properties of the iridum-silane catalytic intermediate [**5F**][$BArF_{24}$] which is involved in the catalytic cycle. As it is shown in chapter 2 (scheme 10) and in the experimental part, we have the spectroscopic (NMR) evidence for the formation of [**5F**][$BArF_{24}$], though no X-ray structure of this adduct has been obtained yet. However, current effort is made towards the crystallization of this adduct, which could open the opportunity to study the bonding situation encountred within the silicon-iridium-hydrogen motif, and by this way either confirm or infirm the presence of the "typical" donor-acceptor interaction already evidenced for [**3A**][$BArF_{24}$] and [**5A**][$BArF_{24}$]. Another possibility to consider, though counter-intuitive, is that the true hydride donor during the *hydride transfer step* could actually be the silane $HSiPhH_2$ by its own rather than the iridium complex **13**, which by this way explains why $HSiPhH_2$ is more reactive than $HSiEt_3$ if we postulate that the former would be more "hydridic" than the former within our specific conditions.[322] The strong point of the latter explanation is that **13** was showed to be formed whatever the silane involved, thus supporting the idea of $HSiPhH_2$ as being the true hydride donor. The uncertainty however is, what could be the relative hydricity of both silanes *relative* to the *in situ* generated carbocations [**C**]$^+$? Another issues raised by this explanation are, what could be the fate of **13** in that case? How would the catalytic intermediate [**5F**][$BArF_{24}$] be regenerated if **13** does not act as the hydride donor? It is evident that the situation regarding the so-called *hydride transfer step* is not clear yet since several potential hydride donors are present and/or generated in this complex catalytic medium. What is the real hydride source for the C–F bond formation? Further experiments and computational studies will be conducted, especially the ones which could verify the relative hydricity of $HSiPhH_2$ and $HSiEt_3$ when compared to **13**. Before answering to these questions, we have already started to exploit the C–F bond methodology that we reported herein for its application to other type of reactions, like the C–C bond formation and the use of boranes instead of silanes for example.

[322] The hydricity (hydride ability) of $HSiEt_3$ has been generally found higher than $HSiPhH_2$, but the estimation of these values hardly depends on the reference reaction and/or the theoretical calculations the authors have chosen. In our opinion, the relative hydridicity of both silanes may change from one chemical system (especially if it is a complex system like ours) to another depending on the relative species with which they could interact/react. For relevant work on the determination of hydricity of silanes (including $HSiEt_3$ and $HSiPhH_2$), see: a) Gusev, D. G.; Ozerov, O. V. Calculated Hydride and Fluoride Affinities of a Series of Carbenium and Silylium Cations in the Gas Phase and in C_6H_5Cl Solution. *Chem. - A Eur. J.* **2011**, *17* (2), 634–640. In this paper, the authors calculated a HA (hydride affinity in the gas phase, kcal•mol^{-1}) of 213.2 for Et_3Si^+, and 226.7 for $PhSiH_2^+$. b) Mayr, H.; Bug, T.; Gotta, M. F.; Hering, N.; Irrgang, B.; Janker, B.; Kempf, B.; Loos, R.; Ofial, A. R.; Remennikov, G.; Schimmel, H. Reference Scales for the Characterization of Cationic Electrophiles and Neutral Nucleophiles. *J. Am. Chem. Soc.* **2001**, *123* (39), 9500–9512. In this paper, the authors determined the rate constant *k* of reaction between silanes and (4-methoxyphenyl)(phenyl)methylium which was found to be lower with $HSiPhH_2$ (35.6 $M^{-1}•s^{-1}$, 20 °C, CH_2Cl_2) than whith $HSiEt_3$ (5290.0 $M^{-1}•s^{-1}$, 20 °C, CH_2Cl_2).

5 General conclusions and perspectives

We have discovered a new family of highly active iridium(III)-based precatalysts, [**2**][$BArF_{24}$] and [**4**][$BArF_{24}$]. These iridacycles are ionic in nature with the cationic moieties [**2**]$^+$ and [**4**]$^+$ being associated with the weakly coordinating anion [$BArF_{24}$]$^-$. Notably, these ionic iridacycles were found to be very stable so that their handling under air whether in solution or as solid powder was possible. Apart from the remarkable stability of [**2**][$BArF_{24}$] and [**4**][$BArF_{24}$], the relative simplicity of their molecular structures allowed us to develop a very simple and convenient synthetic protocol for their preparation on gram scale. [**2**][$BArF_{24}$] and [**4**][$BArF_{24}$] were fully analytically characterized and their molecular structures determined by X-ray diffraction analysis of their single crystals. A series of related ionic iridacycles [**2**][X] (X = PF_6, BF_4, BPh_4, OTf), [**4**][X] (X = BPh_4, OTf), [**6**][$BArF_{24}$], [**8**][$BArF_{24}$], [**10**][$BArF_{24}$] and [**12**][OTf], and the ionic rhodacycle [**2'**][$BArF_{24}$] (scheme 4b) were also conveniently prepared and fully (or partially for few of them) analytically characterized. The molecular structures of [**2**][BPh_4], [**2**][BF_4], [**2'**][$BArF_{24}$], [**4**][BPh_4] and [**6**][$BArF_{24}$] were determined by single crystal X-ray diffraction analysis.

Among all the ionic metallacycles described in this thesis manuscript, [**4**][$BArF_{24}$] was found to be the best precatalyst for the *O*Si reaction of 1-phenylpropanol with triethylsilane (and most presumably for other alcohols), which is characterized by the very high TOF_t of ~1.16×10^6 h^{-1} (t ~3.4 s; TON = 1093). This remarkable activity is to our knowledge unprecedented for an iridium-based (pre)catalyst in the alcohol *O*Si reaction. The mechanism of the latter reaction (using benzyl alcohol and [**2**][$BArF_{24}$])) has been investigated. A plausible catalytic cycle for this reaction has been proposed based on findings of the kinetic catalytic study. By using the piezometry set-up described in scheme 6, the absolute pressure of the released hydrogen gas was directly monitored over time under various catalytic conditions, thereby providing useful kinetic informations of the catalytic system. Therefore, kinetic studies showed a second order in catalyst, a normal primary kinetic isotope effect (KIE) of $k_H^{init}/k_D^{init} = 2.7 \pm 0.2$ for benzyl alcohol and an inverse IKIE value of $k_H^{init}/k_D^{init} = 0.73 \pm 0.01$ for triethylsilane. The *O*Si reaction of alcohols proved to be completely inhibited using acetonitrile as solvent or certain additives such as phenylacetylene, *N*-methyl-1-phenylmethanimine and aniline. In contrast, addition of acetophenone to the *O*Si reaction mixture had no effect on its rate efficiency. These inhibition studies shed a new light on the observation made in the tandem catalysis described in scheme

1, which showed that the *O*Si reaction of methanol did not occur. A plausible explanation is that the presence of potential substrates for the (hydro)silylation reaction such as aniline and phenylacetylene completely change the reaction profile of the system, so that the *O*Si of methanol becomes by far the less favored silylation reaction pathway *within the conditions of catalysis*. On the other hand, we have shown that [**4**][$BArF_{24}$] is a convenient precatalyst for the *N*-silylation of aniline at room temperature. Since the nucleophilicity of the nitrogen atom is known to be increased upon *N*-silylation,[323] *N*-silylamines can be considered as potentially reactive substrates within the tandem alkyne-hydroamination – imine-hydrosilylation system reported by our group in 2012.[324] Furthermore, the latter tandem reaction has been proven to be catalyzed by [**4**][$BArF_{24}$] as well, though with less efficiency.

We have demonstrated the critical role played by the anion X of [**2**][X] salts (where X = $BArF_{24}$, BPh_4, BF_4, PF_6, OTf) in the effectiveness of reactions catalyzed *via* the H–Si bond activation catalysis. Investigations of reactions between [**2**][X] salts and triethylsilane afforded clear evidence for the existence of a silylium-abstraction pathway of X anions. For example, the fact that [**2**][BF_4] is inactive in catalysis is explained by the irreversible formation of $FSiEt_3$ from $[BF_4]^-$ and $[Et_3Si]^+$ of transient [**3A**][BF_4]. Similarly, the species Et_3SiOTf showed to form between $[OTf]^-$ and $[Et_3Si]^+$ of transient [**3A**][OTf]. As the precatalyst [**2**][OTf] has shown similar activity as for [**2**][$BArF_{24}$] (for *O*-silylation of alcohols), Et_3SiOTf may be considered as the real source of silylium in this case since it is known to behave as such in catalytic organic reactions (Eqs. 3–4).[325] As shown in equation 3 below, the potential of Et_3SiOTf (**A**) to act as an efficient silylium transfer agent in the catalytic *O*-silylation reaction of alcohols can be tentatively explained by its reaction with the released acetonitrile ligand **B** to afford the ionic Lewis complex **C** (Eq. 3). Complex **C**, though less abundant due to equilibrium in favor of **A**, is however a stronger silylium donor than **A** because of the lower Lewis basicity of **B** as compared to $[OTf]^-$, so that its reaction with alcohols **D** of higher Lewis basicity than $[OTf]^-$ displaces the overall process to the formation of **E** (Eq. 4).

[323] Rajeswari, S.; Jones, R. J.; Cava, M. P. A New Synthesis of Amides from Acyl Fluorides and N-Silylamines. *Tetrahedron Lett.* **1987**, *28* (43), 5099–5102.
[324] Iali, W.; Paglia, F. La; Goff, X.-F. Le; Sredojević, D.; Pfeffer, M.; Djukic, J.-P. Room Temperature Tandem Hydroamination and Hydrosilation/protodesilation Catalysis by a Tricarbonylchromium-Bound Iridacycle. *Chem. Commun.* **2012**, *48* (83), 10310.
[325] Dilman, A. D.; Ioffe, S. L. Carbon-Carbon Bond Forming Reactions Mediated by Silicon Lewis Acids. *Chem. Rev.* **2003**, *103* (3), 733–772.

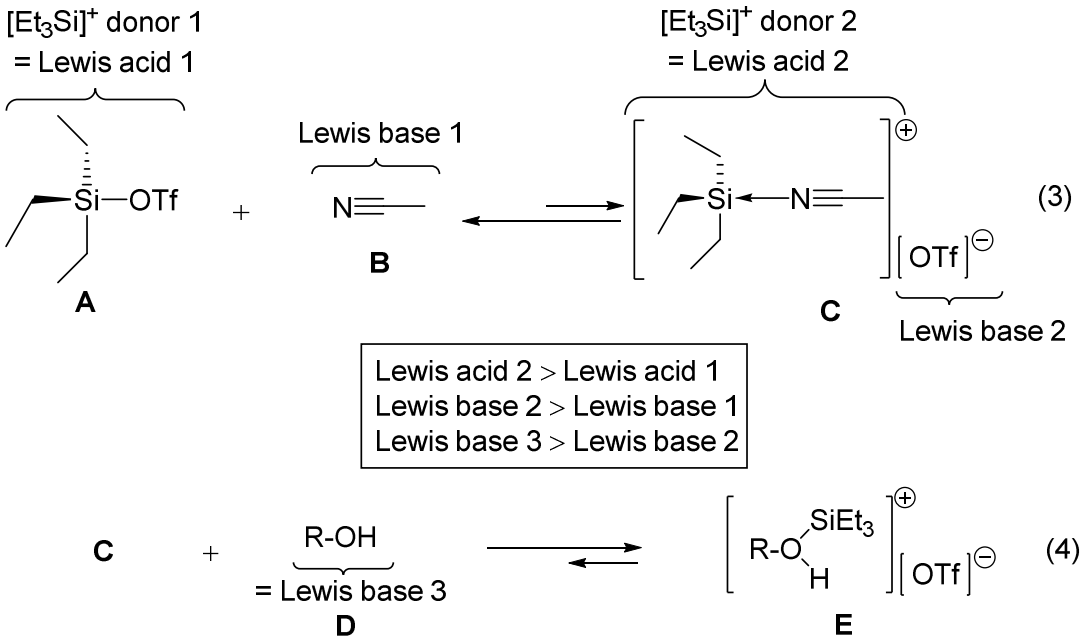

While the higher catalytic activity of [**2**][$BArF_{24}$] is mostly explained by the absence of reaction between [$BArF_{24}$]$^-$ and [Et_3Si]$^+$ in intermediate [**2**][$BArF_{24}$], the relative inactivity of [**2**][BPh_4] as precatalyst cannot be clearly rationalized at this stage, even though one can putatively make the assumption that [BPh_4]$^-$ and [Et_3Si]$^+$ in intermediate [**2A**][BPh_4] (observed by NMR spectroscopy) may react with each other as well (no spectroscopic evidence).

We have successfully identified important active and inactive iridium-silane intermediates. Upon stoichiometric reactions of the catalytically active precatalysts [**2**][$BArF_{24}$] and [**4**][$BArF_{24}$] with triethylsilane at low temperature, single crystals have been obtained and their respective molecular structures [**3A**][$BArF_{24}$] and [**5A**][$BArF_{24}$] determined by X-ray diffraction analysis. The structures of the related diastereoisomers [**3A'**][$BArF_{24}$] and [**5A'**][$BArF_{24}$] were also obtained even though the quality of the acquisition data proved to be insufficient. The molecular structures of the inactive hydrido-bridged iridium complexes [**3B**][OTf] and [**5B**][$BArF_{24}$] were also obtained by X-ray diffraction studies. Relative ease of abstraction of the silylium moiety [Et_3Si]$^+$ in [**3A**][$BArF_{24}$] upon reaction with relatively weak Lewis bases such as [OTf]$^-$ and DMAP have suggested the involvement of an Ir(III)- rather than an Ir(V)-based intermediate. The latter assumption was supported by deep investigation of the electronic structure of [**3A**][$BArF_{24}$] by state-of-the-art DFT methods, including various basis sets and functionals. All the data converge to the best formulation for [**3A**][$BArF_{24}$] as the one displaying a cohesive hydridoiridium(III)→silylium donor-acceptor complex, wherein the Ir—H bond has been calculated to be more stronger than Ir—Si and Si—H (very small covalent character) bonds. As

suggested by theoretical studies, the catalytic intermediate [**5A**][$BArF_{24}$] has been shown to feature the similar structural formulation as for [**3A**][$BArF_{24}$], that is a hydridoiridium(III)→silylium donor-acceptor. Similar computations studies conducted on the X-ray structures of [**3B**][OTf] and the Templeton's[326] complex [**4**→Ag←**4**][OTf] were consistent with the Lewis base donor property of the hydrido-iridacyclic complex **4**, thus suggesting a donor-acceptor Lewis pair as the most realistic structural formulation of these complexes as well.

Complexes [**2**][$BArF_{24}$] and [**4**][$BArF_{24}$] have been shown to be highly active precatalysts for the hydrosilylation of several (hetero)aryl nitriles and carbonyls (aldehydes and ketones), and for the C(sp^3)─F bond activation (hydrodefluorination) of unactivated fluorocarbons. Notably, very high rate efficiencies and broad substrate scope applicability has been demonstrated for each hydrosilylation catalytic system. Remarkably we reported the first examples of an iridium-based homogenous precatalyst for the hydrosilylation of nitriles as well as the first example of a catalytic solvent-free C(sp^3)─F bond activation of the unactivated fluorocyclohexane substrate. Also, the unprecedented tandem *O*Si ─ C(sp^3)─F bond activation of 2-fluorocyclohexanol and the convenient C(sp^3)─F bond activation of fluoroheptane have been described. In general [**4**][$BArF_{24}$] has been shown to be a more efficient precatalyst than [**2**][$BArF_{24}$].

It has been proposed that the catalytic reactions mediated by [**2**][$BArF_{24}$] and [**4**][$BArF_{24}$] (*O*Si of alcohols, hydrosilylation of carbonyls and nitriles, C(sp^3)─F bond activation of fluorocarbons) all involve as key catalytic intermediates the donor-acceptor complexes [**3A**][$BArF_{24}$] and [**5A**][$BArF_{24}$] respectively, which, based on their bifunctional property to behave as both silylium and hydride donors, rationally explain most of the reported results.

In future studies, some selected fundamental questions raised by the studies described in this thesis manuscript should be investigated: 1) What does explain the catalytic inactivity of [**2**][BPh_4] as compared to [**2**][$BArF_{24}$]? 2) what are the origins of the better catalytic activity of [**4**][$BArF_{24}$] when compared to [**2**][$BArF_{24}$]? 3) What does explain the better reactivity of $HSiPhH_2$ as compared to $HSiEt_3$ in the catalytic C(sp^3)─F bond activation of fluorocarbons?

[326] Turlington, C. R.; Harrison, D. P.; White, P. S.; Brookhart, M.; Templeton, J. L. Probing the Oxidation Chemistry of Half-Sandwich Iridium Complexes with Oxygen Atom Transfer Reagents. *Inorg. Chem.* **2013**, *52* (19), 11351–11360.

Overall, the results disclosed in this thesis rely on solid evidence for the involvement of original iridium-silane catalytic intermediates of relevant activity in the convenient activation[327] of O—H, C=O, C≡N, and C—F bonds. Combined experimental and theoretical studies of these intermediates and their related reactions between silanes and precatalysts point towards a Lewis donor-acceptor structural formulation of the type [Ir(III)H]→[SiR_3]. As suggested by computations studies (in collaboration with the group of Stephan Grimme), the formation of the latter intermediates is proposed to proceed *via* the heterolytic bond cleavage of the H—Si bond, resulting in sequential transfers of the hydride (H) from $HSiR_3$ to [Ir(III)][$BArF_{24}$] to form the neutral Lewis donor [Ir(III)H] followed by the trapping of the electrophilic Lewis acid [SiR_3][$BArF_{24}$] by [Ir(III)H].

As the claim made in this thesis[328] still raises some debate among researchers working in the field of silane organometallic complexes, we provide some crucial clues in support. Generation of stable electrophilic silylium cations of sufficient activity is becoming an intense and challenging research topic in organometallic catalysis.[329] A long standing paradigm, particularly within the field of organometallic chemistry, entails that reactions between electro-deficient (electrophilic) late transition-metal (TM) complexes and "reactive" substrates such as silanes proceed oxidatively at the TM upon *cleavage* of the E—R bond (E= C, H, Si, halogen, etc), that is to say that an increase by 2 of the formal oxidation state at the TM is systemically considered to take place (for example Ir(III)→Ir(V)). Although the well-established formalisms of oxidative addition[330] and oxidation state[331] proved to be very helpful until now, especially for the interpretation of organometallic catalytic mechanisms, they frequently proved to be of a limited applicability[332] mainly due to the inherent approximations of the theoretical model on which they are based. In parallel, within the community of organic chemists, there was a famous

[327] The term activation used here does not necessary mean total cleavage of the bond (as it the case for O–H and C–F bonds), but also refers to the relative increase in reactivity of the bond upon reaction/interaction with an "activating" group such as "Et_3Si^+".
[328] Hamdaoui, M.; Ney, M.; Sarda, V.; Karmazin, L.; Bailly, C.; Sieffert, N.; Dohm, S.; Hansen, A.; Grimme, S.; Djukic, J.-P. Evidence of a Donor (Ir–H)→SiR_3 Interaction in a Trapped Ir(III) Silane Catalytic Intermediate. *Organometallics* **2016**, *35* (13), 2207–2223.
[329] Lee, V. Y.; Sekiguchi, A. In *Organometallic Compounds of Low-Coordinate Si, Ge, Sn and Pb*; Wiley, 2010.
[330] a) Labinger, J. A. Tutorial on Oxidative Addition. *Organometallics* **2015**, *34* (20), 4784–4795. b) Tolman, C. A. The 16 and 18 Electron Rule in Organometallic Chemistry and Homogeneous Catalysis. *Chem. Soc. Rev.* **1972**, *1* (3), 337.
[331] Karen, P.; McArdle, P.; Takats, J. Toward a Comprehensive Definition of Oxidation State (IUPAC Technical Report). *Pure Appl. Chem.* **2014**, *86* (6), 1017–1081.
[332] a) Webster, A. J.; Mueller, C. M.; Foegen, N. P.; Sit, P. H. L.; Speetzen, E. D.; Cunningham, D. W.; D'Acchioli, J. S. Oxidation States "naturally": A Natural Bond Orbital Method for Determining Transition Metal Oxidation States. *Polyhedron* **2016**, *114*, 128–132. b) Karen, P. Oxidation State, A Long-Standing Issue! *Angew. Chem. Int. Ed.* **2015**, *54* (16), 4716–4726.

controversy known as the “silylium ion problem”, [333] which had the beneficial effect of reaching at least an important consensus. The latter consensus was that since tri-coordinated silylium cations $[R_3Si]^+$ are highly electrophilic (Lewis acids), they have to be generated in solution under careful choice of conditions such as the use of “weakly coordinating anions” (such as halogenated carboranes)[334] and the least electron-donor (Lewis basic) solvents possible (such as benzene). As it has been shown in the introduction of chapter 3, hydrosilylation of carbonyls catalyzed by organometallic complexes were conducted without special attention to the conclusions of the “silylium ion problem” controversy. Also, most of the organometallic intermediates proposed in most catalytic cycles of hydrosilylation reactions are generally invoked as oxidative addition products thus neglecting the possibility that they could behave as a source of silylium cations by preferentially using the traditional view of inner-sphere catalysis. We do not claim that all the systems reported in the literature have to be viewed as donor-acceptor complexes, we now considered that it is one possibility in transition-metal based hydrosilylation catalysis. It should be kept in mind that electrophilic silylium cations may potentially be involved, so that a proper choice of conditions should be made.

[333] a) Reed, C. A. The Silylium Ion Problem, R_3Si^+. Bridging Organic and Inorganic Chemistry. *Acc. Chem. Res.* **1998**, *31* (6), 325–332. b) Xie, Z.; Bau, R.; Benesi, A.; Reed, C. A. The Silylium Ion (R_3Si^+) Problem: Effect of Alkyl Substituents R. *Organometallics* **1995**, *14* (20), 3933–3941. c) Lambert, J. B.; Kania, L.; Zhang, S. Modern Approaches to Silylium Cations in Condensed Phase. *Chem. Rev.* **1995**, *95* (5), 1191–1201. d) Olah, G. A.; Li, X.-Y.; Wang, Q.; Rasul, G.; Prakash, G. K. S. Trisilyloxonium Ions: Preparation, NMR Spectroscopy, Ab Initio/IGLO Studies, and Their Role in Cationic Polymerization of Cyclosiloxanes. *J. Am. Chem. Soc.* **1995**, *117* (35), 8962–8966.

[334] Douvris, C.; Ozerov, O. V. Hydrodefluorination of Perfluoroalkyl Groups Using Silylium-Carborane Catalysts. *Science* **2008**, *321* (5893), 1188–1190.

6 Experimental part

6.1 General considerations

6.1.1 Materials and methods

All experiments were conducted using dry argon and vacuum atmospheres *via* standard Schlenk lines and glovebox techniques. All glassware was cleaned and oven-dried prior to use. All organic chemicals were purchased from Sigma-Aldrich, Alfa Aesar, TCI and Fluka. $IrCl_3$ was purchased from Pressure Chemical Co. Dicalite 4158 was purchased from Carlo Erba Reagents. All solvents were distilled over sodium or CaH_2 under argon before use. Deuterated solvents were dried over sodium or CaH_2, filtered over activated neutral alumina, and stored under argon before use. All of the alcohols used in catalysis were purified by a bulb-to-bulb distillation over a minimal amount of CaH_2 and stored under argon before use. ^{1}H (300, 400, 500, and 600 MHz), ^{11}B (128 MHz), ^{13}C (75 and 126 MHz), ^{19}F (282 MHz), ^{31}P (121 and 162 MHz), and ^{29}Si (119 MHz) NMR spectra were measured on Bruker DPX 300 and 400, Avance I 500, and Avance III 600 spectrometers. Chemical shifts (expressed in parts per million) were referenced against solvent peaks or external reference standards ($CF_3C_6H_5$ in $CDCl_3$ for ^{19}F, Me_4Si in $CDCl_3$ for ^{29}Si, and $NaBH_4$ in D_2O for ^{11}B). The abbreviations used for NMR data stand for: s, singlet; d, doublet; t, triplet; q, quartet; qt, quintet; m, multiplet. Mass spectra were run on a MicroTOF Bruker Daltonics spectrometer, using a TOF-ESI coupling analysis system. Elemental analyses were achieved with Thermo Scientific FLASH 2000 CHNS/O analyzers.

6.1.2 NMR Diffusion-Ordered Spectroscopy (DOSY NMR)

Measurements of hydrodynamic diffusion coefficients were performed on a Bruker Avance III 600 MHz spectrometer, equipped with a BBFO z gradient probe, developing a pulse field gradient of 5 G $(A \cdot cm)^{-1}$. The samples were analyzed in a 2.5 mm sample NMR tube' thermostated at 298 K. Diffusion NMR data were acquired using a stimulated echo pulse sequence with bipolar z gradients. Limited Eddy current delay was fixed to 5 ms, and the gradient recovery delay was set to 500 μs. A total recycling delay of 3 s was applied between scans. The gradient strength varied linearly between 1 and 34 $G \cdot cm^{-1}$ in 34 experiments. The

diffusion time and the duration of the sinusoidal gradients were optimized for each sample. Typically, the diffusion time was set between 90 and 150 ms and the half-gradient delay was set between 850 and 1300 μs. Hydrodynamic diffusion coefficients were determined by two different methods either from direct reading of 2D-DOSY plots or analytically as described below. 2D-DOSY plots were generated by the DOSY module of the software NMRNotebook, using inverse Laplace transform (ILT) driven by maximum entropy, to build the diffusion dimension. The analytical method corresponds to the graphs depicted in figures 4a and 4b of the manuscript, which show the variation of $\ln(I/I_0)$ as a function of G^2 (relative intensities (I/I_0) were measured for a set of 34 gradient strength values G). By applying a linear fitting to each correlation curve,[335,336] one can extract the value of the hydrodynamic diffusion coefficient D according to $\ln(I/I_0) = \gamma_X^2 \bullet \delta_2 \bullet (\Delta - \delta/3 - \tau/2) \bullet D \bullet G^2$, where γ_X is the gyromagnetic ratio of the X nucleus, δ is the length of the gradient pulse, G is the gradient strength, Δ is the delay between the midpoints of the gradients, τ is the delay between two pulses, and D is the hydrodynamic diffusion coefficient. Under our experimental conditions, the parameters used were as follows: $\gamma_{1H}(BArF_{24}^-) = \gamma_{1H}(BF_4^-) = 2.67522128 \times 10^8$ rad•s^{-1}•T^{-1};[337] $\gamma_{19F}(BArF_{24}^-) = \gamma_{19F}(BF_4^-) = 2.518148 \times 10^8$ rad•rad•s^{-1} T^{-1};[337] $\delta_{19F}(BArF_{24}^-) = 2.6 \times 10^{-3}$ s; $\delta_{1H}(BArF_{24}^-) = 2.3 \times 10^{-3}$ s; $\Delta_{19F}(BArF_{24}^-) = 0.17$ s; $\Delta_{1H}(BArF_{24}^-) = 0.15$ s; $\delta_{1H} = \delta_{19F}(BF_4^-) = 2.2 \times 10^{-3}$ s; $\Delta_{1H}(BF_4^-) = 0.13$ s; $\Delta_{19F}(BF_4^-) = 0.14$ s; G in T•μm^{-1} (34 pulse experiments between 1.749×10^8 and 3.323×10^7 with an incremental separation range of 9.6×10^{-2}); $\tau_{19F}(BArF_{24}^-) = \tau_{19F}(BF_4^-) = 5.285 \times 10^{-2}$ s; $\tau_{1H}(BArF_{24}^-) = \tau_{1H}(BF_4^-) = 5.250 \times 10^{-3}$ s. Plotting $\ln(I/I_0)/C$ as a function of G^2 (where $C = \gamma_X^2 \bullet \delta_2 \bullet (\Delta - \delta/3 - \tau/2)$) gives a negative slope, the absolute value of which is the hydrodynamic diffusion coefficient D expressed in μm^2•s^{-1}: $\ln(I/I_0)/C = -D \bullet G^2$.

6.1.3 X ray Diffraction analytical data

X-ray diffraction data collection was carried out on a Bruker APEX II DUO Kappa-CCD diffractometer equipped with an Oxford Cryosystem liquid N_2 device, using Mo-Kα radiation (λ = 0.71073 Å). The crystal–detector distance was 38 mm. The cell parameters were determined (APEX2 software)[338] from reflections taken from 3 sets of 12 frames, each at 10 s exposure.

[335] Pregosin, P. S. NMR Spectroscopy and Ion Pairing: Measuring and Understanding How Ions Interact. *Pure Appl. Chem.* **2009**, *81* (4), 615–633.
[336] Wu, D. H.; Chen, A. D.; Johnson, C. S. An Improved Difiusion-Qrdered Spectroscopy Experiment. *J. Magn. Reson. A* **1995**, *115*, 260-264.
[337] Harris, R. K.; Becker, E. D.; De Menezes, S. M. C.; Goodfellow, R.; Granger, P. Commission on Molecular Structure and Spectroscopy. *Pure Appl. Chem.* **2001**, *73*, 1795-1818.
[338] "M86-E01078 APEX2 User Manual", Bruker AXS Inc., 2006.

The structures were solved by direct methods using the program SHELXS-2013.[339] The refinement and all further calculations were carried out using SHELXL-2013.[340] For compounds [**3A**][$BArF_{24}$], [**5A**][$BArF_{24}$], [**5A'**][$BArF_{24}$] and [**5B**][$BArF_{24}$] the hydride H1A was located from Fourier difference maps and fixed with the AFIX 1 constraint. For compound [**3B**][OTf], the hydride H1 was located from Fourier difference maps and its position refined. The other H atoms were included in calculated positions and treated as riding atoms using SHELXL default parameters. The non-H atoms were refined anisotropically, using weighted full-matrix least squares on F^2. A semiempirical absorption correction was applied using SADABS in APEX2;[333] transmission factors Tmin/Tmax = 0.6270/0.7463, 0.6387/0.7462, 0.6650/0.7463, and 0.6242/0.7467. More collection and refinement data for each structure can be found in the appendix.

6.1.4 Isothermal Titration Calorimetry (ITC)

Isothermal Titration Calorimetry. All measurements were carried out with a Waters-SAS nanoITC device equipped with two stainless steel Hastealloy cells of 1 mL volume each (measurement and reference cells) placed in a dry glovebox filled with argon. Solutions of [**2**][$BArF_{24}$] were prepared by sonication of suspensions of the complexes in dry and degassed PhCl and were subsequently thoroughly degassed under moderate reduced pressure. In a typical titration, a solution of $HSiEt_3$ was placed in the servo-controlled syringe and injected sequentially into a less concentrated solution of complex [**2**][$BArF_{24}$] in PhCl. The volume injected was set so that the heat release did not reach the saturation level of the device. Every injection of silane solution required a time delay to allow the relaxation of the cell to thermal equilibrium prior to subsequent injection. Time delays below 1000 s generally produced a baseline drift due to uncompensated heat. Such a drift indicative of a slow chemical process could be reduced by increasing the time delay to 1500 s. The enthalpy of reaction was calculated by summing the integration of each thermal response over the molar content after subtraction of the dilution response produced in the last section of the calorigram (figure 18), which corresponds to the addition of further volumes of $HSiEt_3$ solution. The reported value of reaction enthalpy results from three independent ITC experiments.

[339] Sheldrick, G. M. Phase annealing in SHELX-90: direct methods for larger structures. *Acta Crystallogr., Sect. A* **1990**, *A46*, 467-473.
[340] Sheldrick, G. M. A short history of SHELX. *Acta Cryst.* **2008**, *A64*, 112-122.

6.1.5 Computational Methods

Computations were performed with the methods of density functional theory using the SCM-ADF2013.01[341] and Gaussian09[342] (revision D01) packages. The PBE functional[343] and the TPSS[344] functional implemented in the Amsterdam Density Functional package[345] (ADF2013 version) and augmented with Grimme's DFT-D3(BJ) implementation of dispersion with a Becke–Johnson (BJ) damping function were used in all geometry optimizations.[346],[347] Corminboeuf's PBE0[348]-dDsC[349] hybrid functional (ADF) was also used for geometry optimizations as well as for QTAIM and NCI analyses. Geometry optimizations by energy gradient minimization were carried out in all cases with integration grid accuracy comprised between 4.5 and 7.5, an energy gradient convergence criterion of 10^{-3} au, and a tight to very tight SCF convergence criterion. Counterpoise correction for basis set superposition error (BSSE) was neglected throughout this study. Within the PBE scheme, electron correlation was treated within the local density approximation (LDA) in the PW92[350] parametrization. With ADF2013.01, unless otherwise stated, all computations were carried out using scalar relativistic corrections within the zeroth order regular approximation for relativistic effects[351] with ad hoc all-electron (abbreviated ae) single and double polarization function triple-ζ Slater type basis sets (TZP and TZ2P). ETS-NOCV[352] analyses as well as calculations of vibrational modes were performed with optimized geometries using ADF2013 subroutines. Vibrational modes were

[341] SCM: Theoretical Chemistry, Vrije Universiteit, Amsterdam, The Netherlands, 2013.
[342] Pople, J. A. In *Gaussian 09*; Gaussian, Inc.: Pittsburgh, PA, 2009.
[343] Perdew, J. P.; Burke, K.; Ernzerhof, M. Generalized Gradient Approximation Made Simple. *Phys. Rev. Lett.* **1996**, *77*, 3865-3868.
[344] Tao, J.; Perdew, J. P.; Staroverov, V. N.; Scuseria, G. E. Climbing the Density Functional Ladder: Nonempirical Meta–Generalized Gradient Approximation Designed for Molecules and Solids. *Phys. Rev. Lett.* **2003**, *91*, 146401.
[345] te Velde, G.; Bickelhaupt, F. M.; Baerends, E. J.; Fonseca Guerra, C.; van Gisbergen, S. J. A.; Snijders, J. G.; Ziegler, T. Chemistry with ADF. *J. Comp. Chem.* **2001**, *22*, 931-967.
[346] Grimme, S.; Antony, J.; Ehrlich, S.; Krieg, H. A consistent and accurate ab initio parametrization of density functional dispersion correction (DFT-D) for the 94 elements H-Pu. *J. Chem. Phys.* **2010**, *132*, 154104.
[347] Grimme, S.; Ehrlich, S.; Goerigk, L. Effect of the damping function in dispersion corrected density functional theory. *J. Comp. Chem.* **2011**, *32*, 1456-1465.
[348] a) Ernzerhof, M.; Scuseria, G. E. Assessment of the Perdew–Burke–Ernzerhof exchange-correlation functional. *J. Chem. Phys.* **1999**, *110*, 5029-5036. b) Adamo, C.; Barone, V. Toward reliable density functional methods without adjustable parameters: The PBE0 mode. *J. Chem. Phys.* **1999**, *110*, 6158.
[349] Steinmann, S. N.; Corminboeuf, C. Comprehensive Benchmarking of a Density-Dependent Dispersion Correction. *J. Chem. Theor. Comp.* **2011**, *7*, 3567-3577.
[350] Perdew, J. P.; Wang, Y. Accurate and simple analytic representation of the electron-gas correlation energy. *Phys. Rev. B* **1992**, *45*, 13244-13249.
[351] a) van Lenthe, E.; Ehlers, A.; Baerends, E.-J. Contracted Gaussian basis sets for molecular calculations. I. Second row atoms, Z=11–18. *J. Chem. Phys.* **1999**, *110*, 8943-8953. b) van Lenthe, E.; Baerends, E. J.; Snijders, J. G. Relativistic total energy using regular approximations. *J. Chem. Phys.* **1994**, *101*, 9783-9792. c) van Lenthe, E.; Baerends, E. J.; Snijders, J. G. Relativistic regular two-component Hamiltonians. *J. Chem. Phys.* **1993**, *99*, 4597-4610.
[352] a) Mitoraj, M. P.; Michalak, A.; Ziegler, T. On the Nature of the Agostic Bond between Metal Centers and β-Hydrogen Atoms in Alkyl Complexes. An Analysis Based on the Extended Transition State Method and the Natural Orbitals for Chemical Valence Scheme (ETS-NOCV). *Organometallics* **2009**, *28*, 3727-3733. b) Mitoraj, M. P.; Michalak, A.; Ziegler, T. A Combined Charge and Energy Decomposition Scheme for Bond Analysis. *J. Chem. Theory Comput.* **2009**, *5*, 962-975.

analytically computed to verify that the optimized geometries were related to energy minima: statistical thermodynamic data at T = 298.15 K and P = 1 atm were extracted for further determination of enthalpies and variations of Gibbs free enthalpies by conventional methods. The COSMO model[353] of solvation was used for the computation of iondissociation thermochemistries. The geometries of ion pairs were all computed at the ZORA-PBE-D3(BJ)/ae-TZP level and their minimum energy nature confirmed by the absence of any imaginary frequency above 50 $i$cm^{-1} in their computed vibrational modes. Natural population analyses (NPA) as well as Wiberg index determinations were performed with geometries of models relaxed at the ZORA-PBE-D3(BJ) level using all-electron TZP basis sets with the GENNBO[354] 6.0 module of ADF. QTAIM11,[355] and NCI[356] region plot analyses were carried out using the modules embedded within ADF2013. Representations of molecular structures and isosurfaces were produced with ADFview2013. QTAIM analyses were performed on three geometries of [**3**A]$^+$, optimized at different levels. Figure 19b depicts the geometry computed at the PBE0-dDsC/ae-TZP level. The complex was also reoptimized at the PBE0-D3/SDD and PBE-D3/ SDD levels for comparison. These levels consist of the PBE or the PBE0 functionals, respectively, augmented with the "-D3" correction. Three basis sets were considered: def2-TZVPP,[357] 6-311+G**, and 6-311++G**,[358] on all elements except Ir. The Stuttgart/Dresden (SDD)[359] effective core potential (ECP) and its associated basis set were employed on Ir. The wave functions were then calculated by performing single-point calculations on these geometries to generate the ".wfx" files required for subsequent QTAIM analyses. The electron density (ρ_β), the Laplacian of the electron density ($\nabla^2\rho_\beta$), and the bond ellipticity (ε) at bond critical points were computed, along with delocalization indexes (δ(A,B)) between selected pairs of atoms. These calculations were performed with the AIMAll package (version 15.09.27).[360] QTAIM analyses were also carried out with and without scalar relativistic corrections for basis

[353] Klamt, A.; Schuurmann, G. COSMO: a new approach to dielectric screening in solvents with explicit expressions for the screening energy and its gradient. *J. Chem. Soc., Perkin Trans. 2* **1993**, 799-805.
[354] Weinhold, F. In *Encyclopedia of Computational Chemistry*; von Ragué-Schleyer, P., Allinger, N. L., Clark, T., Gasteiger, J., Kollman, P. A., Schaefer, H. F., Schreiner, P. R., Eds.; John Wiley & Sons, Chichester, UK: 1998; Vol. 3, p 1792-1811.
[355] Bader, R. F. W.; Streitwieser, A.; Neuhaus, A.; Laidig, K. E.; Speers, P. *J. Am. Chem. Soc.* **1996**, *118*, 4959-4965.
[356] a) Contreras-Garcia, J.; Johnson, E. R.; Keinan, S.; Chaudret, R.; Piquemal, J. P.; Beratan, D. N.; Yang, W. *J. Chem. Theor. Comput.* **2011**, *7*, 625-632. b) Johnson, E.; Keinan, S.; Mori-Sanchez, P.; Contreras-Garcia, J.; Cohen, A. J.; Yang, W. *J. Am. Chem. Soc.* **2010**, *132*, 6498-6506.
[357] Weigend, F.; Ahlrichs, R. Balanced basis sets of split valence, triple zeta valence and quadruple zeta valence quality for H to Rn: Design and assessment of accuracy. *Phys. Chem. Chem. Phys.* **2005**, *7*, 3297-3305.
[358] a) Clark, T.; Chandrasekhar, J.; Spitznagel, G. W.; von Ragué-Schleyer, P. Efficient diffuse function-augmented basis sets for anion calculations. III. The 3-21+G basis set for first-row elements, Li–F. *J. Comp. Chem.* **1983**, *4*, 294-301. b) McLean, A. D.; Chandler, G. S. Contracted Gaussian basis sets for molecular calculations. I. Second row atoms, Z=11–18. *J. Chem. Phys.* **1980**, *72*, 5639-5648. c) Krishnan, R.; Binkley, J. S.; Seeger, R.; Pople, J. A. Self-consistent molecular orbital methods. XX. A basis set for correlated wave functions. *J. Chem. Phys.* **1980**, *72*, 650-654.
[359] Andrae, D.; Häußermann, U.; Dolg, M.; Stoll, H.; Preuß, H. Energy-adjustedab initio pseudopotentials for the second and third row transition elements. *Theor. Chim. Acta* **1990**, *77*, 123-141.
[360] Keith, T. A.; TK Gristmill Software: Overland Park KS, USA, 2016.

sets, starting from geometries optimized at the (ZORA) PBE0-dDsC level with all-electron TZP and TZ2P basis sets except in the case of [**4**→Ag←**4**]$^+$, for which QTAIM analysis was performed by a single point calculation with a geometry optimized at the ZORA-PBE-D3(BJ)/ae-TZP level. All DFT calculations of reaction enthalpies were performed with the TURBOMOLE 7.0 suite of programs.[361] The geometry optimizations were carried out using the PBEh-3c density functional composite method.[362] Single-point energies were obtained at the B3LYP[363] level associated with the extended quadruple-ζ basis set def2-QZVP.[364] The resolution-of-identity (RI) approximation for the Coulomb integrals[365] with matching default auxiliary basis sets[366] was applied. For integration of the exchange-correlation contribution, the numerical quadrature grid m4 was employed for B3LYP. For DFT calculations with the PBEh-3c functional, the D3 dispersion-correction scheme,[367] applying the Becke–Johnson (BJ) damping,[368,369] was used. For evaluation of the single-point energies the nonlocal (NL) van der Waals functional approach by Vydrov and van Voorhis[370] DFT-NL[371] was employed nonself-consistently (i.e., calculating the NL energy once in a post-SCF manner) for B3LYP. Computations of the harmonic vibrational frequencies were performed at the PBEh-3c level. Thermal corrections from energy to enthalpy were obtained by a coupled rigid-rotor–harmonic-oscillator approximation for each molecule in the gas phase.[372] The PBEh-3c vibrational frequencies were scaled by a factor of 0.95. The COSMO-RS continuum solvation model45,[373]

---

[361] Furche, F.; Ahlrichs, R.; Hättig, C.; Klopper, W.; Sierka, M.; Weigend, F. Turbomole. *WIREs Comput. Mol. Sci.* **2014**, *4*, 91-100.

[362] Grimme, S.; Brandenburg, J. G.; Bannwarth, C.; Hansen, A. Consistent structures and interactions by density functional theory with small atomic orbital basis sets. *J. Chem. Phys.* **2015**, *143*, 054107.

[363] a) Becke, A. D. Density-functional thermochemistry. III. The role of exact exchange. *J. Chem. Phys.* **1993**, *98*, 5648-5652. b) Lee, C.; Yang, W.; Parr, R. G. Development of the Colle-Salvetti correlation-energy formula into a functional of the electron density. *Phys. Rev. B* **1988**, *37*, 785-789. c) Stephens, P. J.; Devlin, F. J.; Chabalowski, C. F.; Frisch, M. J. Ab Initio Calculation of Vibrational Absorption and Circular Dichroism Spectra Using Density Functional Force Fields. *J. Phys. Chem.* **1994**, *98*, 11623-11627.

[364] Weigend, F.; Ahlrichs, R. Balanced basis sets of split valence, triple zeta valence and quadruple zeta valence quality for H to Rn: Design and assessment of accuracy. *Phys. Chem. Chem. Phys.* **2005**, *7*, 3297-3305.

[365] Eichkorn, K.; Treutler, O.; Öhm, H.; Häser, M.; Ahlrichs, R. Auxiliary basis sets to approximate Coulomb potentials. *Chem. Phys. Lett.* **1995**, *242*, 652-660.

[366] Weigend, F. Accurate Coulomb-fitting basis sets for H to Rn*Phys. Chem. Chem. Phys.* **2006**, *8*, 1057-1065.

[367] Grimme, S.; Antony, J.; Ehrlich, S.; Krieg, H. *J.* A consistent and accurate ab initio parametrization of density functional dispersion correction (DFT-D) for the 94 elements H-Pu. *Chem. Phys.* **2010**, *132*, 154104.

[368] Grimme, S.; Ehrlich, S.; Goerigk, L. Effect of the damping function in dispersion corrected density functional theory. *J. Comp. Chem.* **2011**, *32*, 1456-1465.

[369] a) Becke, A. D.; Johnson, E. R. A density-functional model of the dispersion interaction. *J. Chem. Phys.* **2005**, *123*, 154101. b) Johnson, E. R.; Becke, A. D. A post-Hartree-Fock model of intermolecular interactions: Inclusion of higher-order corrections. *J. Chem. Phys.* **2005**, *123*, 024101.

[370] Vydrov, O. A.; vanVoorhis, T. Nonlocal van der Waals density functional: The simpler the better. *J. Chem. Phys.* **2010**, *133*, 244103.

[371] Hujo, W.; Grimme, S. Performance of the van der Waals Density Functional VV10 and (hybrid)GGA Variants for Thermochemistry and Noncovalent Interactions. *J. Chem. Theory Comput.* **2011**, *7*, 3866.

[372] Grimme, S. Supramolecular Binding Thermodynamics by Dispersion-Corrected Density Functional Theory. *Chem. Eur. J.* **2012**, *18*, 9955-9964.

[373] Eckert, F.; Klamt, A. Fast solvent screening via quantum chemistry: COSMO-RS approach. *AIChE J.* **2002**, *48*, 369-385.

was used as implemented in COSMOtherm 2016[374] to obtain all solvation enthalpies. For this purpose single-point calculations employing the default BP8695/def-TZVP[375] level of theory were performed on the optimized gas-phase geometries for each molecule. The solvation contribution was then added to the gas-phase enthalpies.

6.2 Experiments related to Chapter 2: Evidence of a donor-acceptor interaction Ir(H)→SiR_3 in catalytic intermediates of relevant activity

6.2.1 Synthesis of [Cp*Ir(μ-Cl)Cl]$_2$

[Cp*Ir(μ-Cl)Cl]$_2$ was synthesized from $IrCl_3$ and 1,2,3,4,5-pentamethylcyclopenta-1,3-diene (HCp*) following the procedure **I** (scheme 3), as reported in the literature.[376]

6.2.2 Synthesis of the ligand **L**H**3**

The ligand 4-(4-(*tert*-butyl)pyridin-2-yl)-*N*,*N*-dimethylaniline **L**H**3** was previously synthesized by Dr. Wissam Iali and used as such. The ligand **L**H**3** was prepared from 4-(*tert*-butyl)pyridine and 4-bromo-*N*,*N*-dimethylaniline following the procedure reported in the literature.[377]

6.2.3 Synthesis of the ligand **L**H**5**

The ligand 2-(1*H*-inden-3-yl)pyridine **L**H**5** was prepared by the acid-assisted cyclodehydration of 3-phenyl-1-(pyridin-2-yl)propan-1-one following the procedure reported in the literature.[378] Its ^{1}H NMR data matched those already reported.[378]

6.2.4 Synthesis of neutral iridacycles [(κ^2-(C,N)-(**L**)Ir(III)Cl]

[374] Eckert, F.; Klamt, A. In *COSMOtherm, Version C3.0, Release 16.01*; COSMOlogic GmbH & Co. KG: Leverkusen, Germany, 2016.
[375] Schäfer, A.; Huber, C.; Ahlrichs, R. Fully optimized contracted Gaussian basis sets of triple zeta valence quality for atoms Li to Kr. *J. Chem. Phys.* **1994**, *100*, 5829-5835.
[376] White, C.; Yates, A.; Maitlis, P. M.; Heinekey, D. M. (η^5-Pentamethylcyclopentadienyl)Rhodium and -Iridium Compounds. In *Inorganic Syntheses*; John Wiley & Sons, Inc., 2007; pp 228–234.
[377] Djukic, J.-P.; Iali, W.; Pfeffer, M.; Le Goff, X.-F. Synthesis of Planar Chiral Iridacycles by Cationic Metal π-Coordination: Facial Selectivity, and Conformational and Stereochemical Consequences. *Chem. - A Eur. J.* **2012**, *18* (19), 6063–6078.
[378] Boblak, K. N.; Klumpp, D. A. Cyclodehydrations Leading to Indene Products Having N-Heterocyclic Substituents. *J. Org. Chem.* **2014**, *79* (12), 5852–5857.

6.2.4.1 General procedure **II** (scheme 3)[379]

A Schlenk flask was charged with the ligand **L**H (1 equiv.), the iridium precursor [Cp*Ir(μ-Cl)Cl]$_2$ (0.6 equiv.) and anhydrous NaOAc (3 equiv.). To this mixture was added ~10–15 mL of CH_2Cl_2. After a vigorous stirring at room temperature or heating at 50 °C for a minimum period of 16 h, the reaction mixture was filtrated over Celite or Dicalite followed by removal of the solvent. The resulting residue was then purified by recrystallization with CH_2Cl_2/pentane and/or washing with *n*-pentane or *n*-hexane.

6.2.4.2 **1**

The iridacycle **1** was prepared following the general procedure **II.** Its ^{1}H NMR data matched those previously reported.[380]

6.2.4.3 **3**

The iridacycle **3** was prepared following the general procedure **II.** Its ^{1}H NMR data matched those previously reported.[380]

6.2.4.4 **5**

The iridacycle **5** was prepared following the general procedure **II.** Its ^{1}H NMR data matched those previously reported.[377]

6.2.4.5 **7**

The complex **7** was prepared following the general procedure **II** from the ligand **L**H**4** upon heating at 50 °C for 48 h: [Cp*Ir(μ-Cl)Cl]$_2$ (287 mg, 0.36 mmol), **L**H**4** (150 mg, 0.65 mmol), NaOAc (160 mg, 1.95 mmol). The product **7** was obtained as a yellow/orange powder in 60% yield (231 mg). **Anal. Calcd for $C_{27}H_{25}ClIrN$•1/10(CH_2Cl_2)**: C, 54.57; H, 4.25; N, 2.37. **Found**: C, 54.76; H, 4.43; N, 2.37. **^{1}H NMR (500 MHz, 298 K, $CDCl_3$)**: δ = 8.97 (d, 1H, *J* = 5.3 Hz, H-C=N), 8.78 (d, 1H, *J* = 8.4 Hz, H_{Ar}), 8.64 (d, 1H, *J* = 8.4 Hz, H_{Ar}), 8.54 (d, 1H, *J* = 8.4 Hz, H_{Ar}),

[379] Davies, D. L.; Al-Duaij, O.; Fawcett, J.; Giardiello, M.; Hilton, S. T.; Russell, D. R. Room-Temperature Cyclometallation of Amines, Imines and Oxazolines with [$MCl_2Cp^*]_2$ (M = Rh, Ir) and [$RuCl_2$(*p*-cymene)]$_2$. *Dalt. Trans.* **2003**, *2* (21), 4132–4138.
[380] Li, L.; Brennessel, W. W.; Jones, W. D. An Efficient Low-Temperature Route to Polycyclic Isoquinoline Salt Synthesis via C-H Activation with [$Cp^*MCl_2]_2$ (M = Rh, Ir). *J. Am. Chem. Soc.* **2008**, *130* (37), 12414–12419.

8.16 (d, 1H, J = 8.0 Hz, H_{Ar}), 8.05 (d, 1H, J = 7.2 Hz, H_{Ar}), 7.72 (t, 1H, J = 7.2 Hz, H_{Ar}), 7.62–7.67 (m, 2H, H_{Ar}), 7.52 (d, 1H, J = 8.1 Hz, H_{Ar}), 7.50 (d, 1H, J = 8.1 Hz, H_{Ar}), 1.75 (s, 15H, Cp-*Me*$_5$). **^{13}C NMR (126 MHz, 298 K, $CDCl_3$)**: δ = 161.9 (C, Ar), 158.4 (C, Ar), 149.8 (H*C*=N, Ar), 140.3 (C, Ar), 133.5 (CH, Ar), 132.1 (C, Ar), 132.0 (C, Ar), 131.2 (CH, Ar), 128.5 (CH, Ar), 128.1 (C, Ar), 127.1 (CH, Ar), 126.1 (C, Ar), 124.1 (CH, Ar), 123.4 (CH, Ar), 122.0 (C-H PhPy), 115.7 (CH, Ar), 88.7 (*Cp*-Me$_5$), 8.9 (Cp- *Me*$_5$). **HRMS-ESI calcd for $C_{27}H_{25}ClIrN$** ([**7**$^{\bullet}$]$^+$) (m/z): 591.1292. **Found**: 591.1320. **HRMS-ESI calcd for $C_{27}H_{25}IrN$** ([**7**–Cl]$^+$) (m/z): 556.1612. **Found**: 556.1638.

6.2.4.6 **9**

The complex **9** was prepared following the general procedure **II** from the ligand **L**H**5** at room temperature for 16 h: [Cp*Ir(μ-Cl)Cl]$_2$ (327 mg, 0.41 mmol), **L**H**5** (122.6 mg, 0.63 mmol), NaOAc (168 mg, 2.05 mmol). After a crystallization in CH_2Cl_2/pentane at –30 °C overnight, the product **9** was obtained as an orange/red solid in 83% yield (290 mg). **Anal. Calcd for $C_{24}H_{25}ClIrN$•2/5 (CH_2Cl_2)**: C, 49.75; H, 4.41; N, 2.38. **Found**: C, 49.64; H, 4.52; N, 2.28. **^{1}H NMR (400 MHz, 298 K, $CDCl_3$)**: δ = 8.65 (d, 1H, J = 6.0 Hz, H–C=N), 7.85 (d, 1H, J = 8.4 Hz, H_{Ar}), 7.64 (t, 1H, J = 8.4 Hz, H_{Ar}), 7.58 (d, 1H, J = 7.7 Hz, H_{Ar}), 7.46 (d, 1H, J = 7.4 Hz, H_{Ar}), 7.50 (t, 1H, J = 7.4 Hz, H_{Ar}), 7.03 (t, 1H, J = 7.4 Hz, H_{Ar}), 6.93 (m, 1H, H_{Ar}), 4.04 (d, 1H, J = 23.0 Hz, H of C*H*$_2$ in C,N ligand), 3.81 (d, 1H, J = 23.0 Hz, H of C*H*$_2$ in C,N ligand), 1.77 (s, 15H, Cp-*Me*$_5$). **MS-ESI calcd for $C_{24}H_{25}ClIrN$** ([**9**$^{\bullet}$]$^+$) (m/z): 555.13. **Found**: 555.13. **MS-ESI calcd for $C_{24}H_{25}IrN$** ([**9**–Cl]$^+$) (m/z): 520.16. **Found**: 520.16.

6.2.4.7 **11**

The iridacycle **11** was prepared following the general procedure **II.** Its ^{1}H NMR data matched those previously reported.[381]

6.2.5 Synthesis of ionic iridacycles complexes [(κ^2-(C,N)-(**L**)Ir(III)NCMe][X]

6.2.5.1 General procedure **III** (scheme 3)[382]

[381] Liu, Z.; Habtemariam, A.; Pizarro, A. M.; Clarkson, G. J.; Sadler, P. J. Organometallic Iridium(III) Cyclopentadienyl Anticancer Complexes Containing C,N-Chelating Ligands. *Organometallics* **2011**, *30* (17), 4702–4710.
[382] Hamdaoui, M.; Ney, M.; Sarda, V.; Karmazin, L.; Bailly, C.; Sieffert, N.; Dohm, S.; Hansen, A.; Grimme, S.; Djukic, J.-P. Evidence of a Donor–Acceptor (Ir–H)→SiR_3 Interaction in a Trapped Ir(III) Silane Catalytic Intermediate. *Organometallics* **2016**, *35* (13), 2207–2223.

In a Schlenk flask an equimolar mixture of [(κ^2-(C,N)-(**L**)Ir(III)Cl] and [CX] (CX = Na[$BArF_{24}$], Na[BPh_4], Ag[PF_6], Ag[BF_4] or Ag[OTf]) was dissolved in acetonitrile (~7–10 mL). The resulting mixture was vigorously stirred at room temperature within a period not exceeding 4 h, unless otherwise stated. The resultingThe complex suspension was filtered through a pad of Dicalite, and the solvent was removed from the filtrate under reduced pressure. The solid was either recrystallized in a mixture of CH_2Cl_2 and *n*-hexane or *n*-pentane or washed with *n*-hexane or *n*-pentane, to afford an analytically pure compound.

6.2.5.2 [**2**][$BArF_{24}$]

The ionic iridacycle [**2**][$BArF_{24}$] was prepared following the general procedure **III**:[382] **1** (507.2 mg, 0.981 mmol) and Na[$BArF_{24}$] (869.3 mg, 0.981 mmol), room temperature, 2 h. The desired compound was recrystallized at low temperature (~ –20 °C) using a mixture of CH_2Cl_2 and *n*-hexane, giving rise to a yellow powder in 83% yield (1.129 g). Monocrystals were grown by diffusion of diisopropyl ether vapors into a solution of [**2**][$BArF_{24}$] in acetone. **Anal. Calcd for $C_{55}H_{38}BF_{24}IrN_2$**: C, 47.67; H, 2.76; N, 2.02. **Found**: C, 47.61; H, 2.74; N, 1.98. **^{1}H NMR (500 MHz, 298 K, CD_2Cl_2)**: δ = 8.61 (d, ^{1}H, 1H, J = 6.0 Hz, H–C=N PhPy), 7.91 (m, 1H, H_{Ar} PhPy), 7.85 (m, 1H, H_{Ar} PhPy), 7.74 (m, 10H, $2H_{Ar}$ PhPy + $8H_{Ar}$ $BArF_{24}$), 7.57 (m, 4H, $BArF_{24}$), 7.27–7.30 (m, 1H, H_{Ar} PhPy), 7.18–7.23 (m, 2H, H_{Ar} PhPy), 2.23 (s, 3H, Ir-NC*Me*), 1.62 (s, 15H, Cp-*Me*$_5$). **^{13}C NMR (126 MHz, 298 K, CD_2Cl_2)**: δ = 166.0 (C, PhPy), 161.5–162.7 (1:1:1:1 quartet, C–B $BArF_{24}$, $^1J_{C-B}$ = 50 Hz), 156.6 (C, PhPy), 151.9 (H–C=N, PhPy), 145.0 (C, PhPy), 139.6 (*C*–H, PhPy), 136.0 (*C*-H, PhPy), 135.2 (m, $C_{H\text{-}ortho}$ $BArF_{24}$), 132.1 (*C*–H, PhPy), 128.9–129.6 (q, *C*–CF_3 $BArF_{24}$, $^2J_{C-F}$ = 31 Hz), 124.9 (*C*–H, PhPy), 124.5 (*C*–H, PhPy), 124.0 (*C*–H, PhPy), 124.03 (q, *C*–CF_3 $BArF_{24}$, $^1J_{C-F}$ = 272 Hz), 120.3 (*C*–H PhPy), 118.3 (Ir-N*C*Me), 117.9 (m, $C_{H\text{-}para}$ $BArF_{24}$), 91.8 (*Cp*-Me_5), 8.9 (Cp-*Me*$_5$), 4.2 (Ir-NC*Me*). **^{19}F NMR (282 MHz, 298 K, CD_2Cl_2)**: δ = –63.8 (s, CF_3 $BArF_{24}$). **^{11}B NMR (128 MHz, 298 K, CD_2Cl_2)**: δ = –6.6. **HRMS-ESI calcd for $C_{23}H_{26}IrN_2$** ([**2**]$^+$) (m/z): 523.1721. **Found**: 523.1738. **HRMS-ESI calcd for $C_{32}H_{12}BF_{24}$** ([$BArF_{24}$]$^-$) (m/z): 863.0649. **Found**: 863.0723.

6.2.5.3 [**2**][BF_4]

The ionic iridacycle [**2**][BF_4] was prepared following the general procedure **III**:[382] **1** (230 mg, 0.445 mmol) and Ag[BF_4] (87 mg, 0.445 mmol), room temperature, 1 h. The desired compound was obtained after washing with cold pentane. [**2**][BF_4] was isolated as orange crystals in 80%

yield (214 mg). Monocrystals were obtained by slow diffusion of *n*-heptane into a solution of [**2**][BF_4] in CH_2Cl_2. **Anal. Calcd for $C_{23}H_{26}BF_4IrN_2$**: C, 45.32; H, 4.30; N, 4.60. **Found**: C, 45.30; H, 4.34; N, 4.25. **^{1}H NMR (500 MHz, 298 K, CD_2Cl_2)**: δ = 8.74 (d, 1H, H–C=N PhPy, J = 5.6 Hz), 7.94–7.89 (m, 2 H, H_{Ar} PhPy), 7.78–7.74 (m, 2H, H_{Ar} PhPy), 7.34 (m, 1H, H_{Ar} PhPy), 7.28 (m, 1H, H_{Ar} PhPy), 7.19 (m, 1H, H_{Ar} PhPy), 2.32 (s, 3H, Ir-NC*Me*), 1.70 (s, 15H, Cp-*Me*$_5$). **^{13}C NMR (126 MHz, 298 K, CD_2Cl_2)**: δ = 167.6 (C PhPy), 156.9 (C PhPy), 152.6 (H–*C*=N, PhPy), 145.3 (C, PhPy), 139.6 (*C*–H, PhPy), 136.1 (*C*–H, PhPy), 131.8 (*C*–H, PhPy), 124.8 (*C*–H, PhPy), 124.3 (*C*–H, PhPy), 124.2 (*C*–H, PhPy), 120.1 (*C*–H, PhPy), 118.9 (Ir–N*C*Me), 91.7 (*Cp*-Me_5), 8.9 (Cp-*Me*$_5$), 4.2 (Ir-NC*Me*). **^{19}F NMR (282 MHz, 298 K, CD_2Cl_2)**: δ = –153.8 (s, $^{11}BF_4$), –153.8 (s, $^{10}BF_4$). **^{11}B NMR (128 MHz, 298 K, CD_2Cl_2)**: δ = –1.1. **HRMS-ESI calcd for $C_{23}H_{26}IrN_2$** ([**2**]$^+$) (m/z): 523.1721. Found: 523.1764. **HRMS-ESI calcd for $C_{21}H_{23}IrN$** ({[**2**]–CH_3CN}$^+$): 482.1455. **Found**: 482.1490.

6.2.5.4 [**2**][OTf]

The ionic iridacycle [**2**][OTf] was prepared following the general procedure **III**:[382] **1** (200 mg, 0.387 mmol) and Ag[OTf] (99.4 mg, 0.387 mmol), room temperature, 1 h. The desired compound was obtained after washing with cold *n*-pentane. [**2**][OTf] was isolated as yellow crystals (218 mg, 84%). **Anal. Calcd for $C_{24}H_{26}F_3Ir_1N_2O_3S_1$**: C, 42.91; H, 3.90; N, 4.17. **Found**: C, 42.95; H, 3.93; N, 4.14. **HRMS-ESI calcd for $C_{21}H_{23}IrN$** ({[**2**]**–**CH_3CN}$^+$) (m/z): 482.1455. **Found**: 482.1466. **HRMS-ESI calcd for CF_3O_3S** ([OTf]$^-$) (m/z): 148.9515. **Found**: 148.9521. Analytical data matched those previously reported by K.-Y. Sau et al.[383]

6.2.5.5 [**2**][BPh_4]

The ionic iridacycle [**2**][BPh_4] was prepared following the general procedure **III**: **1** (242 mg, 0.468 mmol) and Na[BPh_4] (160.0 mg, 0.468 mmol), room temperature, 4 h. The desired compound was recrystallized at low temperature (~ –20 °C) using a mixture of CH_2Cl_2 and *n*-hexane, giving rise to a yellow powder in 76% yield (0.299 g). Yellow monocrystals were grown by diffusion of *n*-hexane into a solution of [**2**][BPh_4] in CH_2Cl_2. **Anal. Calcd for $C_{47}H_{46}BIrN_2$**: C, 67.05; H, 5.51; N, 3.31. **Found**: C, 66.70; H, 5.49; N, 3.09. **^{1}H NMR (500 MHz, 298 K, CD_2Cl_2)**: δ = 8.59 (d, 1H, J = 5.8 Hz, H_{Ar} PhPy), 7.87 (m, 1 H_{Ar} PhPy), 7.79 (d, 1H, J = 8.0 Hz, H_{Ar} PhPy), 7.75

[383] Sau, Y. K.; Yi, X. Y.; Chan, K. W.; Lai, C. S.; Williams, I. D.; Leung, W. H. Insertion of Nitrene and Chalcogenolate Groups into the Ir-C σ Bond in a Cyclometalated iridium(III) Complex. *J. Organomet. Chem.* **2010**, *695* (9), 1399–1404.

(m, 2H, H_{Ar} PhPy), 7.29 (m, 9H, H_{Ar} PhPy + BPh_4), 7.23 (t, 1H, J = 8.0 Hz, H_{Ar} PhPy), 7.17 (t, 1H, J =8.0 Hz, H_{Ar} PhPy), 6.98 (t, 8H, J =7.4 Hz, H_{Ar} BPh_4), 6.84 (t, 4H, J =7.4 Hz, H_{Ar} BPh_4), 1.67 (s, 15H, Cp-*Me*$_5$), 1.62 (s, 3H, Ir-NC*Me*). **^{13}C NMR (126 MHz, 298K, CD_2Cl_2)**: δ = 167.8 (*C*, PhPy), 164.5 (1:1:1:1 quartet, *C*–B BPh_4, $^1J_{C-B}$ = 49.8 Hz), 156.6 (*C*, PhPy), 151.9 (H–*C*=N, PhPy), 145.1 (*C*, PhPy), 139.8 (H–*C*, PhPy), 136.2 (H_{ortho}–*C*, BPh_4), 135.9 (H–*C*, PhPy), 132.0 (*C*, PhPy), 126.0 (H_{meta}–*C*, BPh_4), 125.0 (H–*C*, PhPy),124.5 (H–*C*, PhPy), 124.2 (H–*C*, PhPy), 122.1 (H_{para}–*C*, BPh_4), 120.3 (H–*C*, PhPy), 118.9 (Ir-N*C*Me), 91.6 (*Cp*-Me_5), 9.0 (Cp-*Me*$_5$), 3.4 (Ir-NC*Me*). **^{11}B (128 MHz, 298 K, CD_2Cl_2)**: δ = –6.6 (m). **HRMS-ESI calcd for $C_{23}H_{26}IrN_2$** ([**2**]$^+$) (m/z): 523.1721. **Found**: 523.1720. **HRMS-ESI calcd for $C_{24}H_{20}B$** ($[BPh_4]^-$) (m/z): 319.1657. **Found**: 319.1628.

6.2.5.6 [**2**][PF_6]

The ionic iridacycle [**2**][PF_6] was prepared following the general procedure **III**: **1** (103 mg, 0.200 mmol) and Ag[PF_6] (50.6 mg, 0.261 mmol), room temperature, 1 h. The desired compound was washed with cold *n*-hexane, giving rise to a yellow powder in 81% yield (0.108 g). **Anal. Calcd for $C_{23}H_{26}F_6Ir_1N_2P_1$**: C, 41.38; H, 3.93; N, 4.20. **Found:** C, 41.56; H, 3.97; N, 4.15. **HRMS-ESI calcd for $C_{23}H_{26}IrN_2P$** ([**2**]$^+$) (m/z): 523.1721. **Found**: 523.1703. **HRMS-ESI calcd for F_6P_1** ($[PF_6]^-$) (m/z): 144.9636. **Found**: 144.9636. Analytical data matched those previously reported by L. S. Park-Gehrke et al.[384]

6.2.5.7 [**4**][$BArF_{24}$]

The ionic iridacycle [**4**][$BArF_{24}$] was prepared following the general procedure **III**: **3** (386 mg, 0.713 mmol) and Na[$BArF_{24}$] (623.2 mg, 0.713 mmol), room temperature, 2 h. After one recrystallization with a mixture of CH_2Cl_2 and *n*-pentane and washing tree times with *n*-pentane, [**4**][$BArF_{24}$] was isolated as a yellow powder in 71% yield (707 mg). Monocrystals were grown by slow diffusion of hexane and benzene into a solution of [**4**][$BArF_{24}$] in 1,2-dichloroethane. **Anal. Calcd for $C_{57}H_{38}BF_{24}IrN_2$·(1/10 CH_2Cl_2)**: C, 48.35; H, 2.71; N, 1.98. **Found**: C, 48.56; H, 2.72; N, 1.99. **^{1}H NMR (500 MHz, 298 K, CD_2Cl_2)**: δ = 8.89 (dd, 1H, J_1 = 5.3 Hz, J_2 = 1.2 Hz, H–C=N B[h]Q), 8.36 (dd, 1H, J_1 = 8.0 Hz, J_2 = 1.1 Hz, H_{Ar} B[h]Q), 8.01 (dd, 1H, J_1 = 6.9 Hz, J_2 = 0.9 Hz, HAr B[h]Q), 7.92 (d, 1H, J = 8.7 Hz, H_{Ar} B[h]Q), 7.73 (m, 9 H, 1H, H_{Ar} B[h]Q + 8H

[384] Park-Gehrke, L. S.; Freudenthal, J.; Kaminsky, W.; Dipasquale, A. G.; Mayer, J. M. Synthesis and Oxidation of CpIrIII Compounds: Functionalization of a Cp Methyl Group. *Dalt. Trans.* **2009**, *0* (11), 1972–1983.

$BArF_{24}$), 7.67–7.70 (m, 2H, H_{Ar} B[h]Q), 7.56 (m, 4 H, $BArF_{24}$), 7.61 (dd, 1H, J_1 = 7.9 Hz, J_2 = 5.3 Hz, H_{Ar} B[h]Q), 2.12 (s, 3H, IrNC*Me*), 1.73 (s, 15H, Cp-*Me*$_5$). **^{13}C NMR (126 MHz, 298K, CD_2Cl_2)**: δ = 161.5–162.7 (1:1:1:1 quartet, *C*–B $BArF_{24}$, $^1J_{C-B}$ = 49.8 Hz), 157.6 (*C*–N, B[h]Q), 154.2 (C, B[h]Q), 150.2 (H–*C*=N, B[h]Q), 142.3 (C, B[h]Q), 138.4 (*C*–H, B[h]Q), 135.2 (m, $C_{H\text{-}ortho}$ BArF24), 134.8 (C, B[h]Q),133.1 (*C*–H, B[h]Q), 131.4 (*C*–H, B[h]Q), 130.6 (*C*–H, B[h]Q),128.9–129.6 (q, *C*–CF_3 $BArF_{24}$, $^2J_{C-F}$ = 31.5 Hz, $^3J_{C-B}$ = 3.0 Hz), 128.1 (C, B[h]Q), 125.0 (q, *C*F_3 $BArF_{24}$, $^1J_{C-F}$ = 272.5 Hz), 124.1 (*C*–H, B[h]Q), 122.9 (*C*–H, B[h]Q), 122.5 (*C*–H, B[h]Q), 118.5 (Ir-N*C*Me), 117.9 (m, $C_{H\text{-}para}$ $BArF_{24}$), 91.6 (*Cp*-Me_5), 9.1 (Cp-*Me*$_5$), 4.2 (Ir-NC*Me*). **^{19}F NMR (282 MHz, 298 K, CD_2Cl_2)**: δ = –63.8 (s, CF_3 $BArF_{24}$). **^{11}B NMR (128 MHz, 298 K, CD_2Cl_2)**: δ = –6.6 (bs). **HRMS-ESI calcd for $C_{25}H_{26}IrN_2$** ([**4**]$^+$) (m/z): 547.1721. **Found**: 547.1716. **HRMS-ESI calcd for $C_{32}H_{12}BF_{24}$** ([$BArF_{24}$]$^-$) (m/z): 863.0649. **Found**: 863.0656.

6.2.5.8 [**4**][BPh_4]

The ionic iridacycle [**4**][BPh_4] was prepared following the general procedure **III**: **3** (93.5 mg, 0.173 mmol) and Na[BPh_4] (342,2 mg, 0.173 mmol), room temperature, for 21 h. After washing three times with *n*-pentane, [**4**][BPh_4] was isolated as a yellow powder in 76% yield (113 mg). Monocrystals were grown by slow diffusion of hexane and benzene into a solution of [**4**][BPh_4] in 1,2-dichloroethane. **Anal. Calcd for $C_{49}H_{46}BIrN_2\cdot(1/3CH_2Cl_2)$**: C, 66.26; H, 5.26 ; N, 3.13. **Found**: C, 66.49; H, 5.24; N, 2.96. **^{1}H (400 MHz, 298 K, $CDCl_3$)**: δ = 8.77 (d, 1H, *J* = 5.4 Hz, H_{Ar} B[h]Q), 8.13 (d, 1 H, *J* = 8.1 Hz, H_{Ar} B[h]Q), 7.93 (d, 1H, *J* = 7.0 Hz, H_{Ar} B[h]Q), 7.9 (d, 1H, *J* = 8.7 Hz, H_{Ar} B[h]Q), 7.73 (d, 1H, *J* =7.6 Hz, H_{Ar} B[h]Q), 7.68 (d, 1H, *J* = 7.5 Hz, H_{Ar} B[h]Q), 7.64 (d, 1H, *J* = 8.9 Hz, H_{Ar} B[h]Q), 7.29–7.27 (m, 6H, H_{Ar} B[h]Q), 6.83 (t, 10H, *J* = 7.3 Hz, H_{Ar} B[h]Q + BPh_4), 6.75 (t, 5H, *J* = 7.0 Hz, H_{Ar} B[h]Q + BPh_4), 2.0 (s, 3H, Ir-NC*Me*), 1.72 (s, 15H, Cp-*Me*$_5$). **^{11}B (128 MHz, 298 K, $CDCl_3$)**: δ = –6.5 (m). **HRMS-ESI calcd for $C_{25}H_{26}IrN_2$** ([**4**]$^+$) (m/z): 547.1721. **Found**: 547.1758. **HRMS-ESI calcd for $C_{24}H_{20}B$** ([BPh_4]$^-$) (m/z): 319.1657. **Found**: 319.1655.

6.2.5.9 [**4**][OTf]

Using the general procedure **III**, [**4**][OTf] was prepared by using the following conditions: **3** (93.5 mg, 0.173 mmol), Ag[OTf] (342,2 mg, 0.173 mmol), room temperature for 2 h. After washing tree times with *n*-pentane, [**4**][OTf] was obtained as a yellow powder in 76% yield (113 mg). **Anal. Calcd for $C_{26}H_{26}F_3IrN_2O_3S\cdot1/10(CH_2Cl_2)$**: C, 44.51; H, 3.75; N, 3.98. Found: C, 44.81;

H, 3.77; N, 4.03. **^{1}H (400 MHz, 298 K, $CDCl_3$)**: δ = 8.44 (d, 1H, J = 8.9 Hz, H_{Ar} B[h]Q), 8.27 (d, 1H, J = 8.7 Hz, H_{Ar} B[h]Q), 7.95 (m, 5H, H_{Ar} B[h]Q), 7.70 (t, 1H, J = 8.1 Hz, H_{Ar} B[h]Q), 7.37 (t,1H, J = 7.3 Hz, H_{Ar} B[h]Q), 7.29 (d, 1H, J = 7.6 Hz, H_{Ar} B[h]Q), 2.43 (s, 3H, Ir-NC*Me*), 1.58 (s, 15H, Cp-*Me$_5$*). **^{13}C (126 MHz, 298 K, $CDCl_3$)**: δ = 156.8 (C, B[h]Q), 154.4 (C, B[h]Q), 151.6 (*C*–H, B[h]Q), 142.1 (C, B[h]Q), 137.7 (*C*–H, B[h]Q),134.2 (C, B[h]Q), 132.7 (*C*–H, B[h]Q), 130.7 (*C*–H, B[h]Q), 129.9 (*C*–H, B[h]Q), 127.3 (C, B[h]Q), 123.9 (*C*–H, B[h]Q), 123.3 (*C*–H, B[h]Q), 121.9 (*C*–H, B[h]Q), 119.0 (Ir-N*C*Me), 91.1 (*Cp*-Me$_5$), 9.0 (Cp-*Me$_5$*), 4.1 (Ir-NC*Me*). **^{19}F{1H} (282 MHz, 298 K, $CDCl_3$)**: δ = –78.9 (C*F*$_3$, [OTf]). **HRMS-ESI (m/z) calcd for $C_{25}H_{26}IrN_2$** ([**4**]$^+$): 547.1721. **Found**: 547.1655. **HRMS-ESI (m/z) calcd for CF_3O_3S** ([OTf]$^-$): 148.9515. **Found**: 148.9530.

6.2.5.10 [**6**][$BArF_{24}$]

The ionic iridacycle [**6**][$BArF_{24}$] was prepared following the general procedure **III**: **5** (100 mg, 0.162 mmol) and Na[$BArF_{24}$] (146.0 mg, 0.176 mmol), room temperature, 3 h. After one recrystallization with a mixture of CH_2Cl_2 and *n*-pentane (~ –20 °C) and washing three times with *n*-pentane, [**6**][$BArF_{24}$] was isolated as a yellowish powder in 61% yield (147 mg). Monocrystals were grown by slow diffusion of *n*-heptane and benzene into a solution of [**6**][$BArF_{24}$] in 1,2-dichloroethane. **Anal. Calcd for $C_{61}H_{51}BF_{24}IrN_3 \cdot 4/5(CH_2Cl_2)$**: C, 47.80; H, 3.41; N, 2.71. **Found**: C, 47.64; H, 3.89; N, 2.62. **^{1}H NMR (500 MHz, 298 K, $CDCl_3$)**: δ = 8.25 (d, 1H, J = 6.3 Hz, H–C=N ^{tBu}PhPy), 7.68 (m, 8H, $BArF_{24}$), 7.58 (m, 1H, H_{Ar} ^{tBu}PhPy), 7.54 (d, 1H, J = 8.6 Hz, HAr ^{tBu}PhPy), 7.50 (m, 4 H, $BArF_{24}$), 6.96–6.97 (m, 2H, H_{Ar} ^{tBu}PhPy), 6.52 (dd, 1H, J_1 = 8.6 Hz, J = 2.5 Hz, H_{Ar} ^{tBu}PhPy), 3.03 (s, 6H, NMe_2 of ^{tBu}PhPy), 2.13 (s, 3H, IrNC*Me*), 1.60 (s, 15H, Cp-*Me$_5$*), 1.33 (s, 9H, ^{t}Bu of ^{tBu}PhPy). **^{13}C NMR (126 MHz, 298K, $CDCl_3$)**: δ = 167.5 (C, ^{tBu}PhPy), 163.5 (C, ^{tBu}PhPy), 161.3 (1:1:1:1 quartet, *C*–B $BArF_{24}$, $^1J_{C-B}$ = 49.8 Hz), 157.9 (C, ^{tBu}PhPy), 152.4 (C, ^{tBu}PhPy), 150.2 (H–*C*=N, ^{tBu}PhPy), 134.9 (*C*–H, ^{tBu}PhPy), 132.7 (C, ^{tBu}PhPy), 129.0 (q, *C*–CF_3 $BArF_{24}$, $^2J_{C-F}$ = 32.1 Hz), 125.7 (*C*–H, ^{tBu}PhPy), 124.7(q, *C*F_3 $BArF_{24}$, $^1J_{C-F}$ = 273.0 Hz), 118.9 (*C*–H, ^{tBu}PhPy), 117.6 (m, *C*$_{H\text{-}para}$ $BArF_{24}$), 117.1 (Ir-N*C*Me), 114.1 (*C*–H, ^{tBu}PhPy), 108.1 (*C*–H, ^{tBu}PhPy), 91.0 (*Cp*-Me_5), 40.3 (*C*H_3, NMe_2 of ^{tBu}PhPy), 35.3 (*C*$(CH_3)_3$, ^{t}Bu of ^{tBu}PhPy), 30.4 (C(*C*$H_3)_3$, ^{t}Bu of ^{tBu}PhPy), 8.8 (Cp-*Me$_5$*), 3.7 (Ir-NC*Me*). **^{19}F NMR (282 MHz, 298 K, CD_2Cl_2)**: δ = –63.8 (s, CF_3 $BArF_{24}$). **^{11}B NMR (128 MHz, 298 K, $CDCl_3$)**: δ = –6.61 (m). **HRMS-ESI calcd for $C_{29}H_{39}IrN_3$** ([**4**]$^+$) (m/z): 622.2769. **Found**: 622.2720. **HRMS-ESI calcd for $C_{32}H_{12}BF_{24}$** ([$BArF_{24}$]$^-$) (m/z): 863.0649. **Found**: 863.0664.

6.2.5.11 [**8**][$BArF_{24}$]

The ionic iridacycle [**8**][$BArF_{24}$] was prepared following the general procedure **III**: **7** (100 mg, 0.169 mmol) and Na[$BArF_{24}$] (150.0 mg, 0.169 mmol), 50 °C, 5 h. After one recrystallization with a mixture of CH_2Cl_2 and *n*-pentane (~ –30 °C) and washing one time with *n*-pentane, [**8**][$BArF_{24}$] was isolated as an orange/yellow powder. **Anal. Calcd for $C_{61}H_{40}BF_{24}IrN_2$•4/5(CH_2Cl_2)**: C, 48.58; H, 2.74; N, 1.83. **Found**: C, 48.22; H, 2.70; N, 1.59. **^{1}H (500 MHz, 298 K, acetone-d_6)**: δ = 9.33 (d, 1H, J = 8.3 Hz, H_{Ar}), 9.28 (d, 1H, J = 5.5 Hz, H_{Ar}), 8.86 (t, 2H, J = 7.6 Hz, H_{Ar}), 8.46 (d, 1H, J = 8.0 Hz, H_{Ar}), 8.13 (d, 1H, J = 7.3 Hz, H_{Ar}), 7.85–7.91 (m, 2H, H_{Ar}), 7.79 (m; 1H_{Ar} + 8H $BArF_{24}$), 7.73 (t, 1H, J = 7.5 Hz, H_{Ar}), 7.68 (m, 4H, $BArF_{24}$), 2.41 (s, 3H, Ir-NC*Me*), 1.86 (s, 15H, Cp-*Me*$_5$). **^{13}C NMR (126 MHz, 298 K, acetone-d_6)**: δ = 162.6 (1:1:1:1 quartet, *C*–B $BArF_{24}$, $^1J_{C-B}$ = 49.6 Hz), 158.7 (C, Ar), 156.3 (C, Ar), 152.4 (H–*C*=N, Ar), 141.3 (C, Ar), 135.5 (*C*–H, Ar), 134.64 (*C*–H, Ar), 134.58 (*C*–H, Ar), 133.1 (C, Ar), 132.22 (C, Ar, overlapping signal), 132.19 (*C*–H, Ar, overlapping signal), 130.1 (*C*–H, Ar), 130.0 (q, *C*–CF_3 $BArF_{24}$, $^2J_{C-F}$ = 32.3 Hz), 128.8 (*C*–H, Ar), 128.7 (C, Ar), 127.4 (C, Ar), 125.4 (q, *C*F_3 $BArF_{24}$, $^1J_{C-F}$ = 271.5 Hz), 125.0 (*C*–H, Ar), 124.9 (*C*–H, Ar), 124.4 (*C*–H, Ar), 118.4 (m, *C*$_{H\text{-}para}$ $BArF_{24}$), 118.3 (Ir-N*C*Me), 92.3 (*Cp*-Me_5), 10.0 (Cp-*Me*$_5$), 3.4 (Ir-NC*Me*). **^{19}F{^{1}H} (282 MHz, 298 K, acetone-d_6)**: δ = –64.22 (s, C*F*$_3$ $BArF_{24}$). **^{11}B NMR (128 MHz, 298 K, acetone-d_6)**: δ = –6.54 (m). **HRMS-ESI calcd for $C_{29}H_{28}IrN_2$** ([**8**]$^+$) (m/z): 597.1887. **Found**: 597.1914. **HRMS-ESI calcd for $C_{32}H_{12}BF_{24}$** ([$BArF_{24}$]$^-$) (m/z): 863.0649. **Found**: 863.0649.

6.2.5.12 [**10**][$BArF_{24}$]

The ionic iridacycle [**10**][$BArF_{24}$] was prepared following the general procedure **III**: **9** (150 mg, 0.27 mmol) and Na[$BArF_{24}$] (240 mg, 0.27 mmol), room temperature, 20 h. After washing three times with *n*-pentane, [**10**][$BArF_{24}$] was isolated as an orange/red powder in 75% yield (289 mg). **Anal. Calcd for $C_{58}H_{40}BF_{24}IrN_2$•1/2(CH_2Cl_2)**: C, 47.92; H, 2.82; N, 1.91. **Found**: C, 47.80; H, 2.87; N, 1.86. **^{1}H (400 MHz, 298 K, $CDCl_3$)**: δ = 8.52 (d, 1H, J = 5.8 Hz, H_{Ar}), 7.96 (d, 1H, J = 8.0 Hz, H_{Ar}), 7.81 (t, 1H, J = 8.0 Hz, H_{Ar}), 7.70 (m; 8H, $BArF_{24}$), 7.66 (d, 1H, J = 8.0 Hz, H_{Ar}), 7.55 (d, 1H, J = 8.0 Hz, H_{Ar}), 7.53 (m, 4H, $BArF_{24}$), 7.38 (t, 1H, J = 7.5 Hz, H_{Ar}), 7.21 (t, 1H, J = 7.5 Hz, H_{Ar}), 7.01 (m, 1H, H_{Ar}), 4.09 (d, 1H, J = 23.5 Hz, C*H*$_2$ of C,N ligand), 3.73 (d, 1H, J = 23.5 Hz, C*H*$_2$ of C,N ligand), 2.13 (s, 3H, Ir-NC*Me*), 1.72 (s, 15H, Cp-*Me*$_5$). **^{13}C NMR (126 MHz, 298 K, acetone-d_6)**: δ =1861 (C, Ar), 164.0 (C, Ar), 162.6 (1:1:1:1 quartet, *C*–B $BArF_{24}$, $^1J_{C-B}$ = 49.7 Hz), 154.0 (H–*C*=N, Ar), 148.5 (C, Ar), 147.0 (C, Ar), 142.5 (C, Ar), 140.8

(*C*–H, Ar), 135.5 (*C*–H, Ar), 134.58 (*C*–H, Ar), 130.0 (q, *C*–CF_3 $BArF_{24}$, $^2J_{C-F}$ = 31.5 Hz), 127.1 (*C*–H, Ar), 126.4 (C, Ar), 127.4 (C, Ar), 125.5 (q, *C*F_3 $BArF_{24}$, $^1J_{C-F}$ = 271.8 Hz), 124.7 (*C*–H, Ar), 123.9 (*C*–H, Ar), 122.4 (*C*–H, Ar), 120.5 (*C*–H, Ar), 118.5 (m, *C*$_{H\text{-}para}$ $BArF_{24}$), 118.1 (Ir-N*C*Me), 92.8 (*Cp*-Me_5), 45.2 (*C*H_2 of C,N ligand), 9.2 (Cp-*Me*$_5$), 3.5 (Ir-NC*Me*). **$^{19}F\{^1H\}$ (282 MHz, 298 K, acetone-d_6)**: δ = –64.22 (s, C*F*$_3$ $BArF_{24}$). **^{11}B NMR (128 MHz, 298 K, acetone-d_6)**: δ = –6.54 (m). **HRMS-ESI calcd for $C_{26}H_{28}IrN_2$** ([**10**]$^+$) (m/z): 561.1887. **Found**: 561.1887. **HRMS-ESI calcd for $C_{32}H_{12}BF_{24}$** ($[BArF_{24}]^-$) (m/z): 863.0649. **Found**: 863.0675.

6.2.5.13 [**12**][OTf]

The ionic iridacycle [**12**][OTf] was prepared following the general procedure **III**: **9** (150 mg, 0.27 mmol) and Ag[OTf] (240 mg, 0.27 mmol), room temperature, 2 h. After washing three times with *n*-pentane, [**12**][OTf] was isolated as a yellowish powder in 90% yield (89 mg). **^1H NMR (400 MHz, 298 K, $CDCl_3$)**: δ = 8.44 (d, 1H, *J* = 8.9 Hz, H_{Ar}), 8.27 (d, 1H, J = 8.7 Hz, H_{Ar}), 7.95 (m, 5H, H_{Ar}), 7.70 (t, 1H, *J* = 8.1 Hz, H_{Ar}), 7.37 (t,1H, *J* = 7.3 Hz, H_{Ar}), 7.29 (d, 1H, *J* = 7.6 Hz, H_{Ar}), 2.43 (s, 3H, Ir-NC*Me*), 1.58 (s, 15H, Cp-*Me*$_5$). **$^{19}F\{^1H\}$ (300 MHz,298 K, $CDCl_3$):** δ = –78.90.

6.2.6 Synthesis of the ionic rhodacycle [**2'**][$BArF_{24}$]

The ionic rhodacycle [**2'**][$BArF_{24}$] was prepared following the general procedure **III**: **1'** (100 mg, 0.23 mmol) and Na[$BArF_{24}$] (208 mg, 0.23 mmol), room temperature, 18 h. After one recrystallization with a mixture of CH_2Cl_2 and *n*-hexane (~ –20 °C), [**2'**][$BArF_{24}$] was isolated as a yellowish powder in 63% yield (191 mg). Monocrystals were grown by slow diffusion of *n*-heptane and benzene into a solution of [**2'**][$BArF_{24}$] in 1,2-dichloroethane. **Anal. Calcd for $C_{55}H_{38}BF_{24}RhN_2 \cdot 3/4(CH_2Cl_2)$**: C, 49.23; H, 2.93; N, 2.06. **Found**: C, 49.29; H, 2.90; N, 2.05. **^1H NMR (400 MHz, 298 K, acetone-d_6)**: δ = 8.97 (d, 1H, *J* = 5.3 Hz, H–C=N PhPy), 8.18 (d, 1H, *J* = 8.2 Hz, H_{Ar} PhPy), 8.10 (t, 1H, *J* = 7.7 Hz, H_{Ar} PhPy), 7.88 (d, 2H, *J* = 7.7 Hz, H_{Ar} PhPy), 7.79 (m, 8H, H_{Ar} $BArF_{24}$), 7.67 (m, 4H, $BArF_{24}$), 7.62 (t, 1H, *J* = 6.7 Hz, H_{Ar} PhPy), 7.34 (t, 1H, *J* = 7.4 Hz, H_{Ar} PhPy), 7.22 (t, 1H, *J* = 7.5 Hz, H_{Ar} PhPy), 2.40 (s, 3H, Ir-NC*Me*), 1.72 (s, 15H, Cp-*Me*$_5$). **^{19}F NMR (282 MHz, 298 K, CD_2Cl_2)**: δ = –63.8 (s, CF_3 $BArF_{24}$). **^{11}B NMR (128 MHz, 298 K, CD_2Cl_2)**: δ = –6.6. **HRMS-ESI calcd for $C_{23}H_{26}RhN_2$** ([**2'**]$^+$) (m/z): 433.1146. **Found**: 433.1141. **HRMS-ESI calcd for $C_{32}H_{12}BF_{24}$** ($[BArF_{24}]^-$) (m/z): 863.0649. **Found**: 863.0647.

6.2.7 Isolation and characterization of the ionic iridacycle [**2C**][$BArF_{24}$]

In a Schlenk flask, to a solution of [**2**][$BArF_{24}$] (50 mg, 0.036 mmol) in CH_2Cl_2 (~5mL) was dropwise added $HSiEt_3$ (11.5 μl, 0.072 mmol). The color of the solution changed from yellow to red immediately after addition of $HSiEt_3$. The resulting mixture was vigorously stirred at room temperature for 25 minutes. The ^1H analysis (CD_2Cl_2) of this sample showed the formation of [**2B**][$BArF_{24}$] as major product, along with **6** as the product of the bishydrosilylation of CH_3CN. The solvent was then removed under vacuum affording a red/orange powderous sample. Without further purification, then a crystallization of [**2B**][$BArF_{24}$] was attempted by diffusion of *n*-pentane vapors into a solution of CH_2Cl_2 containing the sample. After a storage of the latter tube at –30 °C for a couple of days, yellow crystals were isolated after removal of the liquor. Analysis of the latter crystals revealed to be [**2C**][$BArF_{24}$], instead of [**2B**][$BArF_{24}$]. Full analytic data of crystalline [**2C**][$BArF_{24}$] are as follows: **Anal. Calcd for $C_{55}H_{44}BF_{24}IrN_2$**: C, 47.53; H, 3.05; N, 2.02. **Found**: C, 47.58; H, 3.13; N, 1.86. **^1H NMR (500 MHz, 298 K, CD_2Cl_2)**: δ = 8.61 (d, 1H, J = 5.6 Hz, H–C=N PhPy), 7.97 (d, 1H, J = 8.1 Hz, H_{Ar} PhPy), 7.89 (t, 1H, J = 7.7 Hz, H_{Ar} PhPy), 7.78 (d, 1H, J = 7.7 Hz, H_{Ar} PhPy), 7.74 (m, 1H, H_{Ar} PhPy), 7.72 (m, 8H, H_{Ar} $BArF_{24}$), 7.56 (m, 4H, $BArF_{24}$), 7.22–7.32 (m, 3H, H_{Ar} PhPy), 2.66 (bs, 1H, N$\underline{H_2}$ of $Et(H)_2N$-Ir), 2.54 (bs, 1H, N$\underline{H_2}$ of $Et(H)_2N$-Ir), 2.49 (m, 1H, C$\underline{H_2}$ of $Et(H)_2N$-Ir), 2.36 (m, 1H, C$\underline{H_2}$ of $Et(H)_2N$-Ir), 1.67 (s, 15H, Cp-$\underline{Me_5}$), 0.93 (t, 1H, J = 7.1 Hz, C$\underline{H_3}$ of $Et(H)_2N$-Ir). **^{13}C NMR (126 MHz, 298 K, CD_2Cl_2)**: δ = 167.9 (C, PhPy), 162.1 (1:1:1:1 quartet, C–B $BArF_{24}$, $^1J_{C-B}$ = 50.3 Hz), 159.5 (C, PhPy), 151.7 (H–C=N, PhPy), 144.8 (C, PhPy), 139.8 ($\underline{C}$–H, PhPy), 135.8 ($\underline{C}$-H, PhPy), 135.2 (m, $\underline{C}_{H\text{-ortho}}$ $BArF_{24}$), 132.7 ($\underline{C}$–H, PhPy), 129.2 (q, $\underline{C}$–CF_3 $BArF_{24}$, $^2J_{C-F}$ = 31.8 Hz), 125.5 ($\underline{C}$–H, PhPy), 124.9 ($\underline{C}$–H, PhPy), 124.4 ($\underline{C}$–H, PhPy), 125.0 (q, $\underline{C}$–CF_3 $BArF_{24}$, $^1J_{C-F}$ = 272.3 Hz), 121.7 ($\underline{C}$–H PhPy), 120.7 ($\underline{C}$–H PhPy),117.8 (m, $\underline{C}_{H\text{-para}}$ $BArF_{24}$), 89.8 ($\underline{Cp}$-Me_5), 43.8 ($\underline{C}H_2$, $Et(H)_2N$-Ir), 18.5 ($\underline{C}H_3$, $Et(H)_2N$-Ir), 9.0 (Cp-$\underline{Me_5}$). **^{11}B NMR (128 MHz, 298 K, CD_2Cl_2)**: δ = –6.6. **MS-ESI calcd for $C_{23}H_{30}IrN_2$** ([**2C**]$^+$) (m/z): 527.20. **Found**: 527.20. **MS-ESI calcd for $C_{32}H_{12}BF_{24}$** ([$BArF_{24}$]$^-$) (m/z): 863.06. **Found**: 863.07.

6.2.8 NMR spectra of neutral iridacycles [(κ^2-(C,N)-(**L**)Ir(III)Cl]

6.2.8.1 **7**

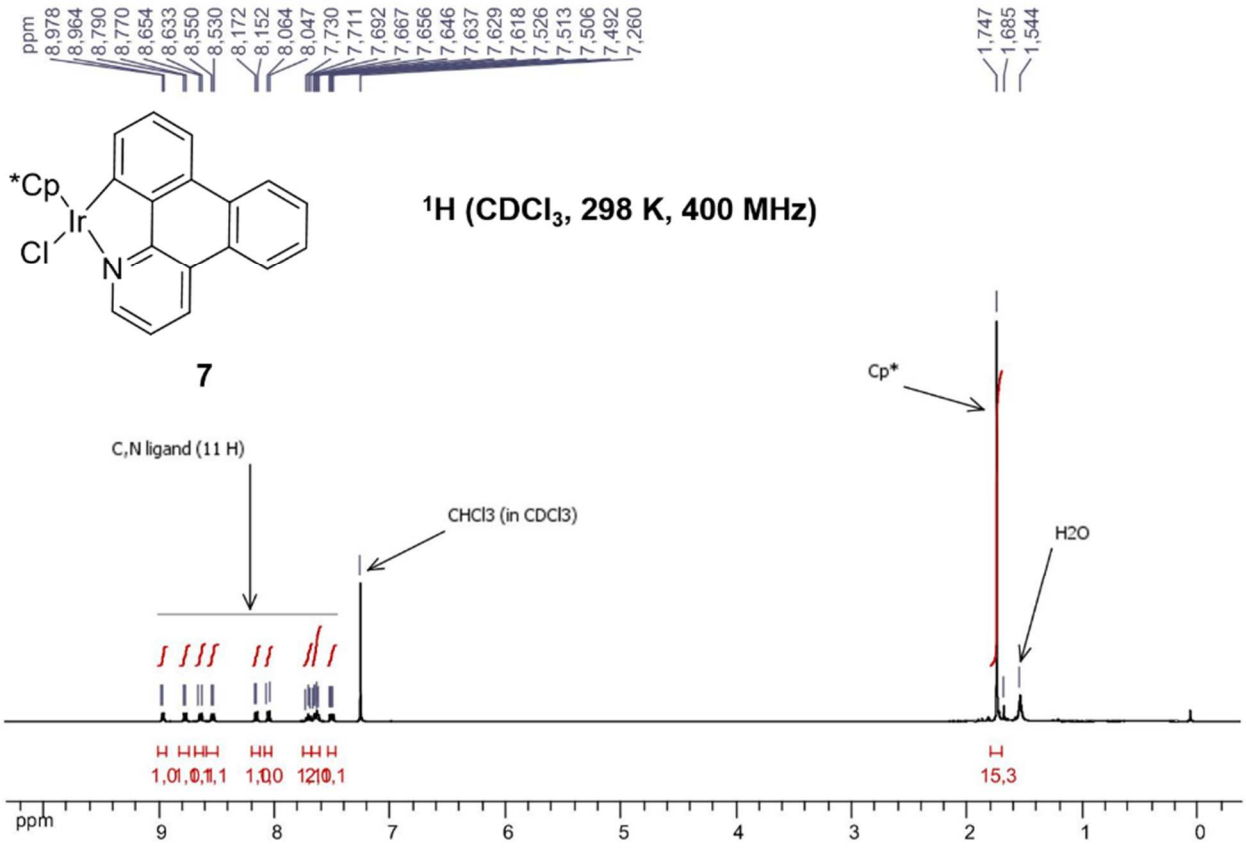
ppm
8,978
8,964
8,790
8,770
8,654
8,633
8,550
8,530
8,172
8,152
8,064
8,047
7,730
7,711
7,692
7,667
7,656
7,646
7,637
7,629
7,618
7,526
7,513
7,506
7,492
7,260
1,747
1,685
1,544
*Cp
Ir
Cl
N
7
¹H (CDCl3, 298 K, 400 MHz)
Cp*
C,N ligand (11 H)
CHCl3 (in CDCl3)
H2O
1,0
1,0
1,1
1,1
1,0
1,0
15,3
ppm
9
8
7
6
5
4
3
2
1
0

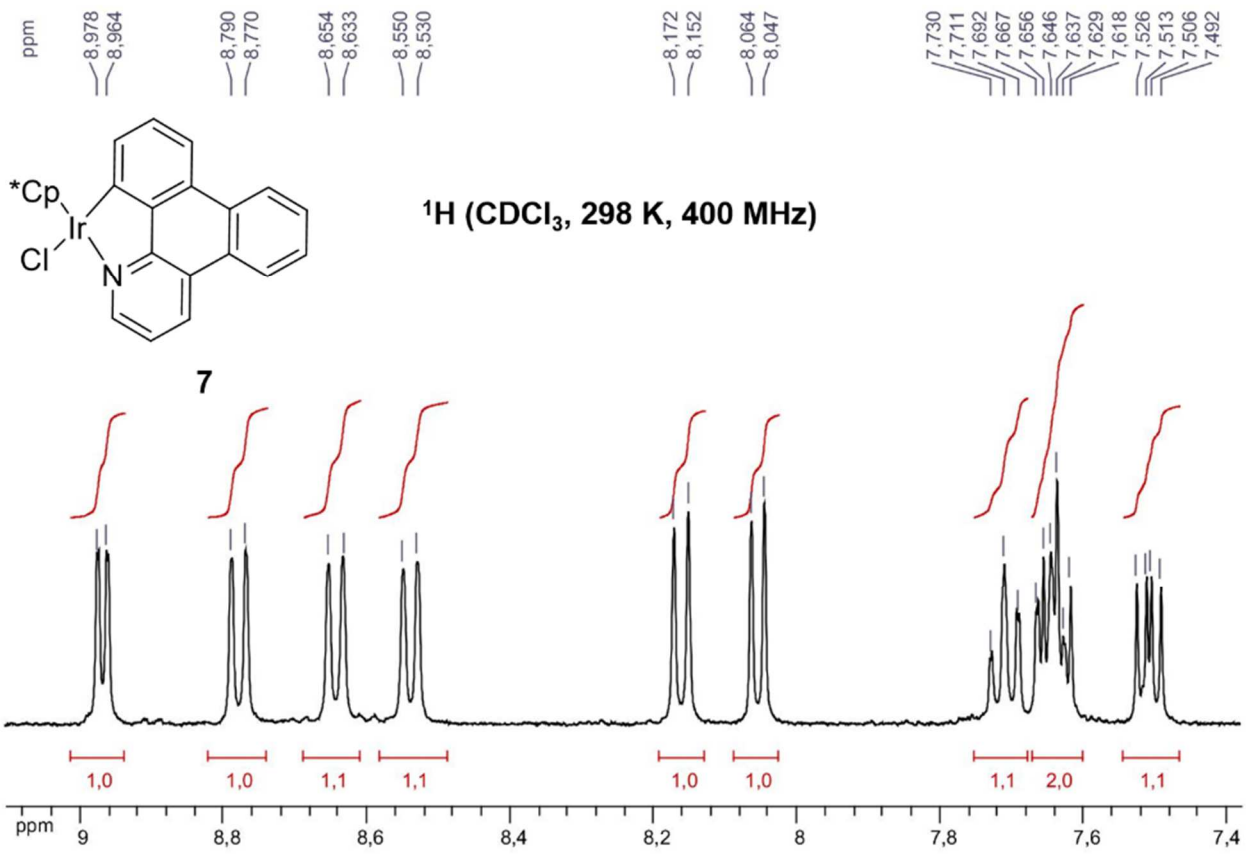
ppm
8,978
8,964
8,790
8,770
8,654
8,633
8,550
8,530
8,172
8,152
8,064
8,047
7,730
7,711
7,692
7,667
7,656
7,646
7,637
7,629
7,618
7,526
7,513
7,506
7,492
*Cp
Ir
Cl
N
7
¹H (CDCl3, 298 K, 400 MHz)
1,0
1,0
1,1
1,1
1,0
1,0
1,1
2,0
1,1
ppm
9
8,8
8,6
8,4
8,2
8
7,8
7,6
7,4

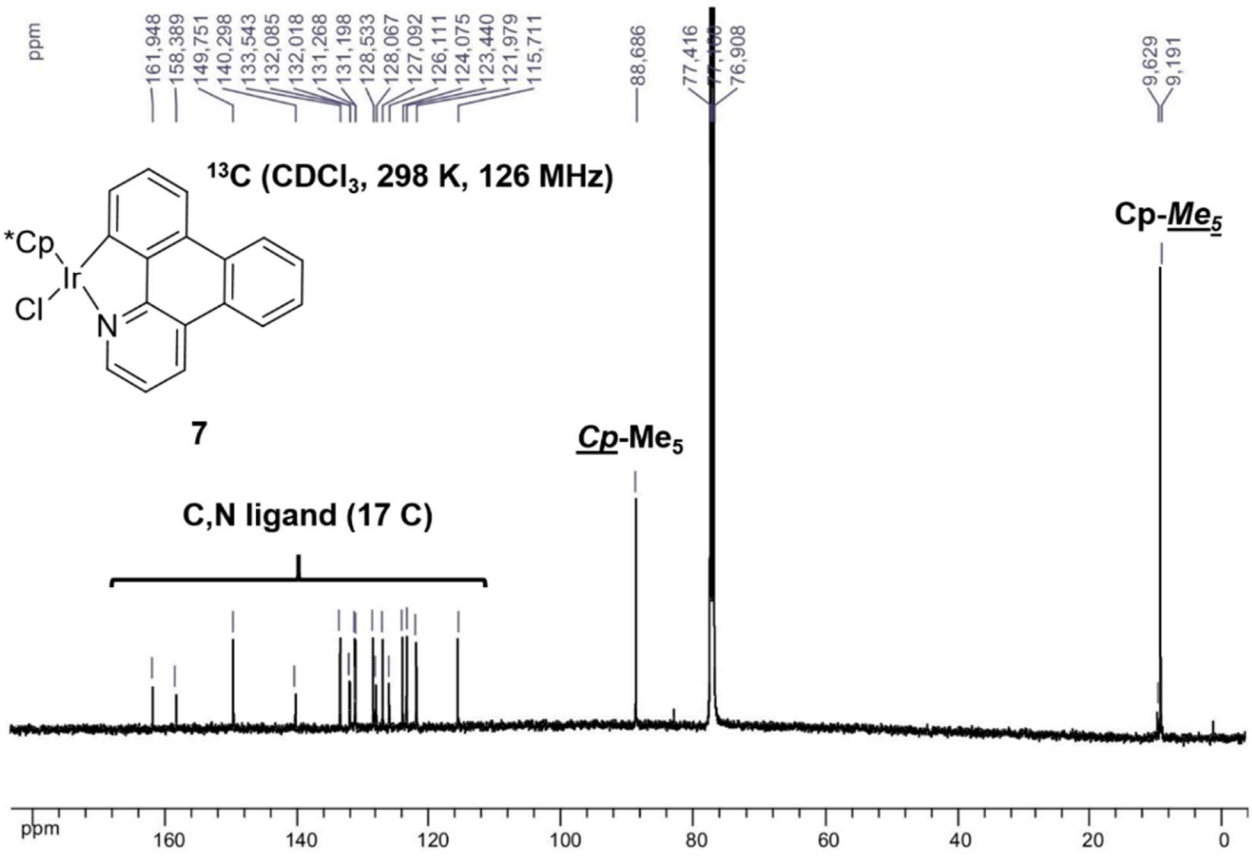
ppm
161,948
158,389
149,751
140,298
133,543
132,085
132,018
131,268
131,198
128,533
128,067
127,092
126,111
124,075
123,440
121,979
115,711
88,686
77,416
76,908
9,629
9,191
13C (CDCl3, 298 K, 126 MHz)
*Cp
Ir
Cl
N
7
Cp-Me5
Cp-Me5
C,N ligand (17 C)
ppm
160
140
120
100
80
60
40
20
0

6.2.8.2 **9**

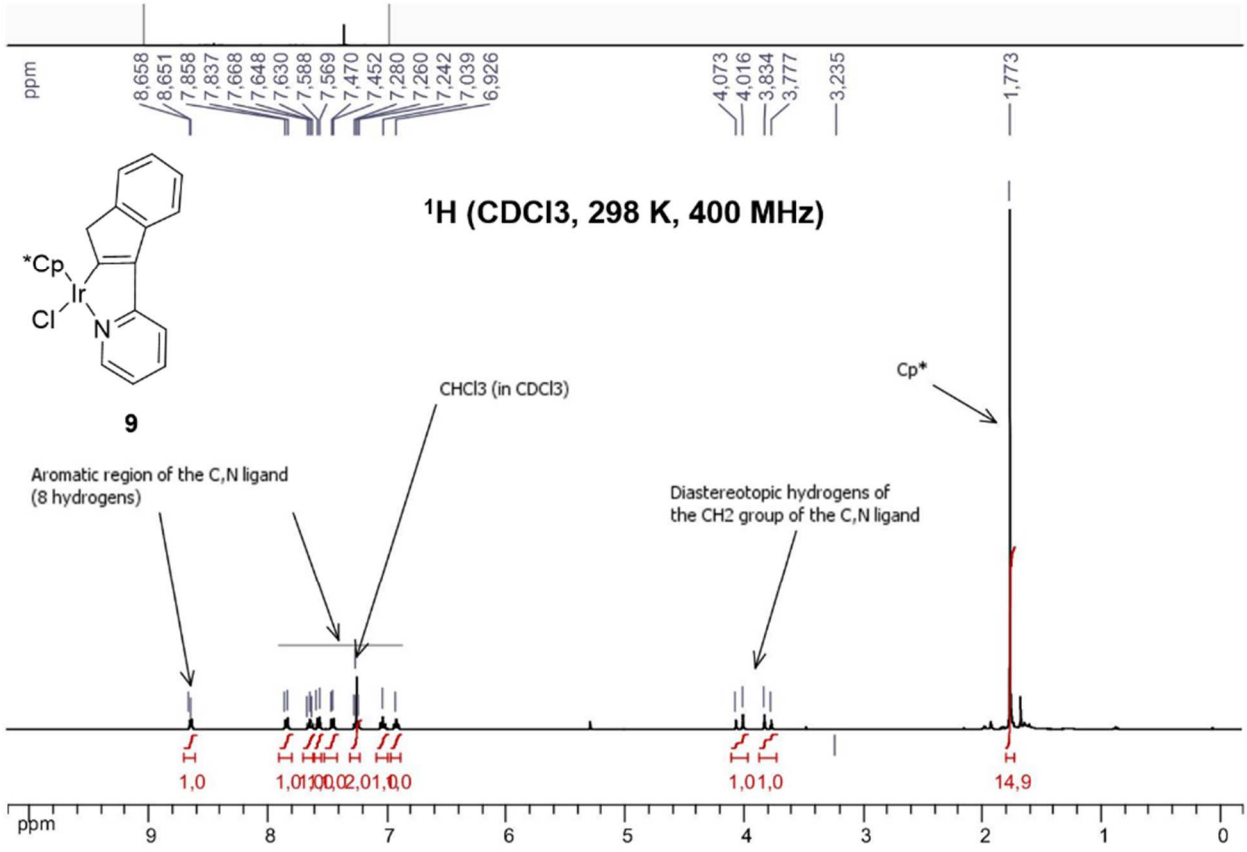
ppm
8,658
8,651
7,858
7,837
7,668
7,648
7,630
7,588
7,569
7,470
7,452
7,280
7,260
7,242
7,039
6,926
4,073
4,016
3,834
3,777
3,235
1,773
*Cp
Ir
Cl
N
9
¹H (CDCl3, 298 K, 400 MHz)
CHCl3 (in CDCl3)
Cp*
Aromatic region of the C,N ligand
(8 hydrogens)
Diastereotopic hydrogens of
the CH2 group of the C,N ligand
1,0
1,01,0
14,9
ppm
9
8
7
6
5
4
3
2
1
0

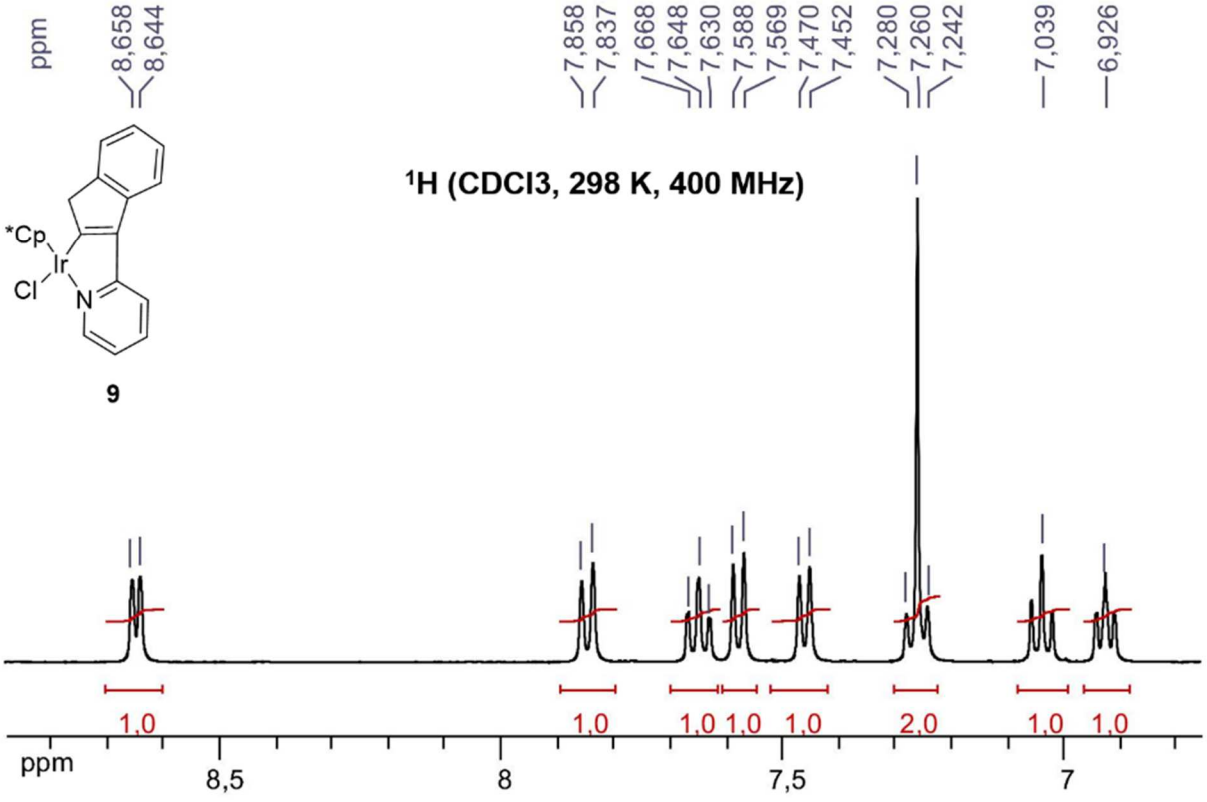
ppm
8,658
8,644
7,858
7,837
7,668
7,648
7,630
7,588
7,569
7,470
7,452
7,280
7,260
7,242
7,039
6,926
*Cp
Ir
Cl
N
9
¹H (CDCl3, 298 K, 400 MHz)
1,0
1,0
1,0
1,0
1,0
2,0
1,0
1,0
ppm
8,5
8
7,5
7

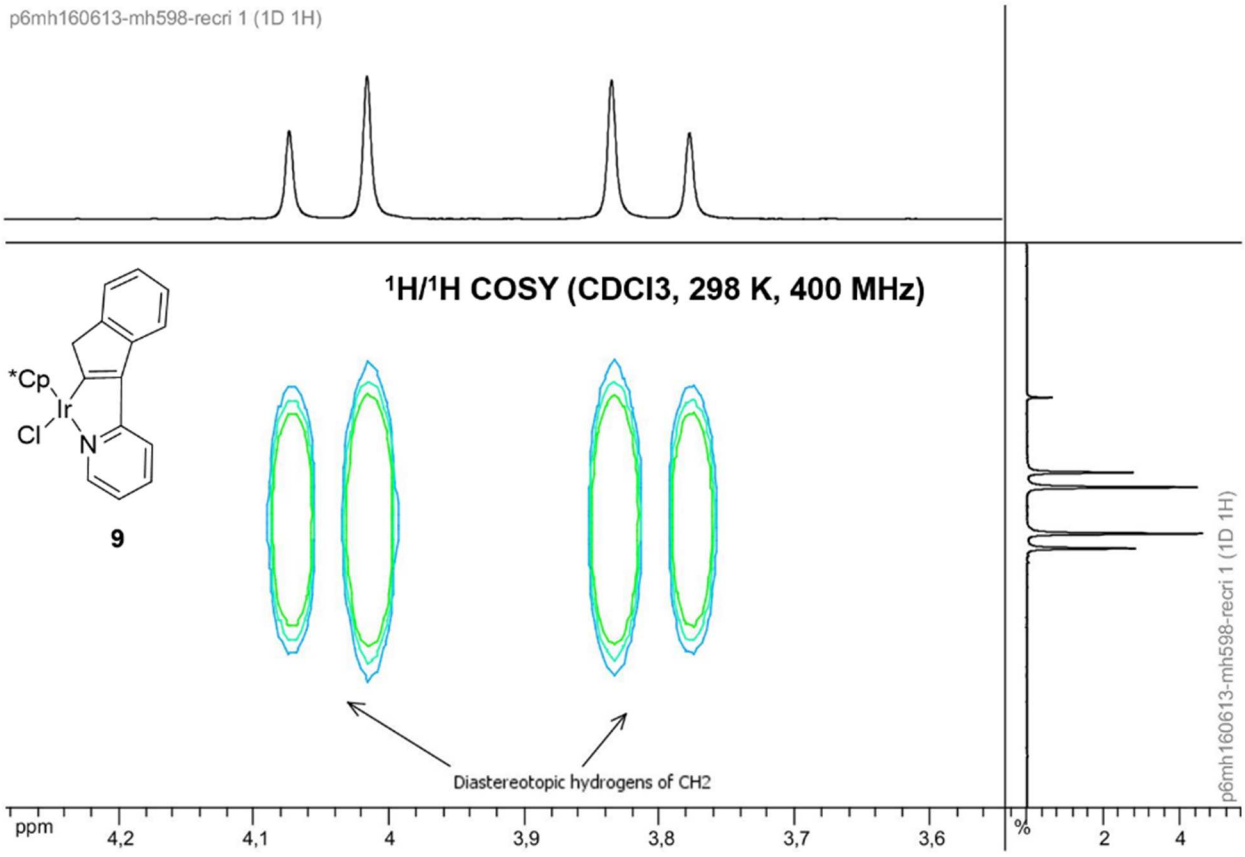
p6mh160613-mh598-recri 1 (1D 1H)
^{1}H/^{1}H COSY (CDCl3, 298 K, 400 MHz)
*Cp
Ir
Cl
N
9
Diastereotopic hydrogens of CH2
ppm
4,2
4,1
4
3,9
3,8
3,7
3,6
%
2
4
p6mh160613-mh598-recri 1 (1D 1H)

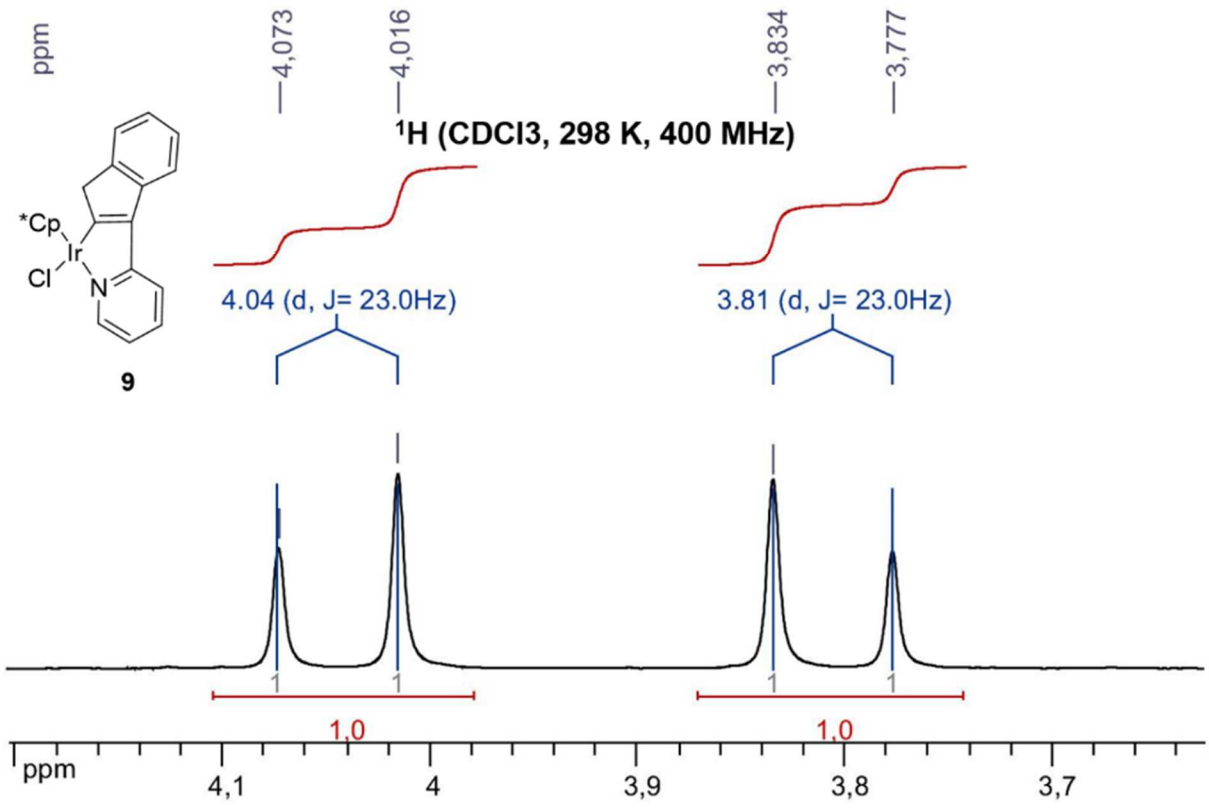
ppm
4,073
4,016
3,834
3,777
^{1}H (CDCl3, 298 K, 400 MHz)
*Cp
Ir
Cl
N
9
4.04 (d, J= 23.0Hz)
3.81 (d, J= 23.0Hz)
1
1
1
1
1,0
1,0
ppm
4,1
4
3,9
3,8
3,7

6.2.9 NMR spectra of ionic iridacycles [(κ^2-(C,N)-(**L**)Ir(III)NCMe][X]

6.2.9.1 [**2**][BArF$_{24}$]

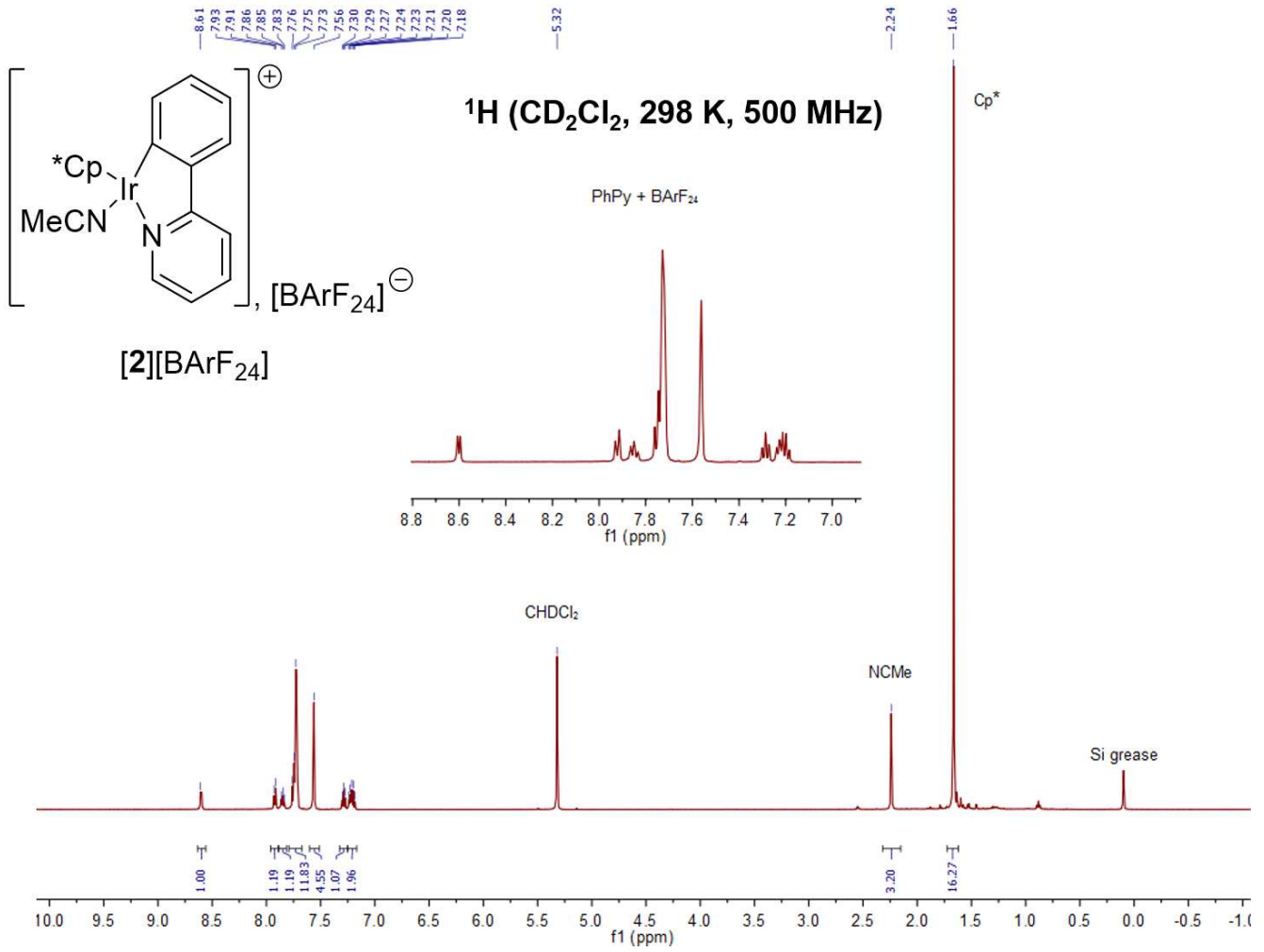

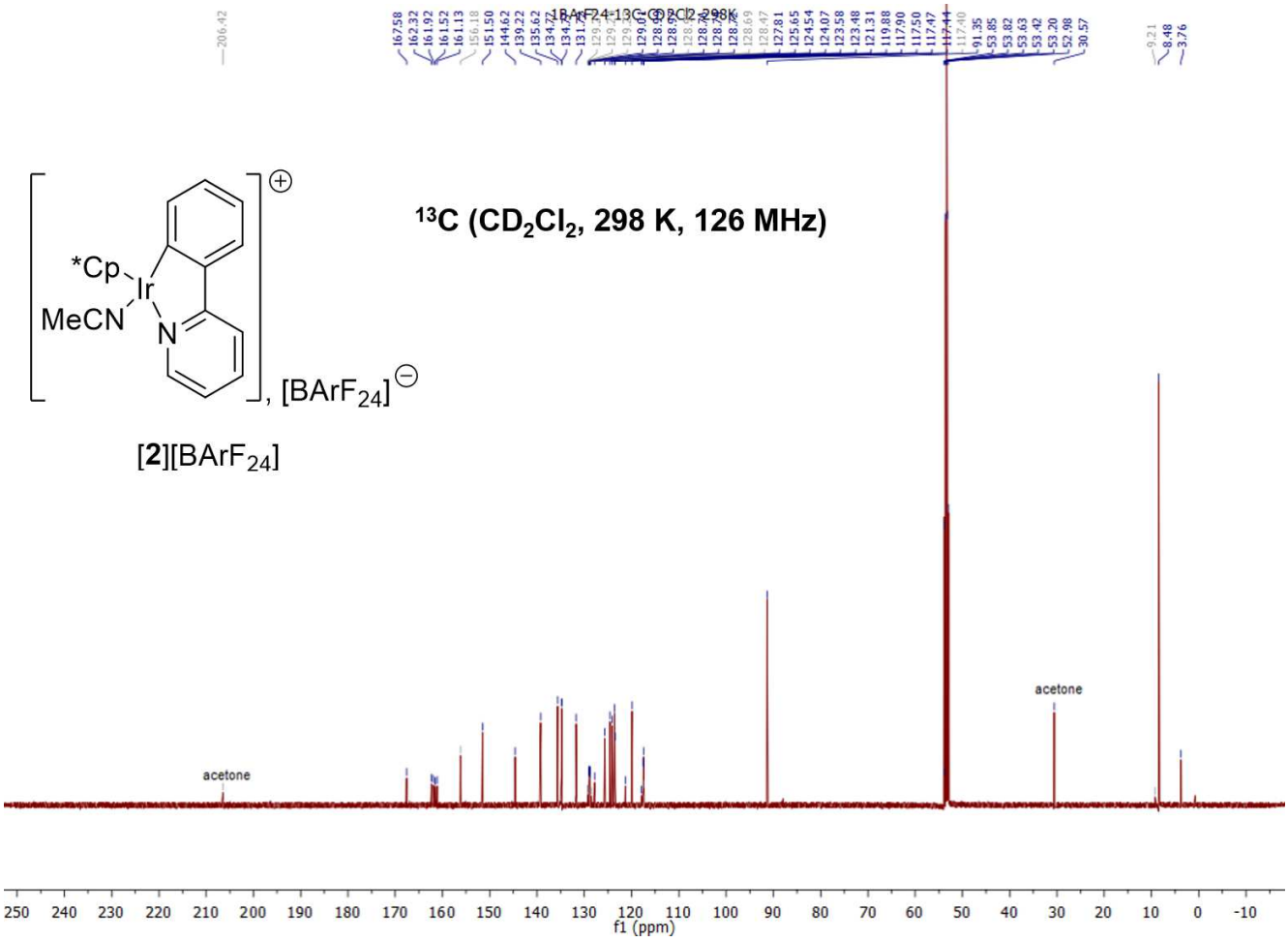
*Cp
Ir
MeCN
N
, [BArF24]
[2][BArF24]
13C (CD2Cl2, 298 K, 126 MHz)
acetone
acetone
f1 (ppm)

1BArF24-19F-CD2Cl2-298K

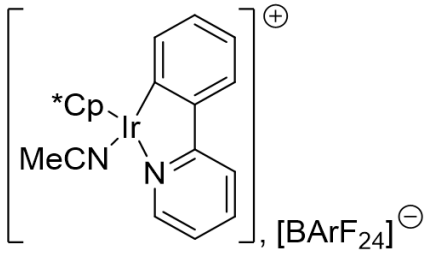

[**2**][$BArF_{24}$]

^{19}F (CD_2Cl_2, 298 K, 282 MHz)

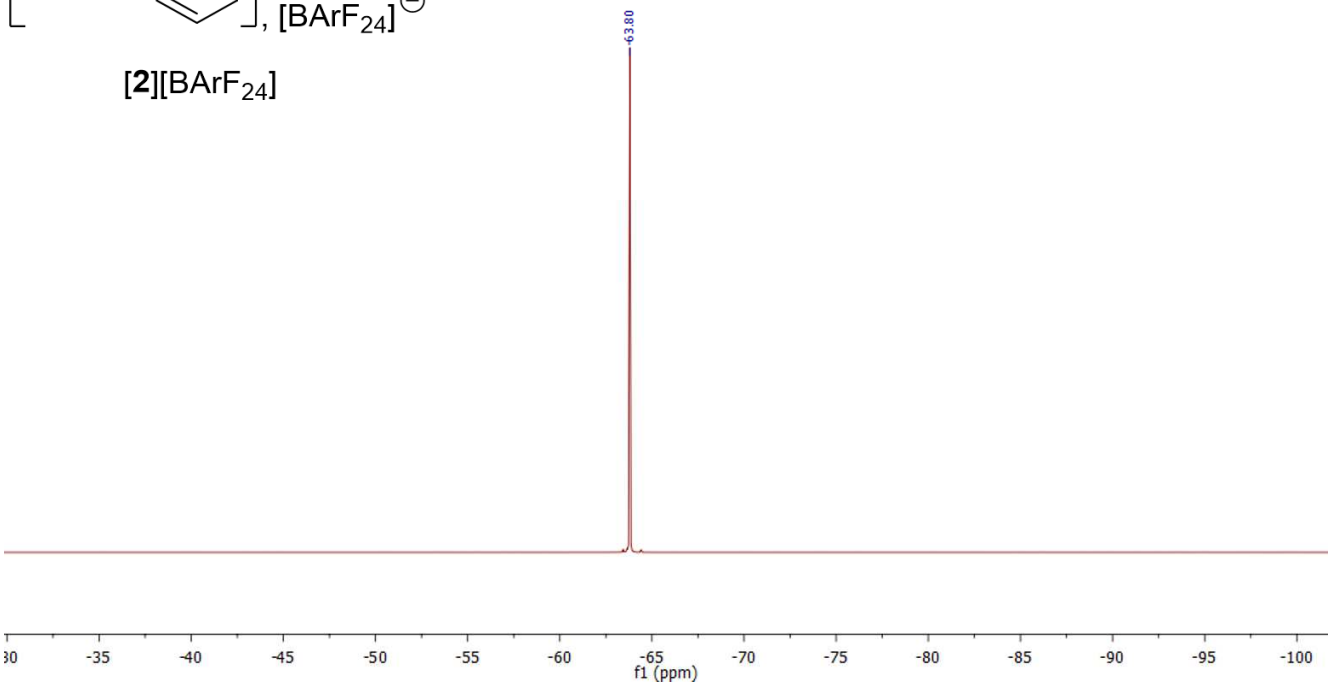

1BArF24-11B-CD2Cl2-298K

^{11}B (CD_2Cl_2, 298 K, 128 MHz)

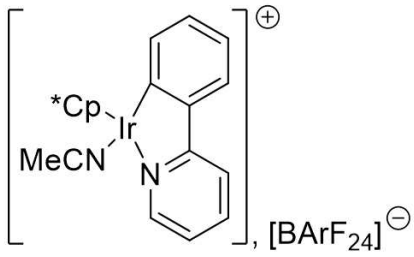

[**2**][$BArF_{24}$]

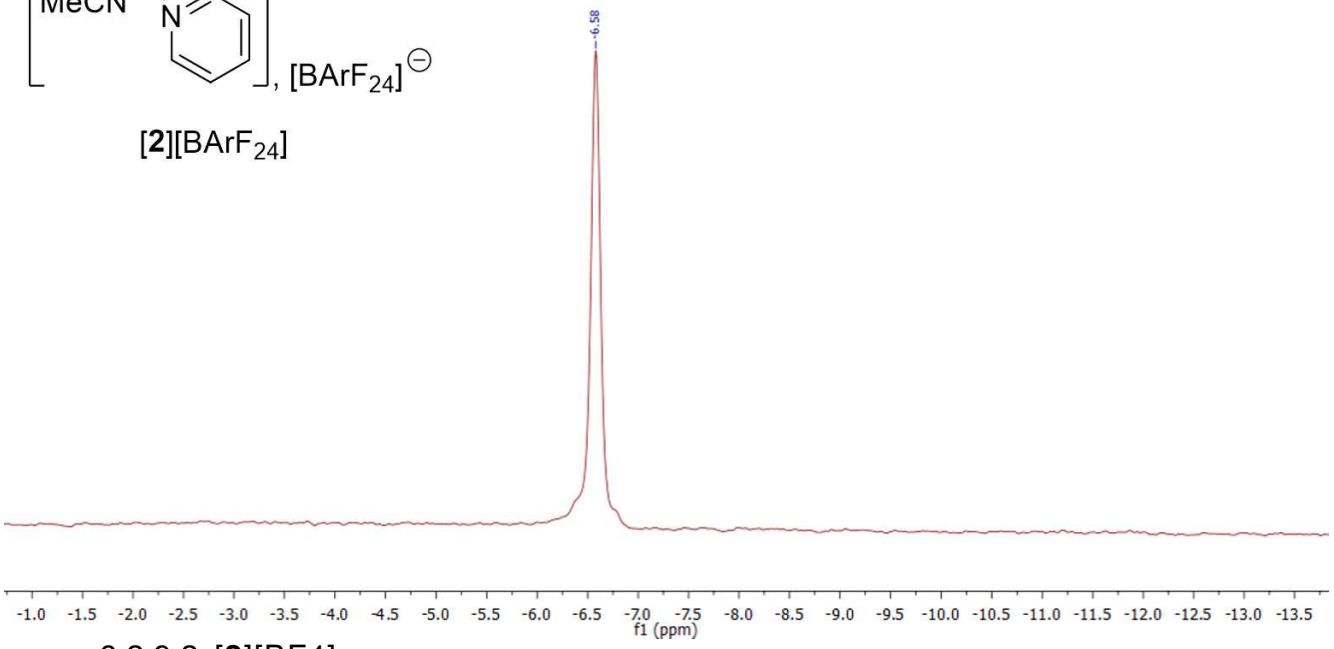

6.2.9.2 [**2**][BF4]

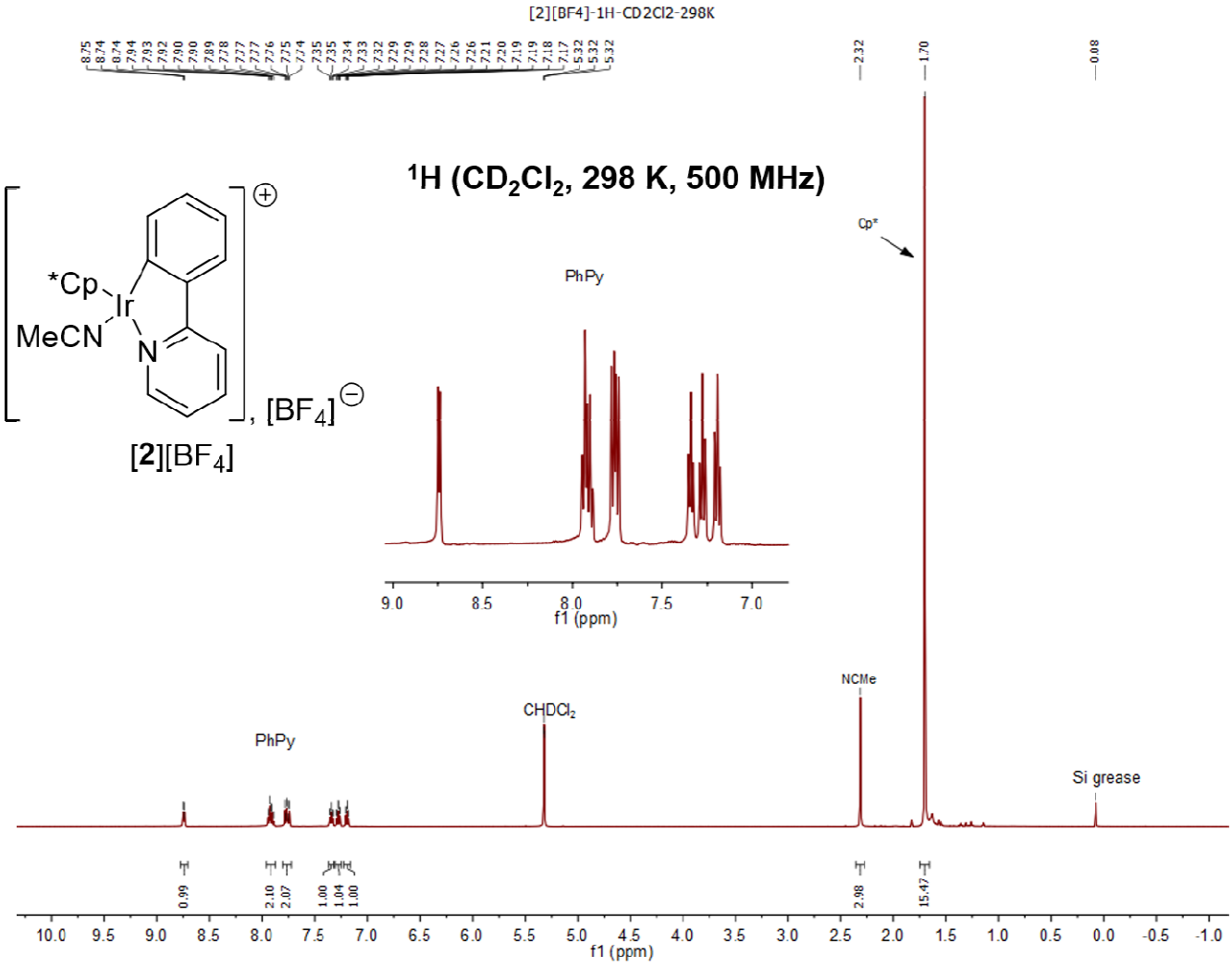
[2][BF4]-1H-CD2Cl2-298K
1H (CD2Cl2, 298 K, 500 MHz)
*Cp
Ir
MeCN
N
, [BF4]
[2][BF4]
PhPy
Cp*
NCMe
CHDCl2
PhPy
Si grease
f1 (ppm)

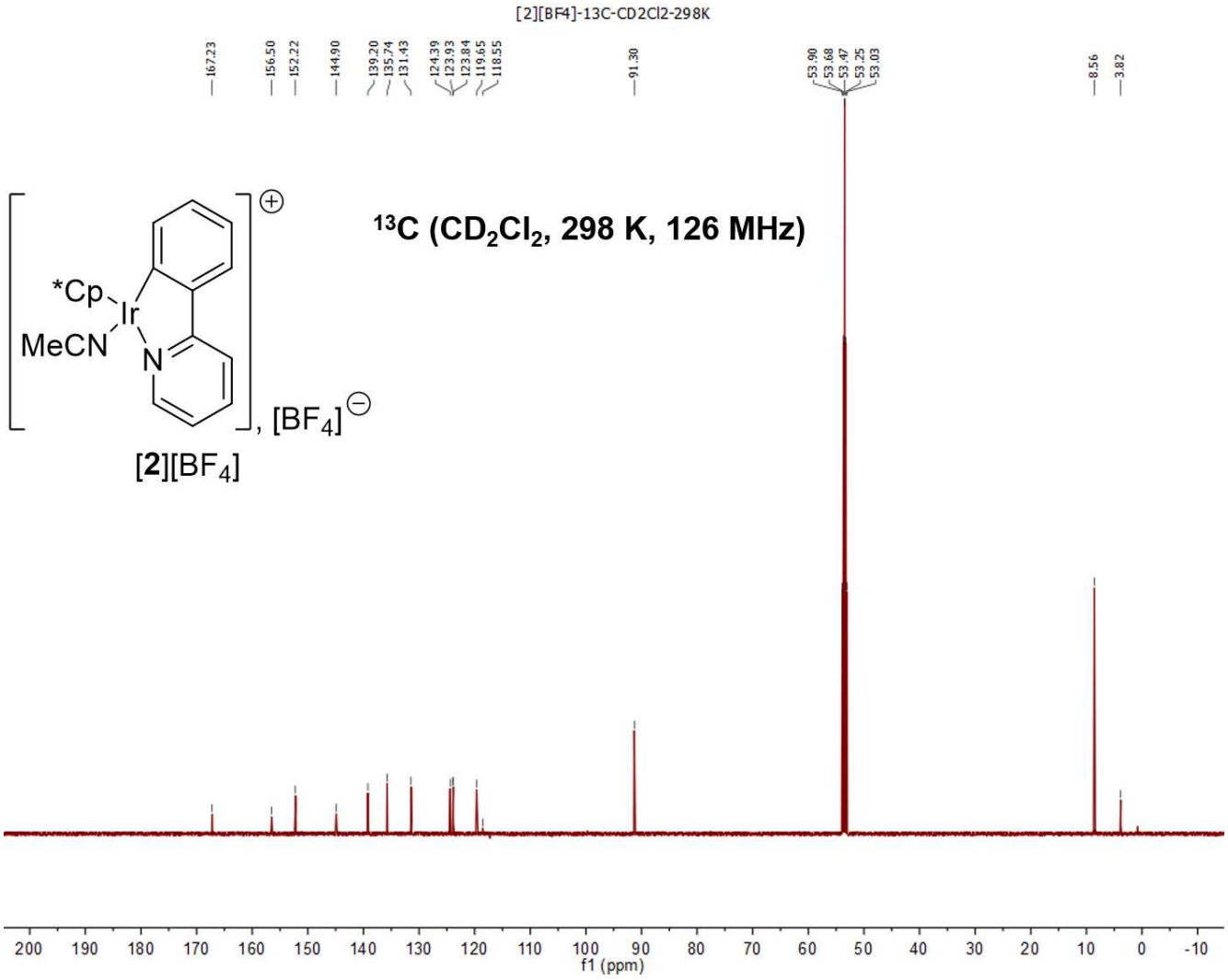
[2][BF4]-13C-CD2Cl2-298K
167.23
156.50
152.22
144.90
139.20
135.74
131.43
124.39
123.93
123.84
119.65
118.55
91.30
53.90
53.68
53.47
53.25
53.03
8.56
3.82
*Cp
Ir
MeCN
N
, [BF4]
[2][BF4]
13C (CD2Cl2, 298 K, 126 MHz)
200 190 180 170 160 150 140 130 120 110 100 90 80 70 60 50 40 30 20 10 0 -10
f1 (ppm)

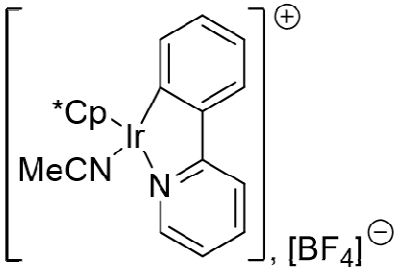

[**2**][BF_4]

^{19}F (CD_2Cl_2, 298 K, 282 MHz)

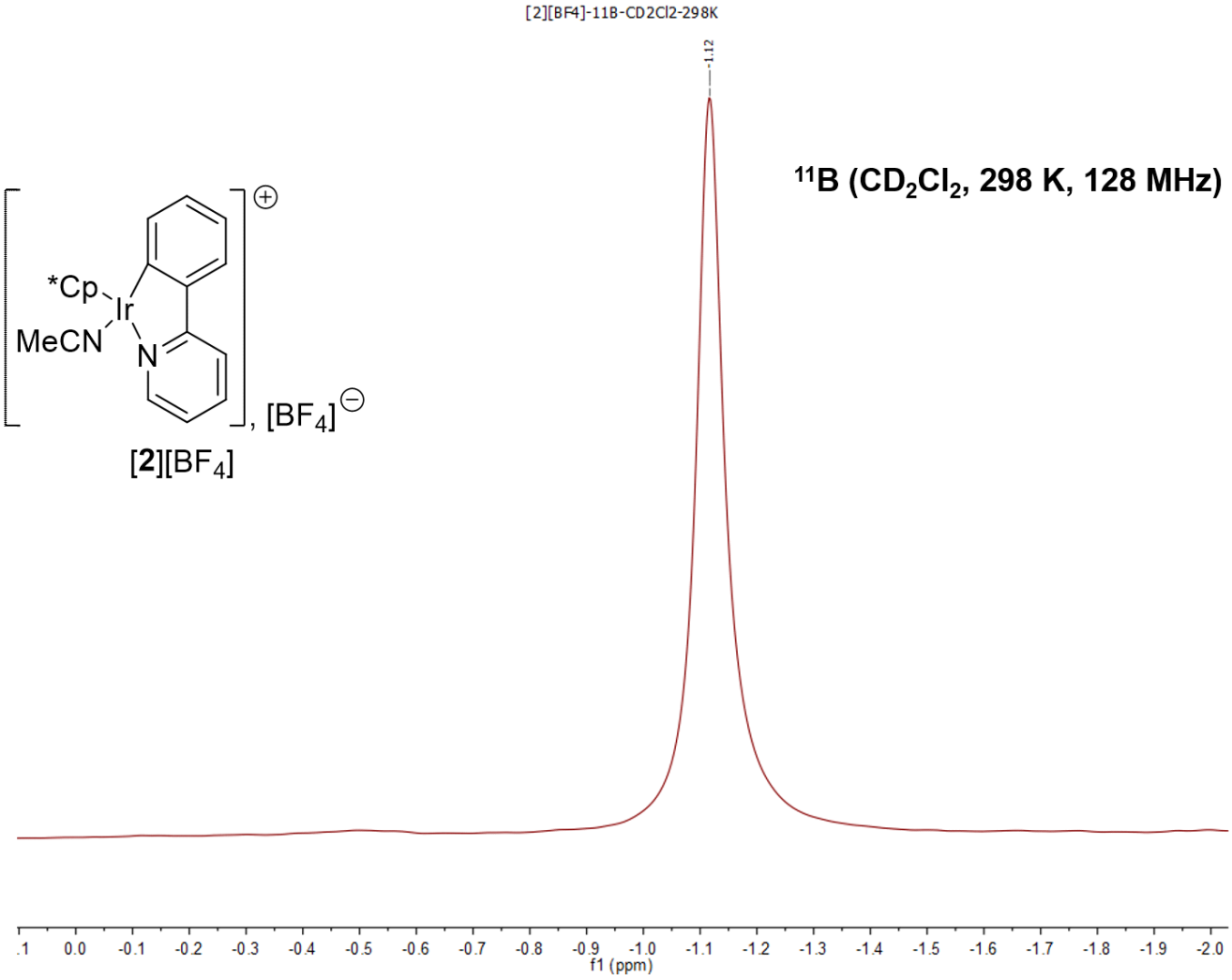
[2][BF4]-11B-CD2Cl2-298K
-1.12
*Cp
Ir
MeCN
N
, [BF4]
[2][BF4]
11B (CD2Cl2, 298 K, 128 MHz)
.1 0.0 -0.1 -0.2 -0.3 -0.4 -0.5 -0.6 -0.7 -0.8 -0.9 -1.0 -1.1 -1.2 -1.3 -1.4 -1.5 -1.6 -1.7 -1.8 -1.9 -2.0
f1 (ppm)

6.2.9.3 [**2**][OTf]

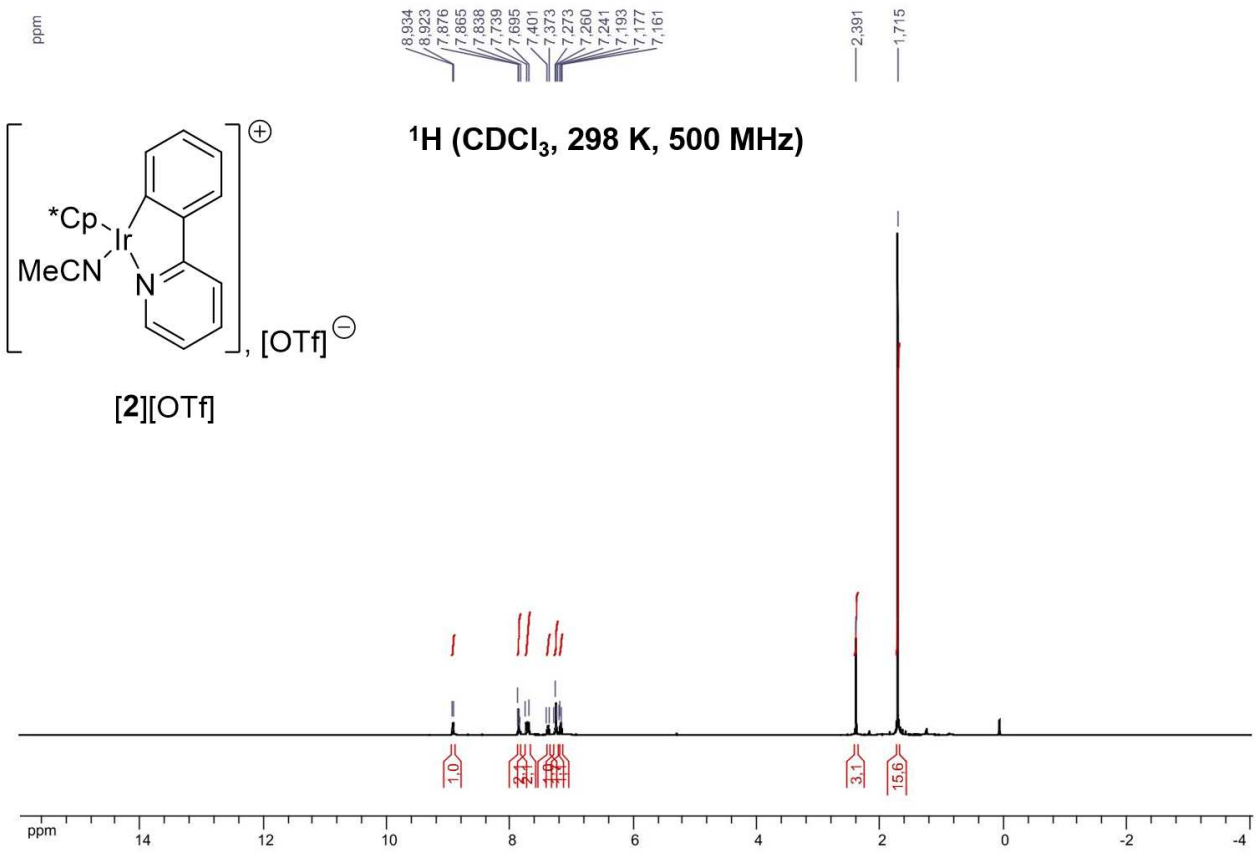

^{1}H ($CDCl_3$, 298 K, 500 MHz)

[**2**][OTf]

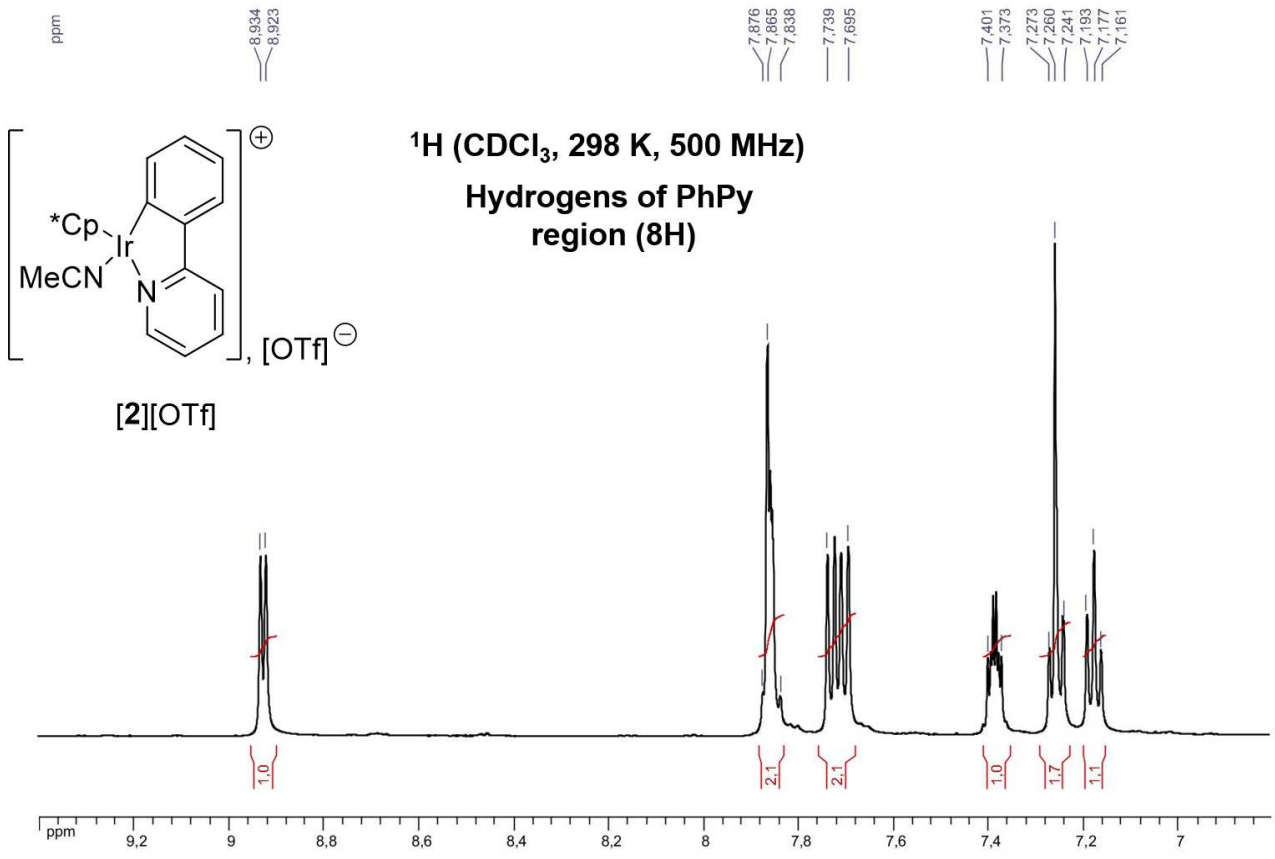
ppm
8,934
8,923
7,876
7,865
7,838
7,739
7,695
7,401
7,373
7,273
7,260
7,241
7,193
7,177
7,161
*Cp
Ir
MeCN
N
, [OTf]
[2][OTf]
1H (CDCl3, 298 K, 500 MHz)
Hydrogens of PhPy
region (8H)
1,0
2,1
2,1
1,0
1,7
1,1
ppm
9,2
9
8,8
8,6
8,4
8,2
8
7,8
7,6
7,4
7,2
7

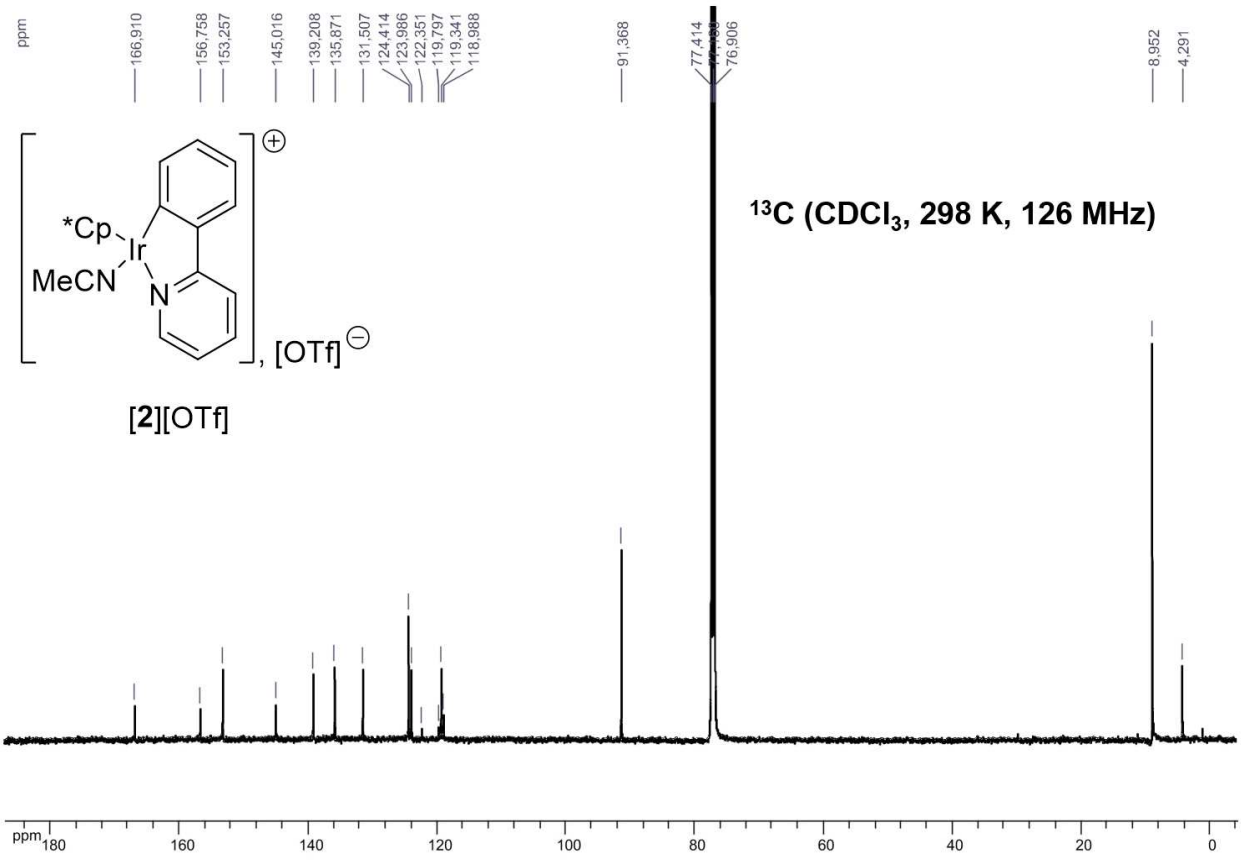
ppm
166,910
156,758
153,257
145,016
139,208
135,871
131,507
124,414
123,986
122,351
119,797
119,341
118,988
91,368
77,414
76,906
8,952
4,291
*Cp
Ir
MeCN
N
, [OTf]
[2][OTf]
13C (CDCl3, 298 K, 126 MHz)
ppm
180
160
140
120
100
80
60
40
20
0

6.2.9.4 [**2**][BPh4]

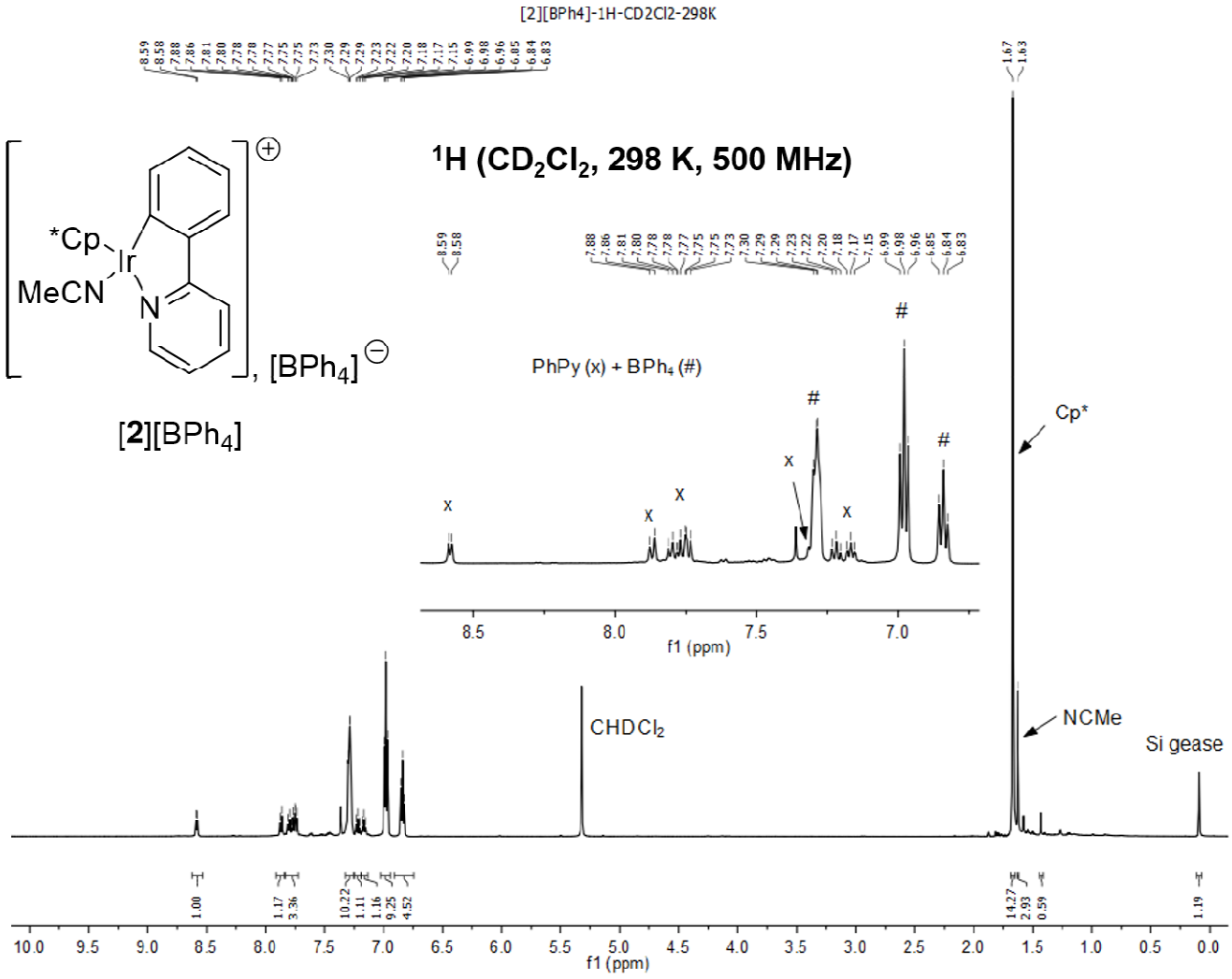
[2][BPh4]-1H-CD2Cl2-298K
*Cp
Ir
MeCN
N
, [BPh4]
[2][BPh4]
1H (CD2Cl2, 298 K, 500 MHz)
PhPy (x) + BPh4 (#)
Cp*
CHDCl2
NCMe
Si gease
f1 (ppm)

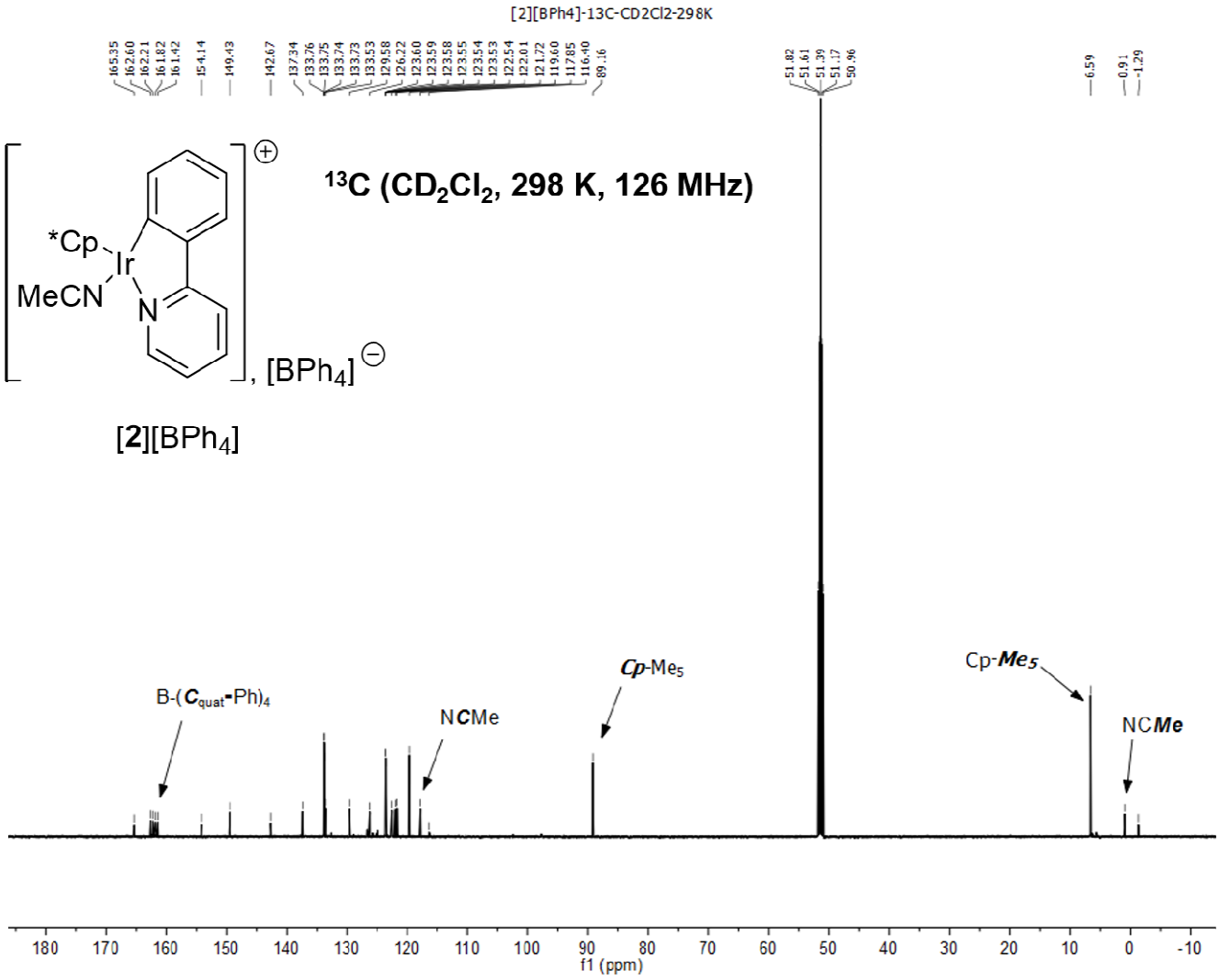
[2][BPh4]-13C-CD2Cl2-298K
*Cp
Ir
MeCN
N
, [BPh4]
13C (CD2Cl2, 298 K, 126 MHz)
[2][BPh4]
B-(Cquat-Ph)4
NCMe
Cp-Me5
Cp-Me5
NCMe
f1 (ppm)

[2][BPh4]-11B-CD2Cl2-298K

-6.55

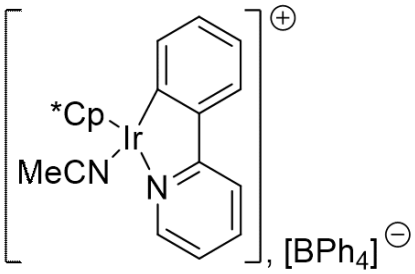

^{11}B (CD_2Cl_2, 298 K, 128 MHz)

[**2**][BPh_4]

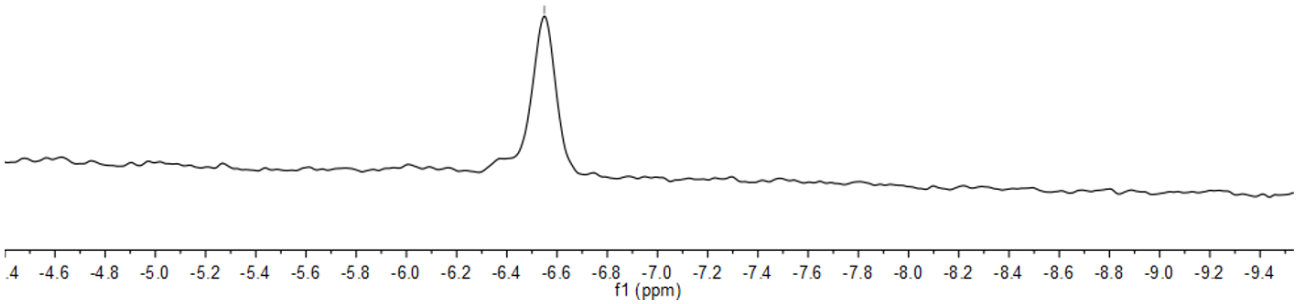

6.2.9.5 [**2**][PF_6]

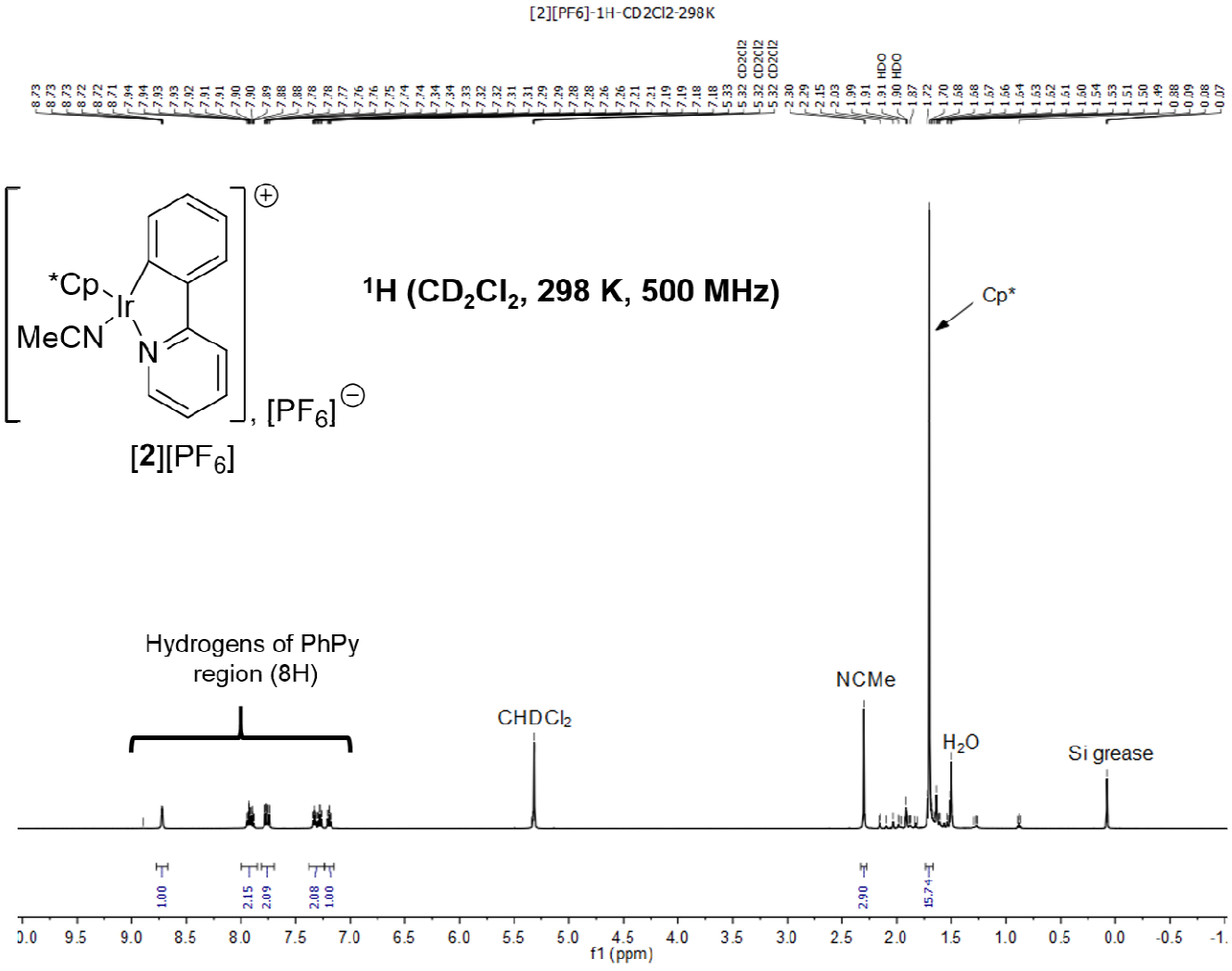
[2][PF6]-1H-CD2Cl2-298K
*Cp
Ir
MeCN
N
, [PF6]
[2][PF6]
1H (CD2Cl2, 298 K, 500 MHz)
Cp*
Hydrogens of PhPy region (8H)
CHDCl2
NCMe
H2O
Si grease
f1 (ppm)

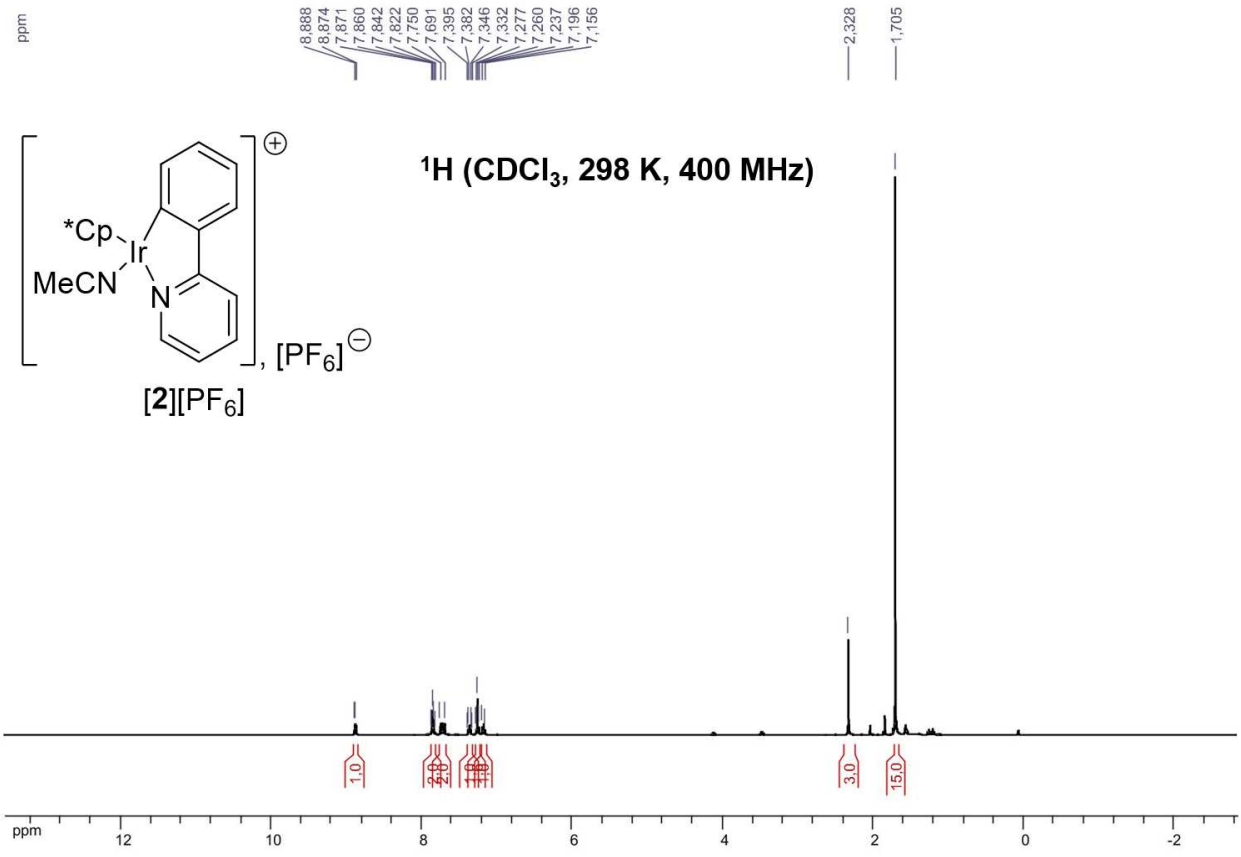
ppm
8,888
8,874
7,871
7,860
7,842
7,822
7,750
7,691
7,395
7,382
7,346
7,332
7,277
7,260
7,237
7,196
7,156
2,328
1,705
*Cp
Ir
MeCN
N
, [PF6]
[2][PF6]
1H (CDCl3, 298 K, 400 MHz)
1,0
2,0
3,0
15,0
ppm
12
10
8
6
4
2
0
-2

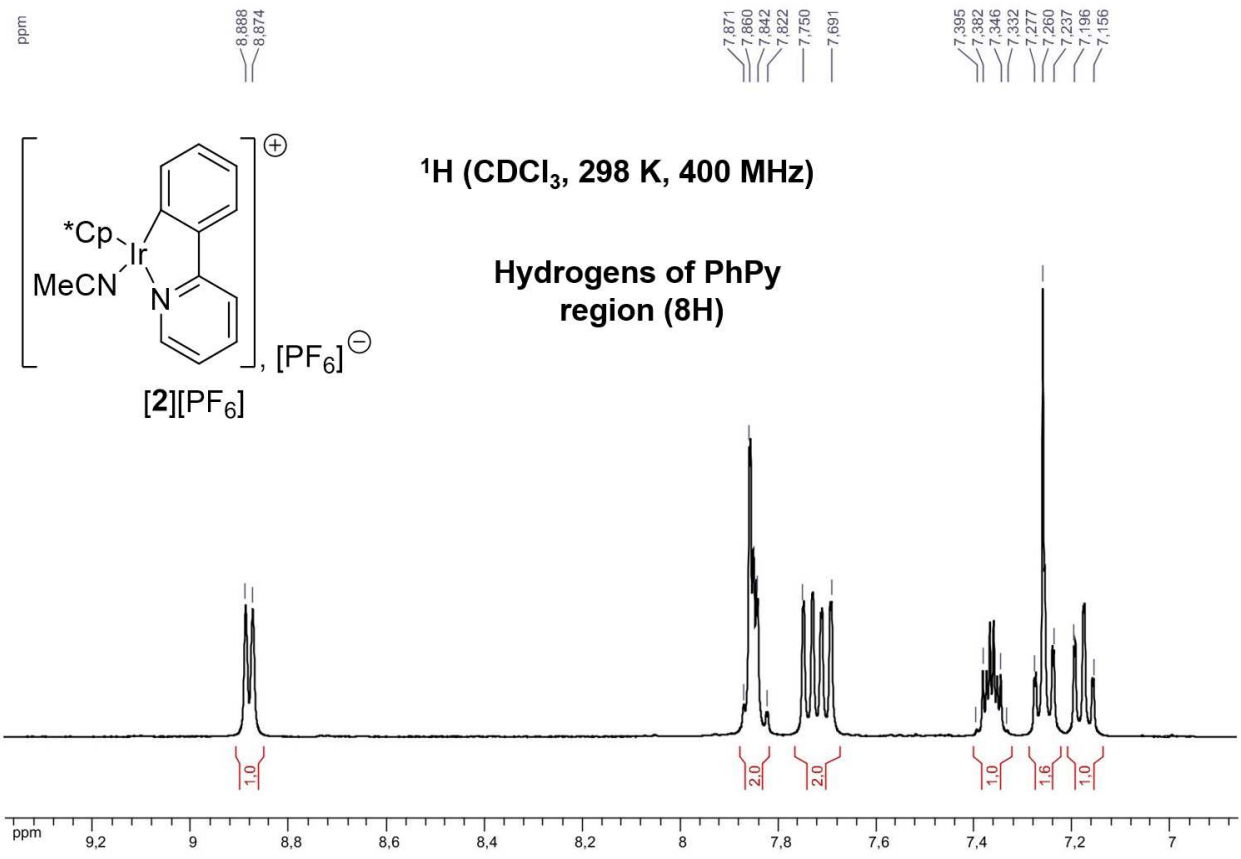
ppm
8,888
8,874
7,871
7,860
7,842
7,822
7,750
7,691
7,395
7,382
7,346
7,332
7,277
7,260
7,237
7,196
7,156
*Cp
Ir
MeCN
N
, [PF6]
[2][PF6]
1H (CDCl3, 298 K, 400 MHz)
Hydrogens of PhPy region (8H)
1,0
2,0
2,0
1,0
1,6
1,0
ppm
9,2
9
8,8
8,6
8,4
8,2
8
7,8
7,6
7,4
7,2
7

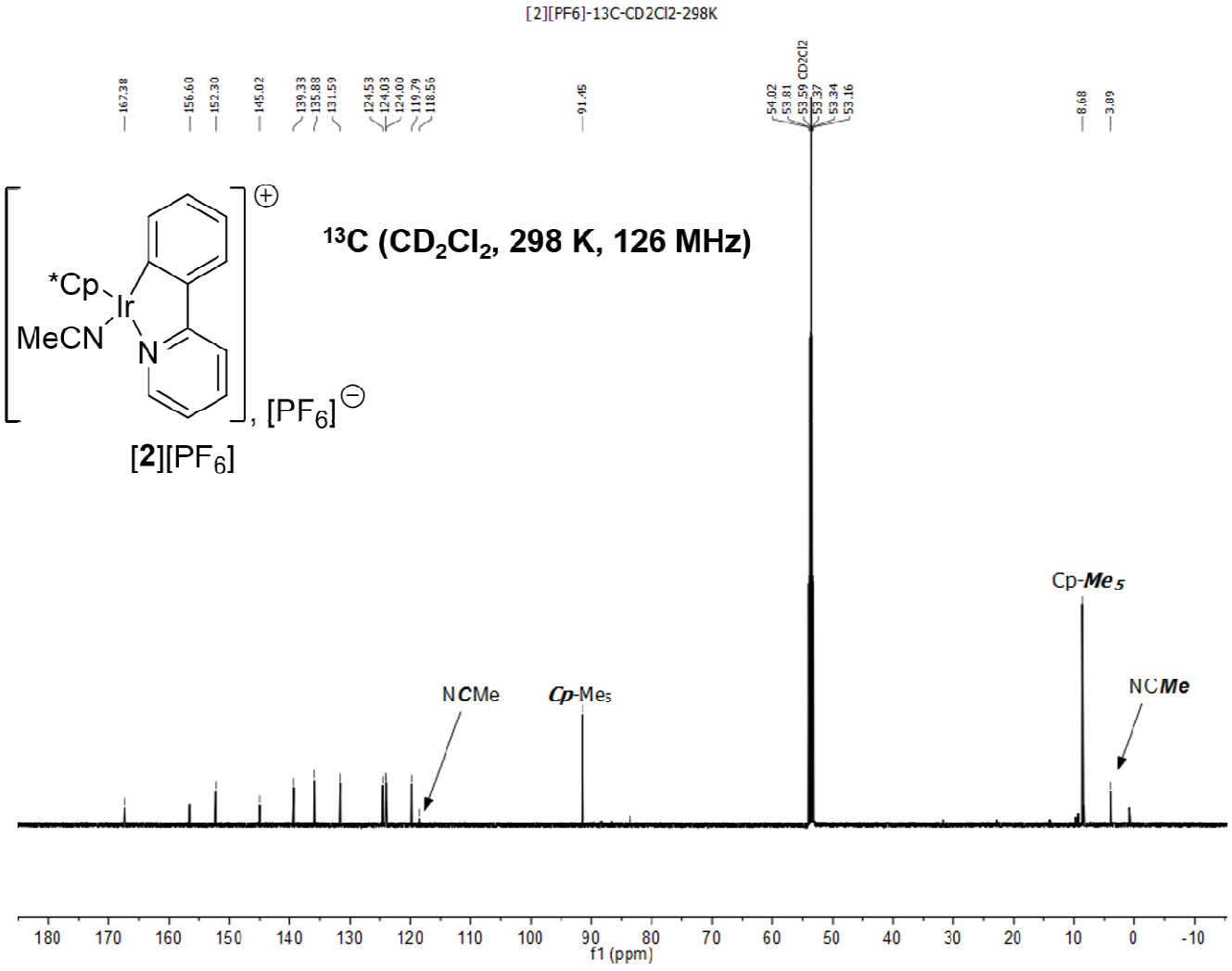
[2][PF6]-13C-CD2Cl2-298K
167.38
156.60
152.30
145.02
139.33
135.88
131.59
124.53
124.03
124.00
119.79
118.56
91.46
54.02
53.81
53.59 CD2Cl2
53.37
53.34
53.16
8.68
3.89
*Cp
Ir
MeCN
N
, [PF6]
[2][PF6]
13C (CD2Cl2, 298 K, 126 MHz)
NCMe
Cp-Me5
Cp-Me5
NCMe
180
170
160
150
140
130
120
110
100
90
80
70
60
50
40
30
20
10
0
-10
f1 (ppm)

[2][PF6]-19F-CD2Cl2-298K

-72.91

-75.42

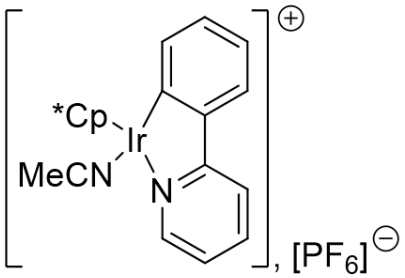

[**2**][PF_6]

^{19}F (CD_2Cl_2, 298 K, 282 MHz)

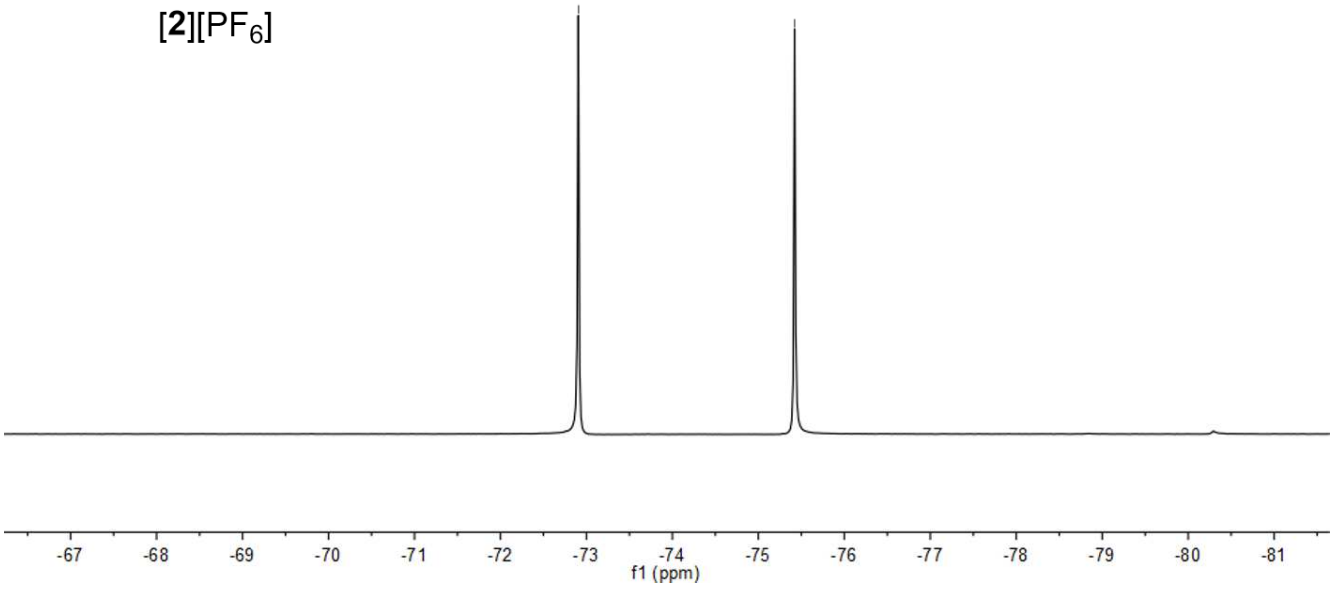

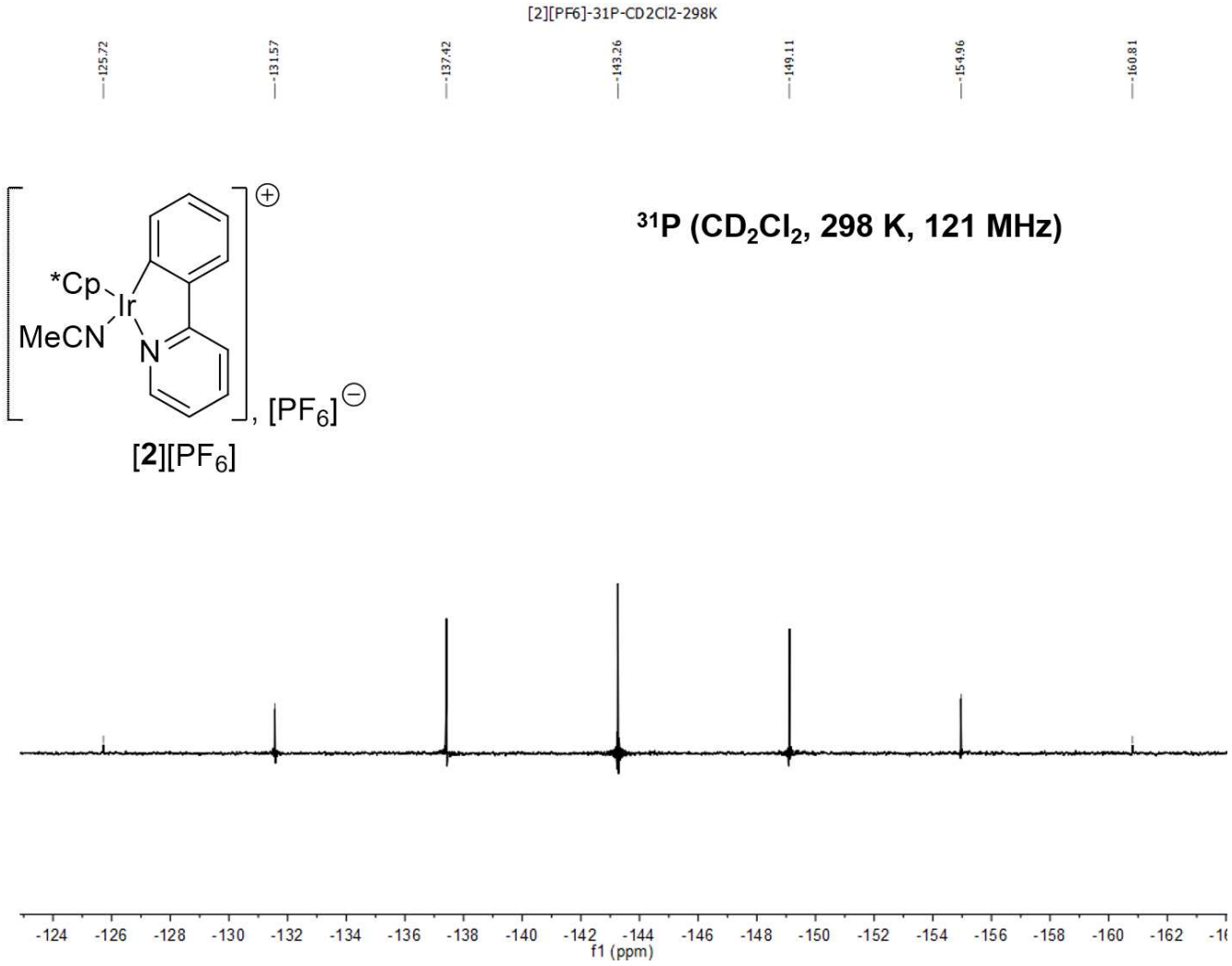

6.2.9.6 [**4**][BArF$_{24}$]

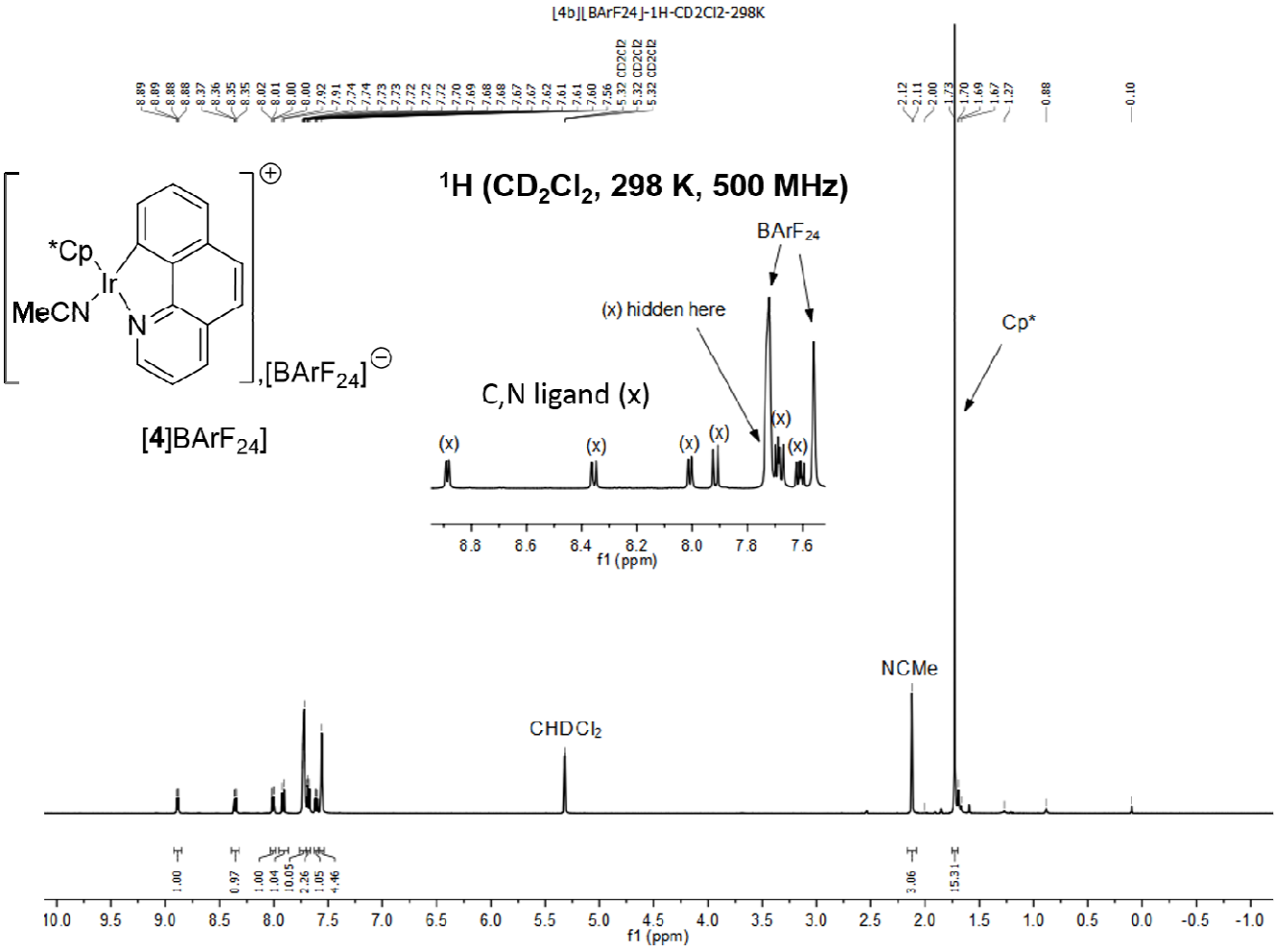
[4b][BArF24]-1H-CD2Cl2-298K
*Cp
Ir
MeCN
N
⊕
⊖
,[BArF24]
[4]BArF24]
1H (CD2Cl2, 298 K, 500 MHz)
BArF24
(x) hidden here
Cp*
C,N ligand (x)
(x)
NCMe
CHDCl2
f1 (ppm)

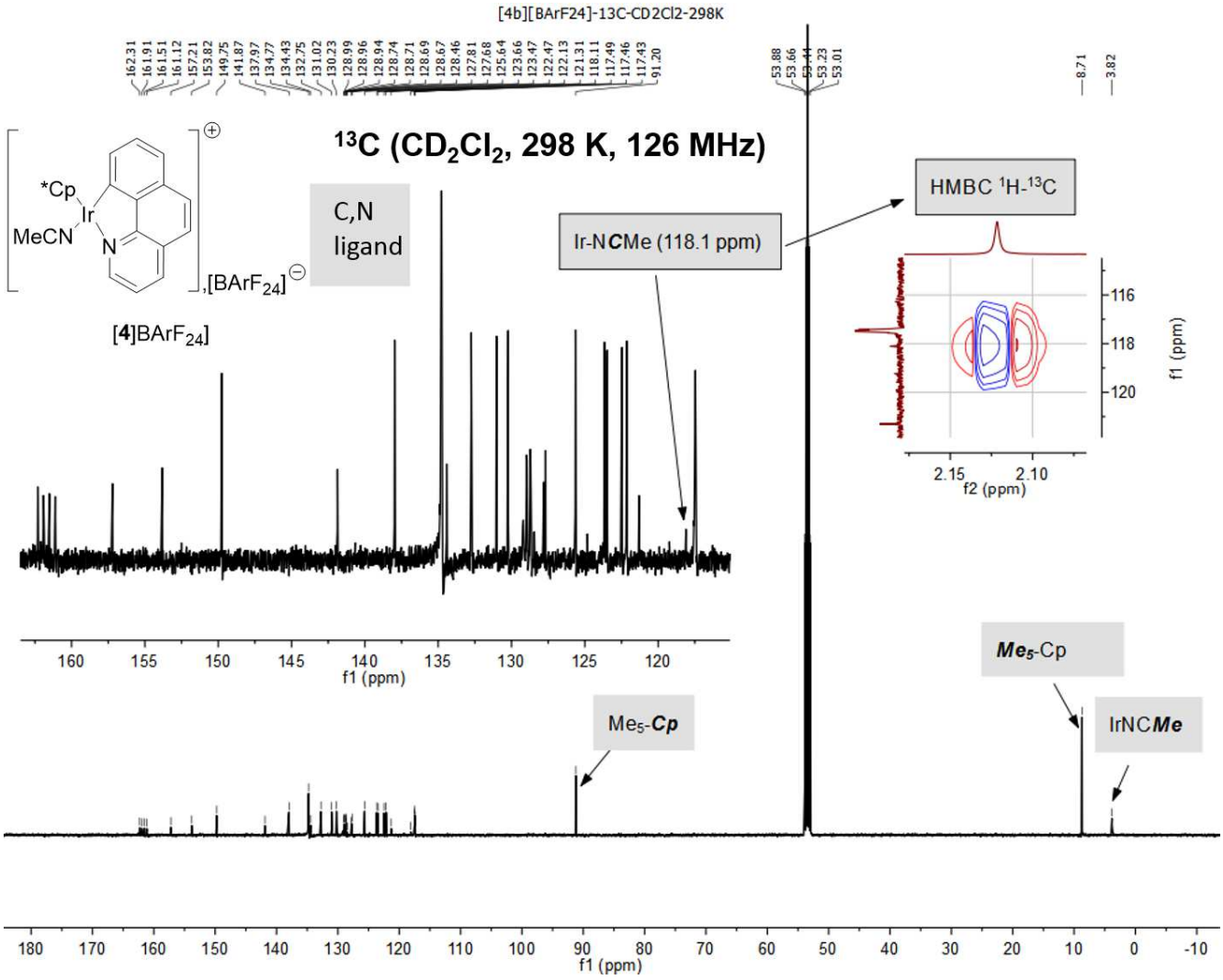
[4b][BArF24]-13C-CD2Cl2-298K
13C (CD2Cl2, 298 K, 126 MHz)
*Cp
Ir
MeCN
N
,[BArF24]
[4]BArF24]
C,N ligand
Ir-NCMe (118.1 ppm)
HMBC 1H-13C
Me5-Cp
IrNCMe
Me5-Cp
f1 (ppm)
f2 (ppm)

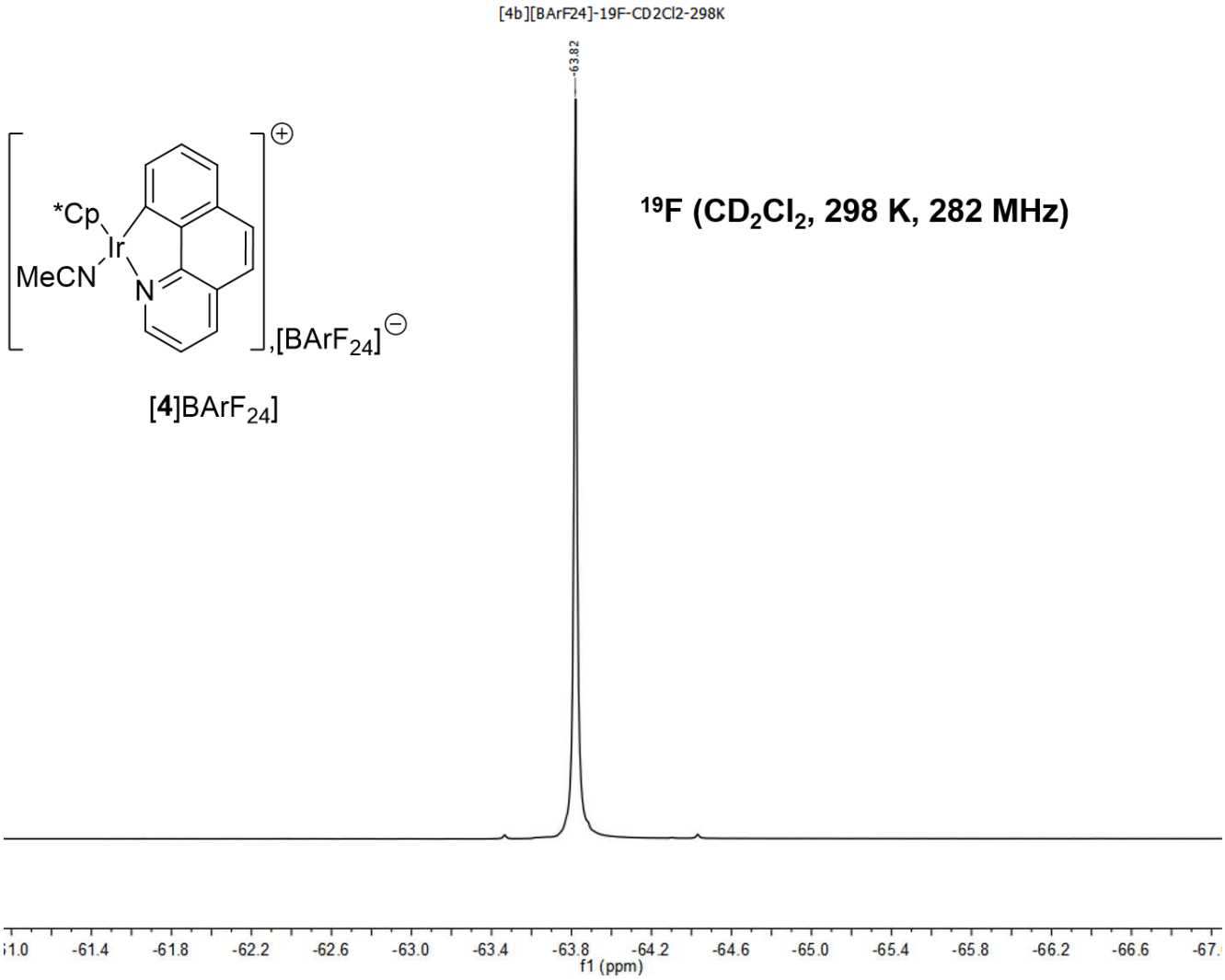

[**4**]BArF$_{24}$]

^{19}F (CD_2Cl_2, 298 K, 282 MHz)

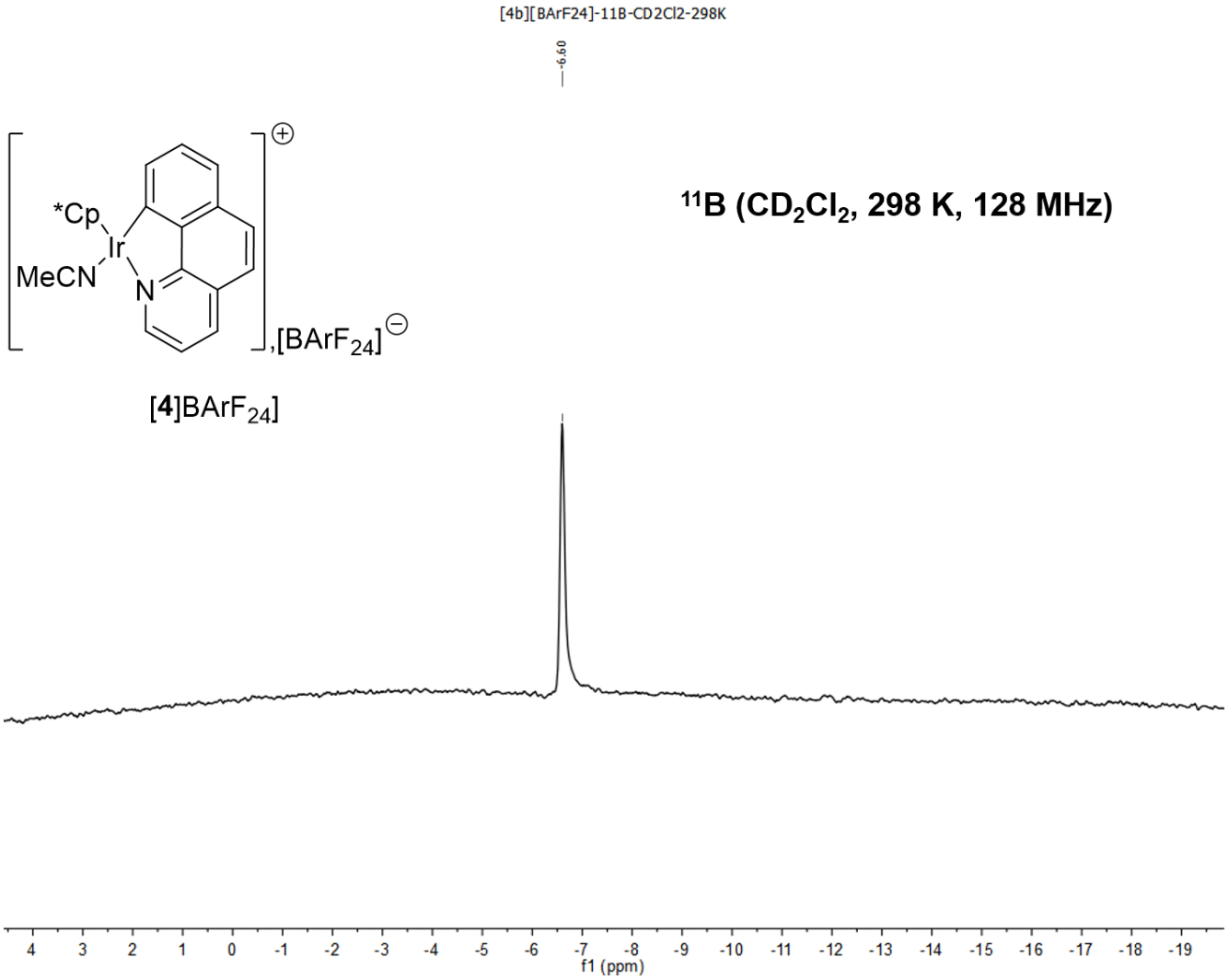
[4b][BArF24]-11B-CD2Cl2-298K
-6.60
*Cp
Ir
MeCN
N
,[BArF24]
11B (CD2Cl2, 298 K, 128 MHz)
[4]BArF24]
4 3 2 1 0 -1 -2 -3 -4 -5 -6 -7 -8 -9 -10 -11 -12 -13 -14 -15 -16 -17 -18 -19
f1 (ppm)

6.2.9.7 [**4**][OTf]

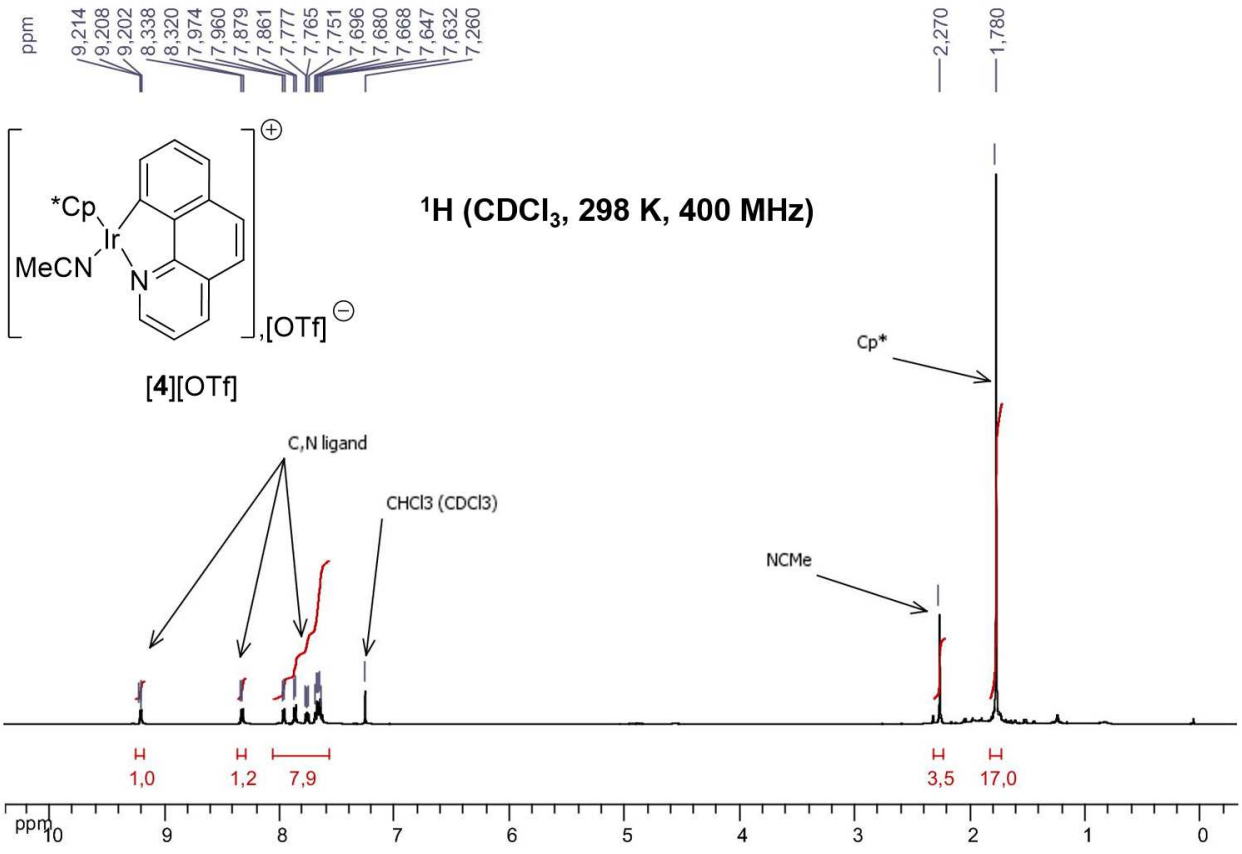
ppm
9,214
9,208
9,202
8,338
8,320
7,974
7,960
7,879
7,861
7,777
7,765
7,751
7,696
7,680
7,668
7,647
7,632
7,260
2,270
1,780
*Cp
Ir
MeCN
N
,[OTf]
[4][OTf]
¹H (CDCl₃, 298 K, 400 MHz)
Cp*
C,N ligand
CHCl3 (CDCl3)
NCMe
1,0
1,2
7,9
3,5
17,0
ppm
10
9
8
7
6
5
4
3
2
1
0

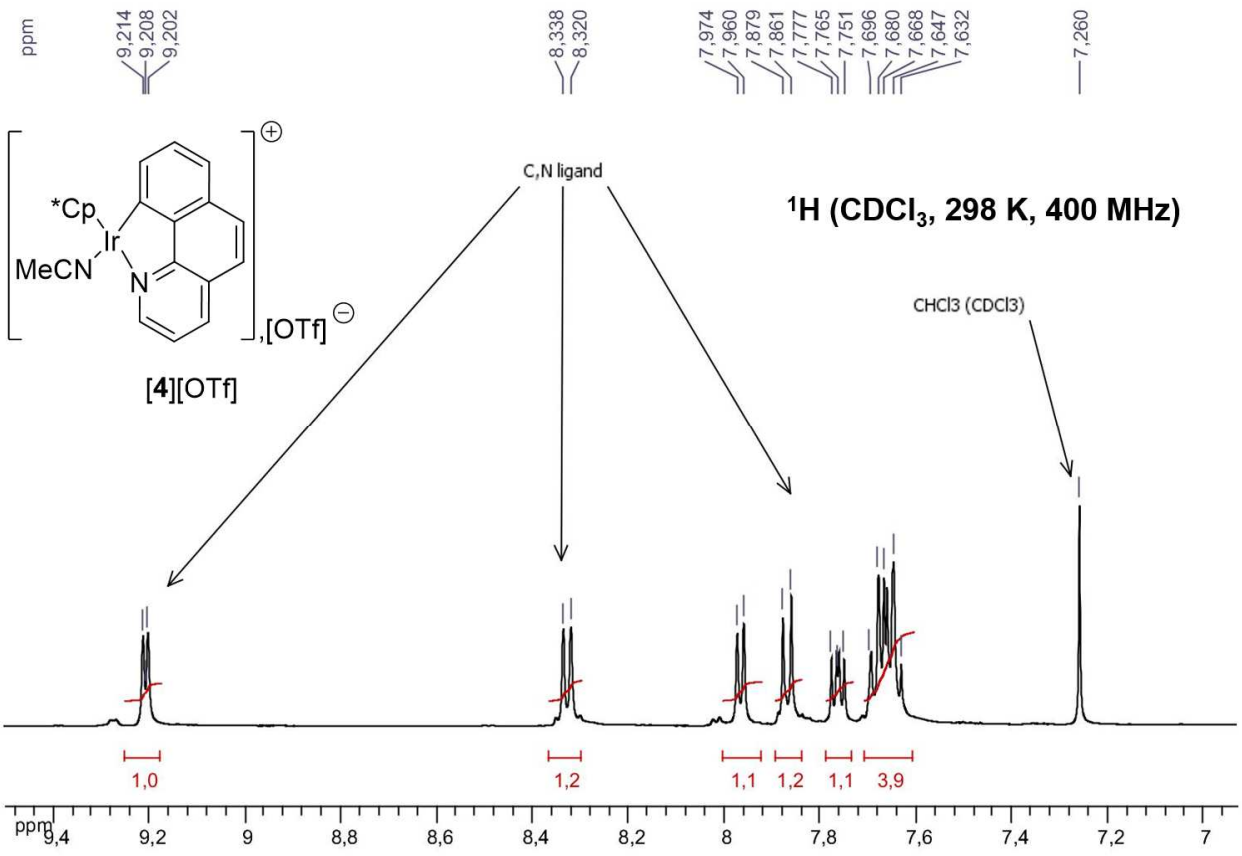
ppm
9,214
9,208
9,202
8,338
8,320
7,974
7,960
7,879
7,861
7,777
7,765
7,751
7,696
7,680
7,668
7,647
7,632
7,260
*Cp
Ir
MeCN
N
⊕
⊖
,[OTf]
[4][OTf]
C,N ligand
CHCl3 (CDCl3)
1H (CDCl3, 298 K, 400 MHz)
1,0
1,2
1,1
1,2
1,1
3,9
ppm
9,4
9,2
9
8,8
8,6
8,4
8,2
8
7,8
7,6
7,4
7,2
7

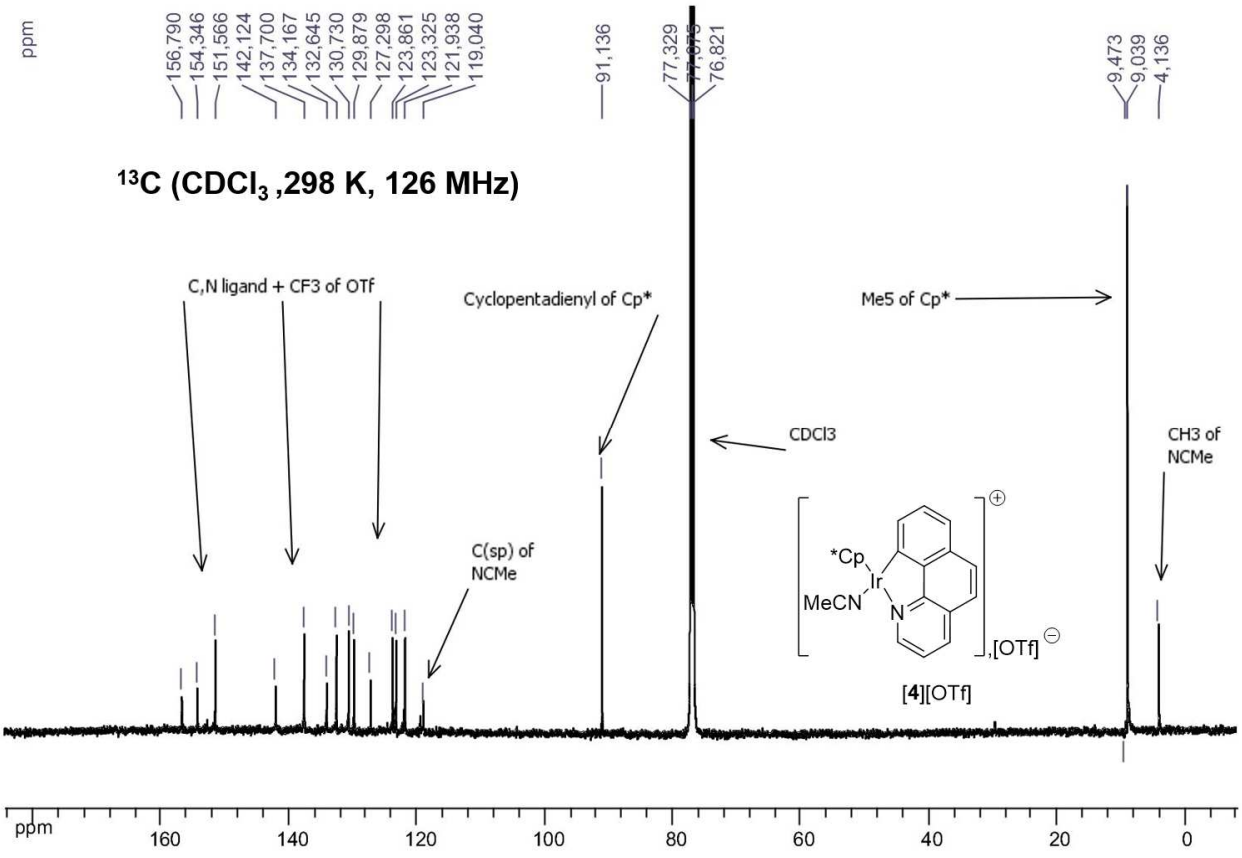
ppm
156,790
154,346
151,566
142,124
137,700
134,167
132,645
130,730
129,879
127,298
123,861
123,325
121,938
119,040
91,136
77,329
77,075
76,821
9,473
9,039
4,136
13C (CDCl3 ,298 K, 126 MHz)
C,N ligand + CF3 of OTf
Cyclopentadienyl of Cp*
Me5 of Cp*
CDCl3
CH3 of NCMe
C(sp) of NCMe
*Cp
Ir
MeCN
N
,[OTf]
[4][OTf]
ppm
160
140
120
100
80
60
40
20
0

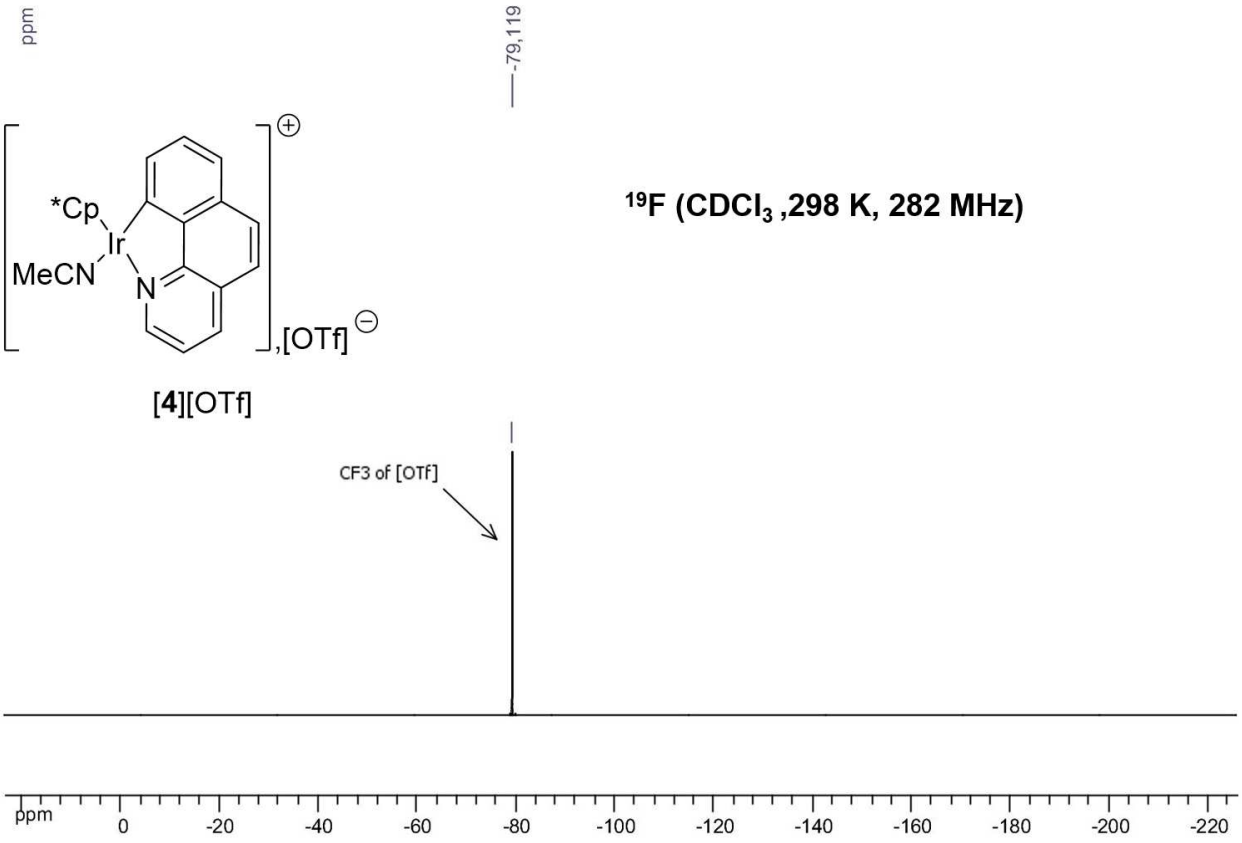

[**4**][OTf]

^{19}F ($CDCl_3$,298 K, 282 MHz)

6.2.9.8 [**4**][BPh_4]

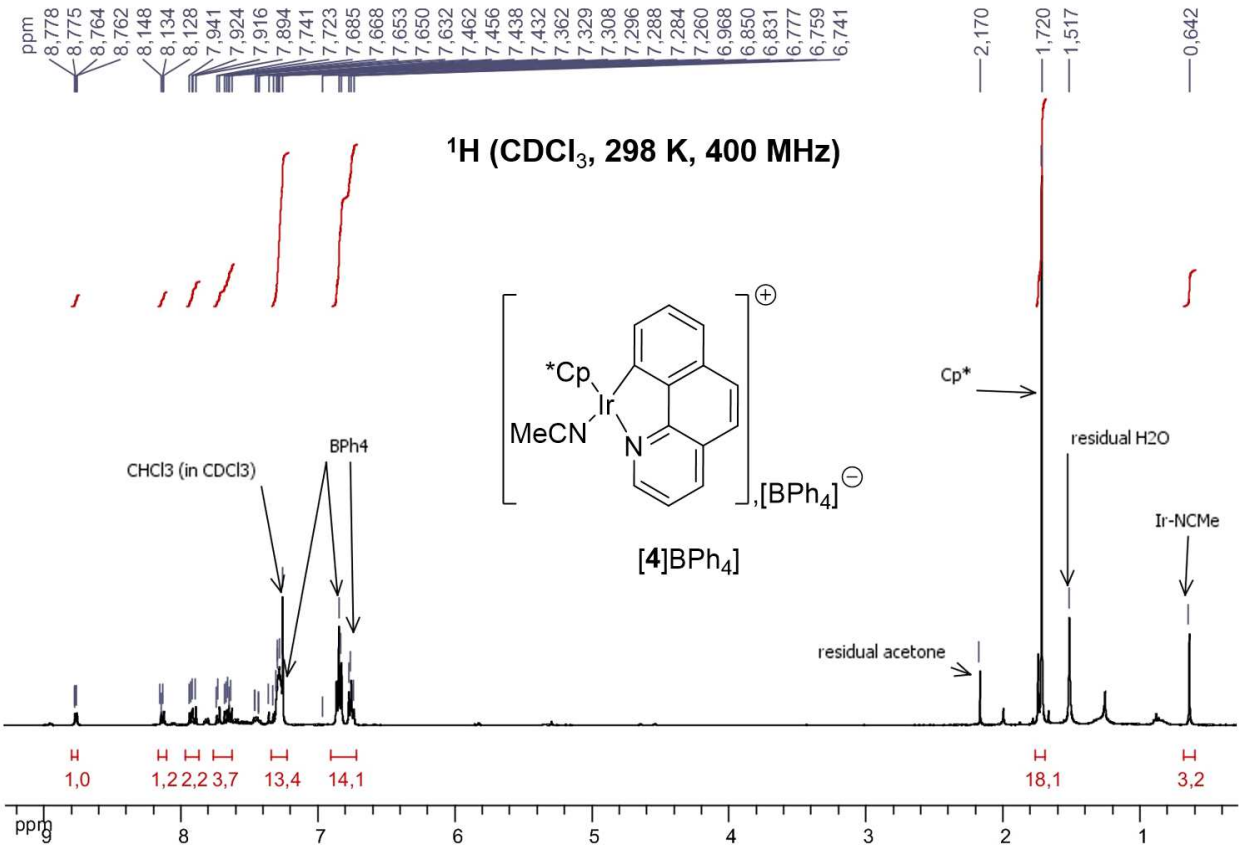
ppm
8,778
8,775
8,764
8,762
8,148
8,134
8,128
7,941
7,924
7,916
7,894
7,741
7,723
7,685
7,668
7,653
7,650
7,632
7,462
7,456
7,438
7,432
7,362
7,329
7,308
7,296
7,288
7,284
7,260
6,968
6,850
6,831
6,777
6,759
6,741
2,170
1,720
1,517
0,642
¹H (CDCl3, 298 K, 400 MHz)
*Cp
Ir
MeCN
N
[BPh4]
[4]BPh4]
Cp*
residual H2O
Ir-NCMe
residual acetone
CHCl3 (in CDCl3)
BPh4
1,0
1,2
2,2
3,7
13,4
14,1
18,1
3,2
ppm
9
8
7
6
5
4
3
2
1

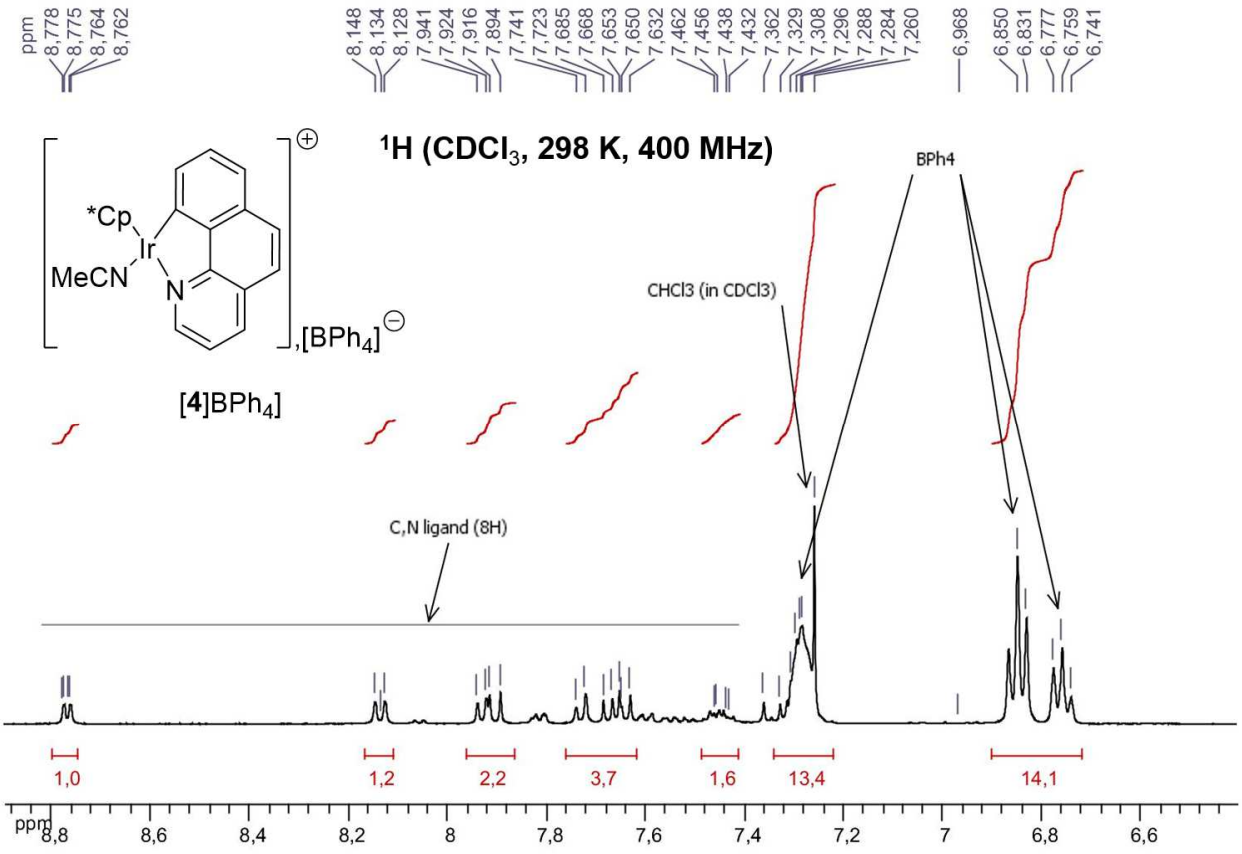
ppm
8,778
8,775
8,764
8,762
8,148
8,134
8,128
7,941
7,924
7,916
7,894
7,741
7,723
7,685
7,668
7,653
7,650
7,632
7,462
7,456
7,438
7,432
7,362
7,329
7,308
7,296
7,288
7,284
7,260
6,968
6,850
6,831
6,777
6,759
6,741
*Cp
Ir
MeCN
N
,[BPh4]
[4]BPh4]
1H (CDCl3, 298 K, 400 MHz)
BPh4
CHCl3 (in CDCl3)
C,N ligand (8H)
1,0
1,2
2,2
3,7
1,6
13,4
14,1
ppm
8,8
8,6
8,4
8,2
8
7,8
7,6
7,4
7,2
7
6,8
6,6

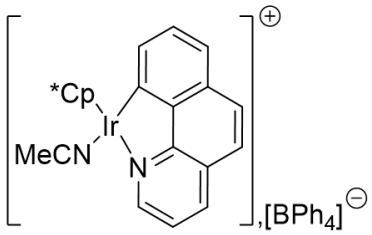

[**4**]BPh_4]

^{11}B ($CDCl_3$, 298 K, 128 MHz)

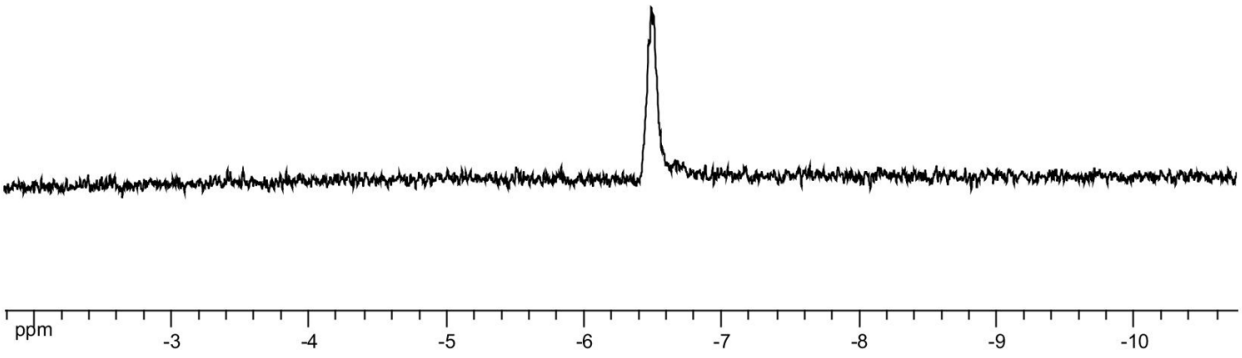

6.2.9.9 [**6**][$BArF_{24}$]

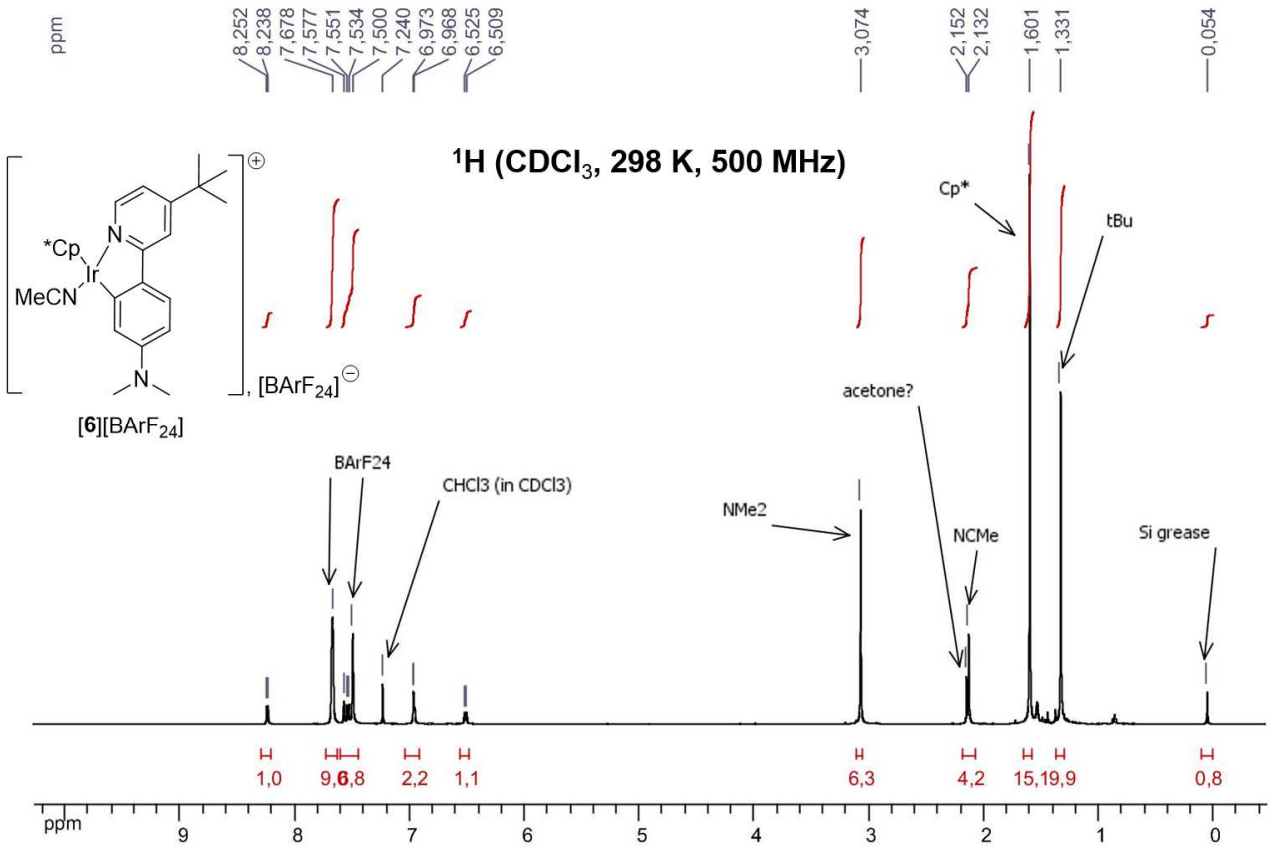
ppm
8,252
8,238
7,678
7,577
7,551
7,534
7,500
7,240
6,973
6,968
6,525
6,509
3,074
2,152
2,132
1,601
1,331
0,054
¹H (CDCl3, 298 K, 500 MHz)
*Cp
Ir
MeCN
N
N
, [BArF24]
[6][BArF24]
Cp*
tBu
acetone?
BArF24
CHCl3 (in CDCl3)
NMe2
NCMe
Si grease
1,0
9,6,8
2,2
1,1
6,3
4,2
15,19,9
0,8
ppm
9
8
7
6
5
4
3
2
1
0

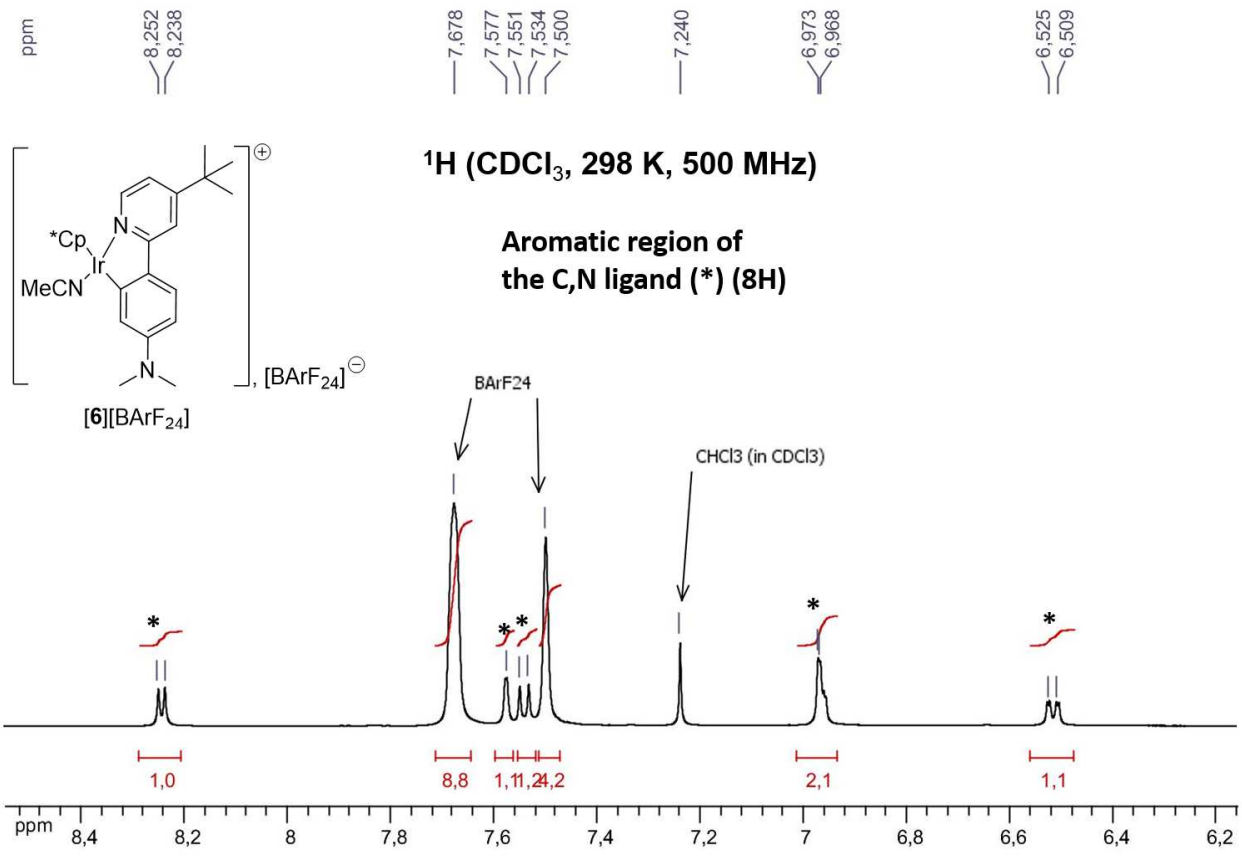
ppm
8,252
8,238
7,678
7,577
7,551
7,534
7,500
7,240
6,973
6,968
6,525
6,509
*Cp
Ir
MeCN
N
N
, [BArF24]
[6][BArF24]
1H (CDCl3, 298 K, 500 MHz)
Aromatic region of
the C,N ligand (*) (8H)
BArF24
CHCl3 (in CDCl3)
*
1,0
8,8
1,1
1,2
4,2
2,1
1,1
ppm
8,4
8,2
8
7,8
7,6
7,4
7,2
7
6,8
6,6
6,4
6,2

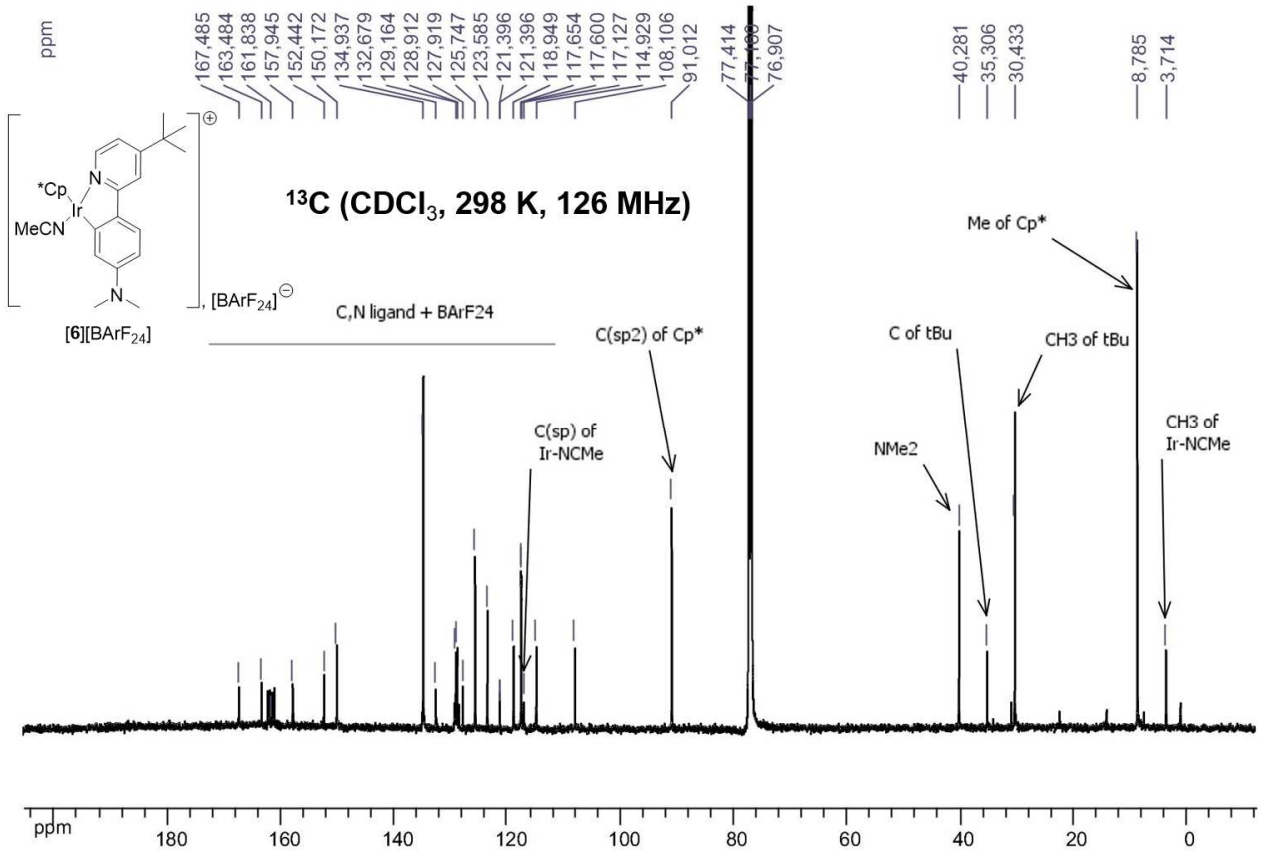
ppm
167,485
163,484
161,838
157,945
152,442
150,172
134,937
132,679
129,164
128,912
127,919
125,747
123,585
121,396
121,396
118,949
117,654
117,600
117,127
114,929
108,106
91,012
77,414
77,166
76,907
40,281
35,306
30,433
8,785
3,714
*Cp
Ir
MeCN
N
N
[BArF24]⊖
[6][BArF24]
13C (CDCl3, 298 K, 126 MHz)
C,N ligand + BArF24
C(sp2) of Cp*
C(sp) of Ir-NCMe
Me of Cp*
C of tBu
CH3 of tBu
NMe2
CH3 of Ir-NCMe
ppm
180
160
140
120
100
80
60
40
20
0

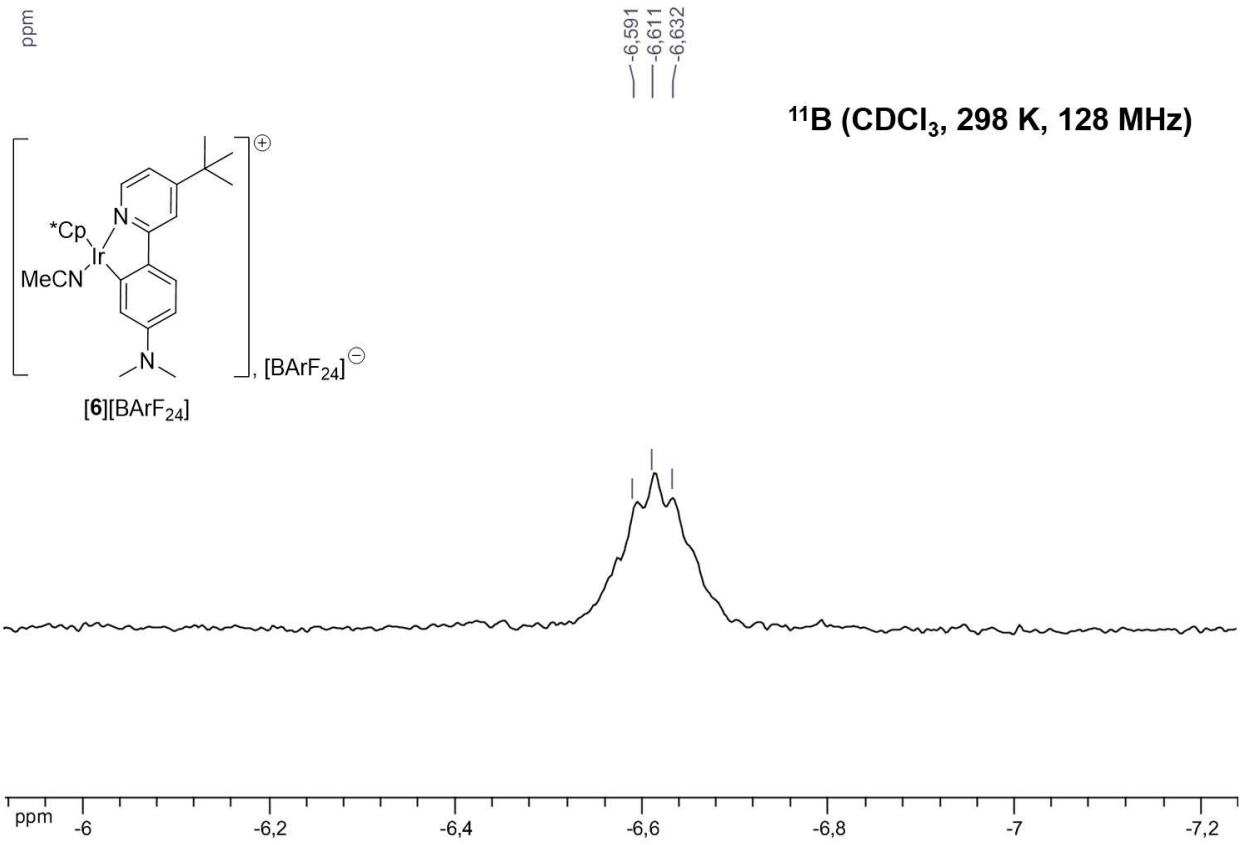

6.2.9.10 [**8**][BArF$_{24}$]

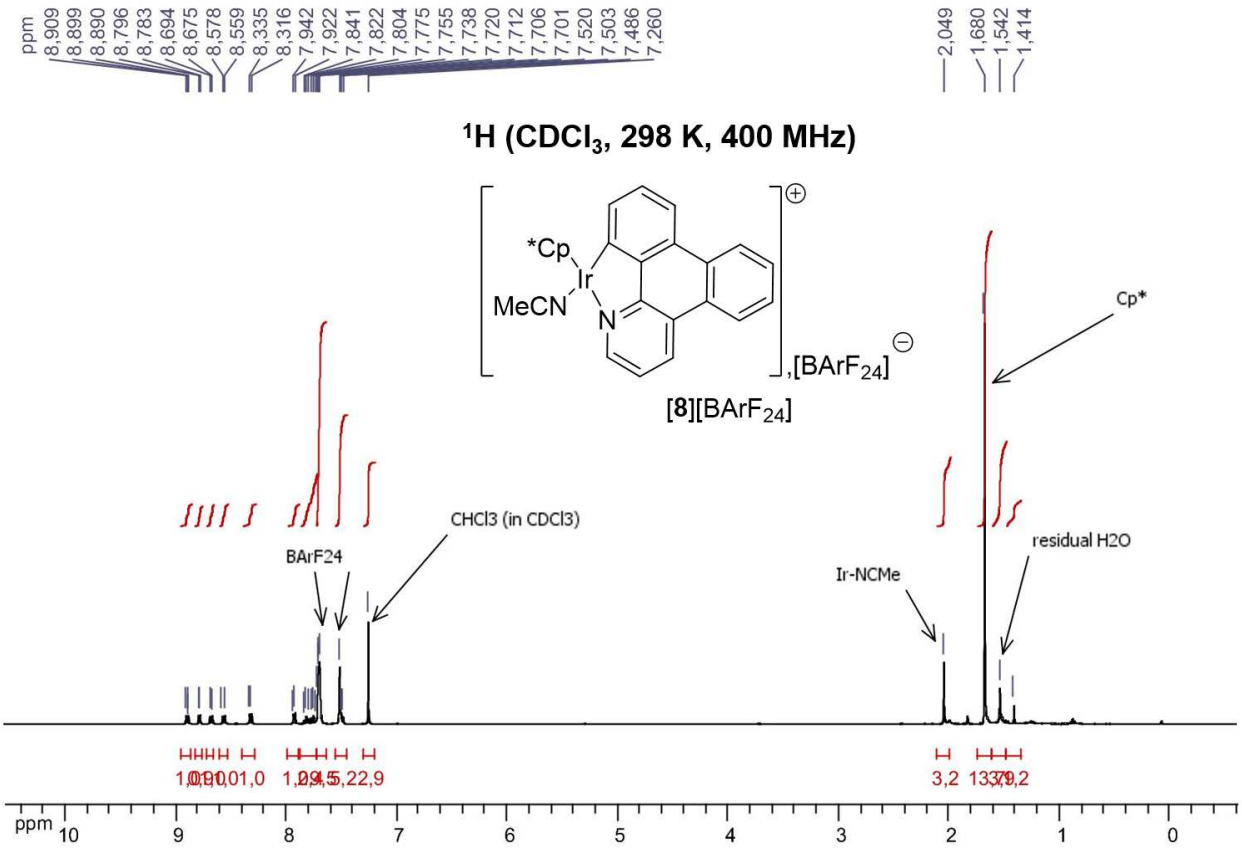
ppm
8,909
8,899
8,890
8,796
8,783
8,694
8,675
8,578
8,559
8,335
8,316
7,942
7,922
7,841
7,822
7,804
7,775
7,755
7,738
7,720
7,712
7,706
7,701
7,520
7,503
7,486
7,260
2,049
1,680
1,542
1,414
¹H (CDCl₃, 298 K, 400 MHz)
*Cp
Ir
MeCN
N
⊕
⊖
,[BArF24]
[8][BArF24]
Cp*
CHCl3 (in CDCl3)
BArF24
Ir-NCMe
residual H2O
3,2
ppm
10
9
8
7
6
5
4
3
2
1
0

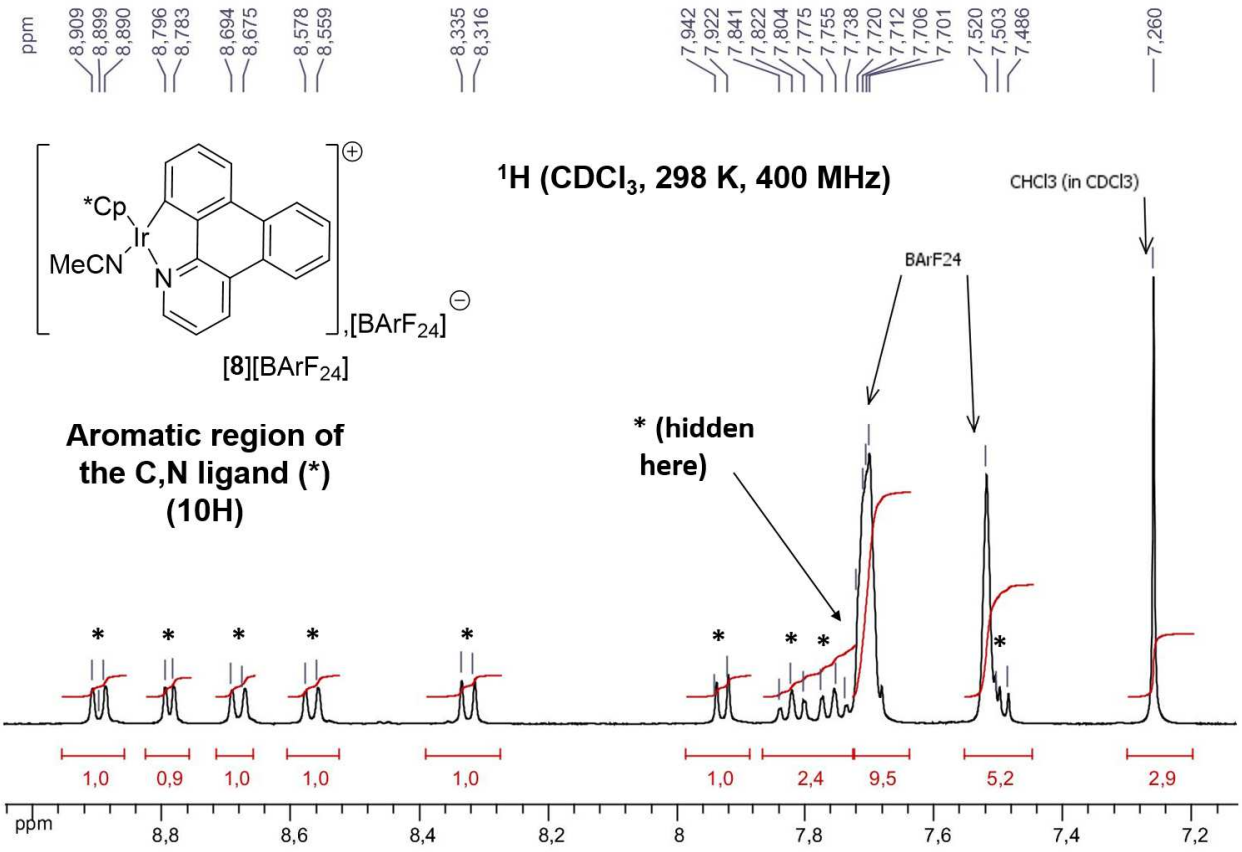
ppm
8,909
8,899
8,890
8,796
8,783
8,694
8,675
8,578
8,559
8,335
8,316
7,942
7,922
7,841
7,822
7,804
7,775
7,755
7,738
7,720
7,712
7,706
7,701
7,520
7,503
7,486
7,260
*Cp
Ir
MeCN
N
,[BArF24]
[8][BArF24]
1H (CDCl3, 298 K, 400 MHz)
CHCl3 (in CDCl3)
BArF24
Aromatic region of the C,N ligand (*) (10H)
* (hidden here)
1,0
0,9
1,0
1,0
1,0
1,0
2,4
9,5
5,2
2,9
ppm
8,8
8,6
8,4
8,2
8
7,8
7,6
7,4
7,2

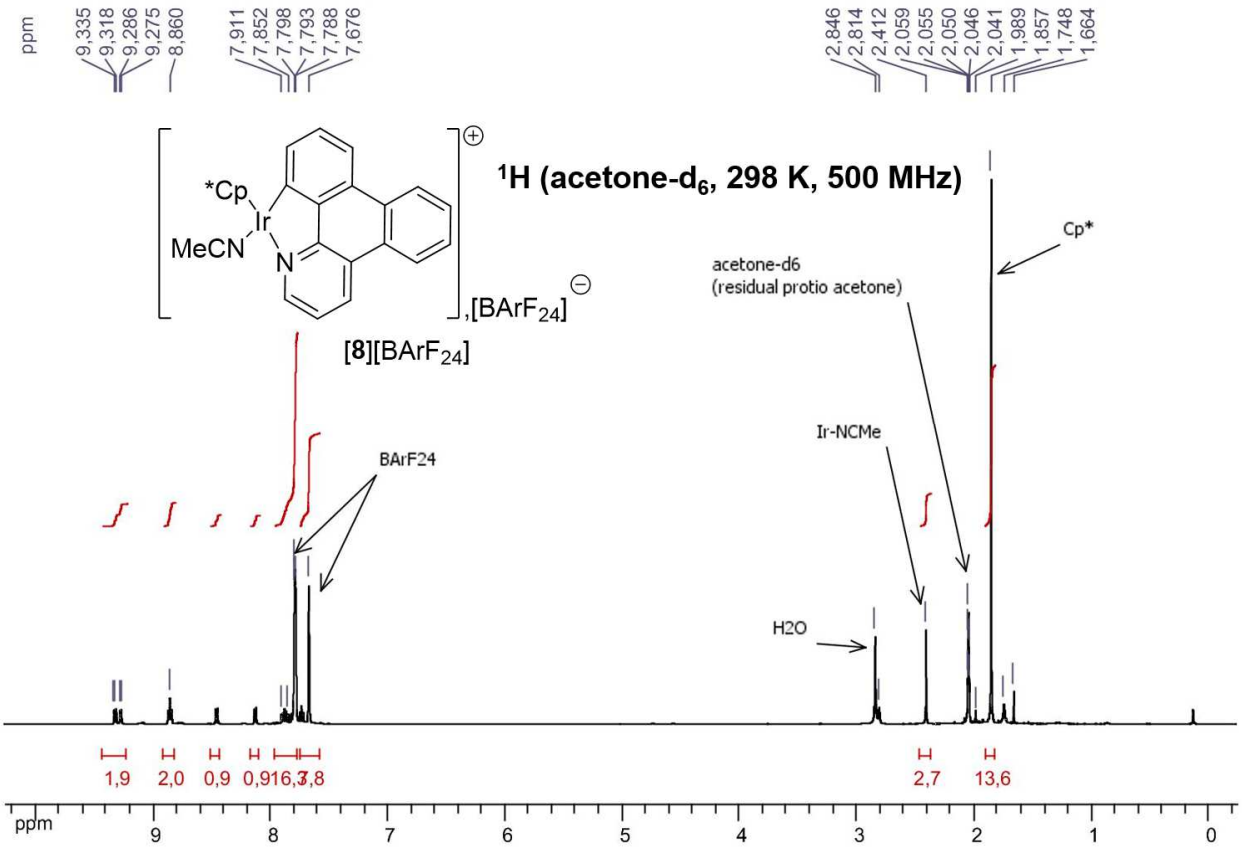
ppm
9,335
9,318
9,286
9,275
8,860
7,911
7,852
7,798
7,793
7,788
7,676
2,846
2,814
2,412
2,059
2,055
2,050
2,046
2,041
1,989
1,857
1,748
1,664
*Cp
Ir
MeCN
N
,[BArF24]
[8][BArF24]
¹H (acetone-d6, 298 K, 500 MHz)
Cp*
acetone-d6
(residual protio acetone)
Ir-NCMe
BArF24
H2O
1,9
2,0
0,9
0,91
6,3
7,8
2,7
13,6
ppm
9
8
7
6
5
4
3
2
1
0

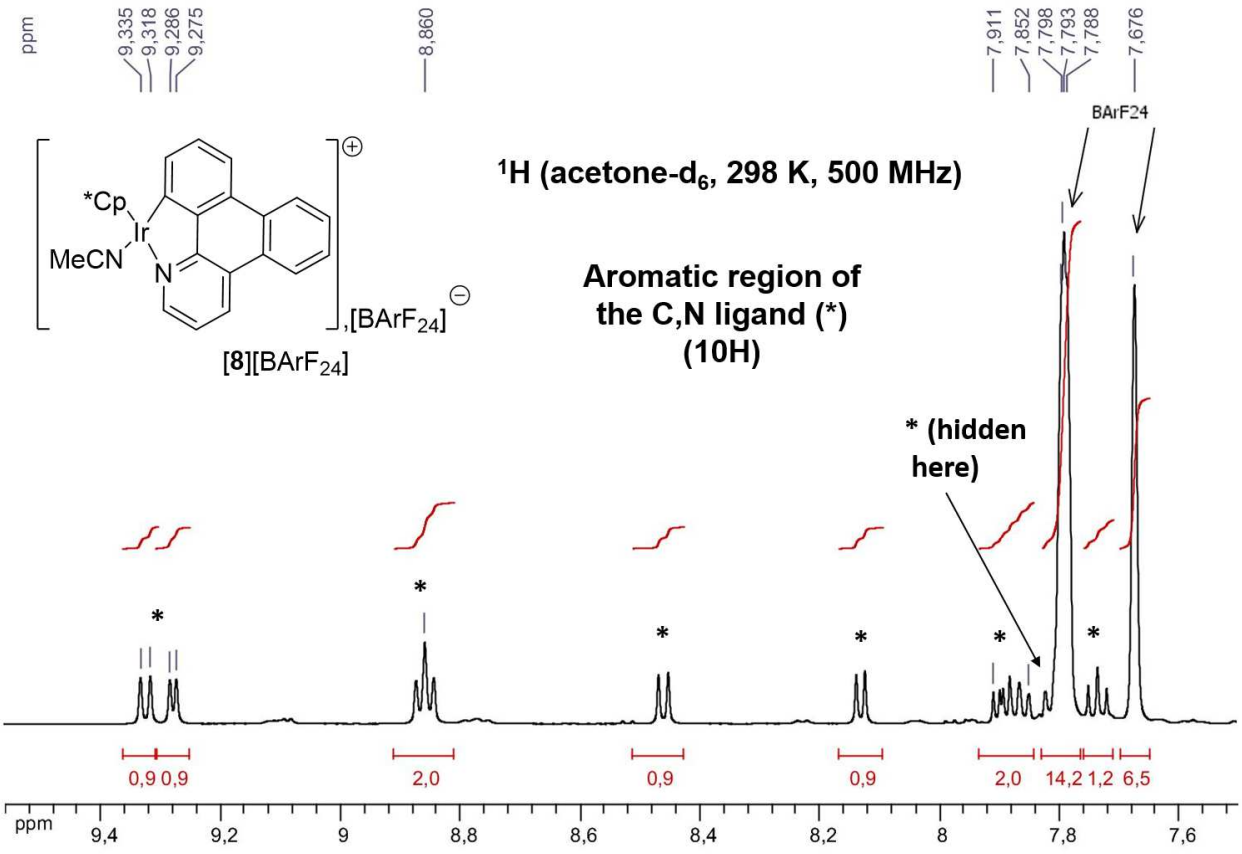
ppm
9,335
9,318
9,286
9,275
8,860
7,911
7,852
7,798
7,793
7,788
7,676
BArF24
*Cp
Ir
MeCN
N
,[BArF24]
[8][BArF24]
1H (acetone-d6, 298 K, 500 MHz)
Aromatic region of the C,N ligand (*) (10H)
* (hidden here)
0,9 0,9
2,0
0,9
0,9
2,0
14,2 1,2 6,5
ppm
9,4
9,2
9
8,8
8,6
8,4
8,2
8
7,8
7,6

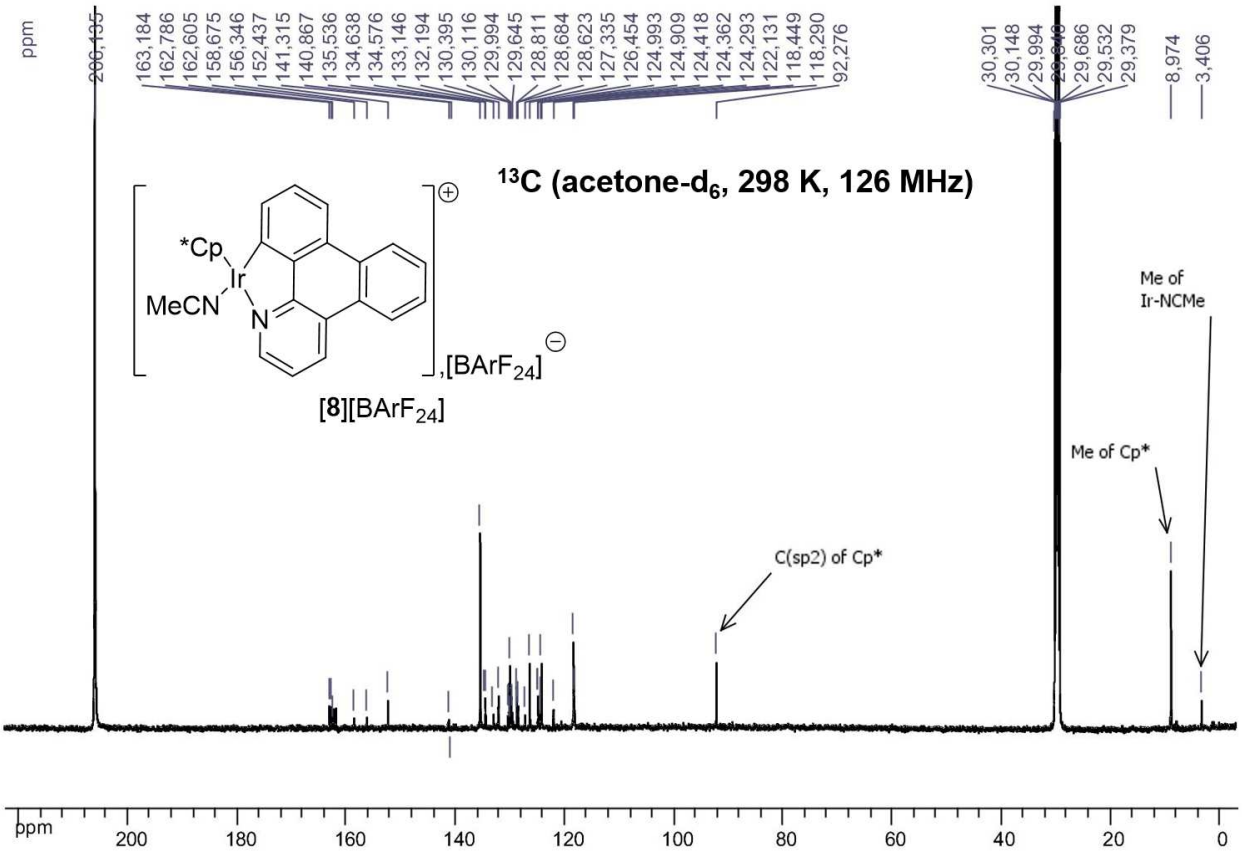
ppm
206,135
163,184
162,786
162,605
158,675
156,346
152,437
141,315
140,867
135,536
134,638
134,576
133,146
132,194
130,395
130,116
129,994
129,645
128,811
128,684
128,623
127,335
126,454
124,993
124,909
124,418
124,362
124,293
122,131
118,449
118,290
92,276
30,301
30,148
29,994
29,840
29,686
29,532
29,379
8,974
3,406
13C (acetone-d6, 298 K, 126 MHz)
*Cp
Ir
MeCN
N
,[BArF24]
[8][BArF24]
Me of Ir-NCMe
Me of Cp*
C(sp2) of Cp*
ppm
200
180
160
140
120
100
80
60
40
20
0

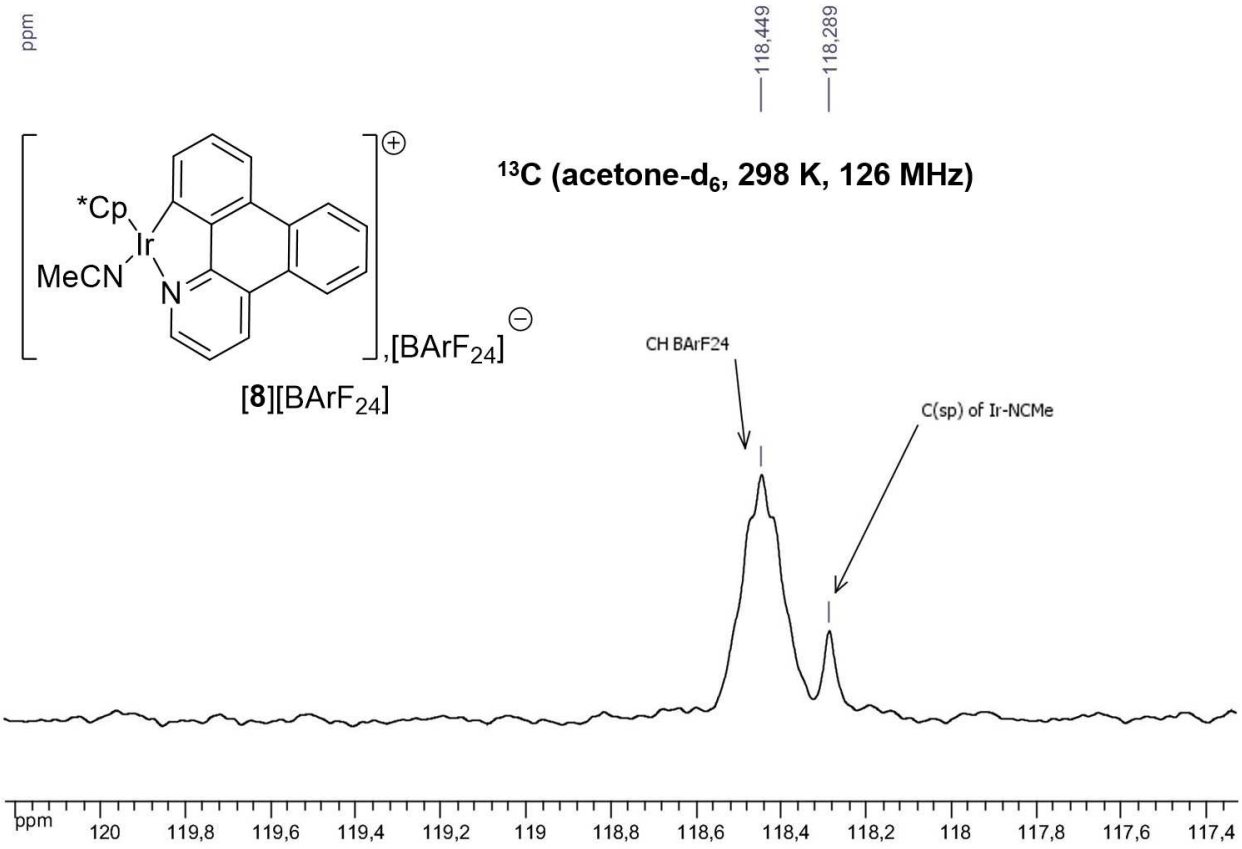
ppm
118,449
118,289
*Cp
Ir
MeCN
N
,[BArF24]
13C (acetone-d6, 298 K, 126 MHz)
CH BArF24
C(sp) of Ir-NCMe
ppm
120
119,8
119,6
119,4
119,2
119
118,8
118,6
118,4
118,2
118
117,8
117,6
117,4

[**8**][BArF$_{24}$]

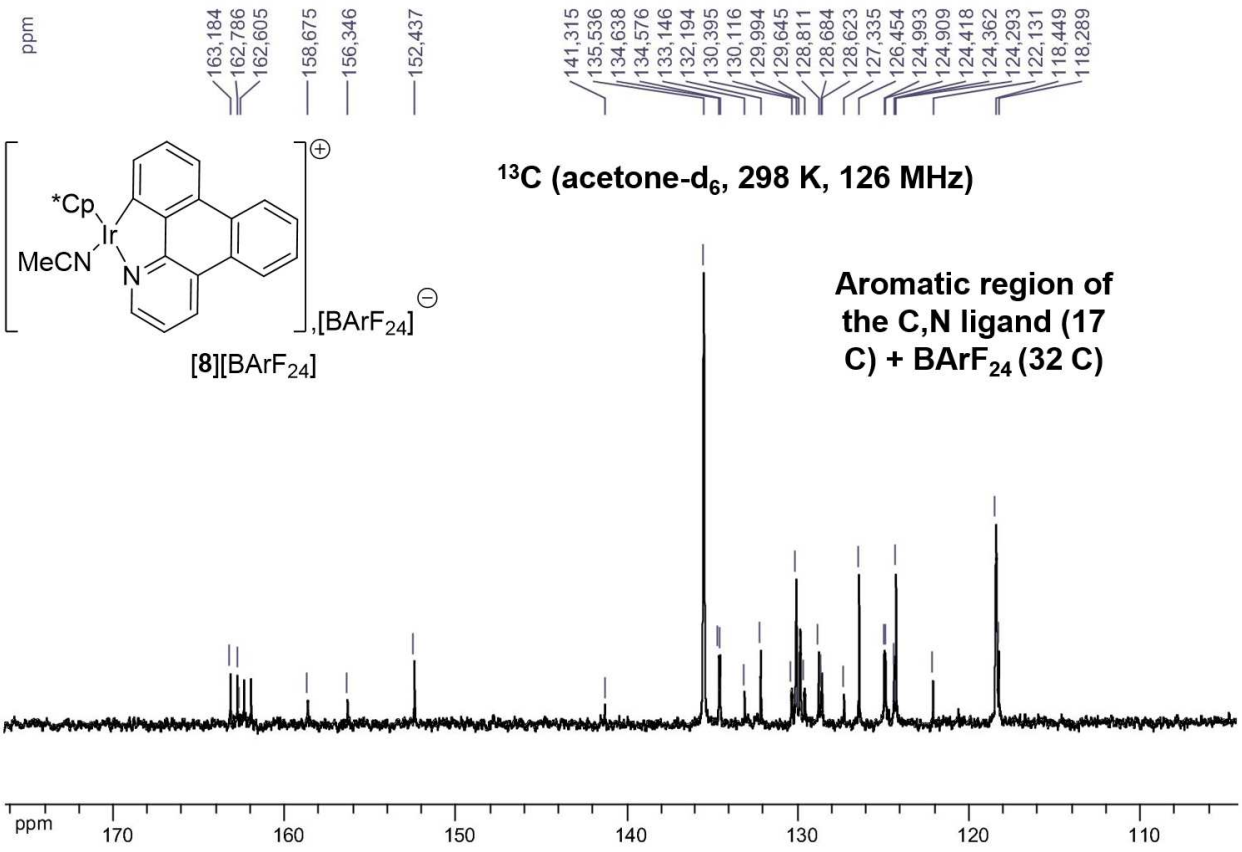
ppm
163,184
162,786
162,605
158,675
156,346
152,437
141,315
135,536
134,638
134,576
133,146
132,194
130,395
130,116
129,994
129,645
128,811
128,684
128,623
127,335
126,454
124,993
124,909
124,418
124,362
124,293
122,131
118,449
118,289
*Cp
Ir
MeCN
N
,[BArF24]
[8][BArF24]
13C (acetone-d6, 298 K, 126 MHz)
Aromatic region of the C,N ligand (17 C) + BArF24 (32 C)
ppm
170
160
150
140
130
120
110

^{19}F (acetone-d_6, 298 K, 282 MHz)

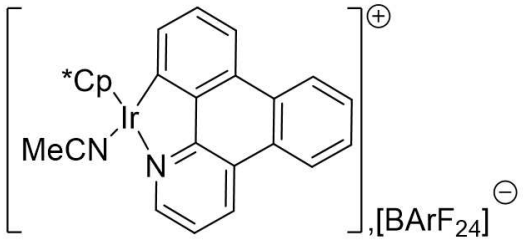

[**8**][$BArF_{24}$]

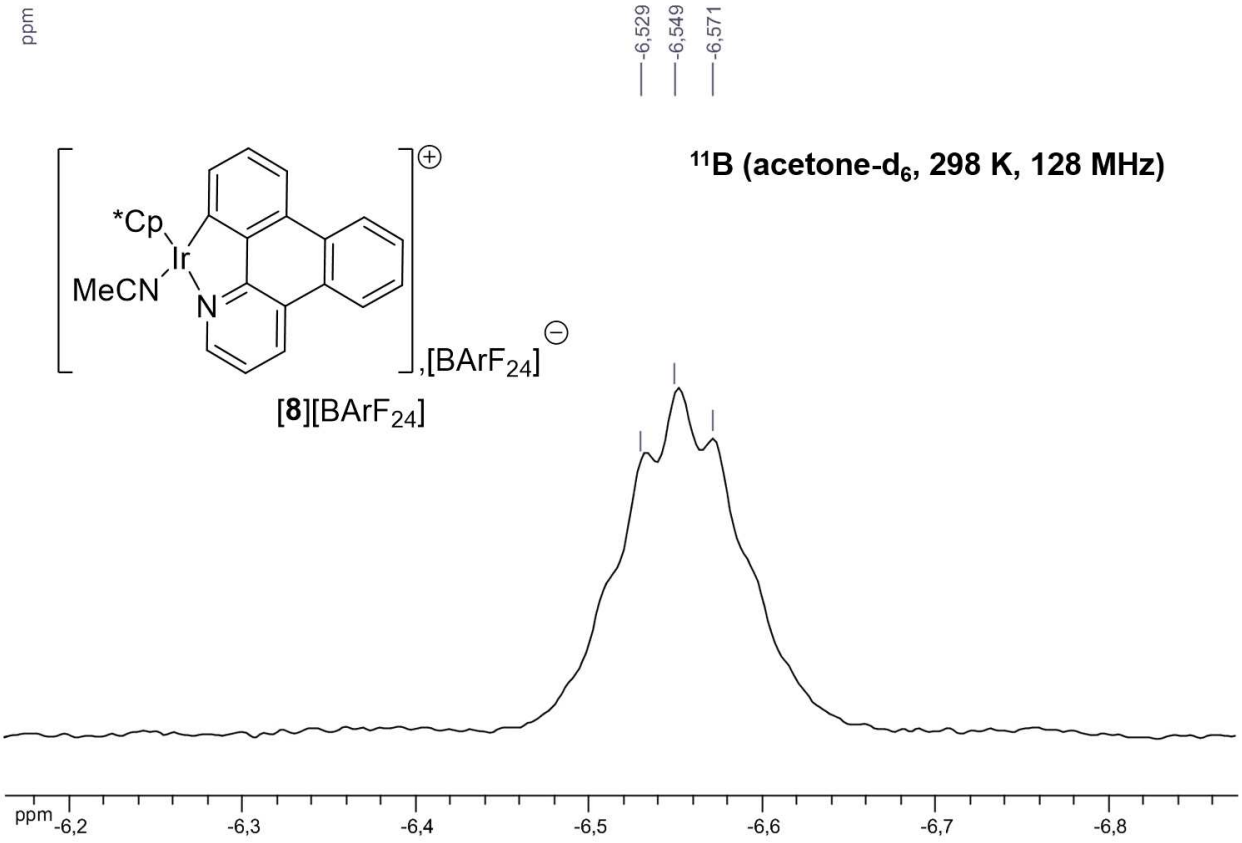

6.2.9.11 [**10**][BArF$_{24}$]

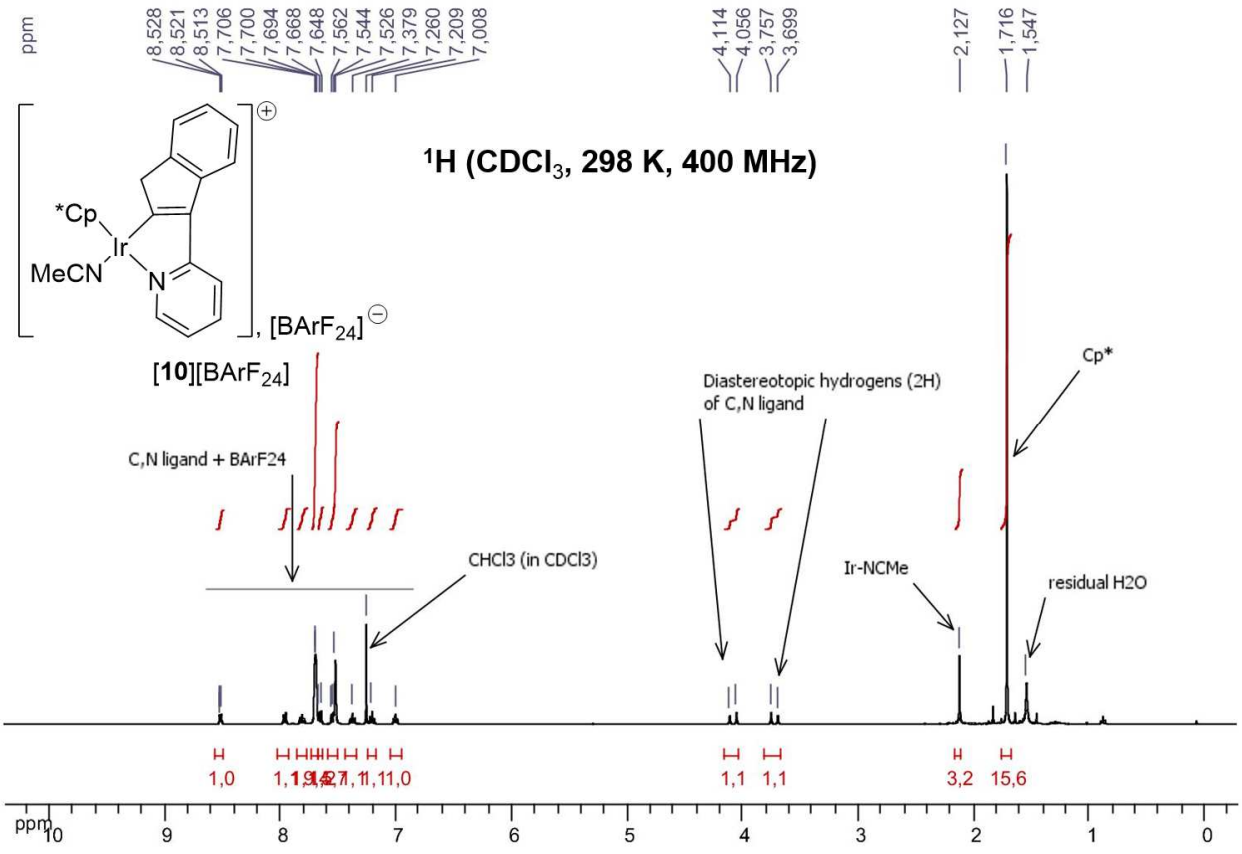
ppm
8,528
8,521
8,513
7,706
7,700
7,694
7,668
7,648
7,562
7,544
7,526
7,379
7,260
7,209
7,008
4,114
4,056
3,757
3,699
2,127
1,716
1,547
*Cp
Ir
MeCN
N
, [BArF24]
[10][BArF24]
¹H (CDCl3, 298 K, 400 MHz)
C,N ligand + BArF24
CHCl3 (in CDCl3)
Diastereotopic hydrogens (2H)
of C,N ligand
Cp*
Ir-NCMe
residual H2O
1,0
1,1
1,1
3,2
15,6
ppm
10
9
8
7
6
5
4
3
2
1
0

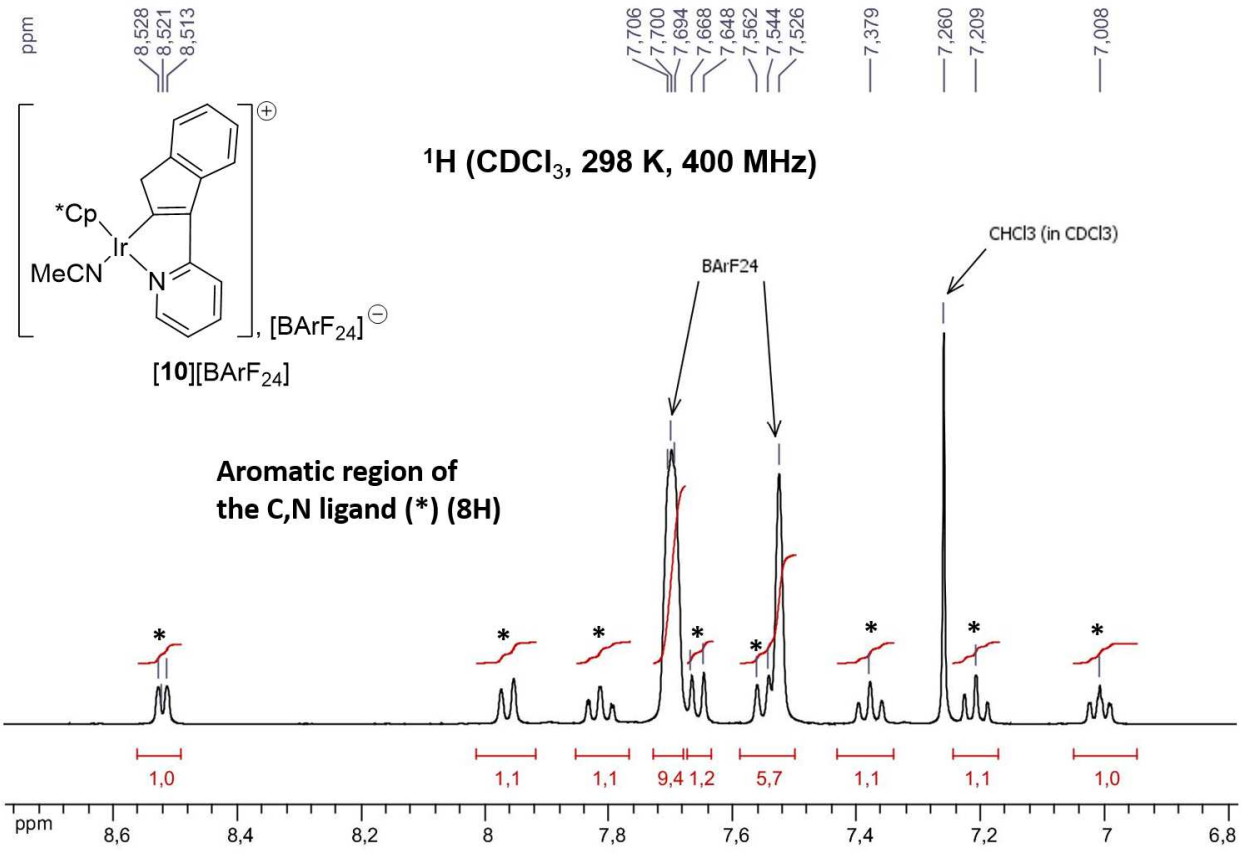
ppm
8,528
8,521
8,513
7,706
7,700
7,694
7,668
7,648
7,562
7,544
7,526
7,379
7,260
7,209
7,008
*Cp
Ir
MeCN
N
, [BArF24]
[10][BArF24]
1H (CDCl3, 298 K, 400 MHz)
BArF24
CHCl3 (in CDCl3)
Aromatic region of
the C,N ligand (*) (8H)
1,0
1,1
1,1
9,4
1,2
5,7
1,1
1,1
1,0
ppm
8,6
8,4
8,2
8
7,8
7,6
7,4
7,2
7
6,8

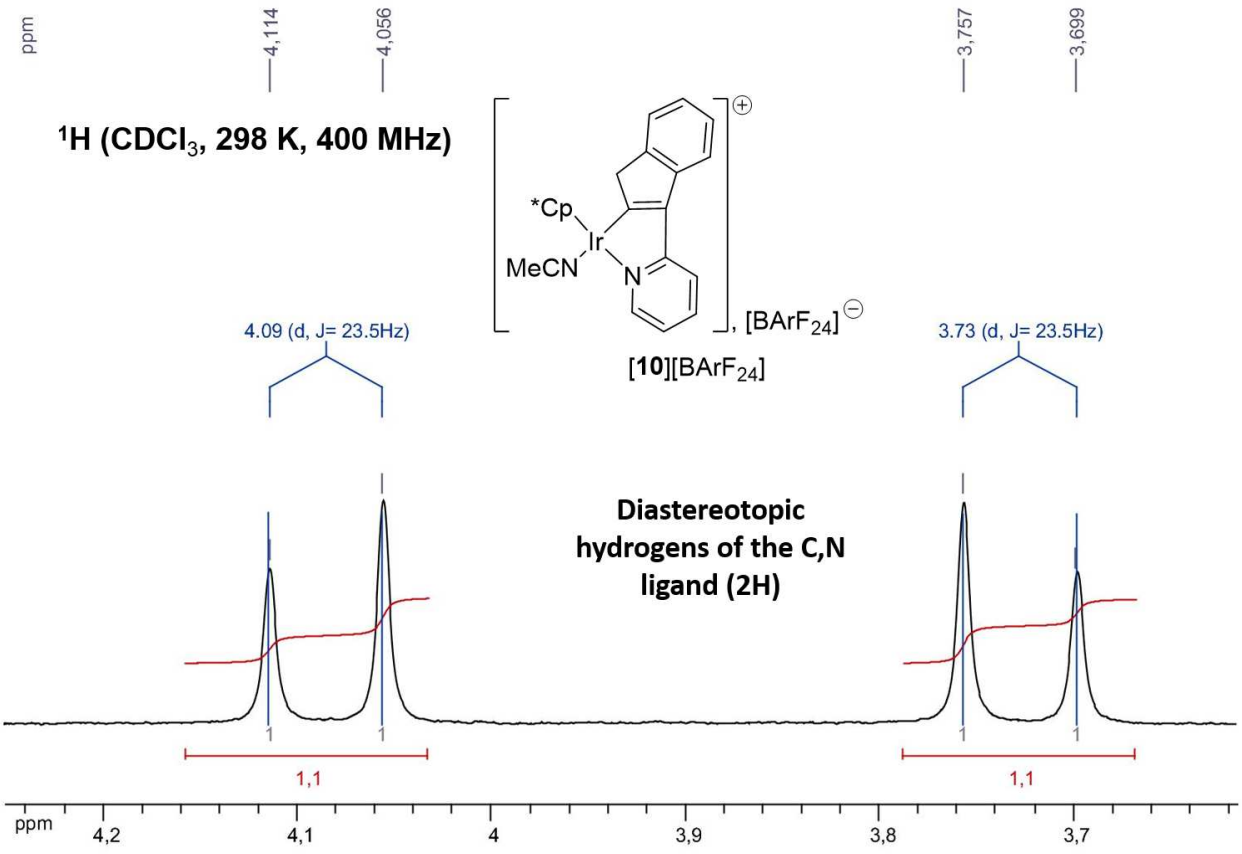
ppm
4,114
4,056
3,757
3,699
¹H (CDCl3, 298 K, 400 MHz)
*Cp
Ir
MeCN
N
, [BArF24]
[10][BArF24]
4.09 (d, J= 23.5Hz)
3.73 (d, J= 23.5Hz)
Diastereotopic hydrogens of the C,N ligand (2H)
1
1
1,1
1
1
1,1
ppm
4,2
4,1
4
3,9
3,8
3,7

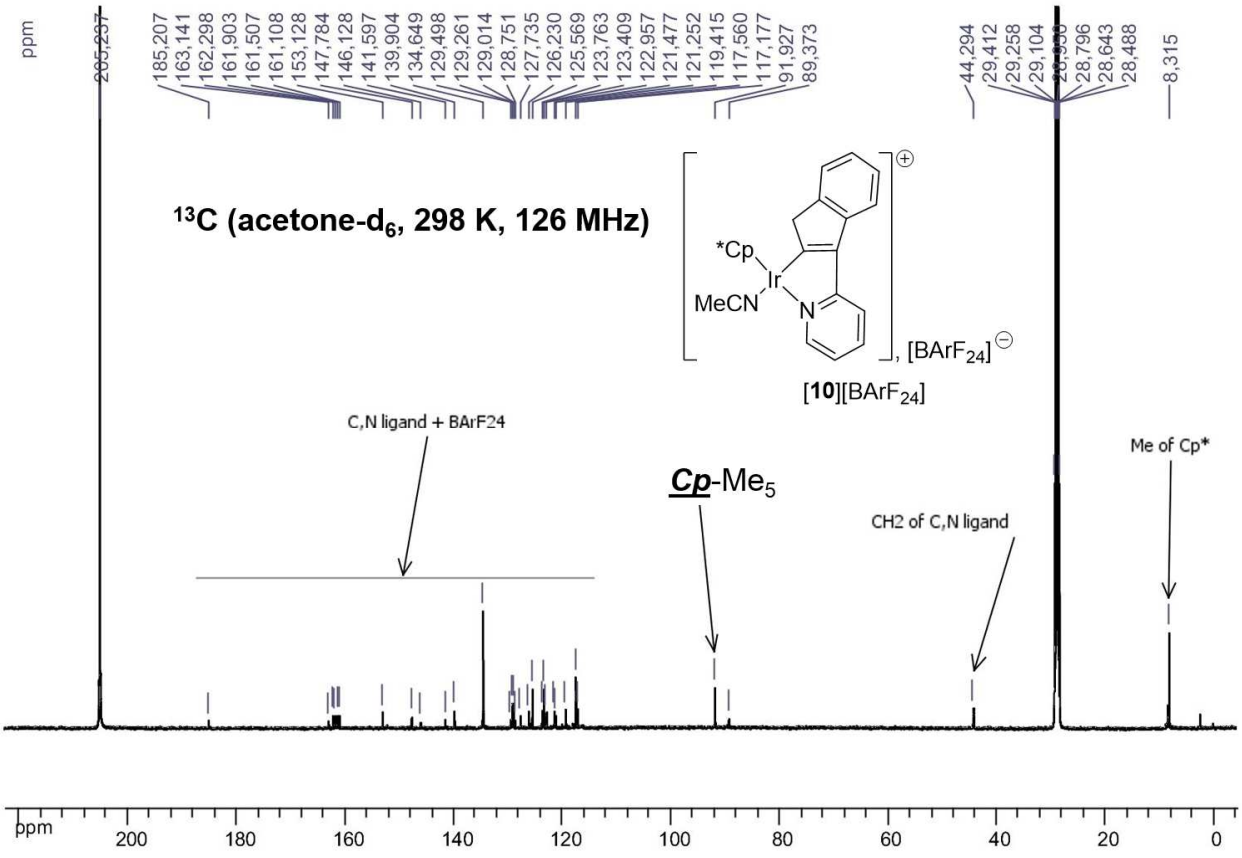
ppm
205,237
185,207
163,141
162,298
161,903
161,507
161,108
153,128
147,784
146,128
141,597
139,904
134,649
129,498
129,261
129,014
128,751
127,735
126,230
125,569
123,763
123,409
122,957
121,477
121,252
119,415
117,560
117,177
91,927
89,373
44,294
29,412
29,258
29,104
28,930
28,796
28,643
28,488
8,315
13C (acetone-d6, 298 K, 126 MHz)
*Cp
Ir
MeCN
N
, [BArF24]
[10][BArF24]
C,N ligand + BArF24
Cp-Me5
CH2 of C,N ligand
Me of Cp*
ppm
200
180
160
140
120
100
80
60
40
20
0

^{19}F (acetone-d_6, 298 K, 282 MHz)

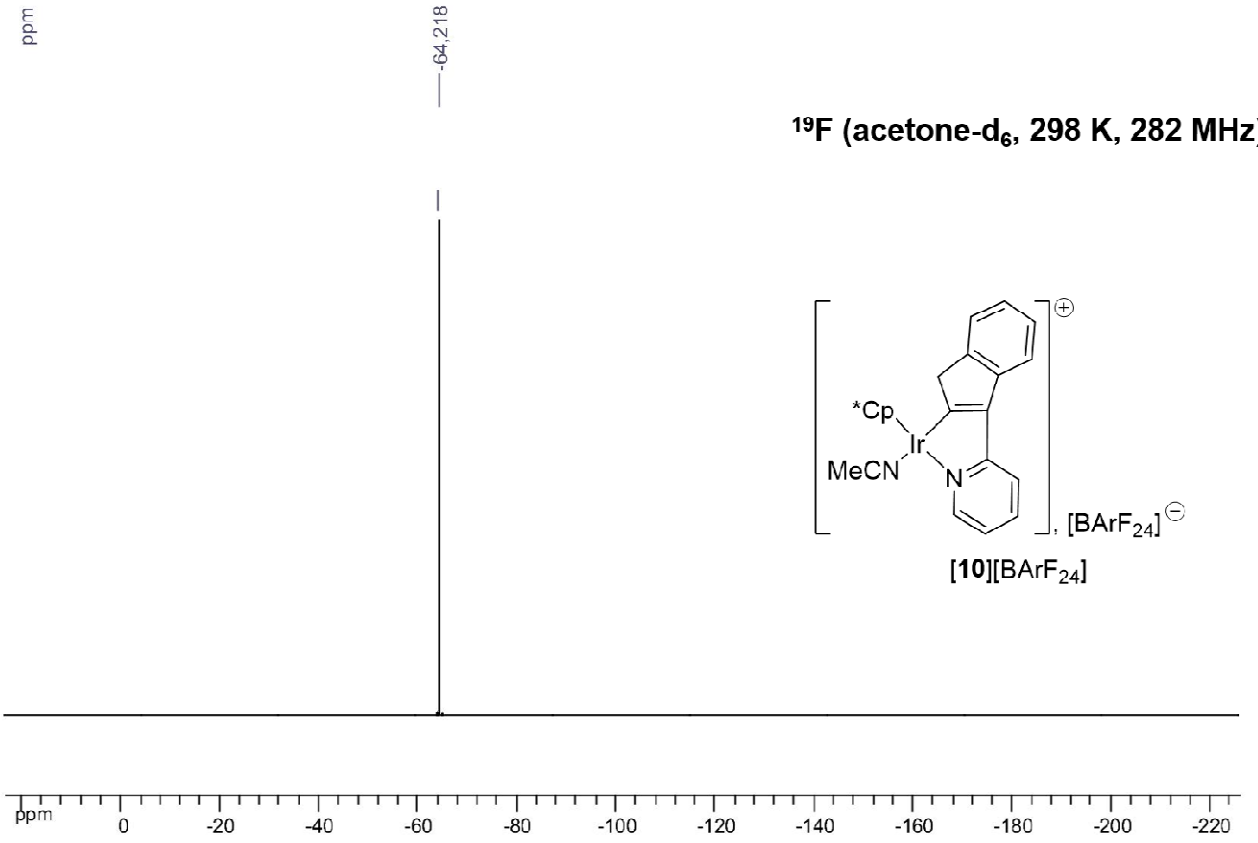

[10][BArF$_{24}$]

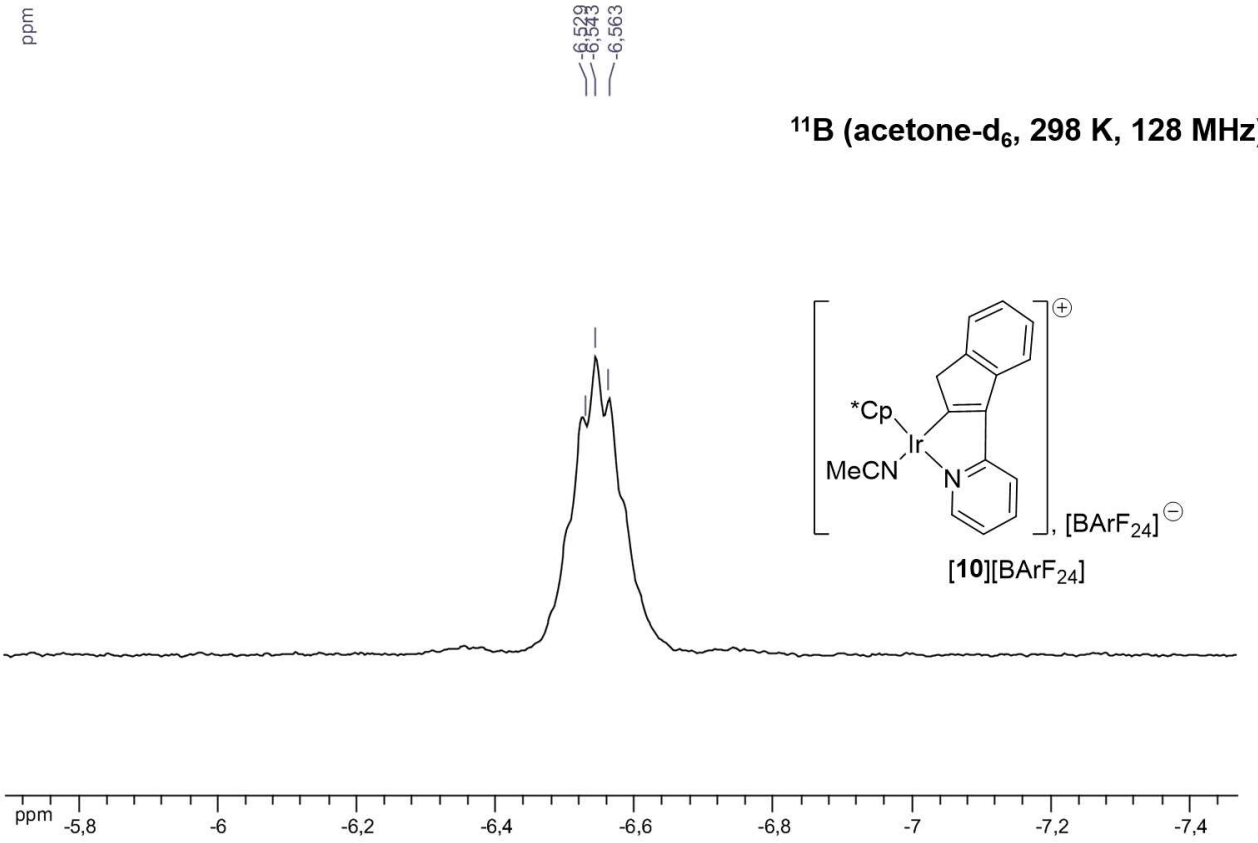
ppm
-6,529
-6,543
-6,563
11B (acetone-d6, 298 K, 128 MHz)
*Cp
Ir
MeCN
N
, [BArF24]
[10][BArF24]
ppm
-5,8
-6
-6,2
-6,4
-6,6
-6,8
-7
-7,2
-7,4

6.2.9.12 [**12**][OTf]

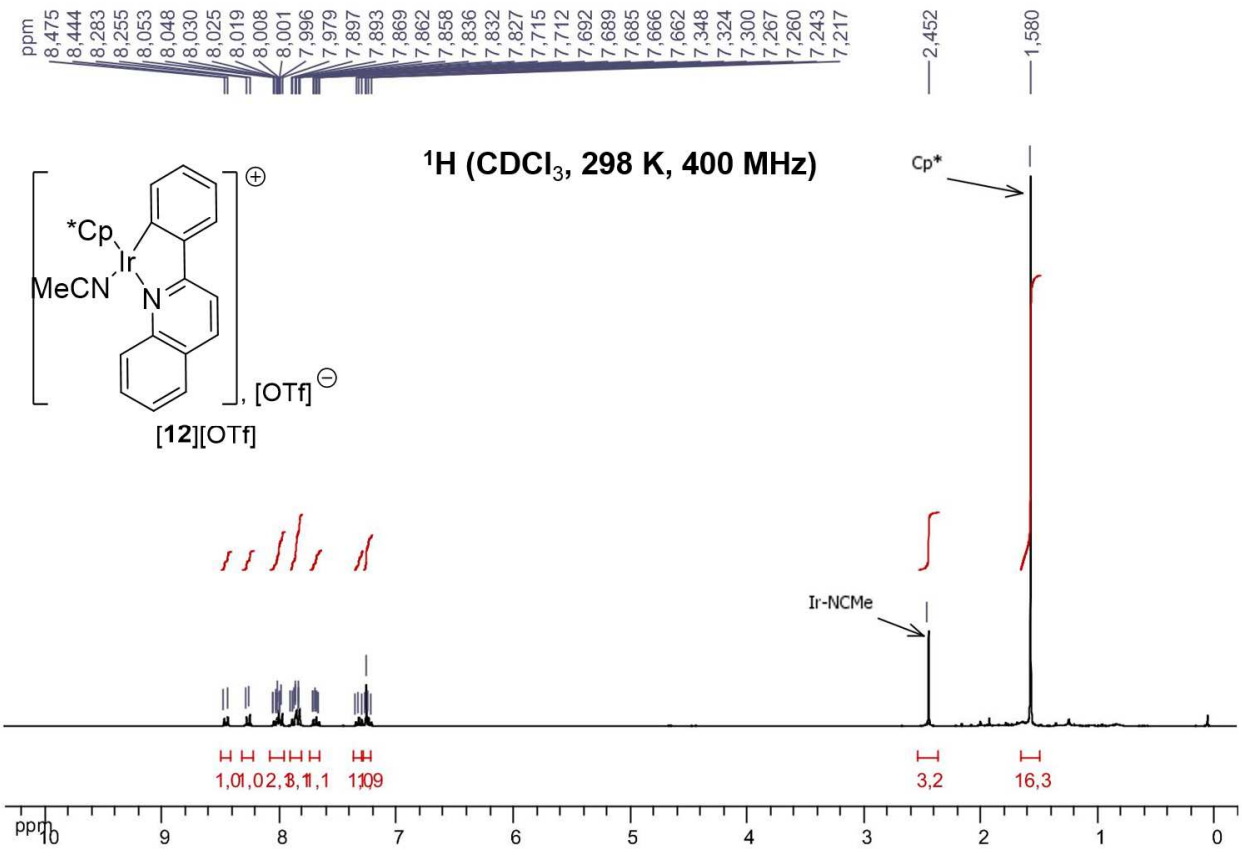
ppm
8,475
8,444
8,283
8,255
8,053
8,048
8,030
8,025
8,019
8,008
8,001
7,996
7,979
7,897
7,893
7,869
7,862
7,858
7,836
7,832
7,827
7,715
7,712
7,692
7,689
7,685
7,666
7,662
7,348
7,324
7,300
7,267
7,260
7,243
7,217
2,452
1,580
¹H (CDCl3, 298 K, 400 MHz)
*Cp
Ir
MeCN
N
[OTf]
[12][OTf]
Cp*
Ir-NCMe
1,0
1,0
2,3
3,1
1,1
1,0
3,2
16,3
ppm
10
9
8
7
6
5
4
3
2
1
0

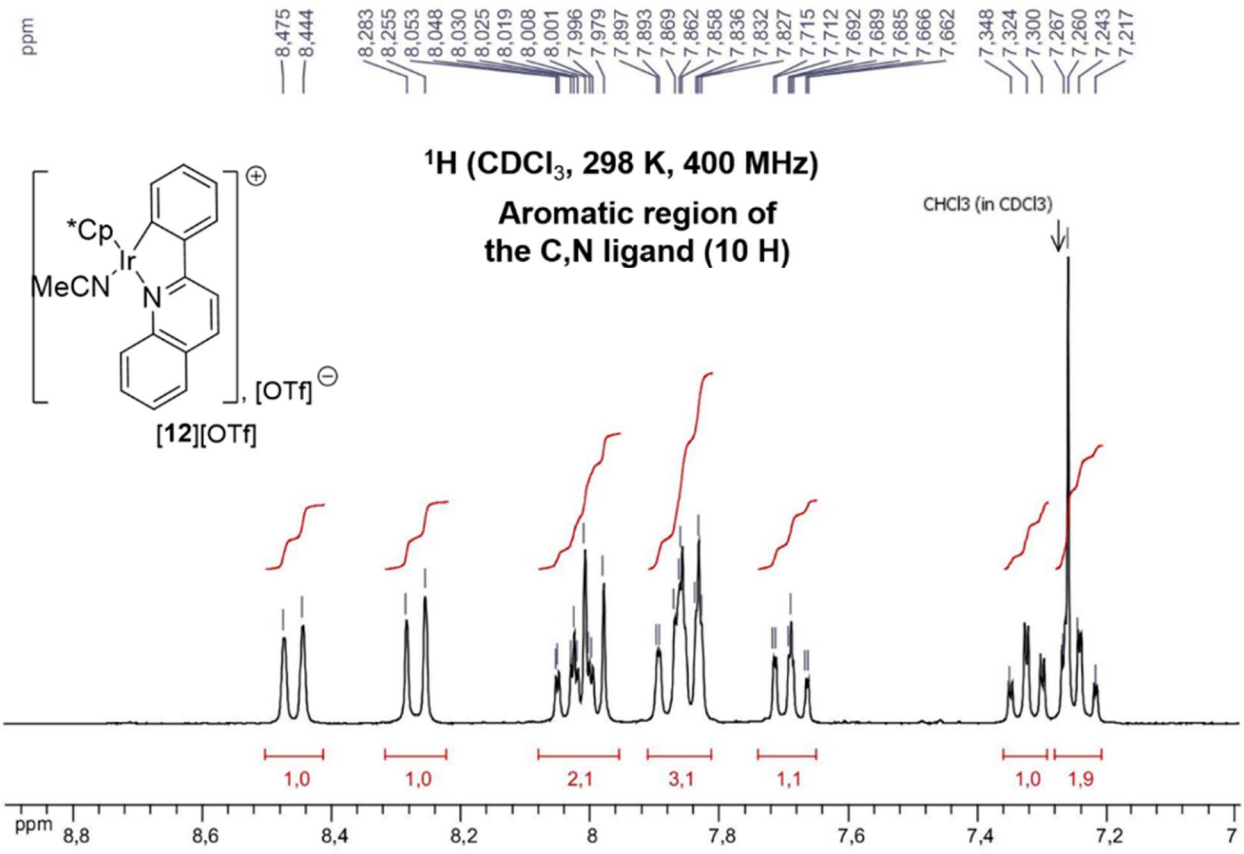
ppm
8,475
8,444
8,283
8,255
8,053
8,048
8,030
8,025
8,019
8,008
8,001
7,996
7,979
7,897
7,893
7,869
7,862
7,858
7,836
7,832
7,827
7,715
7,712
7,692
7,689
7,685
7,666
7,662
7,348
7,324
7,300
7,267
7,260
7,243
7,217
*Cp
Ir
MeCN
N
, [OTf]
[12][OTf]
¹H (CDCl₃, 298 K, 400 MHz)
Aromatic region of
the C,N ligand (10 H)
CHCl3 (in CDCl3)
1,0
1,0
2,1
3,1
1,1
1,0
1,9
ppm
8,8
8,6
8,4
8,2
8
7,8
7,6
7,4
7,2
7

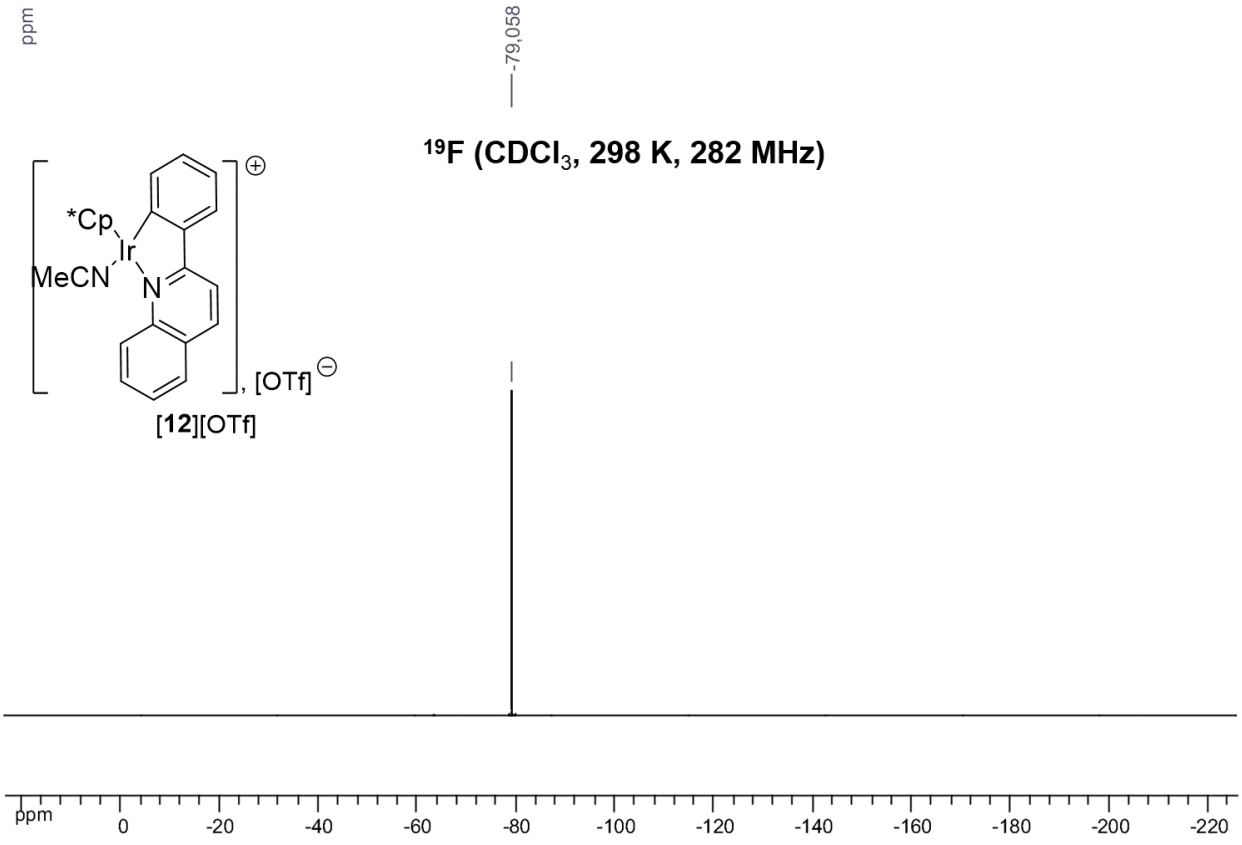

^{19}F ($CDCl_3$, 298 K, 282 MHz)

6.2.10 NMR spectra of the ionic rhodacycle [**2'**][$BArF_{24}$]

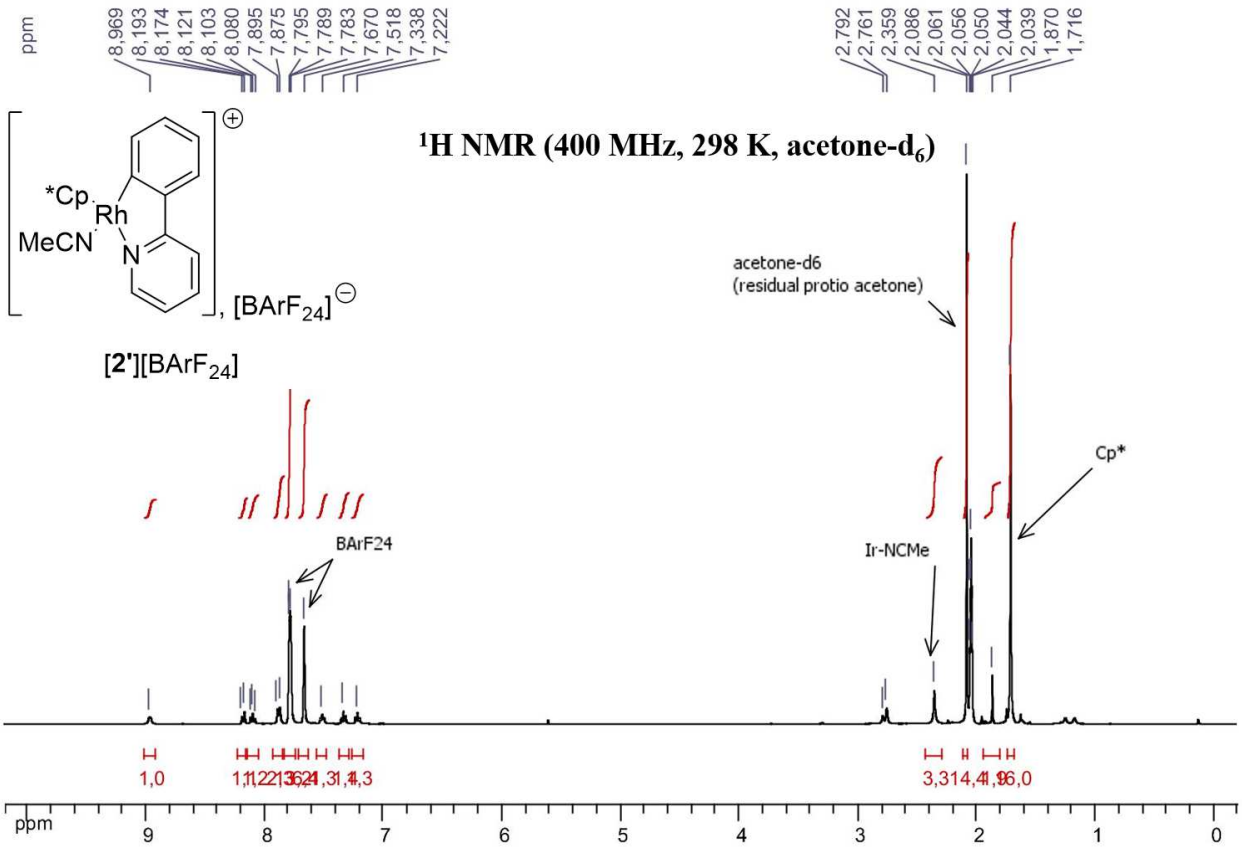
ppm
8,969
8,193
8,174
8,121
8,103
8,080
7,895
7,875
7,795
7,789
7,783
7,670
7,518
7,338
7,222
2,792
2,761
2,359
2,086
2,061
2,056
2,050
2,044
2,039
1,870
1,716
*Cp
Rh
MeCN
N
, [BArF24]
[2'][BArF24]
¹H NMR (400 MHz, 298 K, acetone-d6)
acetone-d6
(residual protio acetone)
Cp*
BArF24
Ir-NCMe
1,0
3,3
14,4
1,9
6,0
ppm
9
8
7
6
5
4
3
2
1
0

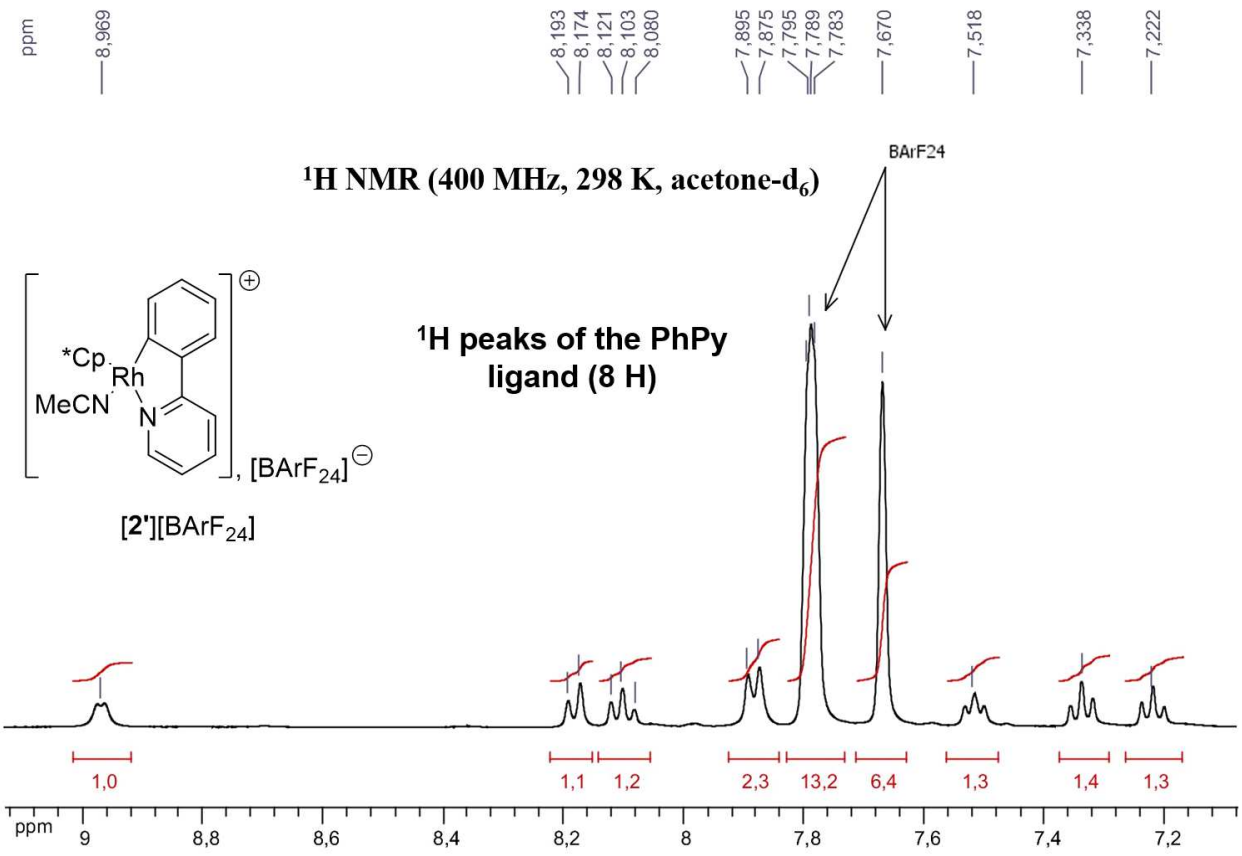

6.2.11 NMR spectra of the ionic iridacycle [**2C**][BArF$_{24}$]

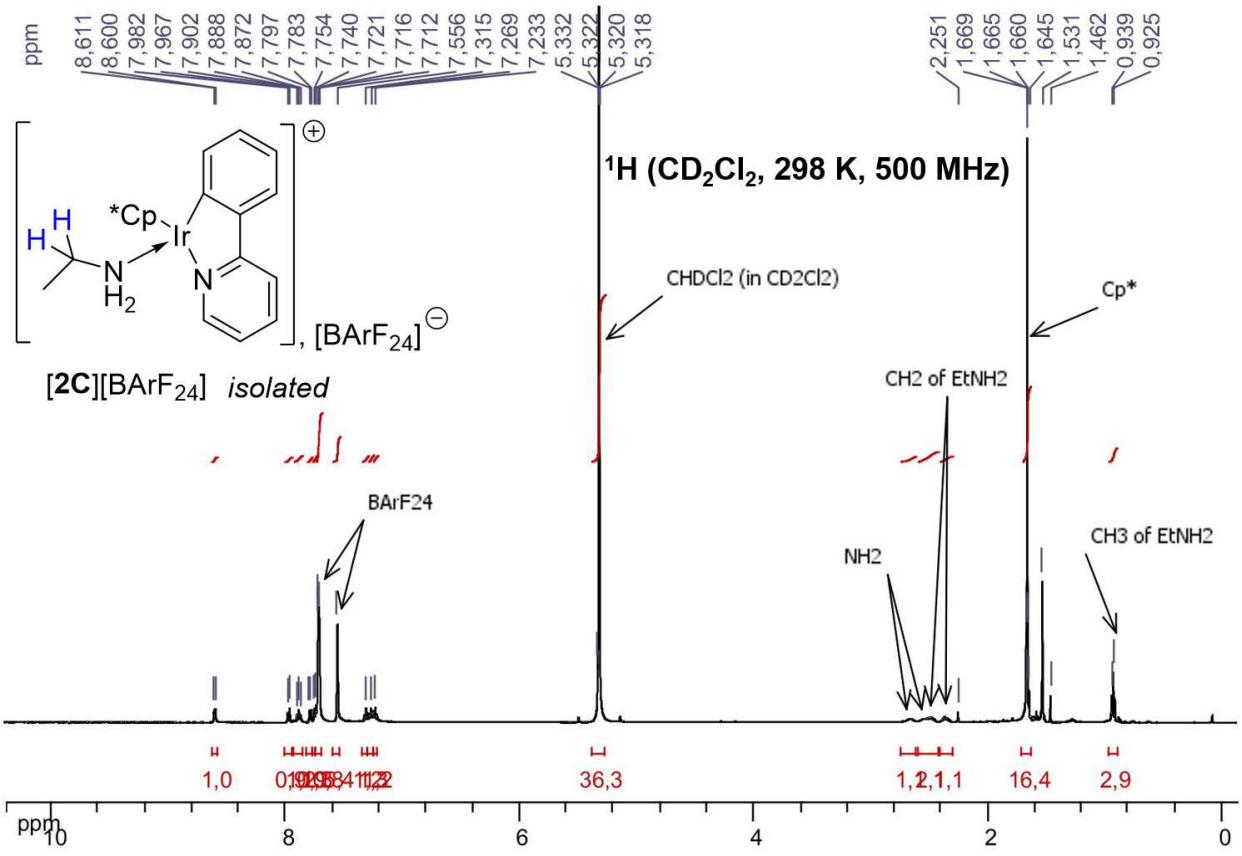
ppm
8,611
8,600
7,982
7,967
7,902
7,888
7,872
7,797
7,783
7,754
7,740
7,721
7,716
7,712
7,556
7,315
7,269
7,233
5,332
5,322
5,320
5,318
2,251
1,669
1,665
1,660
1,645
1,531
1,462
0,939
0,925
*Cp
Ir
H
H
N
H2
N
, [BArF24]
[2C][BArF24] isolated
1H (CD2Cl2, 298 K, 500 MHz)
CHDCl2 (in CD2Cl2)
Cp*
CH2 of EtNH2
BArF24
NH2
CH3 of EtNH2
1,0
36,3
16,4
2,9
ppm
10
8
6
4
2
0

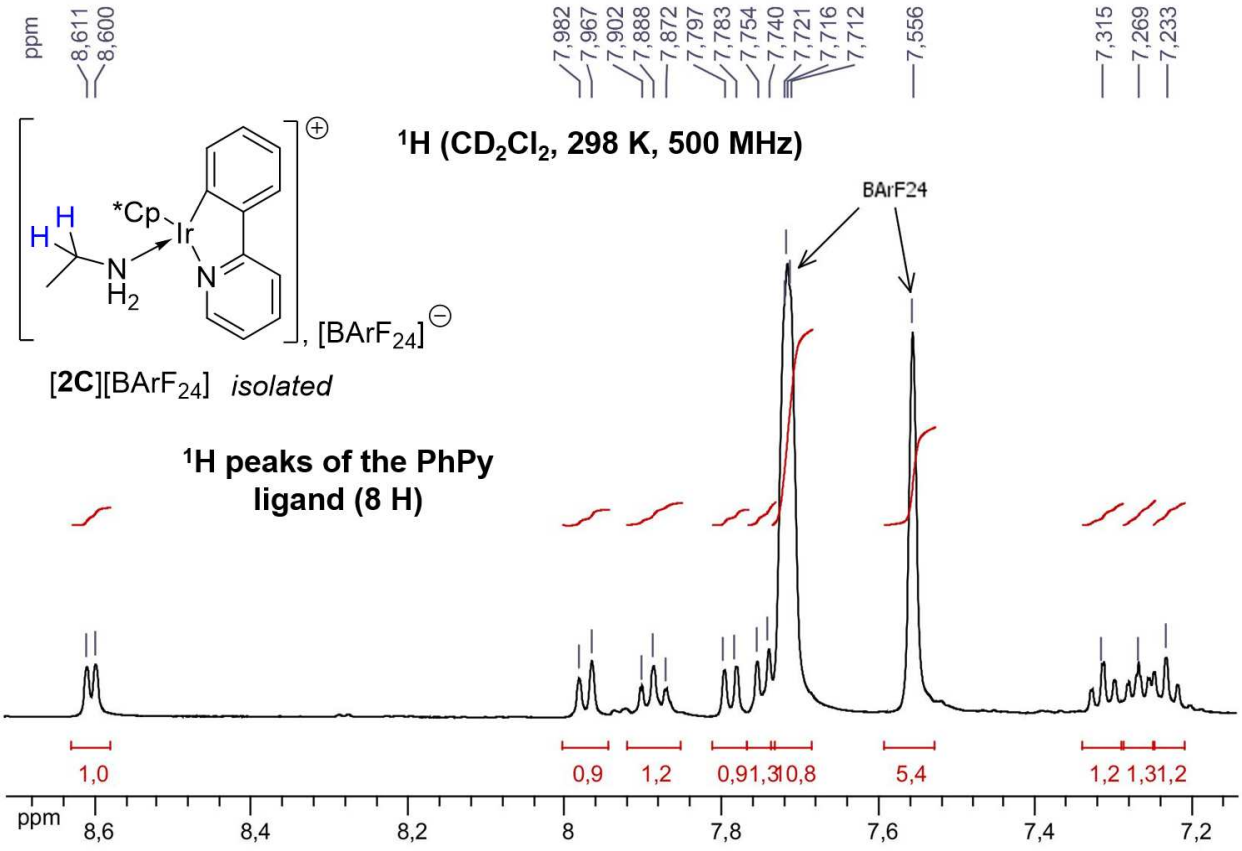
ppm
8,611
8,600
7,982
7,967
7,902
7,888
7,872
7,797
7,783
7,754
7,740
7,721
7,716
7,712
7,556
7,315
7,269
7,233
¹H (CD₂Cl₂, 298 K, 500 MHz)
BArF24
*Cp
Ir
H
H
N
H₂
N
⊕
⊖
, [BArF24]
[2C][BArF24] isolated
¹H peaks of the PhPy ligand (8 H)
1,0
0,9
1,2
0,9
1,3
1
0,8
5,4
1,2
1,3
1,2
ppm
8,6
8,4
8,2
8
7,8
7,6
7,4
7,2

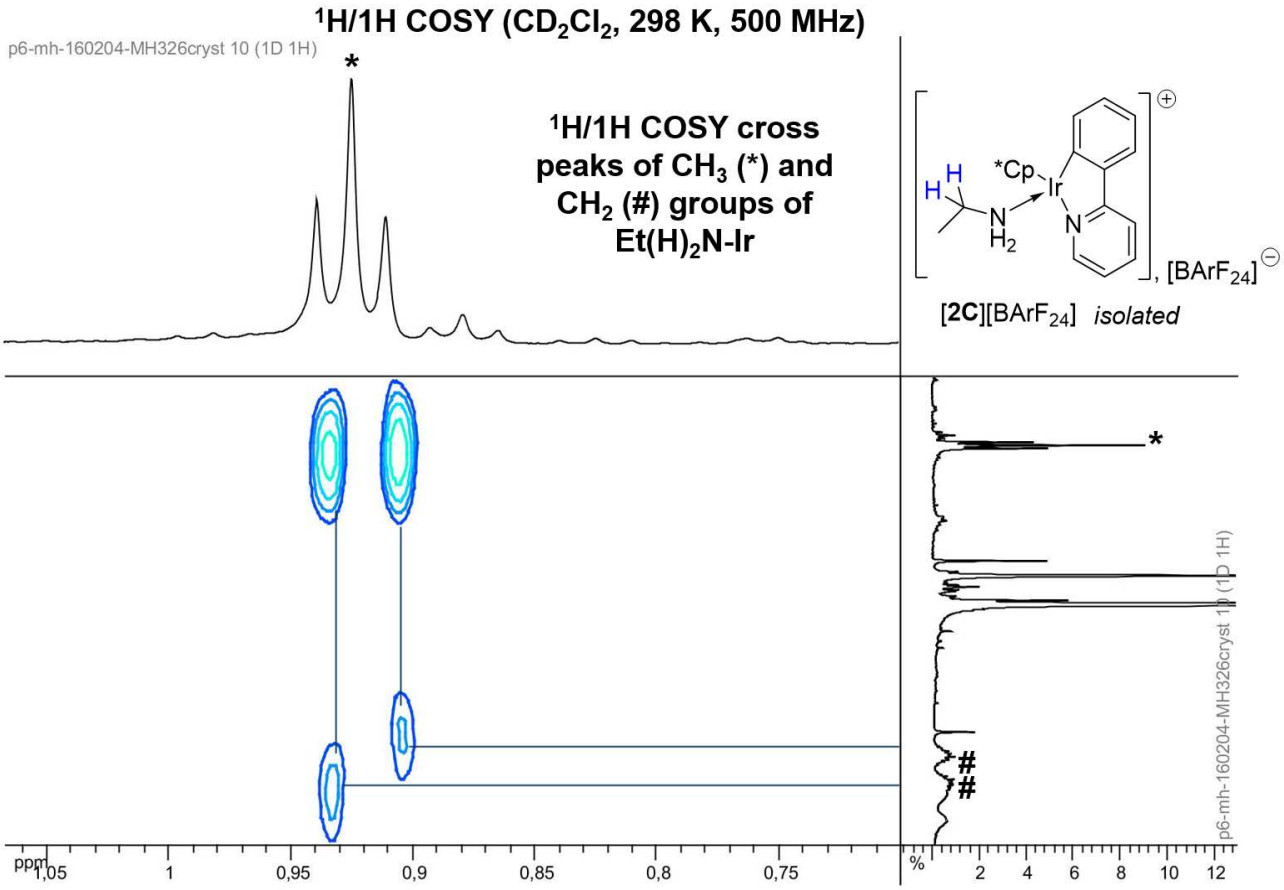
^{1}H/1H COSY (CD_2Cl_2, 298 K, 500 MHz)
p6-mh-160204-MH326cryst 10 (1D 1H)
*
^{1}H/1H COSY cross peaks of CH_3 (*) and CH_2 (#) groups of $Et(H)_2N$-Ir
*Cp
Ir
N
H_2
, $[BArF_{24}]^-$
[2C][$BArF_{24}$] *isolated*
#
#
ppm
1,05
1
0,95
0,9
0,85
0,8
0,75
%
2
4
6
8
10
12

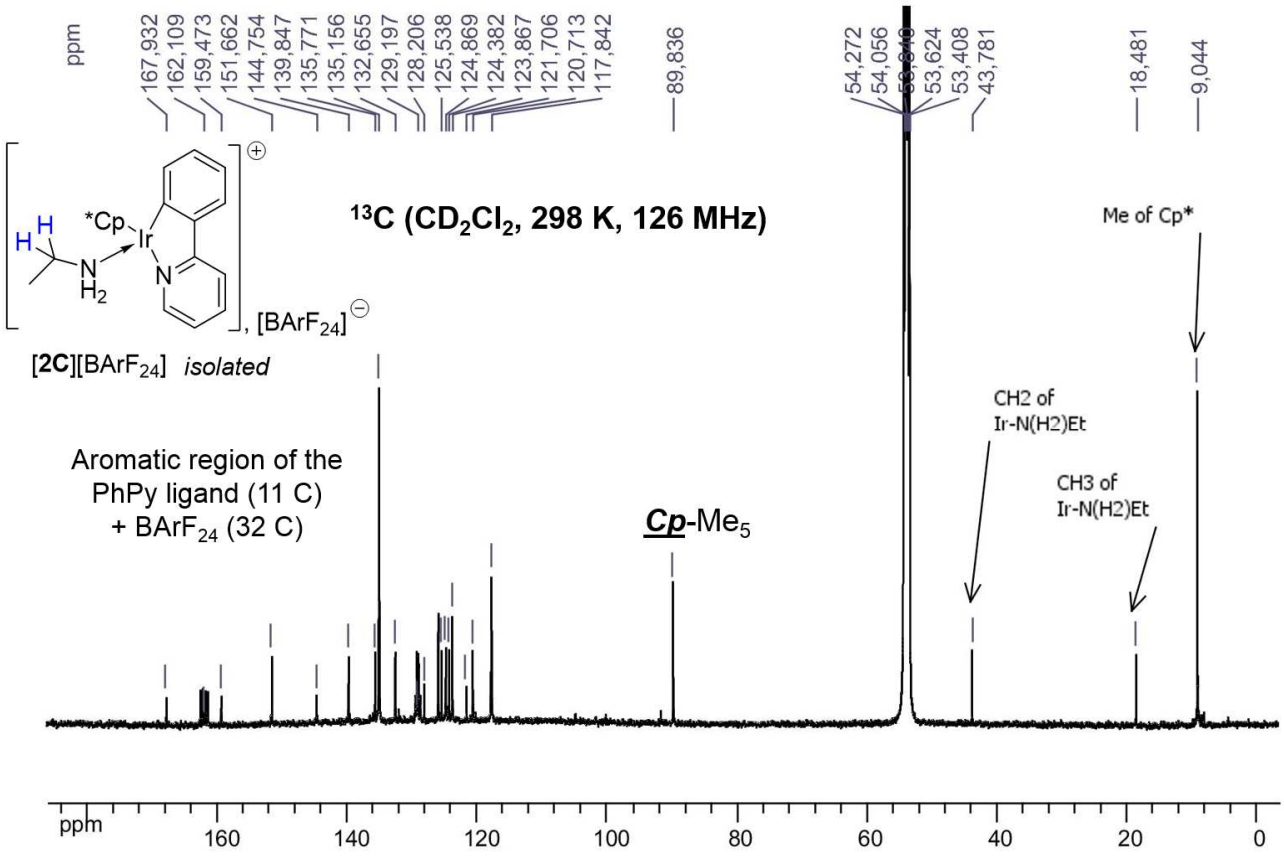
ppm
167,932
162,109
159,473
151,662
144,754
139,847
135,771
135,156
132,655
129,197
128,206
125,538
124,869
124,382
123,867
121,706
120,713
117,842
89,836
54,272
54,056
53,624
53,408
43,781
18,481
9,044
*Cp
Ir
N
H
H
N
H2
, [BArF24]
[2C][BArF24] isolated
13C (CD2Cl2, 298 K, 126 MHz)
Me of Cp*
CH2 of
Ir-N(H2)Et
CH3 of
Ir-N(H2)Et
Aromatic region of the
PhPy ligand (11 C)
+ BArF24 (32 C)
Cp-Me5
ppm
160
140
120
100
80
60
40
20
0

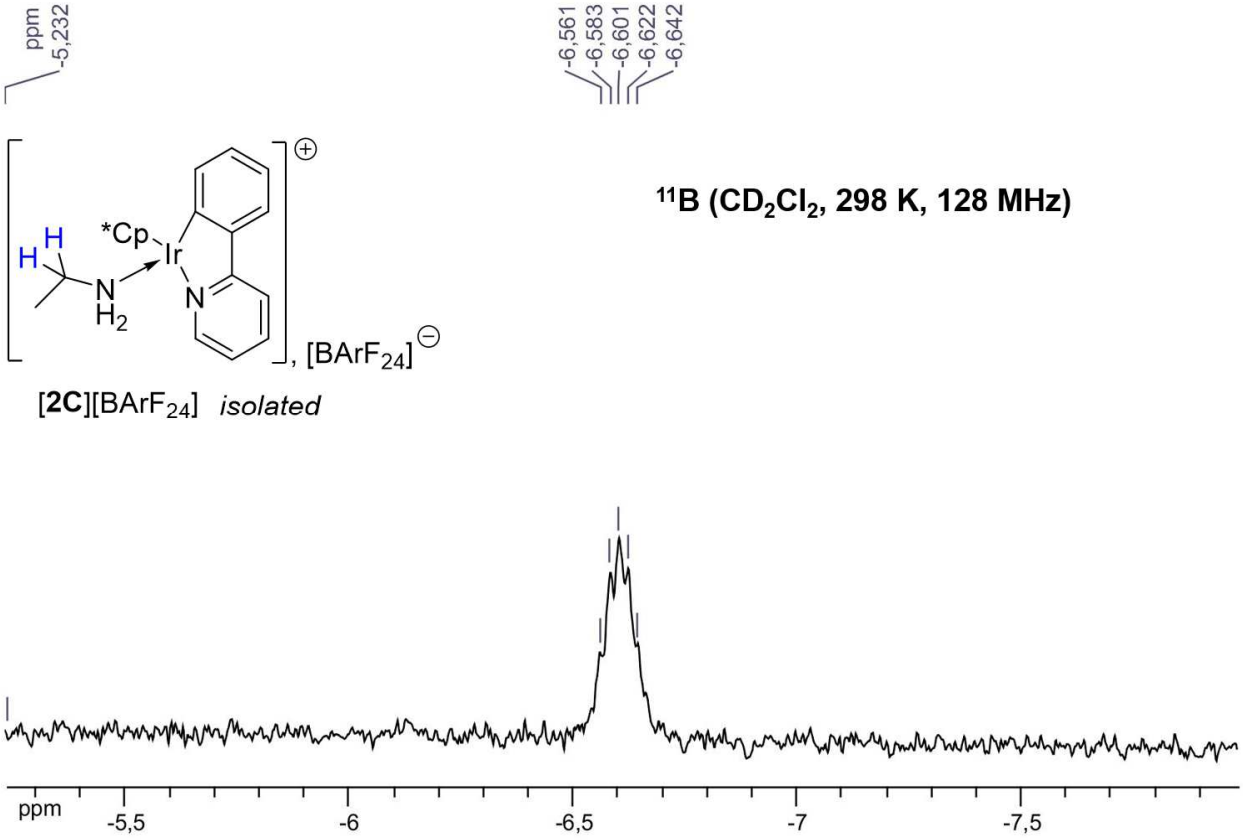

^{11}B (CD_2Cl_2, 298 K, 128 MHz)

[2C][$BArF_{24}$] *isolated*

6.2.12 Catalytic studies of the *O*-silylation of alcohols

6.2.12.1 General procedure for catalysis: monitoring with a piezometric setup

Alcohol (1 equiv) and $HSiEt_3$ (0.5 equiv) were introduced in a small-volume double-walled Schlenk vessel thermostated at 20 °C. After the resulting mixture was slowly stirred for a few minutes, a Mykrolis A332984-007 absolute pressure-tovoltage transducer was airtightly screwed to the neck of the glass vessel and connected to a Pico-Log analog-logic converter/data-logger board interfaced to a computer. This allowed the measurement of the pressure of hydrogen (computed from a linear absolute pressure–output voltage relationship) developed in the known overhead volume of the sealed reactor as a function of time. The absence of leaks was checked by applying a moderate pressure of argon gas. The iridium precatalyst (0.1 mol % relative to $HSiEt_3$) dissolved in 1,2-dichloroethane (0.5 mL) was injected swiftly into the vessel via a lateral glass valve, which was tightly sealed immediately upon injection to avoid gas leaks. Blank control experiments without catalyst were systematically carried out with all alcohols. After each catalytic run the crude reaction mixture was analyzed by ^1H NMR spectroscopy, and the identity of the alkoxysilane was assessed by comparison with data from the literature: $PhCH_2OSiEt_3$,[385] (4-*i*Pr-Ph)CH_2OSiEt_3,[386] (4-MeO-Ph)-CH_2OSiEt_3,[387] $MeOSiEt_3$,[388] $nC_{10}H_{11}OSiEt_3$,[389] and [1-(naphthalen-2-yl)ethoxy]triethylsilane.[390] Kinetic isotopic effects were computed from initial rates of $HSiEt_3$ consumption in solution, which were inferred from an ideal gas law treatment of the developed H_2 (or HD) gas pressure.

6.2.12.2 Silane screening

[385] son, E. A.; Trivedi, E. R.; Corbin, R. A.; Abu-Omar, M. M. Mechanism for Reduction Catalysis by Metal Oxo: Hydrosilation of Organic Carbonyl Groups Catalyzed by a Rhenium(V) Oxo Complex. *J. Am. Chem. Soc.* **2005**, *127*, 15374-15375.
[386] Wright, A.; West, R. New Anionic Rearrangements. XVII. 1,2-Anionic Rearrangements from Oxygen to Carbon in Benzyloxyorganosilanes and Benzyloxyorganogermanes. *J. Am. Chem. Soc.* **1974**, *96*, 3214-3222.
[387] Kennedy-Smith, J. J.; Nolin, K. A.; Gunterman, H. P.; Toste, F. D. Reversing the Role of the Metal-oxygen π-bond. Chemoselective Catalytic Reductions with a Rhenium(V)-Dioxo Complex Joshua J. Kennedy-Smith, Kristine A. Nolin, Haluna P. Gunterman, F. Dean Toste. *J. Am. Chem. Soc.* **2003**, *125*, 4056-4057.
[388] Caseri, W.; Pregosin, P. S. Hydrosilylation chemistry and catalysis with cis-$PtCl_2(PhCH{:}CH_2)_2$. *Organometallics* **1988**, *7*, 1373-1380.
[389] Ito, H.; Watanabe, A.; Sawamura, M. Versatile Dehydrogenative Alcohol Silylation Catalyzed by Cu (I)–Phosphine Complex. *Org. Lett.* **2005**, *7*, 1869-1871.
[390] Diez-Gonzalez, S.; Escudero-Adan, E. C.; Benet-Buchholz, J.; Stevens, E. D.; Slawin, A. M. Z.; Nolan, S. P. [(NHC)CuX] complexes: Synthesis, characterization and catalytic activities in reduction reactions and Click Chemistry. On the advantage of using well-defined catalytic systems. *Dalton Trans.* **2010**, *39*, 7595-7606.

Using the general procedure, the conditions were as follows: benzyl alcohol (1 mL, 9.52 mmol), silane (5.01 mmol), [**2**][$BArF_{24}$] (6.7 mg, 4.8 μmol).

6.2.12.3 Solvent effect

Using the general procedure, the conditions were as follows: benzyl alcohol (1 mL, 9.52 mmol), $HSiEt_3$ (0.8 mL, 5.01 mmol), [**2**][$BArF_{24}$] (6.7 mg, 4.8 μmol), 0.5 mL of solvent (DCE, ACN, PhCl, THF).

6.2.12.4 Screening of the precatalyst [**2**][X]: the effect of the counter-anion X

Using the general procedure, the conditions were as follows: benzyl alcohol (1 mL, 9.52 mmol), $HSiEt_3$ (0.8 mL, 5.01 mmol), precatalyst (4.76 μmol , 0.1 mol).

6.2.12.5 *O*-silylation of alcohols catalyzed by [**2**][$BArF_{24}$]: substrate scope study

Using the general procedure, the conditions were as follows: alcohol (9.52 mmol), $HSiEt_3$ (0.8 mL, 5.01 mmol), [**2**][$BArF_{24}$] (6.7 mg, μmol).

6.2.12.6 Inhibition studies

Using the general procedure, the conditions used were as described in the table below.

Compound		n (mmol)	m (mg) or V (mL)
[**2**][$BArF_{24}$]		0.00476	6.7 mg
Benzyl alcohol		9.52	1 mL
$HSiEt_3$		5.01	0.8 mL
Inhibitor	Aniline	0.0481	0.005 mL
	N-methyl-1-phenylmethanimine	0.0481	0.005 mL
	Phenylacetylene	0.0481	0.005 mL
	Phenyl-1-propyne	0.0481	0.006 mL
	Acetophenone	0.0481	0.0056 mL

6.2.12.7 Kinetic studies

6.2.12.7.1 Order in catalyst

Using the general procedure, the conditions were as follows: benzyl alcohol (1 mL, 9.5 mmol), $HSiEt_3$ (0.8 mL, 5.0 mmol), $c_2(10^{-3}$ M) ([**2**][$BArF_{24}$] in 0.4 mL of DCE): 2.41 (1. 3 mg, 0.02 mol %), 4.81 (2.7 mg, 0.04 mol %), 7.22 (4.0 mg, 0.06 mol %), 9.63 (5,3 mg, 0.08 mol %), 12.0 (6,7 mg, 0.1 mol %), 20 °C.

6.2.12.7.2 Kinetic isotope effect (KIE)

Using the general procedure, the conditions were as follows:

- **Alcohol kinetic isotope effect experiments.** MeOD(H) (405 μL, 10 mmol), $HSiEt_3$ (0.8 mL, 5.01 mmol), [**2**][$BArF_{24}$] (6.9 mg, 5 μmol).

k_H^{init} (MeOH+$HSiEt_3$)	k_D^{init} (MeOD+$HSiEt_3$)	k_H^{init}/k_D^{init}	$<k_H^{init}/k_D^{init}>$
0.02867	0.0115	2.49	2.73±1.8
0.03489	0.01176	2.97	

- **Silane kinetic isotope effect experiment.** MeOH (203 μL, 5.03 mmol), D(H)$SiEt_3$ (400 μL, 2.51 mmol), [**2**][$BArF_{24}$] (3.5 mg, 2.5 μmol).

k_H^{init} (MeOH+$HSiEt_3$)	k_D^{init} (MeOH+$DSiEt_3$)	k_H^{init}/k_D^{init}	$<k_H^{init}/k_D^{init}>$
0.01413	0.001962	0.72	0.73±0.01
0.01462	0.001963	0.74	

6.2.13 Screening of new precatalysts [**2'**][X], [**4**][$BArF_{24}$], [**6**][$BArF_{24}$]

Using the general procedure, the conditions were as follows: 1-phenylpropanol (1.32 mL, 9.52 mmol), $HSiEt_3$ (0.8 mL, 5.01 mmol), precatalyst (4.76 μmol, 0.1 mol).

6.2.14 [**4**][$BArF_{24}$] catalyzed *N*-silylation of aniline with $HSiEt_3$

6.2.14.1 Catalytic procedure

Procedure. In a Schlenk tube, to a mixture of $HSiEt_3$ (0.8 mL, 5.01 mmol) and aniline (0.046 mL, 5.01 mmol) was added a solution of [**2**][$BArF_{24}$] (8.6 mg, 6.1 μmol, 0.1 mol %) in 0.5 mL of CH_2Cl_2. The reaction was allowed to take place at room temperature for a 20 h, after which an aliquot was taken from the reaction mixture for ^1H NMR analysis ($CDCl_3$). A second aliquot was taken for electro-spray ionization (ESI) analysis.

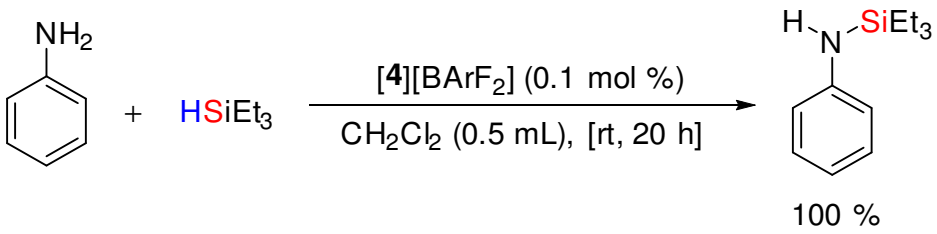

6.2.14.2 Results, discussion and spectra

^{1}H NMR spectroscopy analysis ($CDCl_3$, 298 K, 400 MHz). The product 1,1,1-triethyl-*N*-phenylsilanamine formed selectively and quantitatively as assessed by the presence of its typical ^{1}H peaks in the NMR spectrum (see below).[391] The NMR data are detailed below.

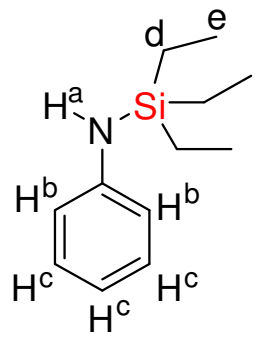

^{1}H NMR data of 1,1,1-triethyl-*N*-phenylsilanamine ($CDCl_3$, 298 K, 400 MHz): δ = 7.15 (t, 2H, H^b, J = 7.7 Hz), 6.68–6.74 (m, 3H, H^c), 3.35 (bs, 1H, H^a), 1.01 (t, 9H, H^e, J = 7.8 Hz), 0.79 (q, 6H, H^d, J = 7.9 Hz).

[391] Iida, A.; Horii, A.; Misaki, T.; Tanabe, Y. Anilinosilanes/TBAF Catalyst: Mild and Powerful Agent for the Silylation of Sterically Hindered Alcohols. *Synthesis (Stuttg).* **2005**, *2005* (16), 2677–2682.

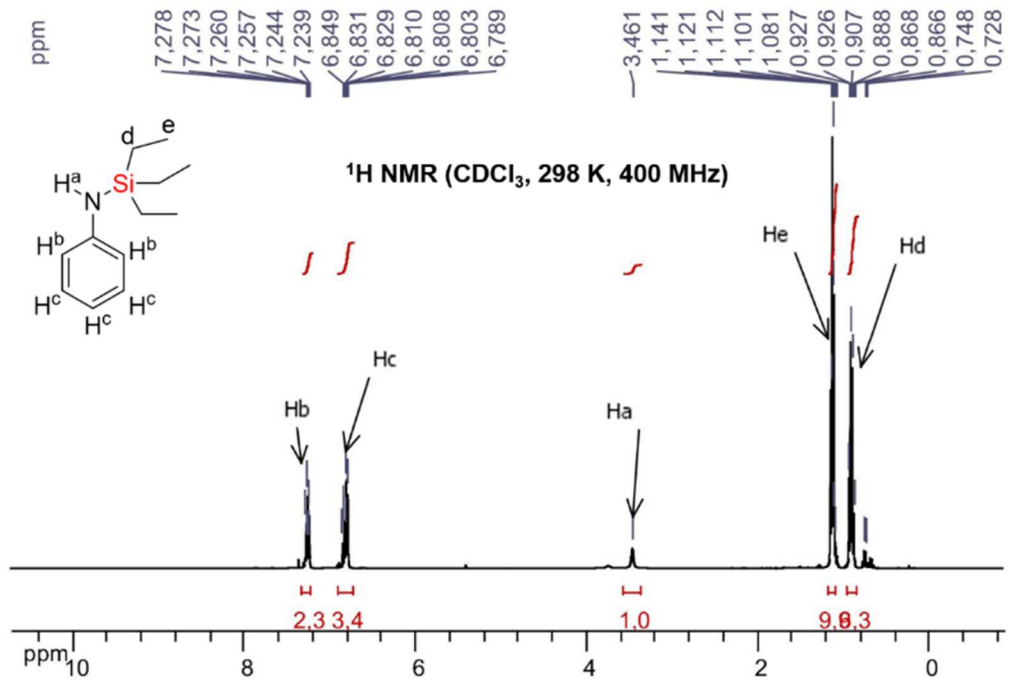

Electro-spray ionization (ESI) analysis. The formation of the product was also evidenced by ESI analysis of the crude reaction mixture (see spectrum below). **MS-ESI calcd for $C_{12}H_{22}NSi$** ($[M+H]^+$) (m/z): 208.15. **Found**: 208.16.

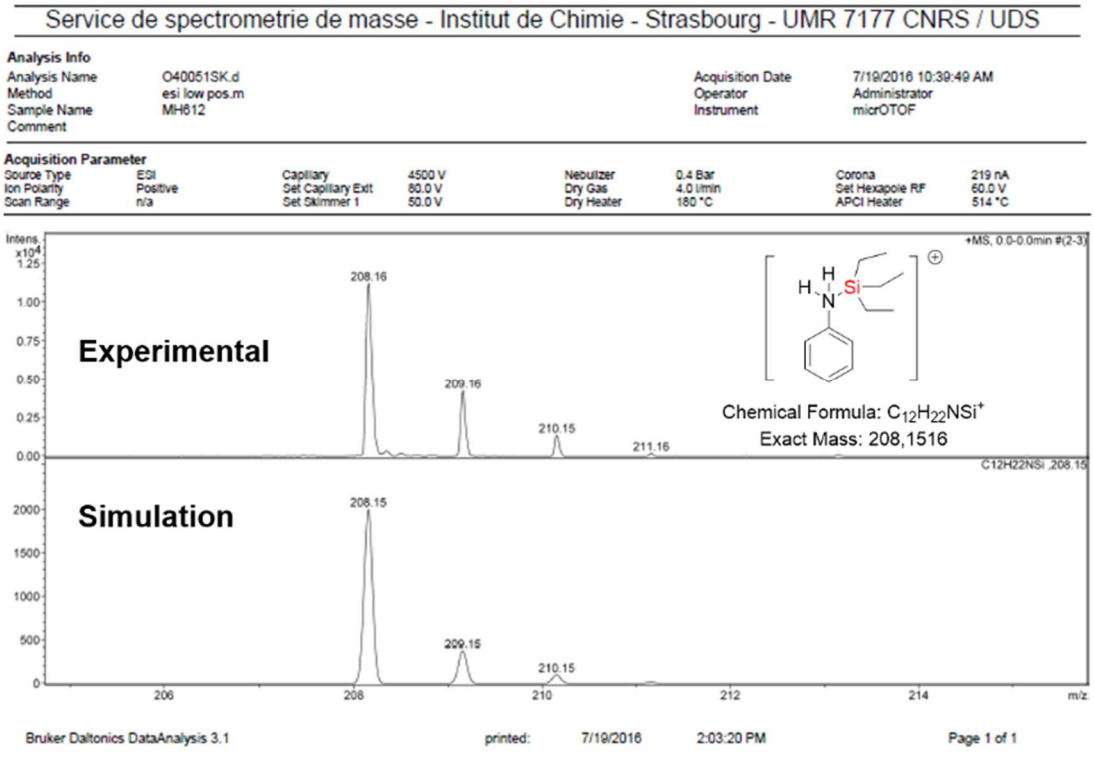

6.2.15 Reactions between iridium metallacycles and silanes ($HSiR_3$)

6.2.15.1 General procedure

In a glovebox, silane $HSiR_3$ (2–3 equiv.) was added to a solution of iridium metallacycle (1 equiv.) in CD_2Cl_2 (0.4–0.65 mL). The resulting solution was shaken and transferred into a J. Young NMR sample tube which was subsequently tightly sealed for analysis.

6.2.15.2 **1** + $HSiEt_3$

Using the general procedure, the conditions of this reaction were as follows: $HSiEt_3$ (10 μL, 62.6 µmol), **1** (15.6 mg, 30.1 μmol), CD_2Cl_2 (0.55 mL). After 20 h of reaction, room temperature ^1H NMR analysis of the reaction revealed no significant reaction, as assessed by the presence of the typical ^1H chemical peaks of **1** accompagnied with hydride peaks at δ = –12.60, –15.27 ppm; the latter peak is characteristic of **4** (see spectrum below). The **1**:**4** ratio amounts ~1:0.3. (see spectra below).

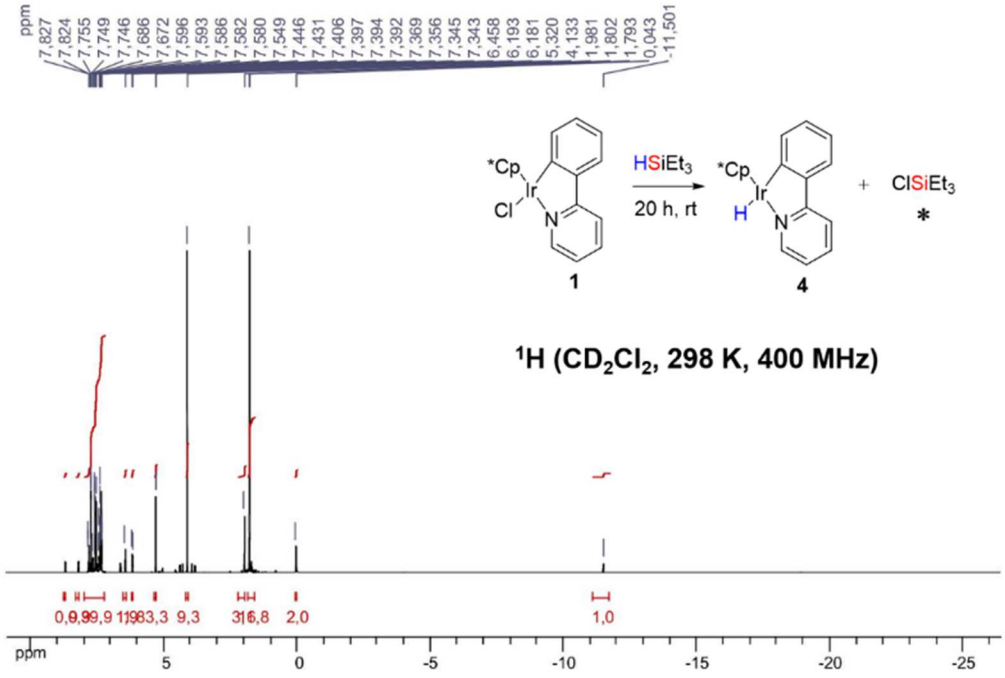

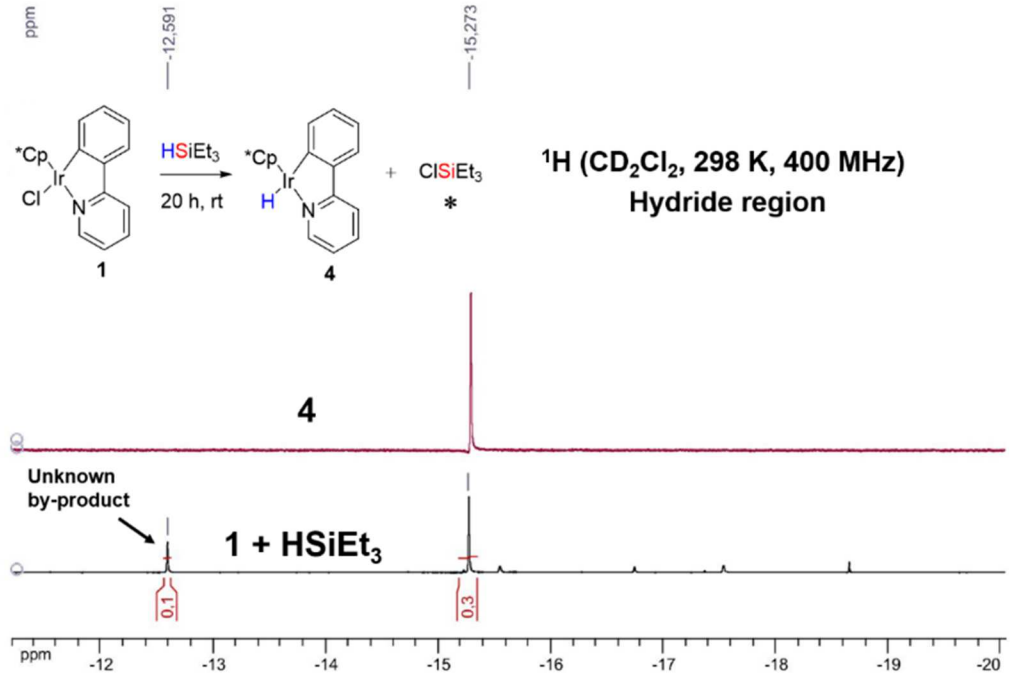
ppm
-12,591
-15,273
*Cp
Ir
Cl
N
1
HSiEt3
20 h, rt
*Cp
Ir
H
N
4
+ ClSiEt3
*
1H (CD2Cl2, 298 K, 400 MHz)
Hydride region
4
Unknown
by-product
1 + HSiEt3
0,1
0,3
ppm
-12
-13
-14
-15
-16
-17
-18
-19
-20

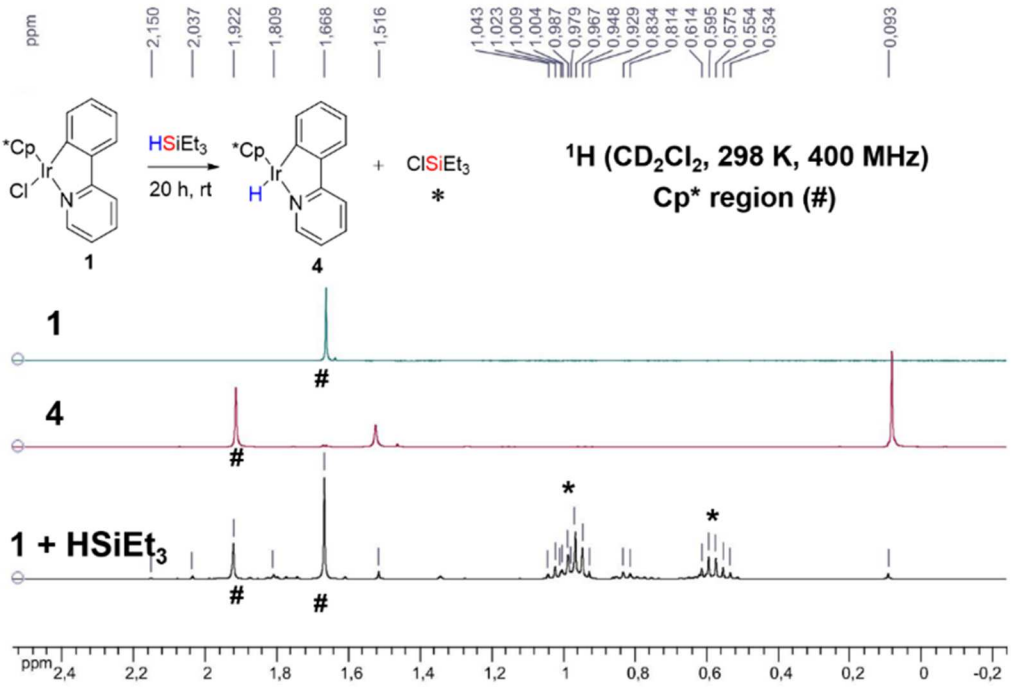
ppm
2,150
2,037
1,922
1,809
1,668
1,516
1,043
1,023
1,009
1,004
0,987
0,979
0,967
0,948
0,929
0,834
0,814
0,614
0,595
0,575
0,554
0,534
0,093
*Cp
Ir
Cl
N
1
HSiEt3
20 h, rt
*Cp
Ir
H
N
4
+ ClSiEt3
*
1H (CD2Cl2, 298 K, 400 MHz)
Cp* region (#)
1
#
4
#
*
*
1 + HSiEt3
#
#
ppm
2,4
2,2
2
1,8
1,6
1,4
1,2
1
0,8
0,6
0,4
0,2
0
-0,2

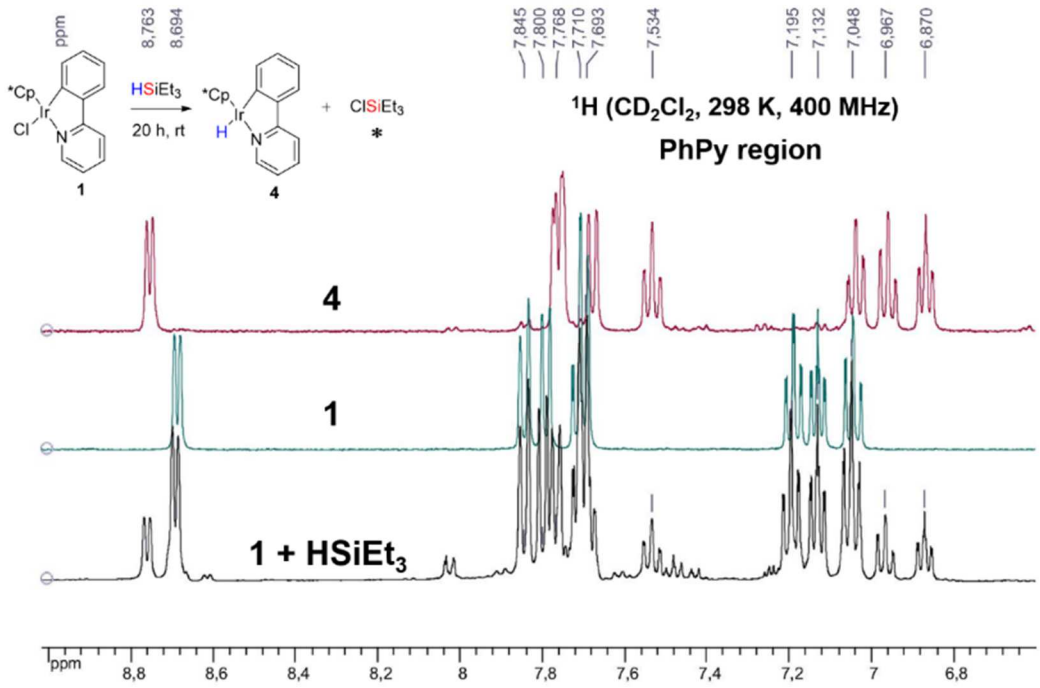

6.2.15.3 [**2**][X] + $HSiR_3$

6.2.15.3.1 Reaction of [**2**][$BArF_{24}$] with $HSiEt_3$

Using the general procedure, the conditions of this reaction were as follows: $HSiEt_3$ (5.8 μL, 36.3 μmol), [**2**][$BArF_{24}$] (25 mg, 18.0 μmol), CD_2Cl_2 (0.5 mL). Low-temperature (–60 °C) NMR analysis of the reaction revealed the spectroscopic evidence for the formation of [**3A**][$BArF_{24}$], [**3B**][$BArF_{24}$] and $(Et_3Si)_2NEt$. The presence of $(Et_3Si)_2NEt$ was confirmed by mass spectroscopy analysis of the reaction mixture. **Data for [3A][$BArF_{24}$] are as follows: ^{1}H NMR (600 MHz, 213 K, CD_2Cl_2)**: δ = 8.43 (d, 1H, H_{Ar} PhPy, J = 5.3 Hz), 7.98 (m, 1H, H_{Ar} PhPy), 7.92 (m, 1H, H_{Ar} PhPy), 7.82 (m, 2H, H_{Ar} PhPy), 7.77 (m, 8H, H_{ortho} $BArF_{24}$), 7.59 (m, 4H, H_{para} $BArF_{24}$), 7.30–7.35 (m, 2H, H_{Ar} PhPy), 7.23–7.27 (m, 1H, H_{Ar} PhPy), 1.71 (s, 15H, Cp-*Me*$_5$), 0.72 (t, 9H, [Ir–H]→[Si(CH_2C*H*$_3$)$_3$], J = 7.8 Hz), 0.42–0.52 (m, 6H, [Ir–H]→[Si(C*H*$_2CH_3$)$_3$], –11.75 (s, 1H, [Ir–*H*]→[Si(CH_2CH_3)$_3$], J_{H-Si} = 20.1 Hz). **^{29}Si coupled-^{1}H dimension of (2D-^{29}Si–^{1}H) HMQC (119 MHz, 213 K, CD_2Cl_2)**: δ = –11.7 (d, 1H, [Ir–*H*]→[Si(CH_2CH_3)$_3$], J_{Si-H} = 20 Hz). **^{29}Si-DEPT NMR (119 MHz, 213 K, CD_2Cl_2)**: δ = 7.1 (d, [Ir–H]→[*Si*(CH_2CH_3)$_3$]). **Data for $(Et_3Si)_2NEt$ are as follows: ^{1}H NMR (600 MHz, 213 K, CD_2Cl_2)**: δ = 2.81 (q, 2H, N–C*H*$_2CH_3$, J = 7 Hz), 0.98 (t, 3H, N–CH_2C*H*$_3$, J = 7 Hz), 0.90 (t, 18H, $SiCH_2C$*H*$_3$, J = 8 Hz), 0.56 (q, 12H, SiC*H*$_2CH_3$,

J = 8 Hz). **^{29}Si-DEPT NMR (119 MHz, 213 K, CD_2Cl_2)**: δ = 10.9 ((Et$_3$*Si*)$_2$NEt). **HRMS-ESI calcd for $C_{14}H_{36}N_1Si_2$** ([M + H]$^+$) (m/z): 274.2381. **Found**: 274.2362.

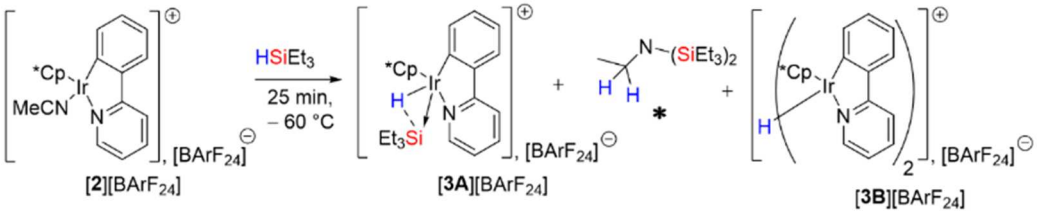

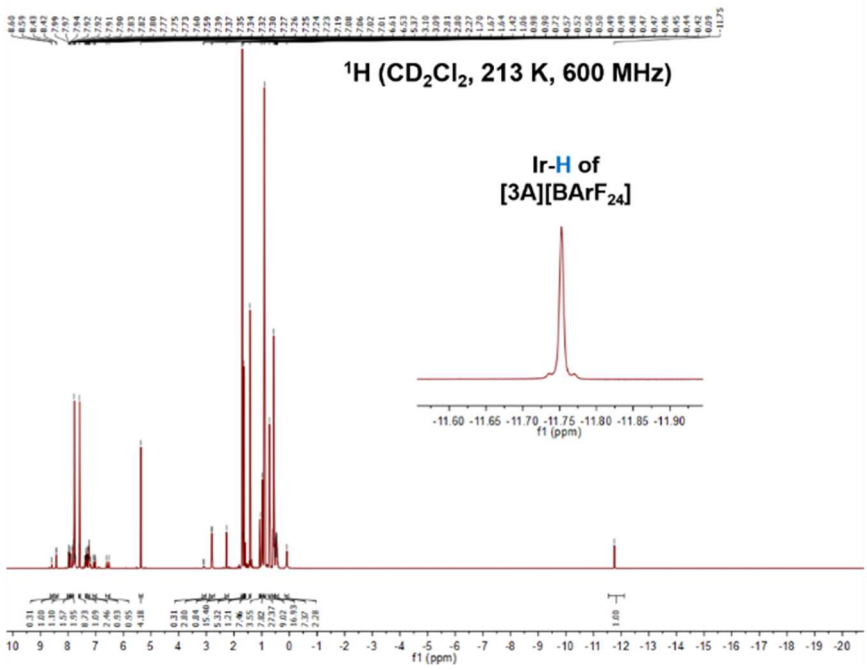

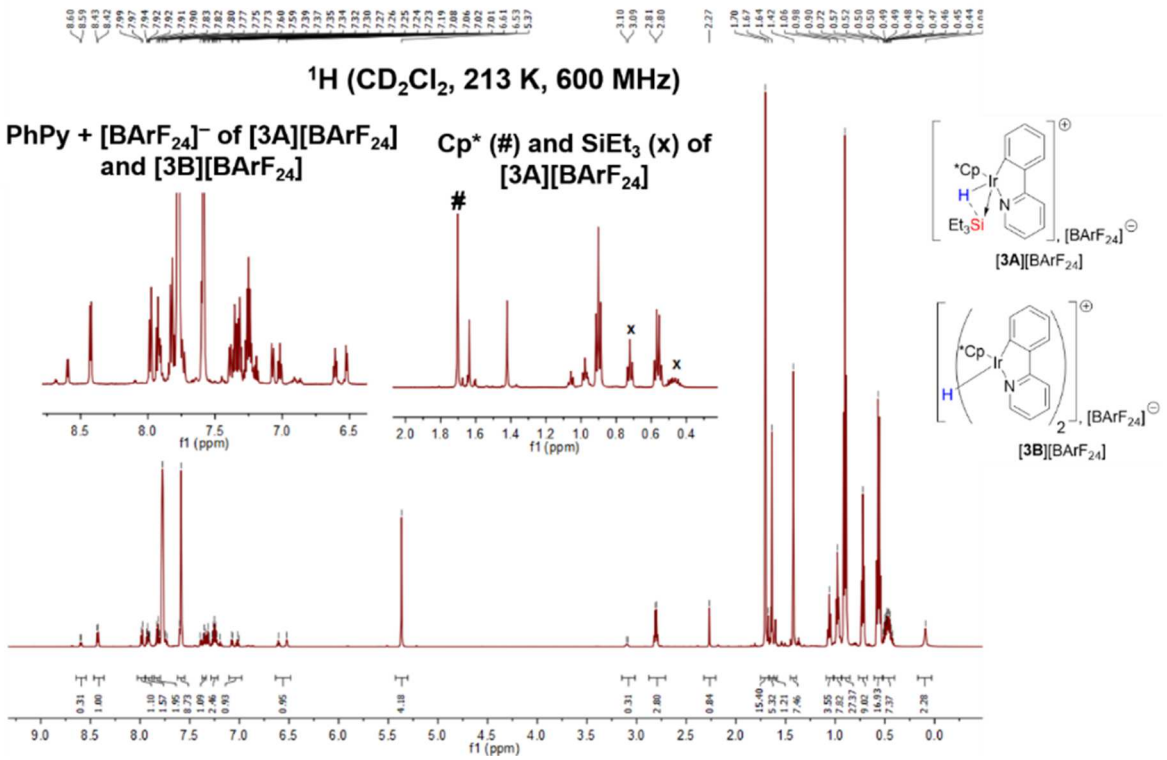
^{1}H (CD_2Cl_2, 213 K, 600 MHz)
PhPy + $[BArF_{24}]^-$ of [3A][$BArF_{24}$] and [3B][$BArF_{24}$]
Cp* (#) and $SiEt_3$ (x) of [3A][$BArF_{24}$]
[3A][$BArF_{24}$]
[3B][$BArF_{24}$]
f1 (ppm)

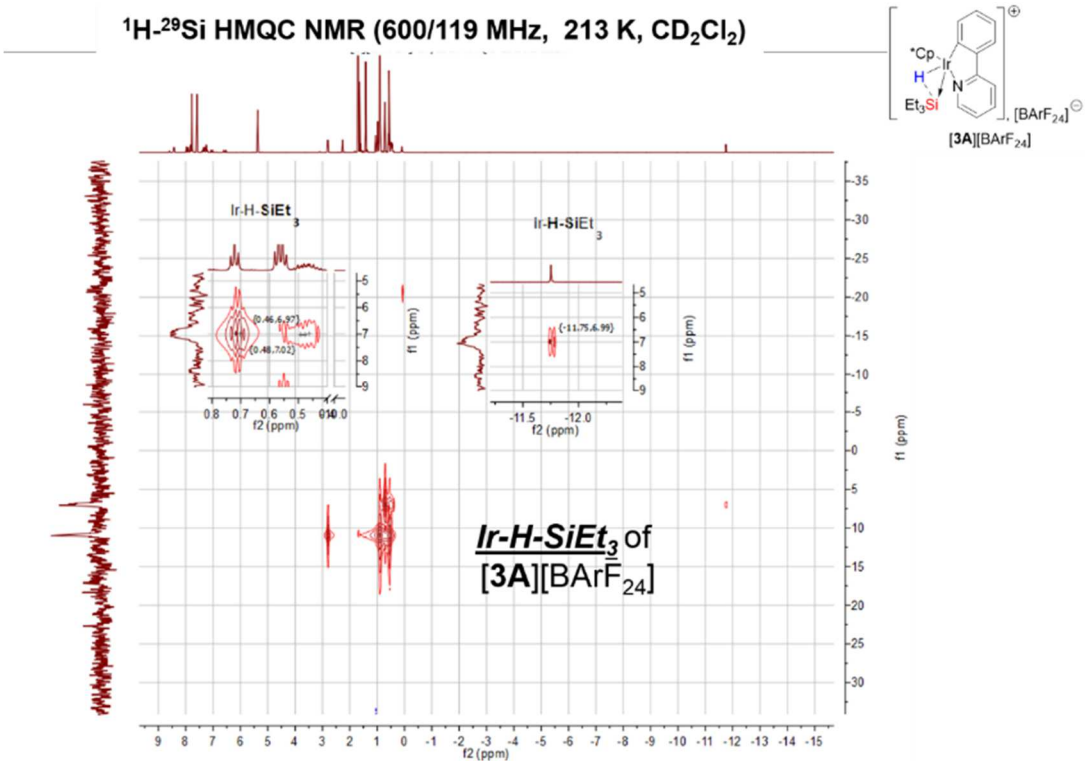
^{1}H-^{29}Si HMQC NMR (600/119 MHz, 213 K, CD_2Cl_2)
Ir-H-SiEt$_3$
Ir-H-SiEt$_3$
Ir-H-SiEt$_3$ of [3A][$BArF_{24}$]
[3A][$BArF_{24}$]
f1 (ppm)
f2 (ppm)

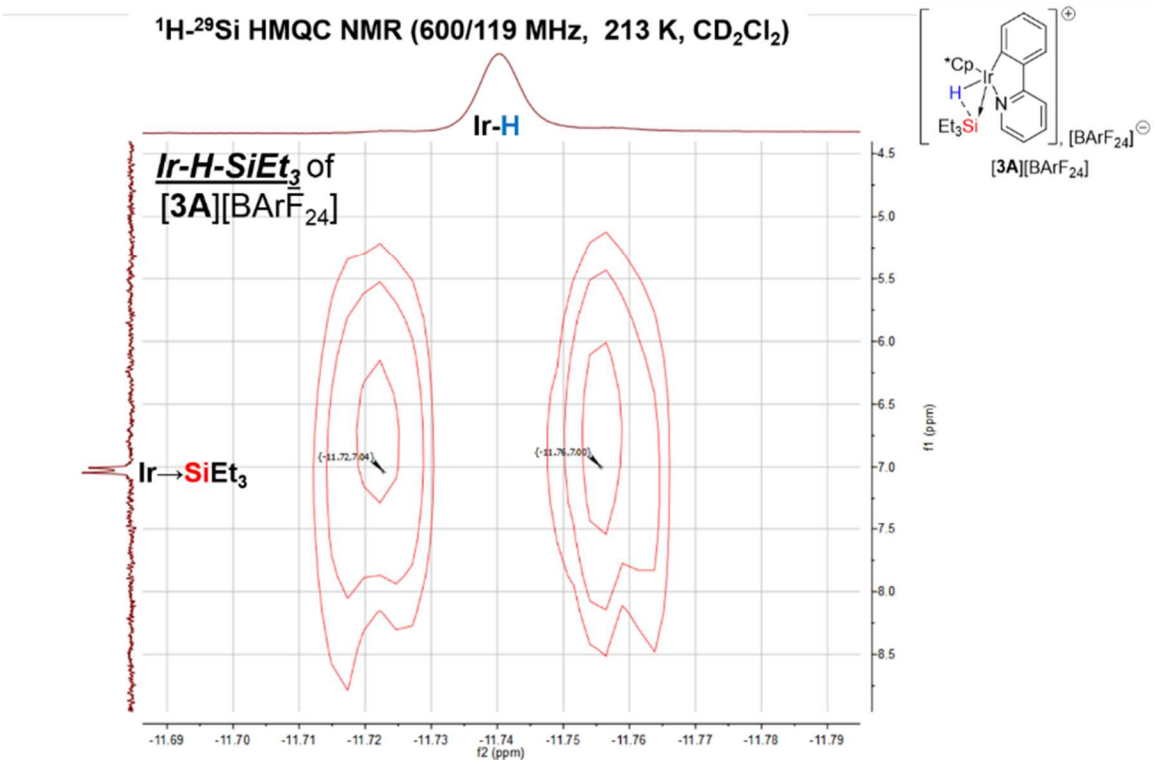

6.2.15.3.2 Reaction of [**2**][BArF$_{24}$] with HSiPh$_3$

Using the general procedure, the conditions of this reaction were as follows: HSiPh$_3$ (31.3 mg, 36.3 µmol), [**2**][BArF$_{24}$] (50 mg, 36.1 μmol), CD_2Cl_2 (0.4 mL). After 50 minutes of reaction, room temperature ^{1}H NMR analysis of the reaction revealed the spectroscopic evidence for the formation of [**3D**][BArF$_{24}$], [**3B**][BArF$_{24}$] and (Ph$_3$Si)$_2$NEt in a ratio of ~1:0.1:1 (see selected NMR spectra below).

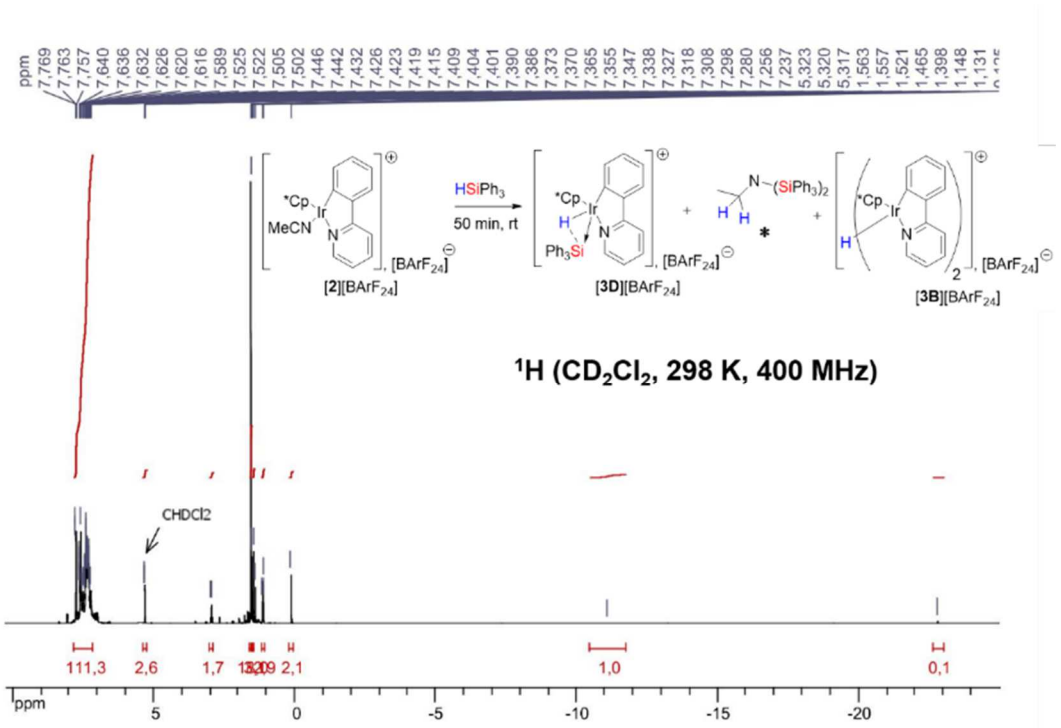
HSiPh3
50 min, rt
[2][BArF24]
[3D][BArF24]
[3B][BArF24]
1H (CD2Cl2, 298 K, 400 MHz)
CHDCl2
111,3
2,6
1,7
2,1
1,0
0,1
ppm

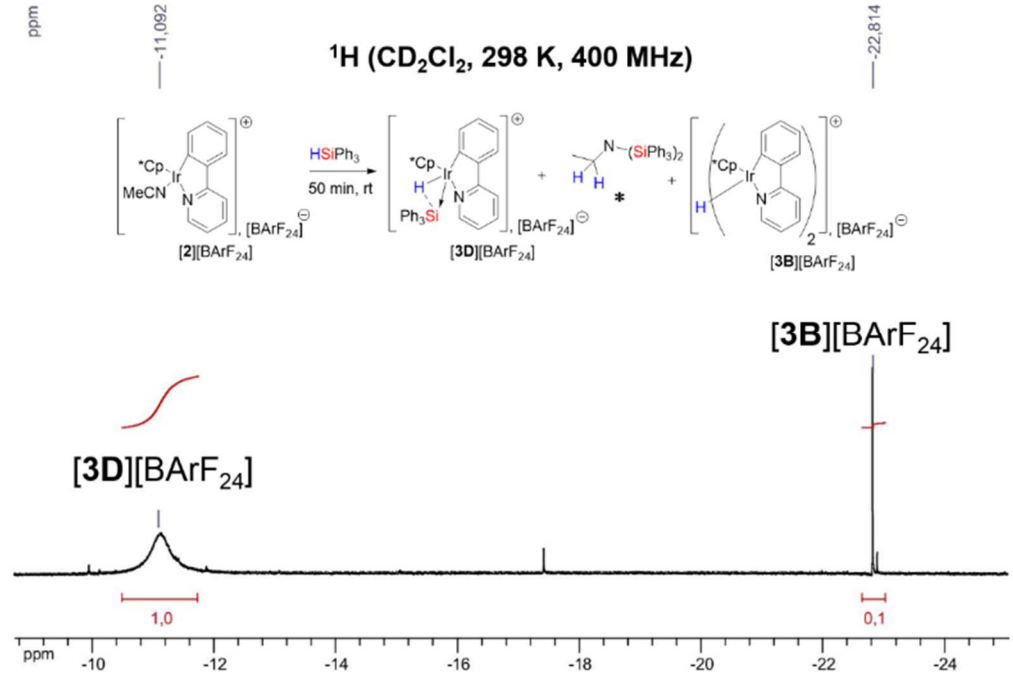
1H (CD2Cl2, 298 K, 400 MHz)
HSiPh3
50 min, rt
[2][BArF24]
[3D][BArF24]
[3B][BArF24]
[3B][BArF24]
[3D][BArF24]
1,0
0,1
ppm

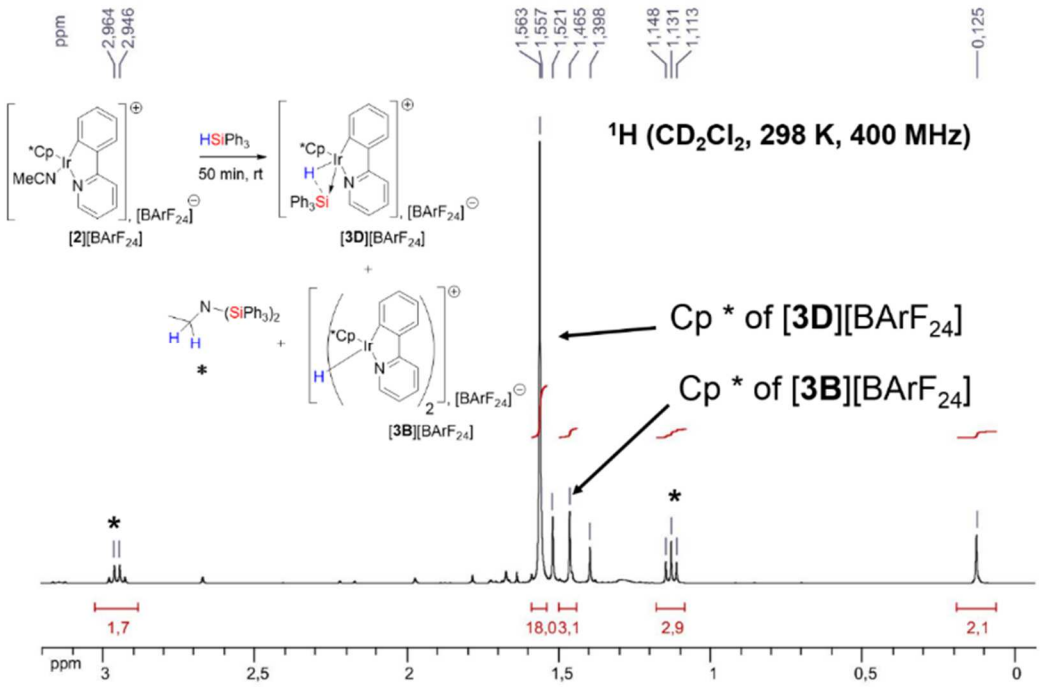

6.2.15.3.3 Reaction of [**2**][BF_4] with $HSiEt_3$

Using the general procedure, the conditions of this reaction were as follows: $HSiEt_3$ (5.6 µL, 35.1 µmol), [**2**][BF_4] (10 mg, 16.4 µmol), CD_2Cl_2 (0.5 mL). Room temperature NMR spectroscopic analysis showed spectroscopic evidence for the formation of **4**, [**3B**][BF_4], $F_3B{\bullet}N(SiEt_3)_2Et$, and $FSiEt_3$. The presence of **4** in the reaction mixture was confirmed by comparing the ^{1}H NMR spectrum of the reaction mixture with that of an authentic sample. The latter compound was synthesized following the procedure found in the literature.[392] The formation of $FSiEt_3$ was confirmed by its characteristic ^{19}F[393] and ^{29}Si NMR signals, which both displayed a doublet with a high coupling constant of 287 Hz. The identity of $F_3B{\bullet}N(SiEt_3)_2Et$ was confirmed by a quartet in the ^{11}B spectrum with a characteristic J_{B-F} coupling constant matching the value observed in the characteristic 1:1:1:1 quartet of the ^{19}F spectrum. Complex [**3B**][BF_4] displayed a hydride signal at around δ = –23 ppm (^{1}H NMR) characteristic of Ir(μ-H)Ir dimers (cf. the synthetic procedure of [**3B**][OTf] and the related spectra). **Data for $FSiEt_3$ are**

[392] Hu, Y.; Li, L.; Shaw, A. P.; Norton, J. R.; Sattler, W.; Rong, Y. Synthesis, Electrochemistry, and Reactivity of New iridium(III) and rhodium(III) Hydrides. *Organometallics* **2012**, *31* (14), 5058–5064.
[393] Vela, J.; Smith, J. M.; Yu, Y.; Ketterer, N. A.; Flaschenriem, C. J.; Lachicotte, R. J.; Holland, P. L. Synthesis and Reactivity of Low-Coordinate Iron(II) Fluoride Complexes and Their Use in the Catalytic Hydrodefluorination of Fluorocarbons. *J. Am. Chem. Soc.* **2005**, *127* (21), 7857–7870. (1)

as follows: ^{1}H NMR (600 MHz, 298 K, CD_2Cl_2): δ = 0.73 (q, 6H, C*H*$_2$), 1.04 (t, 9H, C*H*$_3$). **^{13}C NMR (126 MHz, 298 K, CD_2Cl_2)**: δ = 4.89 (d, *C*H2, $^{2}J_{C\text{-}F}$ = 14.2 Hz), 5.96 (d, CH3, 3JC-F = 2 Hz). **^{19}F NMR (282 MHz, 298 K, CD_2Cl_2)**: δ = –176.9 (s, $^{1}J_{Si\text{-}F}$ = 287 Hz). **^{29}Si-DEPT NMR (119 MHz, 298 K, CD_2Cl_2)**: δ = 33.1 (d, $^{1}J_{Si\text{-}F}$ = 287 Hz). **Data for $F_3B{\bullet}N(SiEt_3)_2Et$ are as follows: ^{1}H NMR (600 MHz, 298 K, CD_2Cl_2)**: δ = 3.13 (q, 2H, N–C*H*$_2$CH$_3$, *J* = 7.2 Hz), 1.09 (t, 3H, N–CH$_2$C*H*$_3$, *J* = 7.1 Hz), 0.97–1.01 (m, 18H, SiCH$_2$C*H*$_3$), 0.64–0.72 (m, 12H, SiC*H*$_2$CH$_3$). **^{19}F NMR (282 MHz, 298 K, CD_2Cl_2)**: δ = –146.4 (q, ^{11}B*F*$_3$ + ^{10}B*F*$_3$, $^{1}J_{B\text{-}F}$ = 20.8 Hz). **^{11}B (128 MHz, 298 K, CD_2Cl_2)**: δ = 0.55 (q, *B*F$_3$, $^{1}J_{B\text{-}F}$ = 20.5 Hz).

^{1}H NMR (CD_2Cl_2) of Et_3SiH + **[2]**[BF_4] recorded on 400 MHz spectrometer at 298 K (green line) compared to the spectra of the authentic samples of **[2]**[BF_4] (CD_2Cl_2, 500 MHz, blue line) and **[4]** (CD_2Cl_2, 400 MHz, red line) : total conversion of **[2]**[BF_4] into **[4]**, **[3B]**[BF_4].

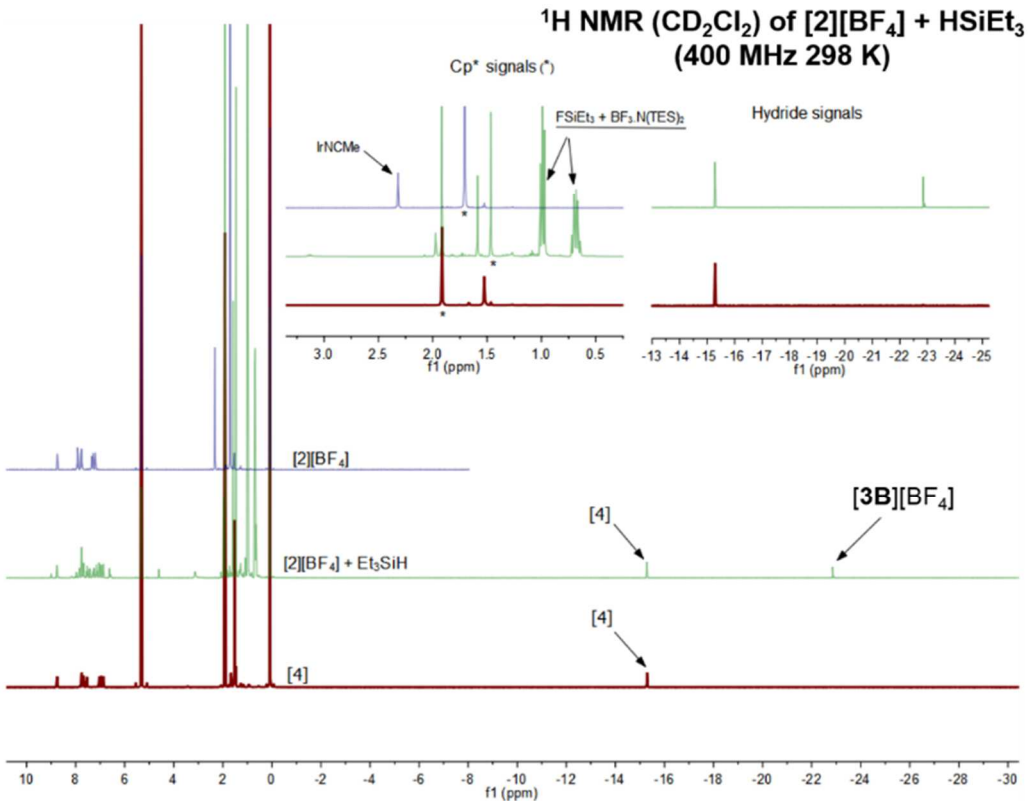

6.2.15.3.4 Reaction of **[2]**[BPh_4] with $HSiEt_3$

Using the general procedure, the conditions of this reaction were as follows: $HSiEt_3$ (8.4 μL, 36.3 μmol), **[2]**[BPh_4] (22.5 mg, 16.2 μmol), CD_2Cl_2 (0.5 mL). After 20 minutes of reaction, room temperature ^{1}H NMR analysis of the reaction revealed the spectroscopic evidence for the formation of **[3A]**[BPh_4], **[3B]**[BPh_4] and $(Et_3Si)_2NEt$ in a ratio of ~0.5:1:2.4 (see selected NMR spectra below).

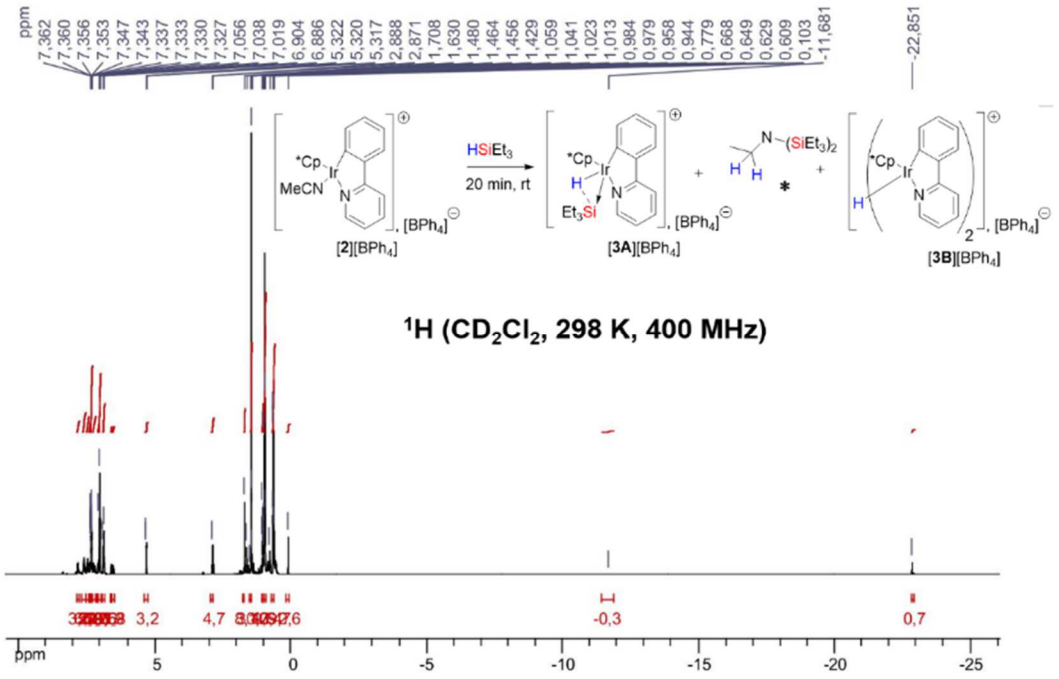
ppm
7,362
7,360
7,356
7,353
7,347
7,343
7,337
7,333
7,330
7,327
7,056
7,038
7,019
6,904
6,886
5,322
5,320
5,317
2,888
2,871
1,708
1,630
1,480
1,464
1,456
1,429
1,059
1,041
1,023
1,013
0,984
0,979
0,958
0,944
0,779
0,668
0,649
0,629
0,609
0,103
-11,681
-22,851
HSiEt3
20 min, rt
[2][BPh4]
[3A][BPh4]
[3B][BPh4]
1H (CD2Cl2, 298 K, 400 MHz)
3,2
4,7
-0,3
0,7
ppm
5
0
-5
-10
-15
-20
-25

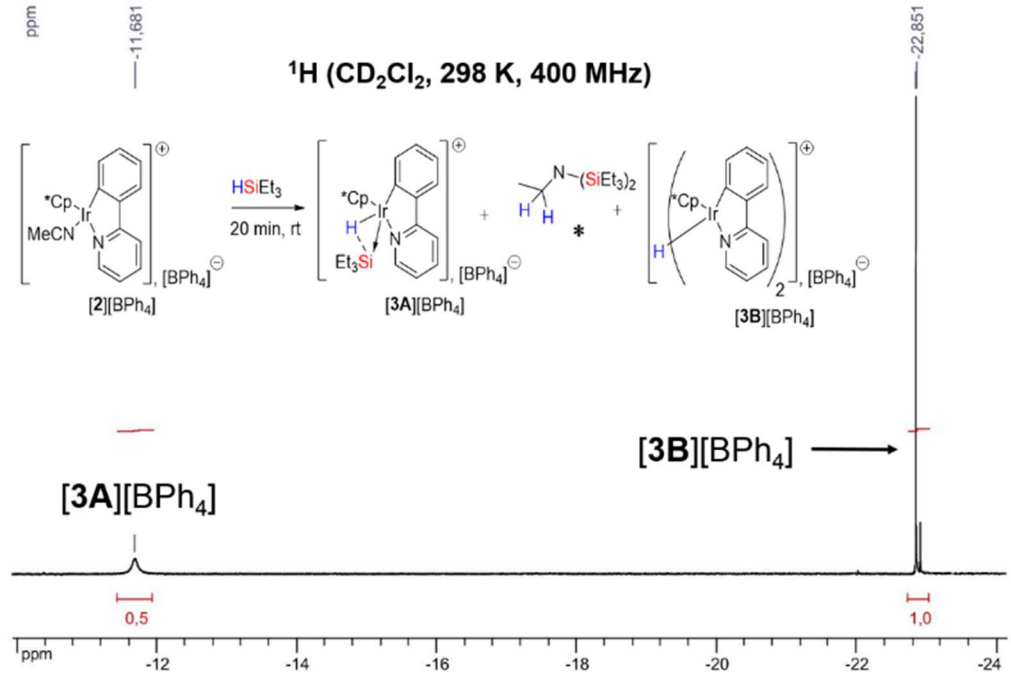
ppm
-11,681
-22,851
1H (CD2Cl2, 298 K, 400 MHz)
HSiEt3
20 min, rt
[2][BPh4]
[3A][BPh4]
[3B][BPh4]
[3A][BPh4]
[3B][BPh4]
0,5
1,0
ppm
-12
-14
-16
-18
-20
-22
-24

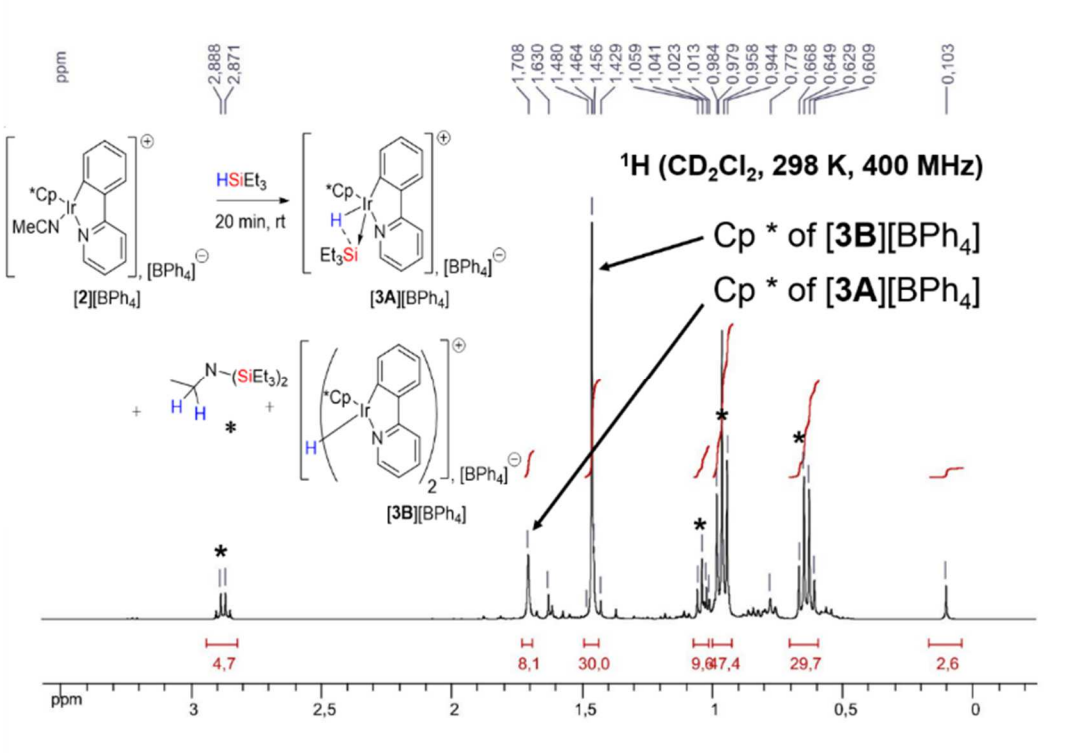
ppm
2,888
2,871
1,708
1,630
1,480
1,464
1,456
1,429
1,059
1,041
1,023
1,013
0,984
0,979
0,958
0,944
0,779
0,668
0,649
0,629
0,609
0,103
^{1}H (CD_2Cl_2, 298 K, 400 MHz)
HSiEt$_3$
20 min, rt
[2][BPh$_4$]
[3A][BPh$_4$]
[3B][BPh$_4$]
Cp * of [3B][BPh$_4$]
Cp * of [3A][BPh$_4$]
4,7
8,1
30,0
9,6
17,4
29,7
2,6
3
2,5
2
1,5
1
0,5
0

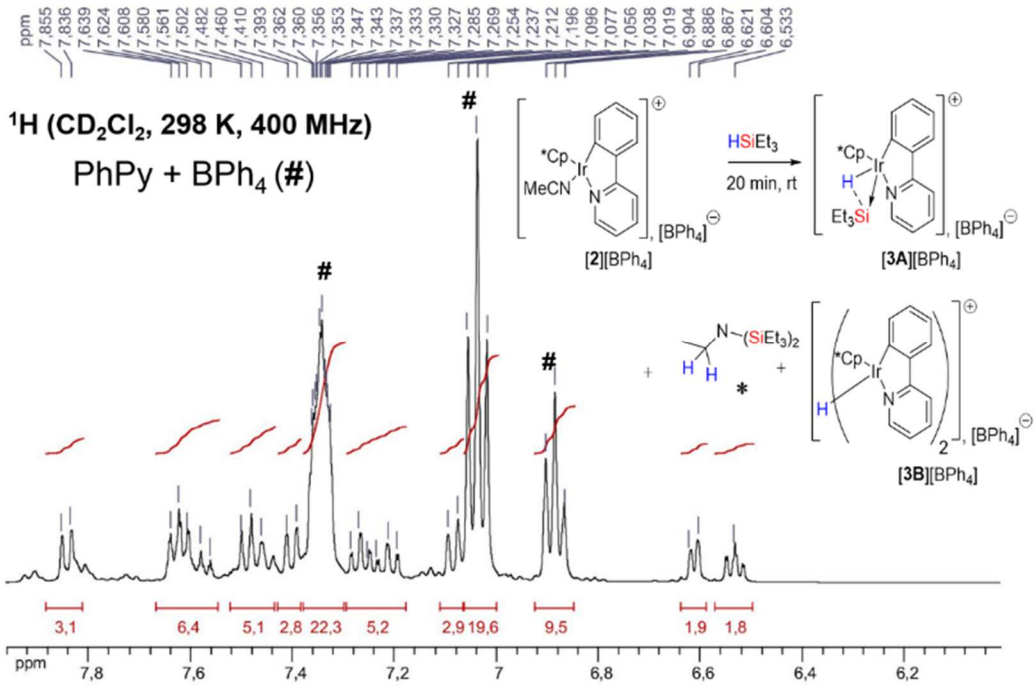
ppm
7,855
7,836
7,639
7,624
7,608
7,580
7,561
7,502
7,482
7,460
7,410
7,393
7,362
7,360
7,356
7,353
7,347
7,343
7,337
7,333
7,330
7,327
7,285
7,269
7,254
7,237
7,212
7,196
7,096
7,077
7,056
7,038
7,019
6,904
6,886
6,867
6,621
6,604
6,533
^{1}H (CD_2Cl_2, 298 K, 400 MHz)
PhPy + BPh$_4$ (#)
HSiEt$_3$
20 min, rt
[2][BPh$_4$]
[3A][BPh$_4$]
[3B][BPh$_4$]
3,1
6,4
5,1
2,8
22,3
5,2
2,9
19,6
9,5
1,9
1,8
7,8
7,6
7,4
7,2
7
6,8
6,6
6,4
6,2

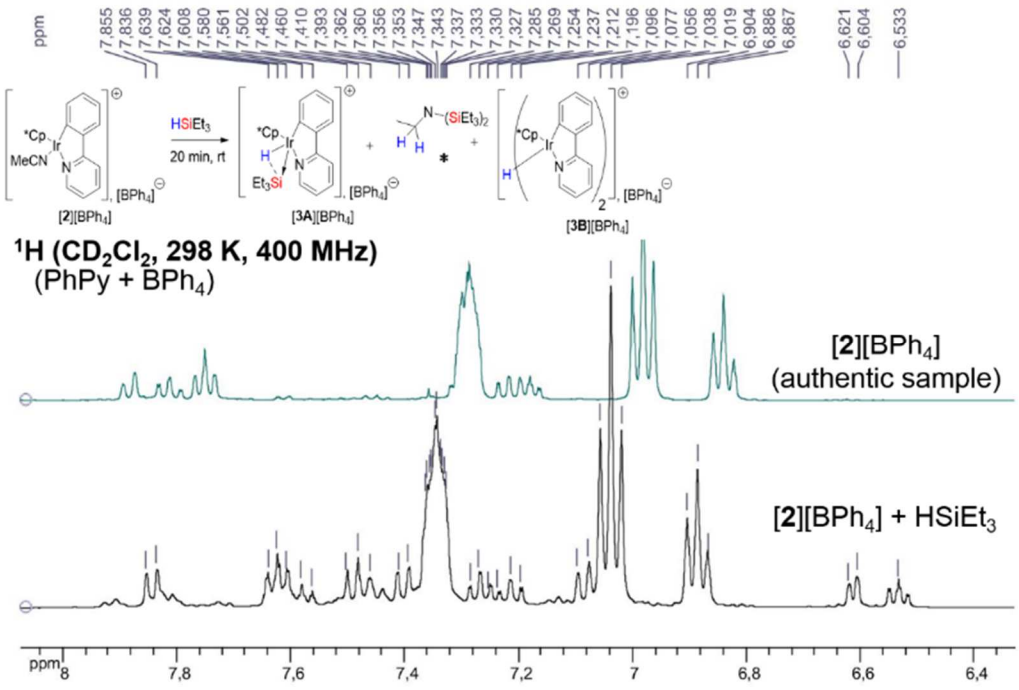

6.2.15.3.5 Reaction of [**2**][OTf] with $HSiEt_3$

Using the general procedure, the conditions of this reaction were as follows: $HSiEt_3$ (8.0 μL, 50.1 μmol), [**2**][OTf] (19.7 mg, 29.2 μmol), CD_2Cl_2 (0.5 mL). Room temperature ^1H NMR spectroscopic analysis displayed the spectroscopic evidence for the formation of **4**, [**3B**][OTf], and Et_3SiOTf. The identity of each of the latter species was assessed by comparison of the ^1H NMR spectra with those of authentic samples (see the related spectra below).

^{1}H NMR (CD_2Cl_2) of Et_3SiH + [**2**][OTf] recorded on 400 MHz spectrometer at 298 K (blue line) compared to the spectra of the authentic samples of [**2**][OTf] (CD_2Cl_2, 500 MHz, red line), [**4**] (CD_2Cl_2, 400 MHz, grease line) and [**3B**][OTf] (CD_2Cl_2, 500 MHz, purple line) : total conversion of [**2**][OTf] into [**4**], [**3B**][OTf].

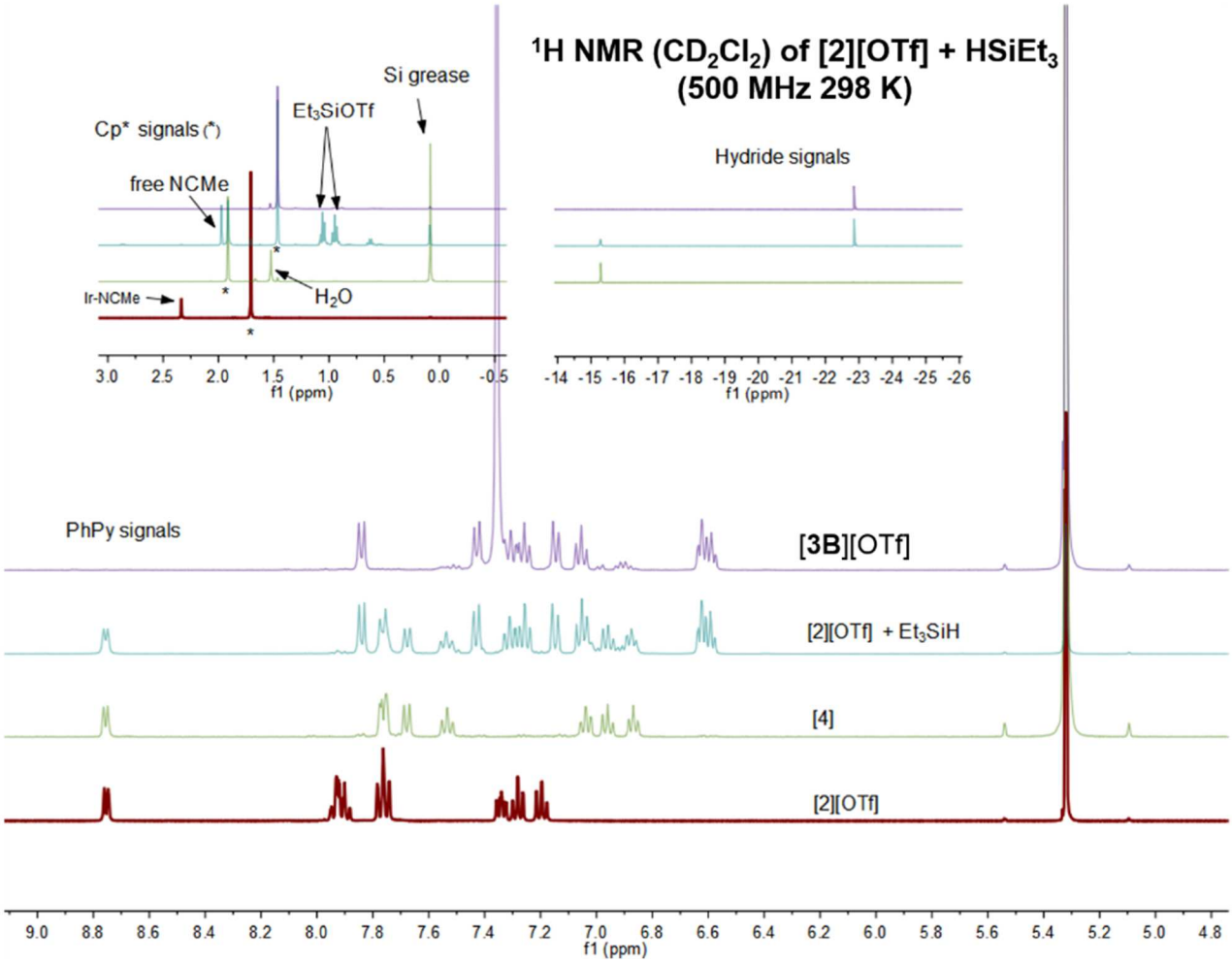

^{1}H NMR (CD_2Cl_2) of Et_3SiH + **[2]**[OTf] recorded on 400 MHz spectrometer at 298 K (down) compared to the ^{1}H NMR (CD_2Cl_2) of Et_3SiOTf recorded in the same conditions (top).

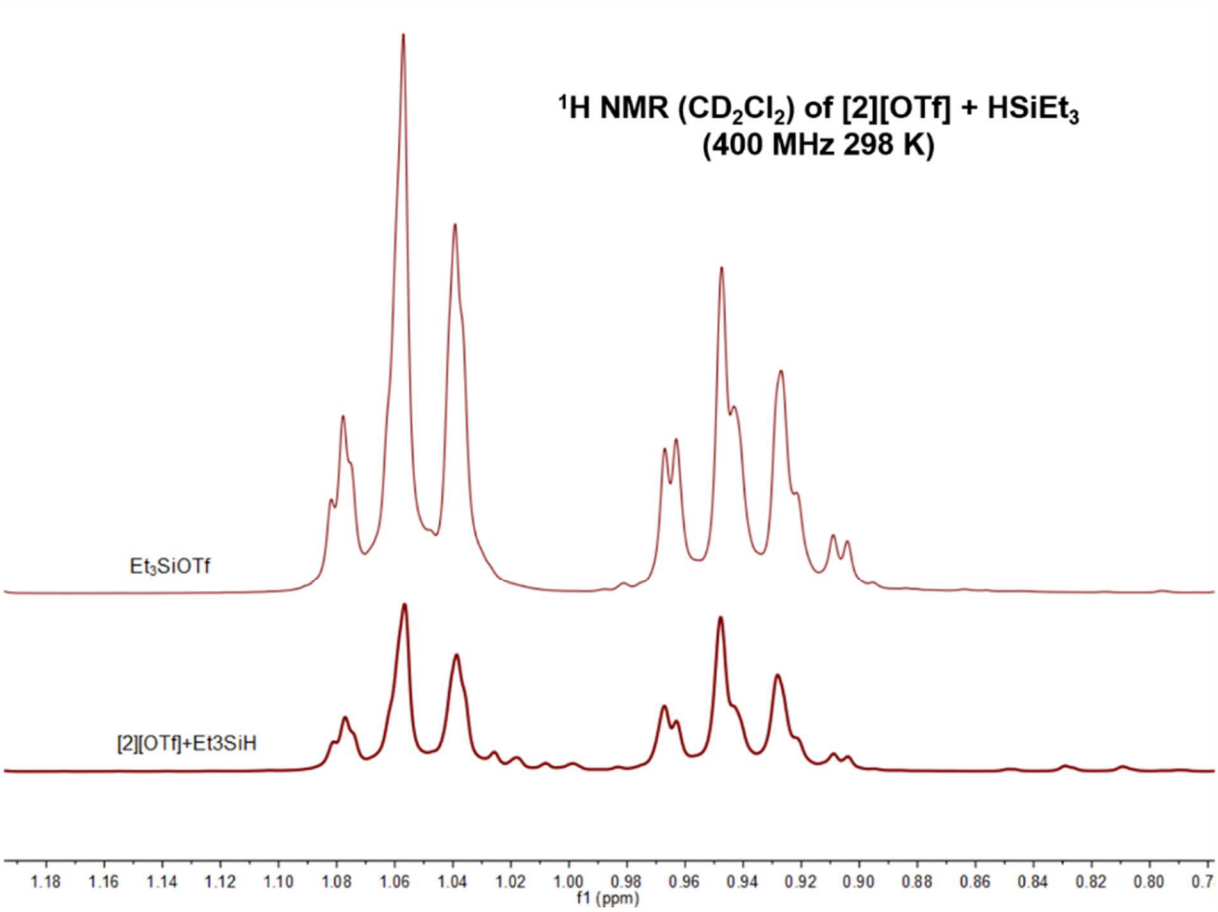

6.2.15.4 [**4**][$BArF_{24}$] + $HSiR_3$

6.2.15.4.1 Reaction of [**4**][$BArF_{24}$] with $PhSiH_3$

Using the general procedure, the conditions of this reaction were as follows: $PhSiH_3$ (15.0 μL, 121.6 μmol), [**4**][$BArF_{24}$] (29 mg, 20.6 μmol), CD_2Cl_2 (0.65 mL). After 25 minutes of reaction, the NMR tube was frozen at < –60 °C. Multinuclear NMR analysis (at –60 °C) of the reaction revealed the total and exclusive conversion of [**4**][$BArF_{24}$] to [**5F**][$BArF_{24}$], along with the released CH_3CN (from [**4**][$BArF_{24}$]) and excess $PhSiH_3$ in a ratio of ~1:1:3 (see selected NMR spectra below). **Data for [5F][$BArF_{24}$] are as follows**: **^{1}H NMR (600 MHz, 213 K, CD_2Cl_2)**: δ = 8.71 (d, 1H, H_{Ar} B[*h*]Q, J = 5.4 Hz), 8.22 (d, 1H, H_{Ar} B[*h*]Q, J = 7.9 Hz), 7.81–7.85 (m, 2H, H_{Ar} B[*h*]Q), 7.75 (m, 8H, H_{ortho} $BArF_{24}$), 7.68 (d, 1H, H_{Ar} B[*h*]Q, J = 8.8 Hz), 7.55 (m, 4H, H_{para} $BArF_{24}$), 7.51 (d, 1H, H_{Ar} B[*h*]Q, J = 8.0 Hz), 7.50 (d, 1H, H_{Ar} B[*h*]Q, J = 8.0 Hz), 7.44 (d, 1H, H_{Ar} B[*h*]Q, J = 8.7 Hz), 6.65 (t, 1H, [Ir-H]→[SiH_2*Ph*], J = 7.5 Hz), 6.46 (t, 2H, [Ir-H]→[SiH_2*Ph*], J

= 7.5 Hz), 6.19 (d, 2H, [Ir-H]→[SiH$_2$*Ph*], J = 7.5 Hz), 4.40 (dd, 1H, [Ir-H]→[Si*H$_2$*Ph], $J^1_{H\text{-}H}$ = 11.8 Hz, $^1J_{H\text{-}Si}$ = 197.0 Hz; $J^2_{H\text{-}H}$ = 2.6 Hz), 3.84 (dd, 1H, [Ir-H]→[Si*H$_2$*Ph], $J^1_{H\text{-}H}$ = 11.8 Hz, $^1J_{H\text{-}Si}$ = 224.0 Hz; $J^2_{H\text{-}H}$ = 2.6 Hz), 1.79 (s, 15H, Cp-*Me$_5$*), –11.50 (bs, 1H, [Ir-*H*]→[SiH$_2$Ph]). **^{29}Si-DEPT NMR (119 MHz, 213 K, CD$_2$Cl$_2$)**: δ = –35.64 (s, [Ir-H]→[*Si*H$_2$Ph]). **Data for "free" PhSiH$_3$ are as follows: ^{1}H NMR (600 MHz, 213 K, CD$_2$Cl$_2$)**: δ = 7.58–7.59 (m, 1H, *Ph*SiH$_3$), 7.44 (m, 2H, *Ph*SiH$_3$), 7.35–7.37 (m, 2H, *Ph*SiH$_3$), 4.13 (s, 3H, *Ph*SiH$_3$, $^1J_{H\text{-}Si}$ = 200.1 Hz). **^{29}Si-DEPT NMR (119 MHz, 213 K, CD$_2$Cl$_2$)**: δ = –58.75 (s, Ph*Si*H$_3$). **Data for "free" CH$_3$CN are as follows: ^{1}H NMR (600 MHz, 213 K, CD$_2$Cl$_2$)**: δ = 1.98 (s, 3H, C*H$_3$*CN).

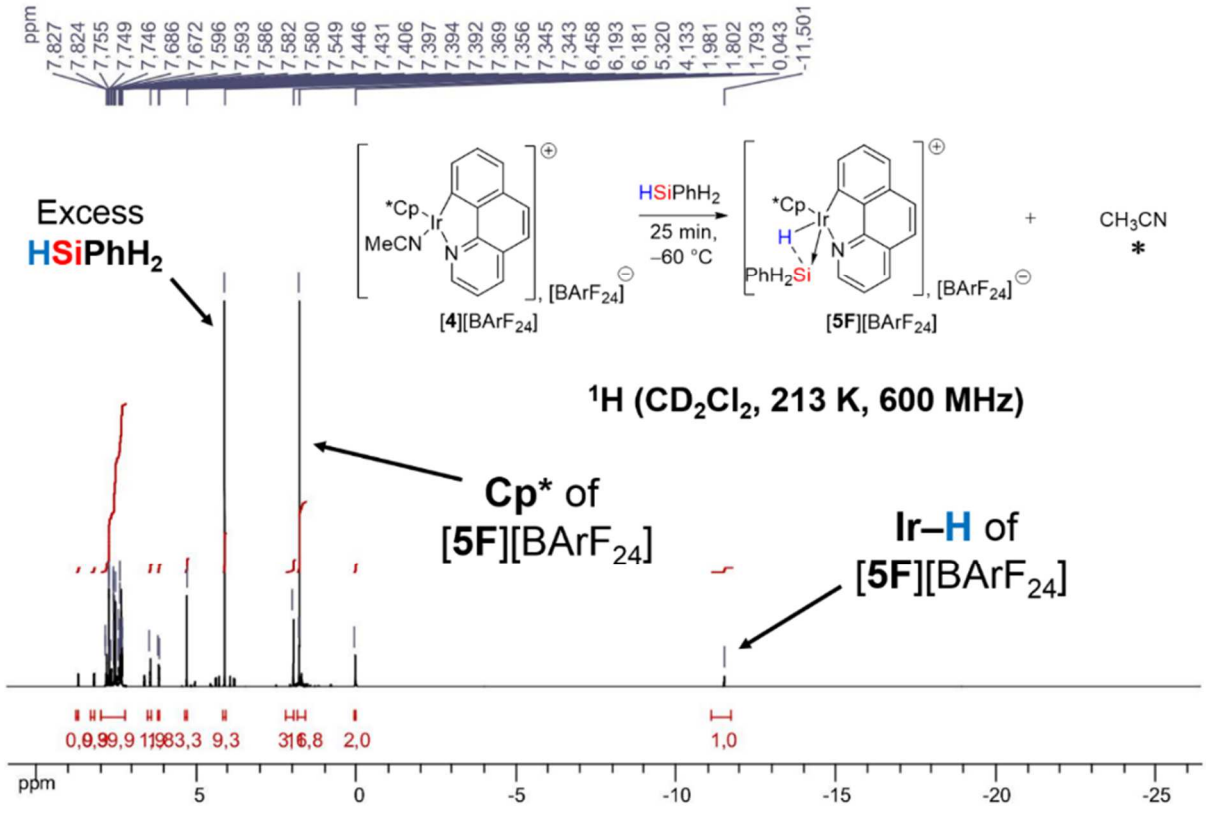

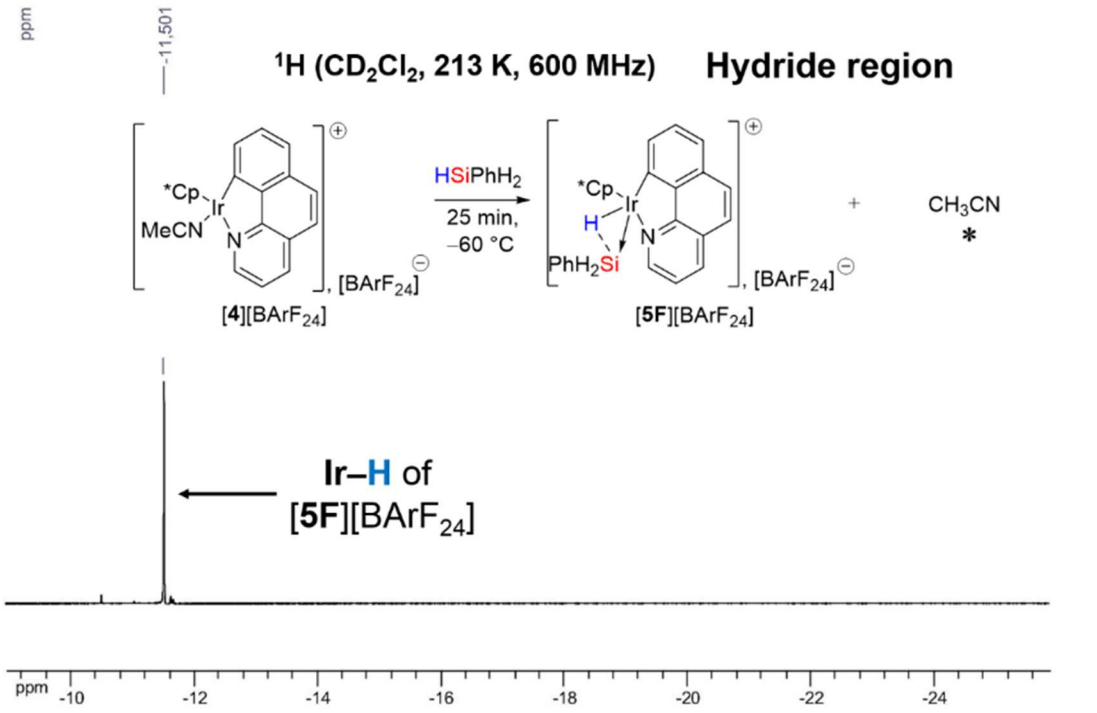
ppm
-11,501
^{1}H (CD_2Cl_2, 213 K, 600 MHz)
Hydride region
*Cp
Ir
MeCN
N
, [$BArF_{24}$]
[4][$BArF_{24}$]
$HSiPhH_2$
25 min,
–60 °C
H
PhH_2Si
[5F][$BArF_{24}$]
CH_3CN
*
Ir–H of
[5F][$BArF_{24}$]
ppm
-10
-12
-14
-16
-18
-20
-22
-24

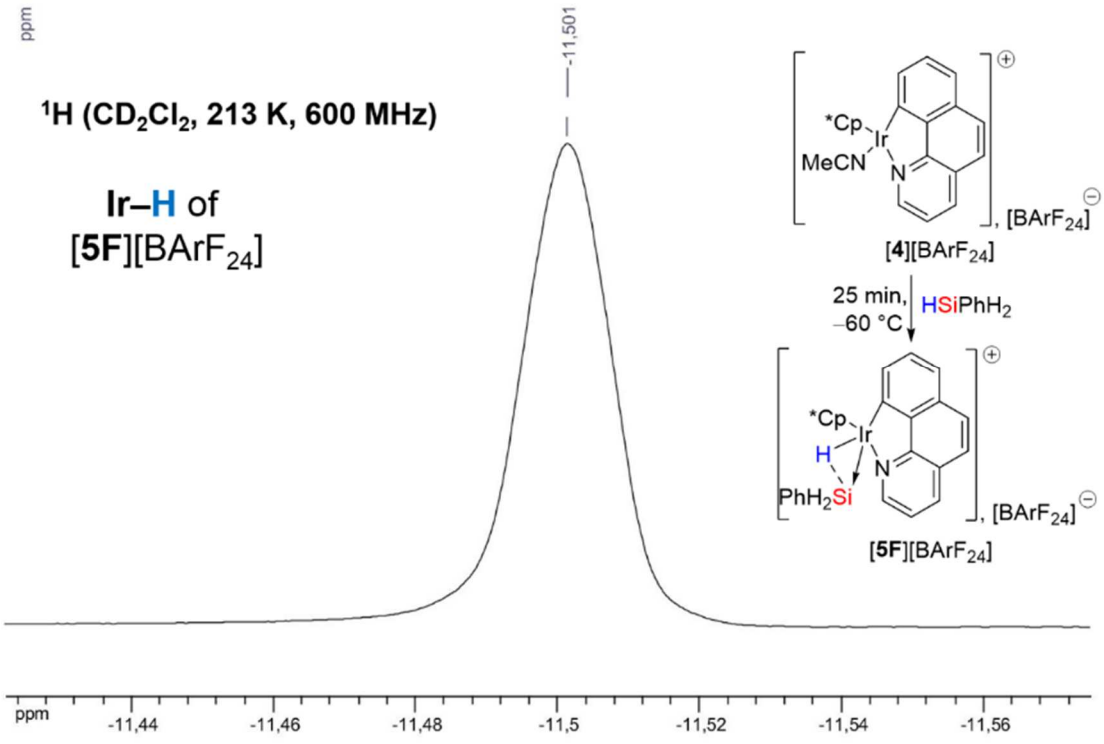
ppm
-11,501
^{1}H (CD_2Cl_2, 213 K, 600 MHz)
Ir–H of
[5F][$BArF_{24}$]
*Cp
Ir
MeCN
N
, [$BArF_{24}$]
[4][$BArF_{24}$]
25 min,
–60 °C
$HSiPhH_2$
H
PhH_2Si
[5F][$BArF_{24}$]
ppm
-11,44
-11,46
-11,48
-11,5
-11,52
-11,54
-11,56

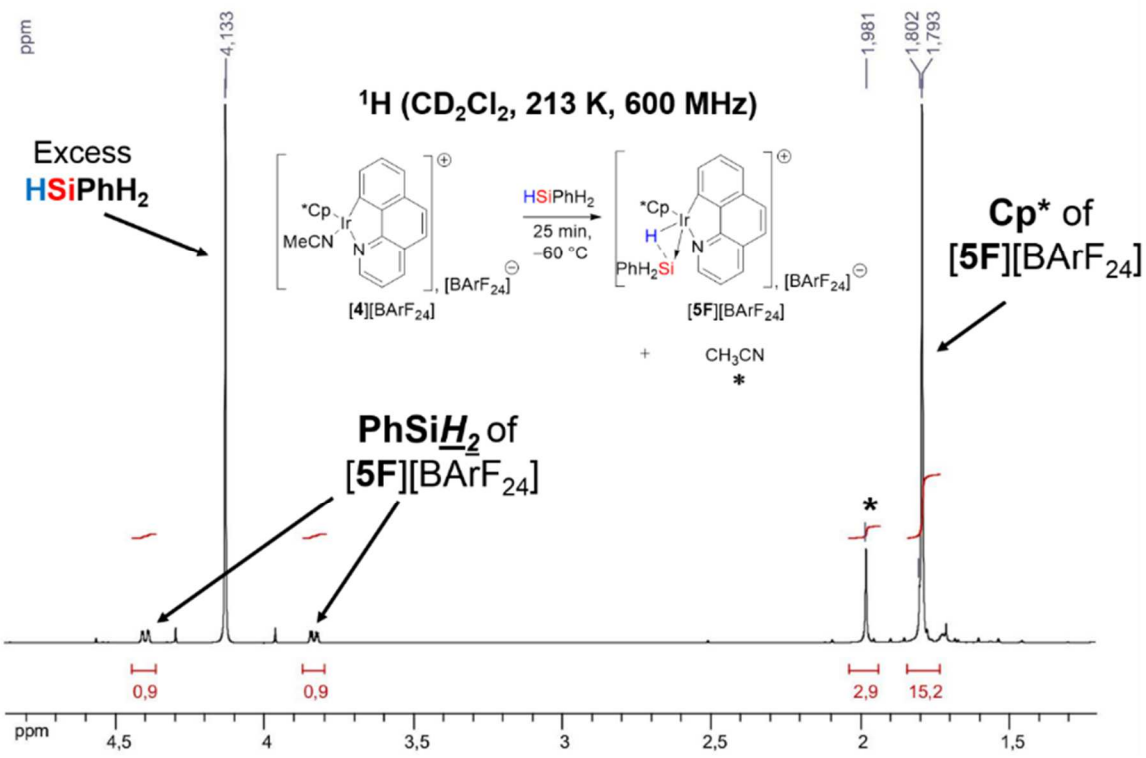
^{1}H (CD_2Cl_2, 213 K, 600 MHz)
Excess
HSiPhH$_2$
HSiPhH$_2$
25 min,
–60 °C
[4][BArF$_{24}$]
[5F][BArF$_{24}$]
CH$_3$CN
*
Cp* of
[5F][BArF$_{24}$]
PhSi*H$_2$* of
[5F][BArF$_{24}$]
4,133
1,981
1,802
1,793
0,9
0,9
2,9
15,2
ppm

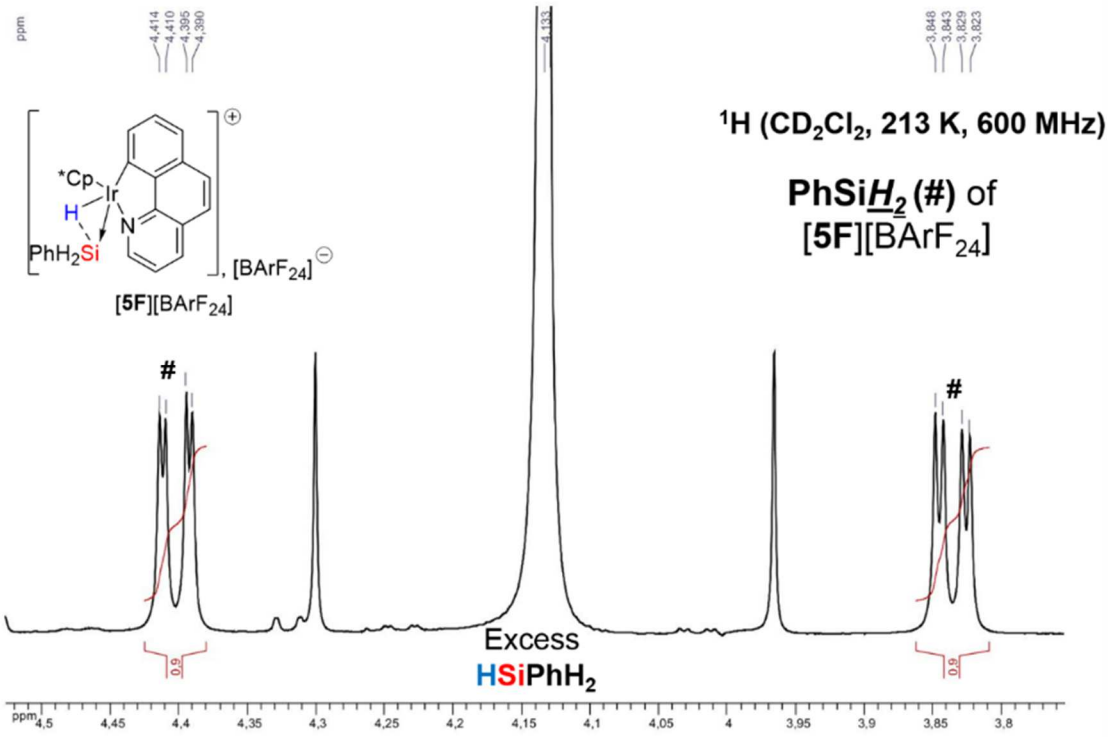
^{1}H (CD_2Cl_2, 213 K, 600 MHz)
PhSi*H$_2$* (#) of
[5F][BArF$_{24}$]
[5F][BArF$_{24}$]
#
#
Excess
HSiPhH$_2$
ppm

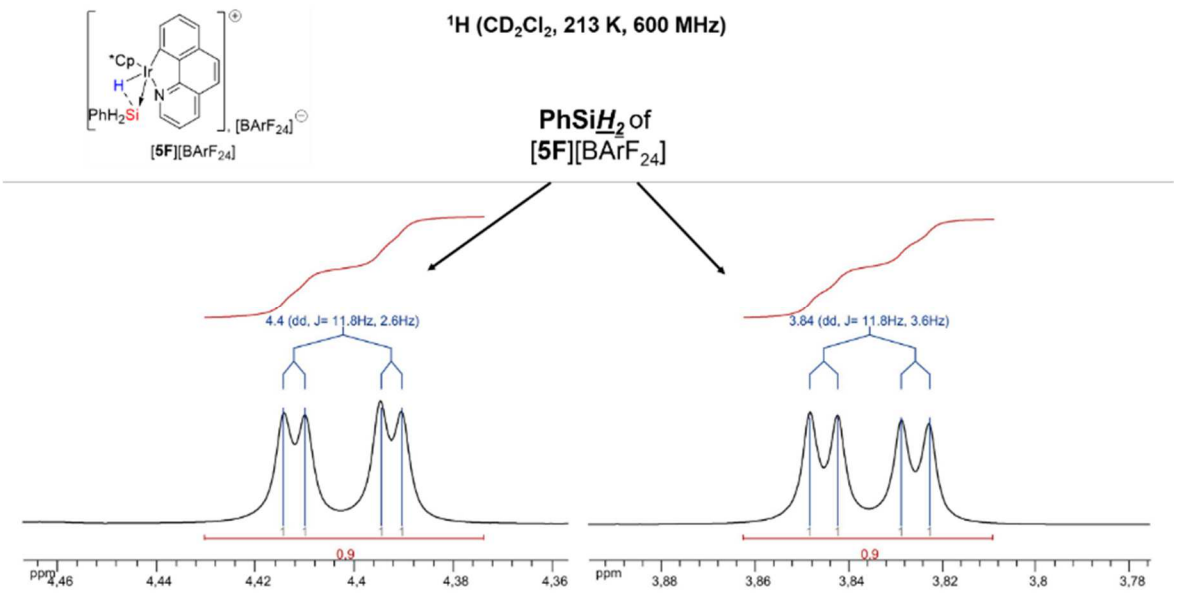
[5F][BArF24]
1H (CD2Cl2, 213 K, 600 MHz)
PhSiH2 of
[5F][BArF24]
4.4 (dd, J= 11.8Hz, 2.6Hz)
3.84 (dd, J= 11.8Hz, 3.6Hz)
0.9
0.9
ppm
4,46
4,44
4,42
4,4
4,38
4,36
ppm
3,88
3,86
3,84
3,82
3,8
3,78

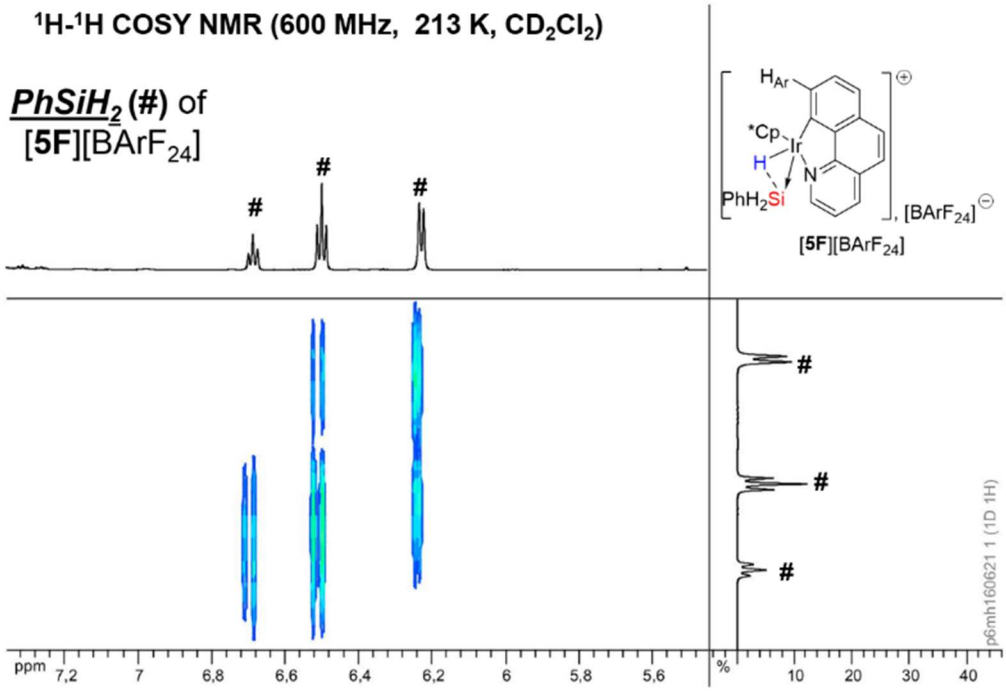
1H-1H COSY NMR (600 MHz, 213 K, CD2Cl2)
PhSiH2 (#) of
[5F][BArF24]
#
#
#
[5F][BArF24]
#
#
#
ppm
7,2
7
6,8
6,6
6,4
6,2
6
5,8
5,6
%
10
20
30
40
p6mh160621 1 (1D 1H)

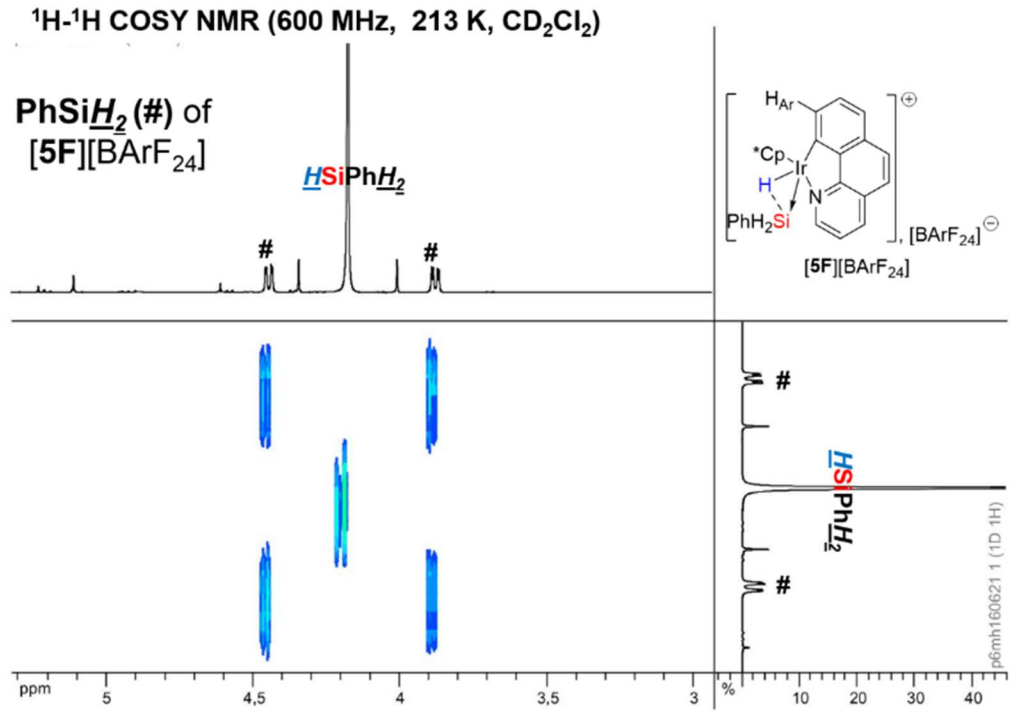
¹H-¹H COSY NMR (600 MHz, 213 K, CD2Cl2)
PhSiH2 (#) of [5F][BArF24]
HSiPhH2
#
#
[5F][BArF24]
ppm
5
4,5
4
3,5
3
%
10
20
30
40
p6mh160621 1 (1D 1H)

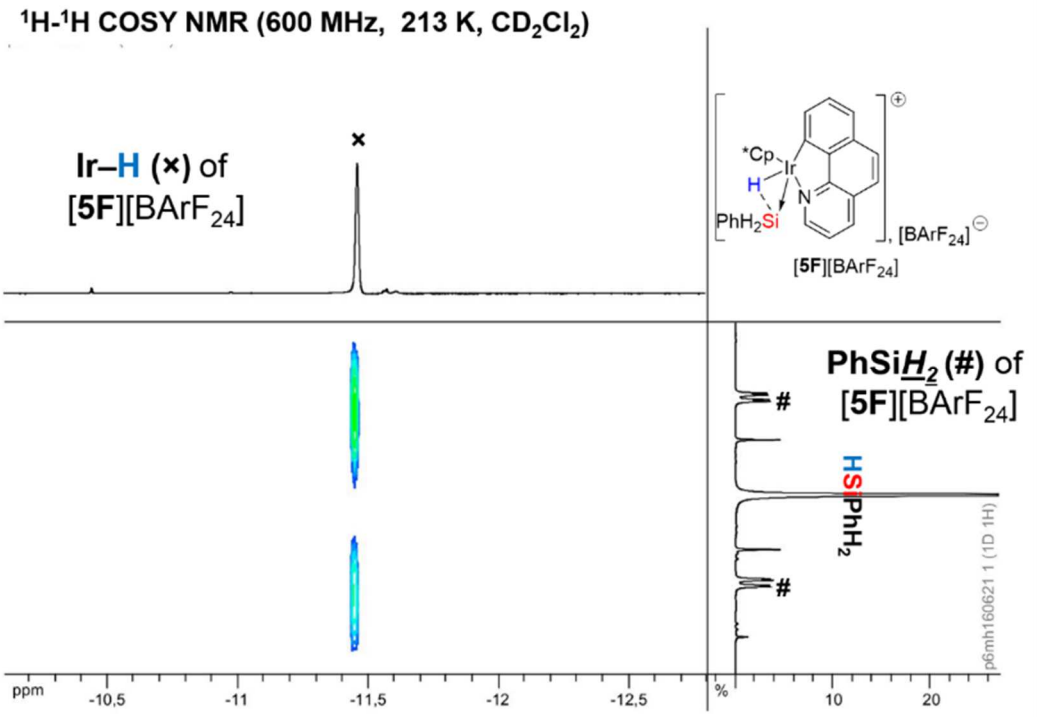
¹H-¹H COSY NMR (600 MHz, 213 K, CD2Cl2)
Ir–H (×) of [5F][BArF24]
×
[5F][BArF24]
PhSiH2 (#) of [5F][BArF24]
#
#
HSiPhH2
ppm
-10,5
-11
-11,5
-12
-12,5
%
10
20
p6mh160621 1 (1D 1H)

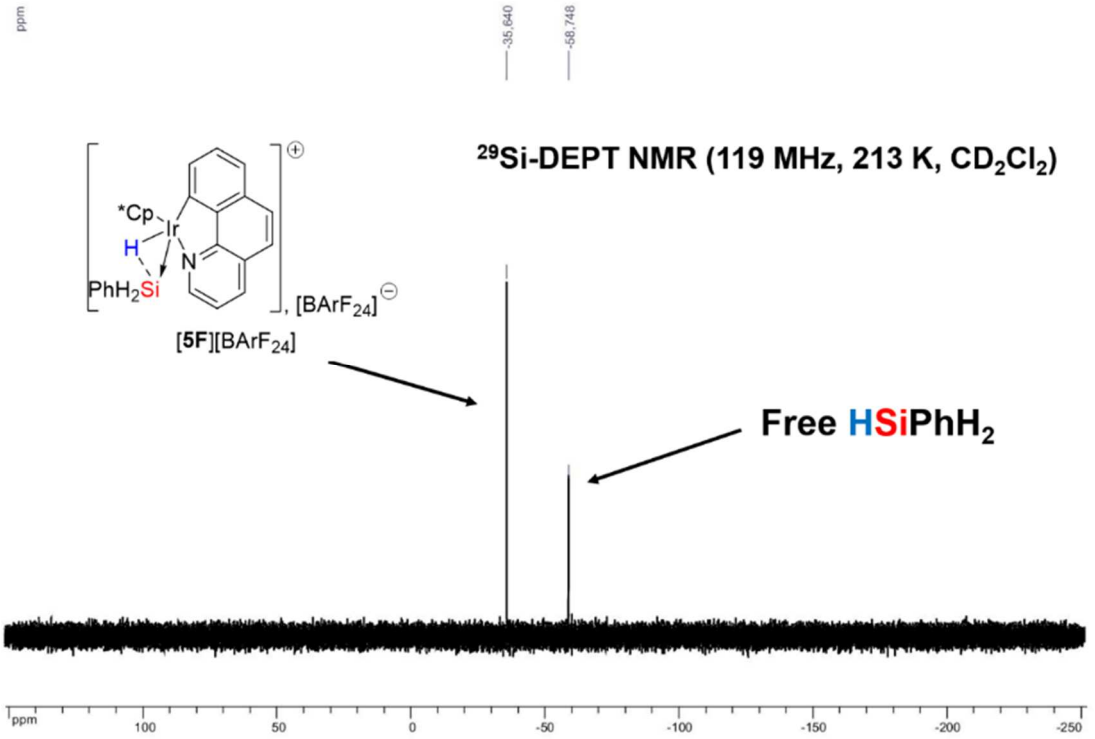
ppm
-35,640
-58,748
*Cp
Ir
H
N
PhH2Si
, [BArF24]
[5F][BArF24]
29Si-DEPT NMR (119 MHz, 213 K, CD2Cl2)
Free HSiPhH2
ppm
100
50
0
-50
-100
-150
-200
-250

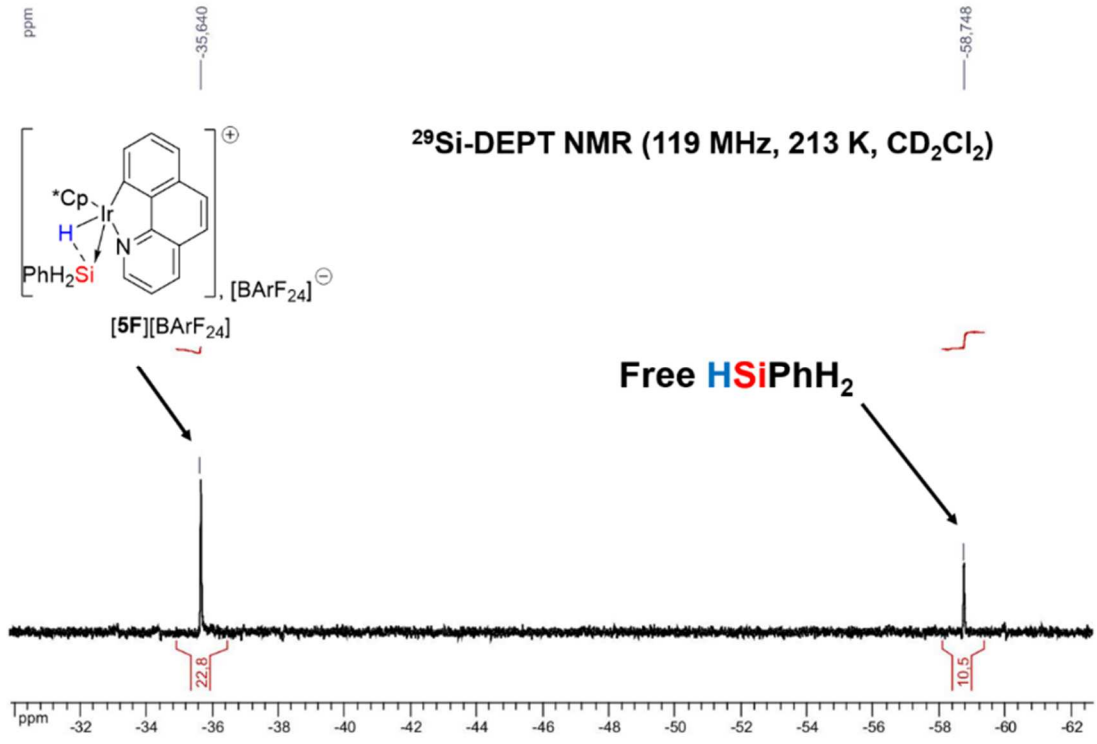
ppm
-35,640
-58,748
*Cp
Ir
H
N
PhH2Si
, [BArF24]
[5F][BArF24]
29Si-DEPT NMR (119 MHz, 213 K, CD2Cl2)
Free HSiPhH2
22,8
10,5
ppm
-32
-34
-36
-38
-40
-42
-44
-46
-48
-50
-52
-54
-56
-58
-60
-62

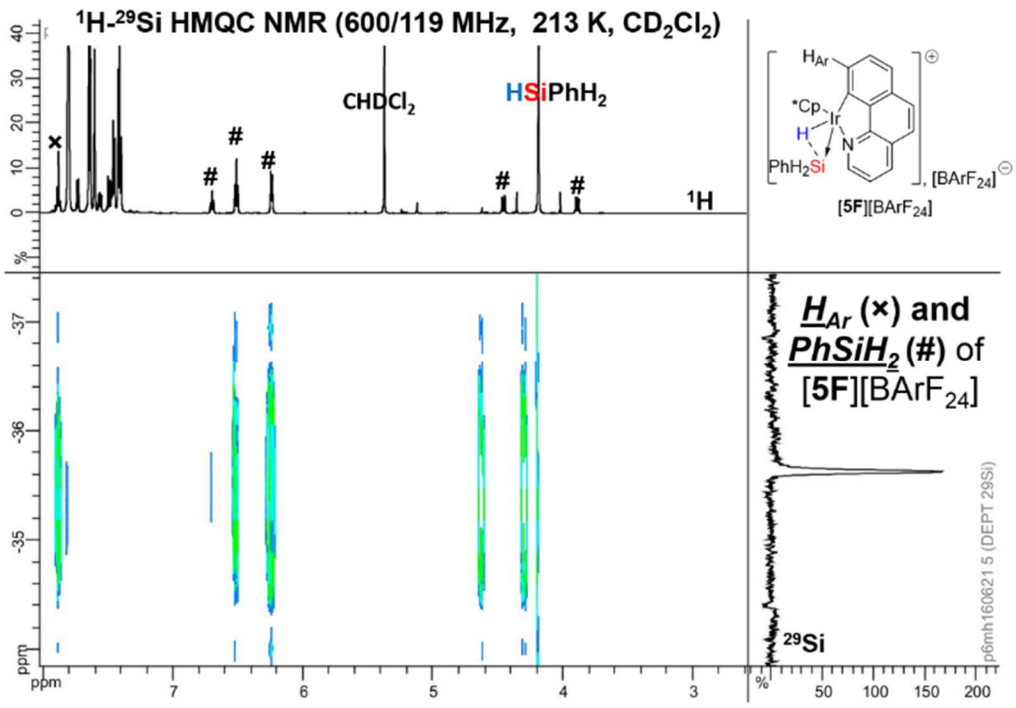

6.2.15.4.2 Reaction of [**4**][BArF$_{24}$] with HSiEt$_3$

Using the general procedure, the conditions of this reaction were as follows: HSiEt$_3$ (4.5 μL, 28.2 μmol), [**4**][BArF$_{24}$] (20 mg, 14.2 μmol), CD_2Cl_2 (0.55 mL). After 25 minutes of reaction, the NMR tube was frozen at < –60 °C. Multinuclear NMR analysis (at –60 °C) of the reaction revealed the total conversion of [**4**][BArF$_{24}$] to [**5A**][BArF$_{24}$], [**5A'**][BArF$_{24}$], [**5B**][BArF$_{24}$], (Et$_3$Si)$_2$NEt along with unconsumed HSiEt$_3$ in a ratio of ~1:1:0.1:1.2:1.2 (see spectra below). [**5A**][BArF$_{24}$] and [**5A'**][BArF$_{24}$] feature identical ^{1}H peaks of H$_{Ar}$ B[*h*]Q (of the C,N ligand) and Cp*, except for bound [Et$_3$Si]$^+$ moieties which feature slightly distinct ^{1}H and ^{29}Si chemical shifts. **Data for [5A][BArF$_{24}$] and [5A'][BArF$_{24}$] were as follows**: **^{1}H NMR (600 MHz, 213 K, CD_2Cl_2)**: δ = 8.67 (d, 2H, H$_{Ar}$ B[*h*]Q, J = 5.3 Hz), 8.38 (d, 2H, H$_{Ar}$ B[*h*]Q, J = 8.0 Hz), 7.90 (d, 2H, H$_{Ar}$ B[*h*]Q, J = 8.8 Hz), 7.8 (t, 4H, H$_{Ar}$ B[*h*]Q, J = 7.4 Hz), 7.73 (m, 16H, H$_{ortho}$ BArF$_{24}$), 7.70 (t, 2H, H$_{Ar}$ B[*h*]Q, J = 8.3 Hz), 7.70 (d, 2H, H$_{Ar}$ B[*h*]Q, J = 8.3 Hz), 7.60 (m, 2H, H$_{Ar}$ B[*h*]Q), 7.54 (m, 8H, H$_{para}$ BArF$_{24}$), 1.69 (s, 30H, Cp-*Me$_5$*), 0.56 (t, 18H [Ir-H]→[Si(CH$_2$C*H$_3$*)$_3$], J = 7.9 Hz), 0.29 (t, 6H [Ir-H]→[Si(C*H$_2$*CH$_3$)$_3$] of [**5A**][BArF$_{24}$]), 0.22 (t, 6H [Ir-H]→[Si(C*H$_2$*CH$_3$)$_3$] of [**5A'**][BArF$_{24}$]), –11.44 (bs, 1H, [Ir-*H*]→[SiEt$_3$]). **^{29}Si-DEPT NMR (119 MHz, 213 K, CD_2Cl_2)**: δ = 6.93 (s, [Ir-H]→[*Si*Et$_3$] of [**5A**][BArF$_{24}$]), 6.90 (s, [Ir-H]→[*Si*Et$_3$] of [**5A'**][BArF$_{24}$]) . **Data for (Et$_3$Si)$_2$NEt) are**

as follows: ^{1}H NMR (600 MHz, 213 K, CD_2Cl_2): δ = 2.81 (q, 2H, N–C*H*$_2$CH$_3$, J = 7.0 Hz), 0.98 (t, 3H, N–CH$_2$C*H*$_3$, J = 7.0 Hz), 0.90 (t, 18H, SiCH$_2$C*H*$_3$, J = 8.0 Hz), 0.56 (q, 12H, SiC*H*$_2$CH$_3$, J = 8.0 Hz). **^{29}Si-DEPT NMR (119 MHz, 213 K, CD_2Cl_2)**: δ = 10.9 ((Et$_3$*Si*)$_2$NEt). **Data for unconsumed-"free" $HSiEt_3$ are as follows: ^{1}H NMR (600 MHz, 213 K, CD_2Cl_2)**: δ = 3.50 (septet, 1H, $^{1}J_{H\text{-}Si}$ = 173.6 Hz), 0.89 (t, 9H, SiCH$_2$C*H*$_3$, J = 8.0 Hz), 0.52 (t, 6H, SiCH$_2$C*H*$_3$, J = 8.0 Hz). **^{29}Si-DEPT NMR (119 MHz, 213 K, CD_2Cl_2)**: δ = 0.0 (s, $HSiEt_3$). A ^{29}Si signal of non-negligible intensity (see ^{1}H-^{29}Si HMQC and ^{29}Si-DEPT spectra) at δ = 9.5 ppm (s) cannot be appropriately attributed to any known molecule.

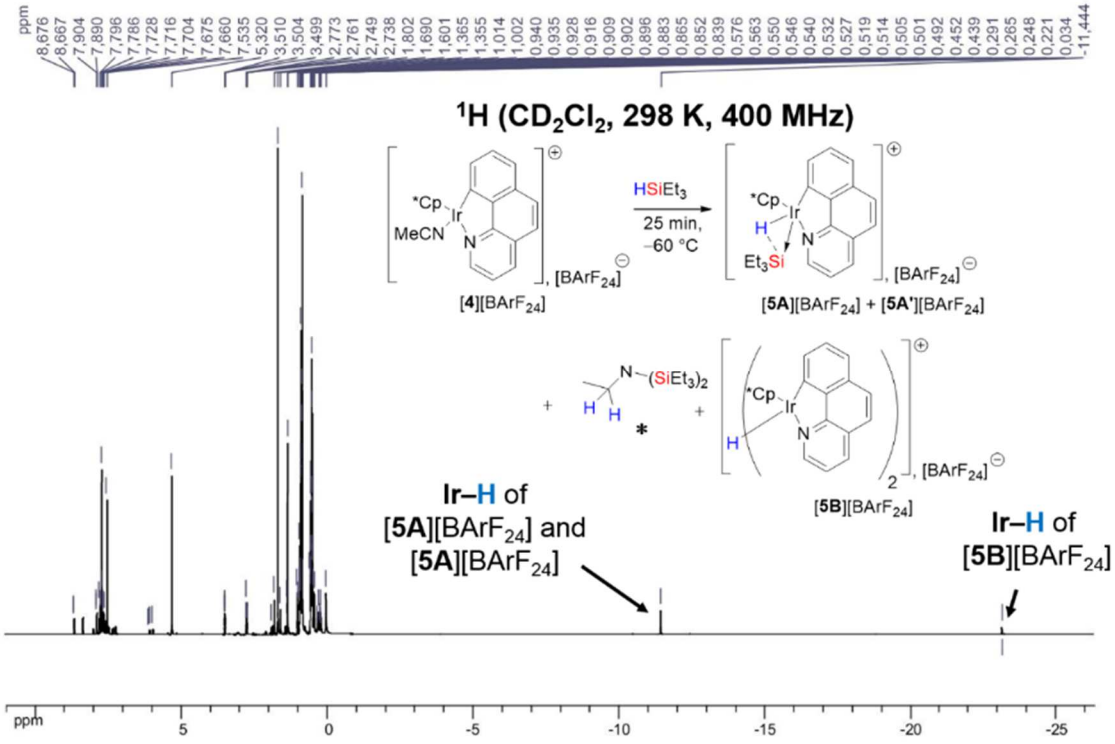

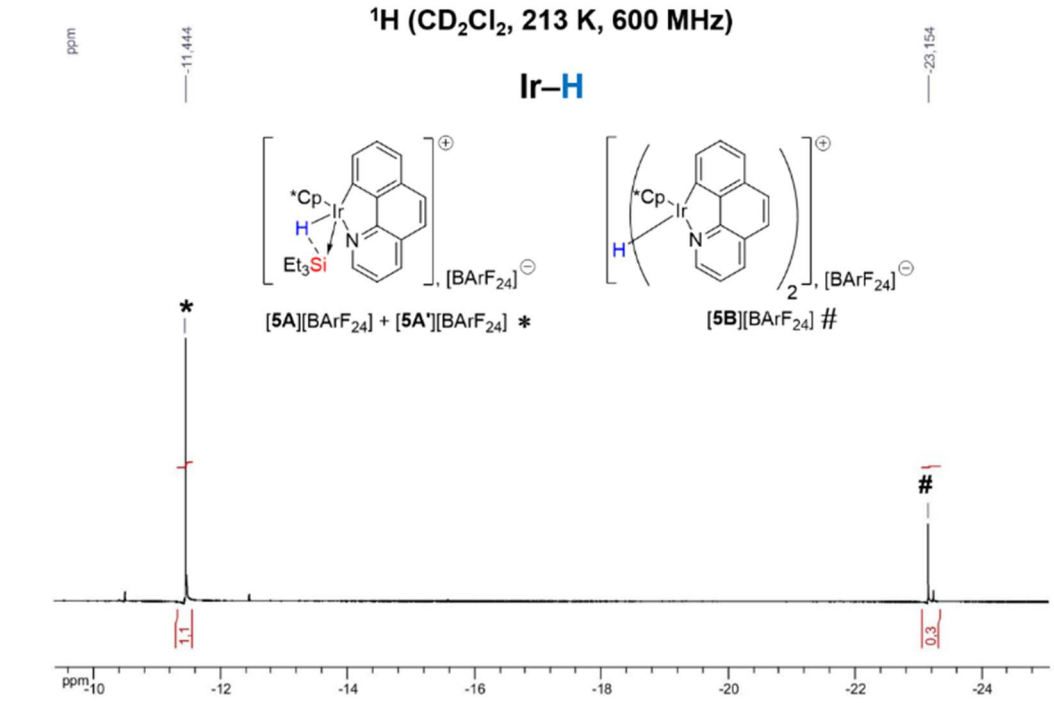
¹H (CD2Cl2, 213 K, 600 MHz)
Ir–H
ppm
-11,444
-23,154
*Cp
Ir
H
N
Et3Si
[BArF24]
2
[5A][BArF24] + [5A'][BArF24] *
[5B][BArF24] #
*
#
1,1
0,3
ppm
-10
-12
-14
-16
-18
-20
-22
-24

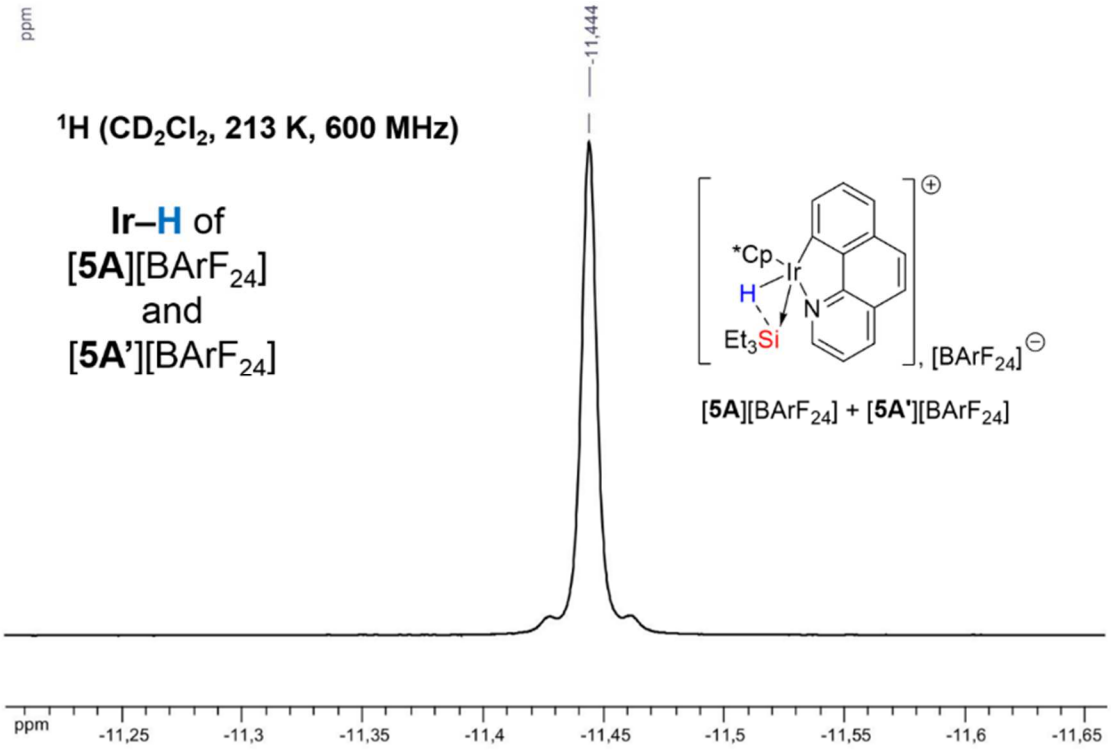
ppm
-11,444
¹H (CD2Cl2, 213 K, 600 MHz)
Ir–H of
[5A][BArF24]
and
[5A'][BArF24]
*Cp
Ir
H
N
Et3Si
[BArF24]
[5A][BArF24] + [5A'][BArF24]
ppm
-11,25
-11,3
-11,35
-11,4
-11,45
-11,5
-11,55
-11,6
-11,65

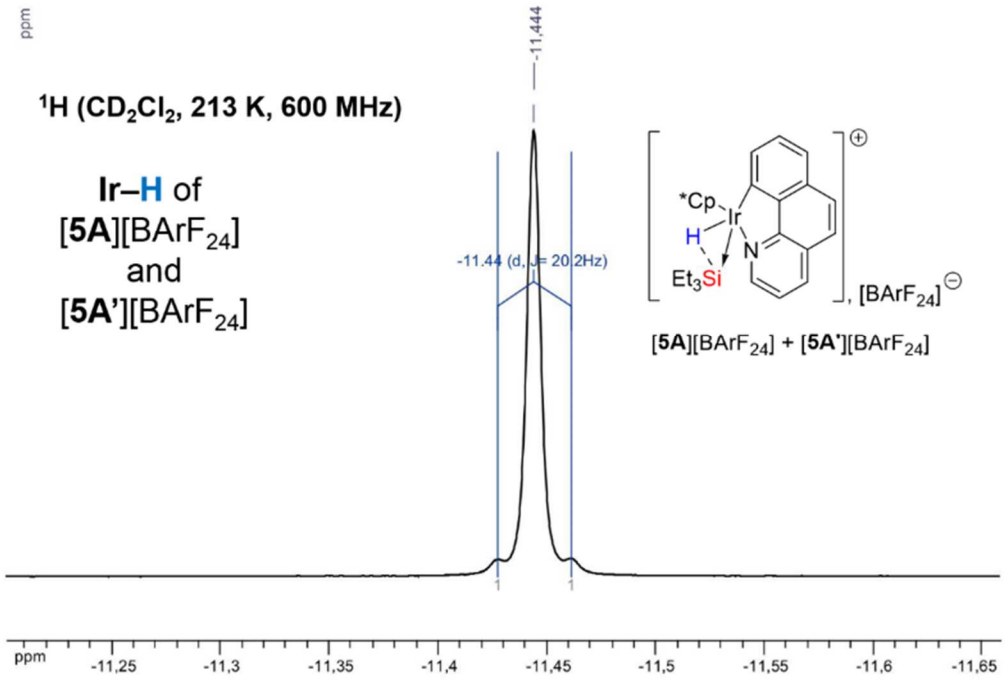
ppm
-11,444
^{1}H (CD_2Cl_2, 213 K, 600 MHz)
Ir–H of
[5A][BArF24]
and
[5A'][BArF24]
-11.44 (d, J = 20.2Hz)
*Cp
Ir
H
N
Et3Si
, [BArF24]
[5A][BArF24] + [5A'][BArF24]
ppm
-11,25
-11,3
-11,35
-11,4
-11,45
-11,5
-11,55
-11,6
-11,65

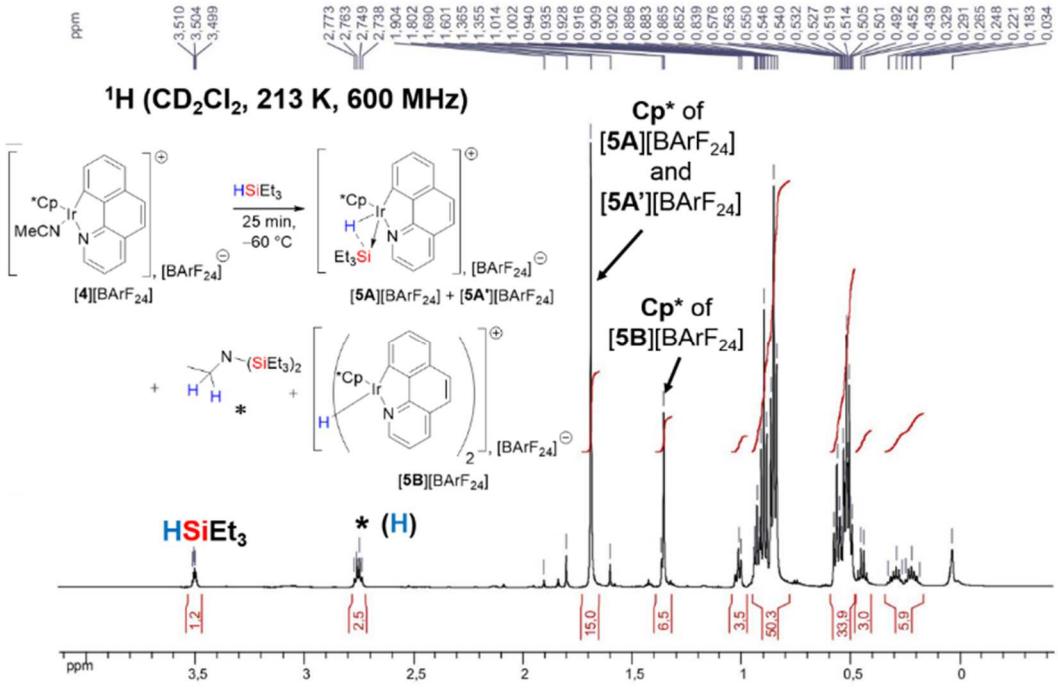
ppm
^{1}H (CD_2Cl_2, 213 K, 600 MHz)
*Cp
Ir
MeCN
N
, [BArF24]
[4][BArF24]
HSiEt3
25 min,
–60 °C
H
Et3Si
[5A][BArF24] + [5A'][BArF24]
Cp* of
[5A][BArF24]
and
[5A'][BArF24]
Cp* of
[5B][BArF24]
N(SiEt3)2
H H
*
2
[5B][BArF24]
HSiEt3
* (H)
1.2
2.5
15.0
6.5
3.5
50.3
33.9
3.0
5.9
ppm
3,5
3
2,5
2
1,5
1
0,5
0

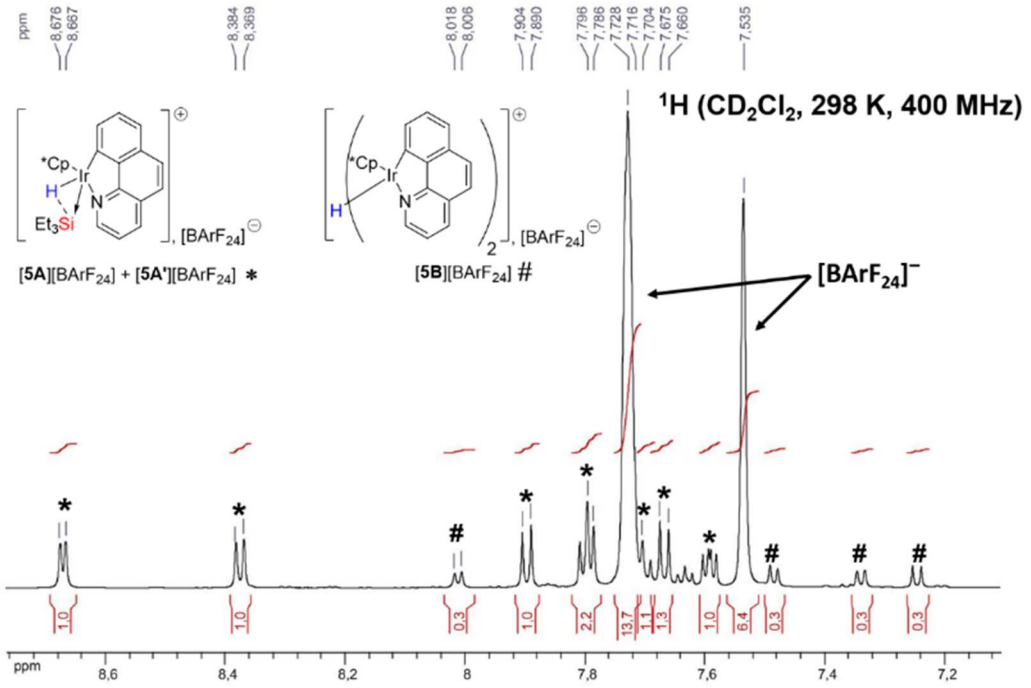
^{1}H (CD_2Cl_2, 298 K, 400 MHz)
[5A][BArF24] + [5A'][BArF24] *
[5B][BArF24] #
[BArF24]⁻
ppm

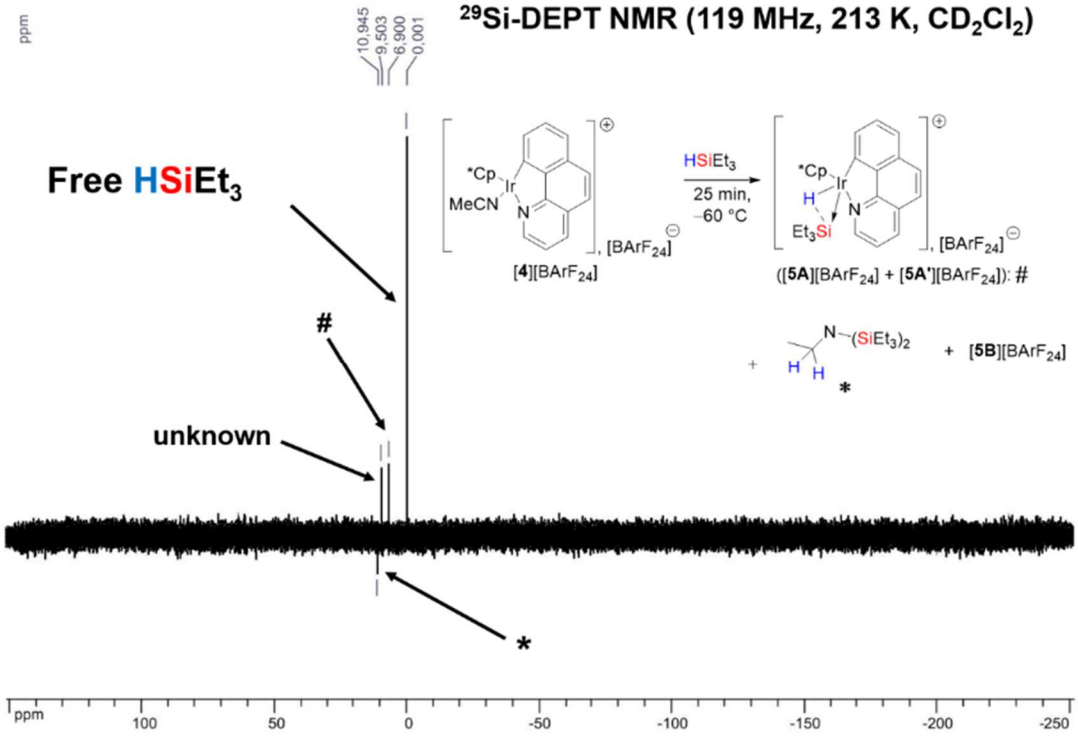
^{29}Si-DEPT NMR (119 MHz, 213 K, CD_2Cl_2)
Free HSiEt3
unknown
[4][BArF24]
HSiEt3
25 min,
–60 °C
([5A][BArF24] + [5A'][BArF24]): #
[5B][BArF24]
ppm

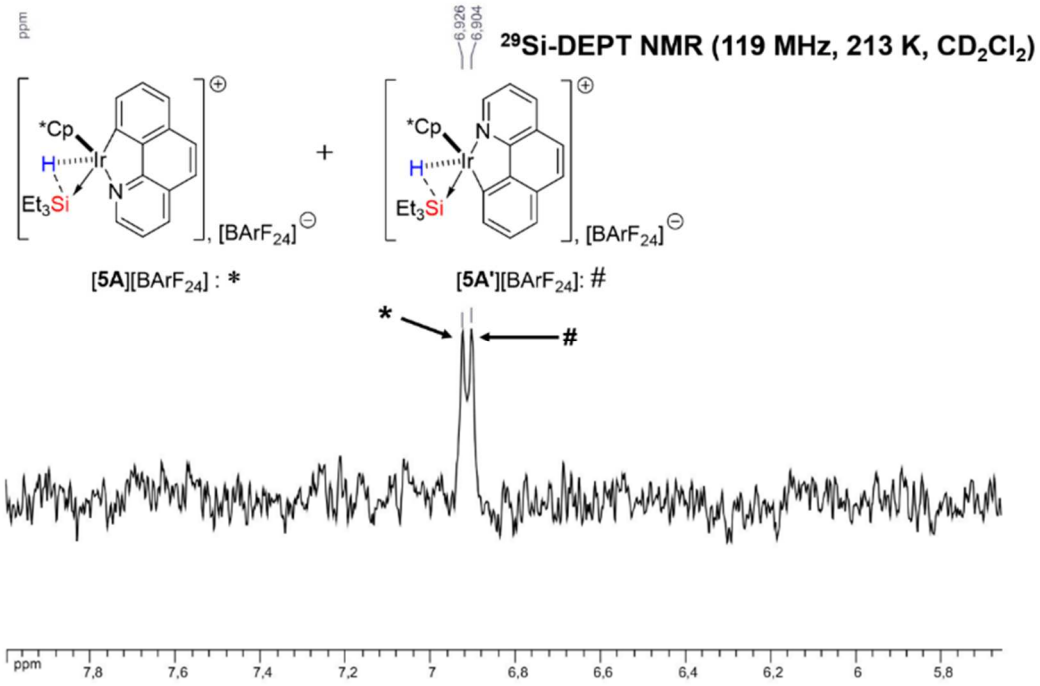
ppm
6.926
6.904
29Si-DEPT NMR (119 MHz, 213 K, CD2Cl2)
*Cp
H
Ir
N
Et3Si
, [BArF24]
[5A][BArF24] : *
[5A'][BArF24]: #
*
#
ppm
7,8
7,6
7,4
7,2
7
6,8
6,6
6,4
6,2
6
5,8

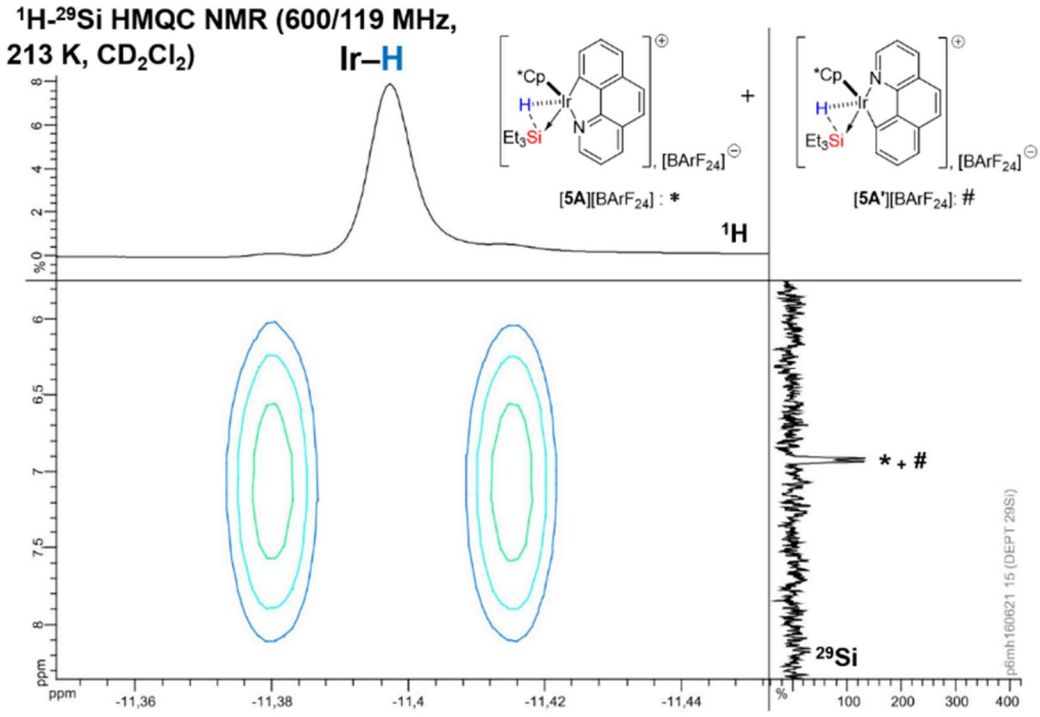
1H-29Si HMQC NMR (600/119 MHz,
213 K, CD2Cl2)
Ir–H
*Cp
H
Ir
N
Et3Si
, [BArF24]
[5A][BArF24] : *
[5A'][BArF24]: #
1H
%
0
2
4
6
8
ppm
6
6,5
7
7,5
8
-11,36
-11,38
-11,4
-11,42
-11,44
* + #
29Si
100
200
300
400
p6mh160621 15 (DEPT 29Si)

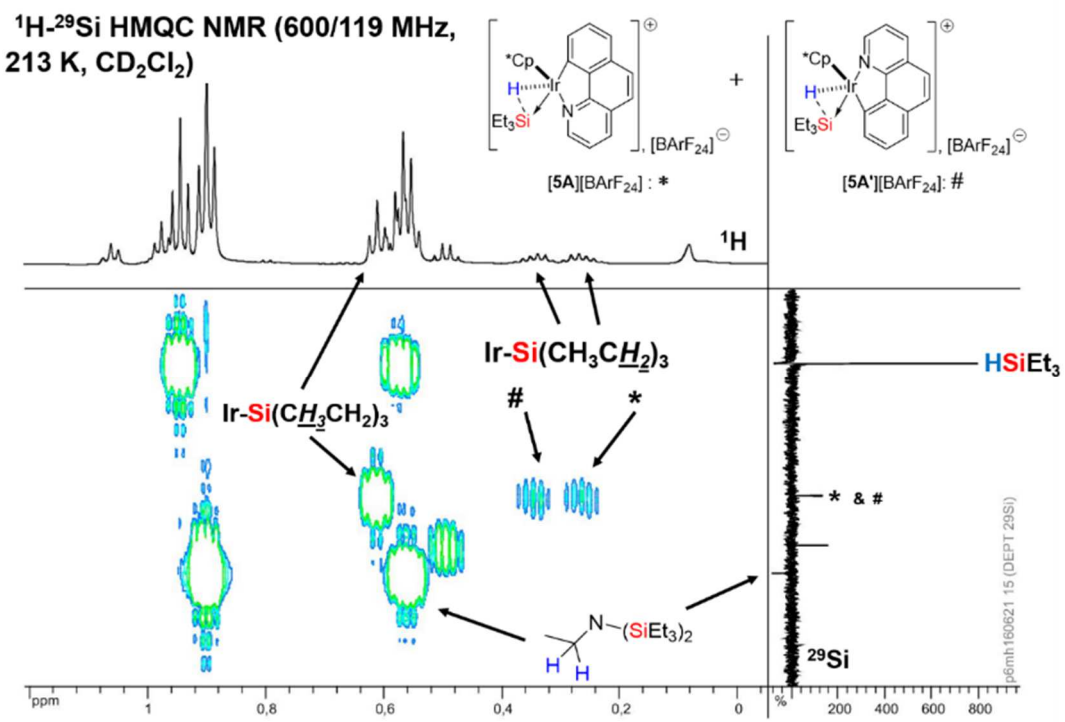
^{1}H-^{29}Si HMQC NMR (600/119 MHz, 213 K, CD_2Cl_2)
[5A][BArF24] : *
[5A'][BArF24]: #
^{1}H
Ir-Si(CH3CH2)3
Ir-Si(CH3CH2)3
#
*
HSiEt3
* & #
N(SiEt3)2
^{29}Si
ppm
1
0,8
0,6
0,4
0,2
0
%
200
400
600
800

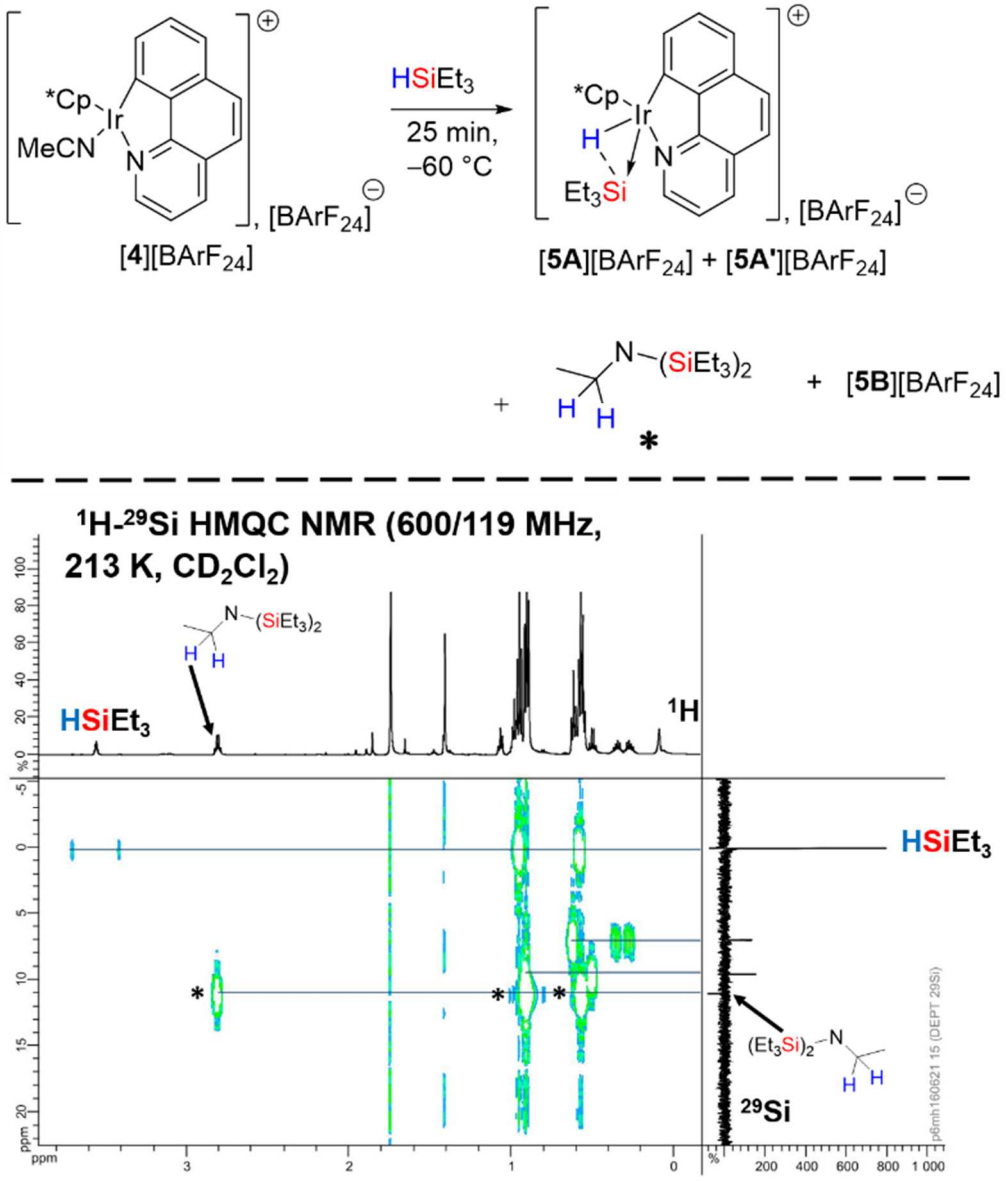

6.2.16 Reactivity of [**3A**][BArF24] with Lewis bases

6.2.16.1 Interaction of 4-*N*,*N*-Dimethylaminopyridine with [**3A**][BArF24]

In a glovebox, $HSiEt_3$ (4.61 μL, 28.9 μmol) was added to a solution of [**2**][BArF24] (20 mg, 14.4 μmol) in CD_2Cl_2 (0.4 mL). The resulting mixture was shaken and transferred into a standard NMR tube, which was then tightly sealed with a septum (t = 0 s or t_0) and analyzed at t_0 + 10 min by ^{1}H NMR spectroscopy at room temperature to verify the presence of [**3A**][BArF24]. A solution of *N*,*N*-dimethylaminopyridine (DMAP) (3.53 mg, 29.0 μmol) in CD_2Cl_2 (0.3 mL) was added via a syringe into the NMR tube, and the resulting solution was vigorously shaken and a

new ^{1}H NMR spectrum was acquired (t_0 + 25 min). Before addition of DMAP, the ratio [**3A**][$BArF_{24}$]:[**3B**][$BArF_{24}$] was 2.6:1 (see NMR spectra). After addition of DMAP the typical signals of [**3A**][$BArF_{24}$] were absent. Only the signals of **4**, [**3B**][$BArF_{24}$], and traces of [**2**][$BArF_{24}$] were observed with a **4**:[**3B**][$BArF_{24}$] ratio of 1.1:1 (see NMR spectrum).

^{1}H NMR (CD_2Cl_2) of Et_3SiH + [**2**][$BArF_{24}$] recorded on 500 MHz spectrometer at 298 K showing the total conversion of [**2**][$BArF_{24}$] into [**3A**][$BArF_{24}$] and [**3B**][$BArF_{24}$] (red line). Addition of DMAP to this mixture gave total conversion of [**3A**][$BArF_{24}$] into [**4**] (green line). The ^{1}H NMR spectrum of the authentic sample of **4** is given for comparison (blue line).

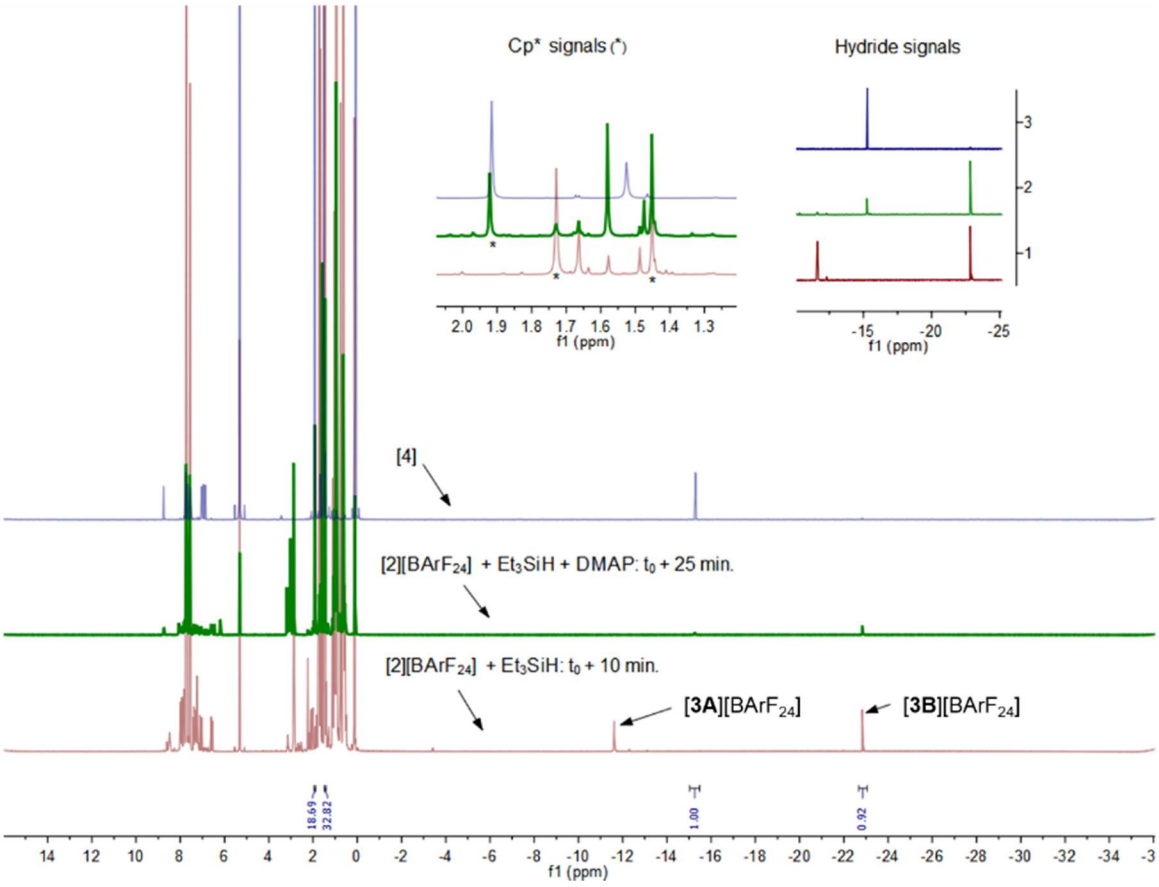

6.2.16.2 Preparation of a Dry Solution of [*n*Bu$_4$N][OTf]

In a glovebox, dry n-tetrabutylammonium bromide [*n*Bu$_4$N][Br] (23 mg, 72.0 *µ*mol) was added to a solution of silver trifluoromethanesulfonate Ag[OTf] (18.5 mg, 72.0 *µ*mol) in dry and degassed CD_2Cl_2 (0.5 mL). The resulting mixture was vigorously shaken to induce the quantitative precipitation of AgBr, which was removed by filtration over a pad of dry Dicalite. The collected filtrate containing [*n*Bu$_4$N][OTf] was used as prepared without further purification.

6.2.16.3 Interaction of [*n*Bu$_4$N][OTf] with [**3A**][BArF$_{24}$]

In a glovebox, HSiEt$_3$ (11.5 µL, 72.0 µmol) was added to solution of [**2**][BArF$_{24}$] (20 mg, 14.0 µmol) in CD_2Cl_2 (0.5 mL). The resulting mixture was shaken and transferred into a standard NMR tube, which was then tightly sealed with a septum (t = 0 s or t_0) and analyzed at t_0 + 15 min by ^{1}H NMR spectroscopy at room temperature to assess the formation of [**3A**][BArF$_{24}$]. A solution of [*n*Bu$_4$N][OTf] (72.0 µmol, vide supra) in CD_2Cl_2 (0.4 mL) was added via a syringe into the NMR sample tube, the resulting solution was vigorously shaken, and a new ^{1}H NMR spectrum was acquired (t_0 + 25 min). Before addition of [*n*Bu$_4$N]-[OTf], the ratio [**3A**][BArF$_{24}$]:[**3B**][BArF$_{24}$] was 7.7:1 (see spectra below). After addition of [*n*Bu$_4$N][OTf] the typical signals of [**3A**][BArF$_{24}$] were absent. Only the signals of **4**, [**3B**][BArF$_{24}$], and traces of HSiEt$_3$ and Et$_3$SiOTf (partially overlapped with the signals of nBu$_4$N$^+$) and [*n*Bu$_4$N][BArF$_{24}$]) were observed with a **4**:[**3B**][BArF$_{24}$] ratio of 50:1 (see spectrum below).

^{1}H NMR (CD_2Cl_2, 400 MHz) spectrum of the mixture of Et_3SiH and [**2**][BArF$_{24}$] at 298 K showing the total conversion of [**2**][BArF$_{24}$] into [**3A**][BArF$_{24}$] and [**3B**][BArF$_{24}$] (red line). Addition of [*n*Bu$_4$N][OTf] to this mixture induced the conversion of [**3A**][BArF$_{24}$] into [**4**] (dark khaki line). The ^{1}H NMR spectra of authentic samples of **4** (green line), Et_3SiOTf (TESOTf, blue line) and [*n*Bu$_4$N][OTf] (purple line) are overlayed for comparison.

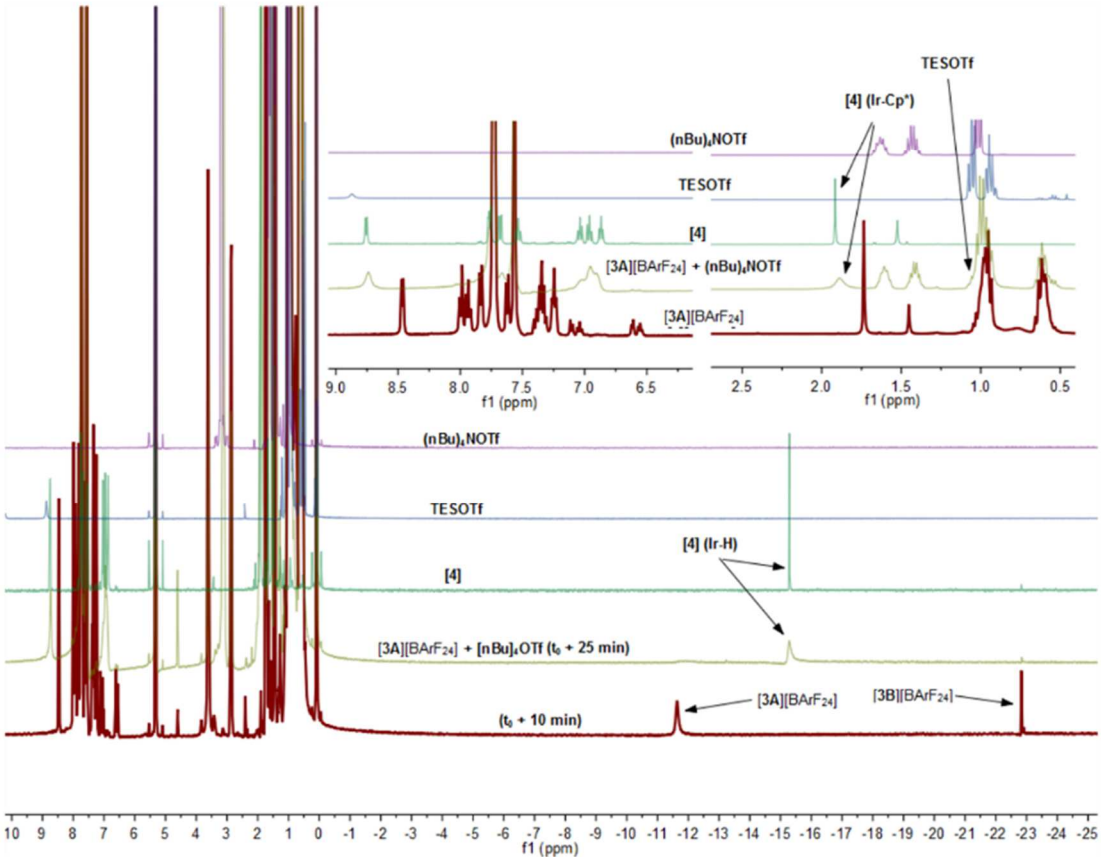

6.2.17.1 [**3B**][OTf] (Optimized Synthesis)

$HSiEt_3$ was added dropwise (70 μL, 0.44 mmol) to a solution of [**2**][OTf] (87 mg, 0.13 mmol) in CH_2Cl_2 (3 mL). A color change from yellow to deep red was observed immediately after addition of $HSiEt_3$. This mixture was stirred at room temperature for 22 h. The resulting solution was concentrated to ca. 1 mL, and benzene (2 mL) and pentane (3 mL) were added. This mixture was left to stand at +4 °C overnight to induce the slow crystallization of [**3B**][OTf], which was collected after removal of the supernatant by suction and dried overnight at room temperature under reduced pressure to afford an analytically pure compound (40 mg, 56% yield). **Anal. Calcd for $C_{43}H_{47}F_3Ir_2N_2O_3S$**: C, 46.39; H, 4.26; N, 2.52. **Found**: C, 46.13; H, 4.25; N, 2.51. **^{1}H NMR (500 MHz, 298 K, CD_2Cl_2)**: δ = 7.84 (d, 2H H–C=N PhPy, J = 7.5 Hz), 7.42 (d, 2H H–C=N PhPy, J = 7.8 Hz), 7.23–7.33 (m, 4H PhPy), 7.14 (d, 2H PhPy, J = 8.0 Hz), 7.05 (m, 2H PhPy), 6.54–6.64 (m, 4H PhPy), 1.46 (s, 30H, Cp-*Me*$_5$), –22.86 (s, 1H Ir(μ-H)Ir). **^{13}C NMR (126 MHz, 298 K, CD_2Cl_2)**: δ = 166.3 (C PhPy), 159.4 (C PhPy), 151.8 (C–H PhPy), 143.7 (C PhPy), 137.1 (C–H PhPy), 136.7 (C–H PhPy), 130.1 (C–H PhPy), 125.1 (C–H PhPy), 122.8 (C–H PhPy), 121.6 (C–H PhPy), 117.3 (C–H PhPy), 91.7 (*Cp*-Me$_5$), 9.3 (Cp-*Me*$_5$). **^{19}F NMR (282 MHz, 298 K, CD_2Cl_2)**: δ = –79.9 (s, 3F C*F*$_3$O$_3$S). **HRMS-ESI (m/z) calcd for $C_{42}H_{47}Ir_2N_2$** ([**3B**]$^+$): 965.2997. **Found**: 965.3018. **HRMS-ESI (m/z) calcd for C*F*$_3$O$_3$S** ([OTf]$^-$): 148.9515. **Found**: 148.9527.

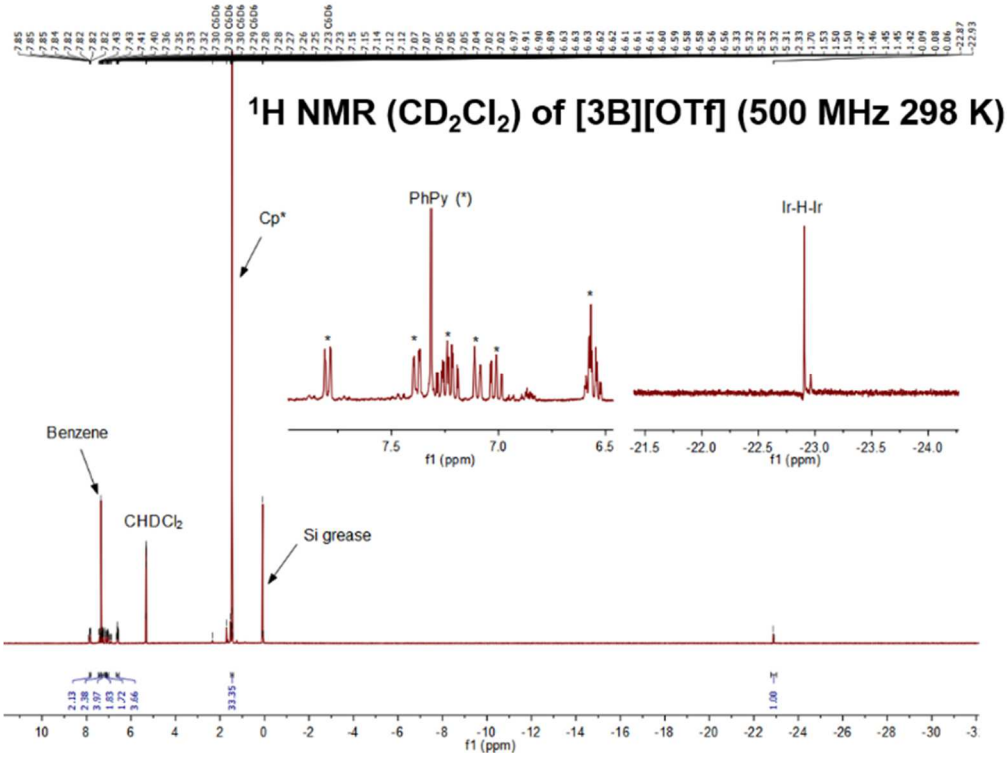
^{1}H NMR (CD_2Cl_2) of [3B][OTf] (500 MHz 298 K)
Cp*
PhPy (*)
Ir-H-Ir
Benzene
$CHDCl_2$
Si grease
f1 (ppm)

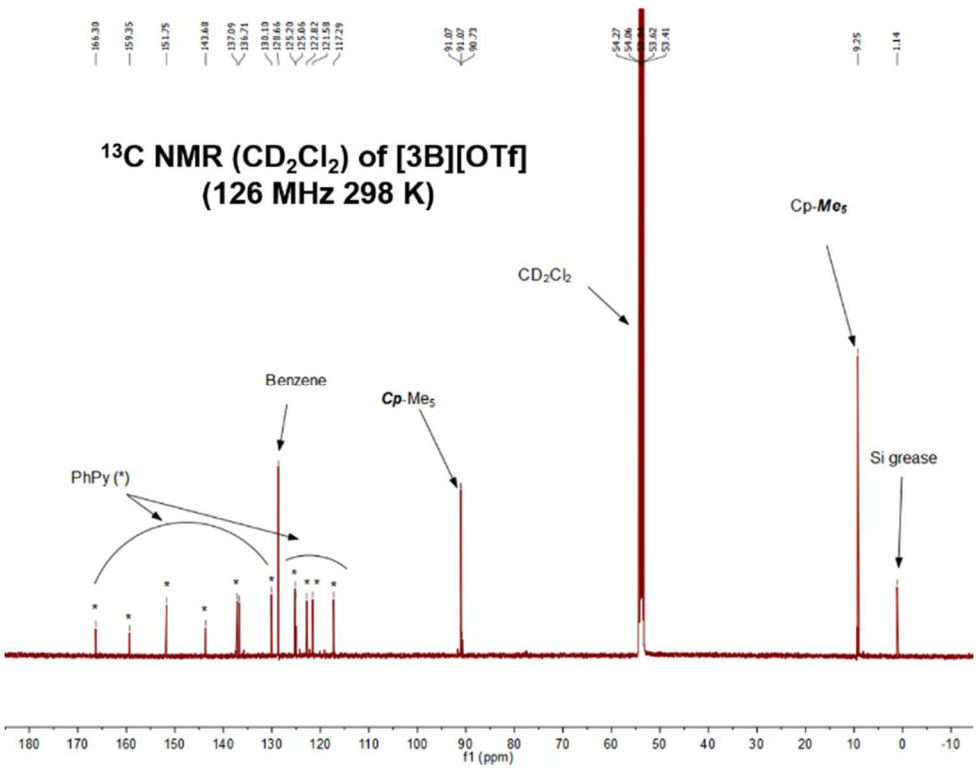
^{13}C NMR (CD_2Cl_2) of [3B][OTf]
(126 MHz 298 K)
Cp-*Me*$_5$
CD_2Cl_2
Benzene
Cp-Me_5
PhPy (*)
Si grease
f1 (ppm)

^{19}F NMR (CD_2Cl_2) of [3B][OTf] (128 MHz 298 K)

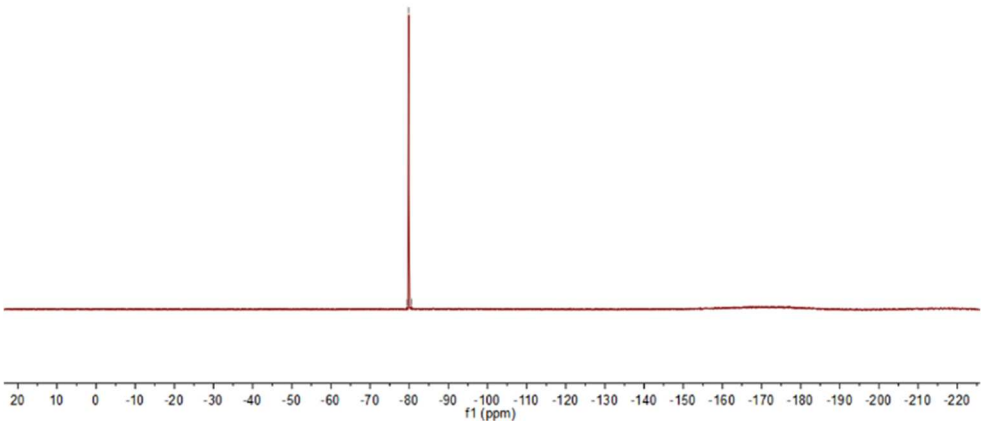

6.3 Experiments related to chapter 3: Hydrosilylation of carbonyls

6.3.1 General procedure

To a mixture of silane (1.1–2.2 equiv.) and carbonyl (1.78 mmol, 1.0 equiv.) substrates was added a solution of the precatalyst (solubilized in 0.5 mL of a given solvent). The reaction was allowed to take place at room temperature for a given time, after which tri-*tert*-butylbenzene was added as internal NMR standard. An aliquot from this solution was taken and mixed with C_6D_6 for NMR analysis. For screening studies, we used [**2**][$BArF_{24}$] as precatalyst.

6.3.2 Optimization studies

6.3.2.1 Comparison of silanes

The influence of the nature of silane on catalysis was studied. For this purpose, only primary and tertiary silanes were screened. All the reactions were conducted at room temperature for 30 minutes following the general procedure: acetophenone (0.2 mL, 1.71 mmol), silane (1.89 mmol), [**2**][$BArF_{24}$] (2.4 mg, 1.71×10^{-3} mmol, 0.1 mol %), CH_2Cl_2 (0.5 mL). The results are summarized in table S1.

Tableau S1. Optimization of silanes for the hydrosilylation of acetophenone. PMHS stands for polymethylhydrosiloxane.

Entry	Silane	Yield (%)
1	$HSiEt_3$	>99
2	$HSiPh_3$	77
3	PMHS	43
4	$HSiPhH_2$	10

From this study, we selected triethylsilane ($HSiEt_3$, entry 1) for next studies as it outperforms other tested silanes (entries 2–4).

6.3.2.2 Comparison of solvents

In this study, a variety of solvents were screened. All the reactions were conducted at room temperature for 30 minutes following the general procedure: acetophenone (0.2 mL, 1.71 mmol), triethylsilane (0.3 mL, 1.89 mmol), [**2**][$BArF_{24}$] (2.4 mg, 1.71×10^{-3} mmol, 0.1 mol %), solvent (0.5 mL). The results are summarized in table S2.

Tableau S2. Optimization of solvents for the hydrosilylation of acetophenone.

Entry	Solvent	Yield (%)
1	Dichloromethane	>99
2	1,2-Dichloroethane	>99
3	Tetrahydrofuran	85
4	Nitromethane	>99
5	Toluene	>99
6	Chlorobenzene	>99
7	Fluorobenzene	>99

This study shows that except tetrahydrofuran (entry 3), all solvents (entries 1, 2 and 4–7) used were compatible with the catalytic system as full completion of the reaction was obtained after 30 minutes at room temperature. Tetrahydrofuran is less compatible probably of its Lewis basic oxygen atom which interacts with the Lewis acidic silylium $[Et_3Si]^+$ moiety of the Lewis pair catalytic species [**3A**][$BArF_{24}$]. Dichloromethane was selected for next studies because of its relative low cost and low boiling point (maybe helpful in case of product isolation) when compared to other solvents.

6.3.2.3 Comparison of precatalysts

6.3.2.3.1 **1** versus [**2**][X]

In this study, different iridium complexes were screened. For this purpose, the neutral complex **1** and salts [**2**][X] (where X = $BArF_{24}$; BF_4; BPh_4; OTf and PF_6) were used. All the reactions were conducted following the general method for 30 minutes in CH_2Cl_2 (0.5 mL): acetophenone

(0.2 mL, 1.71 mmol), triethylsilane (0.3 mL, 1.89 mmol), precatalyst (1.71×10^{-3} mmol, 0.1 mol %). The results are summarized in table S3.

Table S3. Optimization of precatalysts for the hydrosilylation of acetophenone.

Entry	Precatalyst	Yield (%)
1	**1**	<1
2	[**2**][$BArF_{24}$]	>99
3	[**2**][OTf]	53
4	[**2**][BPh_4]	28
5	[**2**][PF_6]	22
6	[**2**][BF_4]	<1

This study shows the higher efficiency of [**2**][$BArF_{24}$] for the hydrosilylation of acetophenone in the conditions used when compared to other salts and **1**. [**4**][X] salts are expected to give similar results as [**2**][X] counterparts. Further comparative studies tend to confirm this assumption. The results are summarized in table S4.

6.3.2.3.2 [**2**][$BArF_{24}$] versus [**4**][$BArF_{24}$]

The reaction between acetophenone and triethylsilane conducted in CH_2Cl_2 (0.5 mL) at room temperature for 30 minutes was catalyzed by [**4**][$BArF_{24}$] as twice faster as [**2**][$BArF_{24}$] (table S4). This observation was confirmed with the reaction between benzyl alcohol and triethylsilane conducted in 1,2-dichloroethane at 20 °C, which was performed tree times faster with [**4**][$BArF_{24}$] than with [**2**][$BArF_{24}$] (table S4). The conditions used for the two reactions were as follows:

- Hydrosilylation of acetophenone (general procedure described above): acetophenone (0.2 mL, 1.71 mmol), triethylsilane (0.3 mL, 1.89 mmol), precatalyst (8.57×10^{-4} mmol, 0.05 mol %).

- *O*-silylation of benzyl alcohol: benzyl alcohol (1 mL, 9.5 mmol), triethylsilane (0.8 mL, (5.0 mmol), precatalyst (4.8×10^{-3} mmol, 0.1 mol %).

Table S4. Comparison of the catalytic performance of [**2**][$BArF_{24}$] versus [**4**][$BArF_{24}$].

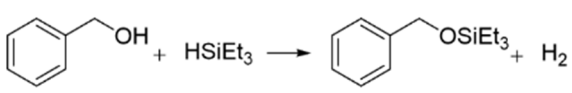		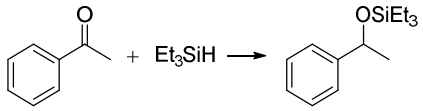	
TOF (h^{-1})		**Yield (%)**	
[**2**][$BArF_{24}$]	[**4**][$BArF_{24}$]	[**2**][$BArF_{24}$]	[**4**][$BArF_{24}$]
105,662	364,490	51	97

6.3.3 Substrate scope study: ketones (table 12)

6.3.3.1 Experimental conditions

The following data detail the experimenl conditions used for the substrate scope study for which the results are reported in table 12. The general procedure for the hydrosilylation of carbonyls described above was used for every substrate. For each catalytic run, the molar quantity of the substrates and the precatalyst, the time and the temperature of the reaction are specified as follows:

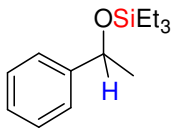 : Acetophenone (0.21 mL, 1.78 mmol), $HSiEt_3$ (0.31 mL, 1.96 mmol), [**4**][$BArF_{24}$] (2.5 mg, 1.77×10^{-3} mmol, 0.1 mol %), 0.4 mL of CH_2Cl_2, 30 min, rt.

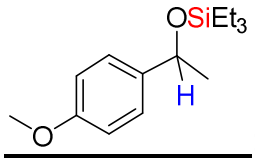

: 4'-Methoxyacetophenone (0.24 mL, 1.78 mmol), $HSiEt_3$ (0.31 mL, 1.96 mmol), [**4**][$BArF_{24}$] (2.5 mg, 1.77×10^{-3} mmol, 0.1 mol %), 0.4 mL of CH_2Cl_2, 30 min, rt.

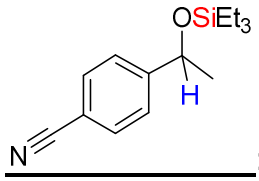

: 4-Acetylbenzonitrile (0.159 g, 1.10 mmol), $HSiEt_3$ (0.19 mL, 1.20 mmol), [**4**][$BArF_{24}$] (7.7 mg, 5.48×10^{-3} mmol, 0.5 mol %), 0.5 mL of CH_2Cl_2, 18 h, rt.

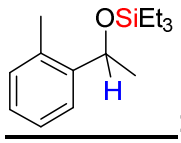

: 2'-Methoxyacetophenone (0.23 mL, 1.78 mmol), $HSiEt_3$ (0.31 mL, 1.96 mmol), [**4**][$BArF_{24}$] (2.5 mg, 1.77×10^{-3} mmol, 0.1 mol %), 0.4 mL of CH_2Cl_2, 30 min, rt.

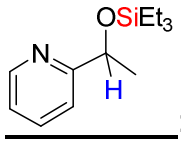

: 2-Acetylpyridine (0.12 mL, 1.10 mmol), $HSiEt_3$ (0.38 mL, 2.41 mmol), [**4**][$BArF_{24}$] (7.7 mg, 5.48×10^{-3} mmol, 0.5 mol %), 0.5 mL of CH_2Cl_2, 18 h, rt.

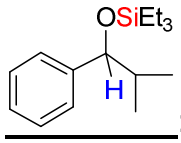

: 2-Methyl-1-phenylpropan-1-one (0.16 mL, 1.10 mmol), $HSiEt_3$ (0.19 mL, 1.20 mmol), [**4**][$BArF_{24}$] (7.7 mg, 5.48×10^{-3} mmol, 0.5 mol %), 0.5 mL of CH_2Cl_2, 30 min, rt.

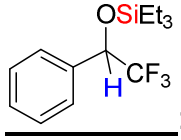

: 2,2,2-Trifluoroacetophenone (0.15 mL, 1.78 mmol), $HSiEt_3$ (0.19 mL, 1.20 mmol), [**4**][$BArF_{24}$] (7.7 mg, 5.48×10^{-3} mmol, 0.5 mol %), 0.5 mL of CH_2Cl_2, 18 h, rt.

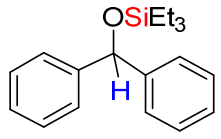

: Benzophenone (0.199 g, 1.78 mmol), $HSiEt_3$ (0.19 mL, 1.20 mmol), [**4**][$BArF_{24}$] (7.7 mg, 5.48×10^{-3} mmol, 0.5 mol %), 0.5 mL of CH_2Cl_2, 30 min, rt.

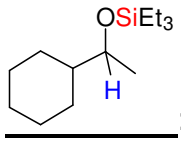

: 1-Cyclohexylethan-1-one (0.10 mL, 1.78 mmol), $HSiEt_3$ (0.31 mL, 1.96 mmol), [**4**][$BArF_{24}$] (2.5 mg, 1.77×10^{-3} mmol, 0.1 mol %), 0.4 mL of CH_2Cl_2, 30 min, rt.

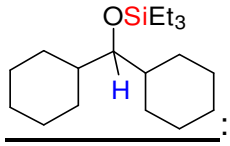

: Dicyclohexylmethanone (0.35 mL, 1.78 mmol), $HSiEt_3$ (0.31 mL, 1.96 mmol), [**4**][$BArF_{24}$] (2.5 mg, 1.77×10^{-3} mmol, 0.1 mol %), 0.4 mL of CH_2Cl_2, 30 min, rt.

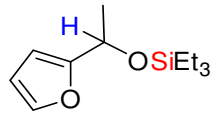

: 2-Acetylfuran (0.11 mL, 1.10 mmol), $HSiEt_3$ (0.19 mL, 1.20 mmol), [**4**][$BArF_{24}$] (7.7 mg, 5.48×10^{-3} mmol, 0.5 mol %), 0.4 mL of CH_2Cl_2, 30 min, rt.

6.3.3.2 NMR data of the products

The structural identity of each silyl ether which is produced during the substrate scope study has been confirmed by ^{1}H NMR analysis. For the products that have been already reported in the literature along with their characterization data, all our ^{1}H NMR data matched those reported (table S5). However, the products for which the NMR spectroscopic data are not published yet, their characteristic ^{1}H NMR chemical shifts (δ, ppm) are provided in table S5. The ^{1}H NMR spectra for all the products are also given in the next section.

Table S5. Hydrosilylation of ketones: NMR spectroscopic data of the products.

Ketone + $HSiEt_3$ 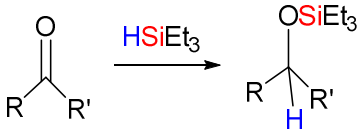	**Our NMR data or related literature references**
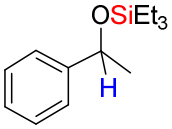	Ison, E. A.; Corbin, R. A.; Abu-Omar, M. M. Hydrogen Production from Hydrolytic Oxidation of Organosilanes Using a Cationic Oxorhenium Catalyst. *J. Am. Chem. Soc.* **2005**, *127* (34), 11938–11939.
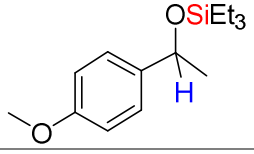	Teci, M.; Lentz, N.; Brenner, E.; Matt, D.; Toupet, L. Alkylfluorenyl Substituted N-Heterocyclic Carbenes in Copper(I) Catalysed Hydrosilylation of Aldehydes and Ketones. *Dalt. Trans.* **2015**, *44* (31), 13991–13998.
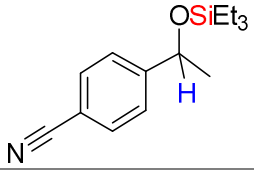	Pérez, M.; Qu, Z. W.; Caputo, C. B.; Podgorny, V.; Hounjet, L. J.; Hansen, A.; Dobrovetsky, R.; Grimme, S.; Stephan, D. W. Hydrosilylation of Ketones, Imines and Nitriles Catalysed by Electrophilic Phosphonium Cations: Functional Group Selectivity and Mechanistic Considerations. *Chem. - A Eur. J.* **2015**, *21* (17), 6491–6500.
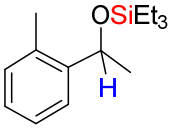	Díez-González, S.; Kaur, H.; Zinn, F. K.; Stevens, E. D.; Nolan, S. P. A Simple and Efficient Copper-Catalyzed Procedure for the Hydrosilylation of Hindered and Functionalized Ketones. *J. Org. Chem.* **2005**, *70* (12), 4784–4796.
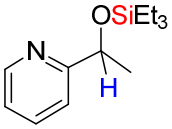	Díez-González, S.; Kaur, H.; Zinn, F. K.; Stevens, E. D.; Nolan, S. P. A Simple and Efficient Copper-Catalyzed Procedure for the Hydrosilylation of Hindered and Functionalized Ketones. *J. Org. Chem.* **2005**, *70* (12), 4784–4796.
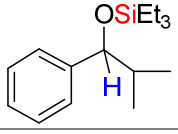	Egbert, J. D.; Nolan, S. P. Tandem Deuteration/Hydrosilylation Reactions Catalyzed by a Rhodium Carbene Complex under Solvent-Free Conditions *Chem. Commun.* **2012**, *48* (22), 2794–2796.
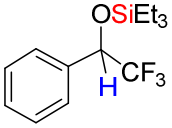	Mallov, I.; Stephan, D. W. Ferrocenyl-Derived Electrophilic Phosphonium Cations (EPCs) as Lewis Acid Catalysts. *Dalt. Trans.* **2016**, *45* (13), 5568–5574.
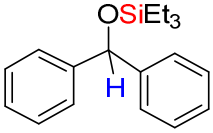	Díez-González, S.; Kaur, H.; Zinn, F. K.; Stevens, E. D.; Nolan, S. P. A Simple and Efficient Copper-Catalyzed Procedure for the Hydrosilylation of Hindered and Functionalized Ketones. *J. Org. Chem.* **2005**, *70* (12), 4784–4796.
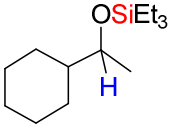	Pérez, M.; Qu, Z. W.; Caputo, C. B.; Podgorny, V.; Hounjet, L. J.; Hansen, A.; Dobrovetsky, R.; Grimme, S.; Stephan, D. W. Hydrosilylation of Ketones, Imines and Nitriles Catalysed by Electrophilic Phosphonium Cations: Functional Group Selectivity and Mechanistic Considerations. *Chem. - A Eur. J.* **2015**, *21* (17), 6491–6500.
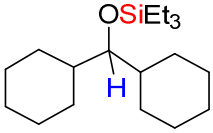	Díez-González, S.; Kaur, H.; Zinn, F. K.; Stevens, E. D.; Nolan, S. P. A Simple and Efficient Copper-Catalyzed Procedure for the Hydrosilylation of Hindered and Functionalized Ketones. *J. Org. Chem.* **2005**, *70* (12), 4784–4796.

6.3.3.3 ^{1}H NMR spectra (C_6D_6, 400 MHz, 298 K)

In this section, we provide the copies of the ^{1}H NMR spectra that were recorded for the reaction mixture of each catalytic run involving the related ketone substrate. Depending on the substrate, the time at which the ^{1}H NMR analysis was done varies from 30 minutes to 18 hours and the molar stoichiometry of $HSiEt_3$ relative to the ketone was either 1.1 or 2.2 equivalents. All the reactions were conducted at room temperature in CH_2Cl_2 (0.4–0.5 mL) as solvent and using [**4**][$BarF_{24}$] (0.1 or 0.5 mol %) as precatalyst. For more details about the general procedure and the specific conditions applied to every catalytic run, see the previous sections of the experimental part (table S5); for the related NMR yields that were determined for every product, the reader is refered to the table 12 of the manuscipt.

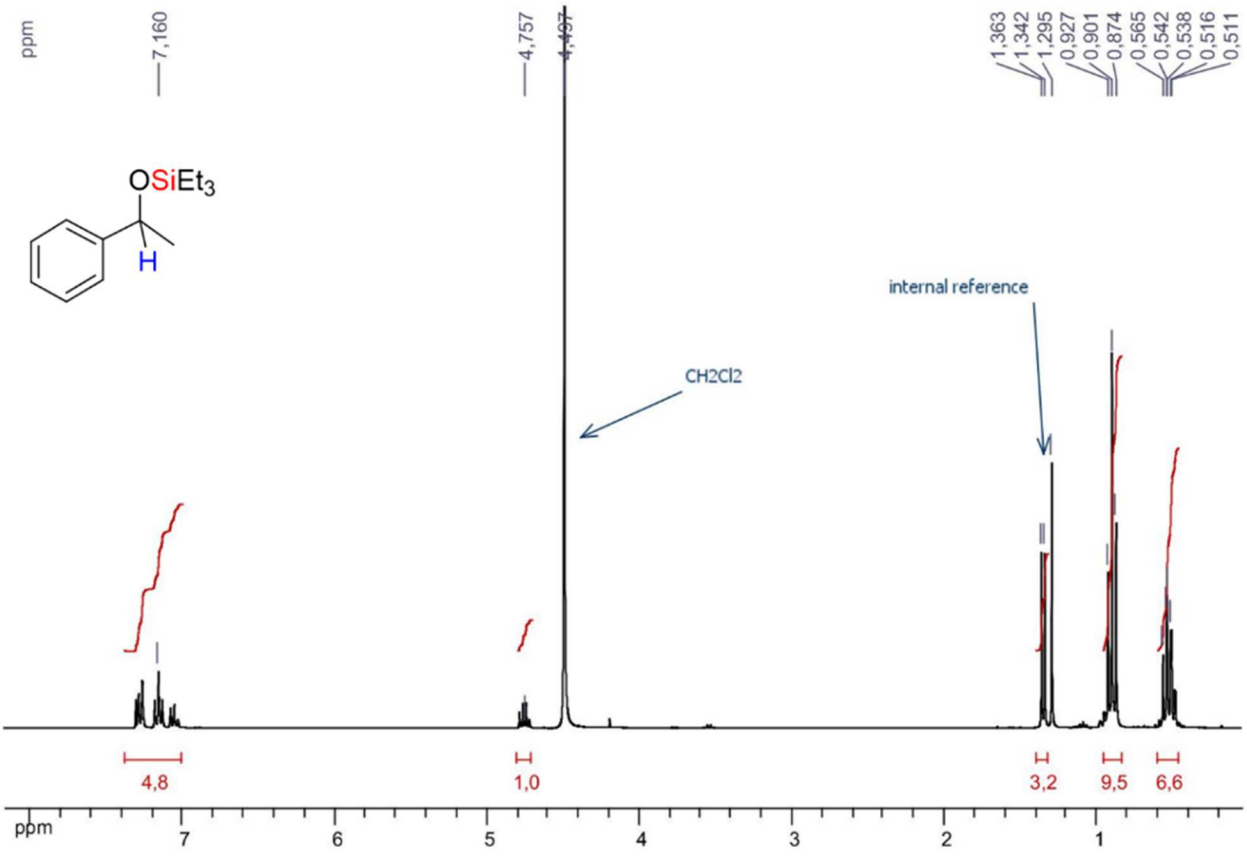
ppm
7,160
4,757
4,497
1,363
1,342
1,295
0,927
0,901
0,874
0,565
0,542
0,538
0,516
0,511
OSiEt3
H
internal reference
CH2Cl2
4,8
1,0
3,2
9,5
6,6
ppm
7
6
5
4
3
2
1

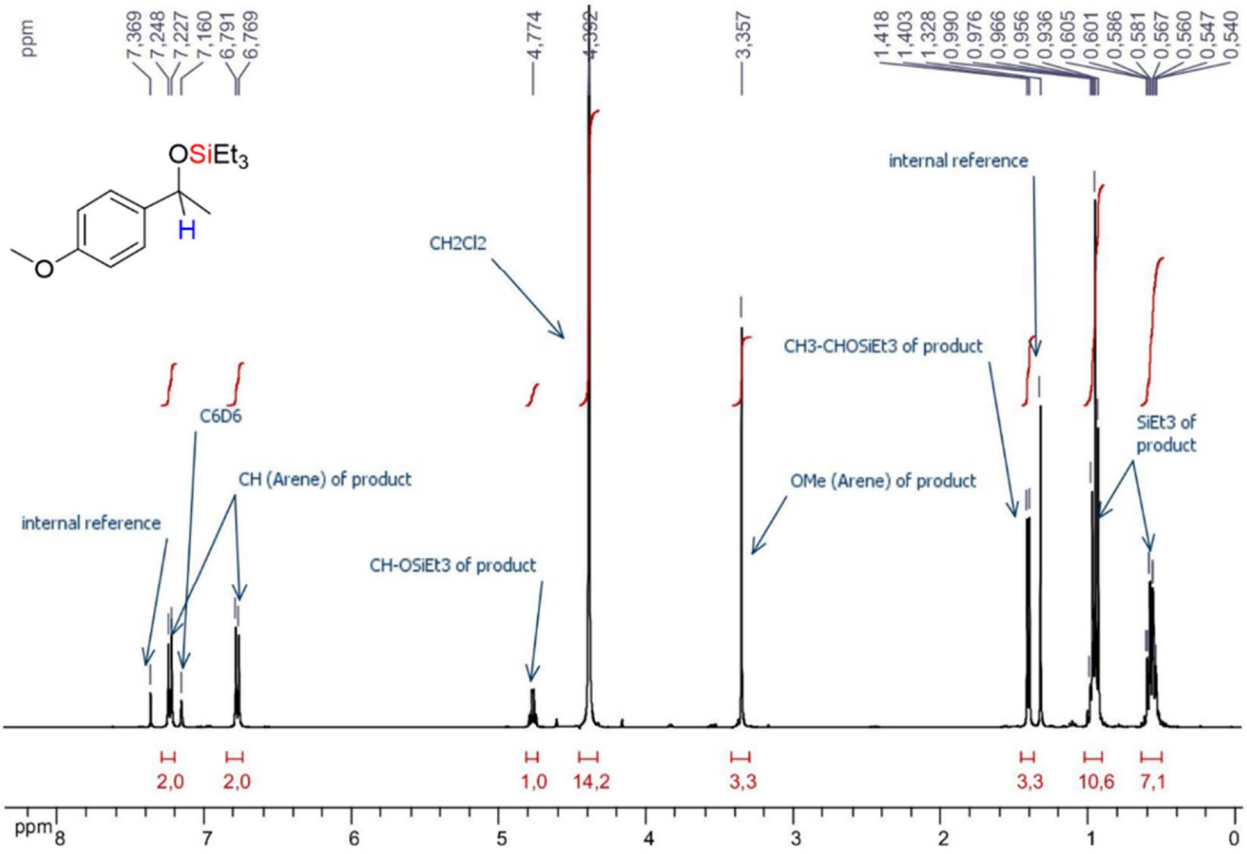
ppm
7,369
7,248
7,227
7,160
6,791
6,769
4,774
4,392
3,357
1,418
1,403
1,328
0,990
0,976
0,966
0,956
0,936
0,605
0,601
0,586
0,581
0,567
0,560
0,547
0,540
OSiEt3
H
O
internal reference
CH2Cl2
CH3-CHOSiEt3 of product
C6D6
CH (Arene) of product
OMe (Arene) of product
SiEt3 of product
internal reference
CH-OSiEt3 of product
2,0
2,0
1,0
14,2
3,3
3,3
10,6
7,1
ppm
8
7
6
5
4
3
2
1
0

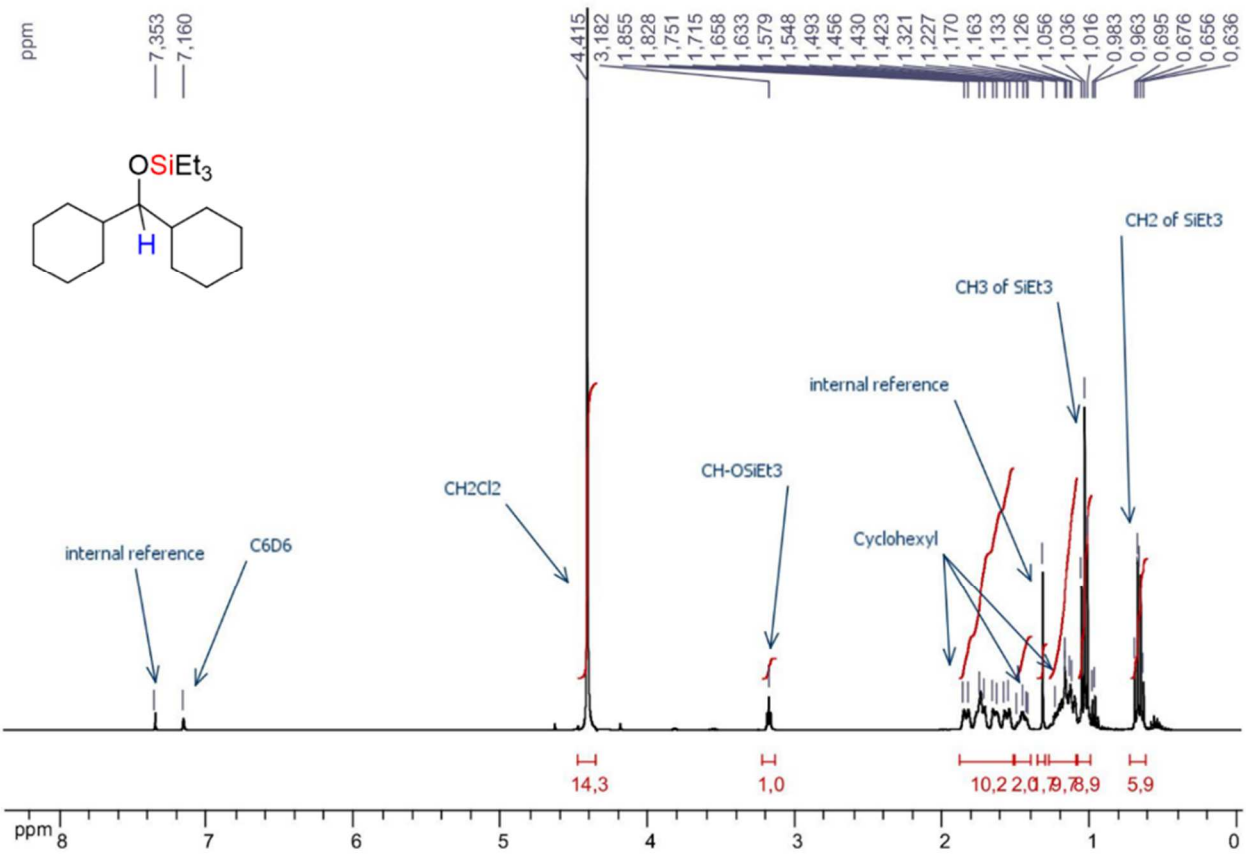
ppm
7,353
7,160
4,415
3,182
1,855
1,828
1,751
1,715
1,658
1,633
1,579
1,548
1,493
1,456
1,430
1,423
1,321
1,227
1,170
1,163
1,133
1,126
1,056
1,036
1,016
0,983
0,963
0,695
0,676
0,656
0,636
OSiEt3
H
CH2 of SiEt3
CH3 of SiEt3
internal reference
CH-OSiEt3
CH2Cl2
Cyclohexyl
internal reference
C6D6
14,3
1,0
5,9
ppm

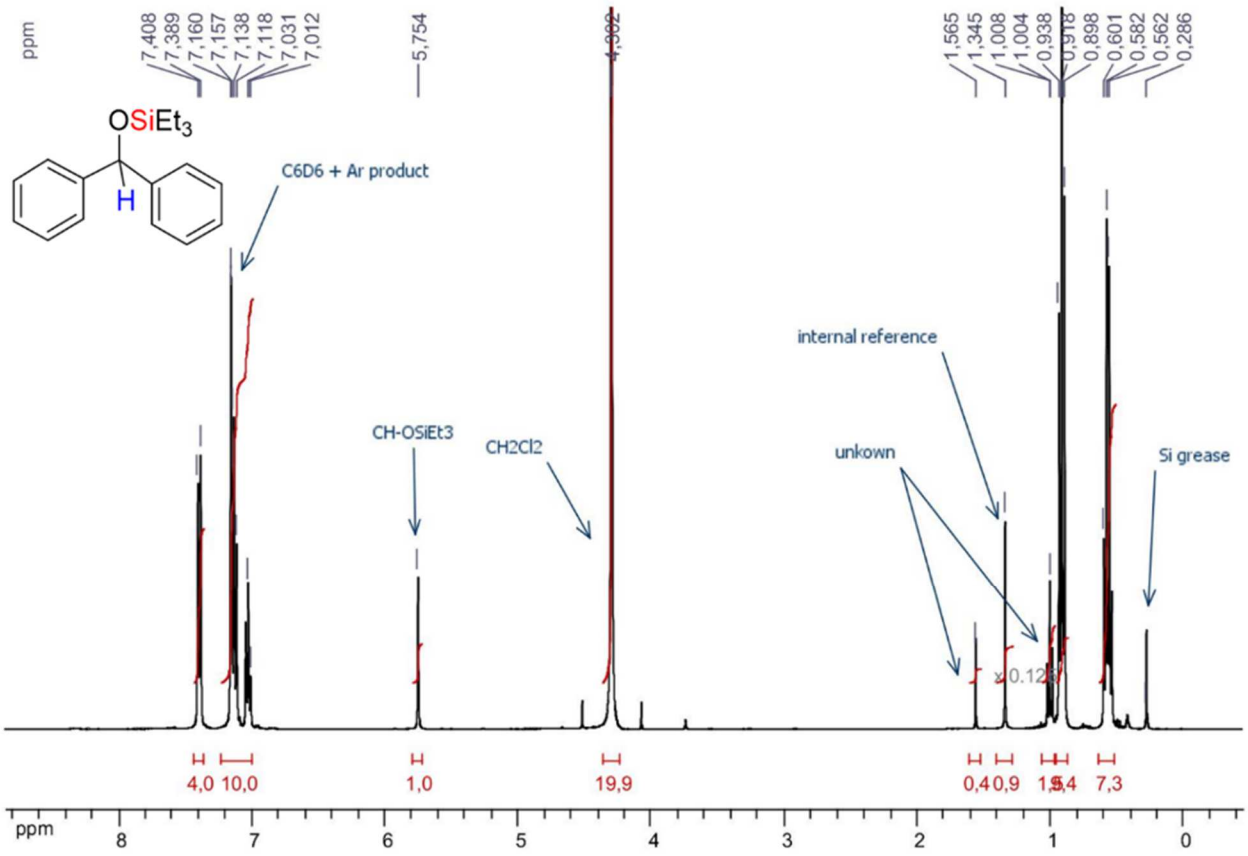
ppm
7,408
7,389
7,160
7,157
7,138
7,118
7,031
7,012
5,754
4,382
1,565
1,345
1,008
1,004
0,938
0,918
0,898
0,601
0,582
0,562
0,286
OSiEt3
H
C6D6 + Ar product
internal reference
CH-OSiEt3
CH2Cl2
unkown
Si grease
4,0
10,0
1,0
19,9
7,3
ppm

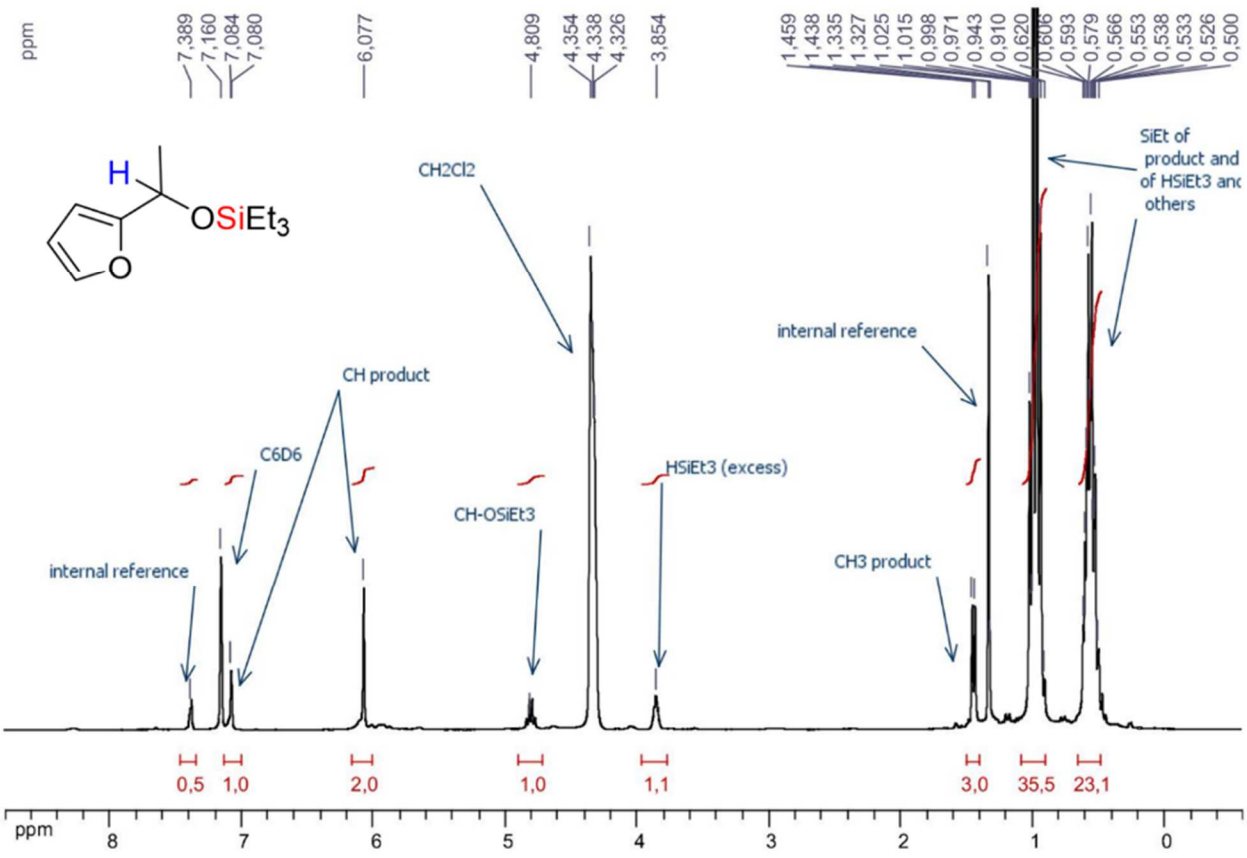
ppm
7,389
7,160
7,084
7,080
6,077
4,809
4,354
4,338
4,326
3,854
1,459
1,438
1,335
1,327
1,025
1,015
0,998
0,971
0,943
0,910
0,620
0,606
0,593
0,579
0,566
0,553
0,538
0,533
0,526
0,500
H
OSiEt3
O
CH2Cl2
SiEt of product and of HSiEt3 and others
internal reference
CH product
C6D6
HSiEt3 (excess)
CH-OSiEt3
internal reference
CH3 product
0,5
1,0
2,0
1,0
1,1
3,0
35,5
23,1
ppm
8
7
6
5
4
3
2
1
0

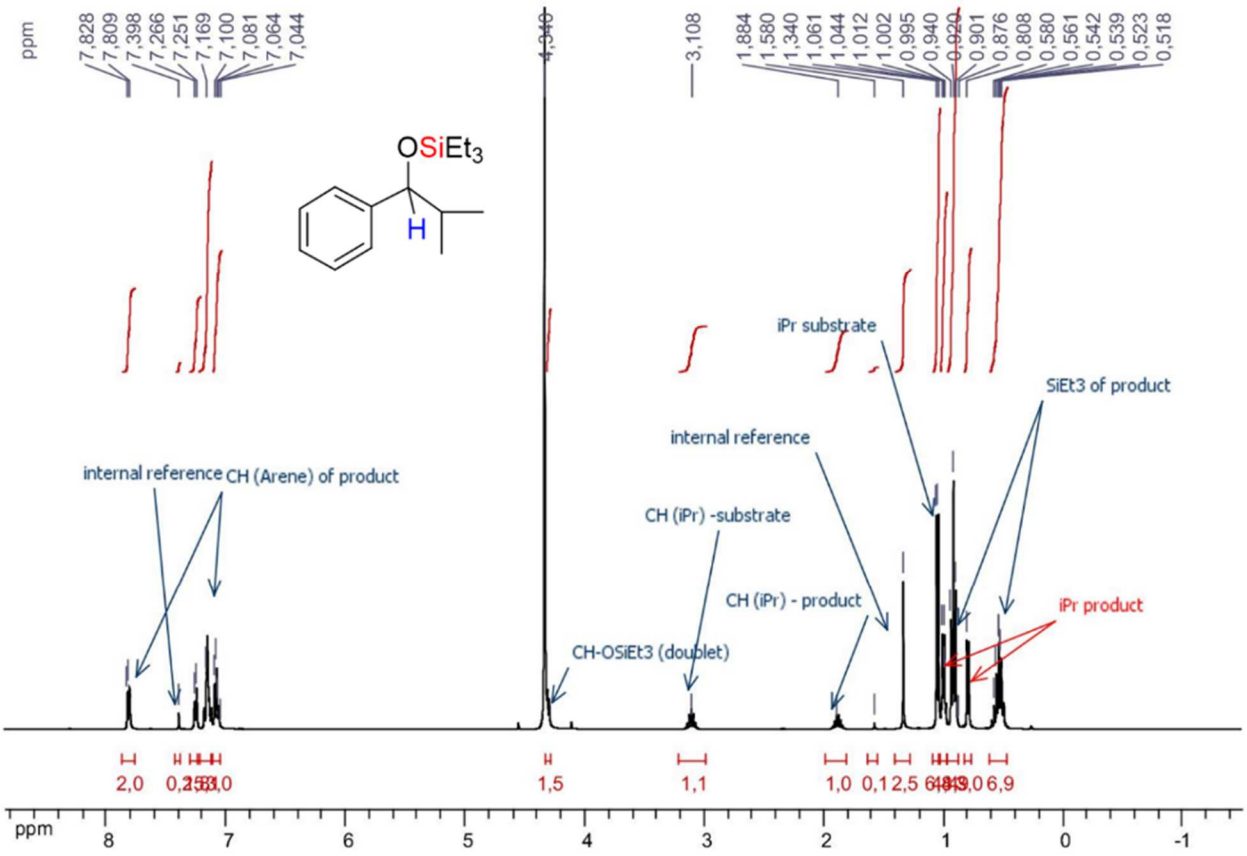
ppm
7,828
7,809
7,398
7,266
7,251
7,169
7,100
7,081
7,064
7,044
4,340
3,108
1,884
1,580
1,340
1,061
1,044
1,012
1,002
0,995
0,940
0,920
0,901
0,876
0,808
0,580
0,561
0,542
0,539
0,523
0,518
OSiEt3
H
iPr substrate
SiEt3 of product
internal reference
internal reference
CH (Arene) of product
CH (iPr) -substrate
CH (iPr) - product
iPr product
CH-OSiEt3 (doublet)
2,0
1,5
1,1
1,0
0,1
2,5
6,9
ppm
8
7
6
5
4
3
2
1
0
-1

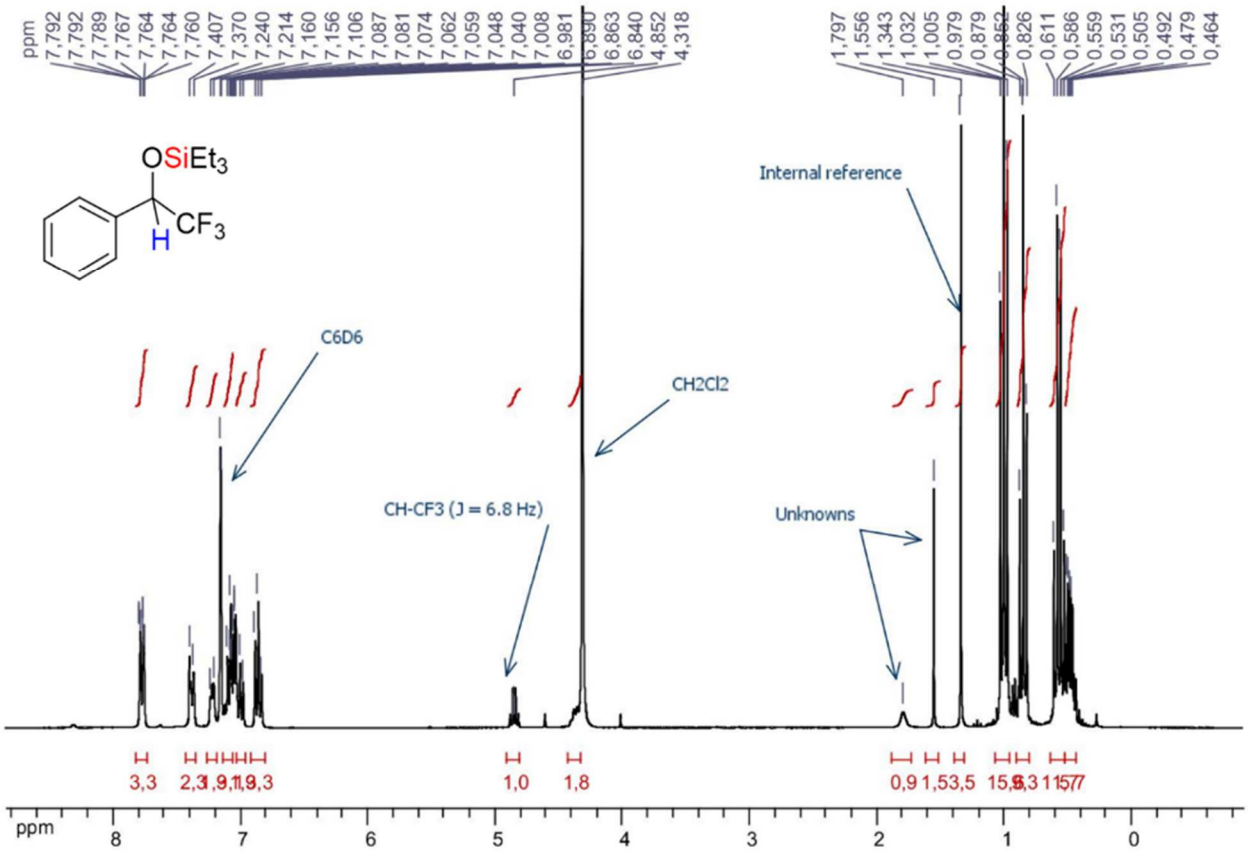
OSiEt3
CF3
H
Internal reference
C6D6
CH2Cl2
CH-CF3 (J = 6.8 Hz)
Unknowns
ppm

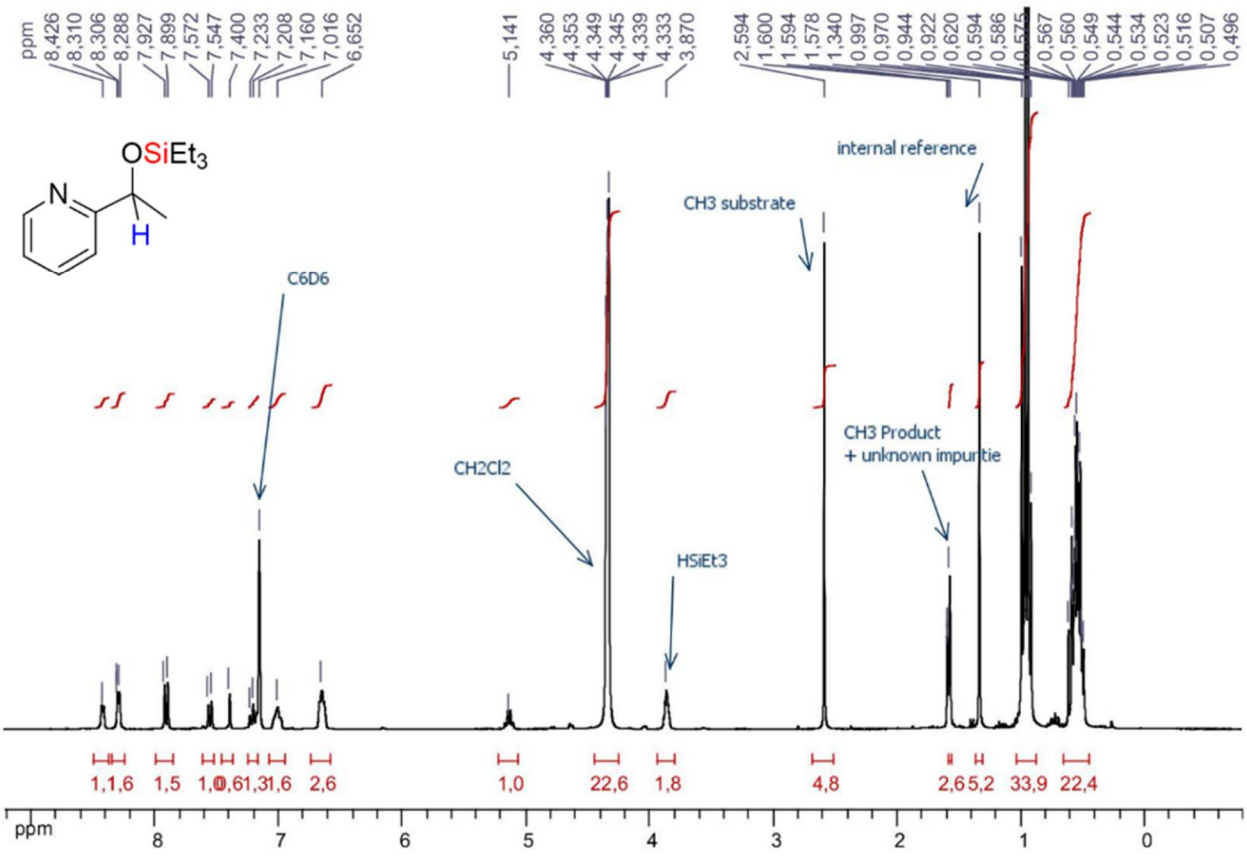
OSiEt3
N
H
internal reference
CH3 substrate
C6D6
CH2Cl2
CH3 Product
+ unknown impurtie
HSiEt3
ppm

6.3.4 Substrate scope study: aldehydes (table 13)

6.3.4.1 Experimental conditions

The following data detail the experimenl conditions used for the substrate scope study for which the results are reported in table 13. The general procedure for the hydrosilylation of carbonyls described above was used for every substrate. For each catalytic run, the molar quantity of the substrates and the precatalyst, the time and the temperature of the reaction are specified as follows:

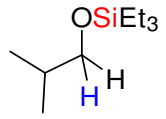

: Isobutyraldehyde (0.10 mL, 1.10 mmol), $HSiEt_3$ (0.38 mL, 2.40 mmol), [**4**][$BArF_{24}$] (7.7 mg, 5.48×10^{-3} mmol, 0.5 mol %), 0.5 mL of CH_2Cl_2, 30 min, rt.

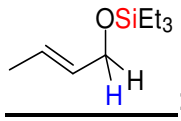

: But-2-enal (0.15 mL, 1.78 mmol), $HSiEt_3$ (0.31 mL, 1.96 mmol), [**4**][$BArF_{24}$] (2.5 mg, 1.77×10^{-3} mmol, 0.1 mol %), 0.4 mL of CH_2Cl_2, 30 min, rt.

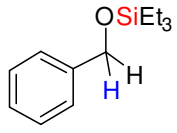

: Benzaldehyde (0.11 mL, 1.10 mmol), $HSiEt_3$ (0.19 mL, 1.20 mmol), [**4**][$BArF_{24}$] (7.7 mg, 5.48×10^{-3} mmol, 0.5 mol %), 0.5 mL of CH_2Cl_2, 30 min, rt.

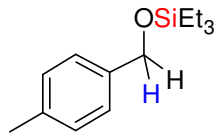

: 4-Methylbenzaldehyde (0.21 mL, 1.78 mmol), $HSiEt_3$ (0.31 mL, 1.96 mmol), [**4**][$BArF_{24}$] (2.5 mg, 1.77×10^{-3} mmol, 0.1 mol %), 0.4 mL of CH_2Cl_2, 30 min, rt.

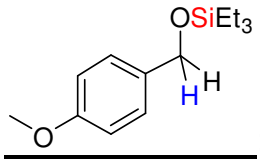

: 4-Methoxybenzaldehyde (0.22 mL, 1.78 mmol), $HSiEt_3$ (0.31 mL, 1.96 mmol), [**4**][$BArF_{24}$] (2.5 mg, 1.77×10^{-3} mmol, 0.1 mol %), 0.4 mL of CH_2Cl_2, 30 min, rt.

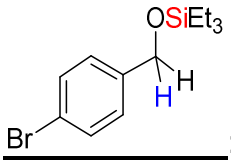

: 4-Bromobenzaldehyde (0.22 g, 1.10 mmol), $HSiEt_3$ (0.38 mL, 2.40 mmol), [**4**][$BArF_{24}$] (7.7 mg, 5.48×10^{-3} mmol, 0.5 mol %), 0.5 mL of CH_2Cl_2, 30 min, rt.

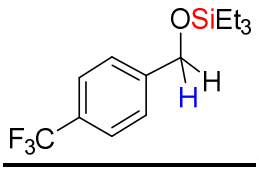

: 4-Trifluoromehylbenzaldehyde (0.15 mL, 1.10 mmol), $HSiEt_3$ (0.19 mL, 1.20 mmol), [**4**][$BArF_{24}$] (7.7 mg, 5.48×10^{-3} mmol, 0.5 mol %), 0.5 mL of CH_2Cl_2, 18 h, rt.

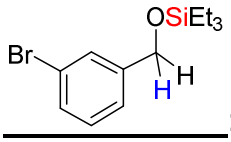

: 3-Bromobenzaldehyde (0.13 mL, 1.10 mmol), $HSiEt_3$ (0.38 mL, 2.41 mmol), [**4**][$BArF_{24}$] (7.7 mg, 5.48×10^{-3} mmol, 0.5 mol %), 0.5 mL of CH_2Cl_2, 2 h, rt.

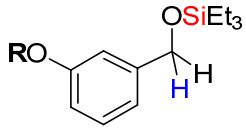

R = H: 17%

R = SiEt$_3$: 83%: 3-Hydroxybenzaldehyde (0.134 g, 1.10 mmol), $HSiEt_3$ (0.38 mL, 2.41 mmol), [**4**][$BArF_{24}$] (7.7 mg, 5.48×10^{-3} mmol, 0.5 mol %), 0.5 mL of CH_2Cl_2, 30 min, rt.

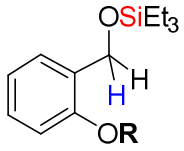

R = H: 39%

R = SiEt$_3$: 61%: 2-Hydroxybenzaldehyde (0.12 mL, 1.10 mmol), $HSiEt_3$ (0.38 mL, 2.41 mmol), [**4**][$BArF_{24}$] (7.7 mg, 5.48×10^{-3} mmol, 0.5 mol %), 0.5 mL of CH_2Cl_2, 30 min, rt.

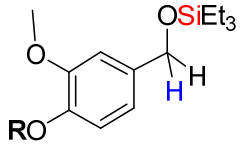

R = H: 75%

R = SiEt$_3$: 25%: 4-Hydroxy-3-methoxybenzaldehyde (0.166 g, 1.10 mmol), $HSiEt_3$ (0.38 mL, 2.41 mmol), [**4**][$BArF_{24}$] (7.7 mg, 5.48×10^{-3} mmol, 0.5 mol %), 0.5 mL of CH_2Cl_2, 30 min, rt.

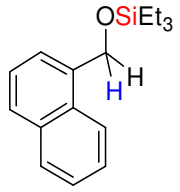

: 1-Naphthaldehyde (0.15 mL, 1.10 mmol), $HSiEt_3$ (0.38 mL, 2.41 mmol), [**4**][$BArF_{24}$] (7.7 mg, 5.48×10^{-3} mmol, 0.5 mol %), 0.5 mL of CH_2Cl_2, 30 min, rt.

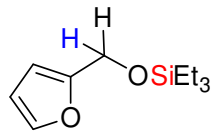

: Furan-2-carbaldehyde (0. 11 mL, 1.33 mmol), $HSiEt_3$ (0.38 mL, 2.41 mmol), [**4**][$BArF_{24}$] (7.7 mg, 5.48×10^{-3} mmol, 0.4 mol %), 0.5 mL of CH_2Cl_2, 2 h, rt.

6.3.4.2 NMR data of the products

The structural identity of each silyl ether which is produced during the substrate scope study has been confirmed by ^{1}H NMR analysis. For the products that have been already reported in the literature along with their characterization data, all our ^{1}H NMR data matched those reported (table S6). However, the products for which the NMR spectroscopic data are not published yet, their characteristic ^{1}H NMR chemical shifts (δ, ppm) are provided in table S6. The ^{1}H NMR spectra for all the products are also given in the next section.

Table S6. Hydrosilylation of aldehydes: NMR spectroscopic data of the products.

Aldehyde + $HSiEt_3$ 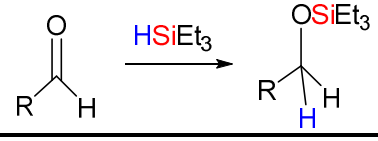	**Our NMR data or related literature references**
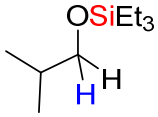	Du, G.; Abu-Omar, M. M. Catalytic Hydrosilylation of Carbonyl Compounds with Cationic Oxorhenium(V) Salen. *Organometallics* **2006**, *25* (20), 4920–4923
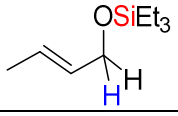	Do, Y.; Han, J.; Rhee, Y. H.; Park, J. Highly Efficient and Chemoselective Ruthenium-Catalyzed Hydrosilylation of Aldehydes. *Adv. Synth. Catal.* **2011**, *353* (18), 3363–3366.
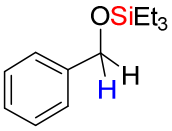	Frainnet, E.; Bourhis, R.; Simonin, F.; Moulines, F. Action de Trialkylsilanes Sur Des Aldehydes Aromatiques En Présence de Catalyseurs Au Nickel. *J. Organomet. Chem.* **1976**, *105* (1), 17–31.
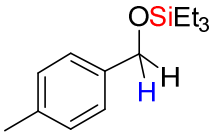	Frainnet, E.; Bourhis, R.; Simonin, F.; Moulines, F. Action de Trialkylsilanes Sur Des Aldehydes Aromatiques En Présence de Catalyseurs Au Nickel. *J. Organomet. Chem.* **1976**, *105* (1), 17–31.
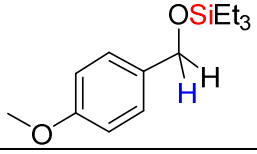	Teci, M.; Lentz, N.; Brenner, E.; Matt, D.; Toupet, L. Alkylfluorenyl Substituted N-Heterocyclic Carbenes in Copper(I) Catalysed Hydrosilylation of Aldehydes and Ketones. *Dalt. Trans.* **2015**, *44* (31), 13991–13998.
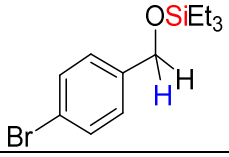	Gevorgyan, V.; Rubin, M.; Liu, J. X.; Yamamoto, Y. A Direct Reduction of Aliphatic Aldehyde, Acyl Chloride, Ester, and Carboxylic Functions into a Methyl Group. *J. Org. Chem.* **2001**, *66* (5), 1672–1675.
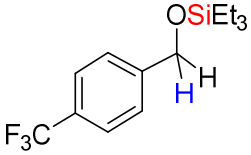	Teci, M.; Lentz, N.; Brenner, E.; Matt, D.; Toupet, L. Alkylfluorenyl Substituted N-Heterocyclic Carbenes in Copper(I) Catalysed Hydrosilylation of Aldehydes and Ketones. *Dalt. Trans.* **2015**, *44* (31), 13991–13998.
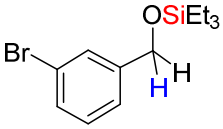	Teci, M.; Lentz, N.; Brenner, E.; Matt, D.; Toupet, L. Alkylfluorenyl Substituted N-Heterocyclic Carbenes in Copper(I) Catalysed Hydrosilylation of Aldehydes and Ketones. *Dalt. Trans.* **2015**, *44* (31), 13991–13998.
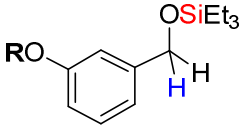 **R = H**: 17% **R = $SiEt_3$**: 83%	• **R = H** (17%): ^1H (C_6D_6, 298 K, 400 MHz), δ = 7.04 (t, 1H, J = 8.0 Hz), 6.86 (d, 1H, J = 8.0 Hz), 6.76 (s, 1H), 6.45 (d, 1H, J = 8.0 Hz), 4.58 (s, 2H), 0.97 (t, 9H, overlapping signals), 0.58–0.64 (q, 6H, overlapping signals). • **R = $SiEt_3$** (83%): ^1H (C_6D_6, 298 K, 400 MHz), δ = 7.14 (s 1H), 7.11 (t, 1H, J = 8.0 Hz), 6.93 (d, 1H, J = 8.0 Hz), 6.82 (d, 1H, J = 8.0 Hz), 4.63 (s, 2H), 1.00 (t, 9H, J = 8.1 Hz), 0.99 (t, 9H, J = 8.1 Hz), 0.72 (q, 6H, J = 8.1 Hz), 0.61 (d, 6H, J = 8.1 Hz).
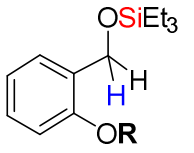 **R = H**: 39% **R = $SiEt_3$**: 61%	• **R = H** (39%): ^1H (C_6D_6, 298 K, 400 MHz), δ = 7.98 (s, 1H), 6.98–7.08 (m, 2H, overlapping signals), 6.78–7.80 (m, 1H, overlapping signals), 6.74 (t, 1H, J = 7.5 Hz), 4.64 (s, 2H, $ArCH_2OSiEt_3$), 0.86 (t, 9H, J = 8.1 Hz), 0.46 (q, 6H, J = 8.1 Hz). • **R = $SiEt_3$** (61%): ^1H (C_6D_6, 298 K, 400 MHz), δ = 7.77 (d 1H, J = 7.6 Hz), 6.78–7.80 (m, 2H, overlapping signals), 6.79 (d, 1H, J = 7.7 Hz), 5.00 (s, 2H, $ArCH_2OSiEt_3$), 1.04 (t, 9H, J = 8.1 Hz), 0.98 (t, 9H, J = 8.1 Hz), 0.68 (q, 12H, J = 8.1 Hz).

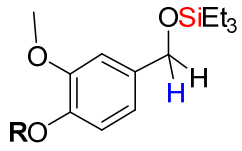 **R = H**: 75% **R = SiEt$_3$**: 25%	• **R = H** (75%): ^{1}H (C_6D_6, 298 K, 400 MHz), δ = 6.96 (d, 2H, J = 8.0 Hz), 6.76 (d, 1H, J = 8.0 Hz), 5.42 (s, 1H, OH), 4.58 (s, 2H, $ArCH_2OSiEt_3$), 3.27 (s, 3H, OMe), 0.91–1.05 (m, 9H, CH_3-CH_2 overlapping signals of $HSiEt_3$ and $OSiEt_3$), 0.75 (q, 6H, J = 7.6 Hz), 0.62 (q, 6H, J = 8.0 Hz). • **R = SiEt$_3$** (25%): ^{1}H (C_6D_6, 298 K, 400 MHz), δ = 6.88–6.90 (m, 2H, overlapping signals), 6.82 (m, 1H, overlapping signals), 4.62 (s, 2H, $ArCH_2OSiEt_3$), 3.44 (s, 3H, OMe), 0.91–1.05 (m, 18H, CH_3-CH_2 overlapping signals of $HSiEt_3$ and $OSiEt_3$), 0.75 (q, 6H, J = 7.6 Hz), 0.50–0.58 (q, 6H, J = 7.6 Hz, overlap with CH_3-CH_2 signals of $HSiEt_3$).
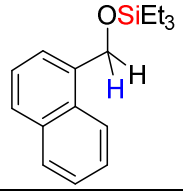	Bajracharya, G. B.; Nogami, T.; Jin, T.; Matsuda, K.; Gevorgyan, V.; Yamamoto, Y. Reduction of Carbonyl Function to a Methyl Group. *Synthesis* **2004**, *2004* (2), 308–311.
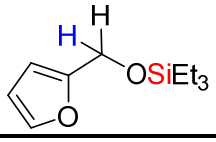	Frainnet, E.; Bourhis, R.; Simonin, F.; Moulines, F. Action de Trialkylsilanes Sur Des Aldehydes Aromatiques En Présence de Catalyseurs Au Nickel. *J. Organomet. Chem.* **1976**, *105* (1), 17–31.

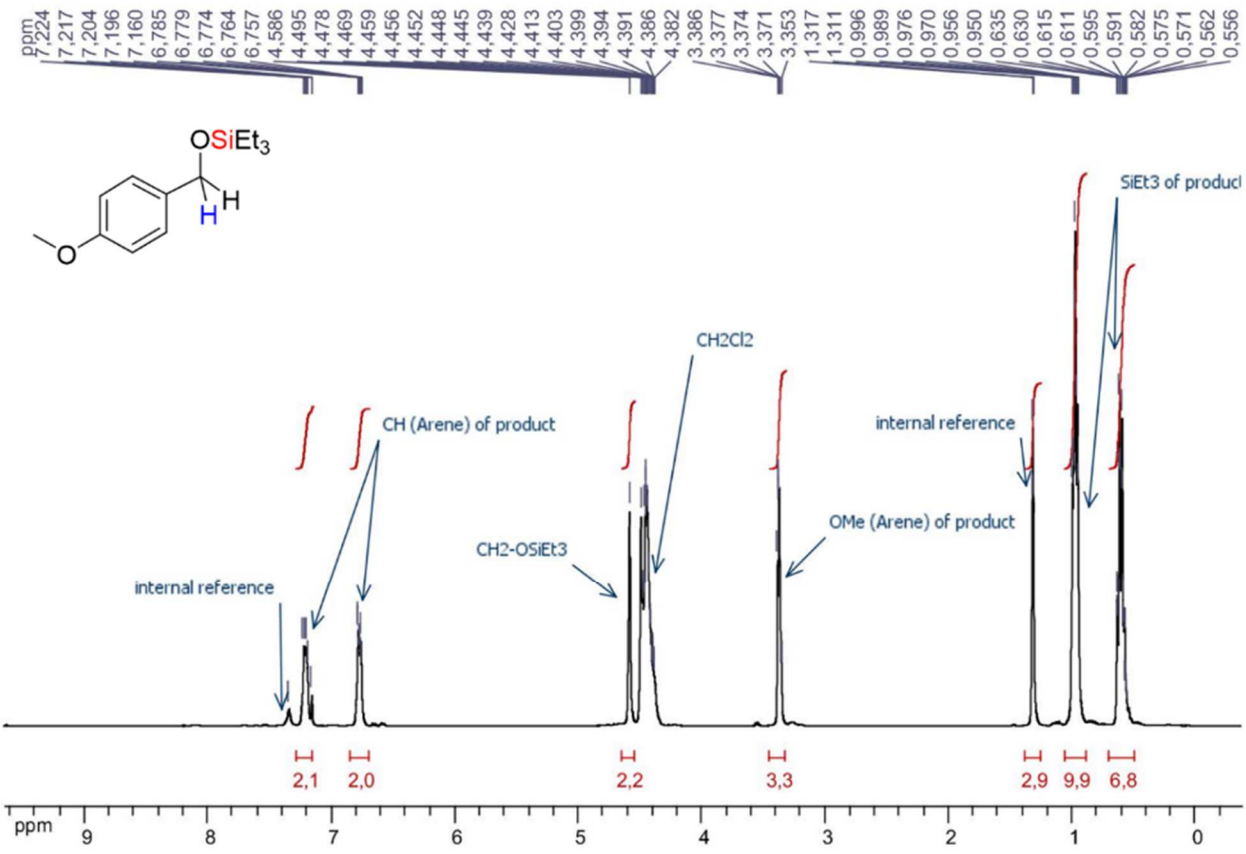
ppm
7,224
7,217
7,204
7,196
7,160
6,785
6,779
6,774
6,764
6,757
4,586
4,495
4,478
4,469
4,459
4,456
4,452
4,448
4,445
4,439
4,428
4,413
4,403
4,399
4,394
4,391
4,386
4,382
3,386
3,377
3,374
3,371
3,353
1,317
1,311
0,996
0,989
0,976
0,970
0,956
0,950
0,635
0,630
0,615
0,611
0,595
0,591
0,582
0,575
0,571
0,562
0,556
OSiEt3
H
H
O
SiEt3 of product
CH2Cl2
CH (Arene) of product
internal reference
OMe (Arene) of product
CH2-OSiEt3
internal reference
2,1
2,0
2,2
3,3
2,9
9,9
6,8
ppm
9
8
7
6
5
4
3
2
1
0

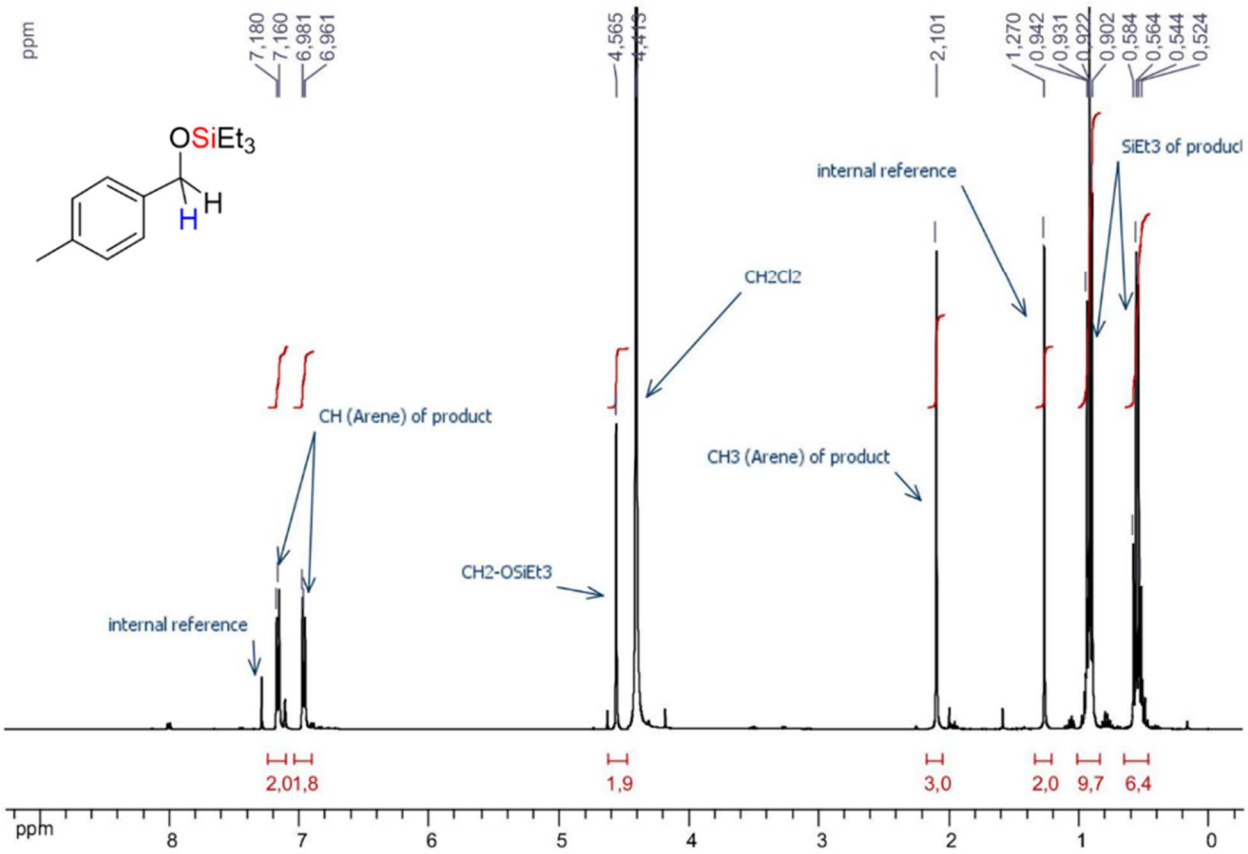
ppm
7,180
7,160
6,981
6,961
4,565
4,413
2,101
1,270
0,942
0,931
0,922
0,902
0,584
0,564
0,544
0,524
OSiEt3
H
H
SiEt3 of product
internal reference
CH2Cl2
CH (Arene) of product
CH3 (Arene) of product
CH2-OSiEt3
internal reference
2,01,8
1,9
3,0
2,0
9,7
6,4
ppm
8
7
6
5
4
3
2
1
0

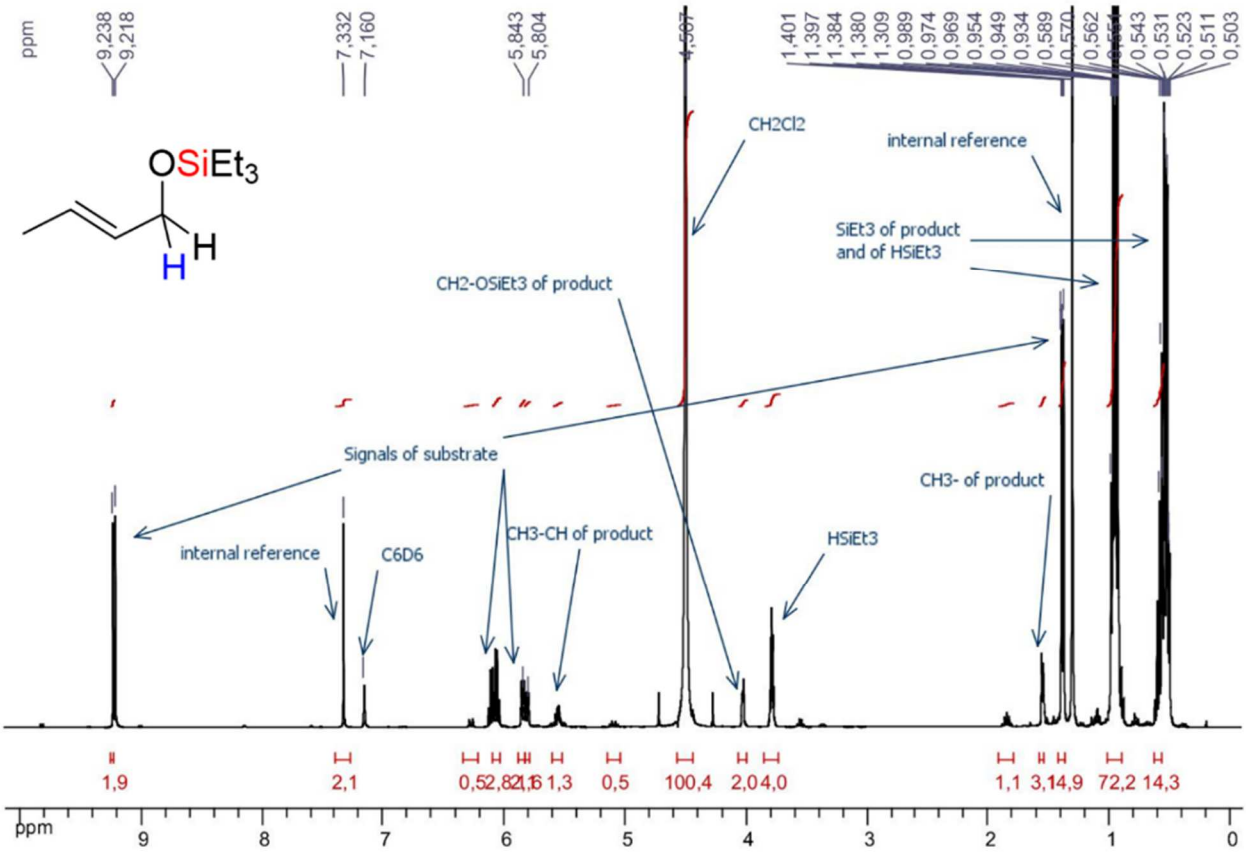
OSiEt3
H
H
CH2Cl2
internal reference
SiEt3 of product
and of HSiEt3
CH2-OSiEt3 of product
Signals of substrate
internal reference
C6D6
CH3-CH of product
HSiEt3
CH3- of product
ppm

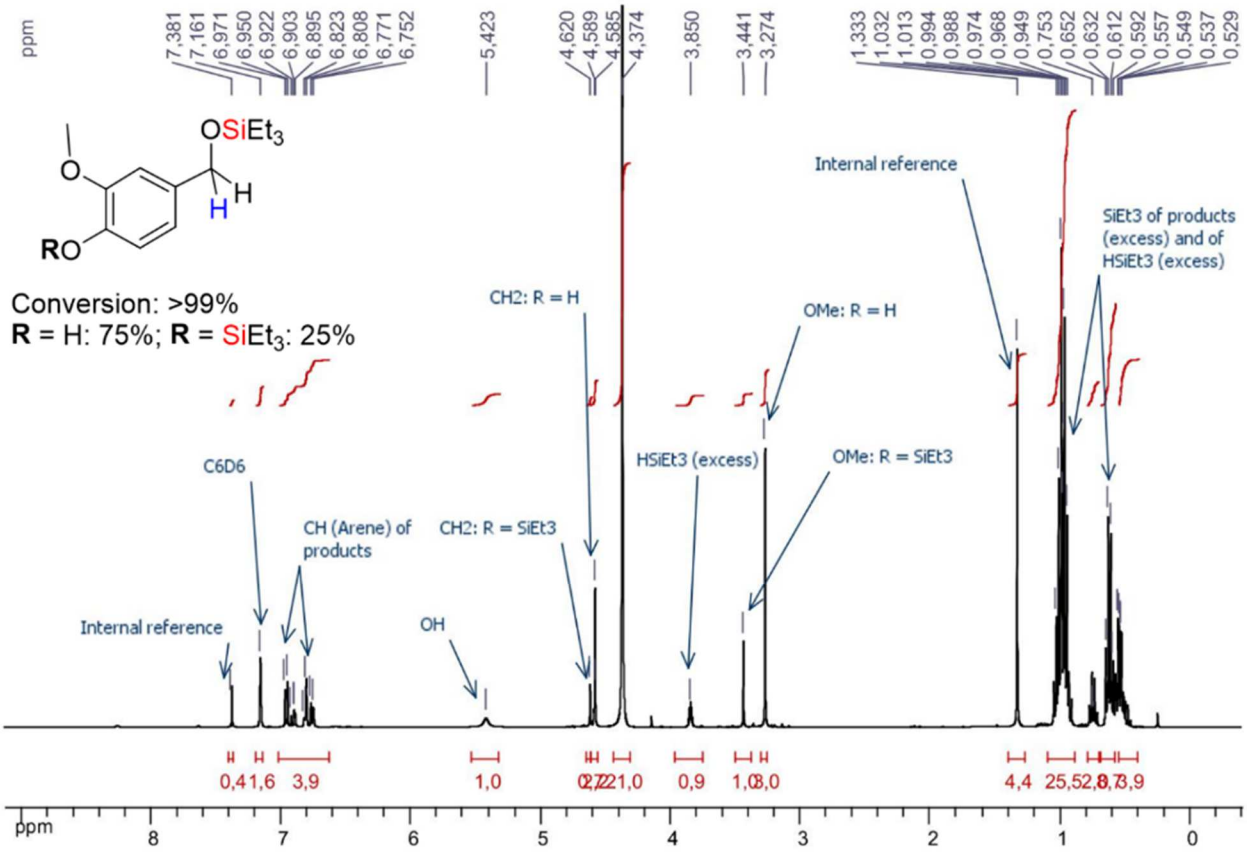
OSiEt3
O
RO
H
Conversion: >99%
R = H: 75%; R = SiEt3: 25%
Internal reference
SiEt3 of products
(excess) and of
HSiEt3 (excess)
CH2: R = H
OMe: R = H
C6D6
HSiEt3 (excess)
OMe: R = SiEt3
CH (Arene) of
products
CH2: R = SiEt3
Internal reference
OH
ppm

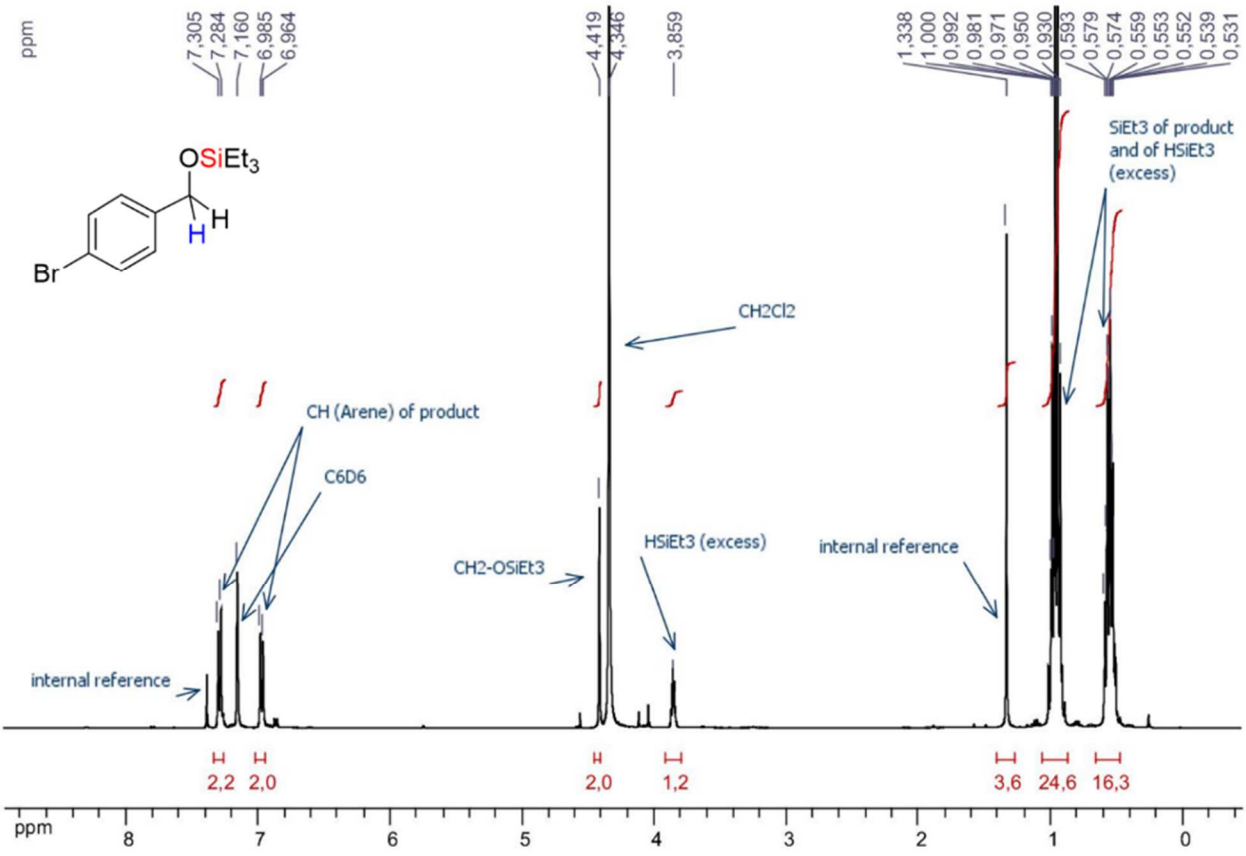
ppm
7,305
7,284
7,160
6,985
6,964
4,419
4,346
3,859
1,338
1,000
0,992
0,981
0,971
0,950
0,930
0,593
0,579
0,574
0,559
0,553
0,552
0,539
0,531
OSiEt3
H
Br
SiEt3 of product and of HSiEt3 (excess)
CH2Cl2
CH (Arene) of product
C6D6
CH2-OSiEt3
HSiEt3 (excess)
internal reference
internal reference
2,2 2,0
2,0 1,2
3,6 24,6 16,3
ppm
8 7 6 5 4 3 2 1 0

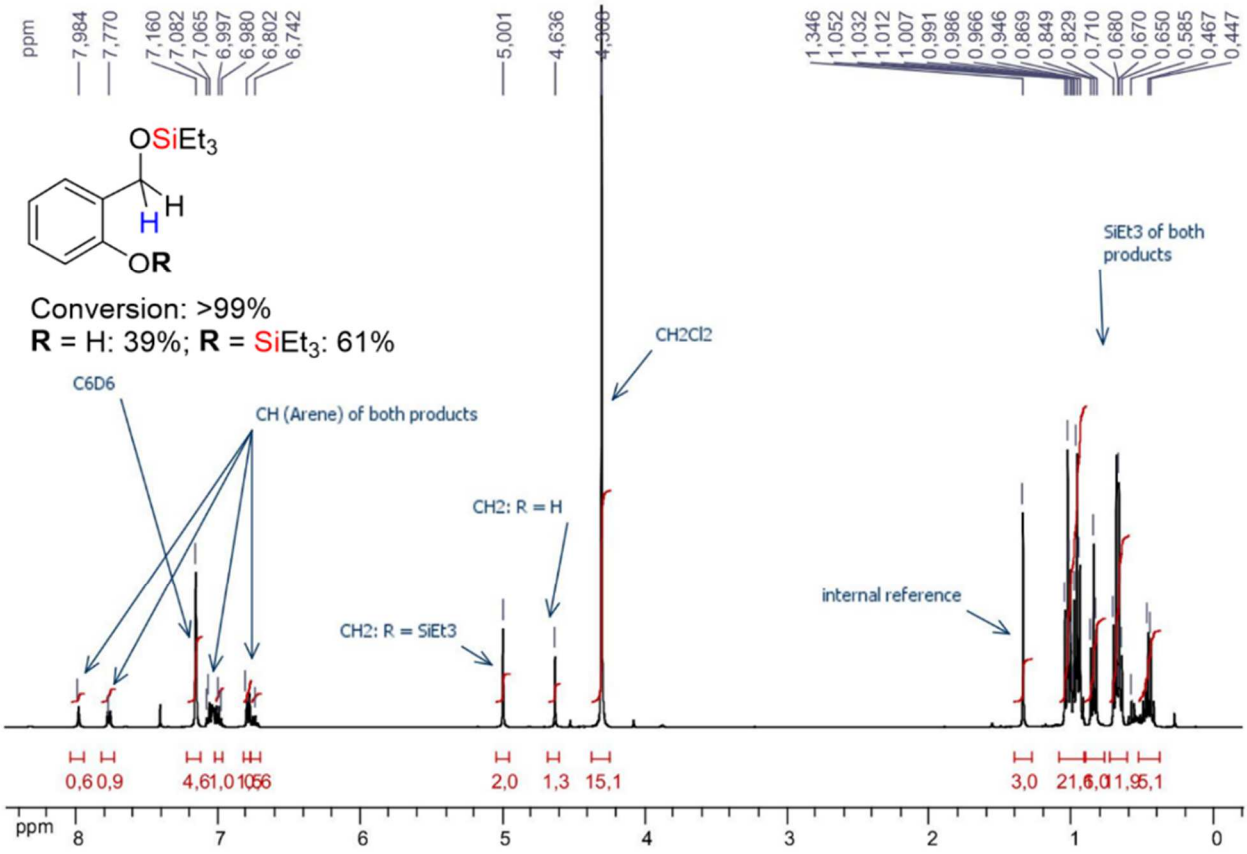
ppm
7,984
7,770
7,160
7,082
7,065
6,997
6,980
6,802
6,742
5,001
4,636
4,366
1,346
1,052
1,032
1,012
1,007
0,991
0,986
0,966
0,946
0,869
0,849
0,829
0,710
0,680
0,670
0,650
0,585
0,467
0,447
OSiEt3
H
OR
Conversion: >99%
R = H: 39%; R = SiEt3: 61%
SiEt3 of both products
CH2Cl2
C6D6
CH (Arene) of both products
CH2: R = H
CH2: R = SiEt3
internal reference
0,6 0,9
4,6 1,0 1,6
2,0 1,3 15,1
3,0 21,6 1,9 5,1
ppm
8 7 6 5 4 3 2 1 0

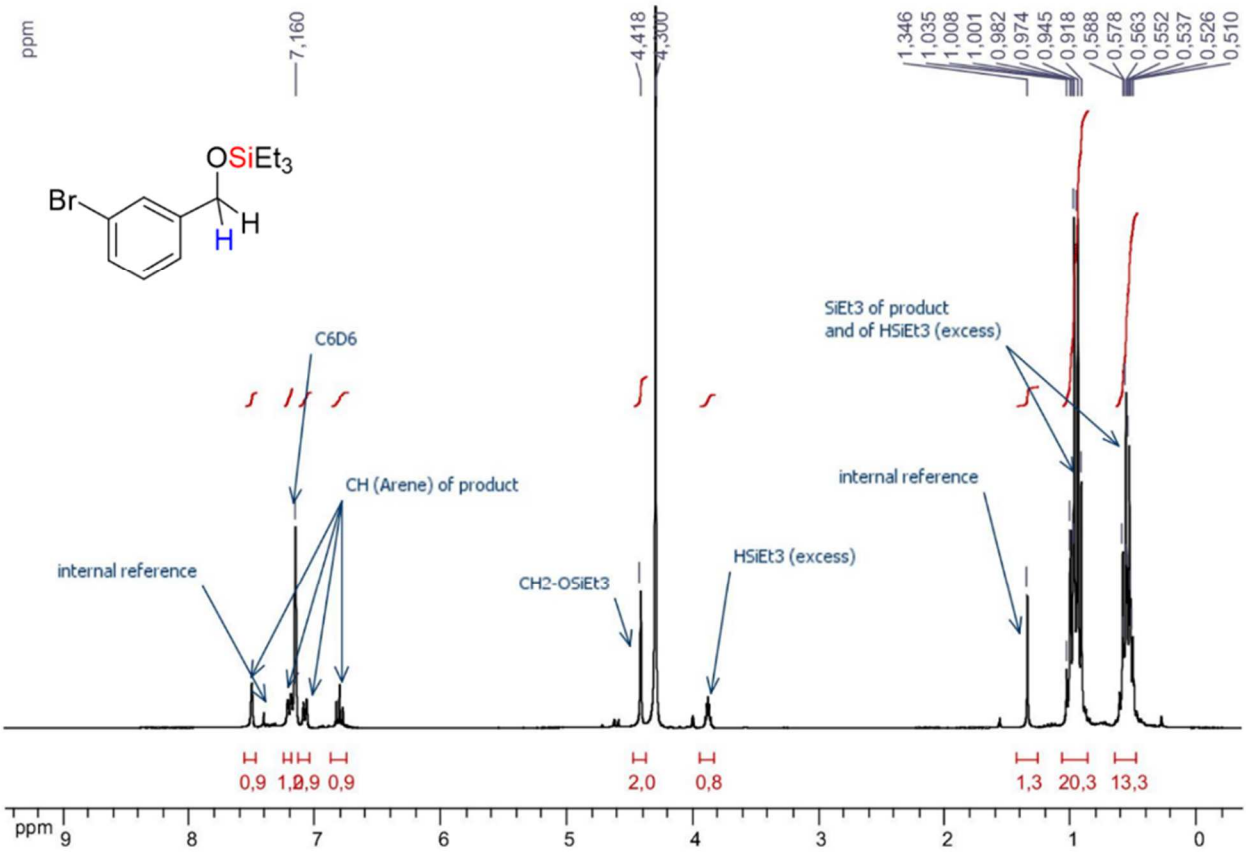
ppm
7,160
4,418
4,300
1,346
1,035
1,008
1,001
0,982
0,974
0,945
0,918
0,588
0,578
0,563
0,552
0,537
0,526
0,510
OSiEt3
Br
H
H
C6D6
CH (Arene) of product
internal reference
CH2-OSiEt3
HSiEt3 (excess)
SiEt3 of product
and of HSiEt3 (excess)
internal reference
0,9
1,2
0,9
0,9
2,0
0,8
1,3
20,3
13,3
ppm
9
8
7
6
5
4
3
2
1
0

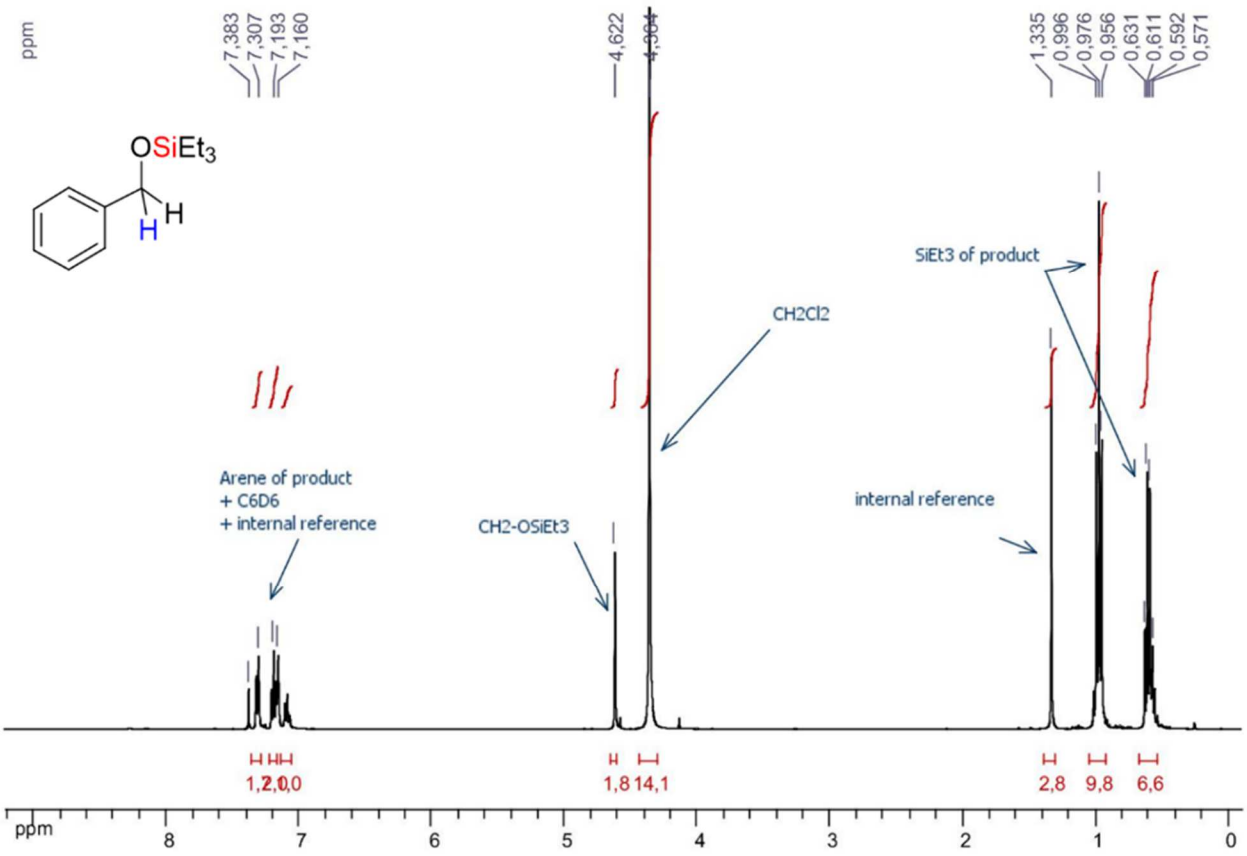
ppm
7,383
7,307
7,193
7,160
4,622
4,304
1,335
0,996
0,976
0,956
0,631
0,611
0,592
0,571
OSiEt3
H
H
SiEt3 of product
CH2Cl2
Arene of product
+ C6D6
+ internal reference
CH2-OSiEt3
internal reference
1,8
14,1
2,8
9,8
6,6
ppm
8
7
6
5
4
3
2
1
0

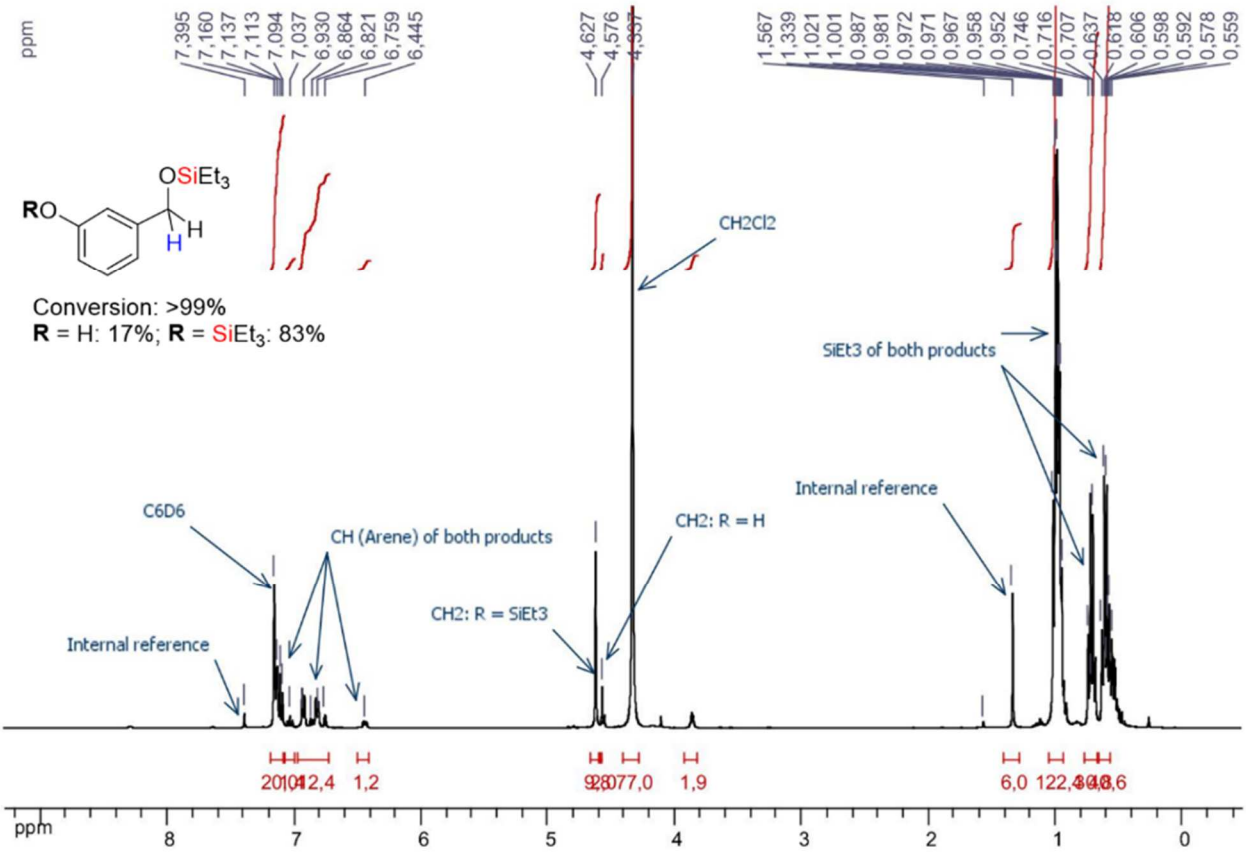
ppm
7,395
7,160
7,137
7,113
7,094
7,037
6,930
6,864
6,821
6,759
6,445
4,627
4,576
4,337
1,567
1,339
1,021
1,001
0,987
0,981
0,972
0,971
0,967
0,958
0,952
0,746
0,716
0,707
0,637
0,618
0,606
0,598
0,592
0,578
0,559
OSiEt3
RO
H
H
Conversion: >99%
R = H: 17%; R = SiEt3: 83%
CH2Cl2
SiEt3 of both products
Internal reference
C6D6
CH (Arene) of both products
CH2: R = H
CH2: R = SiEt3
Internal reference
2,0
1,2
1,9
6,0
ppm
8
7
6
5
4
3
2
1
0

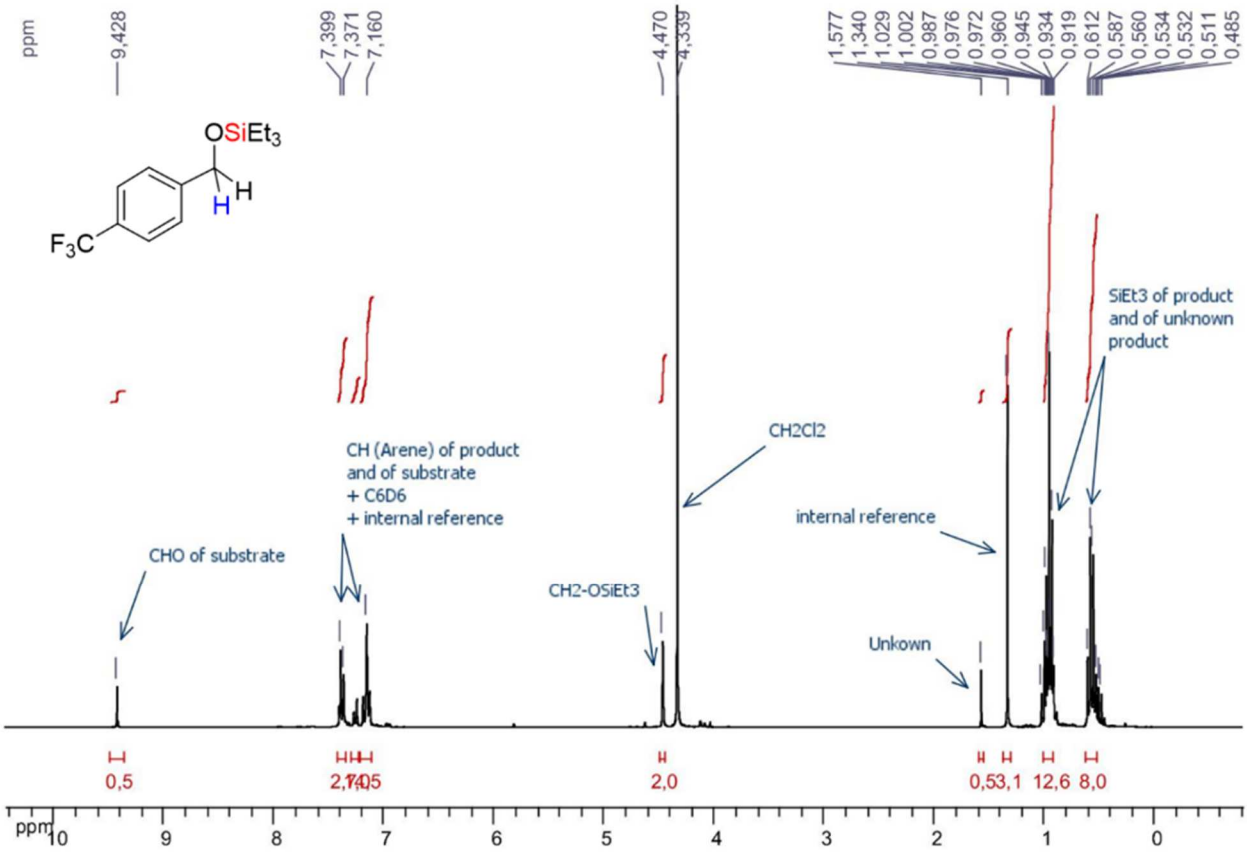
ppm
9,428
7,399
7,371
7,160
4,470
4,339
1,577
1,340
1,029
1,002
0,987
0,976
0,972
0,960
0,945
0,934
0,919
0,612
0,587
0,560
0,534
0,532
0,511
0,485
OSiEt3
H
F3C
SiEt3 of product
and of unknown
product
CH2Cl2
CH (Arene) of product
and of substrate
+ C6D6
+ internal reference
internal reference
CHO of substrate
CH2-OSiEt3
Unkown
0,5
2,0
0,5
3,1
12,6
8,0
ppm
10
9
8
7
6
5
4
3
2
1
0

6.4 Experiments related to Chapter 3: Hydrosilylation of nitriles

6.4.1 General procedure

Unless otherwise specified, to a mixture of silane (1.1–2.2 equiv.) and nitrile (1.92 mmol, 1.0 equiv.) substrates was added a solution of the precatalyst in CH_2Cl_2 (0.5 mL). The reaction was allowed to take place upon heating at a given temperature for a given time, after which tri-*tert*-butylbenzene was added as internal NMR standard. An aliquot from this solution was taken and mixed with C_6D_6 for NMR analysis. For screening studies, we decided to only focus in studying the influence of silanes on catalysis, and have chosen to use [**4**][$BArF_{24}$] as precatalyst because of its better catalytic performance observed in the hydrosilylation of carbonyls, and *O*Si of alcohols.

6.4.2 Comparison of silanes

The influence of the nature of silane on catalysis was studied. For this purpose, only primary and tertiary silanes were screened. All the reactions were conducted at 80 °C for 24 hours following the general procedure: benzonitrile (0.2 mL, 1.94 mmol), silane (4.27 mmol), [**4**][$BArF_{24}$] (27.3 mg, 1.94×10^{-2} mmol, 1 mol %), CH_2Cl_2 (0.5 mL). The results are summarized in table S7.

This study clearly shows that triethylsilane ($HSiEt_3$, entry 1) is the best silane when compared to other tested silanes (entries 2–4). As a consequence, $HSiEt_3$ was used for next studies dealing with hydrosilylation of nitriles.

Tableau S7. Optimization of silanes for the hydrosilylation of benzonitrile. PMHS stands for polymethylhydrosiloxane.

Entry	Silane	Yield (%)
1	$HSiEt_3$	>99
2	$HSiPh_3$	11
3	$HSiPhH_2$	<1
4	PMHS	<1

6.4.3 Comparison of precatalysts: effet of the counter-anion

The influence on catalysis of the counter-anion brought by the precatalyst was studied. For the hydrosilylation of carbonyls, there was a tremendous effect of the counter-anion on catalysis. We aimed at verifying if such effect could be observed for the hydrosilylation of nitriles as well. For this purpose, [**4**][BPh_4] and [**4**][OTf] were synthesized and their performance in catalysis was compared to [**4**][$BArF_{24}$]. All the reactions were conducted following the general method for 24 hours at 70 °C: benzonitrile (0.1 mL, 0.97 mmol), $HSiEt_3$ (0.35 mL, 2.13 mmol), precatalyst (9.7×10^{-3} mmol, 1 mol %), CH_2Cl_2 (0.5 mL). The results are summarized in table S8.

Tableau S8. Optimization of precatalysts for the hydrosilylation of benzonitrile with $HSiEt_3$.

Entry	Precatalyst	Yield (%)
1	[**4**][$BArF_{24}$]	>99
2	[**4**][OTf]	5
3	[**4**][BPh_4]	1

As shown in table S8, there is a clear evidence for a counter-anion effect on the performance of the catalysis. Indeed, [**4**][$BArF_{24}$] showed the best activity (entry 1) when compared to [**4**][OTf] (entry 2) and [**4**][BPh_4] (entry 3) in the hydrosilylation of benzonitrile with $HSiEt_3$. As a consequence, [**4**][$BArF_{24}$] was selected as the precatalyst of choice for next screening studies dealing with the catalytic hydrosilylation of nitriles.

6.4.4 Influence of the proportion of precatalyst

In this study, we wished to know the influence of both the temperature and the proportion of the precatalyst on the course of the reaction. Two values of temperature and five different proportions of precatalyst were chosen as variables for the screening study. We looked at first the influence of the proportion of the precatalyst at room temperature, and then increased the temperature to 70 °C. The proportion of the precatalyst was screened along the series 0.05, 0.1, 0.2, 0.5 and 1 mol % relative to the concentration of benzonitrile. The conditions of each screening catalytic run were as follows: benzonitrile (0.1 mL, 0.97 mmol), silane (0.35 mL, 2.13 mmol), [**4**][$BArF_{24}$] (4.8×10^{-4} mmol, 0.05 mol %; 9.7×10^{-4} mmol, 0.1 mol %; 1.9×10^{-3} mmol, 0.2 mol %; 4.8×10^{-3} mmol, 0.5 mol %; 9.7×10^{-3} mmol, 1 mol %), CH_2Cl_2 (0.5 mL). The reaction progress was monitored at different times by using ^1H NMR. The results are summarized in table S9.

Table S9. Optimization of the proportion of precatalyst for the hydrosilylation of benzonitrile with $HSiEt_3$. (NR = no reaction)

Entry	[4][$BArF_{24}$] (mol %)	Yield (%)					
		25 °C		70 °C			
		2 h	24 h	2 h	4 h	6 h	24 h
1	0.05	NR	NR	5	9	34	40
2	0.1	NR	NR	5	8	16	80
3	0.2	NR	NR	7	14	30	85
4	0.5	NR	NR	16	42	63	>99
5	1.0	NR	NR	41	95	>99	>99

As shown in table S9 (green boxes, entries 4–5), full completion of the reaction between benzonitrile and triethylsilane was obtained when combining a loading of only 0.5 mol % of [**4**][$BArF_{24}$] with a heating at 70 °C for 24 h (entry 4). The combination of 1 mol % of [**4**][$BArF_{24}$] with heating at 70 °C for only 6 h was also an interesting optimization (entry 5). It is also important to notice that a prolonged time of reaction in the latter conditions had no effect of the integrity of the products (1 mol %; 70 °C; 24 h, entry 5). In contrast, no reaction was observed at room temperature at any concentration of [**4**][$BArF_{24}$] used.

6.4.5 Solvent-free hydrosilylation of acetonitrile

6.4.5.1 Catalytic procedures

The reaction described in scheme 30 of the manuscript and in scheme S1 here was carried out following two different procedures.

Procedure 1 ([2][BArF$_{24}$], 1 mol %). To a solution of [**2**][BArF$_{24}$] (135 mg, 0.097 mmol, 1 mol %) in CH_3CN (0.5 mL, 9.7 mmol) was added $HSiEt_3$ (3.1 mL, 19.5 mmol). The reaction mixture was heated at 50 °C for 44 h and then at 80 °C for 100 h (scheme S1a). The reaction mixture was first monitored at two intervals of time: after 1) 20 h at 50 °C and 2) 44 h at 50 °C. Then the temperature of the reaction mixture was increased to 80 °C, after the which the reaction was again monitored at two addtional intervals of time: after 3) 26 h at 80 °C and 4) 100 h at 80 °C. For each analysis, an aliquot from the reaction mixture was taken and mixed with CD_2Cl_2 for NMR analysis.

Procedure 2 ([4][BArF$_{24}$], 1 mol %). To a solution of [**4**][BArF$_{24}$] (53,82 mg, 0.038 mmol, 1 mol %) in CH_3CN (0.20 mL, 3.8 mmol) was added $HSiEt_3$ (1.34 mL, 8.4 mmol). The reaction mixture was heated at 80 °C for 24 h (scheme S1b). For ^{1}H NMR analysis, tri-*tert*-butylbenzene (35.4 mg, 0.144 mmol) was added as internal reference to the reaction mixture, after which an aliquot was taken from this mixture and mixed with C_6D_6.

a) Procedure 1 (^{1}H NMR in CD_2Cl_2)

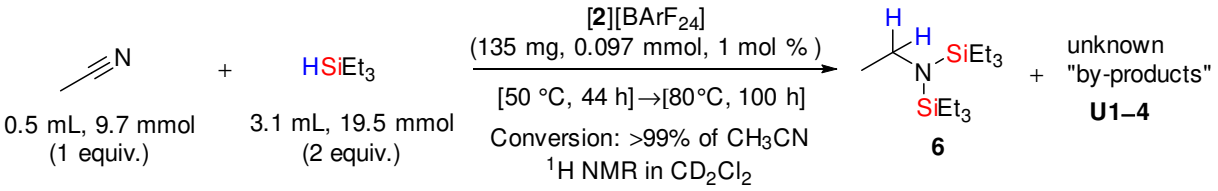

b) Procedure 2 (^{1}H NMR in C_6D_6)

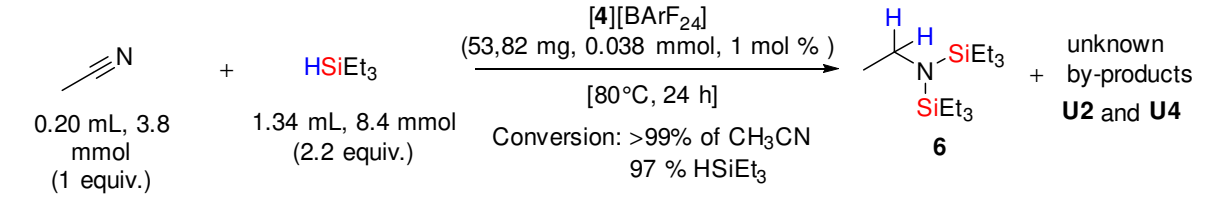

Scheme S1. Hydrosilylation of acetonitrile with $HSiEt_3$ to **6** under solvent-free conditions by using **a)** procedure 1 ([**2**][BArF$_{24}$], 1 % mol) and **b)** procedure 2 ([**4**][BArF$_{24}$], 1 % mol).

6.4.5.2 Characterization and isolation of the products

***N*,1,1,1-tetraethyl-N-(triethylsilyl)silanamine (6).** Using the procedure 1 described above, the presence of the product **6** was assessed by ESI mass analysis of the reaction mixture (see spectrum below). The product **6** was also obtained after the direct vacuum bulb-to-bulb distillation at a temperatue of ~240 °C of the reaction mixture, accompanied however by minor and unkwown product (presumably resulting from the decompostion of **6**). The resulting fraction is as a colorless oil. The identity of **6** was confirmed by ^{1}H NMR analysis of this colorless fraction. After several attempts, **6** was never obtained as a pure compound which is due to the complex nature of the reaction mixture.

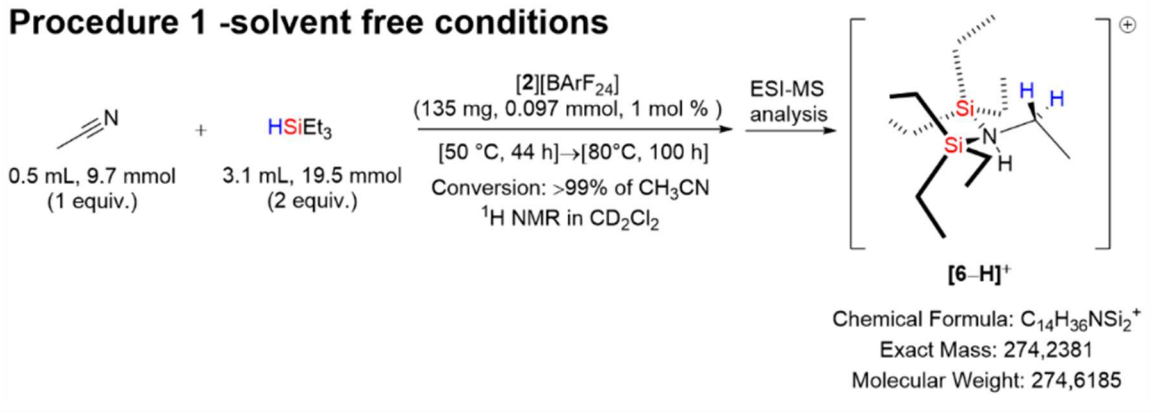

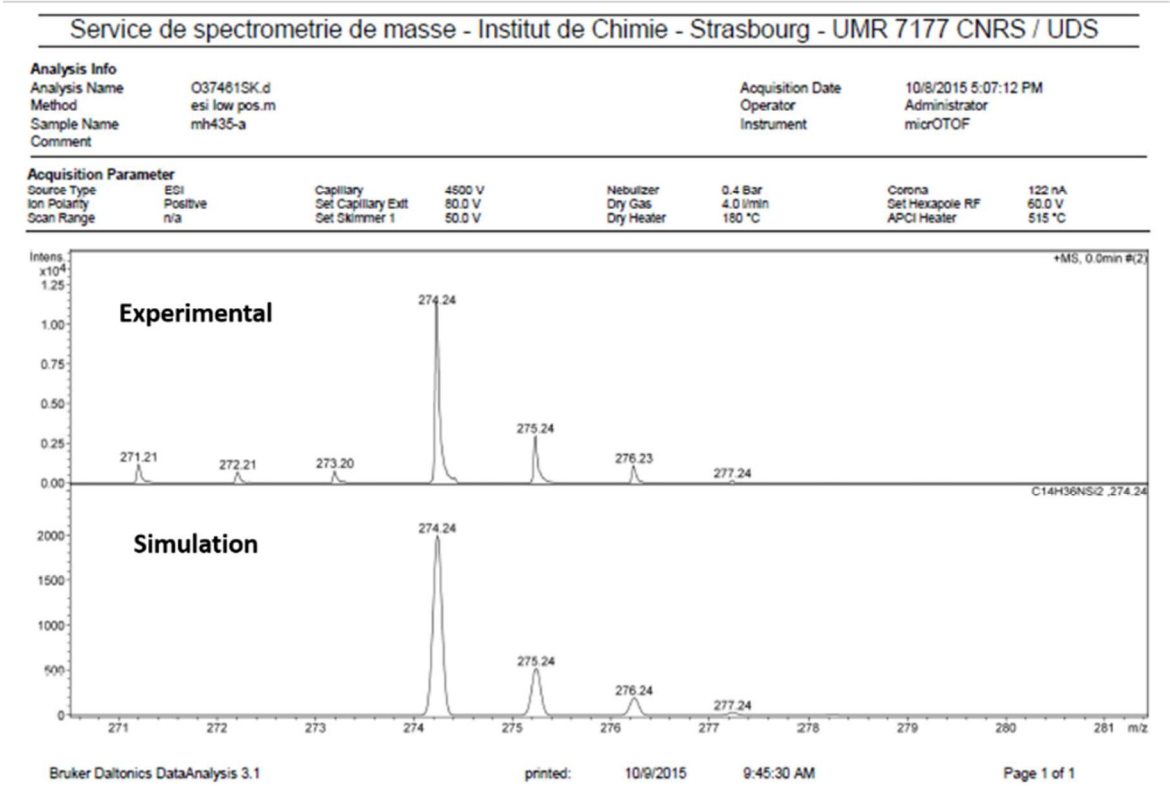

^{1}H NMR data of **6**: δ (C_6D_6, 298 K, 300 MHz) = 2.79 (q, 2H, $CH_3C\underline{H_2}N(TES)_2$, J = 7.1 Hz), 0.94–1.07 (t, 3H of $C\underline{H_3}CH_2N(TES)_2$ + other overlapping signals, J =7.0 Hz), 1.01 (t, 18H, $EtN(SiCH_2C\underline{H_3})_2$ + other overlapping signals, J =7.0 Hz), 0.65 (q, 12H, $EtN(SiC\underline{H_2}CH_3)_2$, J =7.0 Hz).

U2. Using the procedure 1 described above, the product **U2** was also obtained after the direct vacuum bulb-to-bulb distillation at a temperatue of ~70 °C of the reaction mixture, accompanied however by a minor and unknown product (presumably resulting from the decompostion of **U2**) and also by the major by-product $SiEt_4$. The resulting fraction is a colorless oil. We had a deep struggle however in assigning a convenient structure to **U2**, so that its exact identity is still unknown to date. However, its ^{1}H NMR spectrum shows its characteristic quintet signal at δ (CD_2Cl_2, 298 K, 400 MHz) = 2.76 ppm. If we assume that **U2** contains only one $SiEt_3$ group, the ratio of $SiEt_4$/**U2** can be estimated to ~1/0.3. Similarly, assuming that **U2** contains two $SiEt_3$ groups, then the ratio $SiEt_4$/**U2** can now be estimated to ~1/0.2.

^{1}H NMR data of **U2.** An intergation number of 2 was arbitrarily assigned to the quintet peak at δ = 2.76 ppm, so that all the other integration numbers are only relative to this reference number of 2: δ (CD_2Cl_2, 298 K, 400 MHz) = 3.12 (broad s, 0.8 H), 2.76 (quintet, 2H, J = 7.2 Hz), 1.05 (t, 3H, J = 7.2 Hz), 1.01 (t, 4H, J = 8.0 Hz), 0.94 (t, 9H of $RN(SiCH_2C\underline{H_3})_2$, J = 8.0 Hz, overlap with those of $SiEt_4$), 0.72 (q, 3H, J = 8.0 Hz), 0.51 (q, 6H, H of $RN(SiC\underline{H_2}CH_3)_2$, J = 8.0 Hz, overlap with those of $SiEt_4$).

Tetraethylsilane ($SiEt_4$). Using the procedure 1 described above, the product **$SiEt_4$** was cleanly obtained after the direct vacuum bulb-to-bulb distillation at a temperatue of ~100 °C of the reaction mixture. The resulting fraction is a colorless oil. The identity of **$SiEt_4$** was confirmed by ^{1}H NMR and ^{13}C analysis, and the related data matched very well those already reported in the literature.[394]

^{1}H NMR data of **$SiEt_4$:** δ (CD_2Cl_2, 298 K, 400 MHz) = 0.94 (t, 12H of $(SiCH_2C\underline{H_3})_4$, J = 8.0 Hz), 0.54 (q, 8H, $(SiC\underline{H_2}CH_3)_4$, J = 8.0 Hz). ^{13}C NMR δ (CD_2Cl_2, 298 K, 125.8 MHz) = 7.00 (s, 12H $(Si\underline{C}H_2CH_3)_4$), 6.75 (s, 8H, $(SiCH_2\underline{C}H_3)_4$).

[394] Connelly, S. J.; Kaminsky, W.; Heinekey, D. M. Structure and Solution Reactivity of (Triethylsilylium)triethylsilane Cations. *Organometallics* **2013**, *32* (24), 7478–7481.

Ethanamine (6H). Using the procedure 1 described above, the product **6H** was obtained as the hydrolyzed product of **6** when ~1/3 portion of the reaction mixture was stored at –30 °C inside a freezer for 3–4 weeks. **6H** was not isolated. However, its identity was confirmed by its characteristic ^{1}H NMR data as follows: δ (C_6D_6, 298 K, 400 MHz) = 4.93 (broad s, 2H), 3.13 (q, 2H, $CH_3C\underline{H_2}NH_2$, J = 7.2 Hz), 1.12 (t, 2H, $C\underline{H_3}CH_2NH_2$, J = 7.2 Hz).

6.4.5.3 Discussion of the ^{1}H NMR spectra

Procedure 1. Besides the desired product **6** and unconsumed $HSiEt_3$ and CH_3CN substrates, the ^{1}H NMR analysis after 20 h of reaction at 50 °C (see spectrum below) showed the presence of four unidenified peaks. Assuming that each of these four peaks characterizes one single product, we attributed to each unknown product the letter **U** and a number from **1** to **4** (**U1**, **U2**, **U3** and **U4**). The product *N,N*-bis(triethylsilyl)ethylamine **6** ($EtN(TES)_2$) has a characteristic signal at δ = 2.86 ppm (quartet, J = 7.1 Hz, $CH_3C\underline{H_2}N(TES)_2$), and the products **U1**–**4** were characterized by a quartet at δ = 3.1 ppm (J = 7.1 Hz) for **U1**; a quintet at δ = 2.76 ppm (J = 7.2 Hz) for **U2**; a singlet at δ = 2.0 ppm for **U3**, and a singlet at δ = 1.60 ppm for **U4**. These products **U1**–**4** were present during all the process of NMR analysis of the reaction mixture (see spectra below). In table S10 are summarized the relative ^{1}H intergation numbers ($I_{^1H}$) of typical peaks of all the constituents that were observed in the respective NMR spectra of the reaction mixture. Because we know that the quartet signal with a chemical shift at δ = 2.86 ppm belongs to **6**, we systemically attributed a reference $I_{^1H}$ of 2 to this peak in all the NMR spectra, which by this way indicates the relative $I_{^1H}$ of the other peaks that characterize the respective constituents.

The statement made in the manuscript regarding the presence of an apparent concurrent hydrosilylation reaction of CH_3CN within the conditions of this reaction, is revealed to be confirmed from the addditonal data provided in table S10. Indeed, one can notice that there is a non-linear correlation between the respective consumption of acetonitrile and $HSiEt_3$ over time, a fact that does not match the expected linear correlation because these two substrates are supposed to react with each other to afford **6** as the bis hydrosilylation reaction product. We postulate that CH_3CN may react through a concurrent pathway with one of the unknown products **U1**–**U4** or **6**. Interestingly, if we look at even more closely to all the NMR spectra shown below and the ^{1}H intergration number data reported in table S10, and plot the $I_{^1H}$ ratios of **U1**/**U2**, **U1**/**U3** and **U2**/**U3** as a function of time as it is shown in figure S1, we notice that the respective $I_{^1H}$ ratios all remain constant over time. The latter observation can be the result of

the fact that the concentration of **U1**, **U2** and **U3** increases at the same rate. This could also be the indication that **U1**, **U2** and **U3** are actually the same molecule. Furher experiments allowed us to exclude the latter possibility (*vide infra*).

Tableau S10. Monitoring of the change in the relative ^{1}H NMR integration numbers (I_{1H}) as a function of time and temperature of all the constituents observed during the solvent-free hydrosilylation reaction of acetonitrile with $HSiEt_3$. The relative integration number of 2 was arbritrarily attributed to **6** which was taken as a reference constituent.

Conditions		**Relative ^{1}H NMR integration number (I_{1H})**						
T (°C)	**t (h)**	**6**	**U1**	**U2**	**U3**	**U4**	**$HSiEt_3$**	**CH_3CN**
50	20	2	7.2	8.2	8.4	3.9	22.8	18.5
50	44	2	4.2	4.3	4.2	0.6	5.4	0.5
80	26	2	4.1	4.0	4.4	0.9	4.4	0.2
80	100	2	2.7	3.2	3.2	0.5	2.2	0.1

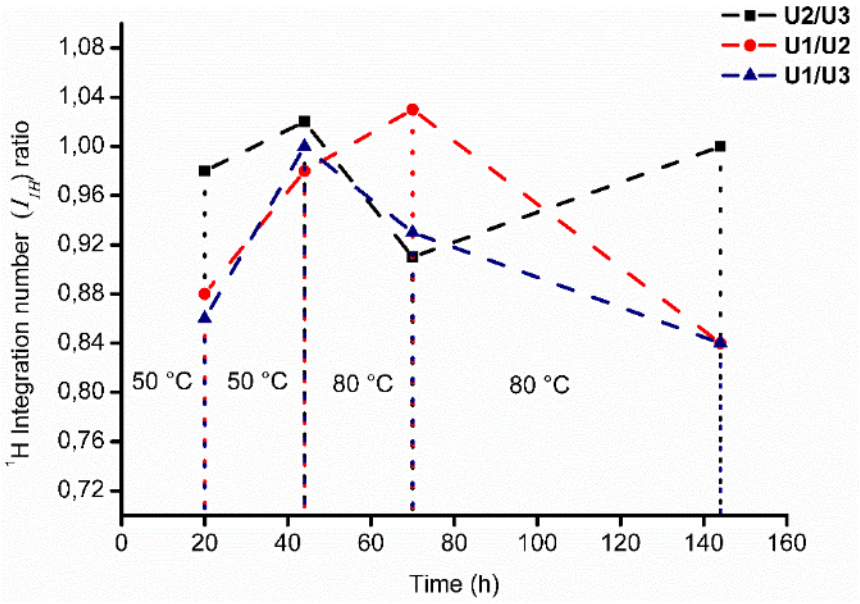

Figure S1. The calculated ratios of the relative ^{1}H NMR integration numbers I_H of **U1**/**U2**, **U1**/**U3** and **U2**/**U3** as a function of time and temperature. The data provided in table S10 were used for this figure.

Procedure 2. The assumption that ^{1}H NMR peaks of **U1**, **U2** and **U3** could actually be connected to a same molecule can be ruled out because when we repeated the reaction in the same solvent-free conditions by using [**4**][$BArF_{24}$] (1 mol %) as preccatalyst instead of [**2**][$BArF_{24}$] and starting with 0.2 mL of CH_3CN instead of 0.5 mL (scheme S1b), the ^{1}H NMR spectroscopic analysis of the reaction mixture generated a different spectrum (see sepectra below). Indeed, this spectrum showed the formation of **6** (~13 % yield) and **U2** as major products, and the typical peaks of **U1** and **U3** were absent. However, the singlet peak at δ = 1.60 ppm which is characteristic of **U4** was still present.

6.4.5.4 ^{1}H NMR spectra

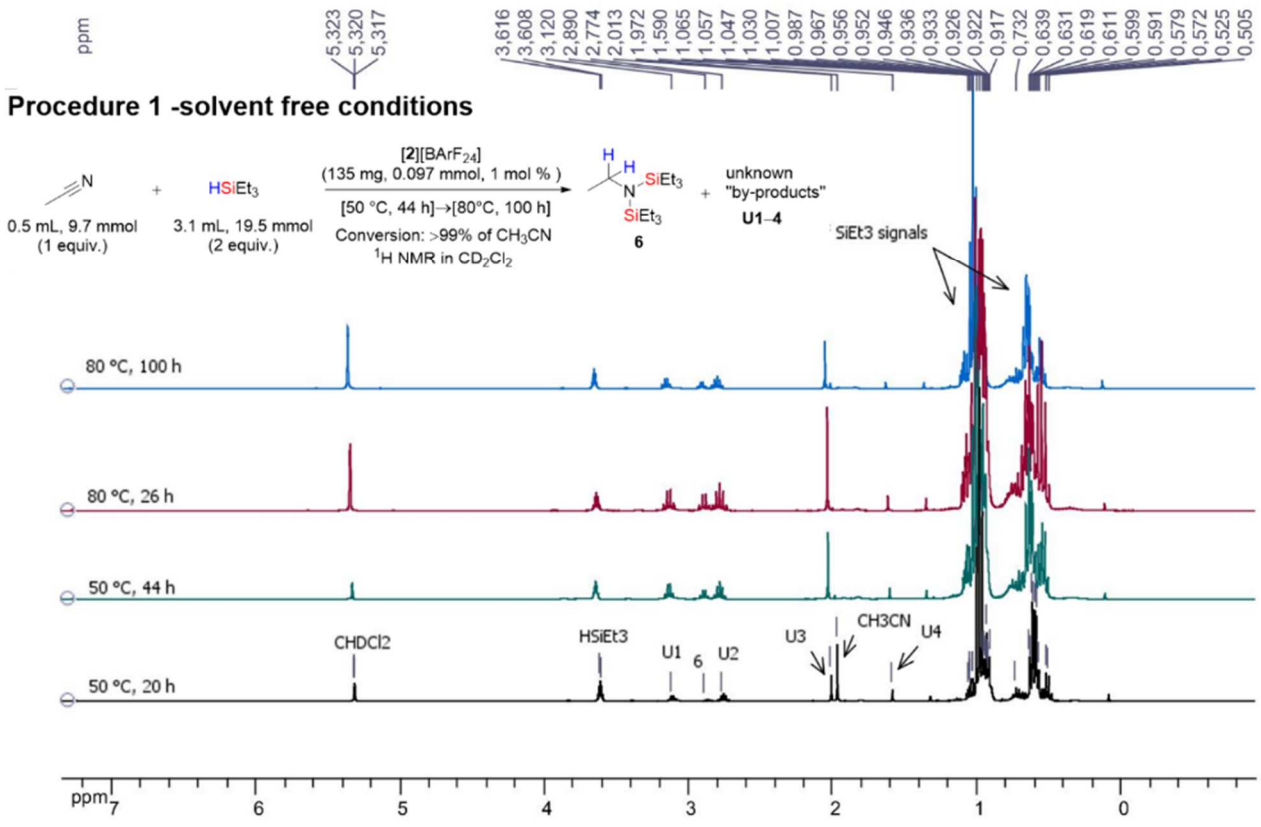
Procedure 1 -solvent free conditions
0.5 mL, 9.7 mmol
(1 equiv.)
HSiEt3
3.1 mL, 19.5 mmol
(2 equiv.)
[2][BArF24]
(135 mg, 0.097 mmol, 1 mol %)
[50 °C, 44 h]→[80°C, 100 h]
Conversion: >99% of CH3CN
1H NMR in CD2Cl2
6
unknown
"by-products"
U1–4
SiEt3 signals
80 °C, 100 h
80 °C, 26 h
50 °C, 44 h
50 °C, 20 h
CHDCl2
HSiEt3
U1
6
U2
U3
CH3CN
U4
ppm

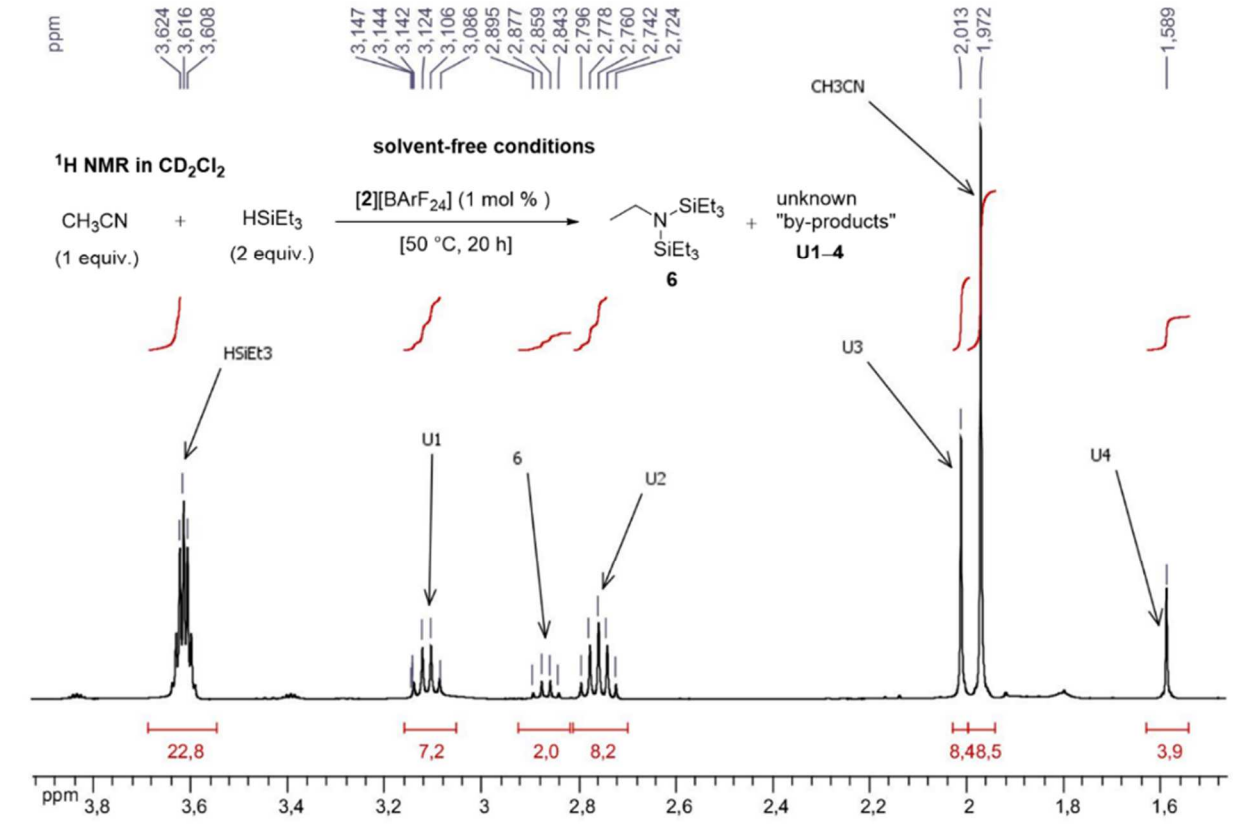
ppm
3,624
3,616
3,608
3,147
3,144
3,142
3,124
3,106
3,086
2,895
2,877
2,859
2,843
2,796
2,778
2,760
2,742
2,724
2,013
1,972
1,589
CH3CN
solvent-free conditions
1H NMR in CD2Cl2
CH3CN
(1 equiv.)
+
HSiEt3
(2 equiv.)
[2][BArF24] (1 mol %)
[50 °C, 20 h]
SiEt3
N
SiEt3
6
+
unknown
"by-products"
U1–4
HSiEt3
U1
6
U2
U3
U4
22,8
7,2
2,0
8,2
8,4
8,5
3,9
ppm
3,8
3,6
3,4
3,2
3
2,8
2,6
2,4
2,2
2
1,8
1,6

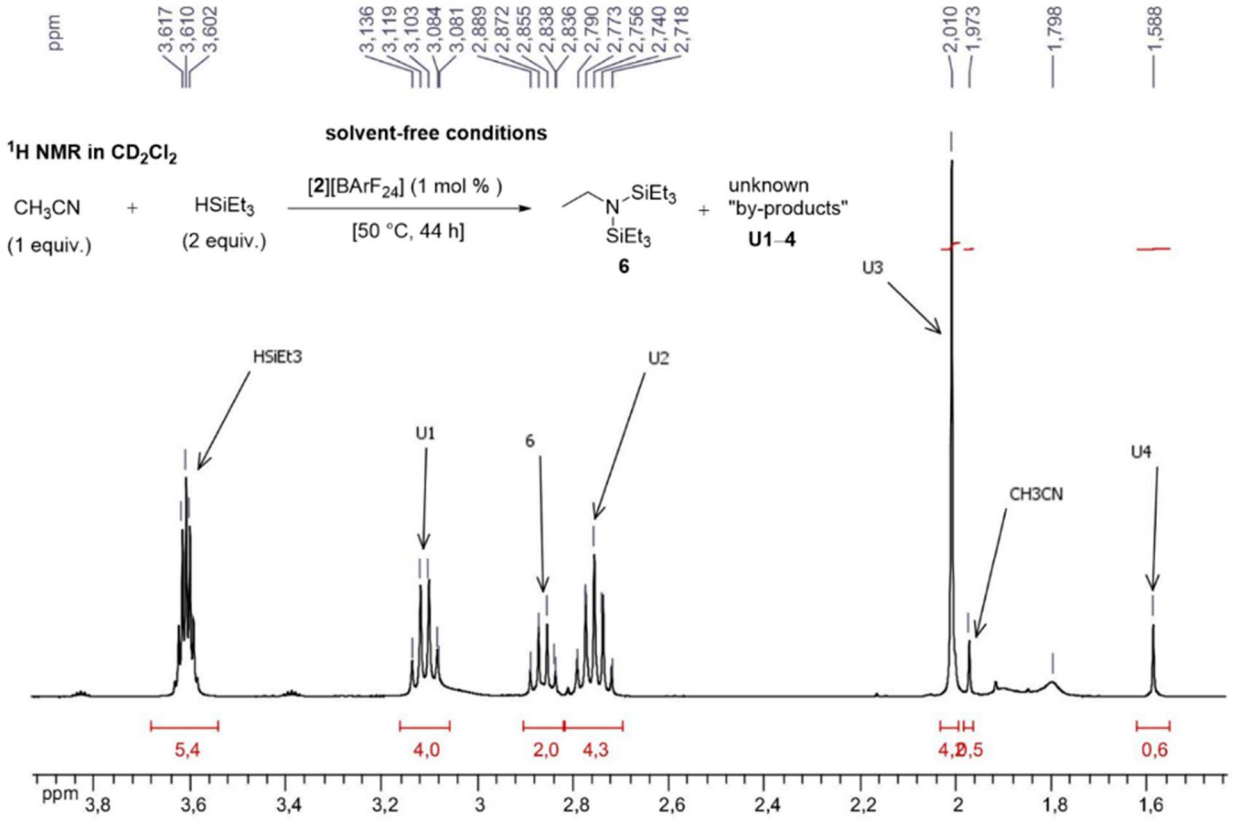
ppm
3,617
3,610
3,602
3,136
3,119
3,103
3,084
3,081
2,889
2,872
2,855
2,838
2,836
2,790
2,773
2,756
2,740
2,718
2,010
1,973
1,798
1,588
solvent-free conditions
1H NMR in CD2Cl2
CH3CN
(1 equiv.)
+
HSiEt3
(2 equiv.)
[2][BArF24] (1 mol %)
[50 °C, 44 h]
SiEt3
N
SiEt3
6
+
unknown
"by-products"
U1–4
U3
HSiEt3
U2
U1
6
U4
CH3CN
5,4
4,0
2,0
4,3
4,2
2,5
0,6
ppm
3,8
3,6
3,4
3,2
3
2,8
2,6
2,4
2,2
2
1,8
1,6

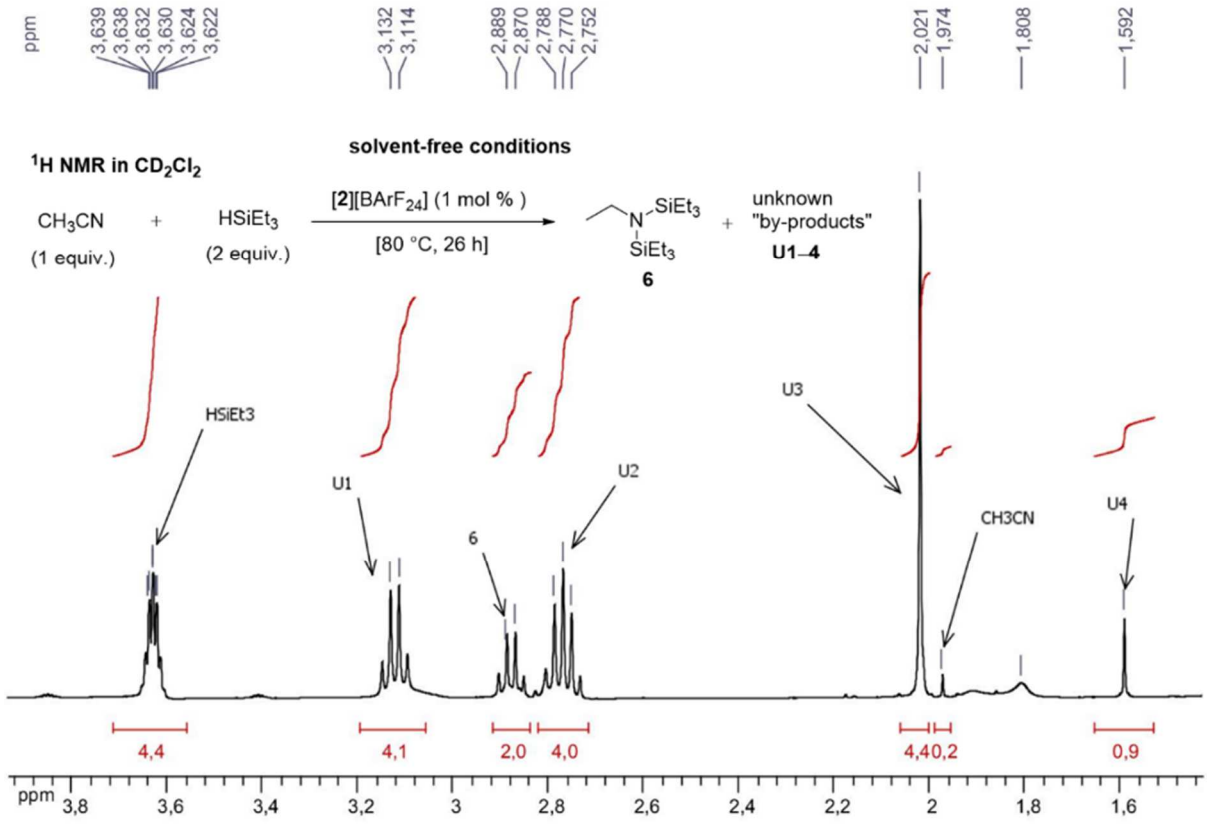
ppm
3,639
3,638
3,632
3,630
3,624
3,622
3,132
3,114
2,889
2,870
2,788
2,770
2,752
2,021
1,974
1,808
1,592
solvent-free conditions
1H NMR in CD2Cl2
CH3CN
(1 equiv.)
+
HSiEt3
(2 equiv.)
[2][BArF24] (1 mol %)
[80 °C, 26 h]
SiEt3
N
SiEt3
6
+
unknown
"by-products"
U1–4
HSiEt3
U1
6
U2
U3
CH3CN
U4
4,4
4,1
2,0
4,0
4,4
0,2
0,9
ppm
3,8
3,6
3,4
3,2
3
2,8
2,6
2,4
2,2
2
1,8
1,6

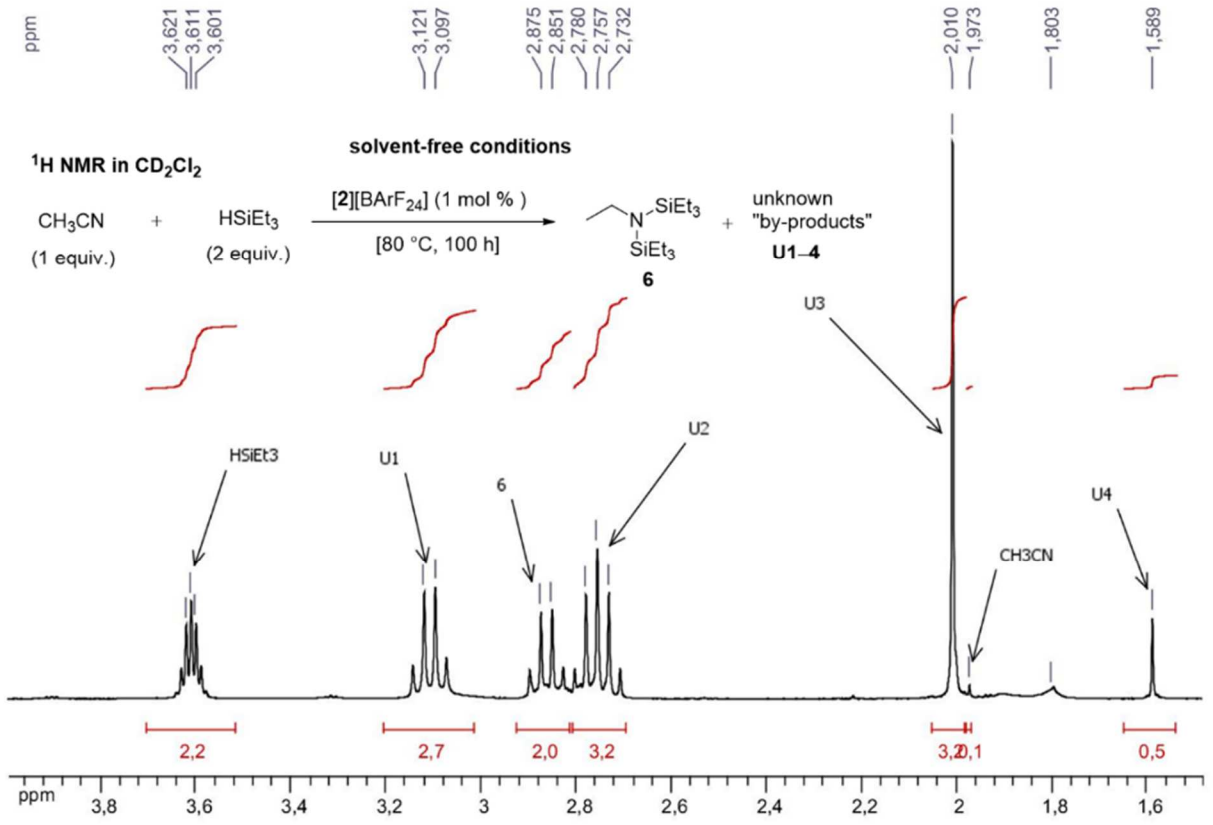
ppm
3,621
3,611
3,601
3,121
3,097
2,875
2,851
2,780
2,757
2,732
2,010
1,973
1,803
1,589
^{1}H NMR in CD_2Cl_2
solvent-free conditions
CH_3CN
(1 equiv.)
+
$HSiEt_3$
(2 equiv.)
[2][$BArF_{24}$] (1 mol %)
[80 °C, 100 h]
$SiEt_3$
N
$SiEt_3$
6
+
unknown
"by-products"
U1–4
U3
HSiEt3
U1
6
U2
U4
CH3CN
2,2
2,7
2,0
3,2
3,2
2,1
0,5
ppm
3,8
3,6
3,4
3,2
3
2,8
2,6
2,4
2,2
2
1,8
1,6

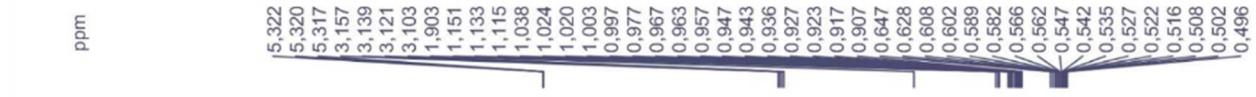
ppm
5,322
5,320
5,317
3,157
3,139
3,121
3,103
1,903
1,151
1,133
1,115
1,038
1,024
1,020
1,003
0,997
0,977
0,967
0,963
0,957
0,947
0,943
0,936
0,927
0,923
0,917
0,907
0,647
0,628
0,608
0,602
0,589
0,582
0,566
0,562
0,547
0,542
0,535
0,527
0,522
0,516
0,508
0,502
0,496

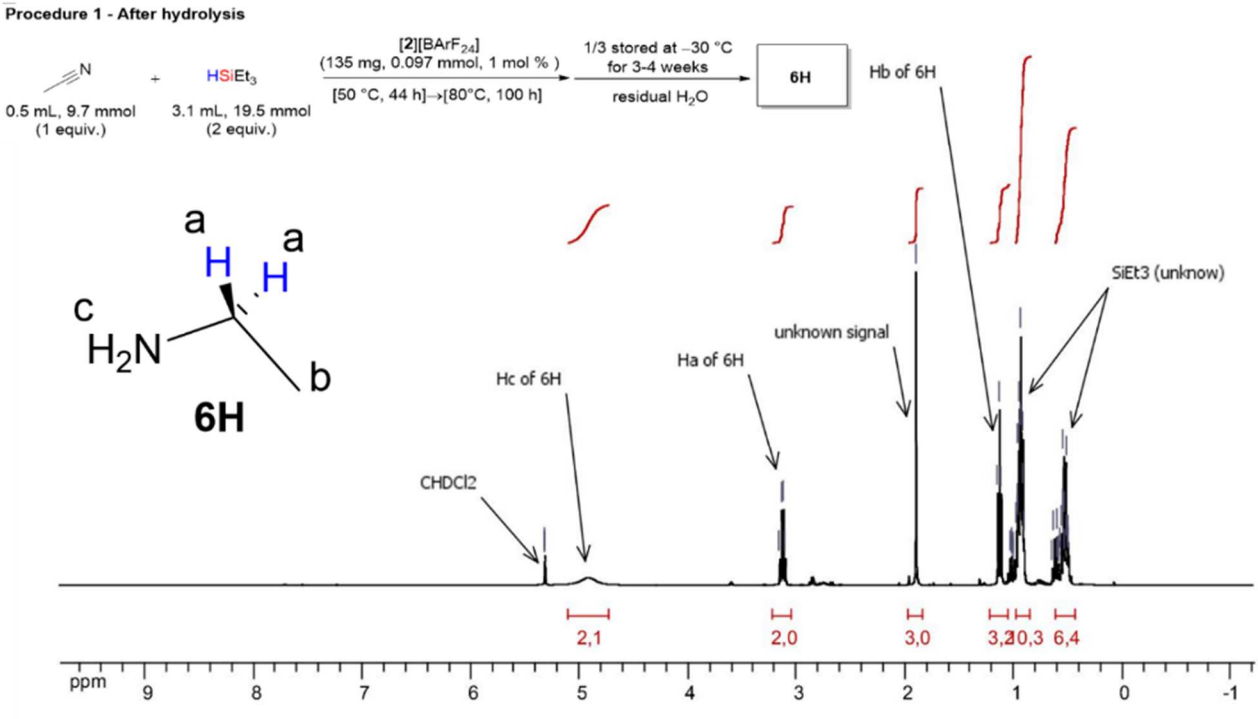
Procedure 1 - After hydrolysis
N
0.5 mL, 9.7 mmol
(1 equiv.)
+
$HSiEt_3$
3.1 mL, 19.5 mmol
(2 equiv.)
[2][$BArF_{24}$]
(135 mg, 0.097 mmol, 1 mol %)
[50 °C, 44 h]→[80°C, 100 h]
1/3 stored at –30 °C
for 3-4 weeks
residual H_2O
6H
Hb of 6H
a
H
H
a
c
H_2N
b
6H
SiEt3 (unknow)
unknown signal
Ha of 6H
Hc of 6H
CHDCl2
2,1
2,0
3,0
3,2
0,3
6,4
ppm
9
8
7
6
5
4
3
2
1
0
-1

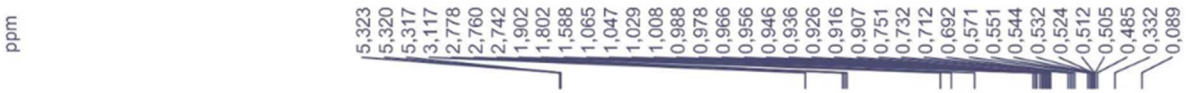

U2

Procedure 1 - After distillation

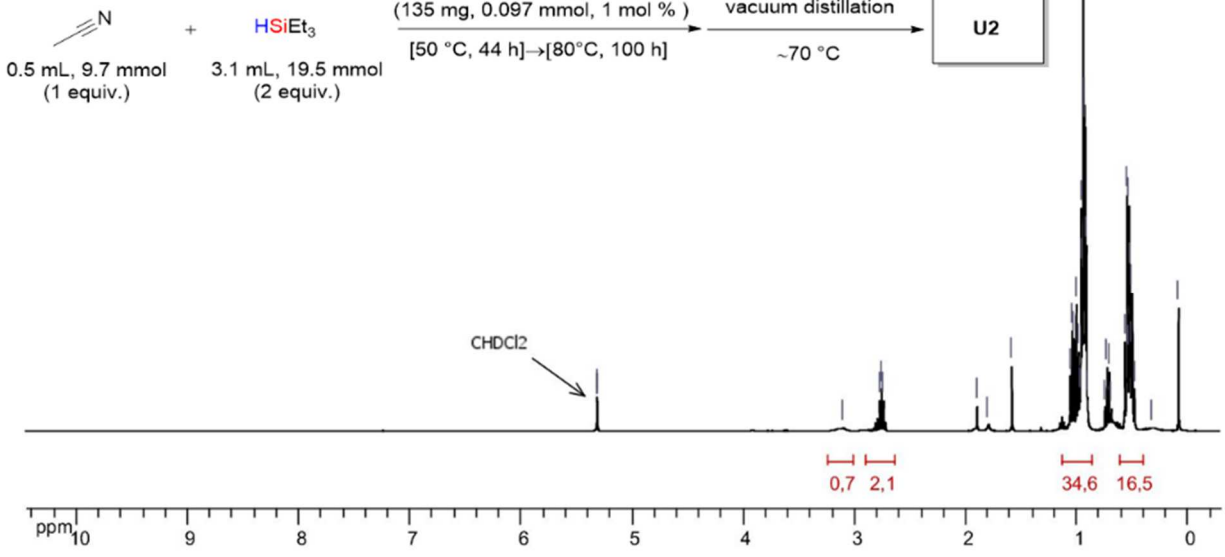

Procedure 1 - After distillation

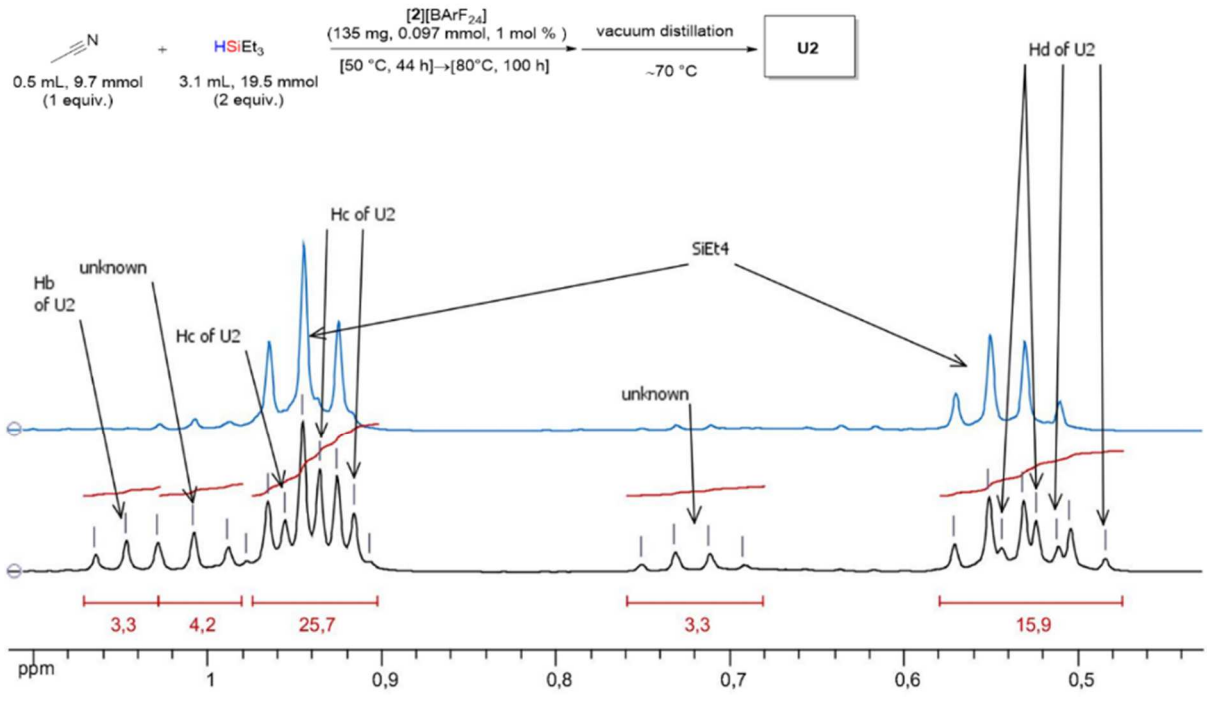

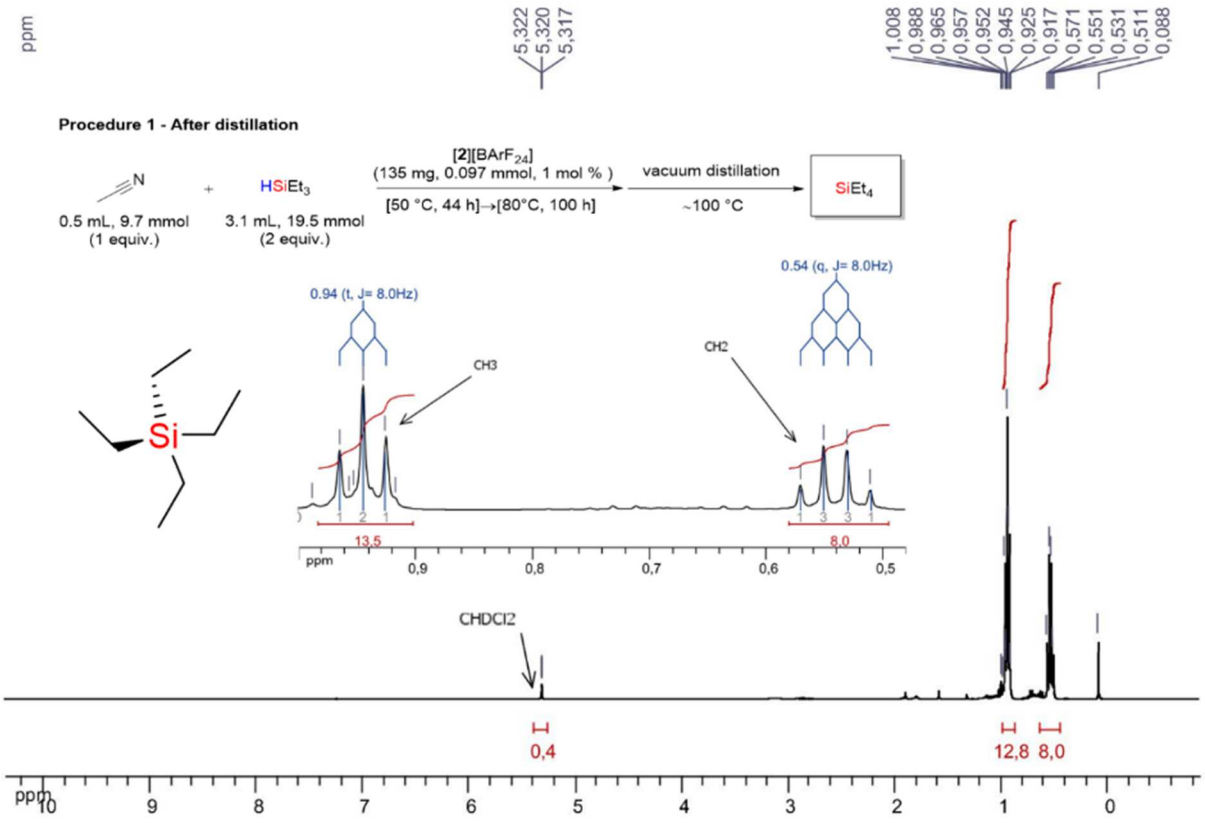
ppm
5,322
5,320
5,317
1,008
0,988
0,965
0,957
0,952
0,945
0,925
0,917
0,571
0,551
0,531
0,511
0,088
Procedure 1 - After distillation
[2][BArF24]
(135 mg, 0.097 mmol, 1 mol %)
[50 °C, 44 h]→[80°C, 100 h]
vacuum distillation
~100 °C
SiEt4
HSiEt3
0.5 mL, 9.7 mmol
(1 equiv.)
3.1 mL, 19.5 mmol
(2 equiv.)
0.94 (t, J= 8.0Hz)
0.54 (q, J= 8.0Hz)
CH3
CH2
Si
13,5
8,0
CHDCl2
0,4
12,8
8,0

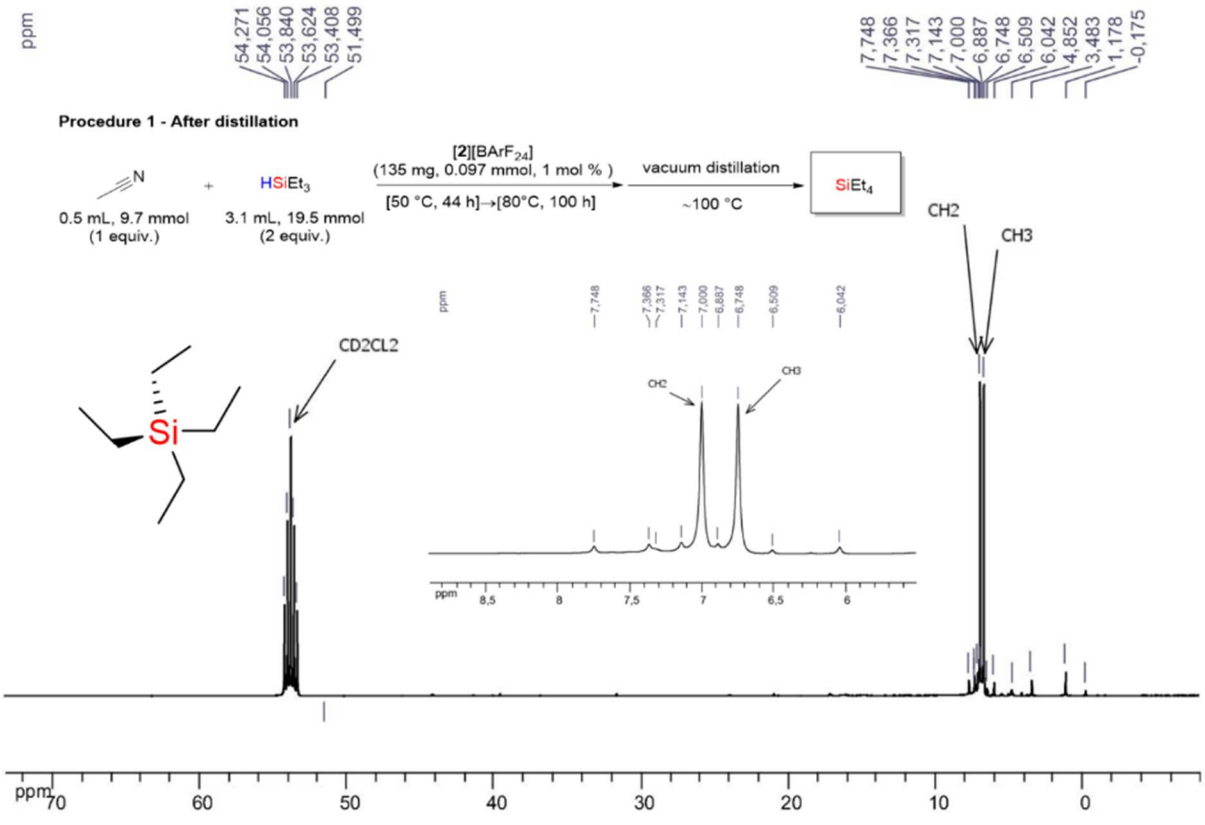
ppm
54,271
54,056
53,840
53,624
53,408
51,499
7,748
7,366
7,317
7,143
7,000
6,887
6,748
6,509
6,042
4,852
3,483
1,178
-0,175
Procedure 1 - After distillation
[2][BArF24]
(135 mg, 0.097 mmol, 1 mol %)
[50 °C, 44 h]→[80°C, 100 h]
vacuum distillation
~100 °C
SiEt4
HSiEt3
0.5 mL, 9.7 mmol
(1 equiv.)
3.1 mL, 19.5 mmol
(2 equiv.)
CH2
CH3
CD2Cl2
Si

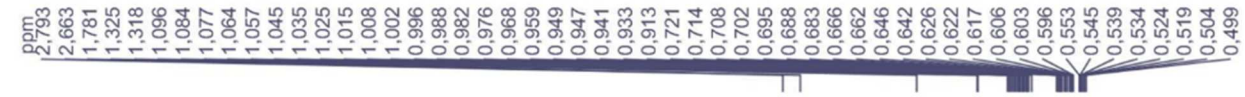
ppm
2,793
2,663
1,781
1,325
1,318
1,096
1,084
1,077
1,064
1,057
1,045
1,035
1,025
1,015
1,008
1,002
0,996
0,988
0,982
0,976
0,968
0,959
0,949
0,947
0,941
0,933
0,913
0,721
0,714
0,708
0,702
0,695
0,688
0,683
0,666
0,662
0,646
0,642
0,626
0,622
0,617
0,606
0,603
0,596
0,553
0,545
0,539
0,534
0,524
0,519
0,504
0,499

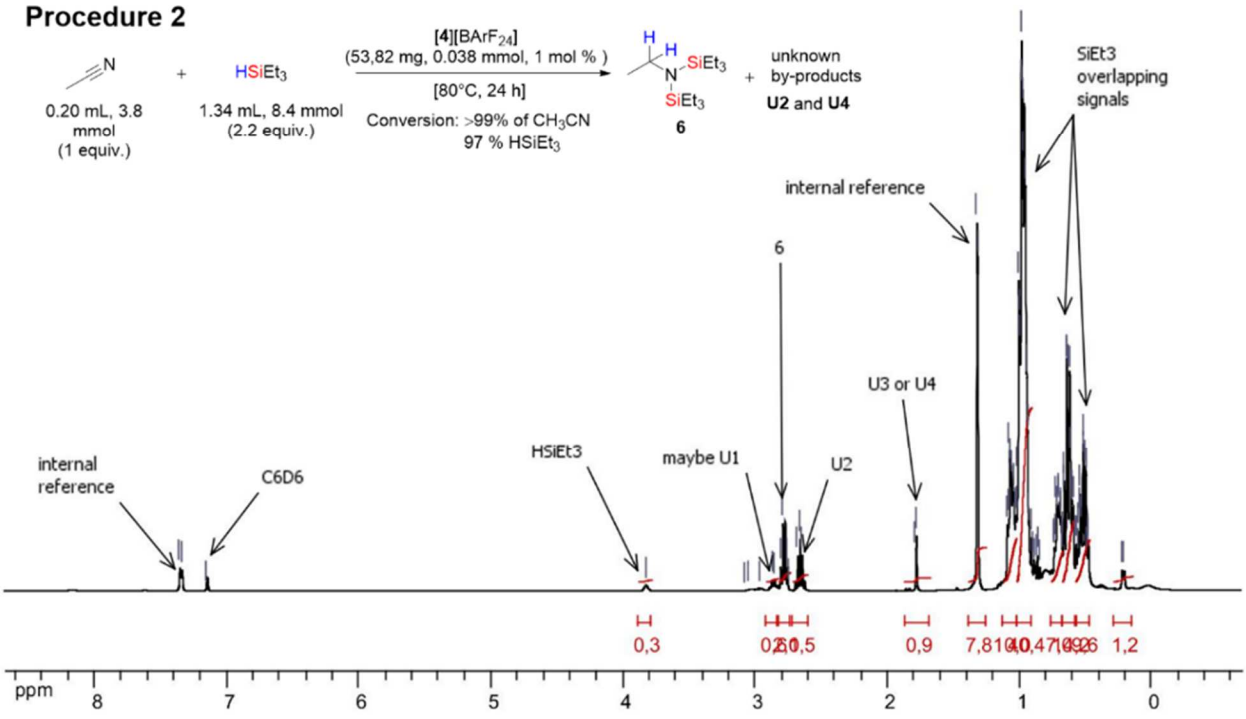
Procedure 2
0.20 mL, 3.8 mmol (1 equiv.)
HSiEt3
1.34 mL, 8.4 mmol (2.2 equiv.)
[4][BArF24]
(53,82 mg, 0.038 mmol, 1 mol %)
[80°C, 24 h]
Conversion: >99% of CH3CN
97 % HSiEt3
6
unknown by-products
U2 and U4
SiEt3 overlapping signals
internal reference
6
U3 or U4
internal reference
C6D6
HSiEt3
maybe U1
U2
0,3
0,9
1,2
ppm
8
7
6
5
4
3
2
1
0

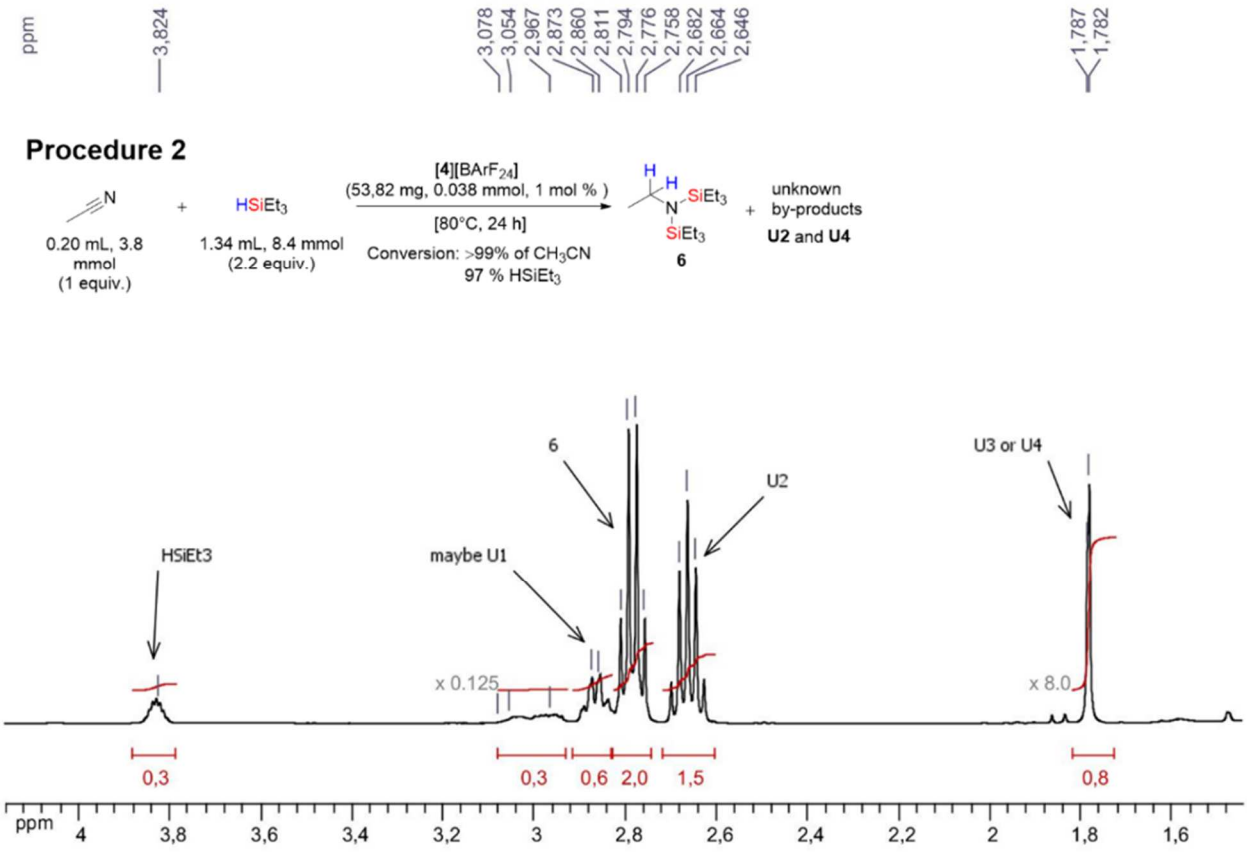

6.4.6 Hydrosilylation of acetonitrile with CH_2Cl_2 as the solvent (table 16)

6.4.6.1 Catalytic procedures

The reaction described in table 16 of the manuscript and in scheme S2 here was carried out following the procedures below.

Procedure 3 ([4][BArF$_{24}$], 1 mol %; HSiEt$_3$). To a mixture of CH_3CN (0.10 mL, 1.92 mmol) and $HSiEt_3$ (0.67 mL, 4.21 mmol) was added a solution of [**4**][$BArF_{24}$] (27.0 mg, 0.019 mmol, 1 mol %) in CH_2Cl_2 (0.5 mL). The reaction mixture was heated at 80 °C for 24 h. For ^1H NMR analysis, tri-*tert*-butylbenzene (41.6 mg, 0.169 mmol) was added as internal reference to the reaction mixture, after which an aliquot was taken from this mixture and mixed with C_6D_6.

Procedure 4 ([4][BArF$_{24}$], 1 mol %; HSiPh$_3$, HSiPhH$_2$, PMHS). To a mixture of CH_3CN (0.10 mL, 1.92 mmol) and $HSiPh_3$ (1.097 g, 4.21 mmol), or $HSiPhH_2$ (0.52 mL g, 4.21 mmol), or

PMHS (0.25 mL, 4.21 mmol) was added a solution of [**4**][$BArF_{24}$] (27.0 mg, 0.019 mmol, 1 mol %) in CH_2Cl_2 (0.5 mL). The reaction mixture was then heated at 80 °C for 24 h. For ^1H NMR analysis, tri-*tert*-butylbenzene (23.8 mg, 0.097 mmol for $HSiPh_3$; 38.8 mg, 0.158 mmol for $HSiPhH_2$; 33.0 mg, 0.134 mmol for PMHS) was added as internal reference to the reaction mixture, after which an aliquot was taken from this mixture and mixed with C_6D_6.

a) Procedure 3 (^1H NMR in C_6D_6)

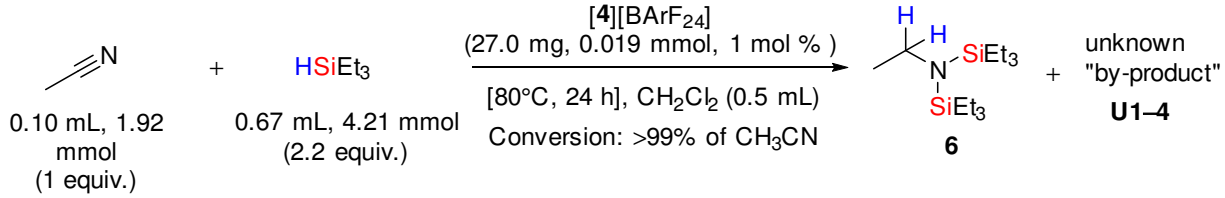

0.10 mL, 1.92 mmol (1 equiv.) + 0.67 mL, 4.21 mmol (2.2 equiv.)

---

b) Procedure 4 (^1H NMR in C_6D_6)

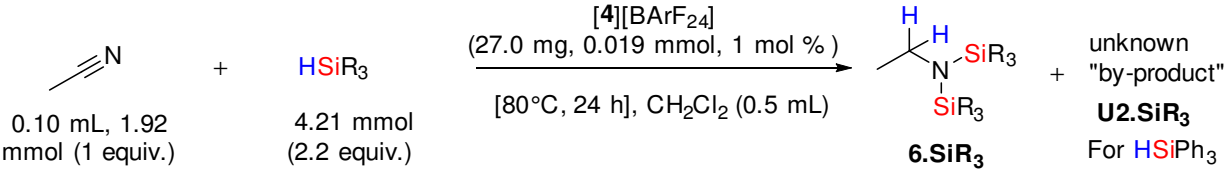

0.10 mL, 1.92 mmol (1 equiv.) + 4.21 mmol (2.2 equiv.)

Scheme S2. Hydrosilylation of acetonitrile with [**4**][$BArF_{24}$] (1 % mol) to **6** under co-solvent conditions by using **a)** procedure 3 ($HSiEt_3$) and **b)** procedure 4 ($HSiPh_3$, $HSiPhH_2$, PMHS).

6.4.6.2 Discussion of the ^1H NMR spectra

Procedure 3 (scheme S2a). The ^1H NMR spectrum showed a similar mixture of products as it has been observed for the solvent-free conditions. Indeed, the product **6** which was estimated to be formed in ~7% was accompanied by **U2** as the major product.

Procedure 4 (scheme S2b). The ^1H NMR spectra showed the expected products **6.SiR$_3$** were formed in ~9% for $HSiPh_3$, ~2% for $HSiPhH_2$. No reaction was observed when PMHS was used as silane. The product **U2.SiR$_3$** was observed only in the case of $HSiPh_3$ as silane.

6.4.7 Hydrosilylation of propionitrile with CH_2Cl_2 as the solvent

6.4.7.1 Catalytic procedures

The reaction described in table 16 of the manuscript and in scheme S3 here was carried out following the procedures below.

Procedure 5 ([4][BArF$_{24}$], 1 mol %; HSiEt$_3$). To a solution of [**4**][BArF$_{24}$] (39,5 mg, 0.028 mmol, 1 mol %) in propionitrile (0.20 mL, 2.8 mmol) was added HSiEt$_3$ (0.98 mL, 6.2 mmol). The reaction mixture was heated at 80 °C for 72 h (scheme S3). For ^{1}H NMR analysis, tri-*tert*-butylbenzene (30.6 mg, 0.124 mmol) was added as internal reference to the reaction mixture, after which an aliquot was taken from this mixture and mixed with C_6D_6. A similar procedure procedure was applied to other silanes, as described below.

Procedure 6 ([4][BArF$_{24}$], 1 mol %; HSiPh$_3$, HSiPhH$_2$, PMHS). To a mixture of propionitrile (0.10 mL, 1.40 mmol) and HSiPh$_3$ (0.803 g, 3.1 mmol), or HPhSiH$_2$ (0. 38 mL g, 3.1 mmol), or PMHS (0.18 mL, 3.1 mmol) was added a solution of [**4**][BArF$_{24}$] (20.0 mg, 0.014 mmol, 1 mol %) in CH_2Cl_2 (0.5 mL). The reaction mixture was then heated at 80 °C for 24 h. For ^{1}H NMR analysis, tri-*tert*-butylbenzene (28.8 mg, 0.109 mmol for HSiPh$_3$; 26.3 mg, 0.107 mmol for HPhSiH$_2$; 22.5 mg, 0.091 mmol for PMHS) was added as internal reference to the reaction mixture, after which an aliquot was taken from this mixture and mixed with C_6D_6.

Procedure 5 (^{1}H NMR in C_6D_6)

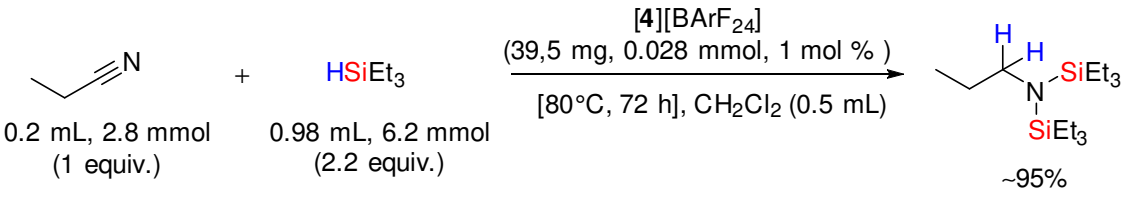

Procedure 6 (^{1}H NMR in C_6D_6)

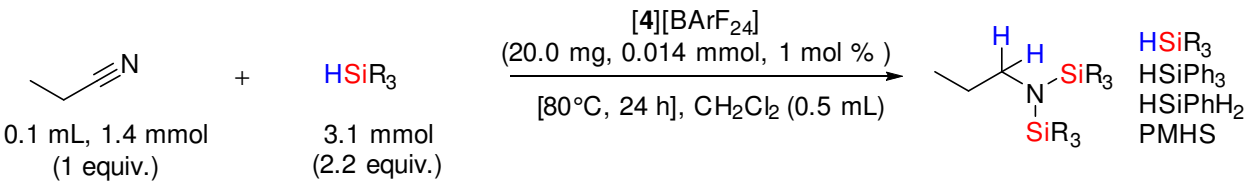

Scheme S3. Catalytic hydrosilylation of propionitrile with [**4**][BArF$_{24}$] (1 % mol) under co-solvent conditions by using **a)** procedure 5 (HSiEt$_3$) and **b)** procedure 6 (HSiPh$_3$, HSiPhH$_2$, PMHS).

6.4.7.2 Discussion of the ^{1}H NMR spectra

Procedure 5 (scheme 3a). The NMR yield of the product 1,1,1-triethyl-*N*-propyl-*N*-(triethylsilyl)silanamine was estimated to ~95%. The product was not isolated. However, its identity was assesed by its characteristic ^{1}H NMR data which are as follows: δ (C_6D_6, 298 K, 400 MHz) = 2.68 (m, 2H, C*H*$_2$N(SiEt$_3$)$_2$), 1.41 (sextuplet of triplets (superimposed multiplet), 2H, C*H*$_2$-CH$_2$N(SiEt$_3$)$_2$), 0.99 (t, 18H, C*H*$_3$-CH$_2$Si(*n*Pr), J = 8.0 Hz), 0.74 (t, 3H, C*H*$_3$-CH$_2$CH$_2$-N(SiEt$_3$)$_2$, J = 7.5 Hz), 0.65 (q, 12H, CH$_3$-C*H*$_2$Si(*n*Pr), J = 8.0 Hz). The related spectrum is shown below along with its molecluar strucutre (represented in scheme S4).

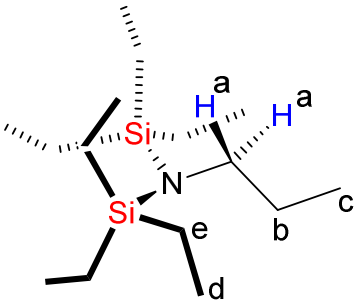

Scheme S4. Molecular structure of 1,1,1-triethyl-*N*-propyl-*N*-(triethylsilyl)silanamine.

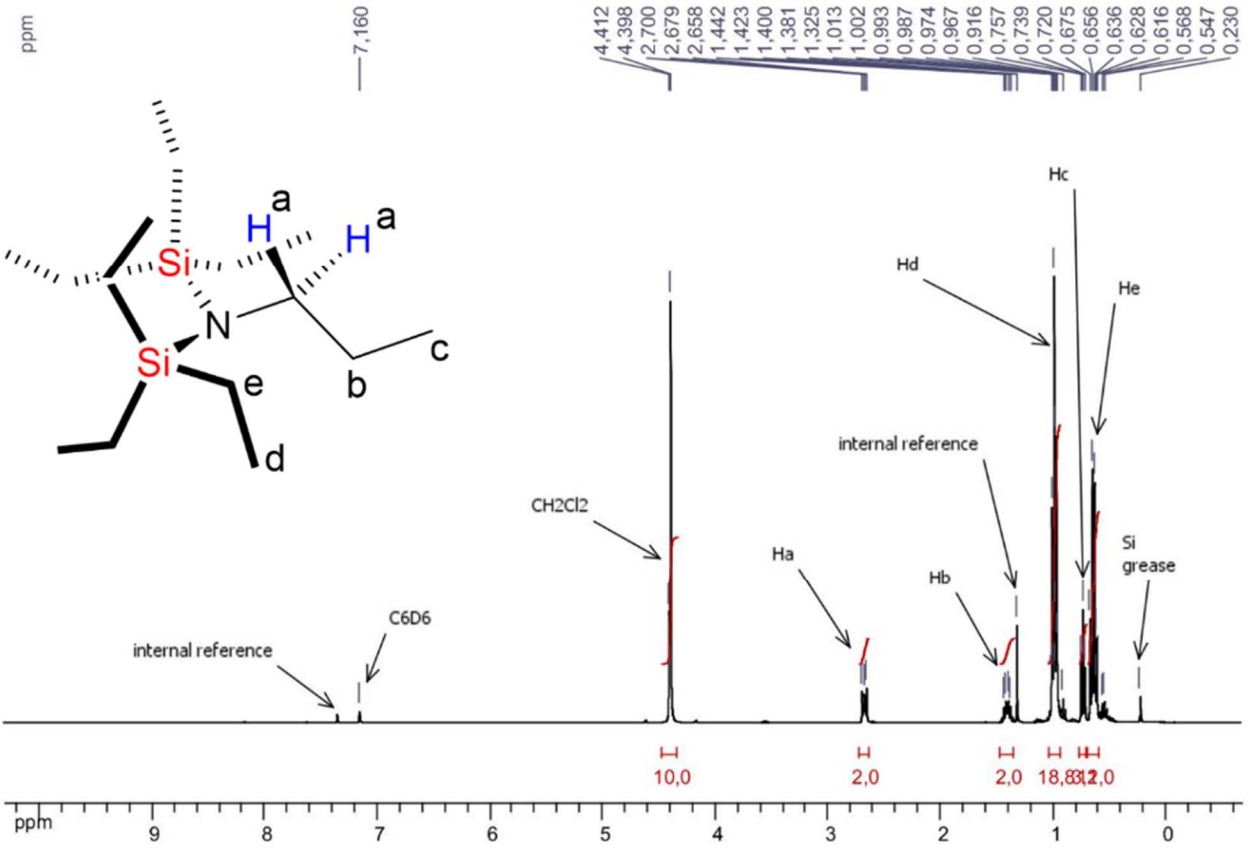

Procedure 6 (scheme 3b). The ^{1}H NMR spectra showed the expected products were formed in ~57% for $HSiPh_3$, ~2% for $HSiPhH_2$. No reaction was observed when PMHS was used as silane.

6.4.8 Solvent-free hydrosilylation of benzonitrile

6.4.8.1 Catalytic procedures

The reaction described in scheme 44 of the manuscript and in scheme S5 here was carried out following procedure.

Procedure 7 ([2][BArF$_{24}$], 1 mol %). To a solution of [**3**][BArF$_{24}$] (135 mg, 0.097 mmol, 1 mol %) in benzonitrile (1 mL, 9.7 mmol) was added $HSiEt_3$ (3.1 mL, 19.5 mmol). The reaction mixture was heated at 50 °C for 20 h and then at 80 °C for 24 h (scheme S5). The reaction mixture was monitored at these two intervals of time. For each analysis, an aliquot from the reaction mixture was taken and mixed with CD_2Cl_2 for NMR analysis.

Procedure 7 (^{1}H NMR in CD_2Cl_2)

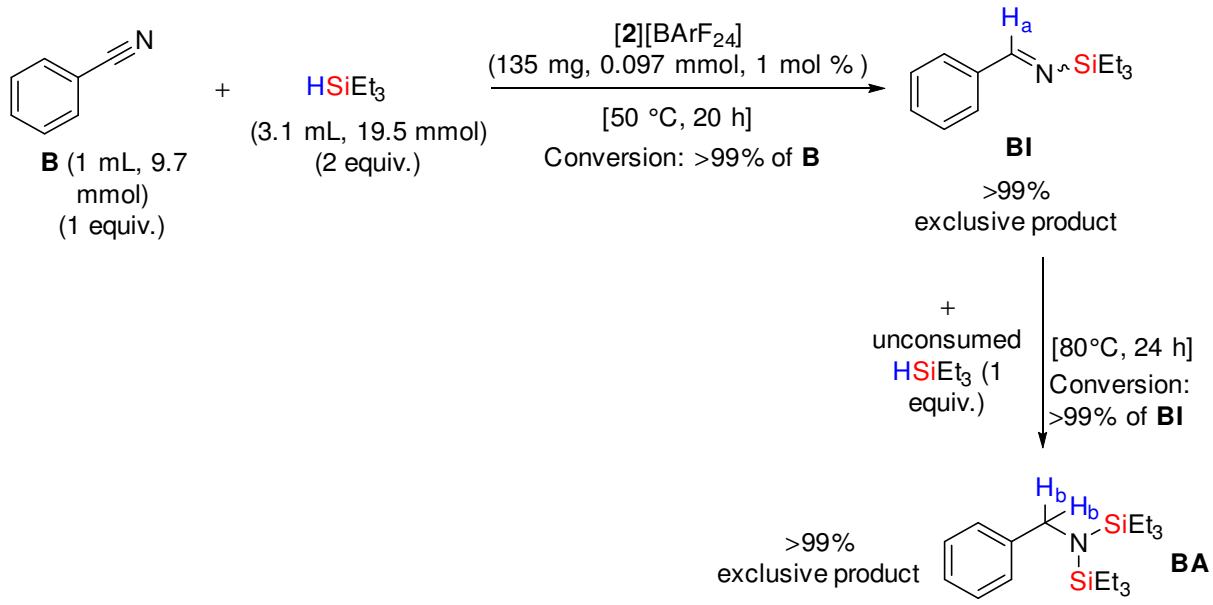

Scheme S5. [**2**][BArF$_{24}$] catalyzed selective hydrosilylation of benzonitrile with $HSiEt_3$ to **BI** and **BA** under solvent-free conditions.

6.4.8.2 Discussion of the ^{1}H NMR spectra

***N*-(triethylsilyl)benzylimine, BI.** Upon heating at 50 °C for 20 h, the ^{1}H NMR spectrum (CD_2Cl_2, 298 K) showed the exclusive formation of the monohydrosilylated product, that is **BI** (PhCHN(TES)) along with unconsumed $HSiEt_3$. The product **BI** was clearly identified because its ^{1}H NMR data perfectly matched those already reported in the literature.[395] An additional heating at 50 °C for 24 h did not result in any change in the reaction mixture as it has been shown by ^{1}H NMR analysis.

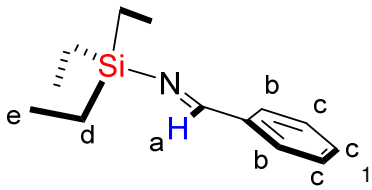

^{1}H NMR data of **BI** (CD_2Cl_2, 298 K, 400 MHz): δ = 9.06 (s, 1H, **H**$_a$), 7.80 (m, 2H, H$_b$), 7.44–7.46 (m, 3H, H$_c$), 0.99 (t, 9H, H$_e$, J = 8.0 Hz), 0.77 (q, 6H, H$_d$, J = 8.0 Hz).

***N*,*N*-bis(triethylsilyl)benzylamine**, **BA**. When the reaction was continued to be heated at 80 °C for 24 h, the ^{1}H NMR analysis (CD_2Cl_2, 298 K) showed the complete conversion of **BI** (>99%) and the exclusive formation of the bishydrosilylated product, that is *N*,*N*-bis(triethylsilyl)benzylamine **BA** ($PhCH_2N(TES)_2$), for which the characteristic chemical shifts data showed to be in accord with those already reported in the literature.[386] The product **BA** was proved to be stable within the reaction mixture, because a prolonged heating at 80 °C for 100 h had not effect on the reaction mixture as evidenced by ^{1}H NMR analysis (see spectra below).

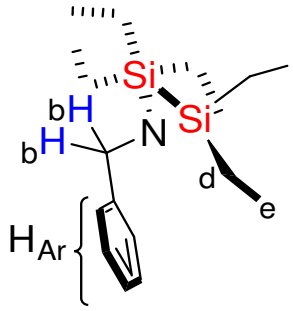

^{1}H NMR data of **BA** (CD_2Cl_2, 298 K, 400 MHz): δ = 7.29–7.40 (m, 4H, H$_{Ar}$), 7.18–7.22 (m, 1H, H$_{Ar}$), 4.20 (s, 2H, **H**$_b$), 0.96–1.01 (m, 18H, H$_e$), 0.64–0.71 (m, 12H, H$_d$).

6.4.8.3 ^{1}H NMR spectra

[395] Pérez, M.; Qu, Z. W.; Caputo, C. B.; Podgorny, V.; Hounjet, L. J.; Hansen, A.; Dobrovetsky, R.; Grimme, S.; Stephan, D. W. Hydrosilylation of Ketones, Imines and Nitriles Catalysed by Electrophilic Phosphonium Cations: Functional Group Selectivity and Mechanistic Considerations. *Chem. - A Eur. J.* **2015**, *21* (17), 6491–6500.

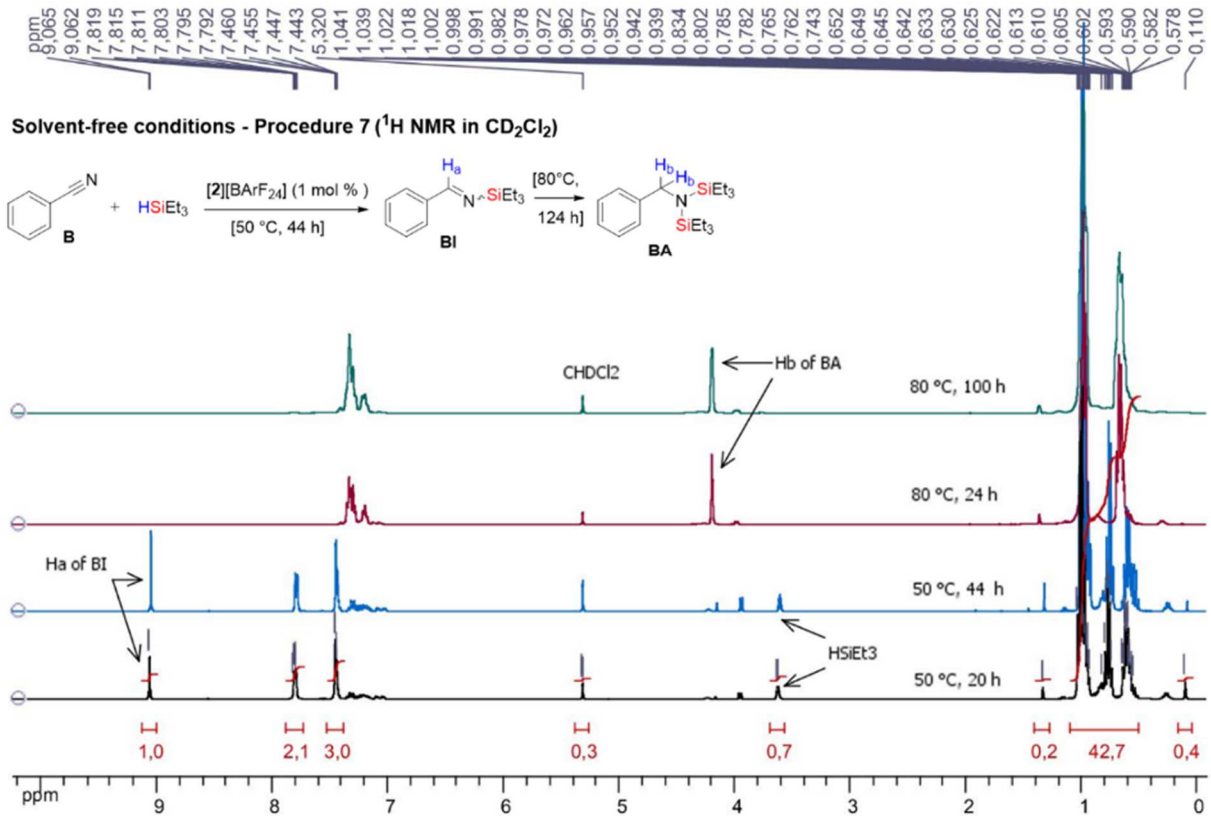
Solvent-free conditions - Procedure 7 (1H NMR in CD2Cl2)
B
HSiEt3
[2][BArF24] (1 mol %)
[50 °C, 44 h]
BI
[80°C, 124 h]
BA
CHDCl2
Hb of BA
80 °C, 100 h
80 °C, 24 h
Ha of BI
50 °C, 44 h
HSiEt3
50 °C, 20 h
1,0
2,1
3,0
0,3
0,7
0,2
42,7
0,4
ppm

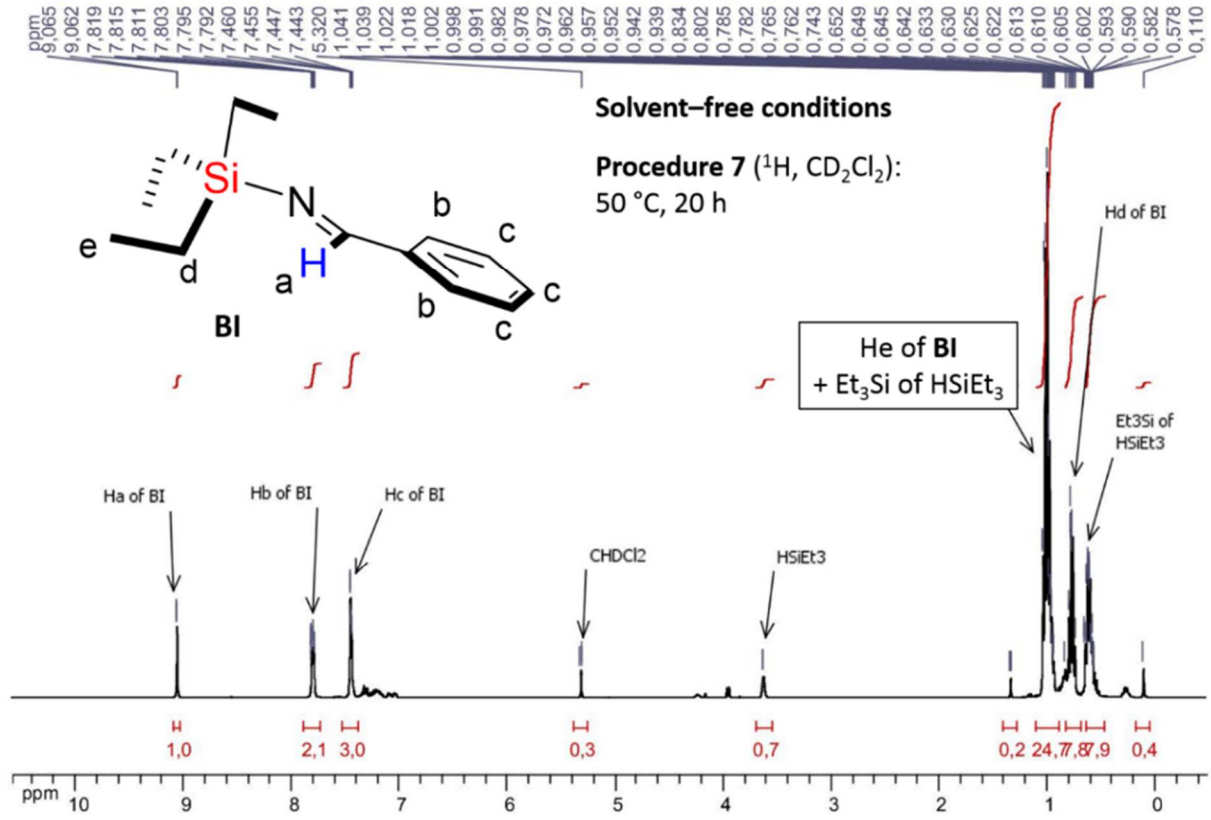
Solvent–free conditions
Procedure 7 (1H, CD2Cl2):
50 °C, 20 h
BI
Hd of BI
He of BI
+ Et3Si of HSiEt3
Et3Si of HSiEt3
Ha of BI
Hb of BI
Hc of BI
CHDCl2
HSiEt3
1,0
2,1
3,0
0,3
0,7
0,2
24,7
7,8
7,9
0,4
ppm

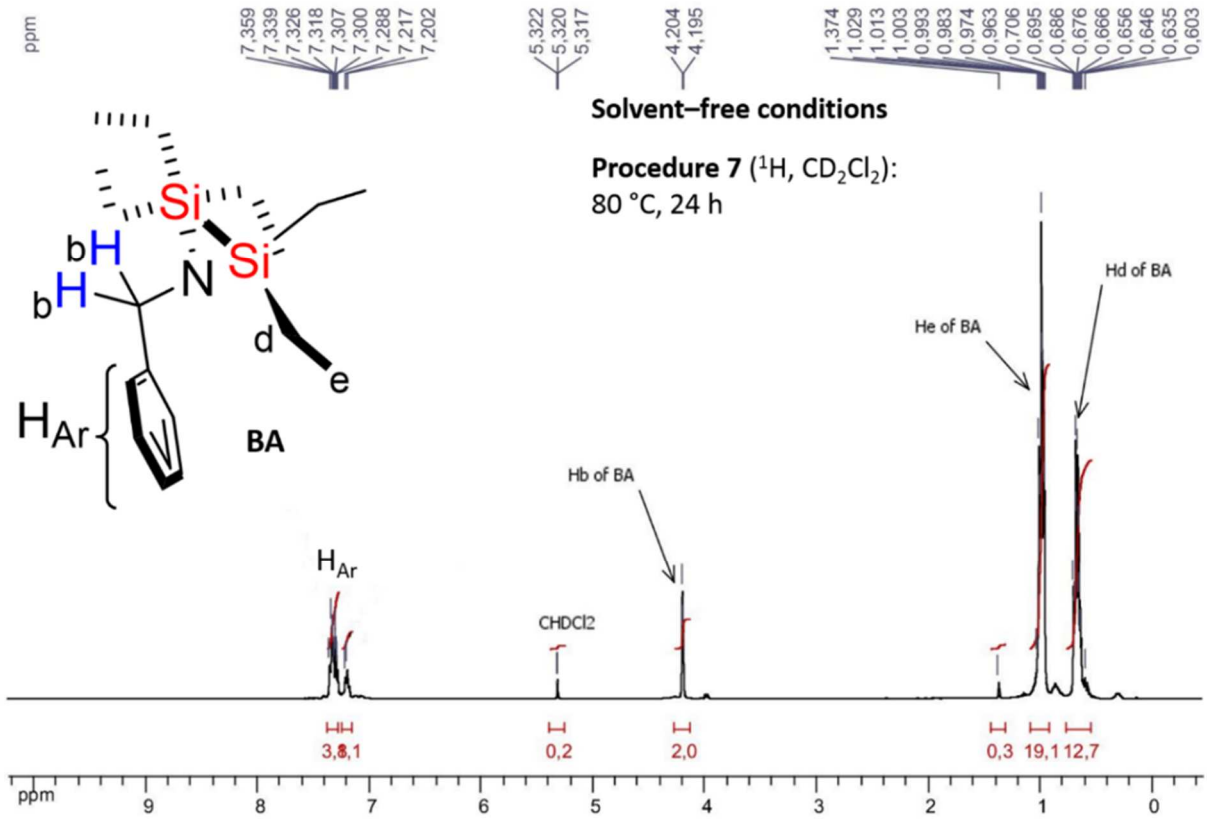
Solvent–free conditions
Procedure 7 (1H, CD2Cl2):
80 °C, 24 h
BA
HAr
Hb of BA
He of BA
Hd of BA
CHDCl2
3,8
1
0,2
2,0
0,3
19,1
12,7
ppm

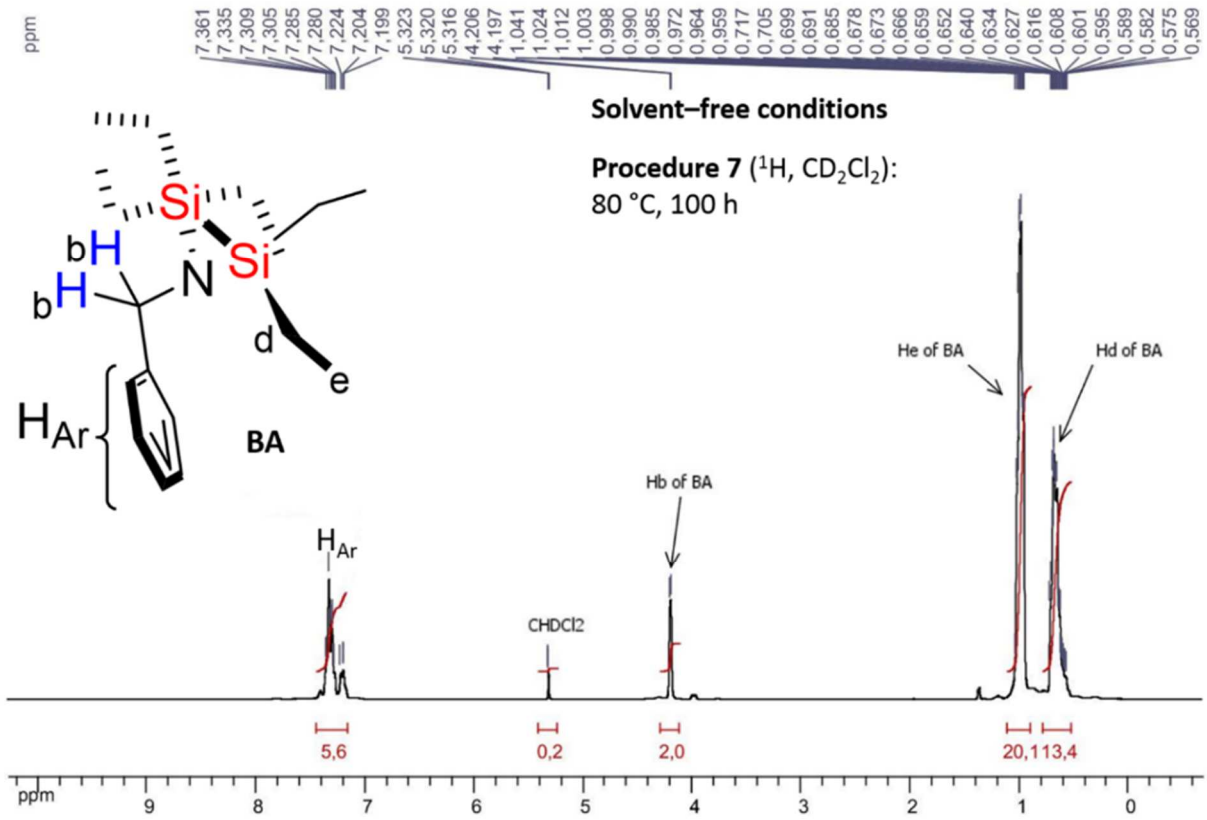
Solvent–free conditions
Procedure 7 (1H, CD2Cl2):
80 °C, 100 h
BA
HAr
Hb of BA
He of BA
Hd of BA
CHDCl2
5,6
0,2
2,0
20,1
13,4
ppm

6.4.9 Hydrosilylation of benzonitrile with CH_2Cl_2 as the solvent ([**4**][$BArF_{24}$], 0.1 mol %)

6.4.9.1 Catalytic procedure

The procedure used here was the same as the one described for the study of the proportion of the precatalyst, as reported above and the results of which are reported in table S9.

Procedure 8 ([4][$BArF_{24}$], 0.1 mol %). To a mixture of benzonitrile (0.10 mL, 0.97 mmol) and $HSiEt_3$ (0.35 mL, 2.13 mmol) was added a solution of [**4**][$BArF_{24}$] (1.4 mg, 0.0097 mmol, 0.1 mol %) in CH_2Cl_2 (0.5 mL). The reaction mixture was heated at 70 °C for 24 h. For ^{1}H NMR analysis, tri-*tert*-butylbenzene (20.3 mg, 0.0824 mmol) was added as internal reference to the reaction mixture, after which an aliquot was taken from this mixture and mixed with C_6D_6.

6.4.9.2 Discussion of the ^{1}H NMR spectrum

The ^{1}H NMR spectrum (C_6D_6, 298 K, 400 MHz) showed the total conversion of benzonitrile to the desired product *N*,*N*-bis(triethylsilyl)benzylamine **BA** (~80% yield), along with an unknown compound (~20% yield) for which a characterisitic singlet peak appeared at δ = 3.55 ppm (see spectrum below). We believe that this latter compound can be considered as intermediate because it was systemically observed when partial conversion of *N*-(triethylsilyl)benzylimine **BI** to **BA** has occured, but no traces of it could be observed when ~99% of **BA** has formed.

6.4.9.3 ^{1}H NMR spectrum

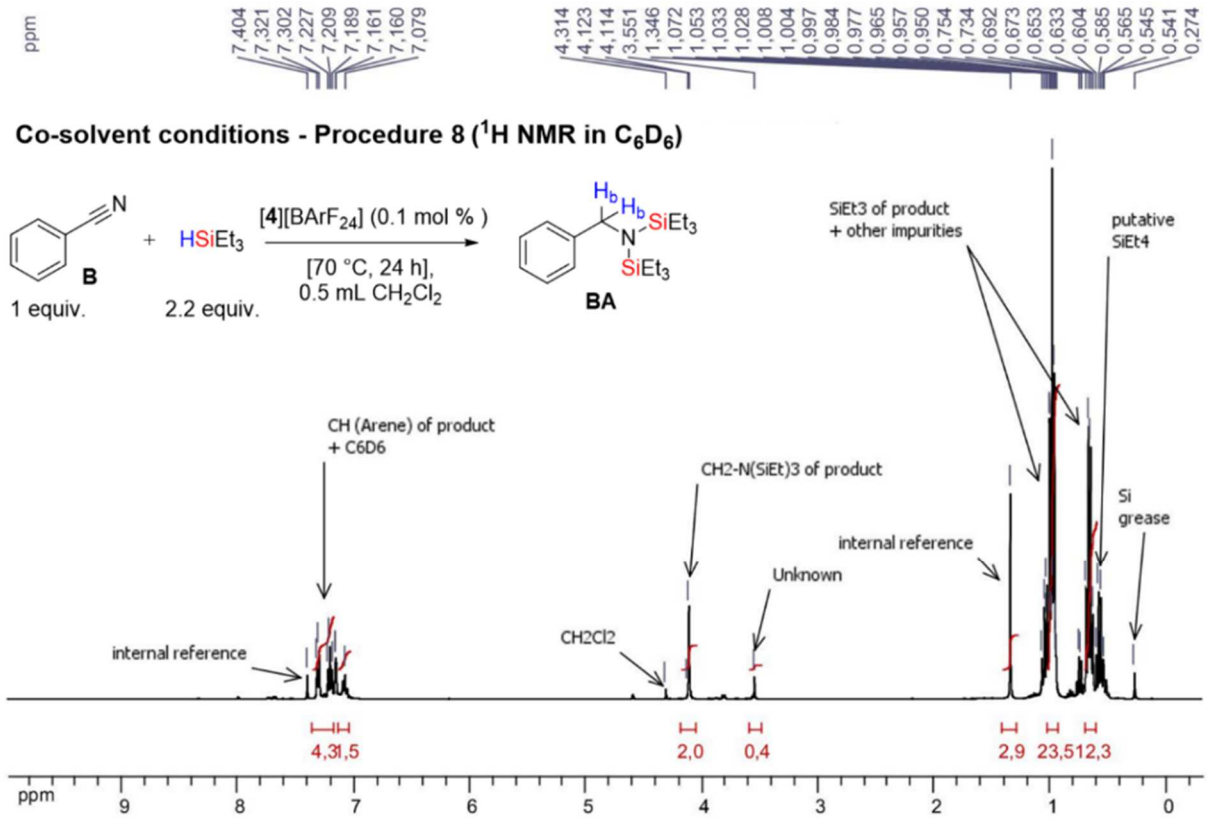

6.4.10 Substrate scope study: hetero(aryl) nitriles (table 17)

6.4.10.1 Experimental conditions

The following data detail the experimenl conditions used for the substrate scope study for which the results are reported in table 17. The general procedure for the catalytic hydrosilylation of nitriles described above was used for every substrate. For each catalytic run, the molar quantity of the substrates and the precatalyst, the time and the temperature of the reaction are specified as follows:

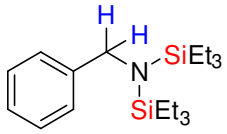

: Benzonitrile (0.10 mL, 0.97 mmol), $HSiEt_3$ (0.35 mL, 2.13 mmol), [**4**][$BArF_{24}$] (1.4 mg, 9.65×10^{-4}, 0.1 mol % mmol; 6.8 mg, 4.85×10^{-3} mmol, 0.5 mol %; or 13.7 mg, 9.70×10^{-3} mmol, 1.0 mol %), 0.5 mL of CH_2Cl_2, 6 h (1.0 mol % of [**4**][$BArF_{24}$]) or 24 h (0.5 mol % of [**4**][$BArF_{24}$]), 70 °C.

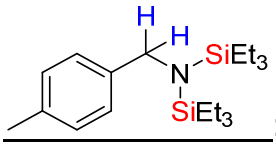

: 4-Methylbenzonitrile (0.10 mL, 0.84 mmol), $HSiEt_3$ (0.30 mL, 1.85 mmol), [**4**][$BArF_{24}$] (5.9 mg, 4.20×10^{-3} mmol, 0.5 mol %), 0.5 mL of CH_2Cl_2, 24 h, 70 °C.

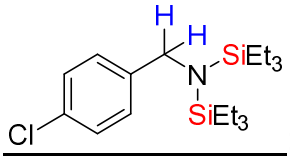

: 4-Chlorobenzonitrile (0.110 g, 0.81 mmol), $HSiEt_3$ (0.60 mL, 3.76 mmol), [**4**][$BArF_{24}$] (5.9 mg, 4.20×10^{-3} mmol, 0.5 mol %), 0.5 mL of CH_2Cl_2, 24 h, 70 °C.

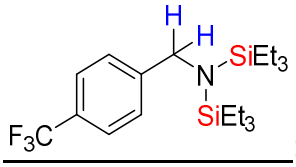

: 4-(Trifluoroethyl)benzonitrile (0.110 g, 0.86 mmol), $HSiEt_3$ (0.60 mL, 3.76 mmol), [**4**][$BArF_{24}$] (5.9 mg, 4.20×10^{-3} mmol, 0.5 mol %), 0.5 mL of CH_2Cl_2, 24 h, 70 °C.

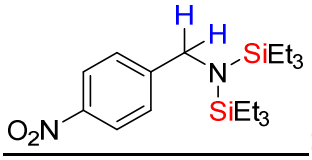

: 4-Nitrobenzonitrile (0.124 g, 0.84 mmol), $HSiEt_3$ (0.30 mL, 1.85 mmol), [**4**][$BArF_{24}$] (5.9 mg, 4.20×10^{-3} mmol, 0.5 mol %), 0.5 mL of CH_2Cl_2, 24 h, 70 °C.

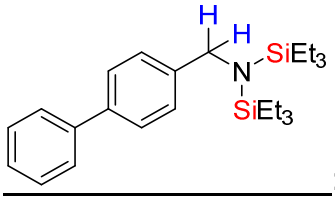

: 4-Phenylbenzonitrile (0.150 g, 0.84 mmol), $HSiEt_3$ (0.30 mL, 1.85 mmol), [**4**][$BArF_{24}$] (5.9 mg, 4.20×10^{-3} mmol, 0.5 mol %), 0.5 mL of CH_2Cl_2, 24 h, 70 °C.

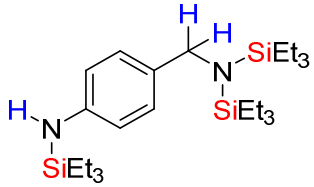

: 4-Aminobenzonitrile (0.100 g, 0.84 mmol), $HSiEt_3$ (0.30 mL, 1.85 mmol), [**4**][$BArF_{24}$] (5.9 mg, 4.20×10^{-3} mmol, 0.5 mol %), 0.5 mL of CH_2Cl_2, 24 h, 70 °C.

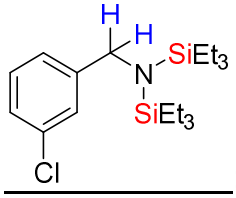

: 3-Chlorobenzonitrile (0.118 g, 0.87 mmol), $HSiEt_3$ (0.60 mL, 3.76 mmol), [**4**][$BArF_{24}$] (5.9 mg, 4.20×10^{-3} mmol, 0.5 mol %), 0.5 mL of CH_2Cl_2, 24 h, 70 °C.

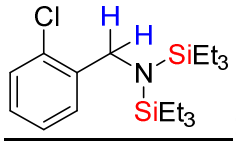

: 2-Chlorobenzonitrile (0.116 g, 0.84 mmol), $HSiEt_3$ (0.30 mL, 1.85 mmol), [**4**][$BArF_{24}$] (5.9 mg, 4.20×10^{-3} mmol, 0.5 mol %), 0.5 mL of CH_2Cl_2, 24 h, 70 °C.

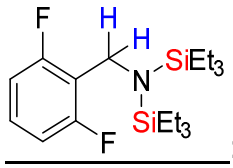

: 2,6-Difluorobenzonitrile (0.117 g, 0.84 mmol), $HSiEt_3$ (0.30 mL, 1.85 mmol), [**4**][$BArF_{24}$] (5.9 mg, 4.20×10^{-3} mmol, 0.5 mol %), 0.5 mL of CH_2Cl_2, 24 h, 70 °C.

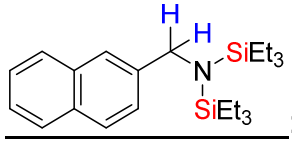

: 2-Naphthonitrile (0.129 g, 0.84 mmol), $HSiEt_3$ (0.30 mL, 1.85 mmol), [**4**][$BArF_{24}$] (5.9 mg, 4.20×10^{-3} mmol, 0.5 mol %), 0.5 mL of CH_2Cl_2, 24 h, 70 °C.

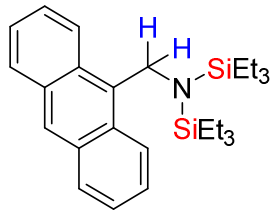

: Anthracene-9-carbonitrile (0.171 g, 0.84 mmol), $HSiEt_3$ (0.30 mL, 1.85 mmol), [**4**][$BArF_{24}$] (5.9 mg, 4.20×10^{-3} mmol, 0.5 mol %), 0.5 mL of CH_2Cl_2, 24 h, 70 °C.

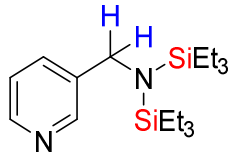

: Picolinonitrile (0.087 g, 0.84 mmol), $HSiEt_3$ (0.30 mL, 1.85 mmol), [**4**][$BArF_{24}$] (5.9 mg, 4.20×10^{-3} mmol, 0.5 mol %), 0.5 mL of CH_2Cl_2, 24 h, 70 °C.

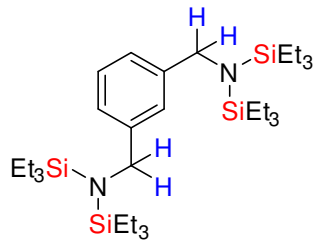

: Isophthalonitrile (0.108 g, 0.84 mmol), $HSiEt_3$ (0.30 mL, 1.85 mmol), [**4**][$BArF_{24}$] (5.9 mg, 4.20×10^{-3} mmol, 0.5 mol %), 0.5 mL of CH_2Cl_2, 24 h, 70 °C.

6.4.10.2 NMR data of the products

The structural identity of each bis(silyl) benzylamine which is produced during the substrate scope study has been confirmed by ^{1}H NMR analysis. For the products that have been already reported in the literature along with their characterization data, all our ^{1}H NMR data matched those reported (table S11). However, the products for which the NMR spectroscopic data are not published yet, their characteristic ^{1}H NMR chemical shifts (δ, ppm) are provided in table S11. The ^{1}H NMR spectra for all the products are also given in the next section.

Table S11. Hydrosilylation of hetero(aryl) nitriles: NMR spectroscopic data of the products.

Nitrile + $HSiEt_3$	**Our NMR data or related literature references**
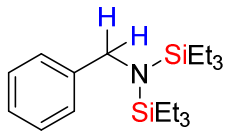	Pérez, M.; Qu, Z. W.; Caputo, C. B.; Podgorny, V.; Hounjet, L. J.; Hansen, A.; Dobrovetsky, R.; Grimme, S.; Stephan, D. W. Hydrosilylation of Ketones, Imines and Nitriles Catalysed by Electrophilic Phosphonium Cations: Functional Group Selectivity and Mechanistic Considerations. *Chem. - A Eur. J.* **2015**, *21* (17), 6491–6500.
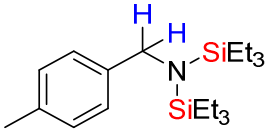	**^{1}H (C_6D_6, 298 K, 400 MHz)**: δ = 7.23 (d, 2H Ar, J = 7.8 Hz), 7.03 (d, 2H Ar, J = 7.8 Hz), 4.11 (s, 2H CH_2), 0.98–1.02 (t, 18H CH_3CH_2Si, J = 7.8 Hz), 0.68 (q, 12H CH_3CH_2Si, J = 7.8 Hz).
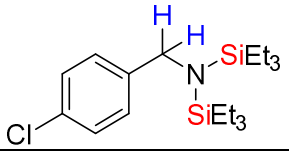	**^{1}H (C_6D_6, 298 K, 400 MHz)**: δ = 7.15–7.19 (m, 2H Ar), 7.08–7.10 (m, 2H Ar), 3.98 (s, 2H CH_2), 0.96 (t, 18H CH_3CH_2Si, J = 8.1 Hz; overlapping with signals of $HSiEt_3$), 0.62 (q, 12H CH_3CH_2Si, J = 8.1 Hz; overlapping v).
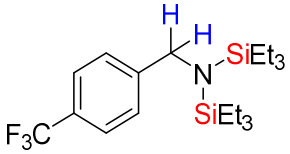	**^{1}H (C_6D_6, 298 K, 400 MHz)**: δ = 7.40 (d, 2H Ar), 7.18 (d, 2H Ar), 3.99 (s, 2H CH_2), 1.01 (t, 18H CH_3CH_2Si, J = 8.1 Hz; overlapping with signals of $HSiEt_3$), 0.59 (q, 12H CH_3CH_2Si, J = 8.1 Hz; overlapping with signals of $HSiEt_3$).
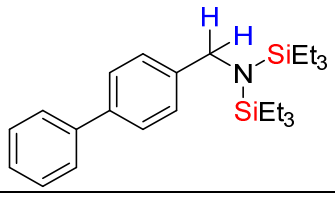	**^{1}H (C_6D_6, 298 K, 400 MHz)**: δ = 7.51 (d, 2H Ar, J = 8.0 Hz), 7.50 (d, 2H Ar, J = 8.0 Hz), 7.37 (d, 2H Ar, J = 8.0 Hz), 7.20–7.24 (m, 3H Ar), 4.17 (s, 2H CH_2), 1.02 (t, 18H CH_3CH_2Si, J = 7.9 Hz), 0.71 (q, 12H CH_3CH_2Si, J = 8.0 Hz).
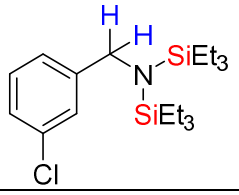	**^{1}H (C_6D_6, 298 K, 400 MHz)**: δ = 7.42 (s, 1H Ar), 7.03 (m, 2H Ar, J = 8.2 Hz), 6.90 (t, 1H Ar, J = 7.7 Hz), 3.97 (s, 2H CH_2), 0.96 (t, 18H CH_3CH_2Si, J = 7.7 Hz; overlapping with other $SiEt_3$-like signals), 0.61 (q, 12H CH_3CH_2Si, J = 7.9 Hz; overlapping with other $SiEt_3$-like signals).
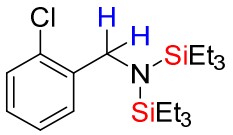	**^{1}H (C_6D_6, 298 K, 400 MHz)**: δ = 7.72 (d, 1H Ar, J = 8.1 Hz), 7.17 (d, 1H Ar, J = 8.1 Hz), 7.07 (t, 1H Ar, J = 7.7 Hz), 6.82 (t, 1H Ar, J = 7.7 Hz), 4.37 (s, 2H CH_2), 0.97 (t, 18H CH_3CH_2Si, J = 7.7 Hz), 0.65 (q, 12H CH_3CH_2Si, J = 7.7 Hz).
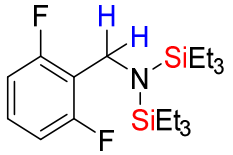	**^{1}H (C_6D_6, 298 K, 400 MHz)**: δ = 6.59-6.62 (m, 1H Ar), 6.48-6.52 (m, 2H Ar), 7.07 (t, 1H Ar, J = 7.7 Hz), 6.82 (t, 1H Ar, J = 7.7 Hz), 4.22 (s, 2H CH_2), 0.99 (t, 18H CH_3CH_2Si, J = 7.7 Hz), 0.71 (q, 12H CH_3CH_2Si, J = 7.7 Hz).
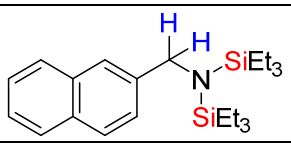	**^{1}H (C_6D_6, 298 K, 400 MHz)**: δ = 7.87 (s, 1H Ar), 7.76 (d, 2H Ar, J = 8.1 Hz), 7.64 (t, 2H Ar, J = 8.1 Hz), 7.23–7.33 (m, 3H Ar), 4.26 (s, 2H CH_2), 1.00 (t, 18H CH_3CH_2Si, J = 8.0 Hz), 0.69 (q, 12H CH_3CH_2Si, J = 8.0 Hz).

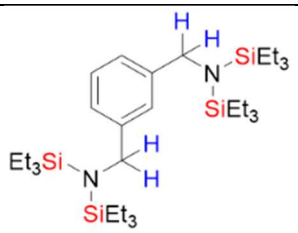

^{1}H (C_6D_6, 298 K, 400 MHz): δ = 7.29 (m, 4H Ar), 4.22 (s, 4H CH_2), 1.01 (t, 36H CH_3CH_2Si, J = 8.0 Hz), 0.70 (q, 24H CH_3CH_2Si, J = 8.0 Hz).

6.4.10.3 ^{1}H NMR spectra (C_6D_6, 400 MHz, 298 K)

In this section, we provide the copies of the ^{1}H NMR spectra that were recorded for the reaction mixture of each catalytic run involving the related nitrile substrate. Depending on the substrate, the time at which the ^{1}H NMR analysis was done varies from 6 to 24 hours and the molar stoichiometry of $HSiEt_3$ relative to the nitrile was either 2.2 or 4.6 equivalents. All the reactions were conducted at 70 °C without solvent or with CH_2Cl_2 (0.5 mL) as solvent and using [**4**][$BarF_{24}$] (0.5 or 1.0 mol %) as precatalyst. For more details about the general procedure and the specific conditions applied to every catalytic run of the specific nitrile substrate, see the previous sections of the experimental part (table S11); for the related NMR yields that were determined for every product, the reader is refered to table 17 of the manuscript.

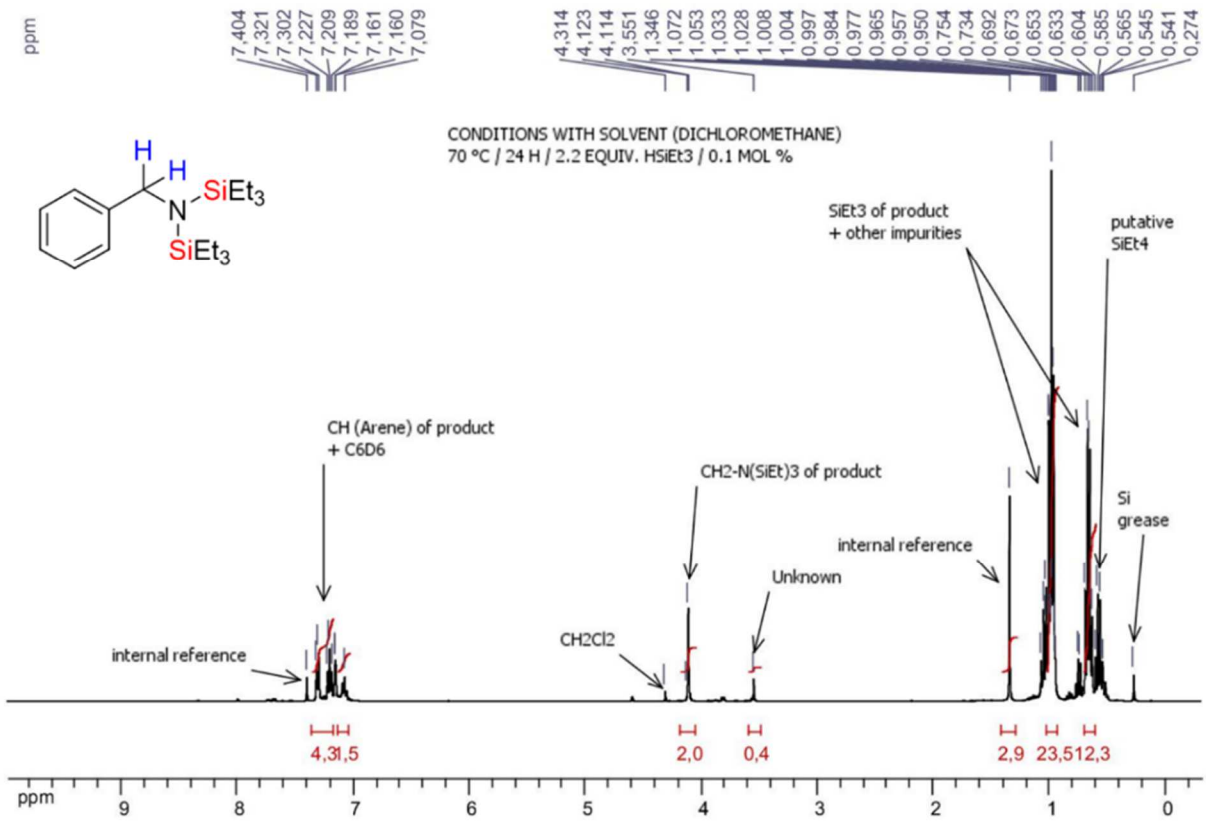

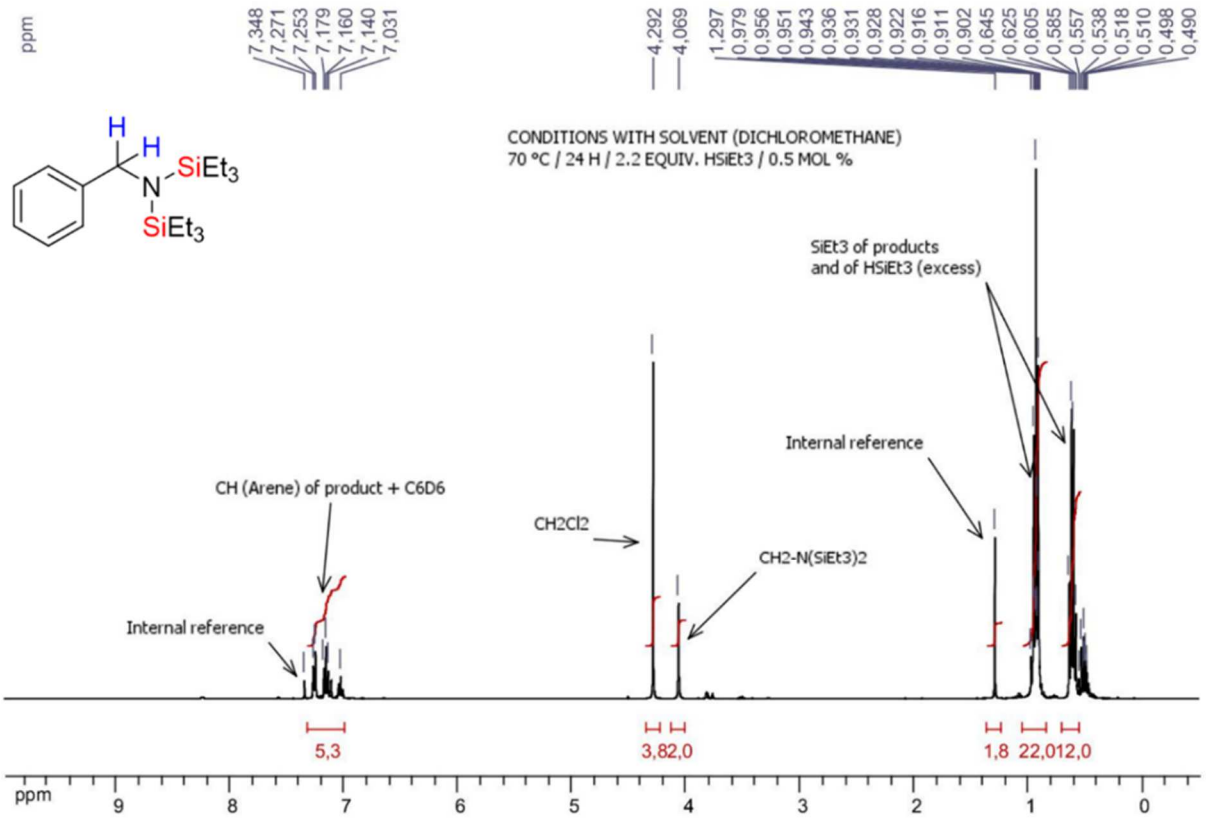
ppm
7,348
7,271
7,253
7,179
7,160
7,140
7,031
4,292
4,069
1,297
0,979
0,956
0,951
0,943
0,936
0,931
0,928
0,922
0,916
0,911
0,902
0,645
0,625
0,605
0,585
0,557
0,538
0,518
0,510
0,498
0,490
H
H
SiEt3
N
SiEt3
CONDITIONS WITH SOLVENT (DICHLOROMETHANE)
70 °C / 24 H / 2.2 EQUIV. HSiEt3 / 0.5 MOL %
SiEt3 of products
and of HSiEt3 (excess)
Internal reference
CH (Arene) of product + C6D6
CH2Cl2
CH2-N(SiEt3)2
Internal reference
5,3
3,82,0
1,8
22,012,0
ppm
9
8
7
6
5
4
3
2
1
0

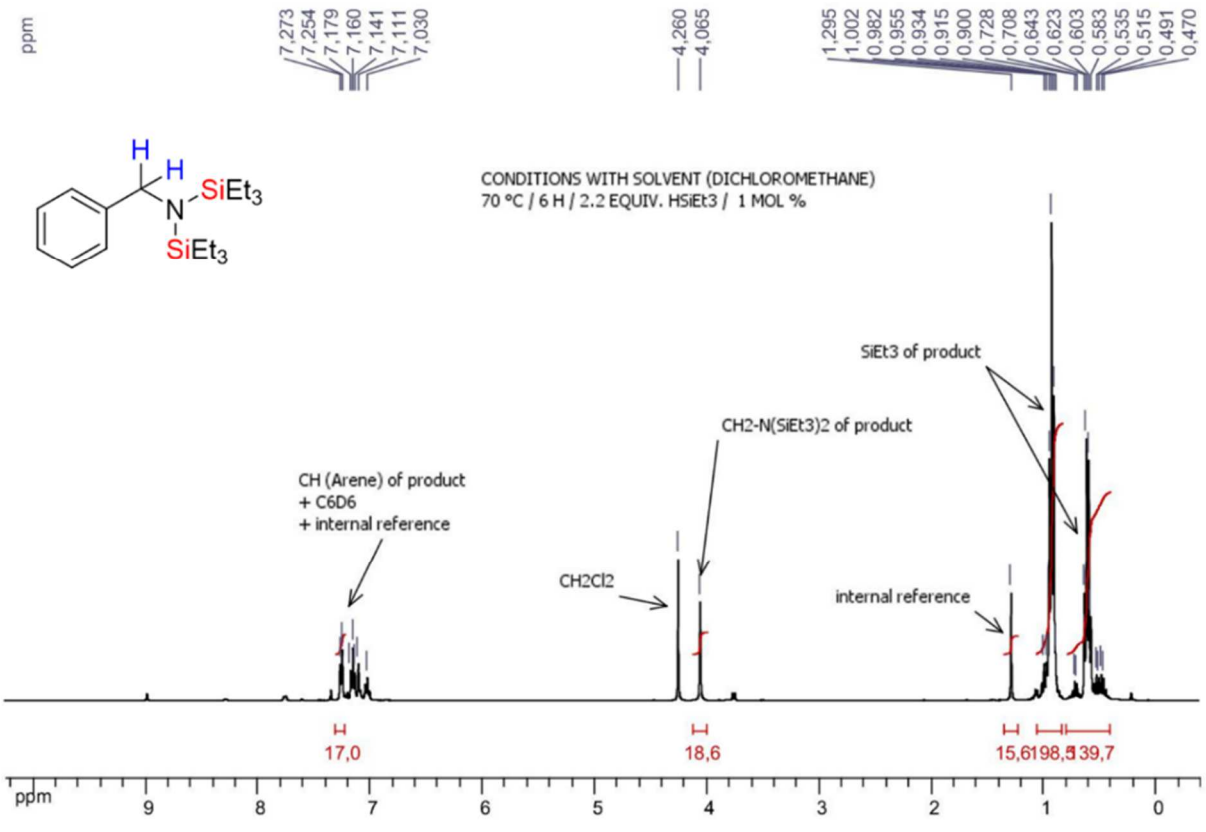
ppm
7,273
7,254
7,179
7,160
7,141
7,111
7,030
4,260
4,065
1,295
1,002
0,982
0,955
0,934
0,915
0,900
0,728
0,708
0,643
0,623
0,603
0,583
0,535
0,515
0,491
0,470
H
H
SiEt3
N
SiEt3
CONDITIONS WITH SOLVENT (DICHLOROMETHANE)
70 °C / 6 H / 2.2 EQUIV. HSiEt3 / 1 MOL %
SiEt3 of product
CH2-N(SiEt3)2 of product
CH (Arene) of product
+ C6D6
+ internal reference
CH2Cl2
internal reference
17,0
18,6
15,6198,5139,7
ppm
9
8
7
6
5
4
3
2
1
0

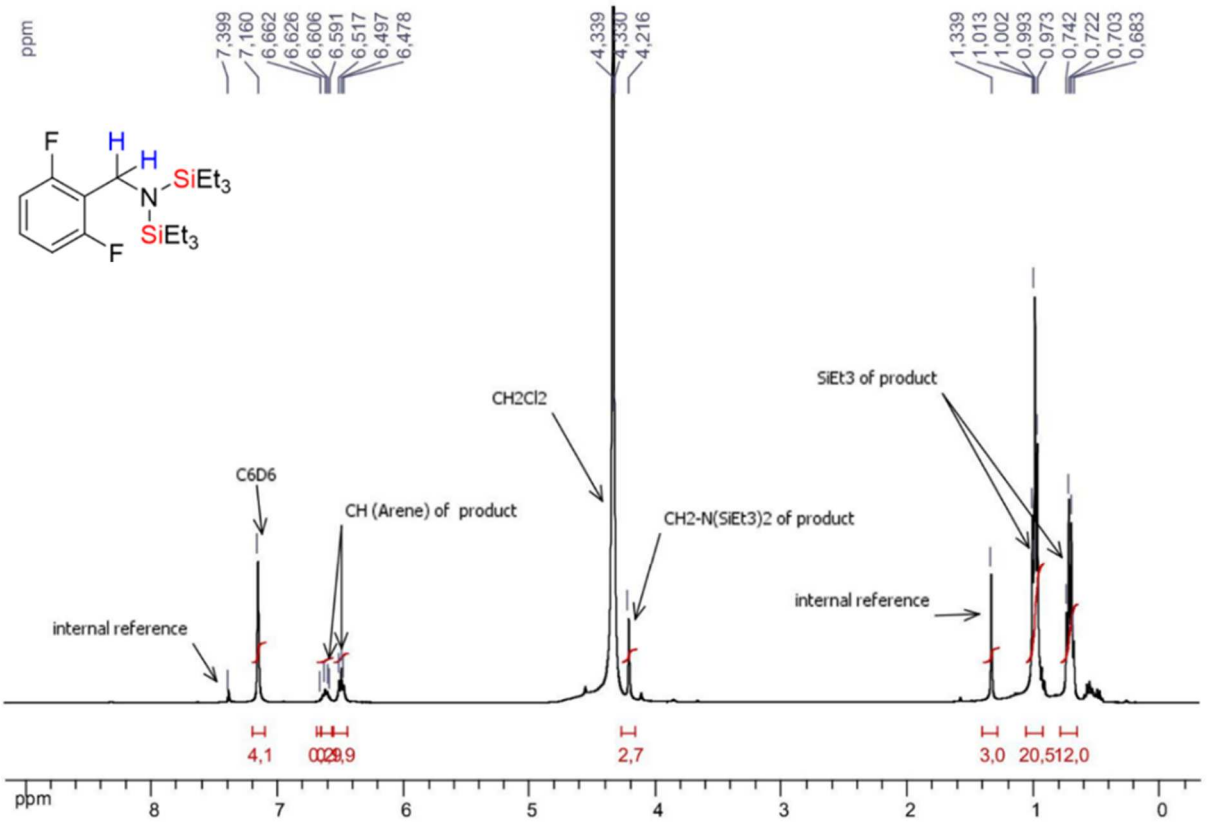
ppm
7,399
7,160
6,662
6,626
6,606
6,591
6,517
6,497
6,478
4,339
4,330
4,216
1,339
1,013
1,002
0,993
0,973
0,742
0,722
0,703
0,683
F
H
H
SiEt3
N
SiEt3
F
C6D6
CH (Arene) of product
CH2Cl2
CH2-N(SiEt3)2 of product
SiEt3 of product
internal reference
internal reference
4,1
2,7
3,0
20,5
12,0
ppm
8
7
6
5
4
3
2
1
0

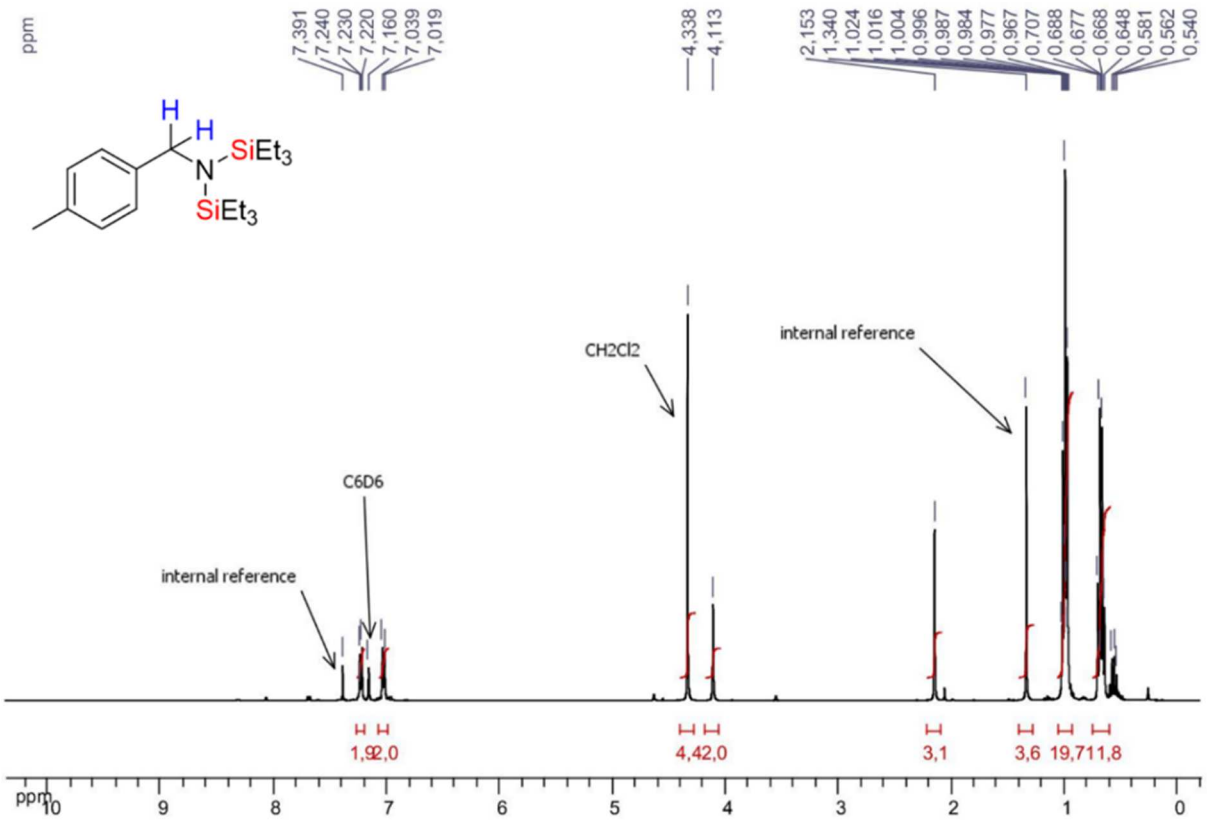
ppm
7,391
7,240
7,230
7,220
7,160
7,039
7,019
4,338
4,113
2,153
1,340
1,024
1,016
1,004
0,996
0,987
0,984
0,977
0,967
0,707
0,688
0,677
0,668
0,648
0,581
0,562
0,540
H
H
SiEt3
N
SiEt3
CH2Cl2
internal reference
C6D6
internal reference
1,9
2,0
4,4
2,0
3,1
3,6
19,7
11,8
ppm
10
9
8
7
6
5
4
3
2
1
0

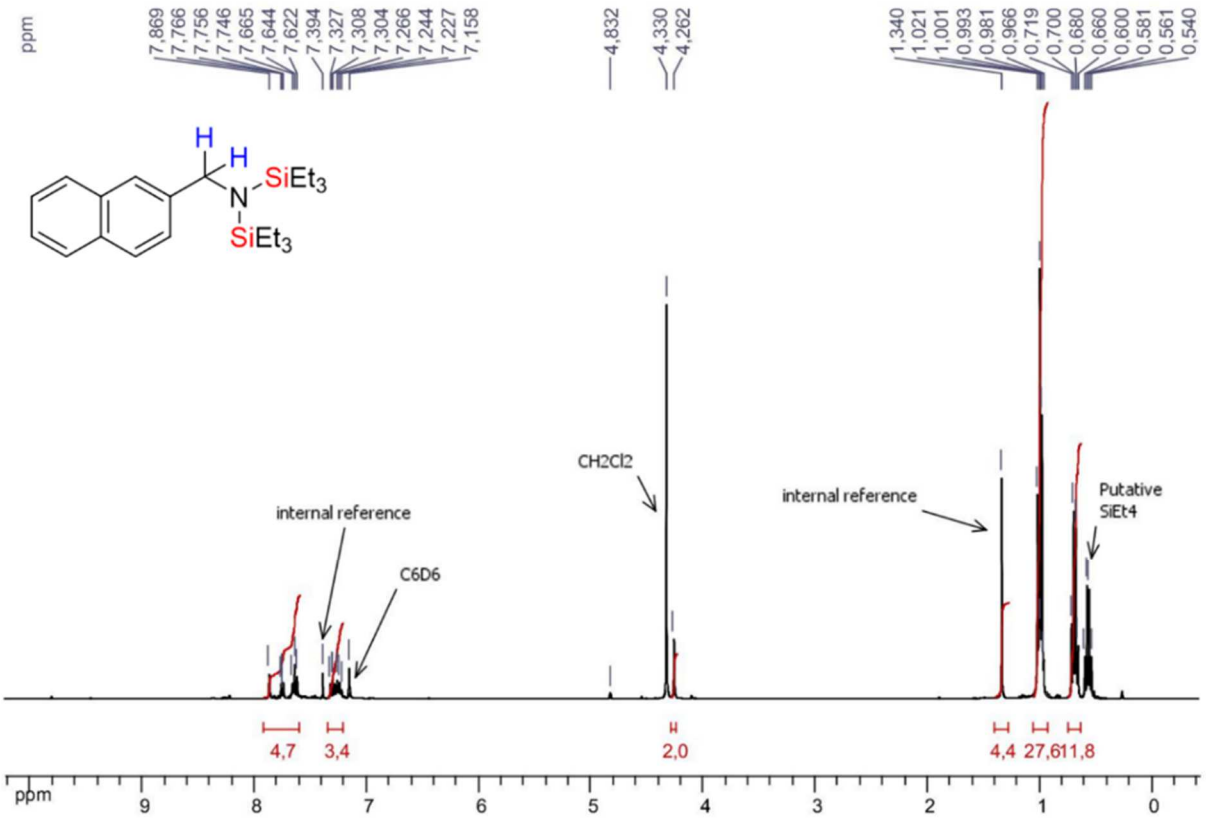
ppm
7,869
7,766
7,756
7,746
7,665
7,644
7,622
7,394
7,327
7,308
7,304
7,266
7,244
7,227
7,158
4,832
4,330
4,262
1,340
1,021
1,001
0,993
0,981
0,966
0,719
0,700
0,680
0,660
0,600
0,581
0,561
0,540
H
H
SiEt3
N
SiEt3
CH2Cl2
internal reference
C6D6
internal reference
Putative
SiEt4
4,7
3,4
2,0
4,4
27,6
11,8
ppm
9
8
7
6
5
4
3
2
1
0

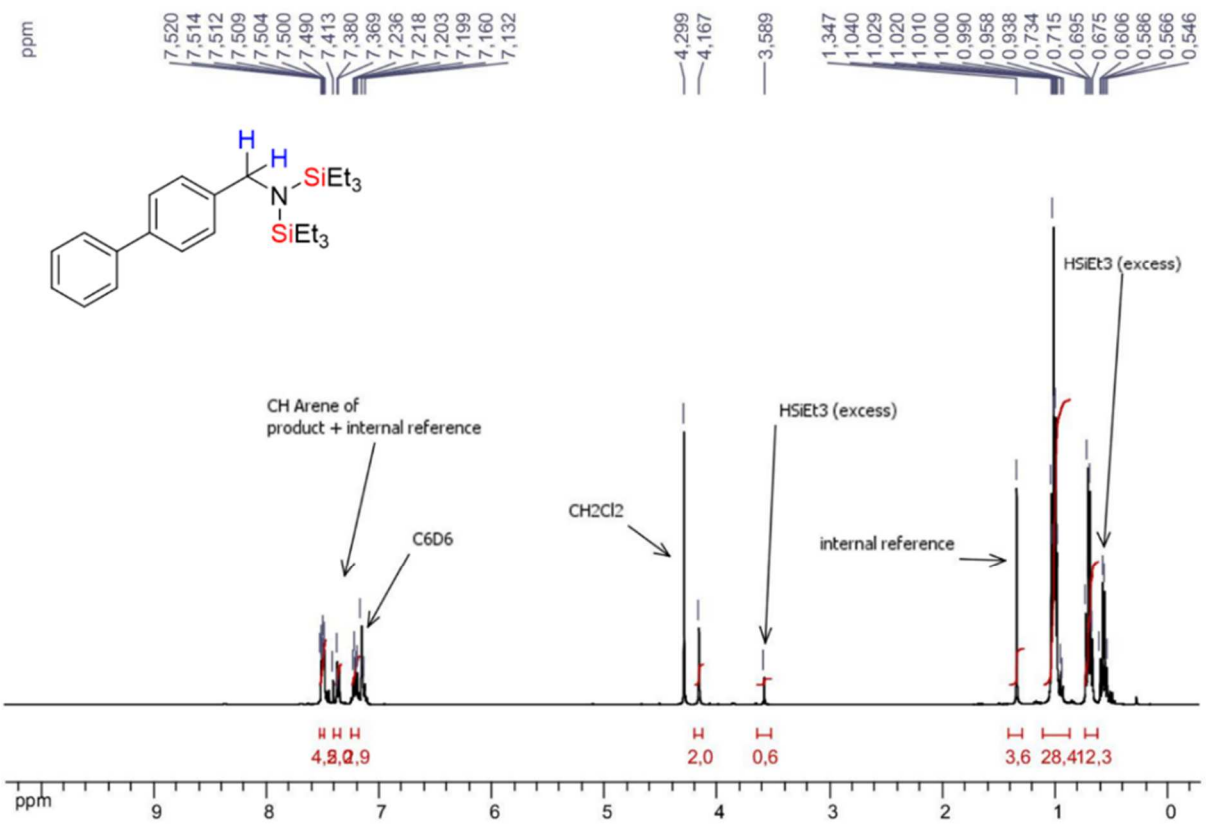
ppm
7,520
7,514
7,512
7,509
7,504
7,500
7,490
7,413
7,380
7,369
7,236
7,218
7,203
7,199
7,160
7,132
4,299
4,167
3,589
1,347
1,040
1,029
1,020
1,010
1,000
0,990
0,958
0,938
0,734
0,715
0,695
0,675
0,606
0,586
0,566
0,546
H
H
SiEt3
N
SiEt3
HSiEt3 (excess)
CH Arene of
product + internal reference
HSiEt3 (excess)
C6D6
CH2Cl2
internal reference
2,0
0,6
3,6
28,4
12,3
ppm
9
8
7
6
5
4
3
2
1
0

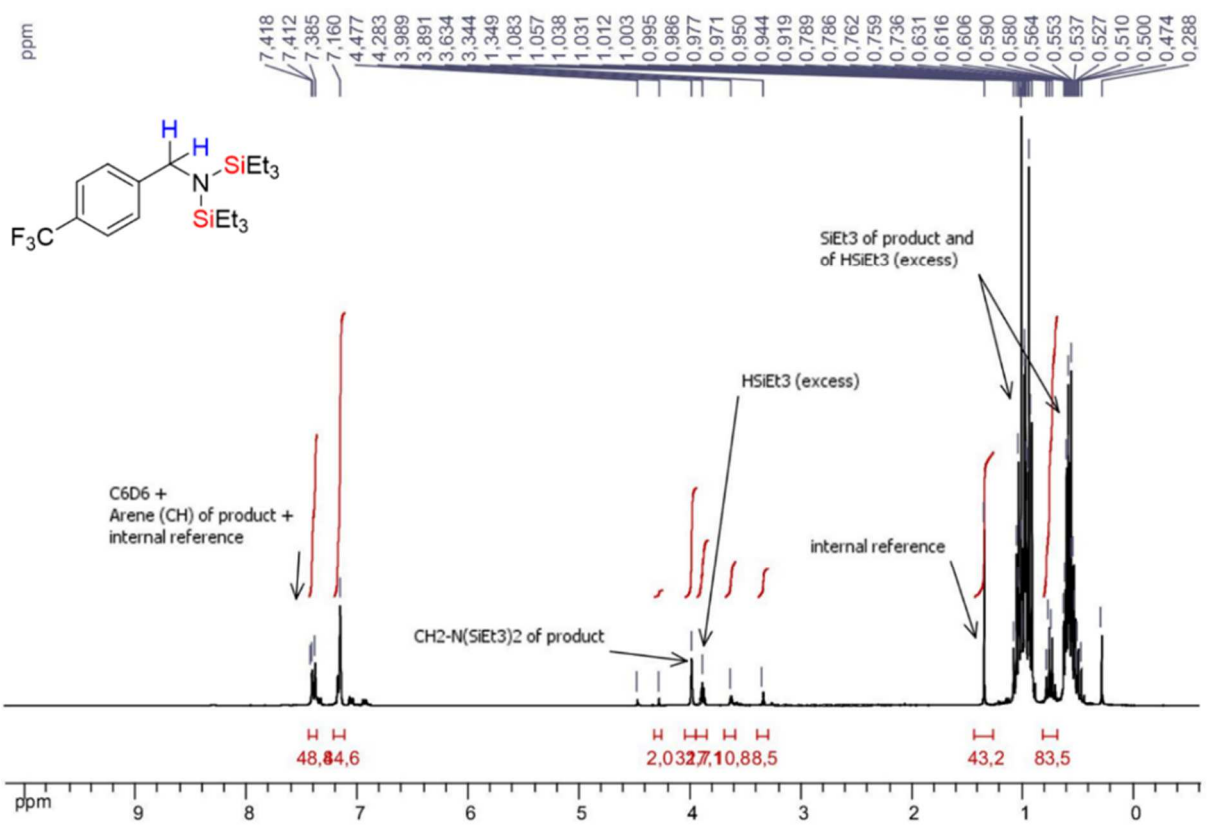
ppm
7,418
7,412
7,385
7,160
4,477
4,283
3,989
3,891
3,634
3,344
1,349
1,083
1,057
1,038
1,031
1,012
1,003
0,995
0,986
0,977
0,971
0,950
0,944
0,919
0,789
0,786
0,762
0,759
0,736
0,631
0,616
0,606
0,590
0,580
0,564
0,553
0,537
0,527
0,510
0,500
0,474
0,288
H
H
SiEt3
N
SiEt3
F3C
SiEt3 of product and
of HSiEt3 (excess)
HSiEt3 (excess)
C6D6 +
Arene (CH) of product +
internal reference
internal reference
CH2-N(SiEt3)2 of product
48,8
4,6
2,0
3
2,7
1,1
0,8
8,5
43,2
83,5
ppm
9
8
7
6
5
4
3
2
1
0

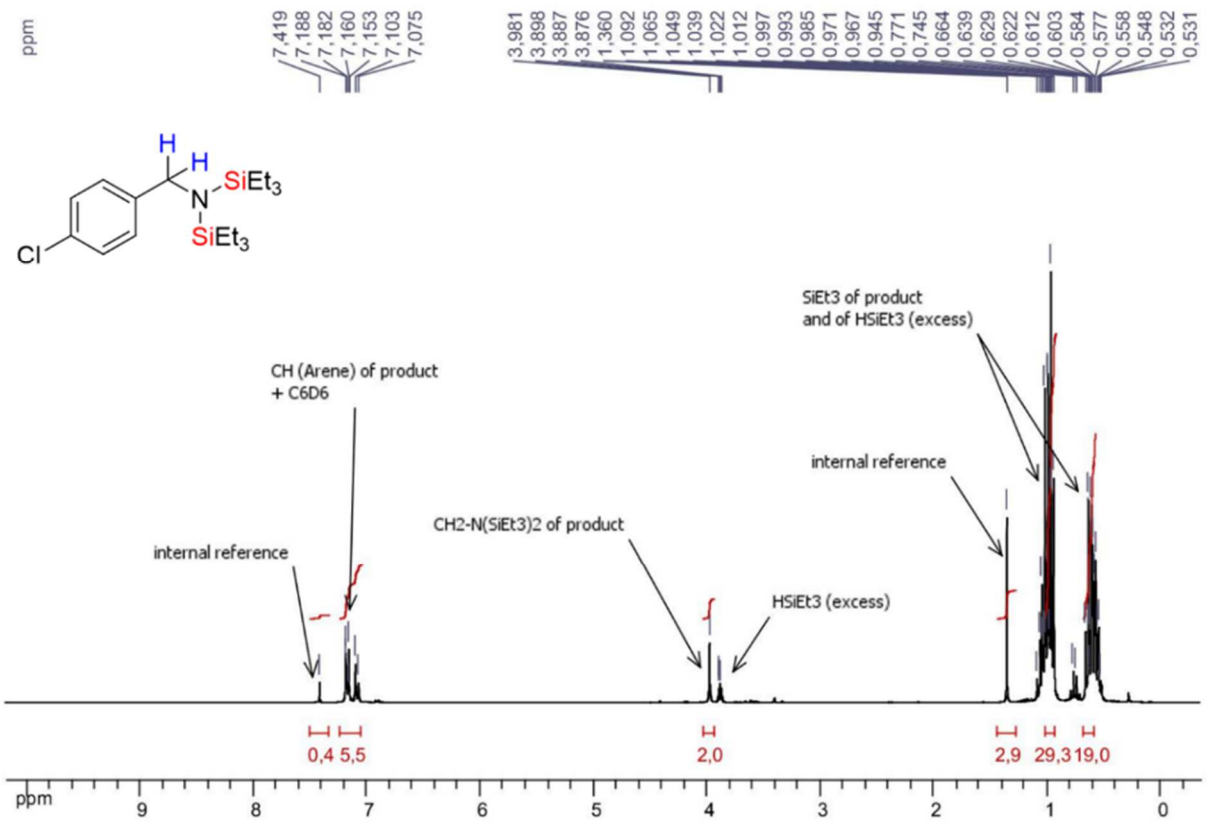
ppm
7,419
7,188
7,182
7,160
7,153
7,103
7,075
3,981
3,898
3,887
3,876
1,360
1,092
1,065
1,049
1,039
1,022
1,012
0,997
0,993
0,985
0,971
0,967
0,945
0,771
0,745
0,664
0,639
0,629
0,622
0,612
0,603
0,584
0,577
0,558
0,548
0,532
0,531
H
H
SiEt3
N
SiEt3
Cl
SiEt3 of product
and of HSiEt3 (excess)
CH (Arene) of product
+ C6D6
internal reference
internal reference
CH2-N(SiEt3)2 of product
HSiEt3 (excess)
0,4
5,5
2,0
2,9
29,3
19,0
ppm
9
8
7
6
5
4
3
2
1
0

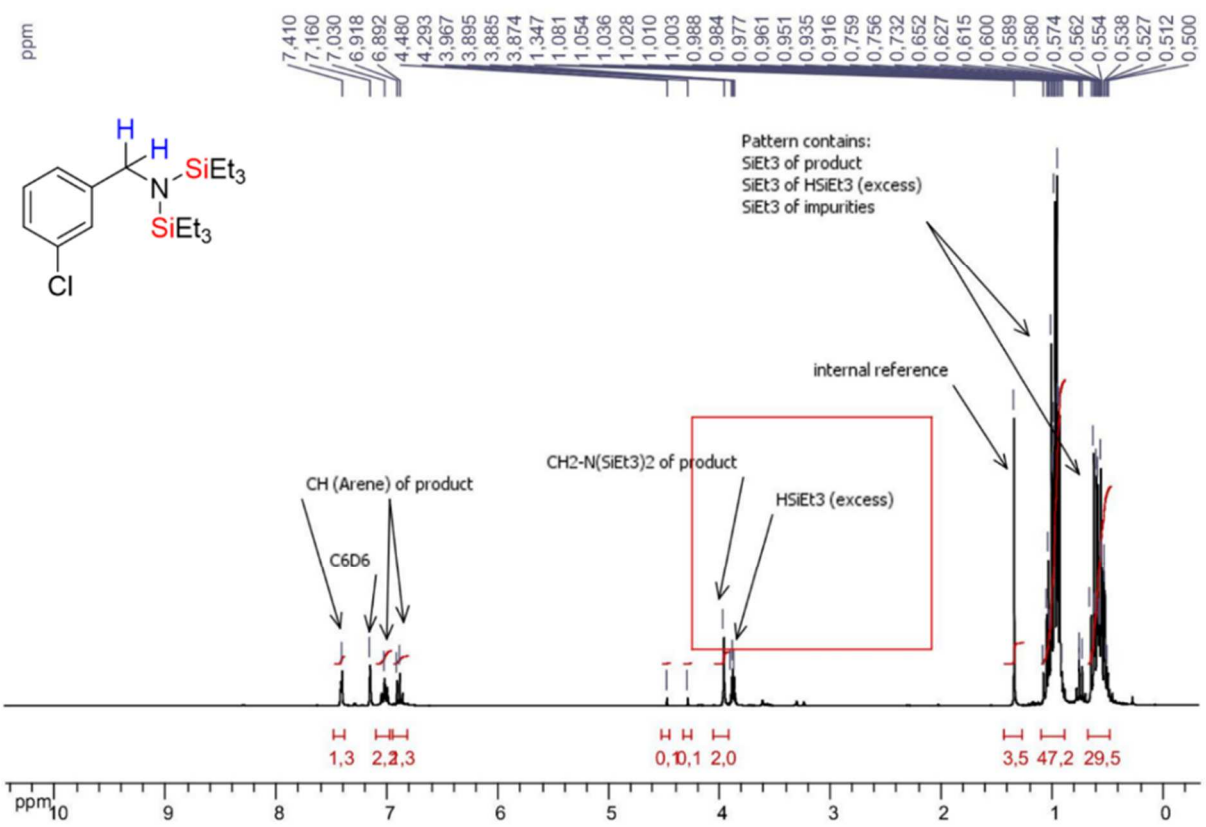
ppm
7,410
7,160
7,030
6,918
6,892
4,480
4,293
3,967
3,895
3,885
3,874
1,347
1,081
1,054
1,036
1,028
1,010
1,003
0,988
0,984
0,977
0,961
0,951
0,935
0,916
0,759
0,756
0,732
0,652
0,627
0,615
0,600
0,589
0,580
0,574
0,562
0,554
0,538
0,527
0,512
0,500
H
H
SiEt3
N
SiEt3
Cl
Pattern contains:
SiEt3 of product
SiEt3 of HSiEt3 (excess)
SiEt3 of impurities
internal reference
CH2-N(SiEt3)2 of product
HSiEt3 (excess)
CH (Arene) of product
C6D6
1,3
2,2
2,3
0,1
0,1
2,0
3,5
47,2
29,5
ppm
10
9
8
7
6
5
4
3
2
1
0

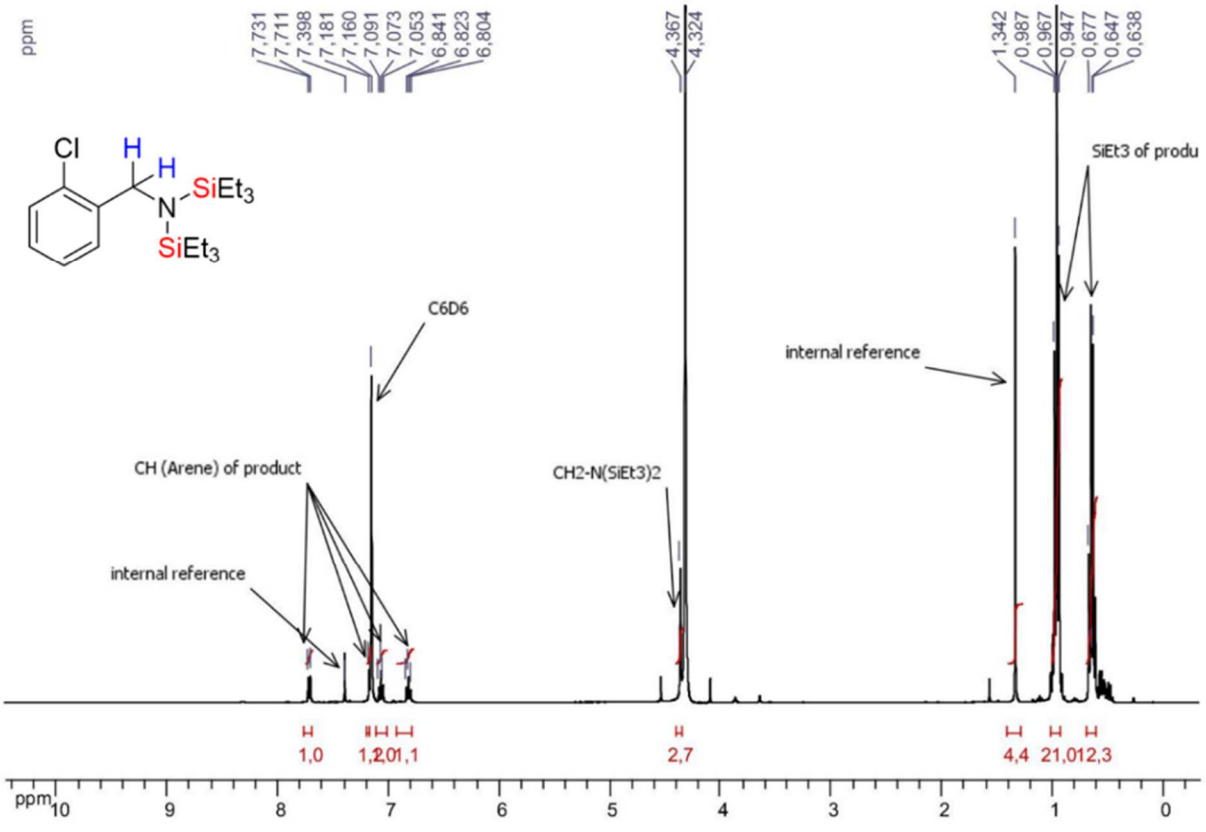
ppm
7,731
7,711
7,398
7,181
7,160
7,091
7,073
7,053
6,841
6,823
6,804
4,367
4,324
1,342
0,987
0,967
0,947
0,677
0,647
0,638
Cl
H
H
SiEt3
N
SiEt3
SiEt3 of produ
C6D6
internal reference
CH (Arene) of product
CH2-N(SiEt3)2
internal reference
1,0
1,2
2,0
1,1
2,7
4,4
21,0
12,3
ppm
10
9
8
7
6
5
4
3
2
1
0

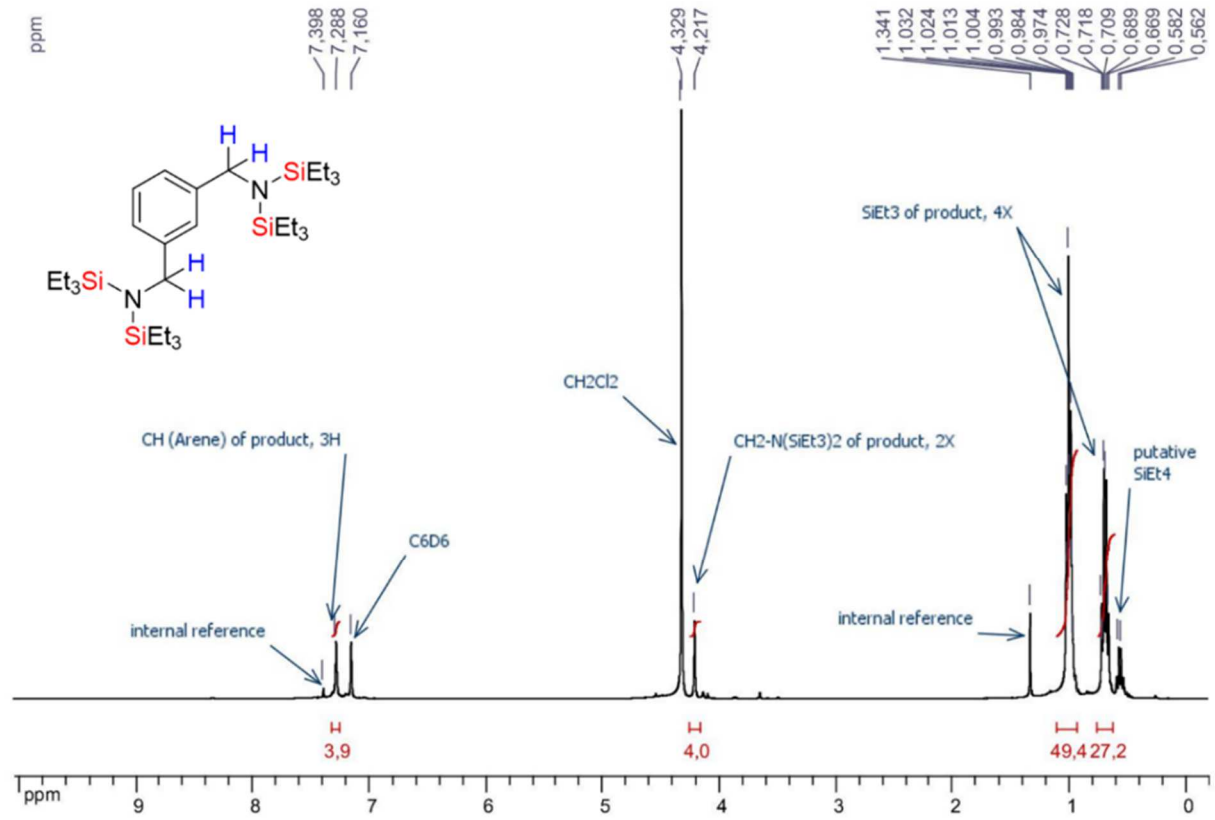
ppm
7,398
7,288
7,160
4,329
4,217
1,341
1,032
1,024
1,013
1,004
0,993
0,984
0,974
0,728
0,718
0,709
0,689
0,669
0,582
0,562
SiEt3 of product, 4X
CH2Cl2
CH (Arene) of product, 3H
CH2-N(SiEt3)2 of product, 2X
putative SiEt4
C6D6
internal reference
internal reference
3,9
4,0
49,4
27,2
ppm

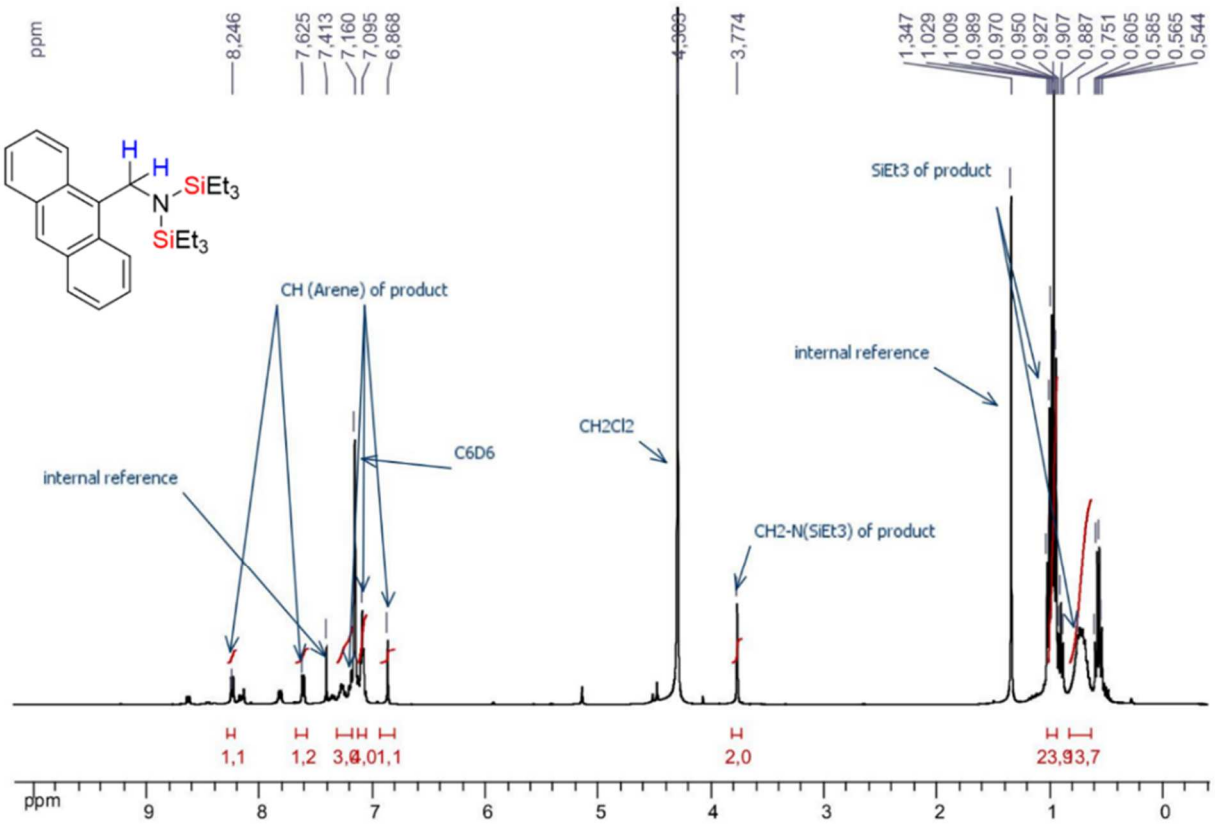
ppm
8,246
7,625
7,413
7,160
7,095
6,868
4,369
3,774
1,347
1,029
1,009
0,989
0,970
0,950
0,927
0,907
0,887
0,751
0,605
0,585
0,565
0,544
SiEt3 of product
CH (Arene) of product
internal reference
CH2Cl2
C6D6
internal reference
CH2-N(SiEt3) of product
1,1
1,2
2,0
23,9
3,7
ppm

6.5 Experiments related to Chapter 4: Catalytic C–F bond activation

6.5.1 Preliminary investigations: HDF reaction of fluorobenzene

6.5.1.1 Catalytic procedures

As depicted in scheme 53 of the manuscript, and in scheme S6 below, the attempt of the HDF reaction of fluorobenzene was carried out following the procedures 1a–b.

Procedure 1a (room temperature). To a solution of [**2**][X] (X = $BArF_{24}$ (20.0 mg, 0.014 mmol, 1.4 mol %), BPh_4 (45 mg, 0.053 mmol, 5.0 mol %), BF_4 (21 mg, 0.034 mmol, 3.2 mol %)) in CD_2Cl_2 (0.4 mL) was dropwise added $HSiEt_3$ (0.34 mL, 2.13 mmol) and fluorobenzene (0.1 mL, 1.07 mmol). During the addition of both substrates, the resulting reaction mixture was characterized by an appreciable effervescence concomittant with a change in color from deep yellow to light red. The reaction mixture was stirred and eventually heated for a given period of time. The reaction mixture was then followed by ^1H and ^{19}F NMR by taking a small aliquot which was diluted with 0.4–0.5 mL of CD_2Cl_2 and transferred under argon to a J-Young NMR tube for analysis.

Procedure 1 - in CD_2Cl_2 (^1H NMR CD_2Cl_2)

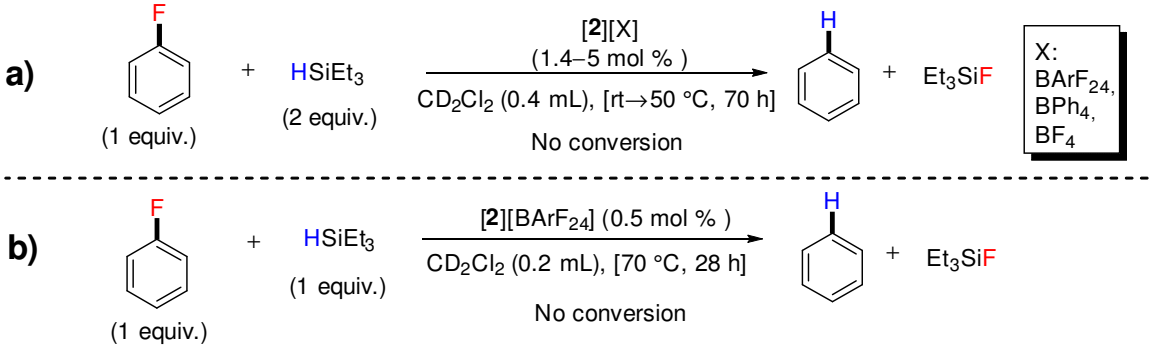

Scheme S6. Attempts of the catalytic HDF reaction of fluorobenzene with $HSiEt_3$ as reducing agent and [**2**][X] (X = $BArF_{24}$, BPh_4, BF_4) as precatalysts.

Procedure 1b (70 °C). To a yellow solution of [**2**][$BArF_{24}$] (20 mg, 0.014 mmol, 0.5 mol %) in CD_2Cl_2 (0.2 mL) was added dropwise $HSiEt_3$ (0.50 mL, 3.13 mmol) and fluorobenzene (0.3 mL, 3.21 mmol). During the addition of both substrates, the resulting reaction mixture was characterized by an appreciable effervescence concomittant with a change in color from deep

yellow to light red. The reaction mixture was stirred and heated at 70 °C for 28 h. The reaction mixture was then followed by ^{1}H and ^{19}F NMR by taking a small aliquot which was diluted with 0.4–0.5 mL of CD_2Cl_2 and transferred under argon to a J-Young NMR tube for analysis.

6.5.1.2 Analysis and discussion of the NMR spectra

Procedures 1a-b. Among the three precatalysts we tested for this reaction, namely [**2**][$BArF_{24}$], [**2**][BF_4] and [**2**][BPh_4], none of them is proved to be an efficient precatalyst either at room temperature (entries 1, 4–5; table S12) or upon prolonged heating at 50–70 °C (entries 2–3; table S12). Indeed, ^{1}H NMR analysis (CD_2Cl_2, 400 MHz, 298 K) of the samples for which the temperature was kept at ~25 °C, the spectra showed the exclusive presence of the characteristic signals of unreacted fluorobenezne (δ 7.21 ppm) and $HSiEt_3$ (Si-*H*, δ 3.65 ppm) in a ratio of 1:2. However, the typical NMR signal of $FSiEt_3$ ($\delta(^{19}F)$ = –176.9 ppm) along with several small peaks within the region of CF_3 groups ($\delta(^{19}F)$ = – 60–64 ppm) were noticed for the samples that were subjected to higher temperatures (50–70 °C, entries 2–3; table S12).

Table S12. Investigation of the catalytic HDF of fluorobenzene with $HSiEt_3$ and [**2**][X] (X = $BArF_{24}$, BF_4, BPh_4) as catalyst system.

Entry	[2](X] (mol %)	T (°C)	t (h)	Conversion. (%)
1	[**2**][$BArF_{24}$] (1.4)	rt	2	<1%
2	[**2**][$BArF_{24}$] (1.4)	60	18	<1%
3	[**2**][$BArF_{24}$] (0.5)	70	28	<1%
4	[**2**][BF_4] (3.2)	rt	2	<1%
5	[**2**][BPh_4] (5.0)	rt	72	<1%

6.5.2 Hexafluorobenzene as internal ^{19}F NMR reference?

6.5.2.1 Catalytic procedures

The reaction we studied is described in scheme S7 below. The goal was to check whether the use of hexafuorobenzene (HFB) as internal reference for ^{19}F NMR spectroscopy is a good choice in a sense that it is not a reactive substrate for the HDF reaction. In this section of work, we describe our investigations towards this goal for various experimental conditions. We used fluorobenzene (C_6H_5F) as substrate because of its inertness towards the catalytic HDF reaction under the conditions we previously described (table S12). Four silanes ($HSiR_3$ = $HSiEt_3$, $HSiPh_3$, $HSiPhH_2$ and PMHS) were tested for the present study.

Procedure 2 - in CH_2Cl_2 (^1H and ^{19}F NMR in CD_2Cl_2)

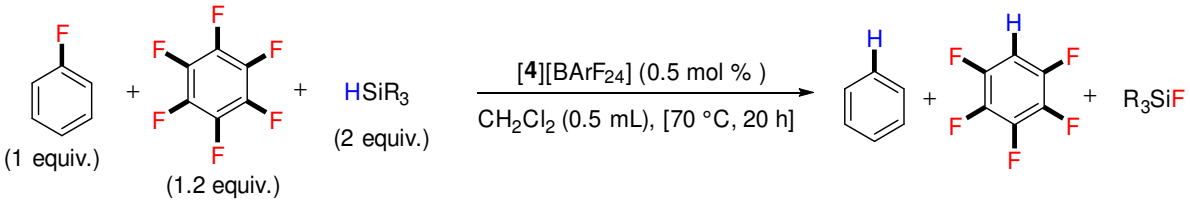

Scheme S12. Investigations of the competitive HDF reaction of fluorobenzene (C_6H_5F) and hexafluorobenzene (HFB) under various catalytic conditions.

Procedure 2 (C_6H_5F + HFB + $HSiR_3$ + [4][$BArF_{24}$]). To a yellow solution of [**4**][$BArF_{24}$] (15.0 mg, 0.011 mmol, 0.5 mol %) in CH_2Cl_2 (0.5 mL) was dropwise added $HSiR_3$ (for $HSiEt_3$: 0.68 mL, 4.24 mmol; for $HSiPh_3$: 1.10 g, 4.24 mmol; for $HSiPhH_2$: 0.52 mL, 4.24 mmol; for PMHS: 0.26 mL, 4.24 mmol), C_6H_5F (0.2 mL, 2.12 mmol) and HFB (0.2 mL, 2.60 mmol). During the addition of the substrates, a marked effervescence concomittant with a change in color from deep yellow to light red were noticed (except when PMHS was used as silane, for which the reaction mixture showed in this case only moderate effervescence and color change). The reaction mixture was stirred at 70 °C for 20 h. The reaction mixture was then followed by ^1H and ^{19}F NMR by taking a small aliquot which was diluted with 0.4–0.5 mL of CD_2Cl_2 and transferred under argon to a J-Young NMR tube for analysis.

6.5.2.2 Results of the study and discussion (table S13)

The results of this study are summarized in table S13 below.

Table S13. Investigation of the catalytic HDF of hexafluorobenzene with $HSiEt_3$ and [**2**][X] (X = $BArF_{24}$, BF_4, BPh_4) as catalyst system: summary of the various conditions that we tested.

Entry	Conditions					
	$HSiR_3$	With [4][$BArF_{24}$] (0.5 mol %)				
		C_6H_5F	HFB	CH_2Cl_2	Conversion (%)	
					C_6H_5F	HFB
1	$HSiEt_3$	yes	yes	yes	<1	<1
2	$HSiPh_3$	yes	yes	yes	<1	<1
3	$HSiPhH_2$	yes	yes	yes	<1	<1
4	PMHS	yes	yes	yes	<1	<1
5	$HSiEt_3$	yes	yes	no	<1	<1
6	$HSiPh_3$	yes	yes	no	<1	<1
7	$HSiPhH_2$	yes	yes	no	<1	<1
8	PMHS	yes	yes	no	<1	<1
9	$HSiPhH_2$	no	yes	yes	<1	<1
10	$HSiPhH_2$	no	yes	no	<1	<1
11	$HSiPhH_2$	yes	no	yes	<1	<1
12	$HSiPhH_2$	yes	no	no	<1	<1
Entry	**$HSiR_3$**	**Without [4][$BArF_{24}$] (0 mol %)**				
		C_6H_5F	HFB	CH_2Cl_2	Conversion (%)	
					C_6H_5F	HFB
13	$HSiPhH_2$	yes	yes	yes	<1	<1
14	$HSiPhH_2$	yes	yes	no	<1	<1

As it is shown in this table, HFB showed any reactivity towards the catalytic HDF reaction whatever the conditions that we used. As a consequence, HFB can be used as an "inert" internal ^{19}F NMR reference for next HDF studies.

6.5.3 Catalytic HDF reaction of 1-fluoroheptane (**1-FH**): CD_2Cl_2 as solvent

6.5.3.1 Catalytic procedure (scheme 53b)

We first started the study by using CD_2Cl_2 as the solvent of the reaction. The conditions of the reaction we studied are described in scheme 53b of the manuscript as well as in scheme S8 and the experimental procedure 3 which are both depicted tbelow.

Procedure 3 - in CD_2Cl_2 (^1H and ^{19}F NMR in CD_2Cl_2)

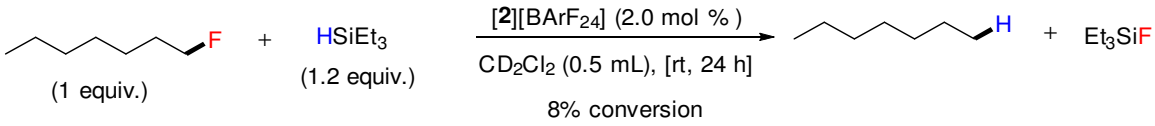

Scheme S8. Investigation of the catalytic HDF reaction of 1-fluoroheptane (**1-FH**) with $HSiEt_3$ and [**2**][$BArF_{24}$] as catalyst system.

Procedure 3 (1-FH + $HSiEt_3$, [2][$BArF_{24}$], CD_2Cl_2). To a yellow solution of [**2**][$BArF_{24}$] (20.0 mg, 0.014 mmol, 2.0 mol %) in CD_2Cl_2 (0.5 mL) was dropwise added $HSiEt_3$ (0.13 mL, 0.82 mmol) and **1-FH** (0.1 mL, 0.68 mmol). During the addition of the substrates, the resulting reaction mixture was characterized by a marked effervescence concomittant with a change in color from deep yellow to light red were noticed. The reaction mixture was stirred at room temperature for 24 h. The reaction mixture was then monitored by ^1H and ^{19}F NMR by taking a small aliquot which was diluted with 0.4–0.5 mL of CD_2Cl_2 and transferred under argon to a J-Young NMR tube for analysis.

6.5.3.2 NMR spectroscopy analysis: results of the study and discussion

Procedure 3. ^1H and ^{19}F NMR spectroscopy analysis (CD_2Cl_2, 298 K, 400 and 300 MHz) revealed that only 8% of **1-FH** was converted. Indeed, the characteristic ^1H NMR and ^{19}F signals of **1-FH** ([CH_2F, doublet of triplets]: δ = 4.0–4.2 ppm, $J^1_{H\text{-}F}$ = 47.5 Hz, $J^3_{H\text{-}H}$ = 6.1; ^{19}F [singlet]: δ = –218.6 ppm) and *n*-heptane (^1H [CH_2, m]: δ = 1.2 ppm; [CH_3, triplet]: δ =0.9 ppm,

$J^{3}_{H\text{-}H}$ = 7.2 Hz) as well as the typical ^{19}F NMR singlet peak of $FSiEt_3$ (^{19}F [singlet]: δ = –176.9 ppm, $J^{1}_{F\text{-}Si}$ = 287 Hz) were observed.

6.5.4 Catalytic HDF reaction of 1-fluoroheptane (**1-FH**): fluorobenzene as solvent

6.5.4.1 Catalytic procedure for the silane screening study (table 18)

We then used fluorobenzene (C_6H_5F) as the solvent of the reaction. Three silanes ($HSiR_3$ = $HSiEt_3$, $HSiPhH_2$ and PMHS) were tested for the present study. The conditions of the reaction we studied are described in table 18 of the manuscript as well as in scheme S9 and the experimental procedure 4 which are both depicted below.

Procedure 4 - in fluorobenzene (C_6H_5F) (^1H and ^{19}F NMR in CD_2Cl_2)

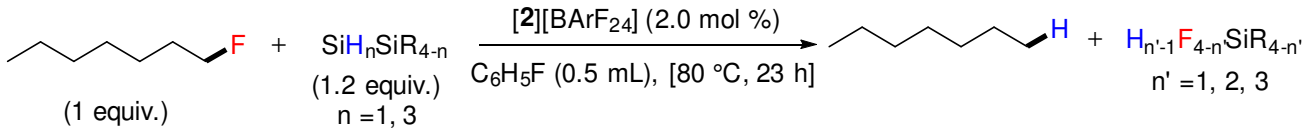

Scheme S9. Investigation of the catalytic HDF reaction of 1-fluoroheptane (**1-FH**) with various silanes $HSiR_3$ and [**2**][$BArF_{24}$] as catalyst system.

Procedure 4 (1-FH + $HSiR_3$, [2][$BArF_{24}$], C_6H_5F). To a solution of [**2**][$BArF_{24}$] (20.0 mg, 0.014 mmol, 2.0 mol %) in C_6H_5F (0.5 mL) was dropwise added $HSiEt_3$ (for $HSiEt_3$: 0.13 mL, 0.82 mmol; for $HSiPhH_2$: 0.11 mL, 0.82 mmol; for PMHS: 0.11 mL, 0.82 mmol) and **1-FH** (0.1 mL, 0.68 mmol). During the addition of the substrates, a marked effervescence concomittant with a change in color from deep yellow to light red were noticed. The reaction mixture was stirred at 80 °C for 23 h. The reaction mixture was then monitored by ^1H and ^{19}F NMR by taking a small aliquot which was diluted with 0.4–0.5 mL of CD_2Cl_2 and transferred under argon to a J-Young NMR tube for analysis.

6.5.4.2 NMR spectroscopy analysis: results of the study and discussion

The results of this study are reported in table 18 of the manuscript. ^1H and ^{19}F NMR spectroscopy analysis showed complete conversion of **1-FH** only in the case of $HSiPhH_2$ as silane. The latter fact was evidenced by the complete disappearance of the typical ^1H and ^{19}F signals of **1-FH** and the appearance of the typical signals of *n*-heptane.

6.5.4.3 Catalytic procedure for [**4**][$BArF_{24}$] as precatalyst (table 20)

We then tested [**4**][$BArF_{24}$] as precatalyst for the reaction between **1-FH** and $HSiPhH_2$. The conditions of the reaction we studied are described in table 20 of the manuscipt as well as in scheme S10 and the experimental procedure 5 which are both depicted below.

Procedure 5 - in C_6H_5F (^1H and ^{19}F NMR in C_6D_6)

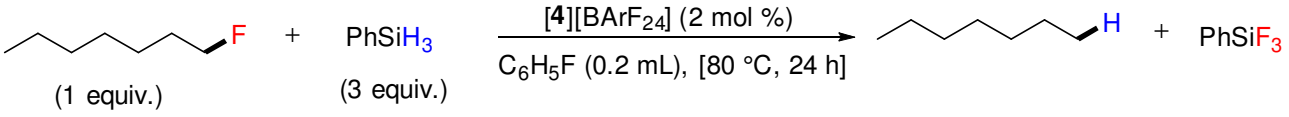

Scheme S10. Investigation of the catalytic HDF reaction of 1-fluoroheptane (**1-FH**) with $HSiPhH_2$ (3 equiv.) and [**4**][$BArF_{24}$] (2 mol %) as the catalyst system.

Procedure 5 (1-FH + $HSiPhH_2$, [4][$BArF_{24}$], C_6H_5F). To a solution of [**4**][$BArF_{24}$] (7.6 mg, 0.0054 mmol, 2.0 mol %) in C_6H_5F (0. 2 mL) was dropwise added $HSiPhH_2$ (0.10 mL, 0.82 mmol) and **1-FH** (0.04 mL, 0.27 mmol). During the addition of the substrates, a marked effervescence concomittant with a change in color from deep yellow to light red were noticed. The reaction mixture was stirred at 80 °C for 24 h. The reaction mixture was then monitored by ^1H and ^{19}F NMR by taking a small aliquot which was mixed with a solution of hexafluorobenzene (0.015 mL, 0.13 mmol) in 0.4–0.5 mL of C_6D_6 and transferred under argon to a J-Young NMR tube for analysis.

The procedure 5 was repeated exactly under the same conditions without using the precacatalyst [**4**][$BArF_{24}$], as described in the following procedure 6.

Procedure 6 (1-FH + $HSiPhH_2$, C_6H_5F). To C_6H_5F (0. 2 mL) was dropwise added $HSiPhH_2$ (0.10 mL, 0.82 mmol) and **1-FH** (0.04 mL, 0.27 mmol). During the addition of the substrates, the resulting reaction mixture was colorless without any noticeable change over time. The reaction mixture was stirred at 80 °C for 24 h. The reaction mixture was then monitored by ^1H and ^{19}F NMR by taking a small aliquot which was mixed with a solution of hexafluorobenzene (0.015 mL, 0.13 mmol) in 0.4–0.5 mL of C_6D_6 and transferred under argon to a J-Young NMR tube for analysis.

6.5.5 Solvent-free catalytic HDF reaction of fluorocyclohexane (**F-Cy**): preliminary results

6.5.5.1 Catalytic procedure related to scheme 58

Herein we detail the experimental conditions used for the reaction we described in scheme 58 of the manuscript as well as in scheme S11 and the experimental procedure 7 which are both depicted tbelow.

Procedure 7 - solvent-free (^{1}H and ^{19}F NMR in C_6D_6)

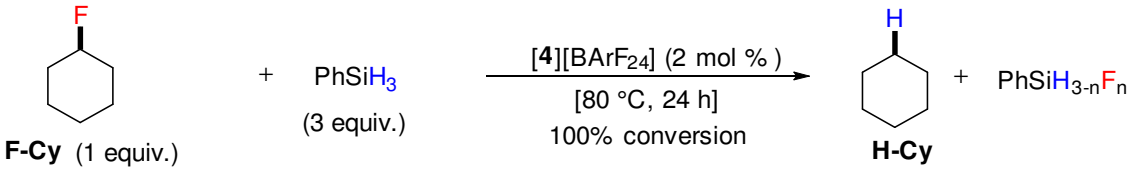

Scheme S11. Investigation of the solvent-free catalytic HDF reaction of fluorocyclohexane (**F-Cy**) with $HSiPhH_2$ as reducing agent and [**4**][$BArF_{24}$] as precatalyst.

Procedure 7 (F-Cy + $HSiPhH_2$, [4][$BArF_{24}$], solvent-free). To a solution of [**4**][$BArF_{24}$] (12.6 mg, 0.0089 mmol, 2.0 mol %) in **F-Cy** (0.05 mL, 0.46 mmol) was dropwise added $HSiPhH_2$ (0.17 mL, 1.37 mmol). During the addition of $HSiPhH_2$, the resulting reaction mixture was characterized by a marked effervescence concomittant without any significant change in color. The reaction mixture was stirred at 80 °C for 24 h. The reaction mixture was then monitored by ^{1}H and ^{19}F NMR by taking a small aliquot which was mixed with a solution of hexafluorobenzene (0.015 mL, 0.13 mmol) in 0.4–0.5 mL of C_6D_6 and transferred under argon to a J-Young NMR tube for analysis.

6.5.6 Solvent-free catalytic HDF reaction of fluorocyclohexane (**F-Cy**): optimization study

6.5.6.1 General catalytic procedure

Several parameters of the solvent-free catalytic HDF reaction of fluorocyclohexane (**F-Cy**) were varied. The general procedure describing the conditions used for every optimization study is provided in scheme S12 and the experimental procedure G depicted below.

Procedure G - solvent-free (^{1}H and ^{19}F NMR in C_6D_6)

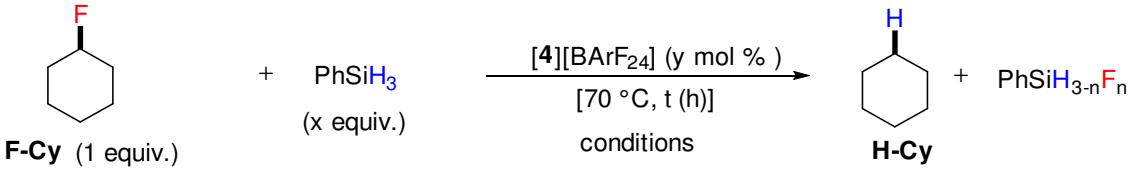

Scheme S12. Optimization study of the solvent-free catalytic HDF reaction of fluorocyclohexane (**F-Cy**) with $HSiPhH_2$ as reducing agent and [**4**][$BArF_{24}$] as precatalyst.

Procedure G (F-Cy, $HSiPhH_2$, [4][$BArF_{24}$], free-solvent). To a solution of [**4**][$BArF_{24}$] (y mol %) in **F-Cy** (0.05 mL, 0.46 mmol) was dropwise added $HSiPhH_2$ (x equiv.). The reaction mixture was stirred at 70 °C for a given time *t* (h). The reaction mixture was then monitored by ^{1}H and ^{19}F NMR by taking a small aliquot which was mixed with a solution of hexafluorobenzene (0.015 mL, 0.13 mmol) in 0.4–0.5 mL of C_6D_6 and transferred under argon to a J-Young NMR tube for analysis.

6.5.6.2 Parameter time *t*

Using the general procedure G (y = mol %; x = equiv), the reaction was followed over time every one hour. It was found that after 1 h, **F-Cy** was totally converted because no characteristic NMR signals (C_6D_6) of it could be identified (C_6D_6) (**F-Cy**: ^{1}H [C*H*F, doublet of septets]: δ = 4.2–4.4 ppm, $J^1_{H\text{-}F}$ = 48.8 Hz, $J^3_{H\text{-}H}$ = 3.9 Hz; ^{19}F [singlet]: δ = –173.9 ppm). ^{19}F NMR analysis revealed the presence of the typical peak of $PhSiF_3$.

6.5.6.3 Parameter x: stoichiometry of $HSiPhH_2$

Using the general procedure G (y = mol %; x = equiv), the stoichiometry x of $HSiPhH_2$ was varied. Figure S2 below shows that $HSiPhH_2$ was conviently converted (91%) when x = 0.5 equivalent.

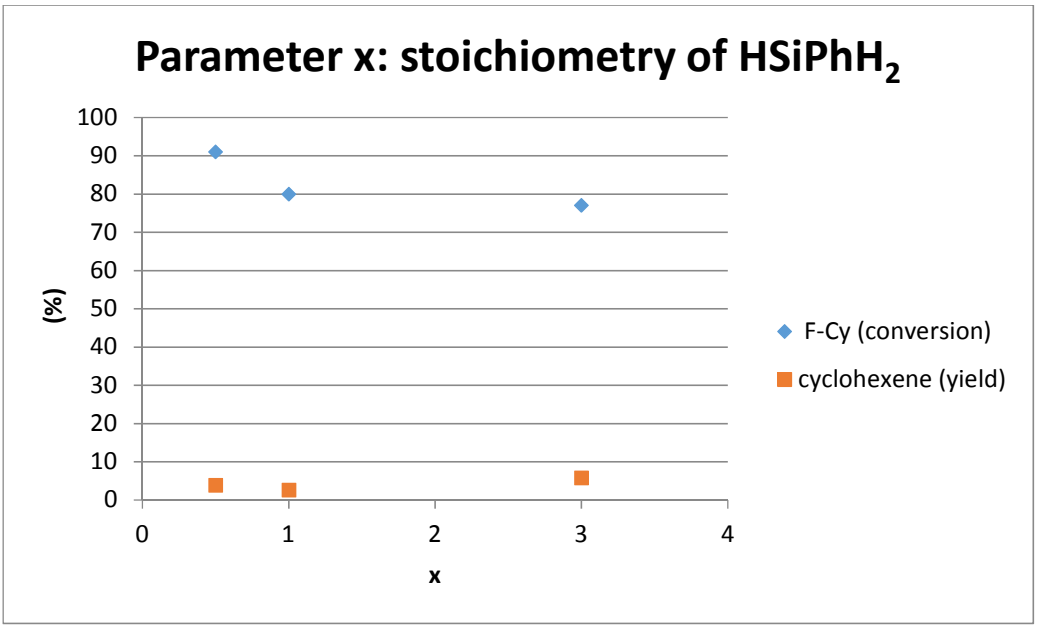

Figure S2. Effect of the variation of the parameter x (stoichiometry of $HSiPhH_2$) on the conversion of **F-Cy** and the production of cyclohexene as by-product.

6.5.6.4 Parameter y: the proportion of [**4**][$BArF_{24}$]

Using the general procedure, the proportion of [**4**][$BArF_{24}$] was varied (parameter y). Figure S3 below shows that **F-Cy** was conviently converted (97%) when y = 0.5 mol %.

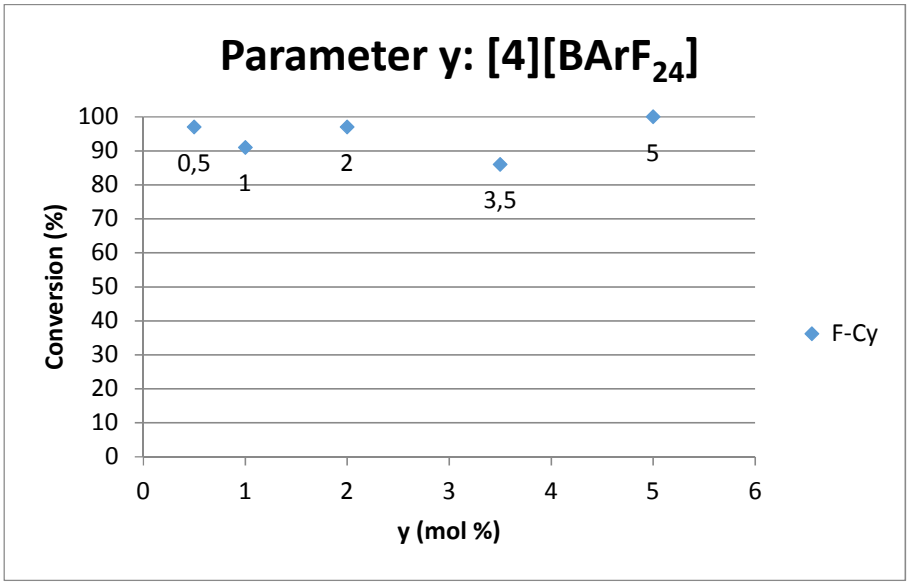

Figure S2. Effect of the variation of parameter x (proportion of [**4**][$BArF_{24}$]) on the conversion of **F-Cy** and the production of cyclohexene as by-product.

6.5.7 Synthesis of ((cyclohexyloxy)methyl)benzene (**CyOBn**) and ((2fluorocyclohexyl)oxy)benzene (**2-FCyOBn**)

The protected alcohols **CyOBn** and **2-FCyOBn** were synthesized following the general procedure G2 below (scheme S13) which was adapted from the procedure previously described in the literature.[396]

Procedure G2 - synthesis of protected alcohols

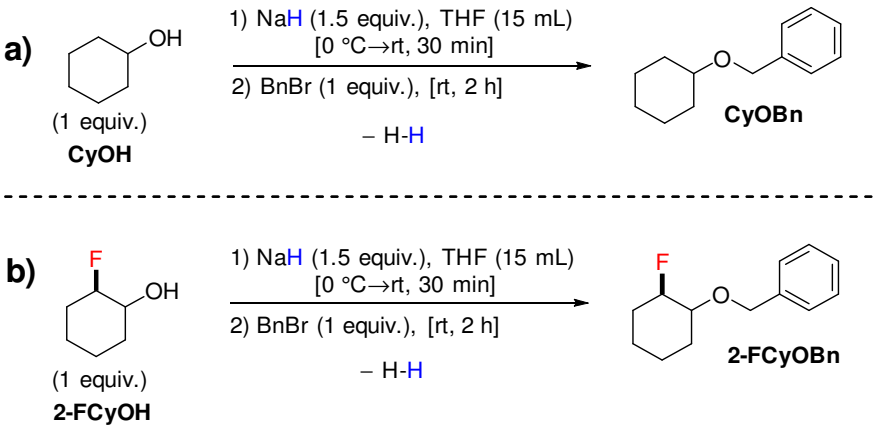

Scheme S13. Synthesis of **CyOBn** and **2-FCyOBn**.

General procedure G2 (a: CyOBn; b: 2-FCyOBn). A Schlenk tube was charged with dry NaH (**a**: 0.260 g, 52.4 mmol; **b**: 1.14 g, 45.8 mmol) and anhydrous THF (~15 mL). The latter solution was cooled down to 0 °C with an ice bath, then the alcohol (**CyOH**: 1.7 mL, 17.0 mmol; **2-FCyOH**: 2 mL, 30.6 mmol) was dropwise added. The resulting mixture was stirred at room temperature for 30 minutes, after which benzyl bromide (BnBr) (3.6 mL, 30.6 mmol) was dropwise added. The resulting mixture was stirred at room temperature for 12 h. Te reaction mixture was then quenched with 20 mL of H_2O and 20 mL of EtOAc. Using an appropriate separating funnel, the aqueous phase (H_2O) and the organic phase (EtOAc) were vigorously shaken, after which the organic phase (OP1) was collected within an appropriate flask. The aqueous phase was further extracted with EtOAc (3 × 15

[396] Lu, P.; Hou, T.; Gu, X.; Li, P. Visible-Light-Promoted Conversion of Alkyl Benzyl Ether to Alkyl Ester or Alcohol via O-α-Sp^3 C–H Cleavage. *Org. Lett.* **2015**, *17* (8), 1954–1957.

mL) and the resulting organic extracts were added to the flask containing OP1. The latter combined organic phase was dried over $MgSO_4$, filtered, and concentrated under vacuum using a rotary evaporator. The resulting solid residue was purified using liquid-solid column chromatography with silica gel as stationary phase: **2-CyOBn**, pentane/dichloromethane (30/70 then 10/90); **2-FCyOBn**, pentane/dichloromethane (60/40 then 20/80). **2-CyOBn** and **2-FCyOBn** were obtained as colorless oils.

2-CyOBn. The ^{1}H NMR data were in accordance with those reported in the literature.[396]

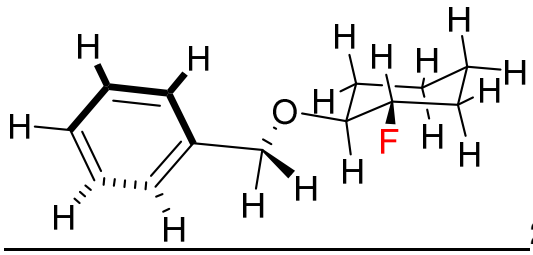

2-FCyOBn. ^{1}H NMR data of ($CDCl_3$, 298 K, 500 MHz): δ = 7.25 (m, 4H, Ar), 7.16 (m, 1H, Ar), 4.59 (dd, 2H, $J^1_{H\text{-}H}$ = 12.3 Hz), 4.36 (doublet of multiplets, 1H, $J^1_{H\text{-}F}$ = 50.7 Hz), 3.34 (m,1H), 1.95 (m, 2H), 1.58 (m, 2H), 1.39 (m, 1H), 1.25 (m, 1H), 1.13 (m, 2H). **^{13}C NMR ($CDCl_3$, 298 K, 126 MHz)**: δ = 138.9 (1C, CH_2-$\underline{C}_{Ar}$), 128.5 (2C, Ar), 127.7 (1C, Ar), 127.6 (1C, Ar), 95.3 (d, $\underline{C}$–F, $J^1_{C\text{-}F}$ = 176.3 Hz), 79.4 (d, (OBn)$\underline{C}H_2$–CF, $J^2_{C\text{-}F}$ = 17.4 Hz), 72.1 ($\underline{C}H_2$-OBn), 30.7 (d, (Cy)$\underline{C}H_2$–CF $J^2_{C\text{-}F}$ = 18.2 Hz), 29.9 (d, $\underline{C}H_2$–CH(OBn)CF, $J^3_{C\text{-}F}$ = 6.6 Hz), 23.4 (1C, $\underline{C}H_2$, Cy), 23.1 (d, $\underline{C}H_2$–CH_2CF, $J^3_{C\text{-}F}$ = 9.8 Hz). **^{19}F NMR ($CDCl_3$, 298 K, 282 MHz)**: δ = –179.9. **HRMS-ESI (m/z) calculated for $C_{13}H_{17}ONa$** ([M+Na]$^+$): 231.12. **Found**: 231.11

7 APPENDIX

In this section, we provide structural informations of the X-ray structures mentioned in the thesis manuscript along with all their related collection and refinement data as well as full geometrical parameters.

7.1 [**2**][$BArF_{24}$]

Data collection: Bruker *APEX2*; cell refinement: Bruker *SAINT*; data reduction: Bruker *SAINT*; program(s) used to solve structure: *SHELXS2013* (Sheldrick, 2013); program(s) used to refine structure: *SHELXL2013* (Sheldrick, 2013); molecular graphics: Bruker *SHELXTL*; software used to prepare material for publication: Bruker *SHELXTL*.

7.1.1 Crystal data

$C_{32}H_{12}BF_{24}\cdot C_{23}H_{26}IrN_2$	$Z = 2$
$M_r = 1385.88$	$F(000) = 1360$
Triclinic, $P\bar{1}$	$D_x = 1.679$ Mg m^{-3}
$a = 12.8467$ (5) Å	Mo $K\alpha$ radiation, $\lambda = 0.71073$ Å
$b = 13.2327$ (5) Å	Cell parameters from 9906 reflections
$c = 17.0526$ (6) Å	$\theta = 2.2–30.2°$
$\alpha = 91.546$ (1)°	$\mu = 2.56$ mm^{-1}
$\beta = 97.457$ (1)°	$T = 173$ K
$\gamma = 107.091$ (1)°	Plate, yellow
$V = 2740.94$ (18) Å^3	0.22 × 0.20 × 0.06 mm

7.1.2 Data collection

Bruker APEX-II CCD diffractometer	17435 independent reflections
Radiation source: sealed tube	14177 reflections with $I > 2\sigma(I)$
Triumph monochromator	$R_{int} = 0.025$
ϕ and ω scans	$\theta_{max} = 31.1°$, $\theta_{min} = 1.6°$
Absorption correction: multi-scan *SADABS*	$h = -10\rightarrow18$
$T_{min} = 0.639$, $T_{max} = 0.746$	$k = -19\rightarrow12$
42350 measured reflections	$l = -24\rightarrow24$

7.1.3 Refinement

Refinement on F^2	Primary atom site location: structure-invariant direct methods
Least-squares matrix: full	Secondary atom site location: difference Fourier map
$R[F^2 > 2\sigma(F^2)] = 0.047$	Hydrogen site location: inferred from neighbouring sites
$wR(F^2) = 0.124$	H-atom parameters constrained
$S = 1.02$	$w = 1/[\sigma^2(F_o^2) + (0.0693P)^2 + 4.0848P]$ where $P = (F_o^2 + 2F_c^2)/3$
17435 reflections	$(\Delta/\sigma)_{max} = 0.001$
739 parameters	$\Delta\rangle_{max} = 1.78$ e Å^{-3}
0 restraints	$\Delta\rangle_{min} = -1.22$ e Å^{-3}

7.1.4 Special details

Geometry. All esds (except the esd in the dihedral angle between two l.s. planes) are estimated using the full covariance matrix. The cell esds are taken into account individually in the estimation of esds in distances, angles and torsion angles; correlations between esds in cell parameters are only used when they are defined by crystal symmetry. An approximate (isotropic) treatment of cell esds is used for estimating esds involving l.s. planes.

7.1.5 **Table A1.** Fractional atomic coordinates and isotropic or equivalent isotropic displacement parameters (Å^2) for [**2**][BArF$_{24}$].

	x	*y*	*z*	U_{iso}*/U_{eq}
C1	0.3975 (4)	0.9328 (4)	0.2793 (3)	0.0470 (11)
H1	0.4558	0.9254	0.3169	0.056*
C2	0.3399 (5)	0.9988 (5)	0.2997 (4)	0.0633 (16)
H2	0.3563	1.0351	0.3507	0.076*
C3	0.2562 (6)	1.0118 (6)	0.2435 (5)	0.075 (2)
H3	0.2172	1.0601	0.2550	0.090*
C4	0.2307 (5)	0.9542 (5)	0.1717 (4)	0.0617 (15)
H4	0.1729	0.9615	0.1337	0.074*
C5	0.2895 (3)	0.8849 (4)	0.1545 (3)	0.0391 (9)
C6	0.2652 (3)	0.8109 (4)	0.0841 (3)	0.0342 (8)
C7	0.1792 (4)	0.8022 (5)	0.0230 (3)	0.0481 (12)
H7	0.1364	0.8498	0.0227	0.058*
C8	0.1568 (4)	0.7237 (5)	-0.0374 (3)	0.0544 (14)
H8	0.0978	0.7167	-0.0789	0.065*

C9	0.2195 (4)	0.6559 (5)	-0.0374 (3)	0.0477 (12)
H9	0.2035	0.6017	-0.0788	0.057*
C10	0.3070 (4)	0.6663 (4)	0.0234 (3)	0.0377 (9)
H10	0.3499	0.6188	0.0227	0.045*
C11	0.3322 (3)	0.7441 (3)	0.0843 (2)	0.0285 (7)
C12	0.6375 (3)	0.8642 (4)	0.2265 (3)	0.0356 (9)
C13	0.6251 (3)	0.7544 (4)	0.2179 (3)	0.0390 (9)
C14	0.5906 (4)	0.7173 (4)	0.1358 (3)	0.0398 (9)
C15	0.5858 (3)	0.8074 (4)	0.0931 (3)	0.0366 (9)
C16	0.6086 (3)	0.8960 (3)	0.1490 (3)	0.0344 (8)
C17	0.6774 (4)	0.9370 (5)	0.3005 (4)	0.0621 (16)
H17A	0.6579	0.8969	0.3467	0.093*
H17B	0.6426	0.9938	0.2972	0.093*
H17C	0.7575	0.9678	0.3059	0.093*
C18	0.6465 (6)	0.6862 (6)	0.2843 (4)	0.0714 (18)
H18A	0.7205	0.6791	0.2857	0.107*
H18B	0.5920	0.6159	0.2753	0.107*
H18C	0.6408	0.7194	0.3350	0.107*
C19	0.5838 (5)	0.6097 (5)	0.1029 (5)	0.0677 (18)
H19A	0.5362	0.5940	0.0516	0.101*
H19B	0.5532	0.5569	0.1397	0.101*
H19C	0.6576	0.6073	0.0960	0.101*
C20	0.5654 (4)	0.8093 (6)	0.0048 (3)	0.0609 (16)
H20A	0.6359	0.8348	-0.0154	0.091*
H20B	0.5210	0.8567	-0.0095	0.091*
H20C	0.5260	0.7376	-0.0186	0.091*
C21	0.6148 (5)	1.0075 (4)	0.1279 (5)	0.0626 (16)
H21A	0.6919	1.0487	0.1279	0.094*
H21B	0.5833	1.0406	0.1671	0.094*
H21C	0.5733	1.0055	0.0752	0.094*
C22	0.3285 (4)	0.6202 (4)	0.2870 (3)	0.0508 (12)
C23	0.2732 (7)	0.5556 (6)	0.3465 (4)	0.090 (3)
H23A	0.3076	0.4999	0.3590	0.135*
H23B	0.1953	0.5233	0.3256	0.135*
H23C	0.2798	0.6005	0.3946	0.135*
C24	-0.0251 (3)	0.6796 (3)	0.7563 (2)	0.0228 (6)
C25	-0.0999 (3)	0.6938 (3)	0.8056 (2)	0.0273 (7)

H25	-0.1209	0.7569	0.8036	0.033*
C26	-0.1442 (3)	0.6188 (3)	0.8571 (3)	0.0332 (8)
C27	-0.1153 (4)	0.5255 (3)	0.8631 (3)	0.0361 (9)
H27	-0.1442	0.4751	0.8994	0.043*
C28	-0.0434 (4)	0.5089 (3)	0.8145 (3)	0.0326 (8)
C29	-0.0005 (3)	0.5832 (3)	0.7615 (2)	0.0271 (7)
H29	0.0470	0.5681	0.7277	0.032*
C30	-0.2259 (5)	0.6375 (4)	0.9061 (4)	0.0533 (14)
C31	-0.0128 (5)	0.4084 (4)	0.8178 (4)	0.0527 (13)
C32	0.1418 (3)	0.7674 (3)	0.6715 (2)	0.0217 (6)
C33	0.2194 (3)	0.7414 (3)	0.7269 (2)	0.0262 (7)
H33	0.1997	0.7192	0.7769	0.031*
C34	0.3244 (3)	0.7474 (3)	0.7105 (2)	0.0309 (8)
C35	0.3587 (3)	0.7834 (3)	0.6403 (3)	0.0323 (8)
H35	0.4303	0.7872	0.6294	0.039*
C36	0.2854 (3)	0.8140 (3)	0.5863 (2)	0.0293 (7)
C37	0.1795 (3)	0.8052 (3)	0.6014 (2)	0.0259 (7)
H37	0.1309	0.8258	0.5627	0.031*
C38	0.4024 (4)	0.7131 (5)	0.7689 (3)	0.0457 (11)
C39	0.3218 (4)	0.8554 (5)	0.5110 (3)	0.0507 (12)
C40	-0.0778 (3)	0.7177 (3)	0.6126 (2)	0.0226 (6)
C41	-0.0686 (3)	0.6502 (3)	0.5514 (2)	0.0249 (7)
H41	-0.0008	0.6351	0.5509	0.030*
C42	-0.1552 (3)	0.6042 (3)	0.4909 (2)	0.0262 (7)
C43	-0.2553 (3)	0.6230 (3)	0.4898 (2)	0.0313 (8)
H43	-0.3149	0.5904	0.4492	0.038*
C44	-0.2668 (3)	0.6904 (4)	0.5491 (3)	0.0341 (9)
C45	-0.1803 (3)	0.7364 (3)	0.6092 (2)	0.0295 (7)
H45	-0.1908	0.7821	0.6494	0.035*
C46	-0.1422 (4)	0.5284 (4)	0.4291 (3)	0.0402 (10)
C47	-0.3734 (4)	0.7128 (6)	0.5480 (4)	0.0636 (17)
C48	0.0263 (3)	0.8853 (3)	0.7161 (2)	0.0221 (6)
C49	0.0116 (3)	0.9556 (3)	0.6583 (2)	0.0281 (7)
H49	-0.0110	0.9290	0.6045	0.034*
C50	0.0289 (3)	1.0622 (3)	0.6772 (2)	0.0318 (8)
C51	0.0594 (3)	1.1048 (3)	0.7551 (3)	0.0340 (8)
H51	0.0692	1.1776	0.7680	0.041*

C52	0.0748 (3)	1.0381 (3)	0.8130 (2)	0.0267 (7)
C53	0.0597 (3)	0.9306 (3)	0.7946 (2)	0.0244 (6)
H53	0.0723	0.8871	0.8359	0.029*
C54	0.0176 (5)	1.1329 (4)	0.6122 (3)	0.0527 (13)
C55	0.1052 (4)	1.0811 (4)	0.8978 (3)	0.0358 (9)
N1	0.3756 (3)	0.8776 (3)	0.2084 (2)	0.0326 (7)
N2	0.3722 (3)	0.6713 (3)	0.2422 (2)	0.0390 (8)
B1	0.0177 (3)	0.7627 (3)	0.6896 (2)	0.0211 (7)
F1	-0.2214 (4)	0.7377 (3)	0.9156 (3)	0.1025 (18)
F2	-0.3261 (3)	0.5823 (5)	0.8799 (4)	0.125 (2)
F3	-0.2114 (5)	0.6075 (4)	0.9799 (3)	0.1076 (18)
F4	0.0098 (7)	0.3869 (5)	0.8960 (6)	0.0730 (11)
F5	-0.0949 (7)	0.3237 (5)	0.7888 (5)	0.0730 (11)
F6	0.0709 (8)	0.4058 (6)	0.7817 (5)	0.0730 (11)
F4B	-0.0350 (9)	0.3513 (6)	0.8764 (7)	0.0730 (11)
F5B	-0.0722 (9)	0.3398 (7)	0.7527 (6)	0.0730 (11)
F6B	0.0961 (10)	0.4273 (7)	0.8132 (6)	0.0730 (11)
F7	0.3703 (7)	0.6914 (8)	0.8380 (5)	0.0858 (11)
F8	0.4230 (7)	0.6262 (7)	0.7397 (5)	0.0858 (11)
F9	0.5016 (6)	0.7855 (7)	0.7845 (5)	0.0858 (11)
F7B	0.4183 (8)	0.7625 (9)	0.8401 (6)	0.0858 (11)
F8B	0.3486 (8)	0.6144 (9)	0.7977 (6)	0.0858 (11)
F9B	0.4790 (8)	0.6839 (9)	0.7408 (6)	0.0858 (11)
F10	0.4153 (6)	0.8461 (6)	0.4953 (4)	0.0826 (11)
F11	0.2477 (6)	0.7999 (6)	0.4455 (4)	0.0826 (11)
F12	0.3193 (5)	0.9522 (8)	0.5011 (5)	0.0826 (11)
F10B	0.4343 (11)	0.9099 (12)	0.5228 (7)	0.0826 (11)
F11B	0.3015 (11)	0.7876 (13)	0.4538 (8)	0.0826 (11)
F12B	0.2742 (11)	0.9329 (15)	0.4847 (9)	0.0826 (11)
F13	-0.1691 (3)	0.4294 (2)	0.4518 (2)	0.0671 (10)
F14	-0.0395 (3)	0.5490 (3)	0.41318 (19)	0.0557 (8)
F15	-0.2061 (4)	0.5263 (4)	0.3602 (2)	0.0869 (15)
F16	-0.4582 (7)	0.6489 (9)	0.5041 (7)	0.1012 (17)
F17	-0.3647 (6)	0.8138 (8)	0.5167 (6)	0.1012 (17)
F18	-0.3955 (7)	0.7353 (9)	0.6184 (7)	0.1012 (17)
F16B	-0.4272 (8)	0.7125 (11)	0.4777 (8)	0.1012 (17)
F17B	-0.4494 (7)	0.6235 (10)	0.5788 (8)	0.1012 (17)

F18B	-0.3771 (9)	0.7893 (11)	0.5942 (10)	0.1012 (17)
F19	0.1145 (9)	1.1673 (6)	0.5824 (5)	0.0837 (12)
F20	-0.0447 (11)	1.0841 (8)	0.5436 (5)	0.0837 (12)
F21	-0.0177 (8)	1.2119 (6)	0.6284 (5)	0.0837 (12)
F19B	0.0897 (12)	1.1294 (7)	0.5560 (6)	0.0837 (12)
F20B	-0.0725 (13)	1.0914 (10)	0.5634 (6)	0.0837 (12)
F21B	0.0524 (10)	1.2354 (8)	0.6351 (6)	0.0837 (12)
F22	0.1646 (4)	1.1832 (3)	0.9050 (2)	0.0734 (11)
F23	0.0191 (3)	1.0724 (4)	0.9340 (2)	0.0788 (13)
F24	0.1678 (3)	1.0334 (3)	0.94166 (18)	0.0584 (8)
Ir1	0.46314 (2)	0.77770 (2)	0.17349 (2)	0.02752 (5)

7.1.6 **Table A2.** Atomic displacement parameters (Å^2) for [**2**][BArF$_{24}$].

	U^{11}	U^{22}	U^{33}	U^{12}	U^{13}	U^{23}
C1	0.041 (2)	0.050 (3)	0.047 (3)	0.009 (2)	0.009 (2)	-0.011 (2)
C2	0.064 (4)	0.062 (4)	0.064 (4)	0.017 (3)	0.020 (3)	-0.022 (3)
C3	0.064 (4)	0.073 (4)	0.101 (6)	0.039 (3)	0.017 (4)	-0.019 (4)
C4	0.046 (3)	0.068 (4)	0.080 (4)	0.032 (3)	0.005 (3)	-0.004 (3)
C5	0.0306 (19)	0.041 (2)	0.047 (3)	0.0115 (18)	0.0095 (18)	0.0049 (19)
C6	0.0232 (16)	0.041 (2)	0.035 (2)	0.0052 (16)	0.0033 (15)	0.0072 (17)
C7	0.036 (2)	0.065 (3)	0.045 (3)	0.018 (2)	0.001 (2)	0.013 (2)
C8	0.036 (2)	0.080 (4)	0.035 (3)	0.004 (2)	-0.0071 (19)	0.012 (3)
C9	0.036 (2)	0.065 (3)	0.028 (2)	-0.003 (2)	0.0008 (18)	-0.003 (2)
C10	0.034 (2)	0.042 (2)	0.031 (2)	0.0035 (17)	0.0033 (16)	-0.0005 (18)
C11	0.0214 (15)	0.0318 (18)	0.0265 (18)	0.0005 (14)	-0.0004 (13)	0.0043 (14)
C12	0.0236 (16)	0.043 (2)	0.036 (2)	0.0083 (16)	-0.0025 (15)	-0.0063 (18)
C13	0.0308 (19)	0.045 (2)	0.044 (2)	0.0172 (18)	-0.0021 (17)	0.0079 (19)
C14	0.035 (2)	0.041 (2)	0.045 (3)	0.0150 (18)	0.0046 (18)	-0.0037 (19)
C15	0.0234 (17)	0.050 (2)	0.034 (2)	0.0085 (17)	0.0042 (15)	0.0016 (18)
C16	0.0227 (16)	0.034 (2)	0.048 (2)	0.0084 (15)	0.0081 (16)	0.0067 (17)
C17	0.034 (2)	0.079 (4)	0.058 (3)	0.004 (3)	-0.007 (2)	-0.031 (3)
C18	0.071 (4)	0.084 (5)	0.068 (4)	0.041 (4)	-0.002 (3)	0.032 (4)
C19	0.058 (3)	0.048 (3)	0.098 (5)	0.020 (3)	0.016 (3)	-0.023 (3)
C20	0.041 (3)	0.102 (5)	0.036 (3)	0.012 (3)	0.010 (2)	0.006 (3)
C21	0.047 (3)	0.039 (3)	0.105 (5)	0.012 (2)	0.020 (3)	0.022 (3)
C22	0.049 (3)	0.049 (3)	0.037 (3)	-0.009 (2)	-0.001 (2)	0.011 (2)

C23	0.095 (5)	0.088 (5)	0.053 (4)	-0.026 (4)	0.005 (4)	0.034 (4)
C24	0.0226 (14)	0.0243 (15)	0.0202 (16)	0.0055 (12)	0.0029 (12)	-0.0008 (12)
C25	0.0265 (16)	0.0272 (17)	0.0276 (18)	0.0060 (14)	0.0075 (14)	-0.0015 (14)
C26	0.0317 (18)	0.034 (2)	0.032 (2)	0.0026 (16)	0.0148 (16)	-0.0009 (16)
C27	0.042 (2)	0.0297 (19)	0.035 (2)	0.0027 (17)	0.0192 (18)	0.0080 (16)
C28	0.040 (2)	0.0229 (17)	0.035 (2)	0.0068 (15)	0.0131 (17)	0.0060 (15)
C29	0.0307 (17)	0.0243 (16)	0.0267 (18)	0.0068 (14)	0.0091 (14)	0.0017 (13)
C30	0.058 (3)	0.043 (3)	0.065 (4)	0.011 (2)	0.040 (3)	0.003 (2)
C31	0.069 (3)	0.030 (2)	0.070 (4)	0.020 (2)	0.033 (3)	0.020 (2)
C32	0.0234 (14)	0.0192 (14)	0.0216 (16)	0.0057 (12)	0.0021 (12)	-0.0007 (12)
C33	0.0254 (16)	0.0290 (17)	0.0230 (17)	0.0069 (14)	0.0014 (13)	0.0022 (14)
C34	0.0242 (16)	0.037 (2)	0.032 (2)	0.0123 (15)	0.0000 (14)	-0.0003 (16)
C35	0.0222 (16)	0.039 (2)	0.037 (2)	0.0096 (15)	0.0081 (15)	0.0031 (17)
C36	0.0264 (16)	0.0330 (19)	0.0285 (19)	0.0067 (14)	0.0088 (14)	0.0067 (15)
C37	0.0245 (15)	0.0284 (17)	0.0258 (17)	0.0088 (13)	0.0045 (13)	0.0060 (14)
C38	0.037 (2)	0.075 (3)	0.034 (2)	0.031 (2)	0.0003 (18)	0.010 (2)
C39	0.047 (3)	0.070 (3)	0.045 (3)	0.024 (3)	0.017 (2)	0.024 (3)
C40	0.0239 (15)	0.0232 (15)	0.0212 (16)	0.0073 (13)	0.0048 (12)	0.0021 (12)
C41	0.0274 (16)	0.0245 (16)	0.0256 (17)	0.0127 (13)	0.0024 (13)	0.0002 (13)
C42	0.0347 (18)	0.0206 (15)	0.0240 (17)	0.0113 (14)	-0.0003 (14)	-0.0010 (13)
C43	0.0302 (18)	0.0333 (19)	0.0289 (19)	0.0109 (15)	-0.0036 (15)	-0.0020 (15)
C44	0.0197 (15)	0.044 (2)	0.038 (2)	0.0125 (16)	-0.0018 (14)	-0.0058 (17)
C45	0.0272 (17)	0.0338 (19)	0.0285 (19)	0.0116 (15)	0.0038 (14)	-0.0060 (15)
C46	0.047 (2)	0.038 (2)	0.037 (2)	0.0214 (19)	-0.0084 (18)	-0.0117 (18)
C47	0.031 (2)	0.095 (5)	0.069 (4)	0.035 (3)	-0.007 (2)	-0.030 (3)
C48	0.0211 (14)	0.0228 (15)	0.0227 (16)	0.0064 (12)	0.0044 (12)	0.0016 (12)
C49	0.0311 (17)	0.0271 (17)	0.0258 (18)	0.0093 (14)	0.0020 (14)	0.0030 (14)
C50	0.0377 (19)	0.0259 (17)	0.033 (2)	0.0123 (15)	0.0030 (16)	0.0084 (15)
C51	0.039 (2)	0.0253 (18)	0.040 (2)	0.0109 (16)	0.0081 (17)	0.0002 (16)
C52	0.0271 (16)	0.0259 (17)	0.0260 (18)	0.0067 (14)	0.0039 (13)	-0.0017 (14)
C53	0.0249 (15)	0.0254 (16)	0.0223 (17)	0.0062 (13)	0.0044 (13)	0.0025 (13)
C54	0.068 (3)	0.040 (3)	0.049 (3)	0.018 (2)	0.000 (3)	0.015 (2)
C55	0.036 (2)	0.037 (2)	0.032 (2)	0.0093 (17)	0.0039 (16)	-0.0073 (17)
N1	0.0291 (15)	0.0358 (17)	0.0305 (17)	0.0061 (14)	0.0047 (13)	-0.0018 (14)
N2	0.0374 (18)	0.0356 (18)	0.0345 (19)	0.0008 (15)	-0.0049 (15)	0.0021 (15)
B1	0.0226 (16)	0.0234 (17)	0.0177 (17)	0.0065 (14)	0.0050 (13)	0.0001 (13)
F1	0.140 (4)	0.070 (2)	0.137 (4)	0.053 (3)	0.106 (4)	0.024 (3)

F2	0.046 (2)	0.164 (5)	0.152 (5)	0.002 (3)	0.049 (3)	-0.051 (4)
F3	0.163 (5)	0.129 (4)	0.073 (3)	0.075 (4)	0.086 (3)	0.035 (3)
F4	0.100 (3)	0.0404 (18)	0.092 (3)	0.0297 (19)	0.037 (2)	0.0218 (19)
F5	0.100 (3)	0.0404 (18)	0.092 (3)	0.0297 (19)	0.037 (2)	0.0218 (19)
F6	0.100 (3)	0.0404 (18)	0.092 (3)	0.0297 (19)	0.037 (2)	0.0218 (19)
F4B	0.100 (3)	0.0404 (18)	0.092 (3)	0.0297 (19)	0.037 (2)	0.0218 (19)
F5B	0.100 (3)	0.0404 (18)	0.092 (3)	0.0297 (19)	0.037 (2)	0.0218 (19)
F6B	0.100 (3)	0.0404 (18)	0.092 (3)	0.0297 (19)	0.037 (2)	0.0218 (19)
F7	0.067 (2)	0.101 (3)	0.087 (2)	0.036 (2)	-0.023 (2)	0.024 (2)
F8	0.067 (2)	0.101 (3)	0.087 (2)	0.036 (2)	-0.023 (2)	0.024 (2)
F9	0.067 (2)	0.101 (3)	0.087 (2)	0.036 (2)	-0.023 (2)	0.024 (2)
F7B	0.067 (2)	0.101 (3)	0.087 (2)	0.036 (2)	-0.023 (2)	0.024 (2)
F8B	0.067 (2)	0.101 (3)	0.087 (2)	0.036 (2)	-0.023 (2)	0.024 (2)
F9B	0.067 (2)	0.101 (3)	0.087 (2)	0.036 (2)	-0.023 (2)	0.024 (2)
F10	0.079 (3)	0.118 (3)	0.063 (2)	0.034 (3)	0.037 (2)	0.041 (2)
F11	0.079 (3)	0.118 (3)	0.063 (2)	0.034 (3)	0.037 (2)	0.041 (2)
F12	0.079 (3)	0.118 (3)	0.063 (2)	0.034 (3)	0.037 (2)	0.041 (2)
F10B	0.079 (3)	0.118 (3)	0.063 (2)	0.034 (3)	0.037 (2)	0.041 (2)
F11B	0.079 (3)	0.118 (3)	0.063 (2)	0.034 (3)	0.037 (2)	0.041 (2)
F12B	0.079 (3)	0.118 (3)	0.063 (2)	0.034 (3)	0.037 (2)	0.041 (2)
F13	0.079 (2)	0.0268 (14)	0.097 (3)	0.0192 (15)	0.015 (2)	-0.0130 (15)
F14	0.0656 (19)	0.0592 (18)	0.0506 (18)	0.0293 (16)	0.0169 (15)	-0.0142 (14)
F15	0.112 (3)	0.119 (3)	0.0451 (19)	0.083 (3)	-0.0375 (19)	-0.046 (2)
F16	0.051 (2)	0.140 (5)	0.127 (4)	0.056 (3)	0.006 (2)	-0.014 (4)
F17	0.051 (2)	0.140 (5)	0.127 (4)	0.056 (3)	0.006 (2)	-0.014 (4)
F18	0.051 (2)	0.140 (5)	0.127 (4)	0.056 (3)	0.006 (2)	-0.014 (4)
F16B	0.051 (2)	0.140 (5)	0.127 (4)	0.056 (3)	0.006 (2)	-0.014 (4)
F17B	0.051 (2)	0.140 (5)	0.127 (4)	0.056 (3)	0.006 (2)	-0.014 (4)
F18B	0.051 (2)	0.140 (5)	0.127 (4)	0.056 (3)	0.006 (2)	-0.014 (4)
F19	0.144 (4)	0.062 (2)	0.052 (2)	0.045 (3)	0.001 (2)	0.0182 (17)
F20	0.144 (4)	0.062 (2)	0.052 (2)	0.045 (3)	0.001 (2)	0.0182 (17)
F21	0.144 (4)	0.062 (2)	0.052 (2)	0.045 (3)	0.001 (2)	0.0182 (17)
F19B	0.144 (4)	0.062 (2)	0.052 (2)	0.045 (3)	0.001 (2)	0.0182 (17)
F20B	0.144 (4)	0.062 (2)	0.052 (2)	0.045 (3)	0.001 (2)	0.0182 (17)
F21B	0.144 (4)	0.062 (2)	0.052 (2)	0.045 (3)	0.001 (2)	0.0182 (17)
F22	0.104 (3)	0.0406 (17)	0.056 (2)	-0.0016 (18)	0.002 (2)	-0.0196 (15)
F23	0.0468 (18)	0.150 (4)	0.0421 (18)	0.033 (2)	0.0140 (14)	-0.021 (2)

F24	0.067 (2)	0.073 (2)	0.0368 (15)	0.0337 (17)	-0.0138 (14)	-0.0156 (14)
Ir1	0.02501 (7)	0.02949 (8)	0.02603 (8)	0.00654 (5)	0.00039 (5)	0.00098 (5)

7.1.7 **Table A3.** Interatomic distances (Å) and angles (deg) for [**2**][$BArF_{24}$].

C1—N1	1.348 (6)	C31—F6	1.315 (11)
C1—C2	1.365 (7)	C31—F5	1.324 (10)
C1—H1	0.9500	C31—F6B	1.359 (13)
C2—C3	1.397 (10)	C31—F4	1.384 (11)
C2—H2	0.9500	C31—F5B	1.399 (13)
C3—C4	1.375 (10)	C32—C37	1.397 (5)
C3—H3	0.9500	C32—C33	1.407 (5)
C4—C5	1.395 (6)	C32—B1	1.647 (5)
C4—H4	0.9500	C33—C34	1.392 (5)
C5—N1	1.372 (6)	C33—H33	0.9500
C5—C6	1.468 (7)	C34—C35	1.378 (6)
C6—C7	1.393 (6)	C34—C38	1.495 (5)
C6—C11	1.404 (5)	C35—C36	1.385 (5)
C7—C8	1.382 (8)	C35—H35	0.9500
C7—H7	0.9500	C36—C37	1.390 (5)
C8—C9	1.371 (8)	C36—C39	1.486 (6)
C8—H8	0.9500	C37—H37	0.9500
C9—C10	1.399 (6)	C38—F9B	1.297 (12)
C9—H9	0.9500	C38—F7	1.309 (10)
C10—C11	1.380 (6)	C38—F7B	1.326 (12)
C10—H10	0.9500	C38—F9	1.340 (9)
C11—Ir1	2.049 (4)	C38—F8	1.350 (10)
C12—C13	1.415 (6)	C38—F8B	1.419 (12)
C12—C16	1.434 (6)	C39—F11B	1.255 (16)
C12—C17	1.503 (7)	C39—F10	1.303 (8)
C12—Ir1	2.249 (4)	C39—F12	1.306 (10)
C13—C14	1.438 (7)	C39—F12B	1.397 (17)
C13—C18	1.515 (7)	C39—F10B	1.398 (15)
C13—Ir1	2.231 (4)	C39—F11	1.400 (10)
C14—C15	1.426 (7)	C40—C41	1.394 (5)
C14—C19	1.491 (7)	C40—C45	1.404 (5)
C14—Ir1	2.178 (4)	C40—B1	1.642 (5)

C15—C16	1.426 (6)	C41—C42	1.395 (5)
C15—C20	1.497 (7)	C41—H41	0.9500
C15—Ir1	2.177 (4)	C42—C43	1.377 (5)
C16—C21	1.509 (6)	C42—C46	1.494 (5)
C16—Ir1	2.153 (4)	C43—C44	1.383 (6)
C17—H17A	0.9800	C43—H43	0.9500
C17—H17B	0.9800	C44—C45	1.389 (5)
C17—H17C	0.9800	C44—C47	1.482 (5)
C18—H18A	0.9800	C45—H45	0.9500
C18—H18B	0.9800	C46—F14	1.331 (6)
C18—H18C	0.9800	C46—F13	1.334 (6)
C19—H19A	0.9800	C46—F15	1.338 (5)
C19—H19B	0.9800	C47—F18B	1.282 (15)
C19—H19C	0.9800	C47—F16	1.293 (11)
C20—H20A	0.9800	C47—F16B	1.303 (14)
C20—H20B	0.9800	C47—F18	1.316 (12)
C20—H20C	0.9800	C47—F17	1.432 (12)
C21—H21A	0.9800	C47—F17B	1.454 (14)
C21—H21B	0.9800	C48—C49	1.405 (5)
C21—H21C	0.9800	C48—C53	1.412 (5)
C22—N2	1.128 (6)	C48—B1	1.641 (5)
C22—C23	1.462 (8)	C49—C50	1.384 (5)
C23—H23A	0.9800	C49—H49	0.9500
C23—H23B	0.9800	C50—C51	1.390 (6)
C23—H23C	0.9800	C50—C54	1.490 (6)
C24—C29	1.404 (5)	C51—C52	1.375 (6)
C24—C25	1.404 (5)	C51—H51	0.9500
C24—B1	1.637 (5)	C52—C53	1.399 (5)
C25—C26	1.388 (6)	C52—C55	1.498 (6)
C25—H25	0.9500	C53—H53	0.9500
C26—C27	1.392 (6)	C54—F21	1.292 (10)
C26—C30	1.494 (6)	C54—F20B	1.298 (16)
C27—C28	1.378 (6)	C54—F21B	1.327 (12)
C27—H27	0.9500	C54—F20	1.356 (13)
C28—C29	1.395 (5)	C54—F19	1.363 (12)
C28—C31	1.493 (6)	C54—F19B	1.425 (14)
C29—H29	0.9500	C55—F23	1.314 (5)

C30—F2	1.292 (7)	C55—F24	1.331 (5)
C30—F1	1.315 (6)	C55—F22	1.336 (6)
C30—F3	1.335 (7)	N1—Ir1	2.091 (3)
C31—F4B	1.280 (12)	N2—Ir1	2.049 (4)
N1—C1—C2	123.1 (5)	C33—C34—C38	120.3 (4)
N1—C1—H1	118.5	C34—C35—C36	117.9 (3)
C2—C1—H1	118.5	C34—C35—H35	121.1
C1—C2—C3	118.3 (5)	C36—C35—H35	121.1
C1—C2—H2	120.8	C35—C36—C37	120.9 (4)
C3—C2—H2	120.8	C35—C36—C39	118.6 (4)
C4—C3—C2	119.4 (5)	C37—C36—C39	120.4 (4)
C4—C3—H3	120.3	C36—C37—C32	122.5 (3)
C2—C3—H3	120.3	C36—C37—H37	118.8
C3—C4—C5	120.2 (6)	C32—C37—H37	118.8
C3—C4—H4	119.9	F9B—C38—F7B	122.4 (7)
C5—C4—H4	119.9	F7—C38—F9	105.7 (6)
N1—C5—C4	119.7 (5)	F7—C38—F8	107.0 (7)
N1—C5—C6	113.8 (4)	F9—C38—F8	104.3 (6)
C4—C5—C6	126.4 (5)	F9B—C38—F8B	97.2 (7)
C7—C6—C11	121.4 (4)	F7B—C38—F8B	91.8 (7)
C7—C6—C5	123.7 (4)	F9B—C38—C34	116.6 (5)
C11—C6—C5	114.8 (4)	F7—C38—C34	115.4 (4)
C8—C7—C6	119.4 (5)	F7B—C38—C34	112.7 (5)
C8—C7—H7	120.3	F9—C38—C34	112.7 (5)
C6—C7—H7	120.3	F8—C38—C34	110.9 (5)
C9—C8—C7	120.3 (4)	F8B—C38—C34	110.6 (5)
C9—C8—H8	119.9	F10—C39—F12	109.6 (6)
C7—C8—H8	119.9	F11B—C39—F12B	105.9 (10)
C8—C9—C10	120.1 (5)	F11B—C39—F10B	109.0 (9)
C8—C9—H9	120.0	F12B—C39—F10B	102.9 (9)
C10—C9—H9	120.0	F10—C39—F11	102.6 (6)
C11—C10—C9	121.3 (4)	F12—C39—F11	101.3 (6)
C11—C10—H10	119.3	F11B—C39—C36	115.6 (7)
C9—C10—H10	119.3	F10—C39—C36	117.0 (5)
C10—C11—C6	117.5 (4)	F12—C39—C36	113.8 (5)
C10—C11—Ir1	126.6 (3)	F12B—C39—C36	112.0 (7)

C6—C11—Ir1	115.8 (3)	F10B—C39—C36	110.7 (6)
C13—C12—C16	106.7 (4)	F11—C39—C36	110.9 (5)
C13—C12—C17	128.1 (5)	C41—C40—C45	115.5 (3)
C16—C12—C17	125.2 (5)	C41—C40—B1	123.5 (3)
C13—C12—Ir1	70.9 (2)	C45—C40—B1	120.7 (3)
C16—C12—Ir1	67.4 (2)	C40—C41—C42	122.4 (3)
C17—C12—Ir1	128.3 (3)	C40—C41—H41	118.8
C12—C13—C14	109.6 (4)	C42—C41—H41	118.8
C12—C13—C18	125.5 (5)	C43—C42—C41	120.7 (3)
C14—C13—C18	124.9 (5)	C43—C42—C46	119.2 (4)
C12—C13—Ir1	72.3 (2)	C41—C42—C46	119.9 (3)
C14—C13—Ir1	69.0 (2)	C42—C43—C44	118.3 (4)
C18—C13—Ir1	125.8 (4)	C42—C43—H43	120.9
C15—C14—C13	106.7 (4)	C44—C43—H43	120.9
C15—C14—C19	127.8 (5)	C43—C44—C45	120.8 (3)
C13—C14—C19	124.5 (5)	C43—C44—C47	118.9 (4)
C15—C14—Ir1	70.8 (2)	C45—C44—C47	120.3 (4)
C13—C14—Ir1	73.0 (2)	C44—C45—C40	122.3 (3)
C19—C14—Ir1	130.2 (4)	C44—C45—H45	118.9
C16—C15—C14	108.1 (4)	C40—C45—H45	118.9
C16—C15—C20	126.1 (5)	F14—C46—F13	105.5 (3)
C14—C15—C20	125.7 (5)	F14—C46—F15	106.8 (4)
C16—C15—Ir1	69.9 (2)	F13—C46—F15	106.5 (4)
C14—C15—Ir1	70.9 (2)	F14—C46—C42	113.6 (4)
C20—C15—Ir1	126.9 (3)	F13—C46—C42	111.4 (4)
C15—C16—C12	108.7 (4)	F15—C46—C42	112.6 (3)
C15—C16—C21	125.0 (5)	F18B—C47—F16B	111.5 (9)
C12—C16—C21	125.9 (5)	F16—C47—F18	112.1 (7)
C15—C16—Ir1	71.7 (2)	F16—C47—F17	104.0 (7)
C12—C16—Ir1	74.6 (2)	F18—C47—F17	97.6 (7)
C21—C16—Ir1	125.5 (3)	F18B—C47—F17B	100.8 (9)
C12—C17—H17A	109.5	F16B—C47—F17B	100.2 (8)
C12—C17—H17B	109.5	F18B—C47—C44	118.1 (6)
H17A—C17—H17B	109.5	F16—C47—C44	117.4 (6)
C12—C17—H17C	109.5	F16B—C47—C44	115.3 (6)
H17A—C17—H17C	109.5	F18—C47—C44	114.3 (6)
H17B—C17—H17C	109.5	F17—C47—C44	109.0 (6)

C13—C18—H18A	109.5	F17B—C47—C44	108.2 (6)
C13—C18—H18B	109.5	C49—C48—C53	115.6 (3)
H18A—C18—H18B	109.5	C49—C48—B1	120.2 (3)
C13—C18—H18C	109.5	C53—C48—B1	123.8 (3)
H18A—C18—H18C	109.5	C50—C49—C48	122.2 (4)
H18B—C18—H18C	109.5	C50—C49—H49	118.9
C14—C19—H19A	109.5	C48—C49—H49	118.9
C14—C19—H19B	109.5	C49—C50—C51	121.3 (4)
H19A—C19—H19B	109.5	C49—C50—C54	119.1 (4)
C14—C19—H19C	109.5	C51—C50—C54	119.5 (4)
H19A—C19—H19C	109.5	C52—C51—C50	117.9 (3)
H19B—C19—H19C	109.5	C52—C51—H51	121.1
C15—C20—H20A	109.5	C50—C51—H51	121.1
C15—C20—H20B	109.5	C51—C52—C53	121.4 (4)
H20A—C20—H20B	109.5	C51—C52—C55	119.2 (3)
C15—C20—H20C	109.5	C53—C52—C55	119.4 (3)
H20A—C20—H20C	109.5	C52—C53—C48	121.6 (3)
H20B—C20—H20C	109.5	C52—C53—H53	119.2
C16—C21—H21A	109.5	C48—C53—H53	119.2
C16—C21—H21B	109.5	F20B—C54—F21B	121.9 (7)
H21A—C21—H21B	109.5	F21—C54—F20	105.8 (7)
C16—C21—H21C	109.5	F21—C54—F19	110.4 (7)
H21A—C21—H21C	109.5	F20—C54—F19	96.5 (7)
H21B—C21—H21C	109.5	F20B—C54—F19B	95.4 (8)
N2—C22—C23	178.7 (6)	F21B—C54—F19B	100.4 (8)
C22—C23—H23A	109.5	F21—C54—C50	116.9 (6)
C22—C23—H23B	109.5	F20B—C54—C50	111.0 (7)
H23A—C23—H23B	109.5	F21B—C54—C50	114.1 (6)
C22—C23—H23C	109.5	F20—C54—C50	115.6 (6)
H23A—C23—H23C	109.5	F19—C54—C50	109.6 (5)
H23B—C23—H23C	109.5	F19B—C54—C50	111.1 (5)
C29—C24—C25	115.3 (3)	F23—C55—F24	105.8 (4)
C29—C24—B1	122.2 (3)	F23—C55—F22	107.4 (4)
C25—C24—B1	122.0 (3)	F24—C55—F22	104.2 (4)
C26—C25—C24	122.3 (3)	F23—C55—C52	112.9 (4)
C26—C25—H25	118.9	F24—C55—C52	113.6 (3)
C24—C25—H25	118.9	F22—C55—C52	112.2 (4)

C25—C26—C27	121.2 (3)	C1—N1—C5	119.1 (4)
C25—C26—C30	119.5 (4)	C1—N1—Ir1	124.6 (3)
C27—C26—C30	119.3 (4)	C5—N1—Ir1	116.2 (3)
C28—C27—C26	117.7 (4)	C22—N2—Ir1	172.4 (4)
C28—C27—H27	121.2	C24—B1—C48	113.1 (3)
C26—C27—H27	121.2	C24—B1—C40	102.7 (3)
C27—C28—C29	121.1 (4)	C48—B1—C40	110.3 (3)
C27—C28—C31	119.2 (4)	C24—B1—C32	112.7 (3)
C29—C28—C31	119.7 (4)	C48—B1—C32	105.1 (3)
C28—C29—C24	122.4 (3)	C40—B1—C32	113.2 (3)
C28—C29—H29	118.8	C11—Ir1—N2	90.78 (15)
C24—C29—H29	118.8	C11—Ir1—N1	78.24 (15)
F2—C30—F1	108.9 (6)	N2—Ir1—N1	84.88 (15)
F2—C30—F3	102.8 (5)	C11—Ir1—C16	114.78 (16)
F1—C30—F3	104.4 (5)	N2—Ir1—C16	154.43 (16)
F2—C30—C26	113.3 (5)	N1—Ir1—C16	98.99 (14)
F1—C30—C26	113.8 (4)	C11—Ir1—C15	94.23 (15)
F3—C30—C26	112.8 (5)	N2—Ir1—C15	146.65 (17)
F6—C31—F5	106.1 (6)	N1—Ir1—C15	128.42 (16)
F4B—C31—F6B	107.6 (8)	C16—Ir1—C15	38.45 (17)
F6—C31—F4	108.4 (7)	C11—Ir1—C14	109.10 (17)
F5—C31—F4	102.7 (6)	N2—Ir1—C14	109.42 (17)
F4B—C31—F5B	102.6 (7)	N1—Ir1—C14	163.36 (16)
F6B—C31—F5B	107.7 (7)	C16—Ir1—C14	64.43 (16)
F4B—C31—C28	118.5 (6)	C15—Ir1—C14	38.23 (17)
F6—C31—C28	116.0 (5)	C11—Ir1—C13	146.71 (17)
F5—C31—C28	113.3 (5)	N2—Ir1—C13	96.53 (16)
F6B—C31—C28	110.8 (6)	N1—Ir1—C13	134.65 (16)
F4—C31—C28	109.5 (5)	C16—Ir1—C13	62.81 (16)
F5B—C31—C28	108.9 (6)	C15—Ir1—C13	62.84 (17)
C37—C32—C33	115.4 (3)	C14—Ir1—C13	38.05 (18)
C37—C32—B1	121.5 (3)	C11—Ir1—C12	152.72 (17)
C33—C32—B1	122.9 (3)	N2—Ir1—C12	116.50 (16)
C34—C33—C32	121.8 (3)	N1—Ir1—C12	102.92 (14)
C34—C33—H33	119.1	C16—Ir1—C12	37.95 (17)
C32—C33—H33	119.1	C15—Ir1—C12	63.32 (16)
C35—C34—C33	121.4 (3)	C14—Ir1—C12	63.54 (16)

C35—C34—C38	118.3 (3)	C13—Ir1—C12	36.82 (16)
N1—C1—C2—C3	-1.7 (9)	C35—C34—C38—F9	50.9 (7)
C1—C2—C3—C4	3.3 (11)	C33—C34—C38—F9	-130.0 (6)
C2—C3—C4—C5	-1.3 (11)	C35—C34—C38—F8	-65.6 (7)
C3—C4—C5—N1	-2.4 (9)	C33—C34—C38—F8	113.5 (6)
C3—C4—C5—C6	173.6 (6)	C35—C34—C38—F8B	-133.3 (7)
N1—C5—C6—C7	178.0 (4)	C33—C34—C38—F8B	45.8 (8)
C4—C5—C6—C7	1.7 (8)	C35—C36—C39—F11B	91.8 (9)
N1—C5—C6—C11	1.1 (6)	C37—C36—C39—F11B	-87.5 (9)
C4—C5—C6—C11	-175.2 (5)	C35—C36—C39—F10	9.7 (8)
C11—C6—C7—C8	2.4 (7)	C37—C36—C39—F10	-169.7 (6)
C5—C6—C7—C8	-174.3 (5)	C35—C36—C39—F12	-119.8 (6)
C6—C7—C8—C9	-0.8 (8)	C37—C36—C39—F12	60.9 (7)
C7—C8—C9—C10	-0.4 (8)	C35—C36—C39—F12B	-146.8 (9)
C8—C9—C10—C11	0.0 (7)	C37—C36—C39—F12B	33.9 (10)
C9—C10—C11—C6	1.5 (6)	C35—C36—C39—F10B	-32.6 (9)
C9—C10—C11—Ir1	-175.3 (3)	C37—C36—C39—F10B	148.1 (8)
C7—C6—C11—C10	-2.7 (6)	C35—C36—C39—F11	126.7 (5)
C5—C6—C11—C10	174.3 (4)	C37—C36—C39—F11	-52.6 (7)
C7—C6—C11—Ir1	174.4 (4)	C45—C40—C41—C42	-0.1 (5)
C5—C6—C11—Ir1	-8.6 (5)	B1—C40—C41—C42	173.1 (3)
C16—C12—C13—C14	1.0 (5)	C40—C41—C42—C43	-0.7 (6)
C17—C12—C13—C14	-176.8 (4)	C40—C41—C42—C46	-177.1 (4)
Ir1—C12—C13—C14	59.1 (3)	C41—C42—C43—C44	1.4 (6)

C16—C12—C13—C18	-179.9 (5)	C46—C42—C43—C44	177.7 (4)
C17—C12—C13—C18	2.4 (8)	C42—C43—C44—C45	-1.2 (7)
Ir1—C12—C13—C18	-121.8 (5)	C42—C43—C44—C47	179.0 (5)
C16—C12—C13—Ir1	-58.1 (3)	C43—C44—C45—C40	0.3 (7)
C17—C12—C13—Ir1	124.1 (5)	C47—C44—C45—C40	-179.8 (5)
C12—C13—C14—C15	2.1 (5)	C41—C40—C45—C44	0.3 (6)
C18—C13—C14—C15	-177.0 (5)	B1—C40—C45—C44	-173.1 (4)
Ir1—C13—C14—C15	63.2 (3)	C43—C42—C46—F14	152.2 (4)
C12—C13—C14—C19	171.4 (5)	C41—C42—C46—F14	-31.4 (6)
C18—C13—C14—C19	-7.7 (8)	C43—C42—C46—F13	-88.9 (5)
Ir1—C13—C14—C19	-127.5 (5)	C41—C42—C46—F13	87.5 (5)
C12—C13—C14—Ir1	-61.1 (3)	C43—C42—C46—F15	30.7 (6)
C18—C13—C14—Ir1	119.8 (5)	C41—C42—C46—F15	-152.9 (4)
C13—C14—C15—C16	-4.4 (5)	C43—C44—C47—F18B	-167.5 (9)
C19—C14—C15—C16	-173.2 (5)	C45—C44—C47—F18B	12.7 (12)
Ir1—C14—C15—C16	60.2 (3)	C43—C44—C47—F16	17.1 (11)
C13—C14—C15—C20	173.0 (4)	C45—C44—C47—F16	-162.7 (8)
C19—C14—C15—C20	4.2 (7)	C43—C44—C47—F16B	-32.1 (11)
Ir1—C14—C15—C20	-122.3 (4)	C45—C44—C47—F16B	148.1 (9)
C13—C14—C15—Ir1	-64.7 (3)	C43—C44—C47—F18	151.3 (7)
C19—C14—C15—Ir1	126.5 (5)	C45—C44—C47—F18	-28.5 (10)
C14—C15—C16—C12	5.1 (4)	C43—C44—C47—F17	-100.7 (7)

C20—C15—C16—C12	-172.3 (4)	C45—C44—C47—F17	79.5 (7)
Ir1—C15—C16—C12	66.0 (3)	C43—C44—C47—F17B	79.0 (8)
C14—C15—C16—C21	178.1 (4)	C45—C44—C47—F17B	-100.8 (7)
C20—C15—C16—C21	0.7 (7)	C53—C48—C49—C50	0.1 (5)
Ir1—C15—C16—C21	-120.9 (4)	B1—C48—C49—C50	-173.3 (3)
C14—C15—C16—Ir1	-60.9 (3)	C48—C49—C50—C51	-1.6 (6)
C20—C15—C16—Ir1	121.7 (4)	C48—C49—C50—C54	176.7 (4)
C13—C12—C16—C15	-3.7 (4)	C49—C50—C51—C52	1.8 (6)
C17—C12—C16—C15	174.1 (4)	C54—C50—C51—C52	-176.5 (4)
Ir1—C12—C16—C15	-64.1 (3)	C50—C51—C52—C53	-0.5 (6)
C13—C12—C16—C21	-176.7 (4)	C50—C51—C52—C55	-178.6 (4)
C17—C12—C16—C21	1.1 (7)	C51—C52—C53—C48	-1.0 (5)
Ir1—C12—C16—C21	123.0 (4)	C55—C52—C53—C48	177.1 (3)
C13—C12—C16—Ir1	60.4 (3)	C49—C48—C53—C52	1.2 (5)
C17—C12—C16—Ir1	-121.8 (4)	B1—C48—C53—C52	174.4 (3)
C29—C24—C25—C26	1.5 (5)	C49—C50—C54—F21	147.8 (7)
B1—C24—C25—C26	173.9 (4)	C51—C50—C54—F21	-33.8 (9)
C24—C25—C26—C27	0.7 (6)	C49—C50—C54—F20B	47.5 (8)
C24—C25—C26—C30	-178.2 (4)	C51—C50—C54—F20B	-134.1 (7)
C25—C26—C27—C28	-1.7 (7)	C49—C50—C54—F21B	-170.0 (7)
C30—C26—C27—C28	177.2 (5)	C51—C50—C54—F21B	8.3 (9)
C26—C27—C28—C29	0.4 (7)	C49—C50—C54—F20	22.1 (8)
C26—C27—C28—C31	-178.4 (5)	C51—C50—C54—F20	-159.5 (6)

C27—C28—C29—C24	2.0 (7)	C49—C50—C54—F19	-85.6 (6)
C31—C28—C29—C24	-179.2 (4)	C51—C50—C54—F19	92.8 (6)
C25—C24—C29—C28	-2.9 (6)	C49—C50—C54—F19B	-57.3 (8)
B1—C24—C29—C28	-175.3 (4)	C51—C50—C54—F19B	121.0 (7)
C25—C26—C30—F2	103.6 (6)	C51—C52—C55—F23	90.5 (5)
C27—C26—C30—F2	-75.4 (7)	C53—C52—C55—F23	-87.7 (5)
C25—C26—C30—F1	-21.6 (8)	C51—C52—C55—F24	-148.9 (4)
C27—C26—C30—F1	159.5 (5)	C53—C52—C55—F24	32.9 (5)
C25—C26—C30—F3	-140.2 (5)	C51—C52—C55—F22	-31.1 (5)
C27—C26—C30—F3	40.8 (7)	C53—C52—C55—F22	150.7 (4)
C27—C28—C31—F4B	-14.6 (10)	C2—C1—N1—C5	-2.0 (8)
C29—C28—C31—F4B	166.6 (7)	C2—C1—N1—Ir1	178.8 (4)
C27—C28—C31—F6	-167.6 (6)	C4—C5—N1—C1	4.1 (7)
C29—C28—C31—F6	13.6 (9)	C6—C5—N1—C1	-172.4 (4)
C27—C28—C31—F5	69.3 (7)	C4—C5—N1—Ir1	-176.7 (4)
C29—C28—C31—F5	-109.5 (6)	C6—C5—N1—Ir1	6.8 (5)
C27—C28—C31—F6B	-139.6 (7)	C29—C24—B1—C48	-155.6 (3)
C29—C28—C31—F6B	41.6 (8)	C25—C24—B1—C48	32.6 (5)
C27—C28—C31—F4	-44.6 (7)	C29—C24—B1—C40	85.6 (4)
C29—C28—C31—F4	136.6 (5)	C25—C24—B1—C40	-86.3 (4)
C27—C28—C31—F5B	102.1 (6)	C29—C24—B1—C32	-36.6 (5)
C29—C28—C31—F5B	-76.7 (7)	C25—C24—B1—C32	151.5 (3)
C37—C32—C33—C34	-3.7 (5)	C49—C48—B1—C24	-150.8 (3)
B1—C32—C33—C34	-179.1 (3)	C53—C48—B1—C24	36.4 (4)
C32—C33—C34—C35	2.8 (6)	C49—C48—B1—C40	-36.4 (4)

C32—C33—C34—C38	-176.3 (4)	C53—C48—B1—C40	150.7 (3)
C33—C34—C35—C36	0.2 (6)	C49—C48—B1—C32	85.9 (4)
C38—C34—C35—C36	179.3 (4)	C53—C48—B1—C32	-87.0 (4)
C34—C35—C36—C37	-2.1 (6)	C41—C40—B1—C24	-96.0 (4)
C34—C35—C36—C39	178.6 (4)	C45—C40—B1—C24	76.8 (4)
C35—C36—C37—C32	1.0 (6)	C41—C40—B1—C48	143.2 (3)
C39—C36—C37—C32	-179.7 (4)	C45—C40—B1—C48	-44.0 (4)
C33—C32—C37—C36	1.8 (5)	C41—C40—B1—C32	25.8 (5)
B1—C32—C37—C36	177.3 (3)	C45—C40—B1—C32	-161.4 (3)
C35—C34—C38—F9B	-23.6 (9)	C37—C32—B1—C24	159.5 (3)
C33—C34—C38—F9B	155.6 (7)	C33—C32—B1—C24	-25.3 (5)
C35—C34—C38—F7	172.4 (7)	C37—C32—B1—C48	-76.9 (4)
C33—C34—C38—F7	-8.4 (9)	C33—C32—B1—C48	98.2 (4)
C35—C34—C38—F7B	125.6 (7)	C37—C32—B1—C40	43.5 (4)
C33—C34—C38—F7B	-55.3 (8)	C33—C32—B1—C40	-141.4 (3)

7.2 [**2**][BPh_4]

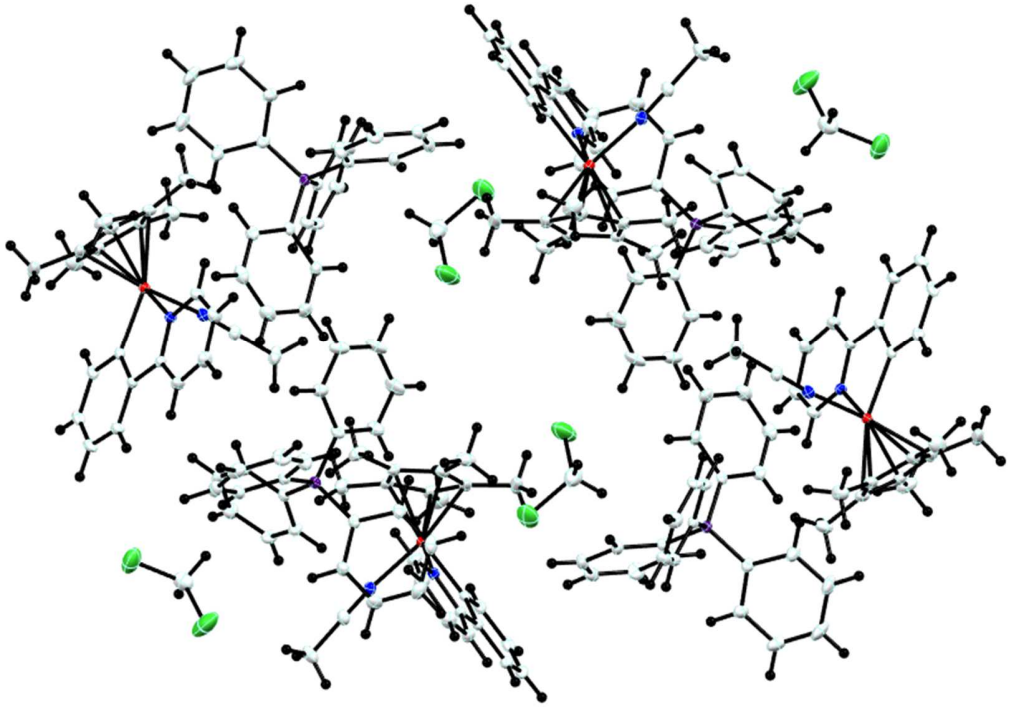

7.2.1 **Figure A4.** Crystal lattice packing of [**2**][BPh_4].

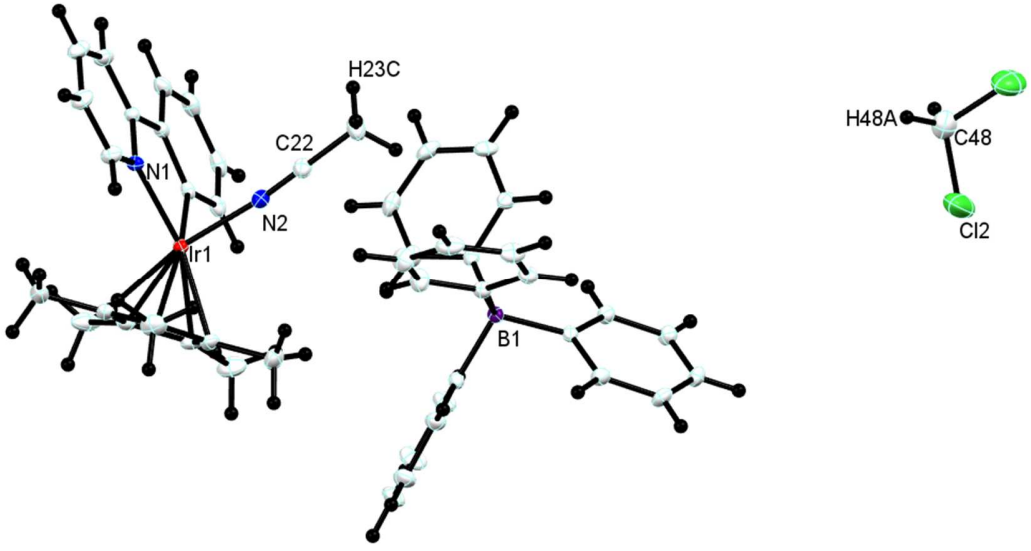

7.2.2 **Figure A5.** Asymmetric unit of [**2**][BPh_4], with all hydrogens and partial numbering of atoms.

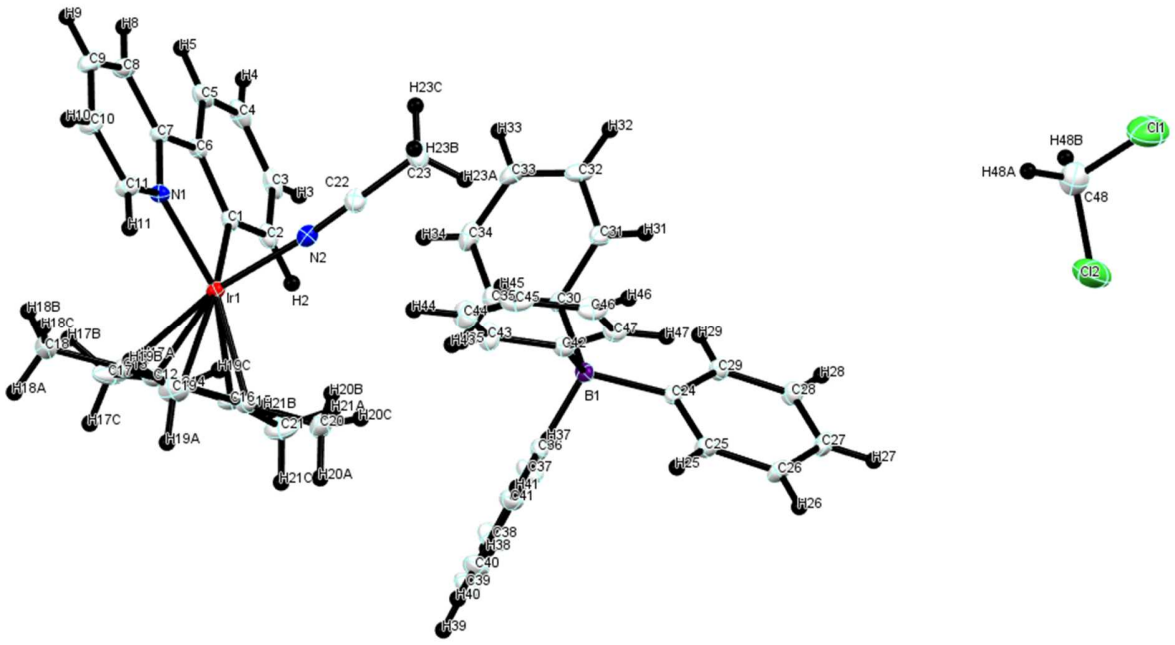

7.2.3 **Figure A6.** Asymmetric unit of [**2**][BPh_4], with all hydrogens and total numbering of atoms.

[**2**][BPh_4]

Data collection: Bruker *APEX2*; cell refinement: Bruker *SAINT*; data reduction: Bruker *SAINT*; program(s) used to solve structure: *SHELXS2013* (Sheldrick, 2013); program(s) used to refine structure: *SHELXL2013* (Sheldrick, 2013); molecular graphics: Bruker *SHELXTL*; software used to prepare material for publication: Bruker *SHELXTL*.

7.2.4 Crystal data

$C_{23}H_{26}IrN_2 \cdot C_{24}H_{20}B \cdot CH_2Cl_2$	$F(000)$ = 1864
M_r = 926.79	D_x = 1.475 Mg m^{-3}
Monoclinic, $P2_1/c$	Mo $K\alpha$ radiation, λ = 0.71073 Å
a = 11.6460 (3) Å	Cell parameters from 9951 reflections
b = 23.1238 (7) Å	θ = 2.6–32.0°
c = 18.5864 (5) Å	μ = 3.36 mm^{-1}

β = 123.485 (1)°	T = 173 K
V = 4174.6 (2) Å^3	Prism, yellow
Z = 4	0.32 × 0.20 × 0.18 mm

7.2.5 Data collection

Bruker APEX-II CCD diffractometer	11492 reflections with $I > 2\sigma(I)$
Radiation source: fine focus sealed tube	R_{int} = 0.034
ϕ and ω scans	θ_{max} = 32.0°, θ_{min} = 1.6°
Absorption correction: multi-scan *SADABS*	h = -17→17
T_{min} = 0.610, T_{max} = 0.746	k = -34→34
59089 measured reflections	l = -27→27
14481 independent reflections	

7.2.6 Refinement

Refinement on F^2	Primary atom site location: structure-invariant direct methods
Least-squares matrix: full	Secondary atom site location: difference Fourier map
$R[F^2 > 2\sigma(F^2)]$ = 0.032	Hydrogen site location: inferred from neighbouring sites
$wR(F^2)$ = 0.062	H-atom parameters constrained
S = 1.03	$w = 1/[\sigma^2(F_o^2) + (0.0244P)^2 + 3.2725P]$ where $P = (F_o^2 + 2F_c^2)/3$
14481 reflections	$(\Delta/\sigma)_{max}$ = 0.002
493 parameters	$\Delta\rangle_{max}$ = 1.61 e Å^{-3}
0 restraints	$\Delta\rangle_{min}$ = -1.05 e Å^{-3}

7.2.7 Special details

Geometry. All esds (except the esd in the dihedral angle between two l.s. planes) are estimated using the full covariance matrix. The cell esds are taken into account individually in the estimation of esds in distances, angles and torsion angles; correlations between esds in cell parameters are only used when they are defined by crystal symmetry. An approximate (isotropic) treatment of cell esds is used for estimating esds involving l.s. planes.

7.2.8 **Table A4.** Fractional atomic coordinates and isotropic or equivalent isotropic displacement parameters (Å^2) for [**2**][BPh_4].

	x	*y*	*z*	U_{iso}*/U_{eq}
C1	-0.0626 (3)	0.04540 (9)	0.68280 (14)	0.0210 (4)
C2	0.0372 (3)	0.01803 (10)	0.67538 (16)	0.0268 (5)
H2	0.1307	0.0187	0.7226	0.032*
C3	0.0013 (3)	-0.01021 (11)	0.59963 (18)	0.0338 (6)
H3	0.0707	-0.0289	0.5961	0.041*
C4	-0.1328 (3)	-0.01152 (11)	0.52984 (18)	0.0345 (6)
H4	-0.1559	-0.0315	0.4788	0.041*
C5	-0.2337 (3)	0.01635 (11)	0.53412 (16)	0.0294 (5)
H5	-0.3263	0.0164	0.4857	0.035*
C6	-0.1985 (3)	0.04461 (9)	0.61043 (14)	0.0213 (4)
C7	-0.2989 (2)	0.07475 (9)	0.62058 (14)	0.0204 (4)
C8	-0.4387 (3)	0.08079 (11)	0.55831 (15)	0.0288 (5)
H8	-0.4774	0.0639	0.5029	0.035*
C9	-0.5211 (3)	0.11108 (12)	0.57663 (18)	0.0346 (6)
H9	-0.6167	0.1153	0.5341	0.042*
C10	-0.4640 (3)	0.13545 (12)	0.65761 (17)	0.0328 (6)
H10	-0.5195	0.1562	0.6717	0.039*
C11	-0.3246 (3)	0.12889 (11)	0.71722 (16)	0.0277 (5)
H11	-0.2844	0.1463	0.7724	0.033*
C12	0.0450 (3)	0.01849 (10)	0.87977 (15)	0.0295 (5)
C13	-0.0408 (3)	0.05430 (12)	0.89519 (15)	0.0290 (5)
C14	0.0208 (3)	0.11081 (11)	0.92211 (14)	0.0266 (5)
C15	0.1429 (3)	0.10956 (11)	0.92112 (14)	0.0268 (5)
C16	0.1603 (3)	0.05304 (12)	0.89650 (15)	0.0298 (5)
C17	0.0251 (4)	-0.04498 (12)	0.86062 (19)	0.0494 (9)
H17A	0.0610	-0.0555	0.8255	0.074*
H17B	-0.0733	-0.0542	0.8290	0.074*
H17C	0.0744	-0.0668	0.9148	0.074*
C18	-0.1679 (3)	0.03419 (15)	0.88854 (18)	0.0452 (8)
H18A	-0.1427	0.0137	0.9415	0.068*
H18B	-0.2191	0.0080	0.8391	0.068*
H18C	-0.2256	0.0676	0.8806	0.068*

C19	-0.0257 (3)	0.15977 (14)	0.95288 (18)	0.0410 (7)
H19A	0.0290	0.1602	1.0161	0.061*
H19B	-0.1231	0.1547	0.9312	0.061*
H19C	-0.0133	0.1964	0.9315	0.061*
C20	0.2391 (3)	0.15917 (13)	0.94385 (18)	0.0386 (6)
H20A	0.3004	0.1623	1.0067	0.058*
H20B	0.1861	0.1950	0.9204	0.058*
H20C	0.2941	0.1528	0.9194	0.058*
C21	0.2857 (3)	0.03239 (16)	0.9008 (2)	0.0482 (8)
H21A	0.3159	0.0621	0.8771	0.072*
H21B	0.2639	-0.0032	0.8671	0.072*
H21C	0.3595	0.0248	0.9610	0.072*
C22	-0.0243 (3)	0.19965 (11)	0.68926 (17)	0.0285 (5)
C23	-0.0280 (3)	0.24787 (12)	0.6377 (2)	0.0406 (7)
H23A	0.0658	0.2570	0.6544	0.061*
H23B	-0.0684	0.2817	0.6474	0.061*
H23C	-0.0840	0.2373	0.5764	0.061*
C24	0.6176 (2)	0.29324 (9)	0.85195 (14)	0.0204 (4)
C25	0.7011 (3)	0.33182 (11)	0.91968 (15)	0.0266 (5)
H25	0.6737	0.3424	0.9575	0.032*
C26	0.8216 (3)	0.35520 (12)	0.93387 (16)	0.0307 (5)
H26	0.8740	0.3815	0.9801	0.037*
C27	0.8659 (3)	0.34033 (12)	0.88078 (17)	0.0313 (5)
H27	0.9479	0.3564	0.8897	0.038*
C28	0.7880 (3)	0.30148 (12)	0.81437 (16)	0.0300 (5)
H28	0.8175	0.2903	0.7779	0.036*
C29	0.6672 (3)	0.27867 (11)	0.80061 (15)	0.0253 (5)
H29	0.6160	0.2521	0.7545	0.030*
C30	0.3827 (2)	0.22859 (10)	0.75166 (14)	0.0208 (4)
C31	0.3417 (3)	0.25336 (10)	0.67181 (15)	0.0270 (5)
H31	0.3751	0.2907	0.6713	0.032*
C32	0.2543 (3)	0.22545 (12)	0.59358 (16)	0.0350 (6)
H32	0.2315	0.2434	0.5413	0.042*
C33	0.2006 (3)	0.17184 (13)	0.59154 (18)	0.0360 (6)
H33	0.1414	0.1525	0.5383	0.043*
C34	0.2341 (3)	0.14691 (12)	0.66796 (19)	0.0356 (6)
H34	0.1960	0.1105	0.6675	0.043*

C35	0.3236 (3)	0.17467 (11)	0.74585 (17)	0.0286 (5)
H35	0.3456	0.1562	0.7976	0.034*
C36	0.5436 (2)	0.22212 (10)	0.92723 (15)	0.0240 (5)
C37	0.6005 (3)	0.16789 (12)	0.93045 (18)	0.0363 (6)
H37	0.5996	0.1552	0.8815	0.044*
C38	0.6579 (4)	0.13191 (15)	1.0021 (2)	0.0498 (8)
H38	0.6933	0.0951	1.0011	0.060*
C39	0.6634 (3)	0.14999 (15)	1.0748 (2)	0.0479 (8)
H39	0.7038	0.1259	1.1244	0.058*
C40	0.6104 (3)	0.20262 (15)	1.07490 (18)	0.0419 (7)
H40	0.6135	0.2151	1.1246	0.050*
C41	0.5516 (3)	0.23821 (12)	1.00217 (16)	0.0323 (6)
H41	0.5157	0.2747	1.0038	0.039*
C42	0.3785 (3)	0.31300 (10)	0.84244 (14)	0.0227 (4)
C43	0.2682 (3)	0.29455 (12)	0.84696 (19)	0.0344 (6)
H43	0.2564	0.2542	0.8503	0.041*
C44	0.1756 (3)	0.33192 (14)	0.84677 (19)	0.0397 (7)
H44	0.1036	0.3172	0.8512	0.048*
C45	0.1876 (3)	0.39056 (13)	0.84009 (17)	0.0381 (7)
H45	0.1248	0.4167	0.8402	0.046*
C46	0.2926 (3)	0.41069 (12)	0.83322 (17)	0.0361 (6)
H46	0.3010	0.4510	0.8274	0.043*
C47	0.3861 (3)	0.37265 (11)	0.83476 (15)	0.0276 (5)
H47	0.4579	0.3878	0.8304	0.033*
C48	0.4210 (4)	0.93761 (17)	0.7645 (2)	0.0547 (9)
H48A	0.3425	0.9379	0.7713	0.066*
H48B	0.4090	0.9043	0.7275	0.066*
N1	-0.2435 (2)	0.09880 (8)	0.70017 (12)	0.0209 (4)
N2	-0.0213 (2)	0.16173 (8)	0.72890 (13)	0.0253 (4)
B1	0.4812 (3)	0.26427 (11)	0.84248 (16)	0.0206 (5)
Ir1	-0.03220 (2)	0.08904 (2)	0.78878 (2)	0.01957 (3)
Cl1	0.42010 (14)	1.00129 (5)	0.71425 (8)	0.0876 (4)
Cl2	0.57214 (16)	0.92938 (6)	0.86430 (8)	0.1058 (5)

7.2.9 **Table A5.** Atomic displacement parameters ($Å^2$) for [**2**][BPh_4].

	U^{11}	U^{22}	U^{33}	U^{12}	U^{13}	U^{23}
C1	0.0263 (12)	0.0164 (9)	0.0261 (10)	0.0005 (9)	0.0181 (10)	0.0027 (8)
C2	0.0320 (14)	0.0232 (11)	0.0346 (12)	0.0024 (10)	0.0242 (12)	0.0028 (9)
C3	0.0537 (19)	0.0232 (11)	0.0489 (16)	0.0006 (12)	0.0437 (16)	0.0009 (11)
C4	0.059 (2)	0.0258 (12)	0.0368 (13)	-0.0067 (12)	0.0380 (15)	-0.0069 (10)
C5	0.0424 (16)	0.0258 (12)	0.0251 (11)	-0.0048 (11)	0.0218 (12)	-0.0023 (9)
C6	0.0289 (12)	0.0177 (9)	0.0197 (9)	-0.0026 (9)	0.0148 (10)	-0.0007 (8)
C7	0.0221 (11)	0.0191 (9)	0.0177 (9)	-0.0015 (8)	0.0096 (9)	0.0010 (7)
C8	0.0256 (13)	0.0290 (13)	0.0225 (10)	-0.0022 (10)	0.0074 (10)	-0.0021 (9)
C9	0.0209 (13)	0.0364 (14)	0.0337 (13)	0.0036 (11)	0.0070 (11)	0.0016 (11)
C10	0.0220 (13)	0.0367 (14)	0.0373 (13)	0.0057 (11)	0.0147 (11)	-0.0022 (11)
C11	0.0243 (13)	0.0326 (12)	0.0248 (11)	0.0052 (10)	0.0127 (10)	-0.0035 (9)
C12	0.0308 (14)	0.0232 (11)	0.0194 (10)	-0.0001 (10)	0.0044 (10)	0.0029 (8)
C13	0.0253 (13)	0.0351 (13)	0.0200 (10)	-0.0042 (11)	0.0083 (10)	0.0044 (9)
C14	0.0252 (13)	0.0325 (12)	0.0182 (10)	-0.0012 (10)	0.0096 (10)	-0.0014 (9)
C15	0.0230 (12)	0.0307 (12)	0.0184 (10)	-0.0026 (10)	0.0063 (9)	-0.0021 (9)
C16	0.0218 (12)	0.0346 (13)	0.0213 (10)	0.0055 (11)	0.0045 (10)	-0.0002 (9)
C17	0.058 (2)	0.0244 (13)	0.0316 (14)	0.0010 (14)	0.0035 (14)	0.0030 (11)
C18	0.0363 (17)	0.063 (2)	0.0308 (13)	-0.0149 (15)	0.0155 (13)	0.0076 (13)
C19	0.0423 (18)	0.0511 (17)	0.0309 (13)	0.0033 (14)	0.0210 (13)	-0.0104 (12)
C20	0.0340 (16)	0.0426 (16)	0.0346 (14)	-0.0137 (13)	0.0160 (13)	-0.0065 (12)
C21	0.0314 (16)	0.060 (2)	0.0410 (16)	0.0170 (15)	0.0125 (14)	-0.0009 (15)
C22	0.0262 (13)	0.0257 (12)	0.0341 (12)	0.0028 (10)	0.0170 (11)	0.0021 (10)
C23	0.0432 (18)	0.0319 (14)	0.0532 (17)	0.0042 (13)	0.0307 (16)	0.0142 (12)
C24	0.0189 (11)	0.0195 (10)	0.0227 (10)	0.0019 (9)	0.0113 (9)	0.0029 (8)
C25	0.0228 (12)	0.0324 (12)	0.0238 (10)	0.0008 (10)	0.0123 (10)	-0.0035 (9)
C26	0.0225 (13)	0.0340 (13)	0.0280 (12)	-0.0042 (11)	0.0092 (10)	-0.0082 (10)
C27	0.0190 (12)	0.0394 (14)	0.0349 (13)	-0.0027 (11)	0.0144 (11)	0.0001 (11)
C28	0.0244 (13)	0.0420 (14)	0.0287 (11)	0.0007 (11)	0.0178 (11)	-0.0021 (10)
C29	0.0236 (12)	0.0298 (12)	0.0253 (10)	-0.0006 (10)	0.0152 (10)	-0.0028 (9)
C30	0.0165 (10)	0.0207 (10)	0.0272 (10)	0.0037 (9)	0.0134 (9)	0.0010 (8)
C31	0.0238 (12)	0.0227 (11)	0.0283 (11)	0.0024 (10)	0.0103 (10)	0.0028 (9)
C32	0.0272 (14)	0.0381 (14)	0.0253 (11)	0.0090 (12)	0.0054 (11)	0.0057 (10)
C33	0.0187 (12)	0.0411 (15)	0.0347 (13)	0.0002 (11)	0.0061 (11)	-0.0096 (11)
C34	0.0285 (14)	0.0301 (13)	0.0515 (16)	-0.0069 (11)	0.0241 (14)	-0.0074 (12)
C35	0.0298 (14)	0.0266 (12)	0.0353 (13)	-0.0026 (10)	0.0218 (12)	-0.0009 (10)
C36	0.0198 (11)	0.0280 (11)	0.0272 (11)	0.0020 (9)	0.0149 (10)	0.0047 (9)

C37	0.0389 (16)	0.0384 (14)	0.0378 (14)	0.0170 (13)	0.0252 (13)	0.0137 (12)
C38	0.052 (2)	0.0454 (18)	0.0537 (19)	0.0261 (16)	0.0304 (17)	0.0263 (15)
C39	0.0406 (18)	0.060 (2)	0.0418 (16)	0.0144 (16)	0.0221 (15)	0.0307 (15)
C40	0.0351 (16)	0.064 (2)	0.0262 (12)	0.0033 (15)	0.0168 (12)	0.0098 (13)
C41	0.0307 (14)	0.0393 (14)	0.0258 (11)	0.0029 (12)	0.0148 (11)	0.0029 (10)
C42	0.0228 (12)	0.0239 (10)	0.0221 (10)	0.0046 (9)	0.0128 (9)	0.0001 (8)
C43	0.0333 (15)	0.0306 (13)	0.0489 (16)	0.0054 (11)	0.0288 (14)	0.0030 (11)
C44	0.0315 (15)	0.0523 (18)	0.0467 (16)	0.0103 (14)	0.0288 (14)	0.0044 (14)
C45	0.0334 (15)	0.0461 (16)	0.0287 (12)	0.0202 (13)	0.0134 (12)	-0.0011 (11)
C46	0.0386 (16)	0.0272 (12)	0.0345 (13)	0.0117 (12)	0.0151 (12)	0.0002 (11)
C47	0.0294 (14)	0.0244 (11)	0.0280 (11)	0.0040 (10)	0.0152 (11)	0.0021 (9)
C48	0.058 (2)	0.057 (2)	0.058 (2)	-0.0095 (18)	0.0371 (19)	-0.0127 (17)
N1	0.0205 (9)	0.0217 (9)	0.0191 (8)	0.0021 (7)	0.0101 (8)	0.0001 (7)
N2	0.0228 (11)	0.0239 (9)	0.0282 (10)	-0.0005 (8)	0.0134 (9)	-0.0025 (8)
B1	0.0200 (12)	0.0215 (11)	0.0232 (11)	0.0044 (10)	0.0138 (10)	0.0025 (9)
Ir1	0.01784 (4)	0.02002 (4)	0.01959 (4)	0.00094 (4)	0.00953 (3)	-0.00042 (3)
Cl1	0.0823 (9)	0.0650 (6)	0.0720 (7)	0.0075 (6)	0.0153 (6)	0.0233 (5)
Cl2	0.1081 (11)	0.1045 (10)	0.0563 (6)	-0.0327 (8)	0.0147 (7)	0.0296 (6)

7.2.10 **Table A6.** Interatomic distances (Å) and angles (deg) for [**2**][BPh_4].

C1—C2	1.396 (3)	C23—H23C	0.9800
C1—C6	1.402 (3)	C24—C29	1.402 (3)
C1—Ir1	2.063 (2)	C24—C25	1.405 (3)
C2—C3	1.391 (3)	C24—B1	1.641 (4)
C2—H2	0.9500	C25—C26	1.387 (4)
C3—C4	1.374 (4)	C25—H25	0.9500
C3—H3	0.9500	C26—C27	1.385 (4)
C4—C5	1.381 (4)	C26—H26	0.9500
C4—H4	0.9500	C27—C28	1.385 (4)
C5—C6	1.402 (3)	C27—H27	0.9500
C5—H5	0.9500	C28—C29	1.388 (3)
C6—C7	1.460 (3)	C28—H28	0.9500
C7—N1	1.364 (3)	C29—H29	0.9500
C7—C8	1.389 (3)	C30—C35	1.400 (3)

C8—C9	1.375 (4)	C30—C31	1.406 (3)
C8—H8	0.9500	C30—B1	1.646 (3)
C9—C10	1.386 (4)	C31—C32	1.390 (4)
C9—H9	0.9500	C31—H31	0.9500
C10—C11	1.378 (4)	C32—C33	1.380 (4)
C10—H10	0.9500	C32—H32	0.9500
C11—N1	1.344 (3)	C33—C34	1.375 (4)
C11—H11	0.9500	C33—H33	0.9500
C12—C16	1.441 (4)	C34—C35	1.389 (4)
C12—C13	1.443 (4)	C34—H34	0.9500
C12—C17	1.498 (4)	C35—H35	0.9500
C12—Ir1	2.157 (2)	C36—C41	1.394 (3)
C13—C14	1.441 (4)	C36—C37	1.404 (4)
C13—C18	1.491 (4)	C36—B1	1.642 (3)
C13—Ir1	2.187 (2)	C37—C38	1.389 (4)
C14—C15	1.433 (4)	C37—H37	0.9500
C14—C19	1.498 (4)	C38—C39	1.383 (5)
C14—Ir1	2.256 (2)	C38—H38	0.9500
C15—C16	1.436 (4)	C39—C40	1.365 (5)
C15—C20	1.493 (4)	C39—H39	0.9500
C15—Ir1	2.213 (2)	C40—C41	1.397 (4)
C16—C21	1.497 (4)	C40—H40	0.9500
C16—Ir1	2.185 (2)	C41—H41	0.9500
C17—H17A	0.9800	C42—C47	1.395 (3)
C17—H17B	0.9800	C42—C43	1.399 (4)
C17—H17C	0.9800	C42—B1	1.643 (3)
C18—H18A	0.9800	C43—C44	1.380 (4)
C18—H18B	0.9800	C43—H43	0.9500
C18—H18C	0.9800	C44—C45	1.376 (4)
C19—H19A	0.9800	C44—H44	0.9500
C19—H19B	0.9800	C45—C46	1.378 (4)
C19—H19C	0.9800	C45—H45	0.9500
C20—H20A	0.9800	C46—C47	1.388 (4)
C20—H20B	0.9800	C46—H46	0.9500
C20—H20C	0.9800	C47—H47	0.9500
C21—H21A	0.9800	C48—Cl2	1.724 (4)
C21—H21B	0.9800	C48—Cl1	1.741 (4)

C21—H21C	0.9800	C48—H48A	0.9900
C22—N2	1.133 (3)	C48—H48B	0.9900
C22—C23	1.456 (4)	N1—Ir1	2.085 (2)
C23—H23A	0.9800	N2—Ir1	2.058 (2)
C23—H23B	0.9800		
C2—C1—C6	117.4 (2)	C25—C26—H26	119.9
C2—C1—Ir1	127.07 (19)	C28—C27—C26	118.5 (2)
C6—C1—Ir1	115.52 (16)	C28—C27—H27	120.7
C3—C2—C1	120.8 (3)	C26—C27—H27	120.7
C3—C2—H2	119.6	C27—C28—C29	120.7 (2)
C1—C2—H2	119.6	C27—C28—H28	119.7
C4—C3—C2	121.1 (3)	C29—C28—H28	119.7
C4—C3—H3	119.4	C28—C29—C24	122.7 (2)
C2—C3—H3	119.4	C28—C29—H29	118.7
C3—C4—C5	119.7 (2)	C24—C29—H29	118.7
C3—C4—H4	120.1	C35—C30—C31	114.5 (2)
C5—C4—H4	120.1	C35—C30—B1	124.1 (2)
C4—C5—C6	119.5 (3)	C31—C30—B1	121.1 (2)
C4—C5—H5	120.2	C32—C31—C30	122.8 (2)
C6—C5—H5	120.2	C32—C31—H31	118.6
C5—C6—C1	121.5 (2)	C30—C31—H31	118.6
C5—C6—C7	123.1 (2)	C33—C32—C31	120.3 (2)
C1—C6—C7	115.49 (19)	C33—C32—H32	119.8
N1—C7—C8	119.9 (2)	C31—C32—H32	119.8
N1—C7—C6	113.7 (2)	C34—C33—C32	118.8 (3)
C8—C7—C6	126.4 (2)	C34—C33—H33	120.6
C9—C8—C7	120.2 (2)	C32—C33—H33	120.6
C9—C8—H8	119.9	C33—C34—C35	120.4 (3)
C7—C8—H8	119.9	C33—C34—H34	119.8
C8—C9—C10	119.6 (3)	C35—C34—H34	119.8
C8—C9—H9	120.2	C34—C35—C30	123.1 (2)
C10—C9—H9	120.2	C34—C35—H35	118.4
C11—C10—C9	118.4 (2)	C30—C35—H35	118.4
C11—C10—H10	120.8	C41—C36—C37	115.2 (2)
C9—C10—H10	120.8	C41—C36—B1	123.4 (2)
N1—C11—C10	122.4 (2)	C37—C36—B1	121.3 (2)

N1—C11—H11	118.8	C38—C37—C36	122.9 (3)
C10—C11—H11	118.8	C38—C37—H37	118.6
C16—C12—C13	107.7 (2)	C36—C37—H37	118.6
C16—C12—C17	126.8 (3)	C39—C38—C37	119.6 (3)
C13—C12—C17	125.2 (3)	C39—C38—H38	120.2
C16—C12—Ir1	71.68 (14)	C37—C38—H38	120.2
C13—C12—Ir1	71.74 (14)	C40—C39—C38	119.6 (3)
C17—C12—Ir1	127.72 (17)	C40—C39—H39	120.2
C14—C13—C12	108.8 (2)	C38—C39—H39	120.2
C14—C13—C18	126.4 (3)	C39—C40—C41	120.3 (3)
C12—C13—C18	124.7 (3)	C39—C40—H40	119.9
C14—C13—Ir1	73.67 (13)	C41—C40—H40	119.9
C12—C13—Ir1	69.47 (13)	C36—C41—C40	122.4 (3)
C18—C13—Ir1	125.33 (18)	C36—C41—H41	118.8
C15—C14—C13	106.5 (2)	C40—C41—H41	118.8
C15—C14—C19	126.2 (2)	C47—C42—C43	114.9 (2)
C13—C14—C19	127.1 (2)	C47—C42—B1	126.2 (2)
C15—C14—Ir1	69.72 (13)	C43—C42—B1	118.9 (2)
C13—C14—Ir1	68.53 (13)	C44—C43—C42	123.4 (3)
C19—C14—Ir1	130.59 (18)	C44—C43—H43	118.3
C14—C15—C16	109.8 (2)	C42—C43—H43	118.3
C14—C15—C20	125.2 (2)	C45—C44—C43	119.9 (3)
C16—C15—C20	125.0 (3)	C45—C44—H44	120.0
C14—C15—Ir1	72.91 (14)	C43—C44—H44	120.0
C16—C15—Ir1	69.88 (13)	C44—C45—C46	118.7 (3)
C20—C15—Ir1	124.53 (18)	C44—C45—H45	120.6
C15—C16—C12	107.2 (2)	C46—C45—H45	120.6
C15—C16—C21	125.4 (3)	C45—C46—C47	120.7 (3)
C12—C16—C21	126.9 (3)	C45—C46—H46	119.7
C15—C16—Ir1	72.03 (14)	C47—C46—H46	119.7
C12—C16—Ir1	69.57 (14)	C46—C47—C42	122.3 (3)
C21—C16—Ir1	130.41 (19)	C46—C47—H47	118.8
C12—C17—H17A	109.5	C42—C47—H47	118.8
C12—C17—H17B	109.5	Cl2—C48—Cl1	111.8 (2)
H17A—C17—H17B	109.5	Cl2—C48—H48A	109.3
C12—C17—H17C	109.5	Cl1—C48—H48A	109.3
H17A—C17—H17C	109.5	Cl2—C48—H48B	109.3

H17B—C17—H17C	109.5	Cl1—C48—H48B	109.3
C13—C18—H18A	109.5	H48A—C48—H48B	107.9
C13—C18—H18B	109.5	C11—N1—C7	119.6 (2)
H18A—C18—H18B	109.5	C11—N1—Ir1	123.14 (16)
C13—C18—H18C	109.5	C7—N1—Ir1	117.27 (16)
H18A—C18—H18C	109.5	C22—N2—Ir1	173.9 (2)
H18B—C18—H18C	109.5	C24—B1—C36	104.43 (19)
C14—C19—H19A	109.5	C24—B1—C42	112.42 (19)
C14—C19—H19B	109.5	C36—B1—C42	110.15 (18)
H19A—C19—H19B	109.5	C24—B1—C30	113.57 (18)
C14—C19—H19C	109.5	C36—B1—C30	112.06 (19)
H19A—C19—H19C	109.5	C42—B1—C30	104.38 (18)
H19B—C19—H19C	109.5	N2—Ir1—C1	84.98 (8)
C15—C20—H20A	109.5	N2—Ir1—N1	83.26 (8)
C15—C20—H20B	109.5	C1—Ir1—N1	78.04 (8)
H20A—C20—H20B	109.5	N2—Ir1—C12	156.67 (10)
C15—C20—H20C	109.5	C1—Ir1—C12	99.00 (9)
H20A—C20—H20C	109.5	N1—Ir1—C12	120.07 (9)
H20B—C20—H20C	109.5	N2—Ir1—C16	117.93 (10)
C16—C21—H21A	109.5	C1—Ir1—C16	103.74 (9)
C16—C21—H21B	109.5	N1—Ir1—C16	158.77 (9)
H21A—C21—H21B	109.5	C12—Ir1—C16	38.75 (10)
C16—C21—H21C	109.5	N2—Ir1—C13	146.73 (9)
H21A—C21—H21C	109.5	C1—Ir1—C13	127.91 (9)
H21B—C21—H21C	109.5	N1—Ir1—C13	97.53 (9)
N2—C22—C23	179.3 (3)	C12—Ir1—C13	38.79 (10)
C22—C23—H23A	109.5	C16—Ir1—C13	64.35 (10)
C22—C23—H23B	109.5	N2—Ir1—C15	97.58 (9)
H23A—C23—H23B	109.5	C1—Ir1—C15	137.19 (10)
C22—C23—H23C	109.5	N1—Ir1—C15	144.77 (9)
H23A—C23—H23C	109.5	C12—Ir1—C15	63.95 (9)
H23B—C23—H23C	109.5	C16—Ir1—C15	38.09 (10)
C29—C24—C25	114.9 (2)	C13—Ir1—C15	63.10 (10)
C29—C24—B1	124.5 (2)	N2—Ir1—C14	110.53 (9)
C25—C24—B1	120.4 (2)	C1—Ir1—C14	163.17 (9)
C26—C25—C24	123.0 (2)	N1—Ir1—C14	109.38 (8)
C26—C25—H25	118.5	C12—Ir1—C14	64.17 (9)

C24—C25—H25	118.5	C16—Ir1—C14	63.75 (9)
C27—C26—C25	120.2 (2)	C13—Ir1—C14	37.81 (9)
C27—C26—H26	119.9	C15—Ir1—C14	37.38 (9)
C6—C1—C2—C3	-1.8 (3)	B1—C24—C25—C26	176.3 (2)
Ir1—C1—C2—C3	179.60 (17)	C24—C25—C26—C27	-0.8 (4)
C1—C2—C3—C4	0.6 (4)	C25—C26—C27—C28	-0.6 (4)
C2—C3—C4—C5	1.0 (4)	C26—C27—C28—C29	1.0 (4)
C3—C4—C5—C6	-1.4 (4)	C27—C28—C29—C24	0.0 (4)
C4—C5—C6—C1	0.2 (3)	C25—C24—C29—C28	-1.3 (4)
C4—C5—C6—C7	-179.6 (2)	B1—C24—C29—C28	-175.7 (2)
C2—C1—C6—C5	1.4 (3)	C35—C30—C31—C32	-2.8 (4)
Ir1—C1—C6—C5	-179.83 (17)	B1—C30—C31—C32	-177.4 (2)
C2—C1—C6—C7	-178.8 (2)	C30—C31—C32—C33	1.9 (4)
Ir1—C1—C6—C7	-0.1 (2)	C31—C32—C33—C34	0.5 (4)
C5—C6—C7—N1	179.3 (2)	C32—C33—C34—C35	-1.7 (4)
C1—C6—C7—N1	-0.4 (3)	C33—C34—C35—C30	0.7 (4)
C5—C6—C7—C8	-1.2 (4)	C31—C30—C35—C34	1.5 (4)
C1—C6—C7—C8	179.0 (2)	B1—C30—C35—C34	176.0 (2)
N1—C7—C8—C9	0.2 (4)	C41—C36—C37—C38	1.4 (4)
C6—C7—C8—C9	-179.2 (2)	B1—C36—C37—C38	178.0 (3)
C7—C8—C9—C10	-0.1 (4)	C36—C37—C38—C39	-1.6 (5)
C8—C9—C10—C11	0.7 (4)	C37—C38—C39—C40	1.0 (5)
C9—C10—C11—N1	-1.5 (4)	C38—C39—C40—C41	-0.3 (5)
C16—C12—C13—C14	-0.5 (3)	C37—C36—C41—C40	-0.8 (4)
C17—C12—C13—C14	172.7 (2)	B1—C36—C41—C40	-177.3 (3)

Ir1—C12—C13—C14	-63.57 (16)	C39—C40—C41—C36	0.3 (5)
C16—C12—C13—C18	-177.5 (2)	C47—C42—C43—C44	-2.0 (4)
C17—C12—C13—C18	-4.3 (4)	B1—C42—C43—C44	-179.6 (3)
Ir1—C12—C13—C18	119.5 (2)	C42—C43—C44—C45	1.4 (5)
C16—C12—C13—Ir1	63.09 (16)	C43—C44—C45—C46	0.3 (4)
C17—C12—C13—Ir1	-123.8 (2)	C44—C45—C46—C47	-1.3 (4)
C12—C13—C14—C15	1.3 (3)	C45—C46—C47—C42	0.6 (4)
C18—C13—C14—C15	178.2 (2)	C43—C42—C47—C46	1.0 (4)
Ir1—C13—C14—C15	-59.65 (16)	B1—C42—C47—C46	178.4 (2)
C12—C13—C14—C19	-173.7 (2)	C10—C11—N1—C7	1.6 (4)
C18—C13—C14—C19	3.2 (4)	C10—C11—N1—Ir1	179.3 (2)
Ir1—C13—C14—C19	125.4 (3)	C8—C7—N1—C11	-0.9 (3)
C12—C13—C14—Ir1	60.91 (16)	C6—C7—N1—C11	178.5 (2)
C18—C13—C14—Ir1	-122.2 (3)	C8—C7—N1—Ir1	-178.76 (17)
C13—C14—C15—C16	-1.6 (3)	C6—C7—N1—Ir1	0.7 (2)
C19—C14—C15—C16	173.4 (2)	C29—C24—B1—C36	107.4 (2)
Ir1—C14—C15—C16	-60.48 (16)	C25—C24—B1—C36	-66.8 (3)
C13—C14—C15—C20	179.5 (2)	C29—C24—B1—C42	-133.2 (2)
C19—C14—C15—C20	-5.5 (4)	C25—C24—B1—C42	52.6 (3)
Ir1—C14—C15—C20	120.6 (2)	C29—C24—B1—C30	-15.0 (3)
C13—C14—C15—Ir1	58.88 (16)	C25—C24—B1—C30	170.9 (2)
C19—C14—C15—Ir1	-126.1 (3)	C41—C36—B1—C24	98.5 (3)
C14—C15—C16—C12	1.3 (3)	C37—C36—B1—C24	-77.8 (3)
C20—C15—C16—C12	-179.7 (2)	C41—C36—B1—C42	-22.4 (3)
Ir1—C15—C16—C12	-61.03 (16)	C37—C36—B1—C42	161.3 (2)
C14—C15—C16—C21	-170.4 (2)	C41—C36—B1—C30	-138.1 (2)

C20—C15—C16—C21	8.6 (4)	C37—C36—B1—C30	45.6 (3)
Ir1—C15—C16—C21	127.3 (3)	C47—C42—B1—C24	11.6 (3)
C14—C15—C16—Ir1	62.34 (17)	C43—C42—B1—C24	-171.2 (2)
C20—C15—C16—Ir1	-118.7 (2)	C47—C42—B1—C36	127.6 (2)
C13—C12—C16—C15	-0.5 (3)	C43—C42—B1—C36	-55.2 (3)
C17—C12—C16—C15	-173.5 (2)	C47—C42—B1—C30	-111.9 (3)
Ir1—C12—C16—C15	62.63 (16)	C43—C42—B1—C30	65.3 (3)
C13—C12—C16—C21	171.0 (2)	C35—C30—B1—C24	136.9 (2)
C17—C12—C16—C21	-2.0 (4)	C31—C30—B1—C24	-49.0 (3)
Ir1—C12—C16—C21	-125.8 (3)	C35—C30—B1—C36	18.8 (3)
C13—C12—C16—Ir1	-63.13 (16)	C31—C30—B1—C36	-167.0 (2)
C17—C12—C16—Ir1	123.9 (3)	C35—C30—B1—C42	-100.4 (3)
C29—C24—C25—C26	1.7 (4)	C31—C30—B1—C42	73.8 (3)

7.3 [**2**][BF_4]

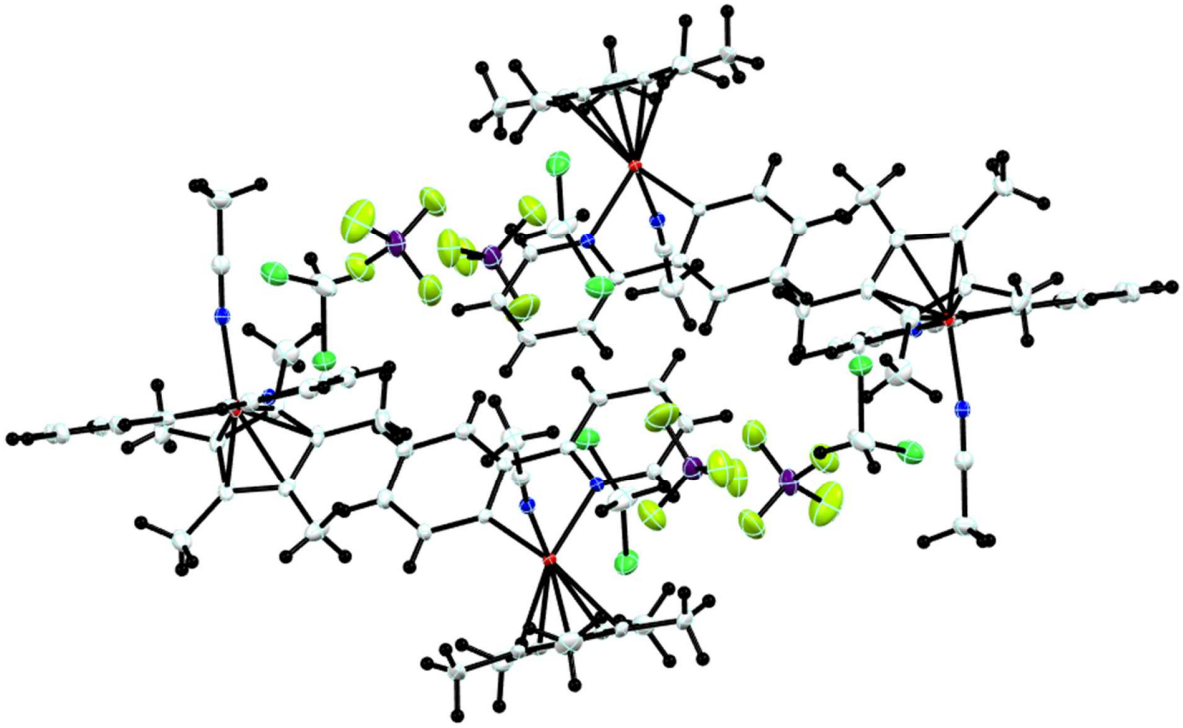

7.3.1 **Figure A7.** Crystal lattice packing of [**2**][BF_4].

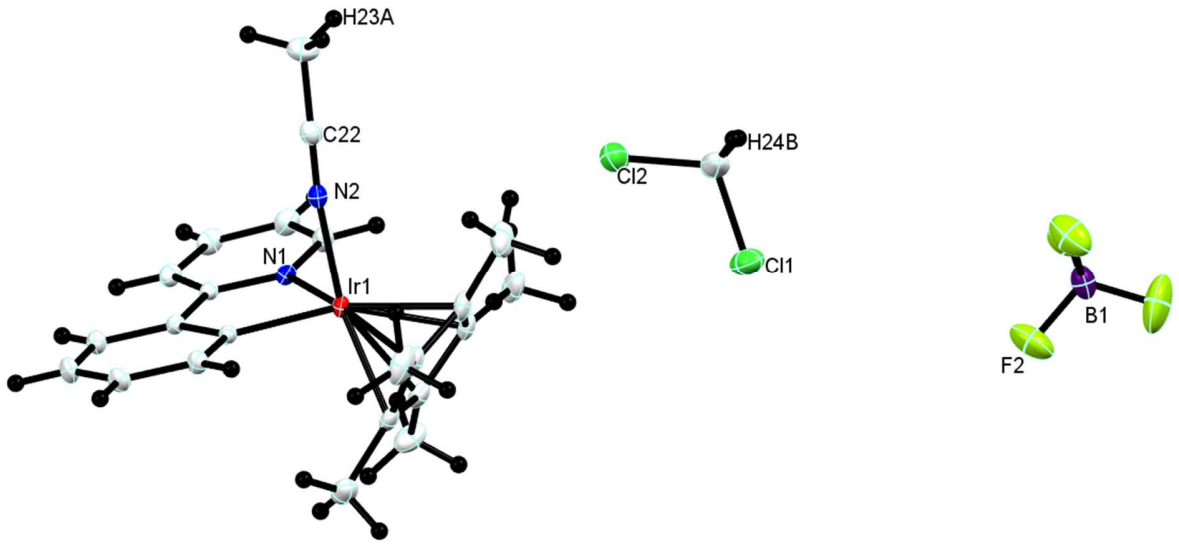

7.3.2 **Figure A8.** Asymmetric unit of [**2**][BF_4], with all hydrogens and partial numbering of atoms.

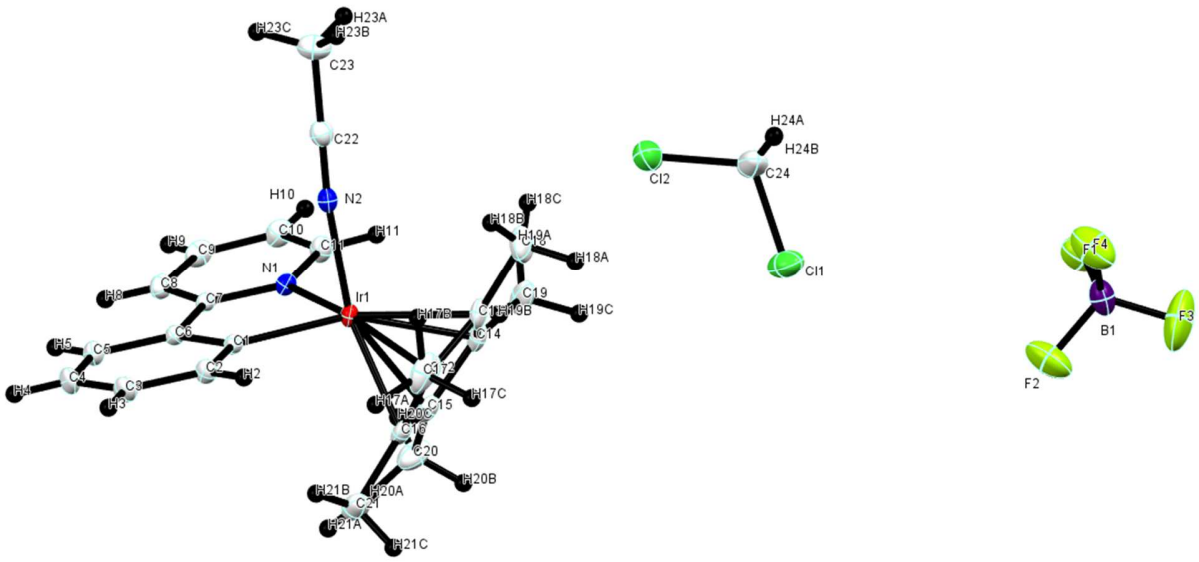

7.3.3 **Figure A9.** Asymmetric unit of [**2**][BF_4], with all hydrogens and total numbering of atoms.

[**2**][BF_4]

Data collection: Bruker *APEX2*; cell refinement: Bruker *SAINT*; data reduction: Bruker *SAINT*; program(s) used to solve structure: *SHELXS2013* (Sheldrick, 2013); program(s) used to refine structure: *SHELXL2013* (Sheldrick, 2013); molecular graphics: Bruker *SHELXTL*; software used to prepare material for publication: Bruker *SHELXTL*.

7.3.4 Crystal data

$C_{23}H_{26}IrN_2 \cdot BF_4 \cdot CH_2Cl_2$	$F(000)$ = 1352
M_r = 694.39	D_x = 1.768 Mg m^{-3}
Monoclinic, $P2_1/c$	Mo $K\alpha$ radiation, λ = 0.71073 Å
a = 14.6676 (5) Å	Cell parameters from 9963 reflections
b = 12.8597 (4) Å	θ = 2.6–32.0°
c = 15.8707 (4) Å	μ = 5.37 mm^{-1}
β = 119.400 (2)°	T = 173 K

V = 2608.02 (14) Å^3	Prism, yellow
Z = 4	0.30 × 0.25 × 0.20 mm

7.3.5 Data collection

Bruker APEX-II CCD diffractometer	7606 reflections with $I > 2\sigma(I)$
Radiation source: fine focus sealed tube	R_{int} = 0.025
ϕ and ω scans	θ_{max} = 32.0°, θ_{min} = 1.6°
Absorption correction: multi-scan *SADABS*	h = -21→21
T_{min} = 0.627, T_{max} = 0.746	k = -19→17
35077 measured reflections	l = -23→23
9049 independent reflections	

7.3.6 Refinement

Refinement on F^2	Primary atom site location: structure-invariant direct methods
Least-squares matrix: full	Secondary atom site location: difference Fourier map
$R[F^2 > 2\sigma(F^2)]$ = 0.030	Hydrogen site location: inferred from neighbouring sites
$wR(F^2)$ = 0.063	H-atom parameters constrained
S = 1.11	$w = 1/[\sigma^2(F_o^2) + (0.0174P)^2 + 6.0988P]$ where $P = (F_o^2 + 2F_c^2)/3$
9049 reflections	$(\Delta/\sigma)_{max}$ = 0.003
313 parameters	$\Delta\rangle_{max}$ = 1.74 e Å^{-3}
0 restraints	$\Delta\rangle_{min}$ = -1.44 e Å^{-3}

7.3.7 Special details

Geometry. All esds (except the esd in the dihedral angle between two l.s. planes) are estimated using the full covariance matrix. The cell esds are taken into account individually in the estimation of esds in distances, angles and torsion angles; correlations between esds in cell parameters are only used when they are defined by crystal symmetry. An approximate (isotropic) treatment of cell esds is used for estimating esds involving l.s. planes.

7.3.8 **Table A7.** Fractional atomic coordinates and isotropic or equivalent isotropic displacement parameters (Å^2) for [**2**][BF_4].

	x	*y*	*z*	U_{iso}*/U_{eq}
C1	0.8060 (2)	0.8903 (2)	0.11931 (19)	0.0203 (5)
C2	0.8837 (2)	0.8746 (3)	0.0936 (2)	0.0262 (6)
H2	0.9235	0.8122	0.1125	0.031*
C3	0.9034 (2)	0.9487 (3)	0.0409 (2)	0.0317 (7)
H3	0.9566	0.9364	0.0244	0.038*
C4	0.8467 (3)	1.0400 (3)	0.0122 (2)	0.0334 (7)
H4	0.8614	1.0903	-0.0233	0.040*
C5	0.7682 (2)	1.0581 (3)	0.0353 (2)	0.0287 (6)
H5	0.7286	1.1206	0.0154	0.034*
C6	0.7482 (2)	0.9834 (2)	0.08826 (19)	0.0215 (5)
C7	0.6634 (2)	0.9927 (2)	0.11185 (19)	0.0211 (5)
C8	0.5944 (2)	1.0763 (2)	0.0890 (2)	0.0276 (6)
H8	0.6010	1.1355	0.0566	0.033*
C9	0.5164 (3)	1.0723 (3)	0.1137 (2)	0.0315 (7)
H9	0.4705	1.1296	0.1002	0.038*
C10	0.5056 (3)	0.9847 (3)	0.1581 (2)	0.0319 (7)
H10	0.4511	0.9801	0.1739	0.038*
C11	0.5753 (2)	0.9037 (3)	0.1791 (2)	0.0280 (6)
H11	0.5673	0.8428	0.2088	0.034*
C12	0.8951 (3)	0.6840 (3)	0.2753 (2)	0.0303 (7)
C13	0.8065 (3)	0.6427 (3)	0.2816 (2)	0.0325 (7)
C14	0.7760 (3)	0.7165 (3)	0.3293 (2)	0.0291 (6)
C15	0.8449 (2)	0.8047 (3)	0.3528 (2)	0.0287 (7)
C16	0.9216 (2)	0.7834 (3)	0.3235 (2)	0.0278 (6)
C17	0.9575 (3)	0.6254 (4)	0.2388 (3)	0.0476 (11)
H17A	0.9974	0.6746	0.2225	0.071*
H17B	0.9099	0.5857	0.1810	0.071*
H17C	1.0057	0.5776	0.2891	0.071*
C18	0.7569 (4)	0.5398 (3)	0.2442 (3)	0.0525 (11)
H18A	0.7940	0.4864	0.2934	0.079*
H18B	0.7606	0.5229	0.1857	0.079*
H18C	0.6835	0.5422	0.2287	0.079*

C19	0.6913 (3)	0.7027 (4)	0.3556 (3)	0.0448 (10)
H19A	0.6300	0.6707	0.3014	0.067*
H19B	0.6720	0.7707	0.3700	0.067*
H19C	0.7168	0.6578	0.4126	0.067*
C20	0.8419 (3)	0.8982 (3)	0.4079 (3)	0.0452 (9)
H20A	0.8863	0.9530	0.4043	0.068*
H20B	0.8677	0.8791	0.4756	0.068*
H20C	0.7698	0.9235	0.3796	0.068*
C21	1.0137 (3)	0.8486 (4)	0.3419 (3)	0.0447 (10)
H21A	1.0020	0.9203	0.3553	0.067*
H21B	1.0229	0.8474	0.2848	0.067*
H21C	1.0766	0.8209	0.3977	0.067*
C22	0.5959 (3)	0.6813 (3)	0.0043 (2)	0.0297 (6)
C23	0.5122 (3)	0.6290 (4)	-0.0799 (3)	0.0463 (9)
H23A	0.4538	0.6146	-0.0682	0.069*
H23B	0.5386	0.5635	-0.0912	0.069*
H23C	0.4881	0.6739	-0.1368	0.069*
C24	0.7950 (4)	0.1768 (5)	0.3032 (3)	0.0688 (16)
H24A	0.7986	0.1066	0.2794	0.083*
H24B	0.7345	0.1780	0.3147	0.083*
N1	0.65431 (18)	0.9086 (2)	0.15885 (17)	0.0216 (5)
N2	0.6600 (2)	0.7224 (2)	0.06967 (18)	0.0243 (5)
B1	0.5966 (4)	0.3422 (4)	0.8918 (4)	0.0466 (11)
F1	0.4993 (2)	0.3853 (3)	0.8642 (2)	0.0730 (9)
F2	0.6630 (3)	0.4208 (3)	0.9005 (3)	0.0813 (10)
F3	0.6258 (4)	0.2895 (3)	0.9741 (3)	0.1106 (15)
F4	0.5856 (3)	0.2743 (3)	0.8188 (3)	0.0811 (10)
Ir1	0.76632 (2)	0.79059 (2)	0.19674 (2)	0.02018 (3)
Cl1	0.90977 (9)	0.19950 (11)	0.41267 (7)	0.0567 (3)
Cl2	0.77480 (9)	0.26778 (9)	0.21475 (9)	0.0543 (3)

7.3.9 **Table A8.** Atomic displacement parameters (Å^2) for [**2**][BF_4].

	U^{11}	U^{22}	U^{33}	U^{12}	U^{13}	U^{23}
C1	0.0191 (11)	0.0239 (14)	0.0172 (11)	-0.0005 (10)	0.0083 (10)	0.0028 (10)

C2	0.0230 (13)	0.0317 (16)	0.0267 (13)	0.0029 (12)	0.0143 (11)	0.0048 (12)
C3	0.0277 (15)	0.040 (2)	0.0323 (15)	-0.0040 (13)	0.0185 (13)	0.0028 (14)
C4	0.0356 (17)	0.0350 (18)	0.0324 (16)	-0.0065 (14)	0.0187 (14)	0.0070 (14)
C5	0.0300 (15)	0.0250 (15)	0.0283 (14)	-0.0020 (12)	0.0123 (12)	0.0053 (12)
C6	0.0203 (12)	0.0218 (14)	0.0188 (11)	-0.0006 (10)	0.0069 (10)	0.0013 (10)
C7	0.0209 (12)	0.0210 (13)	0.0170 (11)	0.0009 (10)	0.0061 (10)	-0.0002 (10)
C8	0.0309 (15)	0.0212 (14)	0.0271 (14)	0.0049 (12)	0.0115 (12)	0.0019 (11)
C9	0.0295 (15)	0.0295 (17)	0.0322 (15)	0.0127 (13)	0.0125 (13)	0.0002 (13)
C10	0.0273 (15)	0.0399 (19)	0.0324 (15)	0.0091 (13)	0.0177 (13)	0.0021 (14)
C11	0.0253 (14)	0.0344 (17)	0.0284 (14)	0.0056 (12)	0.0165 (12)	0.0063 (12)
C12	0.0327 (15)	0.0366 (18)	0.0241 (13)	0.0179 (13)	0.0158 (12)	0.0128 (12)
C13	0.0425 (18)	0.0261 (16)	0.0298 (15)	0.0107 (14)	0.0183 (14)	0.0141 (13)
C14	0.0306 (14)	0.0376 (18)	0.0238 (13)	0.0089 (14)	0.0170 (12)	0.0114 (13)
C15	0.0269 (14)	0.0389 (19)	0.0191 (12)	0.0107 (13)	0.0103 (11)	0.0065 (12)
C16	0.0214 (13)	0.0397 (18)	0.0193 (12)	0.0078 (13)	0.0077 (10)	0.0100 (12)
C17	0.055 (2)	0.056 (3)	0.0409 (19)	0.036 (2)	0.0304 (18)	0.0194 (18)
C18	0.076 (3)	0.0274 (19)	0.053 (2)	0.005 (2)	0.031 (2)	0.0114 (18)
C19	0.0370 (18)	0.073 (3)	0.0331 (17)	0.0065 (19)	0.0240 (15)	0.0187 (19)
C20	0.048 (2)	0.049 (2)	0.0305 (17)	0.0130 (18)	0.0134 (16)	-0.0056 (16)
C21	0.0284 (16)	0.067 (3)	0.0337 (17)	-0.0040 (17)	0.0114 (14)	0.0083 (18)
C22	0.0315 (15)	0.0264 (16)	0.0330 (16)	0.0019 (12)	0.0172 (13)	0.0016 (12)
C23	0.042 (2)	0.046 (2)	0.044 (2)	-0.0103 (18)	0.0158 (17)	-0.0128 (18)
C24	0.045 (2)	0.096 (4)	0.046 (2)	-0.028 (3)	0.007 (2)	0.016 (3)
N1	0.0211 (11)	0.0241 (12)	0.0207 (10)	0.0033 (9)	0.0112 (9)	0.0017 (9)
N2	0.0276 (12)	0.0222 (13)	0.0269 (12)	0.0025 (10)	0.0164 (10)	0.0046 (10)
B1	0.054 (3)	0.039 (3)	0.061 (3)	0.005 (2)	0.039 (2)	0.011 (2)
F1	0.0518 (16)	0.072 (2)	0.098 (2)	0.0039 (15)	0.0382 (16)	-0.0080 (18)
F2	0.076 (2)	0.075 (2)	0.116 (3)	-0.0322 (17)	0.064 (2)	-0.026 (2)
F3	0.169 (4)	0.089 (3)	0.089 (3)	0.052 (3)	0.075 (3)	0.051 (2)
F4	0.097 (2)	0.072 (2)	0.109 (3)	-0.0216 (18)	0.078 (2)	-0.0290 (19)
Ir1	0.02141 (5)	0.02168 (5)	0.02036 (5)	0.00522 (4)	0.01251 (4)	0.00585 (4)
Cl1	0.0445 (5)	0.0829 (9)	0.0368 (5)	-0.0115 (5)	0.0154 (4)	-0.0072 (5)
Cl2	0.0478 (6)	0.0455 (6)	0.0578 (6)	-0.0038 (4)	0.0167 (5)	0.0083 (5)

7.3.10 **Table A9.** Interatomic distances (Å) and angles (deg) for [**2**][BF_4].

C1—C2	1.400 (4)	C15—Ir1	2.167 (3)
C1—C6	1.409 (4)	C16—C21	1.492 (5)
C1—Ir1	2.048 (3)	C16—Ir1	2.178 (3)
C2—C3	1.389 (4)	C17—H17A	0.9800
C2—H2	0.9500	C17—H17B	0.9800
C3—C4	1.380 (5)	C17—H17C	0.9800
C3—H3	0.9500	C18—H18A	0.9800
C4—C5	1.389 (5)	C18—H18B	0.9800
C4—H4	0.9500	C18—H18C	0.9800
C5—C6	1.399 (4)	C19—H19A	0.9800
C5—H5	0.9500	C19—H19B	0.9800
C6—C7	1.469 (4)	C19—H19C	0.9800
C7—N1	1.357 (4)	C20—H20A	0.9800
C7—C8	1.397 (4)	C20—H20B	0.9800
C8—C9	1.380 (5)	C20—H20C	0.9800
C8—H8	0.9500	C21—H21A	0.9800
C9—C10	1.378 (5)	C21—H21B	0.9800
C9—H9	0.9500	C21—H21C	0.9800
C10—C11	1.380 (4)	C22—N2	1.132 (4)
C10—H10	0.9500	C22—C23	1.461 (5)
C11—N1	1.348 (4)	C23—H23A	0.9800
C11—H11	0.9500	C23—H23B	0.9800
C12—C16	1.442 (5)	C23—H23C	0.9800
C12—C13	1.452 (5)	C24—Cl2	1.737 (5)
C12—C17	1.504 (5)	C24—Cl1	1.751 (4)
C12—Ir1	2.165 (3)	C24—H24A	0.9900
C13—C14	1.417 (5)	C24—H24B	0.9900
C13—C18	1.487 (6)	N1—Ir1	2.096 (2)
C13—Ir1	2.236 (3)	N2—Ir1	2.044 (3)
C14—C15	1.441 (5)	B1—F3	1.342 (6)
C14—C19	1.501 (4)	B1—F2	1.363 (6)
C14—Ir1	2.251 (3)	B1—F1	1.386 (6)
C15—C16	1.440 (4)	B1—F4	1.395 (6)
C15—C20	1.498 (5)		

C2—C1—C6	117.2 (3)	C13—C18—H18C	109.5
C2—C1—Ir1	126.6 (2)	H18A—C18—H18C	109.5
C6—C1—Ir1	116.25 (19)	H18B—C18—H18C	109.5
C3—C2—C1	121.1 (3)	C14—C19—H19A	109.5
C3—C2—H2	119.4	C14—C19—H19B	109.5
C1—C2—H2	119.4	H19A—C19—H19B	109.5
C4—C3—C2	120.7 (3)	C14—C19—H19C	109.5
C4—C3—H3	119.6	H19A—C19—H19C	109.5
C2—C3—H3	119.6	H19B—C19—H19C	109.5
C3—C4—C5	120.0 (3)	C15—C20—H20A	109.5
C3—C4—H4	120.0	C15—C20—H20B	109.5
C5—C4—H4	120.0	H20A—C20—H20B	109.5
C4—C5—C6	119.2 (3)	C15—C20—H20C	109.5
C4—C5—H5	120.4	H20A—C20—H20C	109.5
C6—C5—H5	120.4	H20B—C20—H20C	109.5
C5—C6—C1	121.7 (3)	C16—C21—H21A	109.5
C5—C6—C7	123.4 (3)	C16—C21—H21B	109.5
C1—C6—C7	114.8 (2)	H21A—C21—H21B	109.5
N1—C7—C8	120.1 (3)	C16—C21—H21C	109.5
N1—C7—C6	113.6 (2)	H21A—C21—H21C	109.5
C8—C7—C6	126.4 (3)	H21B—C21—H21C	109.5
C9—C8—C7	119.6 (3)	N2—C22—C23	179.3 (4)
C9—C8—H8	120.2	C22—C23—H23A	109.5
C7—C8—H8	120.2	C22—C23—H23B	109.5
C10—C9—C8	119.7 (3)	H23A—C23—H23B	109.5
C10—C9—H9	120.2	C22—C23—H23C	109.5
C8—C9—H9	120.2	H23A—C23—H23C	109.5
C9—C10—C11	118.9 (3)	H23B—C23—H23C	109.5
C9—C10—H10	120.6	Cl2—C24—Cl1	112.9 (3)
C11—C10—H10	120.6	Cl2—C24—H24A	109.0
N1—C11—C10	121.9 (3)	Cl1—C24—H24A	109.0
N1—C11—H11	119.1	Cl2—C24—H24B	109.0
C10—C11—H11	119.1	Cl1—C24—H24B	109.0
C16—C12—C13	107.7 (3)	H24A—C24—H24B	107.8
C16—C12—C17	126.3 (3)	C11—N1—C7	119.8 (3)
C13—C12—C17	125.3 (4)	C11—N1—Ir1	122.8 (2)

C16—C12—Ir1	71.08 (17)	C7—N1—Ir1	117.36 (18)
C13—C12—Ir1	73.39 (17)	C22—N2—Ir1	172.8 (3)
C17—C12—Ir1	128.3 (2)	F3—B1—F2	113.9 (5)
C14—C13—C12	108.7 (3)	F3—B1—F1	107.2 (4)
C14—C13—C18	126.1 (3)	F2—B1—F1	108.0 (4)
C12—C13—C18	125.2 (3)	F3—B1—F4	110.1 (4)
C14—C13—Ir1	72.15 (18)	F2—B1—F4	109.5 (4)
C12—C13—Ir1	68.11 (17)	F1—B1—F4	107.9 (4)
C18—C13—Ir1	125.7 (2)	N2—Ir1—C1	88.88 (10)
C13—C14—C15	107.4 (3)	N2—Ir1—N1	85.23 (10)
C13—C14—C19	126.2 (4)	C1—Ir1—N1	77.77 (10)
C15—C14—C19	126.3 (3)	N2—Ir1—C12	108.87 (12)
C13—C14—Ir1	71.03 (17)	C1—Ir1—C12	108.49 (12)
C15—C14—Ir1	67.85 (16)	N1—Ir1—C12	164.32 (11)
C19—C14—Ir1	129.0 (2)	N2—Ir1—C15	152.09 (12)
C16—C15—C14	109.1 (3)	C1—Ir1—C15	119.03 (12)
C16—C15—C20	126.3 (3)	N1—Ir1—C15	99.74 (11)
C14—C15—C20	124.4 (3)	C12—Ir1—C15	64.60 (12)
C16—C15—Ir1	71.05 (16)	N2—Ir1—C16	146.95 (12)
C14—C15—Ir1	74.12 (17)	C1—Ir1—C16	95.99 (11)
C20—C15—Ir1	125.6 (2)	N1—Ir1—C16	127.76 (11)
C15—C16—C12	106.9 (3)	C12—Ir1—C16	38.79 (13)
C15—C16—C21	127.3 (3)	C15—Ir1—C16	38.70 (11)
C12—C16—C21	125.8 (3)	N2—Ir1—C13	94.44 (12)
C15—C16—Ir1	70.25 (16)	C1—Ir1—C13	145.64 (12)
C12—C16—Ir1	70.13 (17)	N1—Ir1—C13	136.57 (11)
C21—C16—Ir1	126.4 (2)	C12—Ir1—C13	38.50 (13)
C12—C17—H17A	109.5	C15—Ir1—C13	63.09 (13)
C12—C17—H17B	109.5	C16—Ir1—C13	63.94 (13)
H17A—C17—H17B	109.5	N2—Ir1—C14	114.09 (12)
C12—C17—H17C	109.5	C1—Ir1—C14	156.95 (12)
H17A—C17—H17C	109.5	N1—Ir1—C14	104.79 (10)
H17B—C17—H17C	109.5	C12—Ir1—C14	63.71 (11)
C13—C18—H18A	109.5	C15—Ir1—C14	38.03 (13)
C13—C18—H18B	109.5	C16—Ir1—C14	63.97 (12)
H18A—C18—H18B	109.5	C13—Ir1—C14	36.82 (12)

C6—C1—C2—C3	0.9 (4)	Ir1—C13—C14—C19	124.9 (3)
Ir1—C1—C2—C3	-179.8 (2)	C12—C13—C14—Ir1	58.5 (2)
C1—C2—C3—C4	-0.1 (5)	C18—C13—C14—Ir1	-121.6 (3)
C2—C3—C4—C5	-0.5 (5)	C13—C14—C15—C16	-2.6 (3)
C3—C4—C5—C6	0.4 (5)	C19—C14—C15—C16	174.2 (3)
C4—C5—C6—C1	0.4 (5)	Ir1—C14—C15—C16	-62.9 (2)
C4—C5—C6—C7	-176.6 (3)	C13—C14—C15—C20	-177.1 (3)
C2—C1—C6—C5	-1.0 (4)	C19—C14—C15—C20	-0.3 (5)
Ir1—C1—C6—C5	179.6 (2)	Ir1—C14—C15—C20	122.6 (3)
C2—C1—C6—C7	176.2 (3)	C13—C14—C15—Ir1	60.3 (2)
Ir1—C1—C6—C7	-3.1 (3)	C19—C14—C15—Ir1	-122.9 (3)
C5—C6—C7—N1	176.4 (3)	C14—C15—C16—C12	4.0 (3)
C1—C6—C7—N1	-0.8 (3)	C20—C15—C16—C12	178.3 (3)
C5—C6—C7—C8	-2.4 (5)	Ir1—C15—C16—C12	-60.89 (19)
C1—C6—C7—C8	-179.6 (3)	C14—C15—C16—C21	-173.9 (3)
N1—C7—C8—C9	-0.6 (4)	C20—C15—C16—C21	0.5 (5)
C6—C7—C8—C9	178.1 (3)	Ir1—C15—C16—C21	121.2 (3)
C7—C8—C9—C10	-1.9 (5)	C14—C15—C16—Ir1	64.9 (2)
C8—C9—C10—C11	1.7 (5)	C20—C15—C16—Ir1	-120.8 (3)
C9—C10—C11—N1	1.0 (5)	C13—C12—C16—C15	-3.8 (3)
C16—C12—C13—C14	2.2 (3)	C17—C12—C16—C15	-174.9 (3)
C17—C12—C13—C14	173.5 (3)	Ir1—C12—C16—C15	60.97 (19)
Ir1—C12—C13—C14	-61.0 (2)	C13—C12—C16—C21	174.1 (3)
C16—C12—C13—C18	-177.7 (3)	C17—C12—C16—C21	3.0 (5)
C17—C12—C13—C18	-6.4 (5)	Ir1—C12—C16—C21	-121.1 (3)
Ir1—C12—C13—C18	119.1 (3)	C13—C12—C16—Ir1	-64.7 (2)
C16—C12—C13—Ir1	63.2 (2)	C17—C12—C16—Ir1	124.1 (3)
C17—C12—C13—Ir1	-125.5 (3)	C10—C11—N1—C7	-3.5 (5)

C12—C13—C14—C15	0.2 (3)	C10—C11—N1—Ir1	176.5 (2)
C18—C13—C14—C15	-179.9 (3)	C8—C7—N1—C11	3.3 (4)
Ir1—C13—C14—C15	-58.3 (2)	C6—C7—N1—C11	-175.6 (3)
C12—C13—C14—C19	-176.6 (3)	C8—C7—N1—Ir1	-176.8 (2)
C18—C13—C14—C19	3.3 (5)	C6—C7—N1—Ir1	4.4 (3)

7.4 [**2'**][$BArF_{24}$]

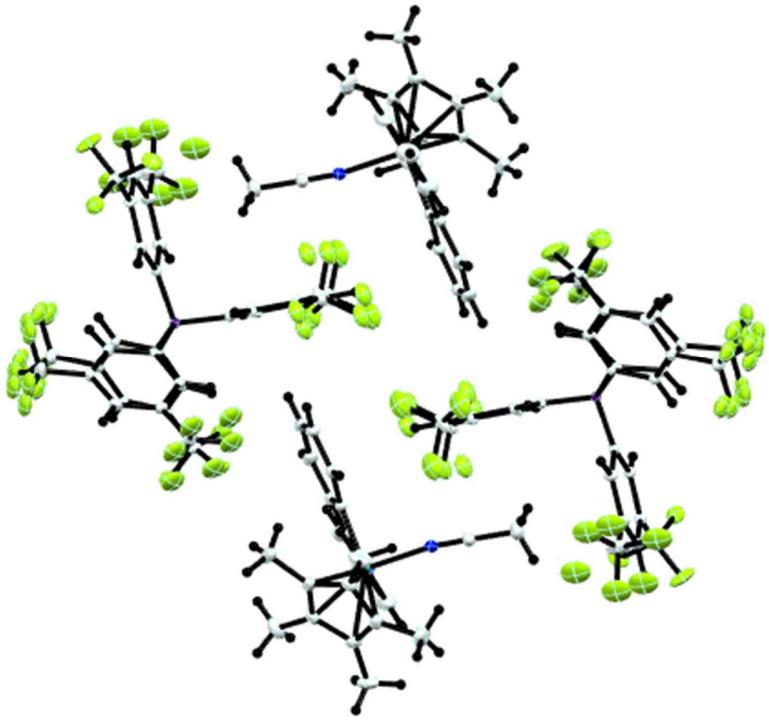

7.4.1 **Figure A10.** Crystal lattice packing of [**2'**][$BArF_{24}$].

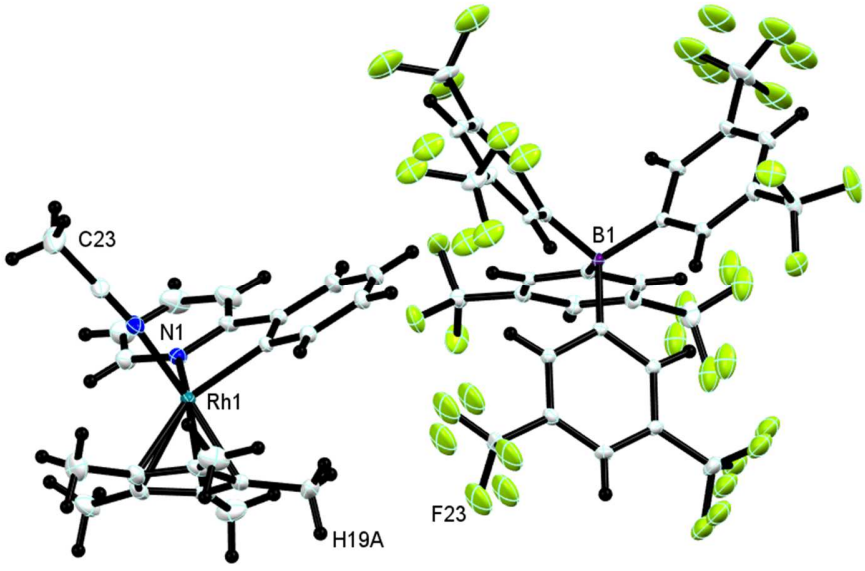

7.4.2 **Figure A11.** Asymmetric unit of [**2'**][$BArF_{24}$], with all hydrogens and partial numbering of atoms.

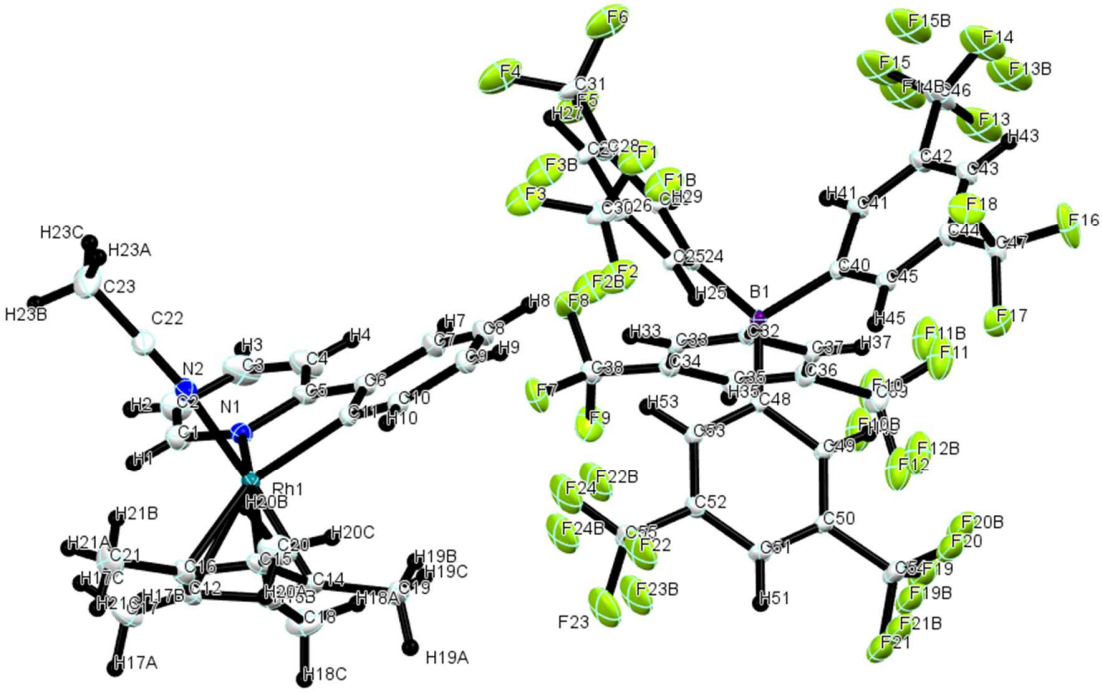

7.4.3 **Figure A12.** Asymmetric unit of [**2'**][BArF$_{24}$], with all hydrogens and total numbering of atoms.

[**2'**][BArF$_{24}$]

Data collection: Bruker *APEX2*; cell refinement: Bruker *SAINT*; data reduction: Bruker *SAINT*; program(s) used to solve structure: *SHELXS2013* (Sheldrick, 2013); program(s) used to refine structure: *SHELXL2013* (Sheldrick, 2013); molecular graphics: *Mercury* (Macrae *et al.*, 2008); software used to prepare material for publication: *SHELXL2013* (Sheldrick, 2013).

7.4.4 Crystal data

$C_{32}H_{12}BF_{24}\cdot C_{23}H_{26}N_2Rh$	$Z = 2$
$M_r = 1296.59$	$F(000) = 1296$
Triclinic, $P\bar{1}$	$D_x = 1.589$ Mg m^{-3}
$a = 12.7624$ (5) Å	Mo $K\alpha$ radiation, $\lambda = 0.71073$ Å
$b = 13.2269$ (6) Å	Cell parameters from 9963 reflections

c = 16.9988 (7) Å	θ = 2.4–29.7°
α = 91.752 (1)°	μ = 0.44 mm^{-1}
β = 97.534 (1)°	T = 173 K
γ = 107.250 (1)°	Prism, yellow
V = 2709.5 (2) Å^3	0.36 × 0.16 × 0.10 mm

7.4.5 Data collection

Bruker APEX-II CCD diffractometer	15767 independent reflections
Radiation source: sealed tube	12927 reflections with $I > 2\sigma(I)$
Triumph monochromator	R_{int} = 0.032
φ and ω scans	θ_{max} = 30.0°, θ_{min} = 1.2°
Absorption correction: multi-scan *SADABS*	h = -17→17
T_{min} = 0.709, T_{max} = 0.746	k = -18→18
74316 measured reflections	l = -23→23

7.4.6 Refinement

Refinement on F^2	Primary atom site location: structure-invariant direct methods
Least-squares matrix: full	Secondary atom site location: difference Fourier map
$R[F^2 > 2\sigma(F^2)]$ = 0.070	Hydrogen site location: inferred from neighbouring sites
$wR(F^2)$ = 0.200	H-atom parameters constrained
S = 1.02	$w = 1/[\sigma^2(F_o^2) + (0.1091P)^2 + 8.299P]$ where $P = (F_o^2 + 2F_c^2)/3$
15767 reflections	$(\Delta/\sigma)_{max} < 0.001$
727 parameters	$\Delta\rangle_{max}$ = 1.90 e Å^{-3}
0 restraints	$\Delta\rangle_{min}$ = -1.99 e Å^{-3}

7.4.7 Special details

Geometry. All esds (except the esd in the dihedral angle between two l.s. planes) are estimated using the full covariance matrix. The cell esds are taken into account individually in the estimation of esds in distances, angles and torsion angles; correlations between esds in cell parameters are only used when they are defined by crystal symmetry. An approximate (isotropic)

treatment of cell esds is used for estimating esds involving l.s. planes.

7.4.8 **Table A10.** Fractional atomic coordinates and isotropic or equivalent isotropic displacement parameters (Å^2) for [**2'**][BArF$_{24}$].

	x	*y*	*z*	U_{iso}*/U_{eq}
C1	0.1025 (4)	0.0682 (4)	0.2176 (2)	0.0368 (9)
H1	0.0451	0.0766	0.1792	0.044*
C2	0.1602 (4)	0.0011 (4)	0.1984 (3)	0.0498 (12)
H2	0.1442	-0.0353	0.1471	0.060*
C3	0.2429 (5)	-0.0130 (5)	0.2552 (4)	0.0574 (14)
H3	0.2822	-0.0611	0.2439	0.069*
C4	0.2672 (4)	0.0441 (4)	0.3286 (3)	0.0482 (11)
H4	0.3236	0.0355	0.3677	0.058*
C5	0.2085 (3)	0.1141 (3)	0.3447 (2)	0.0298 (7)
C6	0.2332 (3)	0.1877 (3)	0.4156 (2)	0.0274 (7)
C7	0.3196 (3)	0.1961 (4)	0.4778 (2)	0.0376 (9)
H7	0.3617	0.1476	0.4784	0.045*
C8	0.3433 (3)	0.2750 (4)	0.5381 (2)	0.0425 (10)
H8	0.4022	0.2813	0.5802	0.051*
C9	0.2816 (3)	0.3452 (4)	0.5378 (2)	0.0375 (9)
H9	0.2987	0.3999	0.5792	0.045*
C10	0.1940 (3)	0.3355 (3)	0.4765 (2)	0.0303 (7)
H10	0.1517	0.3837	0.4765	0.036*
C11	0.1684 (3)	0.2558 (3)	0.41552 (19)	0.0226 (6)
C12	-0.1372 (3)	0.1347 (3)	0.2738 (2)	0.0326 (8)
C13	-0.1059 (3)	0.1063 (3)	0.3525 (3)	0.0317 (8)
C14	-0.0838 (3)	0.1961 (3)	0.4070 (2)	0.0314 (8)
C15	-0.0909 (3)	0.2841 (3)	0.3628 (2)	0.0313 (7)
C16	-0.1271 (3)	0.2436 (4)	0.2802 (2)	0.0346 (8)
C17	-0.1773 (4)	0.0584 (4)	0.2017 (3)	0.0503 (12)
H17A	-0.2579	0.0270	0.1968	0.075*
H17B	-0.1418	0.0021	0.2069	0.075*
H17C	-0.1584	0.0960	0.1543	0.075*
C18	-0.1086 (5)	-0.0034 (4)	0.3754 (4)	0.0529 (13)
H18A	-0.0598	0.0017	0.4259	0.079*

H18B	-0.0832	-0.0393	0.3338	0.079*
H18C	-0.1846	-0.0441	0.3814	0.079*
C19	-0.0632 (4)	0.1981 (5)	0.4961 (3)	0.0502 (13)
H19A	-0.1343	0.1747	0.5165	0.075*
H19B	-0.0224	0.2706	0.5182	0.075*
H19C	-0.0194	0.1505	0.5120	0.075*
C20	-0.0834 (5)	0.3931 (4)	0.3941 (4)	0.0554 (13)
H20A	-0.1582	0.3993	0.3929	0.083*
H20B	-0.0420	0.4455	0.3610	0.083*
H20C	-0.0451	0.4062	0.4490	0.083*
C21	-0.1516 (5)	0.3077 (5)	0.2126 (3)	0.0581 (14)
H21A	-0.1435	0.2742	0.1624	0.087*
H21B	-0.0996	0.3798	0.2211	0.087*
H21C	-0.2276	0.3111	0.2101	0.087*
C22	0.1725 (4)	0.3824 (4)	0.2102 (3)	0.0439 (11)
C23	0.2286 (6)	0.4431 (6)	0.1493 (4)	0.075 (2)
H23A	0.2556	0.5186	0.1674	0.113*
H23B	0.1764	0.4329	0.0999	0.113*
H23C	0.2914	0.4185	0.1397	0.113*
C24	0.5263 (2)	0.3205 (2)	0.74341 (17)	0.0185 (5)
C25	0.5010 (3)	0.4167 (3)	0.73848 (19)	0.0219 (6)
H25	0.4531	0.4316	0.7724	0.026*
C26	0.5437 (3)	0.4906 (3)	0.6856 (2)	0.0260 (6)
C27	0.6167 (3)	0.4736 (3)	0.6365 (2)	0.0306 (7)
H27	0.6460	0.5241	0.6003	0.037*
C28	0.6452 (3)	0.3805 (3)	0.6420 (2)	0.0265 (7)
C29	0.6009 (3)	0.3056 (3)	0.69429 (19)	0.0217 (6)
H29	0.6221	0.2426	0.6966	0.026*
C30	0.5140 (4)	0.5920 (3)	0.6828 (3)	0.0423 (10)
C31	0.7264 (4)	0.3621 (4)	0.5923 (3)	0.0429 (10)
C32	0.4749 (2)	0.1143 (2)	0.78369 (18)	0.0181 (5)
C33	0.4410 (3)	0.0685 (3)	0.70527 (18)	0.0197 (6)
H33	0.4283	0.1120	0.6638	0.024*
C34	0.4254 (3)	-0.0388 (3)	0.68654 (19)	0.0219 (6)
C35	0.4407 (3)	-0.1058 (3)	0.7449 (2)	0.0264 (7)
H35	0.4301	-0.1789	0.7321	0.032*
C36	0.4723 (3)	-0.0621 (3)	0.8233 (2)	0.0258 (6)

C37	0.4897 (3)	0.0450 (3)	0.84191 (19)	0.0220 (6)
H37	0.5124	0.0723	0.8958	0.026*
C38	0.3941 (3)	-0.0832 (3)	0.6015 (2)	0.0283 (7)
C39	0.4824 (4)	-0.1321 (4)	0.8897 (3)	0.0415 (10)
C40	0.5788 (2)	0.2829 (2)	0.88809 (17)	0.0179 (5)
C41	0.6825 (3)	0.2651 (3)	0.89172 (19)	0.0241 (6)
H41	0.6940	0.2200	0.8513	0.029*
C42	0.7689 (3)	0.3118 (3)	0.9530 (2)	0.0277 (7)
C43	0.7574 (3)	0.3789 (3)	1.0131 (2)	0.0254 (6)
H43	0.8170	0.4114	1.0544	0.031*
C44	0.6556 (3)	0.3968 (3)	1.01067 (18)	0.0212 (6)
C45	0.5685 (3)	0.3498 (2)	0.94981 (18)	0.0194 (5)
H45	0.4997	0.3638	0.9503	0.023*
C46	0.8773 (4)	0.2904 (5)	0.9542 (3)	0.0527 (14)
C47	0.6419 (3)	0.4717 (3)	1.0731 (2)	0.0310 (8)
C48	0.3578 (2)	0.2317 (2)	0.82791 (17)	0.0171 (5)
C49	0.3203 (3)	0.1940 (3)	0.89836 (19)	0.0207 (6)
H49	0.3694	0.1739	0.9373	0.025*
C50	0.2136 (3)	0.1848 (3)	0.9133 (2)	0.0231 (6)
C51	0.1391 (3)	0.2143 (3)	0.8590 (2)	0.0260 (7)
H51	0.0667	0.2095	0.8698	0.031*
C52	0.1740 (3)	0.2511 (3)	0.7886 (2)	0.0244 (6)
C53	0.2798 (3)	0.2578 (3)	0.77273 (18)	0.0215 (6)
H53	0.3000	0.2808	0.7229	0.026*
C54	0.1781 (4)	0.1433 (4)	0.9895 (3)	0.0388 (9)
C55	0.0951 (3)	0.2856 (4)	0.7302 (2)	0.0376 (9)
N1	0.1243 (3)	0.1233 (3)	0.28959 (18)	0.0280 (6)
N2	0.1285 (3)	0.3336 (3)	0.2565 (2)	0.0342 (7)
B1	0.4830 (3)	0.2369 (3)	0.81010 (19)	0.0171 (6)
F1	0.5947 (6)	0.6745 (4)	0.7201 (4)	0.0598 (9)
F2	0.4242 (7)	0.5902 (5)	0.7131 (4)	0.0598 (9)
F3	0.4982 (6)	0.6188 (4)	0.6060 (4)	0.0598 (9)
F1B	0.5682 (8)	0.6585 (7)	0.7507 (6)	0.0598 (9)
F2B	0.4021 (10)	0.5709 (8)	0.6859 (6)	0.0598 (9)
F3B	0.5425 (8)	0.6513 (7)	0.6257 (7)	0.0598 (9)
F4	0.7106 (4)	0.3922 (3)	0.5180 (3)	0.0796 (7)
F5	0.7219 (4)	0.2610 (3)	0.5827 (2)	0.0796 (7)

F6	0.8295 (4)	0.4181 (3)	0.6198 (2)	0.0796 (7)
F7	0.3297 (2)	-0.0362 (2)	0.55804 (15)	0.0460 (7)
F8	0.4817 (2)	-0.0730 (3)	0.56487 (16)	0.0594 (9)
F9	0.3358 (3)	-0.1860 (2)	0.59472 (17)	0.0574 (8)
F10	0.5041 (6)	-0.2178 (5)	0.8708 (3)	0.0641 (9)
F11	0.5557 (7)	-0.0819 (5)	0.9541 (3)	0.0641 (9)
F12	0.3877 (6)	-0.1572 (5)	0.9242 (3)	0.0641 (9)
F10B	0.4450 (11)	-0.2365 (9)	0.8629 (6)	0.0641 (9)
F11B	0.5807 (13)	-0.0929 (10)	0.9335 (6)	0.0641 (9)
F12B	0.4141 (13)	-0.1278 (9)	0.9451 (6)	0.0641 (9)
F13	0.8692 (6)	0.1901 (8)	0.9861 (6)	0.0890 (15)
F14	0.9618 (7)	0.3556 (9)	0.9977 (7)	0.0890 (15)
F15	0.8994 (7)	0.2683 (9)	0.8842 (7)	0.0890 (15)
F13B	0.9368 (7)	0.3021 (9)	1.0232 (7)	0.0890 (15)
F14B	0.8822 (7)	0.2179 (9)	0.9050 (8)	0.0890 (15)
F15B	0.9525 (6)	0.3794 (8)	0.9220 (6)	0.0890 (15)
F16	0.7043 (3)	0.4734 (3)	1.14296 (16)	0.0641 (10)
F17	0.5374 (2)	0.4504 (2)	1.08773 (15)	0.0426 (6)
F18	0.6700 (3)	0.5714 (2)	1.05105 (19)	0.0501 (7)
F19	0.2046 (5)	0.0513 (7)	1.0047 (4)	0.0613 (8)
F20	0.2279 (5)	0.2067 (6)	1.0517 (4)	0.0613 (8)
F21	0.0676 (5)	0.1153 (6)	0.9882 (3)	0.0613 (8)
F19B	0.1647 (8)	0.0439 (11)	0.9961 (7)	0.0613 (8)
F20B	0.2642 (8)	0.1911 (10)	1.0557 (6)	0.0613 (8)
F21B	0.0920 (8)	0.1713 (9)	1.0111 (5)	0.0613 (8)
F22	0.0680 (6)	0.3667 (6)	0.7607 (4)	0.0765 (10)
F23	-0.0027 (5)	0.2103 (6)	0.7118 (4)	0.0765 (10)
F24	0.1306 (6)	0.3143 (7)	0.6642 (4)	0.0765 (10)
F22B	0.1486 (8)	0.3841 (9)	0.7027 (6)	0.0765 (10)
F23B	0.0114 (9)	0.3043 (10)	0.7560 (6)	0.0765 (10)
F24B	0.0842 (8)	0.2387 (10)	0.6572 (6)	0.0765 (10)
Rh1	0.03806 (2)	0.22427 (2)	0.32541 (2)	0.02199 (9)

7.4.9 **Table A11.** Atomic displacement parameters ($Å^2$) for [**2'**][$BArF_{24}$].

	U^{11}	U^{22}	U^{33}	U^{12}	U^{13}	U^{23}
C1	0.0331 (19)	0.041 (2)	0.0340 (19)	0.0079 (17)	0.0061 (15)	-0.0069 (16)
C2	0.049 (3)	0.051 (3)	0.049 (3)	0.013 (2)	0.013 (2)	-0.017 (2)
C3	0.046 (3)	0.056 (3)	0.076 (4)	0.025 (2)	0.015 (3)	-0.016 (3)
C4	0.036 (2)	0.051 (3)	0.062 (3)	0.023 (2)	0.003 (2)	-0.005 (2)
C5	0.0213 (15)	0.0327 (19)	0.0354 (18)	0.0081 (14)	0.0049 (13)	0.0021 (15)
C6	0.0208 (15)	0.0342 (19)	0.0257 (15)	0.0060 (13)	0.0028 (12)	0.0050 (13)
C7	0.0271 (18)	0.050 (3)	0.0354 (19)	0.0133 (17)	-0.0004 (15)	0.0094 (18)
C8	0.0285 (19)	0.062 (3)	0.0286 (18)	0.0047 (19)	-0.0062 (15)	0.0083 (18)
C9	0.0321 (19)	0.046 (2)	0.0235 (16)	-0.0029 (17)	0.0002 (14)	-0.0024 (15)
C10	0.0281 (17)	0.0330 (19)	0.0247 (16)	0.0019 (14)	0.0044 (13)	-0.0003 (14)
C11	0.0199 (14)	0.0248 (16)	0.0191 (13)	0.0016 (12)	0.0004 (11)	0.0015 (11)
C12	0.0220 (16)	0.040 (2)	0.0327 (18)	0.0087 (15)	-0.0024 (13)	-0.0066 (15)
C13	0.0216 (16)	0.0291 (18)	0.044 (2)	0.0063 (14)	0.0072 (14)	0.0082 (15)
C14	0.0208 (15)	0.044 (2)	0.0263 (16)	0.0059 (15)	0.0036 (12)	0.0033 (15)
C15	0.0224 (16)	0.0310 (19)	0.041 (2)	0.0089 (14)	0.0049 (14)	-0.0033 (15)
C16	0.0284 (18)	0.043 (2)	0.0357 (19)	0.0158 (16)	0.0018 (14)	0.0102 (16)
C17	0.035 (2)	0.054 (3)	0.051 (3)	0.005 (2)	-0.0046 (19)	-0.021 (2)
C18	0.048 (3)	0.037 (2)	0.080 (4)	0.016 (2)	0.023 (3)	0.021 (2)
C19	0.035 (2)	0.085 (4)	0.0275 (19)	0.012 (2)	0.0087 (16)	0.008 (2)
C20	0.047 (3)	0.042 (3)	0.078 (4)	0.016 (2)	0.012 (3)	-0.015 (3)
C21	0.059 (3)	0.068 (4)	0.054 (3)	0.032 (3)	-0.001 (2)	0.024 (3)
C22	0.042 (2)	0.040 (2)	0.034 (2)	-0.0078 (19)	-0.0032 (17)	0.0101 (17)
C23	0.075 (4)	0.070 (4)	0.050 (3)	-0.023 (3)	-0.002 (3)	0.027 (3)
C24	0.0185 (13)	0.0196 (14)	0.0159 (12)	0.0038 (11)	0.0025 (10)	-0.0004 (10)
C25	0.0239 (14)	0.0198 (14)	0.0216 (14)	0.0046 (12)	0.0070 (11)	0.0009 (11)
C26	0.0302 (17)	0.0202 (15)	0.0276 (16)	0.0055 (13)	0.0089 (13)	0.0041 (12)
C27	0.0352 (19)	0.0277 (18)	0.0278 (16)	0.0035 (15)	0.0142 (14)	0.0050 (13)
C28	0.0250 (15)	0.0282 (17)	0.0256 (15)	0.0032 (13)	0.0126 (12)	0.0003 (13)
C29	0.0196 (14)	0.0218 (15)	0.0230 (14)	0.0043 (11)	0.0056 (11)	-0.0009 (11)
C30	0.051 (3)	0.028 (2)	0.055 (3)	0.0149 (18)	0.024 (2)	0.0137 (18)
C31	0.041 (2)	0.040 (2)	0.048 (2)	0.0040 (18)	0.031 (2)	-0.0004 (19)
C32	0.0164 (12)	0.0192 (14)	0.0185 (13)	0.0051 (11)	0.0026 (10)	0.0002 (10)
C33	0.0198 (13)	0.0196 (14)	0.0194 (13)	0.0056 (11)	0.0030 (10)	0.0014 (11)
C34	0.0219 (14)	0.0209 (15)	0.0223 (14)	0.0058 (12)	0.0030 (11)	-0.0020 (11)
C35	0.0308 (17)	0.0189 (15)	0.0296 (16)	0.0078 (13)	0.0041 (13)	-0.0009 (12)
C36	0.0291 (16)	0.0221 (16)	0.0279 (16)	0.0103 (13)	0.0027 (12)	0.0075 (12)

C37	0.0244 (15)	0.0226 (15)	0.0195 (13)	0.0080 (12)	0.0024 (11)	0.0023 (11)
C38	0.0273 (16)	0.0297 (18)	0.0257 (16)	0.0061 (14)	0.0033 (12)	-0.0055 (13)
C39	0.056 (3)	0.030 (2)	0.039 (2)	0.0164 (19)	-0.0006 (19)	0.0132 (17)
C40	0.0187 (13)	0.0178 (13)	0.0174 (12)	0.0057 (11)	0.0031 (10)	0.0006 (10)
C41	0.0194 (14)	0.0298 (17)	0.0231 (14)	0.0086 (13)	0.0026 (11)	-0.0074 (12)
C42	0.0177 (14)	0.0368 (19)	0.0293 (16)	0.0119 (14)	-0.0011 (12)	-0.0040 (14)
C43	0.0216 (15)	0.0275 (17)	0.0258 (15)	0.0082 (13)	-0.0029 (12)	-0.0010 (13)
C44	0.0276 (15)	0.0181 (14)	0.0193 (13)	0.0105 (12)	0.0009 (11)	-0.0017 (11)
C45	0.0204 (13)	0.0187 (14)	0.0208 (13)	0.0089 (11)	0.0026 (11)	0.0006 (11)
C46	0.0247 (19)	0.081 (4)	0.055 (3)	0.028 (2)	-0.0047 (18)	-0.023 (3)
C47	0.0385 (19)	0.0287 (18)	0.0275 (16)	0.0187 (16)	-0.0065 (14)	-0.0091 (14)
C48	0.0163 (12)	0.0160 (13)	0.0188 (12)	0.0048 (10)	0.0025 (10)	0.0006 (10)
C49	0.0190 (13)	0.0229 (15)	0.0213 (13)	0.0068 (11)	0.0041 (11)	0.0050 (11)
C50	0.0210 (14)	0.0259 (16)	0.0241 (14)	0.0066 (12)	0.0085 (11)	0.0068 (12)
C51	0.0186 (14)	0.0328 (18)	0.0284 (16)	0.0093 (13)	0.0067 (12)	0.0023 (13)
C52	0.0204 (14)	0.0297 (17)	0.0237 (14)	0.0103 (13)	-0.0007 (11)	0.0020 (12)
C53	0.0207 (14)	0.0252 (15)	0.0182 (13)	0.0067 (12)	0.0024 (11)	0.0015 (11)
C54	0.035 (2)	0.055 (3)	0.0329 (19)	0.0175 (19)	0.0161 (16)	0.0204 (18)
C55	0.0274 (18)	0.060 (3)	0.0310 (18)	0.0232 (19)	0.0008 (14)	0.0126 (18)
N1	0.0242 (14)	0.0296 (15)	0.0272 (14)	0.0042 (12)	0.0037 (11)	-0.0013 (12)
N2	0.0303 (16)	0.0323 (17)	0.0317 (16)	-0.0002 (13)	-0.0030 (12)	0.0056 (13)
B1	0.0177 (14)	0.0178 (15)	0.0153 (13)	0.0050 (12)	0.0025 (11)	0.0001 (11)
F1	0.076 (2)	0.0322 (15)	0.081 (3)	0.0226 (15)	0.0306 (18)	0.0176 (14)
F2	0.076 (2)	0.0322 (15)	0.081 (3)	0.0226 (15)	0.0306 (18)	0.0176 (14)
F3	0.076 (2)	0.0322 (15)	0.081 (3)	0.0226 (15)	0.0306 (18)	0.0176 (14)
F1B	0.076 (2)	0.0322 (15)	0.081 (3)	0.0226 (15)	0.0306 (18)	0.0176 (14)
F2B	0.076 (2)	0.0322 (15)	0.081 (3)	0.0226 (15)	0.0306 (18)	0.0176 (14)
F3B	0.076 (2)	0.0322 (15)	0.081 (3)	0.0226 (15)	0.0306 (18)	0.0176 (14)
F4	0.0873 (16)	0.0836 (16)	0.0839 (15)	0.0312 (13)	0.0577 (13)	0.0047 (12)
F5	0.0873 (16)	0.0836 (16)	0.0839 (15)	0.0312 (13)	0.0577 (13)	0.0047 (12)
F6	0.0873 (16)	0.0836 (16)	0.0839 (15)	0.0312 (13)	0.0577 (13)	0.0047 (12)
F7	0.0502 (15)	0.0578 (17)	0.0299 (12)	0.0254 (13)	-0.0122 (11)	-0.0130 (11)
F8	0.0369 (14)	0.108 (3)	0.0332 (13)	0.0216 (16)	0.0111 (11)	-0.0136 (15)
F9	0.084 (2)	0.0312 (14)	0.0414 (15)	-0.0012 (14)	0.0030 (14)	-0.0142 (11)
F10	0.103 (3)	0.0501 (16)	0.0430 (16)	0.0323 (17)	0.0015 (16)	0.0155 (13)
F11	0.103 (3)	0.0501 (16)	0.0430 (16)	0.0323 (17)	0.0015 (16)	0.0155 (13)
F12	0.103 (3)	0.0501 (16)	0.0430 (16)	0.0323 (17)	0.0015 (16)	0.0155 (13)

F10B	0.103 (3)	0.0501 (16)	0.0430 (16)	0.0323 (17)	0.0015 (16)	0.0155 (13)
F11B	0.103 (3)	0.0501 (16)	0.0430 (16)	0.0323 (17)	0.0015 (16)	0.0155 (13)
F12B	0.103 (3)	0.0501 (16)	0.0430 (16)	0.0323 (17)	0.0015 (16)	0.0155 (13)
F13	0.0402 (17)	0.124 (4)	0.114 (3)	0.048 (3)	0.0052 (19)	-0.015 (3)
F14	0.0402 (17)	0.124 (4)	0.114 (3)	0.048 (3)	0.0052 (19)	-0.015 (3)
F15	0.0402 (17)	0.124 (4)	0.114 (3)	0.048 (3)	0.0052 (19)	-0.015 (3)
F13B	0.0402 (17)	0.124 (4)	0.114 (3)	0.048 (3)	0.0052 (19)	-0.015 (3)
F14B	0.0402 (17)	0.124 (4)	0.114 (3)	0.048 (3)	0.0052 (19)	-0.015 (3)
F15B	0.0402 (17)	0.124 (4)	0.114 (3)	0.048 (3)	0.0052 (19)	-0.015 (3)
F16	0.085 (2)	0.088 (2)	0.0313 (13)	0.062 (2)	-0.0235 (14)	-0.0284 (14)
F17	0.0508 (15)	0.0461 (15)	0.0379 (13)	0.0235 (12)	0.0140 (11)	-0.0093 (11)
F18	0.0587 (17)	0.0201 (11)	0.0716 (19)	0.0136 (11)	0.0097 (14)	-0.0100 (12)
F19	0.059 (2)	0.086 (2)	0.0503 (14)	0.027 (2)	0.0279 (18)	0.0295 (13)
F20	0.059 (2)	0.086 (2)	0.0503 (14)	0.027 (2)	0.0279 (18)	0.0295 (13)
F21	0.059 (2)	0.086 (2)	0.0503 (14)	0.027 (2)	0.0279 (18)	0.0295 (13)
F19B	0.059 (2)	0.086 (2)	0.0503 (14)	0.027 (2)	0.0279 (18)	0.0295 (13)
F20B	0.059 (2)	0.086 (2)	0.0503 (14)	0.027 (2)	0.0279 (18)	0.0295 (13)
F21B	0.059 (2)	0.086 (2)	0.0503 (14)	0.027 (2)	0.0279 (18)	0.0295 (13)
F22	0.061 (2)	0.093 (3)	0.076 (2)	0.037 (2)	-0.0234 (16)	0.020 (2)
F23	0.061 (2)	0.093 (3)	0.076 (2)	0.037 (2)	-0.0234 (16)	0.020 (2)
F24	0.061 (2)	0.093 (3)	0.076 (2)	0.037 (2)	-0.0234 (16)	0.020 (2)
F22B	0.061 (2)	0.093 (3)	0.076 (2)	0.037 (2)	-0.0234 (16)	0.020 (2)
F23B	0.061 (2)	0.093 (3)	0.076 (2)	0.037 (2)	-0.0234 (16)	0.020 (2)
F24B	0.061 (2)	0.093 (3)	0.076 (2)	0.037 (2)	-0.0234 (16)	0.020 (2)
Rh1	0.02040 (13)	0.02302 (14)	0.02039 (13)	0.00465 (9)	0.00006 (8)	0.00087 (9)

7.4.10 **Table A12.** Interatomic distances (Å) and angles (deg) for [**2'**][$BArF_{24}$].

C1—N1	1.357 (5)	C30—F2B	1.380 (13)
C1—C2	1.367 (6)	C30—F1B	1.399 (12)
C1—H1	0.9500	C31—F6	1.318 (7)
C2—C3	1.394 (8)	C31—F5	1.326 (6)
C2—H2	0.9500	C31—F4	1.344 (7)
C3—C4	1.386 (8)	C32—C37	1.401 (4)
C3—H3	0.9500	C32—C33	1.405 (4)
C4—C5	1.393 (6)	C32—B1	1.639 (5)

C4—H4	0.9500	C33—C34	1.395 (4)
C5—N1	1.366 (5)	C33—H33	0.9500
C5—C6	1.465 (5)	C34—C35	1.383 (5)
C6—C11	1.392 (5)	C34—C38	1.500 (5)
C6—C7	1.400 (5)	C35—C36	1.395 (5)
C7—C8	1.378 (7)	C35—H35	0.9500
C7—H7	0.9500	C36—C37	1.386 (5)
C8—C9	1.383 (7)	C36—C39	1.498 (5)
C8—H8	0.9500	C37—H37	0.9500
C9—C10	1.398 (5)	C38—F8	1.325 (4)
C9—H9	0.9500	C38—F7	1.334 (5)
C10—C11	1.391 (5)	C38—F9	1.335 (5)
C10—H10	0.9500	C39—F10	1.284 (7)
C11—Rh1	2.042 (3)	C39—F11B	1.321 (16)
C12—C16	1.407 (6)	C39—F11	1.354 (8)
C12—C13	1.438 (6)	C39—F10B	1.362 (12)
C12—C17	1.496 (6)	C39—F12	1.369 (9)
C12—Rh1	2.241 (4)	C39—F12B	1.376 (16)
C13—C14	1.420 (6)	C40—C45	1.397 (4)
C13—C18	1.505 (6)	C40—C41	1.406 (4)
C13—Rh1	2.142 (4)	C40—B1	1.645 (4)
C14—C15	1.423 (6)	C41—C42	1.392 (5)
C14—C19	1.501 (5)	C41—H41	0.9500
C14—Rh1	2.176 (4)	C42—C43	1.385 (5)
C15—C16	1.453 (6)	C42—C46	1.488 (5)
C15—C20	1.494 (6)	C43—C44	1.383 (5)
C15—Rh1	2.181 (4)	C43—H43	0.9500
C16—C21	1.503 (6)	C44—C45	1.394 (4)
C16—Rh1	2.238 (4)	C44—C47	1.492 (4)
C17—H17A	0.9800	C45—H45	0.9500
C17—H17B	0.9800	C46—F14B	1.275 (12)
C17—H17C	0.9800	C46—F14	1.286 (12)
C18—H18A	0.9800	C46—F13B	1.290 (12)
C18—H18B	0.9800	C46—F15	1.304 (13)
C18—H18C	0.9800	C46—F13	1.429 (12)
C19—H19A	0.9800	C46—F15B	1.454 (12)
C19—H19B	0.9800	C47—F16	1.336 (4)

C19—H19C	0.9800	C47—F17	1.338 (5)
C20—H20A	0.9800	C47—F18	1.338 (5)
C20—H20B	0.9800	C48—C49	1.399 (4)
C20—H20C	0.9800	C48—C53	1.403 (4)
C21—H21A	0.9800	C48—B1	1.646 (4)
C21—H21B	0.9800	C49—C50	1.388 (4)
C21—H21C	0.9800	C49—H49	0.9500
C22—N2	1.133 (6)	C50—C51	1.385 (5)
C22—C23	1.460 (7)	C50—C54	1.496 (5)
C23—H23A	0.9800	C51—C52	1.384 (5)
C23—H23B	0.9800	C51—H51	0.9500
C23—H23C	0.9800	C52—C53	1.389 (4)
C24—C29	1.398 (4)	C52—C55	1.499 (5)
C24—C25	1.405 (4)	C53—H53	0.9500
C24—B1	1.641 (5)	C54—F19B	1.285 (14)
C25—C26	1.388 (5)	C54—F20	1.295 (9)
C25—H25	0.9500	C54—F21	1.344 (7)
C26—C27	1.391 (5)	C54—F21B	1.348 (10)
C26—C30	1.498 (5)	C54—F19	1.379 (9)
C27—C28	1.386 (5)	C54—F20B	1.446 (13)
C27—H27	0.9500	C55—F24	1.291 (9)
C28—C29	1.395 (5)	C55—F23B	1.291 (12)
C28—C31	1.488 (5)	C55—F22	1.331 (9)
C29—H29	0.9500	C55—F23	1.337 (8)
C30—F3B	1.288 (11)	C55—F24B	1.341 (12)
C30—F2	1.311 (9)	C55—F22B	1.406 (12)
C30—F1	1.333 (8)	N1—Rh1	2.089 (3)
C30—F3	1.368 (8)	N2—Rh1	2.065 (3)
N1—C1—C2	122.4 (4)	C33—C34—C38	120.1 (3)
N1—C1—H1	118.8	C34—C35—C36	117.6 (3)
C2—C1—H1	118.8	C34—C35—H35	121.2
C1—C2—C3	118.9 (4)	C36—C35—H35	121.2
C1—C2—H2	120.6	C37—C36—C35	121.3 (3)
C3—C2—H2	120.6	C37—C36—C39	118.7 (3)
C4—C3—C2	119.3 (4)	C35—C36—C39	119.9 (3)
C4—C3—H3	120.4	C36—C37—C32	122.1 (3)

C2—C3—H3	120.4	C36—C37—H37	119.0
C3—C4—C5	119.8 (5)	C32—C37—H37	119.0
C3—C4—H4	120.1	F8—C38—F7	106.1 (3)
C5—C4—H4	120.1	F8—C38—F9	107.5 (3)
N1—C5—C4	120.1 (4)	F7—C38—F9	104.8 (3)
N1—C5—C6	114.1 (3)	F8—C38—C34	112.4 (3)
C4—C5—C6	125.6 (4)	F7—C38—C34	113.0 (3)
C11—C6—C7	120.7 (4)	F9—C38—C34	112.4 (3)
C11—C6—C5	115.1 (3)	F10—C39—F11	108.1 (5)
C7—C6—C5	124.1 (4)	F11B—C39—F10B	120.3 (7)
C8—C7—C6	119.7 (4)	F10—C39—F12	109.2 (5)
C8—C7—H7	120.2	F11—C39—F12	98.6 (5)
C6—C7—H7	120.2	F11B—C39—F12B	100.6 (8)
C7—C8—C9	120.3 (4)	F10B—C39—F12B	102.1 (8)
C7—C8—H8	119.8	F10—C39—C36	115.8 (4)
C9—C8—H8	119.8	F11B—C39—C36	109.2 (6)
C8—C9—C10	120.0 (4)	F11—C39—C36	113.9 (4)
C8—C9—H9	120.0	F10B—C39—C36	111.2 (5)
C10—C9—H9	120.0	F12—C39—C36	109.7 (4)
C11—C10—C9	120.4 (4)	F12B—C39—C36	112.6 (6)
C11—C10—H10	119.8	C45—C40—C41	115.7 (3)
C9—C10—H10	119.8	C45—C40—B1	123.6 (3)
C10—C11—C6	118.9 (3)	C41—C40—B1	120.5 (3)
C10—C11—Rh1	125.7 (3)	C42—C41—C40	121.8 (3)
C6—C11—Rh1	115.4 (2)	C42—C41—H41	119.1
C16—C12—C13	106.9 (3)	C40—C41—H41	119.1
C16—C12—C17	128.5 (4)	C43—C42—C41	121.7 (3)
C13—C12—C17	124.5 (4)	C43—C42—C46	118.6 (3)
C16—C12—Rh1	71.6 (2)	C41—C42—C46	119.7 (3)
C13—C12—Rh1	67.1 (2)	C44—C43—C42	117.3 (3)
C17—C12—Rh1	128.3 (3)	C44—C43—H43	121.3
C14—C13—C12	108.9 (3)	C42—C43—H43	121.3
C14—C13—C18	124.9 (4)	C43—C44—C45	121.4 (3)
C12—C13—C18	125.9 (4)	C43—C44—C47	118.5 (3)
C14—C13—Rh1	72.1 (2)	C45—C44—C47	120.1 (3)
C12—C13—Rh1	74.6 (2)	C44—C45—C40	122.2 (3)
C18—C13—Rh1	124.7 (3)	C44—C45—H45	118.9

C13—C14—C15	108.1 (3)	C40—C45—H45	118.9
C13—C14—C19	126.7 (4)	F14B—C46—F13B	117.4 (7)
C15—C14—C19	125.1 (4)	F14—C46—F15	112.0 (7)
C13—C14—Rh1	69.5 (2)	F14—C46—F13	104.3 (7)
C15—C14—Rh1	71.1 (2)	F15—C46—F13	98.2 (7)
C19—C14—Rh1	127.8 (3)	F14B—C46—F15B	97.3 (7)
C14—C15—C16	106.7 (3)	F13B—C46—F15B	95.3 (7)
C14—C15—C20	127.9 (4)	F14B—C46—C42	117.8 (5)
C16—C15—C20	124.5 (4)	F14—C46—C42	117.0 (5)
C14—C15—Rh1	70.8 (2)	F13B—C46—C42	115.5 (5)
C16—C15—Rh1	72.9 (2)	F15—C46—C42	114.2 (5)
C20—C15—Rh1	129.4 (3)	F13—C46—C42	108.8 (5)
C12—C16—C15	109.1 (3)	F15B—C46—C42	108.1 (5)
C12—C16—C21	125.6 (4)	F16—C47—F17	106.4 (3)
C15—C16—C21	125.3 (4)	F16—C47—F18	106.5 (3)
C12—C16—Rh1	71.8 (2)	F17—C47—F18	105.6 (3)
C15—C16—Rh1	68.7 (2)	F16—C47—C44	113.4 (3)
C21—C16—Rh1	126.3 (3)	F17—C47—C44	113.3 (3)
C12—C17—H17A	109.5	F18—C47—C44	111.1 (3)
C12—C17—H17B	109.5	C49—C48—C53	115.5 (3)
H17A—C17—H17B	109.5	C49—C48—B1	121.2 (3)
C12—C17—H17C	109.5	C53—C48—B1	123.2 (3)
H17A—C17—H17C	109.5	C50—C49—C48	122.3 (3)
H17B—C17—H17C	109.5	C50—C49—H49	118.9
C13—C18—H18A	109.5	C48—C49—H49	118.9
C13—C18—H18B	109.5	C51—C50—C49	121.2 (3)
H18A—C18—H18B	109.5	C51—C50—C54	119.0 (3)
C13—C18—H18C	109.5	C49—C50—C54	119.8 (3)
H18A—C18—H18C	109.5	C52—C51—C50	117.6 (3)
H18B—C18—H18C	109.5	C52—C51—H51	121.2
C14—C19—H19A	109.5	C50—C51—H51	121.2
C14—C19—H19B	109.5	C51—C52—C53	121.2 (3)
H19A—C19—H19B	109.5	C51—C52—C55	118.2 (3)
C14—C19—H19C	109.5	C53—C52—C55	120.6 (3)
H19A—C19—H19C	109.5	C52—C53—C48	122.1 (3)
H19B—C19—H19C	109.5	C52—C53—H53	118.9
C15—C20—H20A	109.5	C48—C53—H53	118.9

C15—C20—H20B	109.5	F20—C54—F21	110.2 (5)
H20A—C20—H20B	109.5	F19B—C54—F21B	111.3 (6)
C15—C20—H20C	109.5	F20—C54—F19	103.7 (5)
H20A—C20—H20C	109.5	F21—C54—F19	104.1 (5)
H20B—C20—H20C	109.5	F19B—C54—F20B	101.8 (7)
C16—C21—H21A	109.5	F21B—C54—F20B	101.4 (7)
C16—C21—H21B	109.5	F19B—C54—C50	115.6 (6)
H21A—C21—H21B	109.5	F20—C54—C50	113.6 (4)
C16—C21—H21C	109.5	F21—C54—C50	113.1 (4)
H21A—C21—H21C	109.5	F21B—C54—C50	114.7 (5)
H21B—C21—H21C	109.5	F19—C54—C50	111.3 (4)
N2—C22—C23	178.7 (6)	F20B—C54—C50	110.2 (5)
C22—C23—H23A	109.5	F24—C55—F22	106.5 (6)
C22—C23—H23B	109.5	F24—C55—F23	107.3 (5)
H23A—C23—H23B	109.5	F22—C55—F23	103.2 (5)
C22—C23—H23C	109.5	F23B—C55—F24B	120.7 (7)
H23A—C23—H23C	109.5	F23B—C55—F22B	101.7 (7)
H23B—C23—H23C	109.5	F24B—C55—F22B	90.0 (7)
C29—C24—C25	116.0 (3)	F24—C55—C52	115.1 (4)
C29—C24—B1	121.5 (3)	F23B—C55—C52	117.4 (5)
C25—C24—B1	122.1 (3)	F22—C55—C52	111.7 (4)
C26—C25—C24	122.1 (3)	F23—C55—C52	112.1 (4)
C26—C25—H25	118.9	F24B—C55—C52	111.6 (5)
C24—C25—H25	118.9	F22B—C55—C52	110.6 (4)
C25—C26—C27	121.0 (3)	C1—N1—C5	119.4 (3)
C25—C26—C30	119.9 (3)	C1—N1—Rh1	125.1 (3)
C27—C26—C30	119.1 (3)	C5—N1—Rh1	115.5 (2)
C28—C27—C26	117.9 (3)	C22—N2—Rh1	170.2 (4)
C28—C27—H27	121.1	C32—B1—C24	113.3 (2)
C26—C27—H27	121.1	C32—B1—C40	110.3 (2)
C27—C28—C29	121.1 (3)	C24—B1—C40	102.7 (2)
C27—C28—C31	119.0 (3)	C32—B1—C48	105.2 (2)
C29—C28—C31	119.9 (4)	C24—B1—C48	112.6 (2)
C28—C29—C24	121.9 (3)	C40—B1—C48	112.9 (2)
C28—C29—H29	119.0	C11—Rh1—N2	92.15 (13)
C24—C29—H29	119.0	C11—Rh1—N1	78.56 (13)
F2—C30—F1	106.3 (5)	N2—Rh1—N1	86.32 (14)

F2—C30—F3	106.9 (5)	C11—Rh1—C13	112.42 (14)
F1—C30—F3	104.7 (5)	N2—Rh1—C13	155.44 (14)
F3B—C30—F2B	110.5 (7)	N1—Rh1—C13	98.48 (14)
F3B—C30—F1B	102.9 (7)	C11—Rh1—C14	92.98 (13)
F2B—C30—F1B	105.7 (6)	N2—Rh1—C14	145.15 (16)
F3B—C30—C26	117.8 (5)	N1—Rh1—C14	128.46 (15)
F2—C30—C26	114.9 (4)	C13—Rh1—C14	38.37 (16)
F1—C30—C26	112.7 (4)	C11—Rh1—C15	109.33 (14)
F3—C30—C26	110.7 (4)	N2—Rh1—C15	108.30 (15)
F2B—C30—C26	109.6 (5)	N1—Rh1—C15	162.64 (14)
F1B—C30—C26	109.6 (5)	C13—Rh1—C15	64.34 (15)
F6—C31—F5	108.5 (5)	C14—Rh1—C15	38.13 (16)
F6—C31—F4	103.7 (4)	C11—Rh1—C16	147.52 (15)
F5—C31—F4	104.7 (4)	N2—Rh1—C16	96.33 (14)
F6—C31—C28	112.8 (4)	N1—Rh1—C16	133.14 (14)
F5—C31—C28	113.6 (4)	C13—Rh1—C16	62.89 (15)
F4—C31—C28	112.8 (4)	C14—Rh1—C16	63.04 (14)
C37—C32—C33	115.9 (3)	C15—Rh1—C16	38.37 (15)
C37—C32—B1	119.9 (3)	C11—Rh1—C12	150.64 (15)
C33—C32—B1	123.7 (3)	N2—Rh1—C12	117.21 (14)
C34—C33—C32	121.9 (3)	N1—Rh1—C12	101.77 (13)
C34—C33—H33	119.1	C13—Rh1—C12	38.23 (15)
C32—C33—H33	119.1	C14—Rh1—C12	63.48 (14)
C35—C34—C33	121.3 (3)	C15—Rh1—C12	63.58 (14)
C35—C34—C38	118.7 (3)	C16—Rh1—C12	36.61 (16)
N1—C1—C2—C3	1.3 (8)	C37—C36—C39—F10	-156.6 (5)
C1—C2—C3—C4	-2.3 (9)	C35—C36—C39—F10	26.4 (7)
C2—C3—C4—C5	0.3 (9)	C37—C36—C39—F11B	-55.1 (7)
C3—C4—C5—N1	2.7 (7)	C35—C36—C39—F11B	127.9 (6)
C3—C4—C5—C6	-172.9 (5)	C37—C36—C39—F11	-30.2 (6)
N1—C5—C6—C11	-0.7 (5)	C35—C36—C39—F11	152.8 (5)
C4—C5—C6—C11	175.2 (4)	C37—C36—C39—	169.8 (7)

		F10B	
N1—C5—C6—C7	-176.7 (4)	C35—C36—C39—F10B	-7.2 (8)
C4—C5—C6—C7	-0.9 (7)	C37—C36—C39—F12	79.2 (5)
C11—C6—C7—C8	-2.4 (6)	C35—C36—C39—F12	-97.8 (5)
C5—C6—C7—C8	173.5 (4)	C37—C36—C39—F12B	55.8 (7)
C6—C7—C8—C9	0.5 (7)	C35—C36—C39—F12B	-121.2 (7)
C7—C8—C9—C10	0.7 (7)	C45—C40—C41—C42	-0.2 (5)
C8—C9—C10—C11	-0.1 (6)	B1—C40—C41—C42	173.5 (3)
C9—C10—C11—C6	-1.6 (5)	C40—C41—C42—C43	-0.6 (6)
C9—C10—C11—Rh1	176.0 (3)	C40—C41—C42—C46	180.0 (4)
C7—C6—C11—C10	2.9 (5)	C41—C42—C43—C44	1.0 (6)
C5—C6—C11—C10	-173.3 (3)	C46—C42—C43—C44	-179.6 (4)
C7—C6—C11—Rh1	-175.0 (3)	C42—C43—C44—C45	-0.6 (5)
C5—C6—C11—Rh1	8.9 (4)	C42—C43—C44—C47	-177.9 (3)
C16—C12—C13—C14	3.7 (4)	C43—C44—C45—C40	-0.2 (5)
C17—C12—C13—C14	-173.8 (4)	C47—C44—C45—C40	177.1 (3)
Rh1—C12—C13—C14	64.5 (3)	C41—C40—C45—C44	0.6 (5)
C16—C12—C13—C18	177.1 (4)	B1—C40—C45—C44	-172.9 (3)
C17—C12—C13—C18	-0.3 (6)	C43—C42—C46—F14B	170.8 (8)
Rh1—C12—C13—C18	-122.0 (4)	C41—C42—C46—F14B	-9.8 (10)
C16—C12—C13—Rh1	-60.8 (3)	C43—C42—C46—F14	-17.9 (10)
C17—C12—C13—Rh1	121.7 (4)	C41—C42—C46—F14	161.5 (8)
C12—C13—C14—C15	-5.2 (4)	C43—C42—C46—F13B	24.9 (9)

C18—C13—C14—C15	-178.8 (4)	C41—C42—C46—F13B	-155.6 (7)
Rh1—C13—C14—C15	60.9 (3)	C43—C42—C46—F15	-151.6 (7)
C12—C13—C14—C19	171.4 (4)	C41—C42—C46—F15	27.9 (9)
C18—C13—C14—C19	-2.2 (6)	C43—C42—C46—F13	99.9 (6)
Rh1—C13—C14—C19	-122.5 (4)	C41—C42—C46—F13	-80.6 (6)
C12—C13—C14—Rh1	-66.2 (3)	C43—C42—C46—F15B	-80.4 (6)
C18—C13—C14—Rh1	120.3 (4)	C41—C42—C46—F15B	99.1 (6)
C13—C14—C15—C16	4.7 (4)	C43—C44—C47—F16	-31.1 (5)
C19—C14—C15—C16	-172.0 (4)	C45—C44—C47—F16	151.5 (4)
Rh1—C14—C15—C16	64.6 (3)	C43—C44—C47—F17	-152.5 (3)
C13—C14—C15—C20	174.6 (4)	C45—C44—C47—F17	30.1 (5)
C19—C14—C15—C20	-2.1 (6)	C43—C44—C47—F18	88.8 (4)
Rh1—C14—C15—C20	-125.5 (4)	C45—C44—C47—F18	-88.6 (4)
C13—C14—C15—Rh1	-59.9 (3)	C53—C48—C49—C50	-1.1 (5)
C19—C14—C15—Rh1	123.4 (4)	B1—C48—C49—C50	-177.4 (3)
C13—C12—C16—C15	-0.7 (4)	C48—C49—C50—C51	-0.9 (5)
C17—C12—C16—C15	176.6 (4)	C48—C49—C50—C54	179.6 (4)
Rh1—C12—C16—C15	-58.8 (3)	C49—C50—C51—C52	1.4 (5)
C13—C12—C16—C21	-179.9 (4)	C54—C50—C51—C52	-179.2 (4)
C17—C12—C16—C21	-2.6 (7)	C50—C51—C52—C53	0.3 (5)
Rh1—C12—C16—C21	122.1 (5)	C50—C51—C52—C55	-178.6 (4)
C13—C12—C16—Rh1	58.0 (3)	C51—C52—C53—C48	-2.5 (5)

C17—C12—C16—Rh1	-124.7 (4)	C55—C52—C53—C48	176.4 (4)
C14—C15—C16—C12	-2.4 (4)	C49—C48—C53—C52	2.8 (5)
C20—C15—C16—C12	-172.8 (4)	B1—C48—C53—C52	178.9 (3)
Rh1—C15—C16—C12	60.7 (3)	C51—C50—C54—F19B	109.9 (6)
C14—C15—C16—C21	176.7 (4)	C49—C50—C54—F19B	-70.7 (7)
C20—C15—C16—C21	6.4 (7)	C51—C50—C54—F20	-111.2 (5)
Rh1—C15—C16—C21	-120.2 (4)	C49—C50—C54—F20	68.2 (6)
C14—C15—C16—Rh1	-63.1 (2)	C51—C50—C54—F21	15.3 (7)
C20—C15—C16—Rh1	126.5 (4)	C49—C50—C54—F21	-165.2 (5)
C29—C24—C25—C26	2.7 (5)	C51—C50—C54—F21B	-21.7 (8)
B1—C24—C25—C26	175.6 (3)	C49—C50—C54—F21B	157.8 (6)
C24—C25—C26—C27	-1.9 (6)	C51—C50—C54—F19	132.1 (5)
C24—C25—C26—C30	180.0 (4)	C49—C50—C54—F19	-48.4 (6)
C25—C26—C27—C28	0.0 (6)	C51—C50—C54—F20B	-135.4 (6)
C30—C26—C27—C28	178.2 (4)	C49—C50—C54—F20B	44.1 (7)
C26—C27—C28—C29	0.9 (6)	C51—C52—C55—F24	-176.9 (6)
C26—C27—C28—C31	-177.7 (4)	C53—C52—C55—F24	4.2 (7)
C27—C28—C29—C24	-0.1 (5)	C51—C52—C55—F23B	16.9 (9)
C31—C28—C29—C24	178.6 (4)	C53—C52—C55—F23B	-162.1 (7)
C25—C24—C29—C28	-1.7 (5)	C51—C52—C55—F22	61.5 (6)
B1—C24—C29—C28	-174.7 (3)	C53—C52—C55—F22	-117.5 (5)
C25—C26—C30—F3B	-170.5 (7)	C51—C52—C55—F23	-53.8 (6)

C27—C26—C30—F3B	11.3 (8)	C53—C52—C55—F23	127.3 (5)
C25—C26—C30—F2	-19.7 (7)	C51—C52—C55—F24B	-128.5 (7)
C27—C26—C30—F2	162.1 (5)	C53—C52—C55—F24B	52.6 (8)
C25—C26—C30—F1	102.3 (5)	C51—C52—C55—F22B	132.9 (6)
C27—C26—C30—F1	-75.9 (6)	C53—C52—C55—F22B	-46.0 (7)
C25—C26—C30—F3	-140.9 (4)	C2—C1—N1—C5	1.7 (6)
C27—C26—C30—F3	40.9 (6)	C2—C1—N1—Rh1	-178.3 (4)
C25—C26—C30—F2B	-43.1 (7)	C4—C5—N1—C1	-3.7 (6)
C27—C26—C30—F2B	138.8 (6)	C6—C5—N1—C1	172.4 (3)
C25—C26—C30—F1B	72.4 (6)	C4—C5—N1—Rh1	176.3 (4)
C27—C26—C30—F1B	-105.7 (6)	C6—C5—N1—Rh1	-7.7 (4)
C27—C28—C31—F6	76.1 (6)	C37—C32—B1—C24	150.8 (3)
C29—C28—C31—F6	-102.6 (5)	C33—C32—B1—C24	-36.9 (4)
C27—C28—C31—F5	-160.0 (4)	C37—C32—B1—C40	36.3 (4)
C29—C28—C31—F5	21.4 (6)	C33—C32—B1—C40	-151.4 (3)
C27—C28—C31—F4	-41.0 (6)	C37—C32—B1—C48	-85.8 (3)
C29—C28—C31—F4	140.3 (4)	C33—C32—B1—C48	86.6 (3)
C37—C32—C33—C34	-1.3 (5)	C29—C24—B1—C32	-31.8 (4)
B1—C32—C33—C34	-174.0 (3)	C25—C24—B1—C32	155.6 (3)
C32—C33—C34—C35	1.3 (5)	C29—C24—B1—C40	87.2 (3)
C32—C33—C34—C38	-177.3 (3)	C25—C24—B1—C40	-85.4 (3)
C33—C34—C35—C36	0.0 (5)	C29—C24—B1—C48	-151.1 (3)
C38—C34—C35—C36	178.6 (3)	C25—C24—B1—C48	36.4 (4)
C34—C35—C36—C37	-1.1 (5)	C45—C40—B1—C32	-142.5 (3)
C34—C35—C36—C39	175.8 (4)	C41—C40—B1—C32	44.3 (4)
C35—C36—C37—C32	1.1 (5)	C45—C40—B1—C24	96.4 (3)

C39—C36—C37—C32	-175.9 (3)	C41—C40—B1—C24	-76.7 (3)
C33—C32—C37—C36	0.2 (5)	C45—C40—B1—C48	-25.2 (4)
B1—C32—C37—C36	173.1 (3)	C41—C40—B1—C48	161.7 (3)
C35—C34—C38—F8	-91.9 (4)	C49—C48—B1—C32	77.0 (3)
C33—C34—C38—F8	86.7 (4)	C53—C48—B1—C32	-98.9 (3)
C35—C34—C38—F7	148.0 (3)	C49—C48—B1—C24	-159.1 (3)
C33—C34—C38—F7	-33.4 (5)	C53—C48—B1—C24	25.0 (4)
C35—C34—C38—F9	29.6 (5)	C49—C48—B1—C40	-43.4 (4)
C33—C34—C38—F9	-151.8 (3)	C53—C48—B1—C40	140.7 (3)

7.5 [**6**][$BArF_{24}$]

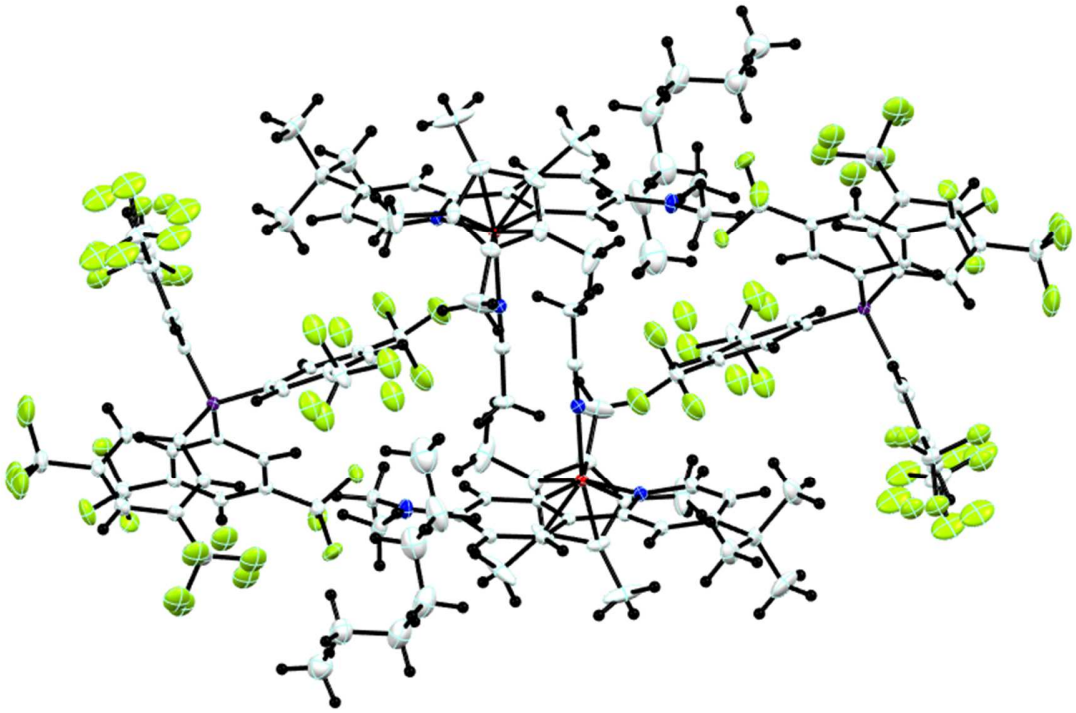

7.5.1 **Figure A13.** Crystal lattice packing of [**6**][$BArF_{24}$].

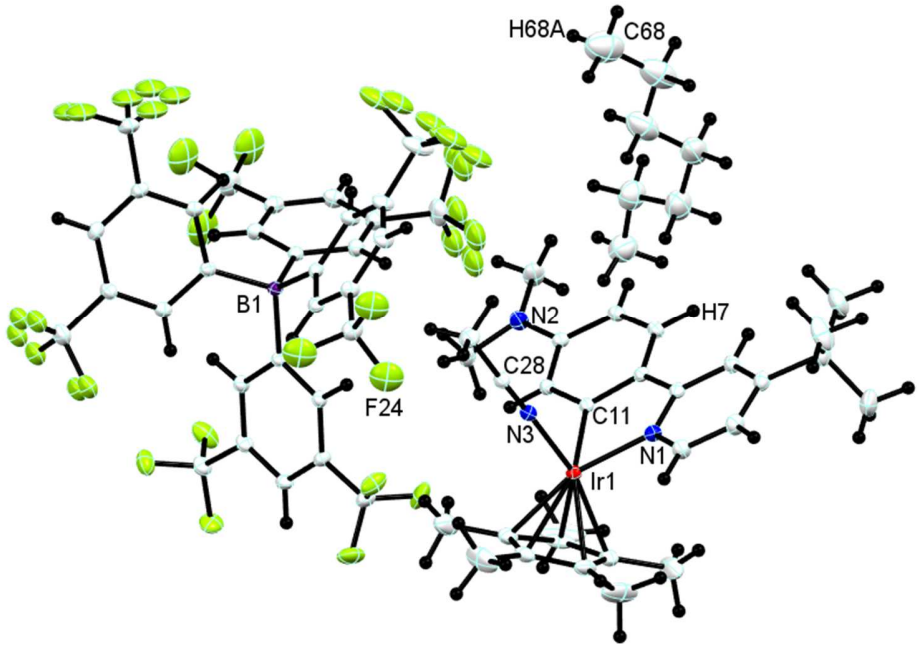

7.5.2 **Figure A14.** Asymmetric unit of [**6**][$BArF_{24}$], with all hydrogens and partial numbering of atoms.

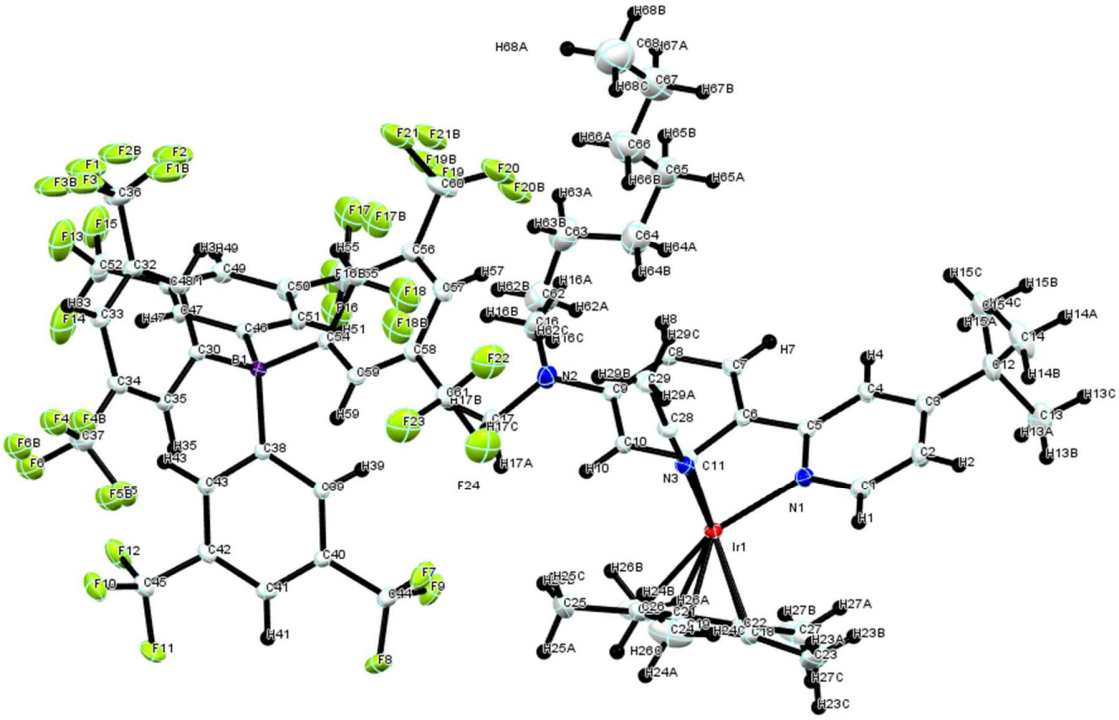

7.5.3 **Figure A15.** Asymmetric unit of [**6**][BArF$_{24}$], with all hydrogens and total numbering of atoms.

[**6**][BArF$_{24}$]

7.5.4 Crystal data

$C_{32}H_{12}BF_{24}\cdot C_{29}H_{39}IrN_3\cdot C_7H_{16}$	$Z = 2$
$M_r = 1585.25$	$F(000) = 1588$
Triclinic, $P\bar{1}$	$D_x = 1.534$ Mg m^{-3}
$a = 14.7520$ (7) Å	Mo $K\alpha$ radiation, $\lambda = 0.71073$ Å
$b = 15.3911$ (7) Å	Cell parameters from 9847 reflections
$c = 16.4500$ (8) Å	$\theta = 2.7$–$29.9°$
$\alpha = 97.200$ (1)°	$\mu = 2.05$ mm^{-1}
$\beta = 96.675$ (1)°	$T = 173$ K
$\gamma = 109.957$ (1)°	Prism, yellow
$V = 3432.0$ (3) Å^3	0.24 × 0.16 × 0.10 mm

7.5.5 Data collection

Bruker APEX-II CCD diffractometer	20031 independent reflections
Radiation source: sealed tube	16368 reflections with $I > 2\sigma(I)$
Triumph monochromator	$R_{int} = 0.046$
ϕ and ω scans	$\theta_{max} = 30.0°$, $\theta_{min} = 1.3°$
Absorption correction: multi-scan *SADABS*	$h = -20 \rightarrow 20$
$T_{min} = 0.669$, $T_{max} = 0.746$	$k = -21 \rightarrow 21$
76738 measured reflections	$l = -23 \rightarrow 23$

7.5.6 Refinement

Refinement on F^2	Primary atom site location: structure-invariant direct methods
Least-squares matrix: full	Secondary atom site location: difference Fourier map
$R[F^2 > 2\sigma(F^2)] = 0.046$	Hydrogen site location: inferred from neighbouring sites
$wR(F^2) = 0.122$	H-atom parameters constrained
$S = 1.02$	$w = 1/[\sigma^2(F_o^2) + (0.0731P)^2 + 2.5831P]$ where $P = (F_o^2 + 2F_c^2)/3$
20031 reflections	$(\Delta/\sigma)_{max} = 0.001$
851 parameters	$\Delta\rangle_{max} = 2.11$ e Å^{-3}
0 restraints	$\Delta\rangle_{min} = -2.20$ e Å^{-3}

7.5.7 Special details

Geometry. All esds (except the esd in the dihedral angle between two l.s. planes) are estimated using the full covariance matrix. The cell esds are taken into account individually in the estimation of esds in distances, angles and torsion angles; correlations between esds in cell parameters are only used when they are defined by crystal symmetry. An approximate (isotropic) treatment of cell esds is used for estimating esds involving l.s. planes.

7.5.8 **Table A13.** Fractional atomic coordinates and isotropic or equivalent isotropic displacement parameters (Å^2) for [**6**][BArF$_{24}$].

	x	*y*	*z*	U_{iso}*/U_{eq}	Occ. (<1)
C1	0.1872 (3)	0.3019 (3)	0.2624 (2)	0.0305 (8)	

H1	0.2123	0.3139	0.2126	0.037*	
C2	0.1002 (3)	0.3137 (3)	0.2722 (3)	0.0339 (9)	
H2	0.0665	0.3332	0.2296	0.041*	
C3	0.0619 (3)	0.2970 (3)	0.3450 (3)	0.0301 (8)	
C4	0.1153 (3)	0.2701 (3)	0.4049 (2)	0.0260 (7)	
H4	0.0920	0.2592	0.4555	0.031*	
C5	0.2032 (3)	0.2586 (3)	0.3924 (2)	0.0233 (7)	
C6	0.2664 (2)	0.2342 (2)	0.4523 (2)	0.0217 (7)	
C7	0.2483 (3)	0.2195 (3)	0.5320 (2)	0.0250 (7)	
H7	0.1883	0.2195	0.5476	0.030*	
C8	0.3162 (3)	0.2051 (3)	0.5881 (2)	0.0256 (7)	
H8	0.3018	0.1936	0.6415	0.031*	
C9	0.4066 (3)	0.2071 (3)	0.5673 (2)	0.0233 (7)	
C10	0.4230 (2)	0.2179 (3)	0.4857 (2)	0.0223 (7)	
H10	0.4826	0.2165	0.4700	0.027*	
C11	0.3540 (2)	0.2306 (2)	0.4275 (2)	0.0210 (6)	
C12	-0.0367 (3)	0.3061 (3)	0.3566 (3)	0.0376 (10)	
C13	-0.1165 (4)	0.2254 (6)	0.2967 (5)	0.079 (2)	
H13A	-0.1164	0.1655	0.3108	0.119*	
H13B	-0.1042	0.2286	0.2397	0.119*	
H13C	-0.1804	0.2303	0.3010	0.119*	
C14	-0.0381 (4)	0.4003 (5)	0.3374 (5)	0.0684 (18)	
H14A	-0.1021	0.4042	0.3427	0.103*	
H14B	-0.0261	0.4055	0.2805	0.103*	
H14C	0.0131	0.4515	0.3766	0.103*	
C15	-0.0565 (4)	0.3007 (5)	0.4448 (4)	0.0539 (14)	
H15A	-0.0578	0.2401	0.4584	0.081*	
H15B	-0.1197	0.3069	0.4493	0.081*	
H15C	-0.0046	0.3516	0.4837	0.081*	
C16	0.4605 (4)	0.1870 (4)	0.7084 (3)	0.0485 (13)	
H16A	0.4339	0.2330	0.7318	0.073*	
H16B	0.5219	0.1948	0.7438	0.073*	
H16C	0.4133	0.1234	0.7055	0.073*	
C17	0.5616 (3)	0.1821 (4)	0.6012 (3)	0.0370 (10)	
H17A	0.5387	0.1213	0.5638	0.056*	
H17B	0.6045	0.1804	0.6506	0.056*	
H17C	0.5979	0.2316	0.5725	0.056*	

C18	0.3386 (3)	0.1890 (3)	0.1701 (2)	0.0363 (10)	
C19	0.4391 (3)	0.2331 (3)	0.1963 (3)	0.0334 (9)	
C20	0.4711 (3)	0.1908 (3)	0.2611 (3)	0.0371 (10)	
C21	0.3870 (4)	0.1146 (3)	0.2723 (3)	0.0426 (11)	
C22	0.3039 (3)	0.1167 (3)	0.2183 (3)	0.0415 (11)	
C23	0.2776 (6)	0.2069 (6)	0.0988 (3)	0.085 (3)	
H23A	0.3080	0.2719	0.0907	0.128*	
H23B	0.2117	0.1966	0.1113	0.128*	
H23C	0.2734	0.1639	0.0481	0.128*	
C24	0.5054 (6)	0.3133 (5)	0.1612 (5)	0.077 (2)	
H24A	0.5458	0.2903	0.1275	0.116*	
H24B	0.5477	0.3629	0.2069	0.116*	
H24C	0.4654	0.3387	0.1264	0.116*	
C25	0.5747 (4)	0.2112 (6)	0.2997 (4)	0.083 (3)	
H25A	0.6057	0.1809	0.2615	0.125*	
H25B	0.5759	0.1869	0.3519	0.125*	
H25C	0.6105	0.2792	0.3109	0.125*	
C26	0.3877 (8)	0.0444 (4)	0.3262 (4)	0.090 (3)	
H26A	0.3204	0.0081	0.3317	0.135*	
H26B	0.4256	0.0767	0.3813	0.135*	
H26C	0.4176	0.0019	0.3013	0.135*	
C27	0.2008 (5)	0.0497 (5)	0.2091 (5)	0.098 (3)	
H27A	0.1562	0.0844	0.2065	0.148*	
H27B	0.1938	0.0172	0.2568	0.148*	
H27C	0.1850	0.0036	0.1578	0.148*	
C28	0.4889 (3)	0.4617 (3)	0.3768 (2)	0.0253 (7)	
C29	0.5437 (3)	0.5615 (3)	0.4077 (3)	0.0396 (10)	
H29A	0.5502	0.5955	0.3609	0.059*	
H29B	0.6089	0.5699	0.4366	0.059*	
H29C	0.5088	0.5860	0.4464	0.059*	
C30	0.9974 (3)	0.3611 (3)	0.7738 (2)	0.0221 (7)	
C31	1.0246 (3)	0.4322 (3)	0.8438 (2)	0.0287 (8)	
H31	0.9802	0.4301	0.8816	0.034*	
C32	1.1149 (3)	0.5059 (3)	0.8596 (2)	0.0313 (8)	
C33	1.1828 (3)	0.5103 (3)	0.8075 (3)	0.0312 (8)	
H33	1.2450	0.5596	0.8190	0.037*	
C34	1.1572 (3)	0.4402 (3)	0.7378 (2)	0.0269 (7)	

C35	1.0670 (3)	0.3676 (3)	0.7214 (2)	0.0243 (7)	
H35	1.0519	0.3208	0.6732	0.029*	
C36	1.1379 (4)	0.5809 (4)	0.9331 (3)	0.0565 (15)	
C37	1.2298 (3)	0.4424 (4)	0.6816 (3)	0.0417 (10)	
C38	0.8743 (2)	0.1962 (2)	0.6776 (2)	0.0204 (6)	
C39	0.8034 (2)	0.1670 (3)	0.6057 (2)	0.0217 (7)	
H39	0.7587	0.1988	0.5990	0.026*	
C40	0.7953 (3)	0.0938 (3)	0.5438 (2)	0.0240 (7)	
C41	0.8573 (3)	0.0437 (3)	0.5513 (2)	0.0264 (7)	
H41	0.8516	-0.0070	0.5092	0.032*	
C42	0.9277 (3)	0.0702 (3)	0.6223 (2)	0.0266 (7)	
C43	0.9367 (3)	0.1448 (3)	0.6833 (2)	0.0238 (7)	
H43	0.9868	0.1618	0.7306	0.029*	
C44	0.7186 (3)	0.0685 (3)	0.4679 (2)	0.0316 (8)	
C45	0.9981 (3)	0.0197 (3)	0.6333 (3)	0.0321 (8)	
C46	0.8583 (3)	0.2311 (3)	0.8345 (2)	0.0225 (7)	
C47	0.9287 (3)	0.2254 (3)	0.8960 (2)	0.0273 (7)	
H47	0.9961	0.2546	0.8931	0.033*	
C48	0.9029 (3)	0.1781 (3)	0.9616 (2)	0.0307 (8)	
C49	0.8067 (3)	0.1354 (3)	0.9689 (2)	0.0333 (9)	
H49	0.7894	0.1037	1.0140	0.040*	
C50	0.7354 (3)	0.1400 (3)	0.9085 (3)	0.0320 (8)	
C51	0.7605 (3)	0.1856 (3)	0.8422 (2)	0.0275 (8)	
H51	0.7100	0.1859	0.8009	0.033*	
C52	0.9803 (4)	0.1722 (4)	1.0238 (3)	0.0472 (12)	
C53	0.6311 (4)	0.0952 (4)	0.9167 (3)	0.0492 (13)	
C54	0.8175 (2)	0.3426 (3)	0.7302 (2)	0.0224 (7)	
C55	0.7656 (3)	0.3738 (3)	0.7865 (2)	0.0288 (8)	
H55	0.7681	0.3576	0.8404	0.035*	
C56	0.7104 (3)	0.4281 (3)	0.7651 (3)	0.0345 (9)	
C57	0.7039 (3)	0.4533 (3)	0.6880 (3)	0.0346 (9)	
H57	0.6656	0.4895	0.6738	0.041*	
C58	0.7548 (3)	0.4242 (3)	0.6319 (2)	0.0271 (7)	
C59	0.8118 (3)	0.3719 (3)	0.6530 (2)	0.0237 (7)	
H59	0.8482	0.3554	0.6137	0.028*	
C60	0.6576 (5)	0.4600 (5)	0.8284 (3)	0.0559 (15)	
C61	0.7453 (3)	0.4451 (3)	0.5459 (3)	0.0337 (9)	

C62	0.3242 (6)	-0.0304 (5)	0.8382 (4)	0.0765 (19)	
H62A	0.2602	-0.0816	0.8255	0.115*	
H62B	0.3682	-0.0455	0.8787	0.115*	
H62C	0.3519	-0.0224	0.7871	0.115*	
C63	0.3122 (5)	0.0590 (6)	0.8738 (4)	0.0736 (19)	
H63A	0.2978	0.0555	0.9309	0.088*	
H63B	0.3745	0.1122	0.8776	0.088*	
C64	0.2322 (5)	0.0774 (6)	0.8229 (5)	0.083 (2)	
H64A	0.1717	0.0211	0.8150	0.100*	
H64B	0.2498	0.0852	0.7672	0.100*	
C65	0.2091 (5)	0.1640 (6)	0.8586 (4)	0.081 (2)	
H65A	0.1544	0.1679	0.8201	0.097*	
H65B	0.1866	0.1544	0.9123	0.097*	
C66	0.2941 (6)	0.2566 (7)	0.8722 (5)	0.087 (2)	
H66A	0.3494	0.2525	0.9098	0.104*	
H66B	0.3155	0.2674	0.8183	0.104*	
C67	0.2707 (7)	0.3376 (7)	0.9082 (5)	0.091 (3)	
H67A	0.2467	0.3257	0.9610	0.110*	
H67B	0.2172	0.3433	0.8695	0.110*	
C68	0.3597 (8)	0.4322 (8)	0.9255 (6)	0.114 (3)	
H68A	0.4133	0.4270	0.9634	0.171*	
H68B	0.3402	0.4827	0.9509	0.171*	
H68C	0.3816	0.4464	0.8731	0.171*	
N1	0.2382 (2)	0.2740 (2)	0.32080 (19)	0.0251 (6)	
N2	0.4787 (3)	0.2013 (3)	0.6258 (2)	0.0346 (8)	
N3	0.4438 (2)	0.3847 (2)	0.35210 (19)	0.0248 (6)	
B1	0.8862 (3)	0.2822 (3)	0.7539 (2)	0.0211 (7)	
F1	1.1451 (6)	0.5406 (6)	1.0059 (5)	0.0911 (15)	0.6
F2	1.0635 (6)	0.6076 (6)	0.9484 (5)	0.0911 (15)	0.6
F3	1.2157 (7)	0.6546 (6)	0.9370 (5)	0.0911 (15)	0.6
F1B	1.0980 (9)	0.6437 (8)	0.9131 (7)	0.0911 (15)	0.4
F2B	1.1071 (9)	0.5613 (9)	0.9997 (9)	0.0911 (15)	0.4
F3B	1.2372 (10)	0.6227 (9)	0.9623 (8)	0.0911 (15)	0.4
F4	1.2991 (4)	0.5214 (6)	0.6849 (4)	0.0523 (7)	0.55
F5	1.1828 (8)	0.4028 (12)	0.6021 (8)	0.0523 (7)	0.55
F6	1.2748 (4)	0.3779 (5)	0.6999 (4)	0.0523 (7)	0.55
F4B	1.2697 (6)	0.5356 (7)	0.6633 (5)	0.0523 (7)	0.45

F5B	1.1994 (10)	0.3968 (15)	0.6063 (9)	0.0523 (7)	0.45
F6B	1.3056 (5)	0.4250 (6)	0.7132 (5)	0.0523 (7)	0.45
F7	0.7044 (2)	0.14429 (19)	0.44561 (17)	0.0478 (7)	
F8	0.7385 (2)	0.0234 (2)	0.40234 (16)	0.0553 (8)	
F9	0.6304 (2)	0.0128 (2)	0.47969 (18)	0.0537 (8)	
F10	1.09047 (19)	0.0759 (2)	0.6339 (2)	0.0485 (7)	
F11	0.9793 (2)	-0.05398 (19)	0.57274 (18)	0.0465 (7)	
F12	0.9984 (2)	-0.0126 (2)	0.70500 (19)	0.0542 (8)	
F13	1.0579 (3)	0.2528 (4)	1.0469 (3)	0.0951 (8)	
F14	1.0224 (3)	0.1134 (4)	0.9945 (3)	0.0951 (8)	
F15	0.9534 (3)	0.1489 (4)	1.0929 (3)	0.0951 (8)	
F16	0.6087 (4)	0.0001 (5)	0.9158 (4)	0.0743 (10)	0.65
F17	0.6095 (4)	0.1231 (5)	0.9874 (4)	0.0743 (10)	0.65
F18	0.5674 (5)	0.1013 (5)	0.8562 (5)	0.0743 (10)	0.65
F16B	0.6042 (8)	0.0203 (10)	0.9530 (8)	0.0743 (10)	0.35
F17B	0.5953 (7)	0.1544 (10)	0.9521 (8)	0.0743 (10)	0.35
F18B	0.5698 (9)	0.0601 (10)	0.8364 (9)	0.0743 (10)	0.35
F19	0.6174 (9)	0.3960 (9)	0.8709 (6)	0.0707 (12)	0.55
F20	0.6012 (6)	0.5024 (6)	0.8003 (4)	0.0707 (12)	0.55
F21	0.7311 (6)	0.5375 (6)	0.8862 (4)	0.0707 (12)	0.55
F19B	0.6404 (11)	0.4115 (12)	0.8897 (7)	0.0707 (12)	0.45
F20B	0.5599 (7)	0.4471 (7)	0.7894 (6)	0.0707 (12)	0.45
F21B	0.6933 (8)	0.5440 (8)	0.8646 (6)	0.0707 (12)	0.45
F22	0.7125 (3)	0.5150 (3)	0.5398 (2)	0.0759 (6)	
F23	0.8289 (3)	0.4721 (3)	0.5171 (2)	0.0759 (6)	
F24	0.6853 (3)	0.3727 (3)	0.4915 (2)	0.0759 (6)	
Ir1	0.36633 (2)	0.24633 (2)	0.30668 (2)	0.02102 (5)	

7.5.9 **Table A14.** Atomic displacement parameters (Å^2) for [**6**][BArF$_{24}$].

	U^{11}	U^{22}	U^{33}	U^{12}	U^{13}	U^{23}
C1	0.0323 (19)	0.034 (2)	0.0282 (18)	0.0143 (17)	0.0048 (14)	0.0103 (16)
C2	0.032 (2)	0.041 (2)	0.0328 (19)	0.0187 (19)	0.0011 (15)	0.0108 (18)
C3	0.0243 (17)	0.028 (2)	0.037 (2)	0.0096 (16)	0.0023 (14)	0.0052 (17)
C4	0.0228 (16)	0.0254 (18)	0.0300 (17)	0.0090 (15)	0.0048 (13)	0.0049 (15)

C5	0.0232 (16)	0.0172 (16)	0.0280 (16)	0.0073 (13)	0.0021 (13)	0.0006 (14)
C6	0.0218 (15)	0.0169 (15)	0.0233 (15)	0.0042 (13)	0.0027 (12)	0.0007 (13)
C7	0.0261 (17)	0.0234 (18)	0.0277 (17)	0.0096 (15)	0.0095 (13)	0.0058 (14)
C8	0.0293 (18)	0.0254 (18)	0.0234 (16)	0.0099 (15)	0.0070 (13)	0.0064 (14)
C9	0.0270 (17)	0.0198 (16)	0.0219 (15)	0.0082 (14)	0.0023 (13)	0.0021 (13)
C10	0.0215 (15)	0.0228 (17)	0.0226 (15)	0.0087 (14)	0.0032 (12)	0.0028 (14)
C11	0.0217 (15)	0.0172 (15)	0.0233 (15)	0.0064 (13)	0.0042 (12)	0.0018 (13)
C12	0.0248 (19)	0.044 (3)	0.049 (2)	0.0175 (19)	0.0042 (17)	0.012 (2)
C13	0.029 (3)	0.096 (5)	0.091 (5)	0.013 (3)	-0.002 (3)	-0.022 (4)
C14	0.055 (3)	0.081 (5)	0.101 (5)	0.048 (3)	0.031 (3)	0.047 (4)
C15	0.040 (3)	0.075 (4)	0.063 (3)	0.034 (3)	0.020 (2)	0.024 (3)
C16	0.042 (2)	0.076 (4)	0.028 (2)	0.021 (3)	0.0016 (18)	0.016 (2)
C17	0.0267 (19)	0.047 (3)	0.039 (2)	0.0144 (19)	0.0003 (16)	0.013 (2)
C18	0.045 (2)	0.046 (3)	0.0224 (17)	0.028 (2)	-0.0011 (16)	-0.0029 (17)
C19	0.041 (2)	0.028 (2)	0.0332 (19)	0.0131 (18)	0.0170 (17)	0.0009 (17)
C20	0.037 (2)	0.046 (3)	0.033 (2)	0.026 (2)	0.0025 (16)	-0.0055 (19)
C21	0.083 (4)	0.024 (2)	0.030 (2)	0.027 (2)	0.021 (2)	0.0056 (17)
C22	0.036 (2)	0.032 (2)	0.047 (2)	0.0033 (19)	0.0166 (19)	-0.010 (2)
C23	0.118 (6)	0.129 (7)	0.030 (2)	0.092 (6)	-0.022 (3)	-0.015 (3)
C24	0.102 (5)	0.050 (4)	0.085 (5)	0.014 (4)	0.067 (4)	0.020 (3)
C25	0.056 (3)	0.134 (7)	0.064 (4)	0.066 (4)	-0.013 (3)	-0.034 (4)
C26	0.206 (9)	0.045 (3)	0.048 (3)	0.074 (5)	0.040 (4)	0.019 (3)
C27	0.059 (4)	0.056 (4)	0.134 (7)	-0.024 (3)	0.049 (4)	-0.054 (4)
C28	0.0248 (17)	0.0194 (17)	0.0304 (17)	0.0060 (14)	0.0082 (13)	0.0029 (14)
C29	0.040 (2)	0.0213 (19)	0.051 (3)	0.0044 (18)	0.0106 (19)	-0.0004 (19)
C30	0.0246 (16)	0.0222 (17)	0.0198 (14)	0.0097 (14)	0.0022 (12)	0.0026 (13)
C31	0.0290 (18)	0.0286 (19)	0.0263 (17)	0.0098 (16)	0.0050 (14)	-0.0021 (15)
C32	0.0309 (19)	0.0267 (19)	0.0290 (18)	0.0058 (16)	0.0024 (14)	-0.0052 (16)
C33	0.0250 (17)	0.0263 (19)	0.035 (2)	0.0035 (16)	0.0023 (15)	-0.0006 (16)
C34	0.0273 (17)	0.0267 (19)	0.0292 (17)	0.0109 (15)	0.0095 (14)	0.0060 (15)
C35	0.0282 (17)	0.0239 (17)	0.0225 (15)	0.0119 (15)	0.0054 (13)	0.0026 (14)
C36	0.047 (3)	0.055 (3)	0.046 (3)	0.003 (3)	0.010 (2)	-0.025 (3)
C37	0.033 (2)	0.045 (3)	0.046 (2)	0.009 (2)	0.0161 (18)	0.005 (2)
C38	0.0229 (15)	0.0183 (16)	0.0215 (15)	0.0092 (13)	0.0034 (12)	0.0035 (13)
C39	0.0205 (15)	0.0207 (16)	0.0246 (16)	0.0084 (13)	0.0030 (12)	0.0048 (14)
C40	0.0266 (17)	0.0210 (17)	0.0214 (15)	0.0068 (14)	0.0008 (13)	0.0009 (14)
C41	0.0312 (18)	0.0211 (17)	0.0260 (17)	0.0091 (15)	0.0068 (14)	0.0001 (14)

C42	0.0288 (18)	0.0234 (18)	0.0326 (18)	0.0142 (15)	0.0082 (14)	0.0068 (15)
C43	0.0240 (16)	0.0252 (18)	0.0246 (16)	0.0117 (14)	0.0029 (13)	0.0055 (14)
C44	0.035 (2)	0.0268 (19)	0.0277 (18)	0.0088 (17)	-0.0024 (15)	-0.0014 (16)
C45	0.033 (2)	0.030 (2)	0.038 (2)	0.0172 (17)	0.0088 (16)	0.0074 (17)
C46	0.0240 (16)	0.0240 (17)	0.0207 (15)	0.0112 (14)	0.0029 (12)	0.0015 (13)
C47	0.0291 (18)	0.032 (2)	0.0231 (16)	0.0156 (16)	0.0019 (13)	0.0044 (15)
C48	0.037 (2)	0.032 (2)	0.0252 (17)	0.0168 (18)	0.0009 (14)	0.0043 (16)
C49	0.042 (2)	0.036 (2)	0.0260 (17)	0.0164 (19)	0.0091 (16)	0.0117 (17)
C50	0.0302 (19)	0.034 (2)	0.0324 (19)	0.0097 (17)	0.0085 (15)	0.0098 (17)
C51	0.0256 (17)	0.030 (2)	0.0276 (17)	0.0120 (16)	0.0029 (13)	0.0041 (15)
C52	0.044 (3)	0.064 (3)	0.037 (2)	0.024 (3)	-0.0042 (19)	0.016 (2)
C53	0.038 (2)	0.063 (3)	0.048 (3)	0.011 (2)	0.017 (2)	0.028 (3)
C54	0.0210 (15)	0.0195 (16)	0.0237 (16)	0.0057 (13)	0.0008 (12)	0.0006 (13)
C55	0.0348 (19)	0.030 (2)	0.0253 (17)	0.0170 (17)	0.0059 (14)	0.0019 (15)
C56	0.043 (2)	0.038 (2)	0.0319 (19)	0.027 (2)	0.0101 (17)	0.0036 (18)
C57	0.038 (2)	0.036 (2)	0.040 (2)	0.0259 (19)	0.0040 (17)	0.0086 (18)
C58	0.0330 (19)	0.0253 (18)	0.0253 (16)	0.0135 (16)	0.0034 (14)	0.0062 (15)
C59	0.0257 (16)	0.0187 (16)	0.0256 (16)	0.0073 (14)	0.0039 (13)	0.0024 (14)
C60	0.090 (4)	0.066 (4)	0.043 (3)	0.062 (4)	0.024 (3)	0.014 (3)
C61	0.041 (2)	0.029 (2)	0.0324 (19)	0.0146 (18)	0.0024 (17)	0.0092 (17)
C62	0.079 (5)	0.075 (5)	0.068 (4)	0.021 (4)	0.008 (3)	0.009 (4)
C63	0.071 (4)	0.084 (5)	0.063 (4)	0.024 (4)	0.003 (3)	0.019 (4)
C64	0.064 (4)	0.114 (7)	0.068 (4)	0.031 (4)	0.003 (3)	0.014 (4)
C65	0.066 (4)	0.122 (7)	0.054 (4)	0.039 (5)	0.005 (3)	0.007 (4)
C66	0.102 (6)	0.117 (7)	0.066 (4)	0.061 (6)	0.032 (4)	0.027 (5)
C67	0.127 (7)	0.133 (8)	0.056 (4)	0.088 (7)	0.029 (4)	0.040 (5)
C68	0.141 (9)	0.137 (10)	0.076 (6)	0.071 (8)	0.008 (6)	0.014 (6)
N1	0.0272 (15)	0.0242 (16)	0.0242 (14)	0.0101 (13)	0.0031 (11)	0.0045 (12)
N2	0.0330 (17)	0.049 (2)	0.0264 (15)	0.0184 (17)	0.0041 (13)	0.0120 (16)
N3	0.0263 (15)	0.0256 (16)	0.0240 (14)	0.0108 (13)	0.0058 (11)	0.0041 (13)
B1	0.0216 (17)	0.0222 (19)	0.0201 (16)	0.0102 (15)	0.0026 (13)	0.0004 (15)
F1	0.093 (3)	0.075 (3)	0.080 (3)	0.018 (2)	0.018 (2)	-0.044 (2)
F2	0.093 (3)	0.075 (3)	0.080 (3)	0.018 (2)	0.018 (2)	-0.044 (2)
F3	0.093 (3)	0.075 (3)	0.080 (3)	0.018 (2)	0.018 (2)	-0.044 (2)
F1B	0.093 (3)	0.075 (3)	0.080 (3)	0.018 (2)	0.018 (2)	-0.044 (2)
F2B	0.093 (3)	0.075 (3)	0.080 (3)	0.018 (2)	0.018 (2)	-0.044 (2)
F3B	0.093 (3)	0.075 (3)	0.080 (3)	0.018 (2)	0.018 (2)	-0.044 (2)

F4	0.042 (2)	0.061 (2)	0.0528 (15)	0.0139 (16)	0.0219 (16)	0.0060 (13)
F5	0.042 (2)	0.061 (2)	0.0528 (15)	0.0139 (16)	0.0219 (16)	0.0060 (13)
F6	0.042 (2)	0.061 (2)	0.0528 (15)	0.0139 (16)	0.0219 (16)	0.0060 (13)
F4B	0.042 (2)	0.061 (2)	0.0528 (15)	0.0139 (16)	0.0219 (16)	0.0060 (13)
F5B	0.042 (2)	0.061 (2)	0.0528 (15)	0.0139 (16)	0.0219 (16)	0.0060 (13)
F6B	0.042 (2)	0.061 (2)	0.0528 (15)	0.0139 (16)	0.0219 (16)	0.0060 (13)
F7	0.0592 (17)	0.0353 (14)	0.0429 (14)	0.0191 (13)	-0.0179 (12)	0.0041 (12)
F8	0.070 (2)	0.068 (2)	0.0278 (12)	0.0362 (17)	-0.0050 (12)	-0.0116 (13)
F9	0.0343 (14)	0.0520 (18)	0.0521 (16)	-0.0070 (13)	-0.0097 (12)	0.0081 (14)
F10	0.0319 (13)	0.0408 (16)	0.076 (2)	0.0172 (12)	0.0127 (13)	0.0080 (15)
F11	0.0522 (16)	0.0347 (14)	0.0585 (17)	0.0287 (13)	0.0065 (13)	-0.0053 (13)
F12	0.0669 (19)	0.074 (2)	0.0537 (17)	0.0542 (18)	0.0236 (14)	0.0332 (16)
F13	0.0801 (16)	0.134 (2)	0.0748 (15)	0.0452 (17)	-0.0161 (12)	0.0398 (16)
F14	0.0801 (16)	0.134 (2)	0.0748 (15)	0.0452 (17)	-0.0161 (12)	0.0398 (16)
F15	0.0801 (16)	0.134 (2)	0.0748 (15)	0.0452 (17)	-0.0161 (12)	0.0398 (16)
F16	0.0449 (12)	0.091 (3)	0.086 (3)	0.0147 (16)	0.0304 (15)	0.025 (2)
F17	0.0449 (12)	0.091 (3)	0.086 (3)	0.0147 (16)	0.0304 (15)	0.025 (2)
F18	0.0449 (12)	0.091 (3)	0.086 (3)	0.0147 (16)	0.0304 (15)	0.025 (2)
F16B	0.0449 (12)	0.091 (3)	0.086 (3)	0.0147 (16)	0.0304 (15)	0.025 (2)
F17B	0.0449 (12)	0.091 (3)	0.086 (3)	0.0147 (16)	0.0304 (15)	0.025 (2)
F18B	0.0449 (12)	0.091 (3)	0.086 (3)	0.0147 (16)	0.0304 (15)	0.025 (2)
F19	0.093 (4)	0.092 (3)	0.060 (2)	0.067 (3)	0.034 (2)	0.014 (2)
F20	0.093 (4)	0.092 (3)	0.060 (2)	0.067 (3)	0.034 (2)	0.014 (2)
F21	0.093 (4)	0.092 (3)	0.060 (2)	0.067 (3)	0.034 (2)	0.014 (2)
F19B	0.093 (4)	0.092 (3)	0.060 (2)	0.067 (3)	0.034 (2)	0.014 (2)
F20B	0.093 (4)	0.092 (3)	0.060 (2)	0.067 (3)	0.034 (2)	0.014 (2)
F21B	0.093 (4)	0.092 (3)	0.060 (2)	0.067 (3)	0.034 (2)	0.014 (2)
F22	0.1046 (17)	0.0831 (16)	0.0532 (11)	0.0410 (14)	0.0155 (11)	0.0369 (11)
F23	0.1046 (17)	0.0831 (16)	0.0532 (11)	0.0410 (14)	0.0155 (11)	0.0369 (11)
F24	0.1046 (17)	0.0831 (16)	0.0532 (11)	0.0410 (14)	0.0155 (11)	0.0369 (11)
Ir1	0.02338 (7)	0.01848 (7)	0.02077 (7)	0.00715 (5)	0.00375 (4)	0.00308 (5)

7.5.10 **Table A15.** Interatomic distances (Å) and angles (deg) for [**6**][$BArF_{24}$].

C1—N1	1.352 (5)	C36—F3B	1.381 (14)

C1—C2	1.380 (6)	C36—F1	1.426 (12)
C1—H1	0.9500	C37—F4	1.284 (9)
C2—C3	1.397 (6)	C37—F5B	1.291 (18)
C2—H2	0.9500	C37—F6B	1.303 (10)
C3—C4	1.381 (5)	C37—F5	1.366 (14)
C3—C12	1.539 (5)	C37—F6	1.412 (9)
C4—C5	1.401 (5)	C37—F4B	1.438 (11)
C4—H4	0.9500	C38—C39	1.397 (5)
C5—N1	1.355 (5)	C38—C43	1.408 (5)
C5—C6	1.449 (5)	C38—B1	1.653 (5)
C6—C7	1.398 (5)	C39—C40	1.383 (5)
C6—C11	1.417 (5)	C39—H39	0.9500
C7—C8	1.376 (5)	C40—C41	1.386 (5)
C7—H7	0.9500	C40—C44	1.498 (5)
C8—C9	1.406 (5)	C41—C42	1.386 (5)
C8—H8	0.9500	C41—H41	0.9500
C9—N2	1.384 (5)	C42—C43	1.385 (5)
C9—C10	1.412 (5)	C42—C45	1.503 (5)
C10—C11	1.396 (5)	C43—H43	0.9500
C10—H10	0.9500	C44—F8	1.324 (5)
C11—Ir1	2.053 (3)	C44—F7	1.340 (5)
C12—C15	1.521 (7)	C44—F9	1.344 (5)
C12—C13	1.525 (7)	C45—F12	1.336 (5)
C12—C14	1.527 (7)	C45—F11	1.339 (5)
C13—H13A	0.9800	C45—F10	1.339 (5)
C13—H13B	0.9800	C46—C47	1.397 (5)
C13—H13C	0.9800	C46—C51	1.401 (5)
C14—H14A	0.9800	C46—B1	1.647 (6)
C14—H14B	0.9800	C47—C48	1.393 (6)
C14—H14C	0.9800	C47—H47	0.9500
C15—H15A	0.9800	C48—C49	1.373 (6)
C15—H15B	0.9800	C48—C52	1.476 (6)
C15—H15C	0.9800	C49—C50	1.386 (6)
C16—N2	1.444 (5)	C49—H49	0.9500
C16—H16A	0.9800	C50—C51	1.389 (5)
C16—H16B	0.9800	C50—C53	1.486 (6)
C16—H16C	0.9800	C51—H51	0.9500

C17—N2	1.441 (5)	C52—F15	1.300 (6)
C17—H17A	0.9800	C52—F14	1.335 (7)
C17—H17B	0.9800	C52—F13	1.344 (7)
C17—H17C	0.9800	C53—F17	1.301 (8)
C18—C19	1.392 (6)	C53—F17B	1.309 (14)
C18—C22	1.434 (7)	C53—F18	1.322 (9)
C18—C23	1.504 (6)	C53—F16B	1.326 (15)
C18—Ir1	2.245 (4)	C53—F16	1.384 (9)
C19—C20	1.432 (6)	C53—F18B	1.438 (15)
C19—C24	1.516 (7)	C54—C59	1.403 (5)
C19—Ir1	2.237 (4)	C54—C55	1.407 (5)
C20—C21	1.435 (7)	C54—B1	1.638 (5)
C20—C25	1.495 (7)	C55—C56	1.399 (6)
C20—Ir1	2.166 (4)	C55—H55	0.9500
C21—C22	1.440 (7)	C56—C57	1.374 (6)
C21—C26	1.484 (7)	C56—C60	1.501 (6)
C21—Ir1	2.168 (4)	C57—C58	1.379 (6)
C22—C27	1.495 (7)	C57—H57	0.9500
C22—Ir1	2.156 (4)	C58—C59	1.394 (5)
C23—H23A	0.9800	C58—C61	1.491 (5)
C23—H23B	0.9800	C59—H59	0.9500
C23—H23C	0.9800	C60—F21B	1.255 (12)
C24—H24A	0.9800	C60—F19	1.297 (15)
C24—H24B	0.9800	C60—F20	1.301 (9)
C24—H24C	0.9800	C60—F19B	1.326 (17)
C25—H25A	0.9800	C60—F20B	1.445 (12)
C25—H25B	0.9800	C60—F21	1.447 (11)
C25—H25C	0.9800	C61—F24	1.311 (6)
C26—H26A	0.9800	C61—F23	1.326 (6)
C26—H26B	0.9800	C61—F22	1.332 (6)
C26—H26C	0.9800	C62—C63	1.502 (10)
C27—H27A	0.9800	C62—H62A	0.9800
C27—H27B	0.9800	C62—H62B	0.9800
C27—H27C	0.9800	C62—H62C	0.9800
C28—N3	1.135 (5)	C63—C64	1.495 (9)
C28—C29	1.461 (6)	C63—H63A	0.9900
C29—H29A	0.9800	C63—H63B	0.9900

C29—H29B	0.9800	C64—C65	1.550 (11)
C29—H29C	0.9800	C64—H64A	0.9900
C30—C31	1.401 (5)	C64—H64B	0.9900
C30—C35	1.402 (5)	C65—C66	1.512 (12)
C30—B1	1.640 (5)	C65—H65A	0.9900
C31—C32	1.394 (6)	C65—H65B	0.9900
C31—H31	0.9500	C66—C67	1.477 (11)
C32—C33	1.382 (6)	C66—H66A	0.9900
C32—C36	1.482 (6)	C66—H66B	0.9900
C33—C34	1.391 (5)	C67—C68	1.559 (13)
C33—H33	0.9500	C67—H67A	0.9900
C34—C35	1.384 (5)	C67—H67B	0.9900
C34—C37	1.488 (5)	C68—H68A	0.9800
C35—H35	0.9500	C68—H68B	0.9800
C36—F2B	1.267 (16)	C68—H68C	0.9800
C36—F3	1.297 (10)	N1—Ir1	2.106 (3)
C36—F2	1.335 (10)	N3—Ir1	2.035 (3)
C36—F1B	1.346 (15)		
N1—C1—C2	122.6 (4)	C40—C39—H39	118.6
N1—C1—H1	118.7	C38—C39—H39	118.6
C2—C1—H1	118.7	C39—C40—C41	120.9 (3)
C1—C2—C3	119.9 (4)	C39—C40—C44	119.4 (3)
C1—C2—H2	120.1	C41—C40—C44	119.7 (3)
C3—C2—H2	120.1	C42—C41—C40	117.7 (3)
C4—C3—C2	117.1 (4)	C42—C41—H41	121.1
C4—C3—C12	121.7 (4)	C40—C41—H41	121.1
C2—C3—C12	121.2 (4)	C43—C42—C41	121.1 (3)
C3—C4—C5	121.3 (4)	C43—C42—C45	118.6 (3)
C3—C4—H4	119.4	C41—C42—C45	120.2 (3)
C5—C4—H4	119.4	C42—C43—C38	122.3 (3)
N1—C5—C4	120.5 (3)	C42—C43—H43	118.9
N1—C5—C6	113.8 (3)	C38—C43—H43	118.9
C4—C5—C6	125.6 (3)	F8—C44—F7	107.4 (3)
C7—C6—C11	119.8 (3)	F8—C44—F9	105.9 (3)
C7—C6—C5	124.4 (3)	F7—C44—F9	104.8 (3)
C11—C6—C5	115.7 (3)	F8—C44—C40	113.6 (3)

C8—C7—C6	121.0 (3)	F7—C44—C40	111.9 (3)
C8—C7—H7	119.5	F9—C44—C40	112.5 (3)
C6—C7—H7	119.5	F12—C45—F11	106.7 (4)
C7—C8—C9	120.6 (3)	F12—C45—F10	106.1 (4)
C7—C8—H8	119.7	F11—C45—F10	106.0 (3)
C9—C8—H8	119.7	F12—C45—C42	112.4 (3)
N2—C9—C8	121.0 (3)	F11—C45—C42	113.3 (3)
N2—C9—C10	120.7 (3)	F10—C45—C42	111.9 (3)
C8—C9—C10	118.3 (3)	C47—C46—C51	116.1 (3)
C11—C10—C9	121.7 (3)	C47—C46—B1	122.9 (3)
C11—C10—H10	119.2	C51—C46—B1	120.9 (3)
C9—C10—H10	119.2	C48—C47—C46	121.8 (4)
C10—C11—C6	118.5 (3)	C48—C47—H47	119.1
C10—C11—Ir1	126.4 (3)	C46—C47—H47	119.1
C6—C11—Ir1	115.1 (2)	C49—C48—C47	121.3 (4)
C15—C12—C13	109.1 (5)	C49—C48—C52	119.2 (4)
C15—C12—C14	107.6 (5)	C47—C48—C52	119.5 (4)
C13—C12—C14	110.2 (5)	C48—C49—C50	118.0 (4)
C15—C12—C3	112.4 (4)	C48—C49—H49	121.0
C13—C12—C3	107.3 (4)	C50—C49—H49	121.0
C14—C12—C3	110.2 (4)	C49—C50—C51	121.0 (4)
C12—C13—H13A	109.5	C49—C50—C53	118.3 (4)
C12—C13—H13B	109.5	C51—C50—C53	120.6 (4)
H13A—C13—H13B	109.5	C50—C51—C46	121.8 (4)
C12—C13—H13C	109.5	C50—C51—H51	119.1
H13A—C13—H13C	109.5	C46—C51—H51	119.1
H13B—C13—H13C	109.5	F15—C52—F14	107.2 (5)
C12—C14—H14A	109.5	F15—C52—F13	105.0 (5)
C12—C14—H14B	109.5	F14—C52—F13	101.2 (5)
H14A—C14—H14B	109.5	F15—C52—C48	115.5 (4)
C12—C14—H14C	109.5	F14—C52—C48	113.0 (4)
H14A—C14—H14C	109.5	F13—C52—C48	113.6 (4)
H14B—C14—H14C	109.5	F17—C53—F18	108.4 (6)
C12—C15—H15A	109.5	F17B—C53—F16B	106.7 (8)
C12—C15—H15B	109.5	F17—C53—F16	102.6 (5)
H15A—C15—H15B	109.5	F18—C53—F16	105.6 (6)
C12—C15—H15C	109.5	F17B—C53—F18B	103.2 (8)

H15A—C15—H15C	109.5	F16B—C53—F18B	101.6 (9)
H15B—C15—H15C	109.5	F17—C53—C50	114.7 (5)
N2—C16—H16A	109.5	F17B—C53—C50	113.1 (7)
N2—C16—H16B	109.5	F18—C53—C50	114.8 (4)
H16A—C16—H16B	109.5	F16B—C53—C50	119.5 (7)
N2—C16—H16C	109.5	F16—C53—C50	109.7 (5)
H16A—C16—H16C	109.5	F18B—C53—C50	110.9 (6)
H16B—C16—H16C	109.5	C59—C54—C55	115.4 (3)
N2—C17—H17A	109.5	C59—C54—B1	121.4 (3)
N2—C17—H17B	109.5	C55—C54—B1	123.1 (3)
H17A—C17—H17B	109.5	C56—C55—C54	121.6 (4)
N2—C17—H17C	109.5	C56—C55—H55	119.2
H17A—C17—H17C	109.5	C54—C55—H55	119.2
H17B—C17—H17C	109.5	C57—C56—C55	121.7 (4)
C19—C18—C22	107.8 (4)	C57—C56—C60	119.4 (4)
C19—C18—C23	126.7 (5)	C55—C56—C60	118.9 (4)
C22—C18—C23	125.3 (5)	C56—C57—C58	117.9 (4)
C19—C18—Ir1	71.6 (2)	C56—C57—H57	121.1
C22—C18—Ir1	67.7 (2)	C58—C57—H57	121.1
C23—C18—Ir1	130.3 (3)	C57—C58—C59	121.1 (4)
C18—C19—C20	109.8 (4)	C57—C58—C61	119.7 (4)
C18—C19—C24	125.3 (5)	C59—C58—C61	119.1 (3)
C20—C19—C24	124.9 (5)	C58—C59—C54	122.4 (3)
C18—C19—Ir1	72.2 (2)	C58—C59—H59	118.8
C20—C19—Ir1	68.4 (2)	C54—C59—H59	118.8
C24—C19—Ir1	126.3 (3)	F19—C60—F20	114.5 (7)
C19—C20—C21	107.1 (4)	F21B—C60—F19B	104.0 (8)
C19—C20—C25	126.3 (5)	F21B—C60—F20B	104.9 (6)
C21—C20—C25	125.9 (5)	F19B—C60—F20B	102.1 (8)
C19—C20—Ir1	73.7 (2)	F19—C60—F21	107.3 (7)
C21—C20—Ir1	70.7 (2)	F20—C60—F21	99.9 (6)
C25—C20—Ir1	128.5 (3)	F21B—C60—C56	118.1 (7)
C20—C21—C22	107.1 (4)	F19—C60—C56	113.1 (6)
C20—C21—C26	125.9 (6)	F20—C60—C56	114.3 (5)
C22—C21—C26	127.0 (6)	F19B—C60—C56	116.3 (7)
C20—C21—Ir1	70.6 (2)	F20B—C60—C56	109.6 (5)
C22—C21—Ir1	70.1 (3)	F21—C60—C56	106.2 (5)

C26—C21—Ir1	126.9 (3)	F24—C61—F23	105.9 (4)
C18—C22—C21	108.1 (4)	F24—C61—F22	106.4 (4)
C18—C22—C27	126.0 (6)	F23—C61—F22	104.1 (4)
C21—C22—C27	125.7 (6)	F24—C61—C58	112.7 (4)
C18—C22—Ir1	74.4 (2)	F23—C61—C58	114.0 (4)
C21—C22—Ir1	71.0 (2)	F22—C61—C58	113.0 (4)
C27—C22—Ir1	124.3 (3)	C63—C62—H62A	109.5
C18—C23—H23A	109.5	C63—C62—H62B	109.5
C18—C23—H23B	109.5	H62A—C62—H62B	109.5
H23A—C23—H23B	109.5	C63—C62—H62C	109.5
C18—C23—H23C	109.5	H62A—C62—H62C	109.5
H23A—C23—H23C	109.5	H62B—C62—H62C	109.5
H23B—C23—H23C	109.5	C64—C63—C62	112.6 (6)
C19—C24—H24A	109.5	C64—C63—H63A	109.1
C19—C24—H24B	109.5	C62—C63—H63A	109.1
H24A—C24—H24B	109.5	C64—C63—H63B	109.1
C19—C24—H24C	109.5	C62—C63—H63B	109.1
H24A—C24—H24C	109.5	H63A—C63—H63B	107.8
H24B—C24—H24C	109.5	C63—C64—C65	116.2 (6)
C20—C25—H25A	109.5	C63—C64—H64A	108.2
C20—C25—H25B	109.5	C65—C64—H64A	108.2
H25A—C25—H25B	109.5	C63—C64—H64B	108.2
C20—C25—H25C	109.5	C65—C64—H64B	108.2
H25A—C25—H25C	109.5	H64A—C64—H64B	107.4
H25B—C25—H25C	109.5	C66—C65—C64	114.7 (6)
C21—C26—H26A	109.5	C66—C65—H65A	108.6
C21—C26—H26B	109.5	C64—C65—H65A	108.6
H26A—C26—H26B	109.5	C66—C65—H65B	108.6
C21—C26—H26C	109.5	C64—C65—H65B	108.6
H26A—C26—H26C	109.5	H65A—C65—H65B	107.6
H26B—C26—H26C	109.5	C67—C66—C65	113.6 (7)
C22—C27—H27A	109.5	C67—C66—H66A	108.9
C22—C27—H27B	109.5	C65—C66—H66A	108.9
H27A—C27—H27B	109.5	C67—C66—H66B	108.9
C22—C27—H27C	109.5	C65—C66—H66B	108.9
H27A—C27—H27C	109.5	H66A—C66—H66B	107.7
H27B—C27—H27C	109.5	C66—C67—C68	113.3 (8)

N3—C28—C29	177.9 (4)	C66—C67—H67A	108.9
C28—C29—H29A	109.5	C68—C67—H67A	108.9
C28—C29—H29B	109.5	C66—C67—H67B	108.9
H29A—C29—H29B	109.5	C68—C67—H67B	108.9
C28—C29—H29C	109.5	H67A—C67—H67B	107.7
H29A—C29—H29C	109.5	C67—C68—H68A	109.5
H29B—C29—H29C	109.5	C67—C68—H68B	109.5
C31—C30—C35	116.1 (3)	H68A—C68—H68B	109.5
C31—C30—B1	119.4 (3)	C67—C68—H68C	109.5
C35—C30—B1	124.3 (3)	H68A—C68—H68C	109.5
C32—C31—C30	121.9 (3)	H68B—C68—H68C	109.5
C32—C31—H31	119.1	C1—N1—C5	118.6 (3)
C30—C31—H31	119.1	C1—N1—Ir1	124.5 (3)
C33—C32—C31	121.0 (4)	C5—N1—Ir1	116.8 (2)
C33—C32—C36	119.7 (4)	C9—N2—C17	121.0 (3)
C31—C32—C36	119.3 (4)	C9—N2—C16	120.6 (3)
C32—C33—C34	117.9 (4)	C17—N2—C16	116.1 (4)
C32—C33—H33	121.0	C28—N3—Ir1	178.4 (3)
C34—C33—H33	121.0	C54—B1—C30	103.5 (3)
C35—C34—C33	121.2 (3)	C54—B1—C46	112.4 (3)
C35—C34—C37	119.9 (4)	C30—B1—C46	111.6 (3)
C33—C34—C37	118.9 (4)	C54—B1—C38	112.6 (3)
C34—C35—C30	122.0 (3)	C30—B1—C38	111.6 (3)
C34—C35—H35	119.0	C46—B1—C38	105.4 (3)
C30—C35—H35	119.0	N3—Ir1—C11	86.82 (13)
F3—C36—F2	109.5 (7)	N3—Ir1—N1	87.89 (12)
F2B—C36—F1B	103.0 (9)	C11—Ir1—N1	77.79 (13)
F2B—C36—F3B	100.3 (9)	N3—Ir1—C22	158.81 (16)
F1B—C36—F3B	112.0 (9)	C11—Ir1—C22	114.06 (17)
F3—C36—F1	109.8 (7)	N1—Ir1—C22	99.62 (15)
F2—C36—F1	96.3 (6)	N3—Ir1—C20	105.24 (16)
F2B—C36—C32	120.2 (7)	C11—Ir1—C20	112.07 (16)
F3—C36—C32	116.2 (5)	N1—Ir1—C20	163.63 (14)
F2—C36—C32	115.0 (5)	C22—Ir1—C20	64.71 (17)
F1B—C36—C32	108.6 (6)	N3—Ir1—C21	141.09 (18)
F3B—C36—C32	112.3 (6)	C11—Ir1—C21	94.96 (15)
F1—C36—C32	108.1 (6)	N1—Ir1—C21	130.54 (17)

F5B—C37—F6B	108.7 (6)	C22—Ir1—C21	38.9 (2)
F4—C37—F5	112.0 (8)	C20—Ir1—C21	38.68 (19)
F4—C37—F6	106.6 (5)	N3—Ir1—C19	97.71 (14)
F5—C37—F6	100.8 (7)	C11—Ir1—C19	149.82 (16)
F5B—C37—F4B	98.4 (10)	N1—Ir1—C19	131.98 (14)
F6B—C37—F4B	104.7 (6)	C22—Ir1—C19	62.57 (16)
F4—C37—C34	117.3 (5)	C20—Ir1—C19	37.93 (17)
F5B—C37—C34	119.0 (7)	C21—Ir1—C19	63.13 (16)
F6B—C37—C34	114.9 (5)	N3—Ir1—C18	121.21 (16)
F5—C37—C34	110.1 (5)	C11—Ir1—C18	151.96 (17)
F6—C37—C34	108.6 (4)	N1—Ir1—C18	101.84 (14)
F4B—C37—C34	109.0 (5)	C22—Ir1—C18	37.95 (18)
C39—C38—C43	115.1 (3)	C20—Ir1—C18	63.14 (16)
C39—C38—B1	124.8 (3)	C21—Ir1—C18	63.60 (17)
C43—C38—B1	120.0 (3)	C19—Ir1—C18	36.19 (16)
C40—C39—C38	122.9 (3)		
N1—C1—C2—C3	0.3 (7)	C41—C42—C43—C38	1.3 (6)
C1—C2—C3—C4	0.9 (6)	C45—C42—C43—C38	179.6 (3)
C1—C2—C3—C12	-177.8 (4)	C39—C38—C43—C42	-0.6 (5)
C2—C3—C4—C5	-1.1 (6)	B1—C38—C43—C42	177.9 (3)
C12—C3—C4—C5	177.6 (4)	C39—C40—C44—F8	157.1 (4)
C3—C4—C5—N1	0.2 (6)	C41—C40—C44—F8	-22.9 (5)
C3—C4—C5—C6	177.5 (4)	C39—C40—C44—F7	35.2 (5)
N1—C5—C6—C7	176.9 (3)	C41—C40—C44—F7	-144.7 (4)
C4—C5—C6—C7	-0.6 (6)	C39—C40—C44—F9	-82.5 (5)
N1—C5—C6—C11	0.2 (5)	C41—C40—C44—F9	97.5 (4)
C4—C5—C6—C11	-177.2 (3)	C43—C42—C45—F12	55.7 (5)
C11—C6—C7—C8	2.5 (6)	C41—C42—C45—F12	-126.0 (4)
C5—C6—C7—C8	-174.0 (4)	C43—C42—C45—F11	176.8 (4)
C6—C7—C8—C9	1.6 (6)	C41—C42—C45—F11	-5.0 (5)
C7—C8—C9—N2	173.9 (4)	C43—C42—C45—F10	-63.5 (5)

C7—C8—C9—C10	-4.2 (6)	C41—C42—C45—F10	114.7 (4)
N2—C9—C10—C11	-175.3 (4)	C51—C46—C47—C48	-0.7 (6)
C8—C9—C10—C11	2.9 (5)	B1—C46—C47—C48	-177.1 (4)
C9—C10—C11—C6	1.1 (5)	C46—C47—C48—C49	-0.5 (6)
C9—C10—C11—Ir1	-179.5 (3)	C46—C47—C48—C52	178.5 (4)
C7—C6—C11—C10	-3.8 (5)	C47—C48—C49—C50	0.6 (6)
C5—C6—C11—C10	173.0 (3)	C52—C48—C49—C50	-178.4 (4)
C7—C6—C11—Ir1	176.8 (3)	C48—C49—C50—C51	0.6 (7)
C5—C6—C11—Ir1	-6.4 (4)	C48—C49—C50—C53	-179.1 (5)
C4—C3—C12—C15	10.8 (6)	C49—C50—C51—C46	-1.8 (6)
C2—C3—C12—C15	-170.6 (4)	C53—C50—C51—C46	177.8 (4)
C4—C3—C12—C13	-109.2 (5)	C47—C46—C51—C50	1.9 (6)
C2—C3—C12—C13	69.5 (6)	B1—C46—C51—C50	178.3 (4)
C4—C3—C12—C14	130.8 (5)	C49—C48—C52—F15	-17.8 (7)
C2—C3—C12—C14	-50.5 (6)	C47—C48—C52—F15	163.2 (5)
C22—C18—C19—C20	0.0 (5)	C49—C48—C52—F14	106.2 (5)
C23—C18—C19—C20	-174.8 (4)	C47—C48—C52—F14	-72.8 (6)
Ir1—C18—C19—C20	58.2 (3)	C49—C48—C52—F13	-139.2 (5)
C22—C18—C19—C24	179.5 (4)	C47—C48—C52—F13	41.8 (6)
C23—C18—C19—C24	4.7 (7)	C49—C50—C53—F17	54.5 (7)
Ir1—C18—C19—C24	-122.3 (5)	C51—C50—C53—F17	-125.2 (6)
C22—C18—C19—Ir1	-58.2 (3)	C49—C50—C53—F17B	96.3 (8)
C23—C18—C19—Ir1	127.0 (5)	C51—C50—C53—F17B	-83.3 (8)

C18—C19—C20—C21	2.7 (5)	C49—C50—C53—F18	-179.0 (5)
C24—C19—C20—C21	-176.7 (4)	C51—C50—C53—F18	1.3 (8)
Ir1—C19—C20—C21	63.3 (3)	C49—C50—C53—F16B	-30.7 (10)
C18—C19—C20—C25	173.3 (4)	C51—C50—C53—F16B	149.7 (8)
C24—C19—C20—C25	-6.2 (7)	C49—C50—C53—F16	-60.3 (6)
Ir1—C19—C20—C25	-126.1 (5)	C51—C50—C53—F16	120.0 (5)
C18—C19—C20—Ir1	-60.6 (3)	C49—C50—C53—F18B	-148.3 (7)
C24—C19—C20—Ir1	120.0 (4)	C51—C50—C53—F18B	32.0 (9)
C19—C20—C21—C22	-4.4 (5)	C59—C54—C55—C56	1.6 (6)
C25—C20—C21—C22	-175.0 (4)	B1—C54—C55—C56	177.7 (4)
Ir1—C20—C21—C22	60.9 (3)	C54—C55—C56—C57	0.3 (7)
C19—C20—C21—C26	172.7 (4)	C54—C55—C56—C60	-179.3 (5)
C25—C20—C21—C26	2.1 (7)	C55—C56—C57—C58	-0.8 (7)
Ir1—C20—C21—C26	-122.0 (5)	C60—C56—C57—C58	178.8 (5)
C19—C20—C21—Ir1	-65.3 (3)	C56—C57—C58—C59	-0.7 (6)
C25—C20—C21—Ir1	124.1 (5)	C56—C57—C58—C61	176.4 (4)
C19—C18—C22—C21	-2.8 (5)	C57—C58—C59—C54	2.7 (6)
C23—C18—C22—C21	172.1 (4)	C61—C58—C59—C54	-174.4 (4)
Ir1—C18—C22—C21	-63.4 (3)	C55—C54—C59—C58	-3.1 (5)
C19—C18—C22—C27	-178.0 (4)	B1—C54—C59—C58	-179.2 (3)
C23—C18—C22—C27	-3.1 (7)	C57—C56—C60—F21B	-75.7 (8)
Ir1—C18—C22—C27	121.4 (5)	C55—C56—C60—F21B	103.9 (7)

C19—C18—C22—Ir1	60.7 (3)	C57—C56—C60—F19	139.9 (7)
C23—C18—C22—Ir1	-124.5 (5)	C55—C56—C60—F19	-40.5 (9)
C20—C21—C22—C18	4.4 (5)	C57—C56—C60—F20	6.5 (9)
C26—C21—C22—C18	-172.6 (4)	C55—C56—C60—F20	-173.9 (6)
Ir1—C21—C22—C18	65.6 (3)	C57—C56—C60—F19B	159.5 (8)
C20—C21—C22—C27	179.6 (4)	C55—C56—C60—F19B	-20.9 (10)
C26—C21—C22—C27	2.6 (8)	C57—C56—C60—F20B	44.3 (8)
Ir1—C21—C22—C27	-119.2 (5)	C55—C56—C60—F20B	-136.1 (6)
C20—C21—C22—Ir1	-61.2 (3)	C57—C56—C60—F21	-102.6 (6)
C26—C21—C22—Ir1	121.7 (5)	C55—C56—C60—F21	77.0 (6)
C35—C30—C31—C32	1.1 (6)	C57—C58—C61—F24	-100.7 (5)
B1—C30—C31—C32	-174.0 (4)	C59—C58—C61—F24	76.5 (5)
C30—C31—C32—C33	-1.9 (7)	C57—C58—C61—F23	138.6 (4)
C30—C31—C32—C36	177.8 (5)	C59—C58—C61—F23	-44.3 (6)
C31—C32—C33—C34	1.6 (6)	C57—C58—C61—F22	20.0 (6)
C36—C32—C33—C34	-178.0 (5)	C59—C58—C61—F22	-162.8 (4)
C32—C33—C34—C35	-0.8 (6)	C62—C63—C64—C65	175.3 (7)
C32—C33—C34—C37	-178.9 (4)	C63—C64—C65—C66	59.5 (9)
C33—C34—C35—C30	0.0 (6)	C64—C65—C66—C67	-178.6 (6)
C37—C34—C35—C30	178.2 (4)	C65—C66—C67—C68	177.7 (6)
C31—C30—C35—C34	-0.2 (5)	C2—C1—N1—C5	-1.2 (6)
B1—C30—C35—C34	174.6 (3)	C2—C1—N1—Ir1	175.9 (3)
C33—C32—C36—	-145.2 (9)	C4—C5—N1—C1	1.0 (5)

F2B			
C31—C32—C36—F2B	35.2 (11)	C6—C5—N1—C1	-176.6 (3)
C33—C32—C36—F3	10.2 (9)	C4—C5—N1—Ir1	-176.4 (3)
C31—C32—C36—F3	-169.4 (6)	C6—C5—N1—Ir1	6.0 (4)
C33—C32—C36—F2	140.1 (7)	C8—C9—N2—C17	165.9 (4)
C31—C32—C36—F2	-39.6 (9)	C10—C9—N2—C17	-16.0 (6)
C33—C32—C36—F1B	96.8 (8)	C8—C9—N2—C16	4.1 (6)
C31—C32—C36—F1B	-82.8 (8)	C10—C9—N2—C16	-177.8 (4)
C33—C32—C36—F3B	-27.6 (10)	C59—C54—B1—C30	75.5 (4)
C31—C32—C36—F3B	152.8 (8)	C55—C54—B1—C30	-100.3 (4)
C33—C32—C36—F1	-113.7 (6)	C59—C54—B1—C46	-163.9 (3)
C31—C32—C36—F1	66.7 (7)	C55—C54—B1—C46	20.2 (5)
C35—C34—C37—F4	161.2 (5)	C59—C54—B1—C38	-45.2 (5)
C33—C34—C37—F4	-20.7 (7)	C55—C54—B1—C38	139.0 (4)
C35—C34—C37—F5B	22.2 (11)	C31—C30—B1—C54	67.3 (4)
C33—C34—C37—F5B	-159.7 (9)	C35—C30—B1—C54	-107.4 (4)
C35—C34—C37—F6B	-109.2 (6)	C31—C30—B1—C46	-53.8 (4)
C33—C34—C37—F6B	69.0 (7)	C35—C30—B1—C46	131.6 (4)
C35—C34—C37—F5	31.5 (9)	C31—C30—B1—C38	-171.4 (3)
C33—C34—C37—F5	-150.3 (8)	C35—C30—B1—C38	14.0 (5)
C35—C34—C37—F6	-77.9 (5)	C47—C46—B1—C54	-140.5 (4)
C33—C34—C37—F6	100.2 (5)	C51—C46—B1—C54	43.3 (5)
C35—C34—C37—F4B	133.7 (5)	C47—C46—B1—C30	-24.8 (5)
C33—C34—C37—F4B	-48.1 (6)	C51—C46—B1—C30	159.1 (3)
C43—C38—C39—C40	-0.8 (5)	C47—C46—B1—C38	96.6 (4)
B1—C38—C39—C40	-179.1 (3)	C51—C46—B1—C38	-79.6 (4)
C38—C39—C40—C41	1.4 (6)	C39—C38—B1—C54	-9.7 (5)
C38—C39—C40—C44	-178.6 (3)	C43—C38—B1—C54	172.1 (3)

C39—C40—C41—C42	-0.6 (6)	C39—C38—B1—C30	-125.5 (4)
C44—C40—C41—C42	179.4 (4)	C43—C38—B1—C30	56.2 (4)
C40—C41—C42—C43	-0.7 (6)	C39—C38—B1—C46	113.2 (4)
C40—C41—C42—C45	-179.0 (4)	C43—C38—B1—C46	-65.1 (4)

7.6 [**4**][$BArF_{24}$]

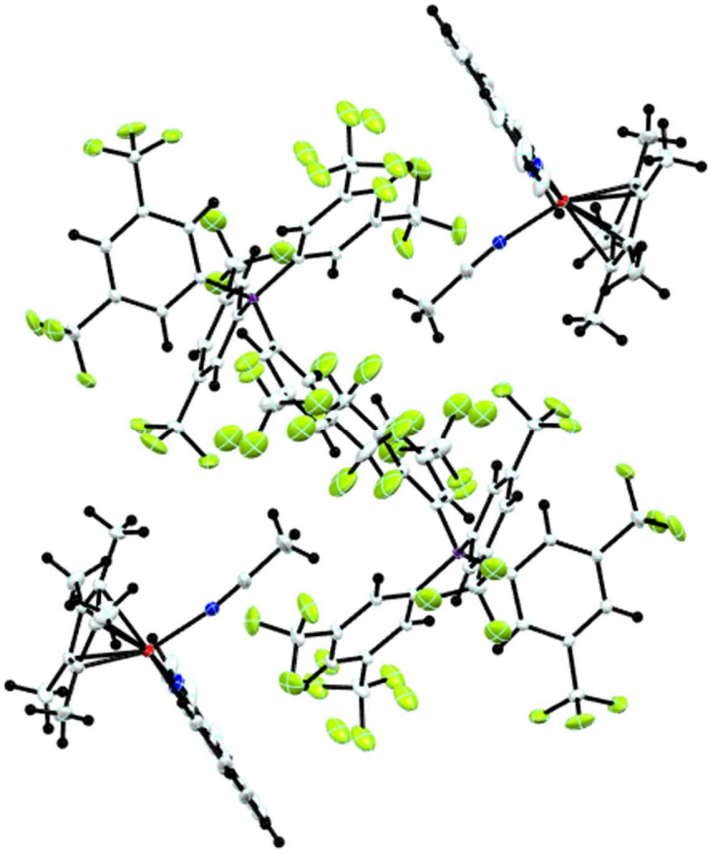

7.6.1 **Figure A16.** Crystal lattice packing of [**4**][$BArF_{24}$].

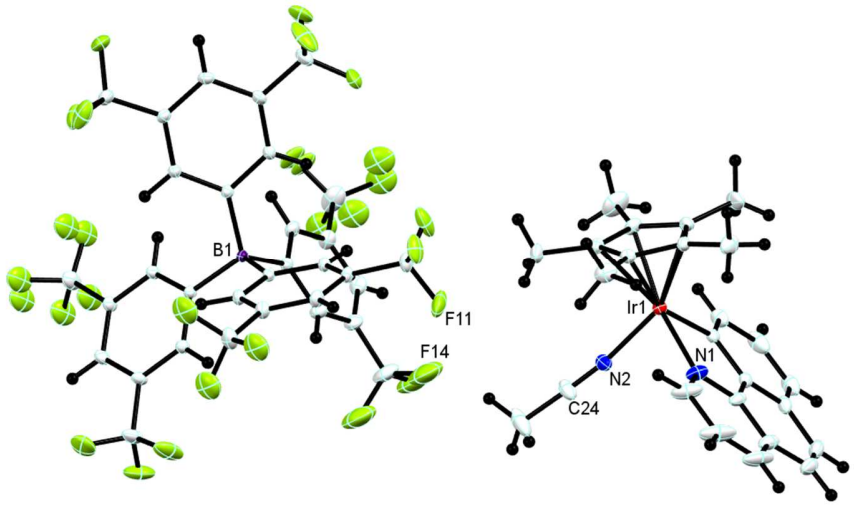

7.6.2 **Figure A17.** Asymmetric unit of [**4**][BArF$_{24}$], with all hydrogens and partial numbering of atoms.

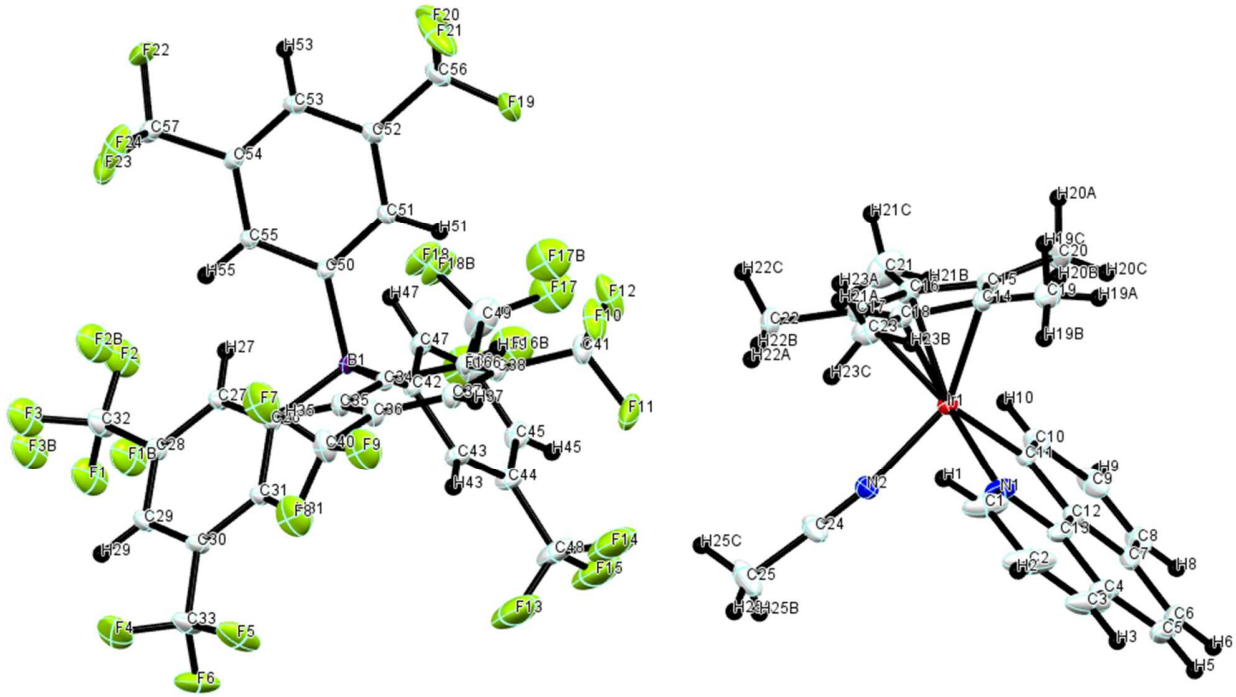

7.6.3 **Figure A18.** Asymmetric unit of [**4**][BArF$_{24}$], with all hydrogens and total numbering of atoms.

[**4**][$BArF_{24}$]

7.6.4 Crystal data

$C_{32}H_{12}BF_{24}\cdot C_{25}H_{26}IrN_2$	$Z = 2$
$M_r = 1409.90$	$F(000) = 1384$
Triclinic, $P\bar{1}$	$D_x = 1.685$ Mg m^{-3}
$a = 12.3318$ (6) Å	Mo $K\alpha$ radiation, $\lambda = 0.71073$ Å
$b = 12.9386$ (6) Å	Cell parameters from 9975 reflections
$c = 18.3704$ (9) Å	$\theta = 2.3–33.9°$
$\alpha = 86.356$ (1)°	$\mu = 2.52$ mm^{-1}
$\beta = 78.921$ (1)°	$T = 173$ K
$\gamma = 75.034$ (1)°	Prism, yellow
$V = 2778.6$ (2) Å^3	0.30 × 0.25 × 0.08 mm

7.6.5 Data collection

Bruker APEX-II CCD diffractometer	22760 independent reflections
Radiation source: sealed tube	19906 reflections with $I > 2\sigma(I)$
Triumph monochromator	$R_{int} = 0.026$
ϕ and ω scans	$\theta_{max} = 34.1°$, $\theta_{min} = 1.6°$
Absorption correction: multi-scan *SADABS*	$h = -19\rightarrow19$
$T_{min} = 0.596$, $T_{max} = 0.747$	$k = -20\rightarrow20$
108274 measured reflections	$l = -28\rightarrow28$

7.6.6 Refinement

Refinement on F^2	Primary atom site location: structure-invariant direct methods
Least-squares matrix: full	Secondary atom site location: difference Fourier map
$R[F^2 > 2\sigma(F^2)] = 0.043$	Hydrogen site location: inferred from neighbouring sites
$wR(F^2) = 0.121$	H-atom parameters constrained
$S = 1.05$	$w = 1/[\sigma^2(F_o^2) + (0.0692P)^2 + 5.3126P]$ where $P = (F_o^2 + 2F_c^2)/3$

22760 reflections	$(\Delta/\sigma)_{max}$ = 0.003
748 parameters	$\Delta\rangle_{max}$ = 3.22 e Å^{-3}
0 restraints	$\Delta\rangle_{min}$ = -3.46 e Å^{-3}

7.6.7 Special details

Geometry. All esds (except the esd in the dihedral angle between two l.s. planes) are estimated using the full covariance matrix. The cell esds are taken into account individually in the estimation of esds in distances, angles and torsion angles; correlations between esds in cell parameters are only used when they are defined by crystal symmetry. An approximate (isotropic) treatment of cell esds is used for estimating esds involving l.s. planes.

7.6.8 **Table A16.** Fractional atomic coordinates and isotropic or equivalent isotropic displacement parameters (Å^2) for **[4]**[BArF$_{24}$].

	x	*y*	*z*	U_{iso}*/U_{eq}	Occ. (<1)
C1	1.1127 (4)	0.2293 (4)	0.8483 (4)	0.0563 (14)	
H1	1.1542	0.1960	0.8032	0.068*	
C2	1.1645 (5)	0.2866 (4)	0.8875 (5)	0.075 (2)	
H2	1.2411	0.2896	0.8694	0.090*	
C3	1.1070 (5)	0.3377 (4)	0.9510 (4)	0.0703 (19)	
H3	1.1431	0.3761	0.9772	0.084*	
C4	0.9950 (5)	0.3337 (3)	0.9775 (3)	0.0520 (13)	
C5	0.9237 (7)	0.3859 (3)	1.0426 (3)	0.0654 (18)	
H5	0.9544	0.4257	1.0715	0.078*	
C6	0.8159 (7)	0.3804 (3)	1.0638 (2)	0.0671 (19)	
H6	0.7716	0.4177	1.1068	0.081*	
C7	0.7634 (5)	0.3191 (3)	1.02336 (19)	0.0476 (11)	
C8	0.6518 (5)	0.3100 (3)	1.0428 (2)	0.0569 (14)	
H8	0.6031	0.3457	1.0852	0.068*	
C9	0.6121 (4)	0.2491 (3)	1.0004 (3)	0.0516 (12)	
H9	0.5357	0.2430	1.0138	0.062*	
C10	0.6830 (3)	0.1956 (3)	0.9372 (2)	0.0331 (7)	
H10	0.6533	0.1544	0.9087	0.040*	
C11	0.7935 (3)	0.2018 (2)	0.91647 (15)	0.0225 (5)	
C12	0.8326 (3)	0.2652 (2)	0.96013 (17)	0.0307 (6)	

C13	0.9462 (4)	0.2736 (2)	0.9372 (2)	0.0349 (7)	
C14	1.0269 (3)	-0.0253 (2)	0.83883 (16)	0.0247 (5)	
C15	0.9113 (3)	-0.0329 (2)	0.85480 (16)	0.0278 (6)	
C16	0.8629 (3)	-0.0010 (3)	0.78920 (18)	0.0278 (6)	
C17	0.9513 (3)	0.0221 (2)	0.73273 (15)	0.0233 (5)	
C18	1.0528 (2)	0.0076 (2)	0.76243 (16)	0.0219 (4)	
C19	1.1113 (4)	-0.0580 (3)	0.8895 (3)	0.0470 (10)	
H19A	1.0708	-0.0580	0.9409	0.071*	
H19B	1.1595	-0.0074	0.8841	0.071*	
H19C	1.1592	-0.1300	0.8769	0.071*	
C20	0.8523 (5)	-0.0750 (3)	0.9247 (2)	0.0507 (12)	
H20A	0.8574	-0.1511	0.9192	0.076*	
H20B	0.7719	-0.0353	0.9349	0.076*	
H20C	0.8890	-0.0664	0.9660	0.076*	
C21	0.7477 (4)	-0.0082 (5)	0.7778 (3)	0.0577 (13)	
H21A	0.7208	0.0459	0.7411	0.087*	
H21B	0.6937	0.0043	0.8249	0.087*	
H21C	0.7536	-0.0796	0.7599	0.087*	
C22	0.9377 (4)	0.0566 (3)	0.65488 (19)	0.0409 (8)	
H22A	0.9910	0.1004	0.6349	0.061*	
H22B	0.8593	0.0987	0.6548	0.061*	
H22C	0.9540	-0.0066	0.6241	0.061*	
C23	1.1665 (3)	0.0166 (3)	0.7209 (2)	0.0389 (8)	
H23A	1.1999	-0.0443	0.6876	0.058*	
H23B	1.2170	0.0167	0.7560	0.058*	
H23C	1.1574	0.0834	0.6917	0.058*	
C24	0.8339 (4)	0.3319 (3)	0.7238 (2)	0.0456 (10)	
C25	0.8009 (7)	0.4147 (5)	0.6689 (3)	0.082 (2)	
H25A	0.8622	0.4512	0.6531	0.124*	
H25B	0.7308	0.4666	0.6907	0.124*	
H25C	0.7875	0.3820	0.6258	0.124*	
C26	0.4726 (2)	0.3468 (2)	0.25475 (14)	0.0187 (4)	
C27	0.3896 (2)	0.3414 (2)	0.21351 (16)	0.0216 (4)	
H27	0.3591	0.2804	0.2193	0.026*	
C28	0.3501 (3)	0.4230 (2)	0.16414 (17)	0.0250 (5)	
C29	0.3910 (3)	0.5141 (2)	0.15453 (18)	0.0270 (5)	
H29	0.3653	0.5689	0.1203	0.032*	

C30	0.4707 (3)	0.5230 (2)	0.19660 (18)	0.0254 (5)	
C31	0.5098 (2)	0.4413 (2)	0.24605 (16)	0.0221 (5)	
H31	0.5633	0.4501	0.2746	0.027*	
C32	0.2628 (4)	0.4118 (3)	0.1210 (2)	0.0417 (9)	
C33	0.5133 (4)	0.6220 (3)	0.1884 (3)	0.0390 (8)	
C34	0.6351 (2)	0.2498 (2)	0.33786 (14)	0.0186 (4)	
C35	0.7263 (2)	0.2767 (2)	0.28880 (15)	0.0221 (5)	
H35	0.7156	0.3025	0.2405	0.026*	
C36	0.8322 (2)	0.2666 (3)	0.30883 (16)	0.0249 (5)	
C37	0.8533 (3)	0.2250 (3)	0.37746 (16)	0.0254 (5)	
H37	0.9257	0.2173	0.3909	0.030*	
C38	0.7654 (2)	0.1950 (2)	0.42608 (15)	0.0223 (5)	
C39	0.6584 (2)	0.2094 (2)	0.40762 (14)	0.0200 (4)	
H39	0.5991	0.1914	0.4432	0.024*	
C40	0.9225 (3)	0.3053 (4)	0.2568 (2)	0.0373 (7)	
C41	0.7870 (3)	0.1491 (3)	0.50064 (17)	0.0316 (6)	
C42	0.4088 (2)	0.2841 (2)	0.38837 (14)	0.0192 (4)	
C43	0.4069 (3)	0.3653 (2)	0.43592 (17)	0.0258 (5)	
H43	0.4687	0.3984	0.4278	0.031*	
C44	0.3169 (3)	0.3988 (3)	0.4948 (2)	0.0318 (6)	
C45	0.2254 (3)	0.3530 (3)	0.50860 (19)	0.0326 (6)	
H45	0.1643	0.3757	0.5489	0.039*	
C46	0.2254 (3)	0.2731 (3)	0.46213 (19)	0.0315 (6)	
C47	0.3151 (3)	0.2398 (3)	0.40325 (16)	0.0257 (5)	
H47	0.3125	0.1849	0.3721	0.031*	
C48	0.3189 (5)	0.4852 (4)	0.5432 (3)	0.0558 (13)	
C49	0.1289 (4)	0.2205 (5)	0.4779 (3)	0.0585 (14)	
C50	0.5251 (2)	0.1325 (2)	0.28677 (14)	0.0185 (4)	
C51	0.5308 (2)	0.0463 (2)	0.33778 (15)	0.0211 (4)	
H51	0.5210	0.0604	0.3891	0.025*	
C52	0.5502 (3)	-0.0587 (2)	0.31597 (16)	0.0231 (5)	
C53	0.5604 (3)	-0.0828 (2)	0.24166 (17)	0.0240 (5)	
H53	0.5706	-0.1542	0.2268	0.029*	
C54	0.5551 (2)	0.0007 (2)	0.19020 (15)	0.0206 (4)	
C55	0.5394 (2)	0.1055 (2)	0.21242 (14)	0.0199 (4)	
H55	0.5383	0.1606	0.1756	0.024*	
C56	0.5642 (4)	-0.1499 (3)	0.3704 (2)	0.0370 (7)	

C57	0.5642 (3)	-0.0208 (3)	0.11001 (17)	0.0278 (5)	
B1	0.5115 (2)	0.2534 (2)	0.31583 (15)	0.0179 (4)	
N1	1.0060 (3)	0.2207 (2)	0.8730 (2)	0.0359 (6)	
N2	0.8608 (3)	0.2643 (2)	0.76559 (16)	0.0315 (5)	
F1	0.1759 (5)	0.4967 (5)	0.1238 (4)	0.0718 (10)	0.65
F2	0.2207 (5)	0.3291 (5)	0.1387 (4)	0.0718 (10)	0.65
F3	0.3068 (5)	0.4130 (5)	0.0460 (4)	0.0718 (10)	0.65
F1B	0.1521 (10)	0.4673 (9)	0.1605 (7)	0.0718 (10)	0.35
F2B	0.2704 (10)	0.3085 (10)	0.1076 (7)	0.0718 (10)	0.35
F3B	0.2614 (11)	0.4607 (9)	0.0571 (7)	0.0718 (10)	0.35
F4	0.5555 (4)	0.6417 (3)	0.1186 (2)	0.0715 (10)	
F5	0.5946 (3)	0.6181 (2)	0.2276 (2)	0.0720 (11)	
F6	0.4313 (3)	0.7089 (2)	0.2111 (2)	0.0685 (9)	
F7	0.9500 (3)	0.2575 (3)	0.1913 (2)	0.0732 (6)	
F8	0.8889 (3)	0.4081 (3)	0.2376 (2)	0.0732 (6)	
F9	1.0194 (3)	0.2885 (3)	0.2815 (2)	0.0732 (6)	
F10	0.8946 (2)	0.0933 (3)	0.49792 (14)	0.0529 (7)	
F11	0.7667 (4)	0.2238 (3)	0.55119 (15)	0.0706 (10)	
F12	0.7227 (3)	0.0835 (3)	0.52862 (17)	0.0649 (9)	
F13	0.3536 (5)	0.5657 (4)	0.5078 (3)	0.1106 (10)	
F14	0.4012 (5)	0.4528 (4)	0.5862 (3)	0.1106 (10)	
F15	0.2283 (5)	0.5167 (4)	0.5927 (3)	0.1106 (10)	
F16	0.0263 (6)	0.3011 (7)	0.4777 (5)	0.0788 (13)	0.55
F17	0.1161 (6)	0.1747 (7)	0.5415 (5)	0.0788 (13)	0.55
F18	0.126 (2)	0.155 (2)	0.4189 (12)	0.054 (2)	0.55
F16B	0.0371 (8)	0.2659 (9)	0.5177 (6)	0.0788 (13)	0.45
F17B	0.1637 (7)	0.1269 (9)	0.5311 (6)	0.0788 (13)	0.45
F18B	0.122 (3)	0.165 (3)	0.4347 (15)	0.054 (2)	0.45
F19	0.5481 (3)	-0.1193 (2)	0.44025 (14)	0.0629 (9)	
F20	0.4934 (3)	-0.2108 (2)	0.36935 (18)	0.0643 (9)	
F21	0.6687 (3)	-0.2152 (3)	0.3554 (2)	0.0773 (12)	
F22	0.5568 (3)	-0.1186 (2)	0.09785 (15)	0.0585 (8)	
F23	0.4814 (2)	0.0457 (2)	0.08024 (13)	0.0501 (6)	
F24	0.6605 (2)	-0.0074 (3)	0.06910 (14)	0.0613 (9)	
Ir1	0.91567 (2)	0.13186 (2)	0.82747 (2)	0.02073 (3)	

7.6.9 **Table A17.** Atomic displacement parameters ($Å^2$) for [**4**][$BArF_{24}$].

	U^{11}	U^{22}	U^{33}	U^{12}	U^{13}	U^{23}
C1	0.0290 (17)	0.0371 (19)	0.105 (4)	-0.0114 (15)	-0.007 (2)	-0.023 (2)
C2	0.043 (2)	0.039 (2)	0.156 (7)	-0.0133 (19)	-0.042 (3)	-0.015 (3)
C3	0.078 (4)	0.0294 (18)	0.126 (5)	-0.013 (2)	-0.074 (4)	-0.002 (2)
C4	0.084 (3)	0.0219 (14)	0.062 (3)	-0.0059 (17)	-0.052 (3)	-0.0001 (15)
C5	0.129 (6)	0.0297 (18)	0.049 (3)	-0.012 (3)	-0.054 (3)	-0.0007 (16)
C6	0.140 (6)	0.0287 (17)	0.0276 (18)	-0.002 (3)	-0.027 (3)	-0.0054 (14)
C7	0.088 (3)	0.0229 (14)	0.0203 (13)	0.0048 (17)	-0.0072 (16)	0.0012 (11)
C8	0.086 (4)	0.0306 (17)	0.0292 (17)	0.0055 (19)	0.021 (2)	-0.0012 (13)
C9	0.049 (2)	0.0372 (18)	0.046 (2)	0.0040 (16)	0.0231 (18)	0.0074 (16)
C10	0.0285 (14)	0.0295 (14)	0.0329 (15)	-0.0022 (11)	0.0067 (12)	0.0023 (11)
C11	0.0259 (12)	0.0183 (10)	0.0209 (11)	-0.0020 (9)	-0.0038 (9)	0.0020 (8)
C12	0.0483 (18)	0.0195 (11)	0.0208 (12)	0.0006 (11)	-0.0109 (12)	0.0017 (9)
C13	0.050 (2)	0.0180 (11)	0.0405 (17)	-0.0012 (12)	-0.0267 (15)	-0.0021 (11)
C14	0.0309 (13)	0.0210 (11)	0.0232 (12)	-0.0038 (10)	-0.0108 (10)	-0.0009 (9)
C15	0.0368 (15)	0.0232 (12)	0.0217 (12)	-0.0114 (11)	0.0043 (11)	-0.0021 (9)
C16	0.0199 (12)	0.0357 (15)	0.0297 (13)	-0.0106 (11)	-0.0014 (10)	-0.0092 (11)
C17	0.0244 (12)	0.0251 (12)	0.0202 (11)	-0.0041 (9)	-0.0059 (9)	-0.0012 (9)
C18	0.0166 (10)	0.0230 (11)	0.0253 (11)	-0.0042 (8)	-0.0026 (9)	-0.0016 (9)
C19	0.060 (3)	0.0356 (18)	0.049 (2)	0.0024 (17)	-0.036 (2)	-0.0018 (15)
C20	0.079 (3)	0.0399 (19)	0.0290 (16)	-0.027 (2)	0.0165 (18)	-0.0008 (14)
C21	0.0271 (17)	0.082 (4)	0.071 (3)	-0.023 (2)	-0.0058 (19)	-0.025 (3)
C22	0.058 (2)	0.0437 (19)	0.0222 (14)	-0.0096 (17)	-0.0157 (14)	0.0027 (13)
C23	0.0225 (14)	0.0422 (18)	0.049 (2)	-0.0102 (13)	0.0080 (13)	-0.0128 (15)
C24	0.058 (2)	0.0293 (16)	0.0322 (16)	0.0079 (15)	0.0061 (16)	0.0052 (13)
C25	0.117 (5)	0.048 (3)	0.044 (3)	0.024 (3)	0.009 (3)	0.019 (2)
C26	0.0203 (10)	0.0173 (9)	0.0197 (10)	-0.0046 (8)	-0.0069 (8)	0.0008 (8)
C27	0.0231 (11)	0.0194 (10)	0.0250 (11)	-0.0066 (9)	-0.0105 (9)	0.0032 (8)
C28	0.0279 (13)	0.0229 (11)	0.0274 (12)	-0.0065 (10)	-0.0144 (10)	0.0044 (9)
C29	0.0318 (14)	0.0208 (11)	0.0303 (13)	-0.0062 (10)	-0.0129 (11)	0.0067 (10)
C30	0.0287 (13)	0.0178 (10)	0.0326 (14)	-0.0084 (9)	-0.0102 (11)	0.0037 (9)
C31	0.0241 (11)	0.0193 (10)	0.0251 (11)	-0.0064 (9)	-0.0090 (9)	0.0015 (9)
C32	0.047 (2)	0.0390 (18)	0.051 (2)	-0.0159 (16)	-0.0335 (18)	0.0132 (16)
C33	0.0433 (19)	0.0242 (13)	0.058 (2)	-0.0163 (13)	-0.0214 (17)	0.0089 (14)
C34	0.0192 (10)	0.0196 (10)	0.0174 (9)	-0.0044 (8)	-0.0048 (8)	-0.0009 (8)
C35	0.0227 (11)	0.0261 (11)	0.0185 (10)	-0.0070 (9)	-0.0057 (9)	0.0017 (9)

C36	0.0199 (11)	0.0329 (13)	0.0228 (11)	-0.0086 (10)	-0.0038 (9)	0.0012 (10)
C37	0.0214 (11)	0.0319 (13)	0.0245 (12)	-0.0069 (10)	-0.0077 (9)	-0.0006 (10)
C38	0.0221 (11)	0.0272 (12)	0.0182 (10)	-0.0044 (9)	-0.0082 (9)	0.0002 (9)
C39	0.0206 (11)	0.0224 (10)	0.0177 (10)	-0.0049 (8)	-0.0062 (8)	0.0008 (8)
C40	0.0292 (15)	0.053 (2)	0.0326 (16)	-0.0184 (15)	-0.0064 (12)	0.0098 (15)
C41	0.0295 (14)	0.0414 (17)	0.0228 (12)	-0.0041 (12)	-0.0108 (11)	0.0048 (11)
C42	0.0186 (10)	0.0205 (10)	0.0192 (10)	-0.0046 (8)	-0.0059 (8)	0.0006 (8)
C43	0.0242 (12)	0.0233 (11)	0.0299 (13)	-0.0071 (10)	-0.0014 (10)	-0.0062 (10)
C44	0.0307 (15)	0.0277 (13)	0.0342 (15)	-0.0052 (11)	0.0018 (12)	-0.0107 (11)
C45	0.0243 (13)	0.0395 (16)	0.0301 (14)	-0.0043 (12)	0.0010 (11)	-0.0051 (12)
C46	0.0220 (13)	0.0443 (17)	0.0303 (14)	-0.0135 (12)	-0.0021 (11)	-0.0027 (12)
C47	0.0232 (12)	0.0331 (14)	0.0236 (12)	-0.0112 (10)	-0.0045 (9)	-0.0041 (10)
C48	0.055 (3)	0.054 (3)	0.059 (3)	-0.022 (2)	0.011 (2)	-0.037 (2)
C49	0.039 (2)	0.093 (4)	0.052 (2)	-0.040 (2)	0.0111 (18)	-0.018 (3)
C50	0.0186 (10)	0.0192 (10)	0.0184 (10)	-0.0051 (8)	-0.0049 (8)	0.0005 (8)
C51	0.0240 (11)	0.0204 (10)	0.0190 (10)	-0.0054 (9)	-0.0048 (9)	0.0023 (8)
C52	0.0256 (12)	0.0195 (10)	0.0246 (11)	-0.0078 (9)	-0.0039 (9)	0.0044 (9)
C53	0.0244 (12)	0.0191 (10)	0.0294 (13)	-0.0084 (9)	-0.0024 (10)	-0.0016 (9)
C54	0.0201 (11)	0.0226 (11)	0.0207 (10)	-0.0078 (9)	-0.0032 (8)	-0.0038 (8)
C55	0.0218 (11)	0.0198 (10)	0.0198 (10)	-0.0075 (8)	-0.0053 (8)	0.0004 (8)
C56	0.047 (2)	0.0252 (13)	0.0354 (16)	-0.0078 (13)	-0.0034 (14)	0.0097 (12)
C57	0.0298 (14)	0.0305 (13)	0.0244 (12)	-0.0108 (11)	-0.0017 (10)	-0.0069 (10)
B1	0.0197 (11)	0.0180 (11)	0.0171 (10)	-0.0050 (9)	-0.0060 (9)	0.0002 (8)
N1	0.0281 (13)	0.0285 (13)	0.0533 (18)	-0.0037 (10)	-0.0134 (12)	-0.0120 (12)
N2	0.0372 (14)	0.0258 (11)	0.0258 (12)	-0.0032 (10)	0.0021 (10)	-0.0009 (9)
F1	0.075 (2)	0.0741 (19)	0.088 (2)	-0.0268 (16)	-0.062 (2)	0.0207 (17)
F2	0.075 (2)	0.0741 (19)	0.088 (2)	-0.0268 (16)	-0.062 (2)	0.0207 (17)
F3	0.075 (2)	0.0741 (19)	0.088 (2)	-0.0268 (16)	-0.062 (2)	0.0207 (17)
F1B	0.075 (2)	0.0741 (19)	0.088 (2)	-0.0268 (16)	-0.062 (2)	0.0207 (17)
F2B	0.075 (2)	0.0741 (19)	0.088 (2)	-0.0268 (16)	-0.062 (2)	0.0207 (17)
F3B	0.075 (2)	0.0741 (19)	0.088 (2)	-0.0268 (16)	-0.062 (2)	0.0207 (17)
F4	0.099 (3)	0.0630 (19)	0.068 (2)	-0.057 (2)	-0.0116 (19)	0.0204 (16)
F5	0.082 (2)	0.0469 (15)	0.119 (3)	-0.0429 (16)	-0.068 (2)	0.0317 (17)
F6	0.073 (2)	0.0232 (11)	0.112 (3)	-0.0137 (12)	-0.021 (2)	-0.0046 (14)
F7	0.0672 (12)	0.0879 (14)	0.0625 (11)	-0.0377 (11)	0.0143 (9)	0.0110 (10)
F8	0.0672 (12)	0.0879 (14)	0.0625 (11)	-0.0377 (11)	0.0143 (9)	0.0110 (10)
F9	0.0672 (12)	0.0879 (14)	0.0625 (11)	-0.0377 (11)	0.0143 (9)	0.0110 (10)

F10	0.0337 (12)	0.0810 (19)	0.0334 (11)	0.0073 (12)	-0.0143 (9)	0.0135 (12)
F11	0.112 (3)	0.0628 (18)	0.0298 (12)	0.0078 (18)	-0.0314 (15)	-0.0109 (12)
F12	0.0587 (17)	0.093 (2)	0.0528 (16)	-0.0347 (17)	-0.0271 (14)	0.0443 (16)
F13	0.150 (3)	0.0838 (17)	0.110 (2)	-0.0520 (18)	-0.0034 (19)	-0.0527 (15)
F14	0.150 (3)	0.0838 (17)	0.110 (2)	-0.0520 (18)	-0.0034 (19)	-0.0527 (15)
F15	0.150 (3)	0.0838 (17)	0.110 (2)	-0.0520 (18)	-0.0034 (19)	-0.0527 (15)
F16	0.0438 (18)	0.101 (4)	0.092 (3)	-0.040 (2)	0.019 (2)	-0.013 (3)
F17	0.0438 (18)	0.101 (4)	0.092 (3)	-0.040 (2)	0.019 (2)	-0.013 (3)
F18	0.042 (2)	0.075 (6)	0.055 (8)	-0.036 (3)	0.000 (6)	-0.031 (5)
F16B	0.0438 (18)	0.101 (4)	0.092 (3)	-0.040 (2)	0.019 (2)	-0.013 (3)
F17B	0.0438 (18)	0.101 (4)	0.092 (3)	-0.040 (2)	0.019 (2)	-0.013 (3)
F18B	0.042 (2)	0.075 (6)	0.055 (8)	-0.036 (3)	0.000 (6)	-0.031 (5)
F19	0.119 (3)	0.0393 (13)	0.0317 (12)	-0.0217 (16)	-0.0181 (14)	0.0149 (10)
F20	0.094 (2)	0.0436 (14)	0.0664 (19)	-0.0430 (16)	-0.0120 (17)	0.0194 (13)
F21	0.0611 (19)	0.0586 (18)	0.081 (2)	0.0193 (15)	0.0020 (16)	0.0406 (17)
F22	0.109 (3)	0.0391 (13)	0.0388 (13)	-0.0317 (15)	-0.0198 (15)	-0.0097 (10)
F23	0.0566 (16)	0.0614 (16)	0.0280 (10)	0.0008 (12)	-0.0169 (10)	-0.0068 (10)
F24	0.0457 (14)	0.112 (3)	0.0331 (12)	-0.0426 (16)	0.0139 (10)	-0.0240 (14)
Ir1	0.01764 (5)	0.02167 (5)	0.02188 (5)	-0.00409 (3)	-0.00188 (3)	-0.00165 (3)

7.6.10 **Table A18.** Interatomic distances (Å) and angles (deg) for [**4**][$BArF_{24}$].

C1—N1	1.338 (5)	C30—C33	1.493 (4)
C1—C2	1.402 (7)	C31—H31	0.9500
C1—H1	0.9500	C32—F3B	1.298 (12)
C2—C3	1.356 (10)	C32—F2	1.303 (7)
C2—H2	0.9500	C32—F1	1.317 (7)
C3—C4	1.387 (9)	C32—F2B	1.351 (13)
C3—H3	0.9500	C32—F3	1.381 (8)
C4—C13	1.414 (5)	C32—F1B	1.444 (14)
C4—C5	1.432 (8)	C33—F4	1.322 (5)
C5—C6	1.331 (10)	C33—F6	1.331 (5)
C5—H5	0.9500	C33—F5	1.333 (5)
C6—C7	1.458 (8)	C34—C35	1.404 (4)
C6—H6	0.9500	C34—C39	1.406 (3)

C7—C8	1.387 (8)	C34—B1	1.639 (4)
C7—C12	1.407 (5)	C35—C36	1.396 (4)
C8—C9	1.376 (8)	C35—H35	0.9500
C8—H8	0.9500	C36—C37	1.384 (4)
C9—C10	1.410 (5)	C36—C40	1.490 (4)
C9—H9	0.9500	C37—C38	1.388 (4)
C10—C11	1.365 (5)	C37—H37	0.9500
C10—H10	0.9500	C38—C39	1.388 (4)
C11—C12	1.408 (4)	C38—C41	1.501 (4)
C11—Ir1	2.073 (3)	C39—H39	0.9500
C12—C13	1.414 (6)	C40—F9	1.321 (5)
C13—N1	1.382 (5)	C40—F7	1.332 (6)
C14—C15	1.427 (5)	C40—F8	1.334 (6)
C14—C18	1.441 (4)	C41—F12	1.322 (5)
C14—C19	1.492 (5)	C41—F11	1.326 (5)
C14—Ir1	2.163 (3)	C41—F10	1.330 (4)
C15—C16	1.437 (5)	C42—C47	1.393 (4)
C15—C20	1.494 (5)	C42—C43	1.401 (4)
C15—Ir1	2.171 (3)	C42—B1	1.642 (4)
C16—C17	1.431 (4)	C43—C44	1.392 (4)
C16—C21	1.502 (5)	C43—H43	0.9500
C16—Ir1	2.186 (3)	C44—C45	1.380 (5)
C17—C18	1.423 (4)	C44—C48	1.480 (5)
C17—C22	1.498 (4)	C45—C46	1.382 (5)
C17—Ir1	2.222 (3)	C45—H45	0.9500
C18—C23	1.492 (4)	C46—C47	1.391 (4)
C18—Ir1	2.222 (3)	C46—C49	1.490 (5)
C19—H19A	0.9800	C47—H47	0.9500
C19—H19B	0.9800	C48—F15	1.288 (7)
C19—H19C	0.9800	C48—F13	1.316 (7)
C20—H20A	0.9800	C48—F14	1.370 (8)
C20—H20B	0.9800	C49—F18B	1.130 (18)
C20—H20C	0.9800	C49—F16B	1.247 (10)
C21—H21A	0.9800	C49—F17	1.277 (10)
C21—H21B	0.9800	C49—F16	1.417 (10)
C21—H21C	0.9800	C49—F18	1.433 (13)
C22—H22A	0.9800	C49—F17B	1.532 (13)

C22—H22B	0.9800	C50—C55	1.398 (4)
C22—H22C	0.9800	C50—C51	1.407 (4)
C23—H23A	0.9800	C50—B1	1.642 (4)
C23—H23B	0.9800	C51—C52	1.388 (4)
C23—H23C	0.9800	C51—H51	0.9500
C24—N2	1.153 (5)	C52—C53	1.394 (4)
C24—C25	1.458 (6)	C52—C56	1.494 (4)
C25—H25A	0.9800	C53—C54	1.386 (4)
C25—H25B	0.9800	C53—H53	0.9500
C25—H25C	0.9800	C54—C55	1.396 (4)
C26—C27	1.403 (4)	C54—C57	1.494 (4)
C26—C31	1.403 (4)	C55—H55	0.9500
C26—B1	1.639 (4)	C56—F20	1.323 (5)
C27—C28	1.398 (4)	C56—F19	1.330 (5)
C27—H27	0.9500	C56—F21	1.334 (5)
C28—C29	1.387 (4)	C57—F24	1.324 (4)
C28—C32	1.494 (4)	C57—F22	1.327 (4)
C29—C30	1.393 (4)	C57—F23	1.335 (4)
C29—H29	0.9500	N1—Ir1	2.099 (3)
C30—C31	1.399 (4)	N2—Ir1	2.034 (3)
N1—C1—C2	121.3 (5)	F6—C33—F5	105.5 (4)
N1—C1—H1	119.3	F4—C33—C30	112.3 (3)
C2—C1—H1	119.3	F6—C33—C30	112.5 (3)
C3—C2—C1	121.1 (5)	F5—C33—C30	113.1 (3)
C3—C2—H2	119.5	C35—C34—C39	115.7 (2)
C1—C2—H2	119.5	C35—C34—B1	124.1 (2)
C2—C3—C4	119.5 (4)	C39—C34—B1	120.0 (2)
C2—C3—H3	120.3	C36—C35—C34	122.1 (2)
C4—C3—H3	120.3	C36—C35—H35	119.0
C3—C4—C13	117.9 (5)	C34—C35—H35	119.0
C3—C4—C5	125.3 (5)	C37—C36—C35	121.0 (3)
C13—C4—C5	116.9 (5)	C37—C36—C40	119.3 (3)
C6—C5—C4	122.0 (4)	C35—C36—C40	119.6 (3)
C6—C5—H5	119.0	C36—C37—C38	117.8 (3)
C4—C5—H5	119.0	C36—C37—H37	121.1
C5—C6—C7	122.3 (5)	C38—C37—H37	121.1

C5—C6—H6	118.8	C37—C38—C39	121.2 (2)
C7—C6—H6	118.8	C37—C38—C41	118.6 (3)
C8—C7—C12	118.4 (4)	C39—C38—C41	120.1 (3)
C8—C7—C6	125.0 (4)	C38—C39—C34	122.1 (3)
C12—C7—C6	116.7 (5)	C38—C39—H39	119.0
C9—C8—C7	119.6 (3)	C34—C39—H39	119.0
C9—C8—H8	120.2	F9—C40—F7	105.3 (4)
C7—C8—H8	120.2	F9—C40—F8	109.3 (4)
C8—C9—C10	121.1 (4)	F7—C40—F8	102.0 (3)
C8—C9—H9	119.4	F9—C40—C36	113.6 (3)
C10—C9—H9	119.4	F7—C40—C36	112.6 (3)
C11—C10—C9	121.1 (4)	F8—C40—C36	113.1 (3)
C11—C10—H10	119.4	F12—C41—F11	105.7 (3)
C9—C10—H10	119.4	F12—C41—F10	106.1 (3)
C10—C11—C12	117.1 (3)	F11—C41—F10	106.6 (3)
C10—C11—Ir1	129.3 (2)	F12—C41—C38	113.3 (3)
C12—C11—Ir1	113.7 (2)	F11—C41—C38	112.7 (3)
C7—C12—C11	122.7 (4)	F10—C41—C38	111.9 (3)
C7—C12—C13	120.5 (4)	C47—C42—C43	116.0 (3)
C11—C12—C13	116.8 (3)	C47—C42—B1	123.6 (2)
N1—C13—C4	122.2 (4)	C43—C42—B1	120.2 (2)
N1—C13—C12	116.2 (3)	C44—C43—C42	121.8 (3)
C4—C13—C12	121.7 (4)	C44—C43—H43	119.1
C15—C14—C18	108.6 (2)	C42—C43—H43	119.1
C15—C14—C19	126.0 (3)	C45—C44—C43	121.0 (3)
C18—C14—C19	125.1 (3)	C45—C44—C48	119.3 (3)
C15—C14—Ir1	71.09 (17)	C43—C44—C48	119.7 (3)
C18—C14—Ir1	73.04 (16)	C44—C45—C46	118.1 (3)
C19—C14—Ir1	127.1 (2)	C44—C45—H45	120.9
C14—C15—C16	107.9 (2)	C46—C45—H45	120.9
C14—C15—C20	126.7 (4)	C45—C46—C47	120.8 (3)
C16—C15—C20	125.2 (4)	C45—C46—C49	118.7 (3)
C14—C15—Ir1	70.45 (16)	C47—C46—C49	120.5 (3)
C16—C15—Ir1	71.30 (18)	C46—C47—C42	122.2 (3)
C20—C15—Ir1	127.6 (2)	C46—C47—H47	118.9
C17—C16—C15	107.3 (3)	C42—C47—H47	118.9
C17—C16—C21	125.7 (3)	F15—C48—F13	112.3 (5)

C15—C16—C21	126.3 (4)	F15—C48—F14	101.6 (5)
C17—C16—Ir1	72.41 (17)	F13—C48—F14	99.0 (5)
C15—C16—Ir1	70.19 (17)	F15—C48—C44	115.4 (4)
C21—C16—Ir1	130.3 (3)	F13—C48—C44	114.5 (4)
C18—C17—C16	109.3 (2)	F14—C48—C44	112.0 (4)
C18—C17—C22	125.9 (3)	F18B—C49—F16B	115.8 (19)
C16—C17—C22	124.8 (3)	F17—C49—F16	105.3 (6)
C18—C17—Ir1	71.31 (16)	F17—C49—F18	112.9 (15)
C16—C17—Ir1	69.71 (17)	F16—C49—F18	100.6 (14)
C22—C17—Ir1	125.0 (2)	F18B—C49—C46	117.9 (18)
C17—C18—C14	106.9 (2)	F16B—C49—C46	119.9 (6)
C17—C18—C23	126.5 (3)	F17—C49—C46	114.9 (5)
C14—C18—C23	126.4 (3)	F16—C49—C46	107.8 (5)
C17—C18—Ir1	71.32 (16)	F18—C49—C46	113.8 (12)
C14—C18—Ir1	68.62 (16)	F18B—C49—F17B	92 (2)
C23—C18—Ir1	128.5 (2)	F16B—C49—F17B	97.1 (7)
C14—C19—H19A	109.5	C46—C49—F17B	106.0 (5)
C14—C19—H19B	109.5	C55—C50—C51	115.4 (2)
H19A—C19—H19B	109.5	C55—C50—B1	124.6 (2)
C14—C19—H19C	109.5	C51—C50—B1	119.8 (2)
H19A—C19—H19C	109.5	C52—C51—C50	122.5 (2)
H19B—C19—H19C	109.5	C52—C51—H51	118.8
C15—C20—H20A	109.5	C50—C51—H51	118.8
C15—C20—H20B	109.5	C51—C52—C53	120.8 (2)
H20A—C20—H20B	109.5	C51—C52—C56	121.6 (3)
C15—C20—H20C	109.5	C53—C52—C56	117.6 (3)
H20A—C20—H20C	109.5	C54—C53—C52	117.9 (2)
H20B—C20—H20C	109.5	C54—C53—H53	121.0
C16—C21—H21A	109.5	C52—C53—H53	121.0
C16—C21—H21B	109.5	C53—C54—C55	120.8 (2)
H21A—C21—H21B	109.5	C53—C54—C57	120.0 (3)
C16—C21—H21C	109.5	C55—C54—C57	119.2 (3)
H21A—C21—H21C	109.5	C54—C55—C50	122.5 (2)
H21B—C21—H21C	109.5	C54—C55—H55	118.7
C17—C22—H22A	109.5	C50—C55—H55	118.7
C17—C22—H22B	109.5	F20—C56—F19	106.1 (3)
H22A—C22—H22B	109.5	F20—C56—F21	105.4 (4)

C17—C22—H22C	109.5	F19—C56—F21	106.9 (4)
H22A—C22—H22C	109.5	F20—C56—C52	113.1 (3)
H22B—C22—H22C	109.5	F19—C56—C52	113.6 (3)
C18—C23—H23A	109.5	F21—C56—C52	111.2 (3)
C18—C23—H23B	109.5	F24—C57—F22	107.6 (3)
H23A—C23—H23B	109.5	F24—C57—F23	105.0 (3)
C18—C23—H23C	109.5	F22—C57—F23	105.6 (3)
H23A—C23—H23C	109.5	F24—C57—C54	112.5 (3)
H23B—C23—H23C	109.5	F22—C57—C54	113.3 (3)
N2—C24—C25	178.0 (5)	F23—C57—C54	112.3 (3)
C24—C25—H25A	109.5	C26—B1—C34	114.0 (2)
C24—C25—H25B	109.5	C26—B1—C42	103.5 (2)
H25A—C25—H25B	109.5	C34—B1—C42	110.4 (2)
C24—C25—H25C	109.5	C26—B1—C50	112.8 (2)
H25A—C25—H25C	109.5	C34—B1—C50	104.8 (2)
H25B—C25—H25C	109.5	C42—B1—C50	111.5 (2)
C27—C26—C31	115.9 (2)	C1—N1—C13	118.0 (4)
C27—C26—B1	121.0 (2)	C1—N1—Ir1	127.9 (3)
C31—C26—B1	122.8 (2)	C13—N1—Ir1	114.1 (3)
C28—C27—C26	122.2 (2)	C24—N2—Ir1	172.3 (3)
C28—C27—H27	118.9	N2—Ir1—C11	88.44 (11)
C26—C27—H27	118.9	N2—Ir1—N1	87.13 (13)
C29—C28—C27	121.0 (3)	C11—Ir1—N1	79.15 (12)
C29—C28—C32	119.4 (3)	N2—Ir1—C14	150.95 (11)
C27—C28—C32	119.6 (3)	C11—Ir1—C14	120.60 (11)
C28—C29—C30	118.0 (3)	N1—Ir1—C14	98.12 (11)
C28—C29—H29	121.0	N2—Ir1—C15	146.55 (13)
C30—C29—H29	121.0	C11—Ir1—C15	97.21 (11)
C29—C30—C31	120.8 (3)	N1—Ir1—C15	126.32 (13)
C29—C30—C33	118.7 (3)	C14—Ir1—C15	38.45 (13)
C31—C30—C33	120.5 (3)	N2—Ir1—C16	108.53 (13)
C30—C31—C26	122.1 (3)	C11—Ir1—C16	108.36 (11)
C30—C31—H31	119.0	N1—Ir1—C16	162.45 (13)
C26—C31—H31	119.0	C14—Ir1—C16	64.35 (12)
F2—C32—F1	107.2 (5)	C15—Ir1—C16	38.50 (13)
F3B—C32—F2B	105.5 (8)	N2—Ir1—C18	112.63 (11)
F2—C32—F3	110.6 (5)	C11—Ir1—C18	158.78 (11)

F1—C32—F3	99.2 (4)	N1—Ir1—C18	103.41 (11)
F3B—C32—F1B	99.8 (7)	C14—Ir1—C18	38.34 (11)
F2B—C32—F1B	113.4 (8)	C15—Ir1—C18	64.01 (11)
F3B—C32—C28	117.8 (6)	C16—Ir1—C18	63.78 (11)
F2—C32—C28	115.4 (3)	N2—Ir1—C17	93.38 (11)
F1—C32—C28	113.5 (4)	C11—Ir1—C17	144.36 (12)
F2B—C32—C28	112.2 (5)	N1—Ir1—C17	136.48 (12)
F3—C32—C28	109.7 (4)	C14—Ir1—C17	63.30 (10)
F1B—C32—C28	107.7 (5)	C15—Ir1—C17	63.42 (11)
F4—C33—F6	105.9 (3)	C16—Ir1—C17	37.89 (11)
F4—C33—F5	106.9 (4)	C18—Ir1—C17	37.37 (10)
N1—C1—C2—C3	-1.8 (9)	C35—C36—C37—C38	-0.8 (5)
C1—C2—C3—C4	-0.2 (9)	C40—C36—C37—C38	176.7 (3)
C2—C3—C4—C13	1.3 (7)	C36—C37—C38—C39	-2.1 (5)
C2—C3—C4—C5	-178.4 (5)	C36—C37—C38—C41	179.7 (3)
C3—C4—C5—C6	178.5 (5)	C37—C38—C39—C34	3.3 (4)
C13—C4—C5—C6	-1.3 (6)	C41—C38—C39—C34	-178.5 (3)
C4—C5—C6—C7	1.3 (7)	C35—C34—C39—C38	-1.3 (4)
C5—C6—C7—C8	179.8 (4)	B1—C34—C39—C38	173.6 (2)
C5—C6—C7—C12	0.1 (6)	C37—C36—C40—F9	4.2 (5)
C12—C7—C8—C9	0.1 (6)	C35—C36—C40—F9	-178.3 (4)
C6—C7—C8—C9	-179.6 (4)	C37—C36—C40—F7	123.7 (4)
C7—C8—C9—C10	0.0 (6)	C35—C36—C40—F7	-58.7 (5)
C8—C9—C10—C11	0.5 (6)	C37—C36—C40—F8	-121.2 (4)
C9—C10—C11—C12	-1.0 (5)	C35—C36—C40—F8	56.3 (5)
C9—C10—C11—Ir1	179.8 (3)	C37—C38—C41—F12	-152.6 (3)
C8—C7—C12—C11	-0.7 (5)	C39—C38—C41—F12	29.1 (5)
C6—C7—C12—C11	179.1 (3)	C37—C38—C41—F11	87.5 (4)
C8—C7—C12—C13	178.8 (3)	C39—C38—C41—F11	-90.8 (4)

C6—C7—C12—C13	-1.5 (5)	C37—C38—C41—F10	-32.7 (4)
C10—C11—C12—C7	1.1 (4)	C39—C38—C41—F10	149.1 (3)
Ir1—C11—C12—C7	-179.6 (2)	C47—C42—C43—C44	0.5 (4)
C10—C11—C12—C13	-178.4 (3)	B1—C42—C43—C44	175.2 (3)
Ir1—C11—C12—C13	1.0 (3)	C42—C43—C44—C45	0.0 (5)
C3—C4—C13—N1	-0.5 (5)	C42—C43—C44—C48	-179.8 (4)
C5—C4—C13—N1	179.2 (3)	C43—C44—C45—C46	-0.3 (5)
C3—C4—C13—C12	-180.0 (4)	C48—C44—C45—C46	179.5 (4)
C5—C4—C13—C12	-0.2 (5)	C44—C45—C46—C47	0.1 (5)
C7—C12—C13—N1	-177.9 (3)	C44—C45—C46—C49	178.1 (4)
C11—C12—C13—N1	1.6 (4)	C45—C46—C47—C42	0.3 (5)
C7—C12—C13—C4	1.6 (5)	C49—C46—C47—C42	-177.6 (4)
C11—C12—C13—C4	-178.9 (3)	C43—C42—C47—C46	-0.6 (4)
C18—C14—C15—C16	-2.1 (3)	B1—C42—C47—C46	-175.2 (3)
C19—C14—C15—C16	-175.5 (3)	C45—C44—C48—F15	-4.9 (8)
Ir1—C14—C15—C16	61.8 (2)	C43—C44—C48—F15	174.9 (5)
C18—C14—C15—C20	173.3 (3)	C45—C44—C48—F13	-137.6 (5)
C19—C14—C15—C20	-0.2 (5)	C43—C44—C48—F13	42.2 (7)
Ir1—C14—C15—C20	-122.9 (3)	C45—C44—C48—F14	110.7 (5)
C18—C14—C15—Ir1	-63.9 (2)	C43—C44—C48—F14	-69.5 (6)
C19—C14—C15—Ir1	122.6 (3)	C45—C46—C49—F18B	170 (3)
C14—C15—C16—C17	2.1 (3)	C47—C46—C49—F18B	-12 (3)

C20—C15—C16—C17	-173.3 (3)	C45—C46—C49—F16B	19.6 (10)
Ir1—C15—C16—C17	63.4 (2)	C47—C46—C49—F16B	-162.4 (8)
C14—C15—C16—C21	172.7 (4)	C45—C46—C49—F17	-59.3 (7)
C20—C15—C16—C21	-2.7 (6)	C47—C46—C49—F17	118.6 (6)
Ir1—C15—C16—C21	-126.0 (4)	C45—C46—C49—F16	57.8 (6)
C14—C15—C16—Ir1	-61.3 (2)	C47—C46—C49—F16	-124.3 (5)
C20—C15—C16—Ir1	123.3 (3)	C45—C46—C49—F18	168.4 (16)
C15—C16—C17—C18	-1.4 (3)	C47—C46—C49—F18	-13.6 (17)
C21—C16—C17—C18	-172.0 (4)	C45—C46—C49—F17B	-88.5 (6)
Ir1—C16—C17—C18	60.6 (2)	C47—C46—C49—F17B	89.4 (6)
C15—C16—C17—C22	178.9 (3)	C55—C50—C51—C52	0.5 (4)
C21—C16—C17—C22	8.3 (6)	B1—C50—C51—C52	-175.4 (3)
Ir1—C16—C17—C22	-119.2 (3)	C50—C51—C52—C53	-2.7 (4)
C15—C16—C17—Ir1	-61.9 (2)	C50—C51—C52—C56	175.6 (3)
C21—C16—C17—Ir1	127.4 (4)	C51—C52—C53—C54	2.6 (4)
C16—C17—C18—C14	0.1 (3)	C56—C52—C53—C54	-175.8 (3)
C22—C17—C18—C14	179.8 (3)	C52—C53—C54—C55	-0.4 (4)
Ir1—C17—C18—C14	59.67 (19)	C52—C53—C54—C57	-179.3 (3)
C16—C17—C18—C23	175.8 (3)	C53—C54—C55—C50	-1.8 (4)
C22—C17—C18—C23	-4.4 (5)	C57—C54—C55—C50	177.1 (3)
Ir1—C17—C18—C23	-124.6 (3)	C51—C50—C55—C54	1.7 (4)
C16—C17—C18—Ir1	-59.6 (2)	B1—C50—C55—C54	177.4 (2)
C22—C17—C18—Ir1	120.2 (3)	C51—C52—C56—	125.6 (4)

		F20	
C15—C14—C18—C17	1.2 (3)	C53—C52—C56—F20	-56.0 (4)
C19—C14—C18—C17	174.8 (3)	C51—C52—C56—F19	4.6 (5)
Ir1—C14—C18—C17	-61.4 (2)	C53—C52—C56—F19	-177.1 (3)
C15—C14—C18—C23	-174.5 (3)	C51—C52—C56—F21	-116.0 (4)
C19—C14—C18—C23	-1.0 (5)	C53—C52—C56—F21	62.3 (5)
Ir1—C14—C18—C23	122.8 (3)	C53—C54—C57—F24	-111.1 (4)
C15—C14—C18—Ir1	62.6 (2)	C55—C54—C57—F24	69.9 (4)
C19—C14—C18—Ir1	-123.8 (3)	C53—C54—C57—F22	11.2 (4)
C31—C26—C27—C28	2.9 (4)	C55—C54—C57—F22	-167.8 (3)
B1—C26—C27—C28	176.3 (3)	C53—C54—C57—F23	130.7 (3)
C26—C27—C28—C29	-0.9 (5)	C55—C54—C57—F23	-48.3 (4)
C26—C27—C28—C32	179.1 (3)	C27—C26—B1—C34	160.5 (2)
C27—C28—C29—C30	-1.2 (5)	C31—C26—B1—C34	-26.5 (4)
C32—C28—C29—C30	178.8 (3)	C27—C26—B1—C42	-79.5 (3)
C28—C29—C30—C31	1.1 (5)	C31—C26—B1—C42	93.5 (3)
C28—C29—C30—C33	-178.4 (3)	C27—C26—B1—C50	41.2 (3)
C29—C30—C31—C26	1.0 (5)	C31—C26—B1—C50	-145.9 (3)
C33—C30—C31—C26	-179.4 (3)	C35—C34—B1—C26	-32.2 (4)
C27—C26—C31—C30	-3.0 (4)	C39—C34—B1—C26	153.3 (2)
B1—C26—C31—C30	-176.3 (3)	C35—C34—B1—C42	-148.2 (3)
C29—C28—C32—F3B	27.7 (9)	C39—C34—B1—C42	37.3 (3)
C27—C28—C32—F3B	-152.2 (8)	C35—C34—B1—C50	91.6 (3)

C29—C28—C32—F2	-173.4 (5)	C39—C34—B1—C50	-82.9 (3)
C27—C28—C32—F2	6.6 (7)	C47—C42—B1—C26	94.8 (3)
C29—C28—C32—F1	-49.1 (6)	C43—C42—B1—C26	-79.5 (3)
C27—C28—C32—F1	130.9 (5)	C47—C42—B1—C34	-142.8 (3)
C29—C28—C32—F2B	150.5 (7)	C43—C42—B1—C34	42.8 (3)
C27—C28—C32—F2B	-29.4 (8)	C47—C42—B1—C50	-26.7 (3)
C29—C28—C32—F3	60.9 (5)	C43—C42—B1—C50	158.9 (2)
C27—C28—C32—F3	-119.1 (4)	C55—C50—B1—C26	19.7 (4)
C29—C28—C32—F1B	-84.1 (6)	C51—C50—B1—C26	-164.8 (2)
C27—C28—C32—F1B	96.0 (6)	C55—C50—B1—C34	-104.8 (3)
C29—C30—C33—F4	-54.6 (5)	C51—C50—B1—C34	70.7 (3)
C31—C30—C33—F4	125.8 (4)	C55—C50—B1—C42	135.7 (3)
C29—C30—C33—F6	64.8 (5)	C51—C50—B1—C42	-48.8 (3)
C31—C30—C33—F6	-114.8 (4)	C2—C1—N1—C13	2.5 (7)
C29—C30—C33—F5	-175.8 (4)	C2—C1—N1—Ir1	-175.8 (4)
C31—C30—C33—F5	4.7 (6)	C4—C13—N1—C1	-1.4 (6)
C39—C34—C35—C36	-1.6 (4)	C12—C13—N1—C1	178.1 (4)
B1—C34—C35—C36	-176.3 (3)	C4—C13—N1—Ir1	177.2 (3)
C34—C35—C36—C37	2.8 (5)	C12—C13—N1—Ir1	-3.3 (4)
C34—C35—C36—C40	-174.7 (3)		

7.7 [**4**][BPh_4]

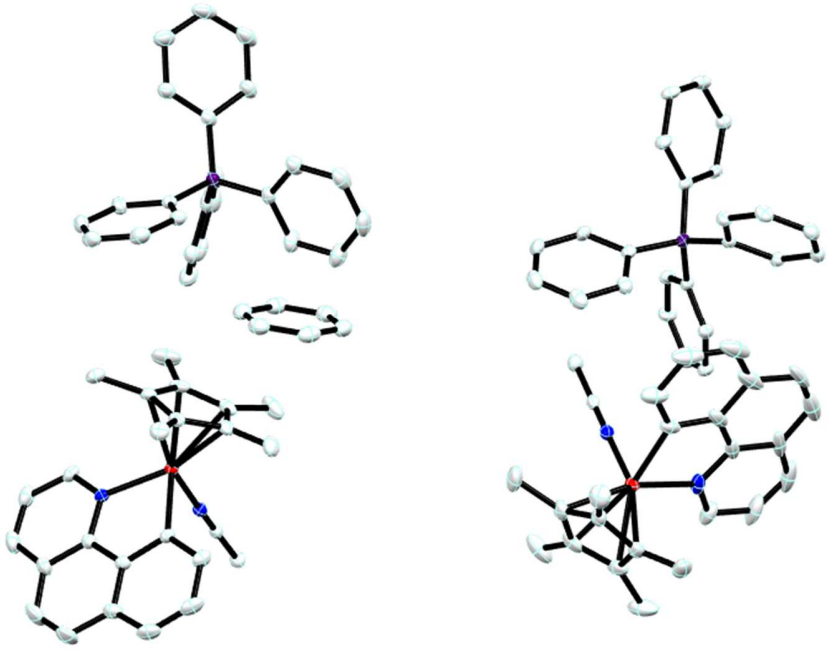

7.7.1 **Figure A19.** Asymmetric unit of [**4**][BPh_4], without hydrogens and without numbering of atoms.

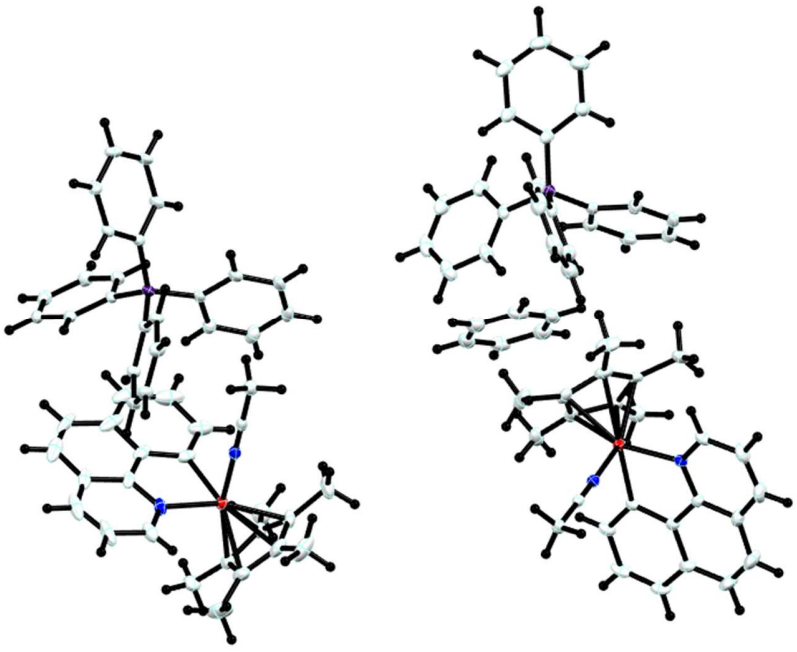

7.7.2 **Figure A20.** Asymmetric unit of [**4**][BPh_4], with all hydrogens and without numbering of atoms.

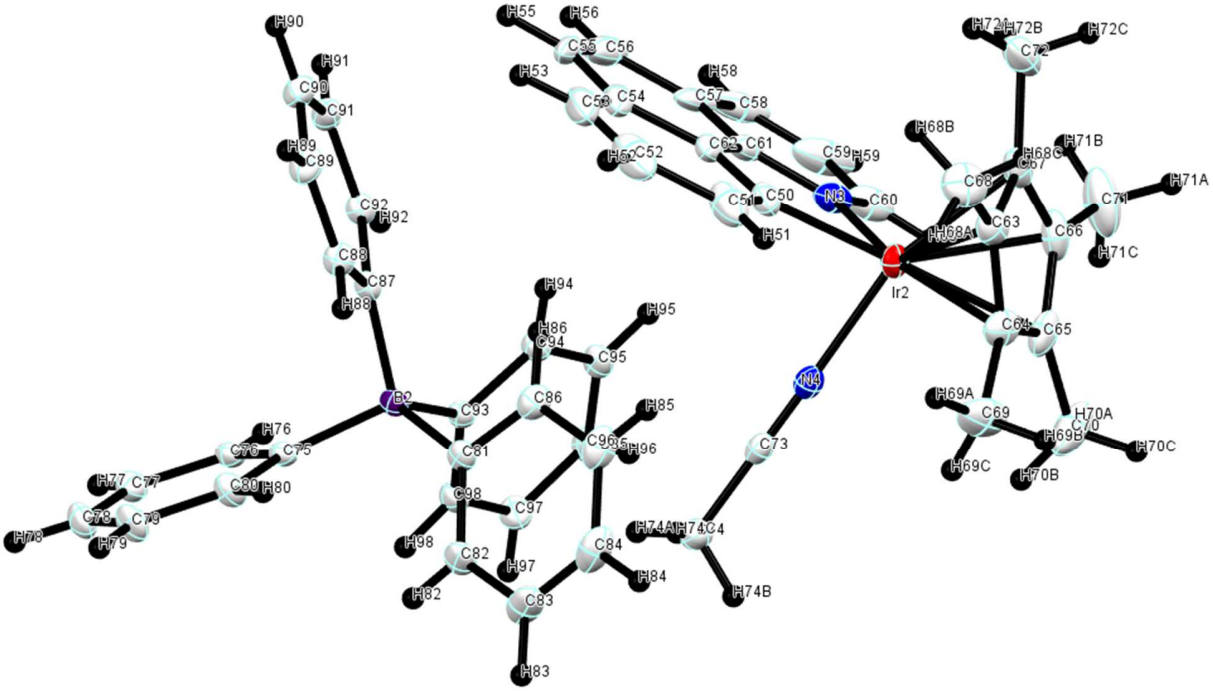

7.7.3 **Figure A21.** Asymmetric unit of [**4**][BPh_4], with all hydrogens and total numbering of atoms.

[**4**][BPh_4]

Data collection: Bruker *APEX2*; cell refinement: Bruker *SAINT*; data reduction: Bruker *SAINT*; program(s) used to solve structure: *SHELXS2013* (Sheldrick, 2013); program(s) used to refine structure: *SHELXL2013* (Sheldrick, 2013); molecular graphics: Bruker *SHELXTL*; software used to prepare material for publication: Bruker *SHELXTL*.

7.7.4 Crystal data

$2(C_{25}H_{26}IrN_2)\cdot 2(C_{24}H_{20}B)\cdot 0.5(C_6H_6)$	$Z = 2$
$M_r = 1770.82$	$F(000) = 1786$
Triclinic, $P\bar{1}$	$D_x = 1.439$ Mg m^{-3}

a = 12.0116 (4) Å	Mo $K\alpha$ radiation, λ = 0.71073 Å
b = 17.9419 (6) Å	Cell parameters from 9986 reflections
c = 19.2603 (6) Å	θ = 2.3–31.9°
α = 92.616 (1)°	μ = 3.30 mm^{-1}
β = 95.995 (1)°	T = 173 K
γ = 97.243 (1)°	Prism, yellow
V = 4087.9 (2) Å^3	0.35 × 0.25 × 0.20 mm

7.7.5 Data collection

Bruker APEX-II CCD diffractometer	20690 reflections with $I > 2\sigma(I)$
Radiation source: fine focus sealed tube	R_{int} = 0.036
ϕ and ω scans	θ_{max} = 32.0°, θ_{min} = 1.5°
Absorption correction: multi-scan *SADABS*	h = -17→17
T_{min} = 0.597, T_{max} = 0.746	k = -26→26
105999 measured reflections	l = -28→28
28306 independent reflections	

7.7.6 Refinement

Refinement on F^2	Primary atom site location: structure-invariant direct methods
Least-squares matrix: full	Secondary atom site location: difference Fourier map
$R[F^2 > 2\sigma(F^2)]$ = 0.035	Hydrogen site location: inferred from neighbouring sites
$wR(F^2)$ = 0.073	H-atom parameters constrained
S = 1.01	$w = 1/[\sigma^2(F_o^2) + (0.0308P)^2 + 2.4408P]$ where $P = (F_o^2 + 2F_c^2)/3$
28306 reflections	$(\Delta/\sigma)_{max}$ = 0.004
994 parameters	$\Delta\rangle_{max}$ = 2.92 e Å^{-3}
0 restraints	$\Delta\rangle_{min}$ = -1.77 e Å^{-3}

7.7.7 Special details

Geometry. All esds (except the esd in the dihedral angle between two l.s. planes) are estimated using the full covariance matrix. The cell esds are taken into account individually in the

estimation of esds in distances, angles and torsion angles; correlations between esds in cell parameters are only used when they are defined by crystal symmetry. An approximate (isotropic) treatment of cell esds is used for estimating esds involving l.s. planes.

7.7.8 **Table A19.** Fractional atomic coordinates and isotropic or equivalent isotropic displacement parameters (Å^2) for [**4**][BPh_4]

	x	*y*	*z*	U_{iso}*/U_{eq}
C1	0.0331 (2)	0.36406 (14)	0.16400 (13)	0.0245 (5)
C2	-0.0382 (2)	0.30330 (17)	0.18197 (17)	0.0376 (7)
H2	-0.0419	0.2944	0.2300	0.045*
C3	-0.1056 (3)	0.25441 (18)	0.1308 (2)	0.0468 (8)
H3	-0.1536	0.2131	0.1451	0.056*
C4	-0.1040 (3)	0.26454 (19)	0.06130 (19)	0.0466 (8)
H4	-0.1513	0.2310	0.0278	0.056*
C5	-0.0325 (2)	0.32454 (18)	0.03944 (16)	0.0385 (7)
C6	-0.0191 (3)	0.3386 (2)	-0.03239 (18)	0.0593 (10)
H6	-0.0637	0.3069	-0.0684	0.071*
C7	0.0536 (4)	0.3946 (3)	-0.04962 (18)	0.0628 (11)
H7	0.0599	0.4014	-0.0978	0.075*
C8	0.1234 (3)	0.4455 (2)	0.00160 (15)	0.0426 (7)
C9	0.2016 (3)	0.5054 (2)	-0.01214 (17)	0.0525 (9)
H9	0.2104	0.5167	-0.0591	0.063*
C10	0.2656 (3)	0.54815 (19)	0.04140 (18)	0.0457 (8)
H10	0.3204	0.5882	0.0318	0.055*
C11	0.2503 (2)	0.53293 (16)	0.11029 (16)	0.0337 (6)
H11	0.2954	0.5632	0.1472	0.040*
C12	0.1107 (2)	0.43313 (16)	0.07254 (13)	0.0277 (5)
C13	0.0344 (2)	0.37339 (15)	0.09187 (13)	0.0272 (5)
C14	0.2171 (3)	0.53400 (19)	0.30838 (15)	0.0392 (7)
C15	0.1926 (3)	0.4642 (2)	0.34004 (14)	0.0404 (8)
C16	0.0747 (3)	0.43733 (18)	0.32595 (14)	0.0364 (7)
C17	0.0248 (2)	0.49138 (16)	0.28330 (13)	0.0296 (6)
C18	0.1125 (2)	0.55036 (16)	0.27283 (14)	0.0309 (6)
C19	0.3278 (3)	0.5842 (3)	0.3163 (2)	0.0664 (12)
H19A	0.3321	0.6188	0.3576	0.100*

H19B	0.3341	0.6132	0.2746	0.100*
H19C	0.3897	0.5535	0.3217	0.100*
C20	0.2762 (4)	0.4247 (3)	0.38386 (18)	0.0676 (13)
H20A	0.3498	0.4328	0.3659	0.101*
H20B	0.2495	0.3706	0.3817	0.101*
H20C	0.2835	0.4449	0.4325	0.101*
C21	0.0128 (4)	0.3721 (2)	0.35815 (17)	0.0542 (10)
H21A	0.0551	0.3289	0.3561	0.081*
H21B	-0.0623	0.3586	0.3323	0.081*
H21C	0.0051	0.3861	0.4070	0.081*
C22	-0.0988 (2)	0.48928 (19)	0.25998 (17)	0.0412 (7)
H22A	-0.1354	0.5123	0.2972	0.062*
H22B	-0.1333	0.4369	0.2498	0.062*
H22C	-0.1085	0.5173	0.2177	0.062*
C23	0.0974 (3)	0.61993 (17)	0.23493 (17)	0.0442 (8)
H23A	0.0936	0.6617	0.2688	0.066*
H23B	0.0273	0.6112	0.2031	0.066*
H23C	0.1615	0.6325	0.2081	0.066*
C24	0.3297 (2)	0.33460 (15)	0.20582 (12)	0.0256 (5)
C25	0.4149 (2)	0.28489 (17)	0.19822 (14)	0.0324 (6)
H25A	0.4700	0.2913	0.2400	0.049*
H25B	0.4534	0.2973	0.1570	0.049*
H25C	0.3787	0.2326	0.1925	0.049*
C26	0.4382 (2)	0.68374 (17)	0.57131 (14)	0.0312 (6)
C27	0.3809 (3)	0.6930 (2)	0.63010 (15)	0.0422 (7)
H27	0.3672	0.7421	0.6443	0.051*
C28	0.3430 (3)	0.6326 (2)	0.66854 (17)	0.0533 (10)
H28	0.3053	0.6413	0.7085	0.064*
C29	0.3601 (3)	0.5607 (2)	0.6490 (2)	0.0536 (10)
H29	0.3358	0.5197	0.6757	0.064*
C30	0.4126 (3)	0.5488 (2)	0.5903 (2)	0.0524 (9)
H30	0.4229	0.4991	0.5755	0.063*
C31	0.4509 (3)	0.60931 (19)	0.55234 (18)	0.0419 (7)
H31	0.4871	0.5996	0.5119	0.050*
C32	0.3826 (2)	0.76626 (15)	0.46326 (13)	0.0290 (6)
C33	0.2693 (2)	0.73576 (17)	0.46299 (15)	0.0339 (6)
H33	0.2481	0.7062	0.5004	0.041*

C34	0.1867 (3)	0.74734 (19)	0.40959 (18)	0.0454 (8)
H34	0.1106	0.7262	0.4115	0.054*
C35	0.2138 (3)	0.78884 (19)	0.35439 (17)	0.0471 (9)
H35	0.1573	0.7960	0.3179	0.056*
C36	0.3238 (3)	0.82001 (19)	0.35244 (16)	0.0455 (8)
H36	0.3437	0.8491	0.3146	0.055*
C37	0.4058 (3)	0.80887 (18)	0.40603 (14)	0.0371 (7)
H37	0.4813	0.8312	0.4038	0.045*
C38	0.5966 (2)	0.73782 (16)	0.49101 (14)	0.0308 (6)
C39	0.5891 (3)	0.69159 (18)	0.42933 (16)	0.0383 (7)
H39	0.5163	0.6727	0.4066	0.046*
C40	0.6831 (3)	0.6723 (2)	0.40008 (19)	0.0484 (8)
H40	0.6738	0.6406	0.3584	0.058*
C41	0.7904 (3)	0.6991 (2)	0.4318 (2)	0.0555 (10)
H41	0.8553	0.6863	0.4121	0.067*
C42	0.8013 (3)	0.7445 (2)	0.4917 (2)	0.0545 (9)
H42	0.8745	0.7631	0.5140	0.065*
C43	0.7066 (3)	0.7637 (2)	0.52066 (17)	0.0435 (8)
H43	0.7172	0.7956	0.5622	0.052*
C44	0.5113 (2)	0.83298 (17)	0.57773 (14)	0.0337 (6)
C45	0.4809 (3)	0.90277 (18)	0.56033 (16)	0.0409 (7)
H45	0.4398	0.9067	0.5161	0.049*
C46	0.5087 (3)	0.9673 (2)	0.60549 (19)	0.0534 (9)
H46	0.4870	1.0139	0.5914	0.064*
C47	0.5671 (3)	0.9635 (2)	0.66995 (19)	0.0587 (10)
H47	0.5845	1.0070	0.7011	0.070*
C48	0.6002 (3)	0.8962 (2)	0.68920 (17)	0.0554 (10)
H48	0.6418	0.8932	0.7335	0.066*
C49	0.5728 (3)	0.8323 (2)	0.64370 (15)	0.0424 (7)
H49	0.5968	0.7864	0.6580	0.051*
C50	0.0877 (3)	0.02898 (18)	0.79401 (16)	0.0399 (7)
C51	0.0140 (3)	0.0772 (2)	0.8103 (2)	0.0624 (11)
H51	-0.0269	0.1008	0.7745	0.075*
C52	-0.0008 (4)	0.0920 (3)	0.8829 (3)	0.0796 (16)
H52	-0.0520	0.1256	0.8946	0.096*
C53	0.0579 (5)	0.0583 (3)	0.9357 (2)	0.091 (2)
H53	0.0464	0.0689	0.9830	0.109*

C54	0.1320 (4)	0.0101 (3)	0.92053 (19)	0.0747 (15)
C55	0.2006 (5)	-0.0284 (3)	0.97193 (18)	0.0815 (18)
H55	0.1913	-0.0215	1.0201	0.098*
C56	0.2750 (5)	-0.0724 (3)	0.9535 (2)	0.0878 (19)
H56	0.3166	-0.0959	0.9890	0.105*
C57	0.2947 (4)	-0.0855 (2)	0.88362 (19)	0.0631 (13)
C58	0.3721 (3)	-0.1295 (2)	0.8590 (3)	0.0747 (15)
H58	0.4174	-0.1548	0.8911	0.090*
C59	0.3831 (3)	-0.1364 (2)	0.7915 (3)	0.0725 (14)
H59	0.4362	-0.1665	0.7758	0.087*
C60	0.3178 (3)	-0.10013 (19)	0.7430 (2)	0.0488 (9)
H60	0.3287	-0.1048	0.6950	0.059*
C61	0.2267 (3)	-0.04995 (19)	0.83217 (16)	0.0440 (8)
C62	0.1468 (3)	-0.0037 (2)	0.84964 (16)	0.0505 (9)
C63	-0.0365 (3)	-0.01555 (18)	0.63994 (15)	0.0366 (7)
C64	0.0378 (3)	0.03044 (19)	0.60338 (15)	0.0409 (7)
C65	0.1214 (3)	-0.0159 (2)	0.58113 (15)	0.0492 (9)
C66	0.0973 (3)	-0.0876 (2)	0.60683 (17)	0.0484 (9)
C67	0.0027 (3)	-0.08731 (18)	0.64756 (15)	0.0406 (7)
C68	-0.1441 (3)	0.0039 (2)	0.6653 (2)	0.0554 (9)
H68A	-0.1454	0.0583	0.6648	0.083*
H68B	-0.1483	-0.0119	0.7132	0.083*
H68C	-0.2089	-0.0222	0.6347	0.083*
C69	0.0302 (3)	0.1100 (2)	0.5839 (2)	0.0636 (11)
H69A	-0.0153	0.1340	0.6156	0.095*
H69B	-0.0053	0.1097	0.5357	0.095*
H69C	0.1062	0.1382	0.5878	0.095*
C70	0.2118 (4)	0.0112 (3)	0.53637 (19)	0.0800 (15)
H70A	0.2728	-0.0203	0.5419	0.120*
H70B	0.2420	0.0636	0.5508	0.120*
H70C	0.1797	0.0080	0.4873	0.120*
C71	0.1551 (4)	-0.1560 (3)	0.5937 (2)	0.0836 (16)
H71A	0.1111	-0.1884	0.5556	0.125*
H71B	0.1609	-0.1839	0.6362	0.125*
H71C	0.2310	-0.1401	0.5808	0.125*
C72	-0.0561 (4)	-0.1531 (2)	0.6808 (2)	0.0607 (11)
H72A	-0.0996	-0.1347	0.7168	0.091*

H72B	0.0000	-0.1827	0.7022	0.091*
H72C	-0.1072	-0.1847	0.6450	0.091*
C73	0.3267 (3)	0.13687 (17)	0.72470 (13)	0.0297 (6)
C74	0.4145 (3)	0.20145 (17)	0.73829 (15)	0.0367 (6)
H74A	0.3935	0.2361	0.7740	0.055*
H74B	0.4227	0.2274	0.6951	0.055*
H74C	0.4863	0.1842	0.7549	0.055*
C75	0.4911 (2)	0.31419 (14)	1.02063 (13)	0.0255 (5)
C76	0.5938 (2)	0.30433 (15)	1.05854 (13)	0.0265 (5)
H76	0.6263	0.2601	1.0483	0.032*
C77	0.6507 (2)	0.35622 (16)	1.11050 (14)	0.0325 (6)
H77	0.7196	0.3467	1.1352	0.039*
C78	0.6059 (3)	0.42181 (17)	1.12587 (16)	0.0383 (7)
H78	0.6434	0.4573	1.1615	0.046*
C79	0.5063 (3)	0.43481 (17)	1.08880 (16)	0.0391 (7)
H79	0.4759	0.4801	1.0982	0.047*
C80	0.4499 (2)	0.38194 (16)	1.03754 (15)	0.0325 (6)
H80	0.3811	0.3921	1.0131	0.039*
C81	0.3412 (2)	0.28157 (15)	0.90302 (13)	0.0290 (6)
C82	0.3802 (3)	0.34653 (17)	0.87063 (15)	0.0393 (7)
H82	0.4497	0.3750	0.8896	0.047*
C83	0.3214 (4)	0.37109 (19)	0.81182 (17)	0.0511 (9)
H83	0.3510	0.4156	0.7915	0.061*
C84	0.2209 (3)	0.3312 (2)	0.78307 (16)	0.0483 (9)
H84	0.1807	0.3477	0.7428	0.058*
C85	0.1788 (3)	0.2670 (2)	0.81324 (16)	0.0461 (8)
H85	0.1089	0.2394	0.7938	0.055*
C86	0.2380 (2)	0.24240 (18)	0.87213 (14)	0.0350 (6)
H86	0.2076	0.1978	0.8919	0.042*
C87	0.3360 (2)	0.20035 (14)	1.01896 (13)	0.0245 (5)
C88	0.2393 (2)	0.22840 (16)	1.03981 (14)	0.0308 (6)
H88	0.2165	0.2720	1.0192	0.037*
C89	0.1758 (2)	0.19498 (19)	1.08917 (15)	0.0372 (7)
H89	0.1111	0.2158	1.1014	0.045*
C90	0.2063 (3)	0.13172 (18)	1.12063 (15)	0.0378 (7)
H90	0.1633	0.1089	1.1546	0.045*
C91	0.3007 (3)	0.10215 (17)	1.10166 (14)	0.0347 (6)

H91	0.3232	0.0588	1.1229	0.042*
C92	0.3625 (2)	0.13572 (15)	1.05177 (13)	0.0272 (5)
H92	0.4261	0.1137	1.0392	0.033*
C93	0.4973 (2)	0.19521 (14)	0.92740 (13)	0.0243 (5)
C94	0.4604 (2)	0.12021 (15)	0.90343 (13)	0.0286 (5)
H94	0.3889	0.0972	0.9138	0.034*
C95	0.5254 (3)	0.07822 (16)	0.86475 (14)	0.0336 (6)
H95	0.4975	0.0276	0.8495	0.040*
C96	0.6298 (3)	0.10947 (17)	0.84852 (15)	0.0363 (7)
H96	0.6744	0.0806	0.8229	0.044*
C97	0.6680 (3)	0.18310 (18)	0.87015 (15)	0.0366 (7)
H97	0.7392	0.2057	0.8588	0.044*
C98	0.6027 (2)	0.22494 (16)	0.90872 (14)	0.0311 (6)
H98	0.6311	0.2758	0.9229	0.037*
C99	0.0108 (3)	0.5569 (2)	0.45446 (18)	0.0510 (9)
H99	0.0182	0.5961	0.4231	0.061*
C100	0.1053 (3)	0.5362 (2)	0.49164 (18)	0.0477 (8)
H100	0.1781	0.5612	0.4859	0.057*
C101	0.0944 (3)	0.4795 (2)	0.53699 (18)	0.0507 (9)
H101	0.1597	0.4653	0.5625	0.061*
N1	0.17402 (18)	0.47706 (12)	0.12624 (11)	0.0255 (4)
N2	0.26309 (18)	0.37307 (13)	0.21260 (11)	0.0261 (4)
N3	0.2394 (2)	-0.05859 (15)	0.76298 (13)	0.0395 (6)
N4	0.2584 (2)	0.08670 (14)	0.71424 (11)	0.0318 (5)
B1	0.4822 (3)	0.75548 (19)	0.52593 (15)	0.0297 (6)
B2	0.4162 (3)	0.24732 (17)	0.96738 (15)	0.0251 (6)
Ir1	0.14468 (2)	0.44260 (2)	0.22653 (2)	0.02344 (3)
Ir2	0.13264 (2)	-0.00262 (2)	0.69704 (2)	0.02910 (3)

7.7.9 **Table A20.** Atomic displacement parameters (Å^2) for [**4**][BPh_4].

	U^{11}	U^{22}	U^{33}	U^{12}	U^{13}	U^{23}
C1	0.0195 (12)	0.0212 (13)	0.0327 (13)	0.0027 (9)	0.0030 (10)	0.0001 (10)
C2	0.0315 (15)	0.0307 (16)	0.0505 (17)	-0.0020 (12)	0.0115 (13)	0.0017 (13)
C3	0.0262 (15)	0.0310 (17)	0.080 (3)	-0.0072 (12)	0.0084 (15)	-0.0071 (16)

C4	0.0273 (15)	0.0408 (19)	0.065 (2)	-0.0020 (13)	-0.0074 (15)	-0.0172 (16)
C5	0.0310 (15)	0.0384 (18)	0.0431 (16)	0.0058 (13)	-0.0066 (12)	-0.0092 (13)
C6	0.065 (2)	0.069 (3)	0.0358 (17)	0.001 (2)	-0.0172 (17)	-0.0145 (17)
C7	0.072 (3)	0.084 (3)	0.0281 (16)	0.004 (2)	-0.0067 (17)	-0.0010 (17)
C8	0.0490 (19)	0.051 (2)	0.0284 (14)	0.0089 (16)	0.0025 (13)	0.0083 (13)
C9	0.065 (2)	0.061 (2)	0.0353 (16)	0.0083 (19)	0.0154 (16)	0.0200 (16)
C10	0.0470 (19)	0.0396 (19)	0.0544 (19)	0.0026 (15)	0.0197 (16)	0.0203 (15)
C11	0.0321 (15)	0.0234 (14)	0.0457 (16)	0.0001 (11)	0.0077 (12)	0.0041 (12)
C12	0.0259 (13)	0.0302 (15)	0.0276 (12)	0.0074 (11)	0.0013 (10)	0.0012 (10)
C13	0.0215 (12)	0.0275 (14)	0.0321 (13)	0.0045 (10)	0.0005 (10)	-0.0030 (10)
C14	0.0317 (15)	0.0454 (19)	0.0373 (15)	0.0066 (13)	-0.0042 (12)	-0.0176 (13)
C15	0.0438 (18)	0.056 (2)	0.0244 (13)	0.0261 (15)	-0.0035 (12)	-0.0080 (13)
C16	0.0503 (19)	0.0381 (17)	0.0247 (12)	0.0191 (14)	0.0066 (12)	-0.0008 (11)
C17	0.0286 (14)	0.0345 (16)	0.0277 (12)	0.0129 (11)	0.0035 (10)	-0.0023 (11)
C18	0.0353 (15)	0.0283 (15)	0.0281 (13)	0.0076 (12)	-0.0007 (11)	-0.0093 (11)
C19	0.039 (2)	0.078 (3)	0.072 (3)	-0.0063 (19)	-0.0066 (18)	-0.035 (2)
C20	0.072 (3)	0.101 (3)	0.0364 (17)	0.054 (3)	-0.0122 (17)	-0.0023 (19)
C21	0.082 (3)	0.052 (2)	0.0363 (16)	0.021 (2)	0.0252 (17)	0.0121 (15)
C22	0.0308 (16)	0.047 (2)	0.0482 (17)	0.0118 (14)	0.0077 (13)	-0.0005 (14)
C23	0.056 (2)	0.0272 (16)	0.0483 (18)	0.0058 (14)	0.0053 (15)	-0.0066 (13)
C24	0.0278 (13)	0.0285 (14)	0.0204 (11)	0.0033 (11)	0.0026 (9)	0.0014 (9)
C25	0.0321 (15)	0.0353 (16)	0.0325 (13)	0.0144 (12)	0.0035 (11)	0.0023 (11)
C26	0.0245 (13)	0.0384 (16)	0.0282 (13)	-0.0032 (11)	-0.0025 (10)	0.0081 (11)
C27	0.0397 (17)	0.049 (2)	0.0342 (15)	-0.0103 (14)	0.0068 (13)	0.0034 (14)
C28	0.045 (2)	0.072 (3)	0.0361 (16)	-0.0231 (18)	0.0081 (14)	0.0095 (16)
C29	0.0384 (19)	0.059 (2)	0.060 (2)	-0.0123 (16)	-0.0035 (16)	0.0325 (19)
C30	0.0375 (18)	0.044 (2)	0.077 (3)	0.0022 (15)	0.0068 (17)	0.0227 (18)
C31	0.0306 (16)	0.0444 (19)	0.0531 (18)	0.0043 (13)	0.0109 (14)	0.0175 (15)
C32	0.0355 (15)	0.0250 (14)	0.0263 (12)	0.0059 (11)	0.0022 (10)	-0.0020 (10)
C33	0.0331 (15)	0.0313 (16)	0.0363 (14)	0.0054 (12)	0.0002 (12)	-0.0030 (12)
C34	0.0350 (17)	0.0378 (18)	0.060 (2)	0.0075 (14)	-0.0090 (15)	-0.0067 (15)
C35	0.056 (2)	0.0384 (19)	0.0443 (17)	0.0192 (16)	-0.0166 (15)	-0.0071 (14)
C36	0.066 (2)	0.0399 (19)	0.0337 (15)	0.0218 (17)	-0.0004 (15)	0.0050 (13)
C37	0.0397 (17)	0.0407 (18)	0.0319 (14)	0.0102 (13)	0.0018 (12)	0.0038 (12)
C38	0.0295 (14)	0.0329 (15)	0.0302 (13)	0.0013 (11)	0.0023 (11)	0.0134 (11)
C39	0.0341 (16)	0.0400 (18)	0.0412 (16)	0.0040 (13)	0.0060 (13)	0.0059 (13)
C40	0.054 (2)	0.041 (2)	0.055 (2)	0.0130 (16)	0.0205 (17)	0.0077 (16)

C41	0.040 (2)	0.058 (2)	0.077 (3)	0.0176 (17)	0.0246 (18)	0.029 (2)
C42	0.0304 (17)	0.072 (3)	0.062 (2)	0.0041 (17)	0.0041 (15)	0.025 (2)
C43	0.0345 (17)	0.053 (2)	0.0414 (17)	-0.0032 (14)	0.0022 (13)	0.0129 (15)
C44	0.0333 (15)	0.0394 (17)	0.0262 (13)	-0.0069 (12)	0.0069 (11)	0.0014 (11)
C45	0.0461 (18)	0.0393 (18)	0.0350 (15)	-0.0024 (14)	0.0051 (13)	-0.0025 (13)
C46	0.063 (2)	0.040 (2)	0.054 (2)	-0.0090 (17)	0.0125 (18)	-0.0068 (16)
C47	0.064 (2)	0.056 (2)	0.047 (2)	-0.0237 (19)	0.0130 (18)	-0.0197 (18)
C48	0.057 (2)	0.068 (3)	0.0309 (16)	-0.0252 (19)	0.0004 (15)	-0.0031 (16)
C49	0.0436 (18)	0.049 (2)	0.0298 (14)	-0.0113 (15)	0.0010 (13)	0.0036 (13)
C50	0.0378 (17)	0.0401 (18)	0.0382 (15)	-0.0081 (13)	0.0085 (13)	-0.0105 (13)
C51	0.052 (2)	0.060 (3)	0.072 (3)	-0.0072 (18)	0.0223 (19)	-0.026 (2)
C52	0.071 (3)	0.070 (3)	0.095 (4)	-0.021 (2)	0.049 (3)	-0.037 (3)
C53	0.113 (4)	0.089 (4)	0.054 (3)	-0.062 (3)	0.038 (3)	-0.029 (3)
C54	0.089 (3)	0.082 (3)	0.0361 (19)	-0.060 (3)	0.020 (2)	-0.0152 (19)
C55	0.111 (4)	0.090 (4)	0.0186 (15)	-0.072 (3)	-0.006 (2)	0.0074 (18)
C56	0.094 (4)	0.094 (4)	0.050 (3)	-0.065 (3)	-0.028 (2)	0.034 (2)
C57	0.061 (2)	0.058 (2)	0.051 (2)	-0.043 (2)	-0.0295 (18)	0.0330 (18)
C58	0.040 (2)	0.060 (3)	0.112 (4)	-0.0209 (19)	-0.036 (2)	0.055 (3)
C59	0.039 (2)	0.052 (2)	0.122 (4)	0.0007 (17)	-0.025 (2)	0.047 (3)
C60	0.0290 (16)	0.0385 (19)	0.077 (2)	0.0038 (13)	-0.0106 (15)	0.0184 (17)
C61	0.0447 (18)	0.0413 (19)	0.0359 (15)	-0.0222 (15)	-0.0144 (13)	0.0148 (13)
C62	0.059 (2)	0.053 (2)	0.0279 (15)	-0.0339 (18)	0.0023 (14)	-0.0016 (14)
C63	0.0341 (16)	0.0385 (17)	0.0357 (14)	0.0075 (13)	-0.0072 (12)	0.0057 (12)
C64	0.0359 (17)	0.050 (2)	0.0359 (15)	0.0089 (14)	-0.0091 (12)	0.0127 (14)
C65	0.0424 (19)	0.078 (3)	0.0250 (14)	0.0096 (18)	-0.0045 (13)	-0.0034 (15)
C66	0.052 (2)	0.051 (2)	0.0396 (16)	0.0227 (17)	-0.0173 (15)	-0.0151 (15)
C67	0.0448 (18)	0.0375 (18)	0.0354 (15)	0.0063 (14)	-0.0145 (13)	-0.0010 (13)
C68	0.0338 (18)	0.066 (3)	0.067 (2)	0.0121 (17)	0.0015 (16)	0.0073 (19)
C69	0.061 (2)	0.057 (2)	0.070 (3)	0.0072 (19)	-0.016 (2)	0.032 (2)
C70	0.055 (2)	0.149 (5)	0.0352 (19)	0.008 (3)	0.0064 (17)	0.006 (2)
C71	0.081 (3)	0.081 (3)	0.086 (3)	0.043 (3)	-0.022 (2)	-0.045 (3)
C72	0.075 (3)	0.036 (2)	0.062 (2)	-0.0070 (18)	-0.017 (2)	0.0023 (17)
C73	0.0389 (16)	0.0310 (15)	0.0222 (12)	0.0134 (13)	0.0055 (11)	0.0049 (10)
C74	0.0432 (17)	0.0346 (17)	0.0334 (14)	0.0036 (13)	0.0098 (12)	0.0041 (12)
C75	0.0292 (13)	0.0200 (13)	0.0282 (12)	0.0024 (10)	0.0089 (10)	0.0014 (10)
C76	0.0302 (14)	0.0195 (13)	0.0308 (12)	0.0025 (10)	0.0085 (10)	0.0021 (10)
C77	0.0300 (14)	0.0317 (15)	0.0349 (14)	0.0002 (11)	0.0035 (11)	0.0020 (11)

C78	0.0412 (17)	0.0310 (16)	0.0399 (15)	-0.0014 (13)	0.0050 (13)	-0.0115 (12)
C79	0.0468 (18)	0.0233 (15)	0.0478 (17)	0.0091 (13)	0.0069 (14)	-0.0091 (12)
C80	0.0331 (15)	0.0248 (14)	0.0405 (15)	0.0099 (11)	0.0030 (12)	-0.0013 (11)
C81	0.0367 (15)	0.0222 (13)	0.0299 (13)	0.0106 (11)	0.0055 (11)	-0.0005 (10)
C82	0.058 (2)	0.0222 (15)	0.0373 (15)	0.0064 (13)	0.0030 (14)	0.0007 (12)
C83	0.093 (3)	0.0270 (17)	0.0382 (16)	0.0219 (18)	0.0104 (18)	0.0082 (13)
C84	0.066 (2)	0.053 (2)	0.0338 (15)	0.0374 (19)	0.0015 (15)	0.0066 (15)
C85	0.0417 (18)	0.062 (2)	0.0370 (16)	0.0210 (16)	-0.0011 (13)	0.0024 (15)
C86	0.0343 (16)	0.0398 (17)	0.0329 (14)	0.0113 (13)	0.0044 (12)	0.0049 (12)
C87	0.0239 (12)	0.0226 (13)	0.0262 (11)	0.0028 (10)	0.0000 (9)	-0.0017 (9)
C88	0.0293 (14)	0.0317 (15)	0.0330 (13)	0.0096 (11)	0.0044 (11)	0.0007 (11)
C89	0.0297 (15)	0.0491 (19)	0.0347 (14)	0.0102 (13)	0.0082 (12)	-0.0015 (13)
C90	0.0409 (17)	0.0437 (18)	0.0285 (13)	0.0006 (14)	0.0088 (12)	0.0017 (12)
C91	0.0455 (17)	0.0300 (15)	0.0278 (13)	0.0054 (13)	-0.0012 (12)	0.0032 (11)
C92	0.0251 (13)	0.0275 (14)	0.0293 (12)	0.0067 (10)	0.0007 (10)	-0.0001 (10)
C93	0.0277 (13)	0.0192 (12)	0.0259 (11)	0.0036 (10)	0.0024 (10)	0.0015 (9)
C94	0.0288 (14)	0.0254 (14)	0.0313 (13)	0.0024 (11)	0.0045 (10)	-0.0005 (10)
C95	0.0457 (17)	0.0230 (14)	0.0336 (14)	0.0098 (12)	0.0062 (12)	-0.0021 (11)
C96	0.0413 (17)	0.0347 (17)	0.0347 (14)	0.0100 (13)	0.0102 (12)	-0.0054 (12)
C97	0.0311 (15)	0.0408 (18)	0.0379 (15)	0.0018 (13)	0.0103 (12)	-0.0032 (13)
C98	0.0355 (15)	0.0230 (14)	0.0341 (14)	0.0000 (11)	0.0066 (11)	-0.0027 (11)
C99	0.074 (3)	0.0361 (19)	0.0455 (18)	0.0093 (18)	0.0169 (18)	-0.0001 (15)
C100	0.0444 (19)	0.041 (2)	0.057 (2)	-0.0029 (15)	0.0187 (16)	-0.0111 (16)
C101	0.051 (2)	0.051 (2)	0.0504 (19)	0.0147 (17)	0.0004 (16)	-0.0092 (17)
N1	0.0234 (11)	0.0231 (11)	0.0300 (11)	0.0030 (9)	0.0042 (8)	-0.0001 (9)
N2	0.0255 (11)	0.0282 (12)	0.0247 (10)	0.0034 (9)	0.0032 (8)	0.0005 (8)
N3	0.0308 (13)	0.0374 (15)	0.0464 (14)	-0.0025 (11)	-0.0123 (11)	0.0165 (11)
N4	0.0393 (14)	0.0320 (14)	0.0260 (11)	0.0119 (11)	0.0025 (10)	0.0041 (9)
B1	0.0293 (16)	0.0324 (17)	0.0263 (14)	0.0001 (13)	0.0018 (12)	0.0039 (12)
B2	0.0270 (15)	0.0201 (14)	0.0283 (13)	0.0038 (11)	0.0037 (11)	0.0001 (11)
Ir1	0.02173 (5)	0.02462 (5)	0.02403 (5)	0.00489 (4)	0.00167 (4)	-0.00115 (4)
Ir2	0.03068 (6)	0.03062 (6)	0.02602 (5)	0.01060 (4)	-0.00437 (4)	0.00107 (4)

7.7.10 **Table A21.** Interatomic distances (Å) and angles (deg) for [**4**][BPh_4]

C1—C2	1.380 (4)	C52—H52	0.9500

C1—C13	1.408 (4)	C53—C54	1.360 (8)
C1—Ir1	2.065 (2)	C53—H53	0.9500
C2—C3	1.404 (4)	C54—C62	1.410 (5)
C2—H2	0.9500	C54—C55	1.474 (7)
C3—C4	1.360 (5)	C55—C56	1.328 (7)
C3—H3	0.9500	C55—H55	0.9500
C4—C5	1.399 (5)	C56—C57	1.405 (7)
C4—H4	0.9500	C56—H56	0.9500
C5—C13	1.416 (4)	C57—C58	1.399 (7)
C5—C6	1.439 (5)	C57—C61	1.441 (5)
C6—C7	1.324 (6)	C58—C59	1.322 (7)
C6—H6	0.9500	C58—H58	0.9500
C7—C8	1.436 (5)	C59—C60	1.393 (4)
C7—H7	0.9500	C59—H59	0.9500
C8—C9	1.390 (5)	C60—N3	1.348 (4)
C8—C12	1.415 (4)	C60—H60	0.9500
C9—C10	1.362 (5)	C61—N3	1.361 (4)
C9—H9	0.9500	C61—C62	1.402 (5)
C10—C11	1.393 (4)	C63—C64	1.405 (5)
C10—H10	0.9500	C63—C67	1.434 (4)
C11—N1	1.339 (4)	C63—C68	1.504 (4)
C11—H11	0.9500	C63—Ir2	2.187 (3)
C12—N1	1.371 (3)	C64—C65	1.466 (5)
C12—C13	1.410 (4)	C64—C69	1.504 (5)
C14—C15	1.428 (5)	C64—Ir2	2.178 (3)
C14—C18	1.437 (4)	C65—C66	1.406 (5)
C14—C19	1.499 (5)	C65—C70	1.504 (5)
C14—Ir1	2.247 (3)	C65—Ir2	2.222 (3)
C15—C16	1.431 (5)	C66—C67	1.447 (5)
C15—C20	1.510 (4)	C66—C71	1.508 (5)
C15—Ir1	2.206 (3)	C66—Ir2	2.228 (3)
C16—C17	1.446 (4)	C67—C72	1.501 (5)
C16—C21	1.500 (5)	C67—Ir2	2.148 (3)
C16—Ir1	2.171 (3)	C68—H68A	0.9800
C17—C18	1.433 (4)	C68—H68B	0.9800
C17—C22	1.501 (4)	C68—H68C	0.9800
C17—Ir1	2.143 (2)	C69—H69A	0.9800

C18—C23	1.496 (4)	C69—H69B	0.9800
C18—Ir1	2.188 (3)	C69—H69C	0.9800
C19—H19A	0.9800	C70—H70A	0.9800
C19—H19B	0.9800	C70—H70B	0.9800
C19—H19C	0.9800	C70—H70C	0.9800
C20—H20A	0.9800	C71—H71A	0.9800
C20—H20B	0.9800	C71—H71B	0.9800
C20—H20C	0.9800	C71—H71C	0.9800
C21—H21A	0.9800	C72—H72A	0.9800
C21—H21B	0.9800	C72—H72B	0.9800
C21—H21C	0.9800	C72—H72C	0.9800
C22—H22A	0.9800	C73—N4	1.134 (4)
C22—H22B	0.9800	C73—C74	1.459 (4)
C22—H22C	0.9800	C74—H74A	0.9800
C23—H23A	0.9800	C74—H74B	0.9800
C23—H23B	0.9800	C74—H74C	0.9800
C23—H23C	0.9800	C75—C76	1.402 (4)
C24—N2	1.134 (3)	C75—C80	1.406 (3)
C24—C25	1.454 (3)	C75—B2	1.650 (4)
C25—H25A	0.9800	C76—C77	1.395 (4)
C25—H25B	0.9800	C76—H76	0.9500
C25—H25C	0.9800	C77—C78	1.386 (4)
C26—C31	1.399 (4)	C77—H77	0.9500
C26—C27	1.400 (4)	C78—C79	1.380 (4)
C26—B1	1.651 (4)	C78—H78	0.9500
C27—C28	1.395 (5)	C79—C80	1.395 (4)
C27—H27	0.9500	C79—H79	0.9500
C28—C29	1.374 (6)	C80—H80	0.9500
C28—H28	0.9500	C81—C82	1.399 (4)
C29—C30	1.371 (5)	C81—C86	1.405 (4)
C29—H29	0.9500	C81—B2	1.644 (4)
C30—C31	1.394 (5)	C82—C83	1.390 (4)
C30—H30	0.9500	C82—H82	0.9500
C31—H31	0.9500	C83—C84	1.373 (5)
C32—C33	1.400 (4)	C83—H83	0.9500
C32—C37	1.402 (4)	C84—C85	1.377 (5)
C32—B1	1.645 (4)	C84—H84	0.9500

C33—C34	1.394 (4)	C85—C86	1.395 (4)
C33—H33	0.9500	C85—H85	0.9500
C34—C35	1.369 (5)	C86—H86	0.9500
C34—H34	0.9500	C87—C92	1.401 (4)
C35—C36	1.373 (5)	C87—C88	1.411 (3)
C35—H35	0.9500	C87—B2	1.643 (4)
C36—C37	1.390 (4)	C88—C89	1.390 (4)
C36—H36	0.9500	C88—H88	0.9500
C37—H37	0.9500	C89—C90	1.382 (4)
C38—C43	1.396 (4)	C89—H89	0.9500
C38—C39	1.406 (4)	C90—C91	1.387 (4)
C38—B1	1.651 (4)	C90—H90	0.9500
C39—C40	1.388 (4)	C91—C92	1.388 (4)
C39—H39	0.9500	C91—H91	0.9500
C40—C41	1.385 (5)	C92—H92	0.9500
C40—H40	0.9500	C93—C98	1.401 (4)
C41—C42	1.368 (5)	C93—C94	1.404 (4)
C41—H41	0.9500	C93—B2	1.654 (4)
C42—C43	1.391 (5)	C94—C95	1.397 (4)
C42—H42	0.9500	C94—H94	0.9500
C43—H43	0.9500	C95—C96	1.380 (4)
C44—C45	1.393 (4)	C95—H95	0.9500
C44—C49	1.402 (4)	C96—C97	1.374 (4)
C44—B1	1.652 (4)	C96—H96	0.9500
C45—C46	1.399 (4)	C97—C98	1.396 (4)
C45—H45	0.9500	C97—H97	0.9500
C46—C47	1.370 (5)	C98—H98	0.9500
C46—H46	0.9500	C99—C101^{i}	1.377 (5)
C47—C48	1.372 (6)	C99—C100	1.379 (5)
C47—H47	0.9500	C99—H99	0.9500
C48—C49	1.394 (5)	C100—C101	1.374 (5)
C48—H48	0.9500	C100—H100	0.9500
C49—H49	0.9500	C101—C99^{i}	1.377 (5)
C50—C51	1.363 (5)	C101—H101	0.9500
C50—C62	1.414 (5)	N1—Ir1	2.106 (2)
C50—Ir2	2.072 (3)	N2—Ir1	2.037 (2)
C51—C52	1.446 (6)	N3—Ir2	2.089 (2)

C51—H51	0.9500	N4—Ir2	2.049 (3)
C52—C53	1.382 (7)		
C2—C1—C13	116.0 (2)	C67—C63—Ir2	69.21 (16)
C2—C1—Ir1	130.1 (2)	C68—C63—Ir2	128.3 (2)
C13—C1—Ir1	113.83 (19)	C63—C64—C65	107.0 (3)
C1—C2—C3	121.4 (3)	C63—C64—C69	127.9 (3)
C1—C2—H2	119.3	C65—C64—C69	124.9 (3)
C3—C2—H2	119.3	C63—C64—Ir2	71.58 (16)
C4—C3—C2	121.9 (3)	C65—C64—Ir2	72.20 (16)
C4—C3—H3	119.1	C69—C64—Ir2	125.6 (2)
C2—C3—H3	119.1	C66—C65—C64	107.7 (3)
C3—C4—C5	119.7 (3)	C66—C65—C70	128.5 (4)
C3—C4—H4	120.2	C64—C65—C70	123.7 (4)
C5—C4—H4	120.2	C66—C65—Ir2	71.80 (18)
C4—C5—C13	117.6 (3)	C64—C65—Ir2	68.89 (16)
C4—C5—C6	124.7 (3)	C70—C65—Ir2	126.4 (2)
C13—C5—C6	117.7 (3)	C65—C66—C67	108.8 (3)
C7—C6—C5	121.8 (3)	C65—C66—C71	127.4 (4)
C7—C6—H6	119.1	C67—C66—C71	123.8 (4)
C5—C6—H6	119.1	C65—C66—Ir2	71.36 (18)
C6—C7—C8	122.6 (3)	C67—C66—Ir2	67.70 (17)
C6—C7—H7	118.7	C71—C66—Ir2	128.3 (2)
C8—C7—H7	118.7	C63—C67—C66	106.4 (3)
C9—C8—C12	117.4 (3)	C63—C67—C72	125.8 (3)
C9—C8—C7	126.1 (3)	C66—C67—C72	127.0 (3)
C12—C8—C7	116.6 (3)	C63—C67—Ir2	72.16 (18)
C10—C9—C8	120.4 (3)	C66—C67—Ir2	73.73 (19)
C10—C9—H9	119.8	C72—C67—Ir2	127.1 (2)
C8—C9—H9	119.8	C63—C68—H68A	109.5
C9—C10—C11	119.7 (3)	C63—C68—H68B	109.5
C9—C10—H10	120.1	H68A—C68—H68B	109.5
C11—C10—H10	120.1	C63—C68—H68C	109.5
N1—C11—C10	122.1 (3)	H68A—C68—H68C	109.5
N1—C11—H11	118.9	H68B—C68—H68C	109.5
C10—C11—H11	118.9	C64—C69—H69A	109.5
N1—C12—C13	116.3 (2)	C64—C69—H69B	109.5

N1—C12—C8	122.0 (3)	H69A—C69—H69B	109.5
C13—C12—C8	121.7 (3)	C64—C69—H69C	109.5
C1—C13—C12	116.8 (2)	H69A—C69—H69C	109.5
C1—C13—C5	123.5 (3)	H69B—C69—H69C	109.5
C12—C13—C5	119.7 (3)	C65—C70—H70A	109.5
C15—C14—C18	106.8 (3)	C65—C70—H70B	109.5
C15—C14—C19	126.7 (3)	H70A—C70—H70B	109.5
C18—C14—C19	126.3 (3)	C65—C70—H70C	109.5
C15—C14—Ir1	69.74 (16)	H70A—C70—H70C	109.5
C18—C14—Ir1	68.88 (15)	H70B—C70—H70C	109.5
C19—C14—Ir1	130.6 (2)	C66—C71—H71A	109.5
C14—C15—C16	109.8 (2)	C66—C71—H71B	109.5
C14—C15—C20	126.1 (3)	H71A—C71—H71B	109.5
C16—C15—C20	124.1 (3)	C66—C71—H71C	109.5
C14—C15—Ir1	72.87 (16)	H71A—C71—H71C	109.5
C16—C15—Ir1	69.62 (15)	H71B—C71—H71C	109.5
C20—C15—Ir1	125.3 (2)	C67—C72—H72A	109.5
C15—C16—C17	106.8 (3)	C67—C72—H72B	109.5
C15—C16—C21	126.1 (3)	H72A—C72—H72B	109.5
C17—C16—C21	126.5 (3)	C67—C72—H72C	109.5
C15—C16—Ir1	72.23 (17)	H72A—C72—H72C	109.5
C17—C16—Ir1	69.38 (15)	H72B—C72—H72C	109.5
C21—C16—Ir1	130.1 (2)	N4—C73—C74	179.9 (4)
C18—C17—C16	107.9 (2)	C73—C74—H74A	109.5
C18—C17—C22	126.2 (3)	C73—C74—H74B	109.5
C16—C17—C22	125.6 (3)	H74A—C74—H74B	109.5
C18—C17—Ir1	72.36 (15)	C73—C74—H74C	109.5
C16—C17—Ir1	71.46 (15)	H74A—C74—H74C	109.5
C22—C17—Ir1	126.04 (19)	H74B—C74—H74C	109.5
C17—C18—C14	108.7 (3)	C76—C75—C80	114.9 (2)
C17—C18—C23	126.0 (3)	C76—C75—B2	122.6 (2)
C14—C18—C23	125.2 (3)	C80—C75—B2	122.1 (2)
C17—C18—Ir1	69.02 (15)	C77—C76—C75	123.4 (2)
C14—C18—Ir1	73.35 (16)	C77—C76—H76	118.3
C23—C18—Ir1	126.34 (19)	C75—C76—H76	118.3
C14—C19—H19A	109.5	C78—C77—C76	119.6 (3)
C14—C19—H19B	109.5	C78—C77—H77	120.2

H19A—C19—H19B	109.5	C76—C77—H77	120.2
C14—C19—H19C	109.5	C79—C78—C77	119.1 (3)
H19A—C19—H19C	109.5	C79—C78—H78	120.4
H19B—C19—H19C	109.5	C77—C78—H78	120.4
C15—C20—H20A	109.5	C78—C79—C80	120.5 (3)
C15—C20—H20B	109.5	C78—C79—H79	119.8
H20A—C20—H20B	109.5	C80—C79—H79	119.8
C15—C20—H20C	109.5	C79—C80—C75	122.5 (3)
H20A—C20—H20C	109.5	C79—C80—H80	118.7
H20B—C20—H20C	109.5	C75—C80—H80	118.7
C16—C21—H21A	109.5	C82—C81—C86	115.5 (3)
C16—C21—H21B	109.5	C82—C81—B2	122.9 (3)
H21A—C21—H21B	109.5	C86—C81—B2	121.3 (3)
C16—C21—H21C	109.5	C83—C82—C81	122.6 (3)
H21A—C21—H21C	109.5	C83—C82—H82	118.7
H21B—C21—H21C	109.5	C81—C82—H82	118.7
C17—C22—H22A	109.5	C84—C83—C82	120.2 (3)
C17—C22—H22B	109.5	C84—C83—H83	119.9
H22A—C22—H22B	109.5	C82—C83—H83	119.9
C17—C22—H22C	109.5	C83—C84—C85	119.3 (3)
H22A—C22—H22C	109.5	C83—C84—H84	120.3
H22B—C22—H22C	109.5	C85—C84—H84	120.3
C18—C23—H23A	109.5	C84—C85—C86	120.4 (3)
C18—C23—H23B	109.5	C84—C85—H85	119.8
H23A—C23—H23B	109.5	C86—C85—H85	119.8
C18—C23—H23C	109.5	C85—C86—C81	122.0 (3)
H23A—C23—H23C	109.5	C85—C86—H86	119.0
H23B—C23—H23C	109.5	C81—C86—H86	119.0
N2—C24—C25	179.1 (3)	C92—C87—C88	114.5 (2)
C24—C25—H25A	109.5	C92—C87—B2	124.3 (2)
C24—C25—H25B	109.5	C88—C87—B2	120.8 (2)
H25A—C25—H25B	109.5	C89—C88—C87	122.8 (3)
C24—C25—H25C	109.5	C89—C88—H88	118.6
H25A—C25—H25C	109.5	C87—C88—H88	118.6
H25B—C25—H25C	109.5	C90—C89—C88	120.5 (3)
C31—C26—C27	115.1 (3)	C90—C89—H89	119.8
C31—C26—B1	122.8 (3)	C88—C89—H89	119.8

C27—C26—B1	122.0 (3)	C89—C90—C91	118.7 (3)
C28—C27—C26	122.3 (3)	C89—C90—H90	120.7
C28—C27—H27	118.8	C91—C90—H90	120.7
C26—C27—H27	118.8	C90—C91—C92	120.1 (3)
C29—C28—C27	120.4 (3)	C90—C91—H91	119.9
C29—C28—H28	119.8	C92—C91—H91	119.9
C27—C28—H28	119.8	C91—C92—C87	123.4 (2)
C30—C29—C28	119.1 (3)	C91—C92—H92	118.3
C30—C29—H29	120.4	C87—C92—H92	118.3
C28—C29—H29	120.4	C98—C93—C94	115.1 (2)
C29—C30—C31	120.2 (4)	C98—C93—B2	122.3 (2)
C29—C30—H30	119.9	C94—C93—B2	122.3 (2)
C31—C30—H30	119.9	C95—C94—C93	122.2 (3)
C30—C31—C26	122.7 (3)	C95—C94—H94	118.9
C30—C31—H31	118.6	C93—C94—H94	118.9
C26—C31—H31	118.6	C96—C95—C94	120.7 (3)
C33—C32—C37	114.9 (3)	C96—C95—H95	119.6
C33—C32—B1	123.7 (3)	C94—C95—H95	119.6
C37—C32—B1	121.4 (3)	C97—C96—C95	118.8 (3)
C34—C33—C32	122.1 (3)	C97—C96—H96	120.6
C34—C33—H33	119.0	C95—C96—H96	120.6
C32—C33—H33	119.0	C96—C97—C98	120.3 (3)
C35—C34—C33	120.9 (3)	C96—C97—H97	119.9
C35—C34—H34	119.6	C98—C97—H97	119.9
C33—C34—H34	119.6	C97—C98—C93	122.9 (3)
C34—C35—C36	119.2 (3)	C97—C98—H98	118.6
C34—C35—H35	120.4	C93—C98—H98	118.6
C36—C35—H35	120.4	C101^{i}—C99—C100	119.7 (3)
C35—C36—C37	119.8 (3)	C101^{i}—C99—H99	120.1
C35—C36—H36	120.1	C100—C99—H99	120.1
C37—C36—H36	120.1	C101—C100—C99	120.0 (3)
C36—C37—C32	123.1 (3)	C101—C100—H100	120.0
C36—C37—H37	118.4	C99—C100—H100	120.0
C32—C37—H37	118.4	C100—C101—C99^{i}	120.2 (3)
C43—C38—C39	114.8 (3)	C100—C101—H101	119.9
C43—C38—B1	124.0 (3)	C99^{i}—C101—H101	119.9
C39—C38—B1	121.1 (2)	C11—N1—C12	118.3 (2)

C40—C39—C38	123.0 (3)	C11—N1—Ir1	127.41 (19)
C40—C39—H39	118.5	C12—N1—Ir1	114.14 (18)
C38—C39—H39	118.5	C24—N2—Ir1	179.0 (2)
C41—C40—C39	119.9 (3)	C60—N3—C61	119.1 (3)
C41—C40—H40	120.1	C60—N3—Ir2	126.1 (2)
C39—C40—H40	120.1	C61—N3—Ir2	114.8 (2)
C42—C41—C40	118.9 (3)	C73—N4—Ir2	178.5 (2)
C42—C41—H41	120.6	C32—B1—C38	109.3 (2)
C40—C41—H41	120.6	C32—B1—C26	109.1 (2)
C41—C42—C43	120.8 (3)	C38—B1—C26	109.1 (2)
C41—C42—H42	119.6	C32—B1—C44	109.7 (2)
C43—C42—H42	119.6	C38—B1—C44	109.7 (2)
C42—C43—C38	122.6 (3)	C26—B1—C44	109.9 (2)
C42—C43—H43	118.7	C87—B2—C81	111.9 (2)
C38—C43—H43	118.7	C87—B2—C75	103.3 (2)
C45—C44—C49	115.0 (3)	C81—B2—C75	112.2 (2)
C45—C44—B1	124.5 (2)	C87—B2—C93	113.7 (2)
C49—C44—B1	120.5 (3)	C81—B2—C93	104.0 (2)
C44—C45—C46	122.6 (3)	C75—B2—C93	112.0 (2)
C44—C45—H45	118.7	N2—Ir1—C1	86.29 (9)
C46—C45—H45	118.7	N2—Ir1—N1	84.82 (8)
C47—C46—C45	120.2 (4)	C1—Ir1—N1	78.95 (9)
C47—C46—H46	119.9	N2—Ir1—C17	154.69 (10)
C45—C46—H46	119.9	C1—Ir1—C17	98.29 (10)
C46—C47—C48	119.4 (3)	N1—Ir1—C17	120.48 (9)
C46—C47—H47	120.3	N2—Ir1—C16	115.53 (9)
C48—C47—H47	120.3	C1—Ir1—C16	102.00 (11)
C47—C48—C49	119.9 (3)	N1—Ir1—C16	159.63 (9)
C47—C48—H48	120.0	C17—Ir1—C16	39.16 (10)
C49—C48—H48	120.0	N2—Ir1—C18	145.62 (10)
C48—C49—C44	122.8 (3)	C1—Ir1—C18	128.02 (10)
C48—C49—H49	118.6	N1—Ir1—C18	98.55 (10)
C44—C49—H49	118.6	C17—Ir1—C18	38.62 (11)
C51—C50—C62	117.9 (3)	C16—Ir1—C18	64.56 (11)
C51—C50—Ir2	129.2 (3)	N2—Ir1—C15	95.23 (9)
C62—C50—Ir2	112.9 (2)	C1—Ir1—C15	135.41 (12)
C50—C51—C52	118.9 (4)	N1—Ir1—C15	145.64 (12)

C50—C51—H51	120.6	C17—Ir1—C15	64.12 (10)
C52—C51—H51	120.6	C16—Ir1—C15	38.15 (12)
C53—C52—C51	121.4 (4)	C18—Ir1—C15	63.12 (11)
C53—C52—H52	119.3	N2—Ir1—C14	108.99 (10)
C51—C52—H52	119.3	C1—Ir1—C14	162.36 (10)
C54—C53—C52	120.7 (4)	N1—Ir1—C14	110.38 (11)
C54—C53—H53	119.7	C17—Ir1—C14	64.12 (11)
C52—C53—H53	119.7	C16—Ir1—C14	63.91 (12)
C53—C54—C62	117.7 (5)	C18—Ir1—C14	37.78 (10)
C53—C54—C55	125.8 (4)	C15—Ir1—C14	37.40 (12)
C62—C54—C55	116.5 (5)	N4—Ir2—C50	86.06 (11)
C56—C55—C54	122.5 (4)	N4—Ir2—N3	85.20 (9)
C56—C55—H55	118.7	C50—Ir2—N3	79.02 (12)
C54—C55—H55	118.7	N4—Ir2—C67	162.98 (11)
C55—C56—C57	122.7 (4)	C50—Ir2—C67	108.14 (13)
C55—C56—H56	118.7	N3—Ir2—C67	106.29 (11)
C57—C56—H56	118.7	N4—Ir2—C64	100.37 (11)
C58—C57—C56	127.1 (4)	C50—Ir2—C64	118.89 (13)
C58—C57—C61	117.0 (4)	N3—Ir2—C64	161.35 (12)
C56—C57—C61	115.9 (5)	C67—Ir2—C64	64.86 (12)
C59—C58—C57	120.8 (3)	N4—Ir2—C63	132.44 (10)
C59—C58—H58	119.6	C50—Ir2—C63	97.31 (12)
C57—C58—H58	119.6	N3—Ir2—C63	142.16 (11)
C58—C59—C60	120.9 (4)	C67—Ir2—C63	38.63 (11)
C58—C59—H59	119.5	C64—Ir2—C63	37.55 (12)
C60—C59—H59	119.5	N4—Ir2—C65	99.22 (12)
N3—C60—C59	121.3 (4)	C50—Ir2—C65	157.69 (13)
N3—C60—H60	119.3	N3—Ir2—C65	122.85 (12)
C59—C60—H60	119.3	C67—Ir2—C65	64.09 (13)
N3—C61—C62	116.2 (3)	C64—Ir2—C65	38.92 (12)
N3—C61—C57	120.7 (4)	C63—Ir2—C65	63.15 (12)
C62—C61—C57	123.0 (3)	N4—Ir2—C66	128.56 (13)
C61—C62—C54	119.4 (4)	C50—Ir2—C66	145.27 (14)
C61—C62—C50	117.1 (3)	N3—Ir2—C66	99.01 (11)
C54—C62—C50	123.5 (4)	C67—Ir2—C66	38.56 (13)
C64—C63—C67	109.6 (3)	C64—Ir2—C66	63.55 (12)
C64—C63—C68	126.8 (3)	C63—Ir2—C66	63.01 (11)

C67—C63—C68	123.6 (3)	C65—Ir2—C66	36.84 (14)
C64—C63—Ir2	70.87 (16)		
C13—C1—C2—C3	-0.4 (4)	C67—C63—C64—C65	5.4 (3)
Ir1—C1—C2—C3	-177.7 (2)	C68—C63—C64—C65	-172.1 (3)
C1—C2—C3—C4	-0.2 (5)	Ir2—C63—C64—C65	63.95 (19)
C2—C3—C4—C5	0.9 (5)	C67—C63—C64—C69	-179.7 (3)
C3—C4—C5—C13	-1.2 (5)	C68—C63—C64—C69	2.8 (5)
C3—C4—C5—C6	176.6 (3)	Ir2—C63—C64—C69	-121.2 (3)
C4—C5—C6—C7	-177.1 (4)	C67—C63—C64—Ir2	-58.5 (2)
C13—C5—C6—C7	0.7 (6)	C68—C63—C64—Ir2	124.0 (3)
C5—C6—C7—C8	-0.5 (7)	C63—C64—C65—C66	-1.9 (3)
C6—C7—C8—C9	-180.0 (4)	C69—C64—C65—C66	-177.0 (3)
C6—C7—C8—C12	-0.2 (6)	Ir2—C64—C65—C66	61.6 (2)
C12—C8—C9—C10	2.4 (5)	C63—C64—C65—C70	176.0 (3)
C7—C8—C9—C10	-177.8 (4)	C69—C64—C65—C70	0.9 (5)
C8—C9—C10—C11	-1.8 (5)	Ir2—C64—C65—C70	-120.5 (3)
C9—C10—C11—N1	0.1 (5)	C63—C64—C65—Ir2	-63.5 (2)
C9—C8—C12—N1	-1.4 (4)	C69—C64—C65—Ir2	121.4 (3)
C7—C8—C12—N1	178.8 (3)	C64—C65—C66—C67	-2.3 (3)
C9—C8—C12—C13	-179.4 (3)	C70—C65—C66—C67	180.0 (3)
C7—C8—C12—C13	0.8 (4)	Ir2—C65—C66—C67	57.5 (2)
C2—C1—C13—C12	-177.1 (2)	C64—C65—C66—C71	175.8 (3)
Ir1—C1—C13—C12	0.6 (3)	C70—C65—C66—C71	-1.9 (5)
C2—C1—C13—C5	0.1 (4)	Ir2—C65—C66—C71	-124.4 (3)
Ir1—C1—C13—C5	177.9 (2)	C64—C65—C66—Ir2	-59.8 (2)
N1—C12—C13—C1	-1.4 (3)	C70—C65—C66—Ir2	122.5 (3)
C8—C12—C13—C1	176.7 (2)	C64—C63—C67—C66	-6.8 (3)

N1—C12—C13—C5	-178.8 (2)	C68—C63—C67—C66	170.8 (3)
C8—C12—C13—C5	-0.7 (4)	Ir2—C63—C67—C66	-66.3 (2)
C4—C5—C13—C1	0.7 (4)	C64—C63—C67—C72	-177.1 (3)
C6—C5—C13—C1	-177.2 (3)	C68—C63—C67—C72	0.4 (5)
C4—C5—C13—C12	177.8 (3)	Ir2—C63—C67—C72	123.3 (3)
C6—C5—C13—C12	-0.1 (4)	C64—C63—C67—Ir2	59.5 (2)
C18—C14—C15—C16	-0.9 (3)	C68—C63—C67—Ir2	-122.9 (3)
C19—C14—C15—C16	173.8 (3)	C65—C66—C67—C63	5.5 (3)
Ir1—C14—C15—C16	-60.10 (19)	C71—C66—C67—C63	-172.7 (3)
C18—C14—C15—C20	-179.2 (3)	Ir2—C66—C67—C63	65.25 (19)
C19—C14—C15—C20	-4.5 (5)	C65—C66—C67—C72	175.7 (3)
Ir1—C14—C15—C20	121.6 (3)	C71—C66—C67—C72	-2.4 (5)
C18—C14—C15—Ir1	59.17 (18)	Ir2—C66—C67—C72	-124.5 (3)
C19—C14—C15—Ir1	-126.1 (3)	C65—C66—C67—Ir2	-59.7 (2)
C14—C15—C16—C17	1.0 (3)	C71—C66—C67—Ir2	122.1 (3)
C20—C15—C16—C17	179.3 (3)	C80—C75—C76—C77	1.5 (4)
Ir1—C15—C16—C17	-61.14 (17)	B2—C75—C76—C77	-171.2 (3)
C14—C15—C16—C21	-170.8 (3)	C75—C76—C77—C78	-0.9 (4)
C20—C15—C16—C21	7.5 (5)	C76—C77—C78—C79	-0.7 (5)
Ir1—C15—C16—C21	127.1 (3)	C77—C78—C79—C80	1.4 (5)
C14—C15—C16—Ir1	62.1 (2)	C78—C79—C80—C75	-0.6 (5)
C20—C15—C16—Ir1	-119.6 (3)	C76—C75—C80—C79	-0.8 (4)
C15—C16—C17—C18	-0.6 (3)	B2—C75—C80—C79	172.0 (3)
C21—C16—C17—C18	171.1 (3)	C86—C81—C82—C83	0.0 (4)
Ir1—C16—C17—C18	-63.62 (18)	B2—C81—C82—C83	173.4 (3)

C15—C16—C17—C22	-175.4 (3)	C81—C82—C83—C84	-0.1 (5)
C21—C16—C17—C22	-3.8 (4)	C82—C83—C84—C85	0.3 (5)
Ir1—C16—C17—C22	121.5 (3)	C83—C84—C85—C86	-0.5 (5)
C15—C16—C17—Ir1	63.01 (18)	C84—C85—C86—C81	0.4 (5)
C21—C16—C17—Ir1	-125.3 (3)	C82—C81—C86—C85	-0.1 (4)
C16—C17—C18—C14	0.0 (3)	B2—C81—C86—C85	-173.7 (3)
C22—C17—C18—C14	174.8 (3)	C92—C87—C88—C89	0.4 (4)
Ir1—C17—C18—C14	-62.99 (18)	B2—C87—C88—C89	-172.9 (3)
C16—C17—C18—C23	-176.6 (2)	C87—C88—C89—C90	0.3 (4)
C22—C17—C18—C23	-1.8 (4)	C88—C89—C90—C91	-0.4 (4)
Ir1—C17—C18—C23	120.4 (3)	C89—C90—C91—C92	-0.3 (4)
C16—C17—C18—Ir1	63.03 (17)	C90—C91—C92—C87	1.1 (4)
C22—C17—C18—Ir1	-122.2 (3)	C88—C87—C92—C91	-1.1 (4)
C15—C14—C18—C17	0.5 (3)	B2—C87—C92—C91	171.9 (2)
C19—C14—C18—C17	-174.2 (3)	C98—C93—C94—C95	1.0 (4)
Ir1—C14—C18—C17	60.26 (18)	B2—C93—C94—C95	174.7 (2)
C15—C14—C18—C23	177.2 (3)	C93—C94—C95—C96	0.0 (4)
C19—C14—C18—C23	2.5 (5)	C94—C95—C96—C97	-1.0 (4)
Ir1—C14—C18—C23	-123.1 (3)	C95—C96—C97—C98	0.9 (5)
C15—C14—C18—Ir1	-59.72 (19)	C96—C97—C98—C93	0.2 (5)
C19—C14—C18—Ir1	125.6 (3)	C94—C93—C98—C97	-1.1 (4)
C31—C26—C27—C28	2.4 (4)	B2—C93—C98—C97	-174.8 (3)
B1—C26—C27—C28	179.7 (3)	C101^{i}—C99—C100—C101	0.0 (5)

C26—C27—C28—C29	-0.8 (5)	C99—C100—C101—C99^{i}	0.0 (5)
C27—C28—C29—C30	-1.4 (5)	C10—C11—N1—C12	1.0 (4)
C28—C29—C30—C31	1.8 (5)	C10—C11—N1—Ir1	176.8 (2)
C29—C30—C31—C26	-0.1 (5)	C13—C12—N1—C11	177.8 (2)
C27—C26—C31—C30	-2.0 (4)	C8—C12—N1—C11	-0.3 (4)
B1—C26—C31—C30	-179.3 (3)	C13—C12—N1—Ir1	1.5 (3)
C37—C32—C33—C34	-0.1 (4)	C8—C12—N1—Ir1	-176.6 (2)
B1—C32—C33—C34	178.7 (3)	C59—C60—N3—C61	2.3 (5)
C32—C33—C34—C35	0.7 (5)	C59—C60—N3—Ir2	-178.7 (3)
C33—C34—C35—C36	-0.8 (5)	C62—C61—N3—C60	177.6 (3)
C34—C35—C36—C37	0.3 (5)	C57—C61—N3—C60	-0.9 (4)
C35—C36—C37—C32	0.4 (5)	C62—C61—N3—Ir2	-1.6 (4)
C33—C32—C37—C36	-0.5 (4)	C57—C61—N3—Ir2	179.9 (2)
B1—C32—C37—C36	-179.2 (3)	C33—C32—B1—C38	137.6 (3)
C43—C38—C39—C40	0.5 (4)	C37—C32—B1—C38	-43.7 (3)
B1—C38—C39—C40	-176.7 (3)	C33—C32—B1—C26	18.3 (4)
C38—C39—C40—C41	-0.3 (5)	C37—C32—B1—C26	-163.0 (2)
C39—C40—C41—C42	0.1 (5)	C33—C32—B1—C44	-102.1 (3)
C40—C41—C42—C43	-0.2 (6)	C37—C32—B1—C44	76.6 (3)
C41—C42—C43—C38	0.5 (5)	C43—C38—B1—C32	144.3 (3)
C39—C38—C43—C42	-0.6 (5)	C39—C38—B1—C32	-38.7 (4)
B1—C38—C43—C42	176.5 (3)	C43—C38—B1—C26	-96.4 (3)
C49—C44—C45—C46	-0.6 (5)	C39—C38—B1—C26	80.6 (3)
B1—C44—C45—C46	-179.1 (3)	C43—C38—B1—C44	24.0 (4)
C44—C45—C46—	-0.6 (5)	C39—C38—B1—C44	-159.0 (3)

C47			
C45—C46—C47—C48	1.4 (6)	C31—C26—B1—C32	86.6 (3)
C46—C47—C48—C49	-1.0 (6)	C27—C26—B1—C32	-90.5 (3)
C47—C48—C49—C44	-0.2 (5)	C31—C26—B1—C38	-32.7 (3)
C45—C44—C49—C48	1.0 (5)	C27—C26—B1—C38	150.1 (3)
B1—C44—C49—C48	179.6 (3)	C31—C26—B1—C44	-153.0 (3)
C62—C50—C51—C52	-0.6 (5)	C27—C26—B1—C44	29.8 (4)
Ir2—C50—C51—C52	-178.2 (3)	C45—C44—B1—C32	-16.8 (4)
C50—C51—C52—C53	0.0 (6)	C49—C44—B1—C32	164.7 (3)
C51—C52—C53—C54	0.2 (7)	C45—C44—B1—C38	103.3 (3)
C52—C53—C54—C62	0.3 (6)	C49—C44—B1—C38	-75.2 (3)
C52—C53—C54—C55	179.1 (4)	C45—C44—B1—C26	-136.8 (3)
C53—C54—C55—C56	-177.1 (4)	C49—C44—B1—C26	44.8 (4)
C62—C54—C55—C56	1.7 (6)	C92—C87—B2—C81	144.5 (2)
C54—C55—C56—C57	0.2 (7)	C88—C87—B2—C81	-42.9 (3)
C55—C56—C57—C58	178.8 (4)	C92—C87—B2—C75	-94.5 (3)
C55—C56—C57—C61	-1.7 (6)	C88—C87—B2—C75	78.0 (3)
C56—C57—C58—C59	-179.2 (4)	C92—C87—B2—C93	27.1 (3)
C61—C57—C58—C59	1.4 (5)	C88—C87—B2—C93	-160.4 (2)
C57—C58—C59—C60	-0.1 (6)	C82—C81—B2—C87	152.3 (2)
C58—C59—C60—N3	-1.8 (6)	C86—C81—B2—C87	-34.6 (3)
C58—C57—C61—N3	-0.9 (5)	C82—C81—B2—C75	36.7 (3)
C56—C57—C61—N3	179.6 (3)	C86—C81—B2—C75	-150.2 (2)
C58—C57—C61—C62	-179.2 (3)	C82—C81—B2—C93	-84.6 (3)
C56—C57—C61—C62	1.2 (5)	C86—C81—B2—C93	88.5 (3)

N3—C61—C62—C54	-177.7 (3)	C76—C75—B2—C87	88.1 (3)
C57—C61—C62—C54	0.7 (5)	C80—C75—B2—C87	-84.1 (3)
N3—C61—C62—C50	0.2 (4)	C76—C75—B2—C81	-151.2 (2)
C57—C61—C62—C50	178.6 (3)	C80—C75—B2—C81	36.6 (3)
C53—C54—C62—C61	176.8 (3)	C76—C75—B2—C93	-34.6 (3)
C55—C54—C62—C61	-2.1 (5)	C80—C75—B2—C93	153.1 (2)
C53—C54—C62—C50	-1.0 (5)	C98—C93—B2—C87	-149.9 (2)
C55—C54—C62—C50	-179.9 (3)	C94—C93—B2—C87	36.8 (3)
C51—C50—C62—C61	-176.6 (3)	C98—C93—B2—C81	88.1 (3)
Ir2—C50—C62—C61	1.3 (4)	C94—C93—B2—C81	-85.2 (3)
C51—C50—C62—C54	1.1 (5)	C98—C93—B2—C75	-33.3 (3)
Ir2—C50—C62—C54	179.1 (3)	C94—C93—B2—C75	153.4 (2)

7.8 [**3B**][OTf]

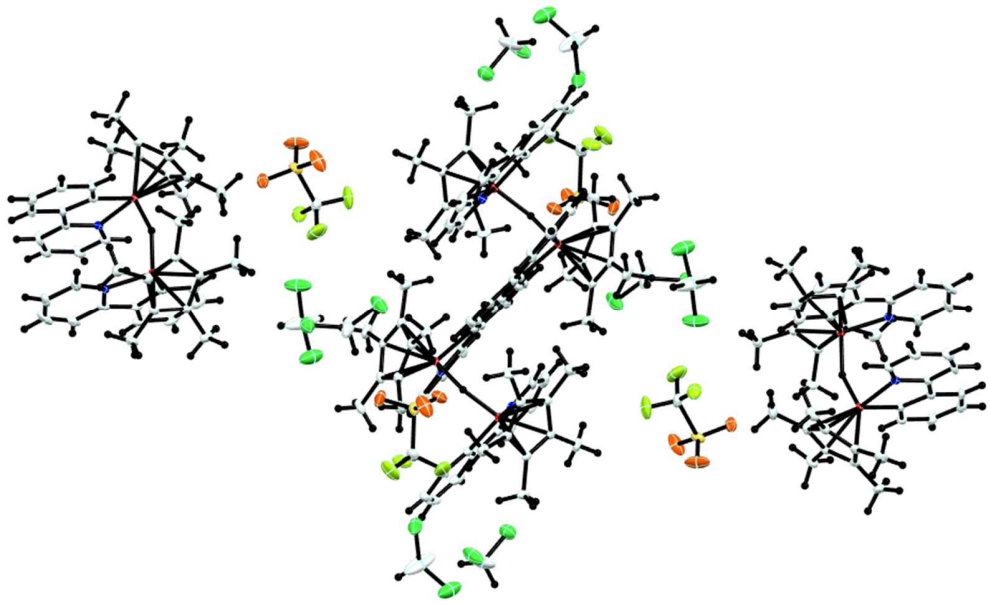

7.8.1 **Figure A22.** Crystal lattice packing of [**3B**][OTf].

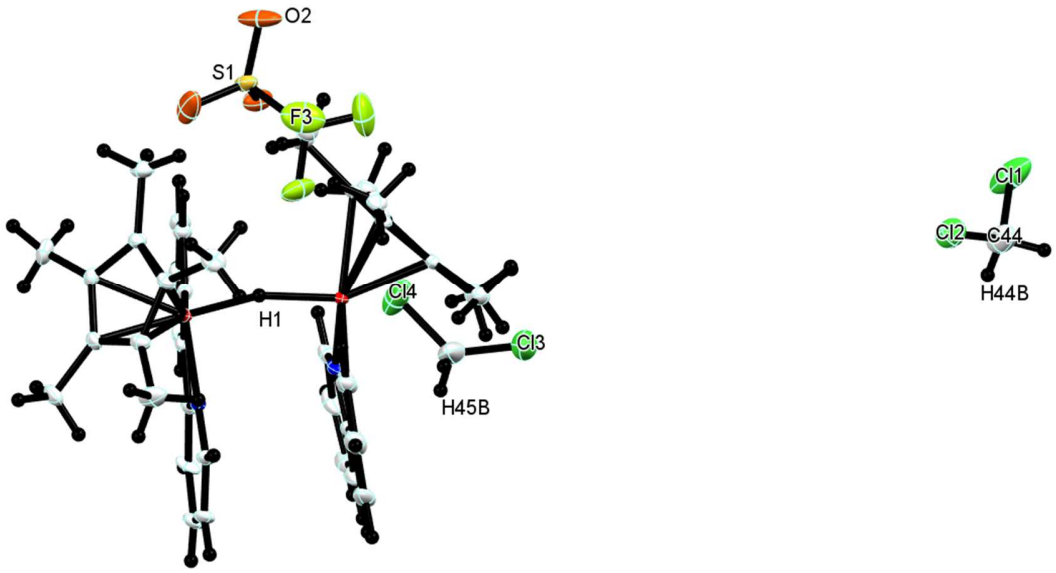

7.8.2 **Figure A23.** Asymmetric unit of [**3B**][OTf], with all hydrogens and partial numbering of atoms.

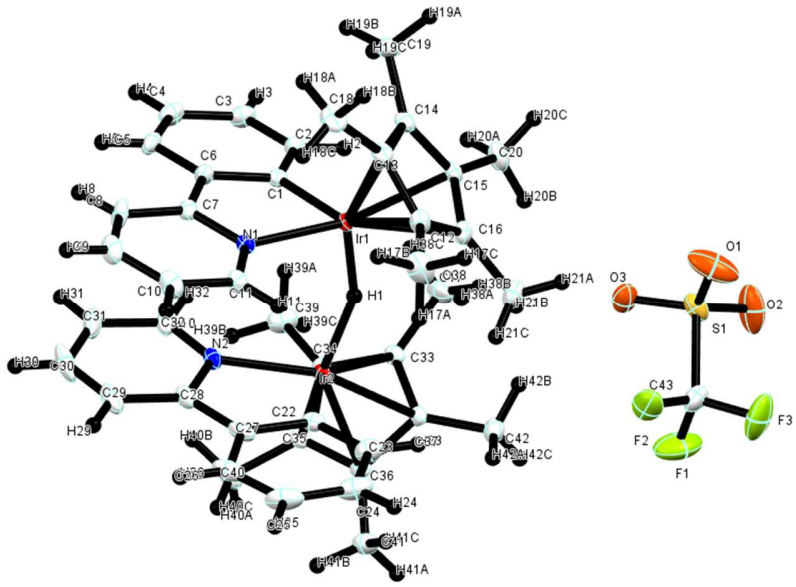

7.8.3 **Figure A24.** Asymmetric unit of [**3B**][OTf], with all hydrogens and total numbering of atoms.

[**3B**][OTf]

7.8.4 Crystal data

$C_{42}H_{47}Ir_2N_2 \cdot CF_3O_3S \cdot 2(CH_2Cl_2)$	$F(000) = 2496$
$M_r = 1283.14$	$D_x = 1.851$ Mg m^{-3}
Monoclinic, $P2_1/c$	Mo $K\alpha$ radiation, $\lambda = 0.71073$ Å
$a = 10.9779$ (9) Å	Cell parameters from 9180 reflections
$b = 23.2754$ (19) Å	$\theta = 2.3$–$34.0°$
$c = 21.0040$ (13) Å	$\mu = 6.11$ mm^{-1}
$\beta = 120.899$ (3)°	$T = 173$ K
$V = 4605.1$ (6) Å^3	Prism, orange
$Z = 4$	0.40 × 0.35 × 0.30 mm

7.8.5 Data collection

Bruker APEX-II CCD diffractometer	15330 reflections with $I > 2\sigma(I)$
Radiation source: fine focus sealed tube	$R_{int} = 0.033$
ϕ and ω scans	$\theta_{max} = 34.1°$, $\theta_{min} = 1.4°$
Absorption correction: multi-scan *SADABS*	$h = -14 \rightarrow 17$
$T_{min} = 0.624$, $T_{max} = 0.747$	$k = -36 \rightarrow 35$
74913 measured reflections	$l = -33 \rightarrow 13$
18826 independent reflections	

7.8.6 Refinement

Refinement on F^2	Primary atom site location: structure-invariant direct methods
Least-squares matrix: full	Secondary atom site location: difference Fourier map
$R[F^2 > 2\sigma(F^2)] = 0.041$	Hydrogen site location: mixed
$wR(F^2) = 0.083$	H atoms treated by a mixture of independent and constrained refinement
$S = 1.15$	$w = 1/[\sigma^2(F_o^2) + (0.021P)^2 + 18.0829P]$ where $P = (F_o^2 + 2F_c^2)/3$
18826 reflections	$(\Delta/\sigma)_{max} = 0.004$
555 parameters	$\Delta\rangle_{max} = 3.40$ e Å^{-3}

0 restraints	$\Delta\rangle_{min}$ = -2.83 e Å^{-3}

7.8.7 Special details

Geometry. All esds (except the esd in the dihedral angle between two l.s. planes) are estimated using the full covariance matrix. The cell esds are taken into account individually in the estimation of esds in distances, angles and torsion angles; correlations between esds in cell parameters are only used when they are defined by crystal symmetry. An approximate (isotropic) treatment of cell esds is used for estimating esds involving l.s. planes.

7.8.8 **Table A22.** Fractional atomic coordinates and isotropic or equivalent isotropic displacement parameters (Å^2) for [**3B**][OTf].

	x	*y*	*z*	U_{iso}*/U_{eq}
C1	0.0927 (4)	1.02589 (16)	0.8763 (2)	0.0215 (7)
C2	0.2258 (4)	1.04711 (18)	0.9298 (2)	0.0258 (8)
H2	0.3059	1.0224	0.9493	0.031*
C3	0.2441 (5)	1.1034 (2)	0.9551 (2)	0.0326 (9)
H3	0.3360	1.1167	0.9911	0.039*
C4	0.1293 (5)	1.1401 (2)	0.9283 (3)	0.0363 (10)
H4	0.1425	1.1784	0.9463	0.044*
C5	-0.0047 (5)	1.12135 (19)	0.8755 (3)	0.0311 (9)
H5	-0.0837	1.1466	0.8567	0.037*
C6	-0.0227 (4)	1.06461 (17)	0.8499 (2)	0.0246 (7)
C7	-0.1588 (4)	1.04145 (17)	0.7919 (2)	0.0231 (7)
C8	-0.2906 (4)	1.06977 (19)	0.7565 (3)	0.0344 (10)
H8	-0.2967	1.1080	0.7704	0.041*
C9	-0.4107 (5)	1.0429 (2)	0.7021 (3)	0.0383 (11)
H9	-0.5006	1.0612	0.6804	0.046*
C10	-0.3981 (4)	0.9888 (2)	0.6798 (3)	0.0342 (10)
H10	-0.4792	0.9700	0.6411	0.041*
C11	-0.2664 (4)	0.96164 (19)	0.7139 (2)	0.0267 (8)
H11	-0.2586	0.9244	0.6978	0.032*
C12	-0.0311 (4)	0.85241 (18)	0.8299 (2)	0.0274 (8)
C13	-0.0440 (4)	0.88652 (18)	0.8842 (2)	0.0268 (8)
C14	0.0967 (4)	0.90449 (18)	0.9401 (2)	0.0267 (8)

C15	0.1947 (4)	0.88497 (17)	0.9188 (2)	0.0254 (7)
C16	0.1138 (4)	0.85183 (17)	0.8513 (2)	0.0267 (8)
C17	-0.1474 (6)	0.8184 (2)	0.7676 (3)	0.0461 (13)
H17A	-0.1387	0.8214	0.7236	0.069*
H17B	-0.2397	0.8337	0.7562	0.069*
H17C	-0.1398	0.7781	0.7824	0.069*
C18	-0.1779 (5)	0.8959 (2)	0.8849 (3)	0.0423 (12)
H18A	-0.1661	0.9289	0.9166	0.064*
H18B	-0.1993	0.8615	0.9044	0.064*
H18C	-0.2561	0.9034	0.8343	0.064*
C19	0.1380 (6)	0.9345 (2)	1.0117 (3)	0.0415 (11)
H19A	0.1852	0.9072	1.0529	0.062*
H19B	0.0528	0.9497	1.0096	0.062*
H19C	0.2029	0.9662	1.0193	0.062*
C20	0.3531 (5)	0.8858 (2)	0.9672 (3)	0.0375 (10)
H20A	0.3849	0.9251	0.9846	0.056*
H20B	0.3957	0.8725	0.9388	0.056*
H20C	0.3822	0.8605	1.0100	0.056*
C21	0.1753 (6)	0.8193 (2)	0.8130 (3)	0.0410 (11)
H21A	0.2050	0.7811	0.8353	0.061*
H21B	0.2576	0.8401	0.8183	0.061*
H21C	0.1036	0.8154	0.7602	0.061*
C22	-0.0467 (4)	0.94867 (19)	0.6370 (2)	0.0255 (8)
C23	-0.0575 (5)	0.8912 (2)	0.6156 (3)	0.0341 (9)
H23	0.0230	0.8668	0.6413	0.041*
C24	-0.1836 (6)	0.8686 (3)	0.5572 (3)	0.0468 (13)
H24	-0.1883	0.8292	0.5442	0.056*
C25	-0.3017 (5)	0.9033 (3)	0.5183 (3)	0.0502 (15)
H25	-0.3864	0.8883	0.4775	0.060*
C26	-0.2957 (5)	0.9595 (3)	0.5389 (3)	0.0460 (14)
H26	-0.3776	0.9831	0.5129	0.055*
C27	-0.1701 (4)	0.9829 (2)	0.5981 (2)	0.0312 (9)
C28	-0.1554 (4)	1.0413 (2)	0.6252 (2)	0.0310 (9)
C29	-0.2597 (5)	1.0837 (3)	0.5966 (3)	0.0475 (14)
H29	-0.3504	1.0757	0.5546	0.057*
C30	-0.2321 (6)	1.1365 (3)	0.6285 (4)	0.0597 (19)
H30	-0.3025	1.1656	0.6077	0.072*

C31	-0.1025 (6)	1.1479 (2)	0.6911 (3)	0.0462 (13)
H31	-0.0835	1.1843	0.7149	0.055*
C32	-0.0005 (5)	1.10493 (19)	0.7184 (3)	0.0333 (9)
H32	0.0897	1.1125	0.7610	0.040*
C33	0.3715 (4)	0.98943 (18)	0.7820 (2)	0.0243 (7)
C34	0.3281 (4)	1.04598 (18)	0.7551 (2)	0.0253 (7)
C35	0.2440 (4)	1.04278 (18)	0.6745 (2)	0.0234 (7)
C36	0.2422 (4)	0.98379 (18)	0.6537 (2)	0.0233 (7)
C37	0.3165 (4)	0.95007 (17)	0.7203 (2)	0.0231 (7)
C38	0.4672 (5)	0.9729 (3)	0.8618 (2)	0.0401 (11)
H38A	0.5661	0.9803	0.8764	0.060*
H38B	0.4551	0.9319	0.8680	0.060*
H38C	0.4429	0.9956	0.8930	0.060*
C39	0.3749 (5)	1.0994 (2)	0.8016 (3)	0.0408 (11)
H39A	0.3636	1.0942	0.8445	0.061*
H39B	0.3170	1.1320	0.7719	0.061*
H39C	0.4749	1.1070	0.8187	0.061*
C40	0.1820 (5)	1.0926 (2)	0.6226 (3)	0.0356 (10)
H40A	0.2512	1.1070	0.6102	0.053*
H40B	0.1582	1.1233	0.6464	0.053*
H40C	0.0958	1.0803	0.5771	0.053*
C41	0.1814 (5)	0.9608 (2)	0.5764 (2)	0.0354 (10)
H41A	0.2587	0.9518	0.5676	0.053*
H41B	0.1191	0.9897	0.5405	0.053*
H41C	0.1268	0.9259	0.5706	0.053*
C42	0.3594 (5)	0.8884 (2)	0.7237 (3)	0.0355 (10)
H42A	0.2798	0.8666	0.6846	0.053*
H42B	0.3855	0.8723	0.7722	0.053*
H42C	0.4408	0.8861	0.7167	0.053*
C43	0.5009 (6)	0.7337 (2)	0.7996 (3)	0.0435 (12)
C44	0.4845 (9)	0.7266 (4)	0.0612 (5)	0.094 (3)
H44A	0.4738	0.7219	0.0117	0.113*
H44B	0.3998	0.7476	0.0537	0.113*
C45	0.0483 (9)	0.7550 (8)	0.5007 (5)	0.174 (8)
H45A	0.0175	0.7147	0.4867	0.209*
H45B	-0.0376	0.7769	0.4900	0.209*
N1	-0.1495 (3)	0.98727 (14)	0.76941 (17)	0.0213 (6)

N2	-0.0256 (3)	1.05299 (15)	0.68623 (19)	0.0252 (6)
O1	0.5078 (6)	0.7204 (3)	0.9212 (3)	0.090 (2)
O2	0.7271 (4)	0.7445 (2)	0.9275 (3)	0.0823 (18)
O3	0.5452 (4)	0.81619 (17)	0.8901 (2)	0.0504 (10)
F1	0.5485 (6)	0.7638 (2)	0.7645 (3)	0.0982 (17)
F2	0.3608 (4)	0.74018 (18)	0.76316 (19)	0.0670 (11)
F3	0.5233 (5)	0.67834 (17)	0.7943 (3)	0.0869 (15)
S1	0.57931 (12)	0.75632 (5)	0.89603 (7)	0.0376 (3)
Cl1	0.6268 (3)	0.76873 (8)	0.11202 (12)	0.1013 (9)
Cl2	0.4810 (2)	0.65924 (8)	0.09375 (10)	0.0698 (5)
Cl3	0.0898 (2)	0.77705 (15)	0.44432 (12)	0.1100 (10)
Cl4	0.1545 (3)	0.75512 (12)	0.59397 (10)	0.1073 (10)
Ir1	0.04185 (2)	0.94448 (2)	0.83531 (2)	0.01813 (3)
Ir2	0.13077 (2)	0.99125 (2)	0.71416 (2)	0.01895 (3)
H1	0.110 (6)	0.955 (2)	0.783 (3)	0.053 (17)*

7.8.9 **Table A23.** Atomic displacement parameters (Å^2) for [**3B**][OTf].

	U^{11}	U^{22}	U^{33}	U^{12}	U^{13}	U^{23}
C1	0.0216 (17)	0.0232 (17)	0.0211 (16)	-0.0016 (13)	0.0119 (14)	-0.0001 (13)
C2	0.0205 (17)	0.029 (2)	0.0253 (17)	-0.0024 (14)	0.0097 (14)	-0.0024 (14)
C3	0.032 (2)	0.033 (2)	0.031 (2)	-0.0084 (18)	0.0150 (18)	-0.0098 (17)
C4	0.047 (3)	0.027 (2)	0.042 (2)	-0.0079 (19)	0.028 (2)	-0.0092 (18)
C5	0.036 (2)	0.026 (2)	0.038 (2)	0.0052 (17)	0.0247 (19)	-0.0017 (16)
C6	0.0265 (19)	0.0228 (18)	0.0249 (17)	0.0024 (14)	0.0135 (15)	-0.0002 (13)
C7	0.0199 (16)	0.0245 (18)	0.0291 (18)	0.0022 (14)	0.0155 (15)	0.0042 (14)
C8	0.0205 (18)	0.027 (2)	0.062 (3)	0.0066 (15)	0.025 (2)	0.0025 (19)
C9	0.0180 (18)	0.049 (3)	0.049 (3)	0.0087 (18)	0.0179 (19)	0.014 (2)
C10	0.0139 (16)	0.045 (3)	0.037 (2)	-0.0036 (17)	0.0080 (16)	0.0070 (19)
C11	0.0161 (16)	0.032 (2)	0.0273 (18)	-0.0011 (14)	0.0075 (14)	0.0016 (15)
C12	0.0220 (18)	0.0235 (18)	0.033 (2)	-0.0018 (14)	0.0114 (16)	0.0019 (15)
C13	0.0242 (18)	0.029 (2)	0.0312 (19)	-0.0023 (15)	0.0168 (16)	0.0065 (15)
C14	0.029 (2)	0.0277 (19)	0.0243 (17)	0.0010 (15)	0.0146 (16)	0.0068 (14)
C15	0.0194 (17)	0.0258 (18)	0.0266 (18)	0.0017 (14)	0.0087 (14)	0.0060 (14)
C16	0.0239 (18)	0.0231 (18)	0.035 (2)	0.0021 (14)	0.0166 (16)	0.0031 (15)

C17	0.037 (3)	0.034 (3)	0.048 (3)	-0.015 (2)	0.008 (2)	-0.004 (2)
C18	0.031 (2)	0.053 (3)	0.053 (3)	0.002 (2)	0.029 (2)	0.016 (2)
C19	0.054 (3)	0.047 (3)	0.027 (2)	0.001 (2)	0.024 (2)	0.0029 (19)
C20	0.023 (2)	0.038 (2)	0.041 (2)	0.0034 (17)	0.0084 (18)	0.0078 (19)
C21	0.043 (3)	0.031 (2)	0.055 (3)	0.006 (2)	0.029 (2)	-0.003 (2)
C22	0.0172 (16)	0.038 (2)	0.0220 (16)	-0.0032 (15)	0.0103 (14)	0.0012 (15)
C23	0.026 (2)	0.041 (3)	0.034 (2)	-0.0118 (18)	0.0148 (18)	-0.0117 (18)
C24	0.041 (3)	0.065 (4)	0.041 (3)	-0.023 (3)	0.025 (2)	-0.023 (2)
C25	0.025 (2)	0.094 (5)	0.030 (2)	-0.022 (3)	0.0128 (19)	-0.021 (3)
C26	0.019 (2)	0.092 (4)	0.024 (2)	-0.002 (2)	0.0091 (17)	0.008 (2)
C27	0.0162 (17)	0.055 (3)	0.0181 (16)	-0.0031 (17)	0.0058 (14)	0.0062 (17)
C28	0.0194 (17)	0.046 (3)	0.0299 (19)	0.0071 (17)	0.0141 (16)	0.0155 (18)
C29	0.030 (2)	0.063 (4)	0.052 (3)	0.019 (2)	0.024 (2)	0.032 (3)
C30	0.040 (3)	0.060 (4)	0.080 (4)	0.023 (3)	0.032 (3)	0.050 (3)
C31	0.057 (3)	0.029 (2)	0.074 (4)	0.018 (2)	0.049 (3)	0.019 (2)
C32	0.033 (2)	0.028 (2)	0.049 (3)	0.0043 (17)	0.029 (2)	0.0100 (18)
C33	0.0136 (15)	0.035 (2)	0.0222 (16)	0.0000 (14)	0.0077 (13)	0.0017 (15)
C34	0.0175 (16)	0.031 (2)	0.0270 (18)	-0.0048 (14)	0.0108 (14)	-0.0019 (15)
C35	0.0162 (15)	0.032 (2)	0.0248 (17)	-0.0009 (14)	0.0123 (14)	0.0044 (14)
C36	0.0149 (15)	0.035 (2)	0.0214 (16)	-0.0007 (14)	0.0105 (13)	0.0011 (14)
C37	0.0148 (15)	0.031 (2)	0.0241 (16)	0.0048 (14)	0.0104 (13)	0.0032 (14)
C38	0.024 (2)	0.061 (3)	0.025 (2)	0.005 (2)	0.0055 (17)	0.006 (2)
C39	0.038 (3)	0.046 (3)	0.041 (3)	-0.015 (2)	0.022 (2)	-0.012 (2)
C40	0.034 (2)	0.037 (2)	0.039 (2)	0.0020 (18)	0.020 (2)	0.0152 (19)
C41	0.025 (2)	0.055 (3)	0.0267 (19)	-0.0023 (19)	0.0131 (17)	-0.0049 (19)
C42	0.031 (2)	0.037 (2)	0.042 (2)	0.0092 (18)	0.022 (2)	0.0058 (19)
C43	0.051 (3)	0.033 (2)	0.055 (3)	0.002 (2)	0.034 (3)	-0.006 (2)
C44	0.068 (5)	0.114 (7)	0.072 (5)	-0.027 (5)	0.015 (4)	0.043 (5)
C45	0.041 (4)	0.42 (2)	0.046 (4)	-0.008 (8)	0.012 (4)	0.039 (8)
N1	0.0169 (14)	0.0248 (15)	0.0216 (14)	-0.0002 (12)	0.0095 (12)	0.0032 (11)
N2	0.0191 (14)	0.0291 (17)	0.0298 (16)	0.0054 (13)	0.0143 (13)	0.0090 (13)
O1	0.092 (4)	0.113 (4)	0.049 (3)	-0.060 (3)	0.025 (3)	0.011 (3)
O2	0.026 (2)	0.059 (3)	0.109 (4)	0.0045 (19)	-0.004 (2)	0.004 (3)
O3	0.044 (2)	0.045 (2)	0.046 (2)	0.0051 (17)	0.0121 (18)	-0.0119 (17)
F1	0.146 (5)	0.105 (4)	0.092 (3)	-0.032 (3)	0.096 (4)	-0.018 (3)
F2	0.050 (2)	0.082 (3)	0.0398 (18)	0.0128 (19)	0.0016 (15)	-0.0148 (17)
F3	0.074 (3)	0.044 (2)	0.126 (4)	0.0059 (19)	0.040 (3)	-0.033 (2)

S1	0.0237 (5)	0.0390 (6)	0.0351 (6)	-0.0059 (4)	0.0043 (4)	0.0079 (5)
Cl1	0.1249 (19)	0.0462 (9)	0.0646 (11)	-0.0137 (11)	-0.0003 (12)	0.0053 (8)
Cl2	0.0732 (11)	0.0599 (10)	0.0642 (10)	-0.0043 (8)	0.0265 (9)	0.0052 (8)
Cl3	0.0714 (14)	0.205 (3)	0.0588 (11)	0.0048 (16)	0.0375 (11)	0.0112 (15)
Cl4	0.1167 (18)	0.1258 (19)	0.0447 (9)	-0.0675 (16)	0.0166 (10)	0.0071 (10)
Ir1	0.01344 (6)	0.02040 (6)	0.01929 (6)	-0.00010 (5)	0.00750 (5)	0.00058 (5)
Ir2	0.01311 (6)	0.02355 (6)	0.01893 (6)	0.00120 (5)	0.00733 (5)	0.00218 (5)

7.8.10 **Table A24.** Interatomic distances (Å) and angles (deg) for [**3B**][OTf].

C1—C2	1.399 (5)	C26—H26	0.9500
C1—C6	1.415 (5)	C27—C28	1.451 (7)
C1—Ir1	2.037 (4)	C28—N2	1.368 (5)
C2—C3	1.389 (6)	C28—C29	1.393 (6)
C2—H2	0.9500	C29—C30	1.357 (10)
C3—C4	1.381 (7)	C29—H29	0.9500
C3—H3	0.9500	C30—C31	1.380 (9)
C4—C5	1.382 (7)	C30—H30	0.9500
C4—H4	0.9500	C31—C32	1.387 (6)
C5—C6	1.401 (6)	C31—H31	0.9500
C5—H5	0.9500	C32—N2	1.343 (6)
C6—C7	1.462 (6)	C32—H32	0.9500
C7—N1	1.368 (5)	C33—C34	1.415 (6)
C7—C8	1.406 (5)	C33—C37	1.443 (6)
C8—C9	1.375 (7)	C33—C38	1.500 (6)
C8—H8	0.9500	C33—Ir2	2.269 (4)
C9—C10	1.375 (7)	C34—C35	1.455 (5)
C9—H9	0.9500	C34—C39	1.499 (6)
C10—C11	1.392 (6)	C34—Ir2	2.267 (4)
C10—H10	0.9500	C35—C36	1.438 (6)
C11—N1	1.351 (5)	C35—C40	1.496 (6)
C11—H11	0.9500	C35—Ir2	2.177 (4)
C12—C16	1.414 (6)	C36—C37	1.437 (5)
C12—C13	1.456 (6)	C36—C41	1.501 (6)
C12—C17	1.500 (6)	C36—Ir2	2.177 (4)
C12—Ir1	2.270 (4)	C37—C42	1.500 (6)
C13—C14	1.441 (6)	C37—Ir2	2.196 (4)

C13—C18	1.494 (6)	C38—H38A	0.9800
C13—Ir1	2.181 (4)	C38—H38B	0.9800
C14—C15	1.435 (6)	C38—H38C	0.9800
C14—C19	1.501 (6)	C39—H39A	0.9800
C14—Ir1	2.171 (4)	C39—H39B	0.9800
C15—C16	1.449 (6)	C39—H39C	0.9800
C15—C20	1.497 (6)	C40—H40A	0.9800
C15—Ir1	2.188 (4)	C40—H40B	0.9800
C16—C21	1.494 (6)	C40—H40C	0.9800
C16—Ir1	2.261 (4)	C41—H41A	0.9800
C17—H17A	0.9800	C41—H41B	0.9800
C17—H17B	0.9800	C41—H41C	0.9800
C17—H17C	0.9800	C42—H42A	0.9800
C18—H18A	0.9800	C42—H42B	0.9800
C18—H18B	0.9800	C42—H42C	0.9800
C18—H18C	0.9800	C43—F1	1.306 (7)
C19—H19A	0.9800	C43—F3	1.327 (6)
C19—H19B	0.9800	C43—F2	1.329 (7)
C19—H19C	0.9800	C43—S1	1.824 (6)
C20—H20A	0.9800	C44—Cl1	1.682 (8)
C20—H20B	0.9800	C44—Cl2	1.719 (8)
C20—H20C	0.9800	C44—H44A	0.9900
C21—H21A	0.9800	C44—H44B	0.9900
C21—H21B	0.9800	C45—Cl3	1.558 (10)
C21—H21C	0.9800	C45—Cl4	1.688 (8)
C22—C23	1.397 (6)	C45—H45A	0.9900
C22—C27	1.414 (6)	C45—H45B	0.9900
C22—Ir2	2.040 (4)	N1—Ir1	2.082 (3)
C23—C24	1.398 (6)	N2—Ir2	2.079 (3)
C23—H23	0.9500	O1—S1	1.422 (5)
C24—C25	1.383 (9)	O2—S1	1.430 (4)
C24—H24	0.9500	O3—S1	1.432 (4)
C25—C26	1.369 (9)	Ir1—H1	1.63 (6)
C25—H25	0.9500	Ir2—H1	1.79 (6)
C26—C27	1.408 (6)		

C2—C1—C6	116.4 (4)	C35—C34—Ir2	67.5 (2)
C2—C1—Ir1	127.9 (3)	C39—C34—Ir2	130.9 (3)
C6—C1—Ir1	115.5 (3)	C36—C35—C34	107.7 (3)

C3—C2—C1	121.8 (4)	C36—C35—C40	126.0 (4)
C3—C2—H2	119.1	C34—C35—C40	126.0 (4)
C1—C2—H2	119.1	C36—C35—Ir2	70.7 (2)
C4—C3—C2	120.4 (4)	C34—C35—Ir2	74.3 (2)
C4—C3—H3	119.8	C40—C35—Ir2	124.8 (3)
C2—C3—H3	119.8	C37—C36—C35	108.2 (3)
C3—C4—C5	120.2 (4)	C37—C36—C41	124.9 (4)
C3—C4—H4	119.9	C35—C36—C41	126.8 (4)
C5—C4—H4	119.9	C37—C36—Ir2	71.5 (2)
C4—C5—C6	119.2 (4)	C35—C36—Ir2	70.7 (2)
C4—C5—H5	120.4	C41—C36—Ir2	126.0 (3)
C6—C5—H5	120.4	C36—C37—C33	107.1 (3)
C5—C6—C1	121.9 (4)	C36—C37—C42	125.2 (4)
C5—C6—C7	123.3 (4)	C33—C37—C42	126.0 (4)
C1—C6—C7	114.7 (3)	C36—C37—Ir2	70.1 (2)
N1—C7—C8	119.3 (4)	C33—C37—Ir2	73.9 (2)
N1—C7—C6	113.7 (3)	C42—C37—Ir2	132.8 (3)
C8—C7—C6	127.0 (4)	C33—C38—H38A	109.5
C9—C8—C7	120.9 (4)	C33—C38—H38B	109.5
C9—C8—H8	119.6	H38A—C38—H38B	109.5
C7—C8—H8	119.6	C33—C38—H38C	109.5
C10—C9—C8	118.6 (4)	H38A—C38—H38C	109.5
C10—C9—H9	120.7	H38B—C38—H38C	109.5
C8—C9—H9	120.7	C34—C39—H39A	109.5
C9—C10—C11	120.0 (4)	C34—C39—H39B	109.5
C9—C10—H10	120.0	H39A—C39—H39B	109.5
C11—C10—H10	120.0	C34—C39—H39C	109.5
N1—C11—C10	121.2 (4)	H39A—C39—H39C	109.5
N1—C11—H11	119.4	H39B—C39—H39C	109.5
C10—C11—H11	119.4	C35—C40—H40A	109.5
C16—C12—C13	107.6 (4)	C35—C40—H40B	109.5
C16—C12—C17	126.0 (4)	H40A—C40—H40B	109.5
C13—C12—C17	126.1 (4)	C35—C40—H40C	109.5
C16—C12—Ir1	71.5 (2)	H40A—C40—H40C	109.5
C13—C12—Ir1	67.6 (2)	H40B—C40—H40C	109.5
C17—C12—Ir1	131.5 (3)	C36—C41—H41A	109.5
C14—C13—C12	107.6 (4)	C36—C41—H41B	109.5
C14—C13—C18	126.7 (4)	H41A—C41—H41B	109.5
C12—C13—C18	125.4 (4)	C36—C41—H41C	109.5

C14—C13—Ir1	70.3 (2)	H41A—C41—H41C	109.5
C12—C13—Ir1	74.3 (2)	H41B—C41—H41C	109.5
C18—C13—Ir1	125.5 (3)	C37—C42—H42A	109.5
C15—C14—C13	108.3 (4)	C37—C42—H42B	109.5
C15—C14—C19	124.8 (4)	H42A—C42—H42B	109.5
C13—C14—C19	126.7 (4)	C37—C42—H42C	109.5
C15—C14—Ir1	71.4 (2)	H42A—C42—H42C	109.5
C13—C14—Ir1	71.0 (2)	H42B—C42—H42C	109.5
C19—C14—Ir1	126.8 (3)	F1—C43—F3	109.2 (5)
C14—C15—C16	107.0 (3)	F1—C43—F2	107.1 (5)
C14—C15—C20	125.3 (4)	F3—C43—F2	105.7 (5)
C16—C15—C20	125.9 (4)	F1—C43—S1	112.0 (4)
C14—C15—Ir1	70.2 (2)	F3—C43—S1	111.8 (4)
C16—C15—Ir1	73.8 (2)	F2—C43—S1	110.7 (4)
C20—C15—Ir1	132.9 (3)	Cl1—C44—Cl2	118.8 (5)
C12—C16—C15	109.3 (4)	Cl1—C44—H44A	107.6
C12—C16—C21	125.4 (4)	Cl2—C44—H44A	107.6
C15—C16—C21	125.2 (4)	Cl1—C44—H44B	107.6
C12—C16—Ir1	72.2 (2)	Cl2—C44—H44B	107.6
C15—C16—Ir1	68.3 (2)	H44A—C44—H44B	107.0
C21—C16—Ir1	128.5 (3)	Cl3—C45—Cl4	125.8 (7)
C12—C17—H17A	109.5	Cl3—C45—H45A	105.9
C12—C17—H17B	109.5	Cl4—C45—H45A	105.9
H17A—C17—H17B	109.5	Cl3—C45—H45B	105.9
C12—C17—H17C	109.5	Cl4—C45—H45B	105.9
H17A—C17—H17C	109.5	H45A—C45—H45B	106.2
H17B—C17—H17C	109.5	C11—N1—C7	119.9 (3)
C13—C18—H18A	109.5	C11—N1—Ir1	123.3 (3)
C13—C18—H18B	109.5	C7—N1—Ir1	116.1 (2)
H18A—C18—H18B	109.5	C32—N2—C28	119.8 (4)
C13—C18—H18C	109.5	C32—N2—Ir2	123.6 (3)
H18A—C18—H18C	109.5	C28—N2—Ir2	116.0 (3)
H18B—C18—H18C	109.5	O1—S1—O2	115.3 (4)
C14—C19—H19A	109.5	O1—S1—O3	115.8 (4)
C14—C19—H19B	109.5	O2—S1—O3	114.3 (3)
H19A—C19—H19B	109.5	O1—S1—C43	101.9 (3)
C14—C19—H19C	109.5	O2—S1—C43	103.5 (3)
H19A—C19—H19C	109.5	O3—S1—C43	103.4 (2)
H19B—C19—H19C	109.5	C1—Ir1—N1	78.46 (14)

C15—C20—H20A	109.5	C1—Ir1—C14	95.60 (15)
C15—C20—H20B	109.5	N1—Ir1—C14	122.61 (14)
H20A—C20—H20B	109.5	C1—Ir1—C13	117.89 (15)
C15—C20—H20C	109.5	N1—Ir1—C13	94.38 (14)
H20A—C20—H20C	109.5	C14—Ir1—C13	38.68 (16)
H20B—C20—H20C	109.5	C1—Ir1—C15	108.63 (15)
C16—C21—H21A	109.5	N1—Ir1—C15	158.82 (14)
C16—C21—H21B	109.5	C14—Ir1—C15	38.45 (15)
H21A—C21—H21B	109.5	C13—Ir1—C15	64.55 (15)
C16—C21—H21C	109.5	C1—Ir1—C16	145.61 (16)
H21A—C21—H21C	109.5	N1—Ir1—C16	135.33 (14)
H21B—C21—H21C	109.5	C14—Ir1—C16	63.05 (16)
C23—C22—C27	117.1 (4)	C13—Ir1—C16	62.79 (15)
C23—C22—Ir2	127.6 (3)	C15—Ir1—C16	37.97 (15)
C27—C22—Ir2	115.2 (3)	C1—Ir1—C12	155.88 (15)
C22—C23—C24	121.6 (5)	N1—Ir1—C12	102.04 (14)
C22—C23—H23	119.2	C14—Ir1—C12	63.48 (16)
C24—C23—H23	119.2	C13—Ir1—C12	38.11 (16)
C25—C24—C23	120.3 (5)	C15—Ir1—C12	63.15 (15)
C25—C24—H24	119.8	C16—Ir1—C12	36.36 (15)
C23—C24—H24	119.8	C1—Ir1—H1	91 (2)
C26—C25—C24	119.5 (5)	N1—Ir1—H1	98 (2)
C26—C25—H25	120.2	C14—Ir1—H1	140 (2)
C24—C25—H25	120.2	C13—Ir1—H1	150 (2)
C25—C26—C27	121.0 (5)	C15—Ir1—H1	102 (2)
C25—C26—H26	119.5	C16—Ir1—H1	90 (2)
C27—C26—H26	119.5	C12—Ir1—H1	112 (2)
C26—C27—C22	120.4 (5)	C22—Ir2—N2	78.37 (16)
C26—C27—C28	124.7 (4)	C22—Ir2—C35	117.60 (15)
C22—C27—C28	114.9 (4)	N2—Ir2—C35	93.57 (14)
N2—C28—C29	119.5 (5)	C22—Ir2—C36	95.20 (15)
N2—C28—C27	114.0 (4)	N2—Ir2—C36	121.38 (14)
C29—C28—C27	126.5 (5)	C35—Ir2—C36	38.59 (15)
C30—C29—C28	120.2 (5)	C22—Ir2—C37	108.25 (16)
C30—C29—H29	119.9	N2—Ir2—C37	157.75 (14)
C28—C29—H29	119.9	C35—Ir2—C37	64.38 (15)
C29—C30—C31	120.4 (5)	C36—Ir2—C37	38.38 (14)
C29—C30—H30	119.8	C22—Ir2—C34	155.60 (15)
C31—C30—H30	119.8	N2—Ir2—C34	102.03 (15)

C30—C31—C32	118.2 (6)	C35—Ir2—C34	38.16 (14)
C30—C31—H31	120.9	C36—Ir2—C34	63.42 (15)
C32—C31—H31	120.9	C37—Ir2—C34	62.98 (15)
N2—C32—C31	121.9 (5)	C22—Ir2—C33	144.97 (16)
N2—C32—H32	119.0	N2—Ir2—C33	135.79 (15)
C31—C32—H32	119.0	C35—Ir2—C33	62.67 (14)
C34—C33—C37	109.4 (3)	C36—Ir2—C33	62.79 (14)
C34—C33—C38	125.7 (4)	C37—Ir2—C33	37.67 (14)
C37—C33—C38	124.8 (4)	C34—Ir2—C33	36.35 (15)
C34—C33—Ir2	71.8 (2)	C22—Ir2—H1	86.9 (19)
C37—C33—Ir2	68.4 (2)	N2—Ir2—H1	97.1 (19)
C38—C33—Ir2	128.9 (3)	C35—Ir2—H1	154.9 (19)
C33—C34—C35	107.4 (3)	C36—Ir2—H1	141.2 (19)
C33—C34—C39	125.4 (4)	C37—Ir2—H1	104.4 (19)
C35—C34—C39	126.9 (4)	C34—Ir2—H1	117.0 (19)
C33—C34—Ir2	71.9 (2)	C33—Ir2—H1	94.4 (19)

C6—C1—C2—C3	-0.7 (6)	C26—C27—C28—N2	176.1 (4)
Ir1—C1—C2—C3	-177.0 (3)	C22—C27—C28—N2	-2.7 (5)
C1—C2—C3—C4	0.7 (7)	C26—C27—C28—C29	-1.8 (7)
C2—C3—C4—C5	-0.6 (7)	C22—C27—C28—C29	179.4 (4)
C3—C4—C5—C6	0.4 (7)	N2—C28—C29—C30	0.8 (7)
C4—C5—C6—C1	-0.4 (6)	C27—C28—C29—C30	178.7 (5)
C4—C5—C6—C7	-177.3 (4)	C28—C29—C30—C31	-2.4 (8)
C2—C1—C6—C5	0.5 (6)	C29—C30—C31—C32	2.4 (8)
Ir1—C1—C6—C5	177.3 (3)	C30—C31—C32—N2	-0.9 (7)
C2—C1—C6—C7	177.6 (3)	C37—C33—C34—C35	-0.1 (4)
Ir1—C1—C6—C7	-5.6 (4)	C38—C33—C34—C35	176.3 (4)
C5—C6—C7—N1	173.0 (4)	Ir2—C33—C34—C35	-58.4 (3)
C1—C6—C7—N1	-4.1 (5)	C37—C33—C34—C39	-174.0 (4)
C5—C6—C7—C8	-3.9 (7)	C38—C33—C34—C39	2.4 (7)
C1—C6—C7—C8	179.0 (4)	Ir2—C33—C34—C39	127.8 (4)
N1—C7—C8—C9	2.8 (7)	C37—C33—C34—Ir2	58.3 (3)
C6—C7—C8—C9	179.5 (4)	C38—C33—C34—Ir2	-125.3 (4)
C7—C8—C9—C10	-3.8 (7)	C33—C34—C35—C36	-2.1 (4)
C8—C9—C10—C11	2.2 (7)	C39—C34—C35—C36	171.6 (4)
C9—C10—C11—N1	0.5 (7)	Ir2—C34—C35—C36	-63.2 (2)
C16—C12—C13—C14	-2.2 (4)	C33—C34—C35—C40	-176.9 (4)
C17—C12—C13—C14	171.3 (4)	C39—C34—C35—C40	-3.2 (7)

Ir1—C12—C13—C14	-62.8 (3)	Ir2—C34—C35—C40	121.9 (4)
C16—C12—C13—C18	-176.7 (4)	C33—C34—C35—Ir2	61.2 (3)
C17—C12—C13—C18	-3.2 (7)	C39—C34—C35—Ir2	-125.1 (4)
Ir1—C12—C13—C18	122.6 (4)	C34—C35—C36—C37	3.5 (4)
C16—C12—C13—Ir1	60.6 (3)	C40—C35—C36—C37	178.3 (4)
C17—C12—C13—Ir1	-125.9 (4)	Ir2—C35—C36—C37	-62.1 (3)
C12—C13—C14—C15	3.4 (4)	C34—C35—C36—C41	-173.3 (4)
C18—C13—C14—C15	177.9 (4)	C40—C35—C36—C41	1.5 (6)
Ir1—C13—C14—C15	-62.0 (3)	Ir2—C35—C36—C41	121.1 (4)
C12—C13—C14—C19	-172.3 (4)	C34—C35—C36—Ir2	65.6 (3)
C18—C13—C14—C19	2.2 (7)	C40—C35—C36—Ir2	-119.6 (4)
Ir1—C13—C14—C19	122.3 (4)	C35—C36—C37—C33	-3.6 (4)
C12—C13—C14—Ir1	65.4 (3)	C41—C36—C37—C33	173.3 (4)
C18—C13—C14—Ir1	-120.1 (4)	Ir2—C36—C37—C33	-65.1 (3)
C13—C14—C15—C16	-3.3 (4)	C35—C36—C37—C42	-169.5 (4)
C19—C14—C15—C16	172.5 (4)	C41—C36—C37—C42	7.4 (6)
Ir1—C14—C15—C16	-65.1 (3)	Ir2—C36—C37—C42	128.9 (4)
C13—C14—C15—C20	-169.1 (4)	C35—C36—C37—Ir2	61.5 (2)
C19—C14—C15—C20	6.7 (7)	C41—C36—C37—Ir2	-121.6 (4)
Ir1—C14—C15—C20	129.2 (4)	C34—C33—C37—C36	2.3 (4)
C13—C14—C15—Ir1	61.7 (3)	C38—C33—C37—C36	-174.1 (4)
C19—C14—C15—Ir1	-122.5 (4)	Ir2—C33—C37—C36	62.6 (2)
C13—C12—C16—C15	0.1 (5)	C34—C33—C37—C42	168.1 (4)
C17—C12—C16—C15	-173.4 (4)	C38—C33—C37—C42	-8.4 (6)
Ir1—C12—C16—C15	58.3 (3)	Ir2—C33—C37—C42	-131.6 (4)
C13—C12—C16—C21	176.8 (4)	C34—C33—C37—Ir2	-60.3 (3)
C17—C12—C16—C21	3.3 (7)	C38—C33—C37—Ir2	123.3 (4)
Ir1—C12—C16—C21	-125.0 (4)	C10—C11—N1—C7	-1.5 (6)
C13—C12—C16—Ir1	-58.2 (3)	C10—C11—N1—Ir1	168.8 (3)
C17—C12—C16—Ir1	128.3 (5)	C8—C7—N1—C11	-0.1 (5)
C14—C15—C16—C12	2.0 (5)	C6—C7—N1—C11	-177.2 (3)
C20—C15—C16—C12	167.6 (4)	C8—C7—N1—Ir1	-171.1 (3)
Ir1—C15—C16—C12	-60.7 (3)	C6—C7—N1—Ir1	11.8 (4)
C14—C15—C16—C21	-174.7 (4)	C31—C32—N2—C28	-0.6 (6)
C20—C15—C16—C21	-9.1 (7)	C31—C32—N2—Ir2	170.4 (3)
Ir1—C15—C16—C21	122.6 (4)	C29—C28—N2—C32	0.6 (6)
C14—C15—C16—Ir1	62.7 (3)	C27—C28—N2—C32	-177.4 (4)
C20—C15—C16—Ir1	-131.7 (4)	C29—C28—N2—Ir2	-171.0 (3)
C27—C22—C23—C24	1.4 (6)	C27—C28—N2—Ir2	10.9 (4)

Ir2—C22—C23—C24	-174.5 (4)	F1—C43—S1—O1	177.2 (5)
C22—C23—C24—C25	0.8 (7)	F3—C43—S1—O1	-59.9 (5)
C23—C24—C25—C26	-2.2 (8)	F2—C43—S1—O1	57.7 (5)
C24—C25—C26—C27	1.5 (7)	F1—C43—S1—O2	-62.8 (5)
C25—C26—C27—C22	0.7 (7)	F3—C43—S1—O2	60.1 (5)
C25—C26—C27—C28	-178.0 (4)	F2—C43—S1—O2	177.7 (4)
C23—C22—C27—C26	-2.1 (6)	F1—C43—S1—O3	56.7 (5)
Ir2—C22—C27—C26	174.3 (3)	F3—C43—S1—O3	179.7 (4)
C23—C22—C27—C28	176.7 (4)	F2—C43—S1—O3	-62.8 (4)
Ir2—C22—C27—C28	-6.9 (4)		

7.9 [**3A**][$BArF_{24}$]

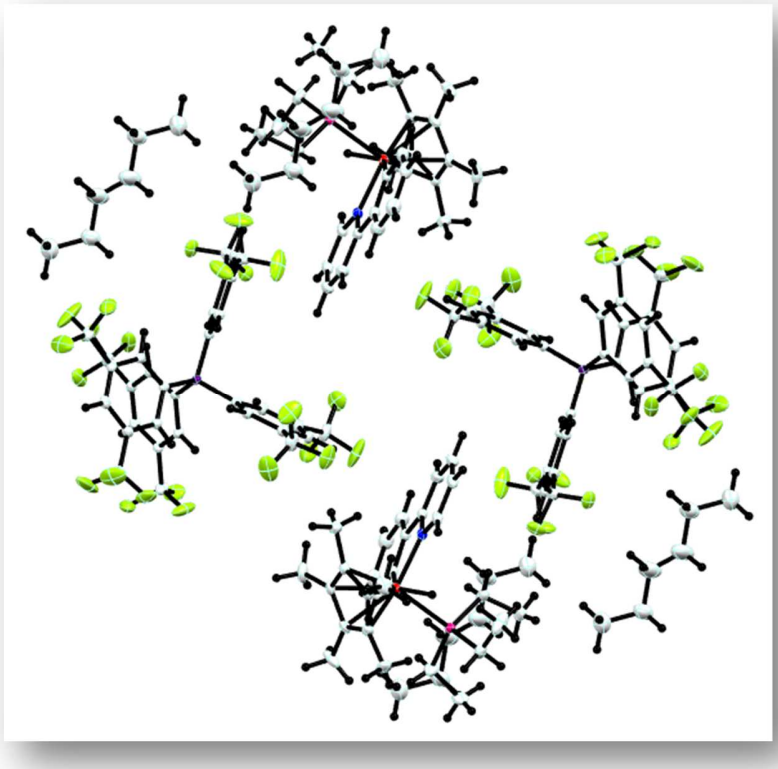

7.9.1 **Figure A25.** Crystal lattice packing of [**3A**][$BArF_{24}$].

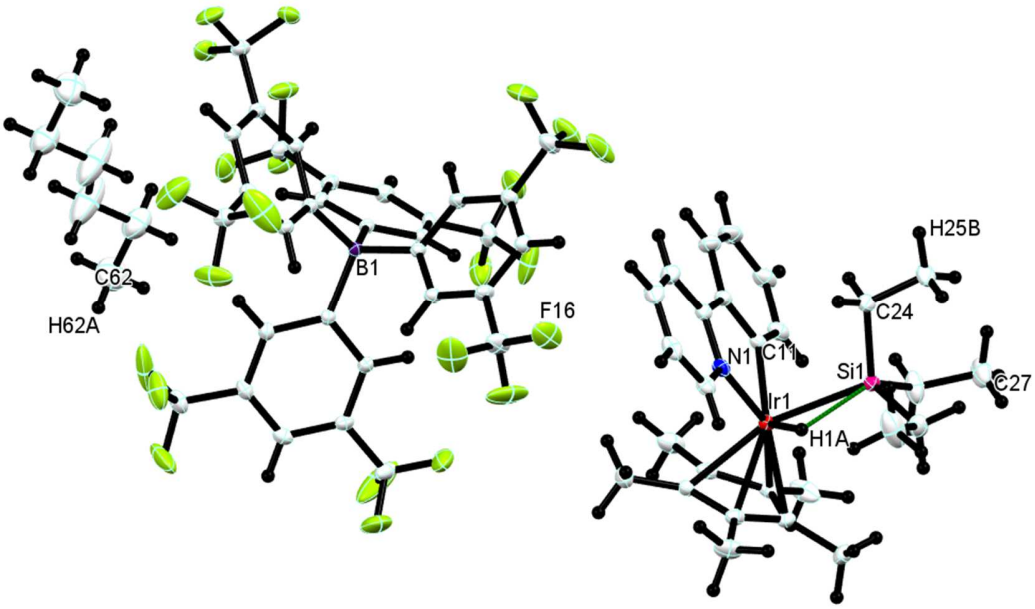

7.9.2 **Figure A26.** Asymmetric unit of [**3A**][BArF$_{24}$], with all hydrogens and partial numbering of atoms. Green dots represent the Si1–H1A interaction (2.10 Å).

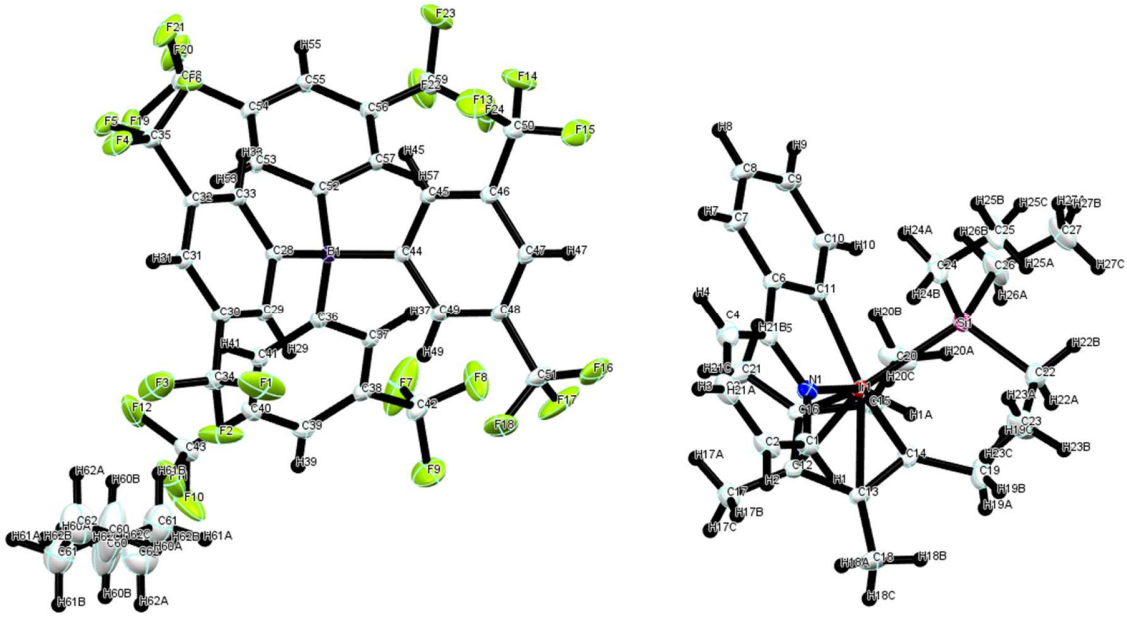

7.9.3 **Figure A27.** Asymmetric unit of [**3A**][BArF$_{24}$], with all hydrogens and total numbering of atoms.

[**3A**][$BArF_{24}$]

7.9.4 Crystal data

$C_{32}H_{12}BF_{24}\cdot C_{27}H_{39}IrNSi\cdot 0.5(C_6H_{14})$	$Z = 2$
$M_r = 1504.19$	$F(000) = 1498$
Triclinic, $P\bar{1}$	$D_x = 1.574$ Mg m^{-3}
$a = 12.614$ (5) Å	Mo $K\alpha$ radiation, $\lambda = 0.71073$ Å
$b = 13.698$ (5) Å	Cell parameters from 9930 reflections
$c = 19.789$ (5) Å	$\theta = 2.5$–$31.9°$
$\alpha = 81.064$ (5)°	$\mu = 2.23$ mm^{-1}
$\beta = 71.685$ (5)°	$T = 173$ K
$\gamma = 79.438$ (5)°	Block, yellow
$V = 3173.5$ (19) Å^3	0.38 × 0.35 × 0.30 mm

7.9.5 Data collection

Bruker APEX-II CCD diffractometer	19600 reflections with $I > 2\sigma(I)$
Radiation source: fine focus sealed tube	$R_{int} = 0.023$
ϕ and ω scans	$\theta_{max} = 32.1°$, $\theta_{min} = 1.5°$
Absorption correction: multi-scan *SADABS*	$h = -18\rightarrow18$
$T_{min} = 0.665$, $T_{max} = 0.746$	$k = -20\rightarrow20$
83067 measured reflections	$l = -29\rightarrow29$
22017 independent reflections	

7.9.6 Refinement

Refinement on F^2	Primary atom site location: structure-invariant direct methods
Least-squares matrix: full	Secondary atom site location: difference Fourier map
$R[F^2 > 2\sigma(F^2)] = 0.033$	Hydrogen site location: mixed
$wR(F^2) = 0.079$	H-atom parameters constrained
$S = 1.04$	$w = 1/[\sigma^2(F_o^2) + (0.0415P)^2 + 2.3317P]$ where $P = (F_o^2 + 2F_c^2)/3$
22017 reflections	$(\Delta/\sigma)_{max} = 0.004$

820 parameters	$\Delta\rangle_{max}$ = 1.69 e Å^{-3}
0 restraints	$\Delta\rangle_{min}$ = -1.29 e Å^{-3}

7.9.7 Special details

Geometry. All esds (except the esd in the dihedral angle between two l.s. planes) are estimated using the full covariance matrix. The cell esds are taken into account individually in the estimation of esds in distances, angles and torsion angles; correlations between esds in cell parameters are only used when they are defined by crystal symmetry. An approximate (isotropic) treatment of cell esds is used for estimating esds involving l.s. planes.

7.9.8 **Table A25.** Fractional atomic coordinates and isotropic or equivalent isotropic displacement parameters (Å^2) for [**3A**][BArF$_{24}$].

	x	*y*	*z*	U_{iso}*/U_{eq}
C1	0.58079 (19)	0.74423 (18)	0.73285 (14)	0.0335 (5)
H1	0.6091	0.7946	0.7474	0.040*
C2	0.6561 (2)	0.6745 (2)	0.69093 (14)	0.0404 (6)
H2	0.7348	0.6777	0.6763	0.049*
C3	0.6149 (3)	0.6002 (2)	0.67072 (15)	0.0454 (7)
H3	0.6652	0.5516	0.6421	0.054*
C4	0.5013 (3)	0.59719 (19)	0.69221 (15)	0.0406 (6)
H4	0.4726	0.5460	0.6789	0.049*
C5	0.42716 (19)	0.66924 (16)	0.73371 (12)	0.0282 (4)
C6	0.3050 (2)	0.67408 (16)	0.75971 (12)	0.0286 (4)
C7	0.2460 (3)	0.6068 (2)	0.74478 (16)	0.0412 (6)
H7	0.2857	0.5547	0.7159	0.049*
C8	0.1309 (3)	0.6163 (2)	0.77201 (17)	0.0468 (7)
H8	0.0906	0.5709	0.7620	0.056*
C9	0.0736 (2)	0.6920 (2)	0.81408 (16)	0.0409 (6)
H9	-0.0062	0.6987	0.8328	0.049*
C10	0.1321 (2)	0.75838 (18)	0.82916 (14)	0.0338 (5)
H10	0.0917	0.8101	0.8582	0.041*
C11	0.24869 (17)	0.75025 (15)	0.80238 (12)	0.0250 (4)
C12	0.38183 (19)	0.97308 (15)	0.71659 (12)	0.0270 (4)
C13	0.42217 (19)	0.99224 (16)	0.77245 (13)	0.0281 (4)
C14	0.3270 (2)	1.00618 (16)	0.83495 (13)	0.0316 (5)

C15	0.22902 (19)	0.99157 (16)	0.81809 (14)	0.0324 (5)
C16	0.26372 (19)	0.97148 (16)	0.74431 (14)	0.0305 (4)
C17	0.4518 (3)	0.9570 (2)	0.64165 (14)	0.0433 (6)
H17A	0.4182	0.9128	0.6223	0.065*
H17B	0.5284	0.9263	0.6415	0.065*
H17C	0.4548	1.0213	0.6119	0.065*
C18	0.5391 (2)	1.0136 (2)	0.7622 (2)	0.0488 (7)
H18A	0.5935	0.9719	0.7271	0.073*
H18B	0.5565	0.9987	0.8079	0.073*
H18C	0.5434	1.0842	0.7448	0.073*
C19	0.3295 (4)	1.0430 (2)	0.90184 (16)	0.0546 (8)
H19A	0.3238	1.1160	0.8951	0.082*
H19B	0.4005	1.0141	0.9122	0.082*
H19C	0.2659	1.0230	0.9419	0.082*
C20	0.1089 (2)	1.0155 (2)	0.8624 (2)	0.0580 (10)
H20A	0.1056	1.0113	0.9129	0.087*
H20B	0.0642	0.9677	0.8565	0.087*
H20C	0.0783	1.0833	0.8468	0.087*
C21	0.1867 (3)	0.9600 (2)	0.7030 (2)	0.0503 (8)
H21A	0.1593	1.0258	0.6823	0.076*
H21B	0.1224	0.9289	0.7350	0.076*
H21C	0.2278	0.9178	0.6645	0.076*
C22	0.4015 (3)	0.7896 (2)	0.98680 (16)	0.0453 (6)
H22A	0.3822	0.8615	0.9936	0.054*
H22B	0.3805	0.7518	1.0348	0.054*
C23	0.5293 (3)	0.7666 (4)	0.9543 (2)	0.0801 (14)
H23A	0.5505	0.6952	0.9485	0.120*
H23B	0.5671	0.7843	0.9861	0.120*
H23C	0.5523	0.8055	0.9075	0.120*
C24	0.3455 (3)	0.62277 (19)	0.92643 (15)	0.0490 (7)
H24A	0.2897	0.6035	0.9070	0.059*
H24B	0.4207	0.6089	0.8914	0.059*
C25	0.3451 (3)	0.5573 (2)	0.99568 (16)	0.0539 (8)
H25A	0.4049	0.5709	1.0132	0.081*
H25B	0.3583	0.4869	0.9871	0.081*
H25C	0.2718	0.5716	1.0315	0.081*
C26	0.1613 (3)	0.7960 (3)	0.98833 (16)	0.0570 (9)

H26A	0.1440	0.8698	0.9838	0.068*
H26B	0.1119	0.7707	0.9669	0.068*
C27	0.1309 (3)	0.7587 (3)	1.06717 (17)	0.0612 (9)
H27A	0.1468	0.6857	1.0728	0.092*
H27B	0.0505	0.7800	1.0897	0.092*
H27C	0.1757	0.7864	1.0900	0.092*
C28	0.18851 (16)	0.69378 (14)	0.27756 (11)	0.0215 (3)
C29	0.30304 (16)	0.70443 (15)	0.24617 (11)	0.0232 (4)
H29	0.3304	0.7586	0.2568	0.028*
C30	0.37741 (16)	0.63891 (15)	0.20027 (11)	0.0239 (4)
C31	0.34164 (17)	0.55878 (15)	0.18274 (11)	0.0249 (4)
H31	0.3922	0.5147	0.1505	0.030*
C32	0.22993 (17)	0.54527 (14)	0.21386 (11)	0.0234 (4)
C33	0.15542 (17)	0.61079 (15)	0.26097 (11)	0.0231 (4)
H33	0.0797	0.5984	0.2824	0.028*
C34	0.49881 (19)	0.65438 (18)	0.17012 (15)	0.0339 (5)
C35	0.1841 (2)	0.46303 (16)	0.19511 (13)	0.0306 (4)
C36	0.12206 (16)	0.88857 (14)	0.30158 (11)	0.0213 (3)
C37	0.08208 (17)	0.96441 (15)	0.34756 (11)	0.0243 (4)
H37	0.0515	0.9465	0.3974	0.029*
C38	0.08564 (18)	1.06466 (15)	0.32267 (12)	0.0267 (4)
C39	0.12923 (19)	1.09423 (16)	0.25008 (13)	0.0296 (4)
H39	0.1325	1.1627	0.2329	0.035*
C40	0.16769 (18)	1.02107 (17)	0.20363 (12)	0.0280 (4)
C41	0.16367 (17)	0.92050 (16)	0.22886 (11)	0.0249 (4)
H41	0.1901	0.8721	0.1955	0.030*
C42	0.0369 (3)	1.14361 (19)	0.37289 (16)	0.0409 (6)
C43	0.2141 (2)	1.0497 (2)	0.12524 (14)	0.0400 (6)
C44	0.14796 (16)	0.74090 (14)	0.40601 (10)	0.0208 (3)
C45	0.11398 (18)	0.65727 (16)	0.45310 (12)	0.0262 (4)
H45	0.0625	0.6217	0.4443	0.031*
C46	0.1529 (2)	0.62441 (16)	0.51239 (12)	0.0285 (4)
C47	0.22855 (19)	0.67348 (17)	0.52722 (12)	0.0286 (4)
H47	0.2551	0.6513	0.5677	0.034*
C48	0.26409 (18)	0.75548 (17)	0.48124 (13)	0.0276 (4)
C49	0.22523 (17)	0.78864 (16)	0.42185 (12)	0.0249 (4)
H49	0.2519	0.8452	0.3912	0.030*

C50	0.1121 (3)	0.5342 (2)	0.56001 (16)	0.0461 (7)
C51	0.3436 (3)	0.8127 (2)	0.49513 (18)	0.0471 (7)
C52	-0.02753 (16)	0.76875 (14)	0.35008 (10)	0.0205 (3)
C53	-0.07376 (17)	0.75470 (15)	0.29711 (11)	0.0238 (4)
H53	-0.0250	0.7440	0.2505	0.029*
C54	-0.18939 (18)	0.75605 (16)	0.31093 (12)	0.0262 (4)
C55	-0.26423 (18)	0.77614 (17)	0.37702 (13)	0.0286 (4)
H55	-0.3431	0.7774	0.3863	0.034*
C56	-0.22050 (17)	0.79432 (16)	0.42917 (11)	0.0257 (4)
C57	-0.10491 (17)	0.78958 (15)	0.41673 (11)	0.0232 (4)
H57	-0.0776	0.8007	0.4541	0.028*
C58	-0.2335 (2)	0.73067 (19)	0.25482 (14)	0.0347 (5)
C59	-0.3019 (2)	0.8187 (2)	0.49981 (13)	0.0368 (5)
C60	0.9684 (6)	0.5426 (6)	-0.0031 (4)	0.134 (3)
H60A	0.9332	0.5382	-0.0405	0.160*
H60B	1.0206	0.5928	-0.0232	0.160*
C61	0.8752 (4)	0.5875 (4)	0.0575 (3)	0.0807 (13)
H61A	0.9052	0.5929	0.0972	0.097*
H61B	0.8152	0.5443	0.0759	0.097*
C62	0.8263 (5)	0.6916 (4)	0.0299 (3)	0.0924 (15)
H62A	0.8855	0.7346	0.0132	0.139*
H62B	0.7644	0.7207	0.0686	0.139*
H62C	0.7978	0.6858	-0.0099	0.139*
B1	0.10764 (18)	0.77203 (16)	0.33367 (12)	0.0208 (4)
N1	0.46747 (16)	0.74263 (14)	0.75375 (10)	0.0275 (4)
F1	0.55864 (19)	0.6142 (3)	0.21245 (17)	0.1105 (12)
F2	0.51270 (16)	0.74880 (14)	0.15745 (15)	0.0777 (8)
F3	0.54842 (17)	0.6178 (2)	0.10838 (15)	0.0913 (10)
F4	0.26409 (15)	0.39792 (13)	0.15719 (11)	0.0529 (5)
F5	0.11273 (16)	0.49839 (13)	0.15618 (10)	0.0476 (4)
F6	0.12483 (14)	0.41002 (11)	0.25298 (9)	0.0419 (4)
F7	-0.0604 (3)	1.1907 (3)	0.36590 (19)	0.1235 (14)
F8	0.0212 (3)	1.11087 (15)	0.43991 (11)	0.0864 (9)
F9	0.0994 (3)	1.21441 (18)	0.36083 (15)	0.0943 (9)
F10	0.2165 (3)	1.14579 (18)	0.10787 (14)	0.1139 (13)
F11	0.31898 (18)	1.0090 (2)	0.09815 (11)	0.0752 (7)
F12	0.1591 (2)	1.0209 (3)	0.08718 (11)	0.1115 (13)

F13	0.1449 (2)	0.45248 (14)	0.52694 (14)	0.0782 (7)
F14	-0.00013 (19)	0.54185 (17)	0.58265 (12)	0.0716 (6)
F15	0.1458 (3)	0.5162 (2)	0.61848 (14)	0.0984 (11)
F16	0.3784 (2)	0.77320 (18)	0.55152 (13)	0.0760 (7)
F17	0.2989 (3)	0.90525 (17)	0.50761 (18)	0.0955 (10)
F18	0.4361 (2)	0.8196 (2)	0.43956 (14)	0.0900 (9)
F19	-0.1745 (2)	0.76221 (19)	0.18817 (10)	0.0683 (6)
F20	-0.33816 (17)	0.77536 (17)	0.25951 (13)	0.0661 (6)
F21	-0.2320 (2)	0.63476 (13)	0.25633 (13)	0.0667 (6)
F22	-0.37875 (18)	0.89848 (18)	0.49309 (11)	0.0700 (6)
F23	-0.36517 (19)	0.74709 (19)	0.53087 (11)	0.0738 (7)
F24	-0.25560 (16)	0.8374 (3)	0.54589 (11)	0.0864 (9)
Si1	0.31250 (5)	0.76027 (4)	0.93409 (3)	0.02638 (11)
Ir1	0.34970 (2)	0.85014 (2)	0.81072 (2)	0.02325 (3)
H1A	0.4352	0.8250	0.8492	0.050*

7.9.9 **Table A26.** Atomic displacement parameters (Å^2) for [**3A**][BArF$_{24}$].

	U^{11}	U^{22}	U^{33}	U^{12}	U^{13}	U^{23}
C1	0.0278 (10)	0.0334 (11)	0.0350 (12)	-0.0012 (8)	-0.0087 (9)	0.0039 (9)
C2	0.0301 (11)	0.0418 (13)	0.0371 (13)	0.0051 (9)	-0.0037 (10)	0.0070 (11)
C3	0.0487 (15)	0.0385 (13)	0.0356 (13)	0.0116 (11)	-0.0034 (11)	-0.0045 (11)
C4	0.0519 (15)	0.0304 (11)	0.0349 (13)	0.0008 (10)	-0.0080 (11)	-0.0078 (10)
C5	0.0344 (10)	0.0239 (9)	0.0248 (10)	-0.0026 (8)	-0.0086 (8)	0.0001 (8)
C6	0.0348 (10)	0.0251 (9)	0.0285 (10)	-0.0089 (8)	-0.0126 (9)	0.0014 (8)
C7	0.0519 (15)	0.0333 (12)	0.0460 (15)	-0.0157 (11)	-0.0192 (12)	-0.0056 (11)
C8	0.0537 (16)	0.0425 (14)	0.0568 (18)	-0.0270 (12)	-0.0257 (14)	0.0013 (13)
C9	0.0351 (12)	0.0428 (13)	0.0514 (16)	-0.0189 (10)	-0.0208 (11)	0.0078 (12)
C10	0.0288 (10)	0.0330 (11)	0.0420 (13)	-0.0105 (8)	-0.0142 (9)	0.0044 (10)
C11	0.0247 (9)	0.0235 (9)	0.0285 (10)	-0.0074 (7)	-0.0112 (8)	0.0042 (7)
C12	0.0311 (10)	0.0216 (8)	0.0296 (10)	-0.0069 (7)	-0.0112 (8)	0.0015 (8)
C13	0.0286 (9)	0.0257 (9)	0.0336 (11)	-0.0058 (7)	-0.0137 (8)	-0.0015 (8)
C14	0.0432 (12)	0.0208 (9)	0.0307 (11)	-0.0027 (8)	-0.0100 (9)	-0.0060 (8)
C15	0.0282 (10)	0.0204 (9)	0.0425 (13)	-0.0013 (7)	-0.0042 (9)	-0.0006 (9)
C16	0.0304 (10)	0.0214 (9)	0.0435 (13)	-0.0048 (7)	-0.0193 (9)	0.0042 (8)

C17	0.0596 (17)	0.0360 (12)	0.0295 (12)	-0.0082 (12)	-0.0073 (12)	0.0006 (10)
C18	0.0379 (13)	0.0420 (14)	0.075 (2)	-0.0171 (11)	-0.0247 (14)	-0.0022 (14)
C19	0.094 (3)	0.0365 (14)	0.0355 (14)	-0.0086 (15)	-0.0187 (16)	-0.0119 (11)
C20	0.0334 (13)	0.0335 (13)	0.081 (2)	0.0067 (10)	0.0087 (14)	0.0028 (14)
C21	0.0577 (17)	0.0380 (13)	0.073 (2)	-0.0163 (12)	-0.0474 (17)	0.0121 (13)
C22	0.0593 (17)	0.0464 (15)	0.0384 (14)	-0.0147 (13)	-0.0250 (13)	0.0020 (11)
C23	0.056 (2)	0.133 (4)	0.060 (2)	-0.040 (2)	-0.0331 (18)	0.030 (2)
C24	0.089 (2)	0.0260 (11)	0.0302 (12)	-0.0051 (13)	-0.0173 (14)	-0.0005 (9)
C25	0.088 (2)	0.0309 (12)	0.0334 (14)	0.0059 (14)	-0.0156 (15)	0.0031 (11)
C26	0.0384 (14)	0.083 (2)	0.0345 (14)	0.0044 (15)	0.0004 (12)	0.0016 (15)
C27	0.0580 (19)	0.064 (2)	0.0381 (16)	0.0060 (15)	0.0104 (14)	-0.0040 (14)
C28	0.0230 (8)	0.0217 (8)	0.0202 (8)	-0.0048 (6)	-0.0064 (7)	-0.0016 (7)
C29	0.0231 (8)	0.0228 (8)	0.0259 (9)	-0.0058 (7)	-0.0074 (7)	-0.0050 (7)
C30	0.0210 (8)	0.0241 (9)	0.0266 (9)	-0.0032 (7)	-0.0065 (7)	-0.0034 (7)
C31	0.0259 (9)	0.0235 (9)	0.0253 (9)	-0.0013 (7)	-0.0077 (7)	-0.0054 (7)
C32	0.0260 (9)	0.0208 (8)	0.0263 (9)	-0.0046 (7)	-0.0105 (7)	-0.0040 (7)
C33	0.0242 (8)	0.0214 (8)	0.0248 (9)	-0.0050 (7)	-0.0081 (7)	-0.0018 (7)
C34	0.0244 (9)	0.0328 (11)	0.0441 (13)	-0.0047 (8)	-0.0067 (9)	-0.0094 (10)
C35	0.0344 (11)	0.0260 (9)	0.0347 (11)	-0.0071 (8)	-0.0118 (9)	-0.0065 (8)
C36	0.0203 (8)	0.0236 (8)	0.0209 (8)	-0.0055 (6)	-0.0059 (7)	-0.0026 (7)
C37	0.0270 (9)	0.0241 (9)	0.0232 (9)	-0.0055 (7)	-0.0074 (7)	-0.0040 (7)
C38	0.0273 (9)	0.0228 (9)	0.0337 (11)	-0.0038 (7)	-0.0125 (8)	-0.0066 (8)
C39	0.0287 (10)	0.0239 (9)	0.0369 (12)	-0.0056 (7)	-0.0126 (9)	0.0028 (8)
C40	0.0249 (9)	0.0310 (10)	0.0253 (10)	-0.0049 (7)	-0.0062 (8)	0.0040 (8)
C41	0.0254 (9)	0.0265 (9)	0.0226 (9)	-0.0037 (7)	-0.0066 (7)	-0.0025 (7)
C42	0.0528 (15)	0.0296 (11)	0.0455 (15)	-0.0015 (10)	-0.0201 (12)	-0.0132 (10)
C43	0.0391 (12)	0.0432 (13)	0.0313 (12)	-0.0086 (10)	-0.0057 (10)	0.0084 (10)
C44	0.0203 (8)	0.0216 (8)	0.0206 (8)	-0.0048 (6)	-0.0049 (7)	-0.0034 (7)
C45	0.0293 (9)	0.0254 (9)	0.0295 (10)	-0.0112 (7)	-0.0132 (8)	-0.0014 (8)
C46	0.0349 (10)	0.0256 (9)	0.0287 (10)	-0.0100 (8)	-0.0139 (9)	0.0022 (8)
C47	0.0323 (10)	0.0295 (10)	0.0296 (10)	-0.0055 (8)	-0.0168 (9)	-0.0021 (8)
C48	0.0258 (9)	0.0298 (10)	0.0328 (11)	-0.0094 (8)	-0.0129 (8)	-0.0048 (8)
C49	0.0235 (8)	0.0260 (9)	0.0279 (10)	-0.0080 (7)	-0.0082 (7)	-0.0038 (8)
C50	0.0638 (18)	0.0429 (14)	0.0442 (15)	-0.0269 (13)	-0.0329 (14)	0.0168 (12)
C51	0.0500 (15)	0.0499 (15)	0.0585 (18)	-0.0231 (13)	-0.0342 (14)	0.0011 (13)
C52	0.0221 (8)	0.0203 (8)	0.0204 (8)	-0.0054 (6)	-0.0069 (7)	-0.0019 (7)
C53	0.0263 (9)	0.0249 (9)	0.0223 (9)	-0.0038 (7)	-0.0092 (7)	-0.0037 (7)

C54	0.0292 (9)	0.0247 (9)	0.0300 (10)	-0.0052 (7)	-0.0147 (8)	-0.0040 (8)
C55	0.0216 (8)	0.0327 (10)	0.0338 (11)	-0.0072 (7)	-0.0102 (8)	-0.0022 (9)
C56	0.0224 (8)	0.0304 (10)	0.0230 (9)	-0.0064 (7)	-0.0043 (7)	-0.0008 (8)
C57	0.0229 (8)	0.0278 (9)	0.0207 (9)	-0.0070 (7)	-0.0073 (7)	-0.0019 (7)
C58	0.0394 (12)	0.0349 (11)	0.0400 (13)	-0.0061 (9)	-0.0237 (10)	-0.0077 (10)
C59	0.0278 (10)	0.0526 (15)	0.0271 (11)	-0.0092 (10)	-0.0036 (9)	-0.0011 (10)
C60	0.115 (5)	0.186 (7)	0.110 (4)	0.064 (4)	-0.058 (4)	-0.093 (5)
C61	0.082 (3)	0.081 (3)	0.078 (3)	0.007 (2)	-0.022 (2)	-0.032 (2)
C62	0.098 (4)	0.083 (3)	0.092 (4)	0.006 (3)	-0.036 (3)	-0.002 (3)
B1	0.0220 (9)	0.0223 (9)	0.0190 (9)	-0.0064 (7)	-0.0050 (7)	-0.0032 (7)
N1	0.0278 (8)	0.0250 (8)	0.0281 (9)	-0.0020 (6)	-0.0088 (7)	0.0013 (7)
F1	0.0465 (12)	0.159 (3)	0.131 (2)	-0.0485 (15)	-0.0555 (14)	0.074 (2)
F2	0.0392 (9)	0.0447 (10)	0.127 (2)	-0.0197 (8)	0.0196 (11)	-0.0193 (11)
F3	0.0402 (10)	0.133 (2)	0.0989 (18)	-0.0337 (12)	0.0260 (11)	-0.0785 (17)
F4	0.0495 (9)	0.0412 (8)	0.0703 (12)	-0.0088 (7)	-0.0061 (8)	-0.0338 (8)
F5	0.0611 (10)	0.0460 (9)	0.0543 (10)	-0.0193 (8)	-0.0384 (9)	-0.0014 (8)
F6	0.0504 (9)	0.0339 (7)	0.0462 (9)	-0.0223 (7)	-0.0146 (7)	0.0021 (6)
F7	0.104 (2)	0.139 (3)	0.154 (3)	0.079 (2)	-0.081 (2)	-0.117 (2)
F8	0.164 (3)	0.0436 (10)	0.0424 (11)	-0.0100 (13)	-0.0137 (14)	-0.0189 (9)
F9	0.146 (2)	0.0567 (13)	0.0880 (18)	-0.0519 (15)	-0.0138 (17)	-0.0285 (12)
F10	0.181 (3)	0.0492 (12)	0.0569 (14)	-0.0096 (16)	0.0256 (17)	0.0212 (11)
F11	0.0521 (11)	0.1129 (19)	0.0370 (10)	0.0030 (12)	0.0058 (8)	0.0052 (11)
F12	0.0916 (18)	0.232 (4)	0.0303 (10)	-0.096 (2)	-0.0255 (11)	0.0303 (16)
F13	0.117 (2)	0.0287 (8)	0.0891 (17)	-0.0237 (10)	-0.0312 (15)	0.0093 (9)
F14	0.0682 (13)	0.0751 (14)	0.0672 (14)	-0.0433 (11)	-0.0113 (11)	0.0265 (11)
F15	0.163 (3)	0.0981 (18)	0.0779 (16)	-0.0890 (19)	-0.0913 (18)	0.0604 (14)
F16	0.0933 (16)	0.0861 (15)	0.0856 (16)	-0.0489 (13)	-0.0702 (14)	0.0163 (12)
F17	0.123 (2)	0.0478 (11)	0.162 (3)	-0.0246 (13)	-0.094 (2)	-0.0228 (14)
F18	0.0634 (13)	0.145 (2)	0.0820 (16)	-0.0738 (16)	-0.0236 (12)	0.0034 (16)
F19	0.0905 (16)	0.0942 (16)	0.0393 (10)	-0.0405 (13)	-0.0341 (10)	-0.0001 (10)
F20	0.0588 (11)	0.0735 (13)	0.0889 (15)	0.0124 (10)	-0.0555 (12)	-0.0319 (12)
F21	0.1112 (18)	0.0313 (8)	0.0875 (15)	-0.0116 (9)	-0.0692 (14)	-0.0097 (9)
F22	0.0637 (12)	0.0808 (14)	0.0424 (10)	0.0253 (11)	0.0003 (9)	-0.0134 (10)
F23	0.0698 (13)	0.0863 (15)	0.0493 (11)	-0.0384 (12)	0.0147 (10)	0.0045 (11)
F24	0.0377 (9)	0.191 (3)	0.0369 (10)	-0.0196 (13)	-0.0023 (8)	-0.0463 (14)
Si1	0.0302 (3)	0.0240 (3)	0.0233 (3)	-0.0024 (2)	-0.0060 (2)	-0.0031 (2)
Ir1	0.02281 (4)	0.02198 (4)	0.02522 (4)	-0.00368 (2)	-0.00765 (3)	-0.00151 (3)

7.9.10 **Table A27.** Interatomic distances (Å) and angles (deg) for [**3A**][BArF$_{24}$].

C1—N1	1.361 (3)	C31—C32	1.383 (3)
C1—C2	1.386 (4)	C31—H31	0.9500
C1—H1	0.9500	C32—C33	1.399 (3)
C2—C3	1.385 (5)	C32—C35	1.498 (3)
C2—H2	0.9500	C33—H33	0.9500
C3—C4	1.367 (4)	C34—F1	1.295 (4)
C3—H3	0.9500	C34—F2	1.312 (3)
C4—C5	1.398 (3)	C34—F3	1.315 (3)
C4—H4	0.9500	C35—F4	1.334 (3)
C5—N1	1.365 (3)	C35—F5	1.341 (3)
C5—C6	1.455 (3)	C35—F6	1.342 (3)
C6—C11	1.390 (3)	C36—C41	1.397 (3)
C6—C7	1.402 (3)	C36—C37	1.405 (3)
C7—C8	1.369 (4)	C36—B1	1.644 (3)
C7—H7	0.9500	C37—C38	1.389 (3)
C8—C9	1.380 (4)	C37—H37	0.9500
C8—H8	0.9500	C38—C39	1.391 (3)
C9—C10	1.389 (3)	C38—C42	1.497 (3)
C9—H9	0.9500	C39—C40	1.383 (3)
C10—C11	1.387 (3)	C39—H39	0.9500
C10—H10	0.9500	C40—C41	1.395 (3)
C11—Ir1	2.089 (2)	C40—C43	1.492 (3)
C12—C16	1.420 (3)	C41—H41	0.9500
C12—C13	1.429 (3)	C42—F8	1.297 (4)
C12—C17	1.495 (3)	C42—F9	1.307 (4)
C12—Ir1	2.296 (2)	C42—F7	1.315 (4)
C13—C14	1.437 (3)	C43—F10	1.311 (4)
C13—C18	1.501 (3)	C43—F12	1.313 (4)
C13—Ir1	2.226 (2)	C43—F11	1.314 (3)
C14—C15	1.431 (4)	C44—C45	1.401 (3)
C14—C19	1.499 (4)	C44—C49	1.402 (3)
C14—Ir1	2.211 (2)	C44—B1	1.636 (3)
C15—C16	1.442 (4)	C45—C46	1.392 (3)
C15—C20	1.498 (3)	C45—H45	0.9500
C15—Ir1	2.227 (2)	C46—C47	1.386 (3)
C16—C21	1.495 (4)	C46—C50	1.499 (3)

C16—Ir1	2.285 (2)	C47—C48	1.379 (3)
C17—H17A	0.9800	C47—H47	0.9500
C17—H17B	0.9800	C48—C49	1.394 (3)
C17—H17C	0.9800	C48—C51	1.492 (3)
C18—H18A	0.9800	C49—H49	0.9500
C18—H18B	0.9800	C50—F13	1.319 (4)
C18—H18C	0.9800	C50—F15	1.327 (3)
C19—H19A	0.9800	C50—F14	1.334 (4)
C19—H19B	0.9800	C51—F17	1.317 (4)
C19—H19C	0.9800	C51—F16	1.328 (4)
C20—H20A	0.9800	C51—F18	1.334 (4)
C20—H20B	0.9800	C52—C53	1.401 (3)
C20—H20C	0.9800	C52—C57	1.407 (3)
C21—H21A	0.9800	C52—B1	1.640 (3)
C21—H21B	0.9800	C53—C54	1.394 (3)
C21—H21C	0.9800	C53—H53	0.9500
C22—C23	1.528 (5)	C54—C55	1.385 (3)
C22—Si1	1.882 (3)	C54—C58	1.497 (3)
C22—H22A	0.9900	C55—C56	1.385 (3)
C22—H22B	0.9900	C55—H55	0.9500
C23—H23A	0.9800	C56—C57	1.391 (3)
C23—H23B	0.9800	C56—C59	1.496 (3)
C23—H23C	0.9800	C57—H57	0.9500
C24—C25	1.516 (4)	C58—F21	1.306 (3)
C24—Si1	1.872 (3)	C58—F20	1.331 (3)
C24—H24A	0.9900	C58—F19	1.343 (3)
C24—H24B	0.9900	C59—F24	1.304 (3)
C25—H25A	0.9800	C59—F23	1.330 (3)
C25—H25B	0.9800	C59—F22	1.341 (3)
C25—H25C	0.9800	C60—C60^{i}	1.299 (12)
C26—C27	1.513 (4)	C60—C61	1.510 (7)
C26—Si1	1.888 (3)	C60—H60A	0.9900
C26—H26A	0.9900	C60—H60B	0.9900
C26—H26B	0.9900	C61—C62	1.536 (7)
C27—H27A	0.9800	C61—H61A	0.9900
C27—H27B	0.9800	C61—H61B	0.9900
C27—H27C	0.9800	C62—H62A	0.9800
C28—C33	1.397 (3)	C62—H62B	0.9800
C28—C29	1.407 (3)	C62—H62C	0.9800

C28—B1	1.637 (3)	N1—Ir1	2.0754 (19)
C29—C30	1.386 (3)	Si1—H1A	2.1000
C29—H29	0.9500	Si1—Ir1	2.5008 (8)
C30—C31	1.388 (3)	Ir1—H1A	1.4698
C30—C34	1.500 (3)		

N1—C1—C2	121.9 (3)	C37—C36—B1	119.90 (17)
N1—C1—H1	119.1	C38—C37—C36	122.3 (2)
C2—C1—H1	119.1	C38—C37—H37	118.8
C3—C2—C1	119.0 (2)	C36—C37—H37	118.8
C3—C2—H2	120.5	C37—C38—C39	120.7 (2)
C1—C2—H2	120.5	C37—C38—C42	120.7 (2)
C4—C3—C2	119.5 (2)	C39—C38—C42	118.5 (2)
C4—C3—H3	120.2	C40—C39—C38	118.0 (2)
C2—C3—H3	120.2	C40—C39—H39	121.0
C3—C4—C5	120.2 (3)	C38—C39—H39	121.0
C3—C4—H4	119.9	C39—C40—C41	121.0 (2)
C5—C4—H4	119.9	C39—C40—C43	119.8 (2)
N1—C5—C4	120.4 (2)	C41—C40—C43	119.2 (2)
N1—C5—C6	114.23 (19)	C40—C41—C36	122.15 (19)
C4—C5—C6	125.4 (2)	C40—C41—H41	118.9
C11—C6—C7	121.0 (2)	C36—C41—H41	118.9
C11—C6—C5	115.29 (19)	F8—C42—F9	105.3 (3)
C7—C6—C5	123.7 (2)	F8—C42—F7	107.5 (3)
C8—C7—C6	119.8 (3)	F9—C42—F7	104.1 (3)
C8—C7—H7	120.1	F8—C42—C38	114.4 (2)
C6—C7—H7	120.1	F9—C42—C38	113.4 (3)
C7—C8—C9	119.8 (2)	F7—C42—C38	111.4 (2)
C7—C8—H8	120.1	F10—C43—F12	107.4 (3)
C9—C8—H8	120.1	F10—C43—F11	104.2 (3)
C8—C9—C10	120.4 (3)	F12—C43—F11	104.0 (3)
C8—C9—H9	119.8	F10—C43—C40	114.0 (2)
C10—C9—H9	119.8	F12—C43—C40	113.0 (2)
C11—C10—C9	120.9 (3)	F11—C43—C40	113.5 (2)
C11—C10—H10	119.5	C45—C44—C49	115.61 (19)
C9—C10—H10	119.5	C45—C44—B1	120.72 (17)
C10—C11—C6	118.0 (2)	C49—C44—B1	123.42 (17)
C10—C11—Ir1	126.53 (17)	C46—C45—C44	122.34 (18)
C6—C11—Ir1	115.15 (15)	C46—C45—H45	118.8

C16—C12—C13	108.5 (2)	C44—C45—H45	118.8
C16—C12—C17	125.6 (2)	C47—C46—C45	120.9 (2)
C13—C12—C17	126.0 (2)	C47—C46—C50	120.3 (2)
C16—C12—Ir1	71.53 (12)	C45—C46—C50	118.8 (2)
C13—C12—Ir1	68.96 (13)	C48—C47—C46	117.8 (2)
C17—C12—Ir1	125.13 (16)	C48—C47—H47	121.1
C12—C13—C14	107.9 (2)	C46—C47—H47	121.1
C12—C13—C18	124.7 (2)	C47—C48—C49	121.42 (19)
C14—C13—C18	126.4 (2)	C47—C48—C51	120.4 (2)
C12—C13—Ir1	74.24 (12)	C49—C48—C51	118.2 (2)
C14—C13—Ir1	70.53 (12)	C48—C49—C44	121.89 (19)
C18—C13—Ir1	129.87 (18)	C48—C49—H49	119.1
C15—C14—C13	107.9 (2)	C44—C49—H49	119.1
C15—C14—C19	126.7 (3)	F13—C50—F15	107.4 (3)
C13—C14—C19	125.0 (3)	F13—C50—F14	104.4 (2)
C15—C14—Ir1	71.79 (12)	F15—C50—F14	106.1 (3)
C13—C14—Ir1	71.69 (12)	F13—C50—C46	112.5 (3)
C19—C14—Ir1	128.27 (18)	F15—C50—C46	113.2 (2)
C14—C15—C16	107.7 (2)	F14—C50—C46	112.6 (2)
C14—C15—C20	126.3 (3)	F17—C51—F16	105.4 (3)
C16—C15—C20	124.6 (3)	F17—C51—F18	105.7 (3)
C14—C15—Ir1	70.59 (13)	F16—C51—F18	106.7 (3)
C16—C15—Ir1	73.58 (12)	F17—C51—C48	112.8 (2)
C20—C15—Ir1	131.79 (17)	F16—C51—C48	113.5 (2)
C12—C16—C15	108.0 (2)	F18—C51—C48	112.2 (3)
C12—C16—C21	126.2 (3)	C53—C52—C57	116.19 (18)
C15—C16—C21	125.5 (2)	C53—C52—B1	122.27 (17)
C12—C16—Ir1	72.36 (13)	C57—C52—B1	121.26 (17)
C15—C16—Ir1	69.19 (13)	C54—C53—C52	121.79 (19)
C21—C16—Ir1	128.03 (16)	C54—C53—H53	119.1
C12—C17—H17A	109.5	C52—C53—H53	119.1
C12—C17—H17B	109.5	C55—C54—C53	121.1 (2)
H17A—C17—H17B	109.5	C55—C54—C58	119.1 (2)
C12—C17—H17C	109.5	C53—C54—C58	119.7 (2)
H17A—C17—H17C	109.5	C54—C55—C56	117.89 (19)
H17B—C17—H17C	109.5	C54—C55—H55	121.1
C13—C18—H18A	109.5	C56—C55—H55	121.1
C13—C18—H18B	109.5	C55—C56—C57	121.40 (19)
H18A—C18—H18B	109.5	C55—C56—C59	117.72 (19)

C13—C18—H18C	109.5	C57—C56—C59	120.9 (2)
H18A—C18—H18C	109.5	C56—C57—C52	121.51 (19)
H18B—C18—H18C	109.5	C56—C57—H57	119.2
C14—C19—H19A	109.5	C52—C57—H57	119.2
C14—C19—H19B	109.5	F21—C58—F20	107.9 (2)
H19A—C19—H19B	109.5	F21—C58—F19	106.6 (2)
C14—C19—H19C	109.5	F20—C58—F19	103.3 (2)
H19A—C19—H19C	109.5	F21—C58—C54	112.9 (2)
H19B—C19—H19C	109.5	F20—C58—C54	112.9 (2)
C15—C20—H20A	109.5	F19—C58—C54	112.7 (2)
C15—C20—H20B	109.5	F24—C59—F23	107.8 (2)
H20A—C20—H20B	109.5	F24—C59—F22	106.2 (3)
C15—C20—H20C	109.5	F23—C59—F22	102.8 (2)
H20A—C20—H20C	109.5	F24—C59—C56	114.7 (2)
H20B—C20—H20C	109.5	F23—C59—C56	112.3 (2)
C16—C21—H21A	109.5	F22—C59—C56	112.2 (2)
C16—C21—H21B	109.5	C60^{i}—C60—C61	124.7 (9)
H21A—C21—H21B	109.5	C60^{i}—C60—H60A	106.1
C16—C21—H21C	109.5	C61—C60—H60A	106.1
H21A—C21—H21C	109.5	C60^{i}—C60—H60B	106.1
H21B—C21—H21C	109.5	C61—C60—H60B	106.1
C23—C22—Si1	116.4 (3)	H60A—C60—H60B	106.3
C23—C22—H22A	108.2	C60—C61—C62	108.9 (5)
Si1—C22—H22A	108.2	C60—C61—H61A	109.9
C23—C22—H22B	108.2	C62—C61—H61A	109.9
Si1—C22—H22B	108.2	C60—C61—H61B	109.9
H22A—C22—H22B	107.3	C62—C61—H61B	109.9
C22—C23—H23A	109.5	H61A—C61—H61B	108.3
C22—C23—H23B	109.5	C61—C62—H62A	109.5
H23A—C23—H23B	109.5	C61—C62—H62B	109.5
C22—C23—H23C	109.5	H62A—C62—H62B	109.5
H23A—C23—H23C	109.5	C61—C62—H62C	109.5
H23B—C23—H23C	109.5	H62A—C62—H62C	109.5
C25—C24—Si1	115.3 (2)	H62B—C62—H62C	109.5
C25—C24—H24A	108.4	C44—B1—C28	104.63 (16)
Si1—C24—H24A	108.4	C44—B1—C52	111.89 (15)
C25—C24—H24B	108.4	C28—B1—C52	113.54 (16)
Si1—C24—H24B	108.4	C44—B1—C36	111.48 (15)
H24A—C24—H24B	107.5	C28—B1—C36	111.68 (16)

C24—C25—H25A	109.5	C52—B1—C36	103.83 (16)
C24—C25—H25B	109.5	C1—N1—C5	118.9 (2)
H25A—C25—H25B	109.5	C1—N1—Ir1	123.75 (16)
C24—C25—H25C	109.5	C5—N1—Ir1	117.25 (15)
H25A—C25—H25C	109.5	C24—Si1—C22	107.11 (15)
H25B—C25—H25C	109.5	C24—Si1—C26	111.18 (18)
C27—C26—Si1	116.4 (2)	C22—Si1—C26	105.75 (16)
C27—C26—H26A	108.2	C24—Si1—H1A	105.7
Si1—C26—H26A	108.2	C22—Si1—H1A	81.4
C27—C26—H26B	108.2	C26—Si1—H1A	137.9
Si1—C26—H26B	108.2	C24—Si1—Ir1	108.40 (9)
H26A—C26—H26B	107.3	C22—Si1—Ir1	113.78 (10)
C26—C27—H27A	109.5	C26—Si1—Ir1	110.59 (11)
C26—C27—H27B	109.5	N1—Ir1—C11	77.60 (8)
H27A—C27—H27B	109.5	N1—Ir1—C14	141.94 (9)
C26—C27—H27C	109.5	C11—Ir1—C14	137.40 (9)
H27A—C27—H27C	109.5	N1—Ir1—C13	105.26 (8)
H27B—C27—H27C	109.5	C11—Ir1—C13	149.81 (8)
C33—C28—C29	115.39 (18)	C14—Ir1—C13	37.78 (9)
C33—C28—B1	125.20 (17)	N1—Ir1—C15	152.66 (9)
C29—C28—B1	119.26 (17)	C11—Ir1—C15	100.73 (9)
C30—C29—C28	122.48 (18)	C14—Ir1—C15	37.63 (9)
C30—C29—H29	118.8	C13—Ir1—C15	62.74 (9)
C28—C29—H29	118.8	N1—Ir1—C16	115.63 (9)
C29—C30—C31	121.05 (18)	C11—Ir1—C16	89.68 (8)
C29—C30—C34	119.17 (18)	C14—Ir1—C16	62.11 (9)
C31—C30—C34	119.77 (19)	C13—Ir1—C16	61.62 (8)
C32—C31—C30	117.79 (18)	C15—Ir1—C16	37.24 (9)
C32—C31—H31	121.1	N1—Ir1—C12	93.74 (8)
C30—C31—H31	121.1	C11—Ir1—C12	113.74 (8)
C31—C32—C33	120.99 (18)	C14—Ir1—C12	61.83 (9)
C31—C32—C35	120.78 (19)	C13—Ir1—C12	36.80 (8)
C33—C32—C35	118.16 (18)	C15—Ir1—C12	61.56 (9)
C28—C33—C32	122.24 (18)	C16—Ir1—C12	36.11 (8)
C28—C33—H33	118.9	N1—Ir1—Si1	99.78 (6)
C32—C33—H33	118.9	C11—Ir1—Si1	80.70 (6)
F1—C34—F2	105.4 (3)	C14—Ir1—Si1	100.60 (7)
F1—C34—F3	106.9 (3)	C13—Ir1—Si1	127.01 (6)
F2—C34—F3	104.8 (3)	C15—Ir1—Si1	106.91 (7)

F1—C34—C30	112.9 (2)	C16—Ir1—Si1	140.35 (7)
F2—C34—C30	113.35 (19)	C12—Ir1—Si1	162.20 (6)
F3—C34—C30	112.8 (2)	N1—Ir1—H1A	76.2
F4—C35—F5	106.5 (2)	C11—Ir1—H1A	124.4
F4—C35—F6	106.65 (19)	C14—Ir1—H1A	88.6
F5—C35—F6	105.39 (19)	C13—Ir1—H1A	84.8
F4—C35—C32	113.21 (19)	C15—Ir1—H1A	123.6
F5—C35—C32	111.83 (19)	C16—Ir1—H1A	146.0
F6—C35—C32	112.74 (19)	C12—Ir1—H1A	116.2
C41—C36—C37	115.74 (18)	Si1—Ir1—H1A	57.0
C41—C36—B1	124.13 (17)		

N1—C1—C2—C3	-1.1 (4)	C37—C38—C42—F7	-104.4 (3)
C1—C2—C3—C4	0.2 (4)	C39—C38—C42—F7	72.3 (4)
C2—C3—C4—C5	0.6 (4)	C39—C40—C43—F10	1.8 (4)
C3—C4—C5—N1	-0.6 (4)	C41—C40—C43—F10	-178.3 (3)
C3—C4—C5—C6	179.9 (2)	C39—C40—C43—F12	-121.1 (3)
N1—C5—C6—C11	-1.8 (3)	C41—C40—C43—F12	58.7 (4)
C4—C5—C6—C11	177.7 (2)	C39—C40—C43—F11	120.8 (3)
N1—C5—C6—C7	179.3 (2)	C41—C40—C43—F11	-59.3 (3)
C4—C5—C6—C7	-1.3 (4)	C49—C44—C45—C46	0.9 (3)
C11—C6—C7—C8	0.5 (4)	B1—C44—C45—C46	175.4 (2)
C5—C6—C7—C8	179.4 (3)	C44—C45—C46—C47	-0.4 (4)
C6—C7—C8—C9	-0.1 (4)	C44—C45—C46—C50	180.0 (2)
C7—C8—C9—C10	-0.2 (5)	C45—C46—C47—C48	-0.2 (3)
C8—C9—C10—C11	0.1 (4)	C50—C46—C47—C48	179.4 (2)
C9—C10—C11—C6	0.4 (4)	C46—C47—C48—C49	0.3 (3)
C9—C10—C11—Ir1	173.67 (19)	C46—C47—C48—C51	178.7 (2)
C7—C6—C11—C10	-0.7 (3)	C47—C48—C49—C44	0.3 (3)
C5—C6—C11—C10	-179.6 (2)	C51—C48—C49—C44	-178.2 (2)
C7—C6—C11—Ir1	-174.73 (19)	C45—C44—C49—C48	-0.9 (3)
C5—C6—C11—Ir1	6.3 (3)	B1—C44—C49—C48	-175.15 (19)
C16—C12—C13—C14	-2.0 (2)	C47—C46—C50—F13	-115.1 (3)
C17—C12—C13—C14	178.2 (2)	C45—C46—C50—F13	64.5 (3)
Ir1—C12—C13—C14	-62.94 (15)	C47—C46—C50—F15	6.9 (4)
C16—C12—C13—C18	-171.1 (2)	C45—C46—C50—F15	-173.5 (3)
C17—C12—C13—C18	9.1 (4)	C47—C46—C50—F14	127.2 (3)
Ir1—C12—C13—C18	127.9 (2)	C45—C46—C50—F14	-53.2 (4)
C16—C12—C13—Ir1	60.91 (15)	C47—C48—C51—F17	-116.3 (3)

C17—C12—C13—Ir1	-118.9 (2)	C49—C48—C51—F17	62.3 (4)
C12—C13—C14—C15	2.3 (2)	C47—C48—C51—F16	3.5 (4)
C18—C13—C14—C15	171.2 (2)	C49—C48—C51—F16	-177.9 (3)
Ir1—C13—C14—C15	-63.09 (15)	C47—C48—C51—F18	124.5 (3)
C12—C13—C14—C19	-170.2 (2)	C49—C48—C51—F18	-57.0 (4)
C18—C13—C14—C19	-1.4 (4)	C57—C52—C53—C54	-3.3 (3)
Ir1—C13—C14—C19	124.4 (3)	B1—C52—C53—C54	-177.37 (18)
C12—C13—C14—Ir1	65.37 (15)	C52—C53—C54—C55	3.1 (3)
C18—C13—C14—Ir1	-125.7 (2)	C52—C53—C54—C58	-174.0 (2)
C13—C14—C15—C16	-1.7 (2)	C53—C54—C55—C56	-0.4 (3)
C19—C14—C15—C16	170.7 (2)	C58—C54—C55—C56	176.7 (2)
Ir1—C14—C15—C16	-64.70 (15)	C54—C55—C56—C57	-2.0 (3)
C13—C14—C15—C20	-168.8 (2)	C54—C55—C56—C59	178.4 (2)
C19—C14—C15—C20	3.6 (4)	C55—C56—C57—C52	1.7 (3)
Ir1—C14—C15—C20	128.2 (2)	C59—C56—C57—C52	-178.7 (2)
C13—C14—C15—Ir1	63.03 (15)	C53—C52—C57—C56	0.9 (3)
C19—C14—C15—Ir1	-124.6 (3)	B1—C52—C57—C56	175.08 (19)
C13—C12—C16—C15	1.0 (2)	C55—C54—C58—F21	-91.4 (3)
C17—C12—C16—C15	-179.2 (2)	C53—C54—C58—F21	85.7 (3)
Ir1—C12—C16—C15	60.30 (15)	C55—C54—C58—F20	31.2 (3)
C13—C12—C16—C21	176.1 (2)	C53—C54—C58—F20	-151.7 (2)
C17—C12—C16—C21	-4.2 (4)	C55—C54—C58—F19	147.7 (2)
Ir1—C12—C16—C21	-124.6 (2)	C53—C54—C58—F19	-35.1 (3)
C13—C12—C16—Ir1	-59.30 (15)	C55—C56—C59—F24	-178.4 (3)
C17—C12—C16—Ir1	120.5 (2)	C57—C56—C59—F24	2.0 (4)
C14—C15—C16—C12	0.4 (2)	C55—C56—C59—F23	58.1 (3)
C20—C15—C16—C12	167.8 (2)	C57—C56—C59—F23	-121.6 (3)
Ir1—C15—C16—C12	-62.32 (15)	C55—C56—C59—F22	-57.1 (3)
C14—C15—C16—C21	-174.7 (2)	C57—C56—C59—F22	123.3 (3)
C20—C15—C16—C21	-7.3 (4)	C60^{i}—C60—C61—C62	176.0 (10)
Ir1—C15—C16—C21	122.6 (2)	C45—C44—B1—C28	-77.5 (2)
C14—C15—C16—Ir1	62.74 (15)	C49—C44—B1—C28	96.5 (2)
C20—C15—C16—Ir1	-129.9 (2)	C45—C44—B1—C52	45.8 (2)
C33—C28—C29—C30	1.8 (3)	C49—C44—B1—C52	-140.16 (19)
B1—C28—C29—C30	177.6 (2)	C45—C44—B1—C36	161.62 (18)
C28—C29—C30—C31	0.2 (3)	C49—C44—B1—C36	-24.4 (3)
C28—C29—C30—C34	-178.8 (2)	C33—C28—B1—C44	103.1 (2)
C29—C30—C31—C32	-1.4 (3)	C29—C28—B1—C44	-72.3 (2)
C34—C30—C31—C32	177.6 (2)	C33—C28—B1—C52	-19.2 (3)

C30—C31—C32—C33	0.5 (3)	C29—C28—B1—C52	165.47 (18)
C30—C31—C32—C35	177.4 (2)	C33—C28—B1—C36	-136.2 (2)
C29—C28—C33—C32	-2.7 (3)	C29—C28—B1—C36	48.5 (2)
B1—C28—C33—C32	-178.22 (19)	C53—C52—B1—C44	-155.26 (18)
C31—C32—C33—C28	1.6 (3)	C57—C52—B1—C44	31.0 (2)
C35—C32—C33—C28	-175.3 (2)	C53—C52—B1—C28	-37.1 (3)
C29—C30—C34—F1	85.0 (3)	C57—C52—B1—C28	149.13 (18)
C31—C30—C34—F1	-94.0 (3)	C53—C52—B1—C36	84.4 (2)
C29—C30—C34—F2	-34.7 (3)	C57—C52—B1—C36	-89.4 (2)
C31—C30—C34—F2	146.2 (3)	C41—C36—B1—C44	138.14 (19)
C29—C30—C34—F3	-153.7 (3)	C37—C36—B1—C44	-47.7 (2)
C31—C30—C34—F3	27.2 (4)	C41—C36—B1—C28	21.5 (3)
C31—C32—C35—F4	10.8 (3)	C37—C36—B1—C28	-164.36 (18)
C33—C32—C35—F4	-172.2 (2)	C41—C36—B1—C52	-101.2 (2)
C31—C32—C35—F5	-109.4 (2)	C37—C36—B1—C52	72.9 (2)
C33—C32—C35—F5	67.5 (3)	C2—C1—N1—C5	1.0 (3)
C31—C32—C35—F6	132.0 (2)	C2—C1—N1—Ir1	-175.78 (18)
C33—C32—C35—F6	-51.0 (3)	C4—C5—N1—C1	-0.2 (3)
C41—C36—C37—C38	-1.3 (3)	C6—C5—N1—C1	179.3 (2)
B1—C36—C37—C38	-175.87 (19)	C4—C5—N1—Ir1	176.84 (18)
C36—C37—C38—C39	0.3 (3)	C6—C5—N1—Ir1	-3.7 (2)
C36—C37—C38—C42	176.9 (2)	C25—C24—Si1—C22	47.7 (3)
C37—C38—C39—C40	0.6 (3)	C25—C24—Si1—C26	-67.4 (3)
C42—C38—C39—C40	-176.1 (2)	C25—C24—Si1—H1A	133.3
C38—C39—C40—C41	-0.5 (3)	C25—C24—Si1—Ir1	170.9 (3)
C38—C39—C40—C43	179.4 (2)	C23—C22—Si1—C24	61.0 (3)
C39—C40—C41—C36	-0.6 (3)	C23—C22—Si1—C26	179.6 (3)
C43—C40—C41—C36	179.5 (2)	C23—C22—Si1—H1A	-42.9
C37—C36—C41—C40	1.4 (3)	C23—C22—Si1—Ir1	-58.8 (3)
B1—C36—C41—C40	175.79 (19)	C27—C26—Si1—C24	67.9 (3)
C37—C38—C42—F8	17.7 (4)	C27—C26—Si1—C22	-48.1 (3)
C39—C38—C42—F8	-165.6 (3)	C27—C26—Si1—H1A	-142.7
C37—C38—C42—F9	138.5 (3)	C27—C26—Si1—Ir1	-171.7 (3)
C39—C38—C42—F9	-44.7 (4)		

7.10[**3A'**][$BArF_{24}$]

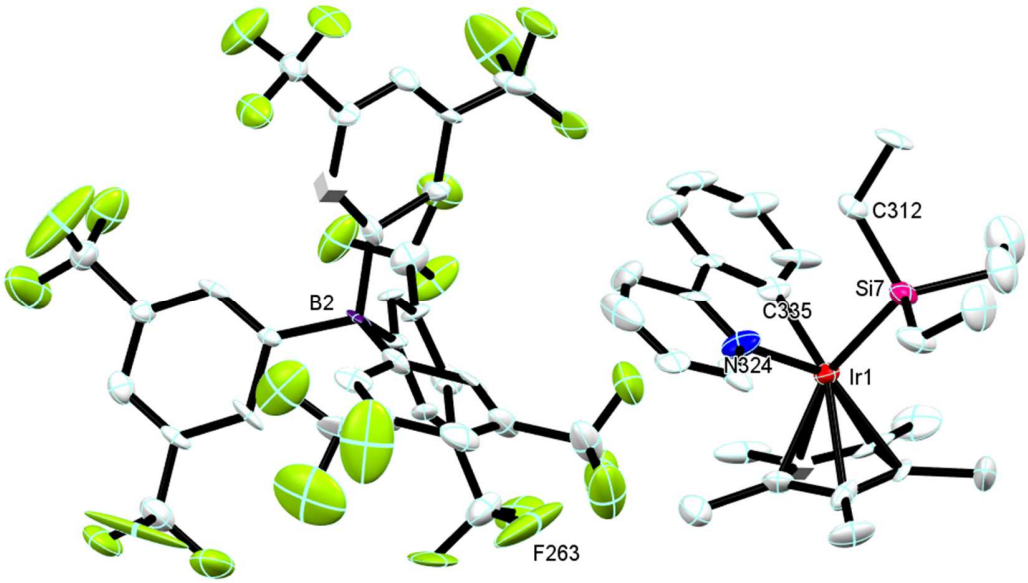

7.10.1 **Figure A28.** Asymmetric unit of [**3A'**][BArF$_{24}$], without hydrogens and with partial numbering of atoms.

[**3A**'][BArF$_{24}$]

7.10.2 Crystal data

$C_{63}BCl_0F_{18.50}IrNSi$	$Z = 8$
$M_r = 1353.24$	$F(000) = 5180$
Monoclinic, $P2_1/c$	$D_x = 1.495$ Mg m^{-3}
$a = 17.5051$ (7) Å	Mo $K\alpha$ radiation, $\lambda = 0.71073$ Å
$b = 37.5922$ (14) Å	$\mu = 2.34$ mm^{-1}
$c = 18.2760$ (7) Å	$T = 173$ K
$\beta = 90.410$ (1)°	0.18 × 0.16 × 0.06 mm
$V = 12026.3$ (8) Å^3	

7.10.3 Data collection

145652 measured reflections	$\theta_{max} = 28.0°$, $\theta_{min} = 1.3°$
28922 independent reflections	$h = -21 \rightarrow 23$
13390 reflections with $I > 2\sigma(I)$	$k = -49 \rightarrow 49$
$R_{int} = 0.182$	$l = -24 \rightarrow 23$

7.10.4 Refinement

Refinement on F^2	1567 parameters
Least-squares matrix: full	0 restraints
$R[F^2 > 2\sigma(F^2)] = 0.207$	$w = 1/[\sigma^2(F_o^2) + (0.2P)^2]$ where $P = (F_o^2 + 2F_c^2)/3$
$wR(F^2) = 0.431$	$(\Delta/\sigma)_{max} = 5.100$
$S = 1.24$	$\Delta\rangle_{max} = 12.72$ e Å^{-3}
28922 reflections	$\Delta\rangle_{min} = -3.40$ e Å^{-3}

7.10.5 Special details

Geometry. All esds (except the esd in the dihedral angle between two l.s. planes) are estimated using the full covariance matrix. The cell esds are taken into account individually in the estimation of esds in distances, angles and torsion angles; correlations between esds in cell parameters are only used when they are defined by crystal symmetry. An approximate (isotropic) treatment of cell esds is used for estimating esds involving l.s. planes.

7.10.6 **Table A28.** Fractional atomic coordinates and isotropic or equivalent isotropic displacement parameters (Å^2) for [**3A'**][BArF$_{24}$].

	x	*y*	*z*	U_{iso}*/U_{eq}
B2	0.0454 (12)	0.8747 (5)	0.0756 (12)	0.031 (5)
B99	0.5477 (12)	0.8728 (5)	0.5782 (12)	0.033 (5)
Ir1	0.01873 (4)	0.61428 (2)	0.10782 (4)	0.0344 (2)
Ir2	0.55993 (6)	0.86033 (2)	0.08411 (5)	0.0617 (4)
C7	0.6141 (10)	0.8734 (4)	0.5169 (8)	0.024 (4)
C1	0.4874 (9)	0.8398 (4)	0.5632 (10)	0.032 (4)
C6	0.4381 (10)	0.8274 (4)	0.6203 (9)	0.033 (4)
C10	0.7375 (11)	0.8722 (5)	0.4168 (11)	0.040 (5)
C11	0.7122 (12)	0.8423 (5)	0.4469 (11)	0.045 (5)
C8	0.6446 (10)	0.9047 (4)	0.4827 (9)	0.032 (4)
C155	-0.1064 (13)	0.6052 (8)	0.1366 (12)	0.069 (7)
C2	0.4741 (10)	0.8255 (4)	0.4941 (8)	0.026 (4)
C165	0.4156 (12)	0.9755 (5)	0.5853 (11)	0.047 (5)
C9	0.7042 (10)	0.9033 (4)	0.4364 (8)	0.029 (4)
C15	0.4280 (11)	0.9570 (5)	0.5193 (10)	0.039 (5)
C175	0.4423 (14)	0.9607 (5)	0.6491 (11)	0.052 (6)
C12	0.6536 (11)	0.8416 (4)	0.4968 (11)	0.039 (5)
C4	0.3782 (11)	0.7851 (5)	0.5382 (11)	0.041 (5)
C18	-0.0168 (11)	0.6129 (5)	0.2269 (11)	0.050 (5)
C17	-0.0100 (12)	0.5792 (5)	0.2001 (12)	0.054 (6)
C144	-0.0715 (14)	0.6300 (6)	0.1798 (11)	0.055 (6)
C5	0.3873 (10)	0.7993 (4)	0.6069 (10)	0.034 (4)
C16	-0.0666 (15)	0.5728 (6)	0.1372 (11)	0.064 (7)
C14	0.4676 (10)	0.9249 (4)	0.5178 (9)	0.031 (4)
C3	0.4217 (12)	0.7980 (4)	0.4827 (9)	0.039 (5)
C148	0.4827 (11)	0.9284 (4)	0.6481 (9)	0.032 (4)
C13	0.4987 (9)	0.9100 (4)	0.5828 (10)	0.034 (4)
C124	0.1521 (11)	0.9032 (5)	-0.0115 (10)	0.043 (5)
C122	-0.0281 (10)	0.9270 (4)	0.0003 (10)	0.034 (4)
C111	-0.0115 (10)	0.8398 (4)	0.0656 (9)	0.030 (4)
C117	-0.0124 (9)	0.9090 (4)	0.0648 (9)	0.027 (4)
C125	0.2094 (11)	0.9019 (4)	-0.0617 (11)	0.041 (5)

C123	0.1118 (11)	0.8744 (4)	0.0129 (10)	0.040 (5)
C112	-0.0334 (10)	0.8277 (4)	-0.0023 (8)	0.028 (4)
C128	0.1397 (12)	0.8409 (4)	-0.0184 (11)	0.045 (5)
C118	-0.0561 (10)	0.9195 (5)	0.1290 (11)	0.046 (5)
C120	-0.1236 (12)	0.9640 (5)	0.0596 (12)	0.049 (6)
C126	0.2317 (12)	0.8702 (5)	-0.0897 (12)	0.048 (5)
C121	-0.0820 (10)	0.9530 (4)	-0.0042 (10)	0.035 (4)
C116	-0.0480 (12)	0.8232 (4)	0.1243 (9)	0.038 (5)
C115	-0.0989 (12)	0.7949 (4)	0.1149 (12)	0.048 (5)
C114	-0.1185 (11)	0.7831 (5)	0.0426 (13)	0.050 (6)
C127	0.1965 (12)	0.8398 (4)	-0.0709 (10)	0.039 (4)
C119	-0.1091 (11)	0.9462 (5)	0.1245 (11)	0.042 (5)
C113	-0.0849 (11)	0.8005 (4)	-0.0136 (9)	0.032 (4)
C216	0.6398 (10)	0.8919 (4)	0.6890 (9)	0.033 (4)
C214	0.6913 (11)	0.8504 (5)	0.7769 (10)	0.043 (5)
C215	0.6823 (12)	0.8841 (6)	0.7485 (10)	0.057 (6)
C212	0.6049 (10)	0.8311 (5)	0.6826 (9)	0.038 (4)
C211	0.5969 (10)	0.8656 (4)	0.6525 (9)	0.029 (4)
C213	0.6523 (9)	0.8241 (5)	0.7440 (9)	0.034 (4)
C225	0.1534 (12)	0.8457 (6)	0.2596 (10)	0.058 (6)
C223	0.1088 (11)	0.9080 (5)	0.1875 (11)	0.051 (5)
C224	0.1143 (11)	0.8434 (5)	0.1884 (10)	0.043 (5)
C222	0.0899 (11)	0.8752 (4)	0.1525 (10)	0.041 (5)
C226	0.1709 (13)	0.8779 (8)	0.2885 (14)	0.074 (7)
C231	0.4158 (15)	0.7828 (6)	0.4068 (14)	0.067 (7)
C240	-0.1032 (16)	0.7890 (7)	-0.0896 (14)	0.067 (8)
C241	-0.0941 (15)	0.9726 (5)	-0.0765 (12)	0.054 (6)
C238	0.7489 (13)	0.8073 (5)	0.4309 (13)	0.049 (6)
C237	0.7335 (13)	0.9368 (5)	0.4036 (12)	0.050 (5)
C242	0.2485 (14)	0.9354 (5)	-0.0896 (13)	0.054 (6)
C236	0.3941 (14)	0.9725 (5)	0.4492 (12)	0.053 (6)
C233	0.6604 (17)	0.7854 (6)	0.7699 (14)	0.068 (8)
F368	0.1165 (13)	0.7876 (5)	0.2935 (11)	0.121 (7)
C232	0.3448 (15)	0.7831 (6)	0.6685 (14)	0.065 (7)
C235	0.4324 (19)	0.9807 (6)	0.7169 (13)	0.085 (10)
C243	-0.1531 (16)	0.9550 (7)	0.1875 (16)	0.076 (8)
C234	0.7243 (15)	0.9144 (8)	0.7873 (12)	0.074 (8)

C244	0.2182 (16)	0.8053 (7)	-0.0968 (16)	0.074 (7)
F275	0.7188 (9)	0.7802 (4)	0.8103 (9)	0.103 (6)
F270	0.3946 (9)	1.0083 (3)	0.4517 (7)	0.084 (5)
F269	0.4379 (13)	0.9642 (4)	0.3934 (8)	0.117 (7)
F274	0.6649 (9)	0.7625 (3)	0.7162 (8)	0.086 (5)
F247	-0.1354 (10)	0.8151 (4)	-0.1299 (8)	0.104 (6)
F250	-0.0978 (11)	0.9515 (4)	-0.1314 (8)	0.108 (6)
F254	0.2430 (8)	0.9624 (3)	-0.0405 (8)	0.079 (4)
F276	0.5997 (9)	0.7765 (3)	0.8053 (9)	0.077 (4)
F248	-0.0375 (10)	0.7821 (4)	-0.1284 (8)	0.086 (5)
F266	0.8085 (8)	0.9370 (4)	0.3942 (9)	0.081 (4)
F267	0.7248 (9)	0.9649 (3)	0.4494 (8)	0.079 (4)
F249	-0.1506 (9)	0.7634 (4)	-0.0963 (8)	0.099 (6)
F265	0.6995 (9)	0.9465 (4)	0.3429 (8)	0.086 (5)
F252	-0.0479 (17)	0.9955 (7)	-0.0861 (12)	0.216 (16)
F253	0.2177 (12)	0.9468 (4)	-0.1492 (9)	0.121 (7)
F261	0.2085 (13)	0.7780 (3)	-0.0566 (11)	0.162 (9)
F268	0.3255 (9)	0.9642 (4)	0.4382 (9)	0.116 (7)
F263	-0.1660 (13)	0.7485 (4)	0.1668 (11)	0.137 (8)
F256	-0.2224 (10)	0.9674 (5)	0.1770 (9)	0.107 (5)
F258	-0.1646 (11)	0.9286 (5)	0.2359 (9)	0.116 (6)
F271	0.7845 (13)	0.8060 (4)	0.3733 (10)	0.132 (8)
F257	-0.1194 (13)	0.9799 (9)	0.2271 (16)	0.26 (2)
F255	0.3214 (9)	0.9315 (3)	-0.0985 (10)	0.097 (5)
F251	-0.1659 (15)	0.9861 (8)	-0.0813 (11)	0.210 (15)
F260	0.1809 (18)	0.7978 (6)	-0.1613 (16)	0.212 (14)
F272	0.7967 (16)	0.7975 (5)	0.4785 (11)	0.200 (13)
F259	0.2831 (11)	0.8039 (4)	-0.1277 (11)	0.114 (6)
F273	0.7054 (11)	0.7799 (4)	0.4309 (16)	0.189 (11)
F262	-0.1828 (19)	0.7992 (6)	0.2119 (15)	0.216 (15)
F264	-0.0890 (16)	0.7704 (9)	0.2272 (13)	0.198 (14)
C247	-0.1377 (17)	0.7772 (7)	0.1802 (15)	0.073 (8)
C245	0.1465 (13)	0.9100 (7)	0.2536 (11)	0.058 (7)
F281	0.2246 (12)	0.7925 (5)	0.2537 (11)	0.127 (7)
F282	0.1916 (14)	0.8113 (5)	0.3596 (9)	0.152 (9)
F277	0.4107 (14)	0.8055 (5)	0.3547 (9)	0.135 (8)
F280	0.3493 (13)	0.7666 (6)	0.3942 (10)	0.178 (10)

C286	0.6837 (15)	0.8500 (5)	0.0927 (13)	0.063 (7)
C284	0.5979 (14)	0.8034 (5)	0.0958 (13)	0.065 (7)
F278	0.4699 (15)	0.7634 (9)	0.3882 (12)	0.235 (17)
C285	0.6568 (13)	0.8229 (7)	0.0515 (12)	0.081 (8)
C289	-0.1038 (16)	0.6704 (6)	0.1957 (15)	0.079 (8)
C290	0.0204 (15)	0.6269 (7)	0.2948 (12)	0.074 (8)
C287	0.6593 (17)	0.8477 (7)	0.1630 (13)	0.088 (9)
C293	-0.1719 (15)	0.6129 (9)	0.0840 (13)	0.096 (10)
C288	0.6000 (16)	0.8199 (5)	0.1679 (12)	0.067 (8)
C291	0.039 (2)	0.5488 (8)	0.2320 (16)	0.120 (12)
C292	-0.0858 (18)	0.5387 (7)	0.0975 (17)	0.097 (10)
Si7	0.1602 (3)	0.60400 (14)	0.0996 (3)	0.0438 (14)
Si4	0.4446 (9)	0.8825 (3)	0.1434 (8)	0.153 (5)
F301	0.3380 (12)	0.8066 (5)	0.7237 (10)	0.133 (8)
F300	0.3836 (14)	0.7584 (7)	0.6983 (13)	0.169 (10)
F305	0.1773 (15)	0.9704 (5)	0.2410 (11)	0.148 (10)
C294	0.5588 (19)	0.7696 (6)	0.0790 (16)	0.098 (10)
F299	0.2828 (11)	0.7703 (6)	0.6541 (10)	0.145 (9)
F303	0.2200 (16)	0.9460 (5)	0.3274 (15)	0.206 (14)
C309	0.3939 (16)	0.9196 (9)	0.0928 (16)	0.108 (11)
F304	0.1178 (19)	0.9534 (7)	0.3275 (18)	0.212 (14)
C298	0.6774 (16)	0.8105 (8)	-0.0251 (14)	0.083 (9)
C297	0.751 (2)	0.8720 (8)	0.0684 (19)	0.109 (11)
C295	0.556 (2)	0.8086 (8)	0.2367 (16)	0.127 (14)
C296	0.687 (2)	0.8707 (7)	0.2283 (18)	0.107 (13)
C310	0.468 (3)	0.8999 (10)	0.242 (2)	0.147 (18)
C308	0.320 (3)	0.9339 (10)	0.128 (3)	0.17 (2)
C302	0.1716 (18)	0.9434 (8)	0.2850 (16)	0.079 (8)
C306	0.332 (3)	0.8325 (12)	0.0900 (19)	0.143 (16)
C307	0.404 (5)	0.864 (3)	0.131 (4)	0.39 (8)
C311	0.427 (4)	0.8894 (12)	0.294 (3)	0.17 (2)
F318	0.4231 (13)	1.0113 (4)	0.7149 (8)	0.127 (7)
F320	0.4055 (12)	0.9617 (5)	0.7709 (9)	0.123 (6)
C313	0.2788 (12)	0.6221 (6)	-0.0069 (12)	0.062 (6)
F323	0.7669 (15)	0.9347 (6)	0.7454 (11)	0.178 (11)
C316	0.1897 (15)	0.5548 (6)	0.0866 (17)	0.085 (9)
F319	0.5044 (14)	0.9834 (5)	0.7595 (10)	0.147 (9)

C315	0.2899 (14)	0.6060 (6)	0.1946 (14)	0.084 (8)
C314	0.2094 (13)	0.6202 (7)	0.1841 (13)	0.067 (7)
F321	0.6902 (12)	0.9395 (6)	0.8081 (17)	0.192 (13)
C312	0.1926 (14)	0.6282 (6)	0.0193 (14)	0.067 (7)
C317	0.1478 (19)	0.5349 (8)	0.0267 (18)	0.108 (11)
F322	0.775 (2)	0.9038 (6)	0.8319 (19)	0.32 (3)
N324	0.0527 (11)	0.6683 (4)	0.0979 (9)	0.058 (5)
N336	0.5738 (11)	0.9134 (4)	0.0583 (8)	0.052 (5)
C342	0.5256 (11)	0.8960 (4)	-0.0545 (9)	0.036 (5)
C347	0.5157 (10)	0.8633 (4)	-0.0220 (9)	0.031 (4)
C341	0.5584 (11)	0.9247 (4)	-0.0107 (10)	0.037 (5)
C335	0.0001 (10)	0.6240 (6)	-0.0011 (11)	0.045 (5)
C340	0.5709 (11)	0.9588 (5)	-0.0354 (11)	0.043 (5)
C344	0.4726 (12)	0.8722 (5)	-0.1665 (11)	0.047 (5)
C343	0.5059 (11)	0.8999 (5)	-0.1295 (10)	0.041 (5)
C346	0.4859 (12)	0.8354 (5)	-0.0589 (11)	0.055 (6)
C345	0.4640 (12)	0.8399 (6)	-0.1315 (11)	0.052 (6)
C337	0.6018 (12)	0.9389 (6)	0.1083 (12)	0.052 (6)
C339	0.6027 (13)	0.9845 (6)	0.0128 (12)	0.055 (6)
C338	0.6182 (14)	0.9740 (5)	0.0861 (11)	0.058 (6)
C325	0.0854 (12)	0.6870 (5)	0.1546 (14)	0.064 (7)
C330	0.0088 (11)	0.6587 (7)	-0.0273 (12)	0.059 (6)
C329	0.0363 (12)	0.6812 (6)	0.0304 (12)	0.057 (6)
C326	0.0967 (14)	0.7233 (6)	0.1467 (15)	0.066 (7)
C334	-0.0221 (14)	0.5996 (8)	-0.0512 (13)	0.076 (7)
C327	0.0800 (18)	0.7379 (6)	0.081 (2)	0.104 (11)
C331	-0.0075 (17)	0.6681 (8)	-0.0950 (16)	0.084 (9)
C328	0.0496 (19)	0.7196 (6)	0.0190 (15)	0.087 (9)
C333	-0.0420 (17)	0.6081 (8)	-0.1251 (15)	0.088 (8)
C332	-0.0316 (16)	0.6418 (12)	-0.1442 (16)	0.102 (12)
C367	0.1777 (19)	0.8103 (7)	0.2936 (14)	0.084 (9)

7.10.7 **Table A29.** Atomic displacement parameters (Å^2) for [**3A'**][BArF$_{24}$].

	U^{11}	U^{22}	U^{33}	U^{12}	U^{13}	U^{23}

B2	0.019 (11)	0.038 (9)	0.036 (12)	0.007 (8)	0.017 (9)	-0.009 (8)
B99	0.030 (12)	0.030 (8)	0.039 (12)	0.001 (8)	-0.004 (10)	-0.005 (8)
Ir1	0.0313 (4)	0.0432 (4)	0.0289 (4)	-0.0013 (3)	0.0036 (3)	0.0062 (3)
Ir2	0.0874 (8)	0.0568 (5)	0.0410 (5)	-0.0130 (5)	-0.0084 (5)	0.0173 (4)
C7	0.024 (10)	0.036 (8)	0.013 (8)	0.001 (7)	0.014 (7)	-0.011 (6)
C1	0.010 (9)	0.037 (8)	0.049 (11)	0.001 (7)	0.014 (8)	-0.010 (7)
C6	0.024 (10)	0.049 (9)	0.027 (10)	-0.005 (8)	0.025 (8)	0.008 (7)
C10	0.029 (11)	0.040 (9)	0.050 (12)	0.009 (8)	0.005 (10)	-0.014 (8)
C11	0.040 (12)	0.053 (11)	0.042 (12)	0.029 (9)	0.016 (10)	0.003 (9)
C8	0.026 (10)	0.040 (9)	0.030 (10)	-0.003 (7)	0.014 (8)	0.007 (7)
C155	0.046 (14)	0.13 (2)	0.035 (13)	-0.005 (14)	0.041 (11)	0.008 (13)
C2	0.033 (11)	0.038 (8)	0.006 (8)	0.006 (7)	0.015 (7)	-0.001 (6)
C165	0.054 (14)	0.043 (10)	0.044 (12)	0.017 (9)	0.015 (11)	0.001 (8)
C9	0.027 (10)	0.045 (9)	0.014 (9)	0.010 (8)	0.017 (7)	0.001 (7)
C15	0.029 (11)	0.049 (10)	0.039 (11)	-0.009 (8)	0.013 (9)	0.002 (8)
C175	0.083 (17)	0.049 (11)	0.025 (11)	0.011 (10)	0.013 (12)	-0.011 (8)
C12	0.037 (12)	0.040 (9)	0.039 (12)	0.007 (8)	0.003 (10)	-0.001 (8)
C4	0.035 (12)	0.050 (10)	0.038 (12)	-0.010 (9)	0.010 (10)	-0.004 (9)
C18	0.033 (12)	0.062 (11)	0.055 (13)	-0.004 (9)	-0.008 (10)	0.034 (9)
C17	0.047 (14)	0.040 (10)	0.075 (16)	0.012 (9)	0.039 (12)	0.045 (10)
C144	0.068 (17)	0.064 (13)	0.032 (12)	0.009 (12)	0.015 (12)	-0.001 (10)
C5	0.028 (11)	0.033 (8)	0.040 (11)	0.002 (7)	0.021 (9)	-0.001 (7)
C16	0.076 (17)	0.083 (16)	0.032 (13)	-0.050 (14)	0.006 (12)	0.023 (11)
C14	0.025 (10)	0.040 (9)	0.028 (10)	0.000 (7)	0.010 (8)	-0.009 (7)
C3	0.060 (14)	0.036 (9)	0.021 (10)	-0.014 (9)	-0.004 (10)	-0.010 (7)
C148	0.043 (12)	0.026 (8)	0.028 (10)	0.002 (7)	0.014 (9)	0.009 (7)
C13	0.007 (9)	0.041 (9)	0.053 (12)	-0.002 (7)	0.016 (8)	-0.008 (8)
C124	0.038 (12)	0.062 (11)	0.031 (11)	-0.034 (9)	0.033 (9)	-0.019 (9)
C122	0.023 (10)	0.037 (8)	0.043 (11)	-0.008 (7)	0.018 (9)	-0.024 (8)
C111	0.026 (10)	0.036 (8)	0.027 (10)	-0.004 (7)	0.016 (8)	0.002 (7)
C117	0.024 (10)	0.026 (7)	0.032 (10)	-0.004 (7)	0.011 (8)	-0.007 (6)
C125	0.031 (11)	0.040 (9)	0.051 (12)	-0.016 (8)	0.011 (9)	-0.004 (8)
C123	0.041 (12)	0.033 (8)	0.047 (12)	0.011 (8)	-0.005 (10)	-0.012 (7)
C112	0.033 (11)	0.035 (8)	0.015 (8)	-0.010 (7)	0.012 (8)	0.005 (6)
C128	0.059 (14)	0.030 (8)	0.047 (12)	-0.007 (8)	0.027 (10)	0.002 (8)
C118	0.020 (10)	0.052 (10)	0.065 (14)	0.014 (8)	0.004 (10)	-0.037 (9)
C120	0.034 (12)	0.051 (10)	0.064 (15)	0.006 (9)	-0.006 (11)	-0.002 (9)

C126	0.038 (13)	0.044 (10)	0.063 (14)	-0.004 (9)	0.026 (11)	-0.006 (10)
C121	0.027 (11)	0.043 (9)	0.035 (11)	0.001 (8)	0.002 (9)	0.001 (8)
C116	0.049 (13)	0.046 (9)	0.021 (10)	0.008 (9)	0.014 (9)	0.005 (7)
C115	0.047 (13)	0.030 (9)	0.067 (15)	-0.005 (9)	0.046 (11)	0.009 (9)
C114	0.032 (12)	0.050 (10)	0.070 (16)	-0.010 (9)	0.002 (11)	-0.008 (10)
C127	0.039 (12)	0.037 (9)	0.040 (11)	0.004 (8)	0.029 (9)	-0.004 (8)
C119	0.020 (11)	0.053 (10)	0.052 (13)	0.007 (9)	0.014 (10)	-0.017 (9)
C113	0.044 (12)	0.032 (8)	0.020 (9)	-0.018 (8)	0.010 (9)	0.005 (7)
C216	0.033 (11)	0.041 (9)	0.024 (9)	-0.004 (8)	0.003 (8)	-0.004 (7)
C214	0.036 (12)	0.065 (12)	0.028 (11)	-0.020 (10)	0.006 (9)	0.002 (9)
C215	0.055 (14)	0.104 (16)	0.012 (9)	-0.026 (12)	0.016 (9)	-0.036 (10)
C212	0.029 (11)	0.057 (10)	0.026 (9)	0.015 (8)	0.003 (8)	0.001 (7)
C211	0.030 (10)	0.038 (8)	0.020 (9)	0.011 (7)	0.012 (8)	-0.007 (6)
C213	0.012 (9)	0.064 (11)	0.027 (10)	0.002 (8)	0.002 (8)	0.013 (8)
C225	0.054 (14)	0.092 (15)	0.029 (11)	0.038 (12)	-0.013 (11)	-0.015 (10)
C223	0.025 (11)	0.064 (11)	0.063 (14)	-0.022 (9)	0.016 (10)	-0.017 (10)
C224	0.027 (11)	0.060 (11)	0.043 (12)	0.022 (9)	0.013 (9)	-0.021 (9)
C222	0.034 (11)	0.042 (9)	0.047 (12)	0.005 (8)	0.007 (9)	-0.018 (8)
C226	0.037 (14)	0.12 (2)	0.065 (17)	0.020 (13)	0.011 (12)	-0.008 (15)
C231	0.069 (17)	0.049 (11)	0.081 (18)	-0.010 (11)	-0.022 (15)	-0.026 (11)
C240	0.063 (19)	0.081 (16)	0.056 (16)	-0.017 (14)	-0.010 (15)	0.003 (13)
C241	0.073 (18)	0.045 (11)	0.045 (14)	0.002 (11)	0.000 (13)	0.002 (9)
C238	0.050 (14)	0.046 (11)	0.053 (14)	0.001 (10)	0.036 (12)	-0.029 (10)
C237	0.049 (15)	0.059 (12)	0.043 (13)	0.021 (10)	0.037 (11)	0.027 (10)
C242	0.049 (15)	0.045 (11)	0.068 (16)	0.003 (10)	0.015 (13)	0.005 (10)
C236	0.061 (16)	0.057 (12)	0.040 (13)	0.026 (11)	-0.001 (12)	0.000 (9)
C233	0.08 (2)	0.063 (14)	0.057 (16)	0.003 (13)	-0.025 (16)	0.029 (12)
F368	0.157 (19)	0.094 (12)	0.111 (15)	0.038 (12)	-0.013 (15)	0.022 (10)
C232	0.058 (17)	0.075 (14)	0.062 (16)	-0.020 (13)	0.013 (13)	0.029 (13)
C235	0.17 (3)	0.055 (13)	0.032 (15)	0.052 (15)	0.003 (17)	-0.001 (10)
C243	0.067 (19)	0.090 (17)	0.07 (2)	0.030 (15)	0.006 (16)	-0.017 (15)
C234	0.062 (17)	0.14 (2)	0.023 (12)	-0.048 (16)	-0.003 (12)	-0.032 (13)
C244	0.060 (18)	0.089 (19)	0.073 (19)	-0.005 (15)	0.041 (15)	-0.018 (16)
F275	0.097 (12)	0.099 (10)	0.111 (12)	-0.004 (8)	-0.057 (11)	0.038 (8)
F270	0.127 (13)	0.051 (7)	0.073 (9)	0.023 (7)	-0.010 (9)	0.010 (6)
F269	0.22 (2)	0.079 (9)	0.050 (10)	0.053 (12)	0.011 (13)	0.010 (7)
F274	0.119 (13)	0.061 (8)	0.079 (10)	0.029 (8)	-0.009 (10)	0.008 (7)

F247	0.148 (16)	0.091 (10)	0.072 (10)	-0.022 (10)	-0.046 (11)	0.026 (8)
F250	0.150 (17)	0.107 (12)	0.066 (10)	-0.013 (11)	-0.039 (11)	0.010 (9)
F254	0.081 (11)	0.052 (7)	0.106 (12)	-0.015 (7)	0.032 (9)	0.000 (7)
F276	0.080 (11)	0.052 (7)	0.098 (12)	-0.002 (7)	0.031 (9)	0.023 (7)
F248	0.093 (12)	0.104 (10)	0.061 (10)	-0.009 (9)	-0.008 (9)	-0.041 (8)
F266	0.046 (9)	0.088 (9)	0.110 (12)	0.010 (7)	0.050 (8)	0.032 (8)
F267	0.092 (12)	0.062 (8)	0.085 (11)	-0.017 (7)	0.050 (9)	-0.001 (7)
F249	0.131 (13)	0.090 (9)	0.076 (9)	-0.081 (9)	-0.032 (10)	0.011 (7)
F265	0.104 (13)	0.087 (9)	0.067 (10)	0.006 (8)	-0.003 (9)	0.033 (7)
F252	0.31 (3)	0.19 (2)	0.144 (17)	-0.18 (2)	-0.13 (2)	0.113 (16)
F253	0.176 (18)	0.099 (12)	0.087 (12)	-0.049 (12)	-0.021 (13)	0.040 (9)
F261	0.29 (2)	0.030 (7)	0.173 (18)	0.055 (10)	0.178 (18)	0.021 (8)
F268	0.078 (12)	0.157 (13)	0.113 (13)	-0.054 (10)	-0.057 (11)	0.088 (10)
F263	0.21 (2)	0.068 (10)	0.137 (17)	-0.048 (12)	0.091 (16)	0.010 (10)
F256	0.079 (12)	0.147 (13)	0.094 (13)	0.060 (10)	0.039 (10)	0.004 (10)
F258	0.125 (16)	0.164 (16)	0.058 (11)	0.052 (12)	0.033 (10)	0.003 (10)
F271	0.22 (2)	0.086 (11)	0.096 (13)	0.081 (13)	0.096 (14)	0.009 (9)
F257	0.120 (19)	0.42 (4)	0.23 (3)	-0.15 (2)	0.143 (19)	-0.28 (3)
F255	0.074 (12)	0.065 (8)	0.152 (15)	-0.025 (8)	0.078 (10)	0.002 (8)
F251	0.21 (2)	0.33 (3)	0.098 (16)	0.20 (3)	0.026 (16)	0.051 (18)
F260	0.22 (3)	0.17 (2)	0.25 (3)	0.03 (2)	-0.01 (3)	-0.15 (2)
F272	0.33 (3)	0.147 (16)	0.121 (15)	0.19 (2)	-0.095 (19)	-0.063 (12)
F259	0.124 (15)	0.067 (9)	0.151 (17)	0.016 (10)	0.098 (13)	-0.016 (10)
F273	0.096 (15)	0.065 (10)	0.41 (3)	0.003 (10)	0.094 (19)	-0.110 (15)
F262	0.33 (4)	0.134 (17)	0.19 (2)	0.07 (2)	0.24 (3)	0.058 (16)
F264	0.17 (2)	0.32 (4)	0.105 (18)	-0.07 (2)	-0.001 (18)	0.14 (2)
C247	0.08 (2)	0.076 (16)	0.066 (17)	-0.012 (14)	0.003 (16)	0.028 (13)
C245	0.034 (14)	0.106 (17)	0.032 (12)	0.023 (12)	-0.006 (11)	-0.024 (11)
F281	0.142 (18)	0.114 (12)	0.126 (16)	0.080 (12)	0.028 (14)	0.018 (11)
F282	0.25 (2)	0.135 (14)	0.074 (12)	0.090 (15)	-0.053 (15)	-0.023 (10)
F277	0.24 (2)	0.114 (14)	0.053 (11)	-0.053 (15)	-0.007 (14)	0.007 (10)
F280	0.21 (2)	0.23 (2)	0.089 (13)	-0.152 (18)	-0.018 (14)	-0.044 (13)
C286	0.084 (19)	0.045 (10)	0.060 (16)	-0.021 (11)	-0.009 (14)	0.008 (10)
C284	0.069 (17)	0.049 (12)	0.076 (17)	0.016 (11)	-0.023 (15)	-0.011 (11)
F278	0.21 (3)	0.38 (4)	0.111 (17)	0.15 (3)	-0.084 (19)	-0.16 (2)
C285	0.050 (15)	0.132 (18)	0.063 (15)	-0.050 (13)	-0.026 (13)	0.071 (13)
C289	0.068 (19)	0.075 (15)	0.09 (2)	0.018 (13)	0.029 (16)	0.010 (13)

C290	0.078 (19)	0.120 (18)	0.024 (12)	-0.026 (15)	-0.004 (13)	0.001 (12)
C287	0.11 (2)	0.106 (18)	0.051 (16)	0.046 (16)	-0.046 (16)	-0.015 (13)
C293	0.038 (15)	0.22 (3)	0.034 (14)	-0.025 (17)	0.007 (11)	0.005 (15)
C288	0.11 (2)	0.039 (10)	0.052 (14)	-0.005 (12)	-0.019 (15)	-0.001 (9)
C291	0.18 (3)	0.09 (2)	0.09 (2)	0.09 (2)	0.05 (2)	0.049 (16)
C292	0.10 (2)	0.089 (18)	0.10 (2)	-0.063 (17)	0.029 (19)	-0.003 (16)
Si7	0.029 (3)	0.057 (3)	0.045 (3)	0.008 (2)	0.003 (3)	-0.003 (2)
Si4	0.216 (12)	0.086 (7)	0.155 (10)	0.005 (6)	-0.103 (9)	0.035 (6)
F301	0.175 (19)	0.142 (14)	0.082 (12)	-0.063 (14)	0.102 (13)	-0.049 (11)
F300	0.13 (2)	0.22 (2)	0.156 (19)	0.028 (17)	0.075 (16)	0.125 (18)
F305	0.25 (3)	0.085 (12)	0.102 (14)	-0.062 (14)	-0.033 (17)	-0.029 (10)
C294	0.13 (3)	0.036 (11)	0.12 (2)	-0.003 (14)	-0.03 (2)	0.018 (12)
F299	0.090 (14)	0.25 (2)	0.095 (15)	-0.108 (15)	0.018 (11)	0.057 (15)
F303	0.25 (3)	0.123 (15)	0.24 (3)	-0.036 (16)	-0.17 (3)	-0.052 (16)
C309	0.059 (19)	0.17 (3)	0.09 (2)	0.040 (19)	0.009 (17)	0.08 (2)
F304	0.23 (3)	0.16 (2)	0.24 (3)	-0.08 (2)	0.03 (3)	-0.14 (2)
C298	0.057 (19)	0.15 (2)	0.037 (15)	0.010 (17)	0.011 (14)	-0.035 (15)
C297	0.11 (3)	0.11 (2)	0.11 (3)	-0.03 (2)	0.04 (2)	-0.008 (19)
C295	0.25 (4)	0.080 (19)	0.049 (18)	0.01 (2)	0.05 (2)	0.027 (14)
C296	0.12 (3)	0.085 (17)	0.11 (3)	0.015 (18)	-0.07 (2)	-0.021 (17)
C310	0.23 (5)	0.11 (3)	0.11 (3)	0.03 (3)	-0.02 (3)	0.00 (2)
C308	0.12 (4)	0.12 (3)	0.27 (6)	0.00 (3)	0.07 (4)	0.10 (3)
C302	0.09 (2)	0.10 (2)	0.046 (17)	-0.012 (16)	0.016 (15)	-0.054 (15)
C306	0.16 (4)	0.19 (4)	0.08 (2)	0.00 (3)	-0.03 (3)	-0.02 (2)
C307	0.36 (12)	0.59 (14)	0.22 (9)	0.42 (11)	-0.19 (10)	-0.21 (10)
C311	0.28 (8)	0.12 (3)	0.12 (4)	-0.02 (4)	0.03 (4)	0.04 (3)
F318	0.25 (2)	0.083 (10)	0.050 (9)	0.071 (12)	-0.011 (12)	-0.026 (7)
F320	0.158 (19)	0.154 (15)	0.058 (11)	-0.026 (13)	0.068 (11)	-0.043 (10)
C313	0.028 (12)	0.110 (17)	0.048 (15)	0.021 (12)	0.021 (10)	-0.012 (13)
F323	0.23 (3)	0.191 (18)	0.111 (15)	-0.168 (19)	0.094 (17)	-0.093 (14)
C316	0.063 (18)	0.073 (15)	0.12 (2)	0.014 (12)	-0.022 (18)	-0.009 (14)
F319	0.19 (2)	0.151 (16)	0.094 (14)	0.041 (15)	-0.038 (16)	-0.067 (12)
C315	0.059 (17)	0.100 (16)	0.093 (18)	0.011 (13)	-0.048 (15)	0.004 (13)
C314	0.036 (14)	0.115 (18)	0.051 (15)	0.015 (13)	0.007 (11)	-0.012 (12)
F321	0.107 (17)	0.162 (16)	0.31 (3)	-0.043 (13)	0.052 (19)	-0.17 (2)
C312	0.049 (17)	0.080 (15)	0.074 (18)	0.028 (13)	0.031 (13)	0.016 (13)
C317	0.10 (3)	0.10 (2)	0.12 (2)	0.012 (18)	-0.03 (2)	-0.020 (17)

F322	0.49 (5)	0.149 (19)	0.32 (4)	-0.18 (3)	-0.31 (4)	0.06 (2)
N324	0.064 (13)	0.062 (10)	0.048 (11)	-0.035 (9)	0.007 (10)	0.005 (8)
N336	0.070 (13)	0.057 (10)	0.028 (9)	0.003 (9)	0.003 (9)	0.004 (7)
C342	0.040 (12)	0.045 (9)	0.022 (10)	0.006 (8)	0.000 (9)	0.012 (7)
C347	0.026 (11)	0.047 (9)	0.020 (9)	-0.019 (8)	0.002 (8)	0.016 (7)
C341	0.035 (12)	0.046 (10)	0.029 (10)	-0.017 (8)	0.011 (9)	0.015 (8)
C335	0.015 (10)	0.077 (13)	0.043 (12)	-0.005 (9)	-0.001 (9)	0.006 (10)
C340	0.038 (12)	0.041 (10)	0.051 (12)	0.011 (8)	0.006 (10)	-0.003 (8)
C344	0.036 (12)	0.061 (12)	0.046 (13)	0.005 (10)	0.003 (10)	0.001 (10)
C343	0.038 (12)	0.052 (10)	0.033 (11)	0.004 (9)	0.007 (9)	-0.002 (8)
C346	0.056 (14)	0.069 (12)	0.040 (12)	-0.036 (10)	0.001 (11)	0.007 (9)
C345	0.038 (13)	0.084 (15)	0.034 (12)	-0.010 (11)	0.010 (10)	-0.002 (10)
C337	0.038 (13)	0.068 (13)	0.050 (14)	-0.003 (10)	-0.003 (11)	0.002 (10)
C339	0.059 (16)	0.064 (13)	0.043 (13)	0.001 (11)	0.008 (12)	-0.006 (10)
C338	0.087 (18)	0.052 (11)	0.034 (12)	-0.001 (11)	0.007 (12)	-0.008 (9)
C325	0.033 (13)	0.049 (11)	0.11 (2)	-0.006 (9)	0.032 (13)	-0.025 (12)
C330	0.020 (11)	0.119 (18)	0.037 (13)	0.027 (11)	0.022 (9)	0.030 (12)
C329	0.037 (13)	0.087 (16)	0.048 (14)	0.018 (11)	0.038 (11)	0.012 (12)
C326	0.054 (16)	0.060 (14)	0.09 (2)	-0.009 (12)	0.049 (14)	0.014 (13)
C334	0.050 (16)	0.15 (2)	0.033 (14)	-0.019 (15)	0.019 (12)	-0.021 (13)
C327	0.11 (3)	0.042 (13)	0.16 (3)	-0.024 (14)	0.07 (2)	-0.035 (17)
C331	0.08 (2)	0.11 (2)	0.063 (19)	-0.013 (16)	0.012 (17)	0.036 (16)
C328	0.13 (3)	0.056 (14)	0.076 (19)	0.008 (15)	0.042 (19)	0.034 (13)
C333	0.07 (2)	0.14 (2)	0.050 (17)	-0.031 (17)	0.020 (15)	0.011 (15)
C332	0.040 (18)	0.22 (4)	0.045 (19)	0.01 (2)	0.021 (14)	0.05 (2)
C367	0.10 (2)	0.096 (18)	0.053 (16)	0.052 (18)	-0.032 (17)	-0.029 (14)

7.10.8 **Table A30.** Interatomic distances (Å) and angles (deg) for [**3A'**][$BArF_{24}$].

B2—C123	1.64 (3)	C231—F278	1.24 (3)
B2—C222	1.60 (3)	C231—F280	1.33 (3)
B2—C111	1.65 (2)	C240—F248	1.38 (3)
B2—C117	1.65 (2)	C240—F247	1.35 (3)
B99—C1	1.65 (2)	C240—F249	1.27 (2)
B99—C211	1.63 (2)	C241—F252	1.19 (3)
B99—C13	1.64 (2)	C241—F250	1.28 (2)

B99—C7	1.62 (3)	C241—F251	1.36 (3)
Ir1—C335	2.048 (19)	C238—F271	1.23 (3)
Ir1—N324	2.125 (15)	C238—F272	1.26 (3)
Ir1—C144	2.15 (2)	C238—F273	1.28 (3)
Ir1—C16	2.228 (19)	C237—F265	1.31 (2)
Ir1—C17	2.202 (17)	C237—F266	1.33 (2)
Ir1—C155	2.28 (2)	C237—F267	1.36 (2)
Ir1—C18	2.27 (2)	C242—F253	1.29 (2)
Ir1—Si7	2.512 (6)	C242—F255	1.30 (3)
Ir2—N336	2.065 (16)	C242—F254	1.36 (2)
Ir2—C347	2.086 (14)	C236—F268	1.25 (3)
Ir2—C288	2.267 (19)	C236—F269	1.32 (3)
Ir2—C286	2.21 (3)	C236—F270	1.35 (2)
Ir2—C284	2.25 (2)	C233—F274	1.31 (3)
Ir2—C287	2.300 (19)	C233—F275	1.27 (2)
Ir2—C285	2.29 (3)	C233—F276	1.29 (3)
Ir2—Si4	2.445 (17)	F368—C367	1.37 (3)
C7—C8	1.44 (2)	C232—F299	1.21 (3)
C7—C12	1.43 (2)	C232—F300	1.27 (3)
C1—C2	1.39 (2)	C232—F301	1.35 (3)
C1—C6	1.44 (2)	C235—F318	1.16 (2)
C6—C5	1.40 (2)	C235—F320	1.31 (3)
C10—C9	1.35 (2)	C235—F319	1.48 (3)
C10—C11	1.33 (3)	C243—F257	1.32 (3)
C11—C12	1.38 (3)	C243—F256	1.31 (3)
C11—C238	1.49 (3)	C243—F258	1.35 (3)
C8—C9	1.35 (2)	C234—F321	1.18 (3)
C155—C144	1.37 (3)	C234—F322	1.27 (3)
C155—C16	1.40 (3)	C234—F323	1.32 (3)
C155—C293	1.52 (3)	C244—F259	1.27 (3)
C2—C3	1.39 (2)	C244—F260	1.37 (3)
C165—C175	1.37 (2)	C244—F261	1.27 (3)
C165—C15	1.41 (3)	F263—C247	1.21 (3)
C9—C237	1.49 (3)	F262—C247	1.28 (3)
C15—C14	1.39 (2)	F264—C247	1.23 (3)
C15—C236	1.52 (2)	C245—C302	1.45 (3)
C175—C235	1.46 (3)	F281—C367	1.29 (3)

C175—C148	1.40 (2)	F282—C367	1.23 (3)
C4—C5	1.37 (2)	C286—C287	1.36 (4)
C4—C3	1.36 (3)	C286—C285	1.35 (3)
C18—C144	1.44 (3)	C286—C297	1.51 (4)
C18—C17	1.36 (3)	C284—C288	1.46 (3)
C18—C290	1.49 (3)	C284—C294	1.47 (3)
C17—C291	1.55 (3)	C284—C285	1.51 (3)
C17—C16	1.53 (3)	C285—C298	1.52 (4)
C144—C289	1.64 (3)	C287—C288	1.48 (4)
C5—C232	1.48 (3)	C287—C296	1.55 (3)
C16—C292	1.51 (3)	C288—C295	1.54 (4)
C14—C13	1.42 (2)	Si7—C314	1.86 (2)
C3—C231	1.50 (3)	Si7—C312	1.82 (3)
C148—C13	1.41 (2)	Si7—C316	1.93 (2)
C124—C125	1.37 (3)	Si4—C307	1.02 (11)
C124—C123	1.37 (3)	Si4—C309	1.89 (3)
C122—C117	1.38 (2)	Si4—C310	1.97 (4)
C122—C121	1.36 (2)	F305—C302	1.30 (3)
C111—C112	1.37 (2)	F303—C302	1.15 (3)
C111—C116	1.40 (3)	F303—F304	1.81 (4)
C117—C118	1.46 (3)	C309—C308	1.54 (5)
C125—C126	1.35 (3)	F304—C302	1.28 (4)
C125—C242	1.52 (3)	C310—C311	1.26 (7)
C123—C128	1.47 (2)	C306—C307	1.88 (10)
C112—C113	1.38 (2)	C313—C312	1.60 (3)
C128—C127	1.39 (3)	C316—C317	1.51 (3)
C118—C119	1.37 (2)	C315—C314	1.52 (3)
C120—C119	1.39 (3)	N324—C329	1.35 (3)
C120—C121	1.44 (3)	N324—C325	1.37 (3)
C126—C127	1.34 (3)	N336—C341	1.36 (2)
C121—C241	1.53 (3)	N336—C337	1.41 (2)
C116—C115	1.40 (3)	C342—C347	1.38 (2)
C115—C114	1.43 (3)	C342—C343	1.42 (2)
C115—C247	1.53 (3)	C342—C341	1.46 (2)
C114—C113	1.35 (3)	C347—C346	1.35 (2)
C127—C244	1.43 (3)	C341—C340	1.38 (2)
C119—C243	1.43 (3)	C335—C334	1.35 (3)

C113—C240	1.49 (3)	C335—C330	1.40 (3)
C216—C215	1.35 (2)	C340—C339	1.42 (3)
C216—C211	1.41 (2)	C344—C345	1.38 (3)
C214—C215	1.38 (3)	C344—C343	1.37 (3)
C214—C213	1.34 (2)	C346—C345	1.39 (3)
C215—C234	1.53 (3)	C337—C338	1.41 (3)
C212—C213	1.41 (2)	C339—C338	1.42 (3)
C212—C211	1.41 (2)	C325—C326	1.38 (3)
C213—C233	1.54 (3)	C330—C331	1.31 (3)
C225—C226	1.35 (3)	C330—C329	1.43 (3)
C225—C224	1.47 (2)	C329—C328	1.48 (3)
C225—C367	1.53 (3)	C326—C327	1.35 (4)
C223—C245	1.37 (2)	C334—C333	1.43 (3)
C223—C222	1.43 (2)	C327—C328	1.42 (4)
C224—C222	1.43 (3)	C331—C332	1.40 (4)
C226—C245	1.43 (3)	C333—C332	1.33 (4)
C231—F277	1.28 (3)		
C123—B2—C222	105.7 (14)	C225—C226—C245	121 (2)
C123—B2—C111	110.3 (14)	F277—C231—F278	104 (3)
C222—B2—C111	113.3 (15)	F277—C231—F280	97 (2)
C123—B2—C117	111.0 (15)	F278—C231—F280	111 (2)
C222—B2—C117	112.9 (14)	F277—C231—C3	115.7 (18)
C111—B2—C117	103.8 (13)	F278—C231—C3	115.3 (19)
C1—B99—C211	110.4 (14)	F280—C231—C3	113 (2)
C1—B99—C13	108.3 (14)	F248—C240—F247	102 (2)
C211—B99—C13	111.9 (14)	F248—C240—F249	111 (2)
C1—B99—C7	110.9 (14)	F247—C240—F249	103.1 (18)
C211—B99—C7	101.6 (14)	F248—C240—C113	111.1 (18)
C13—B99—C7	113.6 (15)	F247—C240—C113	113 (2)
C335—Ir1—N324	77.8 (7)	F249—C240—C113	116 (2)
C335—Ir1—C144	115.7 (8)	F252—C241—F250	111 (3)
N324—Ir1—C144	89.8 (8)	F252—C241—F251	110 (2)
C335—Ir1—C16	104.9 (7)	F250—C241—F251	98 (2)
N324—Ir1—C16	151.4 (10)	F252—C241—C121	112.6 (18)
C144—Ir1—C16	63.1 (10)	F250—C241—C121	112.8 (16)
C335—Ir1—C17	144.7 (8)	F251—C241—C121	111 (2)

N324—Ir1—C17	134.7 (8)	F271—C238—F272	104 (2)
C144—Ir1—C17	61.5 (8)	F271—C238—F273	106 (2)
C16—Ir1—C17	40.5 (8)	F272—C238—F273	99 (2)
C335—Ir1—C155	95.9 (8)	F271—C238—C11	115 (2)
N324—Ir1—C155	115.6 (9)	F272—C238—C11	114.0 (17)
C144—Ir1—C155	35.8 (8)	F273—C238—C11	117 (2)
C16—Ir1—C155	36.2 (9)	F265—C237—F266	109.5 (18)
C17—Ir1—C155	60.6 (8)	F265—C237—F267	104.7 (15)
C335—Ir1—C18	153.4 (7)	F266—C237—F267	101.1 (19)
N324—Ir1—C18	100.6 (7)	F265—C237—C9	115.0 (19)
C144—Ir1—C18	37.8 (7)	F266—C237—C9	113.6 (15)
C16—Ir1—C18	64.1 (8)	F267—C237—C9	111.7 (17)
C17—Ir1—C18	35.4 (7)	F253—C242—F255	110 (2)
C155—Ir1—C18	60.4 (7)	F253—C242—F254	106.2 (17)
C335—Ir1—Si7	96.9 (6)	F255—C242—F254	103.9 (18)
N324—Ir1—Si7	82.3 (6)	F253—C242—C125	111.9 (18)
C144—Ir1—Si7	144.0 (6)	F255—C242—C125	113.2 (17)
C16—Ir1—Si7	124.7 (8)	F254—C242—C125	111 (2)
C17—Ir1—Si7	100.6 (6)	F268—C236—F269	112 (2)
C155—Ir1—Si7	159.9 (7)	F268—C236—F270	105.0 (18)
C18—Ir1—Si7	109.3 (5)	F269—C236—F270	104.9 (19)
N336—Ir2—C347	77.3 (6)	F268—C236—C15	114 (2)
N336—Ir2—C288	140.1 (7)	F269—C236—C15	109.7 (17)
C347—Ir2—C288	140.8 (6)	F270—C236—C15	110.4 (16)
N336—Ir2—C286	93.9 (7)	F274—C233—F275	106 (2)
C347—Ir2—C286	115.7 (8)	F274—C233—F276	105 (2)
C288—Ir2—C286	62.3 (9)	F275—C233—F276	109 (2)
N336—Ir2—C284	154.9 (9)	F274—C233—C213	113.4 (18)
C347—Ir2—C284	104.3 (7)	F275—C233—C213	113.4 (19)
C288—Ir2—C284	37.6 (8)	F276—C233—C213	109 (2)
C286—Ir2—C284	62.4 (8)	F299—C232—F300	106 (2)
N336—Ir2—C287	104.7 (8)	F299—C232—F301	110 (3)
C347—Ir2—C287	150.2 (9)	F300—C232—F301	102 (2)
C288—Ir2—C287	37.7 (9)	F299—C232—C5	117 (2)
C286—Ir2—C287	35.0 (9)	F300—C232—C5	111 (2)
C284—Ir2—C287	61.5 (8)	F301—C232—C5	110.2 (18)
N336—Ir2—C285	116.6 (8)	F318—C235—F320	121 (3)

C347—Ir2—C285	93.5 (7)	F318—C235—C175	120 (2)
C288—Ir2—C285	62.4 (8)	F320—C235—C175	114 (2)
C286—Ir2—C285	35.0 (7)	F318—C235—F319	94 (2)
C284—Ir2—C285	38.7 (9)	F320—C235—F319	87.2 (18)
C287—Ir2—C285	58.5 (8)	C175—C235—F319	112 (2)
N336—Ir2—Si4	82.6 (6)	C119—C243—F257	111 (3)
C347—Ir2—Si4	95.3 (6)	C119—C243—F256	118 (2)
C288—Ir2—Si4	100.5 (8)	F257—C243—F256	104 (2)
C286—Ir2—Si4	147.4 (7)	C119—C243—F258	116 (2)
C284—Ir2—Si4	121.8 (8)	F257—C243—F258	103 (3)
C287—Ir2—Si4	114.5 (8)	F256—C243—F258	102 (3)
C285—Ir2—Si4	160.4 (6)	F321—C234—F322	113 (3)
C8—C7—C12	113.0 (16)	F321—C234—F323	91 (3)
C8—C7—B99	125.6 (14)	F322—C234—F323	99 (3)
C12—C7—B99	121.2 (15)	F321—C234—C215	120 (2)
C2—C1—C6	115.8 (14)	F322—C234—C215	114 (3)
C2—C1—B99	123.1 (17)	F323—C234—C215	115.9 (18)
C6—C1—B99	120.7 (15)	C127—C244—F259	115 (2)
C5—C6—C1	120.2 (16)	C127—C244—F260	110 (2)
C9—C10—C11	118.4 (19)	F259—C244—F260	92 (2)
C12—C11—C10	122.8 (17)	C127—C244—F261	120 (2)
C12—C11—C238	116.0 (18)	F259—C244—F261	110 (2)
C10—C11—C238	121 (2)	F260—C244—F261	105 (3)
C9—C8—C7	122.1 (15)	F263—C247—F264	104 (2)
C144—C155—C16	112 (2)	F263—C247—F262	114 (3)
C144—C155—C293	125 (3)	F264—C247—F262	104 (3)
C16—C155—C293	123 (2)	F263—C247—C115	114 (2)
C144—C155—Ir1	66.7 (14)	F264—C247—C115	109 (2)
C16—C155—Ir1	69.8 (13)	F262—C247—C115	111 (2)
C293—C155—Ir1	123.2 (16)	C223—C245—C302	122 (2)
C3—C2—C1	121.9 (16)	C223—C245—C226	119 (2)
C175—C165—C15	118.3 (17)	C302—C245—C226	118 (2)
C8—C9—C10	122.3 (16)	C287—C286—C285	111 (2)
C8—C9—C237	119.3 (15)	C287—C286—C297	124 (2)
C10—C9—C237	118.3 (17)	C285—C286—C297	121 (3)
C14—C15—C165	121.6 (16)	C287—C286—Ir2	76.3 (16)
C14—C15—C236	120.2 (17)	C285—C286—Ir2	75.8 (15)

C165—C15—C236	118.2 (17)	C297—C286—Ir2	130.9 (19)
C165—C175—C235	118.0 (18)	C288—C284—C294	124 (3)
C165—C175—C148	120.6 (18)	C288—C284—C285	106 (2)
C235—C175—C148	121.2 (17)	C294—C284—C285	129 (2)
C11—C12—C7	121.3 (16)	C288—C284—Ir2	71.8 (11)
C5—C4—C3	118.6 (16)	C294—C284—Ir2	131.6 (16)
C144—C18—C17	105.1 (17)	C285—C284—Ir2	71.9 (14)
C144—C18—C290	129 (2)	C298—C285—C286	131 (2)
C17—C18—C290	126.1 (18)	C298—C285—C284	121 (2)
C144—C18—Ir1	66.5 (12)	C286—C285—C284	108 (2)
C17—C18—Ir1	69.6 (12)	C298—C285—Ir2	127.6 (15)
C290—C18—Ir1	131.8 (16)	C286—C285—Ir2	69.3 (17)
C18—C17—C291	127 (2)	C284—C285—Ir2	69.4 (14)
C18—C17—C16	111.0 (17)	C286—C287—C288	109.2 (19)
C291—C17—C16	122 (2)	C286—C287—C296	126 (3)
C18—C17—Ir1	75.0 (11)	C288—C287—C296	124 (3)
C291—C17—Ir1	127.0 (18)	C286—C287—Ir2	68.7 (13)
C16—C17—Ir1	70.7 (10)	C288—C287—Ir2	69.9 (11)
C155—C144—C18	109 (2)	C296—C287—Ir2	126.6 (17)
C155—C144—C289	125 (2)	C284—C288—C287	105 (2)
C18—C144—C289	122.5 (19)	C284—C288—C295	128 (2)
C155—C144—Ir1	77.6 (14)	C287—C288—C295	127 (2)
C18—C144—Ir1	75.7 (14)	C284—C288—Ir2	70.6 (11)
C289—C144—Ir1	128.2 (16)	C287—C288—Ir2	72.4 (11)
C4—C5—C6	121.5 (17)	C295—C288—Ir2	125 (2)
C4—C5—C232	118.6 (17)	C314—Si7—C312	111.1 (12)
C6—C5—C232	119.8 (17)	C314—Si7—C316	107.0 (11)
C155—C16—C292	129 (2)	C312—Si7—C316	107.0 (13)
C155—C16—C17	100.9 (19)	C314—Si7—Ir1	110.5 (8)
C292—C16—C17	129 (2)	C312—Si7—Ir1	106.5 (8)
C155—C16—Ir1	74.0 (13)	C316—Si7—Ir1	114.7 (8)
C292—C16—Ir1	128.7 (19)	C307—Si4—C309	94 (4)
C17—C16—Ir1	68.9 (10)	C307—Si4—C310	125 (6)
C15—C14—C13	120.9 (16)	C309—Si4—C310	107.6 (16)
C2—C3—C4	121.6 (15)	C307—Si4—Ir2	104 (4)
C2—C3—C231	117.5 (19)	C309—Si4—Ir2	114.9 (12)
C4—C3—C231	120.9 (17)	C310—Si4—Ir2	110.5 (17)

C13—C148—C175	122.6 (15)	C302—F303—F304	44.7 (18)
C148—C13—C14	116.0 (14)	C308—C309—Si4	116 (2)
C148—C13—B99	124.6 (15)	C302—F304—F303	39.2 (16)
C14—C13—B99	119.4 (15)	C311—C310—Si4	118 (4)
C125—C124—C123	124.9 (17)	F303—C302—F305	107 (3)
C117—C122—C121	122.4 (18)	F303—C302—F304	96 (3)
C112—C111—C116	114.7 (15)	F305—C302—F304	102 (3)
C112—C111—B2	121.7 (15)	F303—C302—C245	124 (3)
C116—C111—B2	123.1 (15)	F305—C302—C245	117 (2)
C122—C117—C118	116.7 (15)	F304—C302—C245	106 (3)
C122—C117—B2	127.0 (16)	C306—C307—Si4	169 (9)
C118—C117—B2	116.0 (14)	C317—C316—Si7	115.7 (17)
C126—C125—C124	120.0 (16)	C315—C314—Si7	114.3 (17)
C126—C125—C242	118.0 (19)	C313—C312—Si7	118.0 (16)
C124—C125—C242	121.9 (17)	C329—N324—C325	126.1 (19)
C124—C123—C128	112.3 (19)	C329—N324—Ir1	111.2 (14)
C124—C123—B2	126.3 (15)	C325—N324—Ir1	122.7 (14)
C128—C123—B2	121.1 (16)	C341—N336—C337	117.2 (16)
C113—C112—C111	124.0 (16)	C341—N336—Ir2	119.4 (12)
C127—C128—C123	122.5 (16)	C337—N336—Ir2	123.3 (12)
C119—C118—C117	120.6 (19)	C347—C342—C343	118.5 (15)
C119—C120—C121	117.6 (16)	C347—C342—C341	118.3 (14)
C125—C126—C127	121.1 (19)	C343—C342—C341	123.2 (15)
C122—C121—C120	120.8 (16)	C346—C347—C342	121.9 (15)
C122—C121—C241	119.4 (19)	C346—C347—Ir2	124.2 (12)
C120—C121—C241	119.7 (16)	C342—C347—Ir2	113.6 (11)
C111—C116—C115	122.7 (16)	N336—C341—C340	124.3 (16)
C114—C115—C116	119.8 (18)	N336—C341—C342	110.8 (14)
C114—C115—C247	118.9 (18)	C340—C341—C342	124.8 (15)
C116—C115—C247	121 (2)	C334—C335—C330	116 (2)
C115—C114—C113	116.6 (16)	C334—C335—Ir1	125.4 (18)
C244—C127—C128	116.6 (18)	C330—C335—Ir1	118.8 (15)
C244—C127—C126	124 (2)	C341—C340—C339	119.5 (17)
C128—C127—C126	118.9 (16)	C345—C344—C343	119.3 (18)
C243—C119—C118	119 (2)	C344—C343—C342	119.9 (17)
C243—C119—C120	118.7 (19)	C347—C346—C345	119.1 (17)
C118—C119—C120	122 (2)	C346—C345—C344	121.3 (18)

C112—C113—C114	122.1 (15)	C338—C337—N336	121.3 (18)
C112—C113—C240	119.5 (17)	C340—C339—C338	117.9 (19)
C114—C113—C240	118.4 (16)	C337—C338—C339	119.5 (17)
C215—C216—C211	121.2 (16)	C326—C325—N324	119 (2)
C215—C214—C213	116.8 (16)	C331—C330—C335	123 (2)
C216—C215—C214	124.6 (16)	C331—C330—C329	127 (3)
C216—C215—C234	118 (2)	C335—C330—C329	109.6 (18)
C214—C215—C234	117.2 (18)	N324—C329—C328	116 (2)
C213—C212—C211	122.4 (16)	N324—C329—C330	122 (2)
C216—C211—C212	114.1 (14)	C328—C329—C330	122 (2)
C216—C211—B99	123.7 (14)	C327—C326—C325	118 (2)
C212—C211—B99	121.9 (13)	C335—C334—C333	124 (3)
C214—C213—C212	120.9 (16)	C326—C327—C328	126 (2)
C214—C213—C233	120.9 (15)	C332—C331—C330	118 (3)
C212—C213—C233	118.2 (16)	C329—C328—C327	115 (2)
C226—C225—C224	120 (2)	C332—C333—C334	115 (3)
C226—C225—C367	123.9 (18)	C331—C332—C333	123 (3)
C224—C225—C367	115.7 (18)	F282—C367—F368	100 (3)
C245—C223—C222	123 (2)	F282—C367—F281	117 (2)
C222—C224—C225	119.6 (16)	F368—C367—F281	100 (2)
C223—C222—C224	116.7 (16)	F282—C367—C225	115 (2)
C223—C222—B2	120.9 (16)	F368—C367—C225	109 (2)
C224—C222—B2	122.4 (14)	F281—C367—C225	114 (3)
C1—B99—C7—C8	139.1 (15)	C122—C121—C241—F250	46 (3)
C211—B99—C7—C8	-103.6 (16)	C120—C121—C241—F250	-138 (2)
C13—B99—C7—C8	17 (2)	C122—C121—C241—F251	155 (2)
C1—B99—C7—C12	-47.1 (19)	C120—C121—C241—F251	-29 (3)
C211—B99—C7—C12	70.3 (16)	C12—C11—C238—F271	160 (2)
C13—B99—C7—C12	-169.4 (14)	C10—C11—C238—F271	-23 (3)
C211—B99—C1—C2	-138.4 (17)	C12—C11—C238—F272	-80 (3)
C13—B99—C1—C2	98.8 (19)	C10—C11—C238—F272	97 (3)

C7—B99—C1—C2	-27 (2)	C12—C11—C238—F273	35 (3)
C211—B99—C1—C6	50 (2)	C10—C11—C238—F273	-148 (2)
C13—B99—C1—C6	-73.2 (19)	C8—C9—C237—F265	-87 (2)
C7—B99—C1—C6	161.4 (14)	C10—C9—C237—F265	91 (2)
C2—C1—C6—C5	8 (2)	C8—C9—C237—F266	145.3 (18)
B99—C1—C6—C5	-179.8 (14)	C10—C9—C237—F266	-37 (3)
C9—C10—C11—C12	0 (3)	C8—C9—C237—F267	32 (2)
C9—C10—C11—C238	-176.7 (17)	C10—C9—C237—F267	-150.2 (17)
C12—C7—C8—C9	0 (2)	C126—C125—C242—F253	84 (3)
B99—C7—C8—C9	174.5 (14)	C124—C125—C242—F253	-94 (3)
C6—C1—C2—C3	-6 (2)	C126—C125—C242—F255	-40 (3)
B99—C1—C2—C3	-178.8 (16)	C124—C125—C242—F255	141 (2)
C7—C8—C9—C10	3 (2)	C126—C125—C242—F254	-157.0 (18)
C7—C8—C9—C237	-179.3 (16)	C124—C125—C242—F254	25 (3)
C11—C10—C9—C8	-3 (3)	C14—C15—C236—F268	94 (3)
C11—C10—C9—C237	179.0 (17)	C165—C15—C236—F268	-84 (2)
C175—C165—C15—C14	-1 (3)	C14—C15—C236—F269	-33 (3)
C175—C165—C15—C236	176 (2)	C165—C15—C236—F269	149 (2)
C15—C165—C175—C235	177 (2)	C14—C15—C236—F270	-148.2 (19)
C15—C165—C175—C148	2 (3)	C165—C15—C236—F270	34 (3)
C10—C11—C12—C7	3 (3)	C214—C213—C233—F274	-138 (2)
C238—C11—C12—C7	179.8 (16)	C212—C213—C233—F274	40 (3)

C8—C7—C12—C11	-3 (2)	C214—C213—C233—F275	-16 (4)
B99—C7—C12—C11	-177.4 (15)	C212—C213—C233—F275	161 (2)
C144—C18—C17—C291	-178 (2)	C214—C213—C233—F276	105 (2)
C290—C18—C17—C291	-2 (4)	C212—C213—C233—F276	-77 (3)
Ir1—C18—C17—C291	125 (3)	C4—C5—C232—F299	-32 (3)
C144—C18—C17—C16	-5 (2)	C6—C5—C232—F299	151 (2)
C290—C18—C17—C16	170 (2)	C4—C5—C232—F300	90 (3)
Ir1—C18—C17—C16	-62.0 (15)	C6—C5—C232—F300	-87 (3)
C144—C18—C17—Ir1	57.2 (15)	C4—C5—C232—F301	-158.2 (19)
C290—C18—C17—Ir1	-128 (2)	C6—C5—C232—F301	25 (3)
C16—C155—C144—C18	-15 (3)	C165—C175—C235—F318	-22 (5)
C293—C155—C144—C18	175 (2)	C148—C175—C235—F318	154 (3)
Ir1—C155—C144—C18	-69.8 (17)	C165—C175—C235—F320	133 (3)
C16—C155—C144—C289	-177 (2)	C148—C175—C235—F320	-51 (4)
C293—C155—C144—C289	13 (4)	C165—C175—C235—F319	-130 (2)
Ir1—C155—C144—C289	128 (2)	C148—C175—C235—F319	45 (3)
C16—C155—C144—Ir1	54.8 (17)	C118—C119—C243—F257	90 (3)
C293—C155—C144—Ir1	-115 (2)	C120—C119—C243—F257	-92 (3)
C17—C18—C144—C155	12 (3)	C118—C119—C243—F256	-150 (2)
C290—C18—C144—C155	-163 (2)	C120—C119—C243—F256	28 (3)
Ir1—C18—C144—C155	71.0 (17)	C118—C119—C243—F258	-28 (3)
C17—C18—C144—C289	174 (2)	C120—C119—C243—F258	150 (2)

C290—C18—C144—C289	-1 (4)	C216—C215—C234—F321	56 (4)
Ir1—C18—C144—C289	-126 (2)	C214—C215—C234—F321	-125 (3)
C17—C18—C144—Ir1	-59.2 (16)	C216—C215—C234—F322	-165 (3)
C290—C18—C144—Ir1	126 (2)	C214—C215—C234—F322	14 (4)
C3—C4—C5—C6	2 (3)	C216—C215—C234—F323	-52 (4)
C3—C4—C5—C232	-174.8 (19)	C214—C215—C234—F323	128 (3)
C1—C6—C5—C4	-6 (3)	C128—C127—C244—F259	-161 (2)
C1—C6—C5—C232	171.1 (18)	C126—C127—C244—F259	14 (4)
C144—C155—C16—C292	180 (2)	C128—C127—C244—F260	97 (3)
C293—C155—C16—C292	-10 (4)	C126—C127—C244—F260	-88 (3)
Ir1—C155—C16—C292	-127 (3)	C128—C127—C244—F261	-25 (4)
C144—C155—C16—C17	11 (2)	C126—C127—C244—F261	149 (3)
C293—C155—C16—C17	-179 (2)	C114—C115—C247—F263	19 (3)
Ir1—C155—C16—C17	64.1 (12)	C116—C115—C247—F263	-164 (2)
C144—C155—C16—Ir1	-53.2 (18)	C114—C115—C247—F264	134 (3)
C293—C155—C16—Ir1	117 (2)	C116—C115—C247—F264	-49 (4)
C18—C17—C16—C155	-3 (2)	C114—C115—C247—F262	-112 (3)
C291—C17—C16—C155	170 (2)	C116—C115—C247—F262	65 (3)
Ir1—C17—C16—C155	-68.0 (14)	C222—C223—C245—C302	174 (2)
C18—C17—C16—C292	-172 (3)	C222—C223—C245—C226	2 (4)
C291—C17—C16—C292	1 (4)	C225—C226—C245—C223	-4 (4)
Ir1—C17—C16—C292	123 (3)	C225—C226—C245—C302	-176 (3)

C18—C17—C16—Ir1	64.6 (16)	C287—C286—C285—C298	-169 (2)
C291—C17—C16—Ir1	-122 (2)	C297—C286—C285—C298	-7 (4)
C165—C15—C14—C13	-2 (3)	Ir2—C286—C285—C298	122 (3)
C236—C15—C14—C13	-179.3 (18)	C287—C286—C285—C284	10 (3)
C1—C2—C3—C4	3 (3)	C297—C286—C285—C284	172 (2)
C1—C2—C3—C231	-175.9 (17)	Ir2—C286—C285—C284	-58.9 (15)
C5—C4—C3—C2	-1 (3)	C287—C286—C285—Ir2	68.7 (19)
C5—C4—C3—C231	178.3 (18)	C297—C286—C285—Ir2	-129 (2)
C165—C175—C148—C13	1 (3)	C288—C284—C285—C298	173 (2)
C235—C175—C148—C13	-175 (2)	C294—C284—C285—C298	7 (3)
C175—C148—C13—C14	-4 (3)	Ir2—C284—C285—C298	-122 (2)
C175—C148—C13—B99	178.3 (19)	C288—C284—C285—C286	-6 (2)
C15—C14—C13—C148	4 (3)	C294—C284—C285—C286	-172 (2)
C15—C14—C13—B99	-177.8 (17)	Ir2—C284—C285—C286	58.8 (17)
C1—B99—C13—C148	104.8 (18)	C288—C284—C285—Ir2	-64.4 (13)
C211—B99—C13—C148	-17 (3)	C294—C284—C285—Ir2	129 (2)
C7—B99—C13—C148	-131.4 (17)	C285—C286—C287—C288	-10 (3)
C1—B99—C13—C14	-73 (2)	C297—C286—C287—C288	-171 (2)
C211—B99—C13—C14	165.0 (16)	Ir2—C286—C287—C288	58.2 (16)
C7—B99—C13—C14	51 (2)	C285—C286—C287—C296	171 (2)
C123—B2—C111—C112	-39 (2)	C297—C286—C287—C296	10 (4)
C222—B2—C111—C112	-157.1 (16)	Ir2—C286—C287—C296	-121 (2)

C117—B2—C111—C112	80 (2)	C285—C286—C287—Ir2	-68.4 (19)
C123—B2—C111—C116	149.1 (16)	C297—C286—C287—Ir2	130 (3)
C222—B2—C111—C116	31 (2)	C294—C284—C288—C287	167 (2)
C117—B2—C111—C116	-92.0 (19)	C285—C284—C288—C287	0 (2)
C121—C122—C117—C118	-1 (2)	Ir2—C284—C288—C287	-64.7 (14)
C121—C122—C117—B2	174.0 (16)	C294—C284—C288—C295	-8 (4)
C123—B2—C117—C122	26 (2)	C285—C284—C288—C295	-175 (3)
C222—B2—C117—C122	144.4 (17)	Ir2—C284—C288—C295	120 (3)
C111—B2—C117—C122	-92.5 (19)	C294—C284—C288—Ir2	-128 (2)
C123—B2—C117—C118	-159.4 (14)	C285—C284—C288—Ir2	64.5 (14)
C222—B2—C117—C118	-41 (2)	C286—C287—C288—C284	6 (3)
C111—B2—C117—C118	82.1 (17)	C296—C287—C288—C284	-175 (2)
C123—C124—C125—C126	-2 (3)	Ir2—C287—C288—C284	63.5 (13)
C123—C124—C125—C242	176.3 (18)	C286—C287—C288—C295	-179 (3)
C125—C124—C123—C128	3 (3)	C296—C287—C288—C295	0 (4)
C125—C124—C123—B2	177.1 (17)	Ir2—C287—C288—C295	-121 (3)
C222—B2—C123—C124	-80 (2)	C286—C287—C288—Ir2	-57.5 (17)
C111—B2—C123—C124	157.1 (17)	C296—C287—C288—Ir2	121 (2)
C117—B2—C123—C124	43 (2)	C307—Si4—C309—C308	72 (6)
C222—B2—C123—C128	93.5 (18)	C310—Si4—C309—C308	-57 (4)
C111—B2—C123—C128	-29 (2)	Ir2—Si4—C309—C308	179 (3)
C117—B2—C123—C128	-143.7 (15)	F304—F303—C302—F305	105 (3)

C116—C111—C112—C113	-2 (3)	F304—F303—C302—C245	-114 (5)
B2—C111—C112—C113	-175.1 (16)	F303—F304—C302—F305	-109 (3)
C124—C123—C128—C127	-5 (3)	F303—F304—C302—C245	128 (4)
B2—C123—C128—C127	-179.2 (16)	C223—C245—C302—F303	-157 (4)
C122—C117—C118—C119	-1 (2)	C226—C245—C302—F303	15 (5)
B2—C117—C118—C119	-175.9 (15)	C223—C245—C302—F305	-19 (4)
C124—C125—C126—C127	2 (3)	C226—C245—C302—F305	153 (3)
C242—C125—C126—C127	-175.9 (19)	C223—C245—C302—F304	94 (4)
C117—C122—C121—C120	2 (3)	C226—C245—C302—F304	-94 (3)
C117—C122—C121—C241	177.9 (16)	C309—Si4—C307—C306	50 (30)
C119—C120—C121—C122	-3 (3)	C310—Si4—C307—C306	165 (27)
C119—C120—C121—C241	-178.2 (17)	Ir2—Si4—C307—C306	-67 (29)
C112—C111—C116—C115	4 (3)	C312—Si7—C314—C315	-79 (2)
B2—C111—C116—C115	176.7 (16)	C316—Si7—C314—C315	38 (2)
C111—C116—C115—C114	-3 (3)	Ir1—Si7—C314—C315	163.2 (17)
C111—C116—C115—C247	180 (2)	C314—Si7—C312—C313	68 (2)
C116—C115—C114—C113	1 (3)	C316—Si7—C312—C313	-48 (2)
C247—C115—C114—C113	177 (2)	Ir1—Si7—C312—C313	-171.3 (16)
C123—C128—C127—C244	-180 (2)	C343—C342—C347—C346	-2 (3)
C123—C128—C127—C126	6 (3)	C341—C342—C347—C346	-180 (2)
C125—C126—C127—C244	-178 (2)	C343—C342—C347—Ir2	172.7 (15)
C125—C126—C127—C128	-4 (3)	C341—C342—C347—Ir2	-5 (2)

C117—C118—C119—C243	177.7 (19)	C337—N336—C341—C340	2 (3)
C117—C118—C119—C120	0 (3)	Ir2—N336—C341—C340	-175.1 (16)
C121—C120—C119—C243	-176 (2)	C337—N336—C341—C342	-176.4 (18)
C121—C120—C119—C118	1 (3)	Ir2—N336—C341—C342	6 (2)
C111—C112—C113—C114	0 (3)	C347—C342—C341—N336	0 (3)
C111—C112—C113—C240	-179 (2)	C343—C342—C341—N336	-178.1 (19)
C115—C114—C113—C112	1 (3)	C347—C342—C341—C340	-179 (2)
C115—C114—C113—C240	179.6 (19)	C343—C342—C341—C340	3 (3)
C211—C216—C215—C214	4 (3)	N336—C341—C340—C339	1 (3)
C211—C216—C215—C234	-177 (2)	C342—C341—C340—C339	179 (2)
C213—C214—C215—C216	-3 (3)	C345—C344—C343—C342	-5 (3)
C213—C214—C215—C234	178 (2)	C347—C342—C343—C344	5 (3)
C215—C216—C211—C212	-2 (3)	C341—C342—C343—C344	-178 (2)
C215—C216—C211—B99	-177 (2)	C342—C347—C346—C345	-1 (3)
C213—C212—C211—C216	0 (3)	Ir2—C347—C346—C345	-174.7 (17)
C213—C212—C211—B99	175.0 (19)	C347—C346—C345—C344	1 (4)
C1—B99—C211—C216	-164.9 (17)	C343—C344—C345—C346	2 (3)
C13—B99—C211—C216	-44 (3)	C341—N336—C337—C338	-4 (3)
C7—B99—C211—C216	77 (2)	Ir2—N336—C337—C338	173.0 (17)
C1—B99—C211—C212	21 (3)	C341—C340—C339—C338	-2 (3)
C13—B99—C211—C212	141.2 (17)	N336—C337—C338—C339	3 (4)
C7—B99—C211—C212	-97.2 (19)	C340—C339—C338—C337	0 (4)

C215—C214—C213—C212	1 (3)	C329—N324—C325—C326	7 (4)
C215—C214—C213—C233	178 (2)	Ir1—N324—C325—C326	-171.7 (17)
C211—C212—C213—C214	1 (3)	C334—C335—C330—C331	4 (3)
C211—C212—C213—C233	-177 (2)	Ir1—C335—C330—C331	-175 (2)
C226—C225—C224—C222	-5 (3)	C334—C335—C330—C329	-177 (2)
C367—C225—C224—C222	-180 (2)	Ir1—C335—C330—C329	5 (2)
C245—C223—C222—C224	-2 (3)	C325—N324—C329—C328	-5 (3)
C245—C223—C222—B2	180 (2)	Ir1—N324—C329—C328	173.7 (18)
C225—C224—C222—C223	3 (3)	C325—N324—C329—C330	174 (2)
C225—C224—C222—B2	-179 (2)	Ir1—N324—C329—C330	-7 (3)
C123—B2—C222—C223	91 (2)	C331—C330—C329—N324	-179 (3)
C111—B2—C222—C223	-148.0 (18)	C335—C330—C329—N324	2 (3)
C117—B2—C222—C223	-30 (3)	C331—C330—C329—C328	0 (4)
C123—B2—C222—C224	-87 (2)	C335—C330—C329—C328	-179 (2)
C111—B2—C222—C224	34 (3)	N324—C325—C326—C327	-5 (4)
C117—B2—C222—C224	151.4 (18)	C330—C335—C334—C333	-5 (4)
C224—C225—C226—C245	5 (4)	Ir1—C335—C334—C333	173 (2)
C367—C225—C226—C245	180 (3)	C325—C326—C327—C328	2 (5)
C2—C3—C231—F277	-47 (3)	C335—C330—C331—C332	-3 (4)
C4—C3—C231—F277	134 (2)	C329—C330—C331—C332	178 (2)
C2—C3—C231—F278	74 (3)	N324—C329—C328—C327	1 (4)
C4—C3—C231—F278	-105 (3)	C330—C329—C328—C327	-178 (2)

C2—C3—C231—F280	-158 (2)	C326—C327—C328—C329	0 (5)
C4—C3—C231—F280	23 (3)	C335—C334—C333—C332	5 (4)
C112—C113—C240—F248	51 (3)	C330—C331—C332—C333	3 (5)
C114—C113—C240—F248	-127 (2)	C334—C333—C332—C331	-4 (5)
C112—C113—C240—F247	-62 (3)	C226—C225—C367—F282	23 (5)
C114—C113—C240—F247	120 (2)	C224—C225—C367—F282	-162 (3)
C112—C113—C240—F249	179 (2)	C226—C225—C367—F368	134 (3)
C114—C113—C240—F249	1 (3)	C224—C225—C367—F368	-51 (3)
C122—C121—C241—F252	-81 (3)	C226—C225—C367—F281	-115 (3)
C120—C121—C241—F252	95 (3)	C224—C225—C367—F281	60 (3)

7.11 [**5A**][$BArF_{24}$]

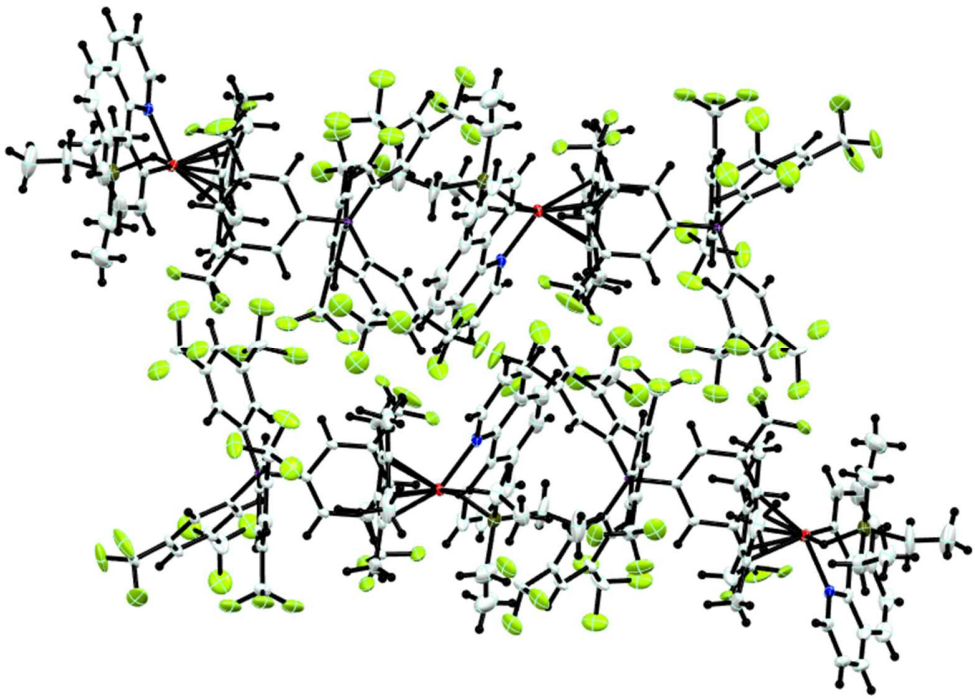

7.11.1 **Figure A29.** Crystal lattice packing of [**5A**][$BArF_{24}$].

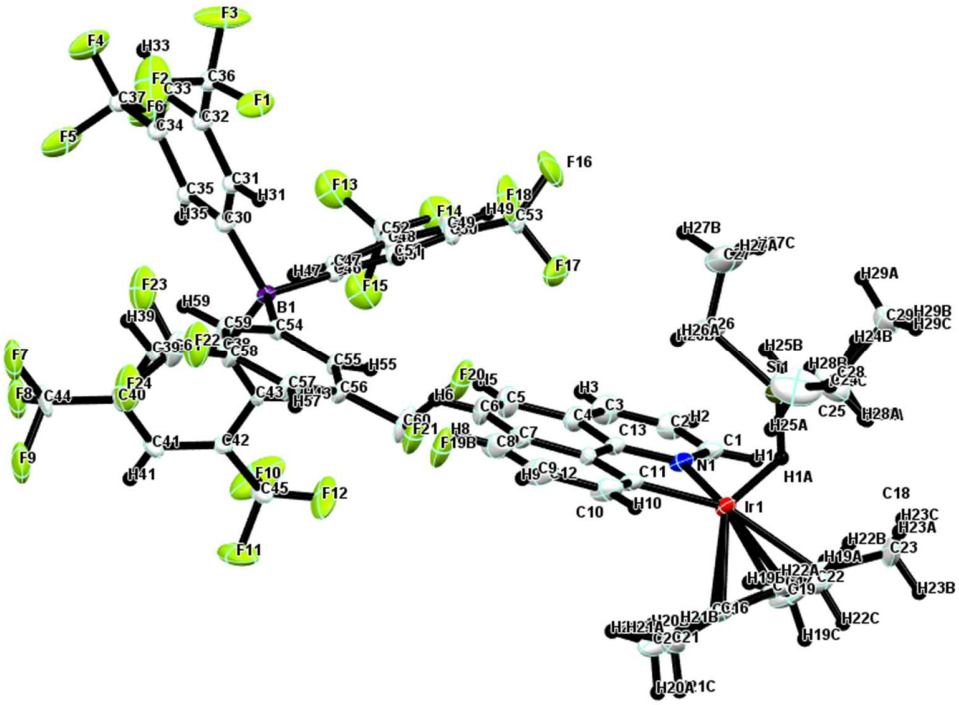

7.11.2 **Figure A30.** Asymmetric unit of [**5A**][BArF$_{24}$], with all hydrogens and total numbering of atoms.

[**5A**][BArF$_{24}$]

Data collection: Bruker *APEX2*; cell refinement: Bruker *SAINT*; data reduction: Bruker *SAINT*; program(s) used to solve structure: *SHELXS2013* (Sheldrick, 2013); program(s) used to refine structure: *SHELXL2013* (Sheldrick, 2013); molecular graphics: *Mercury* (Macrae *et al.*, 2008); software used to prepare material for publication: *SHELXL2013* (Sheldrick, 2013).

7.11.3 Crystal data

$C_{32}H_{12}BF_{24}\cdot C_{29}H_{39}IrNSi$	$F(000)$ = 2944
M_r = 1485.12	D_x = 1.595 Mg m^{-3}
Monoclinic, $P2_1/c$	Mo $K\alpha$ radiation, λ = 0.71073 Å
a = 12.5087 (6) Å	Cell parameters from 9645 reflections
b = 19.5739 (10) Å	θ = 2.4–32.0°

c = 25.5683 (13) Å	μ = 2.29 mm^{-1}
β = 98.955 (1)°	T = 173 K
V = 6183.9 (5) Å^3	Prism, yellow
Z = 4	0.34 × 0.25 × 0.16 mm

7.11.4 Data collection

Bruker APEX-II CCD diffractometer	23408 independent reflections
Radiation source: sealed tube	17366 reflections with $I > 2\sigma(I)$
Triumph monochromator	R_{int} = 0.043
ϕ and ω scans	θ_{max} = 33.1°, θ_{min} = 1.3°
Absorption correction: multi-scan *SADABS*	h = -19→8
T_{min} = 0.622, T_{max} = 0.747	k = -28→30
141138 measured reflections	l = -36→39

7.11.5 Refinement

Refinement on F^2	Primary atom site location: structure-invariant direct methods
Least-squares matrix: full	Secondary atom site location: difference Fourier map
$R[F^2 > 2\sigma(F^2)]$ = 0.066	Hydrogen site location: mixed
$wR(F^2)$ = 0.167	H-atom parameters constrained
S = 1.02	$w = 1/[\sigma^2(F_o^2) + (0.0772P)^2 + 23.8188P]$ where $P = (F_o^2 + 2F_c^2)/3$
23408 reflections	$(\Delta/\sigma)_{max}$ = 0.001
820 parameters	$\Delta\rangle_{max}$ = 5.42 e Å^{-3}
0 restraints	$\Delta\rangle_{min}$ = -2.97 e Å^{-3}

7.11.6 Special details

Geometry. All esds (except the esd in the dihedral angle between two l.s. planes) are estimated using the full covariance matrix. The cell esds are taken into account individually in the estimation of esds in distances, angles and torsion angles; correlations between esds in cell parameters are only used when they are defined by crystal symmetry. An approximate (isotropic) treatment of cell esds is used for estimating esds involving l.s. planes.

7.11.7 **Table A31.** Fractional atomic coordinates and isotropic or equivalent isotropic displacement parameters (Å^2) for [**5A**][BArF$_{24}$].

	x	*y*	*z*	U_{iso}*/U_{eq}	Occ. (<1)
C1	0.7322 (4)	0.5922 (2)	0.48828 (18)	0.0324 (9)	
H1	0.7901	0.5973	0.4685	0.039*	
C2	0.7194 (5)	0.5299 (3)	0.5136 (2)	0.0412 (11)	
H2	0.7673	0.4931	0.5101	0.049*	
C3	0.6376 (5)	0.5216 (3)	0.5437 (2)	0.0430 (12)	
H3	0.6292	0.4792	0.5607	0.052*	
C4	0.5673 (4)	0.5757 (3)	0.54914 (18)	0.0342 (9)	
C5	0.4817 (5)	0.5733 (3)	0.5801 (2)	0.0486 (13)	
H5	0.4691	0.5319	0.5977	0.058*	
C6	0.4187 (4)	0.6275 (3)	0.5852 (2)	0.0468 (13)	
H6	0.3636	0.6241	0.6068	0.056*	
C7	0.4330 (4)	0.6909 (3)	0.55855 (19)	0.0375 (10)	
C8	0.3730 (5)	0.7501 (3)	0.5623 (2)	0.0461 (13)	
H8	0.3163	0.7501	0.5831	0.055*	
C9	0.3955 (5)	0.8086 (3)	0.5362 (2)	0.0474 (13)	
H9	0.3544	0.8488	0.5392	0.057*	
C10	0.4787 (4)	0.8095 (3)	0.5049 (2)	0.0376 (10)	
H10	0.4947	0.8504	0.4877	0.045*	
C11	0.5363 (3)	0.7518 (2)	0.49938 (16)	0.0239 (7)	
C12	0.5148 (3)	0.6939 (2)	0.52660 (17)	0.0281 (8)	
C13	0.5818 (3)	0.6367 (2)	0.52158 (16)	0.0265 (8)	
C14	0.6744 (5)	0.6901 (3)	0.37459 (19)	0.0378 (11)	
C15	0.5625 (4)	0.7001 (2)	0.37672 (17)	0.0329 (9)	
C16	0.5432 (4)	0.7717 (2)	0.37753 (18)	0.0321 (9)	
C17	0.6442 (4)	0.8057 (2)	0.37891 (18)	0.0339 (9)	
C18	0.7261 (4)	0.7540 (3)	0.37689 (19)	0.0385 (11)	
C19	0.7259 (7)	0.6231 (4)	0.3637 (2)	0.070 (2)	
H19A	0.7188	0.6160	0.3254	0.105*	
H19B	0.6897	0.5858	0.3796	0.105*	
H19C	0.8027	0.6239	0.3791	0.105*	
C20	0.4765 (6)	0.6454 (4)	0.3728 (3)	0.066 (2)	
H20A	0.4255	0.6514	0.3400	0.099*	

H20B	0.4376	0.6490	0.4032	0.099*	
H20C	0.5106	0.6003	0.3728	0.099*	
C21	0.4352 (5)	0.8052 (4)	0.3747 (2)	0.0543 (16)	
H21A	0.4445	0.8511	0.3901	0.082*	
H21B	0.3894	0.7779	0.3945	0.082*	
H21C	0.4009	0.8085	0.3376	0.082*	
C22	0.6609 (7)	0.8809 (3)	0.3746 (3)	0.067 (2)	
H22A	0.6537	0.8938	0.3372	0.100*	
H22B	0.7334	0.8930	0.3927	0.100*	
H22C	0.6064	0.9052	0.3912	0.100*	
C23	0.8392 (5)	0.7690 (5)	0.3670 (3)	0.071 (2)	
H23A	0.8865	0.7304	0.3792	0.106*	
H23B	0.8660	0.8103	0.3864	0.106*	
H23C	0.8388	0.7761	0.3291	0.106*	
C24	0.9392 (5)	0.7228 (5)	0.5026 (3)	0.0647 (19)	
H24A	0.9288	0.6727	0.5016	0.078*	
H24B	0.9448	0.7381	0.4662	0.078*	
C25	1.0459 (5)	0.7392 (4)	0.5388 (3)	0.064 (2)	
H25A	1.0632	0.7877	0.5355	0.096*	
H25B	1.1042	0.7113	0.5284	0.096*	
H25C	1.0385	0.7291	0.5756	0.096*	
C26	0.8045 (8)	0.7216 (5)	0.5894 (3)	0.081 (2)	
H26A	0.7777	0.6744	0.5821	0.098*	
H26B	0.8775	0.7180	0.6106	0.098*	
C27	0.7335 (10)	0.7548 (6)	0.6225 (4)	0.106 (4)	
H27A	0.7669	0.7523	0.6597	0.158*	
H27B	0.6634	0.7314	0.6178	0.158*	
H27C	0.7228	0.8027	0.6119	0.158*	
C28	0.8463 (8)	0.8543 (5)	0.5446 (4)	0.056 (2)	0.7
H28A	0.7802	0.8726	0.5565	0.067*	0.7
H28B	0.9046	0.8547	0.5756	0.067*	0.7
C29	0.8775 (11)	0.9013 (6)	0.5040 (5)	0.079 (3)	0.7
H29A	0.9344	0.8801	0.4871	0.118*	0.7
H29B	0.9045	0.9442	0.5209	0.118*	0.7
H29C	0.8143	0.9106	0.4772	0.118*	0.7
C28B	0.879 (2)	0.8502 (12)	0.5124 (10)	0.056 (2)	0.3
H28C	0.9503	0.8546	0.5356	0.067*	0.3

H28D	0.8921	0.8535	0.4752	0.067*	0.3
C29B	0.804 (3)	0.9114 (14)	0.5244 (13)	0.079 (3)	0.3
H29D	0.8234	0.9528	0.5065	0.118*	0.3
H29E	0.8128	0.9194	0.5627	0.118*	0.3
H29F	0.7280	0.8997	0.5114	0.118*	0.3
C30	0.2709 (3)	0.7048 (2)	0.73236 (16)	0.0253 (7)	
C31	0.3532 (4)	0.7537 (2)	0.73141 (18)	0.0303 (9)	
H31	0.3346	0.8008	0.7306	0.036*	
C32	0.4608 (4)	0.7356 (3)	0.7316 (2)	0.0357 (10)	
C33	0.4927 (4)	0.6679 (3)	0.73397 (19)	0.0357 (10)	
H33	0.5660	0.6558	0.7333	0.043*	
C34	0.4155 (3)	0.6184 (2)	0.73730 (18)	0.0307 (9)	
C35	0.3074 (3)	0.6365 (2)	0.73611 (16)	0.0258 (7)	
H35	0.2559	0.6012	0.7379	0.031*	
C36	0.5421 (4)	0.7910 (3)	0.7259 (2)	0.0480 (14)	
C37	0.4459 (4)	0.5460 (3)	0.7420 (2)	0.0422 (11)	
C38	0.1416 (3)	0.7248 (2)	0.79940 (16)	0.0235 (7)	
C39	0.1576 (3)	0.7859 (2)	0.82883 (17)	0.0267 (8)	
H39	0.1638	0.8277	0.8105	0.032*	
C40	0.1646 (3)	0.7873 (2)	0.88328 (18)	0.0280 (8)	
C41	0.1576 (4)	0.7278 (2)	0.91206 (17)	0.0294 (8)	
H41	0.1630	0.7286	0.9495	0.035*	
C42	0.1422 (4)	0.6668 (2)	0.88385 (17)	0.0275 (8)	
C43	0.1348 (3)	0.6655 (2)	0.82940 (16)	0.0258 (7)	
H43	0.1247	0.6228	0.8116	0.031*	
C44	0.1799 (5)	0.8531 (3)	0.9127 (2)	0.0404 (11)	
C45	0.1335 (5)	0.6016 (3)	0.9128 (2)	0.0442 (12)	
C46	0.0658 (3)	0.66258 (19)	0.70522 (15)	0.0207 (6)	
C47	-0.0316 (3)	0.6420 (2)	0.72158 (17)	0.0266 (8)	
H47	-0.0532	0.6629	0.7518	0.032*	
C48	-0.0969 (3)	0.5919 (2)	0.69457 (18)	0.0311 (9)	
C49	-0.0689 (4)	0.5602 (2)	0.65029 (18)	0.0312 (9)	
H49	-0.1130	0.5253	0.6324	0.037*	
C50	0.0254 (3)	0.5808 (2)	0.63282 (17)	0.0284 (8)	
C51	0.0904 (3)	0.6309 (2)	0.65984 (16)	0.0251 (7)	
H51	0.1544	0.6441	0.6468	0.030*	
C52	-0.1977 (5)	0.5707 (3)	0.7139 (2)	0.0486 (14)	

C53	0.0586 (4)	0.5461 (3)	0.5862 (2)	0.0413 (11)	
C54	0.1014 (3)	0.7957 (2)	0.70855 (16)	0.0252 (7)	
C55	0.0105 (4)	0.8277 (2)	0.72388 (18)	0.0304 (8)	
H55	-0.0268	0.8053	0.7486	0.036*	
C56	-0.0265 (4)	0.8908 (2)	0.7044 (2)	0.0337 (9)	
C57	0.0249 (4)	0.9252 (2)	0.6681 (2)	0.0352 (10)	
H57	0.0011	0.9690	0.6554	0.042*	
C58	0.1122 (4)	0.8937 (2)	0.65101 (18)	0.0333 (9)	
C59	0.1482 (4)	0.8300 (2)	0.67019 (17)	0.0297 (8)	
H59	0.2068	0.8091	0.6566	0.036*	
C60	-0.1226 (5)	0.9232 (3)	0.7229 (3)	0.0541 (17)	
C61	0.1713 (5)	0.9301 (3)	0.6135 (3)	0.0509 (15)	
N1	0.6636 (3)	0.6457 (2)	0.49128 (15)	0.0322 (8)	
B1	0.1443 (4)	0.7222 (2)	0.73575 (18)	0.0234 (8)	
F1	0.5229 (3)	0.8486 (2)	0.75159 (19)	0.0740 (12)	
F2	0.5428 (4)	0.8083 (3)	0.67635 (16)	0.0846 (16)	
F3	0.6425 (3)	0.7728 (2)	0.74679 (18)	0.0690 (12)	
F4	0.5474 (6)	0.5336 (4)	0.7390 (3)	0.0850 (12)	0.75
F5	0.4215 (6)	0.5186 (3)	0.7862 (3)	0.0850 (12)	0.75
F6	0.3869 (6)	0.5086 (3)	0.7040 (3)	0.0850 (12)	0.75
F4B	0.4451 (14)	0.5135 (7)	0.6946 (8)	0.061 (2)	0.25
F5B	0.3716 (13)	0.4996 (7)	0.7550 (8)	0.061 (2)	0.25
F6B	0.5474 (15)	0.5318 (8)	0.7674 (8)	0.061 (2)	0.25
F7	0.2076 (4)	0.9047 (2)	0.88415 (18)	0.0737 (7)	
F8	0.2561 (4)	0.8508 (2)	0.95501 (18)	0.0737 (7)	
F9	0.0893 (4)	0.8733 (2)	0.92990 (18)	0.0737 (7)	
F10	0.1839 (5)	0.5501 (2)	0.89466 (18)	0.0947 (18)	
F11	0.1631 (5)	0.6052 (2)	0.96438 (14)	0.0849 (17)	
F12	0.0300 (4)	0.5791 (3)	0.9053 (2)	0.0940 (17)	
F13	-0.2197 (6)	0.6012 (6)	0.7563 (4)	0.0886 (15)	0.65
F14	-0.2026 (6)	0.5035 (5)	0.7235 (4)	0.0886 (15)	0.65
F15	-0.2860 (6)	0.5801 (5)	0.6775 (3)	0.0886 (15)	0.65
F13B	-0.1755 (10)	0.5395 (9)	0.7623 (6)	0.083 (3)	0.35
F14B	-0.2627 (11)	0.5313 (9)	0.6819 (7)	0.083 (3)	0.35
F15B	-0.2495 (10)	0.6253 (9)	0.7318 (7)	0.083 (3)	0.35
F16	0.0907 (6)	0.4827 (4)	0.5970 (3)	0.0742 (12)	0.65
F17	-0.0258 (7)	0.5361 (4)	0.5472 (3)	0.0742 (12)	0.65

F18	0.1352 (6)	0.5799 (4)	0.5655 (3)	0.0742 (12)	0.65
F16B	0.0395 (10)	0.4761 (7)	0.5833 (5)	0.065 (2)	0.35
F17B	0.0016 (11)	0.5661 (7)	0.5405 (5)	0.065 (2)	0.35
F18B	0.1664 (10)	0.5464 (7)	0.5865 (5)	0.065 (2)	0.35
F19	-0.1660 (8)	0.8866 (6)	0.7549 (5)	0.0816 (19)	0.5
F20	-0.2055 (7)	0.9297 (5)	0.6806 (4)	0.0816 (19)	0.5
F21	-0.1025 (8)	0.9892 (7)	0.7355 (5)	0.0816 (19)	0.5
F19B	-0.0966 (7)	0.9322 (6)	0.7803 (4)	0.087 (2)	0.5
F20B	-0.1400 (8)	0.9877 (7)	0.7124 (5)	0.087 (2)	0.5
F21B	-0.2060 (8)	0.8862 (6)	0.7237 (5)	0.087 (2)	0.5
F22	0.2087 (8)	0.8875 (5)	0.5797 (5)	0.0983 (19)	0.65
F23	0.1409 (8)	0.9908 (4)	0.6004 (4)	0.0983 (19)	0.65
F24	0.2807 (7)	0.9380 (5)	0.6336 (4)	0.0983 (19)	0.65
F22B	0.1709 (14)	0.9017 (9)	0.5687 (5)	0.075 (3)	0.35
F23B	0.2324 (14)	0.9760 (8)	0.6341 (4)	0.075 (3)	0.35
F24B	0.0915 (12)	0.9554 (8)	0.5709 (4)	0.075 (3)	0.35
Si1	0.81965 (14)	0.76295 (9)	0.52332 (7)	0.0462 (3)	
Ir1	0.65565 (2)	0.74005 (2)	0.45184 (2)	0.02719 (5)	
H1A	0.7709	0.7382	0.4660	0.050*	

7.11.8 **Table A32.** Atomic displacement parameters (Å^2) for [**5A**][BArF$_{24}$].

	U^{11}	U^{22}	U^{33}	U^{12}	U^{13}	U^{23}
C1	0.036 (2)	0.031 (2)	0.030 (2)	0.0081 (17)	0.0039 (17)	0.0029 (17)
C2	0.054 (3)	0.026 (2)	0.042 (3)	0.011 (2)	0.003 (2)	0.0048 (19)
C3	0.056 (3)	0.027 (2)	0.044 (3)	-0.001 (2)	0.004 (2)	0.012 (2)
C4	0.039 (2)	0.034 (2)	0.029 (2)	-0.0069 (18)	0.0026 (17)	0.0061 (17)
C5	0.051 (3)	0.053 (3)	0.045 (3)	-0.012 (3)	0.014 (2)	0.018 (3)
C6	0.039 (3)	0.064 (4)	0.040 (3)	-0.012 (2)	0.018 (2)	0.007 (2)
C7	0.032 (2)	0.055 (3)	0.026 (2)	-0.004 (2)	0.0091 (17)	-0.002 (2)
C8	0.039 (2)	0.066 (4)	0.037 (2)	0.004 (2)	0.018 (2)	-0.009 (2)
C9	0.048 (3)	0.054 (3)	0.043 (3)	0.020 (2)	0.016 (2)	-0.006 (2)
C10	0.045 (3)	0.034 (2)	0.037 (2)	0.0096 (19)	0.013 (2)	-0.0032 (19)
C11	0.0272 (17)	0.023 (2)	0.0230 (17)	0.0060 (13)	0.0085 (14)	-0.0010 (13)
C12	0.0268 (18)	0.034 (2)	0.0240 (18)	-0.0002 (15)	0.0058 (15)	-0.0005 (16)

C13	0.0301 (19)	0.026 (2)	0.0234 (18)	-0.0008 (15)	0.0032 (15)	0.0025 (15)
C14	0.057 (3)	0.032 (2)	0.027 (2)	0.017 (2)	0.012 (2)	0.0034 (17)
C15	0.045 (2)	0.032 (2)	0.0217 (19)	-0.0080 (18)	0.0059 (17)	0.0006 (16)
C16	0.035 (2)	0.036 (3)	0.0252 (19)	0.0096 (17)	0.0044 (16)	0.0009 (16)
C17	0.046 (2)	0.027 (2)	0.029 (2)	-0.0069 (18)	0.0073 (18)	0.0042 (17)
C18	0.031 (2)	0.060 (3)	0.026 (2)	0.002 (2)	0.0074 (16)	0.010 (2)
C19	0.115 (6)	0.062 (4)	0.035 (3)	0.051 (4)	0.015 (3)	-0.006 (3)
C20	0.084 (5)	0.065 (4)	0.052 (4)	-0.043 (4)	0.017 (3)	-0.006 (3)
C21	0.038 (3)	0.084 (5)	0.040 (3)	0.025 (3)	0.004 (2)	0.005 (3)
C22	0.112 (6)	0.032 (3)	0.053 (4)	-0.015 (3)	0.004 (4)	0.007 (3)
C23	0.034 (3)	0.140 (8)	0.041 (3)	-0.008 (4)	0.012 (2)	0.015 (4)
C24	0.040 (3)	0.101 (6)	0.048 (4)	0.003 (3)	-0.008 (3)	-0.004 (4)
C25	0.040 (3)	0.101 (6)	0.047 (3)	-0.014 (3)	-0.007 (2)	0.018 (3)
C26	0.080 (6)	0.098 (7)	0.061 (5)	0.009 (5)	-0.007 (4)	-0.012 (5)
C27	0.106 (8)	0.154 (11)	0.058 (5)	0.023 (7)	0.017 (5)	-0.022 (6)
C28	0.065 (5)	0.046 (4)	0.054 (5)	-0.009 (4)	0.005 (4)	-0.002 (4)
C29	0.097 (9)	0.053 (6)	0.088 (8)	-0.006 (6)	0.022 (6)	0.009 (5)
C28B	0.065 (5)	0.046 (4)	0.054 (5)	-0.009 (4)	0.005 (4)	-0.002 (4)
C29B	0.097 (9)	0.053 (6)	0.088 (8)	-0.006 (6)	0.022 (6)	0.009 (5)
C30	0.0297 (18)	0.0225 (19)	0.0239 (18)	-0.0041 (14)	0.0045 (14)	-0.0019 (14)
C31	0.0317 (19)	0.030 (2)	0.029 (2)	-0.0091 (15)	0.0049 (16)	-0.0021 (16)
C32	0.0290 (19)	0.046 (3)	0.033 (2)	-0.0131 (18)	0.0068 (17)	-0.0024 (19)
C33	0.0235 (18)	0.053 (3)	0.032 (2)	-0.0014 (18)	0.0071 (16)	-0.004 (2)
C34	0.0241 (18)	0.036 (2)	0.032 (2)	0.0016 (15)	0.0039 (15)	-0.0038 (17)
C35	0.0230 (16)	0.027 (2)	0.0272 (19)	-0.0021 (14)	0.0042 (14)	-0.0029 (15)
C36	0.039 (3)	0.063 (4)	0.044 (3)	-0.024 (2)	0.011 (2)	-0.001 (3)
C37	0.033 (2)	0.043 (3)	0.051 (3)	0.005 (2)	0.008 (2)	-0.007 (2)
C38	0.0242 (16)	0.0196 (18)	0.0273 (18)	-0.0016 (12)	0.0056 (14)	-0.0024 (14)
C39	0.0327 (19)	0.0173 (17)	0.030 (2)	-0.0031 (14)	0.0059 (15)	-0.0021 (15)
C40	0.0288 (18)	0.024 (2)	0.031 (2)	-0.0007 (15)	0.0045 (15)	-0.0079 (16)
C41	0.036 (2)	0.028 (2)	0.0247 (19)	0.0004 (16)	0.0063 (16)	-0.0037 (15)
C42	0.034 (2)	0.0230 (19)	0.0261 (19)	-0.0023 (15)	0.0053 (16)	-0.0021 (15)
C43	0.0326 (19)	0.0176 (17)	0.0270 (19)	-0.0023 (14)	0.0043 (15)	-0.0036 (14)
C44	0.061 (3)	0.025 (2)	0.036 (2)	-0.001 (2)	0.007 (2)	-0.0106 (18)
C45	0.076 (4)	0.030 (2)	0.027 (2)	-0.004 (2)	0.012 (2)	0.0010 (18)
C46	0.0220 (15)	0.0172 (16)	0.0228 (17)	0.0007 (12)	0.0035 (13)	-0.0005 (13)
C47	0.0247 (17)	0.029 (2)	0.0278 (19)	-0.0013 (14)	0.0084 (15)	-0.0038 (15)

C48	0.0246 (18)	0.036 (2)	0.034 (2)	-0.0052 (16)	0.0080 (16)	-0.0034 (17)
C49	0.0300 (19)	0.029 (2)	0.034 (2)	-0.0045 (16)	0.0030 (16)	-0.0075 (17)
C50	0.0279 (18)	0.031 (2)	0.0262 (19)	0.0028 (15)	0.0025 (15)	-0.0081 (16)
C51	0.0225 (16)	0.029 (2)	0.0237 (18)	0.0000 (14)	0.0040 (14)	-0.0039 (15)
C52	0.039 (3)	0.062 (4)	0.048 (3)	-0.022 (2)	0.018 (2)	-0.013 (3)
C53	0.040 (2)	0.044 (3)	0.040 (3)	0.004 (2)	0.006 (2)	-0.018 (2)
C54	0.0307 (18)	0.0193 (18)	0.0256 (18)	0.0013 (14)	0.0041 (15)	0.0017 (14)
C55	0.032 (2)	0.026 (2)	0.036 (2)	0.0017 (15)	0.0118 (17)	0.0066 (16)
C56	0.035 (2)	0.030 (2)	0.040 (2)	0.0069 (17)	0.0162 (19)	0.0057 (18)
C57	0.043 (2)	0.025 (2)	0.040 (2)	0.0065 (17)	0.015 (2)	0.0083 (18)
C58	0.041 (2)	0.032 (2)	0.031 (2)	0.0032 (18)	0.0163 (18)	0.0079 (17)
C59	0.036 (2)	0.027 (2)	0.029 (2)	0.0041 (16)	0.0116 (17)	0.0017 (16)
C60	0.061 (4)	0.037 (3)	0.075 (4)	0.019 (2)	0.042 (3)	0.017 (3)
C61	0.065 (4)	0.040 (3)	0.056 (3)	0.015 (3)	0.036 (3)	0.020 (3)
N1	0.0380 (19)	0.0294 (19)	0.0288 (18)	0.0029 (15)	0.0040 (15)	0.0017 (14)
B1	0.0267 (19)	0.0185 (18)	0.026 (2)	-0.0016 (14)	0.0063 (16)	-0.0015 (15)
F1	0.072 (3)	0.058 (2)	0.096 (3)	-0.038 (2)	0.022 (2)	-0.015 (2)
F2	0.087 (3)	0.119 (4)	0.047 (2)	-0.061 (3)	0.009 (2)	0.016 (2)
F3	0.0354 (17)	0.091 (3)	0.078 (3)	-0.0288 (18)	0.0030 (17)	-0.001 (2)
F4	0.080 (3)	0.057 (2)	0.119 (3)	0.0243 (18)	0.022 (3)	0.001 (2)
F5	0.080 (3)	0.057 (2)	0.119 (3)	0.0243 (18)	0.022 (3)	0.001 (2)
F6	0.080 (3)	0.057 (2)	0.119 (3)	0.0243 (18)	0.022 (3)	0.001 (2)
F4B	0.058 (5)	0.031 (4)	0.095 (8)	0.012 (4)	0.019 (5)	0.000 (4)
F5B	0.058 (5)	0.031 (4)	0.095 (8)	0.012 (4)	0.019 (5)	0.000 (4)
F6B	0.058 (5)	0.031 (4)	0.095 (8)	0.012 (4)	0.019 (5)	0.000 (4)
F7	0.1051 (19)	0.0414 (12)	0.0726 (16)	-0.0070 (12)	0.0073 (14)	-0.0240 (11)
F8	0.1051 (19)	0.0414 (12)	0.0726 (16)	-0.0070 (12)	0.0073 (14)	-0.0240 (11)
F9	0.1051 (19)	0.0414 (12)	0.0726 (16)	-0.0070 (12)	0.0073 (14)	-0.0240 (11)
F10	0.186 (6)	0.038 (2)	0.066 (3)	0.040 (3)	0.041 (3)	0.0191 (19)
F11	0.176 (5)	0.047 (2)	0.0281 (17)	-0.019 (3)	0.004 (2)	0.0115 (15)
F12	0.108 (4)	0.066 (3)	0.109 (4)	-0.040 (3)	0.020 (3)	0.026 (3)
F13	0.058 (3)	0.120 (4)	0.097 (4)	-0.031 (3)	0.039 (2)	-0.003 (3)
F14	0.058 (3)	0.120 (4)	0.097 (4)	-0.031 (3)	0.039 (2)	-0.003 (3)
F15	0.058 (3)	0.120 (4)	0.097 (4)	-0.031 (3)	0.039 (2)	-0.003 (3)
F13B	0.045 (4)	0.115 (7)	0.097 (6)	-0.031 (4)	0.036 (4)	-0.005 (5)
F14B	0.045 (4)	0.115 (7)	0.097 (6)	-0.031 (4)	0.036 (4)	-0.005 (5)
F15B	0.045 (4)	0.115 (7)	0.097 (6)	-0.031 (4)	0.036 (4)	-0.005 (5)

F16	0.076 (3)	0.089 (3)	0.060 (2)	0.004 (2)	0.017 (2)	-0.035 (2)
F17	0.076 (3)	0.089 (3)	0.060 (2)	0.004 (2)	0.017 (2)	-0.035 (2)
F18	0.076 (3)	0.089 (3)	0.060 (2)	0.004 (2)	0.017 (2)	-0.035 (2)
F16B	0.064 (4)	0.076 (5)	0.057 (4)	0.001 (3)	0.013 (3)	-0.042 (4)
F17B	0.064 (4)	0.076 (5)	0.057 (4)	0.001 (3)	0.013 (3)	-0.042 (4)
F18B	0.064 (4)	0.076 (5)	0.057 (4)	0.001 (3)	0.013 (3)	-0.042 (4)
F19	0.056 (3)	0.095 (4)	0.099 (5)	0.035 (3)	0.029 (3)	-0.001 (4)
F20	0.056 (3)	0.095 (4)	0.099 (5)	0.035 (3)	0.029 (3)	-0.001 (4)
F21	0.056 (3)	0.095 (4)	0.099 (5)	0.035 (3)	0.029 (3)	-0.001 (4)
F19B	0.060 (4)	0.097 (5)	0.113 (6)	0.018 (3)	0.040 (3)	-0.020 (4)
F20B	0.060 (4)	0.097 (5)	0.113 (6)	0.018 (3)	0.040 (3)	-0.020 (4)
F21B	0.060 (4)	0.097 (5)	0.113 (6)	0.018 (3)	0.040 (3)	-0.020 (4)
F22	0.102 (4)	0.082 (3)	0.131 (5)	0.024 (3)	0.081 (4)	0.056 (3)
F23	0.102 (4)	0.082 (3)	0.131 (5)	0.024 (3)	0.081 (4)	0.056 (3)
F24	0.102 (4)	0.082 (3)	0.131 (5)	0.024 (3)	0.081 (4)	0.056 (3)
F22B	0.105 (7)	0.091 (6)	0.035 (3)	-0.039 (5)	0.028 (4)	-0.001 (4)
F23B	0.105 (7)	0.091 (6)	0.035 (3)	-0.039 (5)	0.028 (4)	-0.001 (4)
F24B	0.105 (7)	0.091 (6)	0.035 (3)	-0.039 (5)	0.028 (4)	-0.001 (4)
Si1	0.0480 (8)	0.0474 (9)	0.0412 (8)	-0.0089 (7)	0.0010 (6)	-0.0067 (7)
Ir1	0.03062 (8)	0.02693 (8)	0.02560 (8)	0.00359 (6)	0.00936 (5)	0.00316 (6)

7.11.9 **Table A33.** Interatomic distances (Å) and angles (deg) for [**5A**][$BArF_{24}$].

C1—N1	1.363 (6)	C32—C33	1.381 (8)
C1—C2	1.401 (7)	C32—C36	1.510 (7)
C1—H1	0.9500	C33—C34	1.380 (7)
C2—C3	1.382 (8)	C33—H33	0.9500
C2—H2	0.9500	C34—C35	1.394 (6)
C3—C4	1.397 (7)	C34—C37	1.467 (7)
C3—H3	0.9500	C35—H35	0.9500
C4—C13	1.412 (6)	C36—F2	1.313 (7)
C4—C5	1.429 (7)	C36—F3	1.334 (7)
C5—C6	1.341 (9)	C36—F1	1.344 (8)
C5—H5	0.9500	C37—F4	1.306 (9)
C6—C7	1.440 (8)	C37—F5	1.328 (9)
C6—H6	0.9500	C37—F6	1.343 (9)

C7—C8	1.391 (8)	C37—F6B	1.362 (19)
C7—C12	1.407 (6)	C37—F4B	1.368 (19)
C8—C9	1.377 (9)	C37—F5B	1.377 (17)
C8—H8	0.9500	C38—C43	1.401 (6)
C9—C10	1.407 (7)	C38—C39	1.412 (6)
C9—H9	0.9500	C38—B1	1.634 (6)
C10—C11	1.359 (6)	C39—C40	1.382 (6)
C10—H10	0.9500	C39—H39	0.9500
C11—C12	1.378 (6)	C40—C41	1.388 (6)
C11—Ir1	2.079 (4)	C40—C44	1.487 (6)
C12—C13	1.415 (6)	C41—C42	1.393 (6)
C13—N1	1.388 (6)	C41—H41	0.9500
C14—C18	1.406 (8)	C42—C43	1.381 (6)
C14—C15	1.423 (7)	C42—C45	1.488 (7)
C14—C19	1.505 (7)	C43—H43	0.9500
C14—Ir1	2.249 (5)	C44—F7	1.323 (7)
C15—C16	1.424 (7)	C44—F8	1.327 (7)
C15—C20	1.509 (7)	C44—F9	1.338 (7)
C15—Ir1	2.228 (5)	C45—F10	1.311 (7)
C16—C17	1.423 (7)	C45—F11	1.314 (6)
C16—C21	1.493 (7)	C45—F12	1.353 (8)
C16—Ir1	2.267 (4)	C46—C51	1.392 (5)
C17—C18	1.446 (7)	C46—C47	1.407 (5)
C17—C22	1.493 (8)	C46—B1	1.642 (6)
C17—Ir1	2.250 (4)	C47—C48	1.390 (6)
C18—C23	1.504 (7)	C47—H47	0.9500
C18—Ir1	2.247 (5)	C48—C49	1.383 (6)
C19—H19A	0.9800	C48—C52	1.483 (6)
C19—H19B	0.9800	C49—C50	1.385 (6)
C19—H19C	0.9800	C49—H49	0.9500
C20—H20A	0.9800	C50—C51	1.388 (6)
C20—H20B	0.9800	C50—C53	1.486 (6)
C20—H20C	0.9800	C51—H51	0.9500
C21—H21A	0.9800	C52—F13	1.305 (11)
C21—H21B	0.9800	C52—F14B	1.309 (16)
C21—H21C	0.9800	C52—F15	1.341 (11)
C22—H22A	0.9800	C52—F14	1.341 (11)

C22—H22B	0.9800	C52—F15B	1.366 (18)
C22—H22C	0.9800	C52—F13B	1.370 (17)
C23—H23A	0.9800	C53—F16	1.320 (10)
C23—H23B	0.9800	C53—F17B	1.330 (16)
C23—H23C	0.9800	C53—F18	1.340 (10)
C24—C25	1.535 (9)	C53—F18B	1.348 (13)
C24—Si1	1.839 (7)	C53—F17	1.350 (10)
C24—H24A	0.9900	C53—F16B	1.392 (15)
C24—H24B	0.9900	C54—C59	1.391 (6)
C25—H25A	0.9800	C54—C55	1.407 (6)
C25—H25B	0.9800	C54—B1	1.650 (6)
C25—H25C	0.9800	C55—C56	1.384 (6)
C26—C27	1.470 (13)	C55—H55	0.9500
C26—Si1	1.910 (10)	C56—C57	1.382 (6)
C26—H26A	0.9900	C56—C60	1.500 (7)
C26—H26B	0.9900	C57—C58	1.383 (6)
C27—H27A	0.9800	C57—H57	0.9500
C27—H27B	0.9800	C58—C59	1.389 (6)
C27—H27C	0.9800	C58—C61	1.482 (7)
C28—C29	1.485 (15)	C59—H59	0.9500
C28—Si1	1.883 (10)	C60—F19	1.270 (13)
C28—H28A	0.9900	C60—F21B	1.273 (13)
C28—H28B	0.9900	C60—F20B	1.302 (15)
C29—H29A	0.9800	C60—F21	1.346 (15)
C29—H29B	0.9800	C60—F20	1.383 (12)
C29—H29C	0.9800	C60—F19B	1.463 (13)
C28B—C29B	1.59 (4)	C61—F23B	1.242 (14)
C28B—Si1	1.90 (2)	C61—F22B	1.273 (16)
C28B—H28C	0.9900	C61—F23	1.276 (9)
C28B—H28D	0.9900	C61—F22	1.336 (13)
C29B—H29D	0.9800	C61—F24	1.393 (12)
C29B—H29E	0.9800	C61—F24B	1.446 (16)
C29B—H29F	0.9800	N1—Ir1	2.099 (4)
C30—C31	1.410 (6)	F22B—F24B	1.45 (2)
C30—C35	1.411 (6)	Si1—Ir1	2.5657 (16)
C30—B1	1.635 (6)	Si1—H1A	1.5737
C31—C32	1.391 (7)	Ir1—H1A	1.4312

C31—H31	0.9500		
N1—C1—C2	121.6 (4)	F6—C37—C34	111.2 (5)
N1—C1—H1	119.2	F6B—C37—C34	116.6 (8)
C2—C1—H1	119.2	F4B—C37—C34	114.3 (8)
C3—C2—C1	120.5 (5)	F5B—C37—C34	118.7 (7)
C3—C2—H2	119.8	C43—C38—C39	115.2 (4)
C1—C2—H2	119.8	C43—C38—B1	122.2 (3)
C2—C3—C4	119.9 (5)	C39—C38—B1	122.2 (4)
C2—C3—H3	120.1	C40—C39—C38	122.3 (4)
C4—C3—H3	120.1	C40—C39—H39	118.8
C3—C4—C13	117.4 (4)	C38—C39—H39	118.8
C3—C4—C5	124.5 (5)	C39—C40—C41	121.2 (4)
C13—C4—C5	118.1 (5)	C39—C40—C44	120.6 (4)
C6—C5—C4	122.0 (5)	C41—C40—C44	118.2 (4)
C6—C5—H5	119.0	C40—C41—C42	117.4 (4)
C4—C5—H5	119.0	C40—C41—H41	121.3
C5—C6—C7	121.2 (5)	C42—C41—H41	121.3
C5—C6—H6	119.4	C43—C42—C41	121.3 (4)
C7—C6—H6	119.4	C43—C42—C45	119.2 (4)
C8—C7—C12	117.0 (5)	C41—C42—C45	119.5 (4)
C8—C7—C6	125.2 (5)	C42—C43—C38	122.5 (4)
C12—C7—C6	117.8 (5)	C42—C43—H43	118.8
C9—C8—C7	120.4 (5)	C38—C43—H43	118.8
C9—C8—H8	119.8	F7—C44—F8	105.0 (5)
C7—C8—H8	119.8	F7—C44—F9	105.2 (5)
C8—C9—C10	120.7 (5)	F8—C44—F9	106.2 (5)
C8—C9—H9	119.6	F7—C44—C40	114.0 (4)
C10—C9—H9	119.6	F8—C44—C40	113.8 (4)
C11—C10—C9	120.0 (5)	F9—C44—C40	112.0 (4)
C11—C10—H10	120.0	F10—C45—F11	108.8 (5)
C9—C10—H10	120.0	F10—C45—F12	101.7 (5)
C10—C11—C12	118.9 (4)	F11—C45—F12	105.9 (5)
C10—C11—Ir1	126.4 (3)	F10—C45—C42	113.9 (4)
C12—C11—Ir1	114.7 (3)	F11—C45—C42	115.0 (4)
C11—C12—C7	123.0 (4)	F12—C45—C42	110.5 (5)
C11—C12—C13	116.1 (4)	C51—C46—C47	115.8 (4)

C7—C12—C13	120.9 (4)	C51—C46—B1	121.3 (3)
N1—C13—C4	123.3 (4)	C47—C46—B1	122.9 (3)
N1—C13—C12	116.7 (4)	C48—C47—C46	121.6 (4)
C4—C13—C12	120.0 (4)	C48—C47—H47	119.2
C18—C14—C15	109.0 (4)	C46—C47—H47	119.2
C18—C14—C19	125.1 (6)	C49—C48—C47	121.2 (4)
C15—C14—C19	125.3 (6)	C49—C48—C52	119.0 (4)
C18—C14—Ir1	71.7 (3)	C47—C48—C52	119.8 (4)
C15—C14—Ir1	70.7 (3)	C48—C49—C50	118.1 (4)
C19—C14—Ir1	130.3 (4)	C48—C49—H49	121.0
C14—C15—C16	107.8 (4)	C50—C49—H49	121.0
C14—C15—C20	126.5 (5)	C49—C50—C51	120.5 (4)
C16—C15—C20	125.4 (5)	C49—C50—C53	119.0 (4)
C14—C15—Ir1	72.3 (3)	C51—C50—C53	120.5 (4)
C16—C15—Ir1	73.0 (3)	C50—C51—C46	122.8 (4)
C20—C15—Ir1	125.3 (4)	C50—C51—H51	118.6
C17—C16—C15	108.0 (4)	C46—C51—H51	118.6
C17—C16—C21	126.1 (5)	F13—C52—F15	104.9 (7)
C15—C16—C21	125.8 (5)	F13—C52—F14	106.0 (7)
C17—C16—Ir1	71.0 (3)	F15—C52—F14	101.9 (7)
C15—C16—Ir1	70.0 (3)	F14B—C52—F15B	112.9 (10)
C21—C16—Ir1	126.8 (3)	F14B—C52—F13B	108.7 (11)
C16—C17—C18	107.7 (4)	F15B—C52—F13B	94.9 (10)
C16—C17—C22	126.3 (5)	F13—C52—C48	116.7 (5)
C18—C17—C22	125.4 (5)	F14B—C52—C48	115.7 (7)
C16—C17—Ir1	72.3 (3)	F15—C52—C48	112.4 (6)
C18—C17—Ir1	71.1 (3)	F14—C52—C48	113.6 (6)
C22—C17—Ir1	129.2 (4)	F15B—C52—C48	111.4 (7)
C14—C18—C17	107.5 (4)	F13B—C52—C48	111.2 (6)
C14—C18—C23	127.2 (6)	F16—C53—F18	109.5 (6)
C17—C18—C23	124.0 (6)	F17B—C53—F18B	113.7 (9)
C14—C18—Ir1	71.8 (3)	F16—C53—F17	101.3 (6)
C17—C18—Ir1	71.4 (3)	F18—C53—F17	107.7 (6)
C23—C18—Ir1	132.1 (4)	F17B—C53—F16B	100.3 (8)
C14—C19—H19A	109.5	F18B—C53—F16B	99.6 (8)
C14—C19—H19B	109.5	F16—C53—C50	112.1 (5)
H19A—C19—H19B	109.5	F17B—C53—C50	113.0 (6)

C14—C19—H19C	109.5	F18—C53—C50	113.4 (5)
H19A—C19—H19C	109.5	F18B—C53—C50	113.5 (6)
H19B—C19—H19C	109.5	F17—C53—C50	112.0 (5)
C15—C20—H20A	109.5	F16B—C53—C50	115.2 (7)
C15—C20—H20B	109.5	C59—C54—C55	115.3 (4)
H20A—C20—H20B	109.5	C59—C54—B1	125.0 (4)
C15—C20—H20C	109.5	C55—C54—B1	119.7 (3)
H20A—C20—H20C	109.5	C56—C55—C54	122.5 (4)
H20B—C20—H20C	109.5	C56—C55—H55	118.8
C16—C21—H21A	109.5	C54—C55—H55	118.8
C16—C21—H21B	109.5	C57—C56—C55	120.7 (4)
H21A—C21—H21B	109.5	C57—C56—C60	119.1 (4)
C16—C21—H21C	109.5	C55—C56—C60	120.2 (4)
H21A—C21—H21C	109.5	C56—C57—C58	117.9 (4)
H21B—C21—H21C	109.5	C56—C57—H57	121.1
C17—C22—H22A	109.5	C58—C57—H57	121.1
C17—C22—H22B	109.5	C57—C58—C59	121.1 (4)
H22A—C22—H22B	109.5	C57—C58—C61	119.2 (4)
C17—C22—H22C	109.5	C59—C58—C61	119.6 (4)
H22A—C22—H22C	109.5	C58—C59—C54	122.3 (4)
H22B—C22—H22C	109.5	C58—C59—H59	118.9
C18—C23—H23A	109.5	C54—C59—H59	118.9
C18—C23—H23B	109.5	F21B—C60—F20B	116.3 (8)
H23A—C23—H23B	109.5	F19—C60—F21	118.0 (9)
C18—C23—H23C	109.5	F19—C60—F20	102.2 (8)
H23A—C23—H23C	109.5	F21—C60—F20	100.8 (7)
H23B—C23—H23C	109.5	F21B—C60—F19B	96.2 (8)
C25—C24—Si1	114.0 (6)	F20B—C60—F19B	95.3 (9)
C25—C24—H24A	108.8	F19—C60—C56	114.2 (6)
Si1—C24—H24A	108.8	F21B—C60—C56	117.7 (7)
C25—C24—H24B	108.8	F20B—C60—C56	117.5 (6)
Si1—C24—H24B	108.8	F21—C60—C56	110.6 (6)
H24A—C24—H24B	107.7	F20—C60—C56	109.4 (6)
C24—C25—H25A	109.5	F19B—C60—C56	107.7 (6)
C24—C25—H25B	109.5	F23B—C61—F22B	127.8 (10)
H25A—C25—H25B	109.5	F23—C61—F22	122.1 (7)
C24—C25—H25C	109.5	F23—C61—F24	103.2 (8)

H25A—C25—H25C	109.5	F22—C61—F24	83.4 (7)
H25B—C25—H25C	109.5	F23B—C61—F24B	112.2 (10)
C27—C26—Si1	118.3 (8)	F22B—C61—F24B	64.3 (10)
C27—C26—H26A	107.7	F23B—C61—C58	114.2 (7)
Si1—C26—H26A	107.7	F22B—C61—C58	116.1 (9)
C27—C26—H26B	107.7	F23—C61—C58	117.3 (5)
Si1—C26—H26B	107.7	F22—C61—C58	112.2 (6)
H26A—C26—H26B	107.1	F24—C61—C58	112.1 (5)
C26—C27—H27A	109.5	F24B—C61—C58	107.2 (7)
C26—C27—H27B	109.5	C1—N1—C13	117.4 (4)
H27A—C27—H27B	109.5	C1—N1—Ir1	129.2 (3)
C26—C27—H27C	109.5	C13—N1—Ir1	113.3 (3)
H27A—C27—H27C	109.5	C38—B1—C30	103.3 (3)
H27B—C27—H27C	109.5	C38—B1—C46	113.0 (3)
C29—C28—Si1	116.1 (8)	C30—B1—C46	109.8 (3)
C29—C28—H28A	108.3	C38—B1—C54	109.7 (3)
Si1—C28—H28A	108.3	C30—B1—C54	114.4 (3)
C29—C28—H28B	108.3	C46—B1—C54	106.7 (3)
Si1—C28—H28B	108.3	C61—F22B—F24B	63.6 (10)
H28A—C28—H28B	107.4	C61—F24B—F22B	52.1 (8)
C28—C29—H29A	109.5	C24—Si1—C28	112.0 (4)
C28—C29—H29B	109.5	C24—Si1—C28B	89.2 (8)
H29A—C29—H29B	109.5	C24—Si1—C26	105.7 (4)
C28—C29—H29C	109.5	C28—Si1—C26	100.6 (4)
H29A—C29—H29C	109.5	C28B—Si1—C26	127.3 (8)
H29B—C29—H29C	109.5	C24—Si1—Ir1	108.4 (2)
C29B—C28B—Si1	112.9 (17)	C28—Si1—Ir1	117.2 (3)
C29B—C28B—H28C	109.0	C28B—Si1—Ir1	110.0 (7)
Si1—C28B—H28C	109.0	C26—Si1—Ir1	112.2 (3)
C29B—C28B—H28D	109.0	C24—Si1—H1A	79.3
Si1—C28B—H28D	109.0	C28—Si1—H1A	125.9
H28C—C28B—H28D	107.8	C28B—Si1—H1A	104.1
C28B—C29B—H29D	109.5	C26—Si1—H1A	128.0
C28B—C29B—H29E	109.5	Ir1—Si1—H1A	29.7
H29D—C29B—H29E	109.5	C11—Ir1—N1	78.52 (15)
C28B—C29B—H29F	109.5	C11—Ir1—C15	102.47 (17)
H29D—C29B—H29F	109.5	N1—Ir1—C15	94.83 (16)

H29E—C29B—H29F	109.5	C11—Ir1—C18	153.85 (18)
C31—C30—C35	114.6 (4)	N1—Ir1—C18	121.40 (18)
C31—C30—B1	125.1 (4)	C15—Ir1—C18	61.93 (18)
C35—C30—B1	120.0 (3)	C11—Ir1—C14	138.07 (19)
C32—C31—C30	122.3 (4)	N1—Ir1—C14	92.03 (16)
C32—C31—H31	118.8	C15—Ir1—C14	37.06 (19)
C30—C31—H31	118.8	C18—Ir1—C14	36.4 (2)
C33—C32—C31	121.2 (4)	C11—Ir1—C17	117.56 (17)
C33—C32—C36	119.9 (5)	N1—Ir1—C17	153.16 (17)
C31—C32—C36	118.8 (5)	C15—Ir1—C17	61.90 (17)
C34—C33—C32	118.4 (4)	C18—Ir1—C17	37.50 (18)
C34—C33—H33	120.8	C14—Ir1—C17	61.46 (18)
C32—C33—H33	120.8	C11—Ir1—C16	92.96 (16)
C33—C34—C35	120.4 (4)	N1—Ir1—C16	128.31 (17)
C33—C34—C37	120.6 (4)	C15—Ir1—C16	36.92 (17)
C35—C34—C37	119.1 (4)	C18—Ir1—C16	61.73 (17)
C34—C35—C30	123.0 (4)	C14—Ir1—C16	61.23 (17)
C34—C35—H35	118.5	C17—Ir1—C16	36.72 (18)
C30—C35—H35	118.5	C11—Ir1—Si1	97.56 (12)
F2—C36—F3	107.9 (5)	N1—Ir1—Si1	80.72 (12)
F2—C36—F1	106.5 (6)	C15—Ir1—Si1	158.20 (14)
F3—C36—F1	104.9 (5)	C18—Ir1—Si1	102.12 (14)
F2—C36—C32	112.5 (5)	C14—Ir1—Si1	121.36 (15)
F3—C36—C32	112.0 (5)	C17—Ir1—Si1	115.54 (13)
F1—C36—C32	112.5 (4)	C16—Ir1—Si1	150.71 (14)
F4—C37—F5	109.2 (6)	C11—Ir1—H1A	129.9
F4—C37—F6	106.6 (6)	N1—Ir1—H1A	83.4
F5—C37—F6	102.8 (6)	C15—Ir1—H1A	125.5
F6B—C37—F4B	101.8 (11)	C18—Ir1—H1A	72.9
F6B—C37—F5B	111.4 (11)	C14—Ir1—H1A	88.4
F4B—C37—F5B	89.7 (11)	C17—Ir1—H1A	98.9
F4—C37—C34	114.6 (5)	C16—Ir1—H1A	133.5
F5—C37—C34	111.6 (5)	Si1—Ir1—H1A	33.1
N1—C1—C2—C3	-1.6 (8)	C43—C42—C45—F12	-73.5 (6)
C1—C2—C3—C4	-0.3 (8)	C41—C42—C45—F12	106.5 (5)

C2—C3—C4—C13	2.0 (8)	C51—C46—C47—C48	1.6 (6)
C2—C3—C4—C5	-178.6 (5)	B1—C46—C47—C48	179.3 (4)
C3—C4—C5—C6	177.9 (6)	C46—C47—C48—C49	-0.1 (7)
C13—C4—C5—C6	-2.7 (8)	C46—C47—C48—C52	178.7 (5)
C4—C5—C6—C7	1.3 (9)	C47—C48—C49—C50	-1.3 (7)
C5—C6—C7—C8	-178.6 (6)	C52—C48—C49—C50	179.8 (5)
C5—C6—C7—C12	0.5 (8)	C48—C49—C50—C51	1.2 (7)
C12—C7—C8—C9	-0.9 (8)	C48—C49—C50—C53	178.3 (5)
C6—C7—C8—C9	178.2 (6)	C49—C50—C51—C46	0.3 (7)
C7—C8—C9—C10	0.4 (9)	C53—C50—C51—C46	-176.8 (4)
C8—C9—C10—C11	1.5 (9)	C47—C46—C51—C50	-1.7 (6)
C9—C10—C11—C12	-2.8 (7)	B1—C46—C51—C50	-179.4 (4)
C9—C10—C11—Ir1	176.1 (4)	C49—C48—C52—F13	178.8 (8)
C10—C11—C12—C7	2.4 (7)	C47—C48—C52—F13	-0.1 (10)
Ir1—C11—C12—C7	-176.6 (4)	C49—C48—C52—F14B	-11.3 (13)
C10—C11—C12—C13	-176.4 (4)	C47—C48—C52—F14B	169.8 (11)
Ir1—C11—C12—C13	4.5 (5)	C49—C48—C52—F15	-60.0 (8)
C8—C7—C12—C11	-0.5 (7)	C47—C48—C52—F15	121.2 (7)
C6—C7—C12—C11	-179.7 (5)	C49—C48—C52—F14	55.1 (8)
C8—C7—C12—C13	178.3 (5)	C47—C48—C52—F14	-123.8 (7)
C6—C7—C12—C13	-0.9 (7)	C49—C48—C52—F15B	-142.1 (9)
C3—C4—C13—N1	-2.1 (7)	C47—C48—C52—F15B	39.0 (11)
C5—C4—C13—N1	178.4 (5)	C49—C48—C52—F13B	113.3 (9)

C3—C4—C13—C12	-178.4 (4)	C47—C48—C52—F13B	-65.6 (10)
C5—C4—C13—C12	2.2 (7)	C49—C50—C53—F16	-70.1 (7)
C11—C12—C13—N1	2.0 (6)	C51—C50—C53—F16	107.0 (6)
C7—C12—C13—N1	-176.9 (4)	C49—C50—C53—F17B	76.6 (9)
C11—C12—C13—C4	178.5 (4)	C51—C50—C53—F17B	-106.3 (8)
C7—C12—C13—C4	-0.4 (7)	C49—C50—C53—F18	165.2 (6)
C18—C14—C15—C16	3.1 (5)	C51—C50—C53—F18	-17.7 (8)
C19—C14—C15—C16	-168.8 (5)	C49—C50—C53—F18B	-152.0 (9)
Ir1—C14—C15—C16	64.9 (3)	C51—C50—C53—F18B	25.1 (10)
C18—C14—C15—C20	177.0 (5)	C49—C50—C53—F17	43.0 (8)
C19—C14—C15—C20	5.1 (8)	C51—C50—C53—F17	-139.9 (6)
Ir1—C14—C15—C20	-121.2 (5)	C49—C50—C53—F16B	-38.0 (9)
C18—C14—C15—Ir1	-61.8 (3)	C51—C50—C53—F16B	139.1 (8)
C19—C14—C15—Ir1	126.3 (5)	C59—C54—C55—C56	-3.4 (7)
C14—C15—C16—C17	-3.2 (5)	B1—C54—C55—C56	177.0 (4)
C20—C15—C16—C17	-177.2 (5)	C54—C55—C56—C57	0.4 (8)
Ir1—C15—C16—C17	61.2 (3)	C54—C55—C56—C60	-178.8 (5)
C14—C15—C16—C21	174.0 (5)	C55—C56—C57—C58	1.8 (8)
C20—C15—C16—C21	0.0 (8)	C60—C56—C57—C58	-178.9 (6)
Ir1—C15—C16—C21	-121.6 (5)	C56—C57—C58—C59	-0.9 (8)
C14—C15—C16—Ir1	-64.4 (3)	C56—C57—C58—C61	-178.0 (5)
C20—C15—C16—Ir1	121.6 (5)	C57—C58—C59—C54	-2.2 (8)

C15—C16—C17—C18	2.2 (5)	C61—C58—C59—C54	174.9 (5)
C21—C16—C17—C18	-175.0 (5)	C55—C54—C59—C58	4.2 (7)
Ir1—C16—C17—C18	62.7 (3)	B1—C54—C59—C58	-176.2 (4)
C15—C16—C17—C22	173.4 (5)	C57—C56—C60—F19	177.9 (9)
C21—C16—C17—C22	-3.8 (8)	C55—C56—C60—F19	-2.8 (12)
Ir1—C16—C17—C22	-126.0 (5)	C57—C56—C60—F21B	133.2 (9)
C15—C16—C17—Ir1	-60.6 (3)	C55—C56—C60—F21B	-47.5 (12)
C21—C16—C17—Ir1	122.2 (5)	C57—C56—C60—F20B	-13.6 (12)
C15—C14—C18—C17	-1.7 (5)	C55—C56—C60—F20B	165.7 (9)
C19—C14—C18—C17	170.2 (5)	C57—C56—C60—F21	-46.1 (10)
Ir1—C14—C18—C17	-62.9 (3)	C55—C56—C60—F21	133.1 (8)
C15—C14—C18—C23	-169.3 (5)	C57—C56—C60—F20	64.1 (8)
C19—C14—C18—C23	2.6 (9)	C55—C56—C60—F20	-116.7 (7)
Ir1—C14—C18—C23	129.6 (5)	C57—C56—C60—F19B	-119.6 (7)
C15—C14—C18—Ir1	61.2 (3)	C55—C56—C60—F19B	59.7 (8)
C19—C14—C18—Ir1	-126.9 (5)	C57—C58—C61—F23B	76.0 (12)
C16—C17—C18—C14	-0.3 (5)	C59—C58—C61—F23B	-101.2 (11)
C22—C17—C18—C14	-171.6 (5)	C57—C58—C61—F22B	-118.3 (11)
Ir1—C17—C18—C14	63.2 (3)	C59—C58—C61—F22B	64.6 (12)
C16—C17—C18—C23	167.7 (5)	C57—C58—C61—F23	2.9 (11)
C22—C17—C18—C23	-3.6 (8)	C59—C58—C61—F23	-174.3 (8)
Ir1—C17—C18—C23	-128.8 (5)	C57—C58—C61—F22	-146.1 (8)
C16—C17—C18—Ir1	-63.5 (3)	C59—C58—C61—	36.7 (10)

		F22	
C22—C17—C18—Ir1	125.2 (5)	C57—C58—C61—F24	122.0 (7)
C35—C30—C31—C32	3.0 (6)	C59—C58—C61—F24	-55.1 (8)
B1—C30—C31—C32	176.2 (4)	C57—C58—C61—F24B	-49.0 (9)
C30—C31—C32—C33	-1.6 (7)	C59—C58—C61—F24B	133.9 (8)
C30—C31—C32—C36	175.0 (4)	C2—C1—N1—C13	1.5 (7)
C31—C32—C33—C34	-1.3 (7)	C2—C1—N1—Ir1	-173.7 (4)
C36—C32—C33—C34	-177.8 (5)	C4—C13—N1—C1	0.4 (7)
C32—C33—C34—C35	2.5 (7)	C12—C13—N1—C1	176.7 (4)
C32—C33—C34—C37	-177.6 (5)	C4—C13—N1—Ir1	176.3 (3)
C33—C34—C35—C30	-1.0 (7)	C12—C13—N1—Ir1	-7.3 (5)
C37—C34—C35—C30	179.2 (4)	C43—C38—B1—C30	-81.3 (4)
C31—C30—C35—C34	-1.7 (6)	C39—C38—B1—C30	91.7 (4)
B1—C30—C35—C34	-175.3 (4)	C43—C38—B1—C46	37.3 (5)
C33—C32—C36—F2	93.8 (7)	C39—C38—B1—C46	-149.7 (4)
C31—C32—C36—F2	-82.8 (7)	C43—C38—B1—C54	156.3 (4)
C33—C32—C36—F3	-28.0 (7)	C39—C38—B1—C54	-30.7 (5)
C31—C32—C36—F3	155.4 (5)	C31—C30—B1—C38	-89.5 (5)
C33—C32—C36—F1	-145.9 (5)	C35—C30—B1—C38	83.4 (4)
C31—C32—C36—F1	37.5 (7)	C31—C30—B1—C46	149.7 (4)
C33—C34—C37—F4	-4.5 (8)	C35—C30—B1—C46	-37.4 (5)
C35—C34—C37—F4	175.4 (6)	C31—C30—B1—C54	29.7 (6)
C33—C34—C37—F5	120.4 (6)	C35—C30—B1—C54	-157.4 (4)
C35—C34—C37—F5	-59.8 (7)	C51—C46—B1—C38	-150.2 (4)
C33—C34—C37—F6	-125.5 (6)	C47—C46—B1—C38	32.3 (5)
C35—C34—C37—F6	54.4 (7)	C51—C46—B1—C30	-35.5 (5)
C33—C34—C37—F6B	30.5 (11)	C47—C46—B1—C30	147.0 (4)
C35—C34—C37—F6B	-149.6 (10)	C51—C46—B1—C54	89.1 (4)

C33—C34—C37—F4B	-88.0 (10)	C47—C46—B1—C54	-88.5 (4)
C35—C34—C37—F4B	91.9 (10)	C59—C54—B1—C38	137.7 (4)
C33—C34—C37—F5B	168.2 (11)	C55—C54—B1—C38	-42.7 (5)
C35—C34—C37—F5B	-12.0 (13)	C59—C54—B1—C30	22.2 (6)
C43—C38—C39—C40	-0.8 (6)	C55—C54—B1—C30	-158.2 (4)
B1—C38—C39—C40	-174.3 (4)	C59—C54—B1—C46	-99.4 (5)
C38—C39—C40—C41	0.9 (7)	C55—C54—B1—C46	80.2 (5)
C38—C39—C40—C44	-179.1 (4)	F23B—C61—F22B—F24B	-99.0 (15)
C39—C40—C41—C42	-0.6 (6)	F23—C61—F22B—F24B	-31.5 (8)
C44—C40—C41—C42	179.4 (4)	F22—C61—F22B—F24B	-175 (2)
C40—C41—C42—C43	0.3 (7)	F24—C61—F22B—F24B	-138.7 (8)
C40—C41—C42—C45	-179.7 (5)	C58—C61—F22B—F24B	97.5 (9)
C41—C42—C43—C38	-0.3 (7)	F23B—C61—F24B—F22B	122.5 (12)
C45—C42—C43—C38	179.6 (4)	F23—C61—F24B—F22B	137.2 (11)
C39—C38—C43—C42	0.6 (6)	F22—C61—F24B—F22B	2.0 (11)
B1—C38—C43—C42	174.1 (4)	F24—C61—F24B—F22B	81.7 (15)
C39—C40—C44—F7	-13.1 (7)	C58—C61—F24B—F22B	-111.3 (9)
C41—C40—C44—F7	167.0 (5)	C25—C24—Si1—C28	42.7 (7)
C39—C40—C44—F8	-133.4 (5)	C25—C24—Si1—C28B	62.7 (9)
C41—C40—C44—F8	46.7 (7)	C25—C24—Si1—C26	-66.0 (7)
C39—C40—C44—F9	106.2 (5)	C25—C24—Si1—Ir1	173.5 (5)
C41—C40—C44—F9	-73.7 (6)	C29—C28—Si1—C24	60.0 (9)
C43—C42—C45—F10	40.3 (8)	C29—C28—Si1—C28B	16.8 (16)
C41—C42—C45—F10	-139.8 (5)	C29—C28—Si1—C26	171.9 (9)

C43—C42—C45—F11	166.8 (5)	C29—C28—Si1—Ir1	-66.1 (9)
C41—C42—C45—F11	-13.3 (8)		

7.12 [**5A'**][$BArF_{24}$]

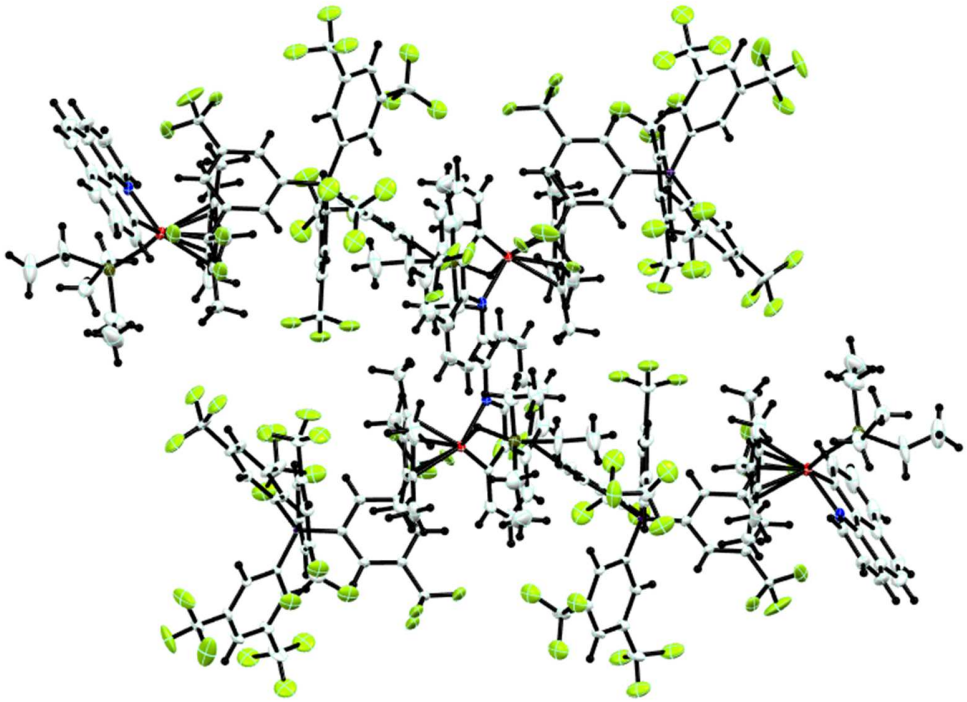

7.12.1 **Figure A31.** Crystal lattice packing of [**5A'**][$BArF_{24}$].

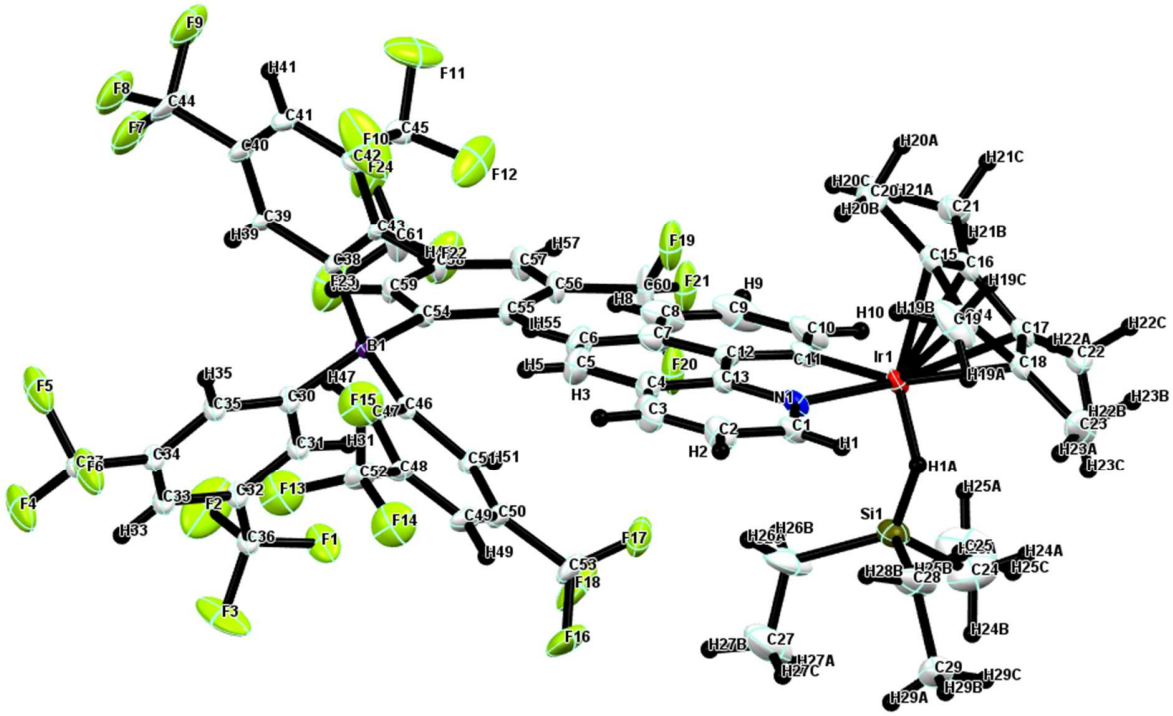

7.12.2 **Figure A32.** Asymmetric unit of [**5A'**][$BArF_{24}$], with all hydrogens and total numbering of atoms.

[**5'**][$BArF_{24}$]

7.12.3 Crystal data

$C_{32}H_{12}BF_{24}\cdot C_{29}H_{39}IrNSi$	$F(000) = 2944$
$M_r = 1485.12$	$D_x = 1.586$ Mg m^{-3}
Monoclinic, $P2_1/c$	Mo $K\alpha$ radiation, $\lambda = 0.71073$ Å
$a = 12.5243$ (4) Å	Cell parameters from 9215 reflections
$b = 19.4902$ (7) Å	$\theta = 2.2–32.0°$
$c = 25.6917$ (9) Å	$\mu = 2.28$ mm^{-1}
$\beta = 97.384$ (1)°	$T = 173$ K
$V = 6219.4$ (4) Å^3	Prism, yellow
$Z = 4$	0.30 × 0.22 × 0.12 mm

7.12.4 Data collection

Bruker APEX-II CCD diffractometer	15492 reflections with $I > 2\sigma(I)$
Radiation source: fine focus sealed tube	$R_{int} = 0.092$
ϕ and ω scans	$\theta_{max} = 32.2°$, $\theta_{min} = 1.3°$
Absorption correction: multi-scan *SADABS*	$h = -18\rightarrow18$
$T_{min} = 0.598$, $T_{max} = 0.746$	$k = -25\rightarrow29$
163836 measured reflections	$l = -38\rightarrow38$
21753 independent reflections	

7.12.5 Refinement

Refinement on F^2	Primary atom site location: structure-invariant direct methods
Least-squares matrix: full	Secondary atom site location: difference Fourier map
$R[F^2 > 2\sigma(F^2)] = 0.146$	Hydrogen site location: mixed
$wR(F^2) = 0.290$	H-atom parameters constrained
$S = 1.24$	$w = 1/[\sigma^2(F_o^2) + (0.064P)^2 + 112.7345P]$ where $P = (F_o^2 + 2F_c^2)/3$
21753 reflections	$(\Delta/\sigma)_{max} = 0.002$
723 parameters	$\Delta\rangle_{max} = 5.46$ e Å^{-3}

0 restraints	$\Delta\rangle_{min}$ = -2.67 e Å^{-3}

Data collection: Bruker *APEX2*; cell refinement: Bruker *SAINT*; data reduction: Bruker *SAINT*; program(s) used to solve structure: *SHELXS2013* (Sheldrick, 2013); program(s) used to refine structure: *SHELXL2013* (Sheldrick, 2013); molecular graphics: Bruker *SHELXTL*; software used to prepare material for publication: Bruker *SHELXTL*.

7.12.6 Special details

Geometry. All esds (except the esd in the dihedral angle between two l.s. planes) are estimated using the full covariance matrix. The cell esds are taken into account individually in the estimation of esds in distances, angles and torsion angles; correlations between esds in cell parameters are only used when they are defined by crystal symmetry. An approximate (isotropic) treatment of cell esds is used for estimating esds involving l.s. planes.

7.12.7 **Table A34.** Fractional atomic coordinates and isotropic or equivalent isotropic displacement parameters (Å^2) for [**5'**][BArF$_{24}$].

	x	*y*	*z*	U_{iso}*/U_{eq}	Occ. (<1)
C1	0.2700 (9)	0.4062 (6)	0.5150 (4)	0.037 (2)	
H1	0.2120	0.4002	0.5350	0.044*	
C2	0.2796 (12)	0.4676 (7)	0.4885 (5)	0.050 (3)	
H2	0.2300	0.5037	0.4920	0.060*	
C3	0.3588 (13)	0.4768 (7)	0.4578 (6)	0.058 (4)	
H3	0.3632	0.5186	0.4392	0.070*	
C4	0.4336 (11)	0.4251 (7)	0.4534 (5)	0.050 (3)	
C5	0.5180 (13)	0.4279 (9)	0.4214 (6)	0.067 (4)	
H5	0.5264	0.4684	0.4017	0.080*	
C6	0.5848 (11)	0.3768 (10)	0.4180 (5)	0.065 (5)	
H6	0.6406	0.3817	0.3964	0.078*	
C7	0.5762 (10)	0.3135 (9)	0.4459 (5)	0.054 (4)	
C8	0.6408 (12)	0.2569 (11)	0.4431 (6)	0.074 (5)	
H8	0.6965	0.2576	0.4213	0.089*	
C9	0.6250 (13)	0.1996 (11)	0.4719 (6)	0.079 (6)	
H9	0.6707	0.1610	0.4700	0.095*	
C10	0.5415 (11)	0.1966 (8)	0.5046 (5)	0.056 (4)	
H10	0.5315	0.1560	0.5239	0.067*	

C11	0.4761 (8)	0.2516 (5)	0.5083 (3)	0.030 (2)	
C12	0.4946 (8)	0.3092 (7)	0.4793 (4)	0.036 (2)	
C13	0.4238 (9)	0.3638 (6)	0.4820 (4)	0.035 (2)	
C14	0.3277 (9)	0.3125 (6)	0.6305 (4)	0.0367 (11)	
C15	0.4394 (9)	0.3017 (6)	0.6301 (4)	0.0367 (11)	
C16	0.4563 (9)	0.2299 (6)	0.6287 (4)	0.0367 (11)	
C17	0.3555 (9)	0.1961 (6)	0.6266 (4)	0.0367 (11)	
C18	0.2745 (9)	0.2499 (6)	0.6272 (4)	0.0367 (11)	
C19	0.2771 (16)	0.3810 (9)	0.6406 (5)	0.079 (6)	
H19A	0.2000	0.3796	0.6277	0.118*	
H19B	0.3116	0.4173	0.6222	0.118*	
H19C	0.2869	0.3905	0.6784	0.118*	
C20	0.5254 (14)	0.3558 (8)	0.6356 (6)	0.070 (5)	
H20A	0.5568	0.3593	0.6725	0.105*	
H20B	0.4938	0.4001	0.6239	0.105*	
H20C	0.5817	0.3435	0.6141	0.105*	
C21	0.5640 (10)	0.1961 (8)	0.6339 (5)	0.052 (3)	
H21A	0.6121	0.2222	0.6141	0.079*	
H21B	0.5563	0.1492	0.6202	0.079*	
H21C	0.5944	0.1947	0.6710	0.079*	
C22	0.3380 (14)	0.1206 (8)	0.6297 (5)	0.064 (4)	
H22A	0.3945	0.0964	0.6139	0.096*	
H22B	0.2675	0.1088	0.6107	0.096*	
H22C	0.3406	0.1069	0.6665	0.096*	
C23	0.1591 (11)	0.2345 (12)	0.6344 (6)	0.090 (7)	
H23A	0.1141	0.2745	0.6239	0.135*	
H23B	0.1548	0.2239	0.6714	0.135*	
H23C	0.1336	0.1950	0.6126	0.135*	
C24	0.1540 (15)	0.1381 (10)	0.4917 (9)	0.091 (6)	
H24A	0.1349	0.1317	0.5276	0.109*	
H24B	0.0874	0.1316	0.4670	0.109*	
C25	0.233 (2)	0.0822 (12)	0.4815 (10)	0.122 (9)	
H25A	0.3004	0.0887	0.5048	0.183*	
H25B	0.2468	0.0846	0.4449	0.183*	
H25C	0.2022	0.0373	0.4883	0.183*	
C26	0.2440 (13)	0.2459 (13)	0.4191 (5)	0.096 (7)	
H26A	0.2652	0.2947	0.4182	0.115*	

H26B	0.3097	0.2184	0.4168	0.115*	
C27	0.1722 (18)	0.2327 (15)	0.3733 (7)	0.122 (10)	
H27A	0.1607	0.1832	0.3694	0.183*	
H27B	0.2026	0.2505	0.3427	0.183*	
H27C	0.1032	0.2554	0.3760	0.183*	
C28	0.0783 (10)	0.2826 (9)	0.4941 (6)	0.064 (4)	
H28A	0.0717	0.2856	0.5320	0.077*	
H28B	0.0909	0.3297	0.4817	0.077*	
C29	-0.0278 (12)	0.2571 (9)	0.4656 (6)	0.070 (4)	
H29A	-0.0232	0.2548	0.4279	0.104*	
H29B	-0.0855	0.2888	0.4720	0.104*	
H29C	-0.0432	0.2114	0.4786	0.104*	
C30	0.8536 (8)	0.2728 (5)	0.2019 (4)	0.0282 (7)	
C31	0.8384 (8)	0.2117 (5)	0.1730 (4)	0.0282 (7)	
H31	0.8310	0.1700	0.1913	0.034*	
C32	0.8338 (8)	0.2099 (5)	0.1192 (4)	0.0282 (7)	
C33	0.8423 (8)	0.2697 (5)	0.0906 (4)	0.0282 (7)	
H33	0.8393	0.2686	0.0535	0.034*	
C34	0.8551 (8)	0.3308 (5)	0.1179 (4)	0.0282 (7)	
C35	0.8610 (8)	0.3324 (5)	0.1723 (4)	0.0282 (7)	
H35	0.8702	0.3752	0.1899	0.034*	
C36	0.8215 (8)	0.1432 (5)	0.0900 (4)	0.0282 (7)	
C37	0.8604 (8)	0.3955 (5)	0.0887 (4)	0.0282 (7)	
C38	0.9294 (6)	0.3340 (4)	0.2952 (3)	0.0181 (15)	
C39	1.0266 (6)	0.3544 (5)	0.2776 (4)	0.0246 (19)	
H39	1.0473	0.3345	0.2467	0.029*	
C40	1.0923 (7)	0.4031 (6)	0.3046 (4)	0.033 (2)	
C41	1.0661 (8)	0.4341 (6)	0.3497 (4)	0.035 (2)	
H41	1.1113	0.4682	0.3675	0.041*	
C42	0.9726 (8)	0.4140 (5)	0.3681 (4)	0.0270 (19)	
C43	0.9065 (6)	0.3647 (5)	0.3415 (3)	0.0210 (17)	
H43	0.8430	0.3515	0.3555	0.025*	
C44	1.1935 (10)	0.4237 (9)	0.2847 (6)	0.063 (4)	
C45	0.9379 (8)	0.4491 (6)	0.4154 (4)	0.037 (2)	
C46	0.7257 (7)	0.2931 (4)	0.2714 (3)	0.0204 (12)	
C47	0.6899 (7)	0.3611 (5)	0.2678 (3)	0.0242 (18)	
H47	0.7416	0.3961	0.2650	0.029*	

C48	0.5839 (7)	0.3803 (5)	0.2681 (4)	0.0273 (19)	
C49	0.5071 (8)	0.3314 (6)	0.2733 (4)	0.036 (2)	
H49	0.4345	0.3443	0.2751	0.043*	
C50	0.5371 (8)	0.2638 (6)	0.2759 (4)	0.035 (2)	
C51	0.6437 (7)	0.2446 (5)	0.2745 (4)	0.0264 (18)	
H51	0.6616	0.1972	0.2756	0.032*	
C52	0.5537 (8)	0.4537 (6)	0.2628 (5)	0.040 (3)	
C53	0.4540 (9)	0.2093 (7)	0.2823 (5)	0.048 (3)	
C54	0.8942 (7)	0.2016 (4)	0.2918 (3)	0.0207 (16)	
C55	0.8522 (7)	0.1675 (5)	0.3326 (4)	0.0265 (19)	
H55	0.7946	0.1883	0.3475	0.032*	
C56	0.8906 (9)	0.1053 (5)	0.3520 (4)	0.032 (2)	
C57	0.9753 (9)	0.0733 (5)	0.3325 (4)	0.037 (2)	
H57	1.0012	0.0301	0.3457	0.044*	
C58	1.0215 (9)	0.1061 (6)	0.2930 (4)	0.034 (2)	
C59	0.9820 (8)	0.1685 (5)	0.2735 (4)	0.0277 (19)	
H59	1.0155	0.1900	0.2467	0.033*	
C60	0.8388 (12)	0.0705 (6)	0.3931 (6)	0.053 (4)	
C61	1.1131 (12)	0.0732 (8)	0.2709 (6)	0.057 (4)	
N1	0.3428 (7)	0.3537 (5)	0.5127 (3)	0.0337 (19)	
B1	0.8501 (8)	0.2740 (5)	0.2657 (4)	0.0204 (12)	
F1	0.7949 (8)	0.0920 (4)	0.1182 (3)	0.063 (2)	
F2	0.9134 (10)	0.1244 (6)	0.0738 (6)	0.120 (5)	
F3	0.7516 (11)	0.1453 (4)	0.0480 (4)	0.105 (4)	
F4	0.863 (2)	0.3889 (10)	0.0383 (8)	0.082 (3)	0.5
F5	0.966 (2)	0.4205 (9)	0.1016 (7)	0.082 (3)	0.5
F6	0.804 (2)	0.4447 (11)	0.1061 (8)	0.082 (3)	0.5
F4B	0.793 (2)	0.3994 (10)	0.0439 (8)	0.082 (3)	0.5
F5B	0.953 (2)	0.4057 (9)	0.0693 (7)	0.082 (3)	0.5
F6B	0.859 (2)	0.4538 (11)	0.1129 (8)	0.082 (3)	0.5
F7	1.2199 (19)	0.3930 (17)	0.2440 (10)	0.090 (4)	0.5
F8	1.2020 (15)	0.4921 (13)	0.2769 (10)	0.090 (4)	0.5
F9	1.2838 (16)	0.4086 (14)	0.3217 (10)	0.090 (4)	0.5
F7B	1.2413 (18)	0.3701 (15)	0.2636 (11)	0.090 (4)	0.5
F8B	1.1741 (15)	0.4549 (13)	0.2366 (10)	0.090 (4)	0.5
F9B	1.2632 (17)	0.4561 (14)	0.3157 (10)	0.090 (4)	0.5
F10	0.9070 (13)	0.5105 (6)	0.4063 (4)	0.130 (6)	

F11	1.0185 (8)	0.4553 (7)	0.4534 (4)	0.102 (4)	
F12	0.8654 (9)	0.4169 (7)	0.4363 (4)	0.112 (5)	
F13	0.5811 (17)	0.4789 (9)	0.2178 (9)	0.076 (3)	0.5
F14	0.4545 (18)	0.4674 (9)	0.2671 (10)	0.076 (3)	0.5
F15	0.6116 (17)	0.4902 (9)	0.3000 (9)	0.076 (3)	0.5
F13B	0.6262 (17)	0.4973 (9)	0.2501 (10)	0.076 (3)	0.5
F14B	0.4602 (18)	0.4651 (9)	0.2336 (9)	0.076 (3)	0.5
F15B	0.5281 (17)	0.4810 (9)	0.3087 (9)	0.076 (3)	0.5
F16	0.3578 (7)	0.2259 (6)	0.2569 (4)	0.085 (3)	
F17	0.4397 (9)	0.2008 (6)	0.3311 (4)	0.094 (4)	
F18	0.4753 (8)	0.1501 (5)	0.2630 (5)	0.089 (3)	
F19	0.8379 (17)	0.1101 (13)	0.4355 (9)	0.081 (3)	0.5
F20	0.7250 (17)	0.0615 (11)	0.3769 (8)	0.081 (3)	0.5
F21	0.8601 (18)	0.0043 (11)	0.3998 (9)	0.081 (3)	0.5
F19B	0.7862 (17)	0.1075 (13)	0.4218 (10)	0.081 (3)	0.5
F20B	0.7811 (19)	0.0228 (12)	0.3785 (8)	0.081 (3)	0.5
F21B	0.9178 (17)	0.0431 (11)	0.4327 (8)	0.081 (3)	0.5
F22	1.1080 (18)	0.0028 (13)	0.2714 (11)	0.087 (3)	0.5
F23	1.1078 (19)	0.0829 (11)	0.2183 (12)	0.087 (3)	0.5
F24	1.2029 (19)	0.0943 (12)	0.2864 (10)	0.087 (3)	0.5
F22B	1.1481 (18)	0.0186 (13)	0.2900 (11)	0.087 (3)	0.5
F23B	1.0808 (19)	0.0536 (11)	0.2176 (12)	0.087 (3)	0.5
F24B	1.1894 (19)	0.1184 (12)	0.2604 (11)	0.087 (3)	0.5
Si1	0.1995 (3)	0.2288 (2)	0.48570 (14)	0.0489 (8)	
Ir1	0.35345 (3)	0.26109 (2)	0.55434 (2)	0.02936 (12)	
H1A	0.2321	0.2649	0.5354	0.050*	

7.12.8 **Table A35.** Atomic displacement parameters (Å^2) for [**5A'**][BArF$_{24}$].

	U^{11}	U^{22}	U^{33}	U^{12}	U^{13}	U^{23}
C1	0.038 (6)	0.041 (6)	0.030 (5)	0.013 (5)	-0.001 (4)	0.003 (4)
C2	0.066 (9)	0.033 (7)	0.051 (7)	0.008 (6)	0.002 (6)	0.007 (5)
C3	0.079 (10)	0.035 (7)	0.060 (8)	-0.005 (7)	0.005 (7)	0.015 (6)
C4	0.056 (8)	0.052 (8)	0.041 (6)	-0.020 (6)	0.007 (5)	0.008 (6)
C5	0.056 (9)	0.084 (12)	0.063 (9)	-0.018 (8)	0.019 (7)	0.011 (8)

C6	0.044 (8)	0.112 (14)	0.045 (7)	-0.025 (8)	0.022 (6)	0.001 (8)
C7	0.035 (6)	0.095 (11)	0.033 (6)	0.001 (6)	0.007 (5)	-0.013 (6)
C8	0.048 (8)	0.128 (16)	0.045 (7)	0.026 (9)	0.003 (6)	-0.018 (10)
C9	0.060 (9)	0.129 (16)	0.048 (8)	0.060 (10)	0.002 (7)	-0.024 (9)
C10	0.058 (8)	0.074 (10)	0.035 (6)	0.039 (7)	0.001 (5)	0.000 (6)
C11	0.035 (5)	0.035 (6)	0.019 (4)	0.014 (4)	0.002 (3)	-0.001 (3)
C12	0.022 (5)	0.066 (8)	0.021 (4)	-0.005 (5)	0.004 (3)	-0.005 (4)
C13	0.035 (5)	0.048 (7)	0.020 (4)	-0.008 (5)	0.002 (4)	0.001 (4)
C14	0.050 (3)	0.043 (3)	0.0175 (17)	0.002 (2)	0.0039 (17)	0.0056 (18)
C15	0.050 (3)	0.043 (3)	0.0175 (17)	0.002 (2)	0.0039 (17)	0.0056 (18)
C16	0.050 (3)	0.043 (3)	0.0175 (17)	0.002 (2)	0.0039 (17)	0.0056 (18)
C17	0.050 (3)	0.043 (3)	0.0175 (17)	0.002 (2)	0.0039 (17)	0.0056 (18)
C18	0.050 (3)	0.043 (3)	0.0175 (17)	0.002 (2)	0.0039 (17)	0.0056 (18)
C19	0.120 (15)	0.084 (12)	0.035 (7)	0.053 (11)	0.022 (8)	0.000 (7)
C20	0.103 (13)	0.059 (10)	0.047 (8)	-0.041 (9)	0.006 (8)	-0.008 (7)
C21	0.038 (6)	0.071 (10)	0.048 (7)	0.012 (6)	0.003 (5)	0.011 (6)
C22	0.089 (11)	0.060 (9)	0.041 (7)	-0.035 (8)	0.001 (7)	0.007 (6)
C23	0.037 (7)	0.18 (2)	0.055 (8)	-0.009 (10)	0.021 (6)	0.022 (11)
C24	0.065 (11)	0.089 (14)	0.115 (16)	-0.011 (10)	-0.005 (11)	-0.028 (12)
C25	0.15 (2)	0.084 (16)	0.12 (2)	0.019 (15)	-0.019 (17)	-0.036 (14)
C26	0.059 (9)	0.20 (2)	0.028 (6)	0.006 (12)	-0.007 (6)	-0.028 (10)
C27	0.091 (15)	0.22 (3)	0.049 (10)	0.018 (17)	-0.003 (9)	0.009 (14)
C28	0.033 (6)	0.096 (12)	0.060 (8)	0.023 (7)	-0.008 (6)	-0.004 (8)
C29	0.045 (8)	0.097 (13)	0.065 (9)	-0.009 (8)	-0.001 (6)	0.015 (9)
C30	0.0371 (18)	0.0206 (17)	0.0277 (15)	-0.0029 (13)	0.0074 (13)	-0.0031 (13)
C31	0.0371 (18)	0.0206 (17)	0.0277 (15)	-0.0029 (13)	0.0074 (13)	-0.0031 (13)
C32	0.0371 (18)	0.0206 (17)	0.0277 (15)	-0.0029 (13)	0.0074 (13)	-0.0031 (13)
C33	0.0371 (18)	0.0206 (17)	0.0277 (15)	-0.0029 (13)	0.0074 (13)	-0.0031 (13)
C34	0.0371 (18)	0.0206 (17)	0.0277 (15)	-0.0029 (13)	0.0074 (13)	-0.0031 (13)
C35	0.0371 (18)	0.0206 (17)	0.0277 (15)	-0.0029 (13)	0.0074 (13)	-0.0031 (13)
C36	0.0371 (18)	0.0206 (17)	0.0277 (15)	-0.0029 (13)	0.0074 (13)	-0.0031 (13)
C37	0.0371 (18)	0.0206 (17)	0.0277 (15)	-0.0029 (13)	0.0074 (13)	-0.0031 (13)
C38	0.016 (4)	0.017 (4)	0.022 (4)	-0.003 (3)	0.004 (3)	-0.002 (3)
C39	0.012 (4)	0.036 (5)	0.027 (4)	0.000 (3)	0.009 (3)	-0.011 (4)
C40	0.017 (4)	0.042 (6)	0.043 (6)	-0.005 (4)	0.010 (4)	-0.008 (5)
C41	0.026 (5)	0.036 (6)	0.041 (5)	-0.007 (4)	0.003 (4)	-0.014 (4)
C42	0.028 (5)	0.031 (5)	0.023 (4)	0.002 (4)	0.003 (3)	-0.009 (4)

C43	0.012 (4)	0.029 (5)	0.023 (4)	0.000 (3)	0.005 (3)	-0.002 (3)
C44	0.025 (6)	0.097 (12)	0.073 (10)	-0.030 (7)	0.025 (6)	-0.031 (9)
C45	0.029 (5)	0.046 (7)	0.036 (5)	0.004 (4)	0.006 (4)	-0.021 (5)
C46	0.030 (3)	0.011 (3)	0.021 (3)	-0.001 (2)	0.003 (2)	0.000 (2)
C47	0.022 (4)	0.028 (5)	0.023 (4)	-0.006 (3)	0.002 (3)	-0.004 (3)
C48	0.019 (4)	0.031 (5)	0.031 (5)	0.000 (3)	0.003 (3)	-0.007 (4)
C49	0.016 (4)	0.048 (7)	0.044 (6)	0.003 (4)	0.007 (4)	-0.010 (5)
C50	0.027 (5)	0.043 (6)	0.036 (5)	-0.014 (4)	0.009 (4)	-0.006 (5)
C51	0.030 (4)	0.020 (5)	0.030 (4)	-0.004 (3)	0.005 (3)	-0.003 (3)
C52	0.021 (5)	0.039 (6)	0.060 (7)	0.008 (4)	0.007 (5)	-0.006 (5)
C53	0.032 (6)	0.057 (8)	0.059 (8)	-0.021 (5)	0.017 (5)	-0.007 (6)
C54	0.020 (4)	0.014 (4)	0.028 (4)	0.004 (3)	0.004 (3)	0.000 (3)
C55	0.024 (4)	0.031 (5)	0.027 (4)	0.002 (4)	0.013 (3)	0.001 (4)
C56	0.042 (6)	0.029 (5)	0.029 (5)	0.001 (4)	0.017 (4)	0.006 (4)
C57	0.046 (6)	0.024 (5)	0.042 (6)	0.013 (4)	0.014 (5)	0.013 (4)
C58	0.038 (6)	0.032 (6)	0.035 (5)	0.007 (4)	0.020 (4)	0.009 (4)
C59	0.027 (5)	0.027 (5)	0.031 (5)	0.000 (4)	0.010 (4)	0.010 (4)
C60	0.074 (9)	0.028 (6)	0.067 (8)	0.013 (6)	0.046 (7)	0.026 (6)
C61	0.055 (8)	0.050 (8)	0.073 (9)	0.027 (6)	0.037 (7)	0.030 (7)
N1	0.041 (5)	0.038 (5)	0.022 (4)	0.009 (4)	0.003 (3)	0.001 (3)
B1	0.030 (3)	0.011 (3)	0.021 (3)	-0.001 (2)	0.003 (2)	0.000 (2)
F1	0.115 (7)	0.024 (4)	0.048 (4)	-0.015 (4)	0.003 (4)	-0.011 (3)
F2	0.131 (10)	0.070 (7)	0.175 (13)	-0.011 (7)	0.084 (9)	-0.070 (8)
F3	0.199 (12)	0.035 (5)	0.061 (5)	-0.012 (6)	-0.061 (7)	-0.015 (4)
F4	0.158 (12)	0.042 (4)	0.046 (4)	-0.024 (5)	0.011 (6)	0.014 (3)
F5	0.158 (12)	0.042 (4)	0.046 (4)	-0.024 (5)	0.011 (6)	0.014 (3)
F6	0.158 (12)	0.042 (4)	0.046 (4)	-0.024 (5)	0.011 (6)	0.014 (3)
F4B	0.158 (12)	0.042 (4)	0.046 (4)	-0.024 (5)	0.011 (6)	0.014 (3)
F5B	0.158 (12)	0.042 (4)	0.046 (4)	-0.024 (5)	0.011 (6)	0.014 (3)
F6B	0.158 (12)	0.042 (4)	0.046 (4)	-0.024 (5)	0.011 (6)	0.014 (3)
F7	0.050 (5)	0.119 (11)	0.111 (9)	-0.028 (6)	0.044 (5)	-0.006 (7)
F8	0.050 (5)	0.119 (11)	0.111 (9)	-0.028 (6)	0.044 (5)	-0.006 (7)
F9	0.050 (5)	0.119 (11)	0.111 (9)	-0.028 (6)	0.044 (5)	-0.006 (7)
F7B	0.050 (5)	0.119 (11)	0.111 (9)	-0.028 (6)	0.044 (5)	-0.006 (7)
F8B	0.050 (5)	0.119 (11)	0.111 (9)	-0.028 (6)	0.044 (5)	-0.006 (7)
F9B	0.050 (5)	0.119 (11)	0.111 (9)	-0.028 (6)	0.044 (5)	-0.006 (7)
F10	0.233 (15)	0.091 (8)	0.077 (7)	0.104 (10)	0.059 (9)	-0.003 (6)

F11	0.076 (6)	0.173 (12)	0.051 (5)	0.024 (7)	-0.013 (5)	-0.063 (6)
F12	0.119 (9)	0.144 (10)	0.091 (7)	-0.065 (8)	0.078 (7)	-0.079 (7)
F13	0.083 (6)	0.038 (4)	0.109 (8)	0.023 (4)	0.012 (6)	-0.003 (5)
F14	0.083 (6)	0.038 (4)	0.109 (8)	0.023 (4)	0.012 (6)	-0.003 (5)
F15	0.083 (6)	0.038 (4)	0.109 (8)	0.023 (4)	0.012 (6)	-0.003 (5)
F13B	0.083 (6)	0.038 (4)	0.109 (8)	0.023 (4)	0.012 (6)	-0.003 (5)
F14B	0.083 (6)	0.038 (4)	0.109 (8)	0.023 (4)	0.012 (6)	-0.003 (5)
F15B	0.083 (6)	0.038 (4)	0.109 (8)	0.023 (4)	0.012 (6)	-0.003 (5)
F16	0.038 (4)	0.104 (8)	0.111 (8)	-0.034 (5)	-0.002 (5)	0.008 (6)
F17	0.106 (8)	0.125 (9)	0.053 (5)	-0.074 (7)	0.023 (5)	0.004 (5)
F18	0.070 (6)	0.059 (6)	0.149 (10)	-0.039 (5)	0.053 (6)	-0.028 (6)
F19	0.085 (8)	0.086 (6)	0.083 (6)	0.002 (5)	0.054 (6)	0.033 (5)
F20	0.085 (8)	0.086 (6)	0.083 (6)	0.002 (5)	0.054 (6)	0.033 (5)
F21	0.085 (8)	0.086 (6)	0.083 (6)	0.002 (5)	0.054 (6)	0.033 (5)
F19B	0.085 (8)	0.086 (6)	0.083 (6)	0.002 (5)	0.054 (6)	0.033 (5)
F20B	0.085 (8)	0.086 (6)	0.083 (6)	0.002 (5)	0.054 (6)	0.033 (5)
F21B	0.085 (8)	0.086 (6)	0.083 (6)	0.002 (5)	0.054 (6)	0.033 (5)
F22	0.075 (7)	0.067 (8)	0.131 (10)	0.012 (5)	0.060 (7)	-0.008 (6)
F23	0.075 (7)	0.067 (8)	0.131 (10)	0.012 (5)	0.060 (7)	-0.008 (6)
F24	0.075 (7)	0.067 (8)	0.131 (10)	0.012 (5)	0.060 (7)	-0.008 (6)
F22B	0.075 (7)	0.067 (8)	0.131 (10)	0.012 (5)	0.060 (7)	-0.008 (6)
F23B	0.075 (7)	0.067 (8)	0.131 (10)	0.012 (5)	0.060 (7)	-0.008 (6)
F24B	0.075 (7)	0.067 (8)	0.131 (10)	0.012 (5)	0.060 (7)	-0.008 (6)
Si1	0.052 (2)	0.056 (2)	0.0372 (16)	-0.0031 (17)	0.0007 (14)	-0.0070 (15)
Ir1	0.03142 (19)	0.0345 (2)	0.02275 (16)	0.00684 (17)	0.00582 (12)	0.00529 (16)

7.12.9 **Table A36.** Interatomic distances (Å) and angles (deg) for [**5A'**][BArF$_{24}$].

C1—N1	1.376 (13)	C33—H33	0.9500
C1—C2	1.390 (17)	C34—C35	1.392 (13)
C1—H1	0.9500	C34—C37	1.474 (14)
C2—C3	1.36 (2)	C35—H35	0.9500
C2—H2	0.9500	C36—F3	1.300 (13)
C3—C4	1.39 (2)	C36—F1	1.300 (12)
C3—H3	0.9500	C36—F2	1.324 (14)
C4—C13	1.415 (16)	C37—F6B	1.30 (3)

C4—C5	1.423 (19)	C37—F6	1.30 (3)
C5—C6	1.31 (2)	C37—F4	1.31 (2)
C5—H5	0.9500	C37—F5B	1.33 (2)
C6—C7	1.44 (2)	C37—F4B	1.34 (2)
C6—H6	0.9500	C37—F5	1.41 (3)
C7—C8	1.38 (2)	C38—C43	1.395 (11)
C7—C12	1.419 (15)	C38—C39	1.410 (11)
C8—C9	1.37 (3)	C38—B1	1.652 (12)
C8—H8	0.9500	C39—C40	1.382 (13)
C9—C10	1.42 (2)	C39—H39	0.9500
C9—H9	0.9500	C40—C41	1.383 (14)
C10—C11	1.360 (15)	C40—C44	1.483 (14)
C10—H10	0.9500	C41—C42	1.374 (14)
C11—C12	1.382 (15)	C41—H41	0.9500
C11—Ir1	2.064 (9)	C42—C43	1.387 (12)
C12—C13	1.394 (16)	C42—C45	1.508 (13)
C13—N1	1.376 (13)	C43—H43	0.9500
C14—C18	1.388 (16)	C44—F9B	1.27 (3)
C14—C15	1.415 (16)	C44—F7	1.29 (3)
C14—C19	1.515 (18)	C44—F7B	1.35 (3)
C14—Ir1	2.258 (10)	C44—F8	1.35 (3)
C15—C16	1.417 (16)	C44—F8B	1.37 (3)
C15—C20	1.501 (18)	C44—F9	1.41 (3)
C15—Ir1	2.244 (10)	C45—F10	1.270 (15)
C16—C17	1.418 (16)	C45—F12	1.277 (15)
C16—C21	1.492 (16)	C45—F11	1.317 (13)
C16—Ir1	2.246 (10)	C46—C47	1.398 (13)
C17—C18	1.460 (16)	C46—C51	1.406 (12)
C17—C22	1.492 (18)	C46—B1	1.627 (13)
C17—Ir1	2.244 (10)	C47—C48	1.380 (13)
C18—C23	1.511 (17)	C47—H47	0.9500
C18—Ir1	2.237 (10)	C48—C49	1.373 (14)
C19—H19A	0.9800	C48—C52	1.481 (15)
C19—H19B	0.9800	C49—C50	1.370 (17)
C19—H19C	0.9800	C49—H49	0.9500
C20—H20A	0.9800	C50—C51	1.391 (14)
C20—H20B	0.9800	C50—C53	1.512 (15)

C20—H20C	0.9800	C51—H51	0.9500
C21—H21A	0.9800	C52—F14	1.29 (2)
C21—H21B	0.9800	C52—F13B	1.32 (2)
C21—H21C	0.9800	C52—F14B	1.33 (2)
C22—H22A	0.9800	C52—F15	1.33 (2)
C22—H22B	0.9800	C52—F13	1.34 (2)
C22—H22C	0.9800	C52—F15B	1.37 (2)
C23—H23A	0.9800	C53—F18	1.297 (16)
C23—H23B	0.9800	C53—F17	1.301 (15)
C23—H23C	0.9800	C53—F16	1.333 (16)
C24—C25	1.52 (3)	C54—C55	1.401 (12)
C24—Si1	1.87 (2)	C54—C59	1.405 (12)
C24—H24A	0.9900	C54—B1	1.628 (12)
C24—H24B	0.9900	C55—C56	1.374 (14)
C25—H25A	0.9800	C55—H55	0.9500
C25—H25B	0.9800	C56—C57	1.380 (14)
C25—H25C	0.9800	C56—C60	1.472 (14)
C26—C27	1.41 (2)	C57—C58	1.387 (14)
C26—Si1	1.897 (16)	C57—H57	0.9500
C26—H26A	0.9900	C58—C59	1.382 (14)
C26—H26B	0.9900	C58—C61	1.489 (15)
C27—H27A	0.9800	C59—H59	0.9500
C27—H27B	0.9800	C60—F20B	1.21 (3)
C27—H27C	0.9800	C60—F19B	1.27 (3)
C28—C29	1.515 (19)	C60—F21	1.33 (2)
C28—Si1	1.880 (14)	C60—F19	1.34 (3)
C28—H28A	0.9900	C60—F21B	1.43 (3)
C28—H28B	0.9900	C60—F20	1.44 (3)
C29—H29A	0.9800	C61—F24	1.22 (3)
C29—H29B	0.9800	C61—F22B	1.23 (3)
C29—H29C	0.9800	C61—F24B	1.35 (3)
C30—C35	1.397 (13)	C61—F23	1.36 (3)
C30—C31	1.402 (13)	C61—F22	1.37 (3)
C30—B1	1.646 (13)	C61—F23B	1.43 (3)
C31—C32	1.377 (13)	N1—Ir1	2.095 (9)
C31—H31	0.9500	Si1—Ir1	2.520 (4)
C32—C33	1.388 (13)	Si1—H1A	1.4693

C32—C36	1.499 (13)	Ir1—H1A	1.5368
C33—C34	1.380 (13)		
N1—C1—C2	121.3 (11)	F5—C37—C34	106.2 (10)
N1—C1—H1	119.4	C43—C38—C39	115.6 (7)
C2—C1—H1	119.4	C43—C38—B1	121.2 (7)
C3—C2—C1	120.9 (12)	C39—C38—B1	123.1 (7)
C3—C2—H2	119.5	C40—C39—C38	121.0 (8)
C1—C2—H2	119.5	C40—C39—H39	119.5
C2—C3—C4	120.2 (12)	C38—C39—H39	119.5
C2—C3—H3	119.9	C39—C40—C41	122.1 (9)
C4—C3—H3	119.9	C39—C40—C44	119.5 (10)
C3—C4—C13	117.7 (12)	C41—C40—C44	118.4 (10)
C3—C4—C5	125.3 (13)	C42—C41—C40	117.8 (9)
C13—C4—C5	117.0 (14)	C42—C41—H41	121.1
C6—C5—C4	122.5 (15)	C40—C41—H41	121.1
C6—C5—H5	118.8	C41—C42—C43	120.7 (8)
C4—C5—H5	118.8	C41—C42—C45	119.6 (9)
C5—C6—C7	122.0 (12)	C43—C42—C45	119.6 (9)
C5—C6—H6	119.0	C42—C43—C38	122.8 (8)
C7—C6—H6	119.0	C42—C43—H43	118.6
C8—C7—C12	117.1 (15)	C38—C43—H43	118.6
C8—C7—C6	125.5 (14)	F9B—C44—F7B	109.4 (18)
C12—C7—C6	117.4 (13)	F7—C44—F8	107.7 (19)
C9—C8—C7	120.1 (14)	F9B—C44—F8B	111.8 (19)
C9—C8—H8	120.0	F7B—C44—F8B	91.0 (17)
C7—C8—H8	120.0	F7—C44—F9	100.6 (19)
C8—C9—C10	121.4 (14)	F8—C44—F9	103.5 (16)
C8—C9—H9	119.3	F9B—C44—C40	117.9 (14)
C10—C9—H9	119.3	F7—C44—C40	118.4 (15)
C11—C10—C9	120.2 (15)	F7B—C44—C40	111.8 (15)
C11—C10—H10	119.9	F8—C44—C40	113.9 (14)
C9—C10—H10	119.9	F8B—C44—C40	111.8 (13)
C10—C11—C12	117.3 (10)	F9—C44—C40	111.0 (15)
C10—C11—Ir1	127.6 (9)	F10—C45—F12	109.0 (12)
C12—C11—Ir1	115.1 (7)	F10—C45—F11	103.6 (12)
C11—C12—C13	116.2 (9)	F12—C45—F11	104.6 (12)

C11—C12—C7	123.9 (12)	F10—C45—C42	113.0 (10)
C13—C12—C7	119.8 (12)	F12—C45—C42	114.2 (9)
N1—C13—C12	116.1 (10)	F11—C45—C42	111.5 (9)
N1—C13—C4	122.5 (11)	C47—C46—C51	114.2 (8)
C12—C13—C4	121.4 (10)	C47—C46—B1	120.9 (7)
C18—C14—C15	109.6 (10)	C51—C46—B1	124.5 (8)
C18—C14—C19	125.3 (13)	C48—C47—C46	123.9 (9)
C15—C14—C19	124.6 (13)	C48—C47—H47	118.0
C18—C14—Ir1	71.2 (6)	C46—C47—H47	118.0
C15—C14—Ir1	71.2 (6)	C49—C48—C47	119.9 (9)
C19—C14—Ir1	130.5 (8)	C49—C48—C52	120.3 (9)
C14—C15—C16	107.3 (10)	C47—C48—C52	119.8 (9)
C14—C15—C20	126.3 (12)	C50—C49—C48	118.8 (9)
C16—C15—C20	126.1 (12)	C50—C49—H49	120.6
C14—C15—Ir1	72.2 (6)	C48—C49—H49	120.6
C16—C15—Ir1	71.7 (6)	C49—C50—C51	121.1 (9)
C20—C15—Ir1	126.1 (8)	C49—C50—C53	119.5 (10)
C15—C16—C17	109.0 (10)	C51—C50—C53	119.3 (11)
C15—C16—C21	124.8 (11)	C50—C51—C46	122.0 (9)
C17—C16—C21	126.0 (11)	C50—C51—H51	119.0
C15—C16—Ir1	71.5 (6)	C46—C51—H51	119.0
C17—C16—Ir1	71.5 (6)	F13B—C52—F14B	109.8 (16)
C21—C16—Ir1	127.5 (8)	F14—C52—F15	105.6 (15)
C16—C17—C18	106.4 (10)	F14—C52—F13	110.7 (16)
C16—C17—C22	126.3 (12)	F15—C52—F13	104.4 (15)
C18—C17—C22	126.9 (12)	F13B—C52—F15B	102.0 (15)
C16—C17—Ir1	71.7 (6)	F14B—C52—F15B	97.7 (14)
C18—C17—Ir1	70.7 (5)	F14—C52—C48	115.5 (13)
C22—C17—Ir1	127.9 (8)	F13B—C52—C48	118.1 (11)
C14—C18—C17	107.7 (10)	F14B—C52—C48	114.2 (12)
C14—C18—C23	128.8 (13)	F15—C52—C48	110.0 (11)
C17—C18—C23	122.4 (13)	F13—C52—C48	110.0 (11)
C14—C18—Ir1	72.8 (6)	F15B—C52—C48	112.5 (12)
C17—C18—Ir1	71.3 (6)	F18—C53—F17	108.5 (13)
C23—C18—Ir1	130.9 (8)	F18—C53—F16	104.2 (11)
C14—C19—H19A	109.5	F17—C53—F16	106.0 (11)
C14—C19—H19B	109.5	F18—C53—C50	113.9 (10)

H19A—C19—H19B	109.5	F17—C53—C50	112.1 (10)
C14—C19—H19C	109.5	F16—C53—C50	111.6 (12)
H19A—C19—H19C	109.5	C55—C54—C59	114.6 (8)
H19B—C19—H19C	109.5	C55—C54—B1	125.4 (8)
C15—C20—H20A	109.5	C59—C54—B1	120.0 (8)
C15—C20—H20B	109.5	C56—C55—C54	122.9 (8)
H20A—C20—H20B	109.5	C56—C55—H55	118.5
C15—C20—H20C	109.5	C54—C55—H55	118.5
H20A—C20—H20C	109.5	C55—C56—C57	121.0 (9)
H20B—C20—H20C	109.5	C55—C56—C60	120.1 (9)
C16—C21—H21A	109.5	C57—C56—C60	118.8 (10)
C16—C21—H21B	109.5	C56—C57—C58	118.1 (9)
H21A—C21—H21B	109.5	C56—C57—H57	121.0
C16—C21—H21C	109.5	C58—C57—H57	121.0
H21A—C21—H21C	109.5	C59—C58—C57	120.4 (9)
H21B—C21—H21C	109.5	C59—C58—C61	119.9 (9)
C17—C22—H22A	109.5	C57—C58—C61	119.7 (10)
C17—C22—H22B	109.5	C58—C59—C54	122.9 (8)
H22A—C22—H22B	109.5	C58—C59—H59	118.6
C17—C22—H22C	109.5	C54—C59—H59	118.6
H22A—C22—H22C	109.5	F20B—C60—F19B	106.4 (17)
H22B—C22—H22C	109.5	F21—C60—F19	118.6 (17)
C18—C23—H23A	109.5	F20B—C60—F21B	105.3 (16)
C18—C23—H23B	109.5	F19B—C60—F21B	99.3 (17)
H23A—C23—H23B	109.5	F21—C60—F20	95.4 (16)
C18—C23—H23C	109.5	F19—C60—F20	101.1 (15)
H23A—C23—H23C	109.5	F20B—C60—C56	115.7 (15)
H23B—C23—H23C	109.5	F19B—C60—C56	117.6 (13)
C25—C24—Si1	116.9 (16)	F21—C60—C56	116.2 (12)
C25—C24—H24A	108.1	F19—C60—C56	111.7 (14)
Si1—C24—H24A	108.1	F21B—C60—C56	110.8 (12)
C25—C24—H24B	108.1	F20—C60—C56	111.0 (13)
Si1—C24—H24B	108.1	F22B—C61—F24B	114.7 (18)
H24A—C24—H24B	107.3	F24—C61—F23	101.8 (17)
C24—C25—H25A	109.5	F24—C61—F22	112.1 (18)
C24—C25—H25B	109.5	F23—C61—F22	98.7 (19)
H25A—C25—H25B	109.5	F22B—C61—F23B	101.1 (19)

C24—C25—H25C	109.5	F24B—C61—F23B	96.0 (16)
H25A—C25—H25C	109.5	F24—C61—C58	117.1 (17)
H25B—C25—H25C	109.5	F22B—C61—C58	118.3 (15)
C27—C26—Si1	119.4 (15)	F24B—C61—C58	113.3 (14)
C27—C26—H26A	107.5	F23—C61—C58	112.3 (14)
Si1—C26—H26A	107.5	F22—C61—C58	112.8 (14)
C27—C26—H26B	107.5	F23B—C61—C58	110.2 (14)
Si1—C26—H26B	107.5	C13—N1—C1	117.4 (10)
H26A—C26—H26B	107.0	C13—N1—Ir1	114.4 (7)
C26—C27—H27A	109.5	C1—N1—Ir1	128.1 (7)
C26—C27—H27B	109.5	C46—B1—C54	116.0 (7)
H27A—C27—H27B	109.5	C46—B1—C30	104.0 (7)
C26—C27—H27C	109.5	C54—B1—C30	110.3 (7)
H27A—C27—H27C	109.5	C46—B1—C38	108.8 (7)
H27B—C27—H27C	109.5	C54—B1—C38	105.8 (7)
C29—C28—Si1	115.6 (12)	C30—B1—C38	112.1 (7)
C29—C28—H28A	108.4	C24—Si1—C28	105.0 (8)
Si1—C28—H28A	108.4	C24—Si1—C26	111.6 (10)
C29—C28—H28B	108.4	C28—Si1—C26	109.9 (8)
Si1—C28—H28B	108.4	C24—Si1—Ir1	113.1 (7)
H28A—C28—H28B	107.4	C28—Si1—Ir1	109.7 (5)
C28—C29—H29A	109.5	C26—Si1—Ir1	107.5 (5)
C28—C29—H29B	109.5	C24—Si1—H1A	115.8
H29A—C29—H29B	109.5	C28—Si1—H1A	76.8
C28—C29—H29C	109.5	C26—Si1—H1A	128.3
H29A—C29—H29C	109.5	C11—Ir1—N1	77.7 (4)
H29B—C29—H29C	109.5	C11—Ir1—C18	155.8 (4)
C35—C30—C31	115.6 (8)	N1—Ir1—C18	120.4 (4)
C35—C30—B1	122.8 (8)	C11—Ir1—C15	102.7 (4)
C31—C30—B1	121.4 (8)	N1—Ir1—C15	97.5 (4)
C32—C31—C30	122.6 (9)	C18—Ir1—C15	61.5 (4)
C32—C31—H31	118.7	C11—Ir1—C17	119.5 (4)
C30—C31—H31	118.7	N1—Ir1—C17	154.5 (4)
C31—C32—C33	120.8 (9)	C18—Ir1—C17	38.0 (4)
C31—C32—C36	120.9 (9)	C15—Ir1—C17	61.9 (4)
C33—C32—C36	118.3 (8)	C11—Ir1—C16	94.3 (4)
C34—C33—C32	117.9 (9)	N1—Ir1—C16	131.3 (4)

C34—C33—H33	121.0	C18—Ir1—C16	61.9 (4)
C32—C33—H33	121.0	C15—Ir1—C16	36.8 (4)
C33—C34—C35	121.1 (9)	C17—Ir1—C16	36.8 (4)
C33—C34—C37	119.4 (8)	C11—Ir1—C14	137.4 (4)
C35—C34—C37	119.4 (8)	N1—Ir1—C14	93.0 (4)
C34—C35—C30	121.9 (9)	C18—Ir1—C14	36.0 (4)
C34—C35—H35	119.0	C15—Ir1—C14	36.6 (4)
C30—C35—H35	119.0	C17—Ir1—C14	61.4 (4)
F3—C36—F1	107.0 (9)	C16—Ir1—C14	60.9 (4)
F3—C36—F2	105.5 (11)	C11—Ir1—Si1	97.8 (3)
F1—C36—F2	105.0 (10)	N1—Ir1—Si1	82.2 (3)
F3—C36—C32	113.8 (9)	C18—Ir1—Si1	100.4 (3)
F1—C36—C32	113.8 (8)	C15—Ir1—Si1	159.0 (3)
F2—C36—C32	111.0 (9)	C17—Ir1—Si1	111.4 (3)
F6—C37—F4	119.8 (15)	C16—Ir1—Si1	146.2 (3)
F6B—C37—F5B	96.7 (15)	C14—Ir1—Si1	122.4 (3)
F6B—C37—F4B	108.5 (16)	C11—Ir1—H1A	127.0
F5B—C37—F4B	98.5 (14)	N1—Ir1—H1A	78.5
F6—C37—F5	101.4 (14)	C18—Ir1—H1A	75.2
F4—C37—F5	97.2 (15)	C15—Ir1—H1A	127.0
F6B—C37—C34	120.2 (11)	C17—Ir1—H1A	101.2
F6—C37—C34	113.2 (12)	C16—Ir1—H1A	135.9
F4—C37—C34	115.3 (11)	C14—Ir1—H1A	90.4
F5B—C37—C34	114.6 (11)	Si1—Ir1—H1A	32.2
F4B—C37—C34	114.9 (11)		
N1—C1—C2—C3	2.7 (19)	C41—C40—C44—F7B	144.1 (17)
C1—C2—C3—C4	-2 (2)	C39—C40—C44—F8	124.8 (17)
C2—C3—C4—C13	0 (2)	C41—C40—C44—F8	-55 (2)
C2—C3—C4—C5	178.1 (14)	C39—C40—C44—F8B	64 (2)
C3—C4—C5—C6	-178.4 (15)	C41—C40—C44—F8B	-115.5 (17)
C13—C4—C5—C6	0 (2)	C39—C40—C44—F9	-118.9 (16)
C4—C5—C6—C7	1 (2)	C41—C40—C44—F9	62 (2)
C5—C6—C7—C8	177.9 (15)	C41—C42—C45—F10	70.1 (15)

C5—C6—C7—C12	-3 (2)	C43—C42—C45—F10	-105.9 (14)
C12—C7—C8—C9	0 (2)	C41—C42—C45—F12	-164.6 (12)
C6—C7—C8—C9	179.6 (15)	C43—C42—C45—F12	19.4 (16)
C7—C8—C9—C10	1 (2)	C41—C42—C45—F11	-46.2 (16)
C8—C9—C10—C11	-1 (2)	C43—C42—C45—F11	137.8 (12)
C9—C10—C11—C12	0.0 (18)	C51—C46—C47—C48	1.1 (13)
C9—C10—C11—Ir1	-177.9 (10)	B1—C46—C47—C48	174.6 (8)
C10—C11—C12—C13	177.3 (10)	C46—C47—C48—C49	1.5 (15)
Ir1—C11—C12—C13	-4.4 (12)	C46—C47—C48—C52	-178.6 (9)
C10—C11—C12—C7	0.8 (16)	C47—C48—C49—C50	-2.9 (15)
Ir1—C11—C12—C7	179.1 (9)	C52—C48—C49—C50	177.3 (10)
C8—C7—C12—C11	-0.9 (18)	C48—C49—C50—C51	1.5 (16)
C6—C7—C12—C11	179.5 (11)	C48—C49—C50—C53	179.3 (10)
C8—C7—C12—C13	-177.3 (11)	C49—C50—C51—C46	1.2 (15)
C6—C7—C12—C13	3.2 (17)	C53—C50—C51—C46	-176.5 (9)
C11—C12—C13—N1	-0.8 (14)	C47—C46—C51—C50	-2.5 (13)
C7—C12—C13—N1	175.9 (10)	B1—C46—C51—C50	-175.6 (9)
C11—C12—C13—C4	-179.0 (10)	C49—C48—C52—F14	5 (2)
C7—C12—C13—C4	-2.4 (16)	C47—C48—C52—F14	-175.4 (15)
C3—C4—C13—N1	1.1 (18)	C49—C48—C52—F13B	-170.0 (16)
C5—C4—C13—N1	-177.3 (11)	C47—C48—C52—F13B	10 (2)
C3—C4—C13—C12	179.2 (11)	C49—C48—C52—F14B	-38.6 (18)
C5—C4—C13—C12	0.8 (18)	C47—C48—C52—F14B	141.5 (14)

C18—C14—C15—C16	-2.4 (11)	C49—C48—C52—F15	123.9 (14)
C19—C14—C15—C16	169.8 (10)	C47—C48—C52—F15	-56.0 (17)
Ir1—C14—C15—C16	-63.5 (7)	C49—C48—C52—F13	-121.7 (14)
C18—C14—C15—C20	-176.8 (10)	C47—C48—C52—F13	58.4 (16)
C19—C14—C15—C20	-4.6 (17)	C49—C48—C52—F15B	71.6 (16)
Ir1—C14—C15—C20	122.1 (11)	C47—C48—C52—F15B	-108.3 (14)
C18—C14—C15—Ir1	61.1 (7)	C49—C50—C53—F18	152.6 (12)
C19—C14—C15—Ir1	-126.7 (10)	C51—C50—C53—F18	-29.6 (17)
C14—C15—C16—C17	1.8 (11)	C49—C50—C53—F17	-83.8 (15)
C20—C15—C16—C17	176.2 (10)	C51—C50—C53—F17	94.0 (14)
Ir1—C15—C16—C17	-62.1 (7)	C49—C50—C53—F16	35.0 (16)
C14—C15—C16—C21	-172.8 (10)	C51—C50—C53—F16	-147.2 (11)
C20—C15—C16—C21	1.6 (17)	C59—C54—C55—C56	-2.5 (14)
Ir1—C15—C16—C21	123.4 (10)	B1—C54—C55—C56	177.9 (9)
C14—C15—C16—Ir1	63.9 (7)	C54—C55—C56—C57	1.1 (17)
C20—C15—C16—Ir1	-121.7 (11)	C54—C55—C56—C60	-176.7 (11)
C15—C16—C17—C18	-0.5 (11)	C55—C56—C57—C58	0.7 (18)
C21—C16—C17—C18	173.9 (10)	C60—C56—C57—C58	178.6 (12)
Ir1—C16—C17—C18	-62.6 (6)	C56—C57—C58—C59	-1.0 (18)
C15—C16—C17—C22	-173.8 (10)	C56—C57—C58—C61	-180.0 (13)
C21—C16—C17—C22	0.6 (17)	C57—C58—C59—C54	-0.4 (17)
Ir1—C16—C17—C22	124.1 (11)	C61—C58—C59—C54	178.5 (12)
C15—C16—C17—Ir1	62.1 (7)	C55—C54—C59—	2.1 (14)

		C58	
C21—C16—C17—Ir1	-123.4 (10)	B1—C54—C59—C58	-178.2 (9)
C15—C14—C18—C17	2.1 (11)	C55—C56—C60—F20B	103.5 (18)
C19—C14—C18—C17	-170.0 (10)	C57—C56—C60—F20B	-74 (2)
Ir1—C14—C18—C17	63.2 (6)	C55—C56—C60—F19B	-24 (2)
C15—C14—C18—C23	169.9 (11)	C57—C56—C60—F19B	158.5 (18)
C19—C14—C18—C23	-2.3 (18)	C55—C56—C60—F21	162.5 (17)
Ir1—C14—C18—C23	-129.1 (12)	C57—C56—C60—F21	-15 (2)
C15—C14—C18—Ir1	-61.1 (7)	C55—C56—C60—F19	-57.1 (19)
C19—C14—C18—Ir1	126.8 (11)	C57—C56—C60—F19	125.0 (16)
C16—C17—C18—C14	-1.0 (10)	C55—C56—C60—F21B	-136.8 (14)
C22—C17—C18—C14	172.3 (10)	C57—C56—C60—F21B	45.4 (19)
Ir1—C17—C18—C14	-64.2 (7)	C55—C56—C60—F20	55.0 (18)
C16—C17—C18—C23	-169.7 (10)	C57—C56—C60—F20	-122.9 (15)
C22—C17—C18—C23	3.6 (17)	C59—C58—C61—F24	80 (2)
Ir1—C17—C18—C23	127.1 (11)	C57—C58—C61—F24	-100.9 (19)
C16—C17—C18—Ir1	63.2 (6)	C59—C58—C61—F22B	178.2 (18)
C22—C17—C18—Ir1	-123.5 (11)	C57—C58—C61—F22B	-3 (3)
C35—C30—C31—C32	1.7 (15)	C59—C58—C61—F24B	40 (2)
B1—C30—C31—C32	175.6 (9)	C57—C58—C61—F24B	-141.2 (18)
C30—C31—C32—C33	-1.2 (16)	C59—C58—C61—F23	-37 (2)
C30—C31—C32—C36	177.8 (9)	C57—C58—C61—F23	141.9 (16)
C31—C32—C33—C34	-0.2 (15)	C59—C58—C61—F22	-147.5 (17)

C36—C32—C33—C34	-179.1 (9)	C57—C58—C61—F22	31 (2)
C32—C33—C34—C35	0.9 (15)	C59—C58—C61—F23B	-66.4 (18)
C32—C33—C34—C37	-177.9 (9)	C57—C58—C61—F23B	112.6 (15)
C33—C34—C35—C30	-0.4 (16)	C12—C13—N1—C1	-178.4 (9)
C37—C34—C35—C30	178.4 (10)	C4—C13—N1—C1	-0.1 (15)
C31—C30—C35—C34	-0.9 (15)	C12—C13—N1—Ir1	5.5 (11)
B1—C30—C35—C34	-174.7 (9)	C4—C13—N1—Ir1	-176.3 (9)
C31—C32—C36—F3	135.8 (12)	C2—C1—N1—C13	-1.7 (16)
C33—C32—C36—F3	-45.2 (14)	C2—C1—N1—Ir1	173.8 (9)
C31—C32—C36—F1	12.8 (14)	C47—C46—B1—C54	157.5 (8)
C33—C32—C36—F1	-168.3 (10)	C51—C46—B1—C54	-29.7 (12)
C31—C32—C36—F2	-105.4 (13)	C47—C46—B1—C30	-81.2 (9)
C33—C32—C36—F2	73.6 (13)	C51—C46—B1—C30	91.5 (9)
C33—C34—C37—F6B	171.4 (17)	C47—C46—B1—C38	38.4 (10)
C35—C34—C37—F6B	-7 (2)	C51—C46—B1—C38	-148.8 (8)
C33—C34—C37—F6	136.8 (14)	C55—C54—B1—C46	-23.7 (12)
C35—C34—C37—F6	-42.1 (17)	C59—C54—B1—C46	156.7 (8)
C33—C34—C37—F4	-6.4 (19)	C55—C54—B1—C30	-141.6 (9)
C35—C34—C37—F4	174.8 (16)	C59—C54—B1—C30	38.8 (11)
C33—C34—C37—F5B	-74.1 (15)	C55—C54—B1—C38	97.0 (10)
C35—C34—C37—F5B	107.1 (14)	C59—C54—B1—C38	-82.6 (10)
C33—C34—C37—F4B	39.0 (17)	C35—C30—B1—C46	80.1 (11)
C35—C34—C37—F4B	-139.8 (15)	C31—C30—B1—C46	-93.4 (10)
C33—C34—C37—F5	-112.8 (13)	C35—C30—B1—C54	-154.9 (9)
C35—C34—C37—F5	68.4 (14)	C31—C30—B1—C54	31.6 (12)
C43—C38—C39—C40	-1.4 (14)	C35—C30—B1—C38	-37.3 (12)
B1—C38—C39—C40	-177.6 (9)	C31—C30—B1—C38	149.2 (9)
C38—C39—C40—C41	-0.3 (17)	C43—C38—B1—C46	37.0 (10)

C38—C39—C40—C44	-179.6 (12)	C39—C38—B1—C46	-147.0 (8)
C39—C40—C41—C42	1.4 (17)	C43—C38—B1—C54	-88.4 (9)
C44—C40—C41—C42	-179.3 (12)	C39—C38—B1—C54	87.7 (10)
C40—C41—C42—C43	-0.8 (16)	C43—C38—B1—C30	151.4 (8)
C40—C41—C42—C45	-176.7 (10)	C39—C38—B1—C30	-32.5 (12)
C41—C42—C43—C38	-0.9 (15)	C25—C24—Si1—C28	174.5 (16)
C45—C42—C43—C38	175.0 (9)	C25—C24—Si1—C26	55.4 (19)
C39—C38—C43—C42	2.0 (13)	C25—C24—Si1—Ir1	-65.9 (18)
B1—C38—C43—C42	178.3 (8)	C29—C28—Si1—C24	-42.7 (15)
C39—C40—C44—F9B	-165 (2)	C29—C28—Si1—C26	77.5 (15)
C41—C40—C44—F9B	16 (3)	C29—C28—Si1—Ir1	-164.5 (11)
C39—C40—C44—F7	-3 (3)	C27—C26—Si1—C24	56 (2)
C41—C40—C44—F7	177 (2)	C27—C26—Si1—C28	-60 (2)
C39—C40—C44—F7B	-37 (2)	C27—C26—Si1—Ir1	-179.4 (19)

7.13[**5B**][$BArF_{24}$]

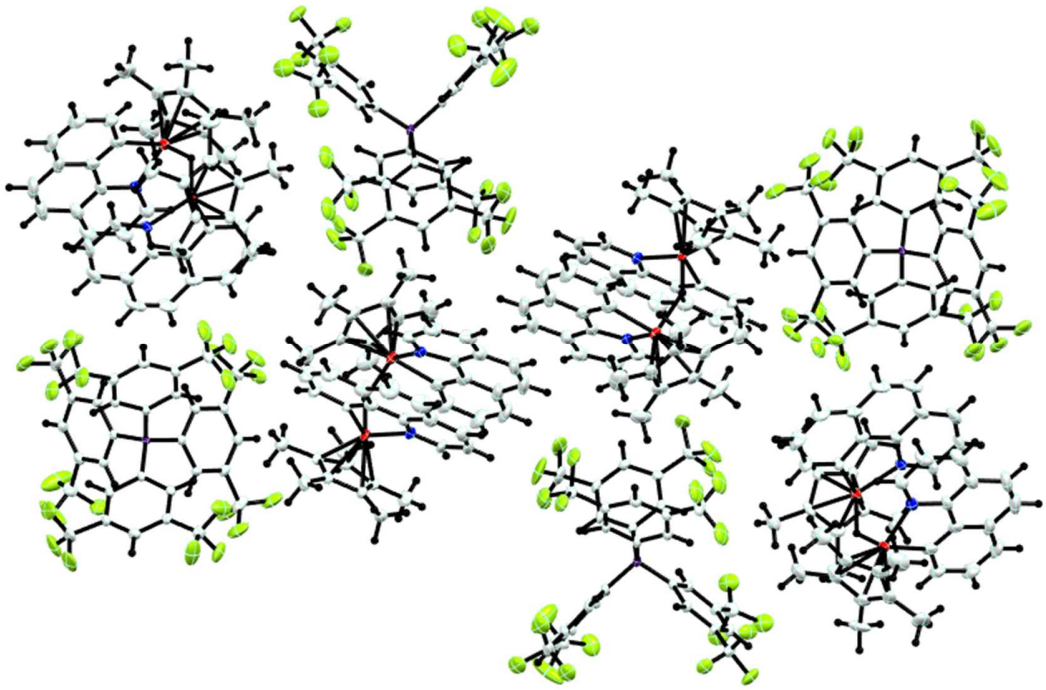

7.13.1 **Figure A33.** Crystal lattice packing of [**5B**][$BArF_{24}$].

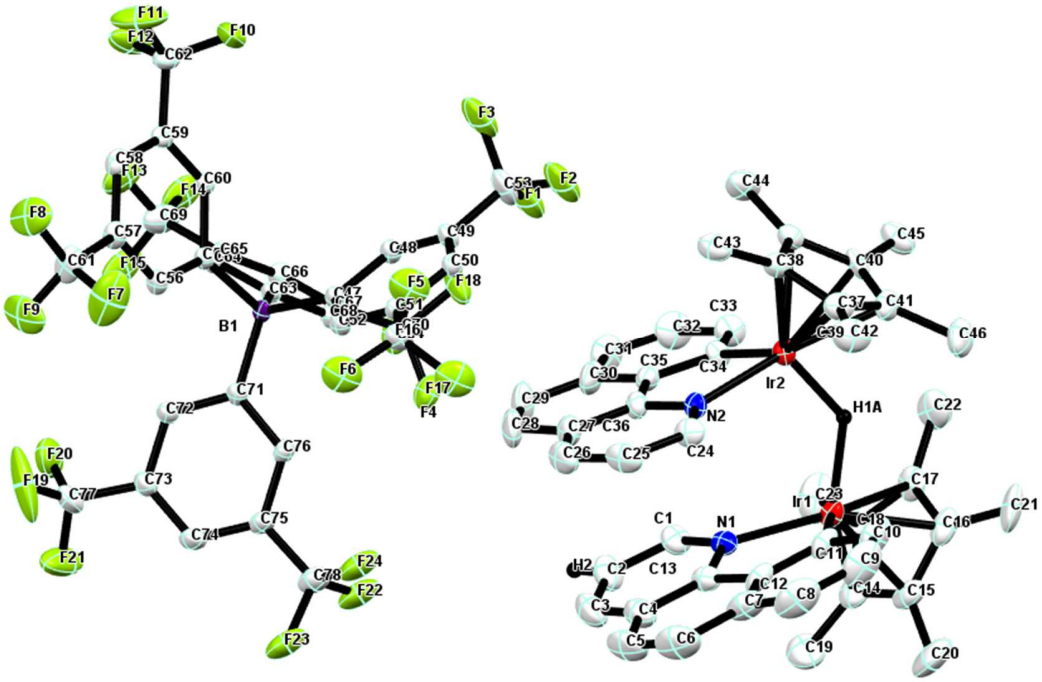

7.13.2 **Figure A34.** Asymmetric unit of [**5B**][BArF$_{24}$], without most of hydrogens and with total numbering of atoms.

[**5B**][BArF$_{24}$]

7.13.3 Crystal data

$C_{32}H_{12}BF_{24}\cdot C_{46}H_{47}Ir_2N_2$	$F(000)$ = 3664
M_r = 1875.48	D_x = 1.719 Mg m^{-3}
Monoclinic, $P2_1/c$	Mo $K\alpha$ radiation, λ = 0.71073 Å
a = 13.1813 (5) Å	Cell parameters from 9787 reflections
b = 14.6406 (6) Å	θ = 2.5–31.5°
c = 37.7769 (14) Å	μ = 3.78 mm^{-1}
β = 96.152 (1)°	T = 173 K
V = 7248.3 (5) Å^3	Prism, red
Z = 4	0.38 × 0.30 × 0.22 mm

7.13.4 Data collection

Bruker APEX-II CCD diffractometer	19373 reflections with $I > 2\sigma(I)$
Radiation source: fine focus sealed tube	$R_{int} = 0.038$
ϕ and ω scans	$\theta_{max} = 32.0°$, $\theta_{min} = 1.5°$
Absorption correction: multi-scan *SADABS*	$h = -19 \rightarrow 19$
$T_{min} = 0.574$, $T_{max} = 0.746$	$k = -21 \rightarrow 21$
175516 measured reflections	$l = -56 \rightarrow 56$
25132 independent reflections	

7.13.5 Refinement

Refinement on F^2	Primary atom site location: structure-invariant direct methods
Least-squares matrix: full	Secondary atom site location: difference Fourier map
$R[F^2 > 2\sigma(F^2)] = 0.082$	Hydrogen site location: mixed
$wR(F^2) = 0.198$	H-atom parameters constrained
$S = 1.22$	$w = 1/[\sigma^2(F_o^2) + (0.0461P)^2 + 90.7306P]$ where $P = (F_o^2 + 2F_c^2)/3$
25132 reflections	$(\Delta/\sigma)_{max} = 0.001$
944 parameters	$\Delta\rangle_{max} = 6.19$ e Å^{-3}
0 restraints	$\Delta\rangle_{min} = -3.48$ e Å^{-3}

Data collection: Bruker *APEX2*; cell refinement: Bruker *SAINT*; data reduction: Bruker *SAINT*; program(s) used to solve structure: *SHELXS2013* (Sheldrick, 2013); program(s) used to refine structure: *SHELXL2013* (Sheldrick, 2013); molecular graphics: Bruker *SHELXTL*; software used to prepare material for publication: Bruker *SHELXTL*.

7.13.6 Special details

Geometry. All esds (except the esd in the dihedral angle between two l.s. planes) are estimated using the full covariance matrix. The cell esds are taken into account individually in the estimation of esds in distances, angles and torsion angles; correlations between esds in cell parameters are only used when they are defined by crystal symmetry. An approximate (isotropic) treatment of cell esds is used for estimating esds involving l.s. planes.

7.13.7 **Table A37.** Fractional atomic coordinates and isotropic or equivalent isotropic displacement parameters (Å^2) for [**5B**][BArF$_{24}$].

	x	*y*	*z*	U_{iso}*/U_{eq}	Occ. (<1)
C1	0.3750 (7)	0.9171 (7)	0.1184 (3)	0.052 (2)	
H1	0.3695	0.9268	0.1429	0.062*	
C2	0.2874 (9)	0.8918 (9)	0.0959 (4)	0.069 (3)	
H2	0.2239	0.8843	0.1054	0.083*	
C3	0.2939 (11)	0.8780 (9)	0.0603 (4)	0.077 (4)	
H3	0.2346	0.8624	0.0450	0.093*	
C4	0.3871 (10)	0.8867 (8)	0.0467 (3)	0.063 (3)	
C5	0.4067 (14)	0.8678 (10)	0.0104 (3)	0.086 (5)	
H5	0.3518	0.8506	-0.0066	0.103*	
C6	0.5017 (16)	0.8743 (11)	0.0005 (3)	0.094 (5)	
H6	0.5118	0.8625	-0.0237	0.112*	
C7	0.5896 (6)	0.8987 (5)	0.02553 (15)	0.070 (4)	
C8	0.6890 (7)	0.9017 (6)	0.01651 (15)	0.089 (5)	
H8	0.7028	0.8861	-0.0069	0.107*	
C9	0.7683 (5)	0.9276 (6)	0.0418 (2)	0.089 (5)	
H9	0.8363	0.9297	0.0356	0.106*	
C10	0.7482 (4)	0.9505 (5)	0.07602 (18)	0.065 (3)	
H10	0.8024	0.9681	0.0933	0.078*	
C11	0.6488 (5)	0.9475 (4)	0.08505 (14)	0.0500 (16)	
C12	0.5695 (4)	0.9216 (4)	0.05980 (18)	0.0500 (16)	
C13	0.4723 (8)	0.9112 (6)	0.0702 (2)	0.046 (2)	
C14	0.5210 (9)	1.1174 (6)	0.1382 (3)	0.056 (3)	
C15	0.6191 (11)	1.1314 (7)	0.1271 (3)	0.063 (3)	
C16	0.6950 (9)	1.0974 (7)	0.1533 (3)	0.060 (3)	
C17	0.6402 (9)	1.0663 (7)	0.1827 (3)	0.054 (2)	
C18	0.5357 (9)	1.0786 (7)	0.1734 (3)	0.057 (3)	
C19	0.4199 (12)	1.1454 (9)	0.1202 (5)	0.091 (5)	
H19A	0.4052	1.2084	0.1268	0.136*	
H19B	0.3670	1.1047	0.1275	0.136*	
H19C	0.4209	1.1416	0.0943	0.136*	
C20	0.6442 (15)	1.1804 (9)	0.0943 (4)	0.100 (5)	
H20A	0.5863	1.1759	0.0758	0.150*	

H20B	0.7046	1.1526	0.0857	0.150*	
H20C	0.6580	1.2449	0.1000	0.150*	
C21	0.8095 (10)	1.1094 (9)	0.1545 (5)	0.088 (5)	
H21A	0.8336	1.0807	0.1335	0.132*	
H21B	0.8430	1.0805	0.1761	0.132*	
H21C	0.8261	1.1746	0.1547	0.132*	
C22	0.6876 (12)	1.0311 (10)	0.2184 (3)	0.082 (4)	
H22A	0.6468	0.9802	0.2260	0.124*	
H22B	0.6892	1.0803	0.2360	0.124*	
H22C	0.7572	1.0102	0.2162	0.124*	
C23	0.4554 (11)	1.0612 (11)	0.1987 (4)	0.092 (5)	
H23A	0.4670	1.0011	0.2098	0.138*	
H23B	0.3874	1.0628	0.1854	0.138*	
H23C	0.4602	1.1085	0.2172	0.138*	
C24	0.5989 (8)	0.7175 (6)	0.0826 (2)	0.048 (2)	
H24	0.6656	0.7329	0.0773	0.057*	
C25	0.5305 (11)	0.6770 (8)	0.0566 (3)	0.064 (3)	
H25	0.5515	0.6644	0.0339	0.076*	
C26	0.4327 (11)	0.6547 (8)	0.0633 (3)	0.069 (3)	
H26	0.3869	0.6269	0.0454	0.083*	
C27	0.4015 (9)	0.6734 (7)	0.0969 (3)	0.056 (3)	
C28	0.3027 (10)	0.6562 (9)	0.1078 (5)	0.082 (4)	
H28	0.2524	0.6277	0.0915	0.099*	
C29	0.2789 (10)	0.6794 (11)	0.1406 (5)	0.086 (4)	
H29	0.2120	0.6676	0.1466	0.103*	
C30	0.3514 (8)	0.7210 (8)	0.1664 (3)	0.061 (3)	
C31	0.3312 (9)	0.7492 (10)	0.2003 (4)	0.072 (3)	
H31	0.2650	0.7414	0.2075	0.087*	
C32	0.4062 (9)	0.7879 (10)	0.2229 (3)	0.072 (4)	
H32	0.3914	0.8053	0.2460	0.087*	
C33	0.5054 (7)	0.8032 (8)	0.2133 (3)	0.051 (2)	
H33	0.5556	0.8315	0.2297	0.061*	
C34	0.5296 (6)	0.7767 (6)	0.1797 (2)	0.0347 (15)	
C35	0.4505 (7)	0.7365 (6)	0.1567 (3)	0.0420 (18)	
C36	0.4746 (7)	0.7137 (6)	0.1222 (2)	0.0400 (17)	
C37	0.8222 (7)	0.7251 (7)	0.1494 (2)	0.0440 (19)	
C38	0.7600 (7)	0.6542 (6)	0.1618 (2)	0.0390 (17)	

C39	0.7378 (6)	0.6780 (6)	0.1971 (2)	0.0391 (17)	
C40	0.7809 (6)	0.7656 (7)	0.2057 (2)	0.045 (2)	
C41	0.8351 (7)	0.7917 (7)	0.1761 (3)	0.048 (2)	
C42	0.8741 (9)	0.7203 (10)	0.1160 (3)	0.069 (3)	
H42A	0.8723	0.7806	0.1046	0.104*	
H42B	0.8387	0.6760	0.0996	0.104*	
H42C	0.9452	0.7013	0.1219	0.104*	
C43	0.7322 (9)	0.5663 (7)	0.1430 (3)	0.057 (3)	
H43A	0.7228	0.5769	0.1173	0.086*	
H43B	0.6687	0.5428	0.1509	0.086*	
H43C	0.7870	0.5217	0.1487	0.086*	
C44	0.6817 (9)	0.6197 (9)	0.2218 (3)	0.062 (3)	
H44A	0.7311	0.5844	0.2375	0.093*	
H44B	0.6355	0.5779	0.2077	0.093*	
H44C	0.6422	0.6591	0.2362	0.093*	
C45	0.7926 (9)	0.8088 (9)	0.2424 (3)	0.065 (3)	
H45A	0.7294	0.8007	0.2535	0.098*	
H45B	0.8068	0.8742	0.2403	0.098*	
H45C	0.8492	0.7796	0.2571	0.098*	
C46	0.9006 (8)	0.8753 (9)	0.1751 (4)	0.077 (4)	
H46A	0.9716	0.8597	0.1832	0.116*	
H46B	0.8768	0.9223	0.1907	0.116*	
H46C	0.8963	0.8986	0.1506	0.116*	
C47	0.1881 (5)	0.3951 (5)	0.11923 (17)	0.0275 (13)	
C48	0.2589 (6)	0.4089 (5)	0.14919 (18)	0.0306 (14)	
H48	0.2348	0.4150	0.1719	0.037*	
C49	0.3634 (6)	0.4140 (6)	0.1467 (2)	0.0354 (16)	
C50	0.4022 (6)	0.4051 (6)	0.1143 (2)	0.0350 (15)	
H50	0.4734	0.4097	0.1126	0.042*	
C51	0.3343 (6)	0.3895 (5)	0.08438 (19)	0.0326 (14)	
C52	0.2306 (5)	0.3846 (5)	0.08697 (17)	0.0289 (13)	
H52	0.1860	0.3737	0.0659	0.035*	
C53	0.4338 (8)	0.4272 (10)	0.1792 (3)	0.061 (3)	
C54	0.3744 (7)	0.3749 (7)	0.0495 (2)	0.0437 (19)	
C55	0.0560 (5)	0.2671 (5)	0.11663 (16)	0.0254 (12)	
C56	0.0306 (6)	0.2232 (5)	0.08385 (18)	0.0323 (14)	
H56	0.0092	0.2593	0.0635	0.039*	

C57	0.0357 (6)	0.1290 (6)	0.08006 (19)	0.0351 (16)	
C58	0.0666 (6)	0.0738 (5)	0.1088 (2)	0.0367 (16)	
H58	0.0709	0.0094	0.1061	0.044*	
C59	0.0912 (5)	0.1148 (5)	0.1418 (2)	0.0301 (14)	
C60	0.0870 (5)	0.2081 (5)	0.14559 (18)	0.0290 (13)	
H60	0.1056	0.2340	0.1684	0.035*	
C61	0.0121 (10)	0.0883 (8)	0.0436 (3)	0.063 (3)	
C62	0.1240 (7)	0.0583 (6)	0.1739 (2)	0.0425 (18)	
C63	0.0237 (5)	0.4153 (5)	0.15756 (17)	0.0265 (12)	
C64	-0.0517 (6)	0.3688 (5)	0.17429 (19)	0.0315 (14)	
H64	-0.0741	0.3105	0.1657	0.038*	
C65	-0.0941 (6)	0.4067 (6)	0.2033 (2)	0.0357 (16)	
C66	-0.0644 (6)	0.4909 (6)	0.2165 (2)	0.0377 (16)	
H66	-0.0937	0.5162	0.2362	0.045*	
C67	0.0087 (6)	0.5379 (5)	0.20054 (19)	0.0326 (14)	
C68	0.0509 (5)	0.5012 (5)	0.17132 (19)	0.0298 (14)	
H68	0.0999	0.5360	0.1604	0.036*	
C69	-0.1727 (9)	0.3531 (9)	0.2201 (3)	0.061 (3)	
C70	0.0462 (7)	0.6282 (6)	0.2148 (2)	0.0417 (18)	
C71	-0.0042 (5)	0.4324 (5)	0.08915 (17)	0.0274 (13)	
C72	-0.1069 (6)	0.4084 (5)	0.08075 (19)	0.0328 (15)	
H72	-0.1324	0.3563	0.0919	0.039*	
C73	-0.1732 (7)	0.4579 (6)	0.0567 (2)	0.0396 (17)	
C74	-0.1381 (7)	0.5335 (6)	0.0398 (2)	0.0433 (19)	
H74	-0.1825	0.5671	0.0231	0.052*	
C75	-0.0370 (7)	0.5597 (6)	0.0476 (2)	0.0386 (17)	
C76	0.0280 (6)	0.5107 (5)	0.07237 (19)	0.0327 (15)	
H76	0.0962	0.5312	0.0780	0.039*	
C77	-0.2824 (8)	0.4270 (9)	0.0493 (3)	0.060 (3)	
C78	0.0023 (10)	0.6413 (7)	0.0308 (2)	0.056 (3)	
N1	0.4654 (6)	0.9277 (5)	0.10609 (19)	0.0399 (15)	
N2	0.5714 (5)	0.7347 (5)	0.11513 (18)	0.0363 (14)	
B1	0.0656 (6)	0.3783 (5)	0.12088 (18)	0.0251 (14)	
F1	0.4043 (12)	0.4892 (14)	0.2015 (4)	0.099 (3)	0.6
F2	0.5301 (14)	0.4430 (14)	0.1744 (4)	0.099 (3)	0.6
F3	0.4404 (11)	0.3481 (13)	0.1993 (4)	0.099 (3)	0.6
F1B	0.3990 (18)	0.419 (2)	0.2095 (6)	0.099 (3)	0.4

F2B	0.4764 (17)	0.514 (2)	0.1790 (5)	0.099 (3)	0.4
F3B	0.522 (2)	0.389 (2)	0.1798 (6)	0.099 (3)	0.4
F4	0.4262 (10)	0.4464 (10)	0.0385 (3)	0.0748 (18)	0.6
F5	0.4489 (10)	0.3112 (10)	0.0508 (3)	0.0748 (18)	0.6
F6	0.3072 (10)	0.3539 (11)	0.0221 (3)	0.0748 (18)	0.6
F4B	0.3400 (15)	0.4460 (15)	0.0276 (4)	0.0748 (18)	0.4
F5B	0.4709 (15)	0.3807 (16)	0.0498 (4)	0.0748 (18)	0.4
F6B	0.3299 (16)	0.3063 (16)	0.0321 (5)	0.0748 (18)	0.4
F7	0.0745 (9)	0.1211 (7)	0.0213 (2)	0.121 (4)	
F8	0.0177 (8)	-0.0001 (5)	0.0432 (2)	0.098 (3)	
F9	-0.0792 (8)	0.1105 (6)	0.0289 (2)	0.103 (3)	
F10	0.1987 (6)	0.0943 (6)	0.1952 (2)	0.100 (3)	
F11	0.1509 (9)	-0.0249 (5)	0.1665 (2)	0.106 (3)	
F12	0.0502 (6)	0.0477 (6)	0.19475 (17)	0.078 (2)	
F13	-0.1704 (10)	0.2687 (9)	0.2181 (4)	0.088 (2)	0.6
F14	-0.1823 (12)	0.3811 (10)	0.2531 (4)	0.088 (2)	0.6
F15	-0.2632 (11)	0.3819 (10)	0.2087 (5)	0.088 (2)	0.6
F13B	-0.2544 (17)	0.3334 (15)	0.1915 (6)	0.088 (2)	0.4
F14B	-0.1389 (16)	0.3274 (15)	0.2545 (6)	0.088 (2)	0.4
F15B	-0.2495 (18)	0.4118 (15)	0.2326 (7)	0.088 (2)	0.4
F16	-0.0151 (5)	0.6660 (5)	0.23684 (18)	0.0671 (18)	
F17	0.0552 (5)	0.6901 (4)	0.18932 (17)	0.0594 (15)	
F18	0.1389 (5)	0.6226 (5)	0.2321 (2)	0.077 (2)	
F19	-0.2917 (7)	0.3537 (10)	0.0313 (3)	0.164 (6)	
F20	-0.3238 (5)	0.4051 (6)	0.0789 (2)	0.090 (3)	
F21	-0.3420 (6)	0.4886 (9)	0.0359 (4)	0.168 (7)	
F22	0.0079 (13)	0.7151 (9)	0.0498 (4)	0.081 (2)	0.6
F23	-0.0501 (12)	0.6667 (9)	0.0001 (4)	0.081 (2)	0.6
F24	0.0999 (11)	0.6317 (8)	0.0223 (3)	0.081 (2)	0.6
F22B	-0.0740 (18)	0.7146 (12)	0.0314 (5)	0.081 (2)	0.4
F23B	-0.0073 (19)	0.6364 (13)	-0.0035 (6)	0.081 (2)	0.4
F24B	0.0570 (18)	0.6943 (14)	0.0549 (6)	0.081 (2)	0.4
Ir1	0.59634 (3)	0.98639 (2)	0.13276 (2)	0.03703 (8)	
Ir2	0.66726 (2)	0.77771 (2)	0.15966 (2)	0.03169 (7)	
H1A	0.6740	0.8996	0.1593	0.050*	

7.13.8 **Table A38.** Atomic displacement parameters ($Å^2$) for [**5B**][$BArF_{24}$].

	U^{11}	U^{22}	U^{33}	U^{12}	U^{13}	U^{23}
C1	0.045 (5)	0.053 (6)	0.058 (6)	0.011 (4)	0.005 (4)	-0.006 (4)
C2	0.043 (5)	0.067 (7)	0.096 (9)	0.009 (5)	-0.001 (6)	-0.012 (7)
C3	0.071 (8)	0.065 (8)	0.088 (9)	0.012 (6)	-0.029 (7)	-0.019 (7)
C4	0.074 (8)	0.054 (6)	0.056 (6)	0.010 (5)	-0.012 (5)	-0.008 (5)
C5	0.131 (13)	0.077 (9)	0.042 (6)	0.016 (9)	-0.025 (7)	-0.011 (6)
C6	0.159 (16)	0.085 (10)	0.035 (5)	0.010 (11)	0.006 (8)	-0.006 (6)
C7	0.125 (11)	0.051 (6)	0.037 (5)	-0.003 (7)	0.018 (6)	0.000 (4)
C8	0.153 (14)	0.077 (9)	0.048 (6)	-0.005 (9)	0.057 (8)	-0.009 (6)
C9	0.112 (11)	0.085 (9)	0.082 (9)	-0.020 (8)	0.070 (9)	-0.017 (7)
C10	0.079 (8)	0.059 (6)	0.066 (7)	-0.017 (6)	0.044 (6)	-0.011 (5)
C11	0.061 (4)	0.027 (3)	0.065 (4)	-0.004 (3)	0.022 (3)	0.000 (3)
C12	0.061 (4)	0.027 (3)	0.065 (4)	-0.004 (3)	0.022 (3)	0.000 (3)
C13	0.066 (6)	0.032 (4)	0.039 (4)	0.007 (4)	-0.002 (4)	-0.008 (3)
C14	0.068 (7)	0.030 (4)	0.072 (7)	0.005 (4)	0.010 (5)	-0.012 (4)
C15	0.104 (9)	0.032 (4)	0.052 (6)	-0.009 (5)	0.004 (6)	-0.006 (4)
C16	0.067 (7)	0.037 (5)	0.080 (7)	-0.011 (4)	0.027 (6)	-0.023 (5)
C17	0.073 (7)	0.046 (5)	0.044 (5)	-0.008 (5)	0.007 (4)	-0.028 (4)
C18	0.068 (7)	0.046 (5)	0.060 (6)	-0.007 (5)	0.023 (5)	-0.028 (5)
C19	0.096 (11)	0.052 (7)	0.121 (13)	0.022 (7)	-0.007 (9)	-0.009 (8)
C20	0.164 (17)	0.045 (7)	0.094 (11)	-0.030 (9)	0.031 (11)	0.002 (7)
C21	0.072 (8)	0.060 (7)	0.134 (13)	-0.039 (6)	0.027 (8)	-0.037 (8)
C22	0.112 (11)	0.075 (9)	0.058 (7)	-0.011 (8)	-0.005 (7)	-0.029 (6)
C23	0.088 (10)	0.094 (10)	0.103 (11)	-0.012 (8)	0.054 (9)	-0.046 (9)
C24	0.067 (6)	0.041 (4)	0.035 (4)	0.006 (4)	0.007 (4)	-0.014 (3)
C25	0.100 (9)	0.053 (6)	0.034 (4)	0.019 (6)	-0.010 (5)	-0.019 (4)
C26	0.086 (9)	0.050 (6)	0.063 (7)	0.000 (6)	-0.023 (6)	-0.020 (5)
C27	0.060 (6)	0.041 (5)	0.065 (6)	-0.010 (4)	-0.009 (5)	-0.009 (4)
C28	0.056 (7)	0.065 (8)	0.119 (12)	-0.028 (6)	-0.019 (7)	-0.011 (8)
C29	0.050 (7)	0.095 (10)	0.112 (12)	-0.036 (7)	0.005 (7)	-0.005 (9)
C30	0.042 (5)	0.058 (6)	0.085 (8)	-0.017 (5)	0.013 (5)	0.006 (6)
C31	0.046 (6)	0.088 (9)	0.088 (9)	-0.009 (6)	0.035 (6)	0.002 (7)
C32	0.056 (6)	0.098 (10)	0.071 (7)	0.006 (6)	0.041 (6)	0.000 (7)
C33	0.045 (5)	0.068 (6)	0.044 (5)	0.003 (4)	0.023 (4)	-0.006 (4)
C34	0.029 (3)	0.044 (4)	0.033 (3)	0.004 (3)	0.008 (3)	-0.006 (3)
C35	0.036 (4)	0.038 (4)	0.052 (5)	-0.004 (3)	0.007 (3)	0.005 (4)

C36	0.043 (4)	0.033 (4)	0.043 (4)	-0.005 (3)	0.001 (3)	-0.009 (3)
C37	0.040 (4)	0.053 (5)	0.042 (4)	0.011 (4)	0.018 (3)	0.002 (4)
C38	0.043 (4)	0.045 (4)	0.030 (4)	0.007 (4)	0.010 (3)	0.000 (3)
C39	0.033 (4)	0.050 (5)	0.034 (4)	0.003 (3)	0.003 (3)	0.000 (3)
C40	0.030 (4)	0.059 (5)	0.042 (4)	0.003 (4)	-0.009 (3)	-0.021 (4)
C41	0.032 (4)	0.048 (5)	0.065 (6)	-0.002 (4)	0.012 (4)	-0.002 (4)
C42	0.062 (7)	0.093 (9)	0.059 (6)	0.018 (6)	0.034 (5)	0.005 (6)
C43	0.073 (7)	0.050 (5)	0.047 (5)	0.019 (5)	-0.003 (5)	-0.008 (4)
C44	0.069 (7)	0.080 (8)	0.039 (5)	0.000 (6)	0.014 (5)	0.009 (5)
C45	0.065 (7)	0.073 (7)	0.054 (6)	0.016 (6)	-0.010 (5)	-0.016 (5)
C46	0.039 (5)	0.078 (9)	0.115 (11)	-0.014 (5)	0.011 (6)	-0.005 (8)
C47	0.030 (3)	0.031 (3)	0.022 (3)	-0.006 (3)	0.003 (2)	-0.001 (2)
C48	0.033 (3)	0.037 (4)	0.023 (3)	-0.006 (3)	0.004 (2)	-0.002 (3)
C49	0.030 (3)	0.044 (4)	0.031 (3)	-0.003 (3)	-0.005 (3)	-0.003 (3)
C50	0.030 (3)	0.039 (4)	0.036 (4)	-0.006 (3)	0.003 (3)	0.003 (3)
C51	0.032 (3)	0.037 (4)	0.030 (3)	0.000 (3)	0.008 (3)	0.001 (3)
C52	0.032 (3)	0.034 (3)	0.020 (3)	-0.002 (3)	0.001 (2)	-0.003 (2)
C53	0.039 (5)	0.105 (9)	0.037 (5)	-0.014 (5)	-0.005 (4)	-0.010 (5)
C54	0.038 (4)	0.063 (6)	0.032 (4)	-0.002 (4)	0.011 (3)	0.002 (4)
C55	0.027 (3)	0.030 (3)	0.020 (3)	-0.004 (2)	0.004 (2)	-0.003 (2)
C56	0.038 (4)	0.039 (4)	0.020 (3)	-0.008 (3)	0.006 (3)	-0.005 (3)
C57	0.044 (4)	0.040 (4)	0.024 (3)	-0.008 (3)	0.013 (3)	-0.009 (3)
C58	0.042 (4)	0.029 (3)	0.041 (4)	-0.001 (3)	0.012 (3)	-0.008 (3)
C59	0.028 (3)	0.030 (3)	0.034 (3)	0.003 (3)	0.007 (3)	0.002 (3)
C60	0.027 (3)	0.035 (4)	0.025 (3)	-0.004 (3)	0.002 (2)	-0.001 (3)
C61	0.095 (9)	0.056 (6)	0.038 (5)	-0.022 (6)	0.011 (5)	-0.025 (4)
C62	0.041 (4)	0.039 (4)	0.047 (5)	0.008 (3)	0.003 (4)	0.009 (4)
C63	0.029 (3)	0.029 (3)	0.022 (3)	-0.003 (2)	0.000 (2)	0.000 (2)
C64	0.037 (4)	0.028 (3)	0.031 (3)	-0.004 (3)	0.008 (3)	0.000 (3)
C65	0.038 (4)	0.037 (4)	0.034 (4)	-0.001 (3)	0.014 (3)	0.005 (3)
C66	0.042 (4)	0.045 (4)	0.027 (3)	0.003 (3)	0.010 (3)	-0.004 (3)
C67	0.034 (4)	0.035 (4)	0.029 (3)	-0.001 (3)	0.002 (3)	-0.009 (3)
C68	0.031 (3)	0.031 (3)	0.028 (3)	-0.006 (3)	0.004 (3)	-0.006 (3)
C69	0.057 (6)	0.072 (7)	0.061 (6)	0.011 (5)	0.033 (5)	0.022 (5)
C70	0.039 (4)	0.044 (5)	0.042 (4)	-0.003 (3)	0.005 (3)	-0.018 (4)
C71	0.032 (3)	0.033 (3)	0.018 (3)	-0.004 (3)	0.004 (2)	-0.003 (2)
C72	0.035 (4)	0.035 (4)	0.028 (3)	-0.004 (3)	0.000 (3)	0.003 (3)

C73	0.042 (4)	0.040 (4)	0.034 (4)	-0.001 (3)	-0.006 (3)	-0.003 (3)
C74	0.057 (5)	0.038 (4)	0.032 (4)	0.002 (4)	-0.008 (3)	0.005 (3)
C75	0.059 (5)	0.033 (4)	0.024 (3)	-0.004 (3)	0.004 (3)	0.003 (3)
C76	0.040 (4)	0.032 (3)	0.027 (3)	-0.010 (3)	0.009 (3)	0.000 (3)
C77	0.043 (5)	0.070 (7)	0.061 (6)	-0.003 (5)	-0.018 (5)	0.009 (5)
C78	0.092 (8)	0.042 (5)	0.034 (4)	-0.005 (5)	0.008 (5)	0.003 (4)
N1	0.047 (4)	0.033 (3)	0.039 (3)	0.006 (3)	0.002 (3)	-0.004 (3)
N2	0.041 (3)	0.034 (3)	0.034 (3)	-0.005 (3)	0.004 (3)	-0.009 (3)
B1	0.030 (3)	0.028 (3)	0.018 (3)	-0.006 (3)	0.004 (3)	-0.005 (2)
F1	0.078 (4)	0.153 (10)	0.058 (4)	-0.009 (6)	-0.033 (3)	-0.006 (5)
F2	0.078 (4)	0.153 (10)	0.058 (4)	-0.009 (6)	-0.033 (3)	-0.006 (5)
F3	0.078 (4)	0.153 (10)	0.058 (4)	-0.009 (6)	-0.033 (3)	-0.006 (5)
F1B	0.078 (4)	0.153 (10)	0.058 (4)	-0.009 (6)	-0.033 (3)	-0.006 (5)
F2B	0.078 (4)	0.153 (10)	0.058 (4)	-0.009 (6)	-0.033 (3)	-0.006 (5)
F3B	0.078 (4)	0.153 (10)	0.058 (4)	-0.009 (6)	-0.033 (3)	-0.006 (5)
F4	0.079 (4)	0.104 (5)	0.046 (3)	0.011 (4)	0.031 (3)	-0.002 (3)
F5	0.079 (4)	0.104 (5)	0.046 (3)	0.011 (4)	0.031 (3)	-0.002 (3)
F6	0.079 (4)	0.104 (5)	0.046 (3)	0.011 (4)	0.031 (3)	-0.002 (3)
F4B	0.079 (4)	0.104 (5)	0.046 (3)	0.011 (4)	0.031 (3)	-0.002 (3)
F5B	0.079 (4)	0.104 (5)	0.046 (3)	0.011 (4)	0.031 (3)	-0.002 (3)
F6B	0.079 (4)	0.104 (5)	0.046 (3)	0.011 (4)	0.031 (3)	-0.002 (3)
F7	0.189 (10)	0.132 (8)	0.052 (4)	-0.065 (7)	0.065 (5)	-0.046 (5)
F8	0.173 (9)	0.052 (4)	0.062 (4)	0.000 (5)	-0.012 (5)	-0.034 (3)
F9	0.143 (8)	0.092 (6)	0.062 (4)	0.011 (5)	-0.043 (5)	-0.038 (4)
F10	0.086 (5)	0.086 (5)	0.112 (6)	-0.028 (4)	-0.063 (5)	0.046 (5)
F11	0.191 (10)	0.064 (5)	0.063 (4)	0.067 (6)	0.019 (5)	0.017 (4)
F12	0.081 (5)	0.108 (6)	0.046 (3)	0.018 (4)	0.013 (3)	0.036 (4)
F13	0.089 (5)	0.074 (5)	0.113 (6)	-0.008 (4)	0.062 (5)	0.025 (4)
F14	0.089 (5)	0.074 (5)	0.113 (6)	-0.008 (4)	0.062 (5)	0.025 (4)
F15	0.089 (5)	0.074 (5)	0.113 (6)	-0.008 (4)	0.062 (5)	0.025 (4)
F13B	0.089 (5)	0.074 (5)	0.113 (6)	-0.008 (4)	0.062 (5)	0.025 (4)
F14B	0.089 (5)	0.074 (5)	0.113 (6)	-0.008 (4)	0.062 (5)	0.025 (4)
F15B	0.089 (5)	0.074 (5)	0.113 (6)	-0.008 (4)	0.062 (5)	0.025 (4)
F16	0.069 (4)	0.064 (4)	0.073 (4)	-0.010 (3)	0.030 (3)	-0.038 (3)
F17	0.068 (4)	0.041 (3)	0.070 (4)	-0.012 (3)	0.012 (3)	-0.013 (3)
F18	0.056 (4)	0.068 (4)	0.098 (5)	0.003 (3)	-0.031 (4)	-0.036 (4)
F19	0.061 (5)	0.244 (15)	0.188 (11)	-0.054 (7)	0.011 (6)	-0.154 (11)

F20	0.056 (4)	0.117 (7)	0.095 (6)	-0.034 (4)	-0.001 (4)	0.016 (5)
F21	0.052 (5)	0.176 (11)	0.265 (15)	-0.012 (6)	-0.031 (7)	0.156 (11)
F22	0.114 (7)	0.052 (4)	0.081 (4)	-0.003 (4)	0.034 (4)	0.027 (3)
F23	0.114 (7)	0.052 (4)	0.081 (4)	-0.003 (4)	0.034 (4)	0.027 (3)
F24	0.114 (7)	0.052 (4)	0.081 (4)	-0.003 (4)	0.034 (4)	0.027 (3)
F22B	0.114 (7)	0.052 (4)	0.081 (4)	-0.003 (4)	0.034 (4)	0.027 (3)
F23B	0.114 (7)	0.052 (4)	0.081 (4)	-0.003 (4)	0.034 (4)	0.027 (3)
F24B	0.114 (7)	0.052 (4)	0.081 (4)	-0.003 (4)	0.034 (4)	0.027 (3)
Ir1	0.04550 (17)	0.03181 (14)	0.03570 (15)	-0.00405 (12)	0.01325 (12)	-0.00787 (11)
Ir2	0.03029 (13)	0.03916 (15)	0.02706 (12)	-0.00096 (11)	0.00974 (9)	-0.00774 (11)

7.13.9 **Table A39.** Interatomic distances (Å) and angles (deg) for [**5B**][$BArF_{24}$].

C1—N1	1.333 (12)	C43—H43B	0.9800
C1—C2	1.407 (15)	C43—H43C	0.9800
C1—H1	0.9500	C44—H44A	0.9800
C2—C3	1.371 (19)	C44—H44B	0.9800
C2—H2	0.9500	C44—H44C	0.9800
C3—C4	1.387 (19)	C45—H45A	0.9800
C3—H3	0.9500	C45—H45B	0.9800
C4—C13	1.401 (14)	C45—H45C	0.9800
C4—C5	1.449 (18)	C46—H46A	0.9800
C5—C6	1.35 (2)	C46—H46B	0.9800
C5—H5	0.9500	C46—H46C	0.9800
C6—C7	1.460 (18)	C47—C48	1.402 (9)
C6—H6	0.9500	C47—C52	1.403 (9)
C7—C8	1.3900	C47—B1	1.641 (10)
C7—C12	1.3900	C48—C49	1.393 (10)
C8—C9	1.3900	C48—H48	0.9500
C8—H8	0.9500	C49—C50	1.384 (11)
C9—C10	1.3900	C49—C53	1.470 (11)
C9—H9	0.9500	C50—C51	1.382 (11)
C10—C11	1.3900	C50—H50	0.9500
C10—H10	0.9500	C51—C52	1.383 (10)
C11—C12	1.3900	C51—C54	1.487 (11)

C11—Ir1	2.078 (4)	C52—H52	0.9500
C12—C13	1.388 (12)	C53—F1B	1.28 (3)
C13—N1	1.389 (11)	C53—F3B	1.29 (3)
C14—C15	1.416 (17)	C53—F2	1.32 (2)
C14—C18	1.439 (16)	C53—F1	1.32 (2)
C14—C19	1.488 (18)	C53—F3	1.38 (2)
C14—Ir1	2.180 (9)	C53—F2B	1.39 (3)
C15—C16	1.419 (17)	C54—F5B	1.27 (2)
C15—C20	1.499 (17)	C54—F6B	1.31 (2)
C15—Ir1	2.157 (10)	C54—F6	1.324 (16)
C16—C17	1.460 (15)	C54—F4	1.340 (16)
C16—C21	1.516 (16)	C54—F5	1.352 (16)
C16—Ir1	2.172 (10)	C54—F4B	1.37 (2)
C17—C18	1.397 (16)	C55—C56	1.403 (9)
C17—C22	1.514 (17)	C55—C60	1.419 (10)
C17—Ir1	2.242 (8)	C55—B1	1.639 (10)
C18—C23	1.522 (16)	C56—C57	1.389 (11)
C18—Ir1	2.254 (9)	C56—H56	0.9500
C19—H19A	0.9800	C57—C58	1.380 (12)
C19—H19B	0.9800	C57—C61	1.502 (11)
C19—H19C	0.9800	C58—C59	1.390 (11)
C20—H20A	0.9800	C58—H58	0.9500
C20—H20B	0.9800	C59—C60	1.376 (10)
C20—H20C	0.9800	C59—C62	1.494 (11)
C21—H21A	0.9800	C60—H60	0.9500
C21—H21B	0.9800	C61—F8	1.297 (13)
C21—H21C	0.9800	C61—F9	1.311 (15)
C22—H22A	0.9800	C61—F7	1.329 (13)
C22—H22B	0.9800	C62—F11	1.307 (11)
C22—H22C	0.9800	C62—F10	1.312 (11)
C23—H23A	0.9800	C62—F12	1.325 (11)
C23—H23B	0.9800	C63—C68	1.393 (9)
C23—H23C	0.9800	C63—C64	1.408 (10)
C24—N2	1.342 (10)	C63—B1	1.638 (10)
C24—C25	1.392 (14)	C64—C65	1.399 (10)
C24—H24	0.9500	C64—H64	0.9500
C25—C26	1.379 (18)	C65—C66	1.370 (12)

C25—H25	0.9500	C65—C69	1.494 (12)
C26—C27	1.402 (17)	C66—C67	1.375 (11)
C26—H26	0.9500	C66—H66	0.9500
C27—C36	1.411 (12)	C67—C68	1.396 (10)
C27—C28	1.428 (18)	C67—C70	1.492 (11)
C28—C29	1.36 (2)	C68—H68	0.9500
C28—H28	0.9500	C69—F13	1.238 (17)
C29—C30	1.425 (17)	C69—F15	1.296 (18)
C29—H29	0.9500	C69—F14	1.332 (18)
C30—C31	1.399 (17)	C69—F14B	1.38 (3)
C30—C35	1.412 (13)	C69—F15B	1.45 (2)
C31—C32	1.359 (19)	C69—F13B	1.47 (3)
C31—H31	0.9500	C70—F18	1.325 (10)
C32—C33	1.412 (13)	C70—F17	1.338 (11)
C32—H32	0.9500	C70—F16	1.339 (10)
C33—C34	1.397 (11)	C71—C76	1.397 (10)
C33—H33	0.9500	C71—C72	1.402 (10)
C34—C35	1.412 (12)	C71—B1	1.636 (10)
C34—Ir2	2.040 (7)	C72—C73	1.395 (11)
C35—C36	1.414 (12)	C72—H72	0.9500
C36—N2	1.366 (11)	C73—C74	1.381 (12)
C37—C41	1.401 (14)	C73—C77	1.506 (13)
C37—C38	1.434 (13)	C74—C75	1.388 (13)
C37—C42	1.499 (12)	C74—H74	0.9500
C37—Ir2	2.255 (8)	C75—C76	1.397 (11)
C38—C39	1.438 (11)	C75—C78	1.475 (12)
C38—C43	1.496 (13)	C76—H76	0.9500
C38—Ir2	2.179 (8)	C77—F21	1.265 (14)
C39—C40	1.426 (13)	C77—F19	1.269 (15)
C39—C44	1.513 (13)	C77—F20	1.334 (14)
C39—Ir2	2.172 (9)	C78—F23B	1.29 (2)
C40—C41	1.439 (14)	C78—F22	1.295 (18)
C40—C45	1.518 (13)	C78—F23	1.337 (18)
C40—Ir2	2.177 (8)	C78—F24B	1.34 (3)
C41—C46	1.502 (15)	C78—F24	1.366 (17)
C41—Ir2	2.242 (9)	C78—F22B	1.47 (2)
C42—H42A	0.9800	N1—Ir1	2.088 (7)

C42—H42B	0.9800	N2—Ir2	2.090 (7)
C42—H42C	0.9800	Ir1—H1A	1.8569
C43—H43A	0.9800	Ir2—H1A	1.7869
N1—C1—C2	121.8 (10)	C50—C49—C53	119.5 (8)
N1—C1—H1	119.1	C48—C49—C53	119.4 (7)
C2—C1—H1	119.1	C51—C50—C49	118.1 (7)
C3—C2—C1	119.7 (12)	C51—C50—H50	120.9
C3—C2—H2	120.1	C49—C50—H50	120.9
C1—C2—H2	120.1	C50—C51—C52	120.6 (7)
C2—C3—C4	120.0 (11)	C50—C51—C54	119.1 (7)
C2—C3—H3	120.0	C52—C51—C54	120.2 (7)
C4—C3—H3	120.0	C51—C52—C47	123.1 (6)
C3—C4—C13	118.1 (11)	C51—C52—H52	118.5
C3—C4—C5	126.0 (12)	C47—C52—H52	118.5
C13—C4—C5	115.9 (13)	F1B—C53—F3B	110.6 (17)
C6—C5—C4	121.0 (13)	F2—C53—F1	108.5 (13)
C6—C5—H5	119.5	F2—C53—F3	102.6 (13)
C4—C5—H5	119.5	F1—C53—F3	103.5 (12)
C5—C6—C7	122.1 (11)	F1B—C53—F2B	105.8 (18)
C5—C6—H6	118.9	F3B—C53—F2B	92.1 (17)
C7—C6—H6	118.9	F1B—C53—C49	118.6 (12)
C8—C7—C12	120.0	F3B—C53—C49	116.4 (14)
C8—C7—C6	123.5 (9)	F2—C53—C49	115.9 (10)
C12—C7—C6	116.5 (9)	F1—C53—C49	114.7 (11)
C7—C8—C9	120.0	F3—C53—C49	110.1 (10)
C7—C8—H8	120.0	F2B—C53—C49	109.5 (12)
C9—C8—H8	120.0	F5B—C54—F6B	116.8 (14)
C10—C9—C8	120.0	F6—C54—F4	105.1 (10)
C10—C9—H9	120.0	F6—C54—F5	106.8 (11)
C8—C9—H9	120.0	F4—C54—F5	99.1 (9)
C9—C10—C11	120.0	F5B—C54—F4B	102.7 (14)
C9—C10—H10	120.0	F6B—C54—F4B	100.3 (13)
C11—C10—H10	120.0	F5B—C54—C51	115.6 (10)
C12—C11—C10	120.0	F6B—C54—C51	112.0 (10)
C12—C11—Ir1	112.0 (4)	F6—C54—C51	117.0 (8)
C10—C11—Ir1	127.9 (4)	F4—C54—C51	113.8 (9)

C13—C12—C11	119.0 (6)	F5—C54—C51	113.2 (8)
C13—C12—C7	120.8 (6)	F4B—C54—C51	107.3 (9)
C11—C12—C7	120.0	C56—C55—C60	115.0 (6)
C12—C13—N1	114.6 (8)	C56—C55—B1	123.3 (6)
C12—C13—C4	123.4 (9)	C60—C55—B1	121.1 (6)
N1—C13—C4	122.0 (10)	C57—C56—C55	122.4 (7)
C15—C14—C18	107.1 (10)	C57—C56—H56	118.8
C15—C14—C19	128.8 (12)	C55—C56—H56	118.8
C18—C14—C19	123.8 (12)	C58—C57—C56	121.0 (7)
C15—C14—Ir1	70.1 (6)	C58—C57—C61	120.2 (8)
C18—C14—Ir1	73.9 (6)	C56—C57—C61	118.7 (8)
C19—C14—Ir1	126.4 (8)	C57—C58—C59	118.2 (7)
C14—C15—C16	109.9 (10)	C57—C58—H58	120.9
C14—C15—C20	127.1 (13)	C59—C58—H58	120.9
C16—C15—C20	122.9 (13)	C60—C59—C58	121.0 (7)
C14—C15—Ir1	71.8 (6)	C60—C59—C62	118.4 (7)
C16—C15—Ir1	71.4 (6)	C58—C59—C62	120.6 (7)
C20—C15—Ir1	126.8 (8)	C59—C60—C55	122.4 (7)
C15—C16—C17	105.7 (10)	C59—C60—H60	118.8
C15—C16—C21	127.3 (12)	C55—C60—H60	118.8
C17—C16—C21	125.8 (12)	F8—C61—F9	107.0 (10)
C15—C16—Ir1	70.3 (6)	F8—C61—F7	108.2 (11)
C17—C16—Ir1	73.3 (5)	F9—C61—F7	104.2 (11)
C21—C16—Ir1	130.8 (7)	F8—C61—C57	113.6 (10)
C18—C17—C16	108.9 (10)	F9—C61—C57	112.3 (9)
C18—C17—C22	124.7 (11)	F7—C61—C57	110.9 (9)
C16—C17—C22	126.4 (11)	F11—C62—F10	107.6 (9)
C18—C17—Ir1	72.4 (5)	F11—C62—F12	104.5 (9)
C16—C17—Ir1	68.1 (5)	F10—C62—F12	103.5 (9)
C22—C17—Ir1	128.0 (8)	F11—C62—C59	113.7 (8)
C17—C18—C14	108.3 (10)	F10—C62—C59	114.1 (8)
C17—C18—C23	123.6 (12)	F12—C62—C59	112.4 (7)
C14—C18—C23	127.8 (12)	C68—C63—C64	115.8 (6)
C17—C18—Ir1	71.4 (5)	C68—C63—B1	121.1 (6)
C14—C18—Ir1	68.3 (5)	C64—C63—B1	122.6 (6)
C23—C18—Ir1	130.5 (8)	C65—C64—C63	121.4 (7)
C14—C19—H19A	109.5	C65—C64—H64	119.3

C14—C19—H19B	109.5	C63—C64—H64	119.3
H19A—C19—H19B	109.5	C66—C65—C64	121.3 (7)
C14—C19—H19C	109.5	C66—C65—C69	120.2 (8)
H19A—C19—H19C	109.5	C64—C65—C69	118.5 (8)
H19B—C19—H19C	109.5	C65—C66—C67	118.5 (7)
C15—C20—H20A	109.5	C65—C66—H66	120.8
C15—C20—H20B	109.5	C67—C66—H66	120.8
H20A—C20—H20B	109.5	C66—C67—C68	120.8 (7)
C15—C20—H20C	109.5	C66—C67—C70	120.3 (7)
H20A—C20—H20C	109.5	C68—C67—C70	118.8 (7)
H20B—C20—H20C	109.5	C63—C68—C67	122.2 (7)
C16—C21—H21A	109.5	C63—C68—H68	118.9
C16—C21—H21B	109.5	C67—C68—H68	118.9
H21A—C21—H21B	109.5	F13—C69—F15	109.4 (15)
C16—C21—H21C	109.5	F13—C69—F14	111.8 (12)
H21A—C21—H21C	109.5	F15—C69—F14	92.0 (12)
H21B—C21—H21C	109.5	F14B—C69—F15B	91.2 (15)
C17—C22—H22A	109.5	F14B—C69—F13B	140.9 (13)
C17—C22—H22B	109.5	F15B—C69—F13B	82.7 (15)
H22A—C22—H22B	109.5	F13—C69—C65	118.4 (10)
C17—C22—H22C	109.5	F15—C69—C65	110.1 (10)
H22A—C22—H22C	109.5	F14—C69—C65	112.0 (11)
H22B—C22—H22C	109.5	F14B—C69—C65	112.0 (12)
C18—C23—H23A	109.5	F15B—C69—C65	111.6 (11)
C18—C23—H23B	109.5	F13B—C69—C65	106.1 (10)
H23A—C23—H23B	109.5	F18—C70—F17	104.3 (8)
C18—C23—H23C	109.5	F18—C70—F16	107.8 (7)
H23A—C23—H23C	109.5	F17—C70—F16	105.8 (8)
H23B—C23—H23C	109.5	F18—C70—C67	112.1 (8)
N2—C24—C25	120.4 (10)	F17—C70—C67	113.1 (7)
N2—C24—H24	119.8	F16—C70—C67	113.2 (7)
C25—C24—H24	119.8	C76—C71—C72	115.9 (7)
C26—C25—C24	121.3 (10)	C76—C71—B1	123.7 (6)
C26—C25—H25	119.4	C72—C71—B1	119.9 (6)
C24—C25—H25	119.4	C73—C72—C71	122.6 (7)
C25—C26—C27	119.4 (10)	C73—C72—H72	118.7
C25—C26—H26	120.3	C71—C72—H72	118.7

C27—C26—H26	120.3	C74—C73—C72	120.0 (8)
C26—C27—C36	116.6 (10)	C74—C73—C77	121.0 (8)
C26—C27—C28	126.1 (11)	C72—C73—C77	118.9 (8)
C36—C27—C28	117.2 (11)	C73—C74—C75	119.0 (8)
C29—C28—C27	121.7 (11)	C73—C74—H74	120.5
C29—C28—H28	119.1	C75—C74—H74	120.5
C27—C28—H28	119.1	C74—C75—C76	120.5 (7)
C28—C29—C30	121.8 (12)	C74—C75—C78	120.4 (8)
C28—C29—H29	119.1	C76—C75—C78	119.1 (8)
C30—C29—H29	119.1	C75—C76—C71	122.0 (7)
C31—C30—C35	117.5 (10)	C75—C76—H76	119.0
C31—C30—C29	124.9 (11)	C71—C76—H76	119.0
C35—C30—C29	117.6 (12)	F21—C77—F19	111.6 (12)
C32—C31—C30	120.2 (9)	F21—C77—F20	102.3 (12)
C32—C31—H31	119.9	F19—C77—F20	102.7 (12)
C30—C31—H31	119.9	F21—C77—C73	113.6 (10)
C31—C32—C33	122.4 (11)	F19—C77—C73	112.9 (10)
C31—C32—H32	118.8	F20—C77—C73	112.7 (8)
C33—C32—H32	118.8	F22—C78—F23	104.2 (12)
C34—C33—C32	119.8 (10)	F23B—C78—F24B	134.5 (16)
C34—C33—H33	120.1	F22—C78—F24	102.6 (12)
C32—C33—H33	120.1	F23—C78—F24	103.6 (11)
C33—C34—C35	116.8 (8)	F23B—C78—F22B	93.7 (14)
C33—C34—Ir2	129.3 (7)	F24B—C78—F22B	83.5 (14)
C35—C34—Ir2	113.7 (6)	F23B—C78—C75	112.8 (12)
C34—C35—C30	123.4 (9)	F22—C78—C75	115.9 (9)
C34—C35—C36	116.2 (7)	F23—C78—C75	115.3 (11)
C30—C35—C36	120.4 (9)	F24B—C78—C75	111.2 (11)
N2—C36—C27	123.1 (9)	F24—C78—C75	113.7 (10)
N2—C36—C35	115.7 (7)	F22B—C78—C75	108.1 (11)
C27—C36—C35	121.2 (9)	C1—N1—C13	118.3 (8)
C41—C37—C38	107.2 (7)	C1—N1—Ir1	127.2 (6)
C41—C37—C42	127.5 (10)	C13—N1—Ir1	113.9 (6)
C38—C37—C42	124.8 (9)	C24—N2—C36	119.1 (8)
C41—C37—Ir2	71.3 (5)	C24—N2—Ir2	126.4 (6)
C38—C37—Ir2	68.3 (5)	C36—N2—Ir2	114.0 (5)
C42—C37—Ir2	131.6 (7)	C71—B1—C63	104.2 (6)

C37—C38—C39	108.0 (8)	C71—B1—C55	112.2 (5)
C37—C38—C43	125.9 (8)	C63—B1—C55	112.4 (5)
C39—C38—C43	125.8 (8)	C71—B1—C47	112.2 (5)
C37—C38—Ir2	74.0 (5)	C63—B1—C47	113.9 (5)
C39—C38—Ir2	70.4 (5)	C55—B1—C47	102.2 (6)
C43—C38—Ir2	126.0 (6)	C11—Ir1—N1	78.7 (3)
C40—C39—C38	108.2 (8)	C11—Ir1—C15	97.0 (4)
C40—C39—C44	125.3 (8)	N1—Ir1—C15	118.3 (4)
C38—C39—C44	126.5 (9)	C11—Ir1—C16	105.8 (3)
C40—C39—Ir2	71.0 (5)	N1—Ir1—C16	155.8 (4)
C38—C39—Ir2	71.0 (5)	C15—Ir1—C16	38.3 (5)
C44—C39—Ir2	125.2 (7)	C11—Ir1—C14	121.4 (4)
C39—C40—C41	106.4 (7)	N1—Ir1—C14	92.7 (4)
C39—C40—C45	125.5 (10)	C15—Ir1—C14	38.1 (5)
C41—C40—C45	126.0 (9)	C16—Ir1—C14	64.5 (4)
C39—C40—Ir2	70.7 (4)	C11—Ir1—C17	142.5 (3)
C41—C40—Ir2	73.5 (5)	N1—Ir1—C17	138.2 (4)
C45—C40—Ir2	133.6 (7)	C15—Ir1—C17	62.9 (4)
C37—C41—C40	110.1 (8)	C16—Ir1—C17	38.6 (4)
C37—C41—C46	125.0 (10)	C14—Ir1—C17	62.6 (4)
C40—C41—C46	124.8 (10)	C11—Ir1—C18	158.5 (4)
C37—C41—Ir2	72.4 (5)	N1—Ir1—C18	103.9 (4)
C40—C41—Ir2	68.5 (5)	C15—Ir1—C18	62.7 (4)
C46—C41—Ir2	128.3 (8)	C16—Ir1—C18	63.3 (4)
C37—C42—H42A	109.5	C14—Ir1—C18	37.8 (4)
C37—C42—H42B	109.5	C17—Ir1—C18	36.2 (4)
H42A—C42—H42B	109.5	C11—Ir1—H1A	93.7
C37—C42—H42C	109.5	N1—Ir1—H1A	111.0
H42A—C42—H42C	109.5	C15—Ir1—H1A	130.7
H42B—C42—H42C	109.5	C16—Ir1—H1A	92.6
C38—C43—H43A	109.5	C14—Ir1—H1A	141.4
C38—C43—H43B	109.5	C17—Ir1—H1A	79.9
H43A—C43—H43B	109.5	C18—Ir1—H1A	104.9
C38—C43—H43C	109.5	C34—Ir2—N2	79.1 (3)
H43A—C43—H43C	109.5	C34—Ir2—C39	95.1 (3)
H43B—C43—H43C	109.5	N2—Ir2—C39	120.2 (3)
C39—C44—H44A	109.5	C34—Ir2—C40	105.5 (3)

C39—C44—H44B	109.5	N2—Ir2—C40	157.4 (3)
H44A—C44—H44B	109.5	C39—Ir2—C40	38.3 (3)
C39—C44—H44C	109.5	C34—Ir2—C38	119.8 (3)
H44A—C44—H44C	109.5	N2—Ir2—C38	94.0 (3)
H44B—C44—H44C	109.5	C39—Ir2—C38	38.6 (3)
C40—C45—H45A	109.5	C40—Ir2—C38	64.3 (3)
C40—C45—H45B	109.5	C34—Ir2—C41	142.0 (3)
H45A—C45—H45B	109.5	N2—Ir2—C41	138.1 (3)
C40—C45—H45C	109.5	C39—Ir2—C41	62.6 (3)
H45A—C45—H45C	109.5	C40—Ir2—C41	38.0 (4)
H45B—C45—H45C	109.5	C38—Ir2—C41	62.1 (3)
C41—C46—H46A	109.5	C34—Ir2—C37	156.9 (3)
C41—C46—H46B	109.5	N2—Ir2—C37	103.8 (3)
H46A—C46—H46B	109.5	C39—Ir2—C37	63.3 (3)
C41—C46—H46C	109.5	C40—Ir2—C37	63.4 (3)
H46A—C46—H46C	109.5	C38—Ir2—C37	37.7 (3)
H46B—C46—H46C	109.5	C41—Ir2—C37	36.3 (4)
C48—C47—C52	115.1 (6)	C34—Ir2—H1A	93.3
C48—C47—B1	124.3 (6)	N2—Ir2—H1A	108.7
C52—C47—B1	120.2 (6)	C39—Ir2—H1A	131.1
C49—C48—C47	122.1 (6)	C40—Ir2—H1A	93.2
C49—C48—H48	118.9	C38—Ir2—H1A	143.2
C47—C48—H48	118.9	C41—Ir2—H1A	82.1
C50—C49—C48	121.0 (7)	C37—Ir2—H1A	107.0
N1—C1—C2—C3	-0.4 (18)	C49—C50—C51—C54	-176.8 (8)
C1—C2—C3—C4	1.6 (19)	C50—C51—C52—C47	0.1 (12)
C2—C3—C4—C13	-1.0 (18)	C54—C51—C52—C47	178.1 (8)
C2—C3—C4—C5	175.3 (13)	C48—C47—C52—C51	-1.4 (11)
C3—C4—C5—C6	-176.7 (14)	B1—C47—C52—C51	-173.8 (7)
C13—C4—C5—C6	0 (2)	C50—C49—C53—F1B	-168 (2)
C4—C5—C6—C7	1 (2)	C48—C49—C53—F1B	11 (2)
C5—C6—C7—C8	176.9 (12)	C50—C49—C53—	-32 (2)

		F3B	
C5—C6—C7—C12	-4.5 (18)	C48—C49—C53—F3B	146.8 (17)
C12—C7—C8—C9	0.0	C50—C49—C53—F2	9.6 (19)
C6—C7—C8—C9	178.6 (10)	C48—C49—C53—F2	-171.6 (14)
C7—C8—C9—C10	0.0	C50—C49—C53—F1	137.4 (13)
C8—C9—C10—C11	0.0	C48—C49—C53—F1	-43.8 (17)
C9—C10—C11—C12	0.0	C50—C49—C53—F3	-106.3 (12)
C9—C10—C11—Ir1	-175.4 (5)	C48—C49—C53—F3	72.5 (14)
C10—C11—C12—C13	174.3 (7)	C50—C49—C53—F2B	70.6 (16)
Ir1—C11—C12—C13	-9.6 (7)	C48—C49—C53—F2B	-110.6 (15)
C10—C11—C12—C7	0.0	C50—C51—C54—F5B	-1.9 (17)
Ir1—C11—C12—C7	176.1 (5)	C52—C51—C54—F5B	-180.0 (14)
C8—C7—C12—C13	-174.2 (7)	C50—C51—C54—F6B	135.1 (13)
C6—C7—C12—C13	7.1 (10)	C52—C51—C54—F6B	-43.0 (15)
C8—C7—C12—C11	0.0	C50—C51—C54—F6	175.4 (11)
C6—C7—C12—C11	-178.7 (9)	C52—C51—C54—F6	-2.6 (15)
C11—C12—C13—N1	-0.5 (10)	C50—C51—C54—F4	-61.6 (12)
C7—C12—C13—N1	173.8 (6)	C52—C51—C54—F4	120.3 (10)
C11—C12—C13—C4	179.0 (8)	C50—C51—C54—F5	50.5 (13)
C7—C12—C13—C4	-6.8 (12)	C52—C51—C54—F5	-127.5 (10)
C3—C4—C13—C12	179.7 (10)	C50—C51—C54—F4B	-115.8 (12)
C5—C4—C13—C12	3.1 (15)	C52—C51—C54—F4B	66.1 (14)
C3—C4—C13—N1	-0.8 (16)	C60—C55—C56—C57	-0.1 (10)
C5—C4—C13—N1	-177.5 (10)	B1—C55—C56—C57	171.5 (7)
C18—C14—C15—C16	3.6 (11)	C55—C56—C57—C58	-0.2 (12)
C19—C14—C15—C16	177.1 (11)	C55—C56—C57—C61	-177.0 (8)
Ir1—C14—C15—C16	-61.6 (7)	C56—C57—C58—C59	0.9 (12)
C18—C14—C15—C20	-172.0 (10)	C61—C57—C58—C59	177.7 (8)

C19—C14—C15—C20	1.5 (18)	C57—C58—C59—C60	-1.4 (11)
Ir1—C14—C15—C20	122.8 (11)	C57—C58—C59—C62	179.3 (7)
C18—C14—C15—Ir1	65.1 (6)	C58—C59—C60—C55	1.2 (11)
C19—C14—C15—Ir1	-121.3 (11)	C62—C59—C60—C55	-179.5 (7)
C14—C15—C16—C17	-3.5 (11)	C56—C55—C60—C59	-0.4 (10)
C20—C15—C16—C17	172.3 (10)	B1—C55—C60—C59	-172.2 (6)
Ir1—C15—C16—C17	-65.4 (6)	C58—C57—C61—F8	4.0 (15)
C14—C15—C16—C21	-171.3 (10)	C56—C57—C61—F8	-179.1 (10)
C20—C15—C16—C21	4.5 (17)	C58—C57—C61—F9	125.8 (10)
Ir1—C15—C16—C21	126.9 (11)	C56—C57—C61—F9	-57.4 (13)
C14—C15—C16—Ir1	61.8 (7)	C58—C57—C61—F7	-118.1 (11)
C20—C15—C16—Ir1	-122.3 (11)	C56—C57—C61—F7	58.7 (14)
C15—C16—C17—C18	2.1 (10)	C60—C59—C62—F11	-163.3 (9)
C21—C16—C17—C18	170.1 (10)	C58—C59—C62—F11	16.0 (12)
Ir1—C16—C17—C18	-61.2 (6)	C60—C59—C62—F10	-39.3 (11)
C15—C16—C17—C22	-174.8 (10)	C58—C59—C62—F10	140.0 (9)
C21—C16—C17—C22	-6.8 (16)	C60—C59—C62—F12	78.2 (10)
Ir1—C16—C17—C22	121.9 (10)	C58—C59—C62—F12	-102.5 (9)
C15—C16—C17—Ir1	63.3 (7)	C68—C63—C64—C65	-1.3 (11)
C21—C16—C17—Ir1	-128.7 (10)	B1—C63—C64—C65	-173.0 (7)
C16—C17—C18—C14	0.0 (10)	C63—C64—C65—C66	0.4 (12)
C22—C17—C18—C14	177.0 (9)	C63—C64—C65—C69	-179.2 (8)
Ir1—C17—C18—C14	-58.5 (6)	C64—C65—C66—C67	-0.1 (13)
C16—C17—C18—C23	-174.7 (10)	C69—C65—C66—C67	179.5 (9)

C22—C17—C18—C23	2.3 (16)	C65—C66—C67—C68	0.7 (12)
Ir1—C17—C18—C23	126.8 (10)	C65—C66—C67—C70	-177.7 (8)
C16—C17—C18—Ir1	58.5 (6)	C64—C63—C68—C67	1.9 (11)
C22—C17—C18—Ir1	-124.5 (10)	B1—C63—C68—C67	173.8 (7)
C15—C14—C18—C17	-2.1 (10)	C66—C67—C68—C63	-1.7 (12)
C19—C14—C18—C17	-176.1 (10)	C70—C67—C68—C63	176.8 (7)
Ir1—C14—C18—C17	60.5 (7)	C66—C65—C69—F13	-152.2 (13)
C15—C14—C18—C23	172.3 (10)	C64—C65—C69—F13	27.3 (17)
C19—C14—C18—C23	-1.7 (17)	C66—C65—C69—F15	81.0 (15)
Ir1—C14—C18—C23	-125.1 (11)	C64—C65—C69—F15	-99.5 (14)
C15—C14—C18—Ir1	-62.6 (6)	C66—C65—C69—F14	-19.9 (15)
C19—C14—C18—Ir1	123.4 (10)	C64—C65—C69—F14	159.7 (11)
N2—C24—C25—C26	0.9 (16)	C66—C65—C69—F14B	-65.2 (16)
C24—C25—C26—C27	0.2 (17)	C64—C65—C69—F14B	114.4 (14)
C25—C26—C27—C36	-0.7 (16)	C66—C65—C69—F15B	35.4 (19)
C25—C26—C27—C28	178.7 (12)	C64—C65—C69—F15B	-145.1 (15)
C26—C27—C28—C29	-177.9 (14)	C66—C65—C69—F13B	123.8 (13)
C36—C27—C28—C29	2 (2)	C64—C65—C69—F13B	-56.6 (14)
C27—C28—C29—C30	-1 (2)	C66—C67—C70—F18	105.7 (9)
C28—C29—C30—C31	177.9 (15)	C68—C67—C70—F18	-72.7 (10)
C28—C29—C30—C35	-1 (2)	C66—C67—C70—F17	-136.7 (8)
C35—C30—C31—C32	-1.6 (19)	C68—C67—C70—F17	44.8 (11)
C29—C30—C31—	179.7 (14)	C66—C67—C70—	-16.4 (12)

C32		F16	
C30—C31—C32—C33	2 (2)	C68—C67—C70—F16	165.1 (8)
C31—C32—C33—C34	-1 (2)	C76—C71—C72—C73	1.2 (11)
C32—C33—C34—C35	1.1 (15)	B1—C71—C72—C73	173.1 (7)
C32—C33—C34—Ir2	-173.4 (9)	C71—C72—C73—C74	0.6 (13)
C33—C34—C35—C30	-1.3 (14)	C71—C72—C73—C77	-180.0 (8)
Ir2—C34—C35—C30	174.0 (8)	C72—C73—C74—C75	-0.9 (13)
C33—C34—C35—C36	177.3 (9)	C77—C73—C74—C75	179.6 (9)
Ir2—C34—C35—C36	-7.4 (10)	C73—C74—C75—C76	-0.4 (13)
C31—C30—C35—C34	1.6 (16)	C73—C74—C75—C78	-178.6 (8)
C29—C30—C35—C34	-179.6 (11)	C74—C75—C76—C71	2.3 (12)
C31—C30—C35—C36	-176.9 (10)	C78—C75—C76—C71	-179.6 (8)
C29—C30—C35—C36	1.8 (16)	C72—C71—C76—C75	-2.6 (11)
C26—C27—C36—N2	0.4 (15)	B1—C71—C76—C75	-174.2 (7)
C28—C27—C36—N2	-179.2 (10)	C74—C73—C77—F21	-20.0 (17)
C26—C27—C36—C35	179.1 (9)	C72—C73—C77—F21	160.5 (12)
C28—C27—C36—C35	-0.4 (15)	C74—C73—C77—F19	108.4 (13)
C34—C35—C36—N2	-1.1 (12)	C72—C73—C77—F19	-71.1 (14)
C30—C35—C36—N2	177.6 (9)	C74—C73—C77—F20	-135.8 (10)
C34—C35—C36—C27	-179.9 (9)	C72—C73—C77—F20	44.7 (14)
C30—C35—C36—C27	-1.2 (14)	C74—C75—C78—F23B	-58.6 (17)
C41—C37—C38—C39	-1.6 (10)	C76—C75—C78—F23B	123.2 (15)
C42—C37—C38—C39	170.9 (9)	C74—C75—C78—F22	99.2 (14)

Ir2—C37—C38—C39	-62.6 (6)	C76—C75—C78—F22	-79.0 (15)
C41—C37—C38—C43	-175.7 (9)	C74—C75—C78—F23	-22.8 (15)
C42—C37—C38—C43	-3.3 (15)	C76—C75—C78—F23	159.0 (10)
Ir2—C37—C38—C43	123.2 (9)	C74—C75—C78—F24B	133.4 (14)
C41—C37—C38—Ir2	61.1 (6)	C76—C75—C78—F24B	-44.7 (16)
C42—C37—C38—Ir2	-126.4 (10)	C74—C75—C78—F24	-142.3 (10)
C37—C38—C39—C40	3.4 (10)	C76—C75—C78—F24	39.6 (13)
C43—C38—C39—C40	177.5 (8)	C74—C75—C78—F22B	43.5 (14)
Ir2—C38—C39—C40	-61.6 (6)	C76—C75—C78—F22B	-134.6 (12)
C37—C38—C39—C44	-174.8 (9)	C2—C1—N1—C13	-1.4 (14)
C43—C38—C39—C44	-0.6 (15)	C2—C1—N1—Ir1	168.3 (8)
Ir2—C38—C39—C44	120.2 (9)	C12—C13—N1—C1	-178.5 (8)
C37—C38—C39—Ir2	65.0 (6)	C4—C13—N1—C1	2.1 (13)
C43—C38—C39—Ir2	-120.8 (9)	C12—C13—N1—Ir1	10.5 (9)
C38—C39—C40—C41	-3.8 (10)	C4—C13—N1—Ir1	-169.0 (8)
C44—C39—C40—C41	174.4 (9)	C25—C24—N2—C36	-1.2 (13)
Ir2—C39—C40—C41	-65.4 (6)	C25—C24—N2—Ir2	170.9 (7)
C38—C39—C40—C45	-168.0 (9)	C27—C36—N2—C24	0.6 (13)
C44—C39—C40—C45	10.2 (14)	C35—C36—N2—C24	-178.1 (8)
Ir2—C39—C40—C45	130.4 (9)	C27—C36—N2—Ir2	-172.4 (7)
C38—C39—C40—Ir2	61.6 (6)	C35—C36—N2—Ir2	8.8 (10)
C44—C39—C40—Ir2	-120.2 (9)	C76—C71—B1—C63	98.8 (7)
C38—C37—C41—C40	-0.8 (11)	C72—C71—B1—C63	-72.5 (8)
C42—C37—C41—C40	-173.0 (10)	C76—C71—B1—C55	-139.3 (7)
Ir2—C37—C41—C40	58.3 (6)	C72—C71—B1—C55	49.4 (8)
C38—C37—C41—	176.0 (10)	C76—C71—B1—C47	-24.9 (9)

C46			
C42—C37—C41—C46	3.8 (17)	C72—C71—B1—C47	163.8 (6)
Ir2—C37—C41—C46	-124.9 (11)	C68—C63—B1—C71	-76.9 (8)
C38—C37—C41—Ir2	-59.1 (6)	C64—C63—B1—C71	94.4 (8)
C42—C37—C41—Ir2	128.7 (10)	C68—C63—B1—C55	161.4 (6)
C39—C40—C41—C37	2.9 (10)	C64—C63—B1—C55	-27.3 (9)
C45—C40—C41—C37	167.0 (9)	C68—C63—B1—C47	45.7 (9)
Ir2—C40—C41—C37	-60.6 (7)	C64—C63—B1—C47	-143.0 (7)
C39—C40—C41—C46	-173.9 (10)	C56—C55—B1—C71	26.1 (9)
C45—C40—C41—C46	-9.8 (16)	C60—C55—B1—C71	-162.8 (6)
Ir2—C40—C41—C46	122.6 (10)	C56—C55—B1—C63	143.2 (7)
C39—C40—C41—Ir2	63.5 (5)	C60—C55—B1—C63	-45.8 (9)
C45—C40—C41—Ir2	-132.4 (10)	C56—C55—B1—C47	-94.3 (7)
C52—C47—C48—C49	1.5 (11)	C60—C55—B1—C47	76.7 (7)
B1—C47—C48—C49	173.6 (7)	C48—C47—B1—C71	139.5 (7)
C47—C48—C49—C50	-0.2 (13)	C52—C47—B1—C71	-48.7 (9)
C47—C48—C49—C53	-179.0 (9)	C48—C47—B1—C63	21.5 (10)
C48—C49—C50—C51	-1.1 (12)	C52—C47—B1—C63	-166.8 (6)
C53—C49—C50—C51	177.7 (9)	C48—C47—B1—C55	-100.1 (8)
C49—C50—C51—C52	1.2 (12)	C52—C47—B1—C55	71.7 (8)

Mustapha HAMDAOUI

ÉTUDE ET APPLICATIONS DE LA RÉACTION D'ACTIVATION DES SILANES PAR LES IRIDACYCLES

Une contribution á l'élaboration de catalyseurs multicompétents

Résumé en français

Une nouvelle famille de précatalyseurs à base d'Ir(III) a été découverte. La facilité de leur préparation, leur remarquable stabilité, et surtout leur excellente efficacité catalytique dans plusieurs réactions, c.-à-d. la *O*-silylation d'alcools, l'hydrosilylation de fonctions C=O et C≡N et l'activation de la liaison C–F, constituent un ensemble de propriétés que d'autres précatalyseurs organométalliques similaires connus à ce jour ne possèdent pas. Le fait le plus significatif est la mise en évidence expérimentale et théorique que les espèces catalytiques impliquées fonctionnement comme une paire de Lewis du type donneur–accepteur [Ir(III)H]→[SiR_3]. Dans ce cas le ligand silylium doit être considéré comme un ligand Z en appliquant le formalisme de Green, ce qui suggère un état d'oxidation formel de +III pour l'atome d'iridium. Cette thèse a contribué à une meilleure compréhension de la chimie du silylium appliquée à la chimie organométallique, et a abouti à l'émergence d'un nouveau champ de recherche qui pourra permettre l'élaboration de nouveaux précatalyseurs multicompétents.

Mots clés :

iridacycles ioniques — catalyse homogène — *O*-silylation — hydrosilylation — activation C–F — intermédiaires donneur-accepteur — [Ir(III)H]→[SiR_3] — ion silylium — ligand Z.

Résumé en anglais

A new family of highly active iridacyclic Ir(III) precatalysts has been discovered. Notably, these ionic iridacycles are very stable so that their handling under air whether in solution or as solid powder is possible. The relative simplicity of their molecular structures allows their preparation on gram scale through a very simple and convenient synthetic protocol. We identified important iridium-silane intermediates involved in the catalysis of various reactions, e.g. the *O*-silylation of alcohols, the hydrosilylation of C=O and C≡N functions, and the activation of the C(sp^3)–F bond of fluorocarbons. Experimental and theoretical studies of these intermediates point towards a Lewis donor-acceptor structural formulation of the type [Ir(III)H]→[SiR_3]. These results constitute a significant contribution to the design of future multicompetent precatalysts, and provide an original insight to the bonding within the Si–Ir–H motif by considering the silylium ion $[SiR_3]^+$ as a Z-type ligand rather than a "traditional" X ligand.

Key Words:

ionic iridacycles — homogeneous catalysis — *O*-silylation — hydrosilylation — C–F bond activation — donor-acceptor intermediates — [Ir(III)H]→[SiR_3] — silylium ion — Z ligand.